PROCEEDINGS

13th International Congress on

Neutron Capture Therapy

"A new option against cancer"

Florence, 2-7 November 2008

Edited by A. Zonta, S. Altieri, L. Roveda and R. Barth

ENEA
Italian National Agency for New Technologies,
Energy and the Environment

13th International Congress on Neutron Capture Therapy
"A new option against cancer"
November 2-7, 2008, Florence, Italy
Proceedings

Edited by Aris Zonta, Saverio Altieri, Laura Roveda, Rolf Barth

2008 ENEA
Italian National Agency for New Technologies,
Energy and the Environment

ISBN: 88-8286-167-8

Index

PRESIDENT'S ADDRESS
BNCT: A New Option Against Cancer

Dear Participants in the ICNCT-13,

On behalf of the President, the Secretary General, and the Organizing Committee, I am glad to welcome you in Florence for the traditional congress of ISNCT. It is a honor to host all of you in one of the most beautiful cities in Italy, rich in history, art and traditions. In this occasion Florence will also be the location of a high level meeting in the field of life sciences.

For the first time the International Congress on Neutron Capture Therapy is being held in Italy. BNCT in Italy has a long history, and a number of research projects dedicated to the development of new clinical applications. First of all I would like to remind you that in Pavia two patients were treated with a challenging and powerful technique that was absolutely innovative. The idea was to exploit the selectivity of the dose delivery due to the boron bio-distribution to treat a diffuse pathology, that is, a tumor that is not responsive to the standard treatments and that is not surgically removable. The originality of the idea and the obtained results opened new possibilities, and many new projects began to apply BNCT to forms of cancer different than Glioblastoma and the brain tumors. Nowadays, BNCT appears to be the only option in the case of head and neck recurrent cancers, skin melanoma and diffuse liver metastases. All over the world new clinical trials have been started with increasing effectiveness in terms of tumor remission and survival of the patients. This is surely a new phase of BNCT, and we are glad that its innovations and its practical results in the treatment of an increasing number of patients can be presented at ICNCT-13. This is why the clinical topic has a strong relevance in the scientific programme: the plenary session and the round table are meant to discuss the clinical results, exchange experiences and hopefully, create new collaborations. This is also the motivation of the title that I chose for this edition of the congress: BNCT is finally becoming "a new option against cancer".

The clinical aspect is, of course, only one of the many implications of BNCT. Following the tradition of the past congresses and the pluralism of the papers that have been sent to the Congress, different scientific sections are dedicated to many different topics. In particular, the contributions, presented either orally or as posters, are divided into Clinical Matters, Medical Physics, Nuclear Engineering, Treatment Planning and Mathematical Modeling, Boron Imaging, Chemistry and Pharmacology, Biology, Neutron Sources and Beam Dosimetry. In all these fields, the BNCT research is advancing, for example testing new drugs and developing neutron sources based on accelerator facilities. The joining of these efforts will lead to a BNCT that can be a real treatment option for the patients: the selectivity could be improved, and the facilities for the irradiations could be more accessible because available inside the hospitals. All these ambitious goals are pursued all over the world, and representatives of the majority of the research groups are attending and giving their contribution to ICNCT-13.

It is my convinced opinion that the quality of an International Congress such as ICNCT depends not only on its scientific programme but also on the human potentiality that it can express. For this reason we invested our time and resources to encourage young people, help researchers from developing countries and acknowledge the work of great personalities in the BNCT community.

During our social banquet, in a moment in which everyone will relax and enjoy our Italian typical food and wine, we will give 10 Fairchild, a Larsson and a Hatanaka Awards.

Let me finally express my deepest acknowledgment to all the people who have worked hard for ICNCT-13, in particular to the members of the Organizing, the Scientific and the Local Committees. Thank you also to Mrs Giuseppina Cardinale, Mrs Alena Papova and Mrs Patrizia Paolacci of Lazzi Agency, who made all the arrangements for the congress and for the social events with high competence and ability. Finally, I would like to thank you all, for your enthusiasm and your invaluable scientific and human contribution to ICNCT-13.

Prof. Aris Zonta
ISNCT and ICNCT-13 president

CLINICAL MATTERS/BIOMEDICAL APPLICATION

Current practices and future directions of therapeutic strategy in glioblastoma: survival benefit and indication of BNCT

Akira Matsumura[1], Tetsuya Yamamoto[1], Takao Tsurubuchi[1], Masahide Matsuda[1], Makoto Shirakawa[1], Kei Nakai[1], Kiyoshi Endo[1], Koichi Tokuue[2], Koji Tsuboi[2]

[1]*Department of Neurosurgery, Graduate School of Comprehensive Human Science, and* [2]*Proton Medical Research Center, University of Tsukuba, Tennodai 1-1-1, Tsukuba City, Ibaraki 305-8575, Japan*

Abstract

Since 1998, we are performing clinical studies on treatment of GBM using conventional fractionated photon radiation therapy (CRT), proton beam therapy (PBT) or boron neutron capture therapy (BNCT). We investigated whether these radiation modalities improves the survival of patients with GBM.

Sixty-eight cases of newly diagnosed GBM have been treated in our institution. After surgery, radiation therapy was performed using CRT with a dose of 60.0-61.2Gy (n=36), hyperfractionated PBT concomitant with fractionated photon irradiation with a total dose of 92.4Gy (n=17), or a single fraction of BNCT (n=15). In PBT, the surrounding volume of 2-cm from main tumor mass and the the volume of perifocal edema were irradiated at dose of 70Gy and 60Gy, respectively.

The median OS time of the case series of BNCT for GBM has been reported as 13 M to 20.7 M. In this study, the median OS and median time to MR change (TTM) for all patients were 25.7 M and 11.9 M, respectively. The 1- and 2-year survival rates were 85.7% and 45.5%, respectively. On the other hand, in the patients who underwent CRT and ACNU-based chemotherapy, OS and 2-year survival rate was 14.2M and 17.9%, respectively. In the patients who underwent high-dose PBT, OS and 2-year survival rate was 21.3M and 38.5%, respectively.

The present small case series of selected patients showed survival benefit after BNCT. The comparison using previously reported prognostic factor-based classifications suggest that outcome of BNCT in terms of survival appeared to have non-inferiority compared to the standard therapy. With respect to the case series as a high-dose radiation trial, the outcome (OS: 9.5 M to 25 M) of previously reported may still comparable to that of BNCT. Randomized trials of comparably selected patients are required to demonstrate conclusively that prolonged survival is a result of this tumor-selective radiotherapy.

Keywords: Glioblastoma, BNCT, radiation therapy, proton, SRS

1. Introduction

Glioblastoma multiforme (GBM) is one of the most frequent primary brain tumors in adults. Despite recent advancements in multidisciplinary therapy, GBM is still an incurable disease that recurs easily and is often lethal. Since 1998, we have been performing clinical studies on treatment of GBM using conventional fractionated photon radiation therapy (CRT), proton beam therapy (PBT) or boron neutron capture therapy (BNCT). In this retrospective analysis, we investigated whether these radiation modalities improve the survival of patients with GBM.

2. Materials and Methods

Sixty-eight cases of newly diagnosed GBM have been treated in our institution. After surgery, radiation therapy was performed using CRT with a dose of 60.0-61.2 Gy (n=36), hyperfractionated PBT concomitant with fractionated photon irradiation with a total dose of 92.4 Gy (n=17), or a single fraction of BNCT (n=15). Eight of 15 patients underwent external beam BNCT with an averaged dose of approximately 30 Gy followed by 30 Gy fractionated photon irradiation. In PBT, a 2-cm margin around the main tumor mass and the volume of perifocal edema were irradiated at doses of 70 Gy and 60 Gy, respectively. In BNCT, the boron uptake

in the tumor and normal brain was determined by the blood sodium borocaptate (BSH) level and boronophenylalanine (BPA) positron emission tomography. The BNCT radiation dose was assessed by the JAEA computer dosimetry system (JCDS), which calculates the dose distribution based on the neutron beam intensity and the boron levels in tissue.

3. Results and Discussion

Concomitant and adjuvant use of temozolomide with conventional photon radiotherapy, the new standard post-operative therapy for GBM has been shown to have a significant survival advantage compared to radiotherapy alone, and shows minimal additional toxicity. The median OS time in a randomized control trial was 14.6 M with temozolomide plus radiotherapy and 12.1 M with radiotherapy alone (Stupp et al., 2005). There is an urgent need for a tumor-selective therapy that would encompass the main tumor mass as well as microscopic invasion while avoiding radiation damage to the surrounding normal brain tissue.

Recent clinical studies on BNCT have focused on high-grade glioma, and to the best of our knowledge, no clinical data have yet been published on NCT in a randomized controlled trial. The median OS time of the case series of BNCT for GBM has been reported as 13 M to 20.7 M. In this study, the median OS and median time to MR change (TTM) for all patients were 25.7 M and 11.9 M, respectively. The 1- and 2-year survival rates were 85.7% and 45.5%, respectively. On the other hand, in the patients who underwent CRT and ACNU-based chemotherapy, the OS and 2-year survival rate were 14.2M and 17.9%, respectively. In the patients who underwent high-dose PBT, the OS and 2-year survival rate were 21.3M and 38.5%, respectively.

The results of the present study could not be directly compared to those of historical controls or to those previously reported in the literature because of the small number of patients, which was a major limitation. However, the prognostic factor-based classification used to compare this study to similar small cohorts (Fitzek, et al., 1999, Curran et al., 1993, Mirimanoff, et al., 2006) suggest that these relatively positive data are unlikely to reflect patient selection alone. Curran et al. reported that the OS after surgery and several radiation regimens using 60 Gy to 81.6 Gy for 1578 patients entered in three RTOG trials were categorized into 4 (III to VI) of 6 classes with median OSs for Classes III, IV, V and VI of 17.9, 11.1, 8.9 and 4.6M, respectively. The most favorable 2-year rate (35%) was also scored in Class III. Moreover, in high-dose radiation therapy using a proton beam, RTOG prognostic Classes III, IV and V had median OSs of 23, 17 and 14 M, respectively, and Class III had a 2-year survival rate of 34% (ref). In the present series, only 2 of 15 patients (13.3%) were categorized as RTOG Class III. It is noteworthy that the median OS (25.7 M) and 2-year survival rate (57.1%) in the present series appear to be superior to those of RTOG Class III in both standard therapy and reported high-dose therapy. In the patients who underwent standard X-ray radiation and ACNU-based chemotherapy, the OS and 2-year survival rate were 14.2M and 17.9%, respectively. This data is similar to that of standard X-ray radiation with TMZ. The relatively favorable survival rate in CRT may suggest that case selection in the two different protocol therapies (BNCT, PBT) did not caused poor prognosis in the patients underwent CRT.

The dose of radiation required to completely kill intrinsically radioresistant GBM cells has not yet been determined, however, previous reports have shown that at least 90 Gy must be used to achieve better local control (Fitzek, et al., 1999, Tanaka et al., 2005.). In general, such high-dose radiation is considered to be in excess of the tolerance dose of normal brain tissue which is used in conventional fractionated photon radiotherapy. Several randomized trials have shown a survival benefit of conventional fractionated photon radiotherapy at total doses of 45 to 60 Gy; the median OS in these trials was 5.8 M to 15.5 M (Walker, et al., 1980, Kristiansen et al., 1981, Sandberg-Wollheim et al., 1991, Bleehen, et al., 1991). Most subsequent dose escalation studies have been designed as case series of small numbers of selected patients who underwent additional stereotactic radiosurgery, fractionated proton beam radiation or other conformal radiotherapy. The better outcome following these radiotherapies, in which the median OS varies from 9.5 M to 25 M, is in part the result of patient selection (Fitzek, et al., 1999, Tanaka et al., 2005, Nwokedi e al., 2002, Baumert et al., 2003, Souhami et al., 2004).

Aggressiveness of salvage therapy following the tumor progression may influence the outcome in terms of OS. In this series, treatment of tumor progression included neurosurgical resection (n=7, 47%) and chemotherapy (n=5, 33%), and no patient underwent a second course of radiation. In the “proven” standard therapy, concomitant and adjuvant use of temozolomide with conventional photon radiotherapy, 23% of patients underwent a second surgery, and 58% of patients received chemotherapy (Stupp et al., 2005).

Prolonged survival can be achieved primarily by the first multidisciplinary therapy, resulting in prolonged TTM (11.9 M). However, in our institutional experience, enlargement or enhancement of the enhanced area on the Gd-enhancement MR image after high-dose radiotherapy (BNCT, PBT) is less related to viable tumor recurrence than to radiation-induced responses such as gliosis or radiation necrosis with a residual tumor nest and a diminished Ki-67 MIB-1 index compared to the pre-irradiation value. Because MR imaging has a low specificity for detecting tumor recurrence, TTM was introduced for progression free survival in this study. We believe there is a better chance of performing salvage therapy such as a second surgery and/or chemotherapy in a patient with MRI-based tumor progression. Moreover, a less viable tumor may re-grow more gradually when the salvage therapy induces a complete response of the tumor.

4. Conclusions

The present small case series of selected patients demonstrated the survival benefit of BNCT. The comparison using previously reported prognostic factor-based classifications suggested that the outcome of BNCT in terms of survival was at least as good and perhaps better than the standard therapy. With respect to previously reported high-dose radiation trial with a small numbers of patient, the outcome (OS: 9.5 M to 25 M) of previously reported trials may still be comparable to that of BNCT. Randomized trials of comparably selected patients are required to demonstrate conclusively that prolonged survival is a result of this tumor-selective radiotherapy.

Acknowledgements

This study was supported in part by a Grant-in-Aid from the Ministry of Education, Science and Culture, Japan (20390379).

References

Stupp, R., Mason, W.P., van den Bent, M.J., et al., 2005. Radiotherapy plus concomitant and adjuvant temozolomide for glioblastoma. N Engl J Med 352: 987-96.

Fitzek, M.M., Thornton, A.F., Rabinov, J.D., et al. 1999. Accelerated fractionated proton/photon irradiation to 90 cobalt gray equivalent for glioblastoma multiforme: results of a phase II prospective trial. J Neurosurg 91: 251-260.

Tanaka, M., Ino, Y, Nakagawa, K., et al., 2005. High-dose conformal radiotherapy for supratentorial malignant glioma: a historical comparison. Lancet Oncol. 6: 953-960.

Walker, M.D., Green, S.B., Byar, D.P., et al., 1980. Randomized comparisons of radiotherapy and nitrosoureas for the treatment of malignant glioma after surgery. N Engl J Med 303: 1323-1329.

Kristiansen, K., Hagen, S., Kollevold, T., et al., 1981. Combined modality therapy of operated astrocytomas grade III and IV: Confirmation of the value of postoperative irradiation and lack of potentiation of bleomycin on survival time: A prospective multicenter trial of the Scandinavian Glioblastoma Study Group. Cancer 47: 649-652.

Sandberg-Wollheim, M., Malmstrom, P., Stromblad, L.G., et al., 1991. A randomized study of chemotherapy with procarbazine, vincristine, and the lomustine with and without radiation therapy for astrocytoma grade 3 and/or 4. Cancer 68: 22-29.

Bleehen, N.M., Stennning, S.P., 1991. A Medical Research Council trial of two radiotherapy doses in the treatment of grades 3 and 4 astrocytoma. Br J Cancer 64: 769-774.

Nwokedi, E.C., DiBasem, S.J., Jabbour, S., et al., 2002. Gamma knife stereotactic radiosurgery for patients with glioblastoma multiforme. Neurosurgery 50: 41-47.

Baumert, B.G., Lutterbach, J., Bernays, R., et al., 2003. Fractionated stereotactic radiotherapy boost after post-operative radiotherapy in patients with high-grade gliomas. Radiotherapy and Oncology 67: 183-190.

Souhami, L., Seiferheld, W., Brachman, D., et al., 2004. Randomized comparison of stereotactic radiosurgery followed by conventional radiotherapy with carmustine to conventional radiotherapy with carmustine for patients with glioblastoma multiforme: report of Radiation Therapy Oncology Group 93-05 protocol. Int J Radiat Oncol Biol Phys 60: 853-860.

Curran, W.J., Scott, C.B., Horton J., et al., 1993. Recursive partitioning analysis of prognostic factors in three Radiation Therapy Oncology Group Malignant Glioma Trials, J Natl Cancer Inst 85: 704-710.

Mirimanoff, R.O., Gorlia, T., Mason, W., et al., 2006. Radiotherapy and temozolomide for newly diagnosed glioblastoma: Recursive partitioning analysis of the EORTC 26981/22981-NCIC CE3 phase III randomized trial. J Clin Oncol 24: 2563-2569.

Survival benefit from Boron Neutron Capture Therapy for the newly diagnosed glioblastoma patients

Shinji Kawabata[a], Shin-Ichi Miyatake[a], Naosuke Nonoguchi[a], Kyoko Iida[a], Shiro Miyata[a], Kunio Yokoyama[a], Atsushi Doi[a], Yuzo Kuroda[a], Toshihiko Kuroiwa[a], Hiroyuki Michiue[b], Hiroaki Kumada[c], Mitsunori Kirihata[d], Yoshio Imahori[e] , Akira Maruhashi[f], Yoshinori Sakurai[f], Minoru Suzuki[f], Shin-Ichiro Masunaga[f], and Koji Ono[f].

[a] Department of Neurosurgery, Osaka Medical College, *2-7 Daigaku-machi, Takatsuki, Osaka, Japan*
[b] Department of Neurosurgery, Okayama University, *Okayama, Japan*
[c] Research Reactor and Tandem Accelerator, Japan Atomic Energy Agency, *Tohkai, Japan*
[d] Department of Agriculture, Osaka Prefectural University, *Sakai, Japan*
[e] Cancer Intelligence Care Systems, Inc., *Minati-ku, Tokyo, Japan*
[f] Kyoto University Research Reactor Institute, *Kumatori, Osaka, Japan*

Abstract

OBJECTIVE: Since 2002 to 2007, we applied boron neutron capture therapy (BNCT) to >50 cases of malignant gliomas (MGs) with epithermal neutron irradiations. Recently, we showed the early radiographical improvement of malignant glioma patients by our modified BNCT, with simultaneous use of BPA and BSH. In this time, we focused on the survival benefit from BNCT for the newly diagnosed glioblastoma patients.

METHODS: BNCT group including 21 newly histological confirmed glioblastoma patients treated with surgical removal followed by BNCT in Osaka Medical College during 2002- 2006 period. Ten patients were treated with BNCT only, and in the other 11 patients, 20 to 30 Gy fractionated external beam X-ray irradiation (XRT) was performed after BNCT. No chemotherapy was administered until tumor progression was observed.

RESULTS: Treatments were well tolerated. Any kind of acute systemic or local severe toxicity were not demonstrated. Mean over all survival of the patients treated by BNCT was 20.7 and the median was 15.6 months with 2-years survival of 25%. Stratification by RPA criteria showed 6, 6, 8 and 1 patients respectively in class III to VI . Three patients out of 6 in class III and 1 out of 8 in class V are alive at the end point of this study. All the patients in class IV and VI died. Median survival time for the BNCT group compared to the RTOG database was as follows: 20.6 months vs. 17.9 months for class III; 16.9 months vs. 11.1 months for class IV; 13.2 months vs. 8.9 months for class V.

CONCLUSION: The RTOG RPA prognostic criteria were helpful in establishing which class of glioma patients could potentially benefit from BNCT. BNCT showed a survival benefit in all of the RPA classes of the RTOG database not only for the good prognosis group.

Keywords: glioblastoma, Boron Neutron Capture Therapy, external beam X-ray irradiation, BPA, BSH

1. Introduction

To create a breakthrough in the treatment for GB, we have been developing boron neutron capture therapy (BNCT) (Kawabata, 2003, Miyatake, 2005).

Numerous varieties of boron delivery agents have been developed and tested in experimental studies (Doi 2008, Barth, 2005), but only two boron-containing drugs have been used clinically, sodium undecahydro – mercapto – *closo* - dodecaborate ($Na_2B_{12}H_{11}SH$ or sodium borocaptate [BSH]) and 4 - dihydroxy -boryl - phenylalanine (or borono - phenylalanine [BPA]) (Barth, 2005). Each boron compound has defects as a BNCT agent. BSH dose not actively accumulate in GB, but passively accumulates by the destruction of blood brain barrier (BBB). On the other hand, BPA actively accumulates in tumors but its accumulation is significantly weak in the quiescent cell population of a tumor. Therefore, the simultaneous use of both compounds can increase the boron level in tumors while compensating for each other's faults.

The effectiveness of the combined use of BSH and BPA was demonstrated in mouse tumor studies (Ono, 1999). Based on these findings in the experiments , we performed, for the first time ever, a new BNCT, in which BSH and BPA were simultaneously combined, obtaining good tumor

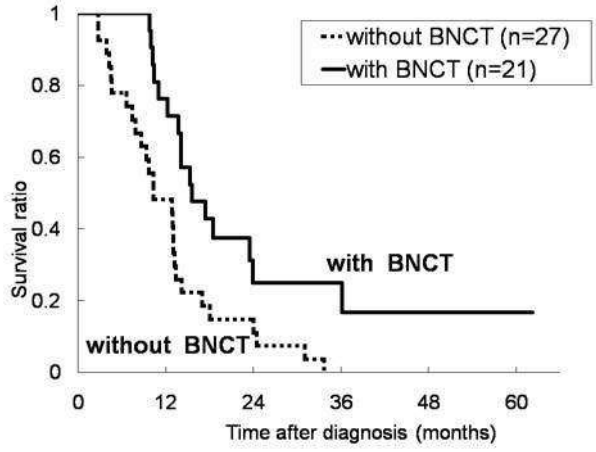

Figure 1 Kaplan-Meier survivals. BNCT (with BNCT) vs our historical control (without BNCT)

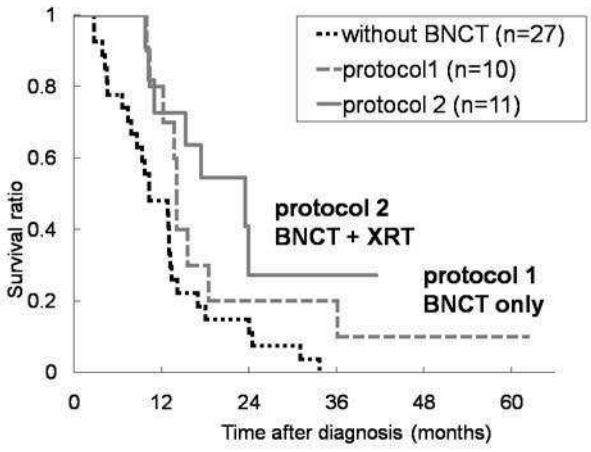

Figure 2 Kaplan-Meier survivals. BNCT with XRT (protocol 2) vs without XRT(protocol 1) and control (without BNCT)

response on MRI, not only for the newly diagnosed malignant gliomas but also for the recurrent cases which had been initially treated by X-ray irradiation therapy (XRT). In our initial protocol, all of the patients received a combination of BSH (100mg/kg) and BPA (250 mg/kg body weight) administered intravenously. BNCT was carried out at the Kyoto University Research Reactor Institute (KURRI) using an epithermal neutron beam 12 hours and 1 hour after the administration of BSH and BPA, respectively. This BNCT showed impressive radiographical shrinkage of the tumor mass, and improved the quality of life for even those patients with recurrent malignant gliomas, as described above and reported previously (Kawabata, 2003, Miyatake, 2005). We achieved a favorable survival benefit for newly diagnosed GB patients with this BNCT protocol, as described below. In the current modified protocol, we applied this BNCT followed by XRT to obtain a more favorable survival benefit for newly diagnosed GB (NDGB) patients. This study was based on experimental animal data showing that a significant therapeutic gain could be obtained when BNCT was combined with an X-ray boost (Barth, 2004).

2. Methods

Our BNCT protocol using both BPA and BSH simultaneously has been described previously (Kawabata, 2003). Our methods were as follows:
First, we started using epithermal neutrons instead of thermal neutrons to obtain good penetration for deep-seated lesions. Second, we simultaneously used 2 different boron compounds (BSH and BPA) with different accumulation mechanisms to the tumor cells (Yokoyama, 2006, Ono, 1999). Third, we utilized a dose simulation work station, the Simulation Environments for Radiotherapy Applications (SERA). Fourth, ^{18}F-labeled BPA positron emission tomography (BPA-PET) was performed for the estimation of the boron compound accumulation prior to neutron irradiation (Imahori, 1998). Fifth, we filled the tumor removed cavity with air to obtain enough neutron flux, especially for the bottom of deep-seated tumors (Sakurai, 2006). Sixth, we developed a central shielding method with a lithium plate at the center of the irradiation field to obtain uniform neutron distribution and increase the neutron flux relatively at the periphery in the radiation field (Ono, 2000). With these modifications, even patients with deep-seated tumors can be treated by BNCT without craniotomy with a short hospital stay. In the present study, the revised protocol was used as a new protocol as follows.

Twelve hours before the neutron irradiation, the patients were administered 100mg/kg of BSH intravenously for one hour. 700mg/kg of BPA was infused continuously to the patients for 6 hours before the irradiation, and they were positioned for neutron irradiation in the reactor (KUR or JRR-4 (Japan Atomic Energy Agency Research Reactor 4)). Just after termination of continuous BPA infusion for 6hrs, neutrons were irradiated. We used the dose-planning workstation to calculate the radiation dose for tumors from the ^{18}F-labeled BPA-positron emission tomography (BPA-PET) data and blood ^{10}B concentrations obtained every 2 hours after BSH administration. We used an epithermal neutron beam. Following this, a 2Gy daily fraction of XRT

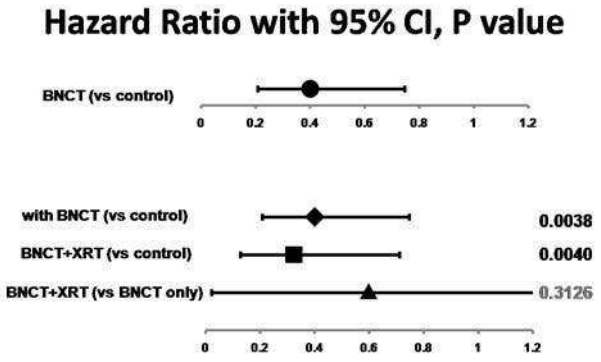

Figure 3 Hazard ratios (Table III&V)

was applied, for a total of 20 to 30Gy. The total dose of XRT was decided based on the BNCT dose for the normal brain. This protocol was approved by the Ethical Committee of Osaka Medical College and also by the Committee for Reactor Medicine in KURRI. In addition, the indication of BNCT for each candidate was discussed by the latter committee. In Protocol 1, we aimed to apply more than 30Gy-Eq for gross tumor volume (GTV) and less than 12 Gy-Eq for normal brain, as BNCT. In Protocol 2, we aimed to apply more than 40Gy-Eq for GTV and less than 15Gy-Eq for normal brain.

Patient enrollment: In the current manuscript, we report the results only for NDGB patients. No chemotherapy was applied for any of the patients until the tumor progression was confirmed histologically or by BPA-PET. Survival time from histologically diagnosed GB was compared with the survival time of the institutional former series of GB patients who were treated by surgical removal followed by XRT and chemotherapy (mainly ACNU) from 1990 to 2006 in Osaka Medical College. In this historical control group, all cases were operated on to aim for the maximum tumor removal, the same as for the cases of the BNCT group. The related Kaplan–Meier curves were calculated and the Logrank test was used for statistical analysis. For the 21 patients who received BNCT, survival time was also compared with the corresponding recursive partitioning analysis (RPA) subclasses by the Radiation Therapy Oncology Group (RTOG) [Curren et al, *J Natl Cancer Inst* 85:704-710, 1993], as the international historical control. Based on this RTOG-RPA, GB was classified into 4 prognostic subgroups (classes III to VI), and the median survival for Classes III, IV, V and VI were 17.9, 11.1, 8.9 and 4.6 months, respectively.

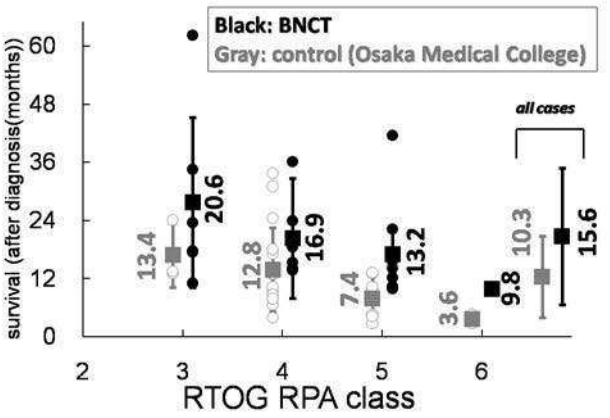

Figure 4 Survival of the corresponding RPA subclasses by RTOG (Curren, 1993)

3. Results

See Tables (I to V)

See Figures (1 to 4)

4. Conclusions

In conclusion, there were 2 major modifications to the current BNCT protocol (Protocol 2) in comparison with our former protocol (Protocol 1). The first modification is a longer term and a larger amount of BPA infusion, and the second is the additional application of XRT. Both modifications probably work synergistically and result in a more favorable survival benefit for GB patients.

Acknowledgements

Grant supports: Grants-in-Aid for Scientific Research for young researchers (B) (18791030 to S.K.), Grants-in-Aid for Scientific Research (B) (16390422 and 19390385 to S-I.M.) from the Japanese Ministry of Education, Science and Culture. Grant-in-Aid for Scientific Research from the Ministry of Health, Labour and Welfare of Japan to S-I.M. (P.I., Hideki Matsui), the Regional Science Promotion Program of the Japan Science and Technology Corporation, as well as by the "Second-term Comprehensive 10-Year Strategy for Cancer Control" of the Ministry of Health, Labor, and Welfare of Japan to S-I.M., the Takeda Science Foundation for Osaka Medical College, Grant-in-Aid for Cancer Research from the Ministry of Education, Culture, Sports, Science, and Technology of Japan (12217065 to K.O.). We thank Yasuko Doi and Eriko Sugane for secretarial assistance.

Reference

Kawabata, S., Miyatake, S., Kajimoto, Y., Kuroda, Y., Kuroiwa, T., Imahori, Y., Kirihata, M., Sakurai, Y., Kobayashi, T., Ono, K., 2003. The early successful treatment of glioblastoma patients with modified boron neutron capture therapy. Report of two cases. **J Neurooncol** 65, 159-165.

Miyatake, S., Kawabata, S., Kajimoto, Y., Aoki, A., Yokoyama, K., Yamada, M., Kuroiwa, T., Tsuji, M., Imahori, Y., Kirihata, M., Sakurai, Y., Masunaga, S., Nagata, K., Maruhashi, A., Ono, K., 2005. Modified boron neutron capture therapy for malignant gliomas performed using epithermal neutron and two boron compounds with different accumulation mechanisms: an efficacy study based on findings on neuroimages. **J Neurosurg** 103, 1000-1009.

Doi, A., Kawabata, S., Iida, K., Yokoyama, K., Kajimoto, Y., Kuroiwa, T., Shirakawa, T., Kirihata, M., Kasaoka, S., Maruyama, K., Kumada, H., Sakurai, Y., Masunaga, S., Ono, K., Miyatake, S., 2008. Tumor-specific targeting of sodium borocaptate (BSH) to malignant glioma by transferrin-PEG liposomes: a modality for boron neutron capture therapy. J. Neurooncol. 87, 287-94.

Ono, K., Masunaga, S., Suzuki, M., Kinashi, Y., Takagaki, M., Akaboshi, M., 1999. The combined effect of boronophenylalanine and borocaptate in boron neutron capture therapy for SCCVII tumors in mice. **Int J Radiat Oncol Biol Phys** 43, 431-436.

Barth, R.F., Coderre, J.A., Vicente, M.G., Blue, T.E., 2005. Boron neutron capture therapy of cancer: current status and future prospects. **Clin Cancer Res** 11, 3987-4002.

Barth, R.F., Grecula, J.C., Yang, W., Rotaru, J.H., Nawrocky, M., Gupta, N., Albertson, B.J., Ferketich, A.K., Moeschberger, M.L., Coderre, J.A., Rofstad, E.K., 2004. Combination of boron neutron capture therapy and external beam radiotherapy for brain tumors. **Int J Radiat Oncol Biol Phys** 58, 267-277.

Yokoyama, K., Miyatake, S., Kajimoto, Y., Kawabata, S., Doi, A., Yoshida, T., Asano, T., Kirihata, M., Ono, K., Kuroiwa, T., 2006. Pharmacokinetic study of BSH and BPA in simultaneous use for BNCT. **J Neurooncol** 78, 227-232.

Imahori, Y., Ueda, S., Ohmori, Y., Sakae, K., Kusuki, T., Kobayashi, T., Takagaki, M., Ono, K., Ido, T., Fujii, R., 1998. Positron emission tomography-based boron neutron capture therapy using boronophenylalanine for high-grade gliomas: part I&II. **Clin Cancer Res** 4, 1825-1841.

Ono, K., Sakurai, Y., Masunaga, S., Kinashi, Y., Takagaki, M., Kobayashi, T., 2000. Improvement of B-10 dose distribution in water phantom irradiated with epithermal neutron beam and its assessment by colonyformation assay: *Program & Abstracts of the Ninth International Symposium on Neutron Capture Therapy for Cancer (Kyoto University Research Reactor Institute).* Osaka, Japan, Kyoto University Research Reactor Institute, pp 197-198.

Sakurai, Y., Ono, K., Miyatake, S., Maruhashi, A., 2006. Improvement effect on the depth-dose distribution by CSF drainage and air infusion of a tumour-removed cavity in boron neutron capture therapy for malignant brain tumours. **Phys Med Biol** 51, 1173-1183.

Table I (See also Figure 1)

	n	Mean ± SD (months)	Median (MST, months)	1 year (%)	2 years (%)
without BNCT	27	12.3±8.1	10.3	48.2	14.8
with BNCT	21	20.7±13.1	15.6	76.2	25.0

Table II (See also Figure 1)

group	n	MST	95%CI (months)	P value (Log-rank test)
without BNCT	27	10.3	(7.4 – 13.2)	
with BNCT	21	15.6	(12.2 – 23.9)	**0.0035**

Table III (See also Figure 3)

	Hazard Ratio	95%CI	P value
with BNCT (vs control)	0.399	(0.206 – 0.746)	**0.0038**

Table IV (see also Figure 2)

group	n	MST	95%CI (months)	P value (Log-rank test)
historical control	27	10.3	(7.4 – 13.2)	
with BNCT only	10	14.1	(9.9 – 18.5)	0.0581
with BNCT plus XRT	11	23.5	(10.2 -)	**0.0103**

Table V (See also Figure 3)

	Hazard Ratio	95%CI	P value
with BNCT (vs control)	0.399	(0.206 – 0.746)	**0.0038**
BNCT+XRT (vs control)	0.323	(0.128 – 0.710)	**0.0040**
BNCT+XRT (vs BNCT only)	0.598	(0.0211 – 1.63)	0.3126

Clinical results of BNCT for malignant brain tumors in children

Y. Nakagawa[a], T.Kageji[b], Y. Mizobuchi[b], S. Nagahiro[b], H. Kumada[c]

[a]Department of Neurosurgery, Kagawa National Children's Hospital, Kagawa, 765-8501, Japan
[a]Department of Neurosurgery, The University of Tokushima, Tokushima, 770-8503, Japan
[c]Department of Research Reactor, Tokai Research Establishment, Japan Atomic Energy Research Institute, Ibaragi, 319-1195, Japan

Abstract

It is very difficult to treat the patients with malignant brain tumor in children, especially under 3-year-old because the conventional irradiation cannot be applied due to the damage of normal brain tissue. However, BNCT has tumor selectivity such as it can make damage only tumor cells. We evaluated the clinical results and courses in patients with malignant glioma under 15-year-old. Among 183 patients with brain tumors treated by our group using BSH-based intra-operative BNCT, twenty-three patients were under 15-year-old. They included 4 patients under 3-year-old. There were 3 cerebral GBMs, 6 anaplastic astrocytomas, 7 primitive neuroectodermal tumors (PNET), 6 pontine gliomas and 1 anaplastic ependymoma. All GBM and PNET patients were died due to CSF and/or CNS dissemination without local tumor regrowth. Five of 6 pontine glioma patients were died. 4 of 6 anaplastic astrocytoma and 1 anaplastic ependymoma patients were alive without tumor recurrence. BNCT can apply to malignant brain tumors in children, especially under 3 year-old instead of conventional radiation. Although it can achieve the local control in the primary site, it cannot prevent CSF dissemination in patients with glioblatoma.

Keywords: BNCT, JCDS, radiation, glioblatoma, children

1. Introduction

Boron neutron capture therapy (BNCT) is a promising modality for the selective irradiation of tumor tissue. Using the heavy-charged particles such as an alpha particle and a lithium nucleus and the selective boron accumulation only in tumor cells, BNCT offers the possibility of selective tumor cell killing without causing damage to adjacent normal brain tissue. In a word, BNCT is an optimal treatment for glioblastoma, which shows invasive character into the healthy normal tissue. We have used BSH (sodium borocaptate; $Na_2B_{12}H_{11}SH$) as a boron carrier. Since 1968, we have treated more than 170 patients with BSH-based intra-operative BNCT. This important clinical trial showed significant improvements over previously reported outcomes and documented the long-term recurrence-free survival of selected patients with malignant glioma. We have reported that the most important factor to prevent the tumor recurrence was BNCT radiation dose at the tumor bulk and invasive lesion, and to avoid the radiation necrosis as an adverse effect was BNCT radiation dose of vasculature at the brain surface. Our recent study demonstrated that the maximum vascular volume dose should be below 12 Gy (as a physical gold wire dose) to avoid radiation necrosis, the optimal mean dose of the GTV and CTV were 26 Gy and 16 Gy (as a physical gold wire dose), respectively for long-term survival in patients with GBM.

Since 1998, epithermal neutron beam has been introduced clinically instead of pure thermal neutron beam for improvement of neutron distribution in a deep site. And also new dose planning system for BNCT was developed instead of gold wire method, which is JAERI Computational Dosimetry System (JCDS). JCDS can evaluate the BNCT radiation dose on CT scan and MRI prior to BNCT.

In general, most of brain tumor has malignant character in case of children. Children are suffered from local recurrence and/or CSF dissemination after surgery, therefore adjuvant treatment such as chemotherapy and radiation have been applied. However, clinical result of malignant brain tumor in children is poor due to biological behavior and resistant of treatment. As a result, it is very difficult to treat the patients with malignant brain tumor in children, especially under 3-year-old because the conventional irradiation cannot be applied due to the damage of normal brain tissue. However, BNCT has tumor selectivity such as it can make damage only tumor cells. We have treated the malignant brain tumor in children with BNCT. We evaluated the clinical results and courses in patients with malignant glioma under 15-year-old.

2. Material and Methods

BSH-based intra-operative BNCT was underwent in more than 180 patients with malignant brain tumors from 1968 to 2005. BSH is administered for one hour by rapid intravenous infusion at 12-15 hours before neutron radiation. On the day of BNCT, patient is taken to the reactor. With the patient under general anesthesia, craniotomy is done; the skin flap and bone flap are reopened. To measure the exact neutron flux at each point of interest, the previously inserted gold wires around tumor tissue are pulled out at 15-20 minutes after full-power operation of the reactor. The neutron beam directly irradiates the lesion. We introduced mixed epithermal and thermal neutron beam since 1998 instead of thermal neutron beam for improvement of neutron beam delivery at deep lesion. BSH-based intra-operative BNCT using mixed neutron beam underwent in 19 patients with malignant brain tumors from 1998 to 2004.

BNCT radiation dose was evaluated with both gold wire and JAERI Computational Dosimetry System (JCDS) methods. The physical radiation dose of the boron n-alpha reaction was estimated retrospectively at each point of gold wire using the neutron fluence, irradiation time and boron concentration in tumor. Gross tumor volume (GTV) was defined as enhanced area on Gd-MRI, clinical target volume (CTV) was defined as high intensity area on T2-MRI. We compared the BNCT radiation dose in patients with or without residual tumor cells.

Among 183 patients with brain tumors treated by our group using BSH-based intra-operative BNCT, twenty-three patients were under 15-year-old. They included 4 patients under 3-year-old. There were 3 cerebral GBMs, 6 anaplastic astrocytomas, 7 primitive neuroectodermal tumors (PNET), 6 pontine gliomas and 1 anaplastic ependymoma.

3. illustrative cases and results

Case1: 1-year-old, female, anaplastic ependymoma

The patient had severe headache and vomiting. An enhanced MRI demonstrated a huge mass in right frontal lobe. After partial resection, BSH-based intra-operative BNCT was done under general anesthesia. The patient was diagnosed as anaplastic ependymoma.

The total dose of 136.4 mg/kg BSH was given to patient intravenously. Irradiation time in was 162.0 min. Blood and tumor boron concentration were 23.0 ppm and 28.0 ppm, respectively. The maximum vascular dose at brain surface was 17.60 Gy(w). Gamma dose was 5.30 Gy(w). The minimum boron physical and weighted total (boron and gamma) dose in GTV (gross tumor volume) were 19.83 Gy and 54.88 Gy(w), respectively. The minimum boron physical and weighted total (boron and gamma) dose in CTV (clinical target volume) were 14.11 Gy and 40.58 Gy(w), respectively.

She was suffered from transient left hemiparesis one year after BNCT. MRA and angiography demonstrated moyamoya phenomenon on right middle cerebral artery. We performed in-direct bypass surgery. 8 years after BNCT, recent MRI demonstrated no tumor recurrence and brain atrophy.

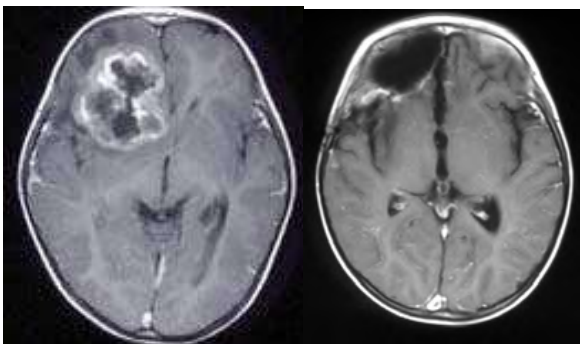

Fig.1. pre BNCT (left), 1 year after BNCT (right)

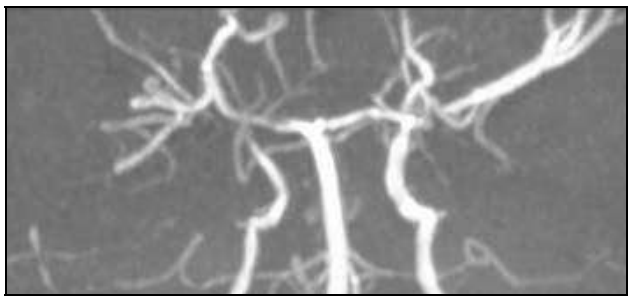

Fig. 2. MRA demonstrated occlusion of right internal carotid artery and severe stenosis of left middle cerebral artery

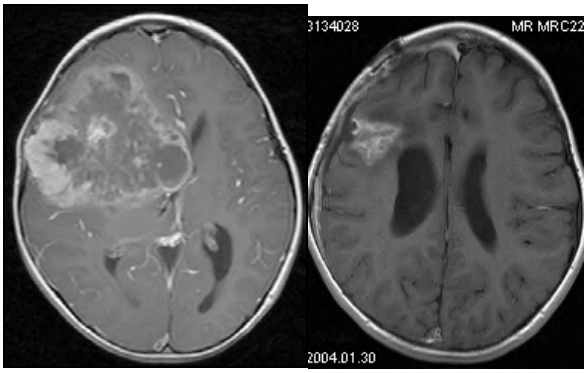

Fig.3. pre BNCT (left), 3 months after BNCT (right)

Case 2: 6-year old, female, glioblastoma

The patient had severe headache and vomiting. An enhanced MRI demonstrated a huge mass in right frontal lobe. After partial resection, BSH-based intra-operative BNCT was done under general anesthesia. The patient was diagnosed as glioblastoma.

The patient had a huge mass in right frontal lobe. BSH-based intra-operative BNCT was done under general anesthesia.

The total dose of 160.0 mg/kg BSH was given to patient intravenously. Irradiation time in was 74.0 min. Blood and tumor boron concentration were 40.0 ppm and 40.0 ppm, respectively. The maximum vascular dose at brain surface was 25.25 Gy(w). Gamma dose was 7.78 Gy(w). The minimum boron physical and weighted total (boron and gamma) dose in GTV (gross tumor volume) were 15.04 Gy and 45.38 Gy(w), respectively. The minimum boron physical and weighted total (boron and gamma) dose in CTV (clinical target volume) were 5.33 Gy and 21.11 Gy(w), respectively.

Abnormal enhancement was recognized 8 months after BNCT. Residual tumor cells were recognized histopathologically in salvage surgery. She was died of CSF dissemination 1 year after BNCT.

All GBM and PNET patients were died. Five of 6 pontine glioma patients were died. 4 of 6 anaplastic astrocytoma and 1 anaplastic ependymoma patients were alive.

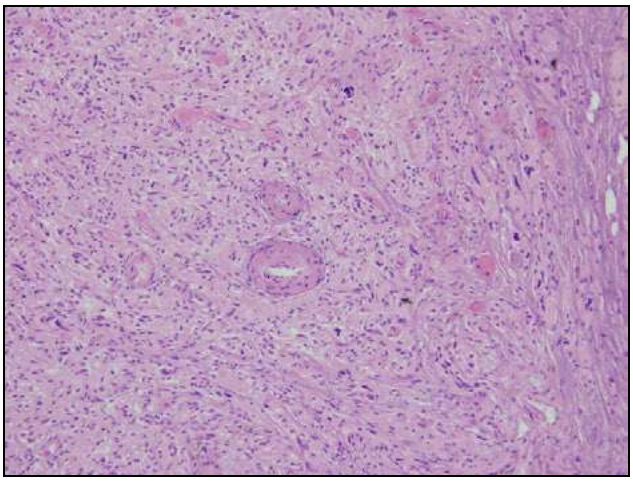

Fig. 4. Histopathological findings in abnormal enhancement area obtained with salvage surgery 6 months after BNCT demonstrated residual tumor cells

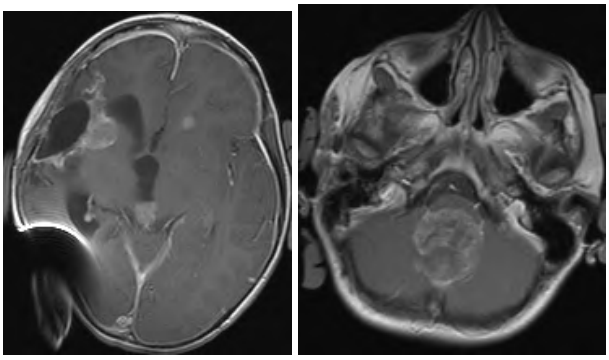

Fig. 5. Both CSF and CNS dissemination were recognized 10 months after BNCT

4. Conclusions

BNCT can apply to malignant brain tumors in children, especially under 3 year-old instead of conventional external beam radiation. Although it can achieve the local control in the primary site, it cannot prevent CSF dissemination in patients with glioblatoma and PNET.

References

Hatanaka H, Nakagawa Y, 1994. Clinical results of long-surviving brain tumor patients who underwent boron neutron capture therapy. Int J Radiat Oncol Biol Phys 28, 1061-1066.

Nakagawa Y, 1994. Boron neutron capture therapy: the past to the present. Int J Radiat Oncol Biol Phys 28, 1217.

Nakagawa Y, Hatanaka H, 1997. Boron neutron capture therapy-clinical brain tumor study. J Neurooncol 33, 105-115.

Nakagawa Y, Pooh K, Kobayshi T, et al., 2003. Clinical review of Japanese experience with boron neutron capture therapy and a proposed strategy using epithermal neutron beams. J. Neurooncol 62, 87-99.

Kageji T, Nagahiro S, Mizozuchi Y, et al.,2006. Boron neutron capture therapy using mixed epithermal and thermal neutron beams in patients with malignant glioma –correlation between radiation dose and radiation injury and clinical outcome-. Int. J. Radiation Oncology Biol. Phys. 65, 1446-1455.

Kageji T, Mizobuchi Y, Nagahiro S, Nakagawa Y, Kumada H, 2006. Correlation between BNCT radiation dose and histopathological findings in BSH-based intra-operative BNCT for malignant glioma. Advances in Neutron Capture Therapy 2006, 35-36.

Acknowledgement

A part of this study was financially supported by the Budget for nuclear research of the ministry of Education, Culture, Sports, Science and Technology based on the screening and counseling by Atomic Energy Commission

Outcome of the First Twelve Patients with Locally Recurred Inoperable Head and Neck Cancer Treated in the Finnish Head and Neck Cancer BNCT Trial

L. Kankaanranta[1], H. Koivunoro[1], T. Seppälä[1], T. Atula[2], A. Mäkitie[2], J. Uusi-Simola[3], M. Kortesniemi[3], P. Välimäki[4], P. Kotiluoto[5], I. Auterinen[5], M. Kouri[1], S. Savolainen[3], H. Joensuu[1]

Departments of [1]Oncology and [2]Otolaryngology, [3]HUS Medical Imaging Centre Helsinki University Central Hospital, [4]Boneca Oy, [5]VTT Technical Research Centre, Espoo, Finland

Background: Head and neck cancer patients whose disease recurs locally after surgery and radiation therapy generally have poor outcome. We evaluated safety and efficacy of boron neutron capture therapy (BNCT) in the treatment of 12 patients who had locally recurred, inoperable head and neck cancer. We have reported earlier results based on a median follow-up time of 14 months (Kankaanranta et al. IJROBP 2007;69:475-82), and now report outcome based on a median follow-up of 31 months.

Patients and Methods: All patients had inoperable, recurred, locally advanced (rT3, rT4 and/or rN2) head and neck cancer. Prior treatments consisted of surgery and conventionally fractionated photon irradiation to a cumulative dose of 56 to 74 Gy administered with or without concomitant chemotherapy. Tumor responses were assessed using the RECIST criteria and adverse effects using the NCI common toxicity grading v3.0. Intravenously administered boronophenylalanine-fructose (BPA-F, 400mg/kg) was used as the boron carrier. Ten patients received BNCT twice; 2 were treated once.

Results: Ten (83%) patients responded to BNCT, and 2 (17%) had tumor growth stabilization for 5.5 and 7.6 months. The median duration of locoregional tumor control was 10 months (range, 1 to 36.0+ months). Six (50%) patients developed metastatic disease. The median survival time was 13 months. Three (25%) patients were alive at the time of the analysis with follow-up of 30+, 31+ and 36+ months as calculated from the date of first BNCT. One of these patients is alive without cancer recurrence (at 36+ months) with a good quality-of-life. One patient developed retinal toxicity, but otherwise no unexpected late toxicity was recorded.

Conclusions: BNCT is effective in the treatment of inoperable, locally advanced head and neck carcinoma that recurs at a previously irradiated site, and deserves further study.

BNCT for skin melanoma in extremities: updated Argentine clinical results

P. R. Menendez[1] , B. M. C. Roth [1] , M. D. Pereira[1-3] , M. R. Casal[1] , S. J. Gonzalez[2], D. B. Feld [2], G. A. Santa Cruz[2], J. Kessler [2] , J. Longhino[2] , H. Blaumann[2] , R. Jimenez Rebagliati[2], O. A. Calzetta Larrieu[2], C. Fernández[2], S. I. Nievas[2], S. J. Liberman [2]

1 - Instituto de Oncologia Angel H. Roffo. Av. San Martín 5481, (1417) Cdad. De Buenos Aires Argentina

2 - Comision Nacional de Energia Atomica, Av. Del Libertador 8250, (1429) Cdad. De Buenos Aires, Argentina

3- Agencia Nacional de Promocion Científica y Tecnológica. PAV 22393, Argentina

As part of phase I/II Melanoma BNCT clinical trial conducted in Argentina in a cooperative effort of the Comision Nacional de Energia Atomica (C.N.E.A.) and the Instituto de Oncologia Angel H. Roffo (IOAHR), 7 patients (6 female – 1 male) received 8 treatment sessions covering 10 anatomical areas located in extremities. Mean age of the patients was 64 years (51-74). The 8 treatments were performed between October 2003 and June 2007. All patients presented multiple subcutaneous skin metastases of melanoma and received an infusion containing 14 gr/m2 of borophenyl-alanine (BPA) followed by the exposition of the area to an hyperthermal neutron beam at the RA-6 reactor. The maximum prescribed dose to normal skin ranged from 16.5 to 24 Gy-eq and Normal Tissue administered dose varied from 15,8 to 27.5 Gy-eq. Taken evaluable nodules, 69.2% of overall response and 30.7% of no changes were seen. The toxicity was acceptable, with 3 out of 10 evaluable areas showing ulceration (30% toxicity grade 3).

Keywords: BNCT, Skin melanomas, BPA-F, Clinical trials

1. Introduction

BNCT project was started in Argentina during 1998. A few years later, in 2003, a clinical trial Phase I/II protocol on cutaneous melanoma begun supported by the Atomic Energy National Comision (CNEA) and the University of Buenos Aires Oncology Institute Angel H. Roffo. The protocol was designed to evaluate the efficacy and toxicity of BNCT for cutaneous skin melanomas in extremities (Gonzalez et al, 2004).

Melanoma is an aggressive disease, that frequently involve distant and locoregional spread, without, in many cases, an useful treatment approach. The binary characteristic of BNCT could be an attractive tool to improve the response over the standard radiotherapy treatment (Hiratsuka J et al, 2000).

The primary end point in this trial was to evaluate tolerability of normal tissue to BNCT and also collecting information regarding tumoral response.

Seven patients (eight irradiation procedures covering ten anatomical areas) having multiple subcutaneous skin metastases on extremities and progressed to initial treatment, were irradiated at the hyperthermal neutron beam of the RA-6 facility after 14 gm/m^2 BPA-fructose infusion.

2. Materials and Methods

2.1 Patients

Six female and one male patients, mean age 64 years (51-74 years), having multiple subcutaneous skin metastasis on right or left leg for all cases and progressed to previous treatment were included in this study. The first patient received two irradiations of one fraction each for two different areas of the leg (October and December 2003). The second patient received one irradiation (one fraction) in June 2004. The third one was irradiated with three consecutive fields at the level of the calf, ankle and foot sole of the right leg on May 2005. Fourth to seventh patients received one fraction covering one location (May,

December 2006, May and June 2007 respectively) as shown in Table 1.

2.2 Patient positioning

A simulation room (SR) for patient positioning procedures was built at Constituyentes Atomic Center (Buenos Aires) with a beam's-eye view window in order to determine distances to the patient's skin reference marks. Templates were built for each field, based on two orthogonal images generated during the beam assignment procedure accomplished with the treatment planning system to reposition the limb at the irradiation room (Bariloche Atomic Center). The patient position was fixed by means of conventional positioning devices.

2.3 Dose prescription

The maximum tolerable dose (MTD) for skin was adopted as the prescription dose, regardless of the boron concentration in the tumor in order to keep skin toxicity at a safe level. A 20 RBE Gy was the dose assumed for 90% of tumor control probability in lesions ≤ 1cm.

The feasibility of a treatment was decided if a therapeutic dose could be administrated to the tumor, keeping the maximum dose to the skin below the prescribed value. Another factor taken into account was the treatment time, which has to be short enough to avoid movement and/or discomfort in the patient.

To evaluate dose distribution in the skin a 5 mm thick layer of tissue was considered. The MTD was scaled from 16.5 to 24 RBE Gy-Eq, as shown in Table 1,

Median follow up was 12 months (4 – 36 m).

2.4 Dose calculation

CT scan of patient's extremity and measured concentration profile of ^{10}B in blood were the key data to design a treatment plan using NCTPlan v. 1.3 treatment planning system (Blaumann HR et al, 2004) and DVH Tool system (Gonzalez S et al, 2004). Considering the above-mentioned dose prescription limit, preliminary treatment time, skin and tumor dose were calculated considering a boron tumor/blood concentration ratio =3.5.

After the irradiation procedure has finished and all blood samples collected, a retrospective patient dosimetry was calculated according to the described procedure(Gonzalez S et al, 2004).

2.5 BPA-F infusion-Patient irradiation

All patients received a ~14g/m^2 BPA-F IV infusion during 90 min. Blood samples were taken before and after the irradiation. Vital signs (pulse oximetry – Heart Rate) were obtained during infusion and irradiation.

Tumor biopsy samples were obtained after the irradiation for boron concentration analysis in some patients. Irradiation times ranged from 50 min up to 85 min.

For estimation of gamma dose distribution, a set of TLDs 700 was put on different parts of the patient's body, outside the external beam port.

Patients follow up consisted in monthly clinical exam, and Image procedures according to medical criteria.

3. Results and discussion

No adverse clinical events were observed during infusion or irradiation procedure.

TLD gamma dose values determined were far below the tolerance values for normal tissues.

Only the first three patients performed tumor biopsy. The range of tumor/blood Boron concentration ratios (T/B) were 1.7 – 2.5 at 2hr 45min after infusion started for patient 1, 2.4 – 4.1 at 5 hr for patient 2 and 2.7 - 3.2 at 10 hr for patient 3. T/B for patient 1 was taken in a separate biodistribution study a few weeks before BNCT.

Although we use a T/B = 3.5, according with our biodistribution results and previous data (Liberman S et al, 2004), the boron concentration into the tumoral cell is just an approximation, as it happens in other BNCT clinical studies.

Table 1 summarizes patient characteristics and outcome of the ten treated areas.

The maximum prescribed dose to normal skin ranged from 16.5 to 24 Gy-eq and Normal Tissue administered dose varied from 15,8 to 27.5 Gy-eq.

Mean difference between maximum tolerable dose and maximum delivered dose (MTD/MDD) was 0.13% (Range -15.3% to +12.7%) obtained from retrospective dose calculation.

Overall response was observed in 69.2% of the nodules defined as a target, with 30.7% of additional no-changed tumours. No progression of disease was observed inside treatment fields along the follow-up (Fig. 1).

Acute grade 3 toxicity (ulceration) was

observed at heel, foot sole and ankle in patients 3, 5 and 7. This could be explained in part by the fact that in this area skin received a higher mean dose and by a different tolerance to radiotherapy for these anatomical areas. Interestingly for patient #3, just grade 1 skin toxicity was observed at the level of the calf, where the mean normal tissue dose was 25.7 Gy-eq, supporting the idea that not just the dose level can explain the different pattern of toxicity. Of note, is the fact that patient 3 suffers vitiligo, a disease that may increase skin sensitivity to radiation therapy. Grade 3 toxity solved slowly, but all patients achieved a complete healing.

As a result of our clinical observations, 24 Gy-eq was considered the prescription dose to normal skin.

Table 1. Patient data, treatment dose and tumor response

Patient	Field	CB	Tum Dose (Gy-Eq9	Clin Response	TIFP (month)	TOFP (month)	Normal Tissue MTD/MDD (Gy-Eq)	Acute Toxicity	Status Post BNCT (May/08) and time of follow-up
#1 D.E.	Lower Leg	11,4	13,4-31,4	21/25 CR 1/25 PR 3/25 NC	3	1	16,5/15,8	G1	Not Alive 18m MTS: Lung
	Upper Leg	12,8	27,4-36,8	NA	< 1m	0	20,0/18,5	G1	
#2 M.A.	Leg	14,7	21,7-51,5	1/11 CR 10/11 NC	7m	NA	22,0/22,6	G1	Not Alive 11m MTS: Inguinal, Pelvic & Liver
#3 L.G.	Calf	15,3	43,1-57,2	4/4 CR 3/3 CR 4/4 CR	-	5m	24,0/25,7	G1	Alive 36m MTS: Inguinal
	Heel	14,0	43,5-48,2				20,0/21,5	G3	
	Foot Sole	13,0	51,0-51,5				20,0/21,2	G3	
#4 M.T.M.	Leg	14,3	16,2-51,1	6/9 CR 1/9 PR 2/9 NC	-	7m	22,0/21,2	G1	Alive 23m MTS: Inguinal
#5 M.C.G.	Heel	16,3	22,7-69,3	10/20 CR 5/20 PR 5/20 NC	-	2m	24,0/27,5	G3	Not Alive 4m MTS: CNS skin
#6 A,E,S,	Thigh	13,6	N1: 37,4-40,79 N2: 25,69-33,11	2/2 CR	-	6m	24,0/20,8	G1	Alive 12m MTS: skin
#7 A.P.	Ankle	14,8	36.4-55.7	1/10 CR 2/10 PR 7/10 NC	-	2m	24,0/23,57	G3	Alive 11m MTS: skin

CB: Average Boron concentration during irradiation
MTD: Maximum tolerable dose
MDD: Maximum delivered dose
NA: Not available
CR: Complete response
PR: Partial response.
CNS: Central Nervous System
NC: No change
PD: Progressive disease
TIFP: Time to in field progression
TOFP: Time outside field progression
Mon: months
MTS: metastatic spread

4. Conclusions

Although we continue to recruit patients for the protocol, data alredy obtained let us conclude that:

a) Toxicity is acceptable for this treatment at the current prescribed dose level.

b) Clinical benefit was found in all the treated areas.

Acknowledgment

Tecnonuclear, for the kindly BPA solution preparation. Julieta Marrero and Paola Babay for the boron concentration measurements in blood samples. This Trial is supported in part by the Agencia de Promocion Cientifica y Tecnologica.

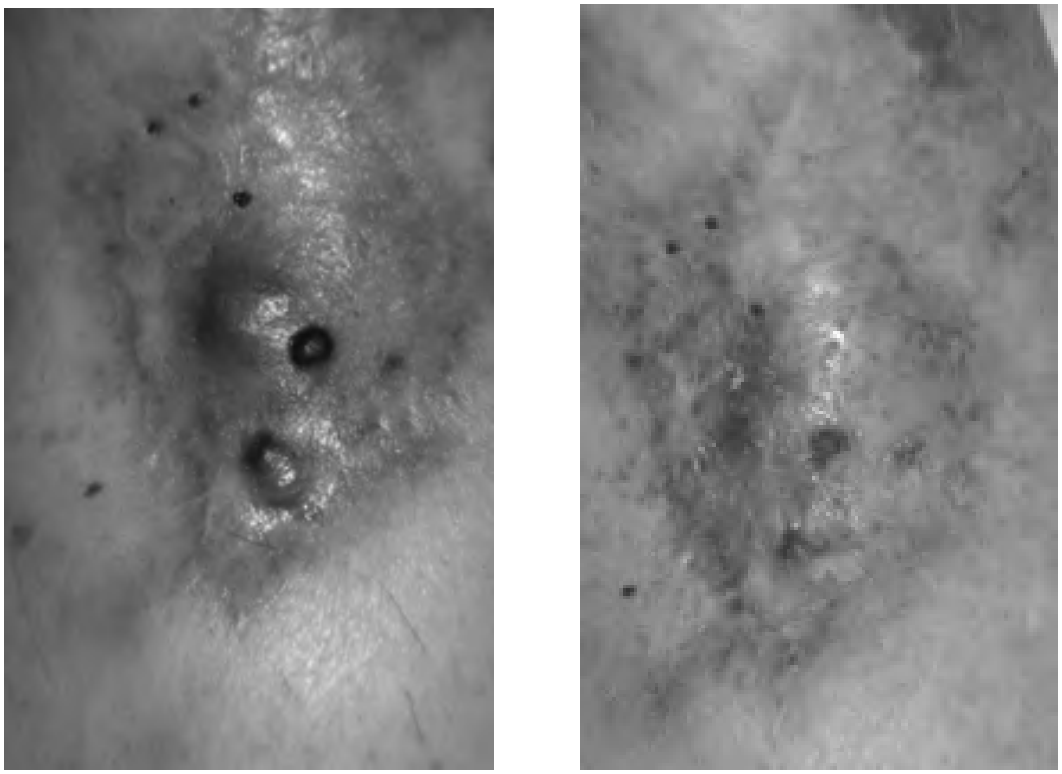

Fig. 1. Patient 4 pictures pre and 4 m. post BNCT

References

H. R. Blaumann, S. J. González, J. Longhino et al. "Boron Neutron Capture Therapy of Skin Melanomas at the RA-6 Reactor: a Procedural Approach to Beam Set Up and Performance Evaluation for Upcoming Clinical Trials," Medical Physics, 31 (1), 70-80 (2004).

J. Hiratsuka, H. Fukuda, T. Kobayashi et al., "Long term outcome of BNCT for malignant melanoma", Proc.9th Int. Symp. on Neutron Capture Therapy for Cancer, Osaka, 165-166 (2000).

S. González, M. Bonomi, G. Santa Cruz et al., "First BNCT Treatment of a Skin Melanoma in Argentina: Dosimetric Analysis and Clinical Outcome," Applied Radiation and Isotopes, 61, 1101-1105 (2004).

S. J. González, G. A. Santa Cruz, W. S. Kiger III et al. "NCTPlan, the New PC Version of MacNCTPlan: Improvements and Verification of a BNCT Treatment Planning System," Proc. 10th Int. Congress on Neutron Capture Therapy for Cancer, Monduzzi Editore, Bologna, 557-561 (2002).

S. J. González, G. A. Santa Cruz, W. S. Kiger III et al. "A New Computational Tool For Constructing Dose-Volume Histograms Using Combinatorial Techniques" Proc. 10th ICNCT, p. 629-633 Monduzzi Editore, Bologna, 2002b.

S. Liberman, S. Dagrosa, R. Jiménez Rebagliati et al., "Biodistribution Studies of Boronophenylalanine -Fructose in Melanoma and Brain Tumor Patients in Argentina," Applied Radiation and Isotopes, 61, 1095-1100 (2004).

Clinical results and radiation dose of BSH, BPA-based non-operative BNCT with additional external beam irradiation

T.Kageji[a], Y. Mizobuchi[a], S. Nagahiro[a], Y. Nakagawa[b], H. Kumada[c]

[a]Department of Neurosurgery, The University of Tokushima, Tokushima, 770-8503, Japan
[b]Department of Neurosurgery, Kagawa National Children's Hospital, Kagawa, 765-8501, Japan
[c]Department of Research Reactor, Tokai Research Establishment, Japan Atomic Energy Research Institute, Ibaragi, 319-1195, Japan

Abstract

We have shifted from BSH (sodium borocaptate)-based intra-operative BNCT (boron neutron capture therapy) (IO-BNCT) to BSH, BPA (boronophenylalanine)-based non-operative BNCT (NO-BNCT) since 2005. In this study, we evaluated the clinical course and outcome of non-operative BNCT with additional external beam irradiation, and analyzed BNCT radiation. We have applied the modified BNCT in 6 patients (7 BNCT treatments) with glioblatoma. 250 mg/kg of BPA and 100mg/kg of BSH were given to patient intravenously (BSH, BPA-based non-operative BNCT: NO-BNCT). BNCT radiation dose was evaluated with physical boron dose and weighted total (boron and gamma) dose JAERI Computational Dosimetry System (JCDS). The minimum boron physical and weighted total (boron and gamma) doses in GTV were 7.8±2.5 Gy and 27.7±8.7 Gy(w), respectively. These doses in CTV were 4.2±1.1 Gy and 15.2±4.3 Gy(w), respectively. 5 patients died of tumor recurrence at the primary site. The mean survival time was 19.6 months after BNCT. Only one patient survived for 14 months with no neurological deficits. There were no patients suffering acute radiation injury. The clinical results of BSH, BPA-based non-operative BNCT with additional external irradiation was equal to that of BSH-based intra-operative BNCT. The former method was safe and carried less adverse effect. A dose-escalation is needed for further improvement of clinical outcome.

Keywords: BNCT, JCDS, radiation, glioblatoma

1. Introduction

Boron neutron capture therapy (BNCT) is a promising modality for the selective irradiation of tumor tissue. Using the heavy-charged particles such as an alpha particle and a lithium nucleus and the selective boron accumulation only in tumor cells, BNCT offers the possibility of selective tumor cell killing without causing damage to adjacent normal brain tissue. In a word, BNCT is an optimal treatment for glioblastoma, which shows invasive character into the healthy normal tissue. We have used BSH (sodium borocaptate; $Na_2B_{12}H_{11}SH$) as a boron carrier. Since 1968, we have treated more than 170 patients with BSH-based intra-operative BNCT. This important clinical trial showed significant improvements over previously reported outcomes and documented the long-term recurrence-free survival of selected patients with malignant glioma. We have reported that the most important factor to prevent the tumor recurrence was BNCT radiation dose at the tumor bulk and invasive lesion, and that, to avoid the radiation necrosis as an adverse effect, it should be considered the BNCT radiation dose of vasculature at the brain surface.

Our recent study demonstrated that the maximum vascular volume dose should be below 12 Gy (as a physical gold wire dose) to avoid radiation necrosis, the optimal mean dose of the GTV and CTV were 26 Gy and 16 Gy (as a physical gold wire dose), respectively for long-term survival in patients with GBM.

Since 1998, epithermal neutron beam has been introduced clinically instead of pure thermal neutron beam for improvement of neutron distribution in a deep site. And also new dose planning system for BNCT was developed instead of gold wire method, which is JAERI Computational Dosimetry System (JCDS). JCDS can evaluate the BNCT radiation dose on CT scan and MRI prior to BNCT.

BPA (boronophenylalanine), has been introduced for clinical BNCT. It can accumulate into tumor cells through passive amino-transportation, so the tumor to blood ratio of BPA is higher than that of BSH. The combination of BPA and epithermal neutron beam makes it possible to introduce non-operative BNCT. Recently new clinical trial has been started using both BSH and BPA simultaneously as boron carriers. It is thought that BSH, BPA-based non-operative BNCT can lead to sufficient radiation dose in comparison with BSH-based intra-operative BNCT.

Since 2005, we have started a new protocol of BSH, BPA-based non-operative BNCT. In this study, we can compare BNCT radiation dose between BSH-based intra-operative BNCT and BSH, BPA-based non-operative BNCT.

2. Material and Methods

19 patients with malignant brain tumors underwent BSH-based intra-operative BNCT using mixed neutron beam from 1998 to 2004. We have applied the modified BNCT in 6 patients (7 BNCT treatments) with glioblatoma. 250 mg/kg of BPA and 100mg/kg of BSH were given to patient intravenously. After NO-BNCT, the patients received additional external radiation of 30 Gy. BNCT radiation dose was evaluated with physical boron dose and weighted total (boron and gamma) dose with JAERI Computational Dosimetry System (JCDS). Irradiation time was prescribed so that normal brain tissue dose did not exceed 12 Gy(w). We analyzed BNCT dose in gross tumor volume (GTV) and clinical target volume (CTV). GTV was coincident with enhancement area on Gd-MRI. CTV was coincident with high intensity area on T2-weighted MRI. External irradiation was applied in three patients after BNCT.

We can compare the BNCT radiation dose between BSH-based intra-operative BNCT (IO-BNCT) and BSH and BPA-based non-operative BNCT (NO-BNCT). Dose ratio indicates the values of IO-BNCT dose divided by NO-BNCT dose.

3. Results

3-1 irradiation time and boron concentration

Irradiation time in IO-BNCT and NO-BNCT were 104.1±39.3 and 29.2±8.8 min., respectively. Blood boron concentration in BPA and BSH were 17.8±5.4 and 33.8±9.1 ppm, respectively in NO-BNCT. Blood boron concentration in BSH NO-BNCT was 29.6±13.2 min.

3-2 skin, normal brain radiation dose

The maximum skin and normal brain tissue dose were 10.3±2.5 and 12.5±2.3 Gy(w) in NO-BNCT, respectively. The maximum vascular dose at brain surface in IO-BNCT was 39.9±12.2 Gy(w). Gamma dose in NO-BNCT and IO-BNCT were 3.1±0.5 Gy(w) and 6.4±3.3 Gy(w), respectively.

3.3 BNCT radiation dose in gross tumor volume (GTV) dose

In NO-BNCT, the minimum boron physical and weighted total (boron and gamma) dose in GTV were 7.8±2.5 Gy and 27.7±8.7 Gy(w), respectively. In comparison, these doses in IO-BNCT were 18.3±5.3 Gy and 52.1±14.2 Gy(w), respectively. The dose ratio between IO-BNCT and NO-BNCT in boron physical dose was 2.35. That in weighted total (boron and gamma) dose was 1.88.

Table 1: GTV radiation dose in boron physical dose (Gy)

	IO-BNCT n=19	NO-BNCT N=7	Dose ratio
maximun	33.8±8.7	19.4±6.2	1.74
minimum	18.3±5.3	7.8±2.5	2.35
average	26.7±6.4	14.5±4.3	1.84

Table 2: GTV radiation dose in weighted total (boron and gamma) dose (Gy(w))

	IO-BNCT n=19	NO-BNCT N=7	Dose ratio
maximun	90.9±22.8	67.9±24.3	1.34
minimum	52.1±14.2	27.7±8.7	1.88
average	71.9±17.1	50.9±16.3	1.41

3-4 BNCT radiation dose in clinical target volume (CTV) dose

In NO-BNCT, The minimum boron physical and weighted total (boron and gamma) dose in CTV were 4.2±1.1 Gy and 15.2±4.3 Gy(w), respectively. In comparison, these doses in IO-BNCT were 11.8±5.6 Gy and 35.8±14.6 Gy(w), respectively. The dose ratio between IO-BNCT and NO-BNCT in boron physical dose was 2.80. That in weighted total (boron and gamma) dose was 2.36

Table 3: CTV radiation dose in boron physical dose (Gy)

	IO-BNCT n=19	NO-BNCT N=7	Dose ratio
maximun	32.8±9.0	19.6±6.0	1.67
minimum	11.8±5.6	4.2±1.1	2.80
average	22.9±5.7	12.4±3.6	1.85

Table 2: GTV radiation dose in weighted total (boron and gamma) dose (Gy(w))

	IO-BNCT n=19	NO-BNCT N=7	Dose ratio
maximun	88.4±22.8	68.7±23.7	1.29
minimum	35.8±14.6	15.2±4.3	2.36
average	57.1±14.3	43.6±14.3	1.31

5 patients died of tumor recurrence at the primary site. The mean survival time was 19.6 months after BNCT. Only one patient survived for 14 months with no neurological deficits. There were no patients suffering acute radiation injury.

4. Discussion

We have reported the correlation between boron neutron capture therapy (BNCT) radiation dose and histopathological findings of autopsy or salvage surgery. Postmortem study revealed that none of the patients manifested local regrowth in the primary site. One patient showed no tumor cells, only radiation necrosis. Two patients showed CSF dissemination. Residual tumor cells were recognized close to tumor cavity in two patients. Histopathological investigation of salvage surgery revealed no tumor cells in two patients. One patient, who died of massive CSF dissemination, demonstrated tumor cells.

There were 4 patients, who demonstrated residual tumor cells histopathologically, in autopsy or salvage surgery. The maximum and minimum GTV doses in patients with residual tumor cells were 72.1±12.8 and 46.4±6.7 Gy(w), respectively. The CTV doses in those patients were 70.6±20.6 and 31.9±11.5 Gy(w), respectively.

There were 3 patients, who demonstrated no tumor cells histopathologically, in autopsy or salvage surgery. The maximum and minimum GTV doses in patients with no residual tumor cells were 120.1±22.8 and 68.0±14.8 Gy(w), respectively. These CTV doses were 113.2±28.5 and 45.2±26.6 Gy(w), respectively We concluded that the BNCT dose is the most important factor for long-term survival in patients with GBM. For the complete remission of GBM after BNCT, the minimum GTV and CTV dose should be 65 Gy(w) and 45 Gy(w) as a boron JCDS dose, respectively.

NO-BNCT is a less invasive treatment modality than IO-BNCT, so high-risk patients such as aged, low-ADL and advanced stage patients can receive BNCT. We think it is very important to clarify if NO-BNCT can achieve the cure of GBM or not.

In this study, we revealed that the BNCT radiation dose of NO-BNCT is insufficient for the long-survival or complete cure. The main reason of limited radiation dose of NO-BNCT is normal and healthy brain tissue damage. BPA can accumulate in tumor tissue in higher concentration than BSH, however, it can accumulate in skin and normal brain tissue. As a result, we cannot increase the radiation dose without limitation. On the other hand, with our new modality, non-operative BNCT with additional external beam irradiation can be a promising method without adverse effect.

This study demonstrated that the combination dose of NO-BNCT and external beam could reach the dose of IO-BNCT. We stress that clinical outcome of new method can be comparable or even superior to IO-BNCT.

5. Conclusion

The clinical results of BSH, BPA-based non-operative BNCT with additional external irradiation was equal to that of BSH-based intra-operative BNCT.

The former method was safe and with less adverse effect. A dose-escalation is needed for further improvement of clinical outcome.

Acknowledgement

A part of this study was financially supported by the Budget for nuclear research of the ministry of Education, Culture, Sports, Science and Technology based on the screening and counseling by Atomic Energy Commission

References

Hatanaka H, Nakagawa Y, 1994. Clinical results of long-surviving brain tumor patients who underwent boron neutron capture therapy. Int J Radiat Oncol Biol Phys 28, 1061-1066.

Nakagawa Y, 1994. Boron neutron capture therapy: the past to the present. Int J Radiat Oncol Biol Phys 28, 1217.

Nakagawa Y, Hatanaka H, 1997. Boron neutron capture therapy-clinical brain tumor study. J Neurooncol 33, 105-115.

Nakagawa Y, Pooh K, Kobayshi T, et al., 2003. Clinical review of Japanese experience with boron neutron capture therapy and a proposed strategy using epithermal neutron beams. J. Neurooncol 62, 87-99.

Kageji T, Nagahiro S, Mizozuchi Y, et al.,2006. Boron neutron capture therapy using mixed epithermal and thermal neutron beams in patients with malignant glioma –correlation between radiation dose and radiation injury and clinical outcome-. Int. J. Radiation Oncology Biol. Phys. 65, 1446-1455.

Kageji T, Mizobuchi Y, Nagahiro S, Nakagawa Y, Kumada H, 2006. Correlation between BNCT radiation dose and histopathological findings in BSH-based intra-operative BNCT for malignant glioma. Advances in Neutron Capture Therapy 2006, 35-36.

BPA-Based BNCT in the Treatment of Glioblastoma Multiforme: A Dose Escalation Study

L. Kankaanranta[1], H. Koivunoro[1], M. Kortesniemi[2], P. Välimäki[3], T. Seppälä[1], P. Kotiluoto[4], I. Auterinen[4], M. Kouri[1], S. Savolainen[2], H. Joensuu[1]

[1]Department of Oncology, [2]HUS Medical Imaging Centre, Helsinki University Central Hospital
[3]Boneca Oy, [4]VTT Technical Research Centre, Espoo, Finland

Purpose: We evaluated safety and efficacy of escalating doses of boronophenylalanine fructose (BPA-f) as the boron carrier for BNCT in the treatment of glioblastoma multiforme (GBM). The highest tolerated dose of BPA-f is unknown in this setting.

Patients and Methods: Patients with histologically diagnosed GBM were eligible to this prospective, phase I-II single-centre trial. BNCT was given a few weeks after brain surgery. No conventional radiotherapy or cancer chemotherapy was allowed. The first 12 patients received BPA-F 290 mg/kg, following which the BPA-f dose was planned to be escalated as follows: 330 mg/kg (n=1), 360 mg/kg (n=3), 400 mg/kg (n=3), 450 mg/kg (n=3), and 500 mg/kg (n=3). Further 6 patients were planned to be treated at the level of maximum tolerated dose -1 (MTD-1). BPA-f was administered intravenously as 2-hr infusion prior to epithermal neutron irradiation at the FiR 1 BNCT facility. The normal brain average maximum dose was restricted to 10 Gy (W). The NCI common toxicity grading v2.0 was used in evaluating adverse effects. ClinicalTrials.gov trial identifier NCT00115453.

Results: Thirty patients were entered in May 1999 to April 2005. The MTD was reached at 500 mg/kg, where 3 of the 8 patients developed severe central nervous system toxicity (grade 3, n= 2; grade 4, n=1). All but one patient have died. The patient alive received BPA-f 500 mg/kg and has been followed up for 39.0 months following BNCT. No association between the BPA-f dose and duration of survival is evident in this small series. The median survival times are 13.4, 11.0, 16.9, 21.9 and 14.7 months in the dose groups of 290, 330/360, 400, 450 and 500 mg/kg, respectively.

Conclusion: The MTD is reached at the BPA-f dose level of 500 mg/kg, when BPA-f is administered intravenously over 2 hours prior to neutron irradiation. The dose of 450 mg/kg was selected to be used in further studies.

Boron Neutron Capture Therapy for Head and Neck Epithelial Carcinomas other than SCC

Teruhito Aihara, M.D.[1] Junichi Hiratsuka, M.D.[2] Suetaka Nishiike, M.D.[1]
Norimasa Morita, M.D.[2] Masako Uno, M.D.[1] Akira Maruhashi, Ph.D.[3]
Hiroaki Kumada, Ph.D.[4] Koji Ono, M.D.[3] and Tamotsu Harada, M.D.[1]

[1]*Departments of Otolaryngology Head and Neck Surgery, and* [2]*Radiation Oncology, Kawasaki Medical School, Okayama, Japan*
[3]*Radiation Oncology Research Laboratory, Research Reactor Institute, Kyoto University, Osaka, Japan*
[4]*Department of Research Reactor, Tokai Research Establishment, Ibaragi, Japan*

1. Background

Advanced head and neck carcinoma are often radio-/chemo-resistant and show extensive growth, requiring a wide resection including surrounding normal tissues. To avoid severe impairment of head and neck structures, it is necessary to explore new treatment for advanced head and neck carcinoma. Mishima first proposed employing boron neutron capture therapy (BNCT) for malignant melanomas utilizing the specific melanin synthesis activity of melanoma cells[1]. Kato et al.[2] began BNCT using both BSH (Na2B12H11SH) and BPA (para-boronophenylalanine) for recurrent parotid gland carcinoma for the first time and reported excellent preliminary results. On the basis of the encouraging results of their pioneering clinical trial, our many years' experience with melanoma BNCT and the trend toward em-phasizing the quality of life after treatment, we also be-gan treating our patients with BNCT using BPA alone[3]. Based on the reports of successful BNCT for mucoepidermoid carcinoma of the parotid gland, we have been conducting BNCT clinical trial for recurrent or locally advanced epithelial carcinomas in the head and neck since October 2003.

2.Patients and Methods

Six patients were treated with BNCT at KUR and JRR-4 from October 2003 to September 2007. The histologic type of (recurrent or primary) carcinoma, region, and TNM staging of each patient were as follows: *Patient 1*: high grade mucoepidermoid carcinoma; submandibular grand, rN2a, *Patient 2*: adenoid cystic carcinoma (ACC); submandibular grand; rT3, *Patient 3*: ACC; maxillary sinus; rT4, *Patient 4*: acinic cell carcinoma; palotid gland; T4N0M0, *Patient 5*: ACC; lacrimal sac; T4N0M0, *Patient 6*: ACC; maxillary sinus; T4N0M0 (Table1).

The tumor/normal-tissue boron concentration ratio (T/N ratio) obtained from ^{18}F-BPA-PET study was adopted for dose estimation before neutron irradiation and dose evaluation after BNCT using SERA or JCDS(Fig2a,b). Neutron irradiation was performed using an epithermal beam at a reactor power of 5.0 MW (KUR) or 3.5 MW (JRR-4) after intravenous administration of BPA in fructose solution at a dose of 500 mg/kg body weight. The tumor dose at the deepest part and the dose of both normal skin and mucosa were planned more than 20 Gy-Eq and less than 15 Gy-Eq, respectively (Table 1) (Fig.2a,2b).

Fig2a. 18F-BPA-PET(Patient4: parotid Cancer. T/N ratio = 5)

4. Results

All patients demonstrated regional complete response (CR). *Patient 6* suffered from dermatitis (grade 2 RTOG/EORTC acute reaction) that exceeded the tolerance level. However, dermatitis was cured within a few months after BNCT. *Patient 1* had brain involvement 12 months after BNCT. Patient3 showed metastasis to the lung. *Patient 4* had local recurrence of the neck 17 months after BNCT.

At present, all the patients are living, surviving 12 to 56 months after BNCT (Table 2).

Case	Tumor site	Age/Sex	Histology	TNM	T/N	Initial Treatment
1	submandibular gland	49/F	MC(HG)	rN2a	2.9	Op+Ch
2	submandibular gland	54/F	ACC	rT3	3.8	Op+Ch+Rt
3	Maxillary sinus	44/M	ACC	rT4	2.5	Op+Rt
4	parotid gland	74/F	AC	T4N0M0	5	
5	Lacrimal sac	58/M	ACC	T4N0M0	3.5	
6	Maxillary sinus	50/F	ACC	T4N0M0	2.5	

Table 1. Patient characteristics

MC(HG): mucoepider*moid carcinoma(high grade malignancy)* ACC*:adenoid cystic carcinoma,* AC*:acinic cell carcinoma,* Op*:operation,* Ch*:chemothera*py, Rt*:radiotherapy*

Case	Histology	Tumor Response	Complications: (RTOG/EORTC score)	Follow-up
1	MC(HG)	CR	G1	56m (distant;brain:12m)
2	ACC	CR	G1	17m
3	ACC	CR	G2	12m (distant;lung:12m)
4	AC	CR	G1	24m (local;17m)
5	ACC	CR	G1	17m
6	ACC	CR	G2	15m

Table 2. Therapeutic effect

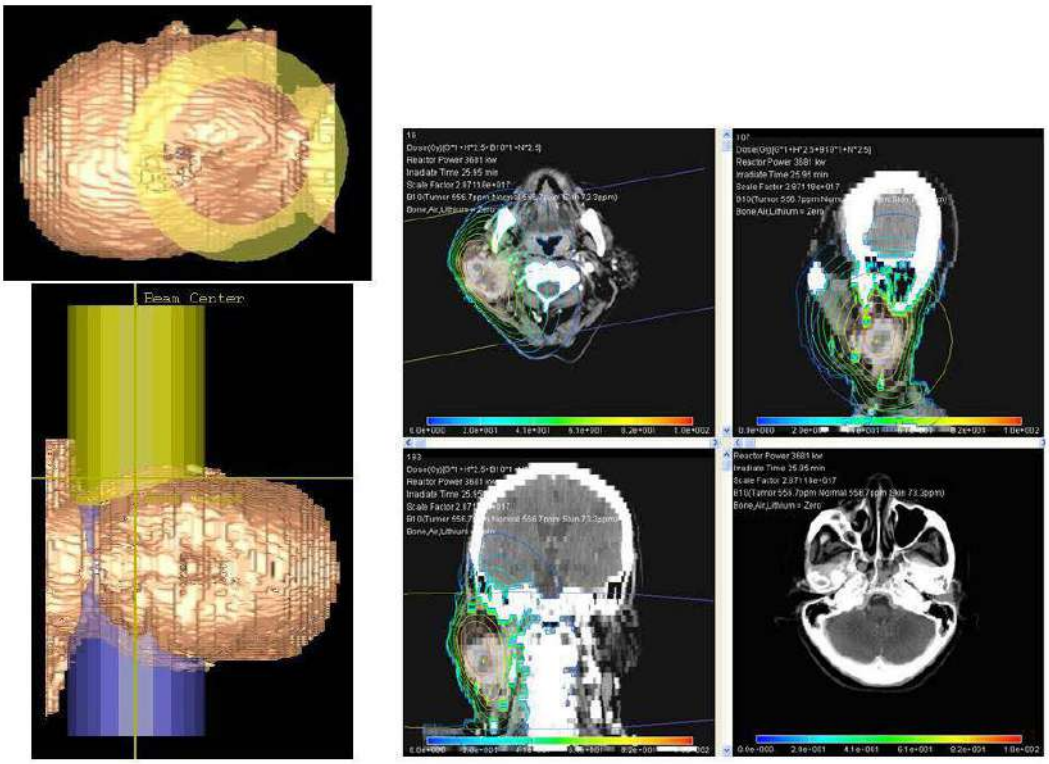

Fig2b. We calculate the radiation dose of the patient in SERA based on CT(Patient4)

4. Conclusion

This study shows that BNCT is a quite effective therapy for the epithelial carcinomas of the head and neck. Based on the promising results and the sample size, further research is warranted on this method. Our results validate the efficacy of BNCT in the treatment of patients with advanced head and neck carcinoma. This is a report of only thirteen patients and additional long-term follow-up is required to assess this treatment. We have estimated T/N boron ratio using 18F-BPA-PET in every cases.

The T/N ratios measured are the values of BPA alone. If T/N ratio was more than 2.5, according to our adaptation, it is thought that therapy effect is good. We believe that head and neck tumors are suitable for BNCT and that such excellent results will have a great impact on patients in the near future.

References

[1] Y Mishima, Pigment Cell Res., 1 (1973) 215-221.

[2] I Kato, et. al., Applied Radiation and Isotopes, 61 (2004) 1069-1073.

[3] T. Aihara, et al., Head and Neck, 28 (2006) 850-855.

Feasible Evaluation of Neutron Capture Therapy for Local Recurrenced Breast Cancer

H.Yanagie[1,2], H. Kumada[3], Y. Sakurai[4], T. Nakamura[3], Y. Furuya[5], H. Sugiyama[2], K. Ono[6], S. Takamoto[2,7], M. Eriguchi[2,8], and H. Takahashi[1,2]

[1]*Department of Nuclear Engineering & Management, Graduate School of Engineering, The University of Tokyo,Tokyo, JAPAN*
[2] *Cooperative Unit of Medicine & Engineering, The University of Tokyo Hospital, Tokyo, JAPAN*
[3]*Japan Atomic Research Institute, Ibaraki, JAPAN*
[4]*Department of Physics, Sapporo Medical University, Hokkaido, JAPAN*
[5]*Department of Surgery, Satukidai Hospital, Chiba, JAPAN*
[6] *Research Reactor Institute, Kyoto University, Osaka, JAPAN*
[7]*Department of Cardiac Surgery, The University of Tokyo Hospital, Tokyo, JAPAN*
[8]*Department of Microbiology, Syowa University School of Pharmaceutical Sciences, Tokyo, JAPAN*

Corresponding Author: Hironobu Yanagie, MD, PhD ; TEL: +81-3-5800-9194 ;
FAX: +81-3-5800-9195 ; E-mail: yanagie@n.t.u-tokyo.ac.jp

Abstract

Local recurrence breast cancer is one of the most difficult condition to cure and there is a need for new therapy. If sufficient boron compound can be targeted to the tumor, Boron Neutron Capture Therapy (BNCT) can be applied to local recurrenced breast cancer. In this study, we performed a preliminary dosimetry with a phantom model of the mammary gland at Kyoto University Research Reactor (KUR), and a feasibility dosimetry with JCDS at JRR4 reactor of Japan Atomic Research Institute.

We performed preliminary dosimetry of a phantom model of the mammary gland with thermal neutron irradiation (OO-0011 mode) on LiF collimation at KUR. The thermal neutron flux was 5.16 E+08 cm-2s-1 at the surface of phantom. The blood boron concentration is estimated to 30 ppm, tumor boron concentration is also estimated to 90 ppm according to tumor/blood ratio is 3 and skin/blood ratio is 1.2. Tumor RBE dose is estimated to 47 Gy/h, and skin RBE dose is 12.4 Gy/h.

In case of advanced breast cancer, we performed the feasibility estimation of 3D construction of tumor according to the MRI imaging of a patient with epithermal neutron mode at JRR4. The blood boron concentration (ppm) and tumor/normal tissue ratio are estimated to 24, 3.5, respectively. Skin RBE dose is ristricted to 10 Gy/h, the maximum tumor RBE dose, minimum tumor RBE dose, and mean tumor RBE dose are 42.2, 11.3, and 28.9 Gy-Eq, respectively, in half hour irradiation.

In this study, we showed the possibility to apply BNCT to local recurrenced breast cancer. We can irradiate tumors selectively and safety as possible, reducing the effects on neighboring healthy tissues.

Keywords : Boron Neutron-Capture Therapy (BNCT), Recurrenced & Advanced Breast Cancer, Neutron Dosimetry, Treatment Planning, JCDS, LiF Collimation

1. Introduction

We would like to apply BNCT, to radioresistant conditions as recurring & advanced breast cancer, hepatocellular carcinoma, liver metastases, or lung cancer.

Incidence of breast cancers is increasing, so it is also more important to plan treatment protocols for recurring cases [1,2].

Breast cancer may recur after primary resection both locally (thoracic wall :23%, local lymph nodes :19%) and in distant sites (bone :23%, lung : 18%, and liver : 4%). The treatment of local recurrences may be curative or palliative to avoid the occurrence of bleeding, ulcer formations, bad smelling. Radiation therapy is commonly used to this purpose [3, 4, 5, 6]. Skin ulcer, and bone necrosis may apper after irradiation due to the

lower tolerance of the thoracic wall after mastectomy. So a dose of about 40~50 Gy is recommended for recurrences.

The cytotoxic effect of boron neutron capture therapy (BNCT) is due to a nuclear reaction between ^{10}B and thermal neutrons ($^{10}B + {}^{1}n \rightarrow {}^{7}Li + {}^{4}He$ (α) + 2.31 MeV (93.7 %) / 2.79 MeV (6.3 %)). The resulting lithium ions andαparticles are high linear energy transfer (LET) particles which produce high biological effects. Their short range in tissue (5 - 9 μm) restricts radiation damage to those cells in which boron atoms are located at the time of neutron irradiation. BNCT is performed in patients with malignant brain tumours, melanoma, head & neck cancer [7]. We wish to extend the application of BNCT to the treatment of locally advanced or local recurrence of breast cancer, hepatocellular cell carcinoma, metastatic liver tumor, or lung cancer.

In this study, we evaluate neutron flux dosimetry in horizontal irradiation position using a phantom model of a mammary gland at Kyoto University Research Reactor, and also evaluate the BNCT simulation for a breast cancer patient with MRI images using JCDS at Japan Atomic Energy Research Institute.

2. Materials & Methods

Preparation of Phantom Model:
We used an phantom shaped mammary gland(hight : 4cm, wide : 12 cm). Gold wires and TLDs were attached in 2cm range from the front side of phantom.

Neutron Irradiation
We used thermal neutron mode(OO-0011) for dosimetry of the phantom model [8,9]. Irradiation was performed at Neutron Irradiation Facility of The Kyoto Research Reactor(KKR). Irradiation were performed with LiF collimation(5 cm φ). The thermal neutron flux was measured by gold wire, and the gamma dose rate was measured by TLD. The measured values of neutron gradation depend of the distance from the surface of Phantom.

Neutron dosimetry with JAERI Computational Dosimetry System (JCDS) for a breast cancer patient:
BNCT was simulated in a 64 years patient with a 3 cm tumour in the lower half of the R breast. LiF collimation was used to selectively irradiate the tumor while sparing the adjacent normal organs (lung, heart). The Neutron Beam Facility at JRR4 enables to carry out boron neutron capture therapy with epithermal neutron beam. The JAERI Computational Dosimetry System (JCDS), which can estimate distributions of radiation doses in a patient's head by simulating in order to support the treatment planning for epithermal neutron beam BNCT, was developed. We applied this JCDS for evaluation the neutron dosimetry for this case.

3. Results & Discussion

The clinical BNCT trial is performed at Kyoto University Research Reactor(KUR) at Kumatori, Osaka and Japan Atomic Institute Reactor at Tokai, Ibaragi in Japan. Phantom model reproduced a breast 4cm high, and 12cm wide) (Figure 1). Thermal neutron irradiation mode(OO-0011) was used. Thermal neutron flux was 5.16 x 10^8 n/cm^2/sec at the surface of phantom (Figure 2). In this evaluation, the concentration of 10B is estimated 30 ppm, Tumor/Blood ratio : 3, and Skin/Blood ratio : 1.2. The tumor boron dose is 12.4 Gy/h, tumor RBE dose is 47 Gy/h, skin boron dose is 4.97 Gy/h, and skin RBE dose is 12.4 Gy/h.

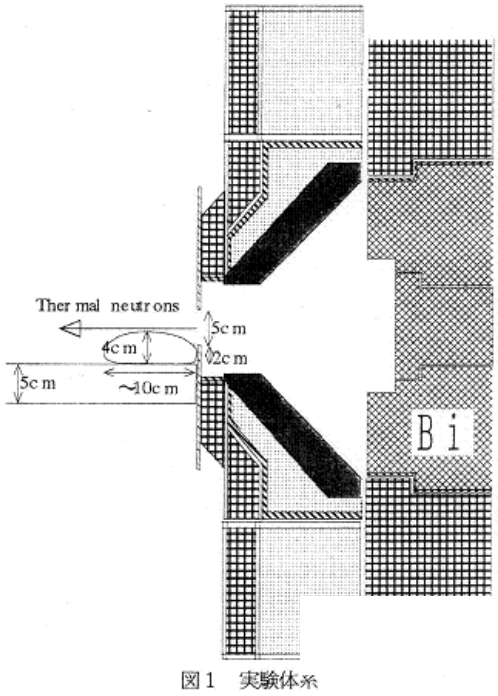

図1 実験体系

Figure 1. Experiment setting of phantom model of mammary gland at KURR

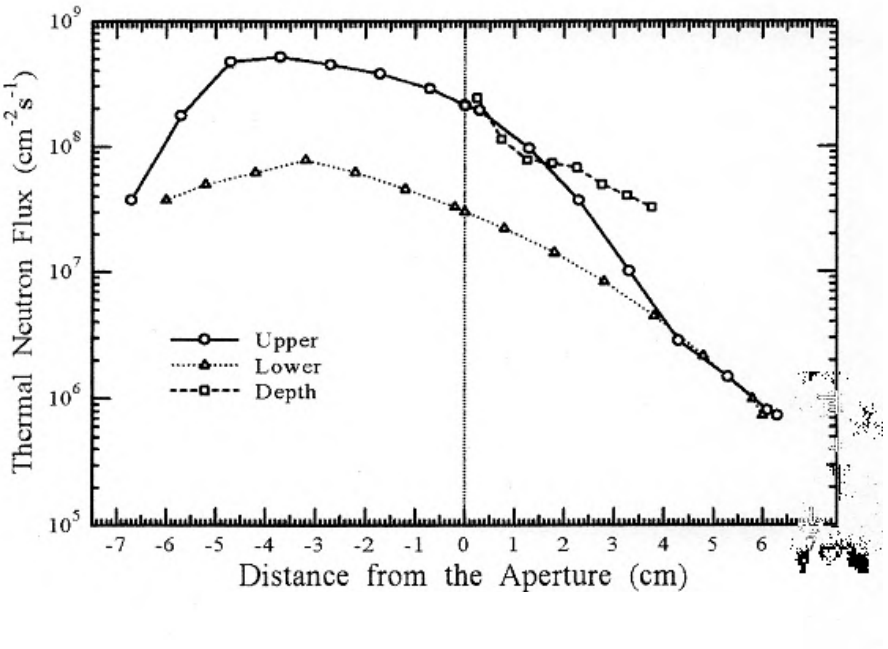

Figure 2. Thermal neutron fluxs of the phantom model of mammary gland at KURR

Thermal neutron mode(OO-0011) was used. At the position that he thermal neutron flux is 5.16 x 10^8 n/cm^2/sec, the tumor RBE dose became 47Gy-Eq on one hour thermal neutron irradiation with the 30 ppm ^{10}B blood concentration at KUR. Thermal neutron irradiation with Void and LiF collimation can be focused to the target field selectively minimizing the irradiation dose to adjacent organs.

Kumada et al had reported that JCDS is a software that creates a 3-dimensional head model of a patient by using CT scan and MRI images, and that generates a input data file automatically calculation of neutron flux and gamma-ray dose distributions in the brain with the Monte Carlo code MCNP, and that displays these dose distributions on the head model for dosimetry by using the MCNP calculation results [10]. JCDS has the following advantages; (1) a detailed 3D model of the patient's head can be easily obtained from the CT and MRI data, (2) the three-dimensional head image is editable to simulate the state of a head after surgery, (3) JCDS can provide information for the Patient Setting System which can support to set the patient to an actual irradiation position swiftly and accurately.

We performed the dosimetry with JCDS in the condition of BNCT using epithermal neutron beams(Figure 3). To decrease the skin side effects, the skinRBE dose limited to 10Gy-Eq.

The minimum tumor RBE dose is 11.3 Gy-Eq, the mean tumor RBE dose is 28.9 Gy-Eq, and the maximum tumor RBE dose is 42.2 Gy-Eq. The two dimensional distributions of neutron beam revealed that the peak of the beam was a little shifted from the tumor site(Figure 4). For calibration of the beam peaks to tumor, t is necessary to perform a few change the beam direction, and addition of some void to the neighbor site of tumors.

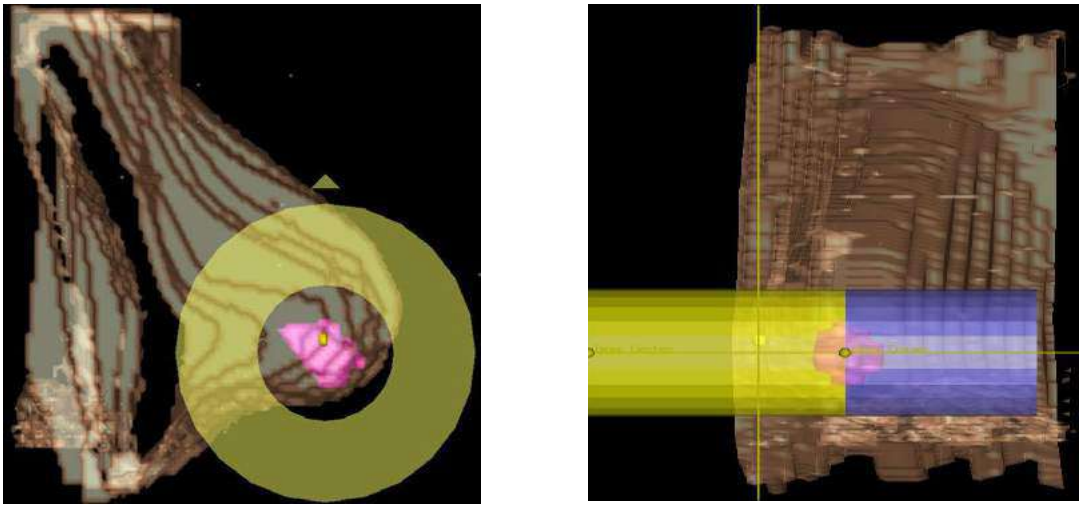

Figure 3. JCDS simulation for rt breast cancer patient. Left : lateral view, Right : frontal view

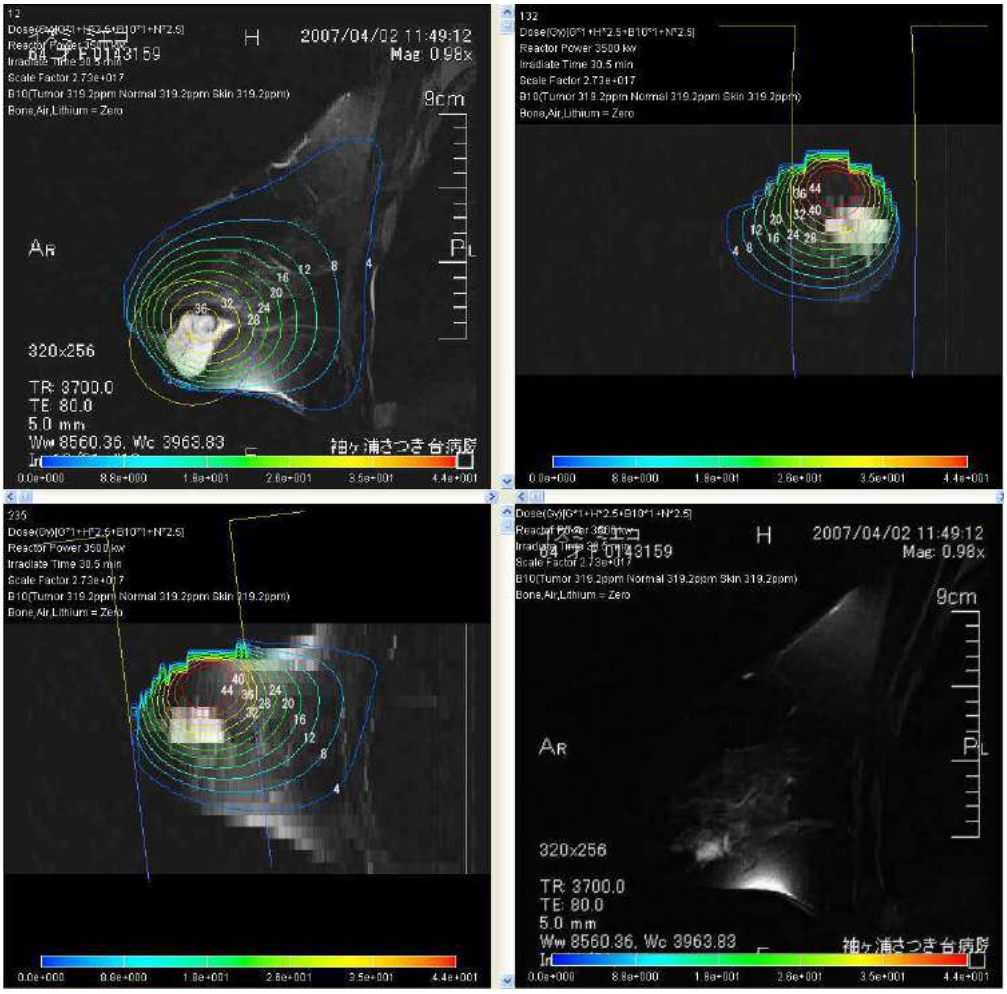

Figure 4. Two dimensional distributions of epithermal neutron beam at JRR4 using JCDS evaluation

We applied the JCDS to dosimetry of epithermal neutron, direction of neutron beam, and patient's positioning on BNCT [11]. We also evaluate the epithermal neutron dose to decreas the skin side effect. High resolution whole body dosimetry system, as JCDS will be very useful to evaluate the thermal neutron dosimetry and the application of BNCT to recurring or advanced breast cancer.

References

Ballo MT, et al., 1999. Local-regional control of recurrent breast carcinoma after mastectomy: does hyperfractionated accelerated radiotherapy improve local control?, Int J Radiat Oncol Biol Phys., 44(1):105-12.

Bristol IJ, et al., 2008. Locoregional Treatment Outcomes After Multimodality Management Of Inflammatory Breast Cancer, Int J Radiat Oncol Biol Phys., [Epub ahead of print]

Kumada H., 2001. The Development of a Computational Dosimetry System for BNCT at JRR-4. Frontiers in Neutron Capture Therapy, Hawthorne et al. (ed), New York, Kluwer Academic, pp611-614.

Liao Z, et al., 2000. Locoregional irradiation for inflammatory breast cancer: effectiveness of dose escalation in decreasing recurrence, Int J Radiat Oncol Biol Phys., 47(5), 1191-200.

Nielsen HM, et al., 2006., Loco-regional recurrence after mastectomy in high-risk breast cancer--risk and prognosis. An analysis of patients from the DBCG 82 b&c randomization trials, Radiother Oncol. 79(2):147-55. Epub 2006 Apr 27.

Ono K., et al., 2002. Results of BNCT to Brain Tumors in KUR. Research and Development in Neutron Capture Therapy, Sauerwein et al.(ed), Bologna, Monduzzi Editore, pp1097-1100.

Sakurai Y. and Kobayashi T., 2000. Characteristics of the KUR Heavy Water Neutron Irradiation facility as a neutron irradiation field with variable energy spectra. Nucl. Instr. Meth. A. 453, 569-596.

Sakurai Y., Kobayashi T., and Ono K., 2002. Study on Accelerator-base neutron Irradiation Field aiming for Wider Application in BNCT – Spectrum Shift and Regional Filtering. Research and Development in Neutron Capture Therapy, Sauerwein et al.(ed), Bologna, Monduzzi Editore, pp259-263.

Touboul E., et al., 1999. Local recurrences and distant metastases after breast-conserving surgery and radiation therapy for early breast cancer, Int J Radiat Oncol Biol Phys., 43(1), 25-38.

Yanagie H, et al., 2007. Evaluation of neutron dosimetry on pancreatic cancer phantom model for application of intraoperative boron neutron-capture therapy, Biomedicine & Pharmacotherapy, 61(9), 505-514.

Willner J, Kiricuta IC, and Kölbl O, 1997., Locoregional recurrence of breast cancer following mastectomy: always a fatal event? Results of univariate and multivariate analysis, Int J Radiat Oncol Biol Phys., 37(4), 853-63.

New Indications for BNCT? Results from the EORTC trial 11001

A. Wittig[a], S.-Y. Sheu[b], G.M. Kaiser[c], S. Lang[d], K.-H. Jöckel[e], R. Moss[f] F. Stecher-Rasmussen[h], J. Rassow[a], L. Collette[i], W. Sauerwein[a]

[a]*Dept. of Radiation Oncology;* [b]*Institute of Pathology and Neuropathology;* [c]*Dept. of General, Visceral and Transplantation Surgery;* [d]*Dept of Otorhinolaryngology Head and Neck Surgery and* [e]*Institute for Medical Informatics, Biometry and Epidemiology University Duisburg-Essen, 45122 Essen, Germany*
[f]*HFR Unit, Institute for Energy, Joint Research Centre, European Commission, Petten, The Netherlands*
[h]*Nuclear Research and consultancy Group (NRG), Petten, The Netherlands*
[i]*European Organisation for Research and Treatment of Cancer (EORTC), Brussels, Belgium*

Abstract

Boron neutron capture therapy (BNCT) is a binary treatment modality that needs two components, a boron compound that selectively transports ^{10}B into tumor cells and thermal neutrons that react with the boron. The selective damage to the tumor is reached by neutron capture reactions releasing high LET-particles with very short range only where ^{10}B is present. Neither ^{10}B nor thermal neutrons alone have any therapeutic effect. Therefore, to develop BNCT towards a treatment modality, the usual trial design is difficult to apply. Instead, innovative trial strategies using surrogate endpoints were developed. In this translational research/phase I study (EORTC 11001) the uptake of 2 compounds that actually are available for BNCT was investigated in squamous cell carcinoma of the head and neck (SCCHN), thyroid cancer and liver metastases of colorectal cancer. Our results indicate that both drugs may be used to treat SCCHN, but not for differentiated thyroid cancer, BPA seems to be an excellent drug in liver metastasis of colorectal cancer. Such data are prerequisite and scientific basis for further developing BNCT. They therefore are of high clinical interest but also relevant for approval of future clinical trials by the regulatory authorities and more of such basic data need to be collected in further clinical trials.

Keywords: translational research, clinical trial, ^{10}B-biodistribution, BS, BPA

1. Introduction

Important progress in cancer treatment may occur by the development of targeted therapies, which aim to selectively destroy tumor cells whilst sparing surrounding healthy tissue, increasing efficacy and decreasing toxicity. One such option is Boron Neutron Capture Therapy (BNCT), which provides through the limited spatial distribution of its effects a highly targeted delivery of radiation, which can selectively kill tumor cells. BNCT is based on the ability of the isotope ^{10}B to capture thermal neutrons with high probability leading to the nuclear reaction $^{10}B(n,\alpha)^{7}Li$. This reaction produces, alpha particles and ^{7}Li-ions, which both have in tissue a high biological effectiveness relative to conventional irradiation. The range of these particles is 10-14 μm only, limiting their effects to approximately one cell diameter.

A prerequisite for such an approach is a selective accumulation of a ^{10}B-carrying compound in the tumor. Therefore, knowledge on the biodistribution of the drug is a prerequisite to develop such treatment option. The paper presents a prospective controlled early clinical trial conducted by the EORTC, which investigates the biodistribution of two boronated compounds. The trial aims to identify tumor entities that may be treated with BNCT due to a selective uptake of the compounds sodium mercaptoundecahydro-closo-dodecaborate (BSH) or para-boronophenylalanine (BPA).

Three solid tumor entities were investigated:

a) squamous cell carcinoma of head and neck (SCCHN)
b) thyroid cancer

c) hepatic metastases of colorectal adenocarcinoma

Treatment of all three tumor entities represent a significant clinical problem and is still challenging.

Advanced squamous cell carcinoma of head and neck (SCCHN) remains among the most treatment refractory tumors [1]. Current treatment involves surgery when the disease is operable, and radio(-chemo)therapy. Research efforts focus on advanced chemotherapy and at irradiation techniques which aim to increase the precision of beam delivery (e.g. intensity modulated radiotherapy, particle irradiation). A specific challenging task with very poor outcome is the treatment of recurrent SCCHN after prior radiotherapy

Recurrences of differentiated thyroid cancer after surgery and radioiodine therapy have the tendency to dedifferentiate and especially to loose their ability to store iodine, which makes treatment challenging. After progressive dedifferentiation the prognosis for these patients is poor, with no curative options available as these tumors respond poorly to currently available chemotherapeutic agents [2].

Hepatic metastases can be treated with curative intention by complete resection of the metastases [3]. However, only 10-15% of all patients can be operated. Local recurrence after surgery due to residual microscopic disease occurs in the majority of patients [4]. Although new cytostatic drugs have a response rate of around 40%, the overall survival benefit is marginal. Up to 90% of patients with liver metastases die from the disease. Selection of liver metastases has moreover been inspired by a research program at the University of Pavia (Italy), which investigate the possibility to cure diffuse hepatic metastases by explanting the liver and irradiating the organ with BNCT followed by an autotransplantation [5-8].

Accepting the hypothesis that BNCT offers a curative chance for actual incurable cases, a preferential delivery of a ^{10}B-containing drug to the tumors should first be demonstrated.

2. Patients and methods

Patients with histological proven SCCHN or thyroid cancer or hepatic metastases of colorectal adenocarcinoma were eligible if surgery was planned. Other eligibility criteria were: age $\geq$ 18 years, WHO performance status $\leq$ 2, adequate hematological values, no severe concomitant disease and absence of toxic effects of previous anticancer therapies. Patients with a history of phenylketonuria, radiation to head and neck or chemotherapy within 3 months prior the planned surgery, were excluded.

Prior to the planned removal of the tumor, groups of patients were infused with either BPA or BSH.

The infusion of drugs in the respective study groups was as follows:

- 50 mg/kg BSH infused within 1 h. Infusion started 12 h prior to tissue sampling.
- 100 mg/kg BPA infused within 1 h. Infusion started 2 h prior to tissue sampling.

Tissue and blood samples were collected and analyzed for the ^{10}B-concentration with prompt gamma ray spectroscopy (PGRA) [9].

Because individual patients did not benefit from their participation in the trial, the number of included patients was kept to a minimum applying descriptive statistics. The primary endpoint was the ^{10}B-concentration measured with PGRS. The secondary endpoint was the toxicity of the ^{10}B-compounds (assessed according to NCI-CTC version 2.1). The clinical trial was conducted in agreement with the Declaration of Helsinki and all applicable laws and regulations. The trial protocol was approved by the Ethics Committee of the University Hospital Duisburg-Essen, Germany.

3. Results

10 patients were infused with BSH, 9 patients with BPA. All patients were eligible and had completed follow-up investigations as planned. Adverse events, which were related to the study medication, did not occur.

In patients suffering from SCCHN after BSH-infusion the mean ^{10}B-concentration ratio tumor/blood was 1.2 ± 0.4. The ^{10}B-concentration ratio between tumor and healthy tissues was 3.6 ± 0.6 for muscle, 1.4 ± 0.5 for skin and 1.0 ± 0.3 for mucosa.

After BPA-infusion the mean ^{10}B-concentration ratio tumor/blood was 4.0 ± 1.7. Mean ^{10}B-concentration ratios between tumor and healthy tissue were 2.1 ± 1.2 for muscle, 1.3 ± 0.5 for skin and 1.4 ±0.01 for mucosa, respectively.

All but one patient with thyroid cancer suffered from differentiated thyroid cancer. After BSH-infusion the mean ^{10}B-concentration ratio tumor/blood was 0.9 ± 0.2. The ^{10}B-concentration ratio between tumor and healthy tissues was 1.9 ± 0.8 for muscle and 0.8 ± 0.2 for skin. After BPA-infusion the mean ^{10}B-concentration ratio tumor/blood was 1.7 ± 0.8. Mean ^{10}B-concentration ratios between tumor and healthy tissue were 0.9 ± 0.3 for muscle and 0.6 ± 0.3 for skin.

In patients suffering from hepatic metastases after BSH-infusion the mean metastasis/blood ratio was 1.1 ± 0.1. In all patients, the ^{10}B-concentration in the liver was slightly higher as compared to blood (^{10}B-concentration ratio liver/blood: 1.4 ± 0.1). In most samples, the ^{10}B-concentration was higher in the normal liver as compared to the metastases (^{10}B-concentration ratio metastasis/liver: 0.7 ± 0.1). The highest ^{10}B-concentration in other healthy tissues was detected in skin (ratio of tumor/skin: 0.86, 1 patient). Low uptake was found in fat (ratio of tumor/fat: 3.9 ± 1.6), muscle of the intestinal wall (ratio of tumor/muscle: 2.0, 1 patient) and in several intestinal polyps (6.7 ± 0.8 ppm, 1 patient), in a patient suffering from familial polyposis syndrome. After BPA-infusion the mean ^{10}B-concentration ratio between metastasis and blood was 2.2 ± 0.4. The mean ratios between metastasis and liver were 1.5 ± 0.3. In all patients, the ^{10}B-concentration in liver was higher as compared to blood (^{10}B-concentration ratio liver/blood: 1.4 ± 0.1). The ^{10}B-concentration in skin was comparable with the ^{10}B-concentration in liver (^{10}B-concentration ratio of tumor/skin: 1.5 ± 0.05), whereas the ^{10}B-concentration ratio of tumor/fat was substantially lower (6.3 ± 2.4). The histological examination of liver metastases showed, that large proportions of the tumor volume consisted of necrosis, mucus and stroma. As BPA is transported actively, only viable cells take up the compound. Consequently, if the ^{10}B-concentration is assessed with a method such as PGRS, which measures the integral concentration within a tissue volume, the measured value does not reflect the ^{10}B-concentration in the viable cells [10]. The discrepancy between integral ^{10}B-concentration in a macroscopic volume and the intracellular ^{10}B-concentration is especially high if the volume of the evaluated tissue contains only a small amount of viable tumor cells, as was the case in metastases of colorectal carcinoma. The proportion of necrosis, mucus, stroma and viable cells was therefore measured (semi quantitative analysis). Then, a ^{10}B-concentration ratio between metastasis and liver was calculated, which was corrected for the proportion of viable tumor cells in the volume of tissue measured [11]. The calculated ^{10}B concentration ratio of metastasis/liver was 6.8.

4. Conclusions

BPA and BSH deliver ^{10}B to SCCHN to an extent that substantiates the potential of BNCT to treat this tumor entity. Mucosa and skin are the most relevant organs at risk for both compounds, whereas high ^{10}B-concentrations in blood reveal the vasculature of healthy organs at risk for a BSH-mediated BNCT. More efforts are necessary to better understand the metabolism of BSH. The simultaneous application of both drugs can be justified.

BPA and BSH do not deliver enough ^{10}B to recurrent differentiated thyroid cancer to justify BNCT. The very poor accumulation of both compounds in the tumor tissue raises the question if prior therapies have changed the perfusion of the area of interest prohibiting the transport of the drugs. Another hypothesis to explain our results for BPA could be a poor expression of the L-amino acid transport protein in this tumor as compared to other malignancies.

BSH does not preferentially accumulate in hepatic metastases of colorectal cancer. BPA is taken up preferentially in liver metastases of colorectal adenocarcinoma to an extent which is high enough for therapeutic BNCT. These findings justify further investigations with the aim to develop the technique towards a treatment modality.

Acknowledgement

The work received financial supported from the European Commission contract QLK3-CT-1999-01067.

References

1 Winquist, E., Oliver, T., Gilbert, R., 2007. Postoperative chemoradiotherapy for advanced squamous cell carcinoma of the head and neck: a systematic review with meta-analysis. Head Neck. 1, 38-46.

2 Ganti, A.K., Chhen, C.E., 2006. Iodine-refractory thyroid carcinoma. Rev Recent Clin Trials. 1, 133-141.

3 Fiorentini, G., Poddie, D.B., Cantore, M., Giovanis, P., Guadagni, S., DeGiorgi, U., Cariallo, A., Dazzi, C., Turci, D., 2001. Locoregional therapy for liver metastases from colorectal cancer: the possibilities of intraarterial chemotherapy, and new hepatic-directed modalities. Hepato-Gastroenterology. 48, 305-312.

4 Ruan, D.T., Warren R.S., 2005. Liver-directed therapies in colorectal cancer. Semin Oncol. 32, 85-94.

5 Nano, R., Barni, S., Chiari, P., Pinelli, T., Fossati, F., Altieri, S., Zonta, C., Prati, U., Roveda, L., Zonta, A., 2004. Efficacy of boron neutron capture therapy on liver metastases of colon adenocarcinoma: optical and ultrastructural study in the rat. Oncol Rep 11, 149-153.

6 Nano, R., Barni, S., Gerzeli, G., Pinelli, T., Altieri, S., Fossati, F., Prati, U., Roveda, L., Zonta, A., 1997. Histiocytic activation following neutron irradiation of boron-enriched rat liver metastases. Ann N Y Acad Sci 832, 274-278.

7 Roveda, L., Prati, U., Bakeine, J., Trotta, F., Marotta, P., Valsecchi, P., Zonta, A., Nano, R., Facoetti, A., Chiari, P., Barni, S., Pinelli, T., Altieri, S., Braghieri, A., Bruschi, P., Fossati, F., Pedroni, P., 2004. How to study boron biodistribution in liver metastases from colorectal cancer. J Chemother. 16 Suppl 5, 15-18.

8 Chiaraviglio, D., De Grazia, F., Zonta, A., Altieri, S., Braghieri, A., Fossati, F., Pedroni, P., Pinelli, T., Perotti, A., Specchariello, M., Perlini, G., Rief, H.. 1989. Evaluation of selective boron absorption in liver tumors. Strahlenther. Onkol. 1989, 170-172.

9 Wittig, A., Michel, J., Moss, R.L., Stecher-Rasmussen, F., Arlinghaus, H.F., Bendel, P., Mauri, P.L., Altieri, S., Hilger, R., Salvadori, P.A., Menichetti, L., Zamenhof, R., Sauerwein, W.A.G., Boron analysis and boron imaging in biological materials for Boron Neutron Capture Therapy (BNCT). Crit Rev Oncol Hemat 2008; doi:10.101016/j.critrevonc.2008.03.004. in press

10 Coderre, J.A., Chanana, A.D., Joel, D.D., Elowitz, E.H., Micca, P.L., Nawrocky, M.M., Chadha, M., Gebbers, J.O., Shady, M., Peress, N.S., Slatkin, D.N., 1998. Biodistribution of boronophenylalanine in patients with glioblastoma multiforme: boron concentration correlates with tumor cellularity. Radiat Res. 149, 163-170.

11 Wittig, A., Malago, M., Collette, L., Huiskamp, R., Bührmann, S., Nievaart, V., Kaiser, G.M., Jöckel, K.H., Schmid, K.W., Ortmann, U., Sauerwein, W.A., 2008. Uptake of two compounds in liver metastases of colorectal adenocarcinoma for extracorporeal irradiation with boron neutron capture therapy (EORTC Trail 11001). Int J Cancer. 122, 1164-1171

Efficacy of BNCT for GBM: Assessment of clinical results from Studsvik, Sweden

K Sköld, B H-Stenstam, J Hopewell, A Z Diaz, V Giusti, and L Pellettieri

Twenty-nine patients with newly diagnosed GBM were treated in a phase II study at Studsvik, Sweden, using a protocol with 6 hour infusion and a total dose of 900 milligram of L-BPA per kilo body weight, prior to irradiation with epithermal neutrons. A report of the study has recently been published by the investigators. In the present report the clinical results have been compared to results from the phase I/II study involving 53 patients at Brookhaven National Laboratory, where a protocol with a 2 hour infusion of L-BPA was used, and with results obtained from a large randomized phase III trial, with conventional radiotherapy combined with concomitant and adjuvant temozolomide as the experimental arm and radiotherapy only as the reference arm. The pre-treatment prognostic status of the patients in the various studies was taken into consideration when comparing the clinical results.

Comparison of the two BNCT studies established a clear advantage of the prolonged infusion protocol used at Studsvik. The median survival time (MST) in the Studsvik study was significantly longer than that observed in the radiotherapy only arm in the phase III study and the level of side effects was similar. The MST was also at least as long as that observed with radiotherapy plus temozolomide and the frequency of WHO grade 3-4 adverse events was more than three times lower in the BNCT study. It is proposed that BNCT should be particularly advantageous in the case of patients with bad performance status (RPA class V), where the benefit of temozolomide is marginal and where the MST in the Studsvik study was significantly longer than that achieved with radiotherapy only. It is suggested that the present results should be verified in a randomized phase III trial.

The Accelerator Based BNCT Project in Kyoto University Reactor Institute

Koji Ono[1], Minoru Suzuki[1], Shin-ichiro Masunaga[1], Yuko Kinashi[1], Genro Kashino[1], Hiroki Tanaka[1], Yoshinori Sakurai[1], Akira Maruhashi[1] , Shin-ichi Miyatake[2], Shinji Kawabata[2], Itsuro Kato[3], Junichi Hiratsuka[4], Teruhito Aihara[4], Mitsunori Kirihata[5], Tomoyuki Asano[6], Toshikazu Suzuki[6], Toshinori Mitsumoto[7], Satoru Yajima[7], Takemi Sato[7]

[1] *Kyoto University Reactor Institute*
[2] *Osaka Medical College*
[3] *Osaka University*
[4] *Kawasaki Medical College*
[5] *Osaka Prefecture University*
[6] *Stella Pharma*
[7] *Sumitomo Heavy Industry*

In Japan, BNCT by epithermal neutron was started in Kyoto University Research Reactor Institute in 2001. Especially, the first success in the world of BNCT for recurrent head and neck cancer accelerated clinical BNCT research, and the cases increased explosively. We also applied BNCT to liver cancers with multiple lesions or lung cancers including malignant mesothelioma. To advance BNCT research further, the project of accelerator based BNCT was started.

An accelerator maker manufactures a cyclotron with an acceleration proton energy of 30MeV and an electric current of 2mA, and the high-speed proton obtained with the cyclotron is made to collide with Be target. The neutrons are slowed down to obtain the epithermal neutrons for BNCT. Moreover, BPA and BSH, which are other important factors in BNCT, are manufactured by the drug manufacturing company according to manufacturing process of a drug for medical use GMP. Preparations are started in order to begin the clinical trial for the approval as medical device and drugs from authority in the spring of 2009.

As compared with the tumor dose distribution given by KUR neutrons on the condition of 10 Gy-Eq at the highest normal brain dose, cyclotron neutron BNCT system can give 20 Gy-Eq of tumor dose at the cerebrum median section in place of <15 Gy-Eq in KUR.

If the neutrons are also delivered from contra-lateral side on the same condition, the sum total dose at the median section will reach 40 Gy-Eq. This dose is aimed as the minimum tumor dose in the present clinical BNCT research.

Expansion of an indication of tumors and improvement in the anti-tumor effects can be easily expected.

Feasibility of Boron Neutron Capture Therapy for malignant spinal tumors

Kei Nakai[1], Hiroaki Kumada[2], Tetsuya Yamamoto[1], Akira Matsumura[1]

[1] *Department of Neurosurgery, Institute of Clinical Medicine, Graduate school of Comprehensive Human Sciences, University of Tsukuba, 1-1-1 Tennodai, Tsukuba, Ibaraki, 305-8575, Japan*
[2] *Japan Atomic Energy Agency, Tokai Research and Development Center, Tokai, Ibaraki, Japan*

Abstract

Treatment of malignant spinal cord tumors is currently ineffective. The characteristics of the spine are its seriality, small volume, and vulnerability: severe QOL impairment can be brought about by small neuronal damage. The present study aimed to investigate the feasibility of BNCT as a tumor-selective charged particle therapy for spinal cord tumors from the view point of protecting the normal spine.

A previous report suggested the tolerance dose of the spinal cord was 13.8Gy-Eq for radiation myelopathy; a dose as high as 11Gy-Eq demonstrated no spinal cord damage in an experimental animal model. We calculated the tumor dose and the normal spinal cord dose on a virtual model of a spinal cord tumor patient with a JCDS treatment planning system. The present study made use of boronophenylalanine (BPA). In these calculations, conditions were set as follows: tumor/normal (T/N) ratio of 3.5, blood boron concentration of 12 ppm, tumor boron concentration of 42 ppm, and relative biological effectiveness (RBE) values for tumor and normal spinal cord of 3.8 and 1.35, respectively. We examined how to optimize neutron irradiation by changing the beam direction and number.

In our theoretical example, simple opposed two-field irradiation achieved 28.0Gy-Eq as a minimum tumor dose and 7.3Gy-Eq as a maximum normal spinal dose. The BNCT for the spinal cord tumor was therefore feasible when a sufficient T/N ratio could be achieved. The use of F-BPA PET imaging for spinal tumor patients is supported by this study.

Keywords: Feasible, BNCT, Spinal tumor, JCDS,

1. Introduction

Spinal cord tumors are relatively rare and account for 2% of all central nervous system tumors, one-third of which are located in the intramedullary compartment. The spinal cord has the characteristic of integrated neuronal axons existing within a diameter of about 2cm. Since both ascending and descending spinal cord pathways are interrupted, neurologic dysfunction may be produced distally. The majority of primary spinal cord tumors are ependymomas and astrocytomas. Approximately one-half of all ependymomas occur somewhere in the cervical or thoracic spinal cord. Spinal ependymomas are associated with a better prognosis than cerebral lesions, particularly when complete resection is possible. Postoperative radiotherapy may be useful when complete resection cannot be achieved, but both early and delayed relapses can occur. Astrocytomas are distributed throughout the spinal cord. The clinical course of spinal astrocytic lesions can be predicted by their pathologic features: long-term survival is related to tumor grade. There is a lack of randomized data supporting the use of fractionated radiotherapy for low-grade tumors that are incompletely resected, but all high-grade tumors should receive postoperative radiation.

BNCT has a bimodal form. The first component is selective Boron-10 accumulation in the target tissue, i.e., the malignant tumor. The target tissue is irradiated with a neutron beam. BNCT produces high levels of LET particles in the Boron-10 accumulated tissue. BNCT has been evaluated for various malignant diseases, but no report has described its application to spinal tumors. The objective of this study was to clarify the feasibility of single-fraction or fractioned BNCT in patients with spinal malignant tumor.

2. Material and Methods

In the present study, we constructed treatment plans for 3 different situations of spinal cord tumors using the

JAEA Computational Dosimetry System (JCDS). JCDS is a BNCT simulation system which was developed and has been improved by Japan's Atomic Energy Agency. A three-dimensional model was created from medical CT and MRI images. We defined the postulated spinal tumor as impinging on the cervical cord. The JDCS requires user-defined parameters, namely, boron concentrations, relative biologic effectiveness (RBE) values, and compound biologic effectiveness (CBE) factors of the chosen boron compound. The present study made use of boronophenylalanine (BPA), which has been employed as a boron compound in clinical trials. An epithermal mode beam, 3.5MW of JRR-4, a 12cm collimator, and a shielding module made of lithium fluoride were assumed for calculation. The beam directions were 1) anteroposterior (AP) and 2) posteroanterior (PA). The values used in the simulation are summarized in **Table 1**. The three-dimensional-model is shown in **Figure 1**.

The normal tissue dose limit was set to below 9.0Gy-Eq for each session (fraction). After the MCNP calculation of the beam and target model, the JCDS output was visualized and analysed.

Table 1. RBE and CBE, boron concentration used for this simulation

	B compound	**BPA**
	T/N ratio	3.5

	Boron Concentration	RBE,CBE
Tumor	42	3.8
Normal tissue	12	1.35
Spinal Cord	12	1.35
Mucosa	12	4.9
Bone	0	

T/N ratio = Tumor/ Normal tissue ratio

Figure1. The schema of the spinal cord tumor model

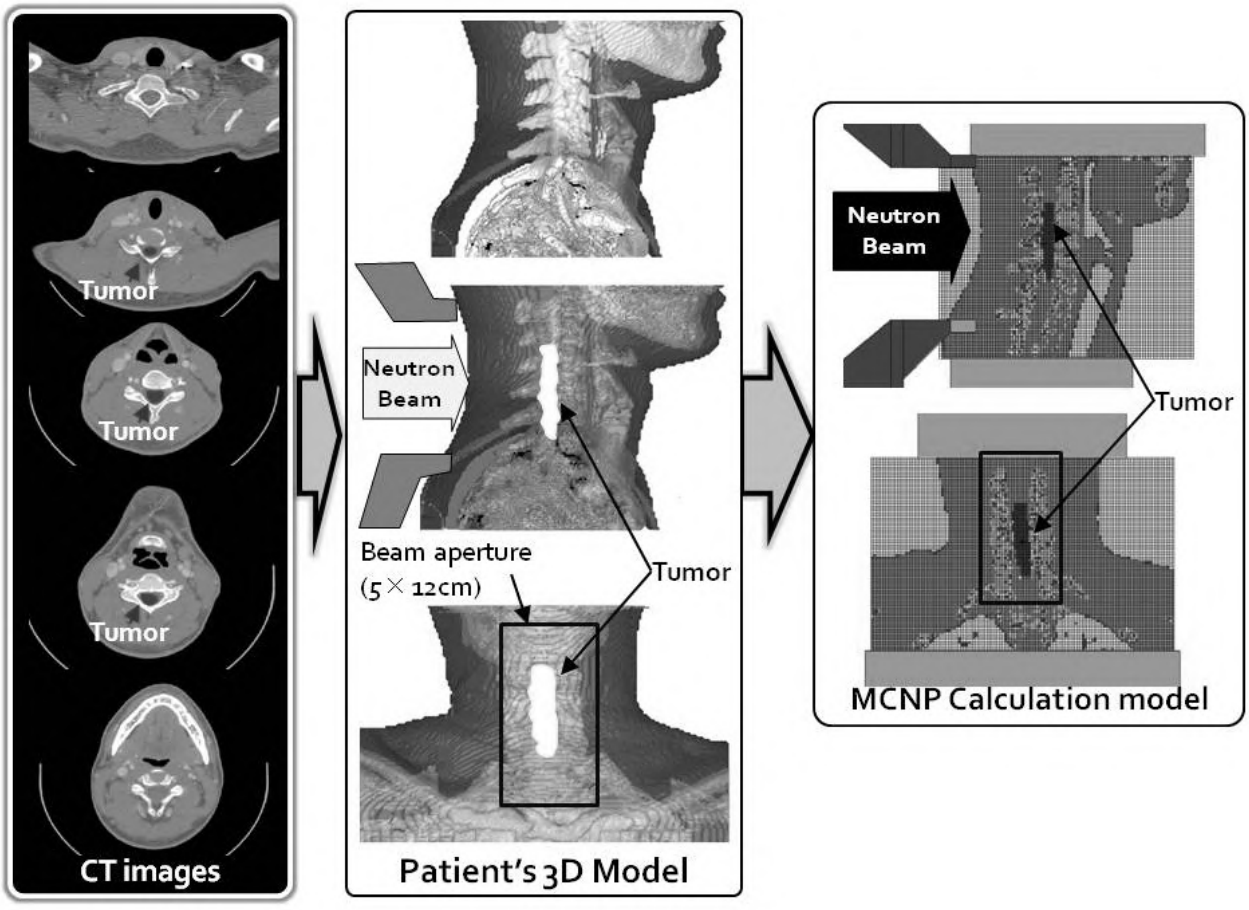

Left: Serial CT image and postulated tumor, **Middle:** Three-dimensional reconstruction of the model, **Right:** voxel model for MCNP calculation

Figure 2. Schematic output of the simulation

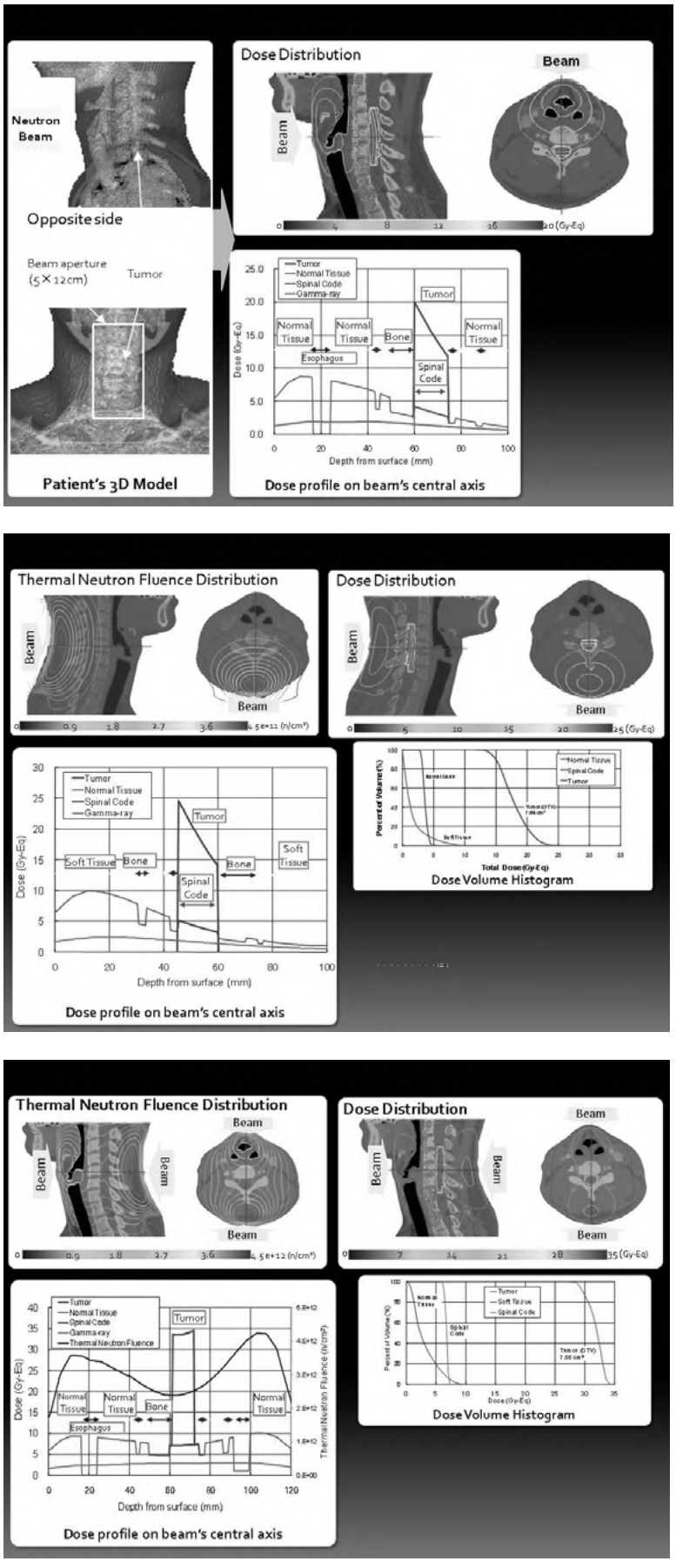

Upper: 3D model, dose distribution and dose profile on beam's axis for anteroposterior irradiation.
Middle: Thermal neutron fluence and dose distribution, dose profile and dose volume histogram for posteroanterior irradiation.
Lower: Thermal neutron fluence and dose distribution, dose profile and dose volume histogram for 2-fraction (AP and PA) irradiation.

3. Results

Table 2 summarizes the tumor dose and normal tissue dose of opposing portal irradiations. The first irradiation was anteroposterior and the second irradiation was posteroanterior. The term "total dose" implied that the 1st (AP) and 2nd (PA) irradiations were performed as a 2-fraction irradiation. Simple opposed two-field irradiation achieved 28.0Gy-Eq as a minimum tumor dose, 7.3Gy-Eq as a maximum normal spinal dose, and 7.4Gy-Eq as a maximum skin dose. The thermal neutron flux was 1.98×10^9 and 1.73×10^9 at the 1st and 2nd irradiation, respectively. Irradiation time was 30 and 38 min at the 1st and 2nd irradiation, respectively; these were tolerable periods without general anaesthesia. The dose distribution and dose profile on the beam's central axis are shown in **Figure 2**. A dose-volume histogram is also shown for AP radiation and opposing portal irradation.

Table 2. Summary of the simulated dose

		Total	1st Irra.	2nd Irra.
Irradiation Time (min)		–	30	38
Tumor Dose (Gy-Eq)	Max.	34.7	22.4	20.5
	Ave.	32.0	16.1	15.9
	Mini.	28.0	11.3	11.3
Normal Tissue (Gy-Eq)	Max.	10.0	9.0	9.0
Spinal Code (Gy-Eq)	Max.	7.3	4.6	4.2
Skin (Gy-Eq)	Max.	7.4	7.0	7.4
Thermal neutron Flux (n/cm^2/s)	Max.	—	1.98×10^9	1.73×10^9
Thermal neutron Fluence (n/cm^2)	Max.	4.24×10^{12}	4.01×10^{12}	4.09×10^{12}

1st Irra. = anteroposterior irradiation, 2nd Irra. = posteroanterior irradiation

4. Discussion

The results showed the feasibility of BNCT for spinal malignant tumor. Coderre et al. reported dose-related changes in the incidence of rats developing myelopathy; they determined the ED_{50} as 13.8 Gy using i.p. BPA administration, and found no spinal damage below 11 Gy-Eq. Morris reported the dose response of the rat spinal cord and radiation damage. They used i.v. BPA. According these data, the ED_{50} for myeloparesis was 12.9 Gy in rats irradiated after i.v. administration of BPA. With a 10 to 20% safety margin, we set 9Gy-Eq as the upper limit for normal tissue exposure in a single session and 10Gy-Eq for the total normal tissue dose. Under this limitation, the simulation achieved a minimum tumor dose of 28.0Gy-Eq.

Fractionated irradiation is suitable for spinal cord tumors BNCT because it reduces the normal tissue damage and concentrates the tumor dose. Compared with single-fraction irradiation, 2-fraction opposing portal irradiation increased the normal tissue dose only 10% while the minimum tumor dose more than doubled.

One limitation of our study concerns the boron distribution. We postulated that tumor boron concentration is 42 ppm and the normal tissue concentration is 12 ppm, but spinal cord vasculature or tissue perfusion circumstances are not the same as those of brain tissue, and the pharmacokinetics of the boron compounds may differ. It is important to determine the BPA pharmacokinetics by an F^{18} PET study and experimentally determine the values that we use here presumptively.

5. Conclusions

BNCT for spinal cord tumor may be feasible if a sufficient tumor/normal tissue ratio can be reached. Opposed two-field irradiation may deliver a sufficient treatment dose to the tumor while keeping the normal spinal cord dose within a safe limit. (e.g. 28Gy vs. 7.3Gy) An F-BPA PET study is warranted to extend this feasibility study to applicability for clinical trials.

References

Schild, SE., Nisi, K., Scheithauer, BW., et al., 1998. The results of radiotherapy for ependymomas: the Mayo Clinic experience. Int J Radiat Oncol Biol Phys 42:953-8.

Rodrigues, GB., Waldron, JN., Wong, CS., Laperriere, NJ., 2000. A retrospective analysis of 52 cases of spinal cord glioma managed with radiation therapy. Int J Radiat Oncol Biol Phys 48:837-42.

Kumada, H., Yamamoto, K., Matsumura, A., Yamamoto, T., Nakagawa, Y., Nakai, K., Kageji, T. 2004. Verification of the computational dosimetry system in JAERI (JCDS) for boron neutron capture therapy. Phys Med Biol. 49:3353-65.

Coderre, JA., Morris, GM., Micca, PL., Fisher, CD., Ross, GA., 1995. Comparative Assessment of Single-Dose and Fractionated boron Neutron Capture Therapy. Rad. Res. 144,310-317.

Morris, GM., Micca, PL., Nawrocky, LE., Weissfloch, LE., Coderre, JA., 2002. Long-Term Infusions of p-Boronophenylalanine for Born Neutron Capture Therapy: Evaluation Using Rat Brain Tumor and Spinal Cord Models. Rad. Res. 158,743-7.

A Cancer Research UK pharmacokinetic study of BPA-mannitol in patients with high grade glioma to optimise uptake parameters for clinical trials of BNCT

G. S. Cruickshank[1], D. Ngoga[1], A. Detta[1], S Green[1], N.D James[1], C Wojnecki[1], J Doran[1], J Hardie[1], M Chester[1], N Graham[1], Z. Ghani[1], G Halbert[2], M Elliot[2], S Ford[2], R Braithwaite[3], TMT Sheehan[3], J Vickerman[4], N Lockyer[4], H. Steinfeldt[5], G. Croswell[5], A. Chopra[5], R Sugar[5] and A Boddy[6]

[1]*University of Birmingham and University Hospital Birmingham, Birmingham, UK*
[2]*CR-UK Formulation Unit, University of Strathclyde, Glasgow, UK*
[3]*Regional Laboratory for Toxicology, Sandwell & West Birmingham Hospitals Trust, Birmingham UK*
[4]*Surface Analysis Research Centre, The University of Manchester, Manchester, UK*
[5]*CR-UK Drug Development Office, London, UK.*
[6]*Northern Institute for Cancer Research, University of Newcastle, Newcastle-Upon-Tyne, UK*

This paper describes results to-date from a human pharmacokinetic study which began recruitment in December 2007. Results are presented for a single patient recruited in December 2007. A second patient was recruited in July 2008 but detailed data are not available at the time of writing. The trial is an open-label, noncomparative, nontherapeutic study of BPA-mannitol in patients with high-grade glioma, who will be undergoing stereotactic brain biopsy as part of the diagnostic process before definitive treatment.
The study investigates the route of infusion (intra venous or intra carotid artery) and in each case will assess the effect of administration of mannitol as a blood-brain barrier disrupter. All cohorts will receive a 2 hr infusion of BPA-mannitol, and for some cohorts an additional mannitol bolus will be administered at the beginning of this infusion.

Measurements are made by Inductively Coupled Plasma Mass Spectrometry (ICP-MS) of ^{10}B concentration in samples of blood, urine, extra-cellular fluid in normal brain (via a dialysis probe), brain tissue around tumour and tumour tissue. Additional analysis of the tumour tissue is performed using Secondary Ion Mass Spectrometry (SIMS).

The first patient was part of the cohort having intravenous (IV) infusion without mannitol bolus. No serious clinical problems were experienced and the assay results can be compared with available patient data from other BNCT centres. In particular we note that the peak ^{10}B concentration in blood was 28.1 mg/mL for a total BPA administration of 350 mg/kg which is very consistent with the previous experience with BPA-fructose reported by the Helsinki group.

Keywords: BPA, BPA-formulation, pharmacokinetic.

Introduction

Data on the pharmacokinetics of boron from BPA administration to humans are limited, and do not in general provide information to assess the infusion routes suggested as beneficial from animal experiments[1-2]. The same studies also suggest that blood brain barrier disruption (BBBD) with mannitol improved uptake of BPA and BSH as well as animal survival in the F98 gliosarcoma model used in the studies. Human data exist to describe boron levels in blood for a range of infusion protocols, however the therapeutic effects of BNCT depend on the differential uptake seen between tumour cells and surrounding brain cells as well as the relative uptake rates between blood, brain and tumour.

The vast majority of data on BPA uptake in humans relates to post-operative pharmacokinetics – the effect of surgery on subsequent BPA distribution being largely unknown. Surgery may disrupt the blood brain barrier and alter the uptake of BPA in normal brain. Furthermore, surgery is followed by a brisk inflammatory reaction and it is known that this may result in uptake of amino acids, with consequent alterations to BPA distribution. BNCT dosimetry in a non-debulked group would therefore be more accurate and better reflect measurable blood boron concentrations.

BPA formulation

BPA is relatively insoluble in aqueous solution so the focus for clinical BNCT studies performed to-date has been on administration of a BPA-fructose solution. In fructose, BPA is soluble to a maximum concentration of approximately 30 mg/ml. Clinical experience with BPA infusions now ranges up to administration of 450 mg/kg body weight over 2 hours[3] or 900 mg/kg over 6 hours[4]. For BPA fructose administration to a 70 kg adult these constitute volumes of infusion of 1.2 to 2.1 litres.

For this study we anticipate escalation of BPA administration levels up to 1050 mg/kg in 2 hours which would lead to a necessary fluid volume for BPA-fructose of 2.45 l. In order to avoid any limitation imposed by tolerable fluid volume, a new BPA formulation was required. A range of excipients were tested for solubility and stability over time. These included fructose, glucose and mannitol. The chosen product for investigation in this study is BPA at 100 mg/ml in 110 mg/ml mannitol. The solution has a pH of 8 ± 0.2. This new formulation therefore allows BPA concentrations more than 3-fold higher than BPA-fructose, reducing the necessary fluid volume load accordingly. Use of BPA-mannitol will also avoid the possible serious adverse reactions in patients with hereditary fructose intolerance.

Pre-clinical studies with this formulation have lead to the determination of the Maximum Tolerated Dose of BPA-mannitol of 1000 mg/kg.

Study Design

This is an open, non-comparative, single-centre, non-therapeutic, Phase I pharmacokinetic study. It will be conducted in two stages:

Stage 1 – Route and BBBD

A 2 x 2 factorial design using a single dose (175 mg/kg/hr for 2 hours) to evaluate:

- Route of delivery: central venous or intra-carotid artery, and
- The effect of BBBD: with or without rapid infusion of 300 ml 20 % w/v mannitol solution via an intra-arterial catheter

There will be three evaluable patients per cohort; up to a maximum of 24 evaluable patients in total if cohorts have to be expanded

Stage 2 – Dose Escalation

Using the optimal route established from Stage 1, a limited dose escalation will be conducted, if required to achieve the study endpoints. The most likely doses, based on current knowledge, being:

- Single dose of 350 mg/kg/hr for 2 hours, and, if required
- Single dose of 525 mg/kg/hr for 2 hours

If it is found that the additional mannitol is of benefit then the mannitol schedule in stage 2 will be the same as that used in stage 1.

Between 15 and 36 patients will be recruited. Eligible patients will be adults aged 45-70 years with a presumptive diagnosis of high-grade glioma and who will be undergoing stereotactic brain biopsy as part of the diagnostic process prior to the definitive treatment.

Biopsy procedures

All patients will be anaesthetised with initial induction using fentanyl (1.5 μg/kg) followed by propofol (titrated slowly to patient response). Gas induction will be by sevoflurane (up to 8 %) in oxygen followed by IV access and fentanyl (1.5 μg/kg). Anesthesia will be maintained by propofol (target-controlled infusion 2.5 μg/ml – 4.0 μg/ml) or sevoflurane (1 % - 3 % inspired) in 50 % oxygen in air.

Samples of blood, urine, cerebro spinal fluid (CSF) or dyalisate of extra-cellular fluid (ECF)) and tissue biopsy samples of tumour and brain around tumour will be collected. For the tissue samples the biopsy will be obtained using a stereotactic image guided procedure. The biopsy needle is a side cutting 2.1r–4 mm Sedan needle that is rotated to produce four biopsy samples at 0^o, 90^o, 180^o, and 270^o axis positions. This study does not require additional needle entries over and above those used as part of standard patient management.

ECF samples are obtained by a dialysis procedure. The probes are placed well away from the main tumour volume and hence measurements are made of the bioavailability of boron in normal brain.

Macroscopic Boron Assays

Analysis of bulk ^{10}B levels will be performed by Inductively-Coupled Plasma Mass Spectrometry (ICP-MS). Analysis of human whole blood for ^{10}B utilises accurate, direct, volumetric pipetting of 100 μl aliquots of the specimen as part of a dilution protocol.

Tissue studies will require solubilisation of weighed samples of individual wet mass unlikely to exceed 100 mg.

Patient and Procedure

Data is presented for one patient, a 72 yr old male with suspected high grade glioma. In order to facilitate assay validation with clinical samples, analysis was performed both of repeat needle biopsy samples, at times of approximately 1 and 1.5 hours following the end of the BPA infusion

Results

The BPA-mannitol formulation was well-tolerated by this patient and no serious toxicity was observed. ICP-MS measurements of boron in whole blood are shown in Figure 1 and are compared with data from other groups. In general the trends observed by other groups are reproduced with BPA-mannitol in this patient.

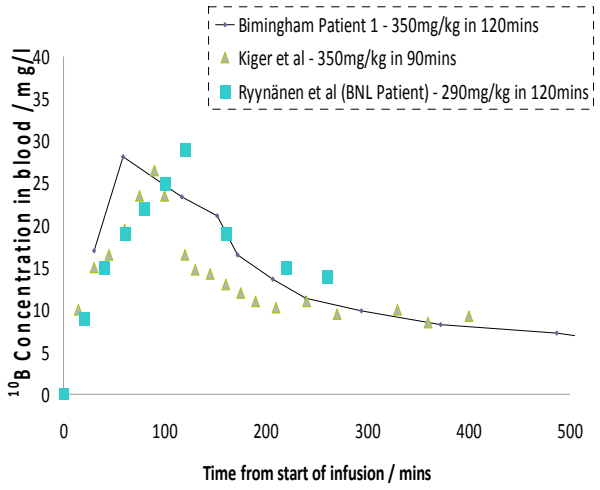

Figure 1. BPA levels in blood for Patient 1 of the Birmingham study with comprable data from Helsinki and MIT

The measurements of boron levels in ECF vs time are shown in Figure 2. These data clearly indicate a peak in bioavialibility of BPA at a time approximately 400 minutes (over 6 hours) after the start of the infusion. Data on further patients will be necessary to corroborate this result.

^{10}B levels in biopsy samples are shown in Table 1. The increased levels for both tumour and border samples at the 1.5 hr compared to the 1 hr time point will be carefully monitored in future patients.

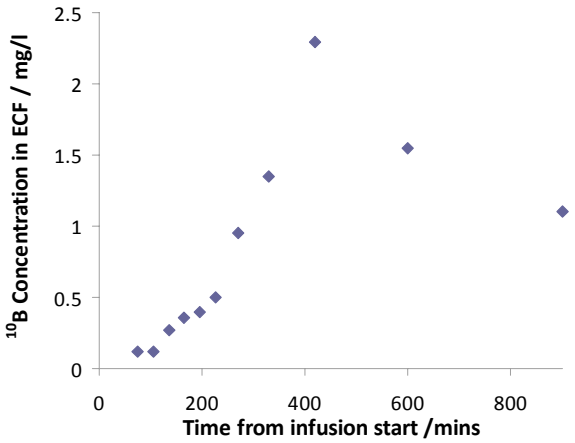

Figure 2. Time-course of Boron concentration in ECF for Patient 1 of the Birmingham study

Time from infusion end (hrs)	Tumour ^{10}B conc (mg/kg)	Border ^{10}B conc. (mg/kg)	Debulk ^{10}B conc (mg/kg)
~ 1	4.6	3.6	-
~ 1.5	6.6	5.2	-
~ 2.25	-	-	4.2

Table 1: ^{10}B levels in biopsy samples

A single measurement of boron level in CSF was made at a time point approx. 2.5 hrs from the infusion end at 1.5 mg/kg

Discussion

The data for BPA-mannitol from this study show similar levels and time-course as previous results from studies using BPA-fructose (as shown in Figure 1). The Birmingham data show a slightly unusual shape to the rising portion of the curve (i.e. from samples taken during the infusion). It is possible that samples for the second and third time-points were swapped – although this was not noticed during the procedure. This will be monitored carefully for subsequent patients.

The maximum BPA level in blood (Figure 2) from our study is entirely consistent with the observations from the Helsinki group derived from BPA-fructose. The peak ^{10}B concentration in blood was 28.1 mg/ml for a total BPA administration of 350 mg/kg. Our data is shown superimposed on the published data from Helsinki (Ryynänen 2002) in Figure 3.

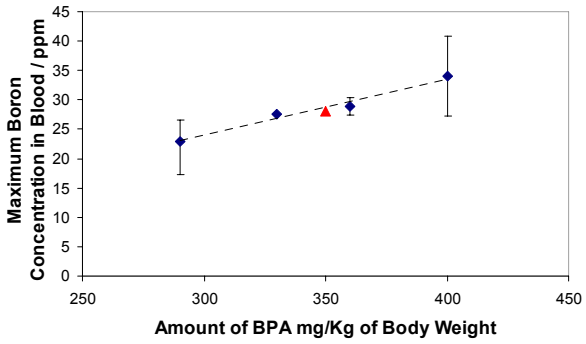

Figure 3. Maximum Blood BPA concentration vs BPA administration as reported by the Helsinki group (solid diamonds) with the result from Birmingham patient 1 superimposed (solid triangle)

Table 1 shows ^{10}B levels in biopsy samples which are relatively low compared to previous published data for Grade IV glioma.

It is important to note at this point that the pathology tissue, sampled with these biopsy samples suggested that this patient was actually suffering from a Grade II glioma. Later clinical experience suggested that the correct diagnosis may in fact have been Grade IV, emphasising the heterogeneity of these complex tumours.

It is also possible that tumour boron levels would continue to increase over time, reflecting the bioavailability of ^{10}B shown by the ECF measurements reported in Figure 2.

Summary

Data from the first patient of a study using a new formulation of BPA in mannitol are presented. No serious clinical problems were experienced and the assay results can be compared with available patient data from other BNCT centres. The time-course of ^{10}B levels in blood is consistent with previous data from BPA-fructose and the peak ^{10}B concentration in blood was 28.1 mg/ml for a total BPA administration of 350 mg/kg which is very consistent with the previously reported results. Boron levels in the ECF of normal brain were found to reach a peak approximately 400 minutes after the start of the BPA infusion.

References

1. Barth RF et al. Cancer Research **57**, 1129 (1997).
2. Barth RF et al. International Journal of Radiation Oncology, Biology, Physics **52**, 858 (2002)
3. Kortesniemi M, Applied Radiation and Isotopes **61**, 823, (2004).
4. Capala J et al J Neuro-Oncol, **62**, 135 (2003)
5. Kiger WS et al. J Neuro Oncology 62: (2003) 171-186
6. Ryynänen P et al. Phys Med Biol 47 (2002) 737-745
7. Ryynänen P. PhD Thesis(2002), University of Helsinki

Boron Biodistribution Study in Colorectal Liver Metastases Patients in Argentina

[a]Jorge E. Cardoso, [b]Susana Nievas, [a]Marcos D. Pereira, [b]Amanda E. Schwint, [b]Veronica A. Trivillin, [b]Emiliano Pozzi, [b]Elisa M. Heber, [b]Andrea Monti Hughes, [a]Pablo Sanchez, [a]Eduardo Bumaschny, [b,c]Maria E. Itoiz, [b]Sara Liberman

[a]Instituto de Oncología Angel H. Roffo, San Martín 5481, 1417 Buenos Aires, Argentina
[b]Comisión Nacional de Energía Atómica, Centro Atómico Constituyentes, Avda. Gral. Paz 1499, San Martin (1650), Prov.. Buenos Aires, Argentina
[c]Department of Oral Pathology, Faculty of Dentistry, University of Buenos Aires, Marcelo T. de Alvear 2142, (1122) Buenos Aires, Argentina

Abstract

Ex-situ BNCT for multifocal unresectable liver metastases employing whole or partial autograft techniques requires knowledge of boron concentrations in healthy liver and metastases following perfusion and immersion in University of Wisconsin (UW) solution, the procedure employed for organ preservation during ex-situ irradiation.

Measurements of boron concentration in blood, liver and metastases following an intravenous infusion of BPA-F in 5 colorectal liver metastases patients scheduled for surgery were performed. Tissue samples were evaluated for boron content pre and post perfusion and immersion in UW. Complementary histological studies were performed. The data showed a dose-dependent BPA uptake in liver, a boron concentration ratio liver/blood close to 1 and a wide spread in the metastases/liver concentration ratios in the range 0.8 to 3.6, partially attributable to histological variations between samples.

Based on the boron concentrations and dose considerations at the RA-3 thermal neutron facility, ex-situ treatment of liver metastases at RA-3 would be feasible.

Keywords: boron neutron capture therapy, unresectable colorectal liver metastases, ^{10}B biodistribution, hepatic autograft.

1. Introduction

Excluding skin tumours, colorectal cancer represents the third more frequent cancer worldwide, and it is the third cause of cancer deaths in both sexes according to the American Cancer Society (2008). Local and distant failure, following initial surgery, is the ultimate cause of death. Near 50% of colon cancer patients will be diagnosed with hepatic metastases, including advanced disease at the presentation and relapses.

Conversely to other distant localizations, hepatic metastases are considered a locoregional disease, as a local treatment can improve the overall survival in this group. Thus, surgery must be performed every time possible as recommended by Chong and Cunningham (2005). Other local techniques have been used to manage hepatic metastases, such as radiofrequency, interstitial radiotherapy or embolization, being limited by technical issues in all cases, especially by the number of lesions or the residual functional liver parenchyma after treatment. Taking into account these points, BNCT could be an attractive approach. The fact that BNCT is a biological targeting technique would confer on it the potential of treating undetectable micrometastases.

The selective ^{10}BPA-F uptake in liver metastases was evaluated by Roveda et al. (2004).

The TAOrMINA project developed and employed a new method for BNCT treatment of multifocal unresectable liver metastases, based on ex-situ irradiation and whole liver autograft by Zonta et al. (2006). The surgeons of the Roffo Institute in Argentina (JEC) propose a new technique based on partial liver autograft (Cardoso

et al. 2007). In situ BNCT treatment of liver metastases is also being considered in the BNCT community.

In all three scenarios boron biodistribution is pivotal to deliver the necessary doses to achieve tumor control (≥ 40 Gy-eq) and spare healthy liver (≤ 15 Gy-eq). In addition, both whole and partial autograft techniques involve liver perfusion with University of Wisconsin solution (UW) and hypothermal preservation in UW during neutron irradiation. Thus, the boron concentration in liver and metastases following UW perfusion and immersion in will reflect a clinical scenario more adequately, issue not been addressed to date.

The aim of the present study was to determine boron concentration in blood, liver and tumor tissue, both pre and post perfusion and immersion in UW, following an intravenous infusion of L-p-boronophenylalanine complexed with fructose (^{10}BPA-F) in patients scheduled for colorectal liver metastases surgery.

2. Materials and Methods

a) Patients

From August 2007 to March 2008, five patients were enrolled in this trial, three males and two females; Table 1 shows the patient data. These trials were performed with approval # 5178/00 addenda July/03/05 from the Argentine National Agency of Drugs, Food and Clinical Technology (ANMAT).

All the patients described in this study were scheduled to undergo surgery for colorectal liver metastases. In each of the patient (P) a diagnosis of adenocarcinoma was confirmed by histopathological analysis and liver CT scans. All P gave informed consent to participate in the study.

Protocol eligibility criteria included normal renal function, absence of cardiovascular disease and phenylketonuria. Blood pressure, temperature and pulse rate were within normal limits in all P at the start of the BPA infusion. P5 had heavy chemotherapy up to six months before surgery.

BPA was administered intravenously (iv) at a dose of 100 mg/kg $_{bw}$ (n=3) or 300 mg/kg $_{bw}$ (n=2), infused over 80 - 90 min. Blood samples for boron analyses were taken during surgery concomitantly with tissue resection, 80-220 minutes after the end of the infusion depending on surgical procedures.

b) BPA-F infusion, boron analysis

^{10}BPA isotopically enriched (>99 at. %) was obtained from Glyconix (New York, NY). A fresh solution of BPA-F was prepared for each P. Boron measurements for blood, liver and tumor tissues were performed by Inductively Coupled Plasma Optical Emission Spectroscopy (ICP-OES) following the same procedure as described previously by Liberman et al. (2004).

c) Tissue sampling and processing

One set of samples was processed for measurement of boron concentration. A second set was fixed in 10% buffered formalin for histological analysis and a third set was stored in liquid nitrogen for future boron microdistribution studies.Tissue samples were evaluated pre and post perfusion and about 2 hrs immersion in UW (UWp) to simulate the clinical scenario of ex-situ irradiation.

Degree of perfusion varied with the surgical procedure and was not always representative of perfusion in an autograft scenario. Sets of paired adjacent tumor samples were taken for P4 and P5 to explore the potential association between boron uptake and histology. There were no detectable metastases (ND) in P1, one set of metastases samples (M_1) was taken for P2 and two sets for P3, P4 and P5 (M_1, M_2).

3. Results

Table 2 summarizes the information of the BPA dose infused to each P, over 80-90 min, tissue extraction time after infusion ended (Te), boron uptake in blood (B), liver (L), metastases (M_1, M_2) and all tissues perfused and immersed in UW solution (UWp) and boron concentration ratios before L/B, M/L and after (UWp) L/B and M/L. Standard deviation of the data is indicated when the number of samples n ≥3. P1-3 received a BPA dose 100mg/kg $_{bw}$, while P4-5 had 300 mg/kg $_{bw}$, clinical dose in the TAORMINA trial (Zonta et al., 2006).

Table 1. Characteristics of the patients

Patient # Age-Gender Weight (kg) Height (m)	Histology	Chem.	Surgery Type # tumors sampled Localization

Table 2. Infusion parameters and boron uptake in tissues with and without UW solution procedure

P#	Te (min)	Blood (µg/g)	Liver (µg/g)	Liver/ Blood	Metastases (µg/g)	Metastases/ Liver	Liver UWp (µg/g)	Metastasis UWp (µg/g)	(Metastases/ Liver) UWp
1	75	5.9±0.1 n=2	6.2±0.6 n=7	1.0±0.1	ND	--	4.3±0.4 n=11	--	--
2	220	3.8±0.3 n=2	3.9±0.7 n=11	1.0±0.2	8.0±02 n=3	2.0±0.2	2.9±0.4 n=8	6.7±0.9 n=7	2.3±0.2
3	127	3.4±0.1 n=2	4.2±0.2 n=6	1.2±0.1	M_1: 10.2 n=1	M_1 :2.4	3±1 n=2	M_1:8±2 n=5	M_1: 3.1±0.4
					M_2: 12±3 n=4	M_2: 2.9±0.2		M_2: 8.7 n=1	M_2: 3.3
4	165	14.7±0.3 n=9	15±1 n=16	1,02±0.07	M_1: 28±3 n=7	M_1 : 1.9±0.1	9.3±0.9 n=12	M_1: 14±4 n=10	M_1 : 1.5±0.3
					M_2:31±10 n=14	M_2 : 2.1±0.3		M_2:14±7 n=10	M_2 :1.5±0.6
*5	169	12.0±0.4 n=6	11.8±0.9 n=3	1.0±0.1	M_1:12.6±0.7 n=5	M_1 : 1.1±0.1	12±1 n=4	M_1: 11±1 n=3	M_1: 0.9±0.1
	187	12.5±0.4 n=9	13.5±0.7 n=4	1.1±0.1	M_2:19±2 n=4	M_2 : 1.4±0.1	11.8±0.6 n=3	M_2: 11.6±0.6 n=3	M_2: 1.0±0.1

P: patients, P1-3: 100mg/kg $_{bw}$, P4-5: 300mg/kg $_{bw}$ BPA, Infusion time 80-90 min, Te: time of sample extraction after end of infusion, UWp: perfused with and immersed in University of Wisconsin solution. M_1, M_2: metastases 1 and 2. * Inefficient UWp.

1 60 - M 60 1.73	ND	Yes	Sampling of hepatic tissue ND tumor
2 70 – M 95 1.80	Moderately/well differentiated adenocarcinoma	No	Left hepatectomy 1 II/III
3 66 - M 84 1.60	Moderately/well differentiated adenocarcinoma (M_1 – M_2)	Yes	Metastasectomy 2 II, III
4 74 - F 77 1.76	M_1: Moderately/well differentiated adenocarcinoma M_2 : Poorly diff.	No	Right hepatectomy 2 V, VII
*5 53 - F 82 1.57	M_1: Well diff. adenocarcinoma M_2: Poorly Differentiated	Yes	Metastasectomy 2 V, III

*Heavy chemotherapy pretreatement. Chem: chemotherapy

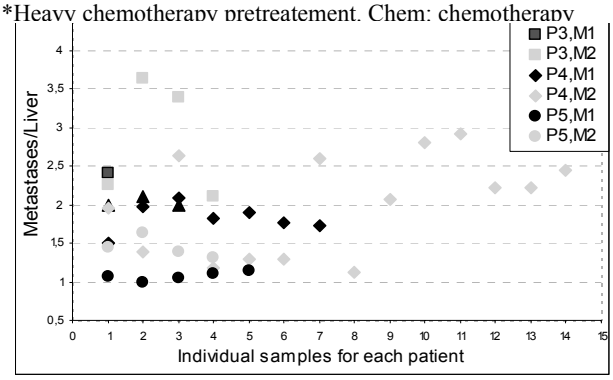

Figure 1. Metastases/Liver individual boron concentration ratio for patients (P) and metastases M_1 and M_2 without UW_p

Figure 1 shows data from individual boron concentration M/L ratios without UW_p. The histological analysis of the tumor samples showed heterogeneity and areas with varying degrees of necrosis, even within the same metastases. Taking into account the individual samples in Figure 1 we found some correlation between boron uptake and histology; i.e. lower boron content was frequently associated to predominantly necrotic samples and poorly differentiated areas were mostly associated to higher boron values.

In Figure 2 data normalized to 100mg/kg $_{bw}$ BPA dose, for B, L, M_1 and M_2 (± SD) are plotted for all patients, at Te. The data is consistent with the heterogeneity shown in Fig.1.

4. **Discussion**

The pharmacokinetics of boron values in blood given in Table 2, within the usual spread for P, is in agreement with Liberman et al. (2004) and Wittig et al. (2008).

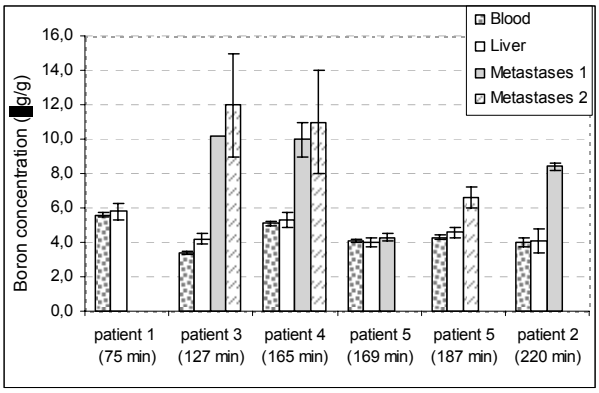

Figure 2. Mean boron concentrations (± SD) normalized to 100 mg/kg BPA, for all patients (n=1 for M_1-P3). Time after infusion is shown for each patient

Mean L/B ratio: 1.05 ± 0.08 (n=6), calculated from Table 2 shows an equivalence between blood and liver boron concentration values for all doses and dose-dependent absolute boron uptake by liver within the conditions of the study.

This L/B constant ratio is markedly relevant in the clinical trials involving whole or partial liver autograft, when ICP is used for boron measurements. Within this context, tissue boron content values can be obtained from the blood measurements that are much faster to perform.

Average M/L ratios in Table 2 are 2.0±06 and 2.3±0.8 for intact and UWp samples respectively. These results show no difference between these groups, within the precision of the measurements.

The boron loss by the UWp calculated from Table 2 is 31±5 % and 38±15% for the liver and metastases respectively. This % lost from the liver vascular system was within the 30% range, consistent with the data reported for liver by Blustajn et al., (1996). The higher dispersion values for the boron loss in the metastases might be partially due to their heterogeneity.

The M/L boron concentration ratios, with and without UWp, were $0.9 \leq M/L \leq 3.3$ or $1.1 \leq M/L \leq 2.9$ respectively (Table 2) Those values are strongly dependent on the histology of the extracted sample. For the individual samples in Fig.1: $0.9 \leq M/L \leq 3.6$.

The analysis of the present samples and previous studies by Roveda et al. (2004) and Wittig et al. (2008) suggest that M/L ratios would be considerably higher if the values reported herein are corrected for percentage of metabolically active tumor parenchyma.

Further microscopic analyses of the samples should be performed, disregarding necrotic and connective tissue, to improve the accuracy of actual effective M/L ratios.

The present data allow us to define the boron concentration conditions, for M and L to achieve tumor control with no L damage.

A preliminary attempt for dose calculation for L and M, assuming a high boron value in Fig. 1 M/L~3.5 and L=10 ppm for 300 mg/kg $_{bw}$ dose as a conservative value, gives a dose in L ≤14 Gy-Eq and in M≥ 46 Gy-Eq, for irradiation in the thermal column of the RA-3 reactor, with a mean flux at the irradiation position of about $(6\pm1).10^9 n.cm^{-2}.s^{-1}$ and a fluence after 12 min irradiation ~ 4.10^{12} $n.cm^{-2}$.

These estimated doses make the ex-situ treatment of liver metastases at RA-3 feasible.

5. Conclusions

Under the conditions of this study we conclude:

a) L/B = 1 for the samples, showing an equivalence between blood and liver values for all the doses.

b) The spread in M/L ratios is strongly dependent on the histology of M.

c) UW_p does not show a significant effect on the M/L ratios.

d) The RA-3 reactor thermal facility provides an adequate neutron flux for ex-situ treatment of liver metastases.

Acknowledgements: The authors wish to thank the the Instituto Biológico Contemporáneo (IBC) for kindly preparing the BPA infusion, the Surgery Team of the Roffo Institute and Marcelo Miller for providing the RA-3 dose data. MDP is a fellow of the Argentine Agency for Science and Technology.

References

Blustajn, J., Cuenod, C.A., Clement, O., Siauve, N., Vuillmin, V., Frija, G., 1997. Measurement of liver blood volume using a macromolecular MRI contrast agent at equilibrium. Magnetic Resonance Imaging **15**, 415-421.

Cancer Facts and Figures 2008. Amer. Cancer Soc.

Cardoso, J.E., Trivillin, V.A., Heber, E.M., Nigg, D.W., Calzetta, O., Blaumann, H., Longhino, J., Itoiz, M.E., Bumaschny, E., Pozzi, E., Schwint, A.E., 2007. Effect BNCT on Normal Liver Regeneration: Towards a Novel Therapy for Liver Metastases. Internat. J. Rad. Biology **83**, 699-706.

Chong, G., Cunningham, D., 2005. Improving long-term outcomes for patients with liver metastases from colorectal cancer. J. Clin. Onc. **23**, 9063-66.

Liberman, S.J., Dagrosa, A., Jiménez Rebagliati, R.A., Bonomi, M.R., Roth, B.M., Turjanski, L., Castiglia, S.J., González, S., Menéndez, P.R., Cabrini, R., Roberti, M.J., Batistoni, D.A., 2004. Biodistribution Studies of Boronophenylalanine-fructose in Melanoma and Brain Tumor Patients in Argentina. Appl. Rad.and Isoto. **61**, 1095-1100.

Roveda, L., Prati, U., Bakeine, J., Trotta, F., Marotta, P., Valsecchi, P., Zonta, A., Nano, R., Facoetti, A., Chiari, P., Barni, S., Pinelli, T., Altieri, S., Braghieri, A., Bruschi, P., Fossati, F., Pedroni, P., 2004. How to Study Boron Biodistribution in Liver Metastases from Colorectal. Cancer. J. Chem. **16**, 15-18.

Wittig, A., Malago, M., Collette, L., Huiskamp, R., Bührmann, S., Nievaart, V., Kaiser, G.M., Jöckel, K.H., Schmid, K.W., Ortmann, U., Sauerwein, W., A., 2008. Uptake of two ^{10}B-compounds in liver metastases of colorectal adenocarcinoma for extracorporeal irradiation with boron neutron capture therapy. Int. J. Cancer **122**, 1164-1171.

Zonta, A., Prati, U., Roveda, L., Ferrari, C., Zonta, S., Clerici, A.M., Zonta,C., Pinelli, T., Fossati, F., Altieri, S., Bortolussi, S., Bruschi,P., Nano, R., Barni, S., Chiari, P., Mazzini, G., 2006. Clinical lessons from the first applications of BNCT on unresectable liver metastases. Journal of Physics: Conference Series **41**, 484-495.

Pharmacokinetics of BSH - results from EORTC trials

W. Sauerwein[1], R.A. Hilger[2], K. Appelmann[3], R. Moss[4], J. Heimans[5], P. Bet[6], A. Wittig[1]

[1] Dept. of Radiation Oncology and [2]Dept. of Medical Oncology University Hospital of Essen, University Duisburg-Essen, Essen, Germany, [3]Nuclear Research and consultancy Group (NRG), Petten, The Netherlands, [4]HFR Unit, Institute for Energy, Joint Research Centre, European Commission, Petten, The Netherlands, [5]Dept. of Neurology and [6]Pharmacy VUmc Amsterdam, The Netherlands

Abstract

BNCT uses the ability of the isotope ^{10}B to capture thermal neutrons leading to the nuclear reaction $^{10}B(n,\alpha)^{7}Li$. This reaction produces ^{4}He- and ^{7}Li- particles with high linear energy transfer (LET) properties and therefore a high biological effectiveness relative to conventional photon irradiation. The short range of these particles limits their effects to one cell diameter, thus providing the potential for a targeted irradiation of tumor cells, if the boron compound is selectively incorporated into the tumor cells. The pharmacokinetics, metabolism and transport into the target cells of the boron carrier are some of the key factors for the success of BNCT. However, little information is available on these mechanisms of the two drugs used for BNCT in humans, BSH and BPA. The blood boron of patients, who have been treated with BSH in the BNCT trials of the EORTC has been analyzed. Non compartmental as well as compartmental analyses were performed. For compartmental analyses, open compartment models with zero-order input and first-order elimination were chosen. In addition, multiple dose calculations were performed. A three-compartment model can best describe the kinetic of BSH in blood. Terminal half-life of BSH was calculated to be 50 – 170 h, the mean ^{10}B-clearance from the blood was 18 +/- 10 ml/min. The intra-individual pharmacokinetic of BSH was linear over the dose range. Multiple infusions of the drug did not influence the pharmacokinetic, thus neither accumulation of the drug, nor a change in clearance were detectable. To describe the pharmacokinetic profile of BSH, a sufficient period of time for blood sampling has to be used. The pharmacokinetic results from this study confirm previous reports after multiple BSH doses.

Keywords: translational research, clinical trial, ^{10}B-biodistribution, BSH pharmacokinetic

1. Introduction

Phase-I and phase-II clinical trials have shown that BNCT can be implemented safely at the clinical level, and preliminary clinical results have been encouraging. One of the drugs used, the boron cluster BSH (Sodium mercaptoundecahydro-closo-dodecaborate, $Na_2{}^{10}B_{12}H_{11}SH$,) [1] has been used to treat malignant glioma [2-4] but also in combination with L-*para*-boronophenylalanine ($C_9H_{12}{}^{10}BNO_4$, BPA) to treat squamous cell carcinoma of head and neck[5]. Since its first clinical application in 1967 neither the pharmacokinetics, nor the metabolism nor the uptake mechanisms of BSH have been fully understood. Originally designed for BNCT of brain tumors, BSH is assumed to target brain lesions by crossing the pathologically damaged blood-brain-barrier (BBB) in the tumor but not the intact BBB that protects healthy brain. Some data on pharmacokinetics are available after a single dose of BSH [6-10]. No human data have been published so far after multiple infusions of BSH in a fractionated treatment schedule. BNCT is clinically attractive only if a sufficiently high concentration of ^{10}B can be delivered preferentially to the tumor, with relatively low concentrations in the surrounding healthy tissue. Besides biodistribution and metabolism, the pharmacokinetic profile of the drug is a prerequisite for a rational clinical application. Knowledge of the pharmacokinetics, moreover, can help one find the ideal time point for the irradiation

at which the ^{10}B tumor-to-blood ratio might be optimal. The effects of dose, infusion time and route of infusion of the drug have to be considered. Such data are necessary to design further clinical trials, improve safety and also to obtain permission from the regulatory authorities to use the drug.

2. Patients and methods

The ^{10}B-concentration in blood after BSH-infusion in patients who where treated in the frame of the EORTC trials 11961 and 11001 were available for analysis. Three different groups of patients can be identified:

Group 1 (EORTC 11961): Patients (n = 14) received a therapeutic dose of BSH prior the resection of a brain tumor. 100 mg BSH/ kg body weight (bw) were given intravenously with an infusion rate of 1 mg/kg bw/min. Sequential blood samples were taken prior and 0-24 h after the infusion. Ten of the fourteen patient who participated in this biodistribution study were later treated with BNCT. Data on uptake in tissues and glioblastoma are available for this cohort[12].

Group 2 (EORTC 11961): Patients (n = 26) received BSH intravenously in 4 fractions on 4 consecutive days of BNCT for a glioblastoma. The mean ^{10}B-concentration in blood over the total irradiation time in 4 fractions was prescribed to be 30 µg/g. To reach this concentration, 100 mg BSH/ kg body weight were infused at a dose rate of 1mg/kg bw /min 8-12 h prior to the first BNCT fraction. The consecutive 3 applications were individually adjusted and prescribed taking into consideration the boron concentration in the blood during the treatment (see fig.1).

Group 3 (EORTC 11001): Patients (n = 10) received a low dose of BSH prior to the planned surgical removal of a tumor. The compound was infused intravenously. The infusion of 50 mg/kg BSH in 1 h started 12 h prior tissue sampling. Blood samples were collected prior and 0-48 hours after the beginning of the infusion. Data on BSH uptake from these patients exist in a multitude of tissues and in different tumors[13]. Long observation periods could be achieved in some cases.

The quality of the study medication was strictly controlled including examination of the identity of the compound by infra-red spectroscopy, monitoring of purity by high pressure liquid chromatography and test for pyrogenicity.

The enrichment of ^{10}B was 99% and was tested with Prompt Gamma Ray Spectrometry and Inductively Coupled Plasma Atomic Emission Spectroscopy (ICP-AES). Injection-solutions were prepared according to standard operating procedures established for the EORTC trials 11961, 11001 and 11011[11]. BSH was dissolved in sterile saline. The solution can be stored for up to 6 h.

In both trials the ^{10}B-concentration in blood was analyzed at the High Flux Reactor HFR Petten with prompt gamma ray spectroscopy (PGRS). PGRS measures the average ^{10}B-concentration in the sample volume by quantification of the 478-keV photon emission during $^{10}B(n,\alpha,\gamma)^{7}Li$ reactions. Before each series of measurements, the system was calibrated using standard samples. Some samples were also measured with ICP-AES. Both methods are established tools for ^{10}B-analysis in biological samples [11].

Pharmacokinetic data were analyzed using the scientific pharmacokinetic software Kinetica 4.1.1. (InnaPhase Corporation, Philadelphia, USA) and the data analysis system TOPFIT 2.0. Non-compartmental as well as compartmental analyses were performed. For compartmental analyses, open compartment models with zero-order input and first-order elimination were chosen. In addition, multiple dose calculations were carried out.

3. Results

Based on a sufficient observation period and adequate numbers of blood drawings, a three-compartment model can best describe the kinetics of BSH in blood. Based on data from 11961, terminal half-life of BSH was calculated to be 50 – 280 h, the mean ^{10}B-clearance from the blood was 18 +/- 10 ml/min. The intra-individual pharmacokinetics of BSH seemed to be linear over the dose range. Multiple infusions of the drug did not influence the pharmacokinetics, thus neither accumulation of the drug, nor a change in clearance were detectable.

An example of the pharmacokinetics of BSH in blood for a fractionated treatment is given in figure 1. According to the EORTC trial 11961the patient (registration number 113) received four consecutive daily applications of BSH (7000 mg, 3000 mg, 2000 mg, and 2000 mg BSH absolute, respectively) prior to each radiation fraction at the HFR in Petten.

Terminal half live was calculated by the use of an open three compartment model with zero-order input and first-order elimination from the central compartment. The total body serum clearance for patient 113 was 16.8 ml/min, peak plasma concentration of the 7000 mg application was calculated to 162 µg/ml, the disposition half-lives were calculated to $t_{1/2\alpha}$ = 3 h, $t_{1/2\beta}$ = 21.4 h, and $t_{1/2\gamma}$ = 248 h, respectively. For detection of the γ-distribution phase, analyses of serum samples between 24 up to 120 h after last administration are necessary.

4. Conclusions

Although BSH has been used clinically for many years, its pharmacokinetics and metabolism is still not fully understood. Pharmacokinetic studies, which have various study designs and are limited in the number of patients, investigate single dose of BSH. To describe the pharmacokinetic profile of BSH, a sufficient period of time for blood sampling has to be used. The pharmacokinetic results from this study confirm those previously reported[14]. However, further investigations seem to be necessary to better understand the γ-distribution phase.

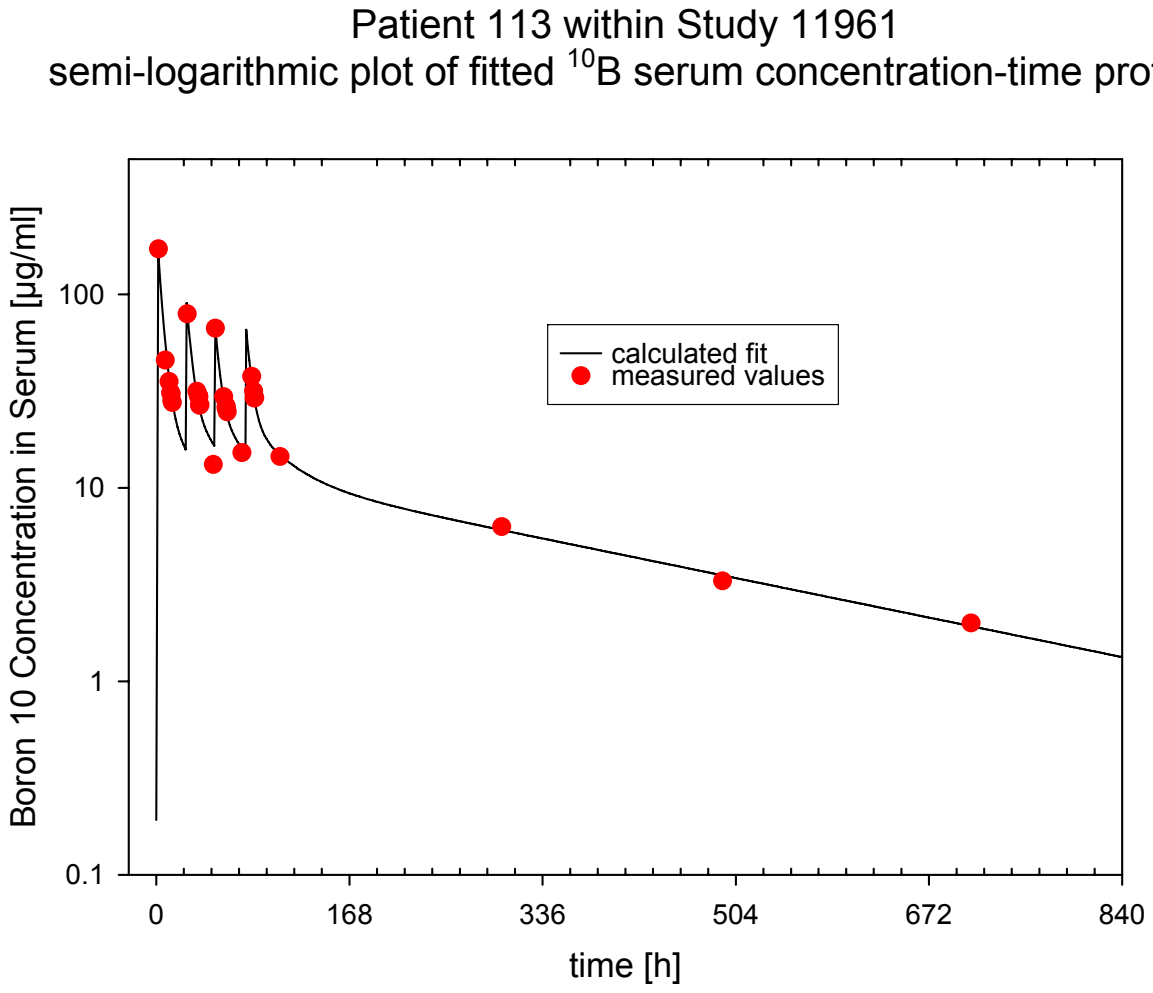

Fig. 1. Semi-logarithmic plot of fitted ^{10}B serum concentration-time profile of patient 113

Acknowledgement

The work received financial supported from the European Commission contract QLK3-CT-1999-01067.

References

1 Hatanaka H, Soloway AH, Sweet H. Incorporation of pyrimidines and boron analogues into brain tumour and brain tissue of mice. An approach to boron-neutron capture therapy. Neurochirurgia Stuttg 1967;10:87-95.

2 Hatanaka H, Sano K. A revised boron-neutron capture therapy for malignant brain tumors. I. Experience on terminally ill patients after Cobalt-60 radiotherapy. J Neurol 1973;204:309-332.

3 Nakagawa Y, Pooh K, Kobayashi T, Kageji T, Uyama S, Matsumura A, Kumada H. Clinical review of the Japanese experience with boron neutron capture therapy and a proposed strategy using epithermal neutron beams. J Neurooncol 2003;62:87-99.

4 Sauerwein W, Zurlo A. The EORTC Boron Neutron Capture Therapy (BNCT) Group: achievements and future projects. Eur J Cancer 2002;38:S31-S34.

5 Suzuki M, Sakurai Y, Nagata K, Kinashi Y, Masunaga S, Ono K, Maruhashi A, Kato I, Fuwa N, Hiratsuka J, Imahori Y. Impact of intra-arterial administration of boron compounds on dose-volume histograms in boron neutron capture therapy for recurrent head-and-neck tumors. Int J Radiat Oncol Biol Phys 2006;66:1523-1527.

6 Goodman JH, Yang W, Barth RF, Gao Z, Boesel CP, Staubus AE, Gupta N, Gahbauer RA, Adams DM, Gibson CR, Ferketich AK, Moeschberger ML, Soloway AH, Carpenter DE, Albertson BJ, Bauer WF, Zhang MZ, Wang CC. Boron neutron capture therapy of brain tumors: biodistribution, pharmacokinetics, and radiation dosimetry sodium borocaptate in patients with gliomas. Neurosurg 2000;47:608-621.

7 Gibson CR, Staubus, A.E., Barth, R.F., Yang. W., Goodman, J.H., Adams, D.M., Ferketich, A.K., Moeschberger, M.L., Gao, Z., Zhang, M.Z., Wang, C.C. Pharmakokinetics of sodium borocaptate, based on boron concentrations, after intravenous administration to glioma patients and simulations to opitmize dosing for neutron capture therapy. J. Pharmacokinetics and Biopharmaceutics 2001.

8 Stragliotto G, Fankhauser H. Biodistribution of Boron Sulfhydryl for Boron Neutron Capture Therapy in Patients with Intracranial Tumors. Neurosurgery 1995;36:285-293.

9 Horn V, Slansky J, Janku I, Strouf O, Sourek K,Tovarys F. Disposition and tissue distribution of boron after infusion of borocaptate sodium in patients with malignant brain tumors. Int J Radiat Oncol Biol Phys 1998;41:631-638.

10 Kageji T, Nagahiro S, Kitamura K, Nakagawa Y, Hatanaka H, Haritz D, Grochulla F, Haselsberger K, Gabel D. Optimal timing of neutron irradiation for boron neutron capture therapy after intravenous infusion of sodium borocaptate in patients with glioblastoma. Int J Radiat Oncol Biol Phys 2001;51:120-130.

11 Wittig A, Michel J, Moss RL, Stecher-Rasmussen F, Arlinghaus HF, Bendel P, Mauri PL, Altieri S, Hilger R, Salvadori PA, Menichetti L, Zamenhof R,W.A.G. S. Boron analysis and boron imaging in biological materials for Boron Neutron Capture Therapy (BNCT). Crit Rev Oncol Hemat 2008. doi:10.101016/j.critrevonc.2008.03.004. in press

12 Hideghéty, K., W. Sauerwein, et al. Tissue uptake of BSH in patients with glioblastoma in the EORTC 11961 phase I BNCT trial." J Neurooncol 2003: **62**(1-2): 145-56.

13 Wittig, A., M. Malago, Collette, L. Huiskamp, R. Bührmann, S. Nievaart, V. Kaiser, G. M. Jöckel, K. H. Schmid, K. W. Ortmann, U. Sauerwein, W. A. Uptake of two 10B-compounds in liver metastases of colorectal adenocarcinoma for extracorporeal irradiation with boron neutron capture therapy (EORTC Trial 11001). Int J Cancer 2008; **122**(5): 1164-71.

14 Gibson, C. R., Staubus, A. E., Barth, R. F., Yang, W., Ferketich, A. K., Moeschberger, M. M. Pharmacokinetics of sodium borocaptate: a critcal..; Journal of Neuro-Oncology2003; 62:157-169.

Dynamic Infrared Imaging of Melanoma and Normal Skin in Patients Treated by BNCT

G.A. Santa Cruz[a], J. Bertotti[b], J. Marín[b], S.J. González[a, h], S. Gossio[c], D. Alvarez[d], B.M.C. Roth[e], P. Menéndez[e], M.D. Pereira[f], M. Albero[g], L. Cubau[g], P. Orellano[g] and S.J. Liberman[a]

[a]*Comisión Nacional de Energía Atómica, Av. del Libertador 8250 (1429), Cdad. de Buenos Aires, Argentina.*
[b]*Facultad de Ingeniería y Ciencias Exactas y Naturales, Universidad Favaloro, Solís 453 (C1078AAI), Cdad. de Buenos Aires, Argentina*
[c]*Dpto. de Física, UBA, Int. Güiraldes 2160, Ciudad Universitaria (1428), Cdad. de Buenos Aires, Argentina*
[d]*Fundación Favaloro, Av. Belgrano 1746 (C1093AAS), Cdad. de Buenos Aires, Argentina*
[e]*Instituto de Oncología Angel H. Roffo, Av. San Martín 5481 (1417), Cdad. de Buenos Aires, Argentina*
[f]*Agencia Nacional de Promoción Científica y Tecnológica, PAV 22393, Argentina*
[g]*INVAP S.E., F.P. Moreno 1089 (R8400AMU), S.C. de Bariloche, Rio Negro, Argentina*
[h]*CONICET, Avda. Rivadavia 1917, (1033) Cdad. de Buenos Aires, Argentina*

Abstract

We recently initiated a program aimed to investigate the suitability of dynamic infrared imaging for following-up nodular melanoma patients treated by BNCT. The reason that makes infrared imaging attractive is the fact that it constitutes a functional and non-invasive imaging method, providing information on the normal and abnormal physiologic response of the nervous and vascular systems, as well as the local metabolic rate and inflammatory processes that ultimately appear as differences in the skin temperature.

An infrared camera, with a focal plane array of 320x240 uncooled ferroelectric detectors and modified optics is employed, with a minimum focus distance of 1.5 m. It provides a video stream of the infrared emission in the 7-14 μm wavelength band. A double blackbody is used as reference for absolute temperature calibration.

After following a protocol for patient preparation and acclimatization, a basal study is performed. Subsequently, the anatomic region of interest is subjected to a provocation test (a cold stimulus), which induces an autonomic vasoconstriction reflex in normal structures, thus enhancing the thermal contrast due to the differences in the vasculature of the different skin regions. Radiation erythema reactions and melanoma nodules possess typically a faster temperature recovery than healthy, non-irradiated skin. However, some other non-pathological structures are also detectable by infrared imaging, (e.g. scars, vessels, arteriovenous anastamoses and injuries), thus requiring a multi-study comparison in order to discriminate the tumor signal. Besides the superficial nodules, which are readily noticeable by infrared imaging, we have detected thermal signals that are coincident with the location of non-palpable nodules, which are observable by CT and ultrasound. Diffuse regions of faster temperature recovery after a cold stimulus were observed between the 3rd and 6th weeks post-BNCT, concurrent with the clinical manifestation of radiation erythema. The location of the erythematous visible and infrared regions is consistent with the three-dimensional dosimetry calculations.

Keywords: Infrared thermography, skin reaction, melanoma

1. Introduction

Medical infrared (IR) thermography is based on the derivation of the spatial and temporal pattern of temperature associated to the IR radiance emitted by the tissue under study. This distribution not only depends on physical parameters, but also on the physiology associated to the homeostatic and metabolic processes and the structure and dynamics of the vascular, tissular and nervous systems. It is affected by internal and external factors and, in the case of a normal tissue, its spatial and temporal

evolution is the manifestation of the organism in an attempt to maintain the homeostasis.

The particular tumor architecture and angiogenesis processes lead to a very dissimilar situation. Inflammation, interstitial hypertension, abnormal vessel morphology and lack of response to homeostatic signals are some of the differences that make tumors to behave differently than normal tissue in terms of heat production and dissipation.

Application of IR thermography for the study of malignant melanoma (MM) has been described by an Italian group (Di Carlo, 1995). They employed a cold patch applied onto the affected area, i.e. a cold stimulus, in order to increase the thermal contrast between normal skin and tumor.

In our BNCT clinical trial for MM, we are exploring the potential of Dynamic IR Imaging (DIRI) for evaluating the early changes in normal skin as well as the tumor evolution after the treatment.

2. Materials and Methods

2.1 Infrared detection equipment

An IR camera (Raytheon PalmIR 250, L3 Comm. Systems) is employed, which uses uncooled ferroelectric detector technology, sensitive to IR radiation in the 7 to 14 μm wavelength band. It focuses targets located within 1.5 m and 3 m distance. The detector is a Focal Plane Array (FPA) composed of 320x240 Barium-Strontium Titanate (BST) ceramic elements. The IR camera provides a video output signal suitable for time-dependent studies. For temperature calibration, a double-cavity black body is used. One of the cavities is electrically heated to temperatures about 40 ºC and the other one is in equilibrium with ambient temperature.

2.2 Protocols in clinical thermography

Clinical thermography is based on the observation of the functional aspects of body thermal regulation. However, environmental, pharmaco-logical, mechanical and even emotional stressors are capable of inducing changes in the skin temperature. Thus, a series of standards and protocols in clinical thermography must be followed for the correct application and interpretation of the results. Information can be found in the International Academy of Clinical Thermology website (IACT).

2.3 Provocation tests

Two different cold stimuli were employed: immersion in water at 15 ºC for 2 minutes or alcohol spray and fan currents over the region, to induce cooling by evaporation. The later was used when no immersion was possible and the skin showed no signs of damage. However, since radiation may induce changes in the skin permeability and can produce severe damage, a system capable of generating cold air currents is presently under design, thus avoiding any contact with the skin of the patient.

2.4 Thermographic procedure

Before any IR study, the patient remains at rest for a period of 15 to 20 minutes, with the body region to be examined exposed to the ambient, in order to reach thermal equilibrium. After that period, a 30-seconds basal study is performed to record the initial temperature distribution. Subsequently, a cold stimulus is applied and another video is acquired for a longer time (3 minutes or more).

Since it is important to compare basal with post-stimulus temperature distributions, the region to study is immobilized and anatomical landmarks are used for image registration.

2.5. Clinical cases

Patient EAS: a 72 years old woman with a history of MM, Breslow 3 mm, Clark 3 at the moment of diagnosis, with several locorregional relapses as subcutaneous nodules through 10 years of follow-up, treated with surgical resection every time. BNCT was performed on May 17th, 2007, for 2 subcutaneous nodules in the right thigh. Complete response was observed at the first assessment, with grade 1 cutaneous toxicity (erythema).

Patient AP: a 66 years old male diagnosed in 2004 for MM, Breslow 3.5 mm, Clark 3, in the left foot. He had presented several local relapses treated with surgical approaches. At the moment of BNCT the patient had multiple subcutaneous nodules in the external maleolar region of the left foot. He was treated by BNCT on June 29th, 2007. Three out of ten nodules reach an objective response. The other nodules had no change after the treatment. The patient presented cutaneous toxicity grade 3 (ulceration), treatment-related.

2.6 BNCT treatment and follow-up

Both patients were treated at the BNCT facility of the RA-6 reactor, Bariloche, Argentina. The patients were followed by clinical inspection, CT and high-resolution Doppler ultrasound. IR studies were carried out before BNCT, weekly during the first month after the treatment, and then monthly.

2.7 Skin reaction assessment

Evaluation of the skin reaction was performed by the clinician during following-up. Additionally, in

order to obtain a semi quantitative measurement, an algorithm (Schaefer, 2006) was implemented to discriminate human skin employing visible images. Briefly, skin hue values lie in a narrow range, and thus small variations of skin color can be visualized by extracting the hue channel from RGB images.

2.8 Thermographic figure of merit for evaluating the skin reaction

During the application of a cold stimulus, the skin temperature drops forced by the change in the boundary condition. After the end of the stimulus, the regions of the skin will recover the temperature with different velocities depending on the local heating sources, which, as explained before, can be of diverse nature. A quantity suitable for comparing studies taken in different days is the following:

$$\alpha\left(t_m, d_n\right) = \left.\frac{\Delta T_{ref} - \Delta T_X}{\Delta T_{ref}}\right|_{t=t_m, d_n} \qquad (2.1)$$

where ΔT_{ref} and ΔT_X are the temperature differences (between basal and t_m seconds after the end of the cold stimulus) of a reference skin region and a particular region X, respectively, taken the day d_n. This quantity reflects the relative difference of recovery velocity between regions.

2.9 Three-dimensional computational dosimetry

Based on the data involved in a BNCT melanoma treatment, 3D representations of the dose distribution in the skin can be performed using the Matlab-based tool described by Gossio et al., (2008.) These reconstructions allow to easily visualize regions of different doses in the skin for studying local toxicities as well as tumor control. Using this tool, a registration of the 3D reconstruction and thermograms of the patient anatomy can be performed to spatially correlate the information provided by DIRI with the absorbed dose in the skin.

2.10 Selected skin regions for evaluation of the erythema

A reference skin region in the thigh of patient EAS that received a non-therapeutic dose was selected, free from surgical scars and distant from the diagnosed melanoma nodules. In order to correlate the erythematous reaction with some thermal signature, skin regions within the treatment field were chosen, at least one-centimeter distance from scars and nodules (see Figure 1). Every region must be identifiable in all IR studies.

2.11 Melanoma nodules

The nodules of patient AP were clearly visible and detectable clinically. For the IR studies, a series of regions close to the larger MM nodules (5 to 8 and 10) were studied, as well as a normal skin region for comparison (see Figure 2).

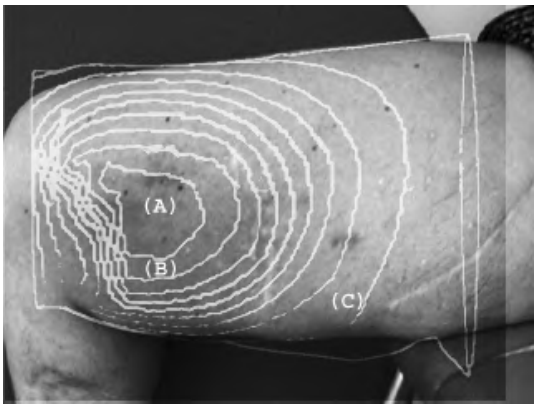

Figure 1. Selected regions (patient EAS) on the skin. (A) and (B) are regions within the treatment field (skin dose greater than 16 Gy-Eq). (C) is a region of low skin dose (less than 2 Gy-Eq). 3D dose reconstruction performed with the tool described in Gossio et al. (2008).

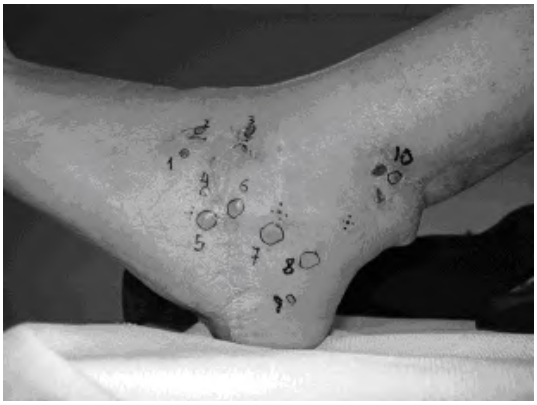

Figure 2. Delineation of MM nodules for patient AP

3. Results

3.1 Evolution of the erythematous reaction

Figure 3 shows the evolution of the quantity given by Eq. (2.1) during the initial follow-up period (30 weeks) for patient EAS, together with the relative difference of hue values.

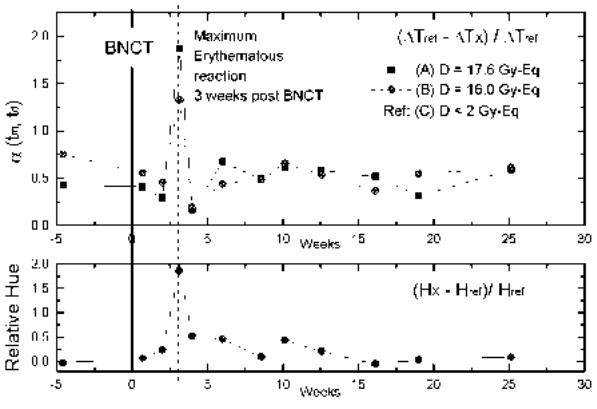

Figure 3. Evolution of the erythematous reaction as observed by IR thermography, compared with measurements of hue values in the corresponding visible images taken during the IR studies

A marked increase is evident at 22 days after BNCT, concomitant with the observed skin color changes. It can be seen that the peak value exceeds unity, because the skin temperature one minute after the cold stimulus within the irradiation field was actually higher than its basal temperature. The same analysis, made on the surgical scars within the field revealed identical behavior (not shown).

3.2 Temperature recovery in MM after cold stimulus

Figure 4 shows the evolution of temperature in selected regions (N5, N8, N10, ROI 5-8 and normal skin) for patient AP, after the cold stimulus (15 ºC water immersion for 2 minutes).

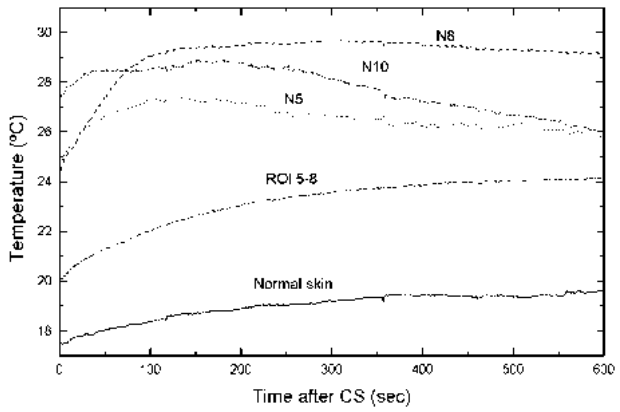

Figure 4. Time-course evolution of temperature after cold stimulus (CS) of the selected regions of patient AP before BNCT. Regions close to the larger nodules were evaluated as a function of time after the cold stimulus. The regions N5, N8 and N10 are areas close to the MM nodules treated by BNCT (see Fig. 3). ROI 5-8 is a mixed region that includes nodules 5 to 8 and part of normal skin.

It is worthy to note that at the beginning of the study, the temperature of the regions in the proximity of the nodules was already 6 to 10 ºC higher than normal skin, and their temperature recovery was much faster that normal tissue.

The region ROI 5-8 contains tumor as well as normal skin, and its temperature is still higher than the normal tissue temperature, but increases slower than the nodules. Figure 5 shows a registration between visible and IR images.

3.3 Comparison of MM thermal signature with other studies

Table I shows a comparison between the detection results of computed tomography, Doppler ultrasound and DIRI, for patient AP. We can see that DIRI has higher sensitivity than Doppler ultrasound and similar to CT.

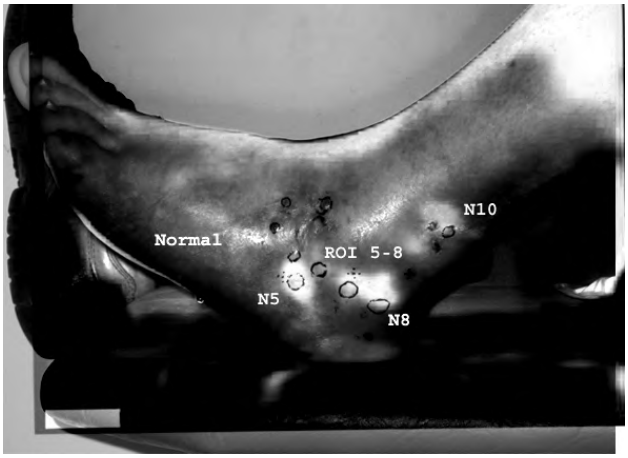

Figure 5. Image registration between a visible image and IR thermography, one minute after the end of the cold stimulus. Temperature recovery in regions around MM nodules is clearly noticeable (white regions)

Table I

Nodule	CT	Ultrasound	DIRI
1	-	-	-
2	-	-	-
3	+	-	-
4	-	-	+
5	+	+	+
6	-	+	+
7	+	+	+
8	+	+	+
9	+	-	+
10	+	-	+

4. Conclusions

These preliminary results show that dynamic IR imaging could be a useful and sensitive tool to study skin toxicities and tumor control in BNCT melanoma treatments.

References

Di Carlo, A., Thermography and the possibilities for its applications in clinical and experimental dermatology. Elsevier Science Inc., 1995.

Gossio, S., Carando, D.G., González S.J., A Computational Dosimetry Tool for the study of tumor doses and skin toxicities in BNCT. Proc. 13th ICNCT, 2008.

IACT. The International Academy of Clinical Thermology. http://www.iact-org.org.

Schaefer, G., Tait, R., Ying Zhu, T. "Overlay of thermal and visual medical images using skin detection and image registration". Proceedings of the 28th IEEE, EMBS Annual International Conference, New York City, USA, Aug 30-Sept 3, 2006.

BPA uptake and distribution in GBM and normal brain is determined by extensive functional LAT-1 transporter expression which does not correlate with proliferative marker PCNA distribution

Detta A[1], Cruickshank GS[1]

[1]*Department of Neurosurgery, School of Medicine, University of Birmingham, Birmingham UK*

Boronophenylalanine (BPA) functions as a vehicle for the delivery of B10 to target cells. Enhanced uptake of BPA into human target GBM tumour cells has been demonstrated. The mechanism of preferential uptake of BPA into tumours is thought to be due to upregulation of the metabolic linked amino acid transporter LAT-1. LAT-1 and tyrosine uptake have also been linked as markers for proliferative activity. In this study we have investigated the distribution of LAT-1 in GBM and normal brain compared to the distribution and incidence of elevated PCNA expression (a proliferative marker). In addition we have tested immediate GBM biopsy tissue and normal brain for uptake of BPA and selectively tested blockade of BPA uptake via LAT-1 with phenylalanine and BCH.

Four populations of cells are identified by dual immunostaining for PCNA and LAT-1. PCNA positive LAT-1 positive, PCNA positive LAT-1 negative (20%) PCNA negative LAT-1 positive, PCNA negative LAT-1 negative. BPA uptake into tumours rose to 30μg/g but much less in normal brain. In both cases uptake was unaffected by tyrosine levels but inhibited by phenylalanine and BCH a specific inhibitor of LAT-1. If inhibition is complete, then most of BPA uptake into GBM is explained by LAT-1 activity

The uptake data confirm the functional importance and specificity of LAT-1 in concentrating BPA in cells, and indicate from the direct competition for uptake between phenylalanine and BPA, that BPA is handled in the same manner as the normal amino acid.

These results indicate a markedly more comprehensive distribution (85% of tumour) of uptake capacity for BPA that does not correlate with proliferative markers. This supports the concept that BPA can act as a more efficient vehicle for BPA entry than was originally thought both in and around the tumour mass. A proportion of PCNA expressing non LAT-1 expressing cells may form a better target for standard radiotherapy or other cell-cycle conditional treatments. This study emphasizes the critical requirement of determining that the potential of BNCT must be based on in vivo biomarker approaches (e.g. LAT-1 distribution) as well as reliable neutron beams.

A novel approach to the study of ^{10}B uptake in human lung by ex-vivo BPA perfusion

P. Borasio[1], G.Giannini[5], F. Ardissone[1], M. Papotti[1], M. Volante[1], C. Fava[1], V. Podio[1], M. Rinaldi[2], M. Boffini[2], G. Izzo[2], V. Tavaglione[1], E. Trevisiol[1], M. Di Franco[3], P.Chiari[4] and A.Zanini[6]

[1] *Università di Torino. Dipartimento di Scienze Cliniche e Biologiche. S. Luigi Orbassano.*
[2] *Università di Torino,Ospedale S. Giovanni Battista, Dipartimento di Cardiochirurgia.*
[3] *SC Farmacia AOU S. Luigi. Orbassano,Torino*
[4] *Dipartimento di Fisica Nucleare e Teorica, Università di Pavia*
[5] *Dipartimento di Fisica, Universita' di Trieste*
[6] *INFN Sez.Torino*

Abstract

Research in BNCT concerns several fields, as uptake of ^{10}B carriers, evaluation of RBE for different tumours, study of response to neutron capture therapy of different pathologies. Up today, experimental data are mainly obtained in animal models. In this work a new technique is proposed, in which human specimens are used to investigate ^{10}B uptake in non-small cell lung cancer. In patients undergoing standard lobectomy for non-small cell lung cancer, the resected pulmonary lobe containing the tumour is perfused with BPA solution under controlled conditions. After resection, perfusion of pulmonary lobe containing the tumour is carried out in an extracorporeal perfusion circuit employing a roller pump and a second pump to maintain a sufficiently high fluid-water temperature (37°C). Isolated lobar arteries and veins are cannulated with paediatric cannulas. Crystalloid priming solution is used with the addition of blood. Ventilation is provided by a paediatric extracorporeal oxygenator. After perfusion, the lung specimen is frozen and several samples, prepared from normal, peritumour and tumour tissue, are placed on Cr-39 thin layers and on slides for the histological analysis. ^{10}B concentration in the samples is evaluated by exposure to thermal neutron field provided in the PhoNeS cavity installed at Elekta PRECISE 25MV e-linac accelerator. This ex-vivo perfusion technique could represent an innovative method to be applied to different tumour pathologies, opening a new experimental field for widely studying BNCT applications in human samples.

Keywords: BNCT, BPA perfusion, lung adenocarcinoma, non-small cell lung cancer. photoneutron source

1. Introduction

Nowadays, BNCT is considered by the scientific community one of the most promising approach to cancer therapy. Unfortunately the possibility of further studies and experiments is reduced because of the small number of available neutron sources able to provide the required energy spectrum and the high neutron flux useful for BNCT application. Moreover, another substantial limit to the progress in BNCT research and applicability to different tumor pathologies is the difficulty encountered in the use of human samples of tumor tissue, because of ethical issues and restriction in drugs uptake in patients.

In this paper a method is proposed, based on extra-body perfusion of BPA in patients surgically treated for non-small cell lung cancer. The method has been applied at the Thoracic Surgery Department of the Ospedale S.Luigi (Orbassano, Torino, Italy), by a staff of surgeons, lung pathologists, clinical-perfusionists and pharmacologists.

The results obtained in two surgical specimens of lung tumors are described. The analysis of the samples, suitably prepared on layers of CR 39 track

detectors (Chan et al., 2006, Giannini et al., 2008, this congress) has been performed by using as thermal neutron source the facility PHONES (Bevilacqua et al. 2006, Zanini et al., 2008 this Congress) applied to the Elekta PRECISE 25 MV accelerator at AOU Molinette Hospital in Torino, Italy.

This new technique could open a new important research field in BNCT: it is evident the great improvement obtained by studying directly the ^{10}B effects on human samples, overcoming the limits of the animal model, as well as the advantage of exploiting an in-hospital neutron source, installed in a Radiotherapy Department. In this way a wide range of BNCT application could be investigated, from analysis of behavior of different ^{10}B carriers, to study of boron compound distribution in tumor cells (peripheral area or nucleus), to test of BNCT effectiveness on different tumor pathologies, to evaluation of RBE factors for different tissues.

2. The perfusion technique

Two patients, with a primary non-small cell lung cancer of adenocarcinoma histology, were included in the study after giving written informed consent in accordance with the regulations of the institutional review board.

After resection, the tumour remained intact in the specimen preparations. Perfusion of the pulmonary lobe was performed in an extracorporeal perfusion circuit employing a roller pump with pulsatile module (350-400 ml/min) and a second pump to maintain a sufficiently high fluid-water temperature (37°C) (fig. 1). In both cases all the lobar arteries and veins are isolated and cannulated with paediatric cannulas (16-18 French).

Fig. 1. Extracorporeal perfusion circuit

Crystalloid priming solution was used (300 ml) with the addition of blood (300 ml). Ventilation was provided with a paediatric extracorporeal oxygenator (0,2/0,3 l/min flow rate, FiO_2 50%). The first lobe (weight 172 g), was continuously perfused (fig. 2) for two hours with a BPA compound of water, fructose and ^{10}B (300 mg BPA/kg tissue). In the second case (weight 166 g, 300 mg BPA/kg tissue) the perfusion was prematurely ended because of a marked flow reduction due to a general extravascular loss of fluid into the pulmonary parenchyma. The net weight gain during the experiment, wet-to-dry weight ratio for lung tissue, pulmonary colour and gas analysis content into the perfusate are the parameters assessed to confirm the stability of the preparations and the quality of the experiments. The bronchial arterial system accounts for about 1% of the cardiac output.

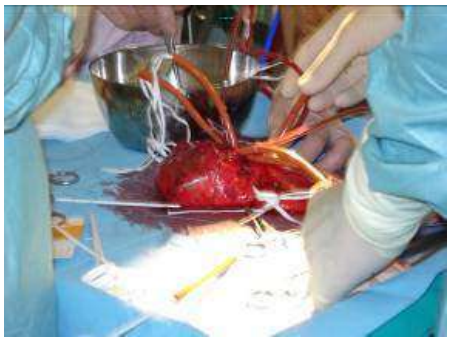

Fig. 2. First lobe perfusion

3. Sample preparation

After BPA perfusion, the biological material is frozen and several samples, prepared from normal, peritumour and tumour tissue, are placed on slides for the histological analysis and on Cr-39 thin layers for irradiation with thermal neutrons produced in PhoNeS treatment cavity (fig. 3).

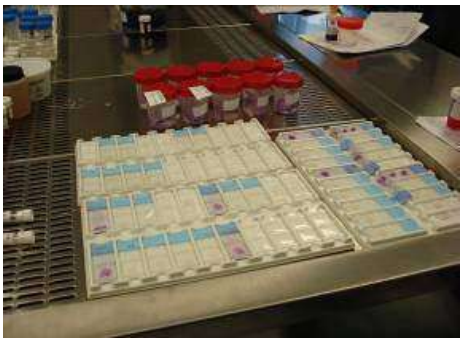

Fig. 3: Samples placed on CR-39 layers

The thickness of samples prepared for irradiation is 5-10 micron, corresponding to the range of the alpha and ^{6}Li particles produced by the reaction of thermal neutrons with ^{10}B. Couples of neighbouring lung samples were cut using Leica cryostat: a section of 10 micron was deposited on glass for morfological analysis by standard ematoxiln-eosin stining (fig. 4); the next 10 micron section was deposited on CR-39 support to be submitted to neutron radiography. The biological samples are placed between two layers of CR39, to double the efficiency of the detector (fig. 5).

Alpha and ^{7}Li secondary particles produced by thermal neutron capture reaction with ^{10}B content in the sample, cause damages on the CR-39 support; after etching with NaOH (6N) these tracks became holes visible by microscope (fig. 6).

Fig. 4. Histological sample

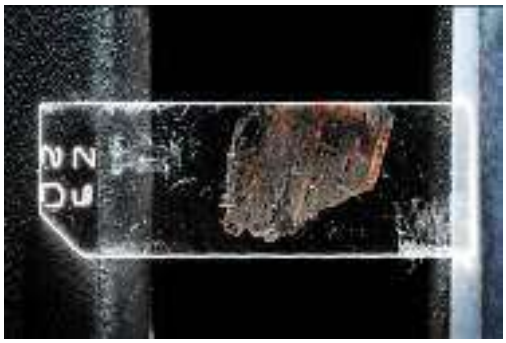

Fig. 5. Histological sample on CR-39 detector

Fig.6. Corresponding image of sample after irradiation

4. The Neutron Source

The neutron source used for the irradiation is constituted by the closed cavity in the PHoNeS photoconverter installed at the head of the Elekta PRECISE 25 MV accelerator. Neutrons are produced in the head of high energy linear accelerators (18 – 25 MV) when the energy of the incident photon is higher than the threshold energy of the (γ,n) reaction (Followill et al. 2002, Zanini et al. 2004). The PhoNeS photoconverter has been designed in view to increase the photoneutron production and to obtain, with suitable moderating materials, an intense thermal neutron field for BNCT application. (Giannini et al. 2006).

A small prototype of photoconverter (fig. 7), easy to be installed and removed from the accelertaor head and suitable to be transported to different radiotherapy departments, has been manufactured (INFN Sez.Trieste Mechanical Laboratory) and equipped with a closed irradiation cavity for biological sample treatment, where a thermal neutron flux 10^{7} n cm^{-2}s^{-1} is produced (Zanini et al., 2008, this Congress).

In fig. 8 it is shown the biological sample positioning inside the irradiation cavity.

Fig. 7. Photoconverter prototype

Fig.8. Biological sample positioning inside the irradiation cavity

After positioning in the cavity, the samples have been irradiated with ~10^{11} cm^{-2} thermal neutron fluence, operating the linac at 400 MU/min and integrating a total of ~7 10^4 MU in ~3 h ~10^4 s.

After etching the CR39 layers for 2h in NaOH (6N) at 90 °C, ~10μm diameter holes, corresponding to α and ^{7}Li products of neutron capture by ^{10}B, are clearly observed at the microscope, with densities of the order of 1-2 10^3 mm^{-2} following the features of the corresponding previously overlaying tissues.

From the analisys of CR-39 detectors it is possible to confirm the efficiency of the ex-vivo perfusion technique and a significant difference in the ^{10}B uptake in tumor and healthy tissue is detected.

^{10}B concentration, calculated both in healthy tissue and tumor tissue is evaluated in (29±3) ppm and (40±3) ppm respectively (Giannini et al. 2008, this Congress). This preliminary result seems to be reasonable considering the short (2 hours) perfusion time.

5. Conclusion

A new technique for BPA perfusion in human tissue is proposed, based on extracorporeal perfusion circuit applied after surgery resection of lung lobe. This technique, joined with the use of PhoNeS neutron source installed at 25 MV linear accelerator, allowed to carry out the analisys of ^{10}B uptake on human primay lung adenocarcinoma inside an hospital department and a ^{10}B concentration in health and tumour tissue of (29±3) ppm and (40±3) ppm respectively is detected after a 2 hours BPA perfusion.

On the base of these promising preliminary results, further experiments are planned to complete the kinetic up-take ^{10}B curve for non-small cell lung cancer, by using different BPA perfusion times (4-6 hours). Moreover, malignant pleural mesotelioma treated by extrapleural pneumonectomy will be studied with the same extracorporeal BPA perfusion method.

In addition, the same procedure could be applied to different organs affected by tumor pathologies and surgically removed following "golden standard ", as liver, kidney, pancreas, etc.

Finally the PhoNeS facility will be used to analize the response to BNCT treatment of human cell cultures treated with BPA or other boron carriers.

Reference

Bevilacqua R., et al. "PhoNeS: A novel approach to BNCT with conventional radiotherapy accelerators" Nuclear Instruments and Methods in Physics Research A 572 p. 231-232 (2007).

Chan K. F., et al. " Alpha-Particle Radiobiologicaal experiments using thin CR-39 detectors" Radiation Protection Dosimetry (2006), Vol. 122, No. 1–4, pp. 160–162

Followill S. et al. 2002 "Neutron source strength measurements for Varian, Simens, Elekta, and General Electric linear accelerators", American College of Medical Physics (PACS Numbers:87.53Qc, 87.52.Ln)

Giannini G. et al. "CR-39 neutron imaging of biological samples at clinical linac's" – 13th International Congress on Neutron Capture Therapy 2-7 November 2008 Florence, Italy.

Giannini G., et al. "Photoneutron Source for In-Hospital BNCT Treatment: feasibility study" – 12th International Congress on Neutron Capture Therapy 9-13 Ottobre 2006 Takamatsu, Kagawa, Japan .

Zanini et al. "Monte Carlo simulation of the photoneutron field in linac radiotherapy treatments with different collimation systems" Phys. Med. Biol. 49 571-582, 2004

Zanini A., et al. "Characterization of a Thermal Cavity in the PhoNeS photo-neutron converter for BNCT research" – 13th International Congress on Neutron Capture Therapy 2-7 November 2008 Florence, Italy.

Boronophenylalanine uptake in C6-glioma model is dramatically increased by L-DOPA preloading

S. Capuani[1,2], T. Gili [1,2], M. Bozzali[3], S. Russo[4], P. Porcari[1], C. Cametti[1,5], E. D'Amore[6], B. Maraviglia[2,5], G. Lazzarino[7], F. S. Pastore[8]

[1]*CNR-INFM SOFT, Physics Department, Univ. of Rome "Sapienza", P.zzale Aldo Moro 2, 00185 Rome, Italy.*
[2]*Enrico Fermi Center, Compendio Viminale 00184, Rome, Italy*
[3]*Neuroimaging Laboratory, Santa Lucia Foundation, Via Ardeatina, 00179 Rome, Italy*
[4]*Victor Horsley Department of Neurosurgery, National Hospital for Neurology and Neurosurgery, Queen Square, WC1N 3BG London, United Kingdom*
[5]*Physics Department, Univ. of Rome "Sapienza", P. le Aldo Moro 2, 00185 Rome, Italy*
[6]*Serv. Qual./Sicurezza Sperim. Anim., Istituto Superiore di Sanità, Viale Regina Elena 299, 00133 Rome, Italy*
[7]*Laboratory of Biochemistry, Department of Chemical Sciences, Univ. of Catania, Viale A. Doria 6, 95125 Catania, Italy*
[8]*Department of Neurosurgery, University "Tor Vergata", Via Montpellier 1, 00133 Rome, Italy*

Abstract

Purpose. Boron Neutron Capture Therapy (BNCT) is a radio-therapeutic modality, based on the cytotoxic effects of $^{10}B(n,\alpha)^{7}Li$ reaction, used for the treatment of malignant gliomas. One of the main limitations for BNCT effectiveness is the insufficient intake of ^{10}B nuclei in the tumour cells. This work was aimed at investigating the use of L-DOPA as enhancer for boronophenylalanine (BPA) uptake in the C6-glioma model. The investigation was first performed *in vitro*, and then extended *in vivo* to the animal model. **Methods and Materials**. BPA accumulation in C6-glioma cells was assessed, using Radiowave Dielectric Spectroscopy, with and without L-DOPA preloading. Two different L-DOPA incubation times (2 and 4 hours) were investigated, and the correspondent effects on BPA accumulation were quantified. C6-glioma cells were also implanted in the brain of 25 rats, and tumor growth was monitored by Magnetic Resonance Imaging. Rats were randomly assigned to two experimental branches: 1) intra-carotid BPA infusion; 2) intracarotid BPA infusion after pre-treatment with L-DOPA, administrated intra-peretoneally 24 hours before BPA infusion. All animals were sacrificed, and assessment of BPA concentrations in tumor tissue, normal brain, and blood samples was performed using High-Performance Liquid Chromatography. **Results.** *In vitro:* L-DOPA preloading induced a massive increase of BPA concentration in C6-glioma cells only after a 4 hour incubation. *In vivo:* in the animal model a significantly higher accumulation of BPA was found in the tumor tissue of rats pre-treated with L-DOPA as compared to the control group ($p<0.0001$). Conversely, no significant difference was found in the normal brain (sampled in both cerebral hemispheres) and blood samples between the two animal groups. **Conclusions.** This study suggests the potential use of L-DOPA as enhancer for BPA accumulation in malignant gliomas eligible for BNCT. According to our results, this new strategy is expected to increase BNCT efficacy in absence of any additional risk of toxicity.

Keywords: C6-glioma, L-DOPA, BPA, MRI, Dielectric Spectroscopy

1. Introduction

Malignant gliomas are the most common primary intracranial neoplasms in humans, and are typically associated with a severe prognosis. Despite advances in microsurgical techniques, radiotherapy and chemotherapy, there has been little improvement in the clinical outcome of patients. Boron Neutron Capture Therapy (BNCT) (Barth, 1999) is a technique based on a targeted radiation approach, which represents an alternative adjuvant therapy for malignant gliomas.

Previous Phase I and Phase II studies have consistently demonstrated no severe effects of BNCT-related toxicity, and some preliminary evidence of therapeutic effectiveness (Busse, 2003; Diaz, 2003; Palmer, 2002; Joensuu 2003). One of the major limitations for BNCT effectiveness is the insufficient incorporation of ^{10}B into the tumor cells,

even considering the most advanced methods of ^{10}B administration. An additional limitation of BNCT is the relatively low specificity of ^{10}B uptake in tumor cells as compared to normal tissues. So far, two different ^{10}B carriers have been used for clinical purposes: the mercapto-undecahydrododecaborate, $Na_2B_{12}H_{11}SH$ (BSH) and the *p*-dihydroxyboryl-phenylalanine $C_9H_{12}BNO_4$ (BPA).

An higher effectiveness of BPA as compared to BSH has been demonstrated in the BNCT of brain malignances (Ono, 1996). This might be explained by a different micro-distribution and tumor incorporation of the two compounds (Capuani, 2002).

BPA is believed to pass through the BBB and cell membranes, and it is found at higher concentration in tumor cells. Conversely, BSH does not penetrate either the BBB or the cellular membranes. Rather, it appears to mainly accumulate in the intracellular space of the bulk tumor, i.e. where the BBB is damaged. The details of the uptake mechanisms for BPA into tumor cells are still not completely understood. There is evidence that such an uptake is supported by a carrier-mediated transport rather than by passive diffusion. Some authors have demonstrated that the administration of L-tyrosine increases the intracellular accumulation of BPA in tumor cells (Papaspyrou, 1994; Wittig, 2000). Moreover, BPA accumulation in 9L rat gliosarcoma cells is enhanced by either pre-treatment with molecules targeted by L or A aminoacid transport systems.

These findings suggest that such transporters work with a substrate-coupled antiport (exchange) mechanism, which is enhanced by preloading of specific aminoacids. L-DOPA is a well known molecule whose chemical structure is similar to that of L-tyrosine and BPA. L-DOPA preloading has been previously demonstrated to improve several times the intracellular accumulation of BPA in 9L rat gliosarcoma cells (Wittig, 2000). Conversely, a simultaneous incubation of 9L gliosarcoma cells with L-DOPA and BPA causes a decrease of intracellular BPA accumulation.

These observations are particularly interesting for their impact on potential clinical applications.

The current work is focused on investigating the potential role of L-DOPA in BNCT (Capuani, in press). We adopted for our experiments the C6 glioma cell line, which has been widely used to evaluate *in vitro* the effects of novel therapies, and to produce animal models based on tumor cells implantation. Specific aims of this study were: A) to replicate in C6 glioma cells the findings previously described in 9L gliosarcoma cells, by demonstrating a significant increase of BPA intracellular accumulation due to L-DOPA preloading (experiment 1); B) to assess *in vivo*, using the C6 glioma cell rat model, the effect of L-DOPA preloading on BPA accumulation in tumors as compared to normal brain tissue (experiment 2). Experiment 1 was conducted using radiowave dielectric spectroscopy (RDS), which allows passive electric parameters of cell membrane to be measured, namely the permittivity (ε_s) and the electrical conductivity of the cell membrane(σ_s), and the electrical conductivity of the intracellular medium (cytosol) (σ_p). Changes of σ_p have been shown as proportional to variations in intracellular BPA content (Capuani, 2002). In experiment 2, BPA quantification in animal tissues was performed using high performance liquid chromatography (HPLC). As previously shown, this technique is a reliable method for analysis of BPA incorporation in several biological tissues, including cerebral samples (Di Pierro, 2000).

Methods and Materials

Experiment 1. A reference sample of C6 glioma cells was first generated to assess the basic characteristics of permittivity and σ_s. Then, equivalent samples were produced to investigate changes of σ_p under five different experimental conditions: a) cells incubated with addition of 2 mmol BPA (condition 1); b) with addition of 50 μg/ml L-DOPA for 2 hours (condition 2); c) with addition of 50 μg/ml of L-DOPA for 4 hours (condition 3); d) with addition of 2 mmol BPA after a 2 hour pre-incubation with 50 μg/ml L-DOPA (condition 4); e) with addition of 2 mmol BPA after a 4 hour pre-incubation with 50 μg/ml L-DOPA (condition 5). RDS was used to assess σ_p in each condition.

This parameter is influenced by the intracellular concentration of BPA and/or L-DOPA. Conductivity cytosol changes were expressed as percentage differences $(\sigma_p^{test}-\sigma_p^{ref})/\sigma_p^{ref}$ between values measured in the test- (σ_p^{test}) and in the reference-sample (σ_p^{ref}) (Figure 1). Experiment 2. Twenty-five male Wistar rats weighing 300-350 grams were used for the current experiment. Each rat underwent a stereotaxic brain implantation of about 10^6 deantigenized C6 glioma cells. Using Magnetic Resonance Imaging (MRI) at 7T, tumor implantation was first assessed five days after surgery (baseline), and tumor growth was followed up by serial longitudinal scans (one every 4 days) When the tumor size reached a minimum diameter of 2.0 mm, rats were randomly assigned to one of the two experimental branches: 1) BPA administration with L-DOPA pre-treatment; or 2) BPA administration without L-DOPA pre-treatment (control group). Animals belonging to the first branch (N=15) received 50 mg/Kg L-DOPA intraperitoneally twenty-four hours before BPA administration. Then, each rat was anesthetized again, and injected in its right internal carotid 300 mg/Kg BPA-fructose complex. Animals belonging to the control branch (N=10), underwent the same procedure with no pre-administration of L-DOPA. All animals were sacrificed 150 min after BPA infusion. Tumor tissue, normal brain, and blood samples were collected for HPLC quantification of BPA (Di Pierro, 2000).

Results

Experiment 1. In Figure 1, mean (±SD) percentage differences between σ_p values measured in test and in reference samples are reported for each condition (Capuani, in press).

Figure 1

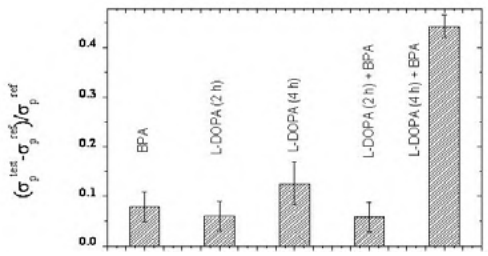

Statistical analysis demonstrated significantly higher σ_p percentage difference values in condition 5 (BPA addition after 4 hour L-DOPA incubation) as compared to any other condition. Moreover, significantly higher σ_p percentage difference values were found in condition 3 (4 hour L-DOPA incubation) compared to condition 2 (2 hour L-DOPA incubation). Experiment 2. Longitudinal MRI scans showed that, on average, tumor lesions reached a diameter ≥2 mm 12 days after surgical implantation. BPA concentrations assessed by HPLC from each sampled tissue (tumor; normal brain; blood) are summarized in Figure 2 for the two experimental groups: rats which received BPA infusion only (group A); rats which received L-DOPA pre-treatment before BPA infusion (group B). BPA accumulation in tumor samples was significantly higher in group B compared to group A ($p<0.0001$). Conversely, no significant difference was found in normal brain and blood samples between the two animal groups.

Figure 2

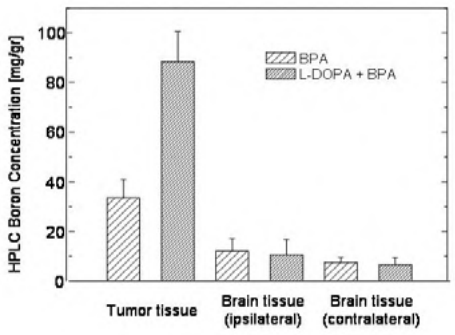

Discussion

The results obtained *in vitro* demonstrate that L-DOPA promotes the cellular uptake of BPA, and extend findings previously observed in 9L gliosarcoma cells (Wittig, 2000). Such an effect is likely to be related to mechanisms of active membrane transport, which are triggered by specific conditions. Our experiments showed that the σ_p changes resulting from the single addition of L-DOPA or BPA to cell cultures are much lower than those observed when a 4 hours L-DOPA preloading preceded BPA administration. It has been previously proposed that both BPA and L-DOPA penetrate trough the cell membrane using two main

mechanisms: by diffusion (slow process, essentially driven by concentration gradients); and by active carries (fast process). Previous experiments, using mouse melanoma cells, suggested the presence of specific membrane antiport carriers with an high affinity for L-substrates, such as L-tyrosine, L-BPA, and L-DOPA (Wittig, 2000). The activation of these carriers is supposed to be driven by a chemical gradient of L-molecules across cell membranes (Wittig, 2000). Our results suggest that 4 hours are needed to reach in C6-glioma cells, by slow diffusion, a critical intracellular concentration of L-DOPA to trigger the faster L-antiport system. The most striking findings of the present work are the convergent results obtained with C6 glioma cells *in vitro* and using the equivalent animal model *in vivo*. L-DOPA pre-administration produced in the rat model an enhancement of tumor BPA accumulation, which was 2.7 times higher than in the control condition (Figure 2). In clinical application, one of the main limitations for BNCT effectiveness is the insufficient accumulation of ^{10}B carrier into the tumor cells. In this perspective, our results are particularly encouraging for planning future BNCT clinical trials in humans. When comparing BPA concentration in blood and normal brain, there was no significant difference between rats which received L-DOPA and rats which did not. This makes the potential use of L-DOPA in BNCT of brain tumors even more attractive. Indeed, the potential ability of L-DOPA to induce a significant increase of BNCT effectiveness (i.e., tumor cells disruption) seems not to be associated with potential side effects (i.e., normal brain tissue damage). So far, different strategies have been proposed to improve BNCT effectiveness (Barth, 2002; Yang, 1997), such as, for example, different approaches of BPA administration (Morris, 2002). These alternative strategies showed an increase of indexes like tumor:brain and tumor:blood BPA concentration, suggesting a potential usefulness for BNCT. However, their potential toxicity has not been fully investigated yet. The current study indicates a remarkable and selective increase of BPA uptake in tumor tissues using L-DOPA, which is a medication associated with modest side effects and low toxicity.

References

Barth, R.F., Soloway, A.H., Goodman, J.H., et al., 1999. Boron neutron capture therapy of brain tumors: an emerging therapeutic modality. Neurosurgery. 44, 433-450.

Barth, R.F., Yang, W., Bartus, R.T., et al., 2002. Neutron capture therapy of intracerebral melanoma: enhanced survival and cure after blood-brain barrier opening to improve delivery of boronophenylalanine. Int. J. Radiat. Oncol. Biol. Phys. 52, 858-868.

Busse, P.M., Harling, O.K, Palmer, M.R., et al., 2003. A critical examination of the results from the Harvard-MIT NCT program phase I clinical trial of neutron capture therapy for intracranial disease. J Neurooncol.62, 111-121.

Capuani, S., Gili, T., Cametti, C., et al., 2002. Radiowave dielectric investigation of boron compounds distribution in cultured tumour cells: Relevance to boron neutron capture therapy. Chem. Phys. Lett. 360, 79-84.

Capuani, S., Gili, T., Bozzali, M., et al., in press. L-DOPA preloading increases the uptake of borophenilalanine in C6 glioma rat model: a new strategy to improve BNCT efficacy. Int. J. Radiat. Oncol. Biol. Phys.

Coderre, J.A., Turcotte, J.C., Riley, K.J., et al., 2003 Boron neutron capture therapy: cellular targeting of high linear energy transfer radiation. Technol. Cancer. Res. Treat. 2, 355-375.

Diaz, A.Z., 2003. Assessment of the results from the phase I/II boron neutron capture therapy trials at the Brookhaven National Laboratory from a clinician's point of view. J Neurooncol. 62, 101-109.

Di Pierro, D., Lazzarino, G., Pastore, F.S., et al., 2000. Determination of boronophenylalanine in biological samples using precolumn o-phthalaldehyde derivatization and reversed-phase high-performance liquid chromatography. Anal. Biochem. 284, 301-306.

Joensuu H, Kankaanranta L, Seppälä T, et al., 2003. Boron neutron capture therapy of brain tumors: clinical trials at the finnish facility using boronophenylalanine. J. Neurooncol. 2003. 62:123-134.

Morris ,G.M., Micca, P.L., Nawrocky, M.M., et al., 2002. Long-term infusions of p-borono phenylalanine for boron neutron capture therapy: evaluation using rat brain tumor and spinal cord models. Radiat. Res. 158, 743-752.

Ono, K., Masunaga, S.I., Kinashi, Y., et al., 1996. Radiobiological evidence suggesting heterogeneous microdistribution of boron compounds in tumors: its relation to quiescent cell population and tumor cure in neutron capture therapy. Int. J. Radiat. Oncol. Biol. Phys. 34, 1081-1086.

Palmer, M.R., Goorley, J.T., Kiger W.S., et al., 2002. Treatment planning and dosimetry for the Harvard-MIT Phase I clinical trial of cranial neutron capture therapy. Int. J. Radiat. Oncol. Biol. Phys. 53, 1361-1379.

Papaspyrou, M., Feinendegen, E.L., Müller-Gärtner, H.W., 1994. Preloading with L-Tyrosine Increases the uptake of Boronophenylalanine in mouse Melanoma Cells. Cancer Res. 54, 6311-6314.

Wittig A., Sauerwein, W.A., Coderre, J.A., 2000. Mechanisms of transport of p-borono-phenylalanine through the cell membrane in vitro. Radiat. Res. 153, 173-180.

Yang, W., Barth, R.F., Rotaru, J.H., et al., 1997. Boron neutron capture therapy of brain tumors: enhanced survival following intracarotid injection of sodium borocaptate with or without blood-brain barrier disruption. Int. J. Radiat. Oncol. Biol. Phys. 37, 663-672.

Effectiveness of Boron Neutron Capture Therapy for Recurrent Head and Neck Malignancies

Itsuro Kato[1], Yusei Fujita[1], Akira Maruhashi[2], Hiroaki Kumada[3], Masatoshi Ohmae[4], Mitsunori Kirihata[5], Yoshio Imahori[6], Minoru Suzuki[2], Yoshinori Sakrai[7],Tetsuro Sumi[1], Soichi Iwai[1], Mitsuhiro Nakazawa[1], Isao Murata[8], Hiroyuki Miyamaru[8] and Koji Ono[2]

[1]*Department of Oral and Maxillofacial Surgery II Osaka University, Graduate School of Dentistry, Osaka, Japan*
[2]*Radiation Oncology Research Laboratory, Research Reactor Institut, Kyoto University, Osaka, Japan*
[3] *Japan Atomic Energy Agency, Tokai Research and Development Center, Ibaraki, Japan*
[4]*Department of Oral and Maxillofacial Surgery, Izimisano Municipal Hospital, Rinku General Hospital, Izumisano, Osaka, Japan*
[5]*Graduate School of Environment and Life Science, Osaka prefectural University, Osaka, Japan*
[6] *Department of Neurosurgery, Kyoto Prefectural University, Kyoto, and CEO of Cancer Intelligence Care Systems, Inc., Tokyo, Japan*
[7]*Graduate School of Medicine, Sapporo Medical University of Medicine, Hokkaido, Japan*
[8]*Division of Electrical, Electronic and Information Engineering, Graduate School of Engineering, Osaka University, Japan*

Abstract

It is necessary to explore new treatments for recurrent head & neck malignancies to avoid severe impairment of oro-facial structures and functions (HNM). Boron neutron capture therapy (BNCT) is tumor-cell targeted radiotherapy that has significant superiority over conventional radiotherapies in principle.

We have treated with 42 times of BNCT for 26 patients (19 squamous cell carcinomas (SCC), 4 salivary gland carcinomas and 3 sarcomas) with a recurrent and far advanced HNM since 2001. Results are (1) ^{10}B concentration of tumor/normal tissue ratios (T/N ratio) of FBPA-PET studies were SCC: 1.8-5.7, sarcoma: 2.5-4.0, parotid tumor: 2.5-3.7. (2) Therapeutic effects were CR: 12cases, PR: 10cases, PD: 3cases NE (not evaluated):1case. Response rate was 85%. (3) Improvement of QOL such as a relief of severe pain, bleeding, and exudates at the local lesion, improvement of PS, disappearance of ulceration, covered with normal skin and preserved oral and maxillofacial functions and tissues. (4) Survival periods after BNCT were 1-72 months (mean: 13.6months). 6-year survival rate was 24% by Kaplan-Meier analysis. (5) Adverse-events were transient mucositis and alopecia in almost cases, 3osteomyelitis and 1brain necrosis were recognized. These results indicate that BNCT represents a new and promising treatment approach for advanced HNM.

Keywords: Head and neck cancer1, BNCT2, Epithermal neutron3, BPA4, BSH5

1. Introduction

Head and neck cancers are the sixth prevalent cancer in the world, with a global yearly incidence of 500,000. Although modest gains in local control and survival have been achieved with appropriate use of surgical intervention combined with radiation therapy and chemotherapy, in the last 20 years, 5-year survival rates for HNM have not improved significantly, remaining at 52% [1]. HNM are often radio- and chemo-resistant, necessitating a wide resection including the surrounding tissues, which results in severe impairment of oro-facial structures and functions. In this context, it is necessary to explore new applications for a full assessment of BNCT which may well benefit HNM. So we had started basic research used human- and murine-squamous carcinoma cell lines [2], [3] as well as other animal experimental model [4].

BNCT is a binary cancer treatment modality that involves the selective accumulation of ^{10}B carriers in tumors followed by irradiation with a epithermal neutron beam. The high energy transfer a α particles and recoiling ^{7}Li nuclei emitted during the capture of a thermal neutron in the ^{10}B (n, α) ^{7}Li reaction which carry an average total kinetic energy of 2.34 MeV, and have a short range (4-9um) of approximately one cell diameter, resulting in induction of a large relative biological effectiveness and selective

destruction of tumor cells containing ^{10}B. The clinical application of BNCT has been limited to advanced brain tumor [5], [6] and malignant melanomas [7]. We, first in the world, reported that six patients with HNM who have been treated with BNCT [8]. The clinical phase I and II trial of BNCT was recently reported [10]. The purpose of this study is to estimate of safety and efficacies of BNCT. We report here clinical results and outcome of 26 patients with HNM, who have been treated with BNCT in the Kyoto University Research Reactor Institute (KUR) and at Japan Atomic Energy Agency (JAEA) Reactor, JRR4 from December, 2001 to December, 2007.

2. Materials and Methods

Patients

The 26 patients with HNM were 19 squamous cell carcinomas (SCCs), 4 Salivary gland carcinomas and 3 sarcomas. All the patients but one had received standard therapy and had developed recurrent HNM for which there were no other treatment options. All the cases had the approval of the ethical committees, medical committee of KUR and that of Osaka University, Graduate School of Dentistry. Characteristics of 26 cases were summarized in Table 1.

^{18}F-BPA PET Study

The accumulation of BPA to tumor and normal tissue was imaged and quantified by ^{18}F- BPA-PET study before BNCT. The synthesis method and preparation of L-^{18}F-BPA and the choice of region of interests (ROIs) are detailed in our previous report [8].

Boron Compounds

A combination of borocaptate sodium (BSH) and para-borono- phenylalanine (BPA) were administered i.v. as ^{10}B-carriers in the first 13 times of BNCT in 10 cases (Table 1) [9]. The administration methods were written in the previous reports [8]. BPA (250mg/kg body weight) in fructose solution were administered intravenously for 1 hour. The epithermal neutron irradiation with KUR was started 12-hour and 1-hour after the administration of BSH and BPA, respectively. In the rest of 16 cases, BPA (250 or 500mg/kg body weight) alone were administered for1 or 2 hours, respectively followed by the epithermal neutron irradiation.

Measurement of Neutron Fluence, ^{10}B-concentration and Dose estimation

The distributions of neutron fluences, the physical doses of neutrons and gamma-rays were calculated by the dose-planning system "SERA" at KUR and "JCDS" at JAEA. Details of estimation methods of neutron fluence, ^{10}B- concentration and CBE and RBE-weighted doses were written in the previous reports [8].

3. Results

The results of all 26 cases are summarized in Table 1. Most of 26cases were recurrent and far advanced HNM such as 15 out of 26cases (58%) developed regional lymph node metastases and 6 out of 15 cases (40%) with lymph nodes metastases developed distant metastases.

So far for 6years, we have treated with 42 times of BNCT for 26 patients with a recurrent HNM since 2001. Results are as follows. (1) ^{10}B concentration of tumor/normal tissue ratios (T/N ratio) of PET studies were SCC: 1.8-5.7, sarcoma: 2.5-4.0, parotid tumor: 2.5-3.7. (2)Regression rates were CR: 12cases (46%), PR: 10cases (39%), PD: 3cases (12%), NE (not evaluated):1case. Response rate was 85%. 9 patients (35%) were disease free survival. (3)BNCT improved QOL, PS and survival periods. (4)Survival periods after BNCT were 1-72 months (mean: 13.6 months). 6-year survival rate was 24% by Kaplan-Meier analysis shown in Figure 1. (5) Adverse events were brain necrosis, osteomyelitis and transient mucositis and alopecia. Aphasia owing to the brain edema and necrosis in case1 had been transiently recovered, after treated with massive dose therapy of vitamin E and steroid hormone.

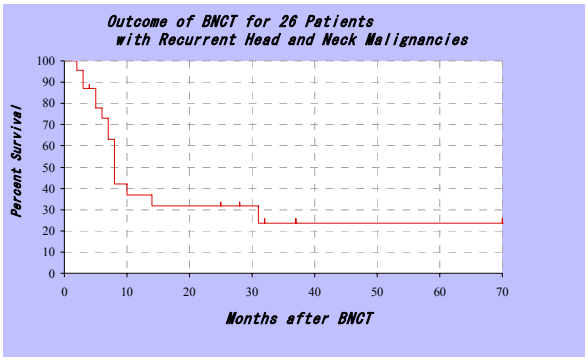

Figure 1. 6-Year Survival Rate of 26 Cases treated with BNCT were 24% by Kaplan-Meier Analysis

Typical cases which had been treated with BNCT are written here the clinical course of a disease.

Case 1: 5 times of BNCT has brought a patient with recurrent huge cancer disease free and long survival.

A 67-year-old woman was diagnosed as muco-epidermoid carcinoma (MEC) of parotid gland in 1998 and underwent a parotidectomy, followed by 45Gy of radiation therapy. In March 1999 the tumor had recurred and additional chemotherapy was ineffective. In October, 2001 the ulcerated tumor had grown to 13.5×12.5×8cm, which caused severe pain, bleeding and mucous exudates.

The first BNCT was performed using epithermal neutron in KUR under the administration of both BSH (5g) and BPA (250mg/kg) in December 2001. Although the tumor had shrunk to 63% during 1 month, the surface of the tumor had partially re-grown, we decided to performe the second BNCT, seated 5mm thickness gelatin-sheet on surface of the tumor in order to compensate insufficient radiation dose at the tumor-surface. The huge tumor had gradually shrunk to 18% of size of the original during one-year with relief of pain, decrease of exudates-secretion from the ulcer, disappearance of tumor ulceration and being covered with normal skin. As the tumor still had partially remained at retroauricular and subauricular portion, the third BNCT with 5mm thickness gelatin-sheet was performed in a sitting posture to set up the tumor closely to the collimator of KUR in December 2002. The tumor had shrunk to 6% and had remained the same size for about 3years [8]. In November 2005, the left neck had suddenly begun to swell with pain, tenderness and redness, PET-CT revealed that tumor had re-grown. The 4th and 5th BNCT had undergone in December 2005 and January 2006, respectively in KUR. The recurrent cervical tumor had been gradually disappeared, however, cervical skin defect had developed in April 2006. In August 2006, internal carotid artery had suddenly ruptured and she was transported to the ICU, which she could escape death. She has been disease free survival for 72 months.

Case 9: BNCT for a carcinoma which developed favorably nerve invasion in case of residual tumor after operation

A 61-year-old woman with a residual maxillary cancer infiltrating into pterygopalatine fossa (T4N1M0, adenoid cystic carcinoma) after maxillectomy was treated with 2 times of BPA mediated BNCT in September and October, 2004 (Figure 2A). In the first BNCT, BPA250mg/kg was administered intravenously (iv) and in the second BNCT, BPA250mg/kg was administered intra-arterially (ia). T/N ratio of ^{10}B concentration was 2.5 and 7.6 respectively. A peak of RBE, CBE-weighted total absorbed dose at the deepest tumor (7cm depth) was 14Gy-Eq in the first and that at deepest tumor (5.5cm depth) was 30Gy-Eq in the second BNCT. A peak of that at normal membrane was 11.6Gy-Eq in the first and that was 7.8 Gy-Eq in the second BNCT, respectively. A residual maxillary cancer and regional lymph node metastasis were disappeared about 7 months after 2 times of BNCT was followed by the chemotherapy (THP-ADR30mg ia, CDDP 48mg, CPA 480mg iv) as shown in Figure 2B. The primary tumor remains disappeared for so far 42 months although bilateral multiple lung metastases have developed 18 months the after first BNCT.

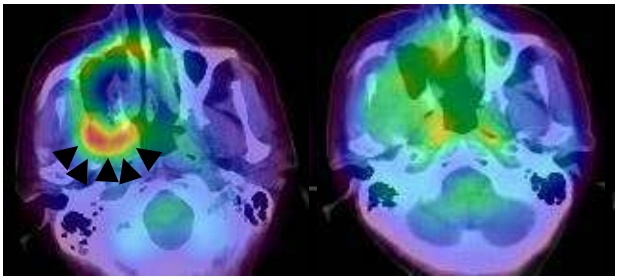

Figure 2A. FBPA-PET study in Case 9 prior to BNCT

A residual maxillary cancer (arrow heads) infiltrating into fossa pterygo-palatina (T4N1M0, adenoid cystic carcinoma) after maxillectomy was treated with 2 times of BPA mediated BNCT followed by the chemotherapy

Figure 2B: 7 months after the first BNCT

A residual maxillary cancer and regional lymph node metastasis remains disappeared for so far 42 months although bilateral multiple lung metastases were developed 18 months after the first BNCT

Case 12: BNCT for third primary carcinoma at head and neck region

A 78-year-old man with a recurrent oro-pharyngeal carcinoma (recurrence of third primary carcinoma) after the treatments for root of tongue carcinoma had no treatment options in January 2005. He had been suffered from the left tongue cancer (first primary carcinoma, T1N0M0) and treated with 70Gy of interstitial Ir-hair pin radiation therapy in 1980. He had treated with 64 Gy of radiation therapy for laryngeal carcinoma (Second primary carcinoma, T1aN0M0) in 1990. In February 2000, tongue carcinoma (third primary carcinoma, T2N1M0) had found and had treated with operation of Lt-Radical neck dissection, hemi-glossectomy, reconstruction of PMMC in March. About 20mm diameter of recurrent exophytic carcinoma at root of tongue had again excised in May, followed by 54Gy of external RT in June-July 2003. T/N ratio of ^{10}B concentration was 4.4. A recurrent oro-pharyngeal carcinoma (T1N0M0, SCC) had treated with 2 times of BPA mediated-BNCT in February and September 2005 in KUR. Both root of tongue carcinoma and middle pharyngeal carcinoma had disappeared 4 months after BNCT. The patient has been disease free survival for 34 months so far.

Case 14: Role of BNCT for the treatment of angiosarcoma

A 59-year-old man with the left maxillary gingival to buccal mucosa was diagnosed as angiosarcoma. Histopathological findings of H&E and immunohistochemical sections indicated that a network of anastomosing channels and solid areas immunoreactive for CD31 and CD34. So pathologists concluded angiosarcoma. T/N ratio of ^{10}B concentration estimated from FBPA-PET study was 2.5. Human recombinant IL-2 was intra-arterially administered and local injected for 2 weeks in April 2005. Aggressive growth was stopped and the tumor was not reduced in the size, treatment effect was NC. The tumor was removed surgically with 1cm safety margin in May 2005, followed by 2 times of BNCT in June and July. 3 times of immunotherapy, just after each BNCT and 1month after second BNCT were treated as adjuvant therapy. The patient has been disease free survival for 30 months so far.

Case 16: Role of BNCT for metastatic node of Rouviere in case of high-grade muco-epidermoid carcinoma

A 56-year-old man with the right buccal carcinoma (T4N2bM0, high-grade mucoepidermoid carcinoma) after operation, chemotherapy, developed metastatic node of Rouviere in July 2005. The patient did not choose surgical operation. T/N ratio estimated from FBPA-PET study was 3.7 (Figure 3A). The patient was treated with BPA mediated BNCT in September, 2005.The lymph node was 5.2cm depth from skin surface and RBE, CBE-weighted total absorbed dose was 22Gy-Eq in metastatic node, that in normal membrane was 12 Gy-Eq. FBPA-PET study at 2 months after BNCT showed no accumulation of FBPA (Figure 3B). The patient remains disease free survival for 27 months so far.

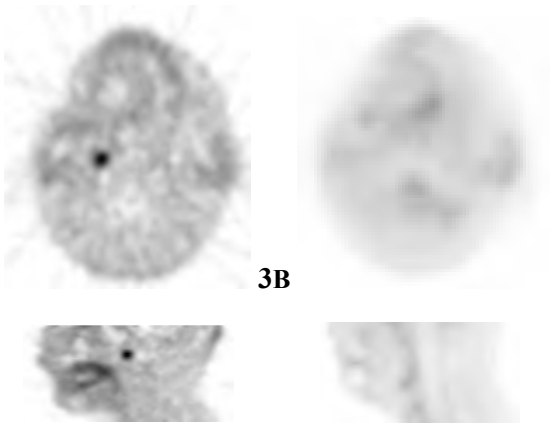

3A **3B**

Figure3A. FBPA-PET-study in Case 16 prior to BNCT

FBPA was accumulated in the Rouviere node

Figure 3B. 2 months after BNCT

No accumulation in the FBPA-PET 2 months after BNCT

Case 22: Role of BNCT for advanced maxillary sinus cancer invaded into orbital fossa and frontal lobe

A 56 year-old man with a recurrent maxillary sinus carcinoma (T4N1M0, SCC) after the trimodal combination therapy (52Gy of external radiationtherapy, CDDP: 113mg total ia and operation). Recurrent cancer was found at ethmoidal sinus and orbital region in November 2005.

Per os administration of TS-1 for 2 weeks and 1 week interval had lead to disappear the tumor on MR images.

As the recurrent tumor had again found at the inside of zygomatic bone, the multi-drug concomitant chemotherapy (TXT, CDDP, 5Fu) did not effective in October 2006. Selective intra-arterial chemotherapy (CDDP+STS) could not continue anymore because of side effects of CDDP such as dyspnea at fourth course of this chemotherapy in February 2007. FBPA-PET study revealed the cancer had a good accumulation and that T/N ratio was 5.7. During this period the tumor had invaded into orbital fossa and frontal lobe (Figure 4A). Then the patient was treated with BPA (500mg/kg) mediated BNCT in Research Reactor, JRR4 at JAEA in March 2007. A peak of RBE, CBE-weighted total absorbed dose at the mean GTV was 77Gy-Eq and lowest dose (5cm depth) was 35Gy-Eq. BNCT was followed by immunotherapy (CD3-LAK) and adjuvant chemotherapy of TS-1 for 6 months. These treatments had brought him complete response (CR) 6 months after BNCT (Figure 4B) and he has not only been disease free survival for 9 months but also he could save his left eye.

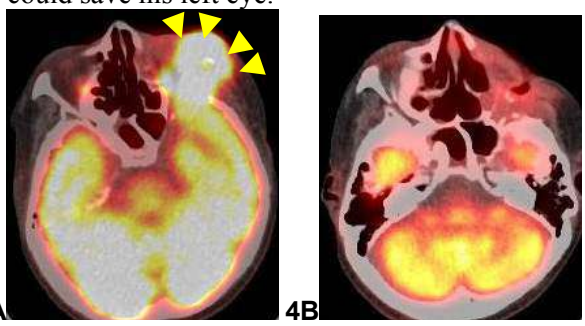

4A 4B

Figure 4A: FDG-PET study in Case 22 prior to BNCT

FDG tracer was accumulated in the left orbital region (arrow heads) and frontal lobe of brain

Figure 4B: 6 months after BNCT

No accumulation of FDG-PET was recognized 6 months after BNCT

4. Conclusions

Treatment modalities for HNM are now mainly limited to surgery, radiotherapy, chemotherapy and their combinations. As there is esthetic preference of patients, which should be considered, it is important for treatment modality to be able to preserve those structures and functions. To avoid severe impairment of oro-facial structures and functions, we had applied BNCT for extended indication for HNM and we could ascertain the effectiveness of BNCT for 22 out of 26 patients with advanced or recurrent HNM for which there were no other treatment options.

Merits of BNCT applying for HNM are as follows.

1. As there are important structures and functions in the head and neck regions and also there is esthetic preference of patients, it is possible for BNCT to preserve those structures and functions.
2. As field cancerization and multiple primaries cancers are especially popular in upper aerodigestive tract, it is important for BNCT to preserve those structures and functions in head and neck region.
3. Patients with a recurrent cancer who had been treated with full dose of radiation therapy could be contraindication for both conventional radiation therapy and the ion-beam therapy, but those who could be indication for BNCT.
4. For patients with the cancer infiltrating preferably into nerve or bone, it is difficult to be cured to get enough surgical margins, but BNCT make it possible to be cured because of tumor-selectivity.
5. Lymph node metastases or skin metastases which are difficult to be removed surgically should be also indication for BNCT.
6. T/N ratio of ^{10}B concentration estimated from FBPA-PET study could make the patients possible to predict their prognosis to some extent, because the higher T/N ratio is the better their prognosis will be.
7. There seemed to be high potential indication for patients with SCC, because their T/N ratios were relatively high such as 1.8-5.7 (mean 3.6).
8. Even if a tumor is radiation-insensitive or chemotherapy-insensitive, enough accumulation of ^{10}B in the tumor tissues should be expected to be good prognosis.
9. BNCT is less-invasive treatment modality compared with surgical operation.

Demerits of BNCT applying for HNM are as follows.

1. As neutron source now depends on research reactor, patients have to go to Research Reactor for BNCT.
2. BNCT is not so effective for deep-seated tumor more than 6cm from surface of the skin.

We are now under construction of the accelerator for BNCT. Many researchers are now investigating new boron compounds, drug delivery systems, administration methods for boron compounds and so on. These results indicated that BNCT represents a new and promising treatment approach even for a huge or far advanced HNM.

References

[1] Smith, D. and Haffty, B.G.. Radiat. Oncol. Invest. 1999; 7:125-144.

[2] Obayashi, S. et al., Delivery of 10 boron to oral squamous cell carcinoma using boronophenyl-alanine and borocaptate sodium for boron neutron capture therapy. Oral Oncology 2004; 40:474-482

[3] Kamida, A. et al., Effects of boron neutron capture therapy on human oral squamous cell carcinoma in a nude mouse model. International Journal of Radiation Biology 2006; 82(1): 21-29

[4] Kreimann E.L., Itoiz ME, et al, Boron neutron capture therapy for the treatment of oral cancer in the hamster cheek pouch medel. Cancer Res 2001, 6:8638-8642

[5] Slatkin, D.N., A history of boron neutron capture therapy of brain tumors. Postulation of a brain radiation dose tolerance limit. Brain 1991; 114:1609-1629

[6] Nakagawa, Y., Hatanaka, H. Boron neutron capture therapy: clinical brain tumor studies. J Neurooncol. 1997; 33: 105-115.

[7]Mishima, Y. et al., Treatment of malignant melanoma by single thermal neutron capture therapy with melanoma- seeking ^{10}B-compound. Lancet 1989; 39:325-333.

[8] Kato, I. et al., Effectiveness of BNCT for recurrent head and neck malignancies. Applied Radiation and Isotopes 2004; 61:1069-1073.

[9] Ono K., et al., The Combined effect of boronophenylalanine and borocaptate in boron neutron capture therapy for SCCVII tumors in mice. Int. J. Radiat. Oncol. Biol. Phys. 1999;43: 431-466

[10] Kankaanranta, L. et al., Boron neutron capture therapy in the treatment of locally recurred head and neck cancer. Int. J. Radiation Oncology Biol. Phys., 2007; 69 : 475-482

Table 1. Treatment Summary of 26 Cases treated with BNCT

Case	Gender	Age	No.	Boron compounds BSH /Body	BPA /kg	Histopathological Diagnosis	History RT (Gy)	Ope Y/N	Longest diameter (cm)	T/N ratio	Irradiation Time mean	Irradiation Time (min)	Criteria for Irradiation time DT:Deepest Tumor, M:Mucosa, S:Skin, N:Normal	Adverse event Mucositis NCI-CTC	Others	% Volume of Original	Survival (months)	Prognosis	Remarks
1	F	67	1	5g	250mg	MEC	50	Y	13.5	3.3	24.8+14.4	60	(DT22.9Gy・S5.5Gy)	<2		63%(1)			
			2	5g	250mg						23+14	75	(DT28Gy・S5.2Gy)	<2		18%(11)		disappearance of ulcer	
			3	5g	250mg					3.5	27~7.14	90	(DT10Gy・S5Gy)	<2	OM	6%(17)			no change in size for 34-month
			4	(−)	500mg					3.3	25	75	DT25Gy・(M17.5Gy)	<2	Brain necrosis				regrowth
			5	(−)	500mg					3.3	25	90→75	M16Gy(DT16Gy)→13.3Gy	<2			72	Alive	
2	M	61	1	5g	250mg	Osteosarcoma	68	Y	10.0	4.0		40		<2		46%(6)	8	DOC	PS:4→PS:2
3	M	56	1	5g	250mg	SCC	70	Y	4.0	1.8	35.4+12	120	(DT21.5Gy・S8Gy)	<2		PD	10	DOC	
4	F	60	1	5g	250mg	SCC	No	Y	11.0	4.4	50−11.4	77	(DT5.7Gy・S5Gy)	<2		27%(1)	1	DOC	disappearance of pain
5	M	73	1	5g	250mg	SCC	60	Y	8.0	4.0	35 11.3	100	DT36.5Gy(87.1Gy)	<2	OM	CR	7	DOI	Distant. Meta.
6	M	51	1	5g	250mg	SCC	No	Y	8.0	4.6	16.3+12	120	DT12.2Gy(N6.8Gy)	<2		NE	5	DOC	Distant. Meta.
7	F	58	1	5g	250mg	IPS	50	Y	7.0	3.1	23.6+12	120	DT14.4Gy(M6.1Gy)	<2		17%(1.5)		prevent eye ball from removing	
			2	5g	250mg					3.1	26.6+12	120	DT20Gy(N8.9Gy)	<2		8%(9)	31	Alive	Recurrence
8	M	53	1	(−)	250mg	MEC	No	Y	8.0	2.8	12	114	DT5.7Gy(N4.7Gy)	<2		8%(3)	3	DOC	Distant. Meta.
9	F	61	1	(−)	250mg	ACC	No	Y	4.0	2.5	15.5	100	DT14Gy(M11.6Gy)	<2		6%(1.5)		shrinkage of Meta.LN	
			2	(−)	250mg	IA			1.5	*7.6	22.3	66	DT30Gy(M7.8Gy)	<2		CR	39	Alive	Distant. Meta.
10	F	51	1	5g	250mg	SCC	No	Y	8.0	3.1	29+12	90	DT15Gy(M12.2Gy)	<2		10%(1.5)	3	DOI	
			2	(−)	250mg	IA			4.0	*4.3	15	60	DT12Gy(M7Gy)	<2					
11	F	77	1	5g	250mg	SCC	50	Y	5.0	4.4	30.3+11.4	51	M13Gy (DT34Gy)	<2		<5%(1)		shrinkage of Meta.LN	
			2	(−)	500mg				2.5		24	60	DT20Gy(M8.6Gy)	<2			6	DOC	Distant. Meta.
12	M	78	1	(−)	500mg	SCC	54	Y	4.0	4.4	24.0	82	DT20Gy(M10.8Gy)	<2		<5%	34	Alive	
			2	(−)	500mg	C-IV			2.0		25.0	60	DT20Gy(M10.6Gy)	<2				third primary carcinoma	
13	M	75	1	5g	500mg	SCC	45	Y	4.5	2.0	35.4+24	73	DT20Gy(M10.9Gy)	3		CR	14	DOC	
			2	(−)	500mg	C-IV			1.5		24.0	90	M12Gy(DT18Gy)	3				Recurrence of Meta. LN	
			3	(−)	500mg				2.0		22.0	90	(DT5.9Gy, M7.0Gy)	3		CR			
14	M	59	1	(−)	250mg*	Angiosarcoma	No	Y	3.0	"2.5"	15.0*	60	M15Gy(DT10.8Gy)	<2		CR	30	Alive	
			2	(−)	500mg				3.0		24.0	45	M15Gy(DT11.3Gy)	<2				treated as adjuvant therapy	
15	M	35	1	(−)	500mg	IA	SCC	85	N	9.0	3.5	IA55	33	M15Gy(DT6・20Gy)	<2		PD	2	DOC	
16	M	56	1	(−)	500mg		MEC	No	Y	0.9	3.7	25.3	60	M12Gy・DT22Gy	<2		CR	27	Alive	Ranvier's LN Meta.
17	M	63	1	(−)	500mg		SCC	64	Y	2.0	2.9	25.3	90	DT30Gy(M15.9Gy)	4			8	DOC	Distant. Meta(Lung).
			2	(−)	500mg					1.0			90	M10Gy(DT18Gy)	4		<5%			Multiple skin metastasis at bilateral neck
18	F	72	1	(−)	500mg	C-IV	SCC	50	Y	2.0	"3.7"	24.0	50	DT30Gy(M12.7Gy)	4		<5%(1)	8	DOC	Meta.LN
			2	(−)	500mg	C-IV				5.0	2.4		90	DT30Gy(M12.7Gy)	4					
			3	(−)	500mg	C-IV				5.0	2.4	18.0	120	DT15Gy	4					
19	M	57	1	(−)	>500	C-IV	SCC	60	Y	7.0	5.7	34.2	60	M15Gy・DT30Gy			<5%(1)	7	DOC	Meta.LN
			2	(−)	>500	C-IV				12.0		36.0	40	DT20Gy(M8.1Gy)	<2		20%			
20	M	55	1	(−)	500(360)		SCC	67	N	12.0	3.0	11.0*	60	DT20Gy(M8.1Gy)	<2		PD	1	DOC	Meta.LN
21	F	85	1	(−)	500mg	C-IV	SCC	74	Y	2.0	2.5	28.7	40	M13Gy	<2	OM	CR	8	DOC	Colon cancer
22	M	56	1	(−)	500mg	C-IV	SCC	52	Y	6.8	5.7	30.2	25	D:9.8(GTV:77, 35Gy)	<2		CR	9	Alive	Invasion to orbital fossa and frontal lobe
23	F	59	1	(−)	500mg	C-IV	SCC	64	Y	8.0	3.3	22.4	25	D:9.9(GTV:27,9.9Gy)	<2		PR	5	Alive	
24	F	57	1	(−)	500mg	C-IV	SCC	40+46	Y	4.0	2.9	19.2	35	D:9.3(GTV:35,17Gy)	<2		CR	7	Alive	Forth Cancer
25	M	47	1	(−)	500mg	C-IV	SCC	60−35	Y	6.0	3.3	24.2	42	D:10.1Gy(GTV59.3, 32.8Gy)	3		CR	5	Alive	
26	M	71	1	(−)	500mg	C-IV	SCC	60	N	5.7	2.9	27.0	36	D:10(GTV:40.1,26.9)	<2		CR	3	Alive	disappearance of pain

MEC: Mucoepidermoid Carcinoma, SCC. Squsmoid Cell Carcinoma, IPS. Inflammatory Fibrosarcoma, ACC: Adenoid Cystic Carcinoma, *:BPA(IA), G.5mmGelatin, T/N: ^{10}B conc. of Tumor/Normal, M: Male, F: Female, IA: Intra arterially, IV: Intra venously, C IV: Continuous IV, PD:Progressive Disease, CR:Complete Response, NE:Not Evaluated, OM: Osteomyelitis, DOC: Dead from cancer, DOI: death from an intercurrent cause

Boron Neutron Capture Therapy for Patients with Melanomas of Head-and-Neck

Kenji Fukutsuji[1], Teruhito Aihara[1], Junichi Hiratsuka[2], Hiroaki Kumada[3], Koji Ono[4], Yoshinori Sakurai[5], Hiroshi Fukuda[6], Norimasa Morita[1], and Yoshinari Imajo[2]

[1] *Department of otolaryngology, and* [2] *Department of Radiation Oncology Kawasaki Medical School, Japan,* [3] *Department of Research Reactor, Tokai Research Establishment, Japan Atomic Energy Research Institute, Japan*
[4] *Radiation Oncology Research Laboratory, Research Reactor Institute, Kyoto University, Japan*
[5] *Department of Physics, Sapporo Medical University School of Medicine, Japan*
[6] *Department of Nuclear Medicine and Radiology, Institute of Development, Aging and Cancer, Tohoku University, Japan*

Abstract

With the approval of the Nuclear Safety Bureau of the Japanese Government and the Medical Ethics Committees of Kawasaki Medical School and Kyoto University, we have conducted clinical trials on patients with mucosal melanomas in head-and-neck at the Japan Research Reactor No. 4 (JRR-4) since 2005.
To date, we have treated 10 patients with head-and-neck mucosal melanomas: 4 with melanomas in the nasal cavity (Nos. 1, 3, 8 and 9), 3 in the paranasal cavity (Nos. 5-7), 2 with metastatic melanomas of the neck lymphnodes (Nos. 4 and 10), and 1 in the lacrimal sac (No. 2).
The tumor/blood ratio obtained from 18F-BPA-PET study was adopted to the dose estimation before neutron irradiation and dose evaluation after BNCT using JCDS. The tumor/blood ratio of 3.0 was adopted when no tumor was detected by PET study due to small tumor volume. Neutron irradiation was performed using an epithermal beam at a reactor power of 3.5 MW after intravenous administration of BPA in fructose solution at a dose of 500 mg/kg body weight. The tumor dose at the deepest part and the dose of both normal skin and mucosa were planned more than 20 Gy-Eq and less than 15 Gy-Eq, respectively.
Four patients (Nos. 1, 3, 5 and 9) showed a complete response (CR) and 5 patients showed a partial response (PR). Only one patient (No. 7) showed no response. Two patients (Nos. 1 and 4) suffered from normal-tissue damage (both grade 2 RTOG/EORTC acute reaction). Both of them were cured within a few months. Four patients (Nos. 4, 5, 9 and 10) died due to distant metastasis. However, no local recurrence of melanoma has been observed in 2 CR patients and no regrowth of melanoma in 2 PR patients.
BNCT is a promising treatment for achieving local control of mucosal melanomas.

1. Background

A critical factor for enhancement of BNCT is the higher incorporation of ^{10}B into tumor cells relative to contiguous normal tissue[1]. ^{10}B-*para*-boronophenylalanine (BPA) accumulation is correlated with the high regulated amino acid transport system (the L system) in tumor cells [2]. Furthermore, BPA is maintained in melanoma cells by forming complexes with the melanin monomers such as 5,6-dihydroxyindole (DHI) and 5,6-dihydoroxyindole-2-carboxylic acid (DHICA) [3]. BNCT which is used clinically for malignant melanoma and uses BPA as the capture agent was developed by Mishima et al [4] who reported successful BNCT treatment of 18 cutaneous melanoma patients. In their study, the melanomas administered BNCT were cutaneous melanomas: nodular, superficial spreading, acral lentiginous, and lentigo maligna melanomas. Based on their treatment regimen and with the approval of the Nuclear Safety Bureau of the Japanese Government and the Medical Ethics Committees of Kawasaki Medical School and Kyoto University, we have conducted clinical trials on patients with mucosal melanomas in head-and-neck at the Japan Research Reactor No. 4 (JRR-4) since 2005.

2. Patients and Methods

To date, we have treated 10 patients with head-and-neck mucosal melanomas: 4 with melanomas in the nasal cavity (Nos. 1, 3, 8 and 9), 3 in the paranasal cavity (Nos. 5-7), 2 with metastatic melanomas of the neck lymphnodes (Nos. 4 and 10), and 1 in the lacrimal sac (No. 2).

Case	Tumor site	Age/Sex	T/N	Stage
1	nasal cavity	55/M	3	rT1
2	lacrimal sac	74/F	3	rT1
3	nasal cavity	73/M	3	T1
4	cervical lymph node	66/M	3	rT1N2b
5	paranasal cavity	73/F	3.1	rT4
6	paranasal cavity	74/M	2.7	rT2
7	paranasal cavity	69/M	3.7	T4
8	nasal cavity	74/F	3	rT1
9	nasal cavity	70/M	2.5	rT1
10	cervical lymph node	72/M	2.5	N2a

Table1. Patient characteristics

The tumor/blood ratio obtained from 18F-BPA-PET study was adopted to the dose estimation before neutron irradiation and dose evaluation after BNCT using JCDS. The tumor/blood ratio of 3.0 was adopted when no tumor was detected by PET study due to small tumor volume. Neutron irradiation was performed using an epithermal beam at a reactor power of 3.5 MW after intravenous administration of BPA in fructose solution at a dose of 500 mg/kg body weight. The tumor dose at the deepest part and the dose of both normal skin and mucosa were planned more than 20 Gy-Eq and less than 15 Gy-Eq, respectively.

3. Results

Four patients (Nos. 1, 3, 5 and 9) showed a complete response (CR) and 5 patients showed a partial response (PR). Only one patient (No. 7) showed no response. Two patients (Nos. 1 and 4) suffered from normal-tissue damage (both grade 2 RTOG/EORTC acute reaction). Both of them were cured within a few months. Four patients (Nos. 4, 5, 9 and 10) died due to distant metastasis. However, no local recurrence of melanoma has been observed in 2 CR patients and no regrowth of melanoma in 2 PR patients.

4. Conclusion

BNCT clinical trials using a thermal beam were conducted on patients with mucosal melanomas by means of BPA at an escalating dose of 500 mg/kg together with an epithermal beam. The clinical trial results indicate that modified melanoma-BNCT is a promising therapy for mucosal as well as cutaneous melanomas. BNCT is a promising treatment for achieving local control of mucosal melanomas.

References

[1] Y. MISHIMA, M. ICHIHASHI, C. HONDA et al., *Progress in Neutron Capture Therapy for Cancer*. pp. 577-683, Plenum. New York. (1992).

[2] A. WITTIG, W.A. SAUERWEIN, J.A. CODERRE et al., "Mechanisms of Transport of p-Borono-Phenylalanine through the Cell Membrane In Vitro," *Radiat Res*., **153**, 173 (2000).

[3] K. YOSHINO, Y. MISHIMA, M. KIMURA et al., *Advances in Neutron Capture Therapy.* pp. 234-238, Elsevier. Amsterdam. (1997).

[4] Y. MISHIMA, C. HONDA, M. ICHIHASHI et al., "Treatment of Malignant Melanoma by Single Thermal Neutron Capture Therapy with Melanoma-Seeking 10B-Compound," *Lancet*., **12**, 388 (1989).

Case	Tumor Response	Complications: (RTOG/EORTC score)	Follow-up	Dead or alive
1	CR	G2	35m	Alive
2	PR	G1	27m(local:27m)	Alive
3	CR	G1	27m(local:14m)	Alive
4	PR	G1	18m(distant;liver:17m)	Dead
5	CR	G1	10m(distant;brain:9m)	Dead
6	PR	G1	9M(distant;lumbar:7m)	Dead
7	NC	G1	17m(local)	Alive
8	PR	G1	17m(local:15m)	Alive
9	CR	G1	7m(distant;lung:6m)	Dead
10	PR	G1＋laryngealedema	6m(distant;brain:6m)	Dead

Table2. Therapeutic effect

Boron neutron capture therapy for recurrent oral cancer and metastasis of cervical lymphnode

Y. Kimura[a], Y. Ariyoshi[a], M. Shimahara[a], S. Miyatake[b], S. Kawabata[b], K. Ono[c], M. Suzuki[c], A. Maruhashi[d]

[a] Department of Dentistry and Oral Surgery, Division of Surgery 2, Osaka Medical College.
[b] Department of Neurosurgery, Division of Surgery 1, Osaka Medical College.2-7 Daigaku-machi Takatsuki city Osaka 569-8686,Japan ,[c] Particle Radiation Oncology Research Center, Research Reactor Institute, Kyoto University.[d] Medical Physics, Department of radiation Life Sciences, Research Reactor Institute, Kyoto University.Kumatori-cho,Sennan-gun,Osaka590-0494,Japan

Abstract

Recurrent oral cancer and metastasis to the cervical lymph nodes often resist chemotherapy and radiotherapy treatments, and invade surrounding tissues. We treated 6 patients with recurrent oral cancer and metastasis to the cervical lymph nodes after conventional treatments in 5 and non-conventional in 1 using BNCT, and herein report our results. In 5 cases, spontaneous pain decreased immediately after BNCT. Osteomyelitis of the maxillary bone and xerostomia did not appear in any of the cases. Mucositis was seen in all, however, it was milder as compared to that seen in cases treated by conventional radiotherapy. The clinical response in our patients ranged from CR-PD. Three of the 6 are alive at the time of writing and we found that BNCT contributed to QOL improvement in all.

Keywords: boron neutron capture therapy (BNCT) ,oral cancer, boronophenylalanine(BPA)

1. Introduction

A radical operation for recurrent and progressive oral cancer is functionally and aesthetically difficult, due to anatomical complexity, while chemotherapy or radiotherapy do not generally result in a radical cure. Oral cancer causes intense pain and makes eating by mouth difficult when advanced, thus markedly reducing patient quality of life (QOL). We have performed boron neutron capture therapy (BNCT) in 6 patients with recurrent oral cancer since introducing the method at our institution in 2005. BNCT is a type of tumor-selective radiotherapy , in which cancer cells are destroyed by alpha and ^{7}Li particles generated by the nuclear reaction between boron (^{10}B) uptake in the tumor and thermal or epithermal neutron.(Coderre J A, et al,1999) It has excellent clinical characteristics and is superior in regard to local control effects. Moreover, pain is controlled with the therapy, while serious mucositis and osteomyelitis of the maxillary bone do not develop.

2. Patients

We treated 6 patients (3 males, 3 females; age range 32-82 years old) with recurrent oral cancer and metastasis to the cervical lymph nodes. Each had suffered a recurrence after conventional therapy, such as surgery, chemotherapy, or radiotherapy, although 1 case was not treated by conventional treatment and included in the present analysis (Table 1). Histopathological findings revealed 2 cases of squamous cell carcinoma, 2 cases of adenocarcinoma, 1 case of mucoepidermoid carcinoma, and 1 case of melanoma. Prior to BNCT, informed consent was obtained from all of the subjects, and the study protocol was approved by the ethical committees of Osaka Medical College and Kyoto University Research Reactor Institute.

3. Methods

The distribution of boronophenylalanine (BPA), used as a boron compound, in the tumor and surrounding healthy tissue can be visualized using a two-dimensional image obtained by an ^{18}F-BPA-PET examination,which was conducted to evaluate BPA uptake in the tumors in all of the present cases (Fig.1) (Imahori,et al,1998). From those results, the

difference in boron concentration (T/N ratio) between the tumor and normal tissues was determined. For the boron compound, BPA at 500 mg/kg of body weight was administered intravenously by drip infusion starting from 2-3 hours before and during irradiation. In Case 2, sodium borocaptate (BSH) at 2g/body weight was used concomitantly. For neutron irradiation, a research reactor (KUR) with an output of 5 MW located at Kyoto University Research Reactor Institute was utilized. We used the BNCT exposure dose planning system SERA for estimating and evaluating the neutron flux distribution, as well as the distribution of the absorbed dose of epithermal neutrons high-speed neutrons and gamma rays. A gold wire set used for measurement was removed at 10 minutes after the start of irradiation to evaluate epithermal neutron flux on a collimator Bi surface at a point 25 cm from the center and at the center of the irradiation field on the affected surface. The full-time exposure dose on the surface adjacent to the affected portion was determined by measuring neutron fluence (nvt) using gold and manganese wires. The absorbed dose of gamma rays was measured using a TLD (BeO), with the gold wire and TLD set in the vicinity of the center of the affected surface. The ^{10}B concentration in blood was determined by collecting venous samples every 30 minutes after BPA administration until just before irradiation, as well as after irradiation for prompt gamma radiation measurement.

Following BNCT, the tumor regression, adverse side effects, survival time, and subjective symptoms were recorded. For evaluating adverse side effects, the Common Terminology Criteria for Adverse Events v3.0 (CTCAE v3.0) was used. Tumor regression was evaluated by CT and MR imaging.

4. Results

T/N ratios calculated on the basis of the ^{18}F-BPA-PET results ranged from 1.9-4.0, with the squamous cell carcinoma cases rated as 3.4-4.0, adenocarcinoma cases as 2.4-3.2, mucoepidermoid carcinoma case as 2.2, and melanoma case as 1.9. The maximum dose to the tumor (Gy-Eq) was 20.1-35.5 Gy-Eq and the minimum 9.12-31.9 Gy-Eq, while the dose to the oral mucosa was 9.03-15.7 Gy-Eq and to the skin was 2.81-7.64 Gy-Eq (Table 2). Tumor reduction was rated as PR in 4 cases, while 1 case was CR and 1 was PD. (Fig.2)Notably, in Case 2 with metastasis to the lymph nodes that was within the BNCT irradiation range, the reduction was rated as CR (Fig.3).

As for clinical improvement, pain was alleviated in all 5 cases in which pain was observed before the study and difficulty eating was improved in each of those. Especially in Cases 1 and 4, the patients, who were forced to stay in the hospital due to pain and difficulty eating, were temporarily discharged after BNCT. In Case 5, bleeding from the tumor was reduced. For adverse side effects, mucositis, fatigue, alopecia, impaired taste, and pharyngeal edema were observed, although none was severe. Neither myelosuppression nor osteomyelitis of the maxillary bone was observed.

Three of the 6 patients survived for a range of 23-29 months after the final BNCT. In Case 1, a tumor in the cervical lymph node was markedly reduced after BNCT, then later became enlarged, which led to death from aspiration pneumonia 4 months later. In Case 2, a tumor in the cervical lymph node was reduced to the level of CR and the patient died from lung metastasis 16 months later. In Case 4, the tumor enlarged after therapy and the patient died 13 months later. The other 3 patients were alive at the time of writing. (Table 3)

5. Discussion

^{10}B, a stable isotope of boron that captures a low-energy neutron, splits off into alpha-particles and Li atomic nuclei. Their ranges are about 9 and 4 micrometer, respectively, which are equivalent to the size of a tumor cell. BNCT makes use of the reaction and selectively destroys tumor cells by causing low-energy neutrons to react with ^{10}B preliminarily uptaken by tumor cells. The therapy was performed for the first time in 1954 by Farr et al. for glioblastoma multiforme, after which Kato et al. began to utilize it for head and neck cancer that had relapsed after initial treatment, and reported 11 cases in 2004.

Oral cancer in the early stage of T1 or T2 is frequently treated with surgery. However, it is difficult to obtain a radical cure for progressive or

recurrent cancer after completion of the initial treatment, even if multimodal approaches such as surgery, radiotherapy, and chemotherapy are used. Accordingly, improvements in therapeutic performance are not encouraging, unless some new therapeutic strategies are developed. We have been performing BNCT treatment for recurrent cancer that relapsed after completion of initial treatment, including surgery, chemotherapy, conventional radiation therapy, and thermotherapy, since 2005.

In BNCT, tumor cells are made to uptake boron and then selectively destroyed. This reduces the impact on normal cells, thus adverse effects can be alleviated. In the present 6 cases, myelosuppression and skin lesions, normally seen with conventional radiation therapy, were not observed. Notably, osteomyelitis of the maxillary bone, which often develops after conventional radiation therapy for oral cancer, was not seen. These findings are extremely significant clinically, as osteomyelitis of the maxillary bone after radiation therapy can induce infection and fracture, which causes difficulty in dealing with the intense pain. In addition, the mucositis and fatigue observed in most cases were mild and rated as grade 2 or lower.

As for clinical response, 4 cases were rated as PR, with 1 case each as PD and CR. Case 2 is quite interesting. In this patient, BNCT was performed for metastasis to the cervical lymph nodes after initial surgery and chemotherapy for melanoma in the maxillary gingiva. With melanoma, the presence of metastasis to the lymph nodes affects the prognosis, as the 5-year survival rate is 39% for cases with metastasis to the lymph nodes, whereas it is 80% for negative cases(Goldsmith,1970). Our patient died from lung metastasis at 16 months after BNCT. However, MR revealed that the metastasis had completely disappeared from the cervical lymph nodes where BNCT was administered (Fig.3), suggesting the effectiveness of BNCT for highly-malignant melanoma.

The mouth has a variety of functions such as eating and talking, as well as aesthetic qualities. These functions are disturbed easily as oral cancer progresses, while QOL is severely affected when pain is added. BNCT is effective not only for reducing the size of the tumor, but also in controlling pain and decreasing bleeding, thus contributing to QOL improvement. The most important goal of this therapy is tumor disappearance, complete cure, and reintegration of the patient into normal life. However, this is yet to be achieved.

The success and failure of BNCT is dependent on if the B^{10} compound can be selectively uptaken by the nuclei of the tumor cells. Miyatake et al(2005). reported using two kinds of boron compounds, BPA and BSH, with BNCT for malignant brain tumors to increase the ^{10}B concentration. In Case 2, we aimed at the cervical lymph nodes as the target and used BPA as the boron compound during the first irradiation. However, since the tumor peak dose was low at 20.1 Gy-Eq, we used BHS concomitantly during the second irradiation. As a result, the tumor peak dose elevated to 35.5 Gy-Eq and the target lymph nodes attained CR.

In the present study, all of the cases were recurrent or metastatic cancer after the completion of an initial treatment, although the number of cases presented is small. We considered that these patients might face difficulties not only with the therapeutic effect on the tumors, but also QOL improvement, if treated by conventional treatment. Although BNCT could not bring about a complete cure it greatly improved the QOL of each patient without causing serious adverse side effects. For BNCT for the stomatognathic region, additional detailed studies are necessary in regard to the method of fixing and positioning the patient. In a future study, we intend to investigate the detailed clinical and basic viewpoints to realize a more effective treatment method.

References

Coderre JA , Morris GM, 1999.The Radiation Biology of Boron Neutron Capture Therapy. Radiation Res.151. 1-18.

Farr LE, Sweet WH, Robertson JS,et al.1954. Neutron Capture Therapy with Boron in the Treatment of Glioblastoma Multiforme. Am J Roentogenol .71. 279,

Goldsmith,H.S.1970.Prognostic significance of lymphnode dissection in the treatment of malignant melanoma.Cancer.26.606-609,

Imahori Y.,Ueda S.,Omori Y.,et al.1998:Fluorine-18-labeled fluoroboronphenylalanine PET in

patients with glioma:J.Nucl.Med.39.325-333.
Kato I, Ono K, Sakurai Y, et al. 2004. Effectiveness of BNCT for recurrent head and neck malignancies. Appl Radiat Isot Nov,61(5).1069-73.
Miyatake S.,Kawabata S.,Kajimoto Y.,et al.2005. Modified boron neutron capture therapy for malignant gliomas performed using epithermal neutron and two boron compounds with different accumulation mechanisms. J Neurosurg.:1000-1009.

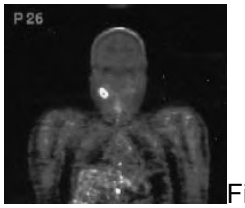

Figure 1. ^{18}F-BPA-PET

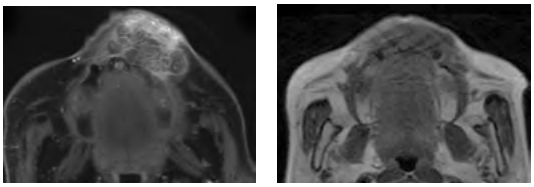
Figure 2. Case 3: Left: MR image taken before BNCT. Right: MR image taken after BNCT.

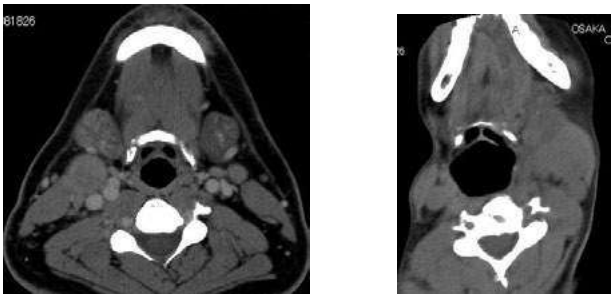

Figure 3. Case 2:Left: MR image taken before BNCT. Right: MR image taken after BNCT.

Table 1. Characteristics of Patients

Case	Age/sex	Location	Histopathological diagnosis	Previous treatment	Symptoms
1	41/M	Cervical lymph node	SqCC	S, CH, Ra	ED, Pa
2	32/M	Cervical lymph node	Melanoma	S, CH	
3	82/F	Upper lip	AC	Th	ED, Pa
4	57/M	Maxilla	SqCC	S, CH, Ra	ED, Pa
5	67/F	Maxilla	MC	S, CH, Ra	ED, Pa、B
6	69/F	Maxilla	AC	S, CH, Ra	ED, Pa

SqCC: squamous cell carcinoma, AC: adenocarcinoma, MC: mucoepidermoid carcinoma,
S: surgery, CH :chemotherapy, Ra: conventional radiotherapy, Th: thermotherapy,
ED: eating disorder, Pa: pain, B: bleeding

Table 2. Parameters of BNCT

Case		Boron compound	T/N ratio of 18F-BPA	**Dose (Gy-Eq)**			
				Skin surface	Oral mucosa	Tumor peak	Tumor minimum
1	1	BPA	4.0	4.93	14.4	39.1	15.0
	2	BPA		2.85	9.52	25.5	10.3
2	1	BPA	1.9	4.6	14.4	20.1	15.7
	2	BPA+BSH		7.64	15.7	35.5	29.0
3	1	BPA	3.2	4.1	15.4	34.6	31.9
	2	BPA		3.59	12.9	28.8	27.9
4	1	BPA	3.4	3.22	9.13	21.6	9.12
	2	BPA		2.81	9.03	21.1	20.4
5	1	BPA	2.2	3.74	15.3	24.8	22.0
6	1	BPA	2.4	7.2	15.0	38.3	17.1

Table 3. Clinical results

Case	Clinical response □	Clinical response□	Adverse side effects (grade)	Outcome (duration after BNCT)
1	PD	DP, IE	M (2), F (1)	Died (4 months)
2	CR		M (3), F (1), AL (1), I (1), PE (2)	Died (16 months)
3	PR	DP, IE	M (2), F (1)	AD
4	PR	DP, IE	M (1), F (1)	Died (13 months)
5	PR	DP, IE, DB	M (1), AL (1)	AD
6	PR	DP, IE	M (2), F (1)	AD

DP: decreased pain, IE: improved eating, DB: decreased bleeding, M: mucositis, F: fatigue, AL: alopecia, I: impaired taste, PE: pharyngeal edema, AD: alive with disease,

Dose distribution and clinical response of glioblastoma treated with external beam boron neutron capture therapy

Masahide Matsuda[1], Tetsuya Yamamoto[1], Hiroaki Kumada[2], Kei Nakai[1], Makoto Shirakawa[1], Takao Tsurubuchi[1], Akira Matsumura[1]

[1] *Department of Neurosurgery, Graduate School of Comprehensive Human Science, University of Tsukuba, Tennodai 1-1-1, Tsukuba, Japan*

[2] *Japan Atomic Energy Agency, Shirakatashirane2-4, Tokai, Japan*

Abstract

The dose distribution and failure pattern after treatment with the external beam BNCT protocol were retrospectively analyzed.

BSH(5g/body) and BPA(250mg/kg) based BNCT was performed in 8 patients with newly diagnosed glioblastoma. The gross tumor volume (GTV) and clinical target volume (CTV)-1 were defined as the residual gadolinium-enhancing volume. CTV-2 and CTV-3 were defined as GTV plus a margin of 2cm and 3cm, respectively. As additional photon irradiation, a total X-ray dose of 30 Gy was given to the T2 high intensity area on MRI.

Five of 8 patients were alive at analysis for a mean follow-up time of 20.3 months. The post-operative median survival time of the 8 patients was 27.9 months (95%CI= 21.0-34.8). The minimum tumor dose of GTV, CTV-2, and CTV-3 averaged 29.8±9.9 Gy, 15.1±5.4 Gy, and 12.4±2.9 Gy, respectively. The minimum tumor non-boron dose of GTV, CTV-2, and CTV-3 averaged 2.0±0.5 Gy, 1.3±0.3 Gy, and 1.1±0.2 Gy, respectively. The maximum normal brain dose, skin dose, and average brain dose were 11.4±1.5 Gy, 9.6±1.4 Gy, and 3.1±0.4 Gy, respectively. The mean minimum dose at the failure site in cases of in-field recurrence (IR) and out-field recurrence (OR) were 26.3±16.7 and 14.9 GyEq, respectively.

The calculated doses at the failure site were at least equal to the tumor control doses which were previously reported. We speculate that the failure pattern was related to an inadequate distribution of boron-10. Further improvement of the microdistribution of boron compounds is expected, and may improve the tumor control by BNCT.

Keywords: Glioblastoma, external beam BNCT, failure pattern

Introduction

The glioblastoma (GBM) is a radioresistant malignant brain tumor that shows wide microscopic invasion to the surrounding normal brain tissue. Investigations have revealed the presence of microscopic invading cells at distances of 2 to 3 cm or even further from the main tumor mass that can be clinically identified by contrast enhancement area on a magnetic resonance image (MRI), and that are found in the microsurgical field during surgical operation (Wallner, 1989. Gasper, 1992. Fitzek, 1999).

A previous study reported that a dose of 90 Gy in accelerated fractionation with photon and proton irradiation almost completely prevented central recurrence, extending the median survival time (MST) of GBM patients to 20 months. In this radiation protocol, recurrence occurred in areas immediately peripheral to the 90 Gy volume, mostly in the 70-80 Gy volume, and radiation necrosis also frequently occurred (Fitzek, 1999). Survival benefit by high-dose photon radiotherapy has been also reported (Tanaka et al., 2005). However, randomized trial with stereotactic radiosurgery followed by photon radiation did not improve the outcome in terms of survival and quality of line (Souhami, 2004).

Our boron neutron capture therapy (BNCT) protocol allows a higher dose compared to conventional radiotherapy (i.e. 60 Gy/30fr) delivered in single session. However, dose analyses such as those performed for proton irradiation have been rarely performed for BNCT and details of the failure pattern after BNCT remain unknown. To determine tumor control dose in GBM patients who underwent BNCT, the relation between the dose

distribution and failure pattern after BNCT were compared in this study.

Materials and Methods

Patient characteristics. The patients consisted of 2 males and 6 females aged 32 to 76 years old (median 65 years), with Karnofsky Performance Scores (KPS) of 50 to 90. All tumors located within 7 cm from the brain surface —with histologically confirmed glioblastoma—were treated with the external beam BNCT; the first case was treated in August, 2005.

Boron administration and boron measurement. Twelve hours before neutron irradiation, sulofhydryl borane $Na_2B_{12}H_{11}SH$ (BSH) (5g/body) in 500 ml saline solution was intravenously injected over 1 hour. A water soluble fructose complex of *p*-dihydroxyboryl-phenylalanine (BPA) (250mg/kg) was also given 1 hour before irradiation. The mean blood boron level during the irradiation was estimated based on a clearance curve delineated by using serial blood samples. These blood samples were measured by inductively coupled plasma atomic emission spectroscopy and prompt gamma-ray spectroscopy.

External beam neutron irradiation. Neutron irradiation was performed in a single fraction using an epithermal beam mode of JRR-4. In the in-air beam characteristics, epithermal neutron flux (0.53eV-10keV) and the γ ray absorbed dose were 2.2×10^9 n $cm^{-2}sec^{-1}$ and 2.4 Sv/h, at a reactor power of 3.5 MW, respectively (Yamamoto, 2003). The gross tumor volume (GTV) and clinical target volume (CTV) -1 were defined as the residual gadolinium-enhancing volume. CTV-2 and CTV-3 were defined as GTV plus a margin of 2cm and 3cm, respectively.

Additional photon irradiation. All cases were given an additional photon dose of 30 Gy in 15 fractions, was delivered to the high intensity area on T2-weighted MR images to compensate for an insufficient dose distribution.

Patient follow-up and data analyses. All patients were followed-up clinically and by MRI every 1-3 months. Neurological events and MRI findings were compared to the dose distributions of the individual dose components. A tumor-to-blood ^{10}B concentration ratio of 1.0 was used to estimate the boron dose delivered to the tumor tissue.

Results and Discussion

The mean follow-up time was 20.3 months, and 5 of 8 patients were alive at analysis. The post-operative median survival time of the 8 patients was 27.9 months (95%CI= 21.0-34.8). The median MRI-progression-free survival time of the 8 patients was 14.8 months (95%CI= 9.7-19.9).

The mean blood boron concentrations of BSH and BPA during irradiation were 34.9 ± 9.6 ppm and 17.4 ± 2.4 ppm, respectively. The minimum tumor doses of GTV, CTV-2, and CTV-3 averaged 29.8 ± 9.9 GyEq, 15.1 ± 5.4 GyEq, and 12.4 ± 2.9 GyEq, respectively. The minimum tumor non-boron doses of GTV, CTV-2, and CTV-3 averaged 2.0 ± 0.5 Gy, 1.3 ± 0.3 Gy, and 1.1 ± 0.2 Gy, respectively (Fig. 1). The maximum normal brain dose, skin dose, and average brain doses were 11.4 ± 1.5 Gy, 9.6 ± 1.4 Gy, and 3.1 ± 0.4 Gy, respectively. In cases with higher blood boron levels related to higher tumor boron dose and lower non-boron dose content, the total BNCT dose had been planned not to exceed a given peak dose to the normal brain.

In the first 24 months of the follow-up period, 6 recurrences were observed, 5 in-field (IR) , defined as tumor progression within CTV-2, and 1 out-field (OR). No difference was seen in the extent of surgical resection, or blood boron level among the 3 groups.

The mean minimum tumor doses of GTV in LC, IR and OR were 32.2 ± 8.5, 30.3 ± 11.7 and 22.1 GyEq, respectively. The mean minimum doses at the failure site in IR and OR were 26.3 ± 16.7 and 14.9 GyEq, respectively (Fig. 2).

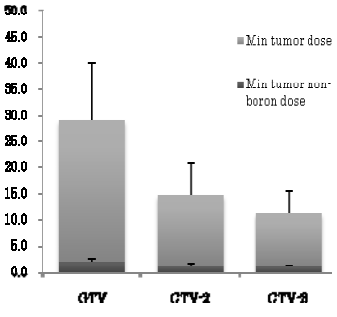

Fig.1 The minimum tumor dose and non-boron dose of 8 patients.

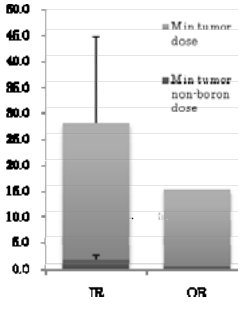

Fig.2 Averaged minimum tumor dose and non-boron dose in 6 patients with tumor recurrence and their failure patterns.

Treatment failure in BNCT may occur because of low boron concentration in tumor, insufficient or heterogeneous delivery of thermal neutrons, heterogeneity of the boron distribution, problems with target setting, and size of the residual tumor. In our series, the calculated doses at the failure site on the assumption that boron distribution was homogeneous were at least equal to the tumor control doses which were previously reported. This suggests that the microdistribution of the boron compound was more heterogeneous than expected, although, theoretical homogeneous preferential accumulation of boron-10 in the tumor cells is essential for tumor control in BNCT. It is speculated that the failure pattern was related to an inadequate distribution of boron-10. In the second case, a recurrence occurred at the site where a calculated dose of 76.4 Gy in single session and X-ray dose of 30 Gy in 15 fractions had been irradiated. From this fact, excessive dose escalation cannot be warranted. In the future, new tumor-targeting boron agents, tumor-targeting delivery systems, and combinations with other modalities such as new chemotherapeutic agents are expected.

Conclusion

In a group of 8 patients treated with external beam BNCT, the post-diagnosis median survival time and the median progression-free survival time were 27.9 months and 14.8 months, respectively.

According to the analysis of the failure patterns, the mean minimum doses at the failure site in cases of IR and OR were 26.3 ± 16.7 and 14.9 GyEq, respectively. When we think based on calculated dose, considerable high dose becomes necessary. Further improvement of the microdistribution of boron compounds is expected before excessive dose escalation.

Acknowledgements

This study was supported in part by a Grant-in-Aid from the Ministry of Education, Science and Culture, Japan (20390379).

Following the 2005 policy of the International Committee of Medical Journal Editors (ICMJE), the later stage of this trial (EB-NCT) was registered with the Japanese authority on clinical trial registration (University Hospital Medical Information Network Clinical Trial Registry: UMIN-CTR; Trial ID: C000000298).

References

Fitzek, M.M., Thornton, A.F., Rabinov, J.D., Lev, M.H., Pardo, F.S., Munzenrider, J.E., Okunieff, P., Bussiere, M., Braun, I., Hochberg, F.H., Hedley-Whyte, E.T., Liebsch, N.J., Harsh, G.R 4th,. 1999. Accelerated fractionated proton/photon irradiation to 90 cobalt gray equivalent for glioblastoma multiforme: results of a phase II prospective trial. J Neurosurg. 91, 251-260.

Gasper, L.E., Fisher, B.J., Macdonald, D.R., LeBer, D.V., Halperin, E.C., Schold Jr., S.C., Cairncross, J.G. 1992. Supratentorial malignant glioma: Patterns of recurrence and implications for external beam local treatment. Int J Radiat Oncol Biol Phys. 24, 55-57.

Oppitz, U., Maessen, D., Zunterer, H., Richter, S., Flentje, M., 1999. 3D-recurrence-patterns of glioblastomas after CT-planned postoperative irradiation. Radiotherapy and Oncology. 53, 53-57.

Souhami, L., Seiferheld, W., Brachman, D., Podgorsak, E.B., Werner-Wasik, M., Lustig, R., Schultz, C.J., Sause, W., Okunieff, P., Buckner, J., Zamorano, L., Mehta, M.P., Curran Jr., W.J. 2004. Randomized comparison of stereotactic radiosurgery followed by conventional radiotherapy with carmustine to conventional radiotherapy with carmustine for patients with glioblastoma multiforme: report of Radiation Therapy Oncology Group 93-05 protocol. Int J Radiat Oncol Biol Phys. 60, 853-860.

Tanaka, M., Ino, Y., Nakagawa, K., Tago, M., Todo, T., 2005. High-dose conformal radiotherapy for supratentorial malignant glioma: a historical comparison. Lancet Oncol. 6, 953-960.

Wallner, K.E., Galicich, J.H., Krol, G., Arbit, E., Malkin, M.G., 1989. Patterns of failure following treatment for glioblastoma multiforme and anaplastic astrocytoma. Int J Radiat Oncol Biol Phys. 16, 1405-1409.

Yamamoto, T., Matsumura, A., Yamamoto, K., Kumada, H., Hori, N., Torii, Y., Shibata, Y., Nose, T. 2003. Characterization of neutron beams for boron neutron capture therapy: In-air radiobiological dosimetry. Radiat Res 160, 70-76.

The peptide modified BSH highly uptaking into the glioma cells

Hiroyuki Michiue[1,3], Tomizawa Kazuhito,[1] Shin-ichi Miyatake[2], Shinji Kawabata[2], Shiro Miyata[2], Tomotugu Ichikawa[3] Toshihiko Kuroiwa[2] ,Isao Date[3], Hideki Matsui[1], Mitsunori Kirihata[4], Koji Ono [5]

[1] *Department of Physiology, Okayama University Graduate School of Medicine, Dentistry and Pharmaceutical Sciences, Japan*
[2] *Department of Neurosurgery, Osaka Medical College, Japan*
[3] *Department of Neurological Surgery, Okayama University Graduate School of Medicine, Dentistry, and Pharmaceutical Sciences, Japan,*
[4] *Department of Agriculture, Osaka Prefectural University, Japan*
[5] *Particle Radiation Oncology Research Center, Research Reactor Institute, Kyoto University, Japan*

Boron neutron capture therapy (BNCT) is a targeted approach to radiotherapy that significantly increases the therapeutic ratio against the malignant brain tumor relative to conventional radiotherapeutic modalities. In our BNCT group, we use the two kinds of Boron compounds in the clinical field (2001, Miyatake et al). One is the boronophenylalanine (BPA) and the other is sodium borocaptate (BSH). These two compounds works in the different uptaking mechanisms and compensates for each other's faults. But one of the most difficult problem is that the BSH can not get into the cell. To improve the effectiveness of BSH delivery, we modified the peptide to the BSH.

We observed the BSH localization in the microscope and confirmed the BSH in the glioma cells. This modified BSH could get into the glioma cell very effectively. We want to show the effectiveness of this modified BSH compound compared to the traditional BSH compound. In future, we think this modified BSH compound can become good help in clinical BNCT field.

Determination of Boronophenylalanin (BPA) in healthy liver and tumour tissue of patients with liver metastasis of colorectal carcinoma

Shahin Minouchehr[1], Gabriele Hampel[2], Christian Schütz[2], Sven Nagels[3], Saverio Altieri[4], Sabina Stella[4], Silva Bortolussi[4], Gerd Otto[1]

[1]Transplantationschirurgie, Johannes Gutenberg-Universität Mainz, D-55131 Mainz, Germany
[2]Institut für Kernchemie, Johannes Gutenberg-Universität Mainz, Fritz-Strassmann-Weg 2, D-55128 Mainz, Germany
[3]Forschungszentrum Karlsruhe GmbH, Hauptabteilung Sicherheit, Postfach 3640, D-76021, Karlsruhe, Germany
[4]Università degli Studi,Dipartimento di Fisica Nucleare e Teorica, Via Bassi,6, 27100 PAVIA, Italy

Patients suffering of colorectal carcinoma develop distant metastases in 50 to 80% with the metastases being confined to the liver in almost half of those cases.

BNCT in patients suffering from multiple liver metastases was established at the University of Pavia with the first case being treated by Pinelli et al in Dec. 2001 [1]. Here, BPA was administered intravenously before explanting the liver and irradiation in the thermal column of the TRIGA-Reactor in Pavia. An accumulation of BPA in tumour vs. healthy liver tissue of 6:1 was determined here. Noteworthy is that the tissue samples were collected before explanting the liver.

The surgical process requires extensive experience in the field of liver transplantation and preservation of the liver during the extracorporeal treatment. This includes perfusion of the liver artery with preservation solution and reducing the liver temperature to 4 °C. The question remains whether there are any wash-out effects during this procedure and if yes, will the accumulation remaining in tumour tissue still be enough for the irradiation therapy?

We plan to implement BNCT for colorectal liver metastases at the University of Mainz on cooperation with the University of Pavia. The conditions in Mainz are excellent as both the transplant center and the irradiation facility are in a close distance.

Our project will be performed in two steps. The first step will be to determine the accumulation of BPA in tumour and healthy liver tissue in patients after partial liver resection and washing the liver specimen with preservation solution. Provided satisfying results we would proceed with step 2 which is to treat a patient with multiple liver metastasis and extracorporeal irradiation of the whole liver.

So far we have obtained the approval of the German Administration for Medical Products (BfArM) and the Ethical Committee for the first part of our project. This is to examine a total of 15 patients with colorectal liver metastases who need a partial liver resection and to determine the accumulation of BPA in tumour and healthy liver tissue. BPA would be administered in a concentration of 200 mg/kg intravenously and blood samples will be collected during the surgical procedure. The liver specimen will be examined at the Institute of Nuclear Chemistry in Mainz with autoradiographic methods and ICP-MS. In case of an accumulation of BPA in tumour vs. healthy liver tissue of at least 3:1 in 3 patients we would proceed with the remaining 12 patients.

Comparison of BNCT and GdNCT efficacy in treatment of canine cancer

V.N. Mitin[a], V.N. Kulakov[b], V.F. Khokhlov[b], I.N. Sheino[b], A.M. Arnopolskaya[a], N.G. Kozlovskaya[a], K.N. Zaitsev[c], A.A. Portnov[c],

[a]*Russian Cancer Research Center of the RAMS, Kashirskoe shosse, 24, 115478 Moscow, Russia*
[b]*State Research Center Institute of Biophysics, Zhivopisnaya ul., 46, 123182 Moscow, Russia*
[c]*Moscow Engineering Physics Institute, Kashirskoe shosse, 31, 115409 Moscow, Russia*

Abstract

In this study, the efficacy of antineoplastic action of Gadolinium NCT and Boron NCT in cases of canine melanoma and osteosarcoma was compared. Spontaneous canine tumors, such as melanoma and osteosarcoma, have clinical features common with human malignancies, so these tumors in dogs can be considered as a clinical model of human melanoma and osteosarcoma. The study has been carried out in 33 dogs with oral cavity melanoma and 9 dogs with osteosarcoma. Dogs with spontaneous melanoma of oral cavity and osteosarcoma of extremities were selected by the results of clinical examination. Irradiation was carried out at the NCT facility of the IRT MEPhI Reactor. Neutron irradiation without boron or gadolinium was chosen as a control method to evaluate the efficacy of NCT.

Keywords: Boron NCT, Gadolinium NCT, Melanoma, Osteosarcoma

1. Introduction

For many forms of cancer diseases, conventional methods of treatment are not effective. Neutron capture therapy with Boron (BNCT) and Gadolinium (GdNCT) appear to be promising methods of cancer treatment. Today there are a lot of clinical studies on BNCT in treatment of different types of cancer, which confirmed the efficacy of this type of NCT, but there are few studies concerning the efficacy of GdNCT (Zhang et al., 2002; Miller et al., 1993).

Every method of NCT has its advantages and disadvantages. Boron and gadolinium used in the compounds in the NCT technology create secondary radiation of different origin in the tumor. In the BNCT technology, a boron-containing drug (BPA-F) is administered intravenously or intraarterially, and atoms of ^{10}B accumulate selectively inside the tumor cells (Kato Ono et al., 2004; Mishima et al., 1989). So, BNCT can precisely mark the tumor borders, and the secondary irradiation created by BNCT kills only tumor cells. Gadolinium-containing drug does not penetrate into the tumor cells and is located only in the intercellular space. In this case, the basic tumor damage is caused by the secondary photon radiation (Khokhlov et al., 1996). However, no clinical studies were conducted to evaluate the clinical efficacy of GdNCT in cancer treatment.

In this study, our purpose was to evaluate and to compare the efficacy of antineoplastic action of the NCT types (BNCT and GdNCT) in most malignant canine tumors.

The study was carried out in dogs with oral cavity melanoma and osteosarcoma – the most malignant canine tumors. In these types of cancer the prognosis is often poor, the life span is no more than 2-3 months and according to latest studies, the incidence of these canine malignancies rises gradually (Withrow et al., 2007).

2. Materials and methods

The study has been carried out in 33 dogs with oral cavity melanoma and 9 dogs with osteosarcoma. Dogs with spontaneous melanoma of oral cavity and osteosarcoma of extremities were selected by the results of clinical examination. In all dogs, II B tumor stage was detected. The diagnosis was confirmed in a histological study of biopsy material.

Dogs with oral melanoma were divided into four groups: 1) 5 dogs treated with neutrons only, 2) 14 dogs treated using BNCT; 3) 14 dogs treated with GdNCT.

In osteosarcoma, two groups were organized: 1) BNCT was applied in 1 dog; 2) GdNCT was performed in 8 dogs with osteosarcoma. In osteosarcoma cases, NCT was included in the complex osteosarcoma treatment.

The plan combines preliminary chemo-radiotherapy, adoptive immunotherapy, regional

administration of BPA (preliminary catheterization of the right iliac artery), wide segmental resection of the right iliac wing with the osteosarcoma lesion, its irradiation outside of the organism in a thermal neutron beam for 45 minutes from each side, reimplantation of the bone and its fixation with hardware, and postoperative chemotherapy. In GdNCT cases of osteosarcoma treatment the plan combines preliminary chemo-radiotherapy, intratumoral administration of Dipentast (Gd–containing drug) by injecting around the tumor immediately prior to irradiation, and irradiation of the patient in a thermal neutron beam (*in vivo* irradiation). Irradiations were carried out at the NCT facility of the IRT MEPhI Reactor. The characteristics of the neutron beam are as follows: thermal neutron flux (E<0.5 eV) 1.1 10^9 n/cm^2/s; epithermal neutron flux (0.5 eV<E<10 keV) 1.6 10^8 n/cm^2/s; fast neutron flux (E>10 keV) 5.8 10^7 n/cm^2/s; fast neutron dose in the beam per thermal neutron 5.6 10^{-13} Gy cm^2/neutron; fast neutron dose in the beam per epithermal neutron 4.2 10^{-12} Gy cm^2/neutron; photon dose per thermal neutron 1.5 10^{-13} Gy cm^2/neutron.

Supportive therapy was provided prior to and after irradiation. The drugs were chosen by the clinician according to the condition of the animal.

During the irradiation, the anesthesiologist controlled the condition of the animal basing on the data of continuous monitoring of primary physiological parameters using Cardiomonitor PRO PAQ encore Model 202 EL, (USA); the position of the animal during the irradiation procedure was controlled telemetrically.

BPA was administered intravenously in melanoma cases or intraarterially in the osteosarcoma case for 2 hours in a dose of 300 mg/kg under X-ray monitoring; the ^{10}B concentration in the tumor was determined by the method of track autoradiography: normal tissue – 9.3 ppm, tumor – 28.5 ppm.

Gd-containg drug - Dipentast was administered intratumorally by injecting around the tumor immediately prior to irradiation, in amounts providing ^{157}Gd concentration in the tumor not less than 10 mg/ml.

Initial anesthesia was induced with ketamine (0.5-1 mg/kg), xylazine (2-4 mg/kg) given intravenously to effect after premedication with atropine sulphate (0.1 mg/kg subcutaneously).

Maintaining anesthesia included intravenous administration of propofol (6-12 mg/kg).

The side effects observed (alopecia, dermatitis, epidermis, radial stomatitis) were treated using conventional methods.

Doses on tumor and surrounding tissues were estimated with use of simple geometrical models of the irradiated body parts of the dogs (Sheino, 2006).

We evaluated the biological tissue effect after the irradiation and the degree of radiation damages.

The rate of incomplete regression (IR) and full regression (FR) and duration of recurrence-free period were assessed in dogs with malignancies.

3. Results and Discussions

After neutron irradiation, we detected alopecia, hyperemia and dermatitis and I stage of radiation damages. In the cases of BNCT, I – II stages of radiation damages were detected with alopecia, tissue depigmentation and ulceration. After the GdNCT treatment, III stage of damages was determined with tissue pigmentation and soft tissues destruction. Obviously, tissue pigmentation is a result of secondary gamma- radiation, which occurs during GdNCT.

Then, antioneoplastic effect was assessed. In cases of melanoma treated with the neutron beam, antineoplastic effect was very low: incomplete regression - in 80% cases, and full regression - in 20% cases. Recurrence was detected in 100% cases. In BNCT group, full regression was diagnosed in 78% of the dogs, and the frequency of recurrence was very low – 14% only in the cases of incomplete regression. In the melanoma group treated by GdNCT, full regression was detected in 44% of the dogs and in 56% - incomplete regression, recurrence was diagnosed in 46% of cases. We evaluated the antineoplastic effect of GdNCT in oral melanoma in comparison with intratumoral concentration of ^{157}Gd compound. The results revealed the dependence of the concentration and antineoplastic effect. The best effect without recurrence we detected, when the concentration of ^{157}Gd in the tumor was 10-12 mg/ml. So, the higher concentration was detected, the lower antitumor effect was revealed. Obviously, this occurrence may be a result of the shielding effect of ^{157}Gd, which has high thermal neutron capture cross-sections. Additionally, dose evaluation in different ^{157}Gd concentrations was performed, which revealed the total dose reduction, when intratumoral ^{157}Gd concentration is more than 12 mg/ml (fig. 1).

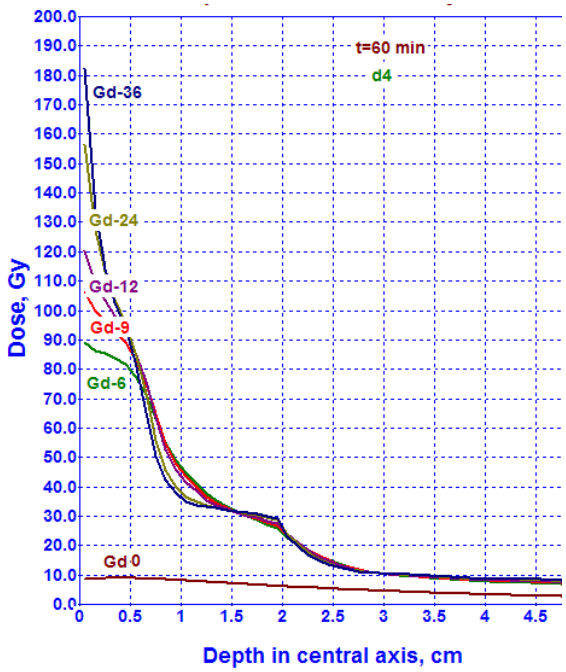

Figure 1. Tumor dose distribution in different ^{157}Gd concentrations

So in the cases of superficial soft-tissue tumors, as malignant melanoma, BNCT is the most effective method of treatment, with low recurrence rate. The mechanism of action provides intracellular boron accumulation, which creates secondary radiation after BNCT, which is localized within the place of location, and that is why optimal for superficial soft-tissue tumors. GdNCT is a promising technology, but in this case the dose of Gd-containing drug should be estimated precisely .

In osteosarcoma cases, BNCT-based complex treatment showed full tumor regression 2.5 months after the irradiation of the bone replant. In GdNCT group, full tumor necrosis was detected in 100% cases.

In canine osteosarcoma, at first we applied BNCT of the excised bone fragment, and complete tumor regression was detected. As soon as we got a good result of NCT of a bone replant, we made an attempt to perform NCT of a bone tumor *in vivo*, without excision, and we chose GdNCT, which later showed full tumor necrosis (fig.2). The main reason of such results was the biological characteristics of osteosarcoma, such as interstitial tumor origin and stromal tumor type. Also, the mechanism of GdNCT provides non-cellular accumulation of ^{157}Gd and secondary radiation in a wide range, which is optimal for such tumors as osteosarcoma, and allows performing GdNCT of the whole organism. Also, in GdNCT groups, no serious side-effects connected with irradiation were detected.

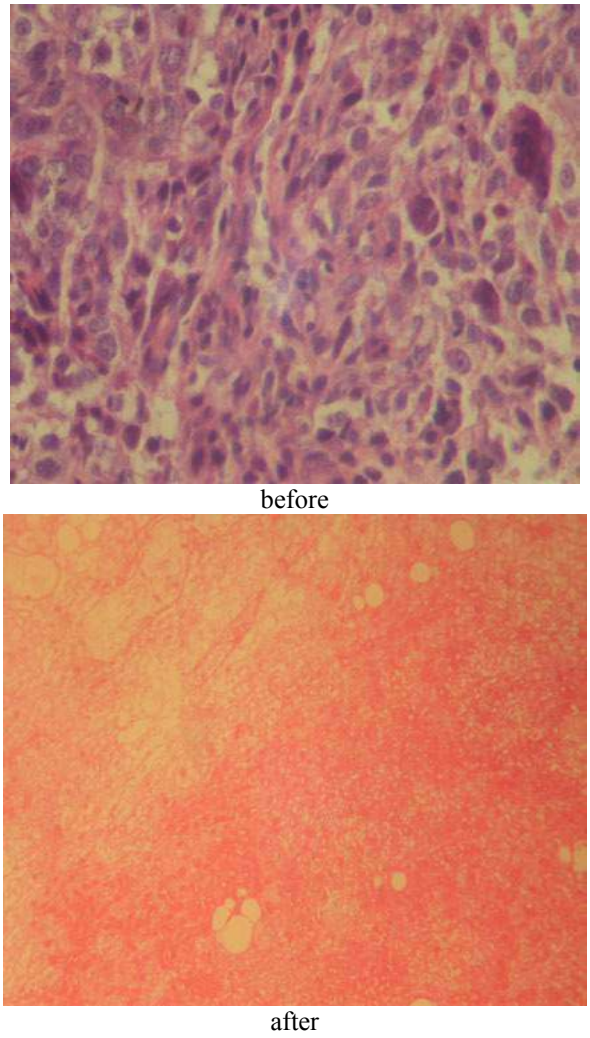

Figure 2. Small cell osteosarcoma. *Hematoxylin-Eosin x 400:* before and after GdNCT (*Total Necrosis-Necrobiosis of tumor bone tissue. IV stage pathomorphism)*

4. Conclusions

Evaluating the biological effect, it was concluded that BNCT induces lower tissue damages and causes tissue depigmentation. GdNCT causes more severe tissue damages and tissue pigmentation, which is obviously a result of secondary radiation of GdNCT.

For soft-tissue, superficial tumors, such as oral melanoma, BNCT is the most effective method of treatment. The effect of GdNCT in melanoma cases is lower and depends on the intratumoral concentration of ^{157}Gd. The optimal ^{157}Gd concentrations are 10-15 mg/ml.

In tumors of interstitial origin, such as canine osteosarcoma, GdNCT appears to be an effective method of treatment, as secondary irradiation is optimal for these tumors. GdNCT gives an opportunity to administer Gd-containg drug intratumorally, to perform in vivo irradiation and to

achieve full tumor necrosis after one course of GdNCT.

For epithelial-cell tumors, such as melanoma, the ^{10}B-containing cell is the main target of damage, and for stromal tumors, such as osteosarcoma, drugs that accumulate in the extracellular space should be administered preferably.

In all cases of malignancies, both NCT types are methods of local tumor treatment, and distant metastases can worsen the results of treatment, so the treatment should always be complex to minimize the risks of tumor dissemination.

Acknowledgements

The work has been carried out with financial support from the Russian Fund for Technology Development of the Ministry of Science and Technologies, and International Science and Technology Center Project #3341.

References

Kato, I., Ono, K., Sakurai, Y. et al., 2004. "Effectiveness of BNCT for recurrent head and neck malignancies", *Applied Radiation and Isotopes,* **61**, 1069 - 1073. 138

Khokhlov V.F, Jashkin P.N., Silin D.I. et al., "Neutron capture therapy with Gd-DTPA in tumor-bearing rats", *Cancer Neutron Capture Therapy*, Edit by Y. Mishima, Plenum Press. N.Y., 865-869,1996..

Miller G.A., Hertel N.E., Wehring B.W. et al., "Gadolinium neutron capture therapy", *Nucl. Techol.,* 103, 320-331, 1993.

Mishima Y., Honda C, Ichiahashi M., Obara H., Hiratsuka J., Fukuda H., Karashima H., Kobayashi T., Kanda K., Yoshino K. Treatment of malignant melanoma by single thermal neutron capture therapy with melanoma-seeking ^{10}B-compound. Lancet. 2: 388-389, 1989

Sheino I.N. Dose-supplementary therapy of malignant tumors. Advances in Neutron Capture therapy, ICNCT-12, Japan, 9-13 October 2006, 531-534.

Withrow S.J., Vial D.M., Withrow & Maceven's small animal clinical oncology –Forth Edition, Elsevier, USA, 2007

Zhang T., Matsumura A., Yamomoto T. et al., "A comparison of in vivo Gd-NCT trial by two targeting compounds: Gd-BOPTA and Gd-DTPA, research and development in neutron capture therapy", in *Research and Development in NCT*, Edit by W. Sauervein, R. Moos, A. Wittig, Monduzzi Editore Intern. Proc. Division, 807-812, 2002.

Survival benefit of boron neutron capture therapy for recurrent malignant gliomas

Shin-Ichi Miyatake[a], Shinji Kawabata[a], Kunio Yokoyama[a], Toshihiko Kuroiwa[a], Hiroyuki Michiue[b], Yoshinori Sakurai[c], Hiroaki Kumada[d], Minoru Suzuki[c], Akira Maruhashi[c)], Mitsunori Kirihata[d], Koji Ono[c]

[a]*Dept of Neurosurgery, Osaka Medical College, 2-7 Daigaku-machi, Takatsuki City, Osaka, 569-8686, Japan*
[b] *Department of Neurosurgery, Okayama University, 2-5-1 Shikata-cho, Okayama 700-8558, Japan*
[c]*Particle Radiation Oncology Research Center, Research Reactor Institute, Kyoto University, Kumatori 590-0494, Japan*
[d]*Department of Research Reactor and Tandem Accelerator, Nuclear Science Institute, Japan Atomic Energy Agency, Tokai, 319-1184, Japan*
[e]*Department of Agriculture, Osaka Prefectural University, Sakai 599-8531,Japan*

Abstract

We have applied boron neutron capture therapy (BNCT) to malignant brain tumors. Here we evaluated the survival benefit of BNCT for recurrent malignant glioma (MG). Since 2002, we have treated 22 cases of recurrent MG with BNCT. Survival time was analyzed with special reference to recursive partitioning analysis (RPA) classification, by Carson *et al*. Median survival times (MSTs) after BNCT for all patients and for glioblastoma as on-study histology at recurrence was 10.8 months (n=22; 95% CI, 7.3 to 12.8 months) and 9.6 months (n=19; 95% CI, 6.9 to 11.4 months), respectively. In our study, MST for the high-risk RPA classes was 9.1 months (n=11; 95% CI, 4.4 to 11.0 months). By contrast, the original journal data showed that the MST of the same RPA classes was 4.4 months (n=129; 95% CI, 3.6 to 5.4 months). BNCT showed a survival benefit for recurrent MG, especially in the high-risk group.

.

Keywords: boronophenylalanine PET, glioblastoma, malignant glioma, recursive partitioning analysis(RPA)

1. Introduction

We have applied a form of tumor-selective particle radiation, boron neutron capture therapy (BNCT), for malignant gliomas (MGs) and malignant meningiomas.

The prognosis of recurrent MGs, especially glioblastoma multiforme (GBM) is poor. We reported the effectiveness of BNCT on neuroimages for MGs, and recently reported the survival benefit of BNCT for newly diagnosed MGs (submitted for publication). Unfortunately, the standard treatment for recurrent MG has not yet been established. Therefore, evaluation of the survival benefit of BNCT for recurrent MGs is difficult.

To evaluate this objectively, we adopted the recursive partitioning analysis (RPA) classification for recurrent MG advocated by Carson *et al.* in a 2007 article in the *Journal of Clinical Oncology*, in which the results of 10 recent protocols of phase-1 and -2 trials applied by the New Approaches to Brain Tumor Therapy CNS Consortium (NABTT) for recurrent MG were summarized (Carson KA, 2008). They included 6 systemic treatment and 4 local treatment trials. Originally this RPA classification was not aimed at the evaluation of the effectiveness of each trial for recurrent MG; however, this RPA classification gave us a uniform background and median survival time (MST) for each recurrent MG-type patient at the time of recurrence. So we classified our recurrent MG patients treated by BNCT and compared their survival to the MSTs presented in the above journal.

2. Patients and methods

Patient enrollment

From 2002 to 2007 we treated a total of 22 cases of recurrent MG using BNCT. Our eligibility criteria for this trial were as follows:

1) age 15 years or older;

2) histologically proven supratentorial MG (GBM, AA, AO, or anaplastic oligodendroglioma,

as on-study histology) that had proved to be progressive or recurrent after radiation therapy;

3) depth of the tumor from scalp less than 6 cm (if the lesion is deeper than 6 cm from the scalp, partial removal or cyst evacuation was applied to fit this criteria, see below);

4) no cerebrospinal fluid (CSF) dissemination at recurrence; 5) estimated life expectancy longer than 3 months, not pregnant or breast feeding, and having a KPS score of 60 or greater.

Clinical regimen of BNCT

In protocol 1, the patients were administered 100mg/kg of sodium borocaptate (BSH) and 250mg/kg of BPA for one hour intravenously 12 hours prior and just prior to neutron irradiation, respectively. In protocol 2, the patients were administered 100mg/kg of BSH intravenously for one hour, 12 hours prior to neutron irradiation and 700mg/kg of BPA continuously for 6 hours before the irradiation. In both protocols, the neutron irradiation time was determined not to exceed 13 Gy-Eq to the normal brain by simulation.

Patient characteristics

The patients' age is 51 (15-67) (median and range), gross tumor volume (GTV) is 42 ml (4.1-64.5) (median and range). In 12 cases surgery was applied before BNCT, as a form of cyst evacuation or partial tumor removal to make a cavity to establish an Ommaya reservoir as described above. Ten cases were administered TMZ, 3 before the relapse and 7 after BNCT.

RPA classification

To objectively evaluate the survival benefit of BNCT for recurrent MG, we classified our BNCT cases according to the RPA classification advocated in some journals (Carson KA, 2008). These classifications can be summarized as follows: class 1, not GBM (initial histology), KPS≥80, frontal (tumor location); RPA class 2, not GBM, KPS≥80, not frontal; RPA class 3, not GBM, KPS≤70; RPA class 4, GBM, Age≤50, KPS≥90; RPA class 5, GBM, Age≤50, 60≤KPS≤80; RPA class 6, GBM, Age≥50, no steroid use; RPA class 7, GBM, Age≥50, steroid use.

3. *Results*

Survival after BNCT and after diagnosis

Survival after BNCT (n=22) and that from initial GBM diagnosis (n=19, on-study histology as GBM) are survayed. MST after BNCT for all patients (n=22) was 10.8 months (95% CI, 7.3 to 12.8 months). MST after BNCT for GBM cases as on-study histology at recurrence (n=19) was 9.6 months (95% CI, 6.9 to 11.4 months). MST after initial GBM diagnosis (n=19) was 19.1 months (95%CI, 11.6 to 23.0 months).

Survival with special reference to RPA classes

The MSTs (months) of our BNCT cases classified according to RPA classes are shown here and compared in each case with the values from Carson *et al.*: Class 1 (n=2): 32.6 versus 25.7 (Carson *et al.*), Class 2 (n=4): 23.7 versus 17.2, Class 3 (n=5): 9.1 versus 3.8, Class 4 (n=3): 10.2 versus 10.4, Class 5 (n=2): 8.5 versus 6.4, Class 7 (n=6): 9.8 versus 4.9. The tendencies in patient survival of our cases after BNCT were very similar to those of the original report in terms of RPA classification. Since our cases were so limited in number, we joined the worst prognosis classes (Class 3 and 7) together into one class. The MST of our cases in this combined class was 9.1 months (n=11; 95% CI, 4.4 to 11.0 months), while that in Carson *et al.* was 4.4 months (n=129; 95% CI, 3.6 to 5.4 months). (Table 1)

4. Discussion

Here we reported the survival benefit of BNCT for recurrent MG cases, mainly GBM. The MST after BNCT for GBM cases as on-study histology at recurrence (n=19) was 9.6 months (95% CI, 6.9 to 11.4 months). In the literature, we found a summary of a large series of 8 phase-2 trials of chemotherapies for recurrent GBM cases (Wong 1999). In this report, the authors mentioned the MST of GBM after relapse as 25 weeks (5.8 months; 95% CI, 21 to 28 weeks, 4.9 to 6.5 months; n=225). In comparison with this result, our data for the survival benefit of BNCT in recurrent GBM was not bad.

As to BNCT for recurrent GBM, 2 small series have been reported in the literature. A Swedish group and a Finnish group reported that MSTs for recurrent GBM after BNCT were 8.7 (n=12) (Pellettieri L, 2008) and 7.5 months (n=7), respectively.

Our data in the current report is almost equal to or somewhat better than the findings in these reports.

MST after BNCT for all patients (n=22) was 10.8 months (95% CI, 7.3 to 12.8 months). We are not sure whether this result is reliable, as this is the result of a small series from a single institution. To evaluate this result as objectively as possible, we applied RPA to our cases as advocated in the literature (Carson KA, 2008). Inclusion criteria for our trial and the ten NABTT phase-1 and -2 trials reported in Carson *et al.* were not very different. Our case numbers for each RPA class were so limited, however, that the MST of our cases in each RPA class were relatively better in comparison with original NABTT results, as listed above. In the original article, RPA class 3 (Not GBM, KPS≤70) and class 7 (GBM, Age≥50, steroid use) showed extremely poor prognosis. The MST of our combined class 3 and class 7 cases was 9.1 months (n=11; 95% CI, 4.4 to 11.0 months), while that in the original article was 4.4 months (n=129; 95% CI, 3.6 to 5.4 months) (Table 1). We can not know whether our current MST data is significantly better than that of each NABTT trial because their raw data were not available. But at least, BNCT showed a good survival benefit even for the highest-risk group, RPA class 3 and 7.

In our 22 cases, we used TMZ in 10 cases, before BNCT in 3 cases and after BNCT in 7. For the former 3 cases, TMZ could not control the tumor growth and methylation-specific PCR showed an unmethylated O6-methylguanine DNA methyltransferase (MGMT) promoter (data not shown). We stopped the administration of TMZ after BNCT as we judged TMZ was not efficacious for these 3 cases. Among the latter 7 cases, only 2 (Cases 1 and 2, both classified as RPA class 1) showed methylated promoter status for MGMT, with good prognoses. For the other 5 cases, we were not sure of the MGMT expression status of the tumor. In the high-risk group in our series (RPA class 3 and 7), 3 cases were administered TMZ after BNCT. Among them, 2 cases showed a relatively short survival after BNCT. We do not deny the meaning of TMZ use at relapse; however, in our series for this high-risk group, the survival benefit of TMZ was limited. In the literature, TMZ has actually shown modest survival benefit at relapse of recurrent GBM reported only 5.4 months prolongation as MST with TMZ at relapse in the report. (Brada M, 2001).

There are several reports with relatively good results for recurrent MG, with an MST of around 10 months after the stereotactic radiosurgery (SRS) or stereotactic radiotherapy (SRT) at relapse. However, there was big difference in GTV at the relapse between these SRS or SRT cases and ours. The median GTV of the former 2 was 10.1 ml and 12.7 ml, while the median GTV of our cases was 42.0 ml. There might also be a difference as to performance status or age between the SRS or SRT reports and our cases. The result of re-irradiation for recurrent GBM was poor. The MST of this report was 26 weeks after the treatment. In addition, BNCT can be applied in only one day. Taken together, BNCT could be one of the promising radiation treatment options for recurrent MG at relapse.

We lost many cases of recurrent MGs after BNCT by CSF dissemination, as we reported (in preparation). In other words, local control by BNCT for even recurrent MG was fairly good. There was a tendency for CSF dissemination to occur in relatively long-term survivors from diagnosis (data not shown). On the other hand, a major problem in BNCT for recurrent MG was the occurrence of radiation necrosis (RN). We experienced RN by BNCT especially for recurrent MG, because the patients had been treated by radiotherapy prior to BNCT. Although BNCT is cell-selective particle radiation, some particle dose is inevitably absorbed by the normal brain tissue. Most of RN could be controlled with medical or surgical treatments as above; however, we lost 3 cases by RN in our series. Preventive medical treatments such as by anticoagulants or by vitamin E must be considered after BNCT, especially for recurrent cases. This is not mentioned in other BNCT reports for recurrent MG; however, it should be seriously considered. In Swedish reports of BNCT for recurrent GBM, the authors mentioned a median time to tumor progression (TP) of 6 months after BNCT, but there was no statement as to how TP was judged in their report. It is very difficult to differentiate RN and TP on MRI, especially with high-dose radiation treatment. So we did not apply the analysis of time to tumor progression in our series. Especially for recurrent cases, if we increase the minimum tumor dose by BNCT, the incidence of RN probably increases, as discussed here. Therefore, it is very difficult to elucidate the most suitable dose of BNCT at relapse. Regardless, RN is a serious problem to be overcome in the field of BNCT.

XRT plus concomitant TMZ (Stupp's regimen) has been the global standard so far for newly diagnosed GBM (Stupp R, 2005). Pellettieri *et al.* reported that BNCT at relapse after Stupp's regimen might be the best treatment of GBM. Also in our series BNCT at relapse showed a good MST after the initial GBM diagnosis of 19.1 months (n=19; 95%CI, 11.6-23.0 months). But it cannot be concluded so easily that BNCT at relapse after Stupp's regimen is the best for the treatment of GBM because 19 cases in our series were referred to our institute at relapse with a significant interval after initial treatments. This interval might prolong the survival after initial GBM diagnosis at a glance.

5. Conclusions

The RPA classification advocated by Carson *et al.* predicted the patient survival trends of our BNCT series; however, BNCT showed the most prominent survival benefit in the high-risk group (RPA classes 3 and 7).

Table 1 Comparison of NABTT trials and our BNCT series

	All patients			RPA 3 + 7		
	MST	95% CI	number in series	MST	95% CI	number in series
NABTT	7.0	6.2 - 8.0	n = 310	4.4	3.6 - 5.4	n = 129
BNCT	10.8	7.3 - 12.8	n = 22	9.1	4.4-11.0	n = 11

References

Brada M, Hoang-Xuan K, Rampling R, DietrichPY, Dirix LY, Macdonald D, et al: Multicenter phase II trial of temozolomide in patients with glioblastoma multiforme at first relapse. **Ann Oncol 12:**259-266, 2001

Carson KA, Grossman SA, Fisher JD, Shaw EG: Prognostic factors for survival in adult patients with recurrent glioma enrolled onto the new approaches to brain tumor therapy CNS consortium phase I and II clinical trials. **J Clin Oncol 25:**2601-2606, 2007

Pellettieri L, B HS, Rezaei A, Giusti V, Skold K: An investigation of boron neutron capture therapy for recurrent glioblastoma multiforme. **Acta Neurol Scand 117:**191-197, 2008

Stupp R, Mason WP, van den Bent MJ, Weller M, Fisher B, Taphoorn MJ, et al: Radiotherapy plus concomitant and adjuvant temozolomide for glioblastoma. **N Engl J Med 352:**987-996, 2005

Wong ET, Hess KR, Gleason MJ, Jaeckle KA, Kyritsis AP, Prados MD, et al: Outcomes and prognostic factors in recurrent glioma patients enrolled onto phase II clinical trials. **J Clin Oncol 17:**2572-2578, 1999

Cost Analysis of Radiotherapy, Carbon Ion Therapy, Proton Therapy and BNCT in Japan

Yoshiaki Nakagawa[a], Hiroyuki Yoshihara[a], Teruyoshi Kageji[b]
Reiko Matsuoka[c], Yoshinobu Nakagawa[d]

a Department of Medical Informatics, Post Graduated School, Kyoto University, Kyoto
b Department of Neurosurgery, The University of Tokushima, 770-8503 Japan
c Association for Nuclear Technology in Medicine, Minatoku Tokyo, Japan

d Department of Neurosurgery, NHO Kagawa National Children's Hospital、Kagawa875-8501

Abstract

It is necessary to estimate financial status to start BNCT as a clinical treatment in a hospital. To evaluate more accurate data on the precise costs of BNCT, we studied the costs of conventional radiotherapy, carbon ion and proton therapy and compare them to BNCT. An aggregate cost calculation of accelerator, buildings, equipments and staff requirements was performed.

Keyword : BNCT, Radiotherapy, Cost analysis,

1. Introduction

BNCT has been carried out at nuclear reactors in clinical trials and research in Japan since 1968. The expenditures have been covered by research funds and expense from ???. Boron compounds have been supplied by pharmaceutical companies. Recent studies have yielded better clinical outcomes and quality of life of patients after BNCT. On the other hand, an accelerator for BNCT has been developed and will be utilized as a medical facility in the near future. A manager of an institute or a hospital must repeatedly estimate the financial status of his institute to decide on the proper management strategy. Then, it is necessary to calculate the cost of the accelerator, building and their depreciation prior to starting accelerator based BNCT in a hospital. Carbon ion therapy and proton therapy were approved as an advanced medical treatment in Japan. The cost of each treatment was decided according to the medical costs such as conventional radiotherapy, chemotherapy and surgical treatment. To evaluate more accurately the data on the precise costs of BNCT, we investigated the cost of accelerator, buildings, equipments and staff requirements of each institute or center.

2. Methods

Facilities: There are two heavy ion medical accelerator centers, four proton centers and two reactors for medical use in Japan (Fig.1). BNCT based on an accelerator is in the planning stage of KUR and a clinic. The cost of radiotherapy per patient was estimated based on accreditation reports of each center.

Classification of the costs:

Cost was subdivided into the cost for the accelerator, building and medical equipment. The depreciation cost of accelerator was calculated over 20 years and building 30 years and equipment over 6 years. There are two plans of accelerator system for BNCT. The cost of the former institute was converted to the BNCT. The other components were institutional maintenance, medical material, personnel cost, personnel welfare, medical appliance maintenance. Personnel costs, broadly classified as doctors, nurses, medical technicians and office workers, were calculated according to the average salary of the hospital or institute[1,2].

Fig 1. Location of heavy ion and proton canter in Japan

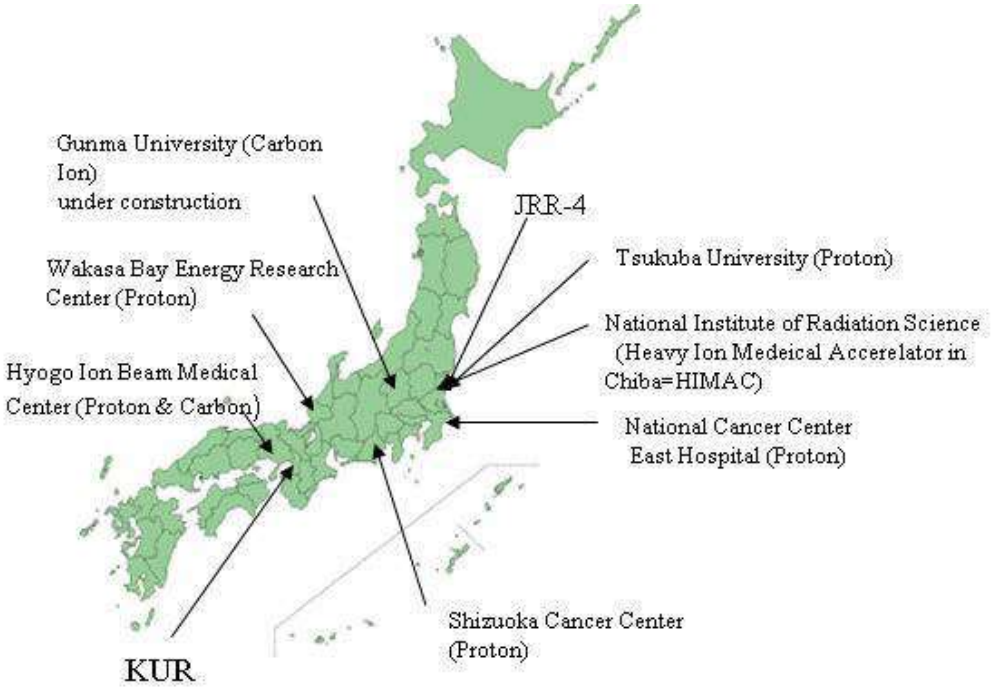

Table 1. Costs and depreciation

				(million yen)		depreciation			
	radiation room	cost of facility	building	equipments	Total cost	facility/ 20years	building/ 30years	equipment / 6years	Total/year
National Institute of Radiation Science (Heavy Ion Medeical Accerelator in Chiba=HIMAC)	5	18,000	14,600	600	32,600	810	438	90	1,338
Tsukuba University (Proton)	3	3,600	2,500	600	6,100	162	75	90	327
National Cancer Center East Hospital (Proton)	3	4,200	4,100	600	8,300	189	123	90	402
Shizuoka Cancer Center (Proton)	3	3,500	2,500	600	6,000	158	75	90	323
Hyogo Ion Beam Medical Center (Proton & Carbon)	6	12,000	16,000	600	28,000	540	480	90	1,110
Wakasa Bay Energy Research Center (Proton)	1	4,760	1,915	600	6,675	214	57	90	362
BNCT plan 1	2	1,200	1,200	400	2,400	54	36	60	150
BNCT plan 2	2	2,000	2,000	400	4,000	90	60	60	210

Table 2. Personnel costs and number of staff

	Proton or Heavy Ion			BNCT	
	No. of person	Cost/person	Total	No. of person	Total
Chief Medical Dr	1	¥15,000,000	¥15,000,000	1	¥15,000,000
Medical Dr.	3	¥12,400,000	¥37,200,000	3	¥37,200,000
Radiation engineer	7	¥4,200,000	¥29,400,000	2	¥8,400,000
Nurse	2	¥5,643,000	¥11,286,000	3	¥16,929,000
Medical Physisist	1	¥7,000,000	¥7,000,000	2	¥14,000,000
Radiation surveyer	1	¥6,500,000	¥6,500,000	1	¥6,500,000
Machien engiher	6	¥4,800,000	¥28,800,000	2	¥9,600,000
Handcraft engiher	2	¥4,200,000	¥8,400,000	0	¥0
Administrative staf	1	¥6,185,000	¥6,185,000	1	¥6,185,000
	24		¥149,771,000	15	¥113,814,000

Table 3. Annual costs of each facility

	depreciation	ruuning cost	maintenance	personal cost	Total
National Institute of Radiation Science (Heavy Ion Medeical Accerelator in Chiba=HIMAC)	1,338	10	180	150	1,678
Tsukuba University (Proton)	327	10	150	150	637
National Cancer Center East Hospital (Proton)	402	10	150	150	712
Shizuoka Cancer Center (Proton)	323	10	150	150	633
Hyogo Ion Beam Medical Center (Proton & Carbon)	1,110	10	180	150	1,450
Wakasa Bay Energy Research Center (Proton)	362	10	150	150	672
BNCT plan 1	150	10	90	101	351
BNCT plan 2	210	10	90	101	411

(million yen)

*running costs include: electricity, lighting and heating expenses and maintenance fees for the accelerator and equipment

Fig. 2. Total cost of irradiation

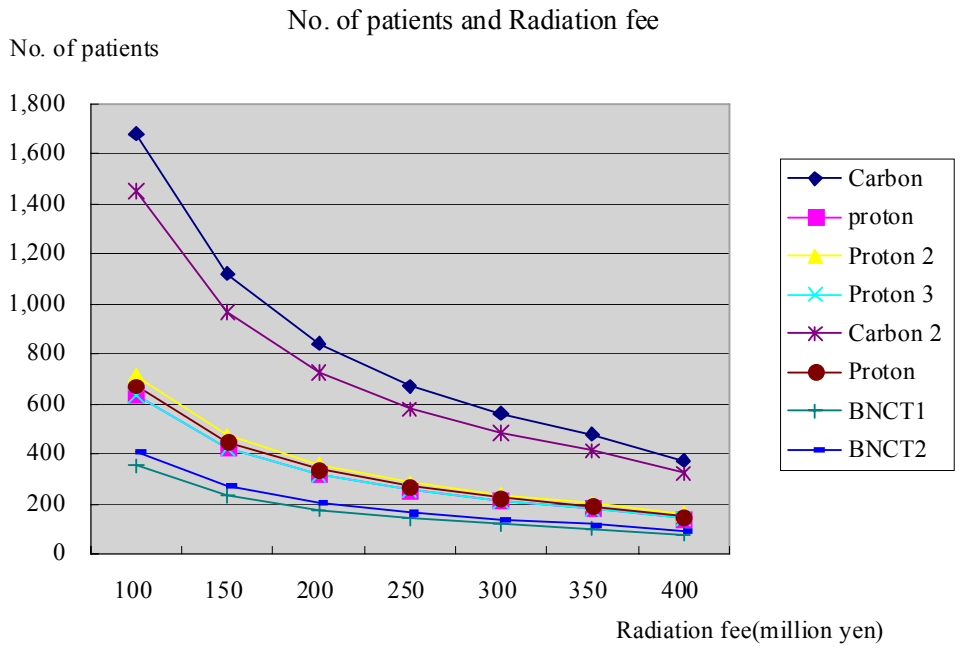

Results

The major cost components are the cost of accelerators or facilities, buildings and equipments. The cost of accelerator for heavy ion was more than 12,000 million yen. It was 3500-4760 million yen for a proton facility (Table 1). The accelerator for BNCT has not been completed but the estimated cost was 1200-2000 million yen.

The cost of building was more than 14000 million yen for heavy ion and 2000-4000 million yen for proton center.

The cost of medical equipment which includes simulator, treatment planning system, dosimetry system and CT scan was decided 600 million yen. Because some equipment or systems were developed in the institutes themselves. The total depreciation cost which includes accelerator, building and equipment was 1338 million yen/year for heavy ion and 323-402 million yen fro proton therapy and 150-21- million yen for BNCT.

The personal cost was calculated using averaged salary in the hospital or national institute. We refereed to HIMAC and Hyogo Ion Beam Medical Center and estimated the number of the staff (table 2). The total personal cost should be varied depend on the number of the staff.

The total costs which include running cost such as electricity, lighting and heating expenses and maintenance fee for accelerator and equipment to function the accelerator as medical facilities were 1678 million yean per year to 351 million yen (table 3).
The cost of each irradiation can be estimated according to the number of the patients (fig. 2).
On the other hand the averaged medical cost which including hospital fee was below:
4.8million yen for operation + chemotherapy + conventional radiotherapy
2.84 million yen for operation + chemotherapy
2.4 million yen for operation

Discussion

The hospital revenue was regarded as the sum of the insurance and cash payments received from patients by hospital for radiotherapy. To calculate the financial balance, it is necessary to balance the cost of each radiation therapy and number of the patients[3]. The medical fees for radiation, surgery and chemotherapy are decided by government in Japan. We can only propose suitable cost according to the financial balance or the cost of the other treatment. The cost for carbon ion therapy is 3.14 million yen and 2.883 million yen for proton therapy. To perform good financial balance, they have to treat more than 400 patients in a year by carbon ion and more than 200 patients by proton therapy (at each facility or total?). We can theoretically treat about 600 patients in a year. However, practically it may be less than 200 patients by BNCT. The cost of BNCT was still not decided but we have estimated that the cost would be more than 2.5 million yen.

4. Conclusions

The costs including accelerator and building for BNCT is much cheaper than that of carbon ion and proton therapy. If we can treat more than 200 patients using accelerator based BNCT in a year, we can demonstrate much better cost performance than heavy ion and proton therapy.

References

1) Nakagawa. Y., Takemura. T., Shirakami G. ,Yoshimura H., The cost analysis and problems of day surgery unit in the University hospital. J. Japan Society for Healthcare Administration 43(4) 331-343, 2006,

2) Nakagawa. Y., Takemura. T., Shirakami G. ,Yoshimura H., The cost analysis and problems of day surgery unit in the University hospital l. J-study of the performance improvement. Japan Society for Healthcare Administration 44(3) 69-78, 2007,

3) Hesteloot K., Lievens Y., Schueren EV. Improved management of radiotherapy departments through accurate cost data. Radiotherapy & Oncology 55 (2000) 251-262

Acknowledgement

A part of this study was financially supported by the Budget for Nuclear Research of the Ministry of Education, Culture, Sports, Science and Technology based on the screening and counseling by Atomic Energy Commission.

Intra-arterial Infusion of Boron-10 (10B) compound in Boron Neutron Capture Therapy for Patient with Maxillary Cancer : A case report

Masatoshi Ohmae[1], Itsuro Kato[2], , Koji Ono[3] Yoshinori Sakurai[3],
Mitsuhiro Nakazawa[2], Yoshiyuki Yura[2]

[1] *Department of Oral and Maxillofacial Surgery, Izumisano Municipal Hospital , Rinku General Medical Center*
[2] *Department of Oral and Maxillofacial Surgery II Osaka University Graduate School of Dentistry*
[3]*Radiation Oncology Research Laboratory, Research Reactor Institute, Kyoto University*

<**Introduction**> We started Boron neutron capture therapy (BNCT) for head and neck malignancies for the first time in the world in 2001 and have achieved successful results. The selective accumulation of 10B-compound into tumor-tissue compared with surrounding normal-tissue(T/N ratio) is especially critical in BNCT. To improve the T/N ratio we administrated boronophenylalanine(BPA) intra-arterially (ia-BPA) and performed BNCT. The T/N ratio was remarkably rose as well as we had expected, and achieved good results.

<**Materials and methods**> 61 year-old woman was diagnosed as having an adenoid cystic carcinoma(ACC) of maxilla and then underwent one course of neoadjuvant chemotherapy and subsequently partial maxillectomy. Histopathological examination and MRI revealed that the tumor mass was partially left in the pterygoid palatal fossa. We tried BNCT on the rest tumor by two different methods of boron compound infusion.

<**Result**>A preferential accumulation of ia-BPA in the tumor was observed (T/N ratio =7.6) compared with that (T/N ratio=2.5) administrated intravenously BPA(iv-BPA) by the 18F-BPA-PET study. She received twice iv-BPA and ia-BPA mediated BNCT with Kyoto University Research Reactor. BNCT caused 97% regression of the tumor and slight side-effect (less than Grade 2 by NCI-CTC) 2 months after BNCT.

<**Conclusion**>Intra-arterial boron compound infusion remarkably raised the T/N ratio which should play crucial role in BNCT.

Boron neutron capture therapy (BNCT) for diffuse or multiple pleural tumors: Case reports of two cases

Minoru Suzuki[1], Kazuo Endo[2], Hiroaki Sato[3], Yoshinori Sakurai[4], Hiroaki Kumada[5], Hiroyuki Kimura[6], Shinichiro Masunaga[1], Yuko Kinashi[1], Kenji Nagata[1], Akira Maruhashi[4], Koji Ono[1]

[1]Particle Radiation Oncology Research Center and [4]Division of Medical Physics, Research Reactor Institute, Kyoto University,
[2]Department of pulmonary medicine and [6]Department of radiology, Hyogo Prefectural Amaga-saki Hospital,
[3]Department of pulmonary medicine, Institute of Clinical Medicine, University of Tsukuba,
[5]Department of Research Reactor, Tokai Research Establishment, Japan Atomic Energy Research Institute

Two patients with diffuse or multiple pleural tumors, malignant pleural mesothelioma (MPM) and lung sarcoma, received boron neutron capture therapy (BNCT). In both cases, due to extensive spread of the tumor through entire pleural space, BNCT was performed twice for treating the tumors in the upper and those in the lower portion on the separate day. In each case, the tumors regressed or remained stable in size for 3-6 months following BNCT. Palliation of chest or back pain and short of breath was successfully provided just within a few days after BNCT. No acute adverse events greater than grade 2 was observed. In patient 1, Grade 2 lung toxicity was observed 7 months after the treatment.

Further clinical study is warranted for revealing the effectiveness of BNCT on palliation or control of pleural tumors.

Boron neutron capture therapy for newly-diagnosed glioblastoma: a pilot study in Tsukuba

Tetsuya Yamamoto, Kei Nakai, Takao Tsurubuchi, Masahide Matsuda, Makoto Shirakawa, Kiyoshi Endo, Akira Matsumura

Department of Neurosurgery, Graduate School of Comprehensive Human Science, University of Tsukuba, Tennodai 1-1-1, Tsukuba City, Ibaraki 305-8575, Japan

Neutron capture therapy (NCT) theoretically allows a unique tumor-cell-selective high-LET particle radiotherapy. The survival benefits and safety of NCT were evaluated in 15 patients with newly diagnosed glioblastoma multiforme (GBM).

Seven patients received intraoperative (IO-) NCT and 8 patients received external beam (EB-) NCT. Sulfhydryl borane (BSH, 5g/body) was administered intravenously 12 hours before neutron irradiation. Additionally, *p*-dihydroxyboryl-phenylalanine (BPA, 250 mg/kg) was given 1 hour before irradiation to the 8 patients who underwent EB-NCT. EB-NCT was combined with fractionated photon irradiation.

Five of 15 patients were alive at analysis for a mean follow-up time of 20.3 M. In 11 of 15 patients followed up for more than one year, 8 (72.7%) maintained their Karnofsky Performance Status (KPS; 90 in 6 and 100 in 2). The median overall survival (OS) and time to MR change (TTM) for all patients were 25.7 M and 11.9 M, respectively. There was no difference in TTM between the IO-NCT (12.0 M) and EB-NCT (11.9 M) groups. The 1- and 2-year survival rates were 85.7% and 45.5%, respectively. Three IO-NCT patients and 1 EB-NCT patient suffered transient orbital swelling accompanied by double vision (Grade 2); 1 of the 3 IO-NCT patients suffered post-epileptic brain swelling (Grade 4) requiring surgical intervention.

This NCT pilot study in 15 patients with newly diagnosed GBM showed survival benefits, suggesting that the neutron capture reaction may function sufficiently to control tumors locally, and that further optimized studies in large series of patients are warranted.

Keywords: Glioblastoma, BNCT

1.Introduction

In the Phase I and Phase II NCT trials for glioblastoma multiforme GBM, the median overall survival (OS) time varied from 13 M to 20.7 M.

Although these values are similar to those of postoperative conventional photon fractionation and standard chemotherapy, they suggest that NCT may be at least partially effective.

In the present pilot study, the survival benefits, safety and dose distribution to the tumor were evaluated in GBM patients who were treated with either the former intra-operative NCT (IO-NCT) or the current less invasive external beam NCT (EB-NCT).

2.Materials and Methods

The BNCT protocols in the present study were approved by the Medical Ethics Committee of the University of Tsukuba, and all participating patients were fully informed and provided their written informed consent. Following the 2005 policy of the International Committee of Medical Journal Editors (ICMJE), the later stage of this trial (EB-NCT) was registered with the Japanese authority on clinical trial registration (University Hospital Medical Information Network Clinical Trial Registry: UMIN-CTR; Trial ID: C000000298).

BSH (5 g/body) was administrated intravenously 12 hours before neutron irradiation. Additionally, a water soluble fructose complex of BPA (250 mg/kg) was given 1 hour before

irradiation for the 8 patients who underwent EB-NCT. ^{18}F-labeled positron emission tomography (PET) was performed prior to EB-NCT in order to calculate the lesion-to-normal ratio of BPA-mediated ^{10}B. A tumor-to-BSH-mediated blood ^{10}B concentration ratio of 1.0 was used to estimate the boron dose to be delivered to the tumor tissue.

Neutron irradiation in both IO- and EB-NCT was performed in a single fraction using an epithermal or epithermal-thermal mixed beam from the Japan Research Reactor No. 4 (JRR-4). Additional photon irradiation, at a total X-ray dose of 30 Gy in 15 fractions or 30.6 Gy in 17 fractions, was given to high-intensity areas on T2-weighted magnetic resonance (MR) images to compensate for an insufficient dose distribution in EB-NCT relative to IO-NCT.

For EB-NCT, the various prescribed doses, including the minimum tumor dose at clinical target volume (CTV)-1, CTV-2 and CTV-3, the maximum normal brain dose, the maximum skin dose and the averaged brain dose, were calculated using the JAEA Computational Dosimetry System (JCDS). CTV-1 was defined as a gross residual or unresected tumor that appeared as a Gd-enhanced area in MR images within three days after surgery. In a cases without a Gd-enhanced area, a 5-mm margin of the post-surgical cavity was defined as CTV-1. CTV-2 (3) was defined as a volume consisting consisting of 2 (1)-cm around CTV-1 (CTV-2).

The median age at primary diagnosis was 57 years (range, 32-76). All patients underwent surgical removal before BNCT. The median age of the IO-NCT patients was 51 years (range, 38-64) and that of the EB-NCT patients was 65 years (range, 32-76). All patients were followed up clinically and by MR imaging every 1-3 M. Survival time and survival rate were estimated using the Kaplan-Meier method to assess the efficacy of NCT. The log-rank test was used to compare survival times in each type of NCT.

3.Results and Discussion

The most common acute adverse event was mild erythema (Grade 1), which was observed in most patients. Three IO-NCT patients and one EB-NCT patient suffered transient orbital swelling accompanied by double vision (Grade 2). Three IO-NCT patients received frontotemporal irradiation without ideal neutron shielding due to skin reflection. One of these three patients suffered post-epileptic brain swelling (Grade 4) requiring surgical intervention.

No serious BSH- or BPA-related toxicity was observed in the present series. It has been reported that the majority of central nervous system toxicities in NCT are acute, self-limiting and primarily related to a temporal increase in intracranial pressure (Coderre et al., 2003). A tumor volume of more than 60 cm^3, an increased average brain dose, and an increased number of irradiation fields were found to lead to a higher incidence of such toxicities. An average brain dose of 6.2 Gy-Eq was associated with a 50% incidence of somnolence. As a consequence of the smaller tumor volume of 18.6$\pm$12.2 cm^3 and rather localized dose planning, lower average brain doses (3.9$\pm$1.8 Gy) were used in the present series compared to previously reported doses. The higher than average brain dose in the IO-NCT group (5.1$\pm$2.2 Gy) compared to the EB-NCT group (3.1$\pm$0.4 Gy) may have contributed to the higher incidence of toxicities.

Five of 15 patients were still alive at analysis, for a mean follow-up time of 20.3 M. Eleven of the 15 patients were followed up for more than one year; among these 11 patients, 8 (72.7%) maintained their KPS (90 in 6 and 100 in 2 cases). The median OS and median time to MR change (TTM) for all patients were 25.7 M and 11.9 M, respectively. There was no significant difference in OS and TTM between the IO-NCT (OS: 23.3 M; TTM: 12.0 M) and EB-NCT (OS: 27.9 M; TTM: 11.9 M) groups, respectively. The 1- and 2-year survival rates were 85.7% and 45.5%, respectively. Hatanaka and Nakagawa treated more than 200 patients with high-grade glioma with BSH-mediated IO-NCT, achieving a median OS of 22.9 M for GBM (Nakagawa et al., 2003). We previously reported 9 patients (GBM in 5, anaplastic astrocytomas in 4) with high-grade gliomas who were treated with BSH-mediated IO-NCT using a mixed epithermal beam of JRR-4 (Yamamoto et al., 2004). The median OS for the 5 GBM patients was 23.2 M. IO-NCT under 2 different protocols reported by Kageji (Kageji et al., 2006) showed median OSs for the higher and lower

dose groups of 19.5 and 15.3 M, respectively. In the present series, additional photon fractionation and the combination of two boron agents were employed in EB-NCT, resulting in similar 2-year survival rates in EB-NCT (50.0%) and IO-NCT (42.9%).

The use of additional photon radiation was based on the experimental data, which showed that the combination of BNCT and photon irradiation could enhance the therapeutic effects in tumor-bearing rats (Barth et al., 2004). BSH biodistribution studies have suggested that the primary mode of selective BSH distribution is passive diffusion from blood to tumor tissue via the disrupted blood brain barrier (BBB) (Hideghety et al., 2003; Joel et al., 1999).

The combination of BPA and BSH as well as a longer infusion of BPA appear to minimize the heterogeneous ^{10}B distribution in both experimental and clinical situations (Barth et al., 2004; Miyatake et al., Busse et al., Capala et al., 2003).

4.Conclusion

This NCT pilot study in 15 patients with newly diagnosed GBM showed survival benefits, suggesting that the neutron capture reaction may function sufficiently to control tumors locally, and that further optimized studies in large series of patients are warranted. No serious adverse events were observed in the patients who were better prepared for neutron shielding. The survival data of EB-NCT, which requires two boron agents and combined X-ray radiation, appear to be identical to those of IO-NCT.

Acknowledgements

This study was supported in part by a Grant-in-Aid from the Ministry of Education, Science and Culture, Japan (20390379).

References

Barth, R.F., Grecula, J.C., Yang, W. et al., 2004. Combination of boron neutron capture therapy and external beam radiotherapy for brain tumors. Int. J. Radiation Oncology Biol. Phys. 58, 267–277.

Busse, P.M., Harling, O.K., Palmer, M.R., et al., 2003. A critical examination of the results from the Harvard-MIT NCT program phase I clinical trial of neutron capture therapy for intracranial disease. Journal of Neuro-Oncology 62, 111–121.

Capala, J.H., Stenstam, B.H., Sköld, K., et al., 2003. Boron neutron capture therapy for glioblastoma multiforme. Journal of Neuro-Oncology 62, 135–144.

Coderre, J.A., Turcotte, J.C., Riley, K.J., et al., 2003. Boron neutron capture therapy: Cellular targeting of high linear energy transfer radiation. Technol Cancer Res T 2, 1-21.

Hideghety, K., Sauerwein, W., Wittig, A., et al., 2003. Tissue uptake of BSH in patients with glioblastoma in the EORTC 11961 phase I BNCT trial. J Neurooncol. 62, 145-56.

Joel, D.D., Coderre, J.A., Micca, P.L., Nawrocky, M.M., 1999. Effect of dose and infusion time on the delivery of p-boronophenylalanine for neutron capture therapy. J Neurooncol. 41, 213-221.

Kageji T., Nagahiro S., Matsuzaki K., et al. , 2006. Boron neutron capture therapy using mixed epithermal and thermal neutron beams in patients with malignant glioma-correlation between radiation dose and radiation injury and clinical outcome. Int. J. Radiat. Oncol. Biol. Phys. 65, 1446-1455.

Miyatake, S., Kawabata, S., Kajimoto, Y., et al.,2005. Modified boron neutron capture therapy for malignant gliomas performed using epithermal neutron and two boron compounds with different accumulation mechanisms: an efficacy study based on findings on neuroimages. J Neurosurg 103, 1000-1009.

Nakagawa Y., Pooh K., Kobayashi T., et al., 2003. Clinical review of the Japanese experience with boron neutron capture therapy and a proposed strategy using epithermal neutron beams. J Neurooncol 62, 87-99.

Yamamoto, T., Matsumura ,A., Nakai, K., et al., 2004. Current Clinical Results of the Tsukuba BNCT Trial. Applied Radiation Isotopes 61: 1089-1093.

Experimental Modified Orthotopic Piggy-back Liver Autotransplantation

L. Roveda[a], A. Zonta[b], F. Staffieri[c], D. Timurian[d], B. DiVenere[d], G.J. Bakeine[e], A.Crovace[c] U. Prati[a]

[a]*Oncologic Surgery, Cancer Center of Excellence Fond. "T.Campanella", Europa Avenue, Catanzaro – CZ-88100 – Italy*
[b] *Department of Surgery, University of Pavia - PV - 27100- Italy*
[c]*Veterinary Surgery Unit, Department of Emergencies and Organs Transplantation, Faculty of Veterinary Medicine, SP per Casamassima km 3, Valenzano – BA - 70010 - Italy,*
[d]*Surgery "Madonna delle Grazie" Hospital, Contrada Cattedra Ambulante, Matera – MT - 75100 - Italy*
[e]*Laboratorio Nazionale di Tecnologie Avanzate e Nanoscienza (TASC), Basovizza - TR - Italy*

Abstract

The classical orthotopic liver autotransplantation is a very challenging and time wasting technique, it includes the division of major hepatic vessels and choledocus, and subsequent reconnection by end to end anastomoses. The caval end to end anastomoses are the most difficult to be performed and the interposition of a prosthesis can be required. We adopted the classical orthotopic liver autotransplantation technique in 2 patients affected with diffused liver metastases from colorectal cancer, for extracorporeal Neutron Capture Therapy (BNCT). The procedure required very long operating times and the extracorporeal circulation set up; furthermore the vena cava reconstruction was performed by the interposition of a goretex-prothesis.
We propose a "modified orthotopic piggy-back technique" to simplify liver reconnection and shorten the operating time.
Materials and Methods: The technique was developed in the swine (25 kg body weight), under general anaesthesia. We performed the resection of the retro-hepatic vena cava with preservation of the caval flow during the anhepatic phase, by interposing a goretex prosthesis. The reconstruction of the V.Cava was then performed by a side-to-side cava-prosthesis anastomosis with lateral clamping of the prosthesis. The procedure was then completed according to the classical technique of liver transplantation.
Results: The mean time for VC reconstruction was 56 (+/- 10) min. and the mean time for side-to-side VC-prothesis anastomosis was 13 (+/- 4) min.
Conclusions: The "modified orthotopic piggy-back technique" can simplify the reimplant of the liver during autotransplantation and shorten the operating time. Furthermore also the time of total extracorporeal circulation is reduced, as during the anhepatic phase and during the side-to-side cava-prothesis anastomosis the flow in the inferior vena cava is uninterrupted.

Keywords: liver autotransplantation technique, ex situ liver surgery, liver malignancies, irresectable liver cancer, BNCT

1. Introduction

The BNCT of diffused liver metastases can be performed only in the isolated liver, thus the treatment includes liver explant and subsequent re-implant after neutron irradiation inside the thermal column of a nuclear reactor. For the re-implant of the liver after the treatment we have adopted the classical technique of orthotopic liver autotransplantation that proved to be very complex, mainly owing to the shortness of the vascular stumps and the use of a prosthesis was required in the reconstruction of the vena cava. An extracorporeal circulation with bypass from the portal vein and the left femoral vein to the left axillary vein, was set up. All this yelded not inconsiderable morbidity and prolonged the operating time.
Thus we propose a modified orthotopic piggy-back technique to simplify this procedure and to shorten the operating time as well as the time of total extracorporeal circulation.

2. Materials and methods

We have developed the method in the swine. After approval by the ethical committee of the Ministry of Health a 4-month old female

Large White pig weighing 20 kg underwent experimental surgery under general anaesthesia. The animal was fasted for 24 hours before induction of anaesthesia.

Anaesthesia. Pre-anaesthetic medication: azaperone (Stresnil 4%; Janssen-Cilag, Beerse, Belgium) 8 mg/kg intramuscularly (IM) and atropine (Atropina Solfato 0.1%; ATI, Bologna, Italy) 0.06 mg/kg IM. After 20 minutes the pig was sedated and in lateral recumbency. An intravenous (IV) catheter was placed into the auricular vein of the right ear and Ringer's lactate solution (10 mL/kg/hour) was infused. General anaesthesia: was induced with fentanyl (Fentanest; Pharmacia & Upjohn, MI, Italy) 4.0 µg/kg IV followed by thiopental (Pentothal Sodium; Gellini, Aprilia, Italy) 10.0 mg/kg IV. After tracheal intubation using a 7.0-mm diameter cuffed endotracheal tube, the pig was connected to a rebreathing circuit and its lungs ventilated mechanically (Ohmeda 7850 ventilator; Datex Ohmeda, Helsinki, Finland). The tidal volume was 20 mL/kg and the respiratory rate was adjusted to maintain end-tidal CO_2 tension (PE¢CO_2) at 4.6–5.9 kPa (35–45 mmHg). Anaesthesia was maintained with sevoflurane (Sevorane; Abbott, Aprilia, Italy) delivered in 100% O_2 and supplemented with fentanyl administered at a constant rate infusion (10 lg kg/1 hour). The right jugular vein and carotid artery were surgically exposed for placement of venous and arterial catheters. The tip of the venous catheter was advanced to the level of the right atrium for the continuous measurement of the central venous pressure (CVP). The correct positioning of the catheter was confirmed by the presence of an appropriate CVP trace. The carotid artery was cannulated with a 14 SWG catheter for continuous arterial pressure monitoring and for withdrawal of blood samples for arterial blood gas analysis (IRMA SL Blood Analysis System; Diametrics Medical, St.Paul, MN, USA). The electrocardiogram, heart rate, haemoglobin saturation of oxygen, PE¢CO2, respiratory gas composition, respiratory rate, tidal volume, airway pressure, systolic arterial blood pressure, CVP were continuously monitored and automatically recorded (Ohmeda Modulus CD; Datex Ohmeda, Helsinki, Finland).

Surgery. During hepatectomy the division of the supra-hepatic and infra-hepatic vena cava was performed; retrohepatic vena cava was removed en-bloc with the liver. The liver was perfused with hypothermic preservation solution (University of Wisconsin) at the back table and the two ends of the retrohepatic vena cava were closed with a running suture (6-0).

The back wall of retro-hepatic vena cava was incised for a length of 3-4 cm including the entry points of the hepatic veins. (fig. 1)

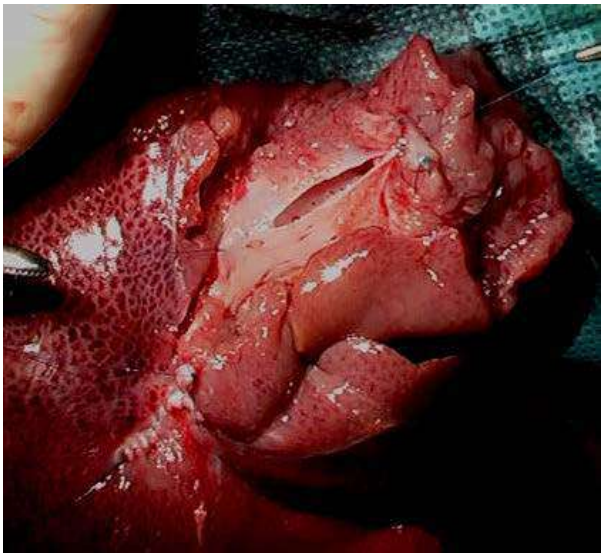

Fig. 1. Back wall of retro-hepatic vena cava

In the meanwhile a caval prosthesis (2 cm in diameter) was used for the cava reconstruction; then the prosthesis was clamped laterally with a Satinsky clamp and was incised for a length of 3-4 cm. (fig. 2).

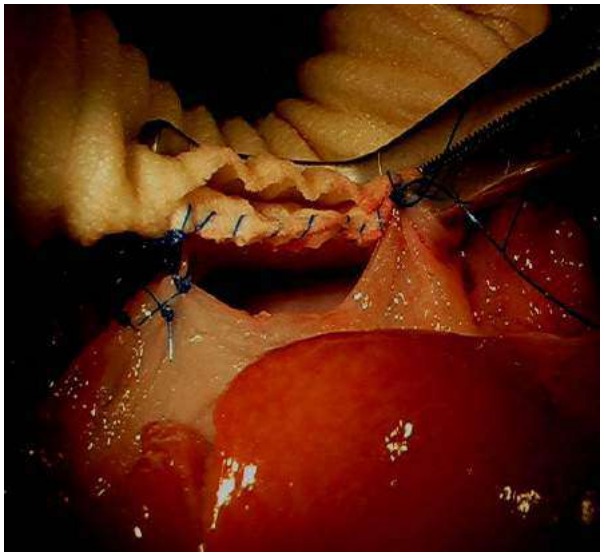

Fig. 2. Lateral clamping of the prosthesis and side-to-side anastomosis

Finally a side-to-side cava-prosthesis anastomosis (running monofilament 4-0 suture) was carried out (Fig. 3).

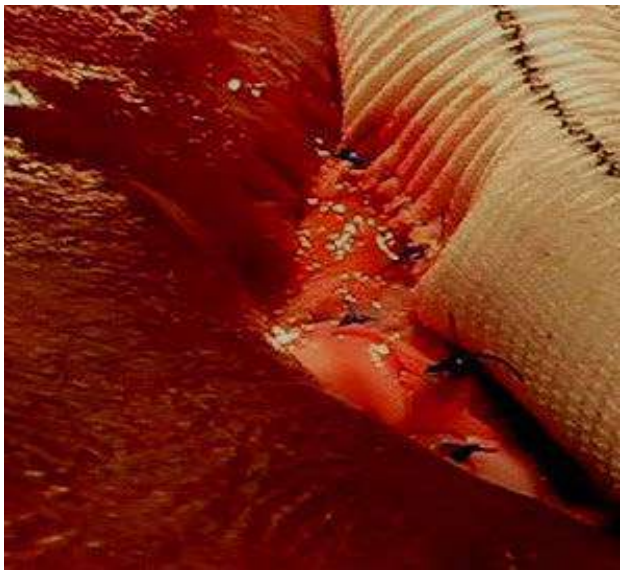

Fig. 3. Side-to-side cava-prosthesis anastomosis

3. Results

The closure of the ends of retrohepatic vena cava required 10 minutes.
The interposition of the caval prosthesis required 56 (+/- 10) min.
The side-to-side cava-prothesis anastomosis with lateral clamping of the prothesis proved to be rather simple and the required time was about 13 (+/- 4) min.

4. Discussion

Ex-vivo liver surgery was developed by R. Pichlmayr in 1988 (Pichlmayr et al., 1988; Pichlmayr et al., 1989; Pichlmayr et al., 1990; Oldhafer et al., 2000) to expand the surgical treatment to otherwise irresectable tumours. The classical orthotopic liver autotransplantation includes the division of retrohepatic vena cava after positioning clamps on the supra-hepatic and infra-hepatic vena cava; the portal vein and hepatic artery are clamped and divided too. Thus the organ can be completely removed from the body with the respective vena cava segment. Finally, after ex situ liver surgery, the liver is reimplanted. During the anhepatic period, a veno-venous bypass connecting the portal vein and inferior vena cava with the axillary vein is set up.
We have adopted this technique to reimplant the liver after BNCT in the isolated organ, to treat liver metastases from colorectal cancer, in 2 patients (Zonta et al., 2006).
The reconstruction of supra-hepatic vena cava was rather difficult because, in contrast to cadaveric liver transplantation, shorter stumps were available for anastomoses, and the interposition of a Goretex-prothesis (20 mm diameter) was required in both patients. The Goretex prothesis was sutured to the supra-hepatic vena cava, then 2 end-to-end anastomoses (cava-prothesis and cava-caval) were required to reconnect the liver.
The mean time for vena cava reconstruction was of about 3 hours in the 2 patients, ECC was manteind for 5h30' and 6h10', while the total operation time was of 21h and 18h40' in the first and second patient respectively.
Post-operative complications in both of the patients were represented mainly by coagulopathy with after-bleeding that in 1 patient required re-laparotomy, jaundice, liver insufficency, renal failure, pleural effusion and femoral vein thrombosis in the site of insertion of the cannula for extracorporeal circulation (ECC).
From our experience we have yelded that the technique of orthotopic liver autotransplantation described by Pichlmayr in 1988 could be improved by the use of a "modified piggy-back technique".
The "piggy-back technique" was developed by Calne (1968) who described a technical modification of caval anastomosis with preservation of the recipient retrohepatic vena cava.
Later on a side-to-side cava-caval anastomosis was introduced by lateral clamping of the recipient vena cava during liver re-implant with preservation of the flow in the vena cava (Belghiti et al., 1992; Lerut et al., 1994; Lerut et al.,1995). This procedure is almost always well tolerated haemodynamically and allows to avoid extracorporeal bypass; a temporary porto-caval shunt can be required in situations with poorly developed porto-systemic collateral circulation to maintain a good haemodynamic stability.
The "modified Piggy-back technique" that we propose includes "en-bloc" dissection of the entire retro-hepatic vena cava with the liver and immediately subsequent vascular reconstruction of the vena cava by the interposition of a Goretex prothesis. This allows an early dismission of total ECC while only the portal decompression is still required. The closure of the two ends of the retro-hepatic vena cava with running sutures is performed at the back table, and finally liver reconnection by "piggy back technique" with a

side-to-side cava-prosthesis anastomosis is completed.
This technique can remarkably shorten the time of total extracorporeal circulation but it is not a reason to completely forget a veno-venous bypass, to avoid the inevitable congestion of the splanchnic system in situations withouth poorly developed porto-systemic collateral circulation.
Anyway the reduced time of total extracorporeal circulation should reduce the risk of potential haemodynamic disruption and circulatory instability.
Furthermore this technique could shorten the time of vascular reconnection of the liver since the vena cava reconstruction, by the interposition of a prothesis, could be carried out during the anahepatic phase when the liver is away for extracorporeal treatment, with reduced risk of intra-oprative bleeding as well as of afterbleeding.
Finally to perform a side-to-side cava-prothesis anastomosis is obviously easier and faster than to perform 2 end-to-end caval anastomoses as required in traditional orthotopic liver autotransplantation.

5. Conclusions

We think that the proposed "modified piggy back technique" could help to simplify the liver reconnection after extracorporeal treatment, as well as to reduce the time of total ECC and the mean operation time, thus permitting earlier extubation and possibly reduction of the rate of post-operative complications (such as afterbleeding, neurological deficits, and wound infections) with a global improvement of the early postoperative outcome.

References

Belghiti, J., Panis, Y., Sauvanet, A., Gayet, B., Fekete, F., 1992. A new technique of side to side caval anastomosis during orthotopic hepatic transplantation without inferior vena caval occlusion. Surg. Gynecol. Obstet. 175,271-272.

Calne, R.Y., William, R., 1968. Liver transplantation in man: observations on technique and organization in five cases. BMJ 4,535.

Lerut, J., de Ville de Goyet, J., Donataccio, M., Reding, R., Otte, J.B., 1994. Piggyback transplantation with side-to-side cavo-cavostomy is an ideal technique for right split liver allograft implantation. J. Am. Coll. Surg. 179,573-576.

Lerut, J.P., Bourlier, P., de Ville de Goyet, J., Laterre, P.F., Reding, R., Otte, J.B., 1995. Improvement of technique for adult orthotopic liver retransplantation. J. Am. Coll. Surg. 180:729-732.

Oldhafer, K.J., Lang, H., Schlitt, H.J., Hauss, J., Raab, R., Klempnauer, J., Pichlmayr, R., 2000. Long-term experience after ex situ liver surgery. Surgery 127:520-527.

Pichlmayr, R., Bretschneider, H.J., Kirchner, E., Ringe, B., Lamesch, P., Gubernatis, G., Hauss, J., Niehaus, K.J., Kaukemuller, J., 1988. Ex situ Operation an der Leber. Eine neue Moglichkeit in der Leber-chirurgie. Langenbecks Arch. Chir. 373,122-126.

Pichlmayr, R., Gubernatis, G., Lamesch, P., Raygrotzi, S., Hauss, J., 1989. Europaisches Thema Leberchirurgie – Neu – entwicklungen in der Leberchirurgie (in situ Protektion und ex situ Operation). Langenbecks Arch. Chir. Suppl. II Verh Dtsch Ges Chir. 257-261.

Pichlmayr, R., Grosse, H., Hauss, J., Gubernatis, G., Lamesch, P., Bretschneider, H.J., 1990. Technique and preliminary results of extracorporeal liver surgery (bench procedure) and of surgery on the in situ perfused liver. Br. J. Surg. 77,21-26.

Zonta, A., Prati, U., Roveda, L., Ferrari, C., Zonta, S., Clerici, A.M., Zonta, C., Pinelli, T., Fossati, F., Altieri, S., 2006. Clinical lessons from the first applications of BNCT on unresectable liver metastases. Journal of Physics: Conference Series 41,484–495. doi:10.1088/1742-6596/41/1/054

Irradiation of an Explanted Pig Liver at the HFR Petten

Ray Moss[1], Gernot Kaiser[2], Sander Nievaart[1], Andrea Wittig[3], Antoaneta Roca[1], Lucien Pott[1], Silvio Nadalin[2], Wolfgang Sauerwein[3]

[1]*HFR Unit, Institute for Energy, JRC Petten, The Netherlands*
[2]*General Surgery & Transplantation, University Hospital Essen, Germany*
[3]*Strahlenklinik, University Essen, Germany*

Abstract

As part of a study between the University Hospital Essen and the JRC Petten to assess the feasibility to perform BNCT on an explanted organ (liver) at the HFR, a liver was taken from a pig in the operating theatre for animals at the Central Animal Facility of the Medical Faculty in Essen, and transported by car to Petten. On arrival 3 hours later, the liver was placed into the special PMMA holder and loaded into the custom-built Liver-Irradiation-Facility (LIF). Air supply provided by cold gun sprays gave a temperature of 5–10 °C around the liver holder throughout the irradiation, which lasted 3 hours exactly. The liver was then brought back to Essen. It was noted that the liver was more radioactive than expected, in comparison to a patient irradiation. The measured radiation level directly following radiation was almost 200μSv/h on contact but after only about 15 minutes, halved to 100μSv/h, due to activated ^{24}Na. The exercise established where improvements are needed, including: writing of Standard Operating Procedures; documentation files fulfilling the legal requirements for human irradiation; a treatment plan; better temperature control, including calibration of the cold guns; but also the need for ready availability of equipment, such as ice and cleansing material (tissue, alcohol, etc.). The overall exercise is one of the first of many procedures, i.e. testing of the transport logistics and the irradiation device (LIF), and should be seen as one of a number of steps needed prior to a full human treatment.

Keywords: BNCT, liver cancer, explanted liver, reactor

1. Introduction

Following the successful demonstration in 2001 by the group of Professor Aris Zonta and co-workers at Pavia Italy [1], who performed extra-corporeal treatment of liver metastases by BNCT, studies have been underway at Petten in collaboration with the University Hospital Essen to ascertain whether such a treatment would be possible at the HFR.

In 2005, a special facility was designed and built to hold the liver during treatment [2]. Unlike the Italian experience, where the liver was placed in the thermal column of the reactor, which effectively surrounds the liver by thermal neutrons only, the design at Petten had to develop a technique to perform the same treatment but using a directed beam of epithermal neutrons. Some initial validation measurements were carried out in 2006, including the cooling of the facility (the liver will need to be kept at a temperature of approximately 4ºC, for over 2 hours) and more sophisticated dosimetry measurements, including gel dosimetry, to validate the neutron and gamma conditions.

A more rigorous test was then performed at the beginning of 2008, whereby a liver was explanted from a pig in the operating theatre of the Department of Transplantation Surgery at the University Hospital Essen, and transported to Petten for irradiation.

This paper reports on the results of this stage of the project and plans for the coming year.

2. Materials and Methods

Liver

For the testing of the logistics and the full irradiation procedure at the HFR (as reported in this paper), a pig liver was used, which was provided by the Central Animal Facility at the University Duisburg-Essen.

In an earlier step in the project, human livers had been placed into the Petten liver holder in one of the operating theatres in the Department of General Surgery and Transplantation, in order to assess the geometric parameters for the final holder design.

Liver Irradiation Facility (LIF)

The major difference between the HFR and the facility at Pavia is that the HFR beam is predominately, a forward directional beam of epithermal neutrons, as opposed to an almost pure thermal neutron field in Pavia. The task at Petten was to construct a facility, which would hold the liver during treatment and would give a homogenous thermal neutron distribution throughout the liver. Design calculations showed that this can be reasonably achieved in a spheroid shaped holder, which would rotate during irradiation. The facility was built during 2005 (see Figure 1).

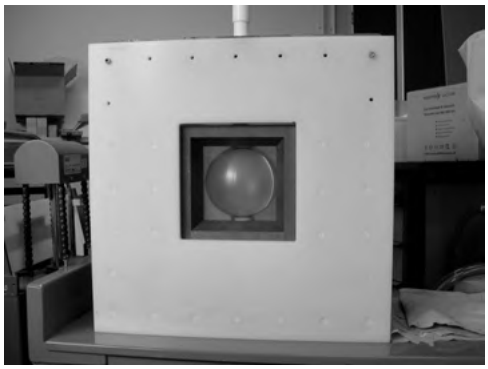

Figure 1: Beam-eye view of Liver Irradiation facility, with the rotating liver holder at the centre of the facility

Cooling

One of the most important criteria during irradiation if that the liver remains cooled at temperatures below 4°C. This led to a device, in fact 2, called a Cold Gun Spray®, which is an ingenious and simple design that by means of the principle of a vortex tube utilises standard compressed air to produce a jet of cold air at more or less zero degrees.

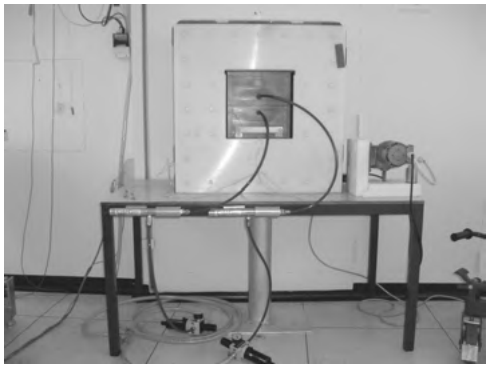

Figure 2: Liver facility with Cold Gun Sprays fitted

Dosimetry

To validate the design calculations, dosimetry measurements using activation foils and gel dosimetry have been performed.

3. Results and Discussion

On 30th January 2008, between 01:00 and 03:00 a.m., a liver was explanted from a pig in the operating theatre of the Department of Transplantation Surgery at the University Hospital Essen. The pig liver was placed into a standard plastic bag, normally used in organ transport, and the bag filled with a copious amount of preservation fluid. This bag was then placed in a second bag, again filled with the fluid, and secured with wire. A third bag was placed around this without fluid. The completed bag was then placed in an organ-transport box, which was partially filled with water and (mushy) ice. At 05:00 a.m., the box was collected and transported to Petten by private car.

The liver arrived in Petten at 08:40 a.m. The box was taken into the reactor building at 08:53 a.m.

Three days earlier, the liver irradiation facility (LIF) had been placed in the BNCT irradiation room and tests had been carried out to familiarise the irradiation team with the operation of the LIF. In particular, testing of the cold gun sprays proved to be trickier than anticipated.

At 09:30 a.m., it was apparent that the liver with the bags was too large for the holder. Also, the second bag was ripped, possibly occurring in the operating theatre, resulting in a large amount of fluid in the third bag. Excess preservation fluid was drained off. This had to be done twice before it was possible to fit the liver into the holder (see Figure 3). During the first attempt to squeeze the liver into the holder, the bags were punctured during the screwing together of the 2 hemispheres. At 09:48 a.m., the holder was loaded into the facility. The air supply to the cold gun sprays was switched on. At 09:50 a.m., the temperature readings of the 4 thermo-couples were already in a range of 5–10 °C. The upper cooling gun required a pressure of 4 bar and the lower one, 3 bar. The irradiation started at 09:55 a.m. and was stopped at 12:55 p.m.

Figure 3: Liver placed into the holder

During the irradiation, the pressure to the cold guns had to be adjusted several times in an attempt to keep the temperatures within the desired range (see Figure 5). The liver left to return to Essen at 13:00 p.m.

Following irradiation, the radioactivity of the liver was measured and it was noted that the level of radioactivity was higher than expected, in comparison to a patient irradiation. The measured radiation level directly following radiation was almost 200μSv/h on contact but decreased after only 15 minutes, to about 100μSv/h. The remaining activity was from ^{24}Na, whose activity decreased gradually over time.

4. Conclusions

The overall purpose in this present phase of the project was to ascertain weaknesses in the logistics and procedures, in order to improve the treatment for additional steps. It was concluded that in general the test procedure had been performed quite successfully. However the following observations were made:

- check lists should be made, preferably in the form of a Standard Operating Procedure, to clarify shortcomings in the requirements and logistical steps during such an irradiation. For example: availability of frozen water (ice), sterile area, second sterile transport box, extra plastic bags for the liver, preservation fluid and scissors and cleaning material (tissue, alcohol, etc.)
- The use of the temperature control system (cold gun sprays) needs to be optimised (more testing) and calibrated
- A documentation file should be developed, i.e. treatment plan, similar to a full “patient-type” run, i.e. labview, dosimetry, entrance via the BNCT Wing, etc

The fact that the liver was more radioactive than expected is not a major cause for concern, as the activity quickly reduced. It would necessary, as it already

is, to complete a radiation transport form, involving alerting the HFR health physicist beforehand.

In collaboration with the University of Duisburg-Essen, following new, promising results [4], it is now the intention to repeat the exercise under a more rigid "medical" test. Thereafter, within 2 years, test involving human livers.

References

1. T. Pinelli, A. Zonta, S. Altieri, S. Barni, A. Braghieri, P. Pedroni, P. Bruschi, P. Chiari, C. Ferrari, F. Fossati, R. Nano, S. Ngnitejeu Tata, U. Prati, G. Ricevuti, L. Roveda and C.Zonta, "TAOrMINA: From the first idea to the application to the human liver," in *Research and Development Neutron Capture Therapy*, edited by W. Sauerwein, R. Moss and A. Wittig, Bologna (Monduzzi Editore), 1065-72 (2002).
2. V. A. Nievaart, R. L. Moss, J. L. Kloosterman, T. H. J. J. Van Der Hagen, H. Van Dam, A. Wittig, M. Malago, W. Sauerwein: Design of a rotating facility for extracorporal treatment of an explanted liver with disseminated metastases by boron neutron capture therapy with an epithermal neutron beam. Radiation Research 166, 81-88, 2006
3. Gambarini G., Daquino G.G., Moss R.L., Carrara M., Nievaart A.V., Vanossi E., "Gel Dosimetry in the BNCT Facility for Extra-Corporal Treatment of Liver Cancer at the HFR Petten", **Radiation Protection Dosimetry, vol 123, Special Issue Neudos-10** (May 2007)**,** 1-6
4. Wittig A, Malago M, Collette L, Huiskamp R, Bührmann S, Nievaart V, Kaiser GM, Jöckel KH, Schmid KW, Ortmann U, Sauerwein WA, "Uptake of two (10)B-compounds in liver metastases of colorectal adeno-carcinoma for extracorporeal irradiation with boron neutron capture therapy (EORTC trial 11001)", **Int J Cancer:** 122, 1164-1171 (2008)

Acknowledgement

The project gained additional funding from the JRC's Innovation Project scheme in 2005.

Figure 5: Chart of one of the 4 thermocouple readings positioned close to the holder during the irradiation period

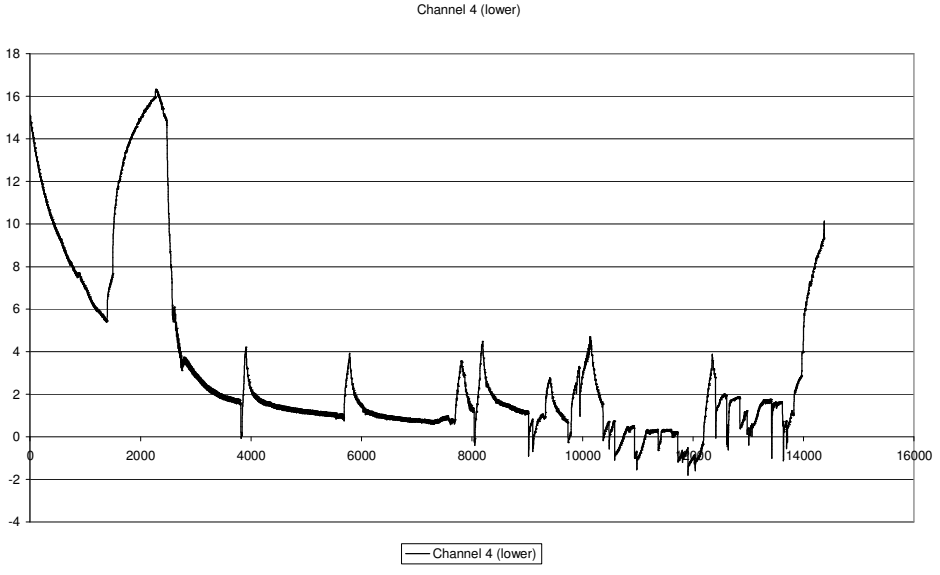

Uptake of BSH and/or BPA in human xenografts on nude mice

Andrea Wittig[1], Gero Hilken[2], René Huiskamp[3], Finn Stecher-Rasmussen[4], Raymond Moss[5], Jürgen Rassow[1], Christian Kriegeskotte[6], Wolfgang Sauerwein[1]

[1]Dept. of Radiation Oncology, University Hospital Essen, University Duisburg-Essen, Germany [2]Central Animal Laboratory, University Hospital Essen, University Duisburg-Essen, Germany
[3]Nuclear Research and consultancy Group (NRG), Petten, The Netherlands
[4]NCT Physics, Alkmar, Netherlands,
[5]HFR Unit, Institute for Energy, Joint Research Centre, European Commission, Petten, The Netherland
[6]Physikalisches Institut, Westfälische Wilhelms-Universität Münster, Münster, Germany

Boron neutron capture therapy (BNCT) relies on the preferential delivery of a ^{10}B-compound to tumor cells. Sound knowledge on the ^{10}B-uptake in tumors but also in surrounding healthy tissues is of fundamental importance for developing the method.

The ^{10}B-uptake as delivered by the compounds sodium mercaptoundecahydro-*closo*-dodecaborate (BSH) and L-para-boronophenylalanine (BPA) was investigated in 4 human tumors (sarcoma (S3), melanoma (MV3), glioblastoma (U87MG), adenocarcinoma (PC-3)) and a murine sarcoma (MuEs) xenografted in nu/nu mice by prompt gamma ray spectroscopy ($n \geq 8$).

After BPA-injection alone ^{10}B-accumulation was observed in all tumors (tumor-blood ratios: 2.0-2.4). BSH injection alone led to tumor-blood ^{10}B-ratios of 0.8 -1.5 with significantly higher ratios for the MV3 and S3 tumors. A co-application of drugs increased the absolute ^{10}B-concentrations in tumors but failed to improve the tissue-blood ^{10}B-ratio.

The significantly different uptake of BSH in different tumors underlines the need to further investigate the possibilities of this drug for BNCT.

Uptake of BSH and BPA in head and neck squamous cell carcinoma in human patients

Andrea Wittig[1], Klaas Appelman[2], Stephan Lang[3], Laurence Collette[4], Sandra Bührmann[5], Karl-Heinz Jöckel[6], Kurt Werner Schmid[7], Uta Ortmann[1], Raymond Moss[8], Wolfgang Sauerwein[1]

[1] *Dept. of Radiation Oncology, University Hospital of Essen, University Duisburg-Essen, Essen, Germany*
[2]*Nuclear Research and consultancy Group (NRG), Petten, The Netherlands*
[3]*Dept. of Otorhinolaryngology, Head and Neck Surgery, University Hospital of Essen, University Duisburg-Essen, Essen, German*
[4]*Statistics Department, European Organisation for Research and Treatment of Cancer (EORTC), Headquarters, Brussels, Belgium*
[5]*Pharmacy of the University Hospital of Essen, University Duisburg-Essen, Essen, Germany*
[6]*Institute for Medical Informatics, Biometry and Epidemiology, University Hospital of Essen, University Duisburg-Essen, Essen, Germany*
[7]*Institute of Pathology and Neuropathology, University Hospital of Essen, University Duisburg-Essen, Essen, Germany*
[8]*HFR Unit, Institute for Energy, Joint Research Centre, European Commission, Petten, The Netherlands*

Purpose: Boron Neutron Capture Therapy (BNCT) might overcome problems encountered with treatment of advanced squamous cell carcinoma of head and neck (SCCHN) especially hypoxia, relative radio-resistance and location near critical organs. This trial investigates the uptake of the compounds sodium mercaptoundecahydro-closo-dodecaborate (BSH) or L-*para*-boronophenylalanine (BPA) in SCCHN.

Experimental Design: In a controlled prospective clinical trial (EORTC 11001) 3 patients were infused with BSH, 3 patients with BPA prior planned resection of the malignant lesion. Samples of tissues and blood were analyzed for the ^{10}B-concentration with prompt gamma ray spectroscopy.

Results: Adverse effects from compounds did not occur. After BPA-infusion the mean ^{10}B-concentration ratio tumor/blood was 4.0 ± 1.7. Mean ^{10}B-concentration ratios between tumor and healthy tissue were 2.1 ± 1.2 for muscle, 1.3 ± 0.5 for skin and 1.4 ±0.01 for mucosa, respectively. After BSH-infusion the mean ^{10}B-concentration ratio tumor/blood was 1.2 ± 0.4. The ^{10}B-concentration ratio between tumor and healthy tissues was 3.6 ± 0.6 for muscle, 1.4 ± 0.5 for skin and 1.0 ±0.3 for mucosa.

Conclusions: BPA and BSH deliver ^{10}B to SCCHN to an extent that substantiates the potential of BNCT to treat this tumor. Mucosa and skin are the most relevant organs at risk for both compounds, whereas high ^{10}B-concentrations in blood reveal the vasculature of healthy organs at risk for a BSH-mediated BNCT. More efforts are necessary to better understand the metabolism of BSH. The simultaneous application of both drugs can be justified.

CNAO: The Italian Hadrontherapy facility

Roberto Orecchia[1,2,3], Sandro Rossi[3], Piero Fossati[1,3]

[1]*Institute of Radiological Sciences, University of Milano, Via a. di Rudinì 8, Milano 20142, Italy*
[2]*European Institute of Oncology, via Ripamonti 435, Milano 20141, Italy*
[3]*National Centre for Oncological Hadrontherapy (CNAO), Via Caminadella 16, Milano 20123, Italy*

Abstract

CNAO will be a dual center capable of providing therapeutic beams of protons and carbon ions with maximum energy of 400 MeV/u. At the beginning, it will be equipped with three treatment rooms with fixed horizontal and vertical beam lines. In a subsequent phase, two more rooms with a rotating gantry are foreseen. An active spot scanning dose delivery system will be employed. Initially, 80% of the treatments will be carried out with carbon ions. All patients will be treated within clinical trials to assess carbon ion indications with an evidence-based methodology. Seven disease-specific working groups have been developed: lung tumors, liver tumors, sarcomas, head and neck tumors, central nervous system lesions, eye tumors and pediatric tumors. The last two groups will be treated mainly with protons. In the first phase, CNAO will focus on head and neck cancers, treating inoperable, residual or recurrent malignant salivary gland tumors, mucosal melanoma, adenocarcinoma and unfavorably located squamous cell carcinoma (SCC) of the nasal and paranasal sinuses. Carbon ions will be employed as a boost in the treatment of locally advanced, poor prognosis, SCC of the hypopharynx and tongue base. Bone and soft tissue sarcomas of the extremity will be treated with a limb-sparing approach, and trunk sarcomas will be treated with exclusive or post-operative irradiation. Skull base tumors (chordoma and chondrosarcoma), recurrent or malignant meningioma and glial tumors will be treated with carbon ions.
After sufficient expertise has been gained in coping with organ motion, CNAO will start treating thoracic and abdominal targets. HCC will be treated in inoperable patients with one or more lesions that can be included in a single CTV. Early stage NSCLC will be treated. In the second phase, two more groups on gynecological malignancies and digestive tumors (esophageal cancer, rectal cancer, pancreatic cancer) will be created.

Keywords*: hadrontherapy, protontherapy, high LET particle beams, carbon ions radiotherapy*

1. Introduction

Hadrontherapy is a kind of high precision radiotherapy that employs subatomic particles called hadrons. The use of positively charged particles beams has been proposed for the first time by the nuclear physicist Robert Wilson in 1946[1] and the first patient has been treated at Lawrence Berkeley Laboratories, CA in 1954[2]. Until the 1990s hadrontherapy was in its pioneering age: treatment was carried out in nuclear physics research centers and could rarely rely on adequate imaging, treatment planning, and patient set-up technologies.
One of the most relevant experiences was conducted at the Massachusetts General Hospital (MGH) in cooperation with Harvard Cyclotron Laboratories (HCL) employing proton beams[3].
Results obtained in this first phase prompted the construction, in 1992 of the first hospital based proton therapy facility in Loma Linda, CA[4]. Since then, more than 50.000 patients have been treated with protons worldwide. Treatments with different species of ions (helium, neon and others) were initially performed at Bevalac, CA[5] but were not subsequently pursued in the USA. The Heavy Ion Medical Accelerator in Chiba (HIMAC) was the first hospital based facility employing ions to start operation in 1994 in Japan[6]. HIMAC has selected carbon ions as the most promising particles. Carbon ions have been employed in another hospital based Japanese centre (Hyogo Ion Beam Medical Centre, HIBMC, Hyogo) and in a physics research centre, Gesellschaft fur Schwerionenforschnung (GSI), Darmstaadt, Germany. More than 3.000 patients have been treated with carbon ions up to now.
Protons and carbon ions are the only two particles that are used in modern hadrontherapy; they have a finite range of penetration in tissues which can be adjusted varying their energy. They have an inverse depth dose profile and deposit most of their energy at the end of their path in the so called Bragg peak. Distal to the Bragg peak dose falls sharply to zero for proton whereas carbon ions show a distal tail in their dose profile due to particle fragmentation.

These physical characteristics permit a very high degree of conformality in dose distribution with an optimal sparing of surrounding healthy tissues. In addition to increased conformality, carbon ions are characterized by an increased relative biological efficacy (RBE). The high RBE is due to their high LET and related high density of ionization that results in clustered damages to the DNA with multiple double strand breaks. This damage is very rarely repaired by cells and results in clonogenic death in a much higher percentage as compared to the damages done by low LET radiations.
A high LET and RBE could result in worse side effects (as is the case for neutron therapy), but hadrons should actually be described as variable LET particles. In fact their LET changes along their path, producing more spaced ionization in the more superficial layers and denser ones near the end of the track; therefore hadrons deliver a low RBE dose to tissues in front of the target and a high RBE dose to the tumor. Carbon ions have the highest ratio between RBE in the Bragg peak and RBE in the entrance channel and therefore have supplanted other ion species in clinical practice.

2. The CNAO facility

CNAO will be a hospital for outpatients treatments with both proton therapy (PT) and carbon ions radiotherapy (CIRT). The basic design of the CNAO accelerator (synchrotron) and lines has been hosted at the European counsel for Nuclear Research (CERN) in the frame of the Proton-Ion Medical Machine Study (PIMMS), from 1996 to 1999[7]. This design has been fully engineered, first by TERA and then by CNAO/INFN (with cooperation of GSI, CERN, University of Pavia and Subatomic and Cosmologic Physics Laboratories / National Institute of Nuclear and Particle Physics (LPSC/IN2P3) Laboratory of Grenoble).

The synchrotron will be the heart of the facility and will be able to accelerate proton and carbon ion to a maximum energy of 400 MeV/u (corresponding to 27 cm penetration depth in water). Three rooms equipped with fixed beam line (two rooms with horizontal beam and one room with vertical and horizontal beam) will be operative, for patient treatment, from the first phase. The facility has been designed to allow a foreseen upgrading with two more rooms equipped with rotating gantries with minimal impact on its daily clinical activities. In every room it will be possible to perform proton therapy and carbon ion radiotherapy (CIRT) and all the devices are designed for both the beams.

Switching between protons and carbon ions on a patient per patient basis will be possible without impacting on the time schedule of the facility. An experimental beam line with a dedicated room will be available from the first phase for radiobiology and physics R&D.

CNAO will employ an active spot scanning system. Two orthogonal magnetic fields will be used to scan the beam in planes parallel to its direction. Magnets will be (?have been) designed to allow scanning of square slices of 20 x 20 cm. Depth will be varied directly by adjusting the beam energy. The smallest step of penetration range achievable will be 0.2 mm. The synchrotron allows varying the energy at each spill, so that every second it will be possible to irradiate a layer of different depth. Scanning magnets, sensors to measure position and intensity of the beam and control systems will be integrated in the nozzle. Different spot size will be available (with a radial size adjustable from 4 mm to 10 mm in steps of 1 mm). The active scanning system and the dose rate have been designed to be able to deliver 2 Gy to a volume of 1 litre in 1 – 1.5 minutes.

Spot scanning allows employing inverse dose optimization algorithms similar to those created for IMRT and therefore to perform the so called intensity modulated particle therapy (IMPT) that enables to fully exploit hadrons favourable physical features. Treatments will be performed with patients immobilized on specially designed couches or chairs (with possibility of a bite block) that will be docked to a state-of the art, 6 degrees of freedom, mobilization device. Set-up verification will be performed with orthogonal KV images of diagnostic quality. Additionally optoelectronic system with markers detection and surface detection capability will be used. CNAO aims to have a high patients through-put.

Design has specifically addressed this issue and dedicated positioning rooms have been built (Computer Aided Positioning, CAP rooms). Patients will be positioned on the couch (or on the chair) outside the treatment room, and will be carried in the treatment room on a trolley predisposed for docking with the mobilization device, thus realizing a time optimization through a pipeline approach.

CNAO will be a centre for therapy and research and will be the first Italian hadrontherapy facility capable of treating deep seated tumours. In the next futures other PT facilities will become available in Italy and the CNAO will devote most of its time to CIRT. At regime 80% of the treatments will be carried out with carbon ions.

3. Indications

Until now hadrontherapy, with protons and especially with carbon ions, has not been a widely available resource and there is no widespread consensus on indications among the oncologists. No phase III prospective randomized trial has ever been conducted to compare hadrontherapy versus other advanced radiotherapy techniques for any disease and there is an ongoing debate on the real necessity, feasibility and ethical issues involved in these trials[8-17]. Available evidence has come from non-prospective, non-randomized mono-institutional phase I or phase II trials. In this setting a new facility has to face the difficult task of creating its own patient selection criteria considering not only published clinical data, but also physical radiobiological and clinical rationale. At CNAO all patients will be treated within clinical trials in order to achieve a twofold goal: to deliver hadrontherapy to the patient that are more likely to benefit from it and to help in producing the evidence necessary to assess its real indications.

Trial design and protocol creation are at present still ongoing at CNAO. Seven disease specific working groups have been created on: head and neck tumors, central nervous system lesions, bone and soft tissue sarcomas, pediatric tumors, eye tumors, lung tumors and liver tumors. Two more groups on gynaecological malignancies and digestive tumours (oesophageal cancer, rectal cancer, pancreatic cancer) will be created in the near future. Each working group is composed of radiation oncologists, medical oncologists, surgeons, diagnostic radiologists and organ-related specialists. The working groups have analyzed the literature and have produced documents with recommendations on tentative indications for trials to be conducted at CNAO. Special care has been taken to consider also alternative available treatments in the effort to propose hadrontherapy to those patients for whom it is reasonable to expect a significant advantage.

Specific features of CNAO patient-set up and beam delivery system poses unique challenges. The absence of the gantry (until the future upgrade) and the availability of the chair for treatments in the sitting position make tumours located in the head the best candidates for the starting phase. Moreover the active scanning system has the potential drawback of increasing the risk of cold and hot spot in the treatment of thoracic and abdominal sites due to the high sensitivity to organ motion. Some protocols will thus be postponed until a reliable organ motion coping strategies is individuated.

Head and neck tumors

Phase II trials will be carried out to reproduce results obtained in other facilities. From a general perspective CIRT will be used to treat volumes macroscopically involved by the tumour whereas low LET radiation will be employed to treat macroscopically normal volumes considered at risk of microscopic involvement. CIRT will therefore be used as sole radiotherapy when there is a very low risk of nodal involvement, otherwise it will be used in combination with other treatment (protons or photons).

The role of high LET particles in the treatment of adenoid cystic carcinoma is well established. Many patients have been treated in the past with neutrontherapy, achieving a high local control at the expenses of heavy toxicity[18-23]. Encouraging results have been obtained at GSI delivering CIRT as a boost after photons IMRT[24]. Inoperable, residual or recurrent adenoid cystic carcinoma will be treated at CNAO with the same approach, using carbon ions as a boost after an initial low let treatment. CNAO will participate in a multicentric phase II trial together with HIT (the upcoming hadrontherapy facility at Heidelberg , Germany) that will be carried out in the framework of a cooperation and research program funded by the European Community.

Malignant mucosal melanoma of the upper aerodigestive tract has been treated at HIMAC with concomitant chemotherapy and CIRT, results (only partially published) have been extremely favourable[25]. CNAO intends to perform a phase II trial reproducing closely the strategy employed at HIMAC. A phase II trial of exclusive CIRT will also be carried out for tumours at low risk of nodal involvement such as unfavourably located head and neck adenocarcinoma, paranasal sinuses squamo-cellular carcinoma (SCC) and osteosarcoma of the mandible[25].

The vast majority of head and neck cancer patient are affected by SCC. The role of hadrontherapy in these patients is not yet clearly defined. Considering the natural history of SCC and its tendency to disseminate to loco-regional lymph-nodes the current philosophy at CNAO is to employ CIRT as a boost to the GTV together with a low LET radiation for the wider CTV. Locally advanced hypopharyngeal SCC has been chosen as the first candidate for a phase II trials adding a CIRT boost to the standard radiochemotherapy . Depending on the result of this trial a future hypothetical trial of CIRT as a boost without chemotherapy could be considered. Locally advance tongue base SCC could

also be treated with the same approach. A future phase III trial of CIRT as a boost without chemotherapy vs. conventional radiochemotherapy could theoretically be performed in a subsequent phase, depending on the results of the phase II trials. Reirradiation is considered a potential application of PT in head and neck and will be carried out at CNAO. It is not foreseen to use CIRT for reirradiation.

Central nervous system lesions (including skull base and paraspinal tumors)

Skull base chordomas and chondrosarcomas have been successfully treated with hadrontherapy, the longest and numerically most relevant experience has been gathered at MGH (Boston, MA). The standard treatment consists of maximum safe resection followed (in case of residual disease) by postoperative protontherapy[26-32], CIRT has been used with promising results at GSI[33]. Chondrosarcomas tend to have a more favourable prognosis. At CNAO, chondrosarcomas will be treated with PT, delivered post operatively with a total dose of 72 GyE and a standard fractionation (1.8 – 2 GyE / Fr). Chordomas will be treated with PT and a dose escalation study from 76 GyE to 80 GyE is foreseen. Subsequently a phase III trial of postoperative PT vs. postoperative CIRT for skull base chordoma is foreseen.

Limited data are available on paraspinal tumours treated with hadrontherapy[34-41], but there is a strong rationale due to the proximity of the spinal cord and nerve roots. At CNAO CIRT will be used for inoperable or macroscopically residual disease whereas PT will be employed only for adjuvant treatments after macroscopically radical resection. Systemic chemotherapy will be employed according to stage and histology.

High grade glial tumours have been treated both with PT[42] and heavy ions beam[43], more recently CIRT has been employed at HIMAC as a boost after photons RT concomitant to temozolamide (TMZ)[44]. A phase II trial of exclusive CIRT is ongoing at NIRS. There is a potential concern on the risk of brain necrosis related to high doses or high LET radiation. In the history of high grade glioma many treatments that seemed promising in phase II trials failed to show any benefit when tested in phase III trials. AT CNAO there is a preliminary program to investigate these tumours in four subsequent phases: 1) phase II trials of PT + TMZ with standard dose and fractionation, 2) dose escalation phase I-II trial of PT +/- TMZ, 3) phase I-II trial of combined PT and CIRT boost +/- TMZ, 4) phase III trial of photons RT vs. PT vs. PT with CIRT boost.

Hadrontherapy has a potential role in the treatment of unresectable, recurrent or residual meningiomas. There is preliminary evidence that doses greater than the conventionally accepted 45-50 Gy may result in better local control. At CNAO a dose escalation study will be performed with PT for atypical or malignant meningioma. If a positive dose response relationship is demonstrated the study will be extended also to benign meningioma.

Bone and soft tissue sarcoma

Both PT and CIRT have been used to treat patients affected by several kind of sarcomas[48-51]. It is too early to draw any conclusion based on sound evidence but the clinical and radiobiological rationale is very strong. At CNAO CIRT will be employed to treat macroscopic disease, i.e. inoperable or incompletely resected tumours. Dose escalation studies have been performed at HIMAC and have been stopped at 73.6 GyE in 16 Fractions over 4 weeks due to the risk of skin toxicity[51]. CNAO employs an active scanning beam delivery system which is potentially less toxic for the skin therefore a dose escalation phase I-II trial will be carried out in the attempt to deliver safely higher doses and improve local control. Retroperitoneal pelvic and spine and head sarcomas of all histology will be treated. Tumors of the extremities will be treated with a limb sparing approach. Chemotherapy will be employed as appropriate to control the risk of metatstatic spread. No concomitant CIRT and chemotherapy is foreseen. In a subsequent step a phase III trials of PT vs. CIRT could provide important evidence on the real need of high LET particles. The ethical issues involved in such a trial need a more thorough investigation, also depending on the results of the preliminary phase I-II studies.

Pediatric tumors

Radiotherapy is at present used in the treatment of many pediatric solid tumours. Developing tissues are extremely sensitive to radiations and radio-induced long term toxicity heavily affects the quality of life in many children that are eventually cured from their disease. In the pediatric population any unnecessary exposure of healthy tissues increases the risk of radio-induced second cancer more than in the adult population, and the longer life expectancy leaves more time for second cancer to develop.

At CNAO pediatric patients will be treated with PT to reduce to the minimum any toxicity on non-target tissues. The active scanning used at CNAO does not employ any passive device in the beam path and reduces to a negligible level the neutron dose that potentially can occur with other delivery

systems; it represents therefore the ideal tool for pediatric treatments. Until more data become available on long term toxicity and the risk of second cancers CIRT will not be employed in children. PT will be used as sole radiotherapy; no randomized trial of PT versus photons RT is foreseen.

PT has already been successfully used in several children cancers including: medulloblastoma[52], skull base and spine chordoma[53-54], craniopharyngioma[55-56], low grade glioma[57-58], rabdomyosarcoma[59] and soft tissue sarcoma[60]. These patients will be treated at CNAO with PT integrated with surgery and chemotherapy with doses and schedules similar to those employed in photons RT. Phase II trials will be carried out focused on reducing early and late toxicity. In a subsequent phase a study of eye sparing PT without surgery is foreseen for retinoblastoma.

Eye tumors

PT is commonly recognized as the standard treatment for choroidal melanoma and its result are equal to those achievable with surgical enucleation[61-72]. Also CIRT has been employed at HIMAC for locally advanced eye melanoma[73]. Up until now, eye treatments have been performed with dedicated passive beam line; at CNAO Choroidal melanoma will be treated with PT using the active spot scanning. Customized gaze fixation devices will be employed. A subsequent study of CIRT for selected patients will be considered when more mature data from HIMAC will become available.

Lung cancer

Highly conformal high dose hypofractionated radiotherapy has been used to treat non small cell lung cancer and preliminary results are very encouraging and potentially comparable with dose of surgical resection. Treatment has been carried out with stereotactic photons RT[73], PT[74-75] and CIRT[76-77]. All published results have refer to patients that were inoperable for either medical or personal reasons. At present the first randomized trials of surgery versus stereotactic RT are about to start in the USA and in Netherlands.

Treatment of thoracic targets with CNAO active scanning system is a very demanding task. Even trivial motion during scanning risk to produce cold spot and jeopardize the local control. Active beam scanning has not as yet been employed to treat lung cancer. CNAO is at present investigating organ motion focusing both on detection (with fluoroscopy and optical infrared devices) and on real time treatment corrections (gating, controlled breathhold, tumour tracking and rescanning). Lung cancer treatment will not be performed in the first phase. In future perspectives stage I NSCLC could be an ideal candidate for a prospective randomized trial of CIRT vs. PT vs. stereotactic photons, but the key issue of organ motion has to be solved before any decision is taken.

Liver cancer

Hadrontherapy has been used in the treatment of poorly differentiated hepatocellular carcinoma employing both PT[78-79] and CIRT[80]. Organ motion due to respiratory cycle can have a major impact on intrahepatic targets displacement. Therefore, consideration similar to those relative to lung cancers apply. CNAO will not be used to treat liver tumours in its first stage of operation, but only when a reliable strategy to deal with organ motion is individualized and sufficient expertise has been gained. In the future all the tumours that are not amenable to surgical excision or catheter based therapies could be treated with CIRT. The first trial to be conducted could be a phase II study for patients with single non resectable lesion greater than 3 cm. Future randomized studies of PT vs. CIRT or of CIRT vs. ablative therapies could be performed, anyway any decision on these trials must be postponed after the appropriate solution of the organ motion issue.

4. Conclusions

CNAO will be a dual centre but will focus its activity on CIRT. Protocol design is still ongoing. At the beginning phase II trials will be carried out to reproduce the results obtained by other hadrontherapy facility. Some areas of interest have been selected for future possible randomized phase III trials such as high grade gliomas, locally advanced hypopharyngeal SCC and stage I NSCLC. Problems associated with organ motion issues are critical for the active scanning delivery system, therefore thoracic and abdominal treatment will not be performed in the initial phase.

References

1.Wilson RR: Radiological use of fast protons. Radiology, 47:487-491,1946

2. Lawrence JH, Tobias CA, Born JL, McCombs RK, Roberts JE, Anger HO, Low-Beer BV, Huggins CB: Pituitary irradiation with high-energy proton beams: a preliminary report. Cancer Res, 18(2): 121-134, 1958.

3. Munzenrider JE, Austin-Seymour M, Blitzer PJ, Gentry R, Goitein M, Gragoudas
ES, Johnson K, Koehler AM, McNulty P, Moulton G: Proton therapy at Harvard. Strahlentherapie, 161(12):756-763, 1985
4. Slater JM, Archambeau JO, Miller DW, Notarus MI, Preston W, Slater JD: The proton treatment center at Loma Linda University Medical Center: rationale for and description of its development. Int J Radiat Oncol Biol Phys, 22(2): 383-389, 1992.
5. Castro JR, Linstadt DE, Bahary J-P: Experience in charged particle irradiation of tumors of the skull base 1977-1992. Int J Radiat Oncol Biol Phys 29:647-655, 1994
6. Tsujii H, Mizoe JE, Kamada T, Baba M, Kato S, Kato H, Tsuji H, Yamada S, Yasuda S, Ohno T, Yanagi T, Hasegawa A, Sugawara T, Ezawa H, Kandatsu S, Yoshikawa K, Kishimoto R, Miyamoto T: Overview of clinical experiences on carbon ion radiotherapy at NIRS. Radiother Oncol, 73 Suppl 2:S41-S49, 2004
7. Badano L, Rossi S: Proton-Ion Medical Machine Study (PIMMS), Part I and II, CERN/PS 1999-010 DI and CERN/PS 2000-007 DR, Geneva.
8. Bentzen SM. Randomized controlled trials in health technology assessment: overkill or overdue? Radiother Oncol. 2008 Feb;86(2):142-7.
9. Goitein M, Cox JD. Should randomized clinical trials be required for proton radiotherapy? J Clin Oncol. 2008 Jan 10;26(2):175-6.
10. Lewis BE. On equipoise and emerging technologies. J Clin Oncol. 2008 May 20;26(15):2590; author reply 2593-6.
11. Macbeth FR, Williams MV. Proton therapy should be tested in randomized trials. J Clin Oncol. 2008 May 20;26(15):2590-1; author reply 2593-6.
12. Morgan JP. A patient's perspective on randomized clinical trials for proton radiotherapy. J Clin Oncol. 2008 May 20;26(15):2592; author reply 2592-3.
13. Tepper JE. Protons and parachutes. J Clin Oncol. 2008 May 20;26(15):2436-7.
14. Glatstein E, Glick J, Kaiser L, Hahn SM. Should randomized clinical trials be required for proton radiotherapy? An alternative view. J Clin Oncol. 2008 May 20;26(15):2438-9.
15. Suit H, Kooy H, Trofimov A, Farr J, Munzenrider J, DeLaney T, Loeffler J, Clasie B, Safai S, Paganetti H. Should positive phase III clinical trial data be required before proton beam therapy is more widely adopted? No. Radiother Oncol. 2008 Feb;86(2):148-53.
16. Glimelius B, Montelius A. Proton beam therapy - do we need the randomised trials and can we do them? Radiother Oncol. 2007 May;83(2):105-9
17. Brada M, Pijls-Johannesma M, De Ruysscher D: Proton therapy in clinical practice: Current clinical evidence. J Clin Oncol 25:965-970, 2007
18. Huber PE, Debus J, Latz D, Zierhut D, Bischof M, Wannenmacher M, Engenhart-Cabillic R. Radiotherapy for advanced adenoid cystic carcinoma: neutrons, photons or mixed beam? Radiother Oncol. 2001 May;59(2):161-7.
19. Prott FJ, Micke O, Haverkamp U, Willich N, Schüller P, Pötter R. Results of fast neutron therapy of adenoid cystic carcinoma of the salivary glands. Anticancer Res. 2000 Sep-Oct;20(5C):3743-9.
20. Marunick MT, Bahu SJ, Aref A. Osteoradionecrosis of the maxillary-orbital complex after neutron beam
radiotherapy. Otolaryngol Head Neck Surg. 2000 Sep;123(3):224-8.
21. Douglas JG, Laramore GE, Austin-Seymour M, Koh W, Stelzer K, Griffin TW. Treatment of locally advanced adenoid cystic carcinoma of the head and neck with neutron radiotherapy. Int J Radiat Oncol Biol Phys. 2000 Feb 1;46(3):551-7.
22. Pötter R, Prott FJ, Micke O, Haverkamp U, Wagner W, Willich N. Results of fast neutron therapy of adenoid cystic carcinoma of the salivary glands. Strahlenther Onkol. 1999 Jun;175 Suppl 2:65-8.
23. Krüll A, Schwarz R, Brackrock S, Engenhart-Cabillic R, Huber P, Prott FJ, Breteau N, Favre A, Lessel A, Koppe H, Auberger T. Neutron therapy in malignant salivary gland tumors: results at European centers.
Recent Results Cancer Res. 1998;150:88-99.
24. Schulz-Ertner D, Nikoghosyan A, Didinger B, Münter M, Jäkel O, Karger CP, Debus J. Therapy strategies for locally advanced adenoid cystic carcinomas using modern radiation therapy techniques. Cancer. 2005 Jul 15;104(2):338-44.
25. Mizoe JE, Tsujii H, Kamada T, Matsuoka Y, Tsuji H, Osaka Y, Hasegawa A, Yamamoto N, Ebihara S, Konno A; Organizing Committee for the Working Group for Head-And-Neck Cancer. Dose escalation

study of carbon ion radiotherapy for locally advanced head-and-neck cancer. Int J Radiat Oncol Biol Phys. 2004 Oct 1;60(2):358-64

26. Rutz HP, Weber DC, Goitein G, Ares C, Bolsi A, Lomax AJ, Pedroni E, Coray A,Hug EB, Timmermann B.

Postoperative spot-scanning proton radiation therapy for chordoma and chondrosarcoma in children and adolescents: initial experience at paul scherrer institute. Int J Radiat Oncol Biol Phys. 2008 May 1;71(1):220-5.

27 . Hug EB. Review of skull base chordomas: prognostic factors and long-term results of proton-beam radiotherapy. Neurosurg Focus. 2001 Mar 15;10(3):E11.

28. Noël G, Feuvret L, Calugaru V, Dhermain F, Mammar H, Haie-Méder C, Ponvert D, Hasboun D, Ferrand R, Nauraye C, Boisserie G, Beaudré A, Gaboriaud G, Mazal A, Habrand JL, Mazeron JJ. Chordomas of the base of the skull and upper cervical spine. One hundred patients irradiated by a 3D conformal technique combining photon and proton beams. Acta Oncol. 2005;44(7):700-8.

29. Weber DC, Rutz HP, Pedroni ES, Bolsi A, Timmermann B, Verwey J, Lomax AJ, Goitein G. Results of spot-scanning proton radiation therapy for chordoma and chondrosarcoma of the skull base: the Paul Scherrer Institut experience. Int J Radiat Oncol Biol Phys. 2005 Oct 1;63(2):401-9.

30 . Igaki H, Tokuuye K, Okumura T, Sugahara S, Kagei K, Hata M, Ohara K, Hashimoto T, Tsuboi K, Takano S, Matsumura A, Akine Y. Clinical results of proton beam therapy for skull base chordoma. Int J Radiat Oncol Biol Phys. 2004 Nov 15;60(4):1120-6.

31. Hug EB, Slater JD. Proton radiation therapy for chordomas and chondrosarcomas of the skull base. Neurosurg Clin N Am. 2000 Oct;11(4):627-38.

32. Munzenrider JE, Liebsch NJ. Proton therapy for tumors of the skull base. Strahlenther Onkol. 1999 Jun;175 Suppl 2:57-63.

33 . Schulz-Ertner D, Karger CP, Feuerhake A, Nikoghosyan A, Combs SE, Jäkel O, Edler L, Scholz M, Debus J.

Effectiveness of carbon ion radiotherapy in the treatment of skull-base chordomas. Int J Radiat Oncol Biol Phys. 2007 Jun 1;68(2):449-57.

34. Isacsson U, Hagberg H, Johansson KA, et al. Potential advantages of protons over conventional radiation beams for paraspinal tumours. Radiother Oncol 1997, 45:63-70.

35. Park L, Delaney TF, Liebsch NJ, Hornicek FJ et al. Sacral chordomas: Impact of high-dose proton/photon-beam radiation therapy combined with or without surgery for primary versus recurrent tumor. Int J Radiat Oncol Biol Phys 2006, 65: 1514-21.

36. Schoenthaler R, Castro J, Petti P, et al. Charged Particle irradiation of sacral chordomas. Int J Radiat Oncol Biol Phys 1993; 26: 291-298.

37. Imai R, Kamada T, Tsuji H, Tsujii H, Tsuburai Y, Tatezaki S; Working Group for Bone and Soft Tissue Sarcomas. Cervical spine osteosarcoma treated with carbon-ion radiotherapy. Lancet Oncol. 2006 Dec;7(12):1034-5.

38 . Imai R, Kamada T, Tsuji H, Yanagi T, Baba M, Miyamoto T, Kato S, Kandatsu S, Mizoe JE, Tsujii H, Tatezaki S; Working Group for Bone, Soft Tissue Sarcomas. Carbon ion radiotherapy for unresectable sacral chordomas.

Clin Cancer Res. 2004 Sep 1;10(17):5741-6.

39. Hug EB, Fitzek MM, Liebsch NJ, Munzenrider JE. Locally challenging osteo- and chondrogenic tumors of the axial skeleton: results of a combined proton and photon radiation tehrapy using three-dimensional treatment planning. Int J Radiat Oncol Biol Phys 1995, 31, 467-476.

40. Park L, Delaney TF, Liebsch NJ, Hornicek FJ et al. Sacral chordomas: Impact of high-dose proton/photon-beam radiation therapy combined with or without surgery for primary versus recurrent tumor. Int J Radiat Oncol Biol Phys 2006, 65: 1514-21.

41. Nowakowski VA, Castro JR, Peti PL, et al. Charged particle radiotherapy of paraspinal tumours. Int J Radiat Oncol Biol Phys 1992; 22: 295-303.

42. Fitzek MM, Thornton AF, Harsh IV G et al. Dose-escalation with proton/photon irradiation for Daumas-Duport lower-grade glioma: results of an institutional phase I/II trial . Int J Radiat Oncol Biol Phys 2001, 51: 131-137.

43. Castro JR, Linstadt DE, Baahry J-P, et al. Experience in charged particle irradiation of tumors of the skull base: 1977-1992. Int J Radiat Oncol Biol Phys 1994; 29: 647-655.

44. Mizoe JE, Tsujii H, Hasegawa A, Yanagi T, Takagi R, Kamada T, Tsuji H, Takakura K; Organizing

Committee of the Central Nervous System Tumor Working Group. Phase I/II clinical trial of carbon ion radiotherapy for malignant gliomas: combined X-ray radiotherapy, chemotherapy, and carbon ion radiotherapy. Int J Radiat Oncol Biol Phys. 2007 Oct 1;69(2):390-6.
45. Miralbel R, Lomax A, Bortfeld T, Modha A, Gutin P. Diagnosis and Treatment of Atypical and Anaplastic Meningiomas: a review. Neurosurgery 2005, 57: 538-550.
46. Noel G, Bollet MA, Calugaru V, Feuvret L, Haie-Meder C, Dhermain F, Ferrand R, Boisserie G, Beaudre A, Mazeron JJ, Habrand JL. Functional outcome of patients with benign meningioma treated by 3D conformal irradiation with a combination of photons and protons. Int J Radiat Oncol Biol Phys. 2005, 62: 1412-422.
47. Weber DC, Lomax AJ, Rutz H: Spot-scanning proton radiation therapy for recurrent, residual or untreated intracranial meningiomas. Radiother Oncol, 71: 251-258, 2004.
48. Patel S, DeLaney TF. Advanced-technology radiation therapy for bone sarcomas. Cancer Control. 2008 Jan;15(1):21-37.

49. Weber DC, Rutz HP, Bolsi A, Pedroni E, Coray A, Jermann M, Lomax AJ, Hug EB,Goitein G. Spot scanning proton therapy in the curative treatment of adult patients with sarcoma: the Paul Scherrer institute experience. Int J Radiat Oncol Biol Phys. 2007 Nov 1;69(3):865-71.

50. DeLaney TF, Park L, Goldberg SI, Hug EB, Liebsch NJ, Munzenrider JE,Suit HD. Radiotherapy for local control of osteosarcoma. Int J Radiat Oncol Biol Phys. 2005 Feb 1;61(2):492-8.
51. Kamada T, Tsujii H, Tsuji H, Yanagi T, Mizoe JE, Miyamoto T, Kato H, Yamada S, Morita S, Yoshikawa K, Kandatsu S, Tateishi A; Working Group for the Bone and Soft Tissue Sarcomas. Efficacy and safety of carbon ion radiotherapy in bone and soft tissue sarcomas. J Clin Oncol. 2002 Nov 15;20(22):4466-71.
52. StClair WH, Adams JA et al: Advantage of protons compared to conventional X-ray or IMRT in the treatment of a pediatric patient with medulloblastoma. Int J Radiat Oncol Biol Phys 58: 727-734, 2004
53. Benk V, Liebsch NJ et al: Base of skull and cervical spine chordomas in children treated by high-dose irradiation. Int J Radiat Oncol Biol Phys 31: 577-581, 1995
54. Hug EB, Sweeney RA et al: Proton radiotherapy in management of pediatric base of skull tumors. Int J Radiat Oncol Biol Phys 52: 1017-1024, 2002
55. Luu QT, Loredo LN, Archambeau JO et al. Fractionnated proton radiation treatment for pediatric craniopahryngioma: preliminary report. J Cancer 2006, 12 (2):155-159
56. Fitzek MM, Linggood RM, Adams J, Munzenrider JE. Combined proton and photon irradiation for craniopharyngioma: long-term results of the early cohort of patients treated at Harvard cyclotron laboratory and Massachusetts General Hospital. In. J. Radiation Oncology Biol. Phys 2006, 64 (5): 1348-1354
57. Fuss M, Hug EB et al: Proton radiation therapy (PRT) for pediatric optic pathway gliomas: comparison with 3D planned conventional photons and a standard photon technique. Int J Radiat Oncol Biol Phys 45: 1117-1126, 1999
58. Hug EB, Muenter MW et al.Conformal proton radiation therapy for pediatric low-grade astrocitomas. Strahlenther Oncol 78: 10-17, 2001
59. Yock T, Schneider R et al: Proton radiotherapy for orbital rabdomiosarcoma: clinical outcome and a dosimetric comparison with photons. Int J Radiat Oncol Biol Phys 62: 1161-1168, 2005
60. Timmermann B, Shuuck A et al: Spot-scanning proton therapy for malignant soft tissue tumors in childhood: first experience at the Paul Sherrer Institute. Int J Radiat Oncol Biol Phys 67: 497-504, 2007
61. Gragoudas ES. Proton beam irradiation of uveal melanomas: the first 30 years. The Weisenfeld Lecture. Invest Ophthalmol Vis Sci. 2006 Nov;47(11):4666-73.
62. Courdi A, Caujolle JP, Grange JD, Diallo-Rosier L, Sahel J, Bacin F, Zur C, Gastaud P, Iborra-Brassart N, Hérault J, Chauvel P. Results of proton therapy of uveal melanomas treated in Nice.Int J Radiat Oncol Biol Phys. 1999 Aug 1;45(1):5-11.
63. Damato B, Kacperek A, Chopra M, Campbell IR, Errington RD. Proton beam radiotherapy of choroidal melanoma: the Liverpool-Clatterbridge experience. Int J Radiat Oncol Biol Phys. 2005 Aug 1;62(5):1405-11.
64. Dendale R, Lumbroso-Le Rouic L, Noel G,

Feuvret L, Levy C, Delacroix S, Meyer A, Nauraye C, Mazal A, Mammar H, Garcia P, D'Hermies F, Frau E, Plancher C, Asselain B, Schlienger P, Mazeron JJ, Desjardins L. Proton beam radiotherapy for uveal melanoma: results of Curie Institut-Orsay proton therapy center (ICPO). Int J Radiat Oncol Biol Phys. 2006 Jul 1;65(3):780-7. Epub 2006 May

65. Egger E, Zografos L, Munkel G, Böhringer T, Bercher L, Chamot L. Results of proton radiotherapy for uveal melanomas. Front Radiat Ther Oncol. 1997;30:111-22.

66. Fuss M, Loredo LN, Blacharski PA, Grove RI, Slater JD. Proton radiation therapy for medium and large choroidal melanoma: preservation of the eye and its functionality. Int J Radiat Oncol Biol Phys. 2001 Mar 15;49(4):1053-9.

67. Gould P. Protons effective on hard-to-treat eye cancers. Lancet Oncol. 2005 Sep;6(9):642.

68. Höcht S, Bechrakis NE, Nausner M, Kreusel KM, Kluge H, Heese J, Heufelder J, Cordini D, Homeyer H, Fuchs H, Martus P, Foerster MH, Wiegel T, Hinkelbein W. Proton therapy of uveal melanomas in Berlin. 5 years of experience at the Hahn-Meitner Institute. Strahlenther Onkol. 2004 Jul;180(7):419-24.

69. Kodjikian L, Roy P, Rouberol F, Garweg JG, Chauvel P, Manon L, Jean-Louis B, Little RE, Sasco AJ, Grange JD. Survival after proton-beam irradiation of uveal melanomas. Am J Ophthalmol. 2004 Jun;137(6):1002-10.

70. Lumbroso-Le Rouic L, Delacroix S, Dendale R, Levy-Gabriel C, Feuvret L, Noel G, Plancher C, Nauraye C, Garcia P, Calugaru V, Asselain B, Desjardins L. Proton beam therapy for iris melanomas. Eye. 2006 Nov;20(11):1300-5.

71. Spatola C, Privitera G, Raffaele L, Salamone V, Cuttone G, Cirrone P, Sabini MG, Lo Nigro S. Clinical application of proton beams in the treatment of uveal melanoma: the first therapies carried out in Italy and preliminary results (CATANA Project). Tumori. 2003 Sep-Oct;89(5):502-9.

72. Munzenrider JE. Uveal melanomas. Conservation treatment. Hematol Oncol Clin North Am. 2001 Apr;15(2):389-402.

73. Lo SS, Fakiris AJ, Papiez L, Abdulrahman R, McGarry RC, Henderson MA, Forquer JA, Hoopes D, Timmerman RD. Stereotactic body radiation therapy for early-stage non-small-cell lung cancer. Expert Rev Anticancer Ther. 2008 Jan;8(1):87-98.

74. Bush DA, Slater JD, Shin BB, Cheek G, Miller DW, Slater JM. Hypofractionated proton beam radiotherapy for stage I lung cancer. Chest. 2004 Oct;126(4):1198-203.

75. Hata M, Tokuuye K, Kagei K, Sugahara S, Nakayama H, Fukumitsu N, Hashimoto T, Mizumoto M, Ohara K, Akine Y. Hypofractionated High-Dose Proton Beam Therapy for Stage I Non-Small-Cell Lung Cancer: preliminary Results of A Phase I/II Clinical Study. Int J Radiat Oncol Biol Phys. 2007 Jul 1;68(3):786-93.

76. Miyamoto T, Baba M, Sugane T, Nakajima M, Yashiro T, Kagei K, Hirasawa N, Sugawara T, Yamamoto N, Koto M, Ezawa H, Kadono K, Tsujii H, Mizoe JE, Yoshikawa K, Kandatsu S, Fujisawa T; Working Group for Lung Cancer. Carbon ion radiotherapy for stage I non-small cell lung cancer using a regimen of four fractions during 1 week. J Thorac Oncol. 2007 Oct;2(10):916-26.

77.Masashi Koto, Tadaaki Miyamoto, Naoyoshi Yamamoto, Hideki Nishimura, Shogo Yamada, Hirohiko Tsujii: Local control and recurrence of stage I non-small cell lung cancer after carbon ion radiotherapy. Radiotherapy and Oncology 71 (2004) 147–156

78.Hata M, Tokuuye K, Sugahara S, Fukumitsu N, Hashimoto T, Ohnishi K, Nemoto K, Ohara K, Matsuzaki Y, Akine Y. Proton beam therapy for hepatocellular carcinoma with limited treatment options. Cancer. 2006 Aug 1;107(3):591-8.

79 Chiba T, Tokuuye K, Matsuzaki Y, Sugahara S, Chuganji Y, Kagei K, Shoda J, Hata M, Abei M, Igaki H, Tanaka N, Akine Y. Proton beam therapy for hepatocellular carcinoma: a retrospective review of 162 patients. Clin Cancer Res. 2005 May 15;11(10):3799-805.

80 Kato H, Tsujii H, Miyamoto T, Mizoe JE, Kamada T, Tsuji H, Yamada S, Kandatsu S, Yoshikawa K, Obata T, Ezawa H, Morita S, Tomizawa M, Morimoto N, Fujita J, Ohto M; Liver Cancer Working Group. Results of the first prospective study of carbon ion radiotherapy for hepatocellular carcinoma with liver cirrhosis. Int J Radiat Oncol Biol Phys. 2004 Aug 1;59(5):1468-76.

Collective Analyses of Clinical Outcomes: Globally Advancing BNCT

Kent J. Riley

Boron neutron capture therapy has successfully developed the scientific infrastructure for clinical programs through multidisciplinary collaborations within individual groups around the world. These centers have independently demonstrated the safety, feasibility and promise of BNCT in clinical trials with small numbers of patients. To advance the modality beyond this stage of development and so facilitate a broader understanding in the radiotherapy community, research must now seek to determine definitive endpoints such as toxicity, tolerance dose, therapeutic response and efficacy. The established system as it exists today is unlikely to fulfill these goals because they require many more patients and greater resources than any one center can sustain. While standardizing treatment protocols across centers would facilitate combining trial data and achieve this aim, this is impractical in the near term due to the independent nature of the various clinical programs already underway and the substantial resources needed that may discourage participation from the new developing centers in the world.

A new type of collaborative effort *between* centers is now needed to both retrospectively and prospectively integrate results of clinical irradiations to advance the overall aims of BNCT. The NCT group from the Massachusetts Institute of Technology (MIT) leads an International Dosimetry Exchange for this purpose that includes groups from clinical centers at the Joint Research Centre (JRC) of the European Commission, Petten (The Netherlands), Nuclear Research Institute, Rez (Czech Republic), VTT, Espoo (Finland), Studsvik, Nyköping (Sweden), Brookhaven National Laboratory (BNL, USA), the Comisión Nacional de Energía Atómica (Argentina), Kyoto University Research Reactor (Japan) and the Japanese Atomic Energy Research Institute (Japan). This group has published a series of reports, culminating in recently completed analyses that evaluated differences in dose specification between centers in Europe and the USA.

Individual dose components calculated from treatment plans formulated by the participating centers were compared to MIT measurements and differences ranged from 4 to 370%. Among centers using BPA, the maximum dose to brain determined for the same nominal specification of 10 Gy(w) is significantly higher than at BNL by 32% (Harvard-MIT), 43% (VTT), 49% (JRC) and 74% (Studsvik). These findings should provide a more accurate interpretation of clinical results reported by the centers and facilitate rigorous collective analyses of trial data for the first time. Each center freely contributed resources and scientific results to this collaboration and the modest efforts have proven worthwhile for both the participants, and the community as a whole.

Another stage in this collaboration is set to begin with physicists renormalizing treatment plans using a common dose specification. Comprehensive analyses of all trial data accrued by each of these centers although now possible in principle may be unrealistic because each center understandably wishes to protect their results and wants to retain control over interpreting therapeutic response. However, simpler, more restricted but nonetheless useful analyses such as dose-limiting toxicity are more feasible if for example, the frequency and severity of adverse events can be separated from data regarding therapeutic outcome and submitted for tabulation together with other centers. Analyses based on these data will help define a more precise specification of dose limits and increase information sharing between clinical programs. This will benefit both existing centers that seek to develop follow-on studies possibly involving different tumors or more advanced boron delivery agents as well as new centers who should be encouraged to participate so as to avoid needlessly duplicating previous studies.

Given the inherent benefits for all participating clinical centers and the entire BNCT research community it is incumbent upon all of us to identify a way to cooperate toward these aims and to advance BNCT while preserving the academic or proprietary interests of each participant.

What is the future for boron neutron capture therapy?

R. F. Barth

Department of Pathology, The Ohio State University, Columbus, Ohio, 43210 USA

Abstract

Over the past 25 years, BNCT research has progressed relatively slowly but steadily with the greatest progress in the field of clinical studies, and specifically its application to a variety of malignancies other than high grade gliomas and melanomas. These include meningiomas, cancers of the head and neck region and under very special circumstances, the treatment of hepatic metastases of colon cancer. However, there are a number of key areas where little, if any, significant progress has been made.

First and foremost among these has been the lack of new boron delivery agents that have advanced to clinical use since the introduction of boronophenylalanine (BPA) for the treatment of melanoma in 1989 and gliomas in the early 1990s. Improvement in drug delivery and the development of the best dosing paradigms for both BPA and sodium borocaptate (BSH) are of major importance and still have not been optimized. This is not only important for brain, but also extracranial tumors.

Dosimetry for BNCT still is based on treating to normal tissue tolerance, based on blood boron values rather than any real time information on the boron content of the residual tumor that is to be irradiated. The ultimate goal would be to move BNCT to the same level as other types of radiation therapy where dosimetry is quite precise.

Another major problem has been the total dependence on nuclear reactors as neutron sources for BNCT, and despite much effort a clinically useful accelerator source has yet to be sited in a hospital and used for therapy. Although there are many reasons for the failure to develop randomized clinical trials, the simple fact of the matter is that until BNCT is put to this test, it will not gain the credibility of a broad community of physicians who are treating cancer patients. Although, the survival statistics for patients with high grade gliomas are almost as dismal now as they were 25 years ago, the introduction of temozolomide in combination with photon irradiation has produced a modest 2.5 month increase in median survival, which raises the bar of what must be achieved in order to make BNCT a clinically useful modality. Obtaining clinical results that are equivalent to external beam photon irradiation will not be sufficient.

Finally, recent experimental studies with the F98 rat glioma combining X-irradiation with intracerebral delivery of carboplatin have yielded survival data that are comparable to the best that we have obtained with BNCT using this brain tumor model. Therefore, the final, and most important question that must be addressed is, “How can BNCT survive as a treatment modality if and when there are more widely applicable and less costly alternatives?”

Keywords: Future of BNCT

1. Introduction: Development of boron delivery agents

The development of boron delivery agents probably is the single greatest need for future progress of BNCT. Sodium borocaptate (BSH) and boronophenylalanine (BPA) were first synthesized over 50 years ago. The first clinical use of BSH was reported by Hiroshi Hatanaka in the 1960's for BNCT of patients with high grade gliomas (Hatanaka, 1976) and BPA was first used clinically by Mishima, *et al.* in 1988-9 to treat patients with cutaneous malignant melanomas (Mishima, et al., 1989). It was not until 1994 that the first clinical trial was initiated at the Brookhaven National Laboratory, Upton, NY to evaluate a BPA-fructose complex for BNCT of patients with GBM (Diaz, 2003). Since then, BPA-fructose has become the most frequently used clinical boron delivery agent for both intra- and extracranial tumors. Although Hatanaka initially administered BSH intra-arterially via the internal carotid artery, it subsequently has been administered intravenously (i.v.) either alone, or more recently in combination with BPA. However, there may be an opportunity to improve upon the delivery of these agents. Experimental animal studies, carried out by my research group using the F98 rat glioma model unequivocally demonstrated that intracarotid (i.c.) administration of both BSH and BPA resulted in higher tumor boron concentrations and tumor to normal brain ratios. As shown in Fig. 1, there were corresponding increases in mean survival times (MSTs) (i.c. BPA + BBB-D 95 d versus 37 d for i.v. BPA) (Barth, R.F., et al., 1997). As shown in Fig. 2, these results were further improved by combining i.c. administration of BPA and BSH with the infusion of a hyperosmotic solution of mannitol to disrupt the blood-brain barrier (BBB-D) (Barth, R.F., et al., 2000). These results demonstrated that improvement in the delivery of BPA and BSH significantly enhanced survival. It remains to be determined whether a similar improvevment in survival can be obtained in patients with GBMs. Dr. Garth Cruickshank and his co-workers at the Queen Elizabeth

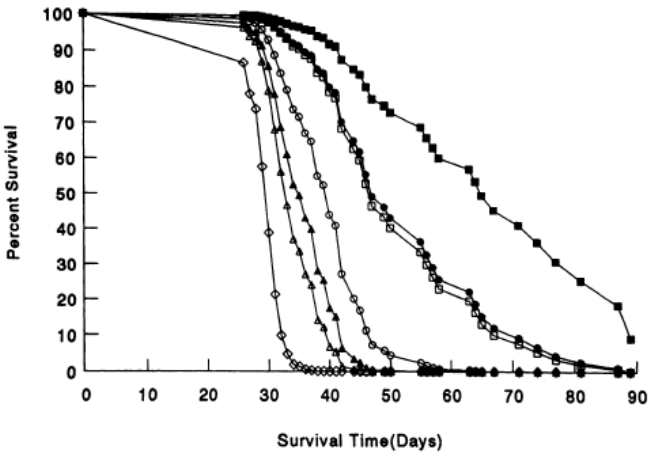

Fig. 1. Cox survival plots of F98 glioma-bearing rats following i.v. or i.c. administration of BPA and BSH with or without BBB-D, followed by neutron irradiation. Cox's proportional hazards model performs a simultaneous fit of the survival curves using all the data points, using a partial likelihood approach. Therefore, the number of data points in each curve includes all of the death times, rather than only those animals in a specific group. Survival time in days after implantation have been plotted for irradiated controls (◊), BSH i.v. (Δ), BPA i.v. (▲), BSH i.c. (○), BPA i.c. (●), BSH i.c. with BBB-D (□), and BPA i.c. with BBB-D (■). Animals that received i.c. BPA + BBB-D had a MST ± SD of 95±95 d (range 46-365) compared to 37±3d and 33±6 d for i.v. BPA and BSH, respectively. (Reprinted from Cancer Res. 57:1129, 1997)

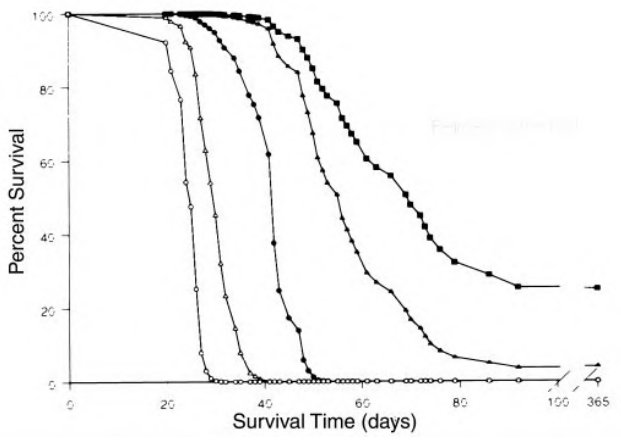

Fig. 2. Cox survival plots of F98 glioma bearing rats following i.v. or i.c. administration of BPA and BSH with or without BBB-D, followed by neutron irradiation. The survival times, in days after implantation, are shown for untreated controls (○), irradiated controls (Δ), BPA + BSH i.v. (●), BPA + BSH i.c. (▲), and BPA + BSH i.c. + BBB-D (■). Animals that received i.c. BPA + BSH + BBB-D had a MST ± SD of 140±133 d (range 48-365 d) compared to 41±4 (range 35-50 d) for rats that received i.v. BPA + BSH. (Reprinted from Intl. J. Rad. Oncol. Biol. & Physics 47:209, 2000)

Hospital in Birmingham, England have plans to evaluate this, but hopefully other clinical investigators also will pursue this line of investigation.

Turning to the development of new, low molecular weight boron delivery agents, this subject has been covered in a recent special issue of *Anti-Cancer Agents in Medicinal Chemistry* (Vicente et al., 2006), and this has been the topic of a number of papers presented at this meeting. Suffice to say, to the best of my knowledge at this time, there is no new boron compound that has reached the stage for evaluation in a Phase I clinical biodistribution study. This is not due to a lack of effort on the part of chemists and biologists, but rather to difficulties more generally associated with drug discovery and pre-clinical evaluation, and more specifically, to the challenges of identifying agents that will attain tumor boron concentrations of ~20 μg/gm with concomitantly low normal brain and blood concentrations.. Pharmaceutical companies have spent vast amounts of money for drug development, and in comparison a relatively small amount of money has been expended for the design and synthesis of new boron compounds for NCT.

Finally, a good part of our own work over the past five years has focused on the development of the high-molecular-weight, epidermal growth factor receptor (EGFR) targeting agents, and this has been summarized by Dr. Weilian Yang. Although *proof-of-principle* has been established for the therapeutic efficacy of boronated anti-EGFR monoclonal antibodies (mAbs), there are significant challenges to their clinical use (Yang et al., 2008). The most important of these relates to their effective delivery, even if administered intracerebrally by convection enhanced delivery (CED). The other, almost equally as important, is variability in EGFR expression from tumor-to-tumor, as well as within individual tumors, and the necessity to target receptor (+) and (-) cells.

2. Problems relating to dosimetry

Although a number of sophisticated computer algorithms have been developed to predict tumor boron concentrations, based on either blood boron levels or the uptake of ^{18}F-BPA by means of positron emission tomography, it still is not possible to determine in real time what the tumor boron concentration will be at the time of treatment. Furthermore, since the dosimetry for BNCT is at the level of individual cancer cells, it is unlikely that this will be possible in the foreseeable future, if ever. Therefore, the current practice of treating to normal brain tolerance is a reasonable approach and its safety has been demonstrated by numerous investigators. However, radiation oncologists require more precise information on the radiation dose delivered to the tumor, and the imprecision of BNCT dosimetry has been one of a number of reasons why the clinical results obtained have been greeted with some skepticism. Nevertheless, the results obtained with head and neck cancers, cutaneous melanomas, and most recently in those few patients with hepatic metastases of colorectal cancer provide convincing evidence of clinical *proof-of-principle* and therapeutic efficacy.

3. Dependence upon nuclear reactors as neutron sources for BNCT

The development of accelerator based neutron sources (ABNS) has been of interest for almost three decades. A number of reports presented at this meeting have described progress in this area, and hopefully at some time in the not-too-distant future, there will be ABNS that will produce epithermal beams with a sufficient flux of neutrons of the appropriate energy that will approximate, if not improve upon those produced by nuclear reactors. The net result of this will be increased clinical interest in BNCT since it will be possible to treat patients in a much more clinically friendly environment than at a nuclear reactor. Furthermore, this increased clinical interest should result in an increase in the number of patients and types of tumors being treated.

4. Development of randomized clinical trials

The greatest single impediment to convincing the broader medical community of the efficacy of BNCT for the treatment of high grade gliomas has been the lack of randomized trials. It took a randomized clinical trial with 573 patients with GBM to establish that surgery followed by the combination of temozolomide and photon irradiation, and then six repetitive cycles of temozolomide, was superior to standard therapy consisting of surgery followed by radiotherapy (Stupp, 2005). This resulted in an increase in overall median survival of only 2.5 months, which doesn't sound like much, but it was statistically significant at the level of $p<0.001$, which convinced even the skeptics! Furthermore, approximately 25% of patients who received this combination therapy were alive at 24 months, which is a more impressive number. I previously believed that one could obtain such a significant improvement in survival with BNCT that a randomized clinical trial would not be necessary. However, a more realistic assessment is that the improvement in survival, if any, in patients with GBM who have been treated with BNCT will be incremental rather than dramatic, and in order to con-

vince a broad medical audience that this is "real," a randomized clinical trial will be necessary. Since clinical BNCT has ended in the United States, and it is unlikely that it will be resumed in the foreseeable future, it remains for physicians in other parts of the world to pick up where we left off; particularly in places like Japan, where they are leading the way clinically, and in Europe, specifically in Finland, and hopefully in China when the clinicians at the Beijing Neurosurgical Institute begin treating patients. The combination of BNCT with external beam photon irradiation was first reported by us in the F98 rat glioma model (Barth et al, 2004), and this approach is now being used clinically in Japan with promising results. Again, in order to obtain convincing data, at least in patients with GBM, it probably will be necessary to carry out randomized clinical trials.

5. Development of new therapeutic approaches

Since there has been such little progress over the past thirty years in the treatment of high grade gliomas, this has been the one thing that has kept BNCT "alive." If there had been a major breakthrough in the treatment of GBMs, one important impetus to continue on with BNCT for brain tumors would have ended. The development of new therapeutic approaches for the treatment of gliomas is an active area of research. Our own recent research has undergone a paradigm shift to a simpler and potentially much more widely applicably approach to treat high grade gliomas. It is based on the findings of my French collaborator, Dr. Helene Elleaume, and her co-workers at the European Synchrotron Radiation Facility (ESRF) in Grenoble, France (Rousseau, et al., 2007). This approach is based on studies carried out using the F98 glioma model whereby either cisplatin or carboplatin was administered intracerebrally by means of CED, and then this was followed by X-irradiation (three fractions of 8 Gy each)with 6 MV photons from a linear accelerator (LINAC) of the tumor bearing, cerebral hemisphere. As shown in Fig. 3, there was a significant enhancement in the survival of treated animals with a MST of 97±15 d. and a 234% increase in life span compared to untreated controls (Rousseau et al., 2007). As shown in Fig. 4, similar data have been obtained by us with whole brain irradiation at a dose of 15 Gy (three fractions of 5 Gy each). Studies are in progress to further optimize this approach.

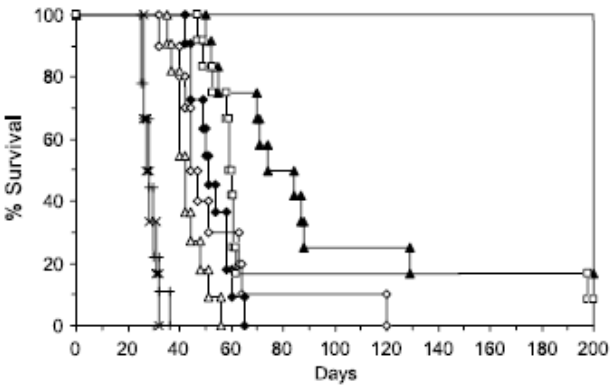

Fig. 3. Kaplan-Meier survival plots for F98 glioma-bearing rats after chemoradiotherapy. Survival times have been plotted in days after implantation for untreated animals (+ and x), CED of carboplatin 20 μg/20 μL alone (◊), irradiation at 6 MV alone (three fractions of 8 Gy; Δ) or in combination with CED of carboplatin 20 μg/20 μL (▲), and irradiation at 80 keV synchrotron X-rays alone (three fractions of 8 Gy; ♦) or in combination with CED of carboplatin 20 μg/20 μL (□). Carboplatin (Reprinted from Clin. Cancer Res. 13:5195, 2007)

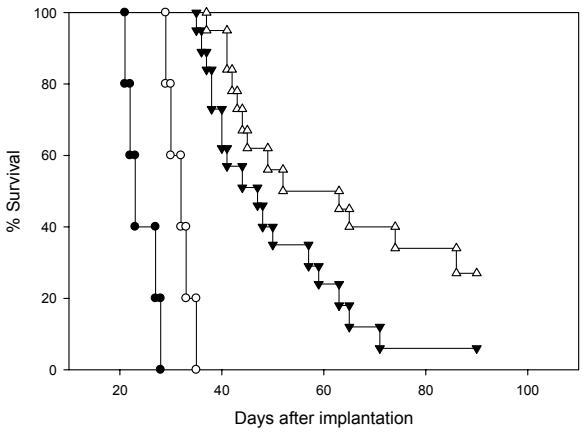

Fig. 4. Kaplan-Meier survival plots for F98 glioma-bearing rats after chemoradiotherapy. Survival times in days after implantation of 10^3 tumor cells have been plotted for untreated controls (●), irradiated control (○), CED of carboplatin (▲), and CED of carboplatin + X-rays (Δ). Animals received three 5 Gy fractions of 6 MV photons beginning 24 hours following CED of carboplatin (20 μg in 20 μL) at a flow rate of 0.33 μL/min. for 30 min. The median survival time was 56 d. for animals that received carboplatin plus X-irradiation compared to 42 d. for i.v. BPA + BSH followed by BNCT (Barth, et al, 2004)

A Phase I clinical study is in the planning stage to evaluate the safety of intracerebral administration of carboplatin by means of CED in patients with GBM, who have recurred, *and* are candidates for a second craniotomy.

If any one of the new therapeutic approaches that currently are being evaluated results in a significant improvement in the survival of patients with high grade gliomas, the proverbial "bar" will have been raised to an even higher level than the modest but significant gain in survival that has been achieved using temozolomide in combination with photon irradiation.

6. Conclusions

In concluding this presentation, I would like to suggest that some consideration be given to combining BNCT with "upfront" temozolomide, followed by repetitive cycles of temozolomide. Such a study was discussed several years ago with Dr. Zhixian Gao and his clinical colleagues at the Beijing Neurosurgical Institute, which is one of the largest neurosurgical centers in the world. The number of GBM patients seen at the BNI exceeds 300 per year and should permit the development of a randomized clinical trial.

What then is the future of BNCT? It probably lies in filling a nitch for those malignancies, whether primary or recurrent, for which there is no effective therapy. One very distinct advantage of BNCT is its ability to selectively deliver a radiation dose to the tumor with a much lower dose to surrounding normal tissues. This is an important feature that makes BNCT particularly attractive for salvage therapy of patients with a variety of malignancies who already have been heavily treated with photon irradiation. In this presentation, I have outlined the problems that I believe are important to solve in order to move forward with BNCT as a treatment modality in the twenty-first century. It is up to investigators, both in basic and clinical research, to come up with solutions to the problems that I have outlined. Finally, it is up to the funding agencies in our various countries to provide the money necessary to carry out these studies. Since by nature I am an optimist, I look forward to continued progress in BNCT, which conceptually is so elegant, but practically is so challenging to implement!

Acknowledgments

The studies described in this report were funded in part by grants from the U.S. Department of Energy and the National Institutes of Health. I would like to thank all of my collaborators over the past 15 years, but especially Dr. Weilian Yang, who has been the closest and most heavily involved in the studies that I have described. Special thanks are due to Laura Martz for expert secretarial assistance in the preparation of this manuscript.

References

Barth, R.F., Yang, W., Rotaru, J.H., Moeschberger, M.L., Joel, D.D., Nawrocky, M.M., Goodman, J.H., and Soloway, A.H., 1997. Boron neutron capture therapy of brain tumors: enhanced survival following intracarotid injection of either sodium borocaptate or boronophenylalanine with or without blood-brain barrier disruption. Cancer Res. 57, 1129 - 1136.

Barth, R.F., Yang, W., Rotaru, J.H., Moeschberger, M.L., Boesel, C.P., Soloway, A.H., Joel, D.D., Nawrocky, M.M., Ono, K., Goodman, J.H. , 2000. Boron neutron capture therapy of brain tumors: enhanced survival and cure following blood-brain barrier disruption and intracarotid injection of sodium borocaptate and boronophenylalanine. Intl. J. Radiat. Oncol. Biol. & Physics 47, 209-218.

Barth, R.F., Grecula, J.C., Yang, W., Rotaru, J.H., Nawrocky, M., Gupta, N., Albertson, B.J., Ferketich, A.K., Moeschberger, M.L., Coderre, J., and Rofstad, E.K. , 2004. Combination of boron neutron capture therapy and external beam radiotherapy for brain tumors. Int'l J. Radiat. Oncol. Biol. & Physics 58, 267-277.

Diaz, A.Z., 2003. Assessment of the results from the phase I/II boron neutron capture therapy trials a the Brookhaven National Laboratory from a clinician's point of view. J. Neurooncol. 62, 101-109.

Hatanaka, H. A., 1975. revised boron-neutron capture therapy for malignant brain tumors: II. Interim clinical result with the patients excluding previous treatments. J. Neurol. 209, 81-94.

Mishima, Y., Ichihashi, M., Tsui, M., Hatta, S., Ueda, M., Honda, C., et al., 1989. Treatment of malignant melanoma by single thermal neutron capture therapy with melanoma-seeking 10B-compound. Lancet 2, 388-389.

Rousseau, J., Boudou, C., Barth, R. F., Balosso, J., Estève, F. and Elleaume, H., 2007. Enhanced survival and cure of F98 glioma-bearing rats following intracerebral delivery of carboplatin in combination with photon irradiation. Clin. Cancer Res. 13, 5195-5201.

Stupp, R., Mason, W.P., van den Bent, MJ, et al., 2005. Radiotherapy plus concomitant and adjuvant temozolomide for glioblastoma. N. Engl. J. Med. 352, 987-996.

Vicente, M.G.H., ed., 2006. Boron in Medicinal Chemistry. Anti-Cancer Agents in Med. Chem. 6, 73-184.

Yang, W., Wu, G., Barth, R. F., Swindall, M. R., Bandyopadhyaya, A. K., Tjarks, W., Tordoff, K., Moeschberger, M., Sferra, T. J., Binns, P. J., Riley, K. J., Ciesielski, M. J., Fenstermaker, R. A., and Wikstrand, C., 2008. Molecular targeting and treatment of composite EGFRvIII and EGFR-positive gliomas using boronated monoclonal antibodies. Clin. Cancer Res. 14, 883-891.

CHEMISTRY AND PHARMACOLOGY

The New and Comprehensive BNCT Program of the International Institute of Nano and Molecular Medicine

M. Frederick Hawthorne [a], Mark W. Lee, Jr.[a]

[a] *International Institute of Nano and Molecular Medicine*
Department of Radiology
1514 Research Park Drive
University of Missouri
Columbia, Missouri 65211, USA

Abstract

In 2006 the University of Missouri Medical School launched the International Institute of Nano and Molecular Medicine (I^2NM^2), headed by the lead author and devoted to a variety of new areas based upon boron chemistry. This effort included the construction of a high-performance thermal neutron beam attached to the 10MW Missouri University Research Reactor (MURR) and coupled to an extensive chemical discovery program dedicated to the design, synthesis and evaluation of new tumor-selective boron agents and methods for their delivery. Success in this area would lead to a proof of principle of BNCT when applied to human therapy. A variety of tumor types would be studied with optimized boron agents.

Keywords: BNCT agent, University of Missouri, neutron, synthesis, biodistribution, therapy

1. Introduction

In 2006 the University of Missouri (MU) initiated a new center for the revived study of BNCT in the United States through the creation of the International institute of Nano and Molecular Medicine (I^2NM^2). This new organization benefits from a strong chemical research program and the collaboration of the MU Medical School, Nuclear Engineering Department, the 10 MW University Reactor (MURR), the Veterinary Medicine School and the Idaho National Laboratory. The I^2NM^2, headed by the lead author, is situated in a new research building very near the MURR and will utilize a new thermal neutron beamline scheduled to be operational in the fall of 2008. The institute is engaged in small animal trials of new boron agents displaying attractive results in biodistribution studies of candidate agents. Initial funding of this venture has been borne by the University of Missouri. The research program of I^2NM^2 involves the BNCT-related research areas of nanoscience, chemistry, pharmacology, imaging, chemical biology, radiation biology and computational chemistry. The I^2NM^2 laboratory will provide analytical services such as tissue analyses for boron using ICP methodology which will, in turn, provide very rapid evaluation of new boron agents in biodistribution studies (Bauer et al., 1990). Promising candidate boron agents that display low toxicity and selective tumor uptake at therapeutic concentrations will be further evaluated in ^{10}B-enriched form using small animal models. Attractive agents providing evidence of enhanced efficacy in these evaluation studies will be further examined elsewhere using large animal models preliminary to eventual human trials. The course of this research will avoid *glioblastoma multiforme*, the principal and nearly exclusive target in BNCT research for the past fifty years (Sweet, 1951).

2. The Current State of BNCT

Numerous studies of the *in-vivo* boron neutron capture reaction have been conducted using a range of animal models extending from mice to humans (Brownell et al., 1978, Barth et al, 1990). Due to the lack of serious evaluation of new boron agent candidates, the field is left with only three boron agents suitable for human use; each arising from the 1955-65 era (Hawthorne and Lee, 2003). These are

boronophenylalanine (BPA), disodium dodecahydrododecaborate thiol (BSH) and disodium decahydrodecaborate (GB-10). Human trials undertaken at this time quite commonly employ commercially available L-BPA. However, the clinical performance of each of these boron agents suffers from low tumor-selectivity when administered at doses sufficient for BNCT. The tumor/blood ratio produced using BPA is generally no greater than 2.4, while BSH and GB-10 are global agents with no tumor-selectivity (Hawthorne and Lee, 2003).

Clearly, new boron agents are required to permit clinically successful BNCT. Of equal importance as new agent types is the exploration of new delivery techniques rather than the traditional intravenous injection (Ozawa et al., 2005).

Current neutron sources which are useful for BNCT research and clinical use are reactor-based and are either thermal or epithermal in energy range, depending on their application. Accelerator-based neutron sources are possible to construct and their further development and construction await a demonstration of BNCT clinical success (Kononov et al., 2006). It is noteworthy that the current rendition of clean, reactor-based neutron sources is well-advanced and probably nearly as optimal as one might ideally achieve. Continued improvements with accelerator-based neutron sources are logical subjects for future work. However, this will require a significant demonstration of success within some segment of BNCT.

3. Possible Success with BNCT

The demonstration of a proof-of-principle with BNCT requires the development of new boron target compounds and complementary delivery methods (Hawthorne and Lee, 2003). The chemistry of boron-agent development and evaluation should be the major emphasis of current efforts in this field. Indeed, throughout the now 50-year course of BNCT investigations, target compounds that have been synthesized, have only received minimal evaluation, typically through biodistribution experiments using small animals coupled with associated observations pertaining to qualitative systemic toxicities. None of these target compounds have ever been investigated using actual BNCT experiments.

A principal objective of the I^2NM^2 will be the development and evaluation of new boron-agents and delivery methods for application in BNCT against a wide range of tumor models. The most promising of these agents, as judged from preliminary biological data, will be evaluated for efficacy against a murine EMT6 tumor model and others as appropriate. In addition, new boron-agents will continually be created within the I^2NM^2 and these will be fully examined, as justified from preliminary biological data. Additionally, promising boron-agents developed by other groups within the international BNCT community may be fully evaluated utilizing the I^2NM^2 facilities and their efficacy compared with existing agents using similar experimental conditions. The ability to perform such thorough evaluations of boron-agents and true "apple-to-apple" comparisons did not previously exist within one organization.

The efforts of the I^2NM^2 will provide a "pipeline" of new agent types for investigations using a wide range of tumor models. An array of delivery methods will be investigated, including intratumoral delivery and nanoparticle-based agents with a variety of targeting methods.

4. I^2NM^2 Facilities

As previously stated, the I^2NM^2 is finalizing the construction of its thermal neutron beamline, which is anticipated to be operational in the fall of 2008. The design and initial measurements of this beamline is the subject of another contribution at this meeting (Nigg et al, this meeting).

In addition to the new I^2NM^2 thermal beamline, the institute has recently occupied its new 30,000 square foot research laboratory building, equipped with several large synthetic, biological and analytical laboratories. The building houses the institute's nuclear magnetic resonance (NMR) suite with new 500 MHz and 400 MHz spectrometers, as well as a mass spectrometry laboratory, with spectrometers equipped with EI, CI, ESI, APCI, and MALDI ionization sources. The I^2NM^2 building also houses a new high-throughput BNCT tissue analysis laboratory, equipped with microwave tissue sample digesters and ICP-OES instruments with a capability of performing several hundred sample analysis per day.

The MURR, the largest academic reactor in the United States, operates nearly continuously and produces a neutron flux of 7×10^{14} n/(cm^2 sec) (Cox and Parkinson, 1973). In addition to conducting research, MURR operates FDA approved cGMP and

GLP programs and produces the radiopharmaceuticals Ceretec™, TheraSphere®, and Quadramet®. Recent installation of a cyclotron adds production of isotopes for PET imaging. The University of Missouri is also home to the top academic Nuclear Engineering Department in the United States.

Adjacent to the I^2NM^2 building and the MURR reactor is a well-equipped small-animal vivarium which will house animals utilized for BNCT investigations. Closely affiliated with I^2NM^2 are the MU Schools of Medicine and Veterinary Medicine. The School of Medicine operates a large on-campus teaching hospital with active clinical programs. The School of Veterinary Medicine operates a 150,000 square foot state-of-the-art small and large animal facility with specialized areas in emergency medicine and surgery, ophthalmology, neurology, oncology, cardiovascular medicine and surgery, orthopedic surgery, and advanced imaging techniques.

4. Conclusions

The presence of the many separate disciplines which comprise the science and engineering of BNCT on the University of Missouri campus coupled with the intense chemical theme of the I^2NM^2 makes this location ideal for a reinvestigation of BNCT research in the United States. The scientific needs are unique, but the available facilities are unique and well-matched for success by the I^2NM^2 and MURR team.

References

Bauer, W. F., Wishard, J. A., Rae, C., Lassahn, N., 1990. Flow injection for sample introduction into inductively coupled plasma for the determination of boron in biological samples. Prog. Neutron Capture Ther. Cancer, [Proc. Int. Symp.], 4th (1992), Meeting Date 1990, 297-300.

Sweet, W.H., 1951. The Use of Nuclear Desintegrations in the Diagnosis and Treatment of Brain Tumor. N. Engl. J. Med., 245, 875-878.

Brownell, G., Zamenhof, R.G., Murray, B.W., Wellum, G.R., 1978. Boron Neutron Capture Therapy. In: Therapy in Nuclear Medicine, R.P. Spencer (ed.), Grune and Stratton, Inc., New York.

Barth, R.F., Solloway, A.H., Fairchild, R.G., 1990. Boron Neutron Capture Therapy of Cancer. Cancer Res. 50, 1061-1070.

Hawthorne, M. F., Lee, M. W., 2003. A critical assessment of boron target compounds for boron neutron capture therapy. Journal of neuro-oncology. 62(1-2), 33-45.

Ozawa, T., Afzal, J., Lamborn, K. R., Bollen, A. W., Bauer, W. F., Koo, M. S., Kahl, S. B., Deen, D. F., 2005. Toxicity, biodistribution, and convection-enhanced delivery of the boronated porphyrin BOPP in the 9L intracerebral rat glioma model. Int. J. Rad. Oncol., Biol. Phys. 63(1), 247-252.

Kononov, V. N., Bokhovko, M. V., Kononov, O. E., Soloviev, N. A., Chu, W. T., Nigg, D., 2006. Accelerator-based fast neutron sources for neutron therapy. Nuclear Instruments & Methods in Physics Research, Section A: Accelerators, Spectrometers, Detectors, and Associated Equipment. 564(1), 525-531.

Cox, E. L., Parkinson, T. F., 1973. Special irradiation facilities at the University of Missouri research reactor facility. Irradiation Facil. Res. Reactors, Proc. Symp., University of Missouri, Columbia, MO, USA, 1972, 39-58.

New dodecaborate cluster lipids and cholesterol derivatives for BNCT

Tanja Schaffran[a], Franziska Lissel[a], Alexander Burghardt[b], Regine Peschka-Süss[b], Rolf Schubert[b], Detlef Gabel[a]

[a]*Department of Chemistry, University of Bremen, D-28357 Bremen, Germany,*
[b] *Institute of Pharmaceutical Sciences, Department of Pharmaceutical Technology and Biopharmacy, University of Freiburg, D-79104 Freiburg, Germany*

Abstract

New dodecaborate cluster lipids B-THF-14, B-Dioxane-14 and B-Pyrane-14 have been synthesized by nucleophilic ring opening reactions of the tetrahydrofurane, dioxane or tetrahydropyrane derivative of the dodecahydro-*closo*-dodecaborate cluster. The lipids, carrying a single negative net charge, have the same lipid backbone and head groups, but varying linkers. Cryo-TEM pictures show formation of boron cluster-containing liposomes from an equimolar mixture of the boron lipid, DPPC and cholesterol. Differential scanning calorimetry shows that B-THF-14 has a main transition temperature of 48.9 °C; no transition can be detected for B-Dioxane-14. B-THF-14 shows toxicity in V79 Chinese hamster cells with an IC_{50} value of 0.38 mM. B-Dioxane-14 is less toxic with an IC_{50} value of 2 mM. In addition, a BNH_3 cholesterol derivative has been synthesized. Physical and biological characterization for this cholesterol derivative is in progress.

Keywords: dodecaborate cluster lipid, DSC, cryo-TEM, cytotoxicity, BNCT

1. Introduction

Boron neutron capture therapy is a radiation therapy for cancer treatment. The short range of the charged particles which are generated in the nuclear reaction between the nontoxic species ^{10}B and thermal neutrons reaches a great biological effect within the cancer cell and without affecting the surrounding tissue. For successful treatment a high amount of boron (approx. 20-30 µg of boron-10 per gram of tumor) is necessary to produce cell death. Several strategies are investigated for the boron transfer system, e.g. antibodies (Soloway et al., 1965; Alam et al., 1989), nucleic acid precursors (Schinazi, 1978) and porphyrin derivatives (Miura et al., 1989; Kahl et al., 1989).

Liposomes show selective localization in tumors (Pathak et al., 2005; Dreher et al., 2006) and might be useful vesicles for boron transfer. We focused on boronated lipids and cholesterol derivatives. In the literature only a few boron-containing lipids and cholesterol derivatives are described. Lemmen et al. (1995) reported a carborane-containing ether lipid and Nakamura et al. (2004) described a nido-carborane cluster lipid. Recently, we published new dodecaborate cluster lipids (Justus et al, 2007) and dodecaborate cluster cholesterol derivatives (Nakamura et al., 2007). A cholesterol-carborane conjugate (Ji et al., 2002) and a cholesterol carborane ester compound (Peacock et al., 2004) have been described before.

In this study we present new dodecaborate cluster lipids and a cholesterol derivative with only one negative charge.

2. Chemistry

The synthesis requires the connection between a derivative of the $B_{12}H_{12}^{2-}$ cluster and a lipid backbone. We used nucleophilic ring opening reactions between the tetrahydrofurane (THF), dioxane and tetrahydropyrane (THP) derivative of the cluster and diethanolamine followed by an esterification at the hydroxyl groups with the acid chloride (Scheme 1).

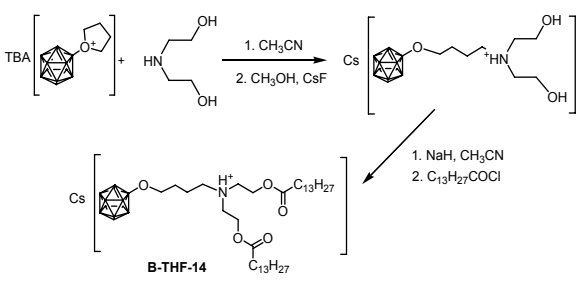

Scheme 1. Synthesis of the dodecaborate cluster lipid B-THF-14

Semioshkin et al. (2007) recently reported reactions of oxonium derivatives with amines, but under different conditions.

The ring opening reactions proceed with a yield of 90-95 % and the esterification, with 35-40 %. The lipids were characterized by MS and NMR spectroscopy. Three new dodecaborate cluster lipids have been obtained the same lipid backbone and head groups, but varying linkers (Scheme 2).

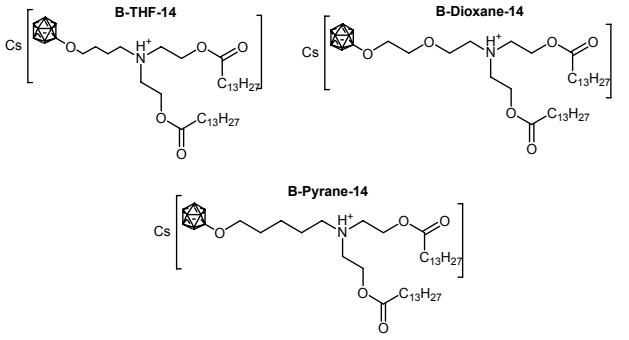

Scheme 2. B-THF-14, B-Dioxane-14, B-Pyrane-14

We have synthesized a new dodecaborate cluster cholesterol derivative with only one negative charge. First the cholesterol reacts with 3-bromo-propionyl chloride in the presence of triethylamine to product 1. Then the ammonioundecahydro-dodecaborate (BNH_3) is deprotonated by sodium hydride and reacts with product 1 to form the BNH_3 cholesterol derivative (Scheme 3).

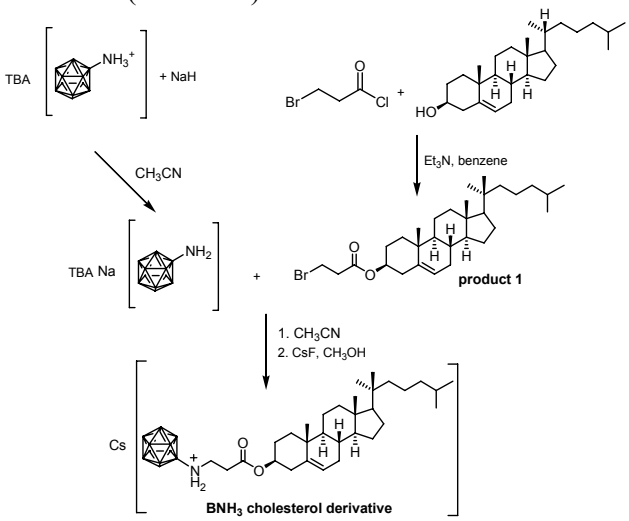

Scheme 3. Synthesis for the BNH_3 cholesterol derivative

Product 1 was first prepared for a mercaptoundeca-hydro-*closo*-dodecaborate-conjugated cholesterol derivative (Nakamura et al. 2007).

The BNH_3 cholesterol dervative was characterized by MS and NMR. The first synthesis step has a yield of 81 % and the yield for the dodecaborate cluster cholesterol derivative is 50 %.

3. Liposomal preparation and toxicity

Liposomes were prepared by hydration of a lipid film followed by extrusion. The cryo-TEM pictures show that preparations of DPPC/cholesterol/boron-containing lipid in the molar ratio of 1:1:1 form liposomes.

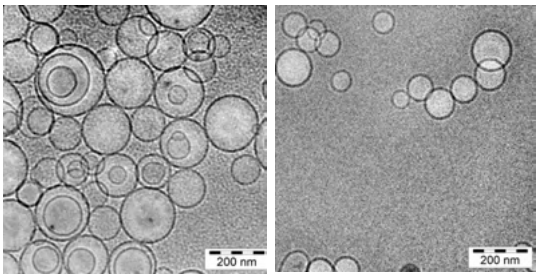

Figure 1. cryo-TEM pictures of DPPC/ cholesterol/ B-THF-14 liposomes (left) and DPPC/cholesterol/ B-Dioxan-14 liposomes (right)

Most of the material forms unilamellar, closed vesicles which exhibit a tolerable size distribution. In the case of B-THF-14 a few multilamellar structures can be observed.

The phase transition temperature of the pure B-THF-14 lipid was determined with differential scanning calorimetric measurements (DSC).

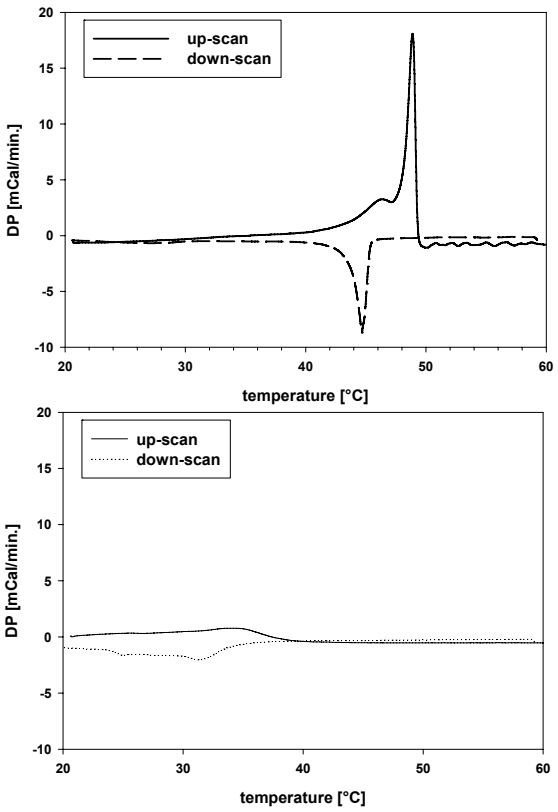

Figure 2. DSC of pure films of B-THF-14 (above) and B-Dioxane-14 (below) (the first up-scan and the first down-scan are shown). Lipid concentration 5 mM.

The DSC data (Figure 2) show a sharp peak at 48.9 °C and a small pre-transition peak at 46 °C. These temperatures are not comparable to other lipids containing the same hydrophobic part. Dimyristoylphosphatidylcholine (DMPC) with the same alkyl chain length has a transition temperature of 24.3 °C. The dodecaborate lipid B-6-14 with a myristoyl chain (recently described by us (Justus et al., 2007)) does not exhibit a pre-transition peak and the main transition is at 18.8 °C, in the same temperature region as DMPC. The temperature difference between the transition peaks in the up- and down scan (approx. 4 degrees) is very remarkable; such strong hysteresis effect is not known yet.

For B-Dioxane-14 the phase transition temperature could not identified. A very broad transition between 20-40 °C with minimal endothermic demand is observed.

Broad transitions are normally found for detergents which are not able to form ordered structures.

Cytotoxicity of the lipids B-THF-14 and B-Dioxane-14 was determined. V79 Chinese hamster cells were exposed to liposomes consist of DPPC/cholesterol/boron-containing lipid (1:1:1) for 24 h. The cell survival was detected by the enzymatic reduction of the WST-1 dye by living cells.

In Figure 3 the toxicity data are shown.

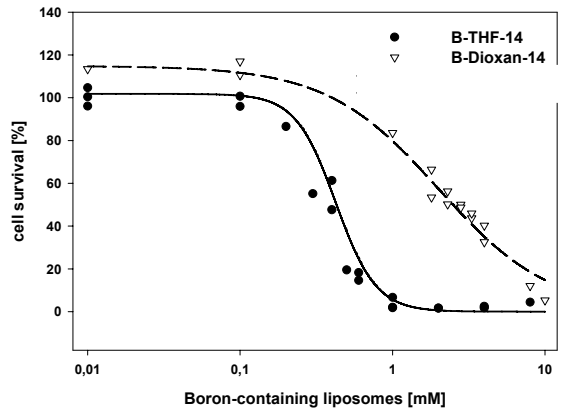

Figure 3. Survival of V79 Chinese hamster cells exposed to B-THF-14 (circles) and B-Dioxane-14 (triangles), respectively. The solid and the dashed lines are the fitted curves from which the IC_{50} value was calculated.

We found that B-THF-14 inhibits the cell growth by 50 % at a concentration of 0.38 mM. B-Dioxane-14 is less toxic and shows toxicity at 2 mM.

Physical and biological characterization for the cholesterol derivative is in progress.

4. Conclusions

New dodecaborate cluster lipids and one cholesterol derivative were obtained. The cryo-TEM pictures demonstrate the possibility to prepare liposomes from dodecaborate cluster lipids in the presence of helper lipids. By means of this liposome formulation a high amount of boron can be transferred to the cancer cells. For successful BNCT 10-30 ppm boron is required which corresponds to approx. $(1\text{-}3)\cdot10^9$ boron atoms for an average mammalian cell (Ipsen et al., 1990). Justus et al. (2007) calculated the boron content for a 100 nm liposome with an equimolar ratio of DSPC, cholesterol and boron lipid. A 100 nm liposome contains $1.6\cdot10^5$ lipid molecules and the effective area per lipid molecule in bilayers is 0.39 nm^2, therefore $6.5\cdot10^5$ boron atoms can be transferred. Only half of that number of boron atoms ($3.8\cdot10^5$) can be encapsulated in 100 nm liposomes at a dodecaborate cluster concentration of 0.1 M. (assuming a volume per liposome of $5.2\cdot10^6$ nm^3)

The liposomes prepared here can most probably be tagged with tumor-seeking entities (Ishida et al., 2001) and thereby a selective tumor accumulation should be possible.

The DSC data show that the headgroup influences the phase transition. Normally the transition temperature depends on the alkyl chain length, thus the temperature increases from DMPC (24 °C) to DSPC (54 °C). B-THF-14 has the same alkyl chain as DMPC but the transition temperature is at 49°C. The DSC data of B-Pyrane-14 which also has a carbon linker between dodecaborate cluster and lipid backbone are very interesting. Perhaps it even has a higher transition temperature as compared to B-THF-14.

B-Dioxane-14 has no characteristic transition and behaves more like a detergent in the DSC. Therefore cryo-TEM pictures of pure boron lipid will be helpful to identify differences in formed structures of B-THF-14 and B-Dioxane-14. For B-THF-14 ordered structures are expected (e.g. liposomes, bilayers); for B-Dioxane-14 disordered structures without transition temperature (such as micelles) appear more probable.

The cell survival data demonstrate that the choice of the lipid head group can influence toxicity. The integration of an oxygen atom in the carbon linker between dodecaborate cluster and lipid moiety decreases the toxicity by a factor of five. In this context it will be interesting to compare the B-Pyrane-14 lipid with B-THF-14, to see whether there is a relation between length of the carbon linker and toxicity.

We prepared the dodecaborate cluster lipids B-6-14 and B-6-16 (Justus et al., 2007) and found a toxicity decrease with longer alkyl chain length. Recently we synthesized B-THF-16 and B-Dioxane-16 with palmitoyl instead of myristoyl chains. Possibly, the toxicity decreases similarly.

We have no data to date about the reasons for toxicity. Perhaps the boron-containing liposomes are completely internalized into the cells or an exchange of boron-containing lipid between liposome and cell membrane occurs. In this case the membrane potential would decrease because of the negative lipid charge and a dysfunction of the membrane channels would be possible. Alternatively, the membrane fluidity could be changed by incorporation of the lipid into the membrane.

The high boron carrying capacity, the low toxicity, and the formation of stable liposomes make dodecaborate cluster lipids attractive agents for BNCT.

References

Alam, F., Barth, R.F., Soloway A.H., 1989. Boron containing immunoconjugates for neutron capture therapy of cancer and immunocytochemistry. Antibody, Immunoconjugates, Radiopharm. 2, 145-163.

Dreher, M.R., Liu, W., Michelich, C.R, Dewhirst, M.W., Yuan, F., Chilkoti, A. 2006. Tumor vascular permeability, accumulation, and penetration of macromolecular drug carriers. J.Natl.Cancer Inst. 98, 335-44.

Ipsen, J.H., Mouritsen, O.G., Bloom, M., 1990. Relationships between lipid membrane area, hydrophobic thickness, and acyl-chain orientational order. The effects of cholesterol. Biophys. J. 57, 405-412.

Ishida, O., Maruyama, K., Tanahashi, H., Iwatsuru, M., Sasaki, K., Eriguchi, M., Yanagie, H. 2001. Liposomes bearing polyethyleneglycol-coupled transferring with intracellular targeting property to the solid tumors in vivo. Pharm. Res. 18, 831-840.

Ji, B.; Peacock, G.; Lu, D.R. 2002. Synthesis of cholesterol-carborane conjugate for targeted drug delivery. Bioorg. Med. Chem. Lett. 12, 2455-2458.

Justus, E., Awad, D., Hohnholt, M., Schaffran, T., Edwards K., Karlsson, G., Damian, L., Gabel, D. 2007. Synthesis, liposomal preparation, and in vitro toxicity of two novel dodecaborate cluster lipids for boron neutron capture therapy. Bioconj. Chem., 1287-93.

Kahl, S.B., Laster, B.H., Kood, M.-S., Warkentien, L.S., Fairchild, R.G., 1989. Distribution of a boronated porphyrin in murine tumors. Clinical Aspects of Neutron Capture Therapy, pp 205-211, Plenum Press, New York.

Lemmen, P.; Weißfloch, L.; Auberger, T.; Probst, T. 1995. Uptake and distribution oft he boron-containing ether lipid B-Et-11-OMe in tumor bearing mice. Anti-Cancer Drugs 6, 744-48.

Miura, M., Gabel, D., Fairchild, R.G., Laster, B.H., Warkentien, L.S., 1989. Synthesis and in vivo studies of a carbonyl porphyrin. Strahlenther. Onkol. 165, 131.

Nakamura, H.; Miyajima, Y.; Takei, T.; Kasaoka, S.; Maruyama, K. 2004. Synthesis and vesicles formation of nido-carborane cluster lipid for boron neutron capture therapy. Chem. Commun., 1910-11.

Nakamura, H.; Ueno, M.; Lee, J.D.; Ban, H.S.; Justus, E.; Fan, P.; Gabel, D. 2007. Synthesis of dodecaborate-conjugated cholesterols for efficient boron delivery in neutron capture therapy. Tetrahedron Lett. 48, 3151-3154.

Pathak, A.P., Artemov, D., Ward, B.D., Jackson, D.G., Neeman, M., Bhujwalla, Z.M, 2005. Characterizing extravascular fluid transport of macromolecules in the tumor interstitium by magnetic resonance imaging. Cancer Res. 65, 1425-32.

Peacock, G.; Sidwell, R.; Pan, G.; Oie, S.; Lu, R. 2004. In vitro uptake of new cholesteryl carborane ester compound by human glioma cell lines. J. Pharm. Sci. 93, 13-19.

Schinazi, R.F., Prusoff, W.H., 1978. Synthesis and properties of boron and silicon substituted uracil of 2′-deoxyuridine. Tetrahedron Lett. 50, 4981-4984.

Semioshkin, A., Nizhnik, E., Godovikov, I., Starikova, Z., Bregadze, V. 2007. Reactions of oxonium derivatives of $[B_{12}H_{12}]^{2-}$ with amines: Synthesis and structure of novel B_{12}based ammonium salts and amino acids. J. Organometal. Chem. 692, 4020-4028.

Soloway, A.H., Brownwell, G.L., Ojemann, R.G., Sweet, W.H., 1965. Boron-slow neutron capture therapy: present status. In Proceedings of the International Symposium of the Preparation and Bio-Medical Application of Labeled Molecules. pp 383-403, Venice, Italy.

Intracellular uptake of a new boronated porphyrin EC032

Takao Tsurubuchi [1], Tetsuya Yamamoto[1], Kei Nakai[1], Fumiyo Yoshida[1], Makiko Miyakawa[1], Makoto Shirakawa[2], Manabu Ueno[3], Masahide Matsuda[1], Yoshinori Nakae[4], Ryuji Asano[4], Akira Matsumura[1]

[1]*Department of Neurosugery, Institute of Clinical medicine, University of Tsukuba, Japan*
[2]*Master's program in Medical Science, University of Tsukuba, Japan*
[3]*Department of Chemistry at Gakushuin University*
[4]*Photochemical Co., Ltd.*

Abstract

We measured the toxicity and intracellular uptake of a newly developed boronated porphyrin EC032, and verified the fluorescence-based boron concentration measuring methods. Toxicity study showed that concentration required to produce a 50% reduction in viability (IC_{50}) of EC032 was more than 0.25 mM. Fluorescence study showed the intracellular uptake of EC032 increased up until 24 hours after its exposure to C6, 9L, U87, and U251 cells. There was also a linear correlation between ICP-AES and fluorescence intensity as an arbitrary unit about measurement of boron concentration.

Fluorescence-based boron concentration measuring methods are very simple and useful methods, especially for screening of slight test dose of porphyrin compounds.

Keywords:boronated porphyrin, fluorescence study, ICP-AES, ^{10}B concentration

1. Introduction

To improve the therapeutic effect of BNCT, sufficient amount of boron and neutron delivery in tumor tissue is important. Several tumor selective porphyrin compounds such as ATN-10 (Yamamoto, 1998), STA-BX909 (Matsumura, 1999) have been reported in our group. We measured the toxicity and intracellular uptake of a newly developed boronated porphyrin EC032 as a new boron carrier. This compound has a tumor selective porphyrin unit and also has a cage of boron. (Figure 1) The fluorescence-based ^{10}B concentration measuring methods was verified.

2. Materials and methods

2.1. Toxicity study

Cytotoxicity effects of EC032 on tumor cells such as C6, 9L rat gliosarcoma cells, and U87, U251 human glioblastoma cells were examined using [3-(4,5-dimethylthiazol-2-yl)-5-(3carboxymethoxyphenyl)-2-(4-sulphophenyl)-2H-tetrazolium, inner salt] (MTS) assay in comparison with sodium borocaptate (BSH) under dark condition. The tumor cells were dispensed into 96-well microplate at a concentration of $5x10^3$ cells/100 μl of supplemented Dulbecco's modified Eagle's medium. The plates were incubated at 37 °Celsius in a humidified CO_2 incubator for 48 hours before the addition of EC032 or BSH. The concentration of EC032 or BSH ranged from 0.25 μM to 2.5 mM. The same series of dilutions was prepared without addition of cells as background control samples. The plates were incubated for an additional 48 hours after which the medium was changed and 20 μl of cell titer 96 aqueous assay system from Promega was added to each sample's well. The absorbance was measured in a microplate reader at 490 nm after 1.5 h. The concentration required to produce a 50% reduction in viability (IC_{50}) was determined.

2.2. Fluorescence study

C6, 9L, U87, U251 cells were incubated with 20 μM EC032 in conditioned medium for 30 min, 1h, 2h, 6h, and 12h in a 96-well microplate. The cultured medium was washed three times with PBS. The cells were pipetted and minced with Triton-X. The fluorescence intensity as an arbitrary unit (a.u.) of the sample in the well was measured by microplate reader. The excitation wave length was 405 nm and the emission wave length was 670±10 nm. Cells of the same condition were trypsinized

and counted. Then the intracellular uptake of EC032 was determined. All experimental procedures were done under dark condition.

2.3. Measurement of boron concentration

We evaluated the correlation between inductively coupled plasma atomic emission spectroscopy (ICP-AES) and fluorescence intensity (a.u.) detected by microplate reader. C6, 9L, U87, and U251 cells were incubated with EC032, which were respectively added to the conditioned medium at a boron concentration of 30μg/ml. The incubation times were 6 and 24 h. The cultures were washed once with PBS. The cells were counted and pretreated by wet ashing method. Then the intracellular boron concentration was measured by ICP-AES. Using another part of the same sample, the fluorescence intensity (a.u.) of the sample was measured by microplate reader under dark condition.

3. Results

Toxicity study: The IC_{50} of EC032 was more than 0.25 mM in 9L, U87, U251, C6 cells. (Figure 2) The IC_{50} of BSH was more than 0.25 mM in U87 and U251 cells and less than 0.25 mM in 9L, C6 cells. (Figure 3)

Fluorescence study: The intracellular uptake of EC032 increased until 24 hours after its exposure to C6, 9L, U87, and U251 cells. (Figure 4) Boron concentrations in cultured glioma cells (C6, 9L, U87, and U251) in the wells of a 96-well microplate after 24 hours incubation with EC032 are shown in Table1.

Measurement of boron concentration: There was a linear correlation between ICP-AES and fluorescence intensity (a.u.) regarding the measurement of boron concentration. (Figure 5)

4. Discussion

As a new boron carrier, EC032 shows low toxicity and time-dependent increase until 24 hours in many glioma cell lines. Fluorescence-based measurement of boron concentration is a very simple and useful method.

BSH and Boronophenylalanine (BPA) are well known boron carriers which have been widely used in recent Boron Neutron Capture Therapy. The toxicity of BSH (Mares, 1992) and BPA (Barth 2004) are known to be very low. No drug has been reported with lower toxicity than these drugs. However, a few studies about the cytotoxicity of BSH *in vitro* have been reported. The IC_{50} of EC032 was more than 0.25 mM, which has lower toxicity than the other boron porphyrins and boron compounds. (Barth, 2004) This indicates that EC032 has low toxicity under dark condition. The IC_{50} of BSH was more than 0.25 mM other than C6 and 9L cells in this study. These datas were slightly lower than previous data. (Mares, 1992) One reason is perhaps that the IC_{50} values of BSH in C6, 9L cells were underestimated because of the clearance of live cells, which decreased their adhesion ability due to ultrastructual changes under high concentrations of BSH. (Mares, 2003) Another is the differences in cellular characteristics among the cell lines.

Serial changes of the intracellular concentration of EC032 in many tumor cell lines showed a time-dependent increase up until 24 hours. According to the report by Yoshida in 2002, BSH shows a homogeneous but low boron concentration pattern in tumor tissues, and BPA shows a heterogeneous but high boron concentration pattern. The uptake pattern of other boronated porphyrins such as porpyrin-cobaltacarborane (Hao, 2007), meso-tetra(4-nido-carboranylphenyl)porphyrin (Vincente, 2002) in tumor cells resembles that with our compound EC032. Other boronated compound such as boronated porphyrin (BOPP) showed an uptake and retention at least 20 times that of BSH. (Fairchild, 1990 and Ceberg, 1995) Although the tumor cell lines and cell numbers are different among these experiments, the estimated intracellular uptake of EC032 seems to be more than that of BOPP. (Hill, 1992 and Nguyen, 1993) Many porphyrin compounds have characteristics suitable for drug targeting because of their affinity to LDL receptors (Spizzirri, 1996 and Shibata, 2001 and Novick, 2006), localization in the intracellular lysosome. (Callahan, 1999), and quantitative detection with fluorescence techniques. Further study of *in vivo* tissue uptake is warranted to determine the appropriate administration dose of EC032 to get acceptable tumor selectivity.

There is a linear correlation between the fluorescence intensity (a.u.) measured by microplate reader and the boron concentration measured by ICP-AES. Measurement of the boron concentration using ICP-AES is a widely used reliable method; our result indicates the reliability of fluorescence based measurement of boron concentration in tumor cells. Moreover, our method is simpler and more convenient than other methods like prompt gamma ray methods and ICP-AES, especially for screening of low test doses of boron compounds.

The new porphyrin EC032 showed low toxicity and time-dependent increase and quantitative results with a fluorescence microplate reader. Therefore, EC032

is a candidate for a boron carrier in Boron Neutron Capture therapy.

4. Conclusion

The new boronated porphyrin EC032 has low cytotoxicity and shows time-dependent uptake in tumor cells. Fluorescence-based boron concentration measuring methods are very simple and useful methods, especially for screening of low test dose of porphyrin compounds.

Acknowledgments

The new boronated porphyrin 'EC032' was kindly provided by the members of Photochemical Co. Ltd., and we thank them for their support in this research. This study was supported in part by a Grant-in-Aid from the Ministry of Education, Science and Culture, Japan (20390379)

References

1. Barth, R.F., Yang W., Al-Madhoun, A.S., Johnsamuel, J., Byun, Y., Chandra, S., Smith D.R., Tjarks, W., Eriksson, S., 2004. Boron-containing nucleosides as potential delivery agents for neutron capture therapy of brain tumors. Cancer Research. 64(1), 6287-6295
2. Ceberg, C.P., Brun, A., Kahl, S.B., Koo. M.S., Person, B.R., Salford, L.G.A., 1995. A cooparative study on the pharmacokinetics and biodistribution of boronated porphyrin (BOPP) and sulfhydryl boron hydride (BSH) in the RG2 rat glioma model. J. Neurosurg. 83, 86-92
3. Callahan, D.E., Forte, T.M., Afzal, S.M.j., Deen, D.F., Kahl, S.B., Bjornstad, K.A., Bauer, W.F., Blakely, E.A., 1999. Boronated protoporphyrin (BOPP): Localization in lysosomes of the human glioma cell line SF-767 with uptake modulated by lipoprotein levels. Int. J. Radiation Oncology Biol. Phys. 45(3), 761-771
4. Fairchild, R.G., Kahl, S.B., Laster, B.H., J. Kalef-Ezra, J., Popenoe, E.A., 1990. In vitro determination of uptake, retention, distribution, biological efficacy, toxicity of boronated compounds for neutron capture therapy: a comparison of porphyrins with sulfhydryl boron hydrides. Cancer Research. 50, 4860－4865
5. Hao, E., Sibrian-Vazquez, M., Serem, W., Garno, J.C., Fronczek, F.R., Vincente, M.G.H., 2007. Synthesis, aggregation and cellular investigation of porphyrin-cobaltacarborane conjugates. Chem. Eur. J. 13, 9035-9042
6. Hill, J.S., Kahl, S.B., Kaye, A.H., Stylli, S.S., Koo, M., Gonzales, M.F., Vardaxis, N.J., Johhson, C.I., 1992. Selective tumor uptake of boronated porphyrin in an animal model of cerebral glioma. PNAS. 89, 1785-1789
7. Mares, V., Baudysova, M., Kvitek, J., Hnatowicz, V., Cervena, J., Vacik, J., Folbergrova, J., 1992. Accumulation of boron-10 in cell cultures exposed to mercaptododecaborate used for the neutron capture therapy. J. Pharmacol. Exp. Therapeutics. 262, 818-822
8. Mares, V., Krajci, D., Lisa, V., 2003. Subcellular targets of mercaptoborate (BSH), a carrier of 10B for neutron capture therapy (BNCT) of brain tumors. Physiol Res. 52(5), 629-635
9. Matsumura, A., Shibata, Y., Yamamoto, T., Yoshida, F., Isobe, T., Nakai, K., Hayakawa, Y., Kiri, M., Shimojo, N., Ono, K., Sakata, I., Nakajima, S., Okumura, M., Nose, T., 1999. A new boronated porphyrin (STA-BX909) for neutron capture therapy: an in vitro survival assay and in vivo tissue uptake study. Cancer Letters. 141, 203-209
10. Novick, S., Laster, B.H., Quastel, M.R., 2006. Postitive cooperativity in the cellular uptake of a boronated porphyrin. The International Journal of Biochemistry & Cell Biology. 38, 1374-1381
11. Nguyen, T., Brownell, G.L., Holden, S.A., Teicher, B.A., 1993. Intracellular distribution of various boron compounds for use in boron neutron capture therapy. Biochemical Pharmacology. 45(1), 147-155
12. Shibata, Y., Matsumura, A., Yoshida, F., Yamamoto, T., Nakai, K., Nose, T., Sakata, I., Nakajima, S., 2001. Competitive uptake of porphyrin and LDL via the LDL receptor in glioma cell lines: flow cytometric analysis. Cancer Lett. 10, 166 (1), 79-87
13. Spizzirri, P.G., Hill, J.S., Kahl, S.B., Ghiggino, K.P., 1996. Photophysics and intracellular distribution of a boronated porphyrin phototherapeutic agent. Photochemistry and photobiology. 64(6), 975-983
14. Vincente, M.G.H., Edwards, B.F., Shetty, S.J., Hou, Y., Boggan, J.E., 2002. Syntheses and preliminary biological studies of four meso-tetra(nido-carboranylmethyl)phenylporphyrins.

Bioorganic & Medicinal Chemistry. 10, 481-492

15. Yamamoto, T., Matsumura, A., Shibata, Y., Fujimori, H., Nakai, K., Yoshida, F., Nose, T., Sakata, T., Nakajima, S., Miwa, N., 1998. Manganese-metalloporphyrin (ATN-10) as a tumor-localizing agent: magnetic resonance imaging and inductively coupled plasma atomic emission spectroscopy study with experimental brain tumors. Neurosurgery. 42(6), 1332-1338
16. Yoshida, F., Matsumura, A., Shibata, Y., Yamamoto, T., Nakauchi, H., Okumura, M., Nose, T., 2002. Cell cycle dependence of boron uptake from two boron compounds used for clinical neutron capture therapy. Cancer Letters. 10;187(1-2), 135-141

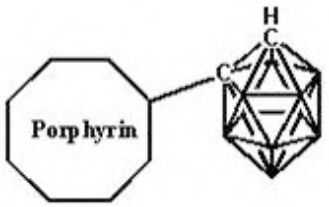

Figure 1 simple constitutional formula of EC032

Apices of the cage mean boron elements

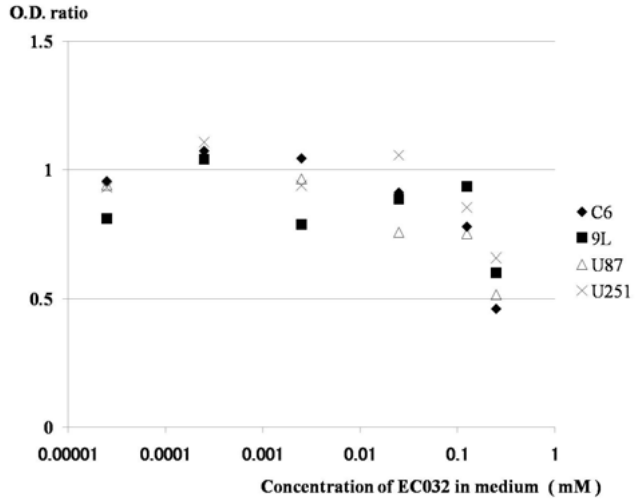

Figure 2 Toxicity study of EC032 using MTS assay

C6	9L	U87	U251
0.4141 (μg B) per 3996 cells	0.2245 (μg B) per 4500 cells	0.4087 (μg B) per 2760 cells	0.2700 (μg B) per 2316 cells

Table 1 Boron concentration in cultured glioma cells (C6, 9L, U87, U251) in the well of 98-well microplate after 24 hours incubation with EC032

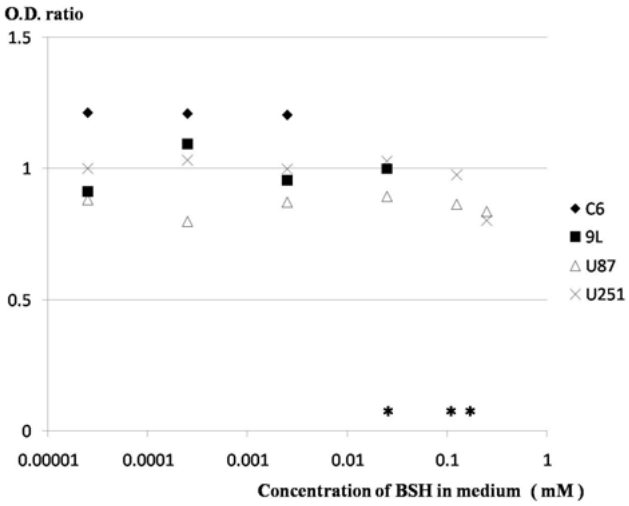

Figure 3 Toxicity study of BSH using MTS assay

An asterisk means the IC50 of BSH beyond 0.0125 mM is not detectable. Double asterisks means the IC50 of BSH beyond 0.125 mM is not detectable.

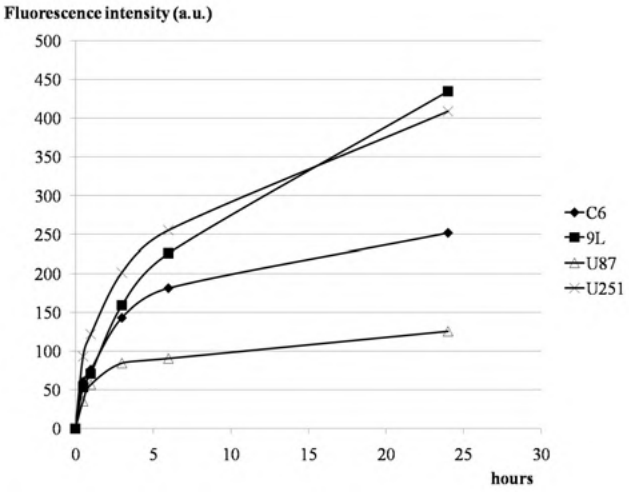

Figure 4 Fluorescence study of EC032 in vitro

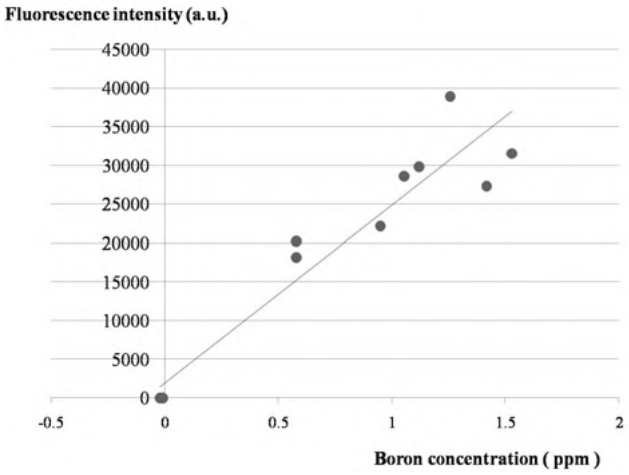

Figure 5 Linear correlation between boron concentration (ppm) measured by ICP-AES and fluorescence intensity (a.u.) (R=0.95404)

Development of Boron Nano Capsules for Neutron Capture Therapy

H. Nakamura[a], M. Ueno[a], H. S. Ban[a], K. Nakai[b,c], K. Tsuruta[c], Y. Kaneda[b], A. Matsumura[c]

[a] *Department of Chemistry, Faculty of Science, Gakushuin University, Mejiro, Tokyo 171-8588, Japan*
[b] *Division of Gene Therapy Science, Graduate School of Medicine, Osaka University, Osaka, 565-0871, Japan*
[c] *Department of Neurosurgery, Institute of Clinical Medicine, University of Tsukuba, Ibaragi, 305-8575, Japan*

Abstract

High accumulation and selective delivery of boron into tumor tissues are the most important requirements to achieve efficient neutron capture therapy of cancers. We focused on liposomal boron delivery system in order to achieve a large amount of boron delivery to tumor. We succeeded in the synthesis of the double-tailed boron cluster lipids **4a-c** and **5a-c**, which has a $B_{12}H_{11}S$-moiety as a hydrophilic function, by *S*-alkylation of $B_{12}H_{11}SH$ (BSH) with bromoacetyl and chloroacetocarbamate derivatives of diacylglycerols. Size distribution of liposomes prepared from the boron cluster lipid **4b**, DMPC, PEG-DSPE, and cholesterol was determined as 100 nm in diameter by an electrophoretic light scattering spectrophotometer. Calcein-encapsulation experiments revealed that these boronated liposomes are stable at 37 °C in FBS solution for 24 h.

Keywords: closo-dodecaborate, boron ion cluster lipids, liposome, mercaptoundecahydrododecaborate, BSH

1. Introduction

Boron neutron capture therapy (BNCT) is a binary cancer treatment based on the nuclear reaction of two essentially nontoxic species, ^{10}B and thermal neutrons (Locher, 1936). The neutron capture reaction by ^{10}B produces an α-particle and a lithium-7 ion bearing approximately 2.4 MeV, and these high linear energy transfer particles afford precise cell killing. Therefore, high accumulation and selective delivery of boron into tumor tissue are the most important requirements to achieve efficient neutron capture therapy of cancers. There are three most important parameters for development of boron compounds: (1) achieving tumor concentrations in the range of 20-35 μg ^{10}B/g; (2) a tumor/normal tissue differential greater than 3-5; (3) sufficiently low toxicity (Barth, 1992). Recently, much attention has been paid for liposomal boron delivery system in order to accumulate a high concentration of boron into tumor. Yanagie (1991) first developed mercaptoundecahydrododecaborate (BSH)-encapsulated egg PC liposomes, which were conjugated with anti-human CEA (carcino-embryonic antigen) monoclonal antibody. Hawthorne (1992) prepared liposomes from DSPC (distearoyl phosphatidylcholine) and cholesterol, in which various boron compounds were encapsulated. Since their initial attempts, various boron clusters-encapsulated liposomes have been developed, such as PEGylated liposomes (Hawthorne, 1994), folate-conjugated liposomes (Lee, 2002), epidermal growth factor (EGF)-conjugated liposomes (Kullberg, 2003), transferrin (TF)-conjugated liposomes (Maruyama, 2004), and Cetuximab-conjugated liposomes (Lee, 2007).

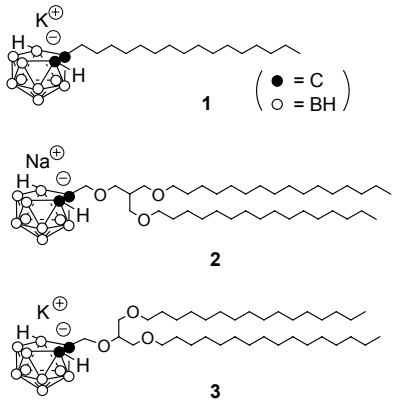

Figure 1. Structures of *nido*-carborane lipids

As an alternative boron delivery system, a system involving the accumulation of boron in the liposomal bilayer is highly potent, because drugs can be encapsulated into the vacant inner cell of a liposome. Furthermore, functionalization of liposomes is possible by combination of lipid contents.

Therefore, boron and drugs may be simultaneously delivered to tumor tissues for BNCT and chemotherapy of cancers. Hawthorne (1995) first introduced *nido*-carborane as a hydrophilic moiety into the amphiphile **1** (Figure 1) and examined liposomal boron delivery in mice using **1** and distearoylphosphatidylcholine (DSPC). We recently developed the *nido*-carborane lipid **2**, which has a double-tailed moiety conjugated with *nido*-carborane as a hydrophilic function (Nakamura, 2004). We investigated active targeting of the boronated liposomes to solid tumors by functionalization of transferrin on the surface of their liposomes and achieved a boron concentration of 22 μg ^{10}B/g tumor by the injection of the liposomes at 7.2 mg ^{10}B/kg body weight with longer survival rates of tumor bearing mice after BNCT (Nakamura, 2006). However, the mice injected at higher boron concentrations resulted in mortality. Hawthorne (2006) also recently reported synthesis of the *nido*-carborane lipid **3** and its unilamellar liposomes. They pointed out the significant toxicity of the lipid **3** liposomes. In order to overcome this problem, we focused on BSH as an alternative hydrophilic function of boron lipids. BSH is a water-soluble divalent anion cluster and significantly lowered toxicity, and thus has been utilized for clinical treatment of BNCT. However, few synthetic examples of BSH derivatives as boron carriers have been reported so far due to difficulty of their functionalizations. Gabel (1991) reported a novel *S*-alkylation of BSH under mild conditions. In this paper, we report synthesis of *closo*-dodecaborate containing boron lipids **4a-c** and **5a-c** and their liposomal property (Figure 2).

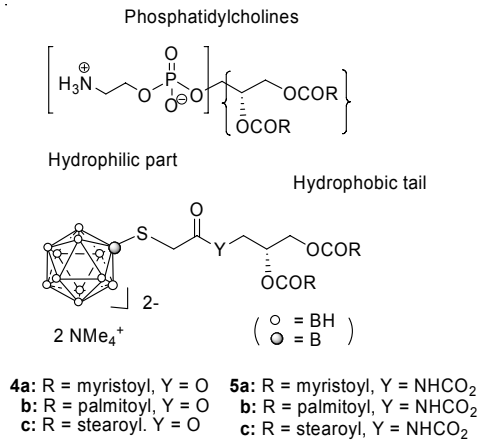

4a: R = myristoyl, Y = O
b: R = palmitoyl, Y = O
c: R = stearoyl. Y = O

5a: R = myristoyl, Y = $NHCO_2$
b: R = palmitoyl, Y = $NHCO_2$
c: R = stearoyl, Y = $NHCO_2$

Figure 2. Design of *closo*-dodecaboryl lipids

2. Chemistry

Our design of the boron lipids is based on biomimetic composition of phosphatidylcholines in order to meet a sufficiently low toxic requirement. Synthesis of the hydrophobic tail functions of **4** is shown in Scheme 1. Reaction of the chiral alcohol **6** with 1.2 equiv of bromoacetyl bromide gave the ester **7**, quantitatively, and the deprotection of **7** was carried out using catalytic amounts of *p*-TsOH in MeOH to give the corresponding diol **8** in 38% yield. The ester formation of the diol **8** with various carboxylic acids was promoted by dicyclohexylcarbodiimide in the presence of catalytic amounts of *N,N*-dimethylaminopyridine in CH_2Cl_2 to afford the precursors **9a-c** in 61-75% yields.

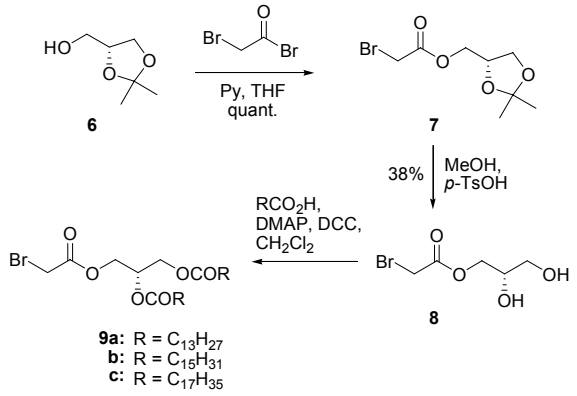

Scheme 1. Synthesis of compounds **9a-c**

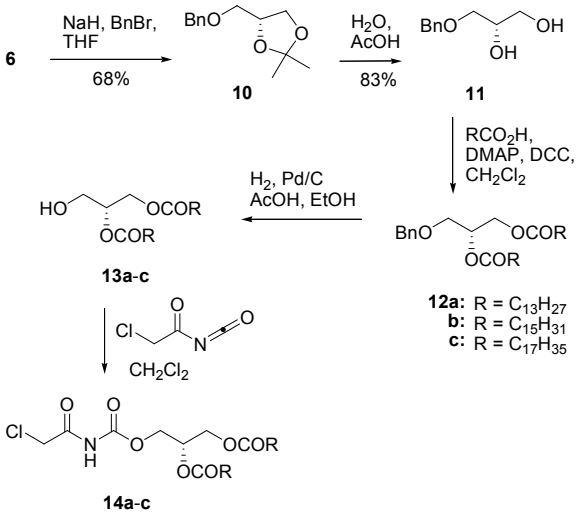

Scheme 2. Synthesis of compounds **14a-c**

Synthesis of the hydrophobic tail functions of **5** is shown in Scheme 2. Alcohol **6** was protected with benzylbromide using NaH and the resulting dioxolane **10** was converted into the diol **11** using aqueous AcOH in 83% yield.

The ester formation of **11** with various carboxylic acids was carried out in a similar manner to give **12a-c**, quantitatively. Deprotection of the benzyl group of **12a-c** by hydrogenation gave the corresponding alcohols **13a-c** (89->99% yields), which reacted with chloroacetyl isocyanate in CH_2Cl_2 to give **14a-c** in 74-98% yields.

Introduction of BSH into the hydrophobic tail functions **9** and **12** was examined using the "activated BSH (**15**)", which was prepared according to the Gabel's protocol, as shown in Scheme 3. *S*-Alkylation of **15** with **9a-c** proceeded in acetonitrile at 70 °C for 12-24 h, giving the corresponding *S*-dialkylated products **16a-c**, which were immediately treated with tetramethylammonium hydroxide (1 equiv.) in acetone to give **4a-c** in 76-91% yields, as tetramethylammonium salts. In a similar manner, the **5a-c** were obtained from **12a-c** in 54-83% yields.

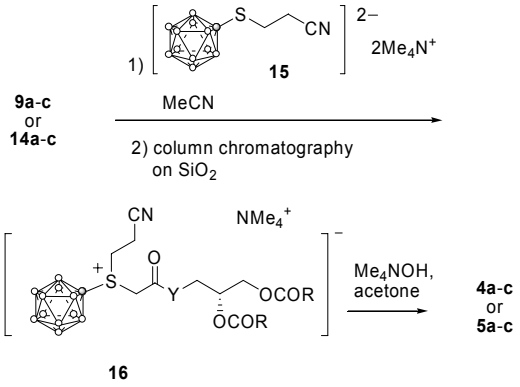

Scheme 3. Synthesis of boron lipids **4** and **5**

3. Preparation and BNCT Effect of Liposomes

Liposomes were prepared from cholesterol, distearoylphosphatidylcholine (DSPC), poly-ethyleneglycol-conjugated distearoylphosphatidyl-ethanolamine (PEG-DSPE) and the boron cluster lipids **4** and **5**, (1/0.75/0.1/0.25) by the reverse-phase evaporation (REV) method. The liposomes obtained were subjected to extrusion 10 times through a polycarbonate membrane of a 100 nm pore size, using an extruder at 60 °C. Purification was accomplished by ultracentrifuging at 200,000 *g* for 60 min at 4 °C, and the pellets obtained were resuspended in PBS buffer. Liposome size was measured with an electrophoretic light scattering spectrophotometer. The liposomes composed of **4** or **5** gave the similar size distributions.

We next investigated the time-dependent biodistribution of the boronated liposomes prepared from **4c** in tumor-bearing mice (male BALB/c mice, 7weeks old), in which colon 26 cells were transplanted into their left thigh, via tail vein at a dose of 20 mg ^{10}B/kg (200 μL of a liposome solution). As shown in Figure 2, enhanced accumulation of ^{10}B was observed in the liver and spleen and this does not conflict with the results of the biodistribution of the boron liposome prepared from **2** (Miyajima, 2006). A high level of ^{10}B concentration (22 ppm) was observed in tumor tissue at 24 h after the administration of boron liposomes. However, enhanced permeability and retention (EPR) effect was not observed and ^{10}B concentrations in tumor gradually decreased along with those in blood.

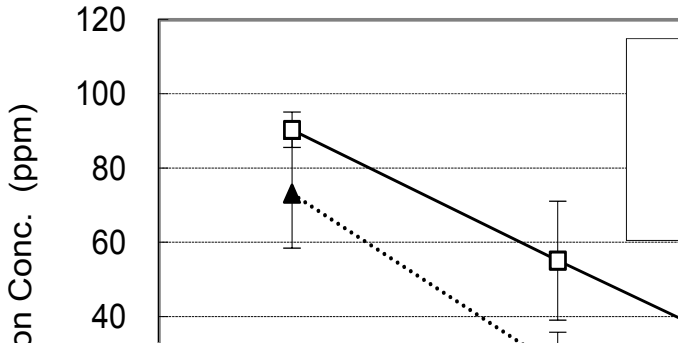

Figure 2. Time course of biodistribution of boron liposomes prepared from **4c** in tumor-bearing mice

Besides the determination of ^{10}B concentration in various organs, the mice were anesthetized 24h after the administration of the boron liposomes and placed in an acrylic mouse holder, where their whole bodies, except their tumor-implanted leg, were shielded with acrylic resin. Neutron irradiation was carried out in JAEA atomic reactor (JRR-4). As shown in Figure 3, tumor growth rate in mice given boron liposomes was significantly suppressed, although administration of saline did not reduce tumor growth after neutron irradiation

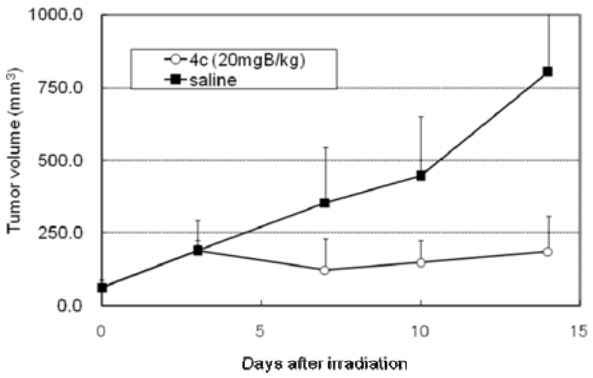

Figure 3. Tumore growth curve of mice bearing colon 26 tumors after i. v. injection of 20 mg ^{10}B/kg of boron liposomes prepared from the boron lipid **4c**, at 24 h after administration, thermal neutron irradiation with 0.9-1.4 x 10^{12} n/cm^2

4. Conclusions

We succeeded in the synthesis of the double-tailed boron cluster lipids **4** and **5**, which have a $B_{12}H_{11}S$-moiety as a hydrophilic function, by *S*-alkylation of BSH with bromoacetyl and chloroacetocarbamate derivatives of diacylglycerols. We invesitigated toxicity of the boron liposomes and found that no mouse died after injection with the boron liposomes at a dose of 20 mg ^{10}B/kg for up to three weeks. Since tumor growth rate in mice administrated with boron liposomes was significantly suppressed after neutron irradiation, boron liposomes have a potential for effective boron delivery vehicle on BNCT.

Acknowledgment

This work was supported by The New Energy and Industrial Technology Development Organization (NEDO) research project of developing a hospital based accelerator for boron neutron capture therapy with advanced drug delivery system.

References

Barth, R. F., Soloway, A. H., Fairchild, R. G., Brugger, R. M., 1992. Boron neutron capture therapy for cancer. Cancer, 70, 2995–3007.

Feakes, D. A., Shelly, K., Knobler, C. B., Hawthorne, M. F., 1994. Na3[B20H17NH3]: synthesis and liposomal delivery to murine tumors. Proc. Natl. Acad. Sci. U S A., 91, 3029–3033.

Feakes, D. A., Shelly, K., Hawthorne, M. F., 1995. Selective boron delivery to murine tumors by lipophilic species incorporated in the membranes of unilamellar liposomes. Proc. Natl. Acad. Sci. U S A., 92, 1367–1370.

Gabel, D., Moller, D., Harfst, S., Rosler, J., Ketz, H., 1993. Synthesis of S-alkyl and S-acyl derivatives of mercaptoundecahydrododecaborate, a possible boron carrier for neutron capture therapy. Inorg. Chem. 32, 2276–2278.

Kullberg, E. B., Carlsson, J., Edwards, K., Capala, J., Sjöberg, S., Gedda, L., 2003. Introductory experiments on ligand liposomes as delivery agents for boron neutron capture therapy. Int. J. Oncol., 23, 461–467.

Locher, G. L., 1936. Biological effects and the therapeutic possibilities of neutrons. Am. J. Roentgenol. 36, 632.

Li, T., Hamdi, J., Hawthorne, M. F., 2006. Unilamellar liposomes with enhanced boron content. Bioconjugate Chem., 17, 15–20.

Maruyama, K., Ishida, O., Kasaoka, S., Takizawa, T., Utoguchi, N., Shinohara, A., Chiba, M., Kobayashi, H., Eriguchi, M., Yanagie, H., 2004. Intracellular targeting of sodium mercaptoundecahydrododecaborate (BSH) to solid tumors by transferrin-PEG liposomes, for boron neutron-capture therapy (BNCT). J. Control. Release, 98, 195–207.

Miyajima, Y., Nakamura, H., Kuwata, Y., Lee, J.-D., Masunaga, S., Ono, K., Maruyama, K., 2006. Transferrin-loaded nido-carborane liposomes: tumor-targeting boron delivery system for neutron capture therapy. Bioconjugate Chem., 17, 1314–1320.

Nakamura, H., Miyajima, Y., Takei, T., Kasaoka, T., Maruyama, K., 2004. Synthesis and vesicle formation of a nido-carborane cluster lipid for boron neutron capture therapy. Chem. Commun., 1910–1911.

Nakamura, H., Lee, J.-D., Ueno, M., Miyajima, Y. Ban, H. S., 2008. Synthesis of *closo*-dodecaboryl lipids and their liposomal formation for boron neutron capture therapy. NanoBiotechnology, 3, 135–145.

Pan, X. Q., Wang, H., Shukla, S., Sekido, M., Adams, D. M., Tjarks, W., Barth, R. F., Lee, R. J., 2002. Boron-containing folate receptor-targeted liposomes as potential delivery agents for neutron capture therapy. Bioconjugate Chem. 13, 435–442.

Pan, X., Wu, G., Yang, W., Barth, R. F., Tjarks, W., Lee, R. J., 2007. Synthesis of cetuximab-immunoliposomes via a cholesterol-based membrane anchor for targeting of EGFR. Bioconjugate Chem., 18, 101–108.

Shelly, K., Feakes, D. A., Hawthorne, M. F., Schmidt, P. G., Krisch, T. A., Bauer, W. F., 1992. Model studies directed toward the boron neutron-capture therapy of cancer: boron delivery to murine tumors with liposomes. Proc. Natl. Acad. Sci. U S A., 89, 9039–9043.

Yanagie, H., Tomita, T., Kobayashi, H., Fujii, Y., Takahashi, T., Hasumi, K, Nariuchi, H., Sekiguchi, M., 1991. Application of boronated anti-CEA immunoliposome to tumor cell growth inhibition in in vitro boron neutron capture therapy model. Br. J. Cancer, 63, 522–526.

Aggregation of Nucleoside-Boron Cluster Conjugates in Aqueous Solutions and its potential effect on behavior as boron carriers for BNCT

Zbigniew J. Lesnikowski[a*], Pavel Matějíček,[b] Petr Cígler,[c] Agnieszka B. Olejniczak,[a] Agnieszka Andrysiak,[a] Blazej Wojtczak,[a] Edyta Paradowska,[a] Mirosława Studzińska,[a] and Karel Procházka[b]

[a]*Laboratory of Molecular Virology and Biological Chemistry, Institute of Medical Biology, Polish Academy of Sciences, 106 Lodowa St., Lodz 93-232, Poland*

[b]*Gilead Sciences and IOCB Research Center, Institute of Organic Chemistry and Biochemistry, AS CR, Flemingovo n. 2, 166 10 Prague 6, Czech Republic and Department of Analytical Chemistry, Institute of Chemical Technology, Prague, Czech Republic*

[c]*Department of Physical and Macromolecular Chemistry, Faculty of Science, Charles University in Prague, Hlavova 2030, 128 43 Prague 2, Czech Republic*

Abstract

A large group of compounds studied as boron carriers for BNCT are boron cluster derivatives or their conjugates with biomolecules. Boron clusters are characterized by exceptional hydrophobicity or at least amphiphilicity, the property which may facilitate the cellular uptake of the carborane-bearing compounds through cellular membranes. Simultaneously, the same quality may promotes formation of different assemblies (aggregates) in aqueous solutions. Herein, we present several new boron-containing nucleoside conjugates and show that some boron-containing nucleoside conjugates have a tendency to associate in water solutions. The size, charge, and exoskeletal pattern of the boron cluster can strongly influence the aggregation. The observed phenomenon can be of importance in better understanding of biological properties of boronated nucleosides and in designing of boronated nucleosides based drugs such as boron carriers for BNCT.

Keywords: carboranes, metallacarboranes, nucleosides, boron carriers, aggregation.

1. Introduction

A number of potential boron carriers for BNCT have been synthesized and tested. Regrettably, in spite of the continuous efforts to develop suitable boron carrying drugs, applications of boron derivatives are mostly limited to two molecules, L-4-(dihydroxyboryl)phenylalanine (BPA) and the sodium salt of thioborane anion ($Na_2B_{12}H_{11}SH$, BSH).

A large group of compounds studied are boron cluster derivatives or their conjugates with biomolecules. Boron clusters are characterized by exceptional hydrophobicity or at least amphiphilicity, the property which may facilitate the cellular uptake of the carborane-bearing compounds through cellular membranes. Simultaneously, the same quality may promote formation of different assemblies (aggregates) in aqueous solutions.

Surprisingly, in spite of extensive biological and pharmaceutical research on boron-cluster-containing conjugates, with few exceptions, very little attention was paid to the solution behavior of these molecules in aqueous media (Matějíček et al., 2006; Bonechi et al., 2007). It is obvious that the aggregation process could reduce the concentration of active boron-containing molecules in the solution, their pharmacokinetics and metabolism.

Herein, we present several new boron-containing nucleoside conjugates and show evidence that some of these conjugates have a tendency to associate in water solutions. The size, charge, and exoskeletal pattern of the boron cluster can strongly influence the aggregation (Matějíček et al., 2008). The observed phenomenon can be of importance in better understanding of biological properties of boronated nucleosides and in designing boronated nucleosides based drugs such as new boron carriers for BNCT.

Table 1 Characterization (partition coefficient *P*, cytotoxicity, aggregation) of new nucleoside/boron cluster conjugates **1**–**7**.

= BH = B = CH = C = Co.

*	Structure	*P*	Cytotoxicity (IC50 μM)			Aggregation
			Vero	A549	HeLa	
1	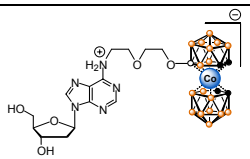	35.12 (±22.89)	>100	88	40	+++
2	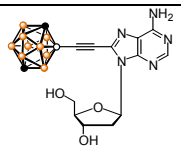	78.1 (±24.3)	>100	>100	>100	+++
3	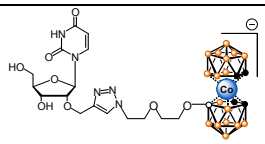	3.85 (±0.61)	>100	>100	>100	++
4	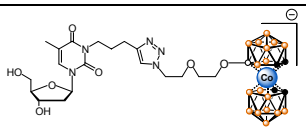	6.38 (±0.65)	80	>100	>100	+
5	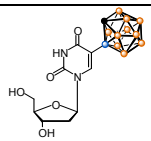	57.0 (±11.9[b])	17.1[c]	ne[d]	ne[d]	+
6	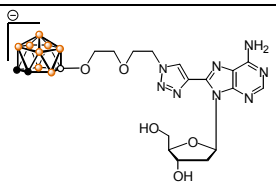	0.17 (±0.02)	ne	ne	ne	-
7	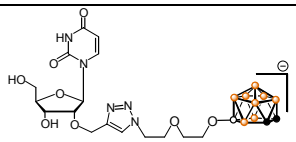	0.02 (±0.01)	>100	>100	>100	-

[a]27.4 (±16.5), Langmuir, **2008**, 24, 2625; [b]Bioorg. Med. Chem. **2005**, *13*, 4168; [c]Int. J. Radiation Oncology Biol. Phys. **1994**, 28, 1113; [d]IC50 = 70.9 in CEM cells and >100 in U253 and 9L cell lines (Int. J. Radiation Oncology Biol. Phys. **1994**, 28, 1113).

2. Synthesis of new boron-containing nucleoside conjugates

Several new boron-containing nucleoside conjugates, as well in pyrimidine as purine series, have been synthesized. 6-*N*-{5-[3-Cobalt(III) bis(1,2-dicarbollide)-8-yl]-3-oxa pentoxy}-2'-*O*-deoxyadenosine (**1**) was obtained from 3',5'-protected 2'-*O*-deoxyadenosine *via* general method of dioxane ring opening in cyclic oxonium derivatives of [3-metal bis(1,2-dicarbollide) (-1)]ate ion followed by deprotection of 3',5'-hydroxyl functions (Olejniczak et al., 2007). Synthesis of 8-[(*p*-dicarba-*closo*-dodecaborane-2-yl)-ethynyl]-2'-deoxyadenosine (**2**) was performed *via* Sonogashira type reaction and will be described in details elsewhere. Compounds 2'-*O*-methyl-(1,2,3-triazol-4-yl)-{4-*N*-{5-[3-cobalt (III) bis(1,2-dicarbollide)-8-yl]-3-oxa-pentoxy}}-uridine (**3**), 3-*N*-propyl-(1,2,3-triazol-4-yl)-{4-*N*-{5-[3-cobalt(III) bis(1,2-dicarbollide)-8-yl]-3-oxa-pentoxy}}-thymidine (**4**), 8-{(1,2,3-triazol-4-yl)-4-*N*-{5-[(7,8-dicarba-*nido*-undecaborane)-10-yl]-3-oxa-pentoxy}}-2'-*O*-deoxyadenosine (**6**) and 2'-*O*-methyl-(1,2,3-triazol-4-yl)-{4-*N*-{5-[(7,8-dicarba-*nido*-undecaborane)-10-yl]-3-oxa-pentoxy}}-uridine (7) were obtained *via* the "click chemistry" approach (Wojtczak et al., 2008). 5-(*o*-Dicarba-*closo*-dodecaborane-1-yl)-2'-deoxyuridine (CDU) (**5**) was obtained as described previously (Yamamoto et al., 1992; Schinazi et al., 1994) (Table 1).

3. Partition coefficient and cytotoxicity measurements

The compound's hydrophobicity was estimated by a simple and commonly-used measurement of partition coefficient *P*, between water and octanol. The partition coefficient is defined as the ratio of the amount of the compound present in the organic phase to that present in the aqueous phase (Dagle et al., 1991). The hydrophobicity of the nucleoside-boron cluster conjugate is strongly affected by the type of the boron cluster: carborane vs. metallacarborane and charged vs. uncharged structure.

Cytotoxicity was established by measurement of 50% inhibition of cell growth (CC_{50}, median cytotoxic concentration) using plaque technique and MTT staining (Berg et al., 1990).

In general, the described nucleoside-boron cluster conjugates are low in toxicity even in rapidly dividing Vero cells which made them potentially useful in further studies as boron carriers in BNCT.

4. Aggregation of selected nucleoside-boron cluster conjugates in aqueous solutions

The aggregation of nucleosides with attached boron clusters was studied using light scattering and atomic force microscopy techniques (Matějíček et al., 2008). Several types of nucleoside-boron cluster conjugates differing in type of nucleoside (purine or pyrimidine), type of boron cluster and its location within the nucleoside molecule were investigated.

While the species containing either the bulky amphiphilic [3-cobalt(III) bis(1,2-dicarbollide)]$^-$ anion or the electroneutral dicarba-*closo*-dodecaboranyl moiety tend to form stable nanoparticles in aqueous solutions to different extent, the compounds bearing the smaller, negatively charged dicarba-*nido*-undecaboranyl moiety as well as the unmodified nucleosides do not aggregate (Table 1).

5. Discussion

The association behavior of the studied compounds can be explained on the basis of boron-cluster properties and overall polarity of individual molecules. The dicarba-*closo*-dodecaboranyl moieties are electroneutral and significantly more hydrophobic than the negatively charged dicarba-*nido*-undecaboranyl ones.

The [3-cobalt(III) bis(1,2-dicarbollide)]$^-$ cluster bears the negative charge, but it retains the strong hydrophobic character due to its bulkiness. In light of the above consideration, one can classify the individual compounds and rationalize the observed behavior.

However, the hydrophobic character of all the mentioned clusters is not strong enough to cause a quantitative aggregation of polar nucleoside phosphates (data not shown), also the solutions of compounds 4 and **5** contain only a small fraction of the aggregates.

The compounds bearing the smaller, negatively charged dicarba-*nido*-undecaboranyl moiety such as **6** and **7**, as well as the unmodified nucleosides U, T and dA used as a control, do not aggregate under condition studied.

4. Conclusions

Several new nucleoside-boron cluster conjugates, including boron rich metallacarborane derivatives, have been described. Nucleoside/metallacarborane conjugate and simple carborane derivatives are characterized by low toxicity and often high lipophilicity, an advantageous and preferred property for potential boron delivering drugs in BNCT (Lesnikowski et al., 2005). The fact that some boron containing conjugates have a tendency to form aggregates in the solution points out the necessity to include measurements of the partition coefficient and/or polydispersity index (PD.I.) into the routine characteristics of these types of molecules.

Acknowledgments

Supported in part by the Polish Ministry of Science and Higher Education (N405 051 32/3592), the Grant Agency of the Czech Republic (203/06/P138), Marie Curie Research and Training Network (505 027, POLYAMPHI), Ministry of Education of the Czech Republic (1M6138896301 and 0021620857).

References

Berg, K., Hansen, M.B., Nielsen, S.E. 1990. A new sensitive bioassay for precise quantification of interferon activity as measured via the mitochondrial dehydrogenase function in cells (MTT-method). APMIS, 98, 156-162.

Bonechi, C., Ristori, S., Martini, S., Panza, L., Martini, G., Rossi, C., Donati, A., 2007. Solution behavior of a sugar-based carborane for boron neutron capture therapy: a nuclear magnetic resonance investigation. Biophys. Chem., 125, 320-327.

Dagle, J. M.; Andracki, M. E.; DeVine, R. J.; Walder, J. A. 1991. Physical properties of oligonucleotides containing phosphoramidite modified inter-nucleoside linkages. Nucl. Acids Res. 19, 1805-1810.

Lesnikowski, Z.J., Paradowska, E., Olejniczak, A.B., Studzińska, M., Seekamp, P., Schüßler, U., Gabel, D., Schinazi, R.F., Plešek, J. 2005. Towards new boron carriers for boron neutron capture therapy: Metallacarboranes and their nucleoside conjugates. Bioorg. Med. Chem., 13, 4168-4175.

Matějíček, P., Cígler, P., Procházka, K., Král, K., 2006. Molecular assembly of metallacarboranes in water: Light scattering and microscopy studies Langmuir, 22, 575-581.

Matějíček, P., Cigler, P., Olejniczak A.B., Andrysiak A., Wojtczak B., Procházka K., Lesnikowski Z.J, 2008. Aggregation Behavior of Nucleoside-Boron Cluster Conjugates in Aqueous Solutions. Langmuir, 24, 2625-2630.

Olejniczak, A. B., Plesek, J., Lesnikowski, Z. J. 2007. Nucleoside-metallacarborane conjugates for base-specific metal-labeling of DNA. Chem. Eur. J., 13, 311-318.

Schinazi, R.F., Goudgaon, N.M., Fulcrand, G., El Kattan, Y., Lesnikowski, Z.J., Moravek, J., Liotta, D.C. 1994. Cellular Pharmacology and Biological Activity of 5-Carboranyl-2'-Deoxyuridine. Intl. J. Radiation Oncol. Biol. Phys., 28, 1113-1120.

Wojtczak, B.A., Andrysiak, A., Grűner, B., Lesnikowski, Z.J. 2008. „Chemical Ligation" – A Versatile Method for Nucleoside Modification With Boron Clusters. Chem. Eur. J. – submitted.

Yamamoto, Y., Seko, T., Nakamura, H., Nemeto, H. 1992. Synthesis of carborane containing nucleoside bases. Heteroatom. Chem., 3, 239-244.

The potential of transferrin-polyethyleneglycol liposomes encapsulating GB-10 as ^{10}B-carriers for boron neutron capture therapy

Shin-ichiro Masunaga[a], Satoshi Kasaoka[b], Kazuo Maruyama[c], David Nigg[d], Yoshinori Sakurai[e], Kenji Nagata[f], Minoru Suzuki[a], Genro Kashino[a], Yuko Kinashi[g], Hiroki Tanaka[e], Akira Maruhashi[e], and Koji Ono[a]

[a]*Particle Radiation Oncology Research Center,* [e]*Department of Medical Physics, and* [g]*Radiation Safety and Control, Research Reactor Institute, Kyoto University, Osaka, Japan*
[b]*Faculty of Pharmaceutical Sciences, Hiroshima International University, Hiroshima, Japan*
[c]*Department of Pharmaceutics, Teikyo University, Kanagawa, Japan*
[d]*Idaho National Engineering and Environmental Laboratory, Idaho Falls, USA*
[f]*Department of Radiology, Ishikiri-Seiki Hospital, Osaka, Japan*

Abstract

Transferrin-polyethyleneglycol (TF-PEG) liposomes showed a prolonged retention in blood circulation, low uptake by reticuloendothelial system and the most enhanced accumulation of ^{10}B in solid tumors. In general, the enhancing effects were significantly greater in total cells than quiescent (Q) cells. In both cells, the enhancing effects of decahydrodecaborate-^{10}B (GB-10)-containing ^{10}B-carriers were significantly greater than mercaptoundecahydrododecaborate-^{10}B (BSH)-containing ^{10}B-carriers, whether loaded in free solution or liposomes. In both cells, whether BSH or GB-10 was employed, the greatest enhancing effect was observed with TF-PEG liposomes followed in decreasing order by PEG liposomes, bare liposomes and free BSH or GB-10 solution. In Q cells, the decrease was remarkable between PEG and bare liposomes. In terms of biodistribution characteristics and tumor cell-killing effect as a whole, including Q cells, GB-10 TF-PEG liposomes were regarded as promising ^{10}B-carriers.

Keywords: Boron neutron capture therapy, Transferrin-polyethyleneglycol liposome, BSH, GB-10, Quiescent cell

1. Introduction

The success in boron neutron capture therapy (BNCT) requires the selective delivery of large amounts of ^{10}B to malignant cells. At the same time, the ^{10}B concentration in the surrounding normal tissue should be kept low to minimize damage to the normal tissue. Various approaches have been employed for the delivery of ^{10}B to tumors, including the use of macromolecules such as monoclonal antibodies, epidermal growth factor and dextran conjugates, and microparticles such as liposomes, low-density lipoprotein complexes, and microcapsules [1]. In particular, the use of liposomes could be a promising approach, as they can carry large quantities of ^{10}B leading to selective localization in tumors [2]. Further, the inclusion of polyethyleneglycol (PEG) was reported to significantly reduce the uptake by the reticuloendothelial system (RES) of liposomes resulting in their prolonged circulation [3]. Recently, a new type of target-sensitive liposome bearing PEG, so-called pendant-type PEG immunoliposomes, in which antibodies or specific ligands are coupled to the extremities of surface-grafted PEG chains, has been reported [4]. In particular, transferrin-coupling pendant-type PEG liposomes (TF-PEG liposomes) were demonstrated to extravasate effectively into solid tumors and internalize into tumor cells [4]. TF-PEG liposomes showed a prolonged circulation and low RES uptake in tumor-bearing mice, resulting in enhanced extravasation of the liposomes into solid tumors.

To make liposomes containing enough ^{10}B, mercaptoundecahydrododecaborate-^{10}B (sodium borocaptate-^{10}B, BSH) or its alternative ^{10}B-compound, decahydrodecaborate-^{10}B (GB-10) [5], was employed as an encapsulated ^{10}B-carrier in the liposomes. GB-10 forms the anion $(B_{10}H_{10})^{-2}$ in aqueous solution. It is manufactured by the oxidation of decaborane and has no special handling or storage requirements. GB-10 is a largely diffusible agent that does not traverse the intact blood brain barrier [5].

It was shown to be non-toxic in dogs [6] and proposed as a boron agent for BNCT and BNCT-enhanced fast neutron therapy [7].

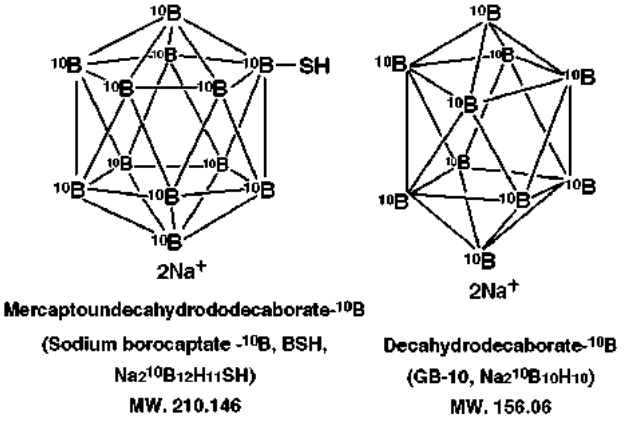

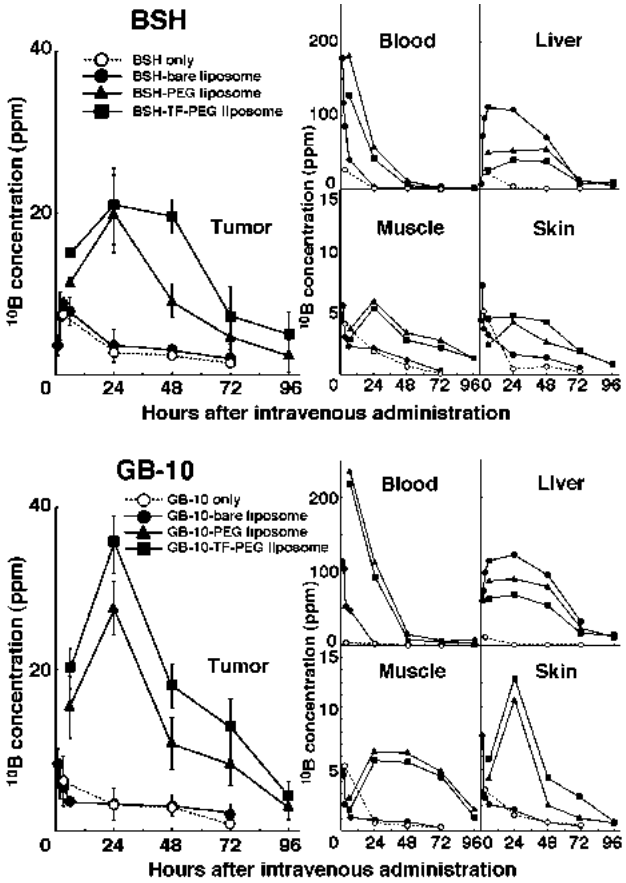

In this study, we examined the potential of liposomes for the selective delivery of therapeutic quantities of ^{10}B to tumors. TF-PEG liposomes and PEG liposomes encapsulating BSH or GB-10 were prepared and their tissue distributions in tumor-bearing mice after intravenous injection were compared with those of conventional liposomes (bare liposomes) and a free BSH or GB-10 solution. Based on the findings in biodistribution studies, we selected a suitable dosage of each ^{10}B-carrier and a time point for starting thermal neutron irradiation for BNCT. We then examined the effects of these ^{10}B-carriers on total [proliferating (P) + quiescent (Q)] and Q tumor cell populations in combination with thermal neutron irradiation, in terms of the surviving fraction (SF) and the micronucleus (MN) frequency, using our own method for selectively detecting the Q cell response to DNA-damaging treatment [8].

2. Materials and Methods

A free BSH or GB-10 solution, bare liposomes, PEG-liposomes or TF-PEG liposomes were injected into SCC VII tumor-bearing mice, and ^{10}B concentrations in the tumors and normal tissues were measured by gamma-ray spectrometry. Meanwhile, tumor-bearing mice were continuously given 5-bromo-2'-deoxyuridine (BrdU) to label all intratumor proliferating cells, then injected with these ^{10}B-carriers containing BSH or GB-10 in the same manner. Right after thermal neutron irradiation, the response of quiescent (Q) cells was assessed in terms of the micronucleus frequency using immunofluorescence staining for BrdU. The frequency in the total tumor cells was determined from the BrdU non-treated tumors [8].

3. Results

Clearance from the blood, and uptake into liver, muscle, and skin of ^{10}B after the intravenous administration of the free BSH or GB-10 solution, bare liposomes, PEG liposomes, and TF-PEG liposomes at a dose of 35 mg ^{10}B/kg was obtained.

The average diameters of liposomes encapsulating BSH or GB-10 were 105-125 nm.

In the case of the intravenous administration of the BSH or GB-10 solution, the disappearance of ^{10}B from the blood stream was very rapid due to high renal clearance. In contrast, the blood levels of ^{10}B remained high for a long time when liposomes were employed. In particular, blood concentrations of ^{10}B were much higher until 48 h after the injection when BSH or GB-10 was loaded in TF-PEG liposomes and PEG liposomes than when loaded in bare liposomes. The ^{10}B concentration in the tumors at 1 h after the injection of free BSH or GB-10 was less than 10 μg/g, and did not increase thereafter. The administration of liposomal BSH or GB-10 increased the accumulation of ^{10}B in solid tumors compared with that of free BSH or GB-10. The time course of the change in the ^{10}B concentration in tumors loaded with BSH and GB-10 were similar except that ^{10}B concentrations were greater 24 h after the loading of GB-10 than BSH in TF-PEG and PEG liposomes. The highest ^{10}B levels in the tumor were obtained with the PEG liposomes and TF-PEG liposomes at 24 h post-injection. The ^{10}B concentration in tumors was 19.9 or 21.1 μg/g using BSH and 27.4 or 35.6 μg/g using GB-10 in the PEG liposomes or TF-PEG liposomes, respectively, and was several times greater than that of each bare liposomes, respectively.

Interestingly, when BSH- or GB-10-loaded TF-PEG liposomes were injected, a high ^{10}B level was maintained in the tumor for a longer period, as observed at 48–72 h after the injection. The long retention produced by TF-PEG liposomes allowed enough time for the blood ^{10}B concentration to reach a low level, resulting in high tumor/blood ratios of much larger than 1.0.

The tumor-to-blood ^{10}B concentration ratios at various hours after injection of liposomal BSH or GB-10

Hours after injection	6	24	48	72
<BSH>				
Bare liposome	0.3	0.7	0.8	0.9
PEG liposome	0.1	0.4	0.9	1.5
TF-PEG liposome	0.1	0.5	1.6	3.0
<GB-10>				
Bare liposome	0.1	0.4	0.8	0.9
PEG liposome	0.1	0.3	0.8	1.4
TF-PEG liposome	0.1	0.4	1.2	2.5

The time course of the change in the ^{10}B concentration in muscle and skin using free BSH or GB-10 solution and bare liposomes was similar to that in tumors. Although ^{10}B concentration themselves were smaller as a whole, the time course of the change in the ^{10}B concentration in muscle and skin on the injection of TF-PEG or PEG liposomes was similar to that in liver and tumors, respectively.

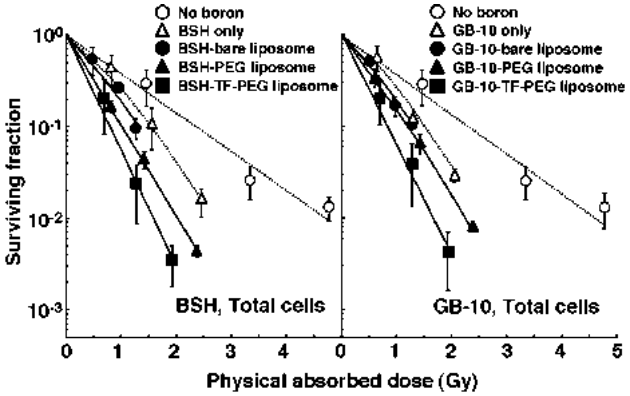

The clonogenic cell survival curves after irradiation with reactor thermal neutron beams following intravenous administration of ^{10}B-carrier containing BSH or GB-10 or without any drug administration were obtained. The micronucleus frequencies after irradiation with reactor thermal neutron beams following intravenous administration of a ^{10}B-carrier containing BSH or GB-10 or without any drug administration for the total and quiescent tumor cell populations were also obtained.

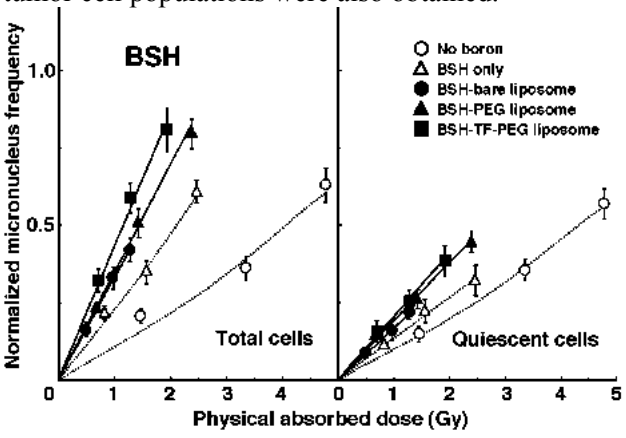

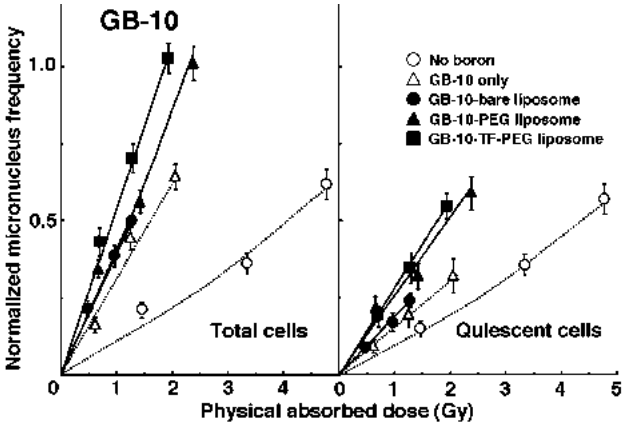

The ^{10}B concentrations in tumors loaded with the free BSH solution only, BSH-bare liposomes, BSH-PEG liposomes, and BSH-TF-PEG liposomes were 12.6 ± 2.1 μg/g, 10.4 ± 1.3 μg/g, 10.4 ± 1.1 μg/g, and 10.3 ± 1.2 μg/g, respectively. Those in tumors loaded with the free GB-10 solution only, GB-10-bare liposomes, GB-10-PEG liposomes, and GB-10-TF-PEG liposomes were 11.2 ± 1.2 μg/g, 9.6 ± 1.0 μg/g, 11.8 ± 1.7 μg/g, and 9.8 ± 0.8 μg/g, respectively. There was no significant difference among these values in irradiated tumors. At the reactor thermal neutron beam irradiation, the ratios of the doses by thermal neutrons, epithermal neutrons, fast neutrons and contaminating gamma-rays to the total physical absorbed dose were 39.1 %, 0.4 %, 11.6 %, and 48.9 %, respectively.

The effects using any ^{10}B-carrier were significantly greater in the total than in Q cell populations ($P < 0.05$). In both populations, the enhancement with GB-10 was significantly greater than that with BSH ($P < 0.05$), whether loaded in the free solution or in liposomes. In both total and Q cell populations, whether BSH or GB-10 was employed, the enhancing effect decreased in the following order; with TF-PEG liposomes > with PEG liposomes > with bare liposomes > with the free BSH or GB-10 solution only. The difference in the enhancing effect was especially remarkable between PEG liposomes and bare liposomes in Q cells.

The effects of ^{10}B-carriers on each end-point

	BSH	GB-10
<Surviving fraction = 0.1>		
Total cells		
Drug only	**1.6 ± 0.1**	**1.8 ± 0.1**
Bare liposome	**2.0 ± 0.05**	**2.1 ± 0.05**
PEG liposome	**2.2 ± 0.1**	**2.4 ± 0.1**
TF-PEG liposome	**2.7 ± 0.15**	**3.0 ± 0.15**
<Normalized micronucleus frequency = 0.2>		
Total cells		
Drug only	**2.1 ± 0.1**	**2.6 ± 0.15**
Bare liposome	**2.9 ± 0.1**	**3.3 ± 0.15**
PEG liposome	**3.2 ± 0.2**	**3.7 ± 0.2**
TF-PEG liposome	**4.0 ± 0.25**	**4.7 ± 0.3**
Quiescent cells		
Drug only	**1.4 ± 0.1**	**1.6 ± 0.1**
Bare liposome	**1.7 ± 0.1**	**1.9 ± 0.1**
PEG liposome	**2.0 ± 0.1**	**2.6 ± 0.15**
TF-PEG liposome	**2.1 ± 0.1**	**2.8 ± 0.15**

Whether BSH or GB-10 was employed, the use of any ^{10}B-carrier widened the difference in sensitivity between the total and Q cell populations significantly, compared with no use of a ^{10}B-carrier ($P < 0.05$). When the free BSH or GB-10 solution only or bare liposomes were used, these differences were similar for the use of GB-10 and BSH. However, when PEG or TF-PEG liposomes were used, these differences were more remarkable with the use of BSH than GB-10.

Dose ratios for quiescent tumor cells relative to the total tumor cell population

	BSH	GB-10
<Normalized micronucleus frequency = 0.2>		
No drug	**1.1 ± 0.1**	
Drug only	**1.8 ± 0.1**	**1.9 ± 0.1**
Bare liposome	**1.95 ± 0.1**	**2.05 ± 0.1**
PEG liposome	**1.85 ± 0.1**	**1.6 ± 0.1**
TF-PEG liposome	**2.1 ± 0.1**	**1.9 ± 0.1**

4. Conclusion

In conclusion, taking the finding that GB-10 was superior to BSH into account, GB-10-containing TF-PEG liposomes appear to be a promising ^{10}B-carrier for BNCT not only in terms of the characteristics of the ^{10}B distribution in tumors and normal tissues but also from the viewpoint of the killing effect on tumor cells including Q cells [9].

References

1. Wu G, Barth RF, Yang W, et al. 2006. Boron containing macromolecules as nanovehicles as delivery agents for neutron capturre therapy. *Anti-Cancer Agents Med Chem*. 6, 167-184.
2. Yanagie H, Tomita T, Kobayashi H, et al. 1997. Inhibition of human pancreatic cancer growth in nude mice by boron neutron capture therapy. *Br. J. Cancer* 75, 660–665.
3. Ishida O, Maruyama K, Sasaki K, et al. 1999. Size-dependent extravasation and interstitial localization of polyethyleneglycol liposomes in solid tumor-bearing mice. *Int J Pharm* 190, 49–56.
4. Maruyama K, Ishida O, Kasaoka S, et al. 2004. Intracellular targeting of sodium mercaptoundecahydrododecaborate (BSH) to solid tumors by transferrin-PEG liposomes, for boron neutron-capture therapy (BNCT) *J Cont Release* 98, 195-335.
5. Trivillin VA, Heber EM, Nigg DW, et al. 2006. Therapeutic success of boron neutron capture therapy (BNCT) mediated by a chemically non-selective boron agent in an experimental model of oral cancer: A new paradigm in BNCT radiobiology. *Radiat Res* 166, 387-396.
6. Stelzer KJ, Gavin PR, Risler R, et al. 2001. Boron neutron capture-enhanced fast neutron therapy (BNC/FNT) for non-small cell lung cancer in canine patients. In: Hawthorne MF, editor. Frontiers in neutron capture therapy. New York: Kluwer Academic/Plenum Publishers; 2001. p. 735–739.
7. Diaz A, Stelzer K, Laramore G, et al. 2002.Pharmacology studies of $Na_2{}^{10}B_{10}H_{10}$ (GB-10) in human tumor patients. In: Monduzzi Editore, editor. Research and development in neutron capture therapy. Proceedings of the 10th International Congress on Neutron Capture Therapy. Bologna, Italy: Litosei–Rastignano; 2002. p. 993–999.
8. Masunaga S, Ono K. 2002. Significance of the response of quiescent cell populations within solid tumors in cancer therapy. *J Radiat Res* 43, 11-25.
9. Masunaga S, Kasaoka S, Maruyama K, et al. 2006. The potential of transferrin-pendant-type polyethyleneglycol liposomes encapsulating decahydrodecaborate-^{10}B (GB-10) as ^{10}B-carriers for boron neutron capture therapy. *Int J Radiat Oncol Biol Phys*, 66, 1515-1522.

A new fabrication technique of boron carbide particles for BNCT agent

Yoshie Ishikawa[a,b], Takeshi Sasaki[a], and Naoto Koshizaki[a]

[a]*Nanotechnology Research Institute (NRI), National Institute of Advanced Industrial Science and Technology (AIST), Tsukuba, Japan*
[b]*Department of Advanced Materials Science, Faculty of Engineering, Kagawa University, Takamatsu, Japan*

Abstract

Boron carbide (B_4C) submicron particles were fabricated by laser irradiation of B particles dispersed in various organic solvents. The particle obtained by laser irradiation in ethyl acetate was encapsulated with 10 nm thick graphite layer. Mean size of obtained B_4C particles depended on laser irradiation time and solvent used as a suspension medium. The particle surface was modified with functional groups, which could be a starting point for further useful molecule connection by simple chemical technique. Thus, the B_4C particles obtained by this technique have a possibility for BNCT agent.

Keywords: boron carbide (B_4C), graphite layer

1. Introduction

Mercaptoundecahyedrododecaborate (BSH) and *p*-boronophenylalanine (BPA) have been the only clinically used chemicals for boron neutron capture therapy (BNCT) because of their safety and specific functions in tumor cells (Morris, 2004; Murayama, 2004). These compounds, however, contain only a small amount of B within their molecules. Because concentrated B in a tumor cell is absolutely imperative for highly effective therapy (Mortensen, 2006a; Mortensen, 2006b), the enormous doses of BSH and BPA for sufficient BNCT impose a strain on the patient. Application of B and B_4C nanoparticles to BNCT is expected to improve the efficiency of therapy, due to the numerous B atoms in these particles (Mortensen, 2006a; Mortensen, 2006b). In addition, B_4C is preferable to B for BNCT because the B surface is gradually oxidized in an *in vivo* environment to form H_3BO_3, causing serious toxicity (Siegel et al., 1986).

Mortenesen et al. (2006a, 2006b) proposed the use of B_4C nanoparticles produced from large B_4C particles by ball milling as a BNCT agent. The B_4C nanoparticles were modified with amino groups and polyvinyl alcohol utilizing the high chemical reactivity of newly exposed surface atoms during the milling process and the hydrophilic behavior of the particle surface.

We have been studying B_4C particle fabrication by pulsed laser irradiation of B particles dispersed in an organic solvent (Ishikawa, 2007). This technique has several advantages over conventional nanoparticle preparation, such as highly pure nanoparticles with less use of chemicals and crystallized nanoparticle formation due to the transient high-temperature process induced by pulsed laser irradiation (Simakin, 2001; Ishikawa, 2006). These features are expected to be suitable for fabricating nanoparticles for biomedical use. It is especially notable that the B_4C particle obtained by this technique has a 10 nm thick graphite surface layer, which is useful for medical functionalization of the particles by facile modification of the graphite layers with various organic molecules. Therefore, B_4C particles obtained by this technique have a possibility for use as a BNCT agent. Here we demonstrate the possibility of our processing technique for size control and surface modification of B_4C particles aiming for a BNCT agent.

2. Experimental

B_4C particle fabrication

Boron carbide particles were prepared by focused laser irradiation of boron powder dispersed in an organic solvent. To do this, 0.24 mg of reagent-grade B powder (99.995 %, Aldrich Chemical Company, Inc.) was dispersed in 6 ml ethyl acetate, ethanol, methanol, 1-propanol,

acetone, acetonitrile, or *N,N*-dimethylformamide (DMF) in a glass vessel. The B powder in organic solvent was then irradiated with the third harmonic (355 nm) of a Nd:YAG (yttrium aluminum garnet) laser operated at 10 Hz with a pulse width of 7 ns. The maximum output on the suspension surface was 1.5 J cm^{-2}. The laser beam was focused 2 mm below the suspension surface using a lens with the focal length of 50 mm. The suspension was agitated using a magnetic stirrer during irradiation. The particles obtained by laser irradiation of B in various solvents were treated with HNO_3 to remove unreacted raw B and by-product H_3BO_3. The solvent was first removed completely using a centrifugal evaporator and the obtained particles were dispersed in 6.2 M HNO_3 for 24 h. At that point, B and H_3BO_3 were completely dissolved in HNO_3, whereas B_4C particles remained undissolved. After the dissolution process, B_4C particles were separated from the supernatant by centrifugation. The collected B_4C particles were repeatedly rinsed with deionized water by centrifugation to remove HNO_3. Obtained B_4C particles after purification were dispersed in deionized water, and the suspension was dropped onto Si substrate and dried in air for x-ray powder diffraction analysis (XRD) and scanning electron microscope (SEM) observation. The suspension was also dropped onto carbon-coated grid for transimission electron microscope (TEM) observation.

B_4C particle surface modification

The B_4C particles purified by the HNO_3 treatment and subsequent rinsing with deionized water were dispersed in an acid mixture consisting of H_2SO_4 and HNO_3 (1:3 in volume) at 70 °C for 2 h. The B_4C particles were then separated from the acid mixture by centrifugation, and rinsed with deionized water to remove the acid mixture. The well-rinsed particles were dried in air. Fourier transform infrared (FTIR) spectra of the B_4C particles was obtained by KBr method.

3. Results and discussion

Figure 1 shows SEM images of (a) raw B particles, and (b) particles obtained by laser irradiation in ethyl acetate for 300 min and subsequent HNO_3 treatment. Connected irregular grains from 50 to 100 nm were observed in particles before the laser irradiation. In contrast, spherical particles 50-400 nm in diameter were formed in ethyl acetate. Mean size of these spherical particles were 237 nm, evaluated from the SEM images of 200 particles. According to XRD measurement, the particles obtained by laser irradiation contained B_4C crystals, whereas raw B powder was amorphous. Similar spherical particles were also obtained by laser irradiation in the other solvents.

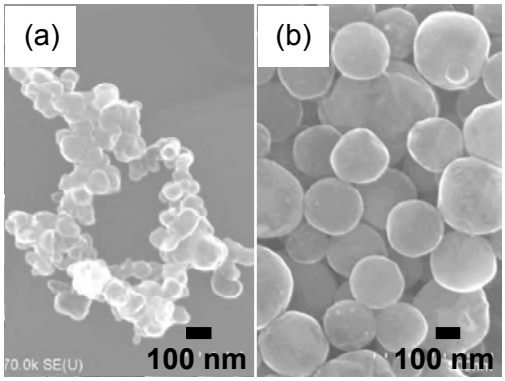

Fig. 1 SEM images of (a) B particles before laser irradiation and (b) particles obtained by laser irradiation in ethyl acetate for 300 min and subsequent HNO_3 treatment

Figure 2 (a) depicts a TEM image of the typical particle obtained by laser irradiation in ethyl acetate for 300 min and subsequent HNO_3 treatment. A high resolution TEM (HRTEM) image of the particle obtained by laser irradiation in ethyl acetate, followed by HNO_3 treatment, is also depicted in Fig. 2 (b). The turbostratic graphite layer was observed on the particle surface with a thickness of 10 nm. Thus, the particle obtained by irradiation in ethyl acetate was firmly encapsulated in a graphite layer.

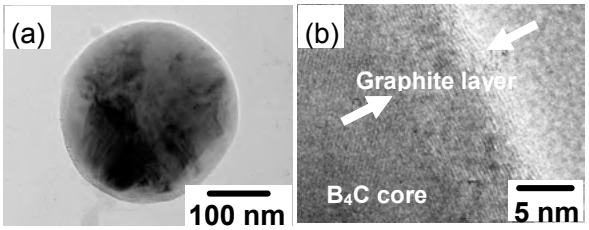

Fig. 2 (a) TEM image of a particle obtained by laser irradiation in ethyl acetate for 300 min, and (b) HRTEM image of the particle surface

The mean size of the B_4C particles obtained by laser irradiation in ethyl acetate increased with the irradiation time from 177 nm (10 min), to 208 nm (60 min), 237 nm (180 min), and 267 nm (300 min). Moreover, the B_4C size depended on solvent for suspension medium. Figure 3 graphs a relationship between dielectric constant (ε) of the solvent and the mean size of B_4C particles obtained in various solvents with 180 min irradiation. The mean particle size decreased with an increase

in the dielectric constant of the solvent. Thus, particle size, which is important for developing BNCT agent application, is controllable by irradiation time and choice of solvent.

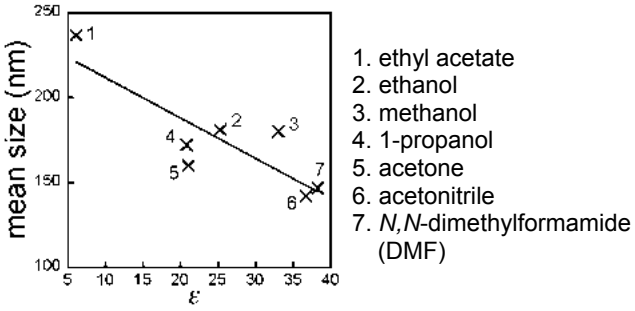

Fig. 3 Influence of solvent dielectric constant on the size of B_4C particle prepared by laser irradiation in various solvents.

Figure 4 illustrates the FTIR spectra of the obtained B_4C particles (a) before and (b) after surface modification by the acid treatment using H_2SO_4 and HNO_3 (1:3 in volume) at 70 °C for 2 h. The peak at 1100 cm^{-1} observed in both particles represents the B-C vibration. New peaks appearing after the acid treatment were at 3100-3700 cm^{-1} (alcohol- derived hydroxyl group stretching vibration), 2800- 3000 cm^{-1} (aliphatic C-H stretching vibration), 1730 cm^{-1} (ester C=O stretching vibration), and 1275 cm^{-1} (ester C-O stretching vibration). A series of peaks at 1330-1500 cm^{-1} probably correspond to aliphatic C- H deformation vibration. These results indicate that the surface of the B_4C particle after the acid treatment was modified with aliphatic compounds having esters and/or OH groups. Thus functional groups on the particle surfaces are useful for further chemical modification for medical functionalization of the particles.

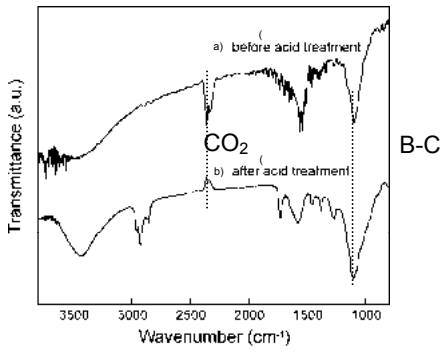

Fig. 4 FTIR spectra of B_4C particles (a) before and (b) after the acid treatment for surface modification.

4. Conclusions

Spherical B_4C particles were obtained by pulsed laser irradiation of B in various organic solvents. The obtained B_4C particles were encapsulated with a 10 nm thick graphite layer. Mean size of the B_4C particles obtained by this technique were controllable from 142 to 267 nm by changing laser irradiation time and the solvent used as a B dispersion medium. Size controllability of the B_4C particle using this technique is important for the development of BNCT agents using particles, because the particle size possibly affects efficiency of BNCT. The surface of the B_4C particle obtained by laser irradiation in ethyl acetate was easily modified with aliphatic compounds having ester and/or OH groups. These functional groups will be useful for further chemical modification for medical functionalization of particles.

Acknowledgement

Part of this study was financially supported by the Budget for Nuclear Research of the Ministry of Education, Culture, Sports, Science and Technology, based on the screening and counseling by the Atomic Energy Commission.

References

Morris, G.M., Micca, P.L. and Coderre, J.A., 2004. The effect of dexamethasone on the uptake of p-boronophenylalanine in the rat brain and intracranial 9L gliosarcoma. Appl. Radiat. Isot. 61, 917-921.

Maruyama K., Ishida O., Kasaoka S., Takizawa T., Utoguchi N., Shinohara A., Chiba M., Kobayashi H., Eriguchi M., Yanagie H., 2004. Intracellular targeting of sodium mercaptoundecahydrododecaborate (BSH) to solid tumors by transferrin-PEG liposomes, for boron neutron-capture therapy (BNCT). J. Controlled Release 98, 195-207.

Mortensen MW, Sorensen PG, Bjorkdahl O, Jensen MR, Gundersen HJG, Bjornholm T., 2006. Preparation and characterization of Boron carbide nanoparticles for use as a novel agent in T cell-guided boron neutron capture therapy. Appl. Radiat. Isot. 64, 315-324.

Mortensen MW, Bjorkdahl O, Sorensen PG, Hansen T, Jensen MR, Gundersen HJG, Bjornholm T., 2006. Functionalization and cellular uptake of boron carbide nanoparticles. The first step toward T cell-guided boron neutron capture therapy. Bioconjugate Chem. 17, 284-290.

Siegel, E., Wason, S., 1986. Boric-acid toxicity. Pedatr. Clin. North Am., 33, 363-367.

Ishikawa Y., Shimizu Y., Sasaki T., Koshizaki N., 2007. Boron carbide spherical particles encapsulated in graphite prepared by pulsed laser irradiation of boron in liquid medium. Appl. Phys. Lett. 91, 161110.

Simakin A.V., Voronov V.V., Shafeev G.A., Brayner R., Bozon-Verduraz F. 2001. Nanodisks of Au and Ag produced by laser ablation in liquid environment. Chem. Phys. Lett. 348, 182-186.

Ishikawa Y., Shimizu Y., Sasaki T., Koshizaki N., 2006. Preparation of zinc oxide nanorods using pulsed laser ablation in water media at high temperature. Colloid Interface Sci. 200, 612-615.

Conjugates of boron clusters with derivatives of natural chlorin and bacteriochlorin

V.I. Bregadze[a], I.B. Sivaev[a], I.A. Lobanova[a], R.A. Titeev[b], D.I. Brittal[b], M.A. Grin[b], A.F. Mironov[b]

[a] *A.N. Nesmeyanov Institute of Organoelement Compounds, Russian Academy of Sciences, 28 Vavilov Str., 119991, Moscow, Russia*
[b] *M.V. Lomonosov Moscow Academy of Fine Chemical Technology, Moscow, Russia*

Abstract

Conjugates of bacteriochlorin *p* and chlorin *e6* with cobalt bis(dicarbollide) anion [3,3'-Co(1,2-$C_2B_9H_{11}$)$_2$]$^-$ were synthesized.

Keywords: polyhedral boron compounds, cobalt bis(dicarbollide) anion, bacteriochlorin p, chlorin e6, boron neutron capture therapy

1. Introduction

Photodynamic therapy (PDT) (Bonnett, 2002) and boron neutron capture therapy (BNCT) (Hawthorne, 1993; Soloway et al., 1998; Bregadze et al., 2006) are promising methods for treating tumors. Both methods are based on the accumulation of special compounds in a tumor, which after specific physical effects (irradiation with light or with a thermal neutron flux) will subsequently acquire enhanced toxicity causing degradation of cancer cells. Thus nowadays the synthesis of porphyrins and phtalocyanines based on boron polyhedra is of particular interest. At present, porphyrin-type compounds are used as photodynamic agents. The efficiency of the latter depends on the nature of light used to irradiate the tumor. The longer wavelength the deeper light penetration into a tissue or tumor. A series of porphyrin and phthalocyanine derivatives containing fragments of polyhedral boron hydrides were synthesized (Bregadze et al., 2001; Giuntini et al., 2005; Hao et al., 2005, 2007; Ratajski et al., 2006; Renner et al., 2006; Tsaryova et al., 2005). However, conjugates of the cobalt bis(dicarbollide) anion with chlorin and bacteriochlorin are not reported to date. The latter have a therapeutic absorption band of 770-840 nm, which provides light penetration into a tissue by 15-20 mm compared to 3-4 mm for porphyrins (Bonnett, 2002). At the same time, cobalt bis(dicarbollide) derivatives contain boron atoms that can capture thermal neutrons and generate α-particles that will degrade the tumor.

The subject of this paper is a design of conjugates of polyhedral boron compounds with chlorin and bacteriochlorin which could be used for delivery of boron to tumor for boron neutron capture therapy (BNCT).

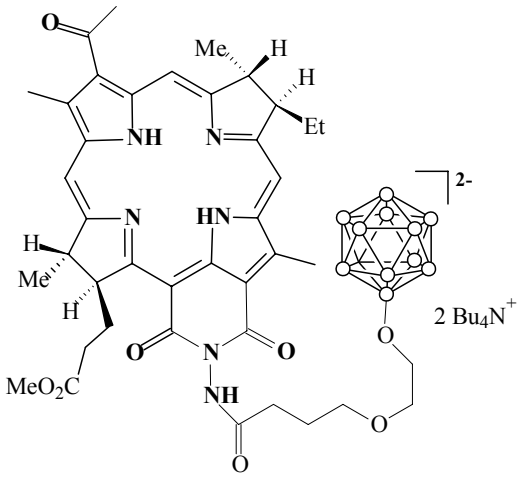

Fig. 1. Conjugate of cycloimide bacteriochlorin with the *closo*-dodecaborate anion

2. Synthesis of cycloimide bacteriochlorin *p* conjugate with the *closo*-dodecaborate anion

Recently the first bacteriochlorin derivative containing fragments of polyhedral boron hydrides was synthesized on the example of cycloimide bacteriochlorin *p* conjugate with the *closo*-dodecaborate anion (Grin et al., 2007) (Fig.1).

Derivatives of the dodecahydro-*closo*-dodecaborate and cobaltdicarbollide anions was shown to be promising candidates for BNCT. Synthesis of their oxonium derivatives is one of the most powerful ways to introduce the reaction centre into boron cage (Semioshkin et al., 2008). Their reactions with various O- and C- nucleophiles gave rise to a great variety of boron cluster derivatives with different functional groups. Boron-containing amino acids (Sivaev et al., 2000, 2002) and phtalocyanines (Semioshkin et al., 2006) were prepared using this method.

3. Conjugates of chlorin and bacteriochlorin with cobalt bis(dicarbollide)

Now new ways of synthesis of conjugates of chlorins and bacteriochlorins with cobalt bis(dicarbollide) anion [3,3'-Co(1,2-$C_2B_9H_{11})_2]^-$ (Sivaev, 1999) were developed. For acylation of exocyclic amino group of bacteriochlorin N-amino cycloimide, cobalt bis(dicarbollide)-based carboxylic acid was prepared by the ring opening reaction of cyclic oxonium derivative of cobalt bis(dicarbollide) with *p*-hydroxybenzoic acid (Fig. 2)

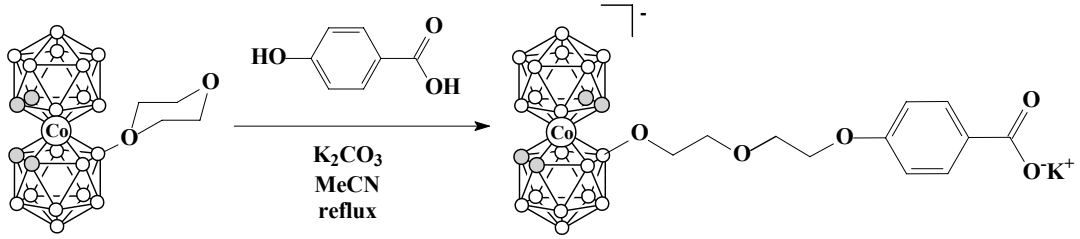

1 **2**

Fig. 2. Dioxane ring disclosure in oxonium derivative of cobaltacarborane

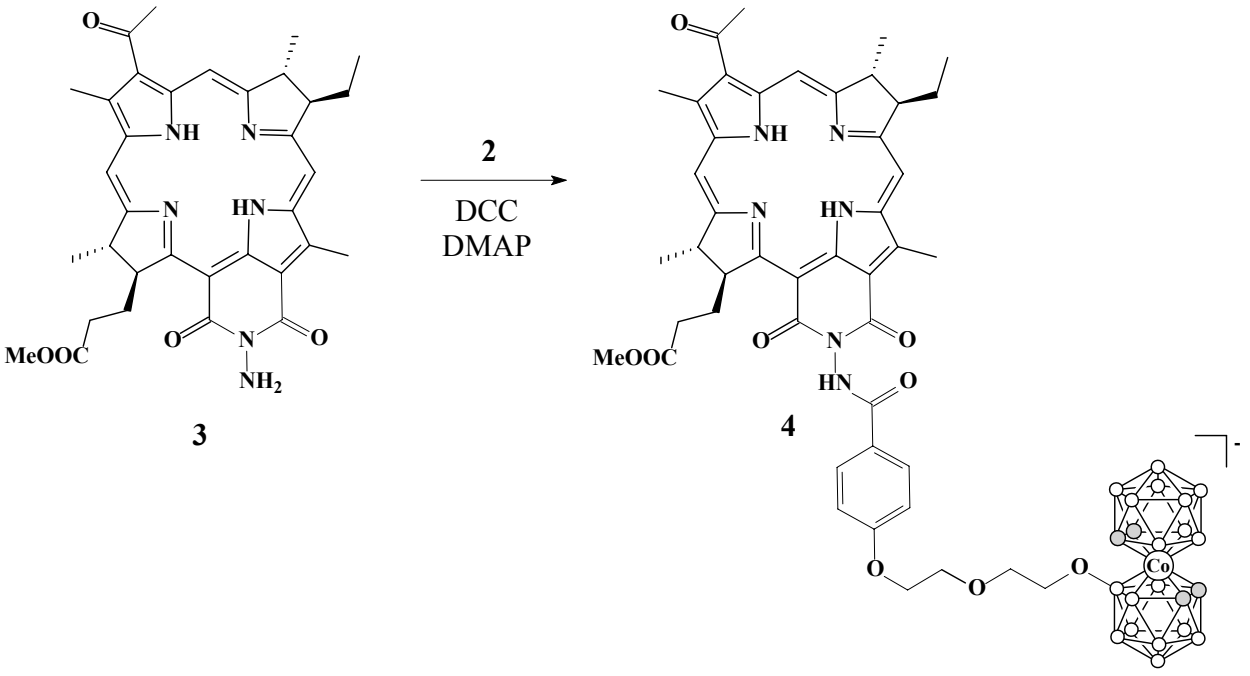

3 **4**

Fig. 3. Synthesis of bacteriochlorin N-amino cycloimide conjugate with derivative of cobalt bis(dicarbollide) anion

Condensation of the acid prepared from **2** with bacteriochlorin N-amino cycloimide (**3**) in the presence of 1,3-dicyclohexylcarbadiimide and N,N-dimethylaminopyridine results in conjugate **4**. (Fig. 3). Compound **4** was isolated by preparative TLC and characterized by IR, UV, ^{1}H and ^{11}B NMR spectra.

Another approach was used for synthesis of chlorin conjugates with cobalt bis(dicarbollide) anion.

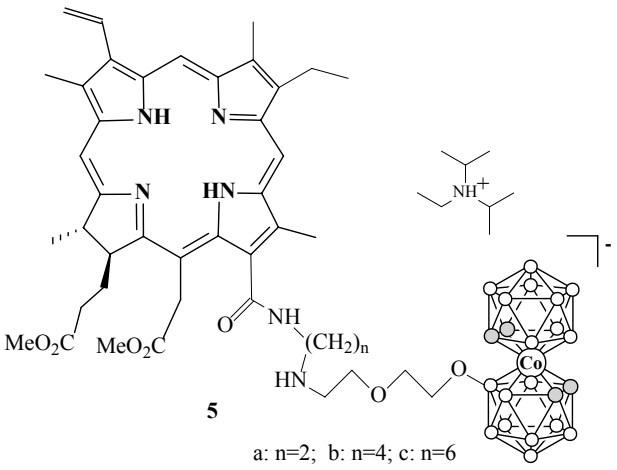

Fig. 4. Conjugate of chlorin *e6* derivatives with cobalt bis(dicarbollide) anion

Aminolysis of pheophorbide *a* with diaminoalkanes $NH_2(CH_2)_nNH_2$ (n=2,4,6) resulted in the corresponding chlorin *e6* derivatives with spacers of different length between the porphyrin macrocycle and terminal amino group (Fig. 4).

The opening 1,4-dioxane ring in cyclic oxonium derivative of cobalt bis(dicarbollide) with these amines gives conjugates **5a, 5b** and **5c,** where the chlorin macrocycle and the boron unit are separated by flexible and rather long spacer. *In vitro* study of the prepared conjugates revealed their effective accumulation in cancer cells.

4. Conclusions

Methods of synthesis of conjugates of cobalt bis(dicarbollide) anion with bacteriochlorin *p* or chlorin *e6* are developed. These conjugates have potential application for photodynamic therapy and boron neutron capture therapy.

Acknowledgments

The authors thank the Russian Foundation for Basic Research (06-03-32459, 07-03-00712) for financial support.

References

Bonnett, R., 2002. Chemical aspects of photodynamic therapy, Gordon and Breach publishers, UK.

Bregadze, V.I., Sivaev, I.B., Gabel, D., Wöhrle, D., 2001. Polyhedral boron derivatives of porphyrins and phthalocyanines. J. Porphyrins and Phthalocyanines 5, 767-781.

Bregadze, V.I., Sivaev, I.B., Glazun, S.A., 2006. Polyhedral boron compounds as potential diagnostic and therapeutic antitumor agents. Anti-Cancer Agents in Medicinal Chemistry 6, 75-109.

Grin, M.A., Semioshkin, A.A., Titeev, R.A., Nizhnik, E.A., Grebenyuk, J.N., Mironov, A.F., Bregadze, V.I., 2007. Synthesis of a cycloimide bacteriochlorin *p* conjugate with the *closo*-dodecaborate anion. Mendeleev Commun. 17, 14-15.

Hao, E., Jensen, T.J., Courtney, B.H., Vicente, M.G.H., 2005. Synthesis and cellular studies of porphyrin-cobaltacarborane conjugates. Bioconjugate Chem. 16, 1495-1502.

Hao, E., Sibrian-Vazquez, M., Serem, W., Garno, J.C., Fronczek, F.R., Vicente, M.G.H., 2007. Synthesis, aggregation and cellular investigations of porphyrin-cobaltacarborane conjugates. Chem. Eur. J. 13, 9035-9047.

Hawthorne, M.F., 1993. The role of chemistry in the development of boron neutron capture therapy of cancer. Angew. Chem. Int. Ed. Engl. 32, 950-984.

Ratajski, M., Osterloh, J., Gabel, D., 2006. Boron-containing chlorins and tetraazaporphyrins: Synthesis and cell uptake of boronated pyropheophorbide a derivatives. Anti-Cancer Agents in Medicinal Chemistry 6, 159-166.

Renner, M.V., Miura, M., Easson, M.V., Vicente, M.G.H., 2006. Recent progress in the syntheses and biological evaluation of boronated porphyrins for boron neutron capture therapy. Anti-Cancer Agents in Medicinal Chemistry 6, 145-157.

Semioshkin, A., Tsaryova, O., Zhidkova, O., Bregadze, V., Wöhrle, D., 2006. Reactions of oxonium derivatives of $[B_{12}H_{12}]^{2-}$ with phenols, and synthesis and photochemical properties of a phthalocyanine containing four $[B_{12}H_{12}]^{2-}$ groups. J. Porphyrins Phthalocyanines 10, 1293-1300.

Semioshkin, A.A., Sivaev, I.B., Bregadze, V.I., 2008. Cyclic oxonium derivatives of polyhedral boron hydrides and their synthetic applications**.** Dalton Trans. 977-992.

Sivaev, I.B., Bregadze V.I., 1999. Chemistry of Cobalt Bis(dicarbollides). A Review, Collect. Czech. Chem. Commun. 64, 783-805.

Sivaev, I.B., Semioshkin, A.A., Brellochs, B., Sjöberg, S., Bregadze, V.I., 2000. Synthesis of oxonium derivatives of the dodecahydro-*closo*-dodecaborate anion $[B_{12}H_{12}]^{2-}$. Tetramethylene oxonium derivative of $[B_{12}H_{12}]^{2-}$ as a convenient precursor for the synthesis of functional compounds for boron neutron capture therapy. Polyhedron 19, 627-632.

Sivaev, I.B., Starikova, Z.A., Sjöberg, S., Bregadze, V.I., 2002. Synthesis of functional derivatives of $[3,3'\text{-}Co(1,2\text{-}C_2B_9H_{11})_2]^-$ anion. J. Organomet. Chem. 649, 1-8.

Soloway, A.H., Tjarks, W., Barnum, B.A., Rong, F.-G., Barth, R.F., Codogni, I.M., Wilson, J.G., 1998. The chemistry of neutron capture therapy. Chem. Rev. 98, 1515-1562.

Tsaryova, O., Semioshkin, A., Wöhrle, D., Bregadze, V., 2005. Synthesis of new carborane-based phthalocyanines and study of their activities in the photooxidation of citronellol. J. Porphyrins Phthalocyanines 9, 268-274.

Synthesis of new dodecahydro-*closo*-dodecaborate cluster containing compounds

Andrea Vöge[1], Detlef Gabel[1]

[1] *Department of Chemistry, University of Bremen, Germany*

When specific compounds for boron neutron capture therapy (BNCT) are to be prepared, the cluster must be covalently attached to organic moieties. $B_{12}H_{11}SH^{2-}$ (BSH) is clinically used for BNCT of glioblastoma and is taken up in tumor tissue without additional target units.
The aim was to synthesize new dodecahydro-*closo*-dodecaborate cluster derivatives with hydrophobic residues so that the grade of accumulation in tumor cells would be higher compared to BSH with the polar thiol group. We suppose that these cluster derivatives pass the cell membrane easier than BSH. The new cluster derivatives shown below could be prepared by palladium catalyzed coupling reactions. They offer the possibility for further modifications.

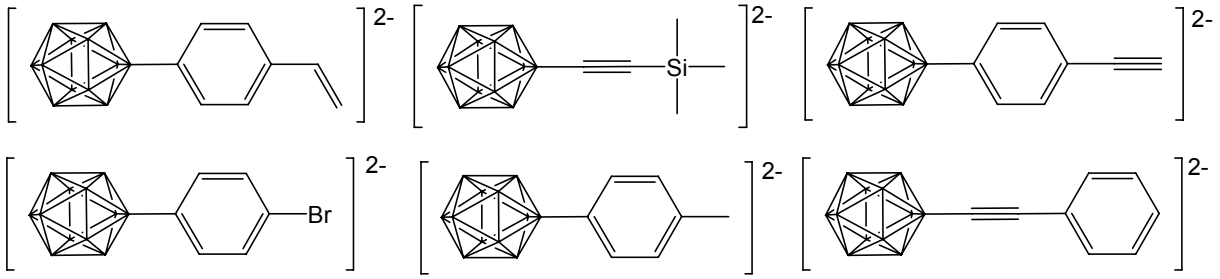

One example for a modification of one of these intermediates is shown below. Fluorinated drugs are used because of their hydrophobicity and the slow degradation, so they are effective for longer time. The fluorine and boron containing compound obtained via a Sonogashira coupling can be a new interesting drug for BNCT.

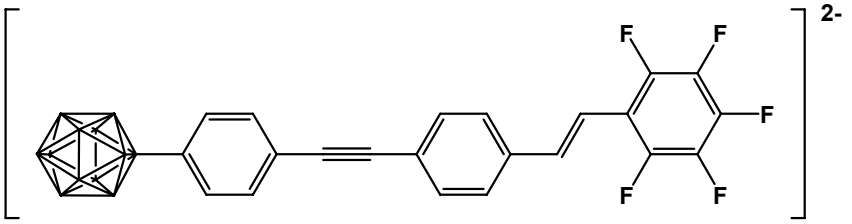

Structural Characterization of Carborane-loaded Liposomes on the Nanoscale Using Scattering Techniques

Julian Oberdisse

Laboratoire des Colloïdes, Verres, et Nanomatériaux
Université Montpellier II/CNRS
F-34091 Montpellier Cedex

Transport and delivery of boron-containing compounds for Boron Neutron Capture Therapy (BNCT) depends on the stability and structural properties of the loaded carriers. In the case of liposome-based delivery, the insertion of drug modifies the physico-chemical equilibrium within the carrier. This is due to the self-organized nature of liposomes, which are formed by self-assembly of amphiphilic molecules such as phospholipids. Properties like spontaneous bilayer curvature and bending elasticity may change upon incorporation of purely hydrophobic or amphiphilic drugs, leading to modifications in bilayer thickness, liposome size, and possibly destruction.

Small angle neutron and X-ray scattering (SANS, SAXS) are powerful methods with nanoscale resolution for the characterization of objects in solution. After a quick introduction to the method, examples of inclusions of (amphiphilic) sugar-based carboranes and (strongly hydrophobic) porphyrazine incorporated into different phospholipid vesicles will be presented and discussed. It will be shown, that incorporated amounts can be deduced from neutron transmission experiments, and that their effect on structural parameters of the liposomes can be directly followed by small angle scattering. It is hoped that these first steps will contribute to the understanding and optimisation of the complex interactions between boron-guest molecules and carrier systems.

Measurement of BPA in the Blood by Fluorometry

○Koji Ono, Genro Kashio, Minoru Suzuki, Shin-ichiro Masunaga, Yuko Kinashi, Noriko Fujii

Kyoto University Research Reactor Institute, Osaka Japan

It is indispensable to know the boron concentration in the blood in BNCT. B-10 and B-10/B-11 are being measured by the prompt gamma-ray spectrometry and ICP, respectively. When using one kind of boron compound, this procedure is sufficient. But, occasionally two kinds of boron compounds, i.e., BPA and BSH, are simultaneously used. In this situation, we have to know the boron concentration originating in each compound in order to translate a physical dose into a biologically X-ray equivalent dose (Gy-Eq). And B-10 concentration must be measured during the short neutron irradiation time. Then, a simple discrimination measuring method of BPA and BSH is strongly desired.

BPA emits fluorescence when it is excited with ultraviolet rays. So, we have an idea to use fluorometry. The solution of BPA-fructose complex was added to the heparinized human blood samples at the B-10 level of 0ppm to 60ppm. Then, small amount of PBS was added to adjust the volume of sample depending upon the volume of BPA solution added at first. Centrifugation was carried out, and plasma was separated, and this plasma was diluted 7 times in volume by 99% ethanol. After vigorous shaking, centrifugation was carried out again. Thereafter, supernatant was filtered with the deproteinization membrane filter. The same ethanol was added to this filtered sample and diluted to 200-350 times finally. This dilution sample was excited with 257nm ultraviolet rays, and the amount of emitted fluorescence of 275nm was measured. The reading value of the 0 ppm fluorescence was equal to it of ethanol. The fluorescence was directly proportional to the boron concentration precisely. Slope of the line depend upon the dilution scale factor of the sample by ethanol, and the measurement sensitivity of B-10 at 0.5 ppm has been achieved. Moreover, BSH did not show measured values.

On-Line Blood Boron Detection using ICP-AES and ICP-MS during BNCT

M. Kortesniemi[1,2], H. Revitzer[3], R. Zilliacus[4], M. Kouri[1,5], S. Savolainen[1,2,6] and S. Linko[5,7],

[1] *Boneca Corporation, Helsinki, Finland*
[2] *HUS Helsinki Medical Imaging Center, University of Helsinki, Finland*
[3] *Helsinki University of Technology, Laboratory of Physical Chemistry and Electrochemistry,*
[4] *VTT Technical Research Centre of Finland, Espoo, Finland*
[5] *Department of Oncology, Helsinki University Central Hospital, Helsinki, Finland*
[6] *Department of Physics, University of Helsinki, Finland*
[7] *Hospital District of Helsinki and Uusimaa, HUSLAB, Helsinki, Finland,*
Espoo Finland

A reliable estimation of the blood boron level for the treatment field is a prerequisite for successful BNCT. The quantification of the boron concentration for such estimation can be done with several methods, including inductively coupled plasma atomic emission spectrometry (ICP-AES), mass spectrometry (ICP-MS), spectrofluorometric and direct current atomic emission spectrometry (DCP-AES) methods, and by prompt gamma photon detection methods.

As part of the ongoing Finnish BNCT clinical trial protocols, the patients were infused with concentrations of 290 to 500 mg BPA per kilogram of total body weight. The boron concentrations were analyzed with ICP-AES and ICP-MS from a total of 73 whole blood samples. The results were compared with each other to assure the congruency of the quantification in case the analyzing method has to be changed during the treatment (e.g. for technical reasons). Additionally, the effect of wet ashing on the outcome was studied.

The average value of samples analyzed with ICP-MS was 6 % lower than with ICP-AES coupled to wet ashing (R^2=0.88). The average value of samples analyzed with ICP-MS without wet ashing was 9 % higher than with ICP-AES (R^2=0.99). The correlation between the results of ICP-MS with wet ashing and ICP-MS or ICP AES without it were good (R^2: 0.97 to 0.98).

The blood boron concentration analyzed with ICP-AES correlated well to the values of ICP-MS with wet ashing of the sample matrix, which is generally the reference method. The feasibility to use these methods parallel during the treatment secures the reliability of the boron quantification, noticing the accuracy requirements of the dose determination for the patient irradiations.

Interaction of charged boron clusters with biologically relevant molecules

Detlef Gabel, Tanja Schaffran, Jingyu Li

[1] *Department of Chemistry, University of Bremen, Germany*

Boron clusters offer the advantage for BNCT that a considerable number of boron atoms can be attached *via* a single chemical bond. Past experience has shown that of the icosahedral structures, *o*-carborane requires solubilizing groups when this cluster should form part of a molecule which is to be transported through the blood stream. The base-degraded *nido*-carborane is anionic, it appears, however, to bear some toxic potential. The dodecaborate anion carries two negative charges, and depending on the counter ions, the cluster and its derivatives are very water-soluble. In view of the charge, it was surprising to find the sulfhydryl derivative BSH being firmly bound to cell membranes and even in the nucleus of cells. More recently, we found that BSH interacts with liposomes as models for cell membranes and induces leakage and aggregation.

We have expanded this investigation to cover other heteroatom substituents and a systematic variation of chain lengths of *N*-substituted derivatives of $B_{12}H_{11}NH_3^-$. The initial interaction appears to be through charge. Depending on the substition of the cluster, hydrophobic effects increase, and the cluster derivatives behave more and more amphiphilicly. Binding to membranes occurs with all derivatives tested. Membrane potentials (measured as zeta potential) as low as –120 mV have been recorded, some of the most negative numbers for liposomes ever measured. Such strong polarization changes of membranes might lead to cellular effects even without further amphiphilic components added.

Surprisingly, the trihexylammonio-undecahydrododecaborate acted also as an efficient inhibor of acetylcholine esterase, despite the fact that the natural substrate, a cation, and the inhibitor, an anion, carry opposite charges.

When using charged clusters as boron carriers, their potential amphiphilic character must be taken into account. A thorough investigation in simple model systems of the toxic potential of the compounds can help to screen compounds and identify possibly detrimental effects.

Synthesis, Toxicology and Biodistribution of the First Porphyrin Bearing the *closo*-Monocarbaborane Anion $[\text{-}CB_{11}H_{11}]^{-1}$

Stephen B. Kahl, Zhen Yao, and Myoung Seo Koo

Department of Pharmaceutical Chemistry, University of California, San Francisco

Of all the boron clusters potentially available as sources of boron for boron neutron capture therapy, derivatives of *closo*-monocarbon carboranes such as $[HCB_{11}H_{11}]^{-1}$ and $[HCB_9H_9]^{-1}$ have received the least attention. These sources, however, offer some potential advantages over the more traditional $B_{10}C_2H_{12}$ isomers. Their inherent permanent mono-anionic charge renders their derivatives considerably more water-soluble, and their higher boron weight percentage and greater resistance to cage degradation compared to 1,2-$B_{10}C_2H_{12}$ are also advantageous. Until recently, the primary barrier to their more widespread application in BNCT has been the lack of a convenient synthesis. Hardie and coworkers recent application of the Brellochs reaction of formaldehyde with *nido*-$B_{10}H_{14}$ now provides a simple, high-yield route to these *closo*-monocarbaborane starting materials.

We will describe the preparation, characterization and preliminary toxicity and biodistribution experiments of the first porphyrin derivative of $[HCB_{11}H_{11}]^{-1}$. Lithiation of the parent anion followed by carbonylation provided the carboxylic acid $[1\text{-}HOOC\text{-}CB_{11}H_{11}]^{-1}$ which was then reacted with oxalyl chloride to provide the corresponding acid chloride. This product was not isolated but was reacted *in situ* with 2,4-bis(1,2-dihydroxyethyl)-6,7-bis[2-(methoxycarbonyl)ethyl]-1,3,5,8-tetramethylporphyrin, a bis-glycol porphyrin that formed the porphyrin framework for our BOPP compound. The resulting anionic, tetra-carborane ester porphyrin is thus the $[\text{-}CB_{11}H_{11}]^{-1}$ analog of BOPP. As expected, it has considerable aqueous solubility. Preliminary toxicology testing demonstrated little systemic toxicity when given by intravenous bolus injection at doses up to 100 mg/kg. We will also describe the results of biodistribution experiments carried with this compound in nude rats bearing the intracerebral U-87 MG human glioma model.

Delivery of a Cholesteryl Ester Mimic to Human Prostate Cells via Low-Density Lipoprotein Receptor Mediated Endocytosis

Ian Gifford[1], Wyatt Vreeland[2], C-K Wang[3], and Mohamad Al-Sheikhly[4]

[1] *Fischell Department of Bioengineering, University of Maryland, USA*
[2] *National Institute of Standards and Technology, Maryland, USA*
[3] *Nuclear Engineering/Medical Physics Program, Georgia Institute of Technology, USA*
[4] *Department of Materials Science and Engineering, University of Maryland, USA*

The use of a boron-containing cholesteryl carborane ester compound (BCH) with boron neutron capture therapy (BNCT) for the treatment of prostate cancer is under investigation. Specifically, the *in vitro* uptake and release kinetics of BCH by human prostate cancer cells (PC-3) and human prostate normal cells (RWPE-1) is under study. For this delivery method, BCH is incorporated into a liposomal formulation and extruded through various membranes to fabricate BCH-containing liposomes of various sizes.

The concentration of BCH in the liposomes, as well as their size, is varied in order to provide the optimum conditions for cellular uptake and retention of the BCH. Size analysis is performed using Asymmetric Field Flow Fractionation (AFFF) combined with multi-angle light scattering (MALS). Following analysis of the liposome sizes, the formulation is added to the growth medium of the cell populations and incubated for varying time scales.

Cellular uptake of the BCH is analyzed using high performance liquid chromatography (HPLC) adapted for the specific detection of BCH and its degradation fragments. Additionally, cells are incubated in fresh media following exposure to the liposomal formulation to quantify the release of the BCH compounds by the cells.

Following this analysis, a comparison can be made between the uptake and release kinetics of the cancerous and normal cell populations to determine the therapeutic ratio and identify an optimal radiation window for subsequent thermal neutron irradiation.

Pharmacokinetic and proteomic profiles of urine samples after application of boron-10 carriers

F. Basilico[1], Erika Redaelli[1], Louise Benazzi[1], A. Wittig[2] and W. Sauerwein[2] and P. L. Mauri[1]

[1] *Institute for Biomedical Technologies, ITB-CNR, Milan, Italy*
[2] *Strahlenklinik, Universitätsklinikum Essen, Germany*

Clinical investigations of the distribution and the metabolism of the ^{10}B-containing compounds that are available for clinical trials (*closo*-undecahydro-1-mercaptododecaborate, BSH, and ^{10}B-phenylalanine, BPA) are very important.

Many efforts had to be made to perform quali-quantitative assay of drugs in fluid and tissue samples. In particular, we have developed a rapid and quantitative method that permits the determination of BSH and BPA, based on flow-injection electrospray tandem mass spectrometry (FI/ESI-MS/MS)[1]. This approach allows, in a short time (about 2 min for analysis) and high sensitivity (LOD 50 fmol), the identification of the main important drugs (^{10}BSH and ^{10}BPA) used in BNCT studies[2].

In addition, for the understanding of the biochemical and physiological differences between tumour and normal cells and using these differences in compound design, synthesis and targeting, it is very important to investigate protein profiles related to different physiological states or to describe the effect of bioactive compounds. In our laboratory, we use shotgun proteomic approach, based on two-dimensional chromatography coupled to tandem mass spectrometry (2DC-MS/MS). This methodology provides a great improvement over gel-based analysis, and it is a powerful technology for clinical proteomic investigations[3].

In this context, urine samples obtained from BNCT patients were investigated to characterize both the level of boron-containing compounds and the protein profiles using FI/ESI-MS/MS and 2DC-MS/MS approaches, respectively. The main results obtained by the "integrated metabolomic and proteomic clinical studies" will be presented.

Boron-containing polymers for conjugation to antibodies

Katy Baumann[1], Detlef Gabel[1]

[1] *Department of Chemistry, University of Bremen, Germany*

Boron neutron capture therapy (BNCT) is a two-step radiotherapy. A selective radiation effect on tumor cells is achieved by first targeting the tumor with non-radioactive ^{10}B and then exposing it to low energy neutrons. For the success of BNCT a key requirement is to selectively deliver a relatively high amount of boron compound to the tumor cells. But to minimize the damage to normal tissue the boron concentration in the surrounding normal tissue cells should be kept low.

In order to improve the efficacy of BNCT, various approaches have been employed to deliver the ^{10}B compounds to the tumor tissue, including the use of macromolecules such as monoclonal antibodies.

The aim of the work is to synthesize polymers containing the dodecaborate cluster. These macromolecules must have functional terminal groups such as carboxy-, hydroxy-, amino- or mercaptogroups for binding them to antibodies.

In order to achieve this, some monomers could be synthesized for polymerization. Examples are an acrylic acid derivative of the hydroxydodecaborate cluster (BOH) **1**, a styrene derivative of the ammoniododecaborate cluster (BNH_3) **3** and epoxy derivatives of BOH and mercaptododecaborate cluster (BSH) **4**.

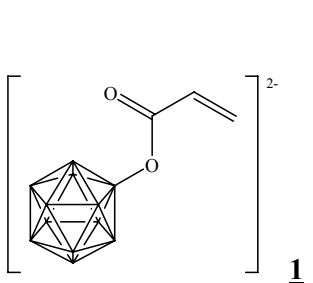

1

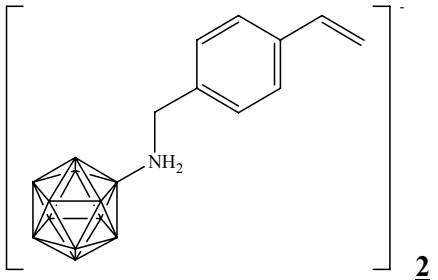

2

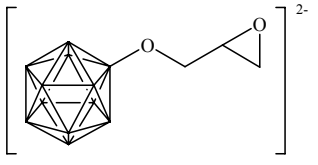

3

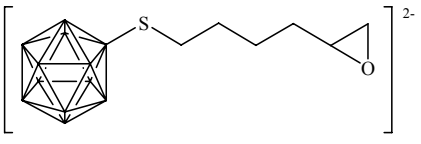

4

The polymerization initiator must contain functional groups to integrate them into the polymers. With these functional groups the synthesized polymers can be bound to the antibodies.

Boronated DNA Metallointercalators for Boron Neutron Capture Therapy

H. Y. Vincent Ching[1], Philippa A. MacKay[1], Louis M. Rendina[1]

[1] *School of Chemistry, The University of Sydney, Australia*

It has been demonstrated that boronated drugs which are localised in the cell nucleus exhibit greater cytotoxic effects upon thermal neutron capture than an equivalent amount of ^{10}B distributed on the cell surface or evenly throughout the cytoplasm. The ability of certain metal complexes containing planar aromatic ligands that bind to DNA by intercalation is well documented. Rendina and co-workers have recently prepared a series of 2,2':6',2"-terpyridineplatinum(II) complexes with thioalkylcarborane ligands, which are able to target chromosomal DNA in tumour cells, and also exhibit *in vitro* anti-cancer properties. This novel class of agents would potentially couple the biological effects of the neutron capture reaction with the avid DNA-binding reaction either additively or perhaps synergistically and, indeed, the platinum may also act as a radiation sensitizer. Furthermore, radiolabels such as ^{195m}Pt can be utilised to monitor cellular uptake and biodistribution of the drug *in vivo*.

Recently we undertook the synthesis, characterisation and biological studies of a related series of boron-rich diimineplatinum(II) complexes containing carboranylpyridylmethanol ligands such as bis[1-(1,12-dicarba-*closo*-dodecaboranyl)4-pyridylmethanol](1,10-phenanthroline)platinum(II) nitrate.

A dramatic improvement in the aqueous solubility of these agents has been successfully achieved by exploiting the host-guest properties of β-cyclodextrin, the cavity of which can readily accommodate the hydrophobic carborane cage. The key results of this work will be presented.

Suitability of boron carriers for boron neutron capture therapy for hepatoma *in situ*: Accumulation of boron in malignant and normal liver cells after treatment with L-boronophenylalanine, sodium borocaptate and boric acid

F.I. Chou[a], H.P. Chung[a] , Y.T. Wang[a], C.W. Chi[c,e], W.Y. Lui[b,d]

a Nuclear Science and Technology Development Center, National Tsing Hua University, Taiwan, Republic of China.

Department of [b] Surgery and [c] Medical Research & Education, Taipei Veterans General Hospital, [d]Department of Surgery and [e]Institute of Pharmacology, School of Medicine, National Yang Ming University; Taiwan, Republic of China.

Abstract

Introduction: Heptocellular carcinoma remains widely prevalent in tropical Africa and south-east Asia. At present, there are no effective treatments for hepatoma and its prognosis is extremely poor unless the tumor was diagnosed in an early stage and resected before metastasis. Therefore, BNCT may provide an alternative therapy for treatment of hepatocellular carcinoma.

Materials and methods: In this study, the suitability of L-boronophenylalanine (BPA), sodium borocaptate (BSH) and boric acid (BA) were evaluated on the basis of organ-specific boron distribution in normal rat tissues. BPA, BSH and BA were administered via intraperitoneal injection into rats with corresponding boron concentrations of 7, 25, and 25 mg/kg body weight, respectively. The intracellular concentrations of BPA, BSH and BA were further examined in human hepatoma HepG2 and liver Clone 9 cell cultures. With the use of 25 ug B/mL media of BPA, BSH and BA, the intracellular uptake of boron in HepG2 and Clone 9 cells was compared.

Results: The accumulation ratios of boron in liver, pancreas and kidney to boron in blood were 0.83, 4.16 and 2.47, respectively in BPA treated rats, and 0.75, 0.35 and 2.89, respectively in BSH treated rats at 3 hours after treatment. However, boron does not appear to accumulate specifically in soft tissues in BA treated rats. The accumulation rates of BPA, BSH and BA in HepG2 cells were higher than that of Clone 9 cells. Boron concentration in BPA, BSH and BA treated HepG2 cells were 1.8, 1.5, and 1.6-fold of Clone 9 cells at 4 h, respectively.

Conclusion: For **in situ** BNCT of hepatoma, normal organs with high boron concentration and adjacent to liver may be damaged in neutron irradiation. BA was more suitable for using as a boron carrier for particular combination treatment with other boron drug for BNCT of hepatoma. These preliminary results provide useful information on future application of BNCT for hepatoma.

Keywords: Hepatoma, BNCT, Boron carriers

1. Introduction

Boron neutron capture therapy (BNCT) is a unique treatment for tumors that can have increased retention of boron containing drugs. BNCT can be used to eliminate tumor cells whose precise location may not be fully known to prevent residual cancer cells from causing tumors to recur. BNCT is based on the nuclear capture reaction that occurs when ^{10}B is irradiated with thermal neutrons to yield alpha particles and recoiling ^{7}Li nuclei with a high linear energy transfer. The alpha particles and recoiling ^{7}Li nuclei have a short mean free path and their radiation energy may be confined to the cell from which they arise; this radiation energy is of lethal magnitude (Davis and Litter, 1970.). BNCT has been applied clinically to some tumors (Kankaanranta et al., 2007; Yamamoto et al., 2008). *In vitro* and *in vivo* tests for oral cancer, melanoma and thyroid cancer have yielded encouraging results (Barth et al., 2005).

In Taiwan, the Tsing-Hua open pool reactor

(THOR) at National Tsing Hua University is being remodeled as a dedicated facility for BNCT, and is ready for use in preclinical trials. Hepatoma, the most common cancer in males and the third most common cancer in females in Taiwan, is a malignant tumor that responds poorly to conventional therapies. BNCT may provide a new approach for hepatoma therapy. Successful clinical applications of BNCT depend upon the selective accumulation of ^{10}B in the tumor, low levels in normal tissues, and the delivery of sufficient thermal neutron fluence to the tumor site. Consequently, BNCT can destroy tumor cells and their processes without compromising close or contiguous normal tissue from which the tumor has arisen. Its success depends mainly on the differential uptake of boron drug between the tumor and normal tissues.

Unless the liver of the patient was surgically isolated and extracorporeally irradiated with thermal neutrons (Pinelli et al., 2002; Wilkinson, 2003), in the BNCT of hepatoma, organs such as the pancreas and spleen which are located close to the liver may be within the irradiation field. The uptake and retention of boron in these organs will be an important factor for design of BNCT for hepatoma. The aim of this investigation was to evaluate the uptake and accumulation of clinically used neutron capture agents such as boronophenylalanine (BPA) and sodium borocaptate (BSH), as well as boric acid (BA) in hepatoma cells. In addition, the bio-distribution of these boron compounds was also evaluated **in vivo**.

2. Material and Methods

2.1. Evaluation of boron concentration in BPA, BSH and BA administered SD Rats

BPA was purchased from Ryscor Science Inc. (North Carolina). BSH was purchased from Katchem Ltd. (Prague, Czech Republic). Boric acid was purchased from Merck Co. (Darmstadt Germany). BSH and boric acid were prepared in aqueous solution. The BPA-fructose solution was prepared as described elsewhere (Coderre et al., 1998). Sprague Dawley rats weighing approximately 300 g were used in this study. BPA and BA were administered in doses of 150 mg/kg, and BSH was administered in doses of 50 mg/kg. The biodistribution of boron was determined at 1 and 3 hours after the intraperitoneal injection of BPA, BSH and BA. Rats were anesthetized by an intraperitoneal injection of chloral-hydrate. Pancreas, spleen, liver, blood, kidney, lung, heart, stomach and small intestine were removed, and tissues were decomposed using a microwave digestion system. Boron concentrations were then assayed using inductively coupled plasma-atomic emission spectroscopy (ICP-AES, OPTIMA 2000 DV, Perkin Elmer Instruments) and were normalized as μg/g of tissue.

2.2. Evaluation of uptake of boron drug in HepG2 and Clone 9 cells

Exponentially growing HepG2 and Clone 9 cells were used in boron drug uptake experiments. Human hepatoma HepG2 cells were grown in 75 cm^2 polystyrene flasks in complete Dulbecco's modified Eagle medium (CDMEM) at 37°C. Rat normal liver Clone 9 cells were grown in Ham's F-12K medium with 2 mM L-glutamine and 10% fetal bovine serum (complete Ham's F12K medium) at 37°C. Cells were treated with 0.125 % (w/v) trypsin in 0.05 % (w/v) EDTA for 5 min at 37°C to detach them from flasks. Cells were then divided into three aliquots and placed in 75 cm^2 flasks with 12 ml media. The medium was replenished on day 2 and 4 after transfer.

BPA, BSH and BA were used as boron drugs to determine the cytotoxicity on HepG2 cells and liver Clone 9 cells. Cell were washed once using culture media, and then incubated in a boron drug-containing media. In each flask, 2 ml of a suitable concentration of boron drugs was mixed with 10 ml of medium to a final boron concentration of 25 μg /ml. Cells were harvested at 2, 4, 6 and 8 h. At each time point, the harvested cells were washed and trypsinized for counting, and lyophilized to measure the concentration of boron. Samples decomposed by the microwave digestion system were then assayed by ICP-AES.

3. Results

3.1 Biodistribution of boron in BA, BSH and BPA-administered SD rats

Figure 1 shows the mean boron concentrations in various tissues of rats at 3 h after injection. In BA-treated rats, boron concentrations in the pancreas, spleen, liver, blood, kidney, lung, heart, stomach and small intestine were 8.9, 10.7, 10.3, 10,6, 16.4, 10,1 10.8, 11.5 and 10.1 μg/g,

respectively. In BSH-treated rats, boron concentrations in the pancreas, spleen, liver, blood, kidney, lung, heart, stomach and small intestine were 2.1, 1.6, 4.3, 5.8, 16.4, 2.9, 1.3, 1.8 and 0.9 μg/g, respectively. In the BPA-treated rats, boron concentrations in the pancreas, spleen, liver, blood, kidney, lung, heart, stomach and small intestine were 17.4, 4.9, 3.5, 4.2, 10.3, 3.5, 3.9, 5.0 and 5.0 μg B/g, respectively. The pancreas had a higher boron concentration than blood; the accumulation ratios of boron in liver, pancreas and kidney to boron in blood were 0.83, 4.16 and 2.47, respectively, in BPA-treated rats. The accumulation ratios of boron in liver, pancreas and kidney to boron in blood were and 0.75, 0.35 and 2.89, respectively, in BSH treated rats at 3 hours post treatment. However, boron did not accumulate specifically in soft tissues in BA-treated rats.

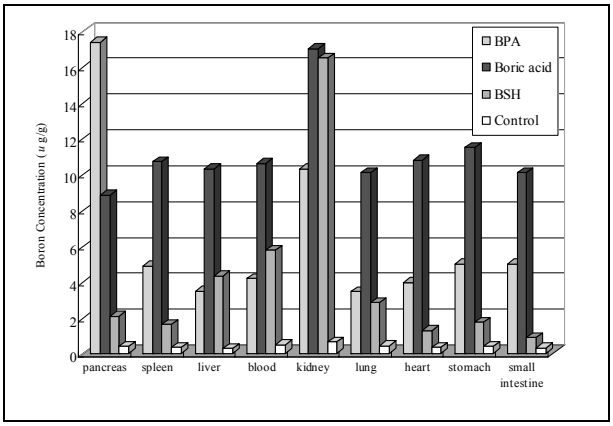

Figure 1. Boron concentration in various tissues and blood of SD rats, as assayed using ICP-AES. Injected doses of BPA, BSH and BA were 7, 25, 25 μg B/g body weight, respectively

3.2 Uptake of BPA, BSH and BA in HepG2 cells and Clone 9 cells

Figure 2 shows the time-dependent uptake of BPA, BSH and BA by HepG2 cells and Clone 9 cells. After 4 hours of treatment the mean boron concentrations in HepG2 cells were 98, 51 and 23 μg/g in the BPA, BA and BSH treatments, respectively; while in Clone 9 cells, the mean boron concentrations were 53, 33 and 15 μg/g in the BPA, BA and BSH treatments, respectively. Boron concentration in BPA, BSH and BA treated HepG2 cells were 1.8, 1.5, and 1.6-times higher than those of Clone 9 cells after 4 hours.

The mean boron concentrations in 8 hour BPA treated HepG2 cells was 124 μg/g, which was about 1.5-times that in Clone 9 cells. The mean boron concentrations in 8 hour BA treated HepG2 cells was 60 μg/g, which was about 1.4 times that in Clone 9 cells. The boron accumulation in BPA and BA treated HepG2 and Clone 9 cells increased with the treatment time. However, the mean boron concentrations of the BSH treated HepG2 cells were 29 μg/g after 8 hours of treatment. BSH-treated Clone 9 cells yielded similar results.

4. Discussion and Conclusions

Although HepG2 cells showed higher uptake and retention of BPA and BSH than Clone 9 liver cells, whether this differential uptake is observed in tumor bearing rats needs further confirmation. Nevertheless, an important finding in this study is that a high uptake of BPA in the pancreas of rat was observed. For the BNCT of hepatoma **in situ**, organs that are adjacent to the liver may be located within the irradiated field. The current treatment planning system cannot avoid the irradiation of pancreas, boron concentrations in tumor and surrounding normal tissues in vivo play a key role in BNCT (Imahori et al., 1998). Consequently, BPA may not be a suitable agent for the BNCT of hepatoma because of the high uptake and retention of BPA in the pancreas. Boric acid may suitable for use as a boron carrier in combination treatment with other boron drugs for the BNCT of hepatoma .

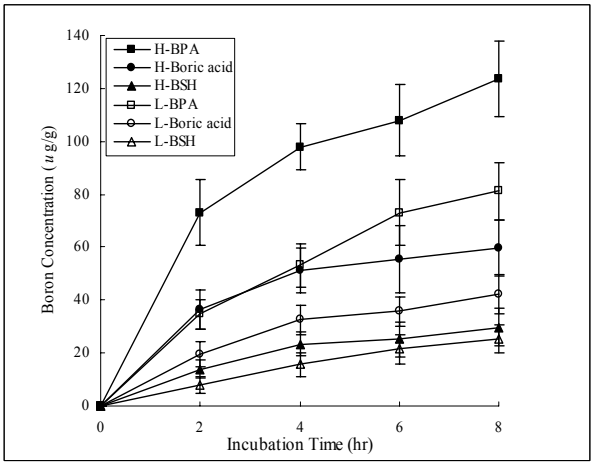

Figure 2. Accumulation of boron in HepG2 and Clone 9 cells as function of incubation time following BSH, BPA and BA treatment at 25 ug B/ml. Data points represent mean ± SD from five replication measurements. H: HepG2 cell, L: Clone 9 liver cell

References

Barth R.F., Coderre J.A., Vicente M.G.H., Blue T.E. 2005. Boron neutron capture therapy of cancer: Current status and future prospects. Clin. Cancer Res. 11, 3987-4002.

Coderre, J.A., Chanana, A.D., Joel, D.D., Elowitz, E.H., Micca, P.L., Nawrocky, M.M., Chadha, M., Gebbers, J.O., Shady, M., Peress, N.S., Slatkin, D.N., 1998. Biodistribution of boronophenylalanine in patients with glioblastoma multiforme: boron concentration correlates with tumor cellularity. Radiat. Res. 149, 163-170.

Davis, M.A., Litter, J.B., 1970. Relative biological effectiveness of the $^{10}B(n, \alpha)\ ^{7}Li$ reaction in HeLa cells. Radiat. Res. 43, 534-553.

Imahori, Y., Ueda, S., Ohmori, Y., Sakae, K., Kusuki, T., Kobayashi, T., Takagaki, M., Ono, K., Ido, T., and Fujii, R., 1998. Positron emission tomography-based boron neutron capture therapy using boronophenylalanine for high-grade gliomas: Part I. Clin. Cancer Res. 4: 1825–1832.

Kankaanranta, L., Seppala, T., Koivunoro, H.,. Saarilahti, K., Atula, T., Collan, J., Salli, E., Kortesniemi, M., Uusi-Simola, J., Mäkitie, A., 2007. Boron neutron capture therapy in the treatment of locally recurred head and neck cancer. Int. J. Radiat. Oncol. Biol. Phys. 69, 475-482.

Pinelli, T., Zonta, A., Altieri, S., Barni, S., Braghieri, A., Pedroni, P., Bruschi, P., Chiari, P., Ferrari, C. and Zonta, C., 2002. TAOrMINA: From the first idea to the application to the human liver. In Research and Development Neutron Capture Therapy (W. Sauerwein, R. Moss and A.

Wittig, Eds.), pp. 1065–1072. Monduzzi Editore, Bologna. Wilkinson, E., 2003. An out-of-body experience. Lancet Oncol. 4, 64 .

Yamamoto T, Nakai K, Matsumura A., 2008. Boron neutron capture therapy for glioblastoma. Cancer Letters. 262, 143-152.

DNA-targeted Gadolinium Compounds for NCT

Ellen L.Crossley[1] and Louis M. Rendina[1]

[1] *School of Chemistry, The University of Sydney, Australia*

^{157}Gd can potentially be used for neutron capture therapy. The advantage of ^{157}Gd is that it possesses the largest effective nuclear cross-section of all naturally-occurring elements (2.55×10^5 barns), approximately sixty times that of ^{10}B. The energetic particles released from the nuclear capture reaction, e.g. Auger electrons, are capable of destroying malignant cells as long as they are localised near key cellular components such as DNA due to their short range. Indeed, it has been demonstrated that if BNCT agents can target chromosomal DNA they are two to five times more effective at achieving cell death than an equivalent amount of agent evenly distributed throughout the cytoplasm.

Recently we have synthesised and fully characterised a novel gadolinium agent linked to a DNA intercalator. Studies have been carried out which show promising cell uptake results with this prototype. A preliminary X-ray fluorescence mapping study of both treated and untreated B16 murine melanoma and A549 human lung carcinoma cells has been performed. The key results of this work will be presented.

Biodistribution of BPA and BSH after single, repeated and simultaneous administrations for neutron-capture therapy of cancer

H. Ichikawa[a], E. Taniguchi[a], T. Fujimoto[b], Y. Fukumori[a]

[a]*Faculty of Pharmaceutical Sciences and Cooperative Research Center of Life Sciences, Kobe Gakuin University, 1-1-3 Minatojima, Chuo-ku, Kobe 650-8586, Japan*
[b]*Department of Orthopaedic Surgery, Hyogo Cancer Center, Akashi, Japan*

Abstract

The effect of administration mode of L-BPA and BSH on the biodistribution in the melanoma-bearing hamsters was investigated. In single intravenous (i.v.) administration, BSH (100 mg BSH/kg) showed no significant retention of ^{10}B in all the tissues, including tumors, while long-term retention of ^{10}B in the tumor, muscle and brain was observed with L-BPA (500 mg BPA/kg). The dose escalation of L-BPA and the simultaneous single administration of L-BPA and BSH were not so effective at increasing boron accumulation in tumor after bolus i.v. injection. The boron concentration in tumor was 41 μg B/g after single bolus i.v. injection even at the dose of 1000 mg BPA/kg. In contrast, two sequential bolus i.v. injections of L-BPA with the dose of 500 mg BPA/kg each was found to be effective at increasing ^{10}B accumulation in the tumor; the maximum ^{10}B concentration in the tumor reached 52 μg B/g at 3 h after the second i.v. injection.

Keywords: Biodistribution, L-BPA, BSH, pharmacokinetics, BNCT

1. Introduction

In clinical neutron capture therapy (NCT), ^{10}B compounds such as p-borono-L-phenylalanine (L-BPA) and disodium undecahydro-mercapto-closo-dodecacarborate (BSH) have been widely used as short-range alpha-particle producing agents. BSH is a cage-shaped compound with 12 boron atoms and an SH group. It is believed that BSH can pass through the disrupted blood-brain-barrier (BBB) and thus accumulate selectively in brain tumor tissue (Yang et al., 1997) and has been clinically utilized for brain tumors. L-BPA is an analog of the essential amino acid phenylalanine and is actively taken up in cells not only as an amino acid analogue for protein synthesis, but also as a tyrosine analogue for melanogenesis. Because of this nature, L-BPA has been clinically utilized for malignant melanoma (Mishima et al., 1989) and brain tumors (Hatanaka and Nakagawa, 1994). In recent years, clinical trials with BPA have been undertaken for several other types of cancers (Kato et al., 2004, Aihara et al., 2006).

In order to make the therapeutic index of NCT sufficient, well-controlled biodistribution of ^{10}B compounds is crucial. Despite the long history of clinical use of L-BPA and BSH worldwide, published data on the precise boron biodistributions are limited. In the present study, fundamental studies on biodistribution of boron after intravenous injections of L-BPA and BSH into tumor-bearing animals were carried out based on the typical dose employed in clinical NCT. Additionally, an optimal mode of administration of ^{10}B compounds was explored.

2. Materials and Methods

L-BPA (10B enriched) and BSH (10B enriched) were kindly supplied by Stella Chemifa Corporation (Osaka, Japan). Fructose, perchloric acid (HClO4, 60%), hydrogen peroxide (H2O2, 30%) and boron standard solution (1000 μg/mL) were purchased from Nacalai Tesque, Inc. (Kyoto, Japan). L-BPA complex with fructose was prepared using known procedures (Yoshino et al., 1989).

All animal experiments were carried out according to the regulations of the Animal Care and Use Committee of Kobe Gakuin University (Kobe, Japan). Female Syrian (golden) hamsters, 5―6 weeks old, were purchased from Japan SLC, Inc. (Shizuoka, Japan). Greene's melanoma (melanotic No. 179 cell, D1-179), which is considered to be a biological and pathological counterpart of human melanoma, was used.

This melanoma was allowed to proliferate

Table 1. ^{10}B concentration-time profiles in blood and tissues after single i.v. administration of BSH (100 mg/kg) and BPA-Fr (500 mg BPA/kg)

		Concentration (μg equiv. of boron/g or ml)						
Tissue		5 min	0.5 hr	1 hr	3 hr	6 hr	12 hr	24 hr
Blood	BSH	102 ± 2	66 ± 13	36 ± 4	16 ± 6	7 ± 3	4 ± 1	2 ± 1
	BPA-Fr	**52 ± 8	**21 ± 4	**19 ± 4	*8 ± 1	5 ± 1	3 ± 1	*1 ± 0.1
Tumor	BSH	27 ± 4	26 ± 6	14 ± 1	6 ± 1	7 ± 1	5 ± 2	3 ± 1
	BPA-Fr	27 ± 5	28 ± 10	*24 ± 5	*36 ± 12	*20 ± 7	13 ± 6	2 ± 0.3
Liver	BSH	198 ± 28	176 ± 15	105 ± 11	26 ± 14	10 ± 3	4 ± 1	2 ± 0.2
	BPA-Fr	**14 ± 0.4	**15 ± 3	**14 ± 1	6 ± 1	*3 ± 1	**2 ± 1	**0.1 ± 0.1
Spleen	BSH	27 ± 3	17 ± 6	8 ± 2	6 ± 1	2 ± 1	2 ± 0.1	1 ± 0.5
	BPA-Fr	*23 ± 1	18 ± 2	**18 ± 1	**9 ± 1	*6 ± 1	3 ± 1	1 ± 0.1
Lung	BSH	61 ± 2	36 ± 8	19 ± 2	10 ± 4	6 ± 2	3 ± 2	2 ± 0.1
	BPA-Fr	**24 ± 4	*17 ± 3	16 ± 2	8 ± 1	5 ± 1	2 ± 1	**0.1 ± 0.1
Kidney	BSH	260 ± 15	139 ± 31	50 ± 6	18 ± 4	9 ± 2	13 ± 0.4	8 ± 0.3
	BPA-Fr	**159 ± 25	*77 ± 2	*65 ± 5	24 ± 3	14 ± 4	**5 ± 2	**1 ± 0.2
Muscle	BSH	9 ± 0.4	6 ± 1	3 ± 1	1 ± 0.4	1 ± 0.4	0.2 ± 0.1	0.1 ± 0.1
	BPA-Fr	**6 ± 1	*8 ± 1	**10 ± 3	**12 ± 0.4	**9 ± 1	**4 ± 1	*1 ± 0.3
Skin	BSH	24 ± 1	27 ± 4	13 ± 2	4 ± 1	3 ± 0.2	1 ± 0.3	1 ± 0.3
	BPA-Fr	**10 ± 0.4	**10 ± 2	**8 ± 1	4 ± 0.4	3 ± 1	1 ± 1	N.D.[a)]
Brain	BSH	2 ± 1	1 ± 0.3	1 ± 0.2	N.D.	N.D.	N.D.	N.D.
	BPA-Fr	3 ± 1	*5 ± 1	*7 ± 2	**9 ± 1	**5 ± 1	*2 ± 1	N.D.

*: P<0.05, **: p<0.01, significantly different from the ^{10}B concentration of BSH.
Each value represents the mean ± S.D. (n=3).

subcutaneously in the left thigh of 5 week old Syrian hamsters, weighing 80-90 g, until it reached 10 mm in diameter (typically at 10 days after implantation).

BSH was dissolved in saline of 10 mg/mL. L-BPA was prepared as a fructose complex (BPA-Fr, 50 mg BPA/mL). BSH (100 mg/kg) or BPA-Fr (500 mg BPA/kg) was i.v. injected via the femoral vein of the hamsters under anesthesia with diethyl ether. These doses of both compounds have been used in clinical NCTs (Yamamoto et al., 2004, Ono et al., 2006). Blood samples were collected by cardiac puncture at 5 min, 0.5, 1, 3, 6, 12 and 24 h after dosing. The hamsters were then sacrificed with diethyl ether, and tissue samples including the liver, spleen, kidney, lung, brain and tumor were removed immediately. Tissues were washed with saline and lightly blotted to remove any excess blood and water. The skin and muscle were removed from the right nates of the hamsters. The livers, kidneys, lungs, brains and tumors were homogenized by a high-speed homogenizer.

Boron analysis was performed by the inductively coupled plasma atomic emission spectrometric (ICP-AES) method. A weighed sample of hamster tissue or homogenate (typically 100-200 mg) was hermetically digested with $HClO_4$ (0.6 mL) and H_2O_2 (1.2 mL) for 24—48 h at 75°C. The resulting solution was diluted with ultra pure water to 5 mL, followed by filtration with a 0.45 μm disposable syringe filter unit.Boron concentration in each sample was determined by ICP-AES (SPS3100, SII NanoTechnology Inc., Japan) at the emission line at 249.773 nm.

3. Results

The biodistribution data of boron after single bolus i.v. administration of BSH (100 mg/kg) and BPA-Fr (500 mg BPA/kg) are summarized in Table 1. I.v. administration of BSH led to the rapidly decreased boron concentration in both the blood and the tissues except for the brain. The boron concentration versus time profiles for the various tissues was similar to that of blood. An extremely high boron concentration was found in the liver and kidney, while the lowest boron concentration was detected in the brain. The BSH concentration in tumor decreased rapidly, similar to the other tissues.

The boron concentration in blood, spleen, kidney, lung and skin also decreased rapidly after i.v. administration of BPA-Fr. A high boron concentration was found in the kidney. However, the B concentration in each tissue, i.e., blood, liver, lung and skin, with BPA-Fr was significantly lower than that with BSH at the same time point after administration. The exception was the spleen, in which the boron concentration was somewhat higher after BPA-Fr administration than after BSH administration. Boron concentrations in muscle and brain increased and reached the highest concentration at 3 h after the administration of BSH-Fr, followed by gradual elimination. Similar trends were found in the concentration-time profile of the tumor. The boron concentration in tumor with BPA-Fr increased and reached 36 μg B/g at 3 h after BPA-Fr administration.

Figure 1 shows the boron concentrations in the tissues at 3 h after rapid single i.v. injection of BPA-Fr at doses of 250, 500 and 1000 mg BPA/kg. The administration at 1000 mg BPA/kg led to a tumor boron concentration of 41 μg B/g, but the dose escalation from 500 to 1000 mg BPA/kg was not effective at increasing tumor accumulation. The trend was similar in the other tissues.

Figure 2 shows the results from the simultaneous administration of both BSH (100 mg BSH/kg) and BPA-Fr (500 mg BPA/kg). The concentrations corresponding to the sum of concentration with each compound were observed in all tissues. In this case, the boron concentration in tumor was 37 μg B/g.

BPA-Fr (500 mg BPA/kg) was i.v. injected twice at a 3-hr interval (total dose, 1000 mg BPA/kg). The second injection was carried out just when the tumor concentration reached the maximum after the first injection. The biodistribution data are listed in Table 2 with the single i.v. injections at two different doses (500 and 1000 mg BPA/kg) for comparison. In all tissues, the boron concentrations after two sequential i.v. injections of BPA were higher than those of a single i.v. injection. The boron concentration in tumor was 52 μg B/g at 3 hr after the second i.v. injection. At 12 h after the second administration, the boron concentration in the tumor was still 20 μg B/g, which is high enough to induce effective NCT.

4. Discussion

BSH is not believed to be retained in all tissues of tumor-bearing hamsters. Relatively rapid elimination from the tissues was observed in the present study, although transiently high boron concentrations were observed in the liver and the kidney. Yamaguchi et al. (1998) studied biodistribution of BSH in normal rats and reported that most of the administered boron was excreted rapidly into urine. High boron concentrations in the kidney observed in this study would relate to the fact that BSH can be rapidly excreted into urine.

Boron was retained longer in tumor, muscle and brain with BPA-Fr. The long retention in tumor and muscle seem to relate to a high cell-uptake and/or cell-affinity of L-BPA as an analog of essential amino acid, phenylalanine. Compared with BSH, BPA accumulation and retention in brain was higher suggesting that L-BPA could pass through the blood-brain barrier slowly. The maximum tumor boron concentration reached 36 μg B/g at 3 h after administration of BPA-Fr, high enough to for effective NCT, since the minimum requirement of boron concentration in NCT is thought to be 20—30 μg B/g in tumor (Barth et al., 1992). The rapid elimination from the blood, the low accumulation in the skin and higher accumulation with longer retention in tumor clearly contributed to the favorable biodistribution characteristics of L-BPA.

Kreimann et al. (2001) reported that the intraperitoneal (i.p.) administration of L-BPA at 1200 mg/kg b.w. led to continuously delivery to an oral pouch tumor and tumor concentrations of 194 μg B/g. In the present study, i.v. administration of more than 500 mg BPA/kg led to the boron concentrations in all tissues leveling off, implying that dose escalation over the 500 mg/kg may not be effective. From this aspect, the common use of a dose of 500 mg BPA/kg for NCT would be reasonable, though the boron accumulation in tumor may depend on administration-route of L-BPA and/or tumor type.

The simultaneous administration of BSH and BPA-Fr has been used in recent clinical NCTs. As evidenced from Fig. 2, the tissue distribution was cumulative, but no additional advantage of simultaneous administration of both compounds was found.

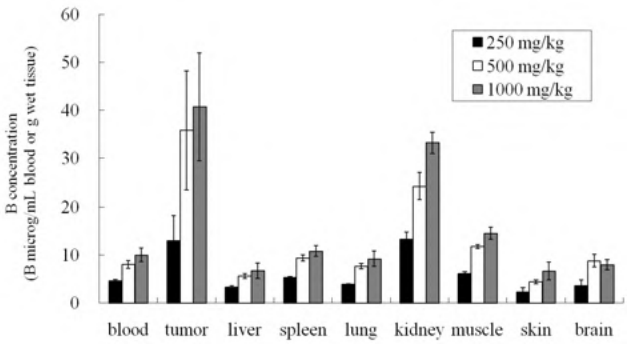

Fig. 1. ^{10}B concentration tissues 3 h after a single i.v. administration of L-BPA at different doses. Each value represents the mean ± S.D. (n=3)

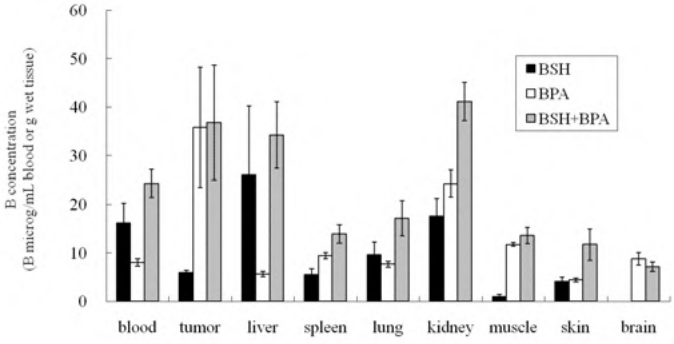

Fig. 2. ^{10}B concentration in various tissues at 3 h after simultaneous i.v. administration of BSH (100 mg/kg) and L-BPA (500 mg/kg). Each value represents the mean ± S.D. (n=3)

Table 2. Effect of dosing frequency on the tissue distribution of ^{10}B concentration at 3 and 12 h after the last i.v. administration of L-BPA

	Concentration (μg equiv. of boron/g or ml)				
	500 mg/kg		500 mg/kg x 2		1000 mg/kg
Tissue	3 hr	12 hr	3 hr	12 hr	3 hr
Blood	8.0 ± 0.8	2.6 ± 0.7	11.9 ± 1.5	3.3 ± 0.4	10.0 ± 1.4
Tumor	35.9 ± 12.4	12.7 ± 6.3	51.8 ± 12.1	19.5 ± 4.1	40.7 ± 11.3
Liver	5.6 ± 0.5	1.6 ± 0.5	8.6 ± 1.6	2.4 ± 0.2	6.8 ± 1.6
Spleen	9.4 ± 0.6	2.7 ± 0.9	13.7 ± 2.3	3.8 ± 0.2	10.8 ± 1.1
Lung	7.7 ± 0.6	2.0 ± 0.8	11.1 ± 1.7	3.1 ± 0.1	9.2 ± 1.6
Kidney	24.3 ± 2.8	4.8 ± 1.6	37.0 ± 6.5	7.8 ± 0.4	33.2 ± 2.2
Muscle	11.7 ± 0.4	3.9 ± 1.1	19.5 ± 2.1	6.3 ± 0.4	14.5 ± 1.3
Skin	4.4 ± 0.4	0.5 ± 0.6	7.4 ± 0.6	2.0 ± 0.2	6.7 ± 1.9
Brain	8.8 ± 1.3	2.0 ± 1.2	12.6 ± 2.8	3.3 ± 0.7	8.0 ± 1.1

This may be because the tumor used in this study was a malignant melanoma.

In case of brain tumors, co-administration of BSH and BPA improved the tumor/normal brain boron ratio over that of BPA administration (Yokoyama et al., 2006).

Two i.v. injections of L-BPA made the boron concentration in the tumor very high: 52 μg B/g at 3 h post-second administration (Table 2). The tumor concentration for the following 9 h continued to be at a level that could be effective in NCT, while the blood and skin concentrations ≤10 μg B/g. In the common clinical NCT, a boron compound solution has been continuously, slowly infused for a few hours. The data from the present study suggested that as an alternative of such a common infusion the repeated rapid injection based on the protocol proposed here would be a way to make NCT more effective.

4. Conclusions

Biodistribution of boron after intravenous injections of BPA and BSH into tumor-bearing animals was studied. BSH revealed relatively rapid elimination from all the tissues while long-term retention of ^{10}B in the tumor, muscle and brain was observed with L-BPA. Among administration modes studied here, twice bolus i.v. injections of L-BPA seemed to be an effective mode of administration to obtain a higher ^{10}B accumulation in the tumor. Formulation considerations with highly concentrated L-BPA injections will be a next issue to apply such an administration mode to clinical NCT.

References

Aihara, T., Hiratsuka, J., Morita, N., Uno, M., Sakurai, Y., Maruhashi, A., Ono, K., and Harada, T., 2006, First clinical case of BNCT for head and neck malignancies using F-18-BPA PET. Head Neck., 28, 850-855.

Barth, R.F., Soloway, A.H., Fairchild, R.G. and Brugger, R.M., 1992. BNCT for cancer – realities and prospects. Cancer, 70, 2995-3007.

Kato, I., Ono K., Sakurai Y., Ohmae M., Maruhashi A., Imahori Y., Kirihata M., Nakazawa M., and Yura Y., 2004. Effectiveness of BNCT for recurrent head and neck malignancies Appl. Rad. Isotpes, 61, 1069-1073.

Kreimann, E.L., Itoiz M.E., Dagrosa A., Garavaglia R., Farias S., Batistoni D., and Schwint A.E., 2001. The hamster cheek pouch as a model of oral cancer for BNCT studies: Selective delivery of boron by BPA. Cancer Res., 61, 8775-8781.

Mishima, Y., Honda C., Ichihashi M., Obara H., Hiratsuka J., Fukuda H., Karashima H., Kobayashi T., Kanda K., and Yoshino K., 1989. Treatment of malignant-melanoma by single thermal-neutron capture therapy with melanoma-seeking B-10-compound. Lancet, 12, 388-389.

Hatanaka, H. and Nakagawa, Y., 1994. Clinical results of long-surviving brain-tumor patients who underwent BNCT. Int. J. Radiat. Oncol. Biol. Phys., 28, 1061-1066.

Ono, K., Masunaga S., Kinashi, Y., Nagata, K., Suzuki, M., Sakurai, Y., Maruhashi, A., Kato, I., Nakazawa, M., Ariyoshi, Y., Kimura, Y., 2006. Neutron irradiation under continuous BPA injection for solving the problem of heterogeneous distribution of BPA. In: Nakagawa,Y., Kobayashi T., and Fukuda H. (Eds.), Advances in NCT, pp. 27-30.

Yamaguchi, T., Nakajima Y., Miyamoto H., Mizobuchi M., Kanazu T., Kadono K., Nakamoto K., and Ikeuchi I., 1998. Distribution and excretion of boron after intravenous administration of disodium BSH to rats. J. Toxicol. Sci., 23, 577-585.

Yamamoto, T., Matsumura A., Nakai K., Shibata Y., Endo K., Sakurai F., Kishi T., Kumada H., Yamamoto K., Torii Y., 2004. Current clinical results of the Tsukuba BNCT trial. Appl. Radiat. Isot., 61, 1089-1093.

Yang, W.L., Barth, R.F., Rotaru, J.H., Moeschberger, M.L., Joel, D.D., Nawrocky, M.M., Goodman, J.H., and Soloway, A.H., 1997. NCT of brain tumors: Enhanced survival following intracarotid injection of BSH with or without blood-brain barrier disruption. Int. J. Radiat. Oncol. Biol. Phys., 37, 663-672.

Yokoyama, K., Miyatake, S.I., Kajimoto, Y., Kawabata, S., Doi, A., Yoshida, T., Asano, T., Kirihata, M., Ono, K., and Kuroiwa, T., 2006. Pharmacokinetic study of BSH and BPA in simultaneous use for BNCT. J. Neurooncol., 78, 227-232.

Yoshino, K., Suzuki A., Mori Y., Kakihana H., Honda C., Mishima Y., Kobayashi T., and Kanda K., 1989. Improvement of solubility of para-BPA by complex-formation with monosaccharides. Strahlenther. Onkol., 165, 127-129.

Delivery of BPA using nanosuspension formulations for neutron-capture therapy of cancer

H. Ichikawa[a], E. Taniguchi[a], T. Fujimoto[b], Y. Fukumori[a]

[a]*Faculty of Pharmaceutical Sciences and Cooperative Research Center of Life Sciences, Kobe Gakuin University, 1-1-3 Minatojima, Chuo-ku, Kobe 650-8586, Japan*
[b]*Department of Orthopaedic Surgery, Hyogo Cancer Center,13-70 Kitaohji-cho, Akashi 673-8558, Japan*

Abstract

The aim of the present study is to explore nanosuspension formulations of L-BPA as an alternative to the solution systems, which can exhibit more beneficial biodistribution of boron, especially a higher accumulation in the tumor than the L-BPA solutions. In order to prepare the nanosuspension formulations, a conventional aqueous suspension containing L-BPA and a stabilizer (either soybean lecithin or Solutol® HS 15) were wet-milled using a planetary ball mill, and then sonicated for 30 min at room temperature. BPA nanosuspensions stabilized with lecithin (BPA-NS-LE) or Solutol® HS 15 (BPA-NS-SO) with the particle size of 366 and 215 nm, respectively, were obtained successfully. Biodistributions of ^{10}B after intravenous (i.v.) administration of the BPA nanosuspension were assessed in melanoma-bearing hamsters. BPA-NS-LE was found to induce high renal toxicity even at the dose of 250 mg BPA/kg. In contrast, no toxicity was observed in the case of BPA-NS-SO at the dose of 250 mg BPA/kg, although such a renal toxicity appeared again at the dose of 500 mg BPA/kg. The maximum boron concentration reached 19 μg B/g in tumor at 3 hr after administration of BPA-NS-SO at 250 mg BPA/kg. This value was significantly high in comparison with that of BPA-fructose complex solution (13 μg B/g in tumor). Although the nanosuspensions were efficient delivery systems, the limitation of dose arising from the renal toxicity will be a critical issue for gaining much higher ^{10}B accumulation in the tumor.

Keywords: BPA, nanosuspension, ball-milling, melanoma, EPR effect

1. Introduction

p-Borono-L-phenylalanine (L-BPA) is an analog of an essential amino acid and actively taken up in tumor cells. Because of this nature, L-BPA has been widely employed as a tumor-specific ^{10}B compound for BNCT. In spite of its excellent tumor accumulation, one pharmaceutical limitation of L-BPA is its poor water-solubility (1.6 g/L) (Yoshino et al., 1989). Typically a high dose such as 500 mg BPA/kg is employed in the clinical NCT. For the clinical use, therefore, L-BPA is complexed with fructose (BPA-Fr) for increasing the water-solubility of L-BPA (Mishima et al., 1989), yet even BPA-Fr is required to be continuously, slowly infused for a few hours. Such a long-term infusion with a large solution volume is a burden on patients and also high in cost.

In the present study, an attempt was made to formulate nanosuspensions composed of L-BPA itself. In this nanosuspension formulation, the dispersing phase is solid particles of L-BPA, so that its volume can be highly reduced as compared with a conventional infusion hitherto employed. This allows one shot injection. Additionally, the nano-sized L-BPA particles can be expected to be accumulated in tumor more efficiently than the dissolved compounds due to the so-called "enhanced penetration and retention effect" (EPR effect) (Matsumura and Maeda, 1986), provided that the nanosuspensions can be formulated so as to possess a long-circulating property in blood. As the first step of the study, nanosuspensions of sparingly water-soluble L-BPA were prepared simply by a wet ball-milling technique. Biodistributions after intravenous injections of the L-BPA nanosuspensions thus prepared were investigated using melanoma-bearing hamsters.

2. Materials and Methods

2.1. Chemicals

L-BPA (^{10}B enriched) was kindly supplied by Stella Chemifa Corporation (Osaka, Japan). Lecithin from soybean (SL, CP reagent grade, phosphatidylcholine content is about 60%) was

purchased from Nacalai Tesque, Inc. (Kyoto, Japan). Macrogol 15 hydroxystearate (Solutol® HS 15) was a gift from BASF (Germany).

2.2. Preparation of BPA nanosuspensions

Nanosuspension preparations were formulated from conventional aqueous L-BPA suspensions (50 mg/mL) containing a surface-active stabilizer. Two different surface-active stabilizers were used: Solutol® HS 15 (50 mg/mL) and SL (25 mg/mL). The conventional aqueous suspensions containing L-BPA and each stabilizer were wet-milled using a planetary ball mill (Planetary micro mill PULVERISETTE 7, Fritsch, Germany). Five mL of the conventional suspensions were placed in a 12-mL agate pot containing 1 mm$^{\phi}$ zirconium oxide balls (30 g). The ball mill apparatus was operated for 6 hr (with Solutol® HS 15) or 1 hr (with SL) at a rotation speed of 632 rpm. Subsequently, the resultant suspensions were sonicated by a water-bath-typed sonicator (BRANSONIC® 2510J-DTH, Branson Ultrasonics Co., CT, USA) for 30 min at room temperature. Particle size of the resultant nanosuspensions was determined using dynamic light scattering particle size analyzer (LB-500, HORIBA, Kyoto, Japan) at 25°C. The L-BPA nanosuspensions stabilized with soybean lecithin and Solutol HS15 were hereafter abbreviated as BPA-NS-LE and BPA-NS-SO, respectively.

2.3. Biodistribution of BPA nanosuspensions

All animal experiments were carried out according to the regulations of the Animal Care and Use Committee of Kobe Gakuin University (Kobe, Japan). Female Syrian (golden) hamsters, 5—6 weeks old, were purchased from Japan SLC, Inc. (Shizuoka, Japan). Greene's melanoma (melanotic No. 179 cell, D_1-179), which is considered to be biological and pathological counterpart of human melanoma, was used. This melanoma was allowed to proliferate subcutaneously in the left thigh of 5 weeks old Syrian hamsters, weighing 80-90 g, until it reached 10 mm in diameter (typically at 10 days after implantation).

The dose of BPA nanosuspensions in the preliminary experiments was 500 or 250 mg BPA/kg. In the detailed biodistribution study, the hamsters were dosed at 250 mg BPA/kg with BPA-NS-SO. An aqueous BPA-fructose complex (BPA-Fr, 50 mg BPA/mL) solution was prepared according to the known procedure (Yoshino et al., 1989) and used as a control dosage form. Each preparation was i.v. injected via the femoral vein of the hamsters under anesthesia with diethyl ether. Blood sample was collected by cardiac puncture at 5 min, 0.5, 1, 3, 6, 12 and 24 hr after dosing. The hamsters were then sacrificed with diethyl ether, and tissue samples including the liver, spleen, kidney, lung, brain and tumor were removed immediately. Tissues were washed with saline and lightly blotted to remove any excess blood and water. The skin and muscle were removed from the right nates of the hamsters. The livers, kidneys, lungs, brains and tumors were homogenized by a high-speed homogenizer.

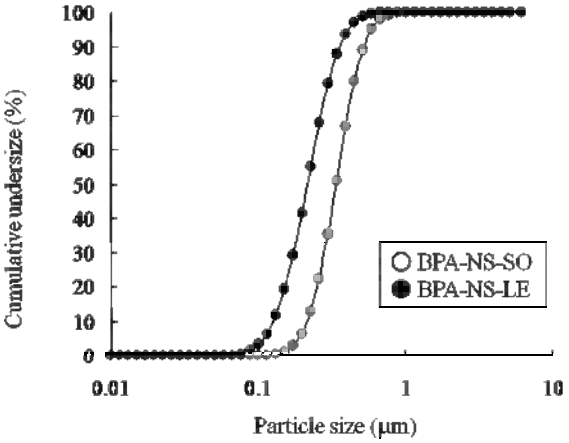

Fig. 1. Particle size distributions of two types of L-BPA nanosuspensions

2.4. Determination of boron

Boron analysis was carried out by the inductively coupled plasma atomic emission spectrometric (ICP-AES) method. A weighed sample of hamster tissues or homogenates (typically 100-200 mg) was hermetically digested with $HClO_4$ (0.6 mL) and H_2O_2 (1.2 mL) for 24—48 hr at 75°C using a dry bath. The resulting solution was diluted with ultra pure water to 5 mL of total volume, followed by filtration with a 0.45 μm disposable syringe filter unit. Boron concentration in each sample was determined by ICP-AES (SPS3100, SII NanoTechnology Inc., Tokyo, Japan). The emission intensity was measured at 249.773 nm. The calibration curves drawn using dilutes of the boron standard solution (1000 μg/mL) were linear in the range of 0.2—100 μg/mL.

3. Results

3.1. Particle size of L-BPA nanosuspensions

Figure 1 shows the particle size distribution achieved by the wet ball-milling. Both SL and Solutol® HS 15 were effective in reducing the particle size. BPA-NS-LE and BPA-NS-SO had mean particle sizes of 215 and 336 nm, respectively.

Table 1. ^{10}B concentration in blood and various tissues at 3 hr after i.v. administration of each formulation at two different doses of L-BPA

3.2. Nanosuspension toxicity

Table 1 lists tissue distributions of boron at 3 hr after i.v. administration of BPA-Fr solution or BPA-nanosupension formulations. All hamsters treated with BPA-NS-LE or BPA-NS-SO at 500 mg BPA/kg and one of three treated with BPA-NS-LE at 250 mg BPA/kg exhibited some necrosis in the kidneys. Two of three animals treated with BPA-NS-LE at 500 mg BPA/kg, and one of three animals treated with BPA-NS-LE at 250 mg BPA/kg or with BPA-NS-SO at 500 mg BPA/kg exhibited hematuria and high boron concentration. The hamsters treated with BPA-NS-SO at 250 mg BPA/kg had no necrotic kidneys. No renal toxicity was seen in the all animals treated with BPA-Fr solution even at the higher dose. These preliminary experiments indicated that boron concentrations were high in all necrotic kidneys, and the treatment with BPA-NS-LE led to higher boron concentration in kidney than that with BPA-NS-SO (Table 1). When compared at 250 mg BPA/kg, the tumor accumulation with the nanosuspensions seemed to be significantly higher than that with the BPA-Fr solution.

3.3. Boron concentration in the blood and tissues

The detailed biodistribution study was carried out with BPA-NS-SO at a lower dose, i.e., 250 mg BPA/kg since BPA-NS-LE showed more serious toxicity, and the side effect was induced at 500 mg BPA/kg even with BPA-NS-SO. The results are shown in Fig. 2. When the hamsters were treated with BPA-NS-SO at 250 mg BPA/kg, the boron level in the liver was significantly higher than those with BPA-Fr at 500 mg BPA/kg. The boron level in the kidney was much higher than that in the other tissues. The peak boron concentration in tumor at 250 mg BPA/kg with BPA-NS-SO was 19 μg B/g at 3 hr after i.v. injection. Pharmacokinetic parameters, T/B ratio and T/N ratio with BPA-NS-SO at 250 mg BPA/kg were summarized in Table 2.

4. Discussions

BPA-NS-LE induced high renal toxicity even at 250 mg BPA/kg (Table 1). On the other hand, BPA-NS-SO exhibited kidney toxicity at the dose of 500 mg BPA/kg, while no toxicity was observed at the of dose 250 mg BPA/kg (Table 1). Thus, the injectable dose of nanosuspensions had to be limited to much lower level than that of BPA-Fr which could be injected at 1000 mg BPA/kg (See our separate paper in the ICNCT13 proceedings) without any toxicity. Although the nanosuspensions were efficient delivery systems of ^{10}B to the tumor (Table 1 and Fig. 2) in comparison with BPA-Fr solution at the same doses, the limitation of dose coming from the toxicity will be a critical issue for gaining much higher ^{10}B accumulation in the tumor. As is well known, the presence of polyethyl-eneglycol (PEG) chains on the surface of particles can lead to a long-term systemic circulation. The surface of BPA-NS-SO particles would be covered with PEG chains, because Solutol® HS 15 has PEG chains. However, no prolonged-circulation effect was observed with BPA-NS-SO (Fig. 2 and Table 2). A possible explanation for the luck of this effect is as follows: most probably Solutol® HS 15 just physically absorbed on the surface of L-BPA particles. Hence its ability of adsorption should be influenced by the environmental condition.

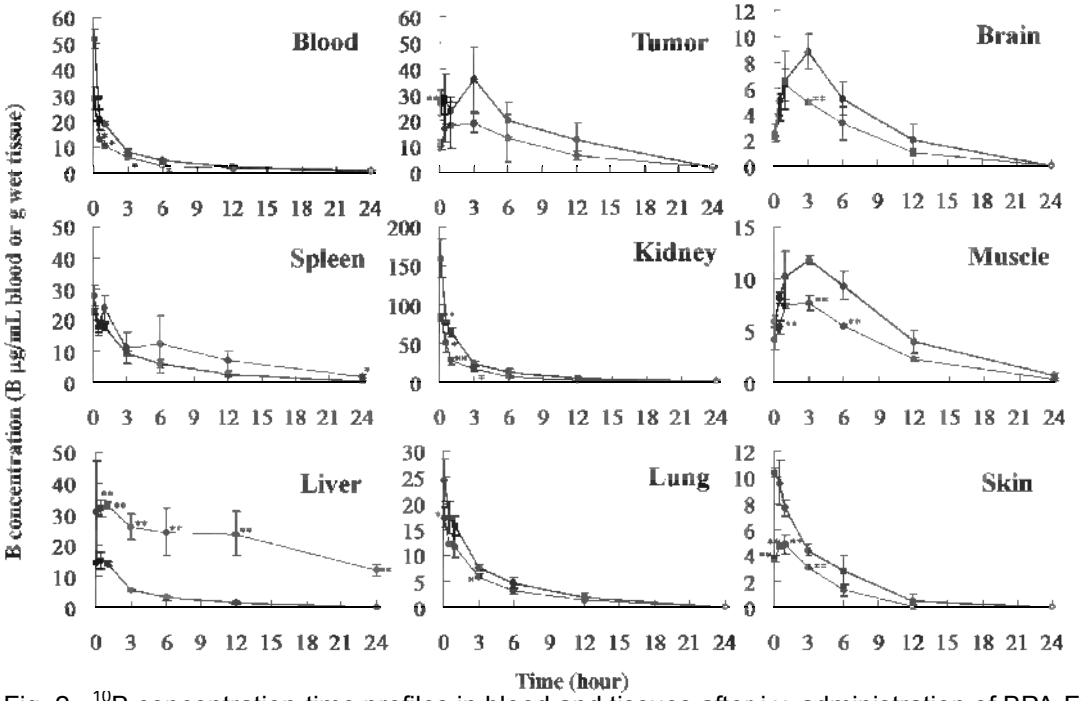

Fig. 2. ^{10}B concentration-time profiles in blood and tissues after i.v. administration of BPA-Fr solution or BPA-NS-SO into tumor-bearing hamsters
*: p<0.05; **: p<0.01, significantly different from the ^{10}B concentration of BPA-Fr. Dose: BPA-Fr, 500 mg BPA/kg b.w. (24 mg ^{10}B/kg b.w.); BPA-NS-SO, 250 mg BPA/kg b.w. (12 mg ^{10}B/kg b.w.). Each value represents the mean ± S.D. (n=3). ●: BPA-Fr; ○: BPA-NS-SO

Since the equilibrium condition may change in the blood after the i.v. injection, the stabilizer molecules were more or less detached from the particle surface in the blood, possibly leading to no prolonged-circulation effect.

The particle sizes of nanosuspensions prepared here did not seem to be small enough to expect the EPR effect. Unfortunately, smaller particles could not be achieved in the wet ball-milling process under the formulations and operating conditions employed here (Fig. 1). Considering the particles size of the present BPA-NS-SO to be 336 nm, it possibly occurred that the L-BPA molecules might distribute into most tissues after dissolving in the blood after the i.v. injection of BPA-NS-SO, while the particulate L-BPA would be trapped in the liver (Fig. 2). Use of nanosuspensions having particles smaller than 100 or less nm should be required to achieve much more accumulation of boron with assistance of EPR effect.

5. Conclusions

The BPA nanosuspensions showed a higher ^{10}B concentration in the tumor when compared to the BPA-Fr solutions at the dose of 250 mg BPA/kg. However, dose escalation of BPA in the nanosuspension formulations gave rise to the renal toxicity. Consequently, the ^{10}B concentration in the tumor did not reach more than 30 μg/g, which is the amount of ^{10}B required for fatal tumor cell damage.

Improvement of the particle characteristics such as a reduced particle size and a stable surface-modification is necessary to increase the ^{10}B concentration in the tumor through the EPR effect.

Table 2. Pharmacokinetic parameters

	AUC_{blood} (μg·h/mL)	AUC_{tumor} (μg·h/mL)	Tumor/ blood	Tumor/ skin
BPA-Fr	116 ± 6	356 ± 96	4.1± 1.1	8.2± 2.8
BPA-NS-SO	*71 ± 1	210 ± 37	3.1± 0.5	6.2± 1.1

References

Matsumura, Y., Maeda, H., 1986. Cancer Res., 46, 6387-6392.

Mishima, Y., Honda, C., Ichihashi, M., Obara, H., Hiratsuka, J., Fukuda, H., Karashima, H., Kobayashi, T., Kanda, K., Yoshino, K. 1989. Lancet, 12, 388-389.

Yoshino, K., Suzuki, A., Mori, Y., Kakihana, H., Honda, C., Mishima, Y., Kobayashi, T., Kanda, K., 1989. Strahlenther. Onkol., 165, 127-129.

Carborane-Containing Phosphonium Salts For Boron Neutron Capture Therapy

Joseph A. Ioppolo[1] and Louis M. Rendina[1]

[1] *School of Chemistry, The University of Sydney, Australia*

Phosphonium salts such as tetraphenylphosphonium (TPP) chloride and methyltriphenylphosphonium (TPMP) iodide are known to accumulate selectively in the mitochondria of cancer cells. This is due to their lipophilic and cationic properties which allow them to traverse the mitochondrial membrane of the tumour cell, in which the membrane potential is generally elevated compared to that of a normal, healthy cell. *In vivo* and *in vitro* uptake studies have shown a high tumour : healthy tissue ratio (~ 40 : 1) for these agents which is approximately an order of magnitude more selective than agents currently being used in the clinic for Boron Neutron Capture Therapy (BNCT). Phosphonium salts containing dicarba-*closo*-dodecaborane (carborane) could act as new cancer-selective, boron delivery agents to mitochondria, organelles that play a critical role in the regulation of apoptosis.

We have recently conducted the synthesis, characterisation, and cell-uptake studies of boronated phosphonium compounds. These include the $[PCH_3Ph_2\text{-}1,12\text{-}C_2B_{10}H_{11}]^+$ I^- salt as well as $[PPh_2CH_3\text{-}7,8\text{-}C_2B_9H_{11}]$ and $[PPh_2CH_3\text{-}7,9\text{-}C_2B_9H_{11}]$ zwitterions. A highly water-soluble derivative containing a tetraethyleneglycol group $[PPh_2(1,12\text{-}C_2B_{10}H_{11})((CH_2CH_2O)_3CH_2CH_2Br]^+$ Br^- has been prepared and characterised, and cell-uptake studies have been undertaken. The key results of this work will be presented.

Disposition of TF-PEG-liposome-BSH in tumor-bearing mice

Y. Ito[a], Y. Kimura[a], T. Shimahara[a], Y. Ariyoshi[a], M. Shimahara[a],
S. Miyatake[b], S. Kawabata[b], S. Kasaoka[c], K. Ono[d]

[a] *Department of Dentistry and Oral Surgery, Osaka Medical College, Japan*
[b] *Department of Neurosurgery,Osaka Medical College,Japan*
[c] *Faculty of Pharmaceutical Sciences,Hiroshima-International University,Japan*
[d] *Particle Radiation Oncology Research Center,Research Reactor Institute,Kyoto University,Japan*

Abstract

Objectives. Boron neutron capture therapy (BNCT) requires high concentration and selective delivery of boron (^{10}B) to the tumor cell. To further improve the drug delivery in BNCT, we conducted a study by devising transferring-conjugated polyethylene-glycol liposomes encapsulating sodium borocaptate (TF-PEG-liposome-BSH). **Materials and Methods.** Cancer-bearing mice were created by implanting SAS, the oral squamous-cell carcinoma (SCC) cell line, under the dorsal skin of BALB/c mice. When the tumor cell mass diameter reached approximately 1 cm, we administrated three types of boron delivery systems (BDS): BSH, PEG-liposome-BSH (PLB) and TG-PEG-liposome-BSH (TPLB). We measured the concentration of ^{10}B over time at the tumor site, blood, and liver. **Result and conclusion**. Results confirmed that ^{10}B concentration is higher in the TPLB group than in the BSH group and that TF-PEG-liposome-BSH is significantly effective as BDS. These findings suggest that BNCT using TF-PEG-liposome-BSH as BDS is an effective therapy for oral SCC.

Keywords: Boron neutron capture therapy (BNCT), mice, BSH, transferrin, polyethylene-glycol, liposome

1. Introduction

To improve the efficacy of boron neutron capture therapy (BNCT) in the treatment of oral malignant tumors, a high concentration of boron uptake is required at the tumor cells. Furthermore, in order to minimize damage to normal cells, it is important that boron specifically concentrates and is retained for a long period of time in the tumor cells, while uptaking with a low concentration in normal cells (Barth et al, 1992). In other words, if boron can be retained only in the tumor cells for as long as possible during exposure, it is assumed that efficacy of BNCT can be improved. Consequently, a delivery system with a long retention time and high selectivity to the tumor cell is desired.

Although many delivery systems that can transport drug agents and can perform targeting have been studied, liposome was selected for this study as it shows high concentration in tumor cells, and can transport a large amount of boron macromolecules.

Since liposomes consist of a lipid membrane derived from a biomembrane, they do not have toxicity or immunogenicity and have excellent biocompatibility. Liposomes are also carriers which can encapsulate a large amount of drug agents without the mediation of chemical bonding (Gabizon et al, 1988). In vivo, however, reticuloendothelial tissues, such as the liver, phagocytize the liposomes. As such, by modifying the PEG into a PEG-Liposome that can be retained in the blood, would reduce phagocytosis, and transport of boron to the tumor cells can be improved. Also, receptors which show high expression for the tumor cell are useful for the transport of the tumor-selective boron compound. Transferrin receptors (TFRs) are known to be overexpressed on the surface of cancer cells with respect to normal cells; by modifying the surface of PEG-Liposomes with transferrin (TF), the resulting liposomes (TF-PEG-Liposomes) targeted at these receptors may be considered to be an effective carrier as cancer targeting (Wagner et al, 1994).

In this study, with the PEG-Liposome and TF-PEG-Liposome modified on the boron compound sodium borocaptate (BSH), concentration at the oral squamous-cell carcinoma (SCC) cell in a cancer-bearing mice model was considered.

2. Materials and Methods

Cells, Animals, and Materials: SAS (from HSRRB) was used as the oral SCC cell line. A medium was mixed 1:1 with DMEM:F-12 MEM, supplemented with 10% FBS and an antibiotic agent. SAS was cultured with the medium at 37℃, 5% CO_2. PEG-Liposome-BSH (PLB), TF-PEG-Liposome-BSH (TPLB), (both provided by Dr. Kasaoka), and BSH were used as boron compound.

Creation of Cancer-Bearing Mice: SAS cells were collected after separating for trypsin EDTA, and then adjusted to 5×10^6 cells/0.1mL. Five-week-old male BALB/c mice were anesthetized by inhalation anesthesia, and the adjusted SAS cells were injected under the dorsal skin.

Boron Compound Administration and Tissue Removal: Experiments were conducted when tumor cell mass diameter on the skin of the cancer-bearing mice reached 1cm. After anesthetizing by inhalation anesthesia, various adjusted boron compounds at 35mg^{10}B/kg (35μg^{10}B /g) were administered to the cancer-bearing mice. The mice were then euthanized with an overdose of anesthesia 24, 48, and 72 hours after administration. Physiological saline was allowed to flow back from the aorta, and then the tumor site, liver, and blood were removed. The removed tissue weight was measured, dissolved in nitric acid, and the sample solutions were used for ICP measuring.

Boron Concentration Measurement: ICP emission spectrometry using an ICP-AES P-5200 (HITACHI) was performed to measure boron concentration. The analytical curve derived from the boron standard solution with a measurement wavelength of 249.773nm was used to measure the concentration. Luminescence intensity of the created sample solution was measured by ICP-AES. Boron concentrations of the solutions were measured according to the analytical curve, and the amount of boron was calculated as the boron concentration per weight of the tissue.

This study was based on the national regulations and guidelines, all experimental procedures were reviewed by the review committee for animal experiments of Osaka Medical Collage.

3. Result and Conclusions

Concentration of boron at the tumor site after 24 hours was higher in the TPLB group than in the BSH group. At the same time, retention of boron in the blood could also be confirmed.

This experiment clearly showed a higher concentration of TF-PEG-Liposome-BSH to the oral SCC cells at the tumor site in vivo. Furthermore, higher retention of TPLB in the blood could also be observed.

According to one study by Maruyama, et al., boron concentrations in the blood and liver when using TPLB were low at 72 hours, but concentration at the tumor site was high. Also, PLB at the tumor site was low at 72 hours, and good retention of TPLB could be confirmed (Maruyama et al, 2004). In the future, the appropriate concentration and length of time to achieve BNCT efficacy, which will have a high concentration at the tumor site while not affecting surrounding tissues, could be estimated for SAS cells by measuring the change in boron concentration in various organs over time.

References

Barth, R. F., Soloway, A. H., Fairchild, R. G. and Brugger, R. M. 1992. Boron neutron capture therapy for cancer. Realities and prospects. Cancer 70: 2995-3007.

Gabizon A. and Papahadjopoulos D. 1988. liposome formulations with prolonged circulation time in blood and enhanced uptake by tumors. Proc Natl Acad Sci USA 85: 6949-6953.

Maruyama K., Ishida O., Kasaoka S., Takizawa T., Utoguchi N., Shinohara M., Chiba M., Kobayashi H., Eriguchi M., Yanagie H., 2004. Intracellular targeting of sodium mercaptoundecahydro-dodecaborate (BSH) to solid tumors by transferring-PEG liposomes, for boron neutron-capture therapy (BNCT). Journal of Controlled Release 98: 195-207

Wagner E., Curiel D., and Cotton M. 1994. Delivery of drugs, proteins and genes into cells using transferring as a ligand for receptor-mediated endocytosis. Advanced Drug Delivery Reviews 14: 113-135.

Effect of Surface Modification on Characteristics of Gadolinium-Loaded Chitosan Nanoparticles for Neutron Capture Therapy of Cancer

H. Ichikawa[a], C. Kanai[a], T. Fujimoto[b], H. Kondoh[c], P. Sharma[d], S.C. Brown[d], B.M. Moudgil[d], Y. Fukumori[a]

[a]*Faculty of Pharmaceutical Sciences and Cooperative Research Center of Life Sciences, Kobe Gakuin University, 1-1-3 Minatojima, Chuo-ku, Kobe 650-8586, Japan*
[b]*Department of Orthopaedic Surgery, Hyogo Cancer Center,13-70 Kitaohji-cho, Akashi 673-8558, Japan*
[c]*Bio-Research, Inc.,5-5-2 Minatojimaminami, Chuo-ku, Kobe 650-0047, Japan*
[d]*Particle Engineering Research Center, University of Florida, Gainesville, FL32611, USA*

Abstract

As a nanoparticulate device for controlled delivery of Gd, we have been developing gadolinium-loaded chitosan nanoparticles (Gd-nanoCPs). The aim of the present study is to apply Gd-nanoCPs to a nano-device for delivering Gd to the tumor site via intravenous injection. For this purpose, a surface modification of the intact Gd-nanoCPs with lecithin was carried out and its effect on the dispersing stability, suppression of Gd-release and cellular interaction behaviours was evaluated. The results demonstrated that lecithin-coating of the Gd-nanoCPs was effective to improve the dispersing stability, to suppress Gd-release in human plasma, and to enhance the cellular association ability of the nanoparticles with the tumor cells without any significant promotion of the cytotoxicity.

Keywords: Gadolinium, chitosan, nanoparticle, lecithin, melanoma cell

1. Introduction

Gadolinium neutron-capture therapy (GdNCT) is currently under development as a potential radiation therapy of cancer. Unlike ^{10}B, ^{157}Gd has several possible advantages, such as the highest thermal neutron-capture cross section among stable nuclides (255000 barns), and the release of the gamma-rays and Auger electrons by the neutron-capture reaction (Greenwood et al., 1978). Consequently, GdNCT may reinforce therapeutic effect by increasing the chance of extensively hitting the target tumor cells with the long-range (>100 μm) photons and/or a locally intensive destruction of DNA in neoplastic cells by short-range and high linear energy transfer electrons (Brugger and Shih, 1989; Martin et al., 1988). In addition, gadolinium has been used as a magnetic resonance imaging (MRI) diagnostic agent, so that it would be possible to coordinate MRI diagnosis with GDNCT by using a functional delivery system of gadolinium (Sharma et al., 2007).

As a nanoparticulate device for controlled delivery of Gd, we have been developing gadolinium-loaded chitosan nanoparticles (Gd-nanoCPs) (Tokumitsu et al., 1999). Our previous studies demonstrated that significant tumor-growth suppression in vivo could be achieved by neutron-capture reaction after intratumoral (i.t.) injection of Gd-nanoCPs (Tokumitsu et al., 2000). However, a complete cure could not be achieved, possibly due to the uneven distribution of Gd in the tumor. Therefore, development of devices capable of delivering Gd to tumors through systemic circulation is strongly required for successful GdNCT.

The ultimate goal of the present study is to apply Gd-nanoCPs to a nano-device for delivering Gd to the tumor site via intravenous injection. Main subjects are to reduce the particle size to be less than 200 nm for utilizing the so-called EPR (enhanced permeation and retention) effect of the tumor (Matsumura and Maeda, 1986), to gain a good dispersing stability as well as to suppress Gd-release from the Gd-nanoCPs in blood-circulation, and to enhance association ability of the Gd-nanoCPs with tumor cells. Our previous study revealed that it was possible to obtain the Gd-nanoCPs with mean particle size of 155 nm by adapting the appropriate preparation conditions (Fukumori et al., 2006). Therefore, the focus of the present study is concentrated on the last three issues. Toward these

issues, a surface modification of the intact Gd-nanoCPs with lecithin was carried out and its effect on the dispersing stability, suppression of Gd-release and cellular interaction behaviours was evaluated.

2. Materials and Methods

Chitosan (100D EL, delacetylation degree of higher than 98%, nominal molecular weight of 10,000) was kindly supplied from Dainichi Seika Co., Ltd. (Japan). Gadopentetic acid (Gd-DTPA) was purchased from Sigma-Aldrich. Soybean lecithin (Nacalai Tesque, Inc., Japan) was used as a surface-modification agent. All other materials were at least of special reagent grades.

Gd-nanoCPs were prepared by using the chitosan and Gd-DTPA through the w/o emulsion-droplet coalescence technique as previously reported (REF). Surface-modification of Gd-nanoCPs with soybean lecithin was carried out by the thin-film hydration method. Briefly, the known amount of soybean lecithin was placed in a round-bottom flask, dissolved in chloroform, and then dried up by a rotary evaporator to give a thin film of soybean lecithin. Separately, the known amount of Gd-nanoCPs was dispersed in phosphate buffer solution (pH 7.0), mixed with the round-bottom flask containing the thin film of soybean lecithin and then sonicated by a bath-type ultrasonicator for 5 min to coat Gd-nanoCPs with soybean lecithin. The mass ratio of Gd-nanoCPs and soybean lecithin was 1:3. The mean particle size and the zeta potential of the lecithin-coated Gd-nanoCPs (LC-Gd-nanoCPs) thus obtained were measured by Zetasizer 3000HSA® (Malvern Instruments Ltd., UK) in water at 25ºC. Gd content of the LC-Gd-nanoCPs was assessed by the ICP-AES (SPS3100, SII NanoTechnology, Inc., Japan).

Release studies were carried out by a dynamic dialysis method. Briefly, the weighed amounts of sample (corresponding to 100 μg of Gd) were added to a cellulose tubing (Molecular weight cut-off size of 300,000) containing human plasma of 5 mL, placed in a centrifugal glass tube pre-filled with 50 mL of human plasma, and then horizontally shaken at 133 times/min at 37ºC. At predetermined time intervals, samples of 5 mL were withdrawn from the external fluid. The amounts of Gd released were determined by the ICP-AES after incineration of each sample.

Cellular toxicity and association behaviour of the intact Gd-nanoCPs and LC-Gd-nanoCPs were assessed using B16F10 mouse melanoma cells that were grown and routinely maintained in Eagle's minimum essential medium (MEM) supplemented with 10% fetal bovine serum (FBS) and 5% L-glutamine in a 90-mm culture dish at 37ºC in atmosphere of 95% air and 5% CO_2. The B16F10 cells were seeded at the density of 5×10^5 cells in a 90-mm culture dish and incubated for 48 h under 5% CO_2 atmosphere at 37ºC. After the culture medium was aspirated, the cells were incubated with 10 ml of the fresh culture medium containing the autoclaved intact Gd-nanoCPs of LC-Gd-nanoCPs with varied Gd concentrations for 0.5, 1, 2, 4, 8 and 12 h under 5% CO_2 atmosphere at 37ºC. Then, the cells were two times washed with 5 ml of PBS to remove unassociated Gd-nanoCPs. Subsequently, the cells were detached from the dish with a trypsin-treatment to obtain the cell suspensions, and then used for cell viability (%) assay, which was expressed as the ratio of the living cell number in the treatment groups to that in the control (untreated) groups. The amounts of Gd associated with the cells (μg Gd/10^6 cells) were determined by the ICP-AES after incineration of the cell samples.

3. Results and Discussion

Mean particle size, zeta potential and Gd content of Gd-nanoCPs before and after coating with soybean lecithin are listed in Table 1. The particle size of the intact Gd-nanoCPs was 196 nm where ultrasonic irradiation was required just before the particle sizing since the intact Gd-nanoCPs tended to be flocculated immediately after preparation. In contrast, the particle sizing was possible for the LC-Gd-nanoCPs even without ultrasonication (the particle size was 216 nm), indicating that the lecithin-coating improved dispersing stability of the intact Gd-nanoCPs. Indeed, the LC-Gd-nanoCPs showed a well-dispersed appearance at least for 1 hr as evidenced from Fig. 1. The zeta potential of the intact Gd-nanoCPs was 27.6 mV, whereas that of the LC-Gd-nanoCPs became a negative value, i.e., −20.1 mV, possibly due to the lecithin-coating. The Gd content of the LC-Gd-nanoCPs was decreased to be 4.7% which was approximately one-fourth of that of the intact Gd-nanoCPs. Obviously this significant

Table 1. Characteristics of Gd-nanoCPs before and after coating with soybean lecithin

	Particle size (nm)	Zeta potential (mV)	Gd content (wt%)
Gd-nanoCPs	196 ± 1	27.6 ± 2.2	20.3 ± 3.3
LC-Gd-nanoCPs	216 ± 3	-20.1 ± 3.5	4.7 ± 0.7

Each value represents the mean±S.D. of three batches.

Fig. 1. Appearance of Gd-nanoCPs before (right) and after (left) coating with soybean lecithin

decrease was consequent of the addition of large amount of soybean lecithin to the Gd-nanoCPs for coating. Considering that the mass ratio of the Gd-nanoCPs and soybean lecithin employed here was 1:3, most of lecithin molecules might be invested to cover the surface of the intact Gd-nanoCPs and thus decrease the Gd content proportionally.

Release profiles of Gd are shown in Fig. 2. The intact Gd-nanoCPs showed a rapid Gd-release with an initial burst of around 50% in the human plasma, and the release was completed within 3 hours. Contrary, Gd-release from the LC-Gd-nanoCPs was strongly suppressed; approximately 80% of Gd still remained in the nanoparticles even at 12 hr followed by the gradual release. Thus, surface modification with lecithin was effective to suppress the Gd-release.

The viability of B16F10 melanoma cells followed by 12-hr exposure to either the intact Gd-nanoCPs or the LC-Gd-nanoCPs is shown in Fig. 3. More than 90% of the cells remained viable in both types of Gd-nanoCPs over a range of feed amount of 10 ppm as Gd, indicating that the lecithin-coating did not affect the cell viability.

Association behaviours of the intact Gd-nanoCPs and the LC-Gd-nanoCPs as a function of incubation

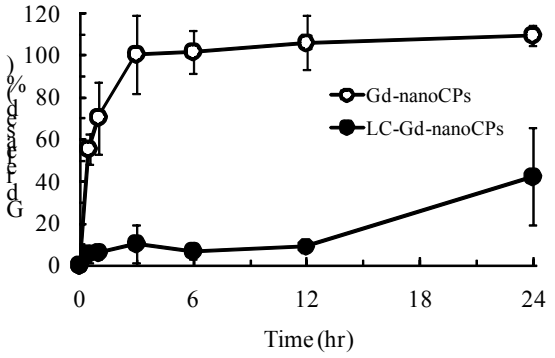

Fig. 2. Effect of lecithin coating on release profiles of Gd from Gd-nanoCPs
Each value indicates the mean ± S.D. (n=3).

time are shown in Fig. 4. In the case of the intact Gd-nanoCPs, the amount of Gd associated with the cells markedly increased until the incubation time reached 2 hr and then decreased slightly. The amount of Gd associated with the cells at 2 hr was almost comparable to the feed amount of Gd, so that almost all the nanoparticles dispersed in the culture medium were associated with the cells, while the number of the cells increased by their proliferation. This would account for the slightly decreased amounts of Gd associated with the cells with time. In contrast, the LC-Gd-nanoCPs showed gradual increase of the amount of Gd associated with the cells with time. The magnitude of the associated amount of Gd in the LC-Gd-nanoCPs was lower in comparison with that in the intact Gd-nanoCPs. At first glance, this seemed to be disadvantage of the lecithin-coating. However, it should be noted that the number of the LC-Gd-nanoCPs associated with the cells at 12-hr incubation was estimated to be approximately 2.5 times higher than that of the intact Gd-nanoCPs, assuming that both the intact Gd-nanoCPs and the LC-Gd-nanoCPs were filled-spheres with a diameter equivalent to their mean particle size, the particle density was the summation mean of the densities of the components, and no Gd release takes place during the association with the cells. This suggested that the LC-Gd-nanoCPs themselves might possess a potentially better association ability with the cells, though the capability of delivering Gd atoms to the cells was less because of their lower Gd content. Further formulation studies to increase Gd content will be crucial for fully utilizing the potentially high cell-association ability of the LC-Gd-nanoCPs and thereby increasing the amount of Gd associated with the cells.

4. Conclusions

Surface modification of the Gd-nanoCPs with soybean lecithin was found to be a useful way to improve the dispersing stability, to suppress Gd-release in human plasma, and to enhance the cellular association ability of the nanoparticles with the tumor cells without any significant promotion of the cytotoxicity. Further formulation studies will be necessary to increase Gd content and to provide a stealth property to the LC-Gd-nanoCPs for enhancing Gd accumulation in tumor sites through the EPR effect.

Acknowledgements

A part of this work was supported by MEXT ("Academic Frontier" Project 2006-2010) and Association for Nuclear Technology in Medicine.

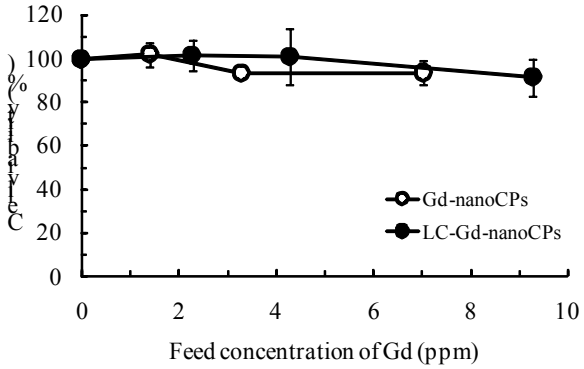

Fig. 3. Cell viability after 12-hr exposure to either intact Gd-nanoCPs or LC-Gd-nanoCPs
Each value indicates the mean ± S.D. (n=3)

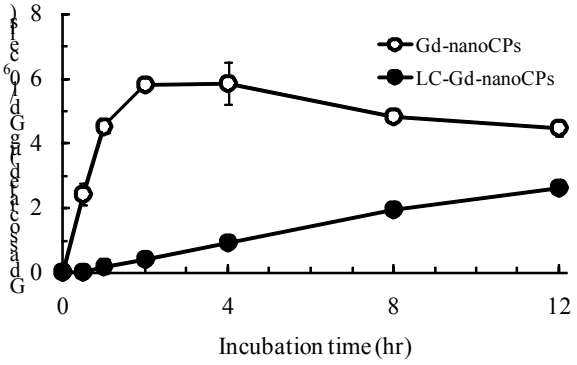

Fig. 4. Effect of lecithin coating on cellular association behaviors of Gd-nanoCPs
Each value indicates the mean ± S.D. (n=3)

References

Brugger, R.M., Shih, J.A., 1989. Evaluation of gadolinium-157 as a neutron capture therapy agent. Strahlenther. Onkol. 165, 153–156.

Fukumori, Y., Ichikawa, H., Nakatani, Y., Yamaguchi, M., Morita, N., Hiratsuka, J., Kondoh, H., Niki, Y., Sakurai, Y., Kobayashi, T., 2006. Gadolinium-loaded chitosan nanoparticles for cancer neutron-capture therapy: pharmaceutical characteristics and in vitro antitumor effect. Proceedings of ACNCT-12 (Advances in Neutron Capture Therapy 2006), pp. 224–227.

Greenwood, R.C., Reich, C.W., Baader, H.A., Koch, H.R., Breitig, D., Schult, O.W.B., Fogelberg, B., Backlin, A., Mampe, W., von Egidy, T., Schreckenbach, K., 1978. Collective and two-quasiparticle states in ^{158}Gd observed through study of radiative neutron capture in ^{157}Gd. Nucl. Phys. A304, 327–428.

Matsumura, Y., Maeda, H., 1986. A new concept for macromolecular therapeutics in cancer chemotherapy: mechanism of tumoritropic accumulation of proteins and the antitumor agent smancs. Cancer Res., 46, 6387-6392.

Martin, R.F., D'cunha, G., Pardee, M., Allen, B.J., 1988. Induction of doublestrand breaks following neutron capture by DNA-bound ^{157}Gd. Int. J. Radiat. Biol. 54, 205–208.

Sharma, P., Brown, S.C., Walter, G., Santra, S., Scott, E., Ichikawa, H., Fukumori, Y., Moudgil, B.M., 2007. Gd nanoparticulates: from magnetic resonance imaging to neutron capture therapy. Adv. Powder Tech. 18, 663–698.

Tokumitsu, H., Ichikawa, H., Fukumori, Y., 1999. Chitosan-gadopentetic acid complex nanoparticles for gadolinium neutron-capture therapy of cancer: preparation by novel emulsion-droplet coalescence technique and characterization. Pharm. Res. 16, 1830–1835.

Tokumitsu, H., Hiratsuka, J., Sakurai, Y., Kobayashi, T., Ichikawa, H., Fukumori, Y., 2000. Gadolinium neutron-capture therapy using novel gadopentetic acid-chitosan complex nanoparticles: in vivo growth suppression of experimental melanoma solid tumor. Cancer Lett. 150, 177–182.

Scheme of Screening Studies of New Compounds

V.N. Kulakov[a], A.A. Lipengolts[a], V.F. Khokhlov[a], I.N. Sheino[a], T.A. Nasonova[a], A.A. Portnov[b], K.N. Zaitsev[b], V.I. Kvasov[b], V.I. Bregadze[c], I.B. Sivayev[c]

[a]*State Research Center – Institute of Biophysics, Moscow, RF*
[b]*Moscow Engineering Physics Institute (State University), Moscow, RF*
[c]*Nesmeyanov Institute of Organoelement Compounds (INEOS RAS), Moscow, RF*

Abstract

An assessment of the solubility in aqueous solutions, acute toxicity, survival rate of a tumor cell suspension after thermal neutron irradiation in aggregate with pharmacokinetic studies in animals with inoculated tumors has become the basis of a screening study of new compounds aimed at selection of promising samples for their further studying. The efficiency of the suggested scheme is illustrated with the example of Na salt of aminoacid derivative of cobalt bis(dicarbollide) - Na[8-$H_2NCH(COOH)CH_2CH_2OCH_2CH_2O$-3,3′-Co(1,2-$C_2B_9H_{10}$)(1′,2′-$C_2B_9H_{11}$)].

Keywords: Screening, toxicity, cell culture, pharmakokinetics

1. Introduction

NCT is in critical need of new ^{10}B-containing agents capable of accumulating in tumor cells in higher concentrations than BPA and BSH. The emergence of new compounds would essentially increase the efficiency of BNCT for the treatment of a primary cancer nidus, which opens way for a wide use of the binary modality NCT in the oncological practice including combinations of NCT with conventional methods of cancer therapy. Screening studies using conventional methods, even at the cellular level, require considerable financial investments, especially if the compounds to be tested are derivatives of polyhedral boron compounds, the synthesis of which is rather complicated. Besides, for the drugs used in binary radiation technologies, the results of cellular-level studies are not always sufficiently correct.

Screening studies require maximum simplicity and availability of research methods in combination with reliability of the results obtained. We suggest the scope of research at the screening stage should include the following: an assessment of the acute toxicity of the compound, cellular level studies, and pharmacokinetic studies in small laboratory animals with inoculated tumors. The purpose of the cellular level studies is to assess the survival rate of a tumor cell culture after an irradiation of the cell suspension at the presence of the compound being investigated. For this purpose, it is rational to use the method developed by us earlier (Korotkevitch et al., 1998). At screening studies, it is possible to limit pharmacokinetic studies with an evaluation of the tumor uptake level. Carrying out such studies is possible with use of compounds with a natural content of ^{10}B.

The efficiency of the suggested approach can be illustrated with the example of Na salt of aminoacid derivative of cobalt bis(dicarbollide) - Na[8-$H_2NCH(COOH)CH_2CH_2OCH_2CH_2O$-3,3′-Co(1,2-$C_2B_9H_{10}$)(1′,2′-$C_2B_9H_{11}$)] (DCC-AA) (Sivaev et al., 2002). The structure of DCC-AA meets the basic requirements to the design of NCT compounds (Kulakov et al., 2001). Good water solubility of its sodium salt, and 18 boron atoms in the structure determined the interest to this compound as a promising BNCT agent.

Materials and methods

A DCC-AA solution of maximum concentration in water or in 0.9% sodium chloride solution contains DCC-AA in amount of 12 mg/ml, which corresponds to a 0.025 M solution. The DCC-AA concentration in the solution was determined by spectrophotometry. The UV-spectrum of DCC-AA has two absorption peaks with $\varepsilon_{280.1nm} = 5.72 \cdot 10^4$ and $\varepsilon_{446.2nm} = 8.06 \cdot 10^2$.

The DCC-AA toxicity was assessed in CBAC57 black mice of 25 g in mass at intravenous and intraperitoneal routes of administration in doses of 1 to 180 mg/kg, in accordance with the regulations in effect in the Russian Federation. The perished animals were dissected for a morphological study.

The cellular level studies have been carried out on a cell culture of murine melanoma B-16 obtained from the bank of cell cultures of the Russian Cancer Research Center (RCRC).

The cells of murine melanoma B-16 grew as a monolayer in glass vials on a mixture of the RPMI-1640 and Eagle's media with addition of 10% veal serum and gentamycin up to the concentration of 80 μg/ml. The grown cells were suspended in 1 ml of physiological solution. One ml of the prepared suspension contained 10^3 melanoma B-16 cells.

The melanoma B-16 cell suspension was put into 1.5-ml plastic vials, and 1 hour prior to irradiation in the MEPhI Reactor beam, the drugs to be compared were added in amounts providing the ^{10}B content in all samples of 26 μg/ml. The irradiation time was 10, 15, and 20 minutes. The control was the non-irradiated suspension of cells. After 72 hours, cells in the microcolonies were counted, and the colony growth rate (CGR) was calculated. The cell survival rate (SC) was determined at 12 days post irradiation.

As a reference for the comparative evaluation of the DCC-AA efficiency, a similar series of experiments has been carried out with BPA-fructose at a standard ^{10}B concentration in the cellular suspension (20 μg/ml).

The pharmacokinetic study of DCC-AA was carried out in female rats (from the Andreyevka Nursery of the Russian Academy of Medical Sciences) of 110 g in mass with S-45 sarcoma inoculated in the thigh. The DCC-AA solution was administered in the animals intratumorally and intravenously in amount of 0.2 ml. The content of ^{10}B in the amount administered was constant and equal to 30 μg. For this study, animals with tumors of 1 cm in diameter were selected. After 5, 15, 30, 60, 90, and 120 minutes, the animals were sacrificed, and samples of organs and tissues were taken for determining the ^{10}B content. The samples of the tumor, muscles, blood, and urine (for rats, with exposure time of 60 minutes and above) were put in polyethylene containers and preserved by adding 0.1 ml of benzyl alcohol. The concentration of ^{10}B in the biological samples was determined on the neutron radiation analysis facility (IRT MEPhI Reactor) with use of monochromatic neutrons. The neutron flux in the position of a sample is $2.7 \cdot 10^6$ n/cm^{2}s. The facility allows determining ^{10}B concentrations at a level of 1 μg/g in biological samples of 1-1.5 ml.

For in vivo studies, mice with B-16 melanoma grafted in the muscles of the shin were used. The irradiation was carried out on the 8-th day after the inoculation of tumors, when their volume was ~ 1 cm^3. In order to assess the growth rate, each two or three days, the tumor sizes were measured in three mutually perpendicular planes, assuming the tumor shape to be ellipsoid. The compounds were administered into the tumor in a total amount of 0.1 ml containing 20 μg of ^{10}B, as 4 injections into different loci of the tumor at ~20-30 minutes prior to irradiation. The irradiation time was 20 minutes.

Results and Discussion

The acute toxicity of DCC-AA was estimated for two routes of administration of the compound to the organism: intravenous and intratumoral.

For the intravenous administration of DCC, the value of LD_{50} was 60±5 mg/kg; for the intraperitoneal administration LD_{50} = 80±10 mg/kg. The morphological examination revealed pathological changes in the lungs of the perished animals for the intravenous administration, and in the intestine for the intraperitoneal administration of DCC-AA.

The in vitro studies were carried out on a melanoma B-16 cell suspension. The suspension of single cells of 0.5 ml in volume with a density of 0.5 million cells/ml was put in plastic ampoules with the internal diameter of 3 mm/ml and irradiated with a neutron flux of the IRT MEPhI Reactor.

The results of the in vitro studies on a cell culture of murine melanoma B-16 has shown DCC-AA to be 2 times more effective than BPA by the criteria of colony growth rate (CGR) and cell survival rate (CSR) (Table 1).

The results presented in Table 1 allow speaking of melanoma growth inhibition at presence of DCC-AA. The efficiency of DCC-AA in suppressing melanoma growth in conditions of the selected method of assessment appears to be much higher compared to the well-known compound BPA. In comparison with BPA, DCC-AA has certain cytotoxicity.

Table 1.
Comparative assessment of the effect of BPA and DCC-AA on murine melanoma B-16 cells at irradiation with a thermal neutron flux. The ^{10}B content in all samples was 26 μg/ml

Radiation dose, Gy	Assessment criterion, % in respect to the control*	BPA	DCC-AA
0	CGR	100	55.2
0	CSR	100	90.4
10	CGR	60.6	36.6
10	CSR	58.3	43.2
15	CGR	48.3	18.9
15	CSR	44.5	20.5
20	CGR	45.6	4.4
20	CSR	45.4	5.7

*The control is a cell suspension without compounds and without irradiation.

At the same time, BNCT of murine melanoma B-16 with DCC-AA was not productive – the effect of the administered DCC-AA on the growth of melanoma after a local irradiation of the tumor in a neutron beam made no difference from the control, which was a neutron irradiation of the tumor without a compound (Fig. 1).

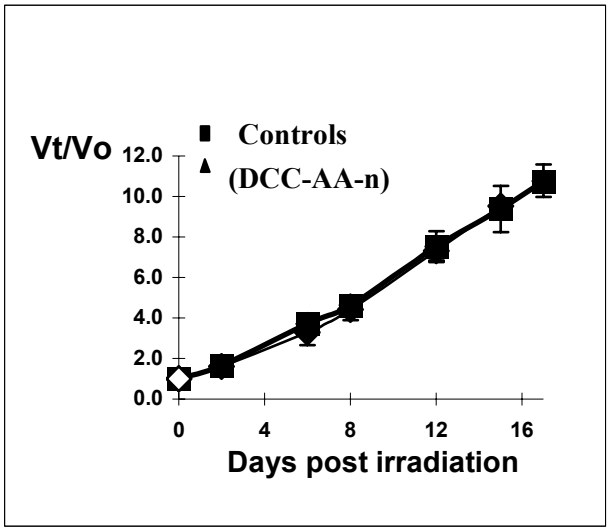

Figure 1. Growth of murine melanoma B-16 after a local irradiation of the tumors in the neutron beam (n) for the case of intratumoral administration of DCC-AA

Apparently, the reason of inefficiency at BNCT can be revealed after pharmacokinetic studies on DCC-AA.

The pharmacokinetic studies were carried out at two routes of DCC-AA administration to the organism - intratumoral and intravenous. The content of ^{10}B in tumor after intravenous administration of DCC-AA was evaluated at 30 minutes after the injection. In 5 minutes after the intratumoral administration of DCC-AA, the concentration of ^{10}B in tumor was at a level of 5 μg/g and smoothly decreased to 3 μg/g by the time of 120 minutes after the DCC-AA administration (Fig. 1). The content of ^{10}B in other tissues of the mice (muscle, blood, urine) did not exceed 1 μg/g. At intravenous administration of DCC-AA, the content of ^{10}B in the tumor tissues, muscles, kidneys, and liver was less than 1 μg/g. The primary amount, more than 60%, of the administered DCC-AA is excreted. The basic route of excretion of DCC-AA is with urine in 5-10 minutes. In all cases, the amount of ^{10}B administered to the animals was the same and equal to 30 μg in a volume of 0.2 ml. The pharmacokinetic study revealed that DCC-AA is not capable of accumulating in the tumor, as it has no tropism for tumors.

The quantitative determination of ^{10}B in the biological samples by prompt gamma-rays was carried out on the facility implemented on the channel HEC-9 of the IRT MEPhI Reactor providing reliable determination of ^{10}B of 1 μg/g and above in a time interval shorter than 2 hours, with an accuracy of not worse than 10%.

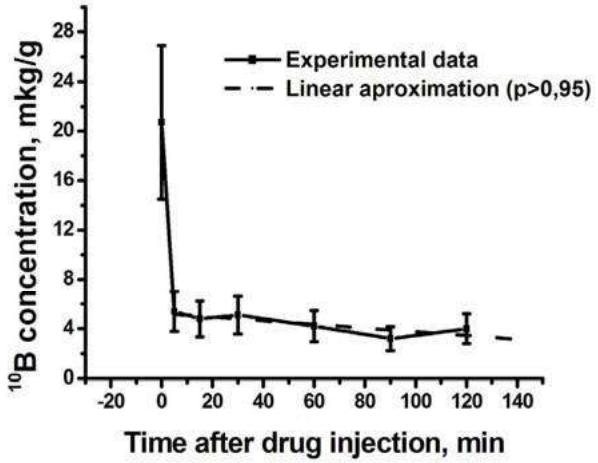

Figure 2. Time history of ^{10}B concentration in a tumor after intratumoral administration of DCC-AA into rats with inoculated S-45 sarcoma

Conclusions

The results of the studies presented above allow selecting potential compounds for neutron capture therapy by the following criteria:

- Solubility in aqueous solutions;
- Acute toxicity;
- Effect of the compound being investigated on the development of the tumor cell culture;
- Degree of accumulation of the compound being investigated in the tumor tissue.

The results obtained convincingly show that limited pharmacokinetic studies should be an obligatory stage of research on feasibility of new NCT compounds. The suggested scheme of screening of potential NCT compounds allows assessing rather simply the prospects of a compound under investigation and expediency of a more detailed study of that compound.

Acknowledgements

The work has been carried out with financial support from International Science and Technology Center Projects #3341 and #3605.

References

1. Korotkevitch, A.O., Malutina, T.S., Kulakov, V.N., Khokhlov, V.F., Experimental estimation of NCT-drug's efficiency 1998. Patent RF № 2144669.
2. Kulakov, V.N., Bregadze, V.I., Sivaev, I.B., Nikitin, S.M., Gol'tyapin, Yu.V., Khokhlov, V.F., 2001. Design of Boron- and Gadolinium-containing Agents for NCT, In: M.F. Hawthorne, K.Shelly, R.J.Wiersema, Frontiers in Neutron Capture Therapy, Kluver Academic/Plenum Publishers, N-Y, V.2, 843-846.
3. Sivaev, I.B., Starikova, Z.A., Sjöberg, S., Bregadze, V.I., 2002. Synthesis of functional derivatives of the [3,3′-Co(1,2-$C_2B_9H_{11})_2$]- anion. J. Organomet. Chem. 649(1), 1-8.

Glycosylated Carbaboranylphosphonates for Use in BNCT-Anti-Cancer Treatment

Johannes Kunig, Sven Stadlbauer, Evamarie Hey-Hawkins

Department of Inorganic Chemistry, Universität Leipzig, Germany

Since the introduction of boron neutron capture theory (BNCT) by *Locher* in 1936, several investigations toward synthesizing useful compounds, including derivatives of amino acids, porphyrins, liposomes, monoclonal antibodies, and epidermal growth factors, were carried out and reviewed. Until now, only BPA (L-*para*-boronophenylalanine), its fructose complex, and BSH (sodium mercapto-*closo*-dodecaboronate) made it into clinical trials on high-grade gliomas and melanomas. Nevertheless, their complete pharmacokinetical behavior and biodistribution are uncertain and need to be further investigated.

Our group focuses on the attachment of glycosides to carbaboranylphosphonates, which combines the boron-bearing part with a hydrophilic, less toxic, and tumor-selective moiety (e.g., Figure 1).

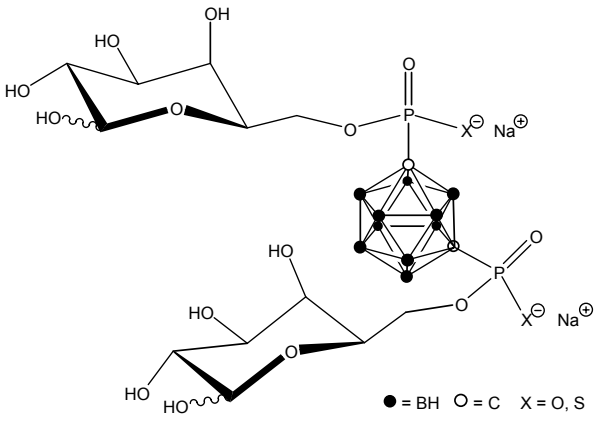

Figure 1. Galactosylphoshonate conjugates of *m*-carbaboranes

Previous work showed that carbaboranylphosphates have higher selectivity for some tumors,[3] but they were still too toxic and lipohilic. It was also observed that galactose derivatives have increased selectivity compared to their pyranose analogues.

Toxicity studies on HeLa cells were carried out and will be presented, as will our current biodistribution studies on BALB/C mice. Toxicity and biodistribution studies on related glucose and mannose derivatives are planned.

Synthesis of complex glycosylated carboranes for BNCT

Federica Campo, Matteo Mossotti, Luigi Panza

Department of Chemical, Food, Pharmaceutical and Pharmacological Sciences, University of Eastern Piedmont, Novara, Italy

Abstract

The synthesis of three different complex glycosylated carboranes has been performed. The synthesis of each carborane begins from a common intermediate obtained by glycosylation of an *o*-carborane functionalized with and hydroxyethyl and an azidopropyl group. The azide allowed the introduction of three moieties that could be useful to get information on the properties of the products or to introduce them into structures that are more complex.

Keywords: carbohydrates, conjugates, probes, synthesis.

1. Introduction

Boron neutron capture therapy (BNCT) is a binary therapeutic strategy for cancer treatment, which exploits the capture of thermal neutron by ^{10}B atoms, resulting in an efficient nuclear reaction destructive for tumor cells (Valliant et al., 2002).

In order to be therapeutically useful, an ideal boronated candidate should have the following properties: high tumor targeting selectivity; low cytotoxicity; high water solubility for intra-arterious administration of the BNCT agent; high uptake by and permanence in cancer cells. Among different boron-containing constructs, carboranes containing carbohydrates have recently raised interest (see e.g. Giovenzana et al., 1999, Tietze et al., 2001, Ronchi et al., 2004).The sugar moiety, in fact, not only is able to confer water solubility to the otherwise hydrophobic boron cluster but also could exert a targeting effect for tumor cells.

In addition to the issue of a compounds tumor targeting properties, one of the major problems in BNCT is the monitoring of the boron containing compounds *in vivo*. In order to have new compounds which can help to face these problems we decided to synthesize new carborane-containing hybrids. The compounds obtained, in addition to the sugar and the carborane, also contain a third moiety constituted of an amino acid or a probe. Such derivatives should allow either the conjugation with peptides or proteins for an improved delivery of the product, or for monitoring the biodistribution of the compound and its metabolic products.

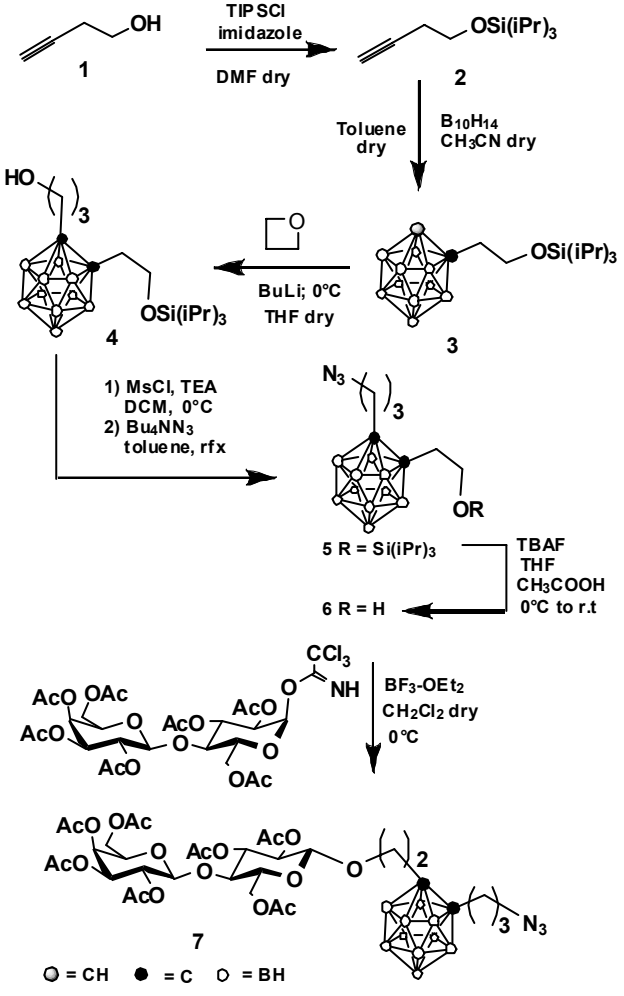

Scheme 1

As a glycosyl moiety, lactose has been chosen as model compound, not only to setup the synthetic scheme, but also because it is known that some tumors overexpress lactose-binding lectins. Different substituents have been linked to a common building block containing a functional group, namely an amino through the formation of an amide bond.

2. Materials and methods

The common precursor containing lactose as well as the carborane part was obtained starting from 3-butyn-1-ol **1**: (Scheme 1). The hydroxyl group of **1** was protected as triisopropylsilylether with TIPSCl and imidazole in DMF to obtain compound **2**. The carborane cage was added to **2** by treatment with decaborane in acetonitrile-toluene at reflux affording compound **3** in a satisfactory 68% yield.

Alkylation of compound **3** with BuLi and oxetane gave, after careful chromatography, monoprotected diol **4** in 81% yield. The free hydroxyl group of **4** was converted into the corresponding azido derivative **5** by conversion to the corresponding mesylate followed by treatment with tetrabutylammonium azide in 78% overall yield.

After deprotection of the silyl ether of **5** with TBAF buffered with acetic acid, the obtained compound **6** was glycosylated with the trichloroacetimidate of heptaacetyl lactose affording the common intermediate **7**.

From **7**, aminoacid functionalyzed derivative **8**, dansyl derivative **10** and nitroxide **12** were obtained with different synthetic procedures (Scheme 2). Condensation with protected glutamic acid was performed by treatment of the azide **7** with tributylphosphine and N-(3-Dimethylaminopropyl)-N'-ethyl-carbodiimide (EDC) to give compound **8** in 67% yield. Reduction of the azido group of **7** and treatment with dansyl chloride afforded compound **9** which was deacetylated to give the final fluorescent derivative **10**.

Reduction of the azido group of **7** and acylation with 4-carboxy-2,2,6,6-tetramethyl-piperidine 1-oxyl (4-carboxy-TEMPO) gave the expected amide

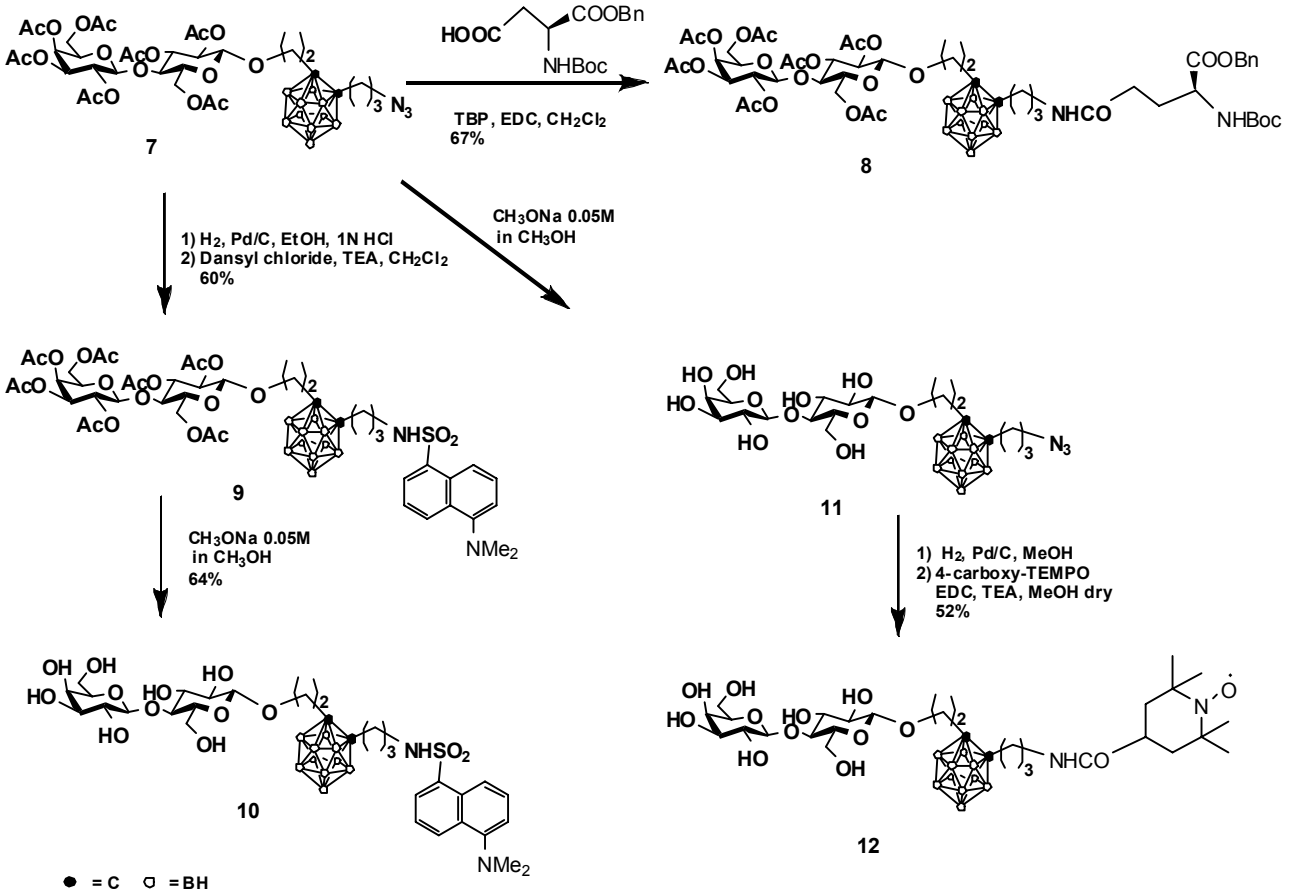

Scheme 2

but the deprotection was very sluggish. So the sequence was inverted by first removing the acetates to give compound **11** which was then treated with Pd and hydrogen to convert the azido group to the corresponding amine and finally condensed with 4-carboxy-TEMPO in the presence of EDC as condensing agent to afford the spin labeled derivative **12**.

Compound **8** will be will be subsequently deprotected for use in peptide synthesis. In fact, after deacetylation and removal of benzyl ester by catalytic hydrogenation the product will be ready for the above mentioned application.

3. Results and discussion

Although many syntheses of hybrid-containing carboranes have appeared in the literature, a common problem is the *in vivo* monitoring of such compounds and, in general, the possibility to get more information on their physicochemical and biological properties.

We describe here the synthesis of three different carborane-carbohydrate hybrids starting from a common intermediate by introduction, besides the carborane cage and a lactose moiety, of three different substituents, which may be useful to better characterize these products from different points of view. Moreover, functionalized derivatives allow their easy incorporation into more complex structures that can be used for delivery of boron-containing entities.

We decided to synthesize:

- a derivative containing a stable nitroxide, which allows the study of the molecule's behavior through electron spin resonance (e.g. when incorporated in liposomes);
- a derivative containing a fluorescent dansyl group in order to monitor the biodistribution of the product
- a conjugate with glutamic acid to be incorporated in proper peptide sequences (or even tested as such).

It is worthy to note that we expect to be able to incorporate such compounds into liposomes similar to our previously reported results (Morandi et al., 2004).

In order to obtain such derivatives we prepared a common intermediate containing a sugar moiety joined to a carborane cage, which is in turn functionalized with a linker ending with an azido group for further conjugation after reduction to an amine.

Common intermediate **7** was obtained from carborane **3** by alkylation with oxetane, after deprotonation with butyl lithium (Kane et al. 1993). Attempts to monofunctionalize *o*-carborane or to monoprotect a diol derived from a double alkylation of carborane did not give satisfactory results.

Standard manipulations gave an intermediate that was glycosylated to afford the desired common intermediate **7**.

Dansyl was introduced according to the above-mentioned strategy, namely azide reduction and sulfonylation and the protected derivative **9** was carefully deacetylated to give the deprotected product **10**. **7** was also efficiently conjugated with protected glutamic acid in the presence of a condensing agent, after treatment with tributylphosphine to form an intermediate iminophosphorane according to a literature procedure (see e.g. Chapuis et al. 2006).

The obtained compound **8** will be differently deprotected whether it will be used as such or for conjugation to peptides.

Finally, nitroxide **12** was prepared following an alternative synthetic pathway. In fact, we were able to obtain the corresponding derivative, protected at the sugar part with the same sequence used for the dansyl derivative. Unfortunately, the deacetylation reaction gave a complex mixture. We decided to invert the sequence by deprotecting the sugar part before azide reduction to give compound **11**. Reduction of the azide and amine acylation with cabossi-TEMPO allowed us to obtain the desired product **12** in acceptable yield.

4. Conclusions

We have been able to synthesize three differently functionalized carborane derivatives, containing either a probe or an appendage for further derivatization. The obtained compounds will be tested *in vitro* to get information on their metabolic behavior.

References

Valliant, J. F.; Guenther, K. J.; King, A. S.; Morel, P.; Schaffer, P.; Sogbei, O. O.; Stephenson, K. A. 2002. The medicinal chemistry of carboranes. Coord. Chem. Rev. 232, 173-230.

Tietze, L. F.; Bothe, U.; Griesbach, U.; Nakaichi, M.; Hasegawa, T.; Nakamura, H.; Yamamoto, Y. 2001. ortho-Carboranyl Glycosides for the Treatment of Cancer by Boron Neutron Capture Therapy. Bioorg. Med. Chem., 9, 1747-1752.

Ronchi, S.; Prosperi, D.; Compostella, F.; Panza, L. 2004. Synthesis of Novel Carborane-hybrids Based on a Triazine Scaffold for Boron Neutron Capture Therapy. Synlett, 1007-1010.

Giovenzana, G.B.;. Lay, L.; Monti, D.; Palmisano, G.; Panza, L. Synthesis of Carboranyl Derivatives of Alkynyl Glycosides as Potential BNCT Agents. Tetrahedron, 55, 14123-14136.

Morandi, S.; Ristori, S.; Berti, D.; Panza, L.; Becciolini, A.; Martini, G. 2004. Association of sugar-based carboranes with cationic liposomes: an electron spin resonance and light scattering study. Biochim. Biophys. Acta 1664, 53-63.

Chapuis, H.; Strazewski, P. 2006. Shorter puromycin analog synthesis by means of an efficient Staudinger–Vilarrasa coupling. Tetrahedron, 62, 12108–12115 and references cited therein.

Kane, R.R.; Dreschsel, K.; Hawthorne, M.F. 1993 Automated Syntheses of Carborane-Derived Homogeneous Oligophosphates: Reagents for Use in the Immunoprotein-Mediated Boron Neutron Capture Therapy (BNCT) of Cancer J. Am. Chem. Soc., 115, 8853-8854.

Boronated Cyclic Peptides As Tumor-Specific Agents for Boron Neutron Capture Therapy

Louis M. Rendina[1], Hugh H. Harris[2], Katrina A. Jolliffe[1], Erin J. Ziolkowski[1]

[1] *School of Chemistry, The University of Sydney, Sydney NSW 2006, Australia*
[2] *School of Chemistry and Physics, The University of Adelaide, Adelaide SA 5005, Australia*

It is well-established that non-selective, biologically-active compounds tethered to a molecule which is capable of selectively binding to tumor-associated markers have been shown to be successful in dramatically improving tumor:organ ratios within a few hours of intravenous drug administration. The present study focusses on combining peptidic ligands with boron-containing entities to afford a new class of conjugates for use in Boron Neutron Capture Therapy (BNCT). To maximise tumor cell destruction, the compound must exhibit some degree of selectivity toward tumors. This requirement may be addressed by using small peptides containing the cyclic RGD motif known to bind to integrin receptors which are over-expressed on tumor cells and are involved in tumor angiogenesis and metastasis. Boronated cyclic peptides thus have the potential to deliver ^{10}B selectively to tumor cells.

We have recently synthesized and characterized a series of compounds consisting of a tumor-targeting cyclic RGD peptide and a variety of boron moieties, as well as heavy-atom analogues for use in cell imaging by means of synchrotron X-ray fluorescence (XRF). The key results of this work will be presented.

Synthesis and evaluation of a novel liposome containing BPA-peptide conjugate for BNCT

Makoto Shirakawa[1], Tetsuya Yamamto[1], Kei Nakai[1], Kenichi Aburai[2], Sho Kawatobi[2], Takao Tsurubuchi[1],Yohei Yamamoto[1], Yuusaku Yokoyama[2], Hiroaki Okuno[2], Akira Matsumura[1]

[1] *University of Tsukuba, Graduate School of Comprehensive Human Sciences, Functional and Regulatory Medical Sciences*
[2] *Faculty of Pharmaceutical Sciences, Toho University*

Abstract

We aimed at securing sufficient concentrations of ^{10}B in BNCT by developing a new drug delivery system. We have designed and developed a novel lipid analog and succeeded in using it to develop the new boron component liposome. It consisted of three different kinds of amino acid derivatives and two fatty acids, and could react directly with the peptide synthesized first on resin by Fmoc solid-phase synthesis. In this study, lipid analog conjugated with HIV-TAT peptide (domain of human immunodeficiency virus TAT protein) and boronophenylalanine (BPA) was synthesized and successfully incorporated into liposomes.

Keywords: boron neutron capture therapy (BNCT), boron delivery system (BDS), liposome, boronophenylalanine (BPA) , HIV-TAT

1. Introduction

Boron neutron capture therapy (BNCT) is a tumor-selective radiation modality which depends on a sufficient cellular uptake of Boron (^{10}B) followed by irradiation with a beam of thermal or epithermal neutrons. ^{4}He and ^{7}Li particles are produced during the neutron capture reaction and damage DNA, which leads to cell killing. Regarding BNCT, the short radiation range of ^{4}He and ^{7}Li particles is decisive for the distribution of ^{10}B. Thus, successful treatment of cancer by BNCT requires the selective delivery of relatively large amounts of ^{10}B compound to malignant cells. The estimated boron concentration required for effective therapy is in the range of 20–30 μg ^{10}B per g tissue. However there have been no ideal boron compounds that fulfill the conditions of low toxicity, water solubility, and low distribution in normal tissue. Therefore, we aimed at securing sufficient concentrations of ^{10}B in BNCT by developing a new drug delivery system.

2. Materials and methods

2.1. Synthesis of lipopeptide

Lipopeptide conjugated with HIV-TAT peptide and boronophenylalanine (BPA) was synthesized on TGS-RAM resin by the Fmoc solid-phase synthesis method using an automatic peptide synthesizer (Shimadzu PSSM-8 Peptide Synthesizer Simultaneous Multiple) (**Figure 1**).

Tryptophan residue was added at the N-terminus of HIV-TAT peptide as a fluorescence probe. BPA was coupled arbitrarily. Then, Fmoc-AEEA (9-fluorenylmethoxycarbonyl-8-amino-3,6-dioxaoctanoic acid, linker domain), 11 Fmoc-Asp-OtBu (hydrophilic domain), and Fmoc-Dap(Fmoc)-OH (glycero mimic domain) were coupled sequentially. Benzotriazole-1-yl-oxy-tris-pyrrolidino-phosphonium hexafluorophosphate (PyBOP), N-hydroxybenzotriazole (HOBt), and N-methyl morpholine (NMM) were used, respectively, for the peptide coupling reaction with 1.0, 1.0, and 1.5 equivalents based on amino acids. Fmoc amino acid and alkyl chain were used for resin in an equivalent of the excess of 7 and 6, respectively. Each coupling reaction was carried out for 30 min. The last condensation reaction with palmitic acid was carried out in a manual mode with the reaction progress checked by a ninhydrin test. De-protection and cleavage of resin were accomplished with a cleavage cocktail (10 mg/mL of 2-methylindole containing trifluoroaceticacid /H_2O/thioanisole/1,2-ethanedithiol/ethylmethyl sulfide/phenol = 82/5/5/3/2/3) for 16 hours at room temperature, then precipitated by adding a large amount of diethyl ether. After the drying procedure, we got a purpose thing.

2.2. Preparation of liposome

The lipid mixture prepared using the constant ratio was dissolved in organic solvent. It was prepared by the

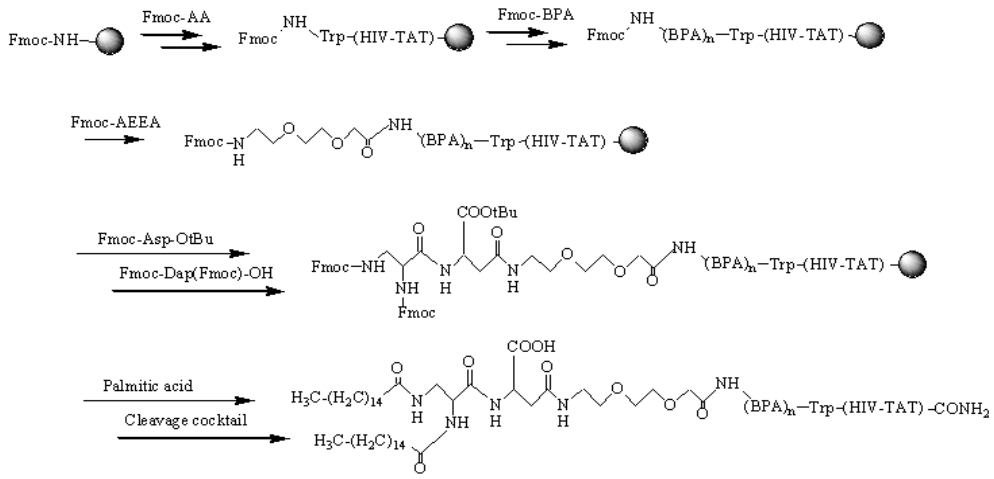

Figure 1. Synthesis of the HIV-TAT and BPA peptide conjugated lipid analog

conventional lipid-film method. The resulting liposomes were extruded through polycarbonate membrane using an extruder, yielding the peptide-modified liposome.

2.3. Gel Filtration Chromatography

The prepared liposome was subjected to size exclusion chromatography, which separated the liposome, micelle and monomolecule fractions, and the content of the lipopeptide was determined (**Figure 2**). The liposome was then measured using the fluorescence of the tryptophan residue of the lipopeptide.

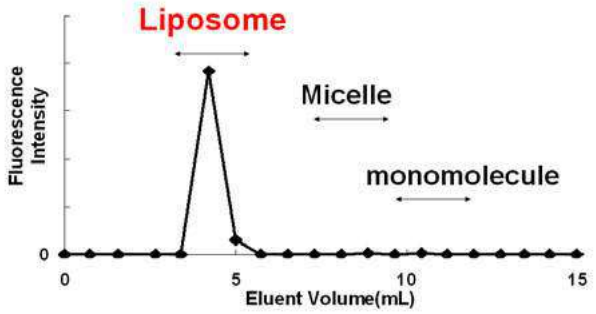

Figure 2. Gel Filtration Chromatography of liposome, micelle and monomolecule

3. Results

3.1. Identification of lipopeptide

In the case of n=5 (B5-TAT), the C8-column used for high performance liquid chromatography (HPLC) analysis showed the main peak (retention time at 13.6 min) accompanied by the existence of some impurities (**Figure 3a**). However, the synthesis of conjugated lipopeptide attached to palmitoyl chain as an anchor domain proceeded very smoothly. HPLC analysis showed almost one peak, and ESI-TOFMS (electrospray ionization mass spectroscopy) showed *m/z* 3504 of the dehydration peak as an exact mass of *m/z* 3522. In addition, ^{1}H NMR analysis (JEOL JMN-AL400) also showed the structure of the lipopeptide; for example, the molar ratio of the TAT-peptide and palmitoyl moiety showed the correct proton ratio of the ortho position on the tyrosine residue (2H as a characteristic signal of the peptide at 6.62 ppm) to the methyl signal at 0.81 ppm in the alkyl chain end (6H as a characteristic signal of the lipid) using an integration value of ^{1}H NMR spectra (**Figure 3b**). The overall yield of the lipopeptide was greater than 70% based on the molar ratio of the amino group on TGS-RAM resin.

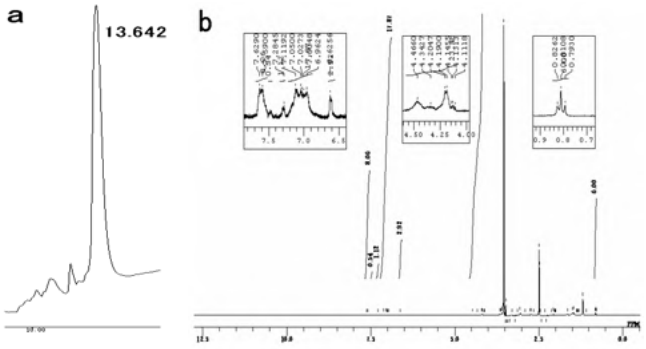

Figure 3. Identification of HIV-TAT peptide and BPA conjugated lipid analog B5-TAT. (a) C8-HPLC, (b) ^{1}H NMR

3.2. Incorporated ratio of lipopeptide

The incorporation of lipopeptide into the liposome was examined. The methods are showed in Figure 2. Synthesized lipopeptide was incorporated into the liposome effectively. The incorporated ratios of lipopeptide to liposome are summarized in Table 1.

Table.1 Liposome formation and lipopeptide incorporated into liposome

Lipopeptide	Theoretical lipopeptide ratio (mol %)	incorporated ratio (%)
B5-TAT	5	66.1
	10	73.4

4. Discussion

We synthesized a new peptide lipid containing multiple BPA components and a TAT domain for use in a boron-containing liposome which can encapsulate a boron compound in its internal water phase. The peptide lipid can be efficiently incorporated into liposomes that are 100 nm in diameter.

HIV-TAT was first developed from reverse transcriptase of HIV. It is a kind of protein transduction domain[3] which can introduce intracellular protein, deoxyribonucleic acid and macromolecular-containing liposome. *Yagi et al.* reported an *in vitro* anti-tumor effect of DOX encapsulated by TAT-modified liposome in 2007.[1] The TAT-conjugating liposome facilitated an *in vitro* gene expression as well as in vivo expression when the same liposome was locally injected[4].

Active targeting against tumor cells using TAT have been evaluated; however, there is no previous report involving a boron-containing TAT liposome or compound.

A sufficient concentration of boron is necessary for successful BNCT. Thus, a material with high boron content generally has an advantage.[2] *Nakamura et al.* developed a double-stranded boron cluster in 2004.[5] In the present study, the peptide lipid synthesized contains only 1 to 5 boron in a single molecule. However, our peptide lipid allows the number of boron to be increased up to n=12 or n=15.

In general, the hydrophilic charge of BSH in a boron-containing liposome has certain difficulty in encapsulating more BSH in the internal water phase of the liposome itself. There has been no previous report involving encapsulated BSH in the internal water phase within a boron liposome. Our peptide modification liposome of the hydrophilic charge is aspartic acid, and it shows high performance in terms of film stability and has a potential advantage in encapsulating BSH in the liposome in which the lipopeptide conjugate BPA.

Further investigation is needed to determine the *in vitro* and *in vivo* toxicity and the boron introduction efficiency.

5. Conclusions

We succeeded in synthesizing a lipopeptide containing boron. This lipopeptide could be incorporated into the liposome effectively. After toxicity testing, these liposomes will be administered to the cells or in vivo as a new BDS candidate.

Acknowledgements

This study was supported in part by a Grant-in Aid from the Ministry of Education, Science and Culture, Japan (20390379), and from the Ministry of Health, Labour and Welfare (20100201).

References

1. Yagi, N.; Yano, Y.; Hatanaka, K.; Yokoyama, Y.; Okuno, H. *Biomed. let.* **2007,** *17, 2590-2593.*

2. Maruyama, K.; Ishida, O.; Kasaoka, S.; Takizawa, T.; Utoguchi, N.; Shinohara, A.; Chiba, M.; Kobayashi, H.; Eriguchi, . *J. Controlled. Release.* **2004,** *98,195-207.*

3. Green, M.; Loewenstein, P. M., *Cell* **1998,** *55, (6), 1179-1888.*

4. Torchilin, V. P.; Levchenko, T. S.; Rammohan, R.; Volodina, N.; Papahadjopoulos-Sternberg, B.; D'Souza, G.. G.. M., *Proc. Nat1. Acad. Sci.U.S.A.* **2003,** *100, (4), 1972-1977.*

5. Lee J.-D. ; Ueno, M.; Miyajima, Y.; Nakamura, H. *Org. let.* **2007,** *9, 323-326.*

6. Wadia, J. S.; Stan, R.V.; Dowdy, S.F., *Nat. Med.* **2004,** *10, (3), 310-315*

7. Eric, L. S.; Steven, F. D., *Pharm. Res.* **2004,** *V21, (3), 389-393.*

8. Fretz, M. M.; Mastrobattista, E.; Koning, G. A.; Jiskoot, W.; Storm, G., *Int. J. Pharm.* **2005,** *298, (2), 305-309.*

9. Kageji, T.; Nagahiro, S.; Otersen, B.; Gabel, D.; Nakaichi, M.; Nakagawa, Y. *J. Neurooncol.* **2002,** *59, (2), 135-142.*

New approach to incorporation of boron in tumor-seeking molecules

Igor B. Sivaev, Andrey A. Semioshkin, Vladimir I. Bregadze

A.N.Nesmeyanov Institute of Organoelement Compounds, Russian Academy of Sciences, 28 Vavilov Str., 119991, Moscow, Russia

Abstract

Cyclic oxonium derivatives of polyhedral boron hydrides have great potential for modification of various types of tumor seeking biomolecules and are very promising starting materials for synthesis of BNCT agents.

Keywords: polyhedral boron hydrides, functionalization, cyclic oxonium derivatives, biomolecules, boron neutron capture therapy

1. Introduction

Polyhedral boron hydride anions have for a long time been considered as potential candidades for boron neutron capture therapy (BNCT) of cancer (Hawthorne, 1993). Up to recently, the main efforts of chemists working on design and synthesis of new BNCT agents were concentrated mainly on $C_2B_{10}H_{12}$. The carboranes can be easily incorporated into organic structures due to the carbon atoms which are available for "normal" organic chemistry. However their extreme lipophilicity often renders potentially bioactive structures containing these clusters water-insoluble (Soloway, 1998; Valliant, 2002). Sodium salts of polyhedral boron hydrides promise well water solubility of BNCT agents on their base, however some complicated chemistry of polyhedral boron hydride anions and absence of convenient ways of their functionalization were the deterrent factors (Sivaev, 2002a). Solution of this problem was found relatively recently when chemistry of cyclic oxonium derivatives of boron hydrides was developed (Semioshkin, 2008).

2. Cyclic oxonium derivatives of polyhedral boron hydrides: synthsis and ring opening

Preparation of the first oxonium derivatives of polyhedral boron hydrides was reported almost 40 years ago (Young, 1969). General approach to their synthesis consists in abstraction of hydride under the treatment with Lewis or Brönsted acids resulting in formation of a carbocation-like centre on the boron atom, which is then subjected to the attack of ether solvent as nucleophile resulting in the corresponding cyclic oxonium derivatives (Fig. 1).

During the last decade, effective methods of synthesis of cyclic oxonium derivatives of the main polyhedral boron hydrides, such as *closo*-dodecaborate $[B_{12}H_{12}]^{2-}$ (Sivaev, 2000; Sivaev, 2008), *closo*-decaborate $[B_{10}H_{10}]^{2-}$ (Bernard, 2004; Zhizhin, 2004), cobalt bis(dicarbollide) $[3,3'\text{-}Co(1,2\text{-}C_2B_9H_{11})_2]^-$ (Plešek, 1997; Teixidor, 2003), 7,8-dicarba-*nido*-undecaborate $[7,8\text{-}C_2B_9H_{12}]^-$ (Zakharkin, 1979; Stogniy, 2007), were elaborated.

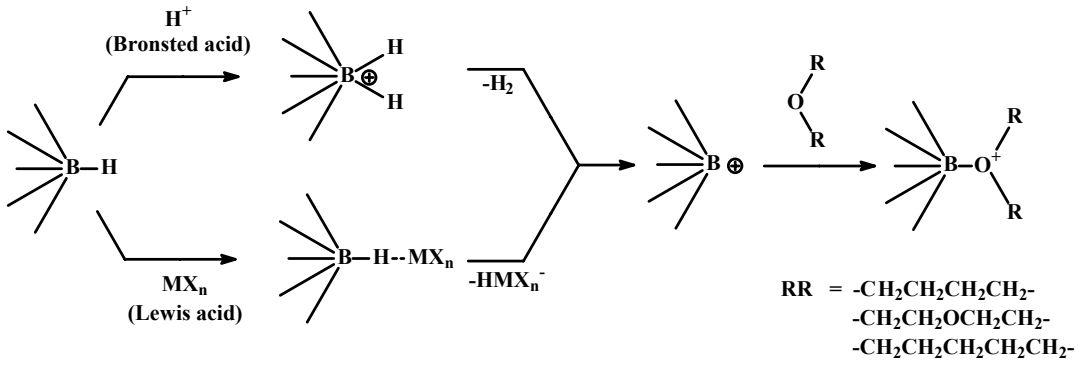

Fig. 1. General scheme of formation of cyclic oxonum derivatives of polyhedral boron hydrides

Trialkyloxonium salts are widely used in organic synthesis as powerful alkylating agents. Despite higher stability of oxonium derivatives of boron hydrides, it was reasonable to suppose that they also could act as alkylating agents. This is especially attractive for the cyclic oxonium derivatives, where breaking one carbon–oxygen bond should result in a moiety having a boron cluster separated from the former carbocationic center by spacer of 4–5 atoms (Fig. 2). In such a way, molecules with a reasonable length spacer between boron cage and property-determining part of molecule could be prepared. Moreover, hydrophilic/lipophilic nature of the spacer can be affected by proper choice of the initial substituent. Thus, the ring-opening of the tetrahydrofuran- and tetrahydropyrane-based derivatives produce compounds with lipophilic spacers between boron cage and bioactive part of molecule, whereas the 1,4-dioxane ring opening with *O*-nucleophiles gives compounds with the -$(CH_2CH_2O)_2$- spacer that can be considered as oligo(ethylene glycol) fragment with reasonable number of ethylene glycol units. Oligo- and poly-(ethylene glycol) fragments are widely used as covalent modifiers of biological macromolecules as well as linkers for preparing bioconjugates with various biologically relevant molecules. In this connection it is rather surprising that active use of this type of compounds in synthesis started only 30 years after they had been prepared for the first time.

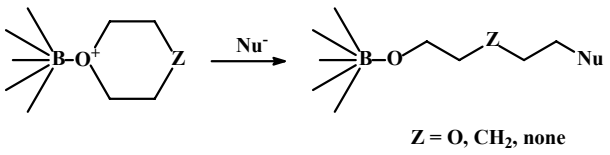

Fig. 2. General scheme of the oxonium ring disclosure in boron hydride derivatives

3. Synthesis of boron-containing biomolecules

In 2000 nucleophilic ring-opening of cyclic oxonium derivatives of *closo*-dodecaborate was proposed to be a new synthetic methodology for the preparation of wide spectrum of its functional derivatives (Sivaev, 2000). Quite soon this methodology was applied to synthesis of functional derivatives of cobalt bis(dicarbollide) (Sivaev, 2002b), *closo*-decaborate (Bernard, 2004), 7,8-dicarba-*nido*-undecaborate (Stogniy, 2007) and some other anionic boron hydrides. At present, this approach is widely used by several research groups for functionalization of different types of polyhedral boron hydrides as well as their attachment to various bioorganic molecules.

There are two different strategies for preparation of boronated biomolecules using cyclic oxonium derivatives of polyhedral boron hydrides. The first one is based on direct reaction of cyclic oxonium derivatives with nucleophilic sites of biomolecules. This strategy was successfully applied to synthesis of boron-containing porphyrins (Hao, 2005; Sibrian-Vazquez, 2006; Hao, 2007) (Fig.3), phthalocyanines (Semioshkin, 2006), and coumarins (Justus, 2007). However, in the case of biomolecules having several nucleophilic sites of close reactivity, such as nucleosides, this strategy can result in mixtures of the ring-opening products (Olejniczak, 2003; Lesnikowski, 2005; Olejniczak, 2007).

The second strategy is based on two step synthesis. The first step is synthesis of polyhedral boron hydride derivatives with various functional groups, whereas the second step is their conjugation with biomolecules using standard methods of organic/bioorganic chemistry. At present, a wide spectrum of polyhedral boron derivatives containing terminal amino (Sivaev, 2000; Sivaev, 2002b; Semioshkin, 2007a), carboxylic (Sivaev, 2000; Grin, 2007; Stogniy, 2007), amino acid (Sivaev, 2000; Sivaev, 2002b), azido (Orlova, 2007), and acetylenic (Semioshkin, 2007b; Sivaev, 2008) functional groups were prepared.

Some of these derivatives were used for preparation of boron-containing porphyrins (Grin, 2007) and carbohydrates (Orlova, 2006) (Fig.4).

4. Conclusions

Cyclic oxonium derivatives of polyhedral boron hydrides are easily available and very promising starting materials for synthesis of various boron-containing biomolecules for boron neutron capture therapy.

Acknowledgements

The authors thank the Russian Foundation for Basic Research (08-03-00463) for financial support.

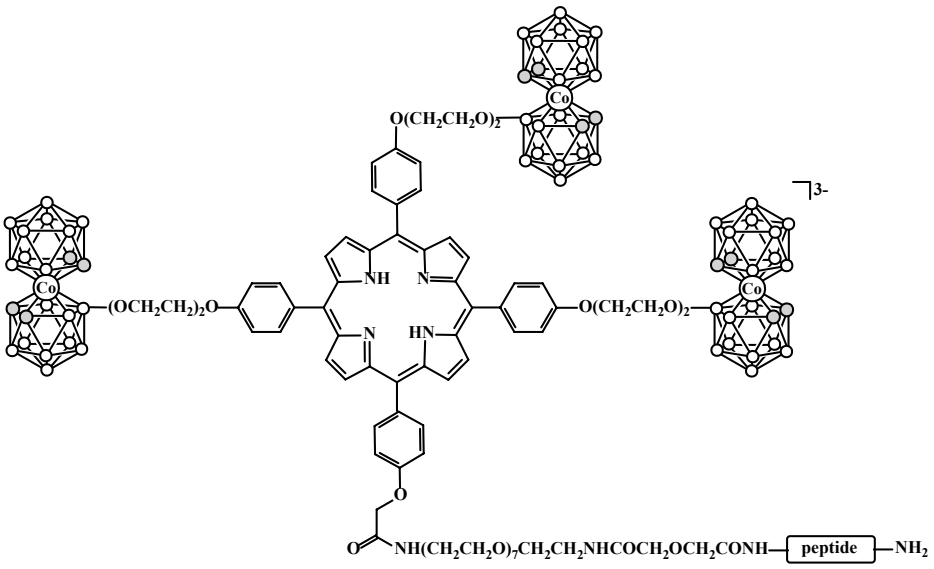

Fig.3. Boron-containing porphyrin-peptide conjugate

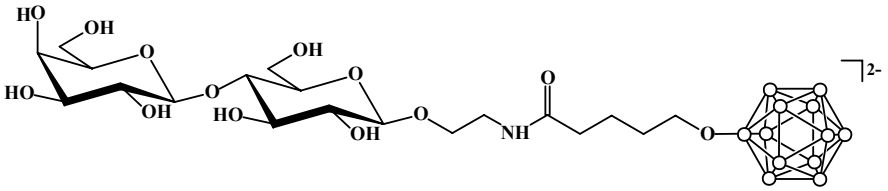

Fig.4. Boron-containing carbohydrate

References

Bernard, R., Cornu, D., Perrin, M., Schaff, J.-P., Miele, P, 2004. Synthesis and X-ray structual characterisation of the tetrametylene oxonium derivative of the hydrodecaborate anion. A versatile route for derivative chemistry of $[B_{10}H_{10}]^{2-}$. J. Organomet. Chem. 689, 2581-2585.

Grin, M.A., Semioshkin, A.A., Titeev, R.A., Nizhnik, E.A., Grebenyuk, J.N., Mironov, A.F., Bregadze, V.I., 2007. Synthesis of a cycloimide bacteriochlorin *p* conjugate with the *closo*-dodecaborate anion. Mendeleev Commun. 17, 14-15.

Hao, E., Jensen, T.J., Courtney, B.H., Vicente, M.G.H., 2005. Synthesis and cellular studies of porphyrin-cobaltacarborane conjugates. Biooconjugate Chem. 16, 1495-1502.

Hao, E., Sibrian-Vazquez, M., Serem, W., Garno, J.C., Fronczek, F.R., Vicente, M.G.H., 2007. Synthesis, aggregation and cellular investigations of porphyrin-cobaltacarborane conjugates. Chem. Eur. J. 13, 9035-9047.

Hawthorne, M.F., 1993. The role of chemistry in the development of boron neutron capture therapy of cancer. Angew. Chem. Int. Ed. Engl. 32, 950-984.

Justus, E., Izteleuova, D.T., Kazantsev, A.V., Axartov, M.M., Lork, E., Gabel, D., 2007. Preparation of carboranyl and dodecaborate derivatives of coumarin. Collect. Czech. Chem. Commun. 72, 1740-1754.

Lesnikowski, Z.J., Paradowska, E., Olejniczak, A.B., Studzinska, M., Seekamp, P., Schüßler, U., Gabel, D., Schinazi, R.F., Plešek, J., 2005. Toward new boron carriers for boron neutron capture therapy: metallacarboranes and their nucleoside conjugates. Bioorg. Med. Chem. 13, 4168-4175.

Olejniczak, A.B., Plešek, J., Křiž, O., Lesnikowski, Z.J., 2003. A Nucleoside conjugate containing a metallacarborane group and its incorporation into a DNA oligonucleotide. Angew. Chem. Int. Ed. 42, 5740-5743.

Olejniczak, A.B., Plešek, J., Lesnikowski, Z.J., 2007. Nucleoside-metallacarborane conjugates for base-specific metal labeling of DNA. Chem. Eur. J. 13, 311-318.

Orlova, A.V., Kondakov, N.N., Zinin, A.I., Kimel,

B.G., Kononov, L.O., Sivaev, I.B., Bregadze, V.I., 2006. A uniform approach to the synthesis of carbohydrate conjugates of polyhedral boron compounds as potential agents for boron neutron capture therapy. Russ. J. Bioorg. Chem. 32, 568-577.

Orlova, A.V., Kondakov, N.N., Kimel, B.G., Kononov, L.O., Kononova, E.G., Sivaev, I.B., Bregadze V.I., 2007. Synthesis of novel derivatives of *closo*-dodecaborate anion with azido group at the terminal position of the spacer. J. Appl. Organomet. Chem. 21, 98-100.

Plešek, J., Heřmanek, S., Franken, A., Cisarova, I., Nachtigal, C., 1997. Dimethyl sulfate induced nucleophilic substitution of the [bis(1,2-dicarbollido)-3-cobalt(1-)]ate ion. Syntheses, properties and structures of its 8,8'-μ-sulfato, 8-phenyl and 8-dioxane derivatives. Collect. Czech. Chem. Commun. 62, 47-56.

Semioshkin, A., Tsaryova, O., Zhidkova, O., Bregadze, V., Wöhrle, D., 2006. Reactions of oxonium derivatives of $[B_{12}H_{12}]^{2-}$ with phenols, and synthesis and photochemical properties of a phthalocyanine containing four $[B_{12}H_{12}]^{2-}$ groups. J. Porphyrins Phthalocyanines 10, 1293-1300.

Semioshkin, A., Nizhnik, E., Godovikov, I., Starikova, Z., Bregadze, V., 2007a. Reactions of oxonium derivatives of $[B_{12}H_{12}]^{2-}$ with amines: Synthesis and structure of novel B_{12}-based ammonium salts and amino acids. J. Organomet. Chem. 692, 4020-4028.

Semioshkin, A.A., Osipov, S.N., Grebenyuk, J.N., Nizhnik, E.A., Godovikov, I.A., Shchetnikov, G.T., Bregadze, V.I., 2007b. An effective approach to 1,2,3-triazole-containing *closo*-dodecaborates. Collect. Czech. Chem. Commun. 72, 1717-1724.

Semioshkin, A.A., Sivaev, I.B., Bregadze, V.I., 2008. Cyclic oxonium derivatives of polyhedral boron hydrides and their synthetic applications**.** Dalton Trans. 977-992.

Sibrian-Vazquez, M., Hao, E., Jensen, Vicente, M.G.H., 2006. Enhanced cellular uptake with a cobaltacarborane-porphyrin-HIV-1 Tat 48-60 conjugate. Biooconjugate Chem. 17, 928-934.

Sivaev, I.B., Semioshkin, A.A., Brellochs, B., Sjöberg, S., Bregadze, V.I., 2000. Synthesis of oxonium derivatives of the dodecahydro-*closo*-dodecaborate anion $[B_{12}H_{12}]^{2-}$. Tetramethylene oxonium derivative of $[B_{12}H_{12}]^{2-}$ as a convenient precursor for the synthesis of functional compounds for boron neutron capture therapy. Polyhedron 19, 627-632.

Sivaev, I.B., Bregadze, V.I., Kuznetsov, N.T., 2002a. Derivatives of the *closo*-Dodecaborate Anion in Their Application in Medicine. Russ. Chem. Bull. 51, 1362-1374.

Sivaev, I.B., Starikova, Z.A., Sjöberg, S., Bregadze, V.I., 2002b. Synthesis of functional derivatives of $[3,3'\text{-}Co(1,2\text{-}C_2B_9H_{11})_2]^-$ anion. J. Organomet. Chem. 649, 1-8.

Sivaev, I.B., Kulikova, N.Yu., Nizhnik, E.A., Vichuzhanin, M.V., Starikova, Z.A., Semioshkin, A.A., Bregadze, V.I., 2008. Practical synthesis of 1,4-dioxane derivative of the *closo*-dodecaborate anion and its ring opening with acetylenic alkoxides. J. Organomet. Chem. 693, 519-525.

Soloway, A.H., Tjarks, W., Barnum, B.A., Rong, F.-G., Barth, R.F., Codogni, I.M., Wilson, J.G., 1998. The chemistry of neutron capture therapy. Chem. Rev. 98, 1515-1562.

Stogniy, M.Yu., Abramova, E.N., Lobanova, I.A., Sivaev, I.B., Bragin, V.I., Petrovskii, P.V., Tsupreva, V.N., Sorokina, O.V., Bregadze, V.I., 2007. Synthesis of functional derivatives of 7,8-dicarba-*nido*-undecaborate anion by ring-opening of its cyclic oxonium derivatives. Collect. Czech. Chem. Commun. 72, 1676-1688.

Teixidor, F., Pedrajas, J., Rojo, I., Viñas, C., Kivekäs, R., Sillanpää, R., Sivaev, I., Bregadze, V., Sjöberg, S., 2003. Chameleonic capacity of $[3,3'\text{-}Co(1,2\text{-}C_2B_9H_{11})_2]^-$ in coordination. Generation of the highly uncommon S(thioether)-Na bond. Organometallics 22, 3414-3423.

Valliant, J.F., Guenther, K.J., King, A.S., Morel, P., Schaffer, P., Sogbein, O.O., Stephenson, K.A., 2002. The medicinal chemistry of carboranes. Coord. Chem. Rev. 232, 173-230.

Young, D.C., Howe, D.V., Hawthorne, M.F., 1969. Ligand derivatives of (3)-1,2-dicarbadodecahydro-undecaborate(1-). J. Am. Chem. Soc. 91, 859–862.

Zakharkin, L.I., Kalinin, V.N., Zhigareva, V.V., 1979. Oxidation of dicarbadodecahydro-*nido*-undecaborate anions by mercuric chloride in tetrahydrofuran and pyridine. Russ. Chem. Bull. 28, 2198–2199.

Zhizhin, K.Yu., Mustyatsa, V.N., Malinina, E.A., Votinova, N.A., Matveev, E.Yu., Goeva, L.V., Polyakova, I.N., Kuznetsov, N.T., 2004. Interaction of *closo*-decaborate anion $B_{10}H_{10}^{2-}$ with cyclic ethers. Russ. J. Inorg. Chem. 49, 180-189.

Boron compound delivery to oral squamous cell carcinoma cells using transferrinconjugated PEG-liposomes

T.Shimahara[a], Y.Ito[a], Y.Ariyoshi[a], Y.Kimura[a], M.Shimahara[a], S.Miyatake[b], S.Kawabata[b], S.Kasaoka[c], K.Ono[d]

[a] *Department of Dentistry and Oral Surgery, Osaka Medical College, Japan*
[b] *Department of Neurosurgery, Osaka Medical College, Japan*
[c] *Faculty of Pharmaceutical Sciences,Hiroshima-International University, Japan*
[d] *Particle Radiation Oncology Research Center,Research Reactor Institute, Kyoto University, Japan*

Abstract

To improve outcomes of boron neutron capture therapy(BNCT), it is critical to selectively deliver boron and increase the absolute value of boron concentration in the tumor. It is pertinent to deliver as much boron compound as possible within the tumor cells. We conducted this study using a drug in which borocaptate sodium (BSH) is encapsulated in transferrin(TF) targeting polyethylene glycol(PEG)-coated liposomes. Our results showed the uptake of ^{10}B over time when delivered by TF-PEG-liposome(BSH) to oral squamous cell carcinoma cells *in vitro*, in comparison with PEG-liposome(BSH) or liposome(BSH) or bare BSH. Findings also indicated that ^{10}B remained in the tumor cells *in vitro* for an extended period of time. Study findings suggest the efficacy of TF-PEG-liposome as a drug carrier and the possibility of improving treatment outcomes of BNCT in the future.

Keywords:Boron neutron capture therapy,liposome,transferring receptor,oral squamous cell carcinoma

1. Introduction

In recent years, advances in medical technology have improved the prognosis for patients with malignant oral tumors. Unfortunately, regular cancer treatment is still unable to control many types of malignant tumors. In a previous study, we reported relatively favorable outcomes after treating five cases of head and neck malignancies, uncontrollable by regular cancer treatment, with boron neutron capture therapy (BNCT)(Ariyoshi et al., 2007).

Borocaptate sodium (BSH) is a boron compound currently used for BNCT(Barth et al., 1992). For this therapy, it is crucial that a high concentration of boron compounds selectively accumulate in tumors, avoidings much as possible accumulation in normal tissues surrounding the tumor prior to neutron irradiation. These conditions are difficult to achieve using the current protocol, whereby a highly concentrated BSH solution is administered intravenously for long periods of time to maintain required concentration in cancer tissues. In order to develop drug delivery system (DDS) technologies for delivering boron compounds to target cancer cells, it is imperative to improve our understanding of potential ways to enclose such drugs in a tissue-selective carrier.

Liposomes were first discovered by Bangham in 1965, and their application as a DDS carrier has been studied widely. Liposomes are ideal drug carriers due to their ability to encapsulate high doses of drugs, their tissue-selectivity, and because they can protect the drugs from potential destruction by the body's immune system. One disadvantage is that liposomes have a tendency to accumulate in the reticuloendothelial systems (RES) of the liver or spleen. Coating liposomal surfaces with polyethylene glycol (PEG) can prevent the accumulation in the RES and thereby enable prolonged retention in the blood.

An effective way of targeting drugs to specific cell types is to conjugate the drugs of interest to

cell-specific receptor ligands or antibodies targeted against these receptors. One of such ligands that is currently of interest is transferrin (TF)(Maruyama et al., 2004) TF is found widely in serum and extracellular fluid, and is an iron-binding protein that supplies iron to cells through TF receptors(Wagner et al., 1994). Relative to normal cells, cancer cells overexpress TF receptors on their cell surface, and thus, conjugation of TF to liposomes should allow for active targeting of these tumor cells. We hypothesize that utilizing TF-PEG-liposome (BSH) would result in selective accumulation of this boron compound in cancer cells. Here, we test this hypothesis by examining *in vitro* TF-PEG-liposome (BSH) delivery to oral squamous cell carcinoma cells.

2. Materials and Methods

Cell culture

SAS cells from a human oral squamous cell carcinoma-derived cell line (HSRRB) were used for this study. Cells were cultured in medium containing 45 % DMEM (Dulbecco's Modified Eagle's Medium, GIBCO), 45 % F-12 (Ham's F12 medium, GIBCO), 10 % FBS (Fetal Bovine Serum, GIBCO), and antibiotics (hereafter DMEM/F12) and incubated in 5 % CO_2 at 37℃. Trypsin-EDTA (0.25 % Trypsin, 1mM EDTA · 4Na, GIBCO) and DPBS (Dulbecco's Phosphate-Buffered Saline, GIBCO) were used to subculture cells. DMEM/F12 without FBS (hereafter DMEM/F12(-FBS)) was used for washing cells. SAS cells were cultured in 6-well plates and used for experiments in the subconfluent stage.

Cellular uptake of boron compounds over time

SAS cells were cultured in media containing one of four different boron compounds: BSH, liposome (BSH), PEG-liposome (BSH), and TF-PEG-liposome (BSH). The amount of boron compounds taken up by cells was determined over different culture periods. Boron concentrations were adjusted to 30 μg ^{10}B/ ml in the culture media (DMEM/F12(-FBS)).

Culture media was removed from the subconfluent 6-well plates, and wells were washed with DMEM/F12(-FBS). The cells were then cultured in the media containing the different boron compounds. Culture media was removed after 1, 3, 6, 12, and 24 hours and cells were washed twice with 4°C DMEM/F12(-FBS). To detach cells, 2 ml of Trypsin was applied, and 2 ml of DMEM/F12(-FBS) was added to harvest the cells. After adding 0.5 ml of nitric acid to the cell-containing solutions, boron concentrations were measured by inductively coupled plasma-atomic emission spectrometry (ICP-AES).

Cellular uptake of the boron compounds upon transferrin (TF) receptor inhibition

To examine the involvement of TF receptors in the uptake of TF-PEG-liposome (BSH) into SAS cells, we used culture media (30 μg ^{10}B/ ml) containing free TF (500 μg) and one of two different boron compounds: PEG-liposome (BSH) or TF-PEG-liposome (BSH). Cells were therefore cultured in four different variations of culture media: PEG-liposome (BSH), PEG-liposome (BSH) + free TF, TF-PEG-liposome (BSH), and TF-PEG liposome (BSH) + free TF. After 6 hours of incubation in these solutions, cells were harvested and the concentration of cellular boron uptake was measured.

Retention of boron compounds in cells

SAS cells were cultured for 24 hours in four different types of culture media containing 30 μg ^{10}B/ ml. The culture media was removed after 24 hours, and cells were washed with DMEM/F12(-FBS). Cells were then cultured in DMEM/F12 without boron compounds, and harvested after 1, 3, 6, and 24 hours. Boron concentrations were measured at each time point to assess the retention capacity of these compounds in SAS cells.

Measuring boron concentrations

Inductively Coupled Plasma-Atomic Emission Spectrometry was used to measure boron concentrations using a P-5200 ICP dual monochromater system (Hitachi, Ltd.). Boron concentrations in sample solutions were determined according to a calibration curve after measuring the emission intensity by ICP-AES. These were calculated as the mass of boron per 10^6 SAS cells (ng/ 10^6cells).

3. Results

Cellular uptake of the boron compounds over time

Cellular uptake of all four boron compounds increased over time. However, a concentration of 40 ng/ 10^6 cells was attained in 1 hour by TF-PEG-liposome (BSH), while other compounds required 3 hours to reach the same concentration. Cellular uptake of TF-PEG-liposome (BSH) after 24 hours was 100ng/10^6cells, while the uptake of other compounds at this time point yielded concentrations of 40 to 60 ng/ 10^6cells, an amount significantly less than that attained with TF-PEG-liposome (BSH) even after 6 hours (Figure 1).

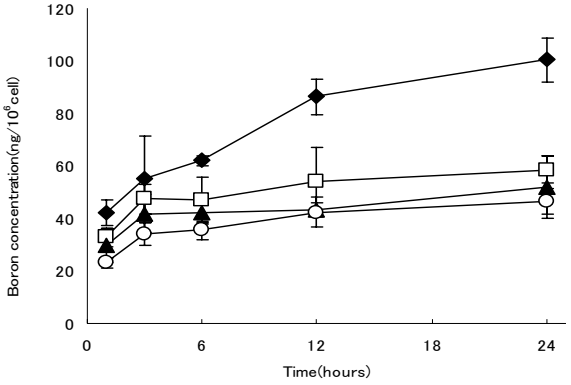

(Figure 1) (◆:TF-PEG-liposome(BSH),□ : PEG-liposome(BSH), ▲ : Liposome(BSH),○: BSH)

Cellular uptake of the boron compounds upon transferrin (TF) receptor

After 6 hours, boron concentrations were 62 ng/ 10^6cells for the TF-PEG-liposome (BSH) group, but significantly lower (39 ng/ 10^6cells) for the TF-PEG-liposome (BSH) + free TF group. No significant difference in uptake was observed between the PEG-liposome (BSH) group (36 ng/ 10^6cells) and the PEG-liposome (BSH) + free TF group (35 ng / 10^6 cells) (Figure 2).

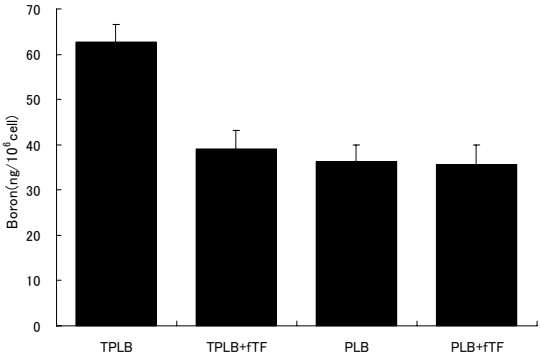

(Figure 2) (TPLB: TF-PEG-liposome(BSH), PLB: PEG-liposome(BSH), fTF:free transferrin)

Retention of the boron compounds after uptake

After culturing for 24 hours in media containing one of four different boron compounds, cellular uptake was 47 ng/ 10^6 cells for BSH , 54 ng/ 10^6 cells for liposome (BSH), 59 ng/ 10^6 cells for PEG-liposome (BSH), and 85 ng/ 10^6 cells for TF-PEG-liposome (BSH). When the original culture medium was replaced with boron-free medium, cellular boron concentration significantly decreased to half of the initial concentration after 1 hour. This was observed in the BSH, liposome (BSH), and PEG-liposome (BSH) treatments. Marked decreases in cellular boron concentrations were not observed after that.

After 24 hours, retention was low for boron compounds not conjugated to a transferrin receptor: 8 ng/ 10^6 cells for BSH, 18 ng/ 10^6 cells for liposome (BSH), and 19 ng/ 10^6 cells for PEG-liposome (BSH). The uptake for TF-PEG-liposome (BSH), on the other hand, decreased to 47 ng/ 10^6 cells after 1 hour, did not change for 6 hours after that, and maintained a high concentration (30 ng/ 10^6 cells) even after 24 hours (Figure 3).

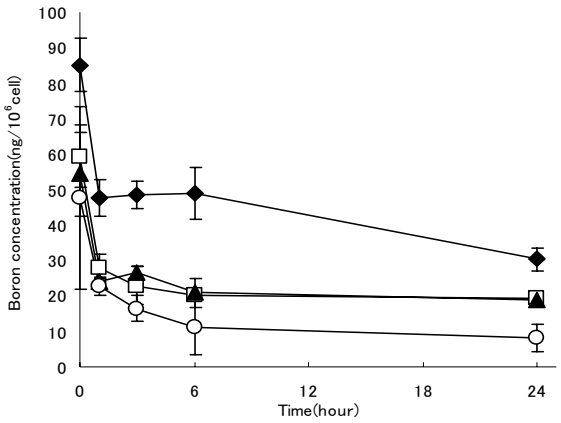

(Figure 3) (◆:TF-PEG-liposome(BSH),□ : PEG-liposome(BSH), ▲ : Liposome(BSH), ○ : BSH)

4. Discussion

While the utility of TF-PEG-liposomes has been studied and assessed by many others(Doi et al., 2008), the application of this knowledge to treat oral cancer has not been reported. Our objective here was to test whether TF-PEG-liposomes could be used effectively to deliver BSH specifically to oral squamous carcinoma cells, and whether the retention of BSH would be sufficient to utilize this method in BNCT.

We found strong evidence to support the idea that the presence of the transferrin receptor allows for increased boron uptake over time. A comparison of cellular uptake of four different boron compounds over time revealed that uptake was increased for TF-PEG-liposome (BSH), and that this uptake was 1.5 to 2 times higher than the 3 other compounds examined (BSH, liposome (BSH), and PEG-liposome (BSH)).

Measuring cellular uptake after TF receptor inhibition allowed us to specifically test the role of the TF receptor in this process. A comparison of uptake of two different boron compounds, PEG-liposome (BSH) and TF-PEG-liposome (BSH), revealed that after the TF receptor was inhibited, no changes occurred in the uptake of PEG-liposome (BSH), but a clear decrease in uptake of TF-PEG-liposome (BSH) was observed. This implies that TF receptors expressed on the surface of SAS cells are the target molecules for TF-PEG-liposome (BSH).

A high retention time of boron compounds in tumor cells is a requirement for the use of ~~if~~ these compounds in BNCT. Although the amount of TF-PEG-liposome (BSH) remaining in cells decreased to approximately one half of the initial amount 1 hour after uptake, this amount did not change for 6 hours. Moreover, after 24 hours, the amount of TF-PEG-liposome (BSH) was 1.5 to 3 times higher than cells treated with the other boron compounds.

By testing *in vitro* the efficacy of TF-PEG-liposome (BSH) to selectively accumulate in oral squamous carcinoma cells, we conclude that TF-PEG-liposome (BSH) is indeed capable of selectively accumulating in tumor cells, and can do so in high concentrations. The tissue-selectivity as well as the ability to remain at high concentrations in cells are both highly necessary characteristics for boron compounds administered in BNCT. We expect that our findings will help to establish a foundation for future *in vivo* studies as well as clinical application.

References

Ariyoshi, Y., Miyatake, S., Kimura, Y., et al, 2007. Boron neutron capture therapy using epithermal neutrons for recurrent cancer in the oral cavity and cervical lymph node metastasis. Oncol. Rep.18,861-866.

Barth, R. F., Soloway, A. H., Fairchild, R. G., et al, 1992. Boron neutron Capture therapy for cancer. Realities and prospects. Cancer. 70, 2995-3007.

Doi, A., Kawabata, S., Iida K., et al, 2008. Tumor-specific targeting of Sodium borocaptate(BSH) to malignant glioma by transferring-PEG liposome: a modality for boron neutron capture therapy. J Neurooncol. 87, 287-294.

Maruyama, K. ,Ishida, O., Kasaoka, S., et al, 2004. Intracellular Targeting of sodium mercapto-undecahydrododecaborate (BSH) to solid tumors by transferring-PEG liposomes,for boron neutron-capture therapy(BNCT). J. Control. Release. 98, 195-207.

Wagner, E., Curiel, D., Cotton, M., 1994. Delivery of drugs, proteins and genes into cells using transferring as a ligand for receptor-mediated endocytosis. Advanced Drug DeliveryReviews. 14, 113- 135.

Enhancement of *p*-Boronophenylalanine Uptake into Subcutaneous Rat Gliosarcomas: Synergy of Benserazide and L-dopa

Lothar E. Weissfloch [a, c], Marta M. Nawrocky [a], Karlheinz Tempel [b], Daniel N. Slatkin [a]

[a] *Medical Department, BNL, Upton, NY 11973, USA,* [b] *Faculty of Veterinary Medicine, University of Munich, 80539 Munich, Germany,* [c] *KLIFOVET AG, 80689 Munich, Germany (present affiliation)*

In Memoriam
Georg Weissfloch
Nov 16, 1928 – Dec 30, 2000

Abstract

A synthetic, boronated analogue of tyrosine, *p*-boronophenylalanine (BPA), selectively accumulates in certain malignant neoplasms, including human glioblastoma multiforme and rat 9L gliosarcoma (9LGS). BPA is used as a boron-10 delivery agent in clinical trials of boron neutron-capture therapy (BNCT). 9LGS cells exposed to levo-dopa (L-dopa) *in vitro* show increased avidity for BPA thereafter. Since L-dopa is rapidly catabolized by dopa decarboxylase, we exposed the rats to the decarboxylase inhibitor benserazide prior to L-dopa to test enhancement of BPA uptake into rat brain 9LGS tumors *in vivo*. Benserazide and L-dopa were injected i.p. sequentially before i.p. administration of BPA into male Fisher 344 rats bearing subcutaneous 9LGS gliosarcomas. Boron concentrations were measured in tumors and blood sampled over a 4 h period after BPA-injection. Pretreated tumors accumulated boron at average concentrations of 69.3 ± 7.6 mg/g 2 h and 80.1 ± 9.1 mg/g 3 h after BPA injection, boron enhancements of 50% ($p = 0.001$) and 65% ($p < 0.001$), respectively, when compared to non-pretreated tumors at the same time points. Analogous pretreatment should be tested as a possible enhancer of boron uptake from BPA into more malignant rat gliomas *in vivo*.

Key words: 9L gliosarcoma, benserazide, BNCT, BPA, L-dopa

1. Introduction

The short range of BNCT particles restricts most of the dose to the boron-loaded cells, selective accumulation of the boron delivery agent in tumor cells and vasculature is key to BNCT, thus (1, 2). The boronated analogue of the neutral amino acid tyrosine, *p*-boronophenylalanine (BPA), has been tested as a delivery agent for BNCT. It has been shown that BPA is taken up preferentially by glioma cells (3). Wittig et al. have shown that BPA accumulation can be doubled in vitro by preloading tumor cells with levo-dopa (L-dopa) (4).

In higher organisms, L-dopa is rapidly catabolized outside cells by dopa decarboxylase to L-dopamine, which neither enters cells nor influences BPA uptake into cells (5). L-dopa administered with a dopa decarboxylase inhibitor like Benserazide yields higher BPA levels in plasma and brain than L-dopa alone (6, 7). Benserazide is already being used to modify the pharmacokinetic properties of L-dopa in patients with Parkinson's disease. The object of the present translational study is to increase the amount of BPA delivered to rat 9LGS tumors through L-dopa preloading assisted by Benserazide. This paper describes the biodistribution of boron in 9LGS-bearing rats following intraperitoneal (i.p.) application of BPA after injections of Benserazide and L-dopa.

2. Materials and Methods

Immunocompetent male Fisher 344 rats of 10 to 12 weeks of age and 260 to 290 g body weight (bw) were used. To initiate subcutaneous (s.c.) tumors, the rats were anesthetized by i.p. injection of 0.1 mL/100 g bw of a mixture of 20 mg Xylazine and 120 mg Ketamine per mL. followed by s.c. injection of ~2.5 x 10^6 9LGS-cells suspended in 0.1 mL of DMEM into four dorsolateral body sites on each rat. BPA containing boron with the natural-abundance boron-10/boron-11 ratio was used. BPA as the pure L-

enantiomer was dissolved in 0.9% NaCl as the fructose complex (BPA-F) at 55 mg BPA/mL and was

administered as a single ~4 mL i.p. injection to deliver 1,000 mg BPA/kg bw. Benserazide was dissolved in 0.9% NaCl to a concentration of 30 mg/mL; the animals received ~0.5 mL of this solution i.p., thus ~50 mg Benserazide per kg bw. To dissolve 10 mg L-dopa per mL physiological saline, 10Vol-% Cremophor EL and 20Vol-% propylene glycol were added as detergents; this mixture was administered to each rat as a single ~3 mL i.p. injection sized to deliver 100 mg/kg bw. Solutions of Benserazide and L-dopa were prepared just before use to minimize oxidation.

Primary Experiment

Administration of BPA, Benserazide, and L-dopa was performed 10 days after tumor inoculation. Rats bearing tumors initially received 50 mg Benserazide per kg bw i.p, followed by 100 mg L-dopa per kg bw i.p. 30 minutes later. Another sixty minutes later, BPA-F was given in one i.p. injection of 1,000 mg BPA/kg bw. Blood and tumor were sampled at four 1-hr intervals starting one hour after the BPA-F-injection, one blood sample and one tumor being acquired at each time point. Under short-term gas anesthesia blood samples were taken from the venous retro-orbital sinus, and each tumor was removed aseptically. Nine rats received drugs according to the schedule described above; seven rats with identically-induced 9LGS tumors served as controls, which received 0.9% NaCl instead of Benserazide and L-dopa at same volume.

Control Experiment

Since Cremophor EL is known to influence other drugs' pharmacokinetics (8-10), a control experiment with three arms of four rats each was carried out. All 12 of the rats in the control experiment bore 9LGS tumors induced as in the primary experiment. In Arm I, instead of Benserazide and L-dopa, similar volumes of 0,9% NaCl were injected i.p. when these drugs would have been administered at 0 min and 30 min as per the protocol described above; BPA was given i.p. at 90 min at the regular dose rate of 1000 mg BPA/kg bw. In Arm II, instead of Benserazide, an equal amount of 0.9% NaCl was given for the first injection. The second drug injection contained 10% Cremophor by volume, only (no L-dopa) and BPA was given at the regular dose rate of 1000 mg BPA/kg bw. as third injection. In Arm III, rats received Benserazide (first injection), Cremophor and L-dopa (second injection), and BPA (third injection). Blood and tumor sampling were performed for all three arms as done in the primary experiment. This control experiment was intended to distinguish the potential pharmacokinetic property of Cremophor, determining the degree of influence on BPA uptake of Cremophor alone (Arm II) vs. that of Benserazide with L-dopa and Cremophor (Arm III). Both DCP-AES (11, 12) and neutron-induced prompt-γ spectrometry (13, 14) were used for boron determinations at BNL.

Calculation of average values for boron of tumor and blood, means, standard deviations, and paired *t*-tests was done with SigmaPlot 2000™ Graphics and Statistics Program. Statistical significance was set at $p < 0.05$.

3. Results

Primary Experiment

At 1, 2, 3, and 4 h after BPA injection, analysis of samples revealed higher boron concentrations in tumor and blood from Benserazide/L-dopa–treated rats than in those from controls receiving only BPA .

Figure 1: Boron uptake in treated and untreated rats

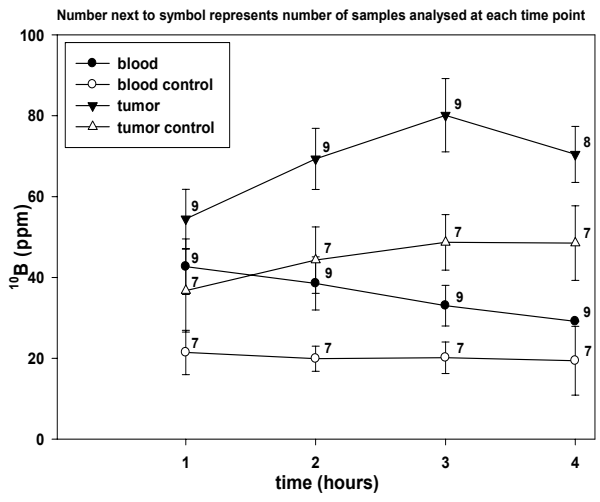

The differences were statistically significant in all cases. Boron in treated tumors accumulated from 1 h to 3 h and declined at 4 h, but at all times exceeded the concentration in untreated tumors ($p \leq 0.01$). Over the 4-hour sampling period, boron in treated rats' blood continuously decreased from 42.7 ± 6.9 ppm at 1 h to 29.1 ± 0.1 ppm at 4 h, whereas that of the untreated rats remained stable at about 20 ppm.

Control Experiment

Tumors treated under control arms I, II, and III showed boron uptake histories similar to those seen in the primary experiment (Fig. 1) with intratumoral boron concentrations in Arm III rats (BPA, Cremophor, and Benserazide) significantly exceeding those in Arm I and Arm II rats. Differences between Arm I and Arm II remained non significant. For example, at 3 h a surplus of 7% was caused by Cremophor (Arm II over Arm I, $p = 0.19$) but of 46% due to Benserazide/L-dopa (Arm III over Arm I, $p < 0.001$).

4. Discussion

The combination of L-dopa and Benserazide was primarily responsible for the enhanced intratumoral BPA uptake in these experiments.

As research has shown Benserazide given in a dose of 50 mg/kg bw inhibits extracerebral dopa decarboxylase activity (7, 15). Further, dopa decarboxylase inhibitors such as Benserazide are in routine clinical use to extend the plasma lifetime of L-dopa administered as treatment for Parkinson's disease. Together, these facts suggest the combination of Benserazide with L-dopa to enhance BPA uptake into tumor cells to increase the efficacy of BPA-based BNCT. This study shows that pretreatment with L-dopa and Benserazide does indeed increase intratumoral boron levels greatly over treatment with BPA alone. Regardless of the precise mechanism of action, such a pretreatment might significantly improve the outcome of BNCT performed 2 to 3 hours after administration of BPA, when intratumoral levels of boron are at their height.

To enhance the solubility of L-dopa in physiological saline, Cremophor EL was used as a biocompatible detergent (16). However, Cremophor has been recognized to exercise some influence on bioavailability and pharmacokinetics of drugs (9, 10). This study has addressed this possibility. The effect is very mild but a far greater, statistically significant excess of boron uptake in tumors treated by Benserazide/L-dopa (Arm III) at 3 h when compared to Arm II (BPA, Cremophor) ($p < 0.01$) or Arm I (BPA, only) ($p < 0.001$) was observed.

This study shows that pretreatment with Benserazide and L-dopa significantly increases uploading of BPA into 9L-gliosarcoma rat tumors in vivo. This was never seen before. It verifies that L-dopa combined with Benserazide has a significant effect on boron uptake by tumor cells in vivo, a result with clear clinical implications

Further studies may be suggested. An experiment should use rats bearing the 9L-glioblastoma in one lobe of their brain. This would allow comparison of treatment effect in the damaged lobe and the healthy opposite lobe, as well as the influence of the blood-brain-barrier. Nude rats instead of immuno-competent Fisher 344 rats could be used, as the 9L-glioblastoma in nude is more infiltrative, thus providing a closer morphological resemblance to human gliomas (17).

Both Benserazide and another dopa decarboxylase inhibitor, Carbidopa, have been reported to not alter the plasma half-life of L-Dopa (6, 18), which is 1 to 3 hours. The delay from administration of L-dopa to administration of BPA should not, therefore, be longer than the 60 minutes used in this study. The decay of L-Dopa has been determined to follow a biexponential elimination pattern after intravascular administration in rat, dog, and man (18 - 20). Due to the similarity in elimination profile of L-Dopa in man and rat (21), further translational research using rats treated with the equivalent of human clinical might be advantageous.

Acknowledgements

This work was supported by the US-Department of Energy under Grant No. DE-AC02-98CH10886. We wish to thank Peggy L. Micca for her unfailing, excellent technical support analyzing numerous samples, and we gratefully acknowledge the contribution of Michiko Miura in enhancing the solubility of L-Dopa by Cremophor.

References

1. Slatkin D.N.: A history of boron neutron capture therapy of brain tumours. Postulation of brain radiation dose tolerance limit. *Brain.* 114, 1609-1629 (1990).
2. Coderre J.A., Chanana A.D., Joel D.D., Elowitz E.H., Micca P.L., Nawrocky M.M., Chadha M., Gebbers J.O., Shady M., et al: Biodistribution of boronophenylalanine in patients with glioblastoma multiforme: boron concentration correlates with tumor cellularity. *Radiat. Res.* 149(2), 163-170 (1998).
3. Coderre J.A., Glass J.D., Fairchild R.G., Micca P.L., Fand I, Joel D: Selective delivery of boron by the melanin precursor analogue *p*-boronophenylalanine to tumors other than melanoma. *Cancer Res.* 50(1), 138-141 (1990).
4. Wittig A, Sauerwein W.A., Coderre J.A.: Mechanisms of transport of *p*-borono-phenylalanine through the cell membrane in-vitro. *Radiat.Res.* 153(2), 173-180 (2000).
5. Standaert D.G., Young A.B, Parkinson´s Disease. In *Goodman & Gilman´s. The Pharmacological Basis of Therapeutics.* pp. 506-513, 9th Edition. The McGraw-Hill Companies, Inc., New York, 1996.
6. Doller H.J., Connor J.D., Lock D.R., Sloviter R.S., Dvorchik B.H., Vesell E.S.: Levodopa pharmacokinetics: Alterations after benserazide, a decarboxylase inhibitor. *Drug Metab. Dispos.* 6(2), 164-168 (1978).
7. Kent A.P., Stern G.M., Webster R.A.: The effect of benserazide on the peripheral and central distribution and metabolism of levodopa after acute and chronic administration in the rat. *Br.J. Pharmacol.* 100(4), 743-748 (1990).
8. Sykes E., Woodburn K., Decker D., Kessel D.: Effects of Cremophor EL on distribution of Taxol to serum lipoproteins. *Br. J. Cancer* 70(3), 401-404 (1994).
9. Badary O.A., Al-Shabanah O.A., Al-Gharably N.M., Elmazar M.M.: Effect of Cremophor EL on the pharmacokinetics, antitumor activity and toxicity of doxorubicin in mice. *Anticancer Drugs.* 9(9), 809-815 (1998).
10. de Vos A.I., Nooter K., Verweij J., Loos W.J., Brouwer E., de Bruijn P., Ruijgrok E.J., van der Burg M.E., Stoter G., et al: Differential modulation of cisplatin accumulation in leukocytes and tumor cell lines by the paclitaxel vehicle Cremophor EL. *Ann. Oncol.* 8(11), 1145-1150 (1997).
11. Barth R.F., Adams D.M., Soloway A.H., Mecherter E.B., Alam F., Anisuzzaman A.K. M.: Determination of boron in tissue using direct-current plasma emission spectroscopy. *Anal. Chem.* 63(9), 890-893 (1991).
12. Bauer W., Micca P., White A.: A rapid method for the direct analysis of boron in whole blood by atomic emission spectroscopy. In: *Advances in neutron capture therapy.* (A. H. Soloway, R. F. Barth, D. E. Carpenter, Eds.) pp. 403-407. Plenum Press, New York, 1993.
13. Kobayashi T., Kanda K.: Microanalysis system of ppm-order ^{10}B concentration in tissue for neutron capture therapy by prompt γ-ray spectrometry. *Nucl. Instrum. Methods.* 204, 525-531 (1983).
14. Fairchild R.G., Gabel D., Laster B.H., Greenberg D, Kiszenick W., Micca P.: Microanalytical techniques for boron analysis using the $^{10}B(n, \square)^{7}Li$ reaction. *Med.Phys.* 13(1), 50-56 (1986).
15. Bartholini G, Burkard W.P., Pletscher A.: Increase of cerebral catecholamines caused by 3,4-dihydroxy-phenylalanine after inhibition of peripheral decarboxylase. *Nature* 215(103), 852-853 (1967).
16. Woodcock D.M., Jefferson S., Linsenmeyer M.E., Crowther P.J., Chojnowski G..M., Williams B., Bertoncello I.: Reversal of the multidrug resistance phenotype with Cremophor EL, a common vehicle for water-insoluble vitamins and drugs. *Cancer Res.* 50(14), 4199-4203 (1990).
17. Saini M., Bellinzona M., Meyer F., Cali G.., Samii M.: Morphometrical characterization of two glioma models in the brain of immuno-competent and immunodeficient rats. *J.Neuro-Oncol.* 42(1), 59-67 (1999).
18. Rose S., Jenner P., Marsden C.D.: Peripheral pharmacokinetic handling and metabolism of L-Dopa in the rat: The effect of route of administration and carbidopa pretreatment. *J.Pharm.Pharmacol.* 43(5), 325-330 (1991).
19. Sasahara K., Nitanai T., Habara T., Morioka T., Nakajima E.: Dosage form design for improvement of bioavailability of levodopa II: bioavailability of marketed levodopa preparations in dogs and Parkinsonian patients. *J.Pharm.Sci.* 69(3), 261-265 (1980).
20. Sasahara K., Nitanai T., Habara T., Morioka T., Nakajima E.: Dosage form design for improvement of bioavailability of levodopa III: influence of dose on pharmacokinetic behaviour of levodopa in dogs and Parkinsonian patients. *J.Pharm.Sci.* 69(12), 1374-1378 (1980).
21. Kuruma I., Bartholini G.., Tissot R., Pletcher A.: Comparative investigation of inhibitors of extracerebral dopa decarboxylase in man and rats. *J.Pharm.Pharmacol.* 24(4), 289-294 (1972).

Carboranyl porphyrazines: synthetic aspects and molecular properties

Pietrangeli Daniela,[a] Giampaolo Ricciardi[a]

[a]*Department of Chemistry, Università della Basilicata, Via N. Sauro 85, 85100 Potenza, Italy*

Abstract

Among the challenges precluding the widespread use of BNCT has been the difficulty in achieving selective delivery of large quantities of boron to malignant cells. In an attempt to address this issue we have recently developed an effective strategy to synthesize a new family of boronated porphyrazines to be delivered through the membrane of cancerous tissues as such or with the help of liposomes. Herein we describe the synthesis and the basic physico-chemical properties of neutral octa-*closo*-carboranyl-alkylthio-porphyrazines as well as of their water-soluble counterparts obtained by mild deboronation of the *closo*-polyedra. Preliminary studies indicate that these compounds show negligible cell toxicity and, compared with BPA, good cellular uptake. This encourages further studies for their evaluation as potential BNCT sensitizers.

Keywords:BNCT, carboranylporphyrazines

1. Introduction

In the last fifteen years several BNCT (BNCT = Boron Neutron Capture Therapy) agents have been proposed (Soloway et al., 1998), including boronated nucleosides, amino acids, peptides, phospholipids, monoclonal antibodies, liposomes (Lee et al., 2007), closomers (Ma et al.,2006), dendrimers, porphyrins (Mao et al., 2007) and phthalocyanines (Giuntini et al., 2005). Recently, we focused on the porphyrazine (Pz) macrocycle – a small-ring tetrapyrrole relatively less studied than the porphyrin analog as a potential carrier of highly boronated chemical functions. Our aim was to design and synthesize Pzs bearing carboranyl-containing pendants, to deliver into cancerous cells with the help of liposomial vectors. In the context of the tetrapyrrolic systems, Pzs – often denoted azaporphyrins – represent an interesting variant. Indeed, Pzs with chemical and physical properties not easily accessible to porphyrins are readily synthesized through template cyclotetramerization of an appropriate dinitrile derivative. In particular, Pzs bearing S, N or O peripheral heteroatoms are readily synthesized. As, in principle, boron-containing Pzs may conjugate the photosensitizing properties of the macrocycle with the BNCT sensitizing capability of the boronated substituents, they have a potential in the multiple approach in the anticancer therapy. Having these considerations in mind, we have undertaken the synthesis of neutral and anionic *o*-carboranyl-porphyrazines. In these nanosized molecules the C(1) atom of the *o*-carborane cage is linked to the Pz ring through a hexylthio tail, whereas the C(2) atom bears *ad hoc* bonded chemical functions. Hexylthio-carboranyl-porphyrazines (HECSPzs) have proven to be efficiently incorporated in liposomes with tunable lipidic formulations, and hence, they do meet an essential prerequisite for being effectively delivered through the membrane of cancerous tissues (Ristori et al., 2007; Salvati et al., 2007). Here the salient synthetic aspects and the basic properties of the investigated carboranyl-porphyrazines are briefly overviewed.

2. Materials and methods

Materials: All chemicals and solvents (Aldrich Chemicals Ldt.) were of reagent grade and used in the syntheses as supplied. *o*-Carborane was purchased from Ryscor Science (USA), 1-methyl-*o*-Carborane and ^{10}B enriched 1-methyl-*o*-Carborane, were purchased from KATCHEM (Czech

Republic). Solvents used in physical measurements were of spectroscopic or HPLC grade. THF was freshly distilled from sodium benzophenone ketyl under nitrogen.

Physical Measurements: ^{1}H and ^{13}C NMR spectra were recorded on an INOVA Varian 500 MHz spectrometer or on a Varian VNMRS-400 MHz spectrometer. $^{10}B\{^{1}H\}$ NMR data were recorded on a Varian VNMRS-400 MHz spectrometer. IR and UV-vis spectra were recorded on FT/IR-460-Plus JASCO and Varian Cary 05E spectrophotometers, respectively.

3. *Neutral* carboranyl-porphyrazines

The synthesis of *closo*-carboranylporphyrazines is a multistep process involving template condensation of an appropriate carboranyl-maleonitrile derivative on $Mg^{II}(n\text{-OPr})_2$. The number and type of synthetic steps vary from one compound to another, mostly depending on the chemical functions appended to the *o*-carborane C(2). We first analyze the rather complicated case in which a hydrogen atom is bonded to the C(2) atom of the carborane cage. The resulting carboranyl-porphyrazines were considered worth investigation because (i) compatibly with the reactivity of the porphyrazine-octathiolate ring, the *o*-carborane C-H protons can be functionalized *in situ*, allowing for a supramolecular chemistry, (ii) these protons may undergo hydrogen bond formation (Ramachandran et al., 2006) that plays an important role in the process of interaction with receptors *in vivo*. Two alternative synthetic sequences for porphyrazines bearing unsubstituited *o*-carborane subunits are outlined in Scheme 1 for the representative case of the [2,3,7,8,12,13, 17,18-octakis-(1,2-dicarba-*closo*-dodecaboranyl)-hexylthio-5,10,15,20-porphyrazine] magnesium (II) complex, MgHECSPz. Initially (pathway A), the *o*-carborane **1** was partially lithiated, then it was treated with TBDMSCl to form the TBDMS-protected carborane **2**. This compound was treated with *n*-butyllithium and, subsequently, *in situ*, with a large excess of 1,6-dibromohexane to give **3** in a 48% overall yield. Spectroscopic characterization data for these intermediate compounds agreed well with the available literature data (Ma et al, 2006). The MgHECSPz precursor, the *cis*-2,3-bis[6-(1-TBDMS-1,2-*closo*-dodecarboran-2-yl)hexylthio]-maleonitrile, **5a**, was obtained in 25% yield by reaction of **3** with dimercaptomaleonitrile disodium salt, $(dmmnt)Na_2$. Cyclotetramerization of **5a** on $Mg^{II}(n\text{-OPr})_2$ (step 4) proved to be the critical synthetic step. This was not unexpected, as the rather prolonged reaction time (>24h) and relatively high temperature (~130°C) normally employed in the template cyclotetramerization of maleonitrile derivatives, are likely to favor effective nucleophilic attack of the $Mg^{II}(n\text{-OPr})_2$ on the *o*-carborane moieties, hence inducing their degradation with formation of anionic (*nido*) species.

In fact, treatment of *o*-carboranes with different nucleophiles, including alkaline metal alkoxides, proves to be a useful synthetic tool for inducing the *closo→nido* conversion of the carborane cage (Hawthorne et al., 1968).

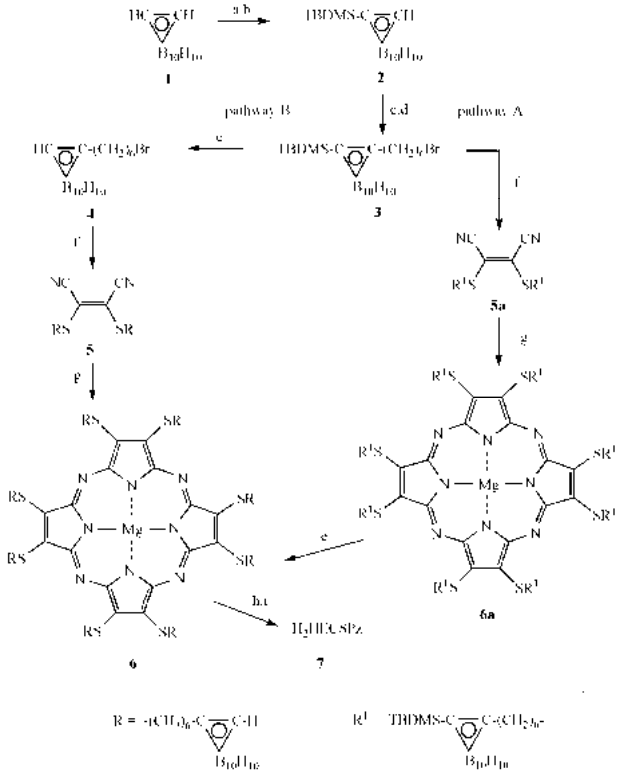

Scheme 1. Synthesis of H_2HECSPz, **7**. Reagents and conditions: (a) *n*-BuLi, THF, under N_2, 0°C-r.t., 0.5 h.; (b) TBDMSiCl, THF, under N_2, 0°C -reflux, overnight; (c) *n*-BuLi, C_6H_6/Et_2O (2:1), under N_2, 0°C-r.t., 0.5 h; (d) $Br(CH_2)_6Br$, C_6H_6/Et_2O (2:1), 0°C C-reflux, overnight. Pathway A: (f) $[dmmnt]Na_2$, MeOH, 0°C-r.t., in the dark, 24 h; (g) $Mg^{II}(n\text{-OPr})_2$, *n*-PrOH, 110°C, 10h; (e) $(Bu)_4NF$, THF, -78°C-r.t.; (h) TFA, $CHCl_3$; (i) NH_3, pH=7, on ice. Pathway B: (e) TBAF, THF, -78°C-r.t.; (f) $[dmmnt]Na_2$, MeOH, 0°C-r.t., in the dark, 24 h; (g) $Mg^{II}(n\text{-OPr})_2$, *n*-PrOH, 110°C, 10h; (h) TFA, $CHCl_3$; (i) NH_3, pH=7, on ice

However, we found that the impact of this by-process can be significantly attenuated by using mild reaction conditions (T <115°C) and a relatively short reaction time (~10h). This procedure, though implying incomplete conversion of **5a** (~ 30% of unreacted **5a** can be retrieved), has the merit to reduce the formation of carborane based byproducts, which are difficult to separate from the desired porphyrazine by chromatography. Tetrabutylammonium fluoride (TBAF) was used to remove the TBDMS protecting group from **6a** to give MgHECSPz in ca. 5% overall yield. In an attempt to test the stability of the carborane C-H group under the cyclotetramerization conditions, the compound **3** was deprotected. Using this strategy (pathway B) the *cis*-2,3-bis[6-(1,2-*closo*-dodecarboran-2-yl)-hexyl-thio]maleonitrile, **5**, was obtained in high yield, due to the enhanced solubility of **4** in methanol which is related to the involvement of the free carboranyl C(2)-H group in hydrogen bonding interactions with the solvent. However, template cyclotetramerization of the maleonitrile derivative **5** on $Mg^{II}(n\text{-}OPr)_2$ (step 5) afforded again the MgHECSPz complex, **6**, in ~5% yield, thus indicating that the C(2)–H and C(2)–TBDMS groups impart to the carborane cage a comparable sensitivity to the basic environment used for the template cyclotetramerization of **5**. That in the isolated Mg^{II} complex, the *o*-carborane cages retain the *closo* structure was confirmed by ^{1}H, ^{13}C, ^{11}B NMR, and IR spectroscopy. The ^{13}C NMR spectrum showed two resonances at δ= 63.6 ppm and δ=40.2 ppm which are the signature of the C-H and C-R (R = hexyl, in the actual case) carbons, respectively, belonging to a neutral *closo*-carborane cage. In turn, the IR spectrum showed the symmetric and intense peak at 2588 cm^{-1} (Figure 1), attributable to the B-H stretching vibration of the *closo o*-carborane cage. Opening the *closo* carborane cage generally induces a red shift of this adsorption, which is found in the vicinity of 2520 cm^{-1} in the *nido* carboranes (Leites, 1992). Finally, ^{11}B NMR spectra showed the typical resonance of *closo*-carborane between -2 and 16 ppm. The MgHECSPz complex **6** was demetallated to obtain the free base carboranylporphyrazine. The procedure, which employs dissolution of the magnesium complex in $CHCl_3$ and TFA, neutralization on ice with 30% ammonia solution, gave H_2MeHECSPz **7** in 11% yield.

Significantly higher yields could be achieved in the synthesis of MgMeHECSPz **11** and its free base derivative H_2MeHECSPz.

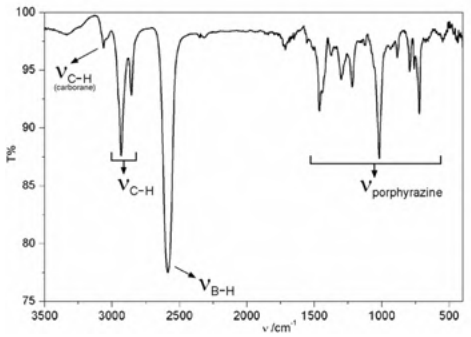

Figure 1: IR spectrum of **6** (thin film supported on KBr disk)

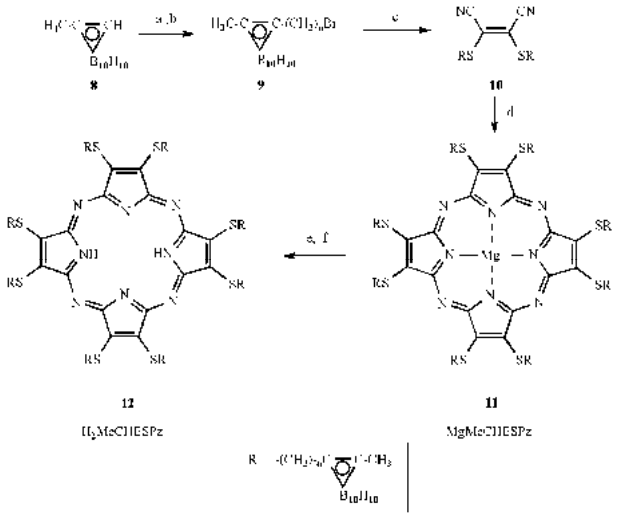

Scheme 2. Synthesis of H_2MeCHESPz, **12**. Reagents and conditions: (a) *n*-BuLi, THF, under Ar, -50°C-r.t., 2h; (b) $Br(CH_2)_6Br$, THF, under Ar, -78°C-r.t., 4h; (c) [dmmnt]Na_2, MeOH/EtOH 8:2, 0°C-r.t., in the dark, 36 h; (d) $Mg^{II}(n\text{-}OPr)_2$, *n*-PrOH

As shown in Scheme 2, **10** was synthesized in three steps. To the lithiated intermediate a large excess of 1,6-dibromohexane was added *in situ* at -78°C and the reaction was carried out at room temperature for several hours.

After removal of the excess 1,6-dibromohexane the brominated product was treated with [dmmnt]Na_2 at room temperature for 36 hours. An MeOH/EtOH 8:2 v:v mixture was used to improve the solubility of **9**. The maleonitrile derivative **10** – at 52% overall yield– was condensed on $Mg^{II}(n\text{-}OPr)_2$ at 90°C. **11** was obtained in 70% yield. The magnesium complex **11** was demetallated as usual to give the corresponding free base H_2MeHECSPz **12** in 18% overall yield. Using ^{10}B enriched 1-Me-*o*-carborane, the synthetic procedure afforded the ^{10}B H_2MeHECSPz **12** in comparable yield, which enables employment of this molecule in *in vitro* and *in vivo* BNCT experiments.

4. *Polyanionic* carboranyl-porphyrazines

Neutral carboranyl-porphyrazines exhibit scarce solubility, if any, both in water and biological solvents that makes the utilization of liposomial carriers for their intracellular delivery necessary. To enhance the solubility of carboranyl-porphyrazines in therapeutic solutions the molecules were converted in their water-soluble counterparts through mild deboronation of the *closo*-polyedra (Scheme 3). In a typical experiment, MgMeCHESPz was treated in EtOH/THF with CsF, a mild deboronating agent. The crude product was dissolved in acetone and passed slowly through a Dowex 50WX4-400 resin in the potassium form to allow for the Cs/K exchange. The *nido*-compound was achieved in 65% yield.

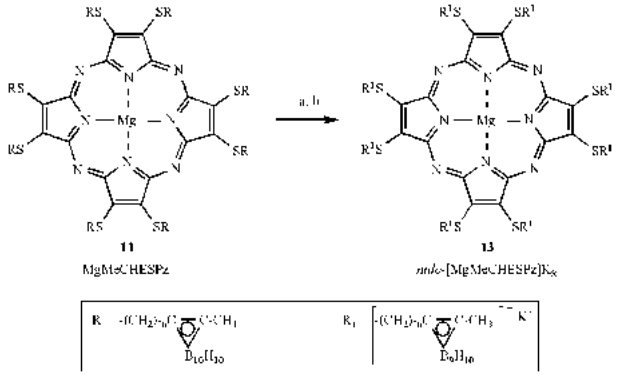

Scheme 3. Synthesis of *nido*-[MgMeCHESPz]K_8 **13**. Reagents and conditions: (a) CsF, THF/EtOH, 80°C, 48h; (b) resin Dowex 50WX4-400 in K^+ form

The IR spectrum of the compound shows the intense IR absorption at 2520 cm^{-1} due to the B–H vibrations of the *nido* cage, while the ^{11}B NMR spectrum is characterized by a twin, broad signal in the range -2.4 to -2.8 ppm associated to the *endo* hydrogen. The *nido*-[MgMeCHESPz]K_8 complex is soluble in acetone, water, methanol, and mixtures of them. It shows a well-resolved UV-vis spectrum in acetone, with the most intense band (Q) peaking at 668 nm. However, the complex tends to aggregate in water, as inferred from the broadening of the main absorptions in the optical spectrum taken in this solvent at pH=7.0. In spite of the significant aggregation, preliminary BNCT studies *in vitro* indicate that the *nido*-species exhibit a good cellular uptake, as compared to borophenylalanine (BPA).

5. Conclusions

New porphyrazines bearing differently functionalized peripheral *o*-carborane cages have been synthesized from readily available starting materials. Preliminary studies indicate that these compounds show negligible cell toxicity and, compared with BPA, a good cellular uptake, which encourages further studies for their evaluation as potential BNCT sensitizers.

Acknowledgment. Financial support by MIUR (PRIN2007, 2007XWBRR4_002) is gratefully acknowledged.

References

Soloway, A. H.,Tjarks, W., Barnum, B. A., Rong, F. G., Barth, R. F., Codogni, I. M.,Wilson, J. G., 1998. The chemistry of neutron capture therapy. Chem. Rev. 98, 1515–1562.

Lee, Jong-Dae, Ueno, M., Miyajima, Y., Nakamura, H., 2007. Synthesis of boron cluster lipids: *closo*-dodecaborate as an alternative hydrophilic function of boronated liposomes for neutron capture therapy. Org. Lett. 9, 323–326.

Ma, L., Hamdi, F., Wong, F., Hawthorne, M.F., 2006. Closomer of high boron content: synthesis, characterization, and potential application as unimolecular nanoparticle delivery vehicles for boron neutron capture therapy. Inorg. Chem. 45, 278–285

Hao, E., Simbrian-Vazquez, M., Serem, W., Garno, J. C., Fronczek, F. R.,Vicente, M. G. H, 2007. Synthesis, aggregation and cellular investigation of porphyrin-cobaltocarborane conjugates. Chem. Eur. J. 13, 9035–9042.

Giuntini, F., Raoul, Y., Dei, D., Municchi, M.,Chiti, G., Fabris, C., Collutti, P., Jori, G., Roncucci, G., 2005. Synthesis of tetrasubstituted Zn(II)-phtalocyanines carrying four carboranyl-units as potential BNCT and PDT agents. Tethraedron Lett. 46, 2979-982

Ristori, S., Salvati, A., Martini, G., Spalla, O., Pietrangeli, D., Rosa, A., Ricciardi, G., 2007. Liposome insertion of a poly-carboranylalkylthio-porphyrazine newly synthesized to improve potentiality in multiple approach cancer therapy. J. Am. Chem. Soc. 129,2728-2729.

Salvati, A., Ristori, S., Oberdisse, J., Spalla, O., Ricciardi, G., Pietrangeli, D., Giustini, M., Martini, G., 2007. Small angle scattering and zeta potential of liposomes loaded with octa(carborayl)porphyrazines. J. Phys. Chem. B. 111, 10357-10364.

Ramachandran, B. M., Knobler, C. B., Hawthorne, M. F., 2006. Example of an intramolecular, non classical C-H···π hydrogen bonding interaction in an arylcarborane derivative. J. Mol. Struct. 785, 167-169.

Hawthorne, M. F., Young, D. C., Garrett, P. M. Owen, D. A., Schwerin, S. G., Tebbe, F. N., Wegner, P. A., 1968. The preparation and characterization of the (3)-1,2- and (3)-1,7-dicarbadodeahydroundecaborate. J. Am. Chem. Soc. 90, 862-868.

Leites, L. A., 1992. Vibrational spectroscopy of carbo-ranes. Chem. Rev. 92, 279-323.

Rational design of boron-rich compounds targeting human thymidine kinase for BNCT

P. Carloni[1], Z. Ghaemi Bafghi[1,2], P. Lupieri[1,2], G. Lattanzi[1,3], G. Giannini[2,4],

[1]*SISSA and INFM DEMOCRITOS, Trieste, Italy*
[2]*Physics Department, University of Trieste, Italy*
[3]*Department of Medical Biochemistry, Biology and Physics, University of Bari, Italy*
[4]*INFN–Trieste, Italy*

The drugs currently used in the clinics for BNCT can discriminate tumor cells versus healthy ones at best in the 5:1 ratio. In most cases, the target is not known. To improve drugs' selectivity, it is imperative to identify molecular target(s) of the drug in the cell nucleus.

In this context, 12 ^{10}B rich analogs of human thymidine kinase 1 (TK1) substrate (thymidine) have been recently designed (Fig.1). TK1's function is the phosphorylation of thymidine to form building blocks of DNA (thymidine monophosphate): one of these analogs has the best kinetic efficiency relative to the natural substrate of TK1, and *in vivo* studies showed that it is efficiently incorporated in cancerous cells. Unfortunately, however, the production of thymidine monophosphate analogs is still much slower than in the natural substrate.

We are using computational methods to design new boron ligands with improved reactivity. We performed docking calculations based on the large X-ray structural information available on the human TK1 and homologous, N. Ostermann *et al.,* enzymes. The compounds turn out to bind similarly to the natural substrate (Fig. 2). We are currently performing molecular dynamics and QM/MM calculations to shed light on the reaction mechanism of the compounds and compare it to that of the natural substrate. Knowledge of the structure of the transition state may allow the design of new ligands with faster reaction kinetics. These in turn may be incorporated faster in cancerous cell nuclei than the current ones. To the best of our knowledge, this is the first computer-aided, structure-based drug design approach in BNCT.

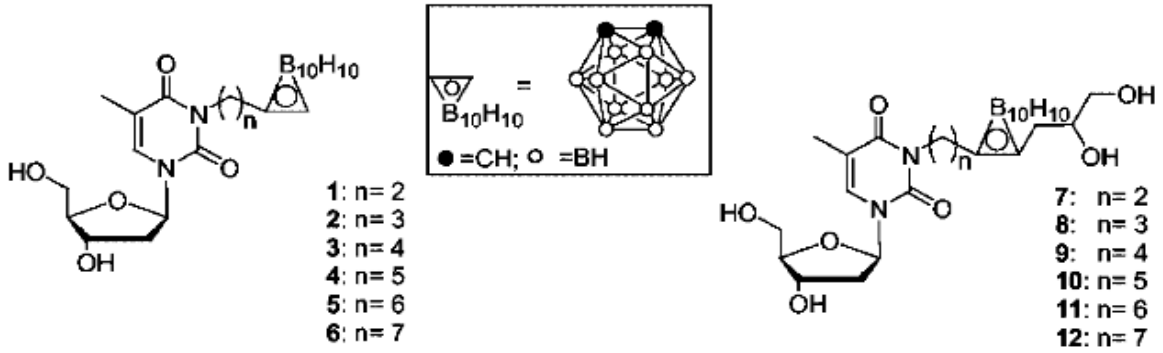

Figure 1: The boron-rich analogs of deoxythymidine drawn for BNCT, as proposed in A.S. Al-Madhoun *et al, Cancer Research* **64**, 6280 (2004)

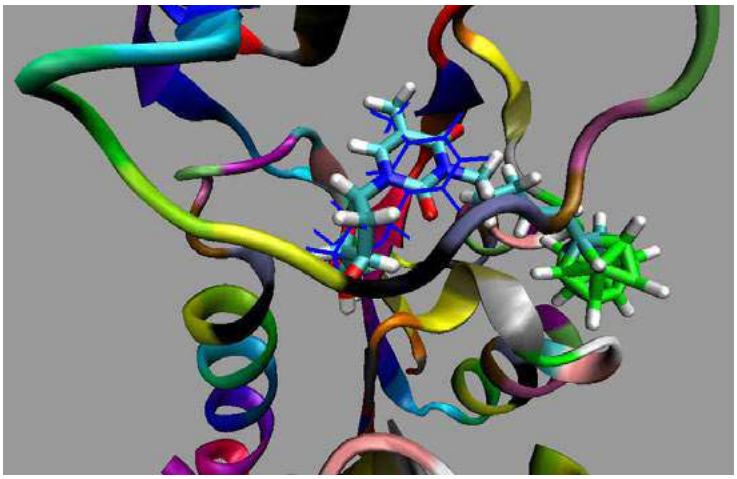

Figure 2: The predicted binding pose of one of the deoxythymidine analogs with a five-methylene spacer between thymine and the boron cage, in comparison with the natural substrate (in blue)

Boron carriers for BNCT: state of the art and new perspectives deriving from nanotechnology

Luigi Manzo[1], Anna F. Castoldi[1], Teresa Coccini[1], Elisa Roda[1], Ferrari Cinzia[2], Clerici Anna Maria[2], Zonta Cecilia[2], Aris Zonta[1]

[1]*Toxicology Division, University of Pavia and IRCCS Fondazione Salvatore Maugeri, Pavia, Italy;*

[2]*Department of Surgery, University of Pavia, Italy*

The efficient treatment of cancer by BNCT demands the selective delivery and marked accumulation of ^{10}B in malignant tumor tissues, whereas the B concentration in the cells of surrounding normal tissue should be kept low to minimize the damage to normal tissue. Clinically, two boron delivery agents have been used for BNCT, namely sodium borocaptate (BSH) and p-borono-phenylalanine (BPA), a dihydroxyboryl derivative of phenylalanine. Both these agents have limitations. To improve the efficacy of the BNCT of cancers, considerable effort has been directed toward the development of new means of selective targeting of ^{10}B to tumors. Ideally, a boron delivery agent for BNCT should fulfill the following conditions: (I) non-toxic at the clinically relevant dose(s) (II) minimum concentration of 20–30 μg of ^{10}B/g per gram of tumor tissue; (III) high tumor/normal tissue and tumor/blood concentration ratios; (IV) rapid clearance from blood circulation and normal tissues, but persistence in tumor; (V) water solubility; and (VI) chemical stability.

In order to meet these requirements, several classes of boron delivery agents have been designed and synthesized over the years. Examples of these compounds include boron-containing amino acids, functionalized polyhedral borane clusters, biochemical precursors of nucleic acids and DNA-binding agents, porphyrin- and carbohydrate- derivatives, peptides, boron-conjugated biological complexes, such as boronated- monoclonal antibodies, -epidermal growth factors, and -carborane oligomers, and liposomes. Promising approaches may come from nanotechnologies and entail the use of targeted and tailored nanoparticles, being developed as “intelligent” drug delivery systems. For example, targeting, imaging and treatment of brain cancer (the latter being difficult to reach by conventional drugs) has been shown to be improved by nanoparticles simultaneously loaded with an anticancer drug and a contrast agent. Notably, a recent study by Mortensen et al (Bioconjugate Chem 2006, 17, 284) has put forward the intriguing hypothesis that *ad hoc* surface modifications of boron carbide nanoparticles may allow their use for, and the development of, T-cell guided BNCT.

Non-tumor specificity of polyhedral borane cages toward C6 cells

Masao Takagaki [a,b], C-G. Yan [b] and Narayan S. Hosmane[b]

[a]*School of Nursing, Aino Gakuin College, Osaka, Japan (m-takagaki@ns-t.aino.ac.jp)*
[b]*Department of Chemistry and Biochemistry, Northern Illinois University, DeKalb, Illinois, USA*

Abstract

Mechanism of tumor uptake of mercaptoborane (BSH), one of the therapeutics for use in boron neutron capture therapy (BNCT) for malignant brain tumors, is contributed by its SH moiety. Nonetheless, the borane cages have no biological activity against the C6 gliosarcoma cell membrane and/or cytoplasimic component. The three dimensional conformation of the borane cages does not possess any biological compatibility.

Keywords: Boron neutron capture therapy, Polyhedral borane, BSH

1. Introduction

Mercaptoborane (BSH) is one of the therapeutics for use in current BNCT. However, controversy remains concerning the actual mechanism of tumor uptake of BSH. Nonetheless, we have recently reported that the T/B ratio was generally less than 1.0 (av. 0.6) for human malignant glioma specimen on our regimen and concluded that the BSH was non-specific boron carrier (Takagaki et al., 1997). We have recently investigated the uptake mechanism and in-vitro BNCT effect of the dianionic dodecahedral borane cage itself (without the SH moiety) and its several cage-degraded and cage-expanded mono- and dianionic derivatives using the C6 gliosarcoma cell line.

2. Polyhedral borane cages

Eight borane derivatives ($(NH_4)_2B_{10}H_{10}$, $NaB_{11}H_{11}$, $K_2B_{11}H_{11}$, $Na^{10}B_{11}H_{14}$, $K_2B_{12}H_{12}$, $Na_2B_{20}H_{18}$, $Na_2B_{22}H_{20}$, $Na_2{}^{10}B_{22}H_{20}$) were synthesized (Yan, unpublished data) in which $K_2B_{12}H_{12}$ was the sulfide-free form of BSH. All compounds were chemically stable and highly water-soluble.

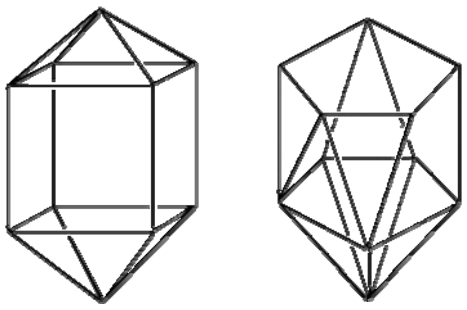

$(NH_4)_2B_{10}H_{10}$ $NaB_{11}H_{11}$

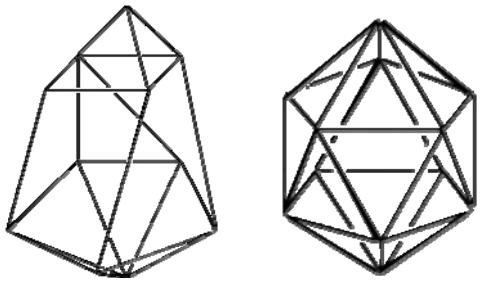

$K_2B_{11}H_{11}$ $K_2B_{12}H_{12}$

3. Cell surviving fraction & toxicity

C6 gliosarcoma cells were incubated in subconfluent condition in standard MEM (Nissui, Tokyo, Japan) supplemented with 10% FCS, in 36 □ 5% carbon dioxide atmosphere overnight. Aliquots of borane anion solutions were incubated for 6 hrs into the Petri dishes respectively for uptake by tumor cells in dose-dependent and/or time-dependent manners. Boron concentration in tumor cells was measured by prompt γ-ray spectroscopy (PGS) and/or ppb-order boron quantitative assay via α autoradiography (ATA) (Takagaki et al., 2001). Boron 10 concentrations in media were confirmed by PGS. The tumor cells were washed twice with PBS after boron loading. Aliquots containing 5×10^3 cells/ml were pipetted into cylindrical Teflon tubes 1 cm in diameter and 3 cm high that did not generate any secondary radiation when subjected to thermal neutron. The inability of cells to adhere to Teflon allows precise quantitative manipulation of cells without trypsinization. The thermal neutron fluence was determined by

averaging the activity of two gold films symmetrically attached to the Teflon tube surface along the thermal neutron axis. The thermal neutron fluence ranged from 0 to 4.2×10^{12} n/cm^2. For estimation of the neutron energy spectra, 8 kinds of activation films and 14 kinds of nuclear reactions were used: ^{197}Au(n, γ)^{198}Au for the thermal neutron regions; ^{115}In(n, γ)^{116m}In, ^{197}Au(n, γ)^{198}Au, ^{58}Fe(n, γ)^{59}Fe and ^{63}Cu(n, γ)^{64}Cu for the epithermal neutron region; and ^{115}In(n, n*)^{116}In, ^{54}Fe(n, p)^{54}Mn, ^{27}Al(n, p)^{27}Mg, ^{27}Al(n, α)^{24}Na, ^{47}Ti(n, p)^{47}Sc, ^{48}Ti(n, p)^{48}Sc, ^{24}Mg(n, p)^{24}Na, ^{63}Cu(n, α)^{60}Co, ^{58}Ni(n, p)^{58}Co and ^{197}Au(n, 2n)^{196}Au for the fast-neutron region. The neutron absorbed dose (Gy) was calculated using the flux-to-dose conversion factor. The chemical composition of the tumors was assumed to be 10.7% hydrogen, 12.1% carbon, 2% nitrogen, 71.4% oxygen and 3.8% others. The γ-ray dose was monitored by thermo-luminescent dosimeters (TLDs) attached to the tubes and ranged from 0 to 5 Sv. Immediately after irradiation, 500 cells were seeded in 6-cm Petri dishes (Corning, NY) and incubated for 10 days in a humidified 37℃ atmosphere of 98% air/5% carbon dioxide to allow colony formation. The colonies were fixed and stained with a 10% formaldehyde/1% toluidine blue solution and then counted microscopically. The IC_{50} (moles/liter), i.e. the concentration that inhibited the growth of C6 gliosarcoma cells by 50% after 3 day of continuous exposure, was determined via CellTiter 96® Aqueous One Solution Cell Proliferation Assay.

4. Results

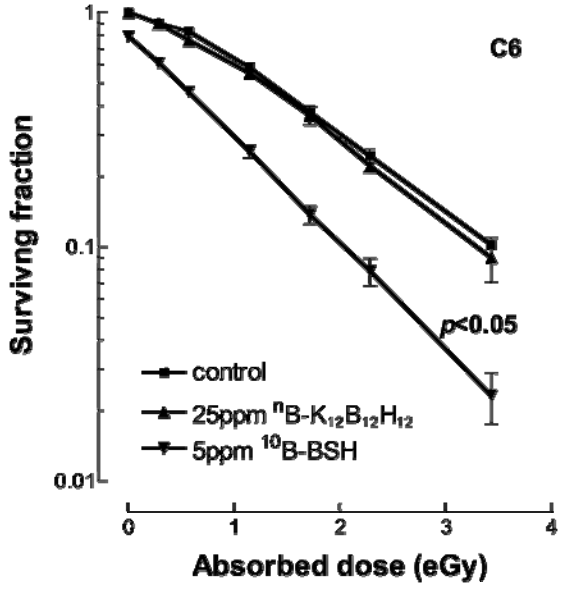

Toxicity of anionic polyhedral borane derivatives to the C6 cells was observed by chamber slide technique, IC_{50}: $(NH_4)_2B_{10}H_{10}$ = $6.66\text{x}10^{-2}$ M, $K_2B_{12}H_{12}$ = $4.54\text{x}10^{-2}$M, BSH=$2.75\text{x}10^{-2}$M. Neither any boron uptake nor null boron enhancement ratio in the tumor cells were observed under our experimental conditions. The boron concentration in tumor cells was under detectable limit by PGS and ATA after boron loading. There was no significant difference of surviving fraction between the groups those who received the borane derivatives and those with the boron-free control group.

BSH might pass through the cell membrane via conjugate form with some amino acid or amine, etc. Borane anion cages themselves are chemically stable, highly water soluble and permeable through the cell membrane. Therefore, use of anionic borane cages as boron carrier part might be beneficial for the accumulation of boron atoms into tumor cells by conjugating with some biological active moiety.

5. Conclusions

The anionic polyhedral borane cages have no biological active moiety against the tumor cell membrane and cytoplasmic component. The borane cages themselves act as only inorganic "materials" whose 3D conformation did not possess any biological compatibility. On the other hand, the BSH could be forced to enter and then remain in the tumor cells via its sulfide-group activity like a "Space Shuttle". It is clear that the sulfhydryl linkage contributes significantly to the toxicity and non-tumor specificity of BSH in the C6 cells.

This paper is dedicated to my Leading Neurosurgeon, the late Dr. Yoshifumi Oda, M.D., Ph.D., Kyoto University by M.T.

References

Takagaki, M., Oda, Y., Miyatake, S., Kobayashi, T., Sakurai, Y., Ohsawa, M., Mori, M., Ono,K., 1997. Boron neutron capture therapy: preliminary study of BNCT with sodium borocaptate ($Na_2B_{12}H_{11}SH$) on glioblastoma. *J. Neuro. Oncol.* 35, 177-185.

Takagaki M, Ono, K., Masunaga, SI., Kinashi, Y., Skurai, T., Kobayashi, T., Miyatake, S., Hashimoto, N., 2001. ^{10}B quantitative determination in the ppb order range by particle tracks reading for boron neutron capture therapy. *Radio. Analy. Nucl. Chem.* 247(2), 389-392.

Carborane derivative drugs inserted in liposome as an effective strategy for Boron Neutron Capture Therapy

S. Altieri[1], M. Balzi[2], S. Bortolussi[1], P. Bruschi[1], L. Ciani[3], A.M. Clerici[4], P.Faraoni[2], C. Ferrari[4], L. Panza[5], D. Pietrangeli[6], G. Ricciardi[6], S. Ristori[3], S.Stella[1]

1) Department of Nuclear and Theoretical Physics, University of Pavia, Pavia, Italy
2) Department of Clinical Physiology, University of Florence, Florence, Italy
3) Department of Chemistry, University of Florence, Florence, Italy
4) Department of Surgery, University of Pavia, Pavia, Italy
5) DISCAFF, University of Oriental Piemonte, Novara, Italy
6) *Department of Chemistry, University of Basilicata, Potenza, Italy*

Liposomes are the most accredited drug delivery system and, currently, the only one approved for clinical trials, though different promising nanosize vectors have been designed and prepared.

In all cases, it has been established that optimising biomedical applications requires extensive physico-chemical characterization at the molecular and meso-scale level. Factors like overall size, surface charge and drug insertion modality are of primary importance to understand the interaction between loaded vectors and cellular or tissutal substrates.

Here we report on the use of three liposomal formulations, made with different lipid components , i.e. the positively charged DOTAP, the zwitterionic DOPC and the negatively charged DOPA, in order to obtain positive, zwiterionic and negative aggregates, respectively. In addition to this, all liposomes contained the zwitterionic phospholipid DOPE as a fusogenic element.

Liposomes were loaded with carborane-derived drugs, i.e. o-closocarboranyl β-lactoside and 1-allyl-o-closocarboranyl-2- hexylthio-porphyrazine and tested for BNCT efficacy on model cell cultures.

The chosen cell line was the DHDK12TRb rat coloncarcinoma cell line, which is able to induce liver metastases in BD-IX rats and has been largely used in recent years to study the uptake capability of standard BNCT drugs, such as borophenyl-alanine (BPA). This cell line therefore represents an interesting model for comparative purposes.

Preliminary experiments were also carried out on the murine melanoma B16F10 cell line.

Boron uptake was determined by measuring alfa particle emission with the alpha spectrometry technique. Fixed amounts of cells were deposited on mylar disks and irradiated in the thermal column of the TRIGA Mark II reactor (University of Pavia). Boron concentration was thus obtained by analyzing the charged particles spectra emitted in the ^{10}B (n, α) $\rightarrow$ ^{7}Li reaction, which were detected by a thin silicon detector.

The results of boron uptake were analyzed in terms of both inserted drug and liposome properties. Toxicity effects were also investigated and a comparison was made with the behaviour of BPA on the same cell lines.

In general, an improved performance of the newly prepared ^{10}B delivery systems was demonstrated.

BORON IMAGING

Positron Emission Tomography: a crucial role for BNCT ?

Luca Menichetti[1], Luca Cionini[2], Wolfgang A. G. Sauerwein [3], Piero A.Salvadori[1]

1. Department of PET and Radiopharmaceutical Chemistry, CNR Institute of Clinical Physiology, Pisa, Italy
2. Unit of Radiotherapy, AOUP-University Hospital, Pisa, Italy
3. Department of Radiation Oncology, University Duisburg-Essen, University Hospital Essen, Germany

Abstract

BNCT is Positron Emission Tomography (PET) has become a key imaging tool in clinical practice and biomedical research to quantify and study biochemical processes in vivo. Physiologically active compounds are tagged with positron emitters (e.g. ^{18}F, ^{11}C, ^{124}I) while maintaining their biological properties, and are administered intravenously in tracer amounts (10^{-9} – 10^{-12} M quantities). The recent physical integration of PET and Computed Tomography (CT) in hybrid PET/CT scanners allows a combined anatomical and functional imaging: nowadays PET molecular imaging is emerging as powerful pharmacological tool in oncology, neurology and for treatment planning as guidance for radiation therapy. The in vivo pharmacokinetics of boron carrier for BNCT and the quantification of ^{10}B in living tissue were performed by PET in the late nineties using compartmental models based on PET data. Nowadays PET and PET/CT have been used to address the issue of pharmacokinetic, metabolism and accumulation of BPA in target tissue. The added value of the use of *L*-^{18}F-BPA and PET/CT in BNCT is to provide key data on the tumour extraction of ^{10}B-BPA versus normal tissue and to predict the efficacy of the treatment based on a single-study patient analysis. Due to the complexity of a binary treatment like BNCT, the role of PET/CT is currently to design new criteria for patient enrolment in treatment protocols: the *L*-^{18}F-BPA/PET methodology could be considered as an important tool in newly designed clinical trials to better estimate the concentration ratio of BPA in the tumour as compared to neighbouring normal tissues. Based on these values for individual patients the decision could be made whether a BNCT treatment could be advantageous due to a selective accumulation of BPA in an individual tumour. This approach, applicable in different tumour entities like melanoma, glioblastoma and head and neck malignancies, make this methodology as reliable prognostic and therapeutic indicator for patient undergoing BNCT.

Keywords: PET; BNCT, BPA, ^{18}F-BPA; glioblastoma; head and neck malignances; treatment planning.

1. Introduction

Positron Emission Tomography (PET) has become a leading imaging modality in clinical practice and biomedical research due to its ability to quantify biochemical processes and study their dynamic evolution in vivo [1]. The integration of PET and Computed Tomography (CT) in hybrid PET/CT scanners covered the practical gap to relate information on radiotracer distribution to anatomy and organ structure. Nowadays, molecular imaging based on PET/CT is entering a new age that moves this modality from the early quest for disease location to approach more effective measurement that may carry to a personalized medicine [2].

Assessing single patient response to therapy and qualifying the patient for the best therapy are some of the most stringent requests of modern healthcare and as a consequence a major concern for healthcare technology and drug developers.

In particular, a strong effort is required to address those pathologies that are still missing adequate treatment, such as incurable and rare diseases. Gliomas include a number of tumors that, due to their anatomical location or malignancy, still are characterised by high mortality and very poor life expectancy [3-5].

Boron Neutron Capture Therapy was proposed quite a long time ago as a possible treatment for lethal brain tumors and first trials started already during 1950's but the lack of boronated molecules that

could efficiently load the necessary ^{10}B-concentration to the lesion while maintaining a very high ratio to healthy tissues proved to be the major limitation. Despite many efforts, the lack of a ^{10}B-carriers highly selective for the tumor and in methodology able to monitor the absolute ^{10}B-concentration in vivo still remains the challenging issues. Only two compounds, although recognized not enough selective, yielded positive results as ^{10}B-carriers: an inorganic salt, disodium mercaptoundecahydrododecaborate (BSH) and, in particular, an aromatic amino acid, 4-dihydroxyborylphenylalanine (BPA). Indeed, BPA appears to be in larger use in early (I, II and I/II phases) clinical trials because its very low toxicity and differential target/non target extraction.

In general, drug development is a very complex and cumbersome activity; developing a product (BPA or a related substance) aimed at being at the same time a drug and a proactive medium in external beam radiotherapy poses relevant difficulties.

The in vivo pharmacokinetics of boron carrier for BNCT and the quantification of ^{10}B in target tissue soon became the hinging point of the effort to optimize the target delivery and then the BNCT efficacy [6-9].

2. Subjects and Methods

The integration of PET and Computed Tomography (CT) in hybrid PET/CT scanners and the added value of providing a direct link of information on radiotracer distribution to anatomy and organ structure and marked also a milestone in the integrated use of molecular imaging both via post-processing approaches such as image fusion and further developing hybrid scanners such as SPECT/CT and PET/MRI.

Nowadays, molecular imaging based on *functional Magnetic Resonance Imaging* (*fMRI*), MRS and PET/CT- is entering a new age that moves modalities from the early quest for disease location to approach exquisite measurement that may be a promising road to personalised medicine [5]. Molecular imaging modalities are regarded as interesting tools to fill the gap of understanding BPA in vivo pharmacokynetics, and attention was mostly paid to Magnetic Resonance Spectroscopy (MRS) and PET.

Although the ability to detect signals from substrates, such it would be for BPA, once administered and extracted by the tumor (and the signal of the aromatic protons of BPA falls outside most of signals coming from the tissues components), still the large voxel dimension (8-10 ml) keeps MRS far from the desired spatial resolution and this together with the low sensitivity (a minimum detectable tissue concentration is estimated at level of 2 mM with 1.5T) make this modality attractive but still to be developed.

PET, featuring high sensitivity of quantitative imaging was also considered a possible tool to study BPA pharmacology. Moreover, the parent BPA had to be labelled with a positron emitter (β+) nucleus in order to be used with PET.

^{18}F-labelled BPA (4-dihydroxyboryl-2-[^{18}F]fluoro-*D,L*-phenylalanine, [^{18}F]BPA) was then labelled using [^{18}F]acetylhypofluorite as electrophilic fluorinating agent and protected BPA as substrate (Ishiwata, 1991). This early experiment obtained promising results on labelled BPA pharmacokinetics and its metabolic stability in vivo. Effect of enantiomeric purity and stereoisomerism was studied soon after (Ishiwata 1992) demonstrating that L-form was superior to racemate.

Trying to improve boronated drug availability and extraction by brain lesions, different BPA formulations were tested and BPA-fructose adduct was selected due to lower side effects and easier administration. A labelled analogue of the adduct, obtained formulating [^{18}F]BPA prepared by electrophilic fluorination with fructose, was studied in vivo with PET (Reddy, 1995).

However, tracer quantification by PET requires specifically designed protocols based on dynamic acquisitions, image correction and proper scanner calibration.

In late 90's PET dynamic studies were performed (Kabalka 1997, Imahori 1998) and first steps in [^{18}F]BPA modelling and quantification [6-9]. *Time activity curves* (*TAC*) were derived from dynamic images, while input function were either based on vascular images (e.g. carotid artery) or obtained by arterial blood sampling.

Tissue and blood data were then analysed using pharmacological models such as a classical four compartments model, extracellular (free and bound) in equilibrium with intracellular (free and bound), that could eventually be reduced to three provided recirculating activity and metabolites were measured in blood. Although, in these preliminary tests, single rate constant were variable from patient to patient global influx constant, considering a Gjedde-Patlak approach on the late portion of *TAC'*s, was rather stable.

This was opening the way to a perspective use of PET evaluation of ^{18}F-BPA tumor extraction and regional distribution as an indicator of BPA uploading by lesions, following the scout approach often used before dose scale up in radiometabolic therapy.

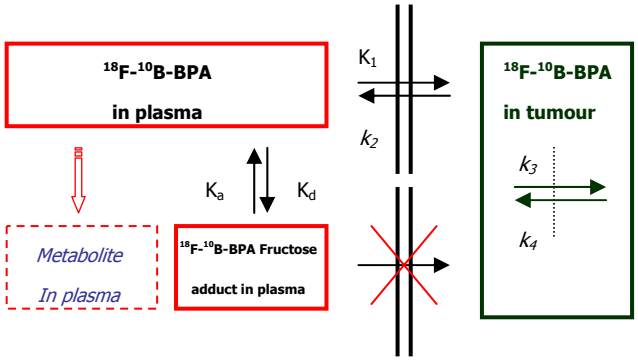

Figure 1: example of three compartment model of L-^{18}F-BPA adopted for assessing the pharmacokinetic of BPA in patients. Rate constants K1 [ml• g-1•min^{-1}], *k2* [min^{-1}], *k3* [min^{-1}], *k4* [min^{-1}] used in the four-parameters model for ^{18}F-^{10}BPA. K_a and K_b represent the dissociation/association process of the fructose-BPA adduct. The ^{10}B extraction in tissues can be calculated from the values of K1, *k2, k3, k4* obtained by PET with ^{18}F-BPA and the input function of *L*-BPA

However, the correlation has to be demonstrated between uptake of ^{18}F-BPA in vivo and the levels of ^{10}B retained by the lesion under the condition of BPA pretreatment used during patient preparation for BNCT as well as the ability of such a technique to account for disease differences and clinical conditions (Takahashi 2003) [10].

Fostering this approach, it was recently shown the potential of PET imaging for the assessment of BPA accumulation in lesions different from high-grade gliomas. 18F-BPA has been used in metastatic malignant melanoma (Busse 2003), head and neck malignancies (Kankaranta 2007), low grade brain tumours -such as schwannoma and meningioma- (Havu-Aurén 2007), and recurrent cancer in the oral cavity (Ariyoshi 2007) and cervical lymph node metastasis (Aihara, 2006). [11-14]

These clinical findings, all based on quantitative studies [15], are addressing the evaluation of transport and accumulation of BPA, and are also providing valuable data to reinforce the statement that PET with ^{18}F-BPA has a future in screening different types of tumour lesion candidate for BNCT.

4. Discussion

The expected added value of the use of ^{18}F-BPA and PET in BNCT is to provide key data on the tumour extraction of ^{10}BPA versus normal tissue. This has two major implication from one side the possibility to predict the efficacy of the treatment based on a single-study, case-by-case patient analysis thus excluding subjects that are expected not to benefit from treatment; from the other side the regional concentration of ^{18}F-BPA, once correlated to the concentration of the boronated drug, would provide a map of regional ^{10}B concentration. This is essential to obtain a meaningful treatment planning (TP). Most TP's have been calculated so far using ^{10}B concentration derived from phantom, averaging ^{10}B concentration on the gross lesion volume obtained from CT or MRI images, or ex vivo punctual measurements, e.g. after surgical excision of the lesion bulk, but facing relevant discrepancies with real situation due to partial volume errors affecting residual mass.

Alternative approaches other than ^{18}F-BPA/PET have been recently investigated to predict the ^{10}B extraction and assessing the metabolic viability with different labeled aminoacids, like as *O*-(2-^{18}F-fluoroethyl)-L-tyrosine [16-19]. The potential use of these indicators may be adopted in centers were the ^{18}F-BPA is not clinically available to screen the patients candidate to BNCT [19]. The labeled aminoacid analogues, can also be adopted after BNCT to monitor the effectiveness of the treatment as aids to differentiate the active and proliferating treated area.

Ability of PET, in particular PET/CT, to give precise and regional indication on viable proliferating tissue and, in perspective, boron-10 mapping means that more precise and well shaped TP's or treatment optimization might be achieved.

BNCT, as a binary treatment, is a per se complex modality; furthermore the patient cohort that may benefit from this treatment is severely ill and difficult to deal with: the role of PET/CT is then to be an important tool in the design of clinical trials to better estimate the concentration ratio of BPA in the tumour as compared to neighbouring normal tissues and to design new criteria for patient enrolment in treatment protocols. Hopefully, this would also contribute to and speed the process of clinical trials progress toward Phase II and Phase III.

References

[1] Hiroshi Watabe, Yoko Ikoma,Yuichi Kimura,Mika Naganawa, Miho Shidahara Annals of Nuclear Medicine Vol. 20, No. 9, 583–588, 2006, "PET kinetic analysis—compartmental model"

[2] Schöder H, Erdi YE, Larson SM, Yeung HW. Eur J Nucl Med Mol Imaging (2003) 30:1419–1437, "PET/CT: a new imaging technology in nuclear medicine"

[3] Michela Lecchi, Piero Fossati, Federica Elisei, Roberto Orecchia, Giovanni Lucignani, Eur J Nucl Med Mol Imaging DOI 10.1007/s00259-007-0631-y "Current concepts on imaging in radiotherapy"

[4] Anca-Ligia Grosu, Morand Piert, Wolfgang A. Weber, Branislav Jeremic, Maria Picchio, Ulrich Schratzenstaller, Frank B. Zimmermann, Markus Schwaiger, Michael Molls , Strahlenther Onkol 2005;181:483–99 "Positron Emission Tomography for Radiation Treatment Planning"

[5] Andreas H. Jacobs, Lutz W. Kracht, Axel Gossmann, Maria A. Ru¨ger, Anne V. Thomas, Alexander Thiel, Karl Herholz . The Journal of the American Society for Experimental NeuroTherapeutics, Vol. 2, 333–347, April 2005 "Imaging in Neurooncology"

[6] George W. Kabalka, Gary T. Smith, Jonathan P. Dyke, William S. Reid, C.P. Desmond Longford. Tony G. Roberts, N. Kesavulu Reddy, Edward Buonocore and Karl F. Hubner, J Nuc Med, 1997; 38:1762-1767 "Evaluation of Fluorine-18-BPA-Fructose for Boron Neutron Capture Treatment Planning"

[7] Yoshio Imahori,2 Satoshi Ueda, Yoshio Ohmori, Kenji Sakae, Tsukasa Kusuki, Tooru Kobayashi, Masao Takagaki, Koji Ono, Tatsuo Ido, Ryou Fujii., Vol. 4, 1825-1832, August 1998 Clinical Cancer Research, "Positron Emission Tomography-based Boron Neutron Capture Therapy Using Boronophenylalanine for High-Grade Gliomas: Part I"

[8] Yoshio Imahori,2 Satoshi Ueda, Yoshio Ohmori, Kenji Sakae, Tsukasa Kusuki, Tooru Kobayashi, Masao Takagaki, Koji Ono, Tatsuo Ido, Ryou Fujii, Vol. 4, 1833-1841, August 1998 Clinical Cancer Research, "Positron Emission Tomography-based Boron Neutron Capture Therapy Using Boronophenylalanine for High-Grade Gliomas: Part II"

[9] Yoshio Imahori, Satoshi Ueda, Yoshio Ohmori, Tsukasa Kusuki, Kqji Ono, Ryou Fujii and Tatsuo Ido , J Nuc Med 1998; 39:325-333 "Fluorine-18-Labeled Fluoroboronophenylalanine PET in Patients with Glioma"

[10] Yoshinobu Takahashi, Yoshio Imahori, Katsuyoshi Mineura, Clinical Cancer Research Vol. 9, 5888–5895, December 1, 2003 "Prognostic and Therapeutic Indicator of Fluoroboronophenylalanine Positron Emission Tomography in Patients with Gliomas"

[11] Yasunori Ariyoshi , Shin-Ichi Miyatake , Yoshihiro Kimura , Takeshi Shimahara , Shinji Kawabata , Kenji Nagata , Minoru Suzuki , Akira Maruhashi , Koji Ono , Masashi Shimahara, Oncol. Rep. 2007 Oct; 18(4):861-6 "Boron Capture Therapy using epitermal neutrons for recurrent cancer in the oral cavity and cervical lymph node metastasis"

[12] Katja Havu-Aurén, Johanna Kiiski, Kaisa Lehtiö, Olli Eskola1, Martti Kulvik, Ville Vuorinen, Vesa Oikonen, Jyrki Vähätalo, Juha Jääskeläinen, Heikki Minn, European Journal of Nuclear Medicine and Molecular Imaging Vol. 34, No. 1, January 2007 Uptake of 4-borono-2-[18F]fluoro-L-phenylalanine in sporadic and neurofibromatosis 2-related schwannoma and meningioma studied with PET

[13] Teruhito Aihara, Junichi Hiratsuka, Norimasa Morita, Masako Uno, Yoshinori Sakurai, PhD,3 Akira Maruhashi, Koji Ono, Tamotsu Harada, Boron Neutron Capture Therapy HEAD & NECK—DOI 10.1002 Sept. 2006 Case Report "First clinical case of boron neutron capture therapy for head and neck malignancies using 18F-BPA PET"

[14] George W. Kabalka, Trent L. Nichols, Gary T. Smith, Laurence F. Miller, Mohammad K. Khan Paul M. Busse, Journal of Neuro-Oncology 62: 187–195, 2003 "The use of positron emission tomography to develop boron neutron capture therapy treatment plans for metastatic malignant melanoma"

[15] Matthias T. Wyss, Silvia Hofer, Martin Hefti, Esther Bartschi, Catrina Uhlmann, Valerie Treyer, Ulrich Roelcke, J Nucl Med 2007; 48:1047–1052 "Spatial Heterogeneity of Low-Grade Gliomas at the Capillary Level: A PET Study on Tumor Blood Flow and Amino Acid Uptake"

[16] Kiichi Ishiwata, T, Hideo Tsukad, Kazuo Kubota, Tadashi Nariai, Norihiro Harada, Kazunori Kawamura, Yuichi Kimura, Keiichi Oda, Ren Iwata, Kenji Ishii, Nuclear Medicine and Biology 31 (2004) 191–198, Evaluation of O-[11C]methyl-L-tyrosine and O-[18F]fluoromethyl-Ltyrosine as tumor imaging tracers by PET

[17] Kiichi Ishiwata, T, Hideo Tsukad, Kazuo Kubota, et al., Nuclear Medicine and Biology 31 (2004) 191–198, Evaluation of O-[11C]methyl-L-tyrosine and O-[18F]fluoromethyl-Ltyrosine as tumor imaging tracers by PET

[18] Kiichi Ishiwata, T, Hideo Tsukad, Kazuo Kubota, et al., Nuclear Medicine and Biology 31 (2004) 191–198, Evaluation of O-[11C]methyl-L-tyrosine and O-[18F]fluoromethyl-Ltyrosine as tumor imaging tracers by PET

[19] Mehrkens JH, Pöpperl G, Rachinger W, Herms J, Seelos K, Tatsch K, Tonn JC, Kreth FW. J Neurooncol. 2008 May;88(1):27-35 The positive predictive value of O-(2-[18F]fluoroethyl)-L-tyrosine (FET) PET in the diagnosis of a glioma recurrence after multimodal treatment.

Basic Methodology for Application to BNCT Using *In Vivo* Boron Imaging

Yoshio Imahori [1,2], Kenichi Kashihara [2], Shin-Ichi Miyatake [1,3], Itsuro Kato [4], Ryo Fujii [1], Masaru Nakamura [1], Ariyoshi Fushimi [5], Kaori Yamashita [5], Tatsuo Ido [6], Takashi Yamashita [2,7], Koji Ono [8]

[1] *Cancer Intelligence Care Systems, Inc.,Tokyo,* [2] *Department of Radiation Oncology*, *Tokyo Radiation Oncology Clinic, Tokyo,* [3] *Department of Neurosurgery, Osaka Medical College, Osaka,* [4] *Department of Oral and Maxillofacial Surgery II, Osaka University,* [5] *Resorttrust, Inc., Nagoya,* [6] *Japan Radioisotope Association, Tokyo,* [7] *Cancer Institute Hospital, Tokyo,* [8] *Kyoto University Research Reactor Institute, Kyoto.*

Boron neutron capture therapy (BNCT) has been reported to be effective in some kind of cancers. Positron emission tomography (PET) is very important method from a view point of evidence-based medicine (EBM). Capacity for taking the boron-10 compound is variety in each cancer so that PET study using fluoroboronophenylalanine (FBPA) is very effective as application to each cancer. In this report, it is a purpose to arrange the methodology for extended application to BNCT.

A basic method for the research of the extended application has been performed by *in vivo* measurement using PET with F-18 labeled FBPA. Each tumor was confirmed histopathologically, and each location was considered with MRI. The optimal administering method was arranged, and intra-venous or intra-arterial injection was performed to a patient with cancer. The time-activity curve was obtained by PET and the kinetic constants were calculated using an assumption kinetic model.

In patients with breast cancer, they were measured by FBPA-PET. Radioactivity accumulated 60 min after intra-venous injection of FBPA. The tumor to normal (T/N) ratio was 4.2. It has demonstrated the possibility to apply BNCT to breast cancer. In patients with oro-pharyngeal cancer, the catheter was put on the external carotid artery, and radioactivity was accumulated after the injection, but gradually decreased. The radioactivity curve in the lesion within the area of external-artery was suited to those of simulation from the model using following "probability equation".

$$P_{B(n+1)} = P_{B(n)}(1 - 2*K_{(B-A)}) + K_{(B-A)}.$$

$$P_{B(n)} = a + b*p^{n}.$$

where $P_{B(n)}$ is probability of a concentration in compartment B (tissue), and A means arterial compartment.

It was able to be confirmed to boron imaging that simulation and the measurement value were corresponding in intra-venous or intra-arterial condition. Further, it may be possible to simulate boron concentration in tumor tissue by the "diffusion equation" for BSH. This method can be performed by the concept of PS-products (permeability-surface area). It may be possible to adopt for practical use.

PET pharmacokinetic analysis to estimate boron concentration in tumor and brain as a guide to plan BNCT for malignant cerebral glioma

Tadashi Nariai[1], Kiichi Ishiwata[2], Yuichi Kimura[3], Motoki Inaji[1], Toshiya Momose[1], Tetsuya Yamamoto[4], Akira Matsumura[4], Kenji Ishii[2], Kikuo Ohno[1]

[1] *Department of Neurosurgery, Tokyo Medical and Dental University, Tokyo, Japan*
[2] *Positron Medical Center, Tokyo Metropolitan Institute of Gerontology, Tokyo, Japan*
[3] *Molecular Imaging Center, National Institute of Radiological Sciences, Chiba, Japan*
[4] *Department of Neurosurgery, University of Tsukuba, Tsukuba, Japan*

Abstract

Introduction: To plan the optimal BNCT for patients with malignant cerebral glioma, estimation of the ratio of boron concentration in tumor tissue against that in the surrounding normal brain (T/N ration of boron) is important. We report a positron emission tomography (PET) imaging method to estimate T/N ratio of tissue boron concentration based on pharmacokinetic analysis of amino acid probes. Methods: Twelve patients with cerebral malignant glioma underwent 60 min dynamic PET scanning of brain after bolus injection of ^{18}F-borono-phenyl-alanine (FBPA) with timed arterial blood sampling. Using kinetic parameters obtained by this scan, T/N ratio of boron concentration elicited by one hour constant infusion of BPA, as performed in BNCT, was simulated by Runge-Kutta algorithm. ^{11}C-methionine (MET) PET scan, which is commonly used in worldwide PET centers as brain tumor imaging tool, was also performed on the same day to compare the image characteristics of FBPA and that of MET. Result: PET glioma images obtained with FBPA and MET are almost identical in all patients by visual inspection. Estimated T/N ratio of tissue boron concentration after one-hour constant infusion of BPA, T/N ratio of FBPA on static condition, and T/N ratio of MET on static condition showed significant linear correlation between each other. Conclusion. T/N ratio of boron concentration that is obtained by constant infusion of BPA during BNCT can be estimated by FBPA PET scan. This ratio can also be estimated by MET-PET imaging. As MET-PET study is available in many clinical PET centers, selection of candidates for BNCT may be possible by MET-PET images. Accurate planning of BNCT may be performed by static images of FBPA PET. Use of PET imaging with amino acid probes may contribute very much to establish an appropriate application of BNCT for patients with malignant glioma.

Keywords: PET, BPA, methionine glioblastoma

1. Introduction

To plan the optimal boron neutron capture therapy (BNCT) for patients with malignant cerebral glioma, estimation of the ratio of boron-10 concentration in tumor tissue against that in the surrounding normal brain (T/N ration of boron) is important. Imahori et al. reported that ^{18}F labelled boronophenylalanine (FBPA) is a suitable imaging probe for positron emission tomography (PET) imaging (Imahori et al. 1998; Imahori et al. 1998). They indicated that, by measuring the T/N ratio of radioactivity of FBPA, T/N ratio of boron-10 obtained by infusion of BPA during BNCT.

Therefore, FBPA PET can be used to screen the appropriate candidate who can be benefited by BNCT. FBPA PET data may be used for dose planning of BNCT (Miyatake et al. 2005).

FBPA is a radiolabelled amino acid analogue that passes through intact blood-brain barrier (BBB) through large amino acid transporter and accumulates in the active tumor cells that invaded beyond the area with BBB disruption. Therefore, amino acid probe can be used to deliver therapeutic agent into malignant glioma as BPA. Positrons labelled amino acids are also used for glioma imaging with PET. T/N of radiolabelled amino acids is reported to correspond well with tumor grade and to predict prognosis of patients with glioma (Nariai et al. 2005).

Among various positron labelled amino acid probes, ^{11}C methionine (MET) is most widely used probe in world wide clinical PET centres because of its

clinical availability (Singhal et al. 2008). As clinical data of MET is accumulated in many institutions including ours (Nariai et al. 2005), we considered that to compare image characteristics of two probes, FBPA and MET, is important to establish the use of PET to plan the optimum BNCT. We also tried to establish an appropriate method to estimate T/N ratio of tissue boron concentration based on pharmacokinetic analysis of amino acid probes using PET

2. Subjects and Methods

Twelve patients with cerebral malignant glioma (11 glioblastoma maltiforme and 1 anaplastic astrocytoma) underwent 60 min dynamic scanning of brain by PET scanner (Headtome V, Shimadzu, Kyoto, Japan) after bolus injection of ^{18}F-borono-phenyl-alanine (FBPA) (250MBq) with timed arterial blood sampling. The transmission data were acquired for each patient with a rotating germanium-68 rod source for attenuation correction. Using kinetic parameters obtained by this scan, T/N ratio of boron concentration elicited by one hour constant infusion of BPA, as performed in BNCT, was simulated by Runge-Kutta algorithm (Press et al. 2002)

^{11}C-methionine (MET) PET scan was also performed on the same day to compare the image characteristics of FBPA and that of MET. PET measurements were carried out by measuring the equilibrated radioactivity 20 min after i.v. MET injection (250 MBq)

FBPA-PET and MET-PET were co-registered using automated image registration program (Ardekani et al. 1995) working on a medical image analysis program Dr. View (Asahi Kasei Information System, Co. Ltd., Tokyo, Japan) working on a personal computer.

Regions of interest were manually placed on the tumor and contralateral normal brain. When tumor is heterogeneous characteristics such with different degree of contrast enhancement in location-by-location, or when a patient bore multiple tumors, multiple regions of interest were taken in single patient.

Ethical committee of Tokyo Metropolitan Institute of Gerontology has approved these clinical research protocols.

3. Results

PET glioma images obtained with FBPA and MET are almost identical in all patients by visual inspection. Some representative images were shown in Figure 1. The estimated T/N ratio of tissue boron concentration after one-hour constant infusion of

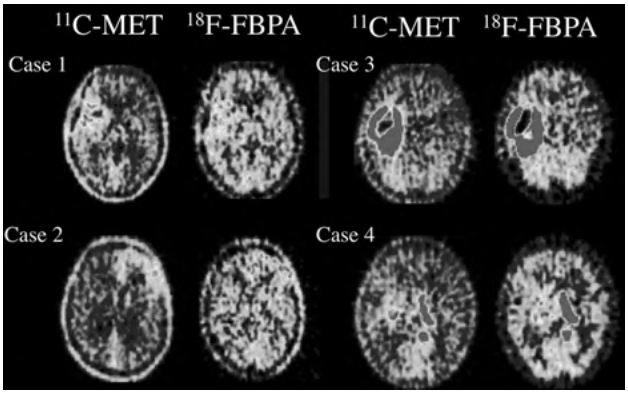

Figure 1. PET images of representative four patients with glioblastoma were displayed. ^{11}C methionine (MET) images and ^{18}F-fluoroboronophenylalanine (FBPA) images were coregistered with each other by image registration program and displayed in side-by-side. By visual inspection, PET tumor images of two different tracers are almost identical

BPA, T/N ratio of FBPA on static condition showed close linear correlation. Correlation coefficient (R^2 =0.89) is high enough to be used in clinical practice (Figure 2). T/N ratio of MET on static condition also showed significant linear correlation with the estimated T/N ratio of tissue boron concentration after one hour constant infusion of BPA.

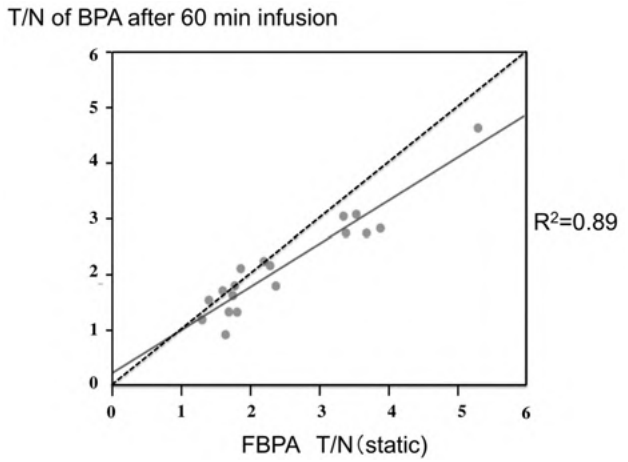

Figure 2. A graph to indicate the relationship between the T/N ratio of FBPA on static PET scan (x-axis) and the T/N ratio of tissue boron concentration after one hour constant infusion of BPA estimated by a pharmacokinetic analysis of dynamic FBPA PET scan (y-axis). Solid line indicates linear regression fit with high correlation coefficient (R^2=0.89). Dotted line indicates line of identity

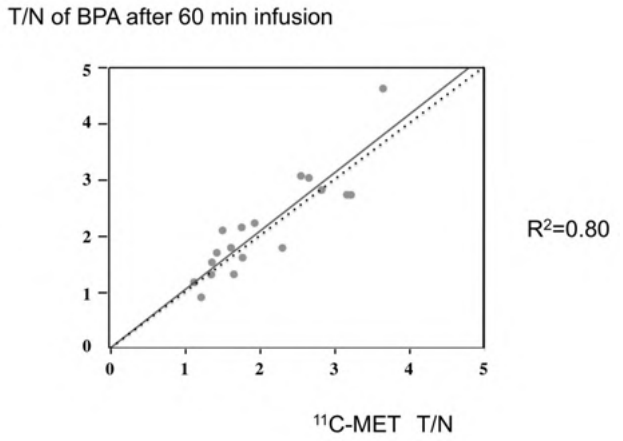

Figure 3. A graph to indicate the relationship between the T/N ratio of MET on static PET scan (x-axis) and the T/N ratio of tissue boron concentration after one-hour constant infusion of BPA estimated by a pharmacokinetic analysis of dynamic FBPA PET scan (y-axis). Solid line indicates linear regression fit with high correlation coefficient (R^2=0.80). Dotted line indicates line of identity

Though the correlation coefficient (R^2=0.80) is slightly lower than that obtained in FBPA PET, it also showed highly close linear correlation and may be fit for screening of BNCT candidates (Figure 3).

4. Discussion

Our present clinical PET research indicated that T/N ratio of boron concentration that is obtained by constant infusion of BPA during BNCT can be estimated by FBPA PET scan. This ratio can also be estimated by MET-PET imaging. As the effectiveness of BNCT for malignant glioma mainly depends on the degree of accumulation of ^{10}B in glioma cell in comparison to the surrounding brain, result of PET amino acid protocol may be an important factor to determine the indication of BNCT.

We have conducted present clinical research as a basis to a basis to establish clinical PET protocol in BNCT. As indicated in the present study, FBPA-PET may be the most reliable indicator to estimate tissue boron concentration. This tracer, however, is not available in most for clinically orientated PET centers to date, and therefore it is not possible to screen all the treatment candidates by this technique. On the other hand, MET-PET study is available in many worldwide clinical PET centers.

Selection of candidates for BNCT may be adequately performed by MET-PET images as sufficient linear regression line displayed in figure 3 indicates.

Use of PET amino acid imaging may not be useful not only for screening the candidates but also inevitable to monitor the effectiveness of BNCT. When BNCT is effective, necrotic tissue may appear. Such necrosis is difficult to differentiate from tumor progression by MRI. Use of amino acid PET, whichever FBPA or MET, is known to be a useful tool to differentiate those two opposite condition (Tsuyuguchi et al. 2004; Miyashita et al. 2008). MET PET is also known to be effective in monitoring the multimodal treatment of malignant glioma by expressing tumor viability by T/N ratio (Nariai et al. 2005; Galldiks et al. 2006). As these reports suggest, PET amino acid imaging may be able to contribute to whole process of BNCT for malignant glioma.

References

Ardekani, B.A., Braun, M., Hutton, B.F., Kanno, I.Iida, H., 1995. A fully automatic multimodality image registration algorithm. J Comput Assist Tomogr 19(4): 615-23

Galldiks, N., Kracht, L.W., Burghaus, L., Thomas, A., Jacobs, A.H., Heiss, W.D.Herholz, K., 2006. Use of 11C-methionine PET to monitor the effects of temozolomide chemotherapy in malignant gliomas. Eur J Nucl Med Mol Imaging 33(5): 516-24

Imahori, Y., Ueda, S., Ohmori, Y., Kusuki, T., Ono, K., Fujii, R.Ido, T., 1998. Fluorine-18-labeled fluoroboronophenylalanine PET in patients with glioma. J Nucl Med 39(2): 325-33

Imahori, Y., Ueda, S., Ohmori, Y., Sakae, K., Kusuki, T., Kobayashi, T., Takagaki, M., Ono, K., Ido, T.Fujii, R., 1998. Positron emission tomography-based boron neutron capture therapy using boronophenylalanine for high-grade gliomas: part I. Clin Cancer Res 4(8): 1825-32

Miyashita, M., Miyatake, S.I., Imahori, Y., Yokoyama, K., Kawabata, S., Kajimoto, Y., Shibata, M.A., Otsuki, Y., Kirihata, M., Ono, K.Kuroiwa, T., 2008. Evaluation of fluoride-labeled boronophenylalanine-PET imaging for the study of radiation effects in patients with glioblastomas. J Neurooncol

Miyatake, S., Kawabata, S., Kajimoto, Y., Aoki, A., Yokoyama, K., Yamada, M., Kuroiwa, T., Tsuji, M., Imahori, Y., Kirihata, M., Sakurai, Y., Masunaga, S., Nagata, K., Maruhashi, A.Ono, K., 2005. Modified boron neutron capture therapy for malignant gliomas performed using epithermal neutron and two boron compounds with different accumulation mechanisms: an efficacy study based on findings on neuroimages. J Neurosurg 103(6): 1000-9

Nariai, T., Tanaka, Y., Wakimoto, H., Aoyagi, M., Tamaki, M., Ishiwata, K., Senda, M., Ishii, K., Hirakawa, K.Ohno, K., 2005. Usefulness of L-[methyl-11C] methionine-positron emission tomography as a biological monitoring tool in the treatment of glioma. J Neurosurg 103(3): 498-507

Press, W., Teukolsky, S., Vettering, W.Flannery, B. 2002. Integration of ordinary differential equations. In (Eds), Numerical Recipes in C++. Cambridge University Press, New York**: pp** 712-755.

Singhal, T., Narayanan, T.K., Jain, V., Mukherjee, J.Mantil, J., 2008. 11C-L-methionine positron emission tomography in the clinical management of cerebral gliomas. Mol Imaging Biol 10(1): 1-18

Tsuyuguchi, N., Takami, T., Sunada, I., Iwai, Y., Yamanaka, K., Tanaka, K., Nishikawa, M., Ohata, K., Torii, K., Morino, M., Nishio, A.Hara, M., 2004. Methionine positron emission tomography for differentiation of recurrent brain tumor and radiation necrosis after stereotactic radiosurgery--in malignant glioma. Ann Nucl Med 18(4): 291-6

In vivo ^{19}F MR Imaging and Spectroscopy for the BNCT optimization

P. Porcari[a,b], S. Capuani[a,b], E. D'Amore[c], M. Lecce[d], A. La Bella[e],
F. Fasano[f], L.M. Migneco[e], R. Campanella[g,h], B. Maraviglia[b,i] and F.S. Pastore[d]

[a]*CNR-INFM SOFT, Physics Department, Sapienza University of Rome, Piazzale Aldo Moro 2,* 00185 *Rome, Italy*
[b]*Enrico Fermi Center, Compendio Viminale 00184, Rome, Italy*
[c]*Service for Biotechnology and Animal Welfare, Istituto Superiore di Sanità, Viale Regina Elena 299, 00133 Rome, Italy*
[d]*Neuroscience Department, Institute of Neurosurgery, University of Rome "Tor Vergata", Via Montpellier 1,00133 Rome, Italy*
[e]*Chemistry Department, Sapienza University of Rome, Piazzale Aldo Moro 2,* 00185 *Rome, Italy*
[f]*Neuroimaging Laboratory, Santa Lucia Foundation, IRCCS Rome, Via Ardeatina 306, 00179 Rome, Italy*
[g]*Physics Department, University of Perugia, Via A. Pascoli, 06123 Perugia, Italy*
[h]*INBB-National Institute Biostructures and Biosystems, Viale Medaglie d'Oro 305, 00136 Roma, Italy*
[i]*Physics Department, Sapienza University of Rome, Piazzale Aldo Moro 2,* 00185 *Rome, Italy*

Abstract

Introduction: Boron Neutron Capture Therapy (BNCT) is a binary radio-therapeutic modality based on the cytotoxic effects of highly ionizing particles released in the $^{10}B(n,\alpha)^{7}Li$ reaction. Aim of this work was to evaluate *in vivo* the spatial distribution and pharmacokinetics of 4-borono-2-fluorophenylalanine (^{19}F-BPA) using ^{19}F magnetic resonance imaging (MRI) and magnetic resonance spectroscopy (MRS) in a C6 tumour-bearing rat. This animal model was employed because it was well characterized and commonly used in the literature to mimic the human glioblastoma. Moreover the effect of L-DOPA as potential enhancer of ^{19}F-BPA tumour uptake was evaluated.

Methods and Materials: Eight male Wistar rats (300-350g) were anesthetized and a C6 cell suspension (10^6 cells in 10µl) was stereotatically implanted in the right hemisphere. Fourteen days after tumour implantation, rats were infused with a ^{19}F-BPA-fr-complex solution (300 mg/kg (bw)) within carotid artery. Two rats were also injected intraperitoneally with a L-DOPA solution (100 mg/kg (bw)) 24 hours before infusion. ^{1}H, ^{19}F-MRI images were acquired at 7T using the Spin-Echo (SE) sequence. (Echo-Time (TE)/Repetition-Time (TR)) were (40/2500)ms and (4.6/1800)ms for ^{1}H and ^{19}F scans respectively. To perform pharmacokinetics studies blood samples were collected from the femoral vein at different times (1-2.5-5h) after infusion.

Results: Boron distribution mapping of ^{19}F-BPA was performed, *in vivo*, using ^{19}F-MRI. Selective ^{19}F-BPA bio-distribution in C6 tumour-bearing rats was revealed by superimposing the ^{19}F image with the corresponding ^{1}H image acquired for the anatomical correlation. Characteristic uptake of ^{19}F-BPA in C6 glioma showed a maximum at 2.5h after infusion as confirmed by both ^{19}F images, collected at different times (2.5-3.5-5h) after infusion, and ^{19}F spectra acquired on blood samples. Furthermore, increased ^{19}F-BPA tumour uptake after L-DOPA pre-treatment was assessed using ^{19}F-MRI.

Conclusion: This study shows the ability of ^{19}F-MRI to selectively map the bio-distribution of ^{19}F-BPA in C6 tumour-bearing rat and provides a useful method to perform pharmacokinetics studies using ^{19}F-MRS.

Keywords: BNCT, BPA, ^{19}F-BPA, L-DOPA, MRI, ^{19}F-MRS, ^{19}F-MRI, glioma, C6 glioma, animal model, rat brain

1. Introduction

BNCT (Barth et al., 1992) is an experimental binary radiation therapy based on the cytotoxic effects of high linear energy transfer (LET) particles released from the $^{10}B(n,\alpha)^{7}Li$ reaction that occurs when ^{10}B captures a thermal neutron.

For BNCT effectiveness a large amount of ^{10}B atoms (at least 10^9 atoms of ^{10}B per targeted cell) (Barth and Soloway, 1997) should be accumulated within tumour cells in order to obtain a maximum tumour-to-brain (T:Br) ^{10}B concentration ratio. Furthermore thermal neutron fluences greater than 10^{12} n·cm^{-2} (Barth and Soloway, 1997) are needed.

Currently, the therapy is mainly used to treat malignant brain gliomas for which the conventional therapies do not provide any substantial benefit. Indeed, their prognosis is very poor with a median survival time (MST) of 6 to 12 months while their treatments are only palliative. For these incurable tumours BNCT represents a potential promise. Nowadays the therapy is being experimented in Phase II clinical trials in several centres around the world and the main challenge of researchers, involved with BNCT, is that of making it a clinically useful treatment modality in the next future. The main problem to be overcame is due to the lack of effective imaging methods to monitor the bio-distribution of ^{10}B-labelled compounds in order to estimate the efficiency of the carrier and the optimal timing of neutron irradiation. This ideal time is when tumour-to-brain (T:Br) ^{10}B concentration ratio achieves the maximum value.

The aim of our work is therefore double in optimizing BNCT therapy.

At first, in order to estimate the optimal timing of neutron irradiation, we proposed a novel imaging method for bio-distribution mapping and pharmacokinetics evaluation of BPA. The strategy used was to map ^{19}F-labelled BPA using ^{19}F NMR in a way similar to Positron Emission Tomography studies (Wang et al. 2004). The feasibility of the method was demonstrated *in vitro* (Porcari et al. 2006). In this paper, *in vivo* pharmacokinetic evaluation and selective bio-distribution of ^{19}F-BPA in C6 tumour-bearing rats were assessed using both ^{19}F MRI and ^{19}F MRS.

Then, in order to improve the effectiveness of the therapy by increasing the BPA tumour intake, the strategy used was to administrate ^{19}F-BPA-fr complex after L-DOPA preloading.

^{19}F MRI images of C6 tumour-bearing rats, acquired after ^{19}F-BPA-fr complex administration to assess the distribution mapping of the compound and to evaluate the effect of L-DOPA as potential enhancer of BPA intake are reported.

2. Materials and methods

Racemic ^{10}B-enriched ^{19}F-BPA (figure 1) was purchased from Katchem Ltd. (Czech Republic) and prepared as fructose complex (Porcari et al., 2006) because of its poor water solubility.

3,4-Dihydroxy-L-phenylalanine (L-DOPA) was purchased from Sigma Aldrich.

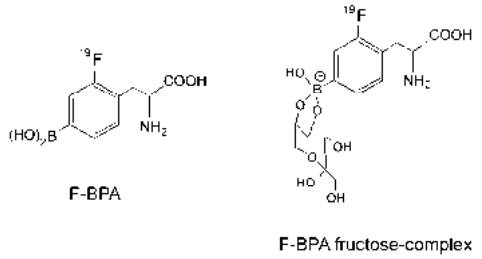

Figure 1. Chemical structures of ^{19}F-BPA and ^{19}F-BPA-fr complex

Animal model

Cell line

C6 cells (Istituto Zooprofilattico Sperimentale "B. Ubertini", Brescia, Italy) were grown in Ham's F10 medium supplemented with horse serum (15%), fetal calf serum (2,5%) and antibiotics in a humidified 5% CO_2 / 95% air at 37°C.

Tumour implantation

Brain tumours were induced in 8 (12-13 weeks old) male Wistar rats (300-350g) by stereotaxic inoculation of C6 glioma cells. All rats were anesthetized intraperitoneally using a mixture of ketamine (90 mg/kg of b.w.) and medetomidine hydrochloride (0.4 mg/kg of b.w.) before being fixed in a stereotaxic frame. A middle scalp incision was made and a C6 cell suspension (10^6 cells in 10 µl) was slowly injected (10 min) with a Hamilton syringe through a small drilled hole into the right hemisphere (2 mm anterior to the right coronal suture, 3 mm lateral to the sagittal suture, 4 mm depth). All procedures related to animal care were performed in accordance with the Legislative Decree 116/92, which represents the Italian enforcement of the European Directive 86/609/EEC.

^{19}F-BPA-fr complex administration

Fourteen days after tumour implantation, each rat was anesthetized again and surgically prepared for ^{19}F-BPA-fr complex infusion. The right internal carotid artery was cannulated and a ^{19}F-BPA-fr complex solution (300 mg/kg b.w.) was

administrated using a constant flow infusion pump. Two hours after infusion, rats underwent both ^{1}H and ^{19}F imaging in order to map ^{19}F-BPA spatial bio-distribution.

Pharmacokinetic studies were carried out by collecting blood samples from the right femoral vein at different times (1, 2.5 and 4 hours) after infusion.

L-DOPA pre-loading

To assess *in vivo* the effect of L-DOPA preloading on the BPA intake, two rats were injected intraperitoneally with a L-DOPA solution (100 mg /kg (bw)) 24 hours before ^{19}F-BPA-fr complex infusion. Rats with comparable tumour volume, assessed by ^{1}H MRI, were assigned to the experiment.

Before infusion, one of them was pre-treated with L-DOPA while the other was not (control). Subsequently both rats underwent ^{1}H and ^{19}F imaging. Histopatological assessment was performed after MRI examination to determine tumour volume. The resulting tumour dimensions were: (1.5, 0.9, 0.8) mm and (1.2, 1, 0.9) mm for L-DOPA pre-treated and not pre-treated rats, respectively.

To evaluate the ^{19}F-BPA uptake in tumour, a phantom containing an aqueous solution of ^{19}F-BPA-fr complex (20 mM) was positioned on the surface coil as a reference during MRI measurements.

Magnetic resonance measurements

In Vivo ^{1}H and ^{19}F imaging were performed using a 7T horizontal bore MR scanner (Bruker Biospec) equipped with a ^{1}H-^{19}F surface coil.

^{19}F MR axial images of rat brain were obtained using Spin Echo (SE) sequence (512 µs hermite 90° selective pulse and 200 µs hard 180° pulse) with repetition time (TR) = 1800 ms, echo time (TE) = 4.3 ms, matrix size (MTX) = 64x64 pixels, field of view (FOV) = 10 cm (in plane resolution = 1.85mm x 1.85 mm), number of slices (NS) = 1 and slice thickness (ST) = 40 mm.

Conventional T2-weighted ^{1}H MR axial images were acquired for anatomical reference with the following acquisition parameters: TR/TE = 2500/40 ms, MTX = 128 x 128 pixels, FOV = 5 x 5 cm (in plane resolution = 391µm x 391µm), NA = 2, NS = 4 and ST = 1.5 mm.

To assess ^{19}F-BPA spatial distribution mapping, ^{1}H and ^{19}F images were processed using Matlab tool in order to superimpose ^{19}F image (in colour levels of low = blue, high = red) on the corresponding anatomical ^{1}H reference (in grey levels).

Because of ^{19}F image was not slice selective, ^{1}H image consisted of the overlapping of all proton slices.

^{19}F NMR spectra of blood samples were collected using a 9.4 T vertical bore high-resolution spectrometer (Bruker Avance-400). All spectra were acquired with 1400 scans, TR = 5s and processed with a LB=1 Hz exponential filter.

3. Results and Discussion

In figure 2, selective ^{10}B bio-distribution mapping of ^{19}F-BPA-fr complex in C6 tumour-bearing rat was shown. ^{1}H axial image (tumour arrowhead) and the superimposition of ^{19}F MR axial image, acquired 2.5 hours after infusion, on its corresponding morphological reference are displayed in figure 2(a) and (b), respectively.

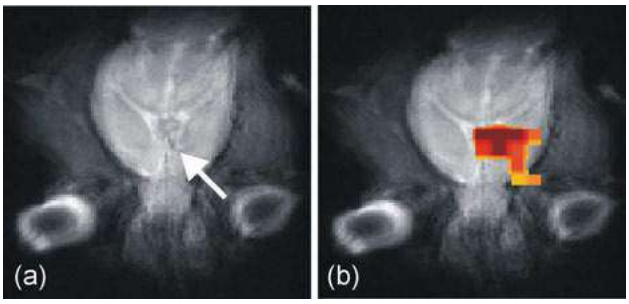

Figure 2. (a) ^{1}H MR axial image of rat brain obtained by overlapping (using Matlab Tool) all proton slices. Tumour was indicated by white arrow.
(b) Superimposition of ^{19}F MR axial image of rat brain (in colour levels: low=blue, high=red) acquired 2.5 hours after infusion on the corresponding morphological ^{1}H reference (in grey levels).

Because of the lack of ^{19}F background signal *in vivo*, the hyper-intense focus in ^{19}F image derived only from the ^{19}F-BPA signal. Furthermore the combination between ^{19}F MR monitoring of rat brain over 4 hours after infusion and the quantification of ^{19}F spectra (not reported) collected on blood samples showed a maximum uptake of ^{19}F-BPA in C6 glioma at 2.5 hours after infusion. As a consequence, these findings demonstrate that 2.5 hour after infusion is the optimal timing for neutron irradiation according to previous results (Hsieh et al. 2005) obtained using PET imaging of ^{18}F-BPA.

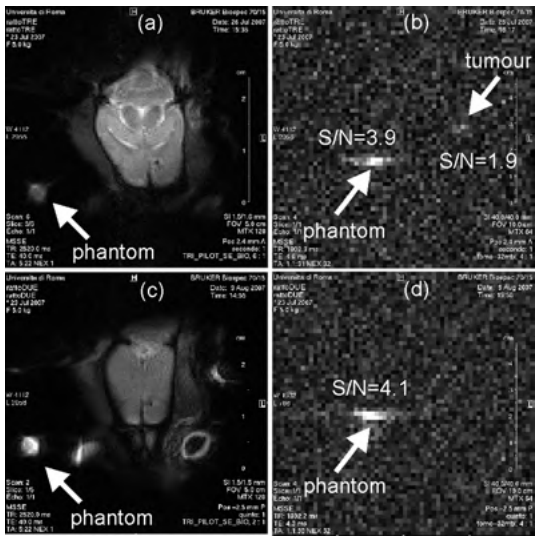

Figure 3. Upper panel: ^{1}H T2-weighted axial reference (a) and ^{19}F axial image (b) of rat brain preloaded with L-DOPA and then infused with ^{19}F-BPA-fr complex.
Down panel: ^{1}H T2-weighted axial reference (c) and ^{19}F axial image (d) of rat brain not preloaded with L-DOPA (control) but infused with ^{19}F-BPA-fr complex.
In both cases a phantom was positioned on the surface coil as a reference. Signal-to-noise (S/N) ratio of both phantom and tumour (figure 3b) and phantom (figure 3d) are reported.

To assess the effect of L-DOPA as potential enhancer of ^{19}F-BPA tumour intake, a preliminary *in vivo* experiments on C6 animal model were carried out. In figure 3, ^{1}H T2-weighted axial references (a and c) and ^{19}F axial images (b and d) of rat brain preloaded with and without L-DOPA are reported, respectively. The comparison between the ^{19}F brain images of L-DOPA pre-treated (figure 3b) and not pre-treated (control, figure 3d) rats was performed. The ^{19}F-BPA tumour signal was observed only in figure 3(b) (L-DOPA preloaded rat) but not in the other case (figure 3d) confirming thus a reasonably increasing of ^{19}F-BPA tumour uptake after L-DOPA administration (Porcari, 2007). The latter was also due to the little dimensions of both tumour volumes (reported above) measured by histopatological assessment performed immediately after imaging.

4. Conclusions

Our *in vivo* results demonstrate that ^{19}F MRI is a useful method for *in vivo* spatial distribution mapping of ^{19}F-BPA. Besides its combination with ^{19}F MRS method provides useful information on ^{19}F-BPA pharmacokinetics. Indeed *in vivo* ^{19}F images and ^{19}F spectra of ^{19}F-BPA-fr complex in C6 animal model, never reported in literature so far, confirmed evidence of maximum uptake in tumour at 2.5 hours after infusion. These findings obtained on small rodents suggest a potential future application of ^{19}F MRI and ^{19}F MRS using ^{19}F-BPA in BNCT clinical trials. Indeed, since ^{19}F NMR can be performed using ^{1}H MR scanner by suitably tuning RF coils, future clinical applications requires only minor MRI improvements to be carried out.

Furthermore, preliminary results on improved ^{19}F-BPA-fr complex uptake in C6 tumour-bearing rat after L-DOPA pre-treatment, was obtained by means of ^{19}F MRI.

References

Barth, R.F., Soloway, A.H., 1997. Boron neutron capture therapy of brain tumours – current status and future prospects. J. Neurooncol. 33, 3-18.

Barth, R.F., Soloway, A.H., Fairchild, R.G., Brugger, R.M., 1992. Boron neuron capture therapy for cancer: Realities and prospects. Cancer 70, 2995-3007.

Hsieh, C.H., Chen, Y.F., Chen, F.D., Hwang, J.J., Chen, J.C., Liu, R.S., Kai, J.J., Chang, C.W., Wang, H.E. 2005. Evaluation of pharmacokinetics of 4-borono-2-(18)F-fluoro-L-phenylalanine for boron neutron capture therapy in a glioma-bearing rat model with hyperosmolar blood-brain barrier disruption. J. Nucl. Med. 46, 1858-65.

Porcari, P., 2007 Multi-nuclear MR Spectroscopy and MR Imaging in rat brain. *In vitro* and *in vivo* results at 9.4T and 7T for the Boron Neutron Capture Therapy (BNCT) optimization. Specialty thesis in Medical Physics.

Porcari, P., Capuani, S., Campanella, R., La Bella, A., Migneco, L.M., Maraviglia, B., 2006. Multi-nuclear MRS and ^{19}F MRI of ^{19}F-labelled and ^{10}B-enriched *p*-boronophenylalanine-fructose complex to optimize boron neutron capture therapy: phantom study at high magnetic field. Phys. Med. Biol. 51, 3141-54.

Wang, H.l., Liao, A.H., Deng, W.P., Chang, P.F., Chen, J.C., Chen, F.D., Liu, R.S., Lee, J.S., Hwang, J.J., 2004. Evaluation of 4-Borono- 2-^{18}F-Fluoro-L-Phenylalanine-Fructose as a probe for boron neutron capture therapy in a glioma-bearing rat model. J. Neurooncol. 45, 302-8.

Calibration of the prompt gamma ray analysis facility in Petten for ^{10}B concentrations up to 2000 ppm

S. Nievaart[a], K. Appelman[a], F. Stecher-Rasmussen[b], W. Sauerwein[c], A. Wittig[c], R. Moss[a]

[a] *Institute for Energy, Joint Research Centre of the European Commission, Petten, the Netherlands*
[b] *NCT Physics, Alkmaar, The Netherlands*
[c] *Department of Radiation Oncology, University Duisburg-Essen, Essen, Germany*

Abstract

At the BNCT facility in Petten, the Netherlands, ^{10}B concentrations in biological materials are measured with the Prompt Gamma Ray Analyses facility, which is situated at one of the horizontal beam tubes of the High Flux Reactor. Up until recently, the quantities of ^{10}B are determined in small samples (20 mg – 1 g) of blood, urine and/or tissues, following calibration of the facility, using certified ^{10}B solutions, with a ^{10}B-concentration ranging from 0 ppm up to 210 ppm and by fitting a calibration curve of a second order polynomial through 8 measurements. The concentrations of blood and tissue were always below the 210 ppm and therefore within the measured calibration range. Recently, urine samples containing up to 2800 ppm were investigated. These values are outside the calibrated range and in a first approach results were based on extrapolation of the fitted curve. For this study, newly certified ^{10}B solutions between 374 ppm and 1972 ppm were measured in order to verify if the previous extrapolation is justified. This appears not to be the case and two calibration curves are necessary. We found that for a ^{10}B-concentration of more than 300 ppm another fitted third order polynomial is needed as beyond this level, the self-shielding of ^{10}B interacts with the measurements. This result is confirmed by simulating the whole set-up with MCNP. With the new calibration curve, materials from patients were analysed retrospectively, resulting in differences of the ^{10}B-concentrations of up to 16%, when compared to the former calibration curve.

Keywords: PGRA, ^{10}B concentration, calibration, Monte Carlo

1. Introduction

The knowledge of the precise ^{10}B concentration in tissues is one of the most important requirements for further developing BNCT. This paper investigates one of the techniques used routinely to determine ^{10}B concentration in tissues and fluids. A dedicated facility was constructed at the BNCT facility in the High Flux Reactor (HFR) in Petten (NL). In front of the so-called Horizontal Beam tube 7 (HB7), thermal neutrons can react with a sample and the eventual prompt gammas can be detected and analyzed by a high purity germanium (HPGe) detector and processing equipment. After proper calibration, this Prompt Gamma Ray Spectroscopy (PGRA) facility can detect the amount of ^{10}B in small volumes of blood, urine or tissues by counting the gammas from the ^{10}B(n,αγ)^{7}Li reaction. In 96% of these reactions, a characteristic 478 keV gamma ray is emitted. PGRA is an established tool for accurately detecting the ^{10}B concentration in biological samples. PGRA has already proven itself as a technique that provides accurately boron concentrations (Raaijmakers et al., Thellier et al and Wittig et al.). In Petten, PGRA is used to determine the ^{10}B-concentration in blood during the irradiation, in urine samples as well as in boron uptake studies on non-irradiated patients (EORTC protocols 11961, 11011 and 11001). Until recently, by far most of the measured concentrations were below 100 ppm and did not exceed the 210 ppm limit to which the facility is calibrated according to certified solutions. Some exceptions of higher ^{10}B concentrations in urine samples were encountered over the last years. Therefore, we intended to analyse these values further, as the calibration curve based on < 210 ppm was suspected to be inadequate due to the shielding effect of ^{10}B above certain values (Ye). After obtaining a certified 1972 ppm ^{10}B solution and accordingly some diluted lower concentrations, the calibration curve could be extended. In this work, after describing briefly the PGRA set up, the new curve is presented by means of measurements as well as simulations.

2. Materials and Methods

The PGRA set-up: The beam tube HB7, in front of where the PGRA facility is constructed, is one of 12 horizontal beam tubes at the Petten reactor. The HFR is of the tank-in-pool type, light water cooled and moderated and operated at 45 MW. The reactor was especially designed for materials testing purposes. Nowadays, besides material testing, reactor fuel irradiation experiments and BNCT, the main task is to produce radio-isotopes for medical purposes in hospitals all over the world. In 2006, the high enriched fuel of the HFR was replaced by low enriched fuel. This had one consequence for HB7 as will be discussed later in this section. In order to get mainly thermal neutrons at the sample position, a so-called neutron mirror is mounted on to the HB7 beam port. Figure 1 provides a schematic overview of this neutron mirror which is constructed out of Permendur® (49 m% natural cobalt, 49 m% natural iron and 2 m% vanadium).

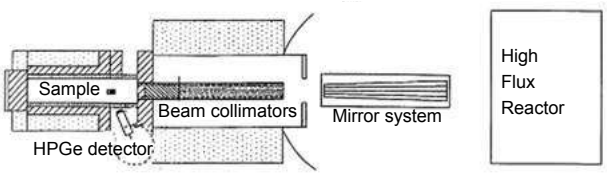

Figure 1. Schematic overview of the neutron mirror in the PGRA facility at the HB7 in Petten

The whole spectrum of neutrons coming from the core is filtered by this filter, whereby only the desired thermal ones reach the sample. More information can be found in Stecher-Rasmussen et el. For shielding purposes, lead and basalt blocks are surrounding the neutron mirror system, also forming a channel around the sample holder. The inside of this channel consists of polyethylene to absorb the neutrons. A huge concrete block is placed at the end of this channel, acting as a beam stop. The neutron spectrum in Petten is Maxwellian-shaped but slightly shifted to lower energies. The dominating neutron energy is around 18 meV (Abrahams et al.). Gammas from the reactor core cannot reach the sample position but other gammas, by neutrons induced, are present and add to the background during the measurements.

In one of the lead blocks of the channel, a cone shaped hole is constructed where a HPGe detector is positioned behind neutron absorbing shielding of polyethylene and lithium powder. The cone shaped hole has a diameter of 50 mm at the side of the detector and 40 mm at the channel side.

The HPGe detector is of the coaxial type and manufactured by Canberra® with a relative efficiency of 20% and a resolution of 2.3 keV (June 2008). The detector is positioned such that it can detect only gammas that travel nearly perpendicular to the main direction of the neutrons that enter the channel.

The data acquisition is performed by the Canberra® Digital Spectrum Analyzer DSA-1000 which is connected to a personal computer on which Genie2K® software is installed. For BNCT purposes, Genie2K® distinguish of course the ^{10}B induced gammas but also, for reference purposes, the hydrogen gamma peak out of a wide spectrum which goes up to around 2.5 MeV. The dead time of the detector system is around 25% of the net counting time. This is automatically taken care of by the system.

Calibration samples: Before measuring ^{10}B concentrations, the detector system needs to be securely calibrated with a Co-60 and Am-241 sources. Certified solutions with increasing ^{10}B concentrations are measured to establish the related count rates. This procedure is performed every time a set of samples is measured as it is directly dependent on the (cycle) status of the reactor. In this context it was noted that the PGRA facility in Petten lost around 40% of its neutron intensity after the fuel transition in 2006. This was due to another configuration of fuel elements in the reactor core, whereby fresh elements are no longer loaded in front of HB7 as previously.

Consequently, longer irradiation/counting times are necessary to obtain the same statistical accuracy as before. Up to recently, the only certified boron solutions used in Petten contain 0.000, 10.579, 21.454, 31.855, 42.037, 85.106, 146.711, 209.862 ppm ^{10}B. Large quantities of these solutions are conserved in plastic bottles and stored in a refrigerator. With the experience over recent years, this way of storing of the solutions has been proven to be stable. The so-called calibration samples are prepared in the same way as the blood, urine and tissue samples; around 1cc of the medium is put into a 1 mm thick walled plastic vial (11.0 mm diameter, 23.0 mm high) using a pipette when fluid.

A precise balance with a milligram scale is used to measure the weight of the content in the vial which is necessary to calculate the ^{10}B concentration in the sample. Lately, an extra 374.600, 544.000, 1020.000 and 1972.000 ppm ^{10}B calibration samples were made under certified conditions in a laboratory in Petten. The mother solution is H_3BO_3 containing 9968 (± 35) µg/ml natural boron of which 19.78% is ^{10}B.

In order to overcome the poor solubility when working with this (high) concentration, 1.5% NH_4OH was added.

The calibration data coming from the 8 samples (< 210 ppm) is obviously curved and is always fitted satisfactorily with a second-order polynomial. Beside a custom made program Comfit, the polynomial least-squares regression in Microsoft Excel® is used to calculate the three coefficients and their accompanying standard deviations of the second order polynomial fit.

Calculations: All measurement set-ups given in this article are simulated by Monte Carlo using MCNP4C (Briesmeister) for counting the 478 keV gammas that leave the vial. The simulation starts after the neutron mirror such that only the channel made of lead, basalt, polyethylene, the concrete stopper and the plastic vial with holder and content is modelled. The neutron source description is taken as described above. All statistical uncertainties of the simulations presented are below 1% in the 95% confidence interval. The accuracy in the count-rates of the measurements is within 5% as will be indicated in the results by error bars.

3. Results

All calibration solutions are prepared under the described certified conditions and measured for 1800 seconds per sample (excluding dead time). The measured count rates are provided in the graph with a Log-Lin scale in Figure 2. Included in the same figure are the simulated ^{10}B concentrations coming from MCNP simulations.

Since the absolute efficiency of the detector system cannot be simulated, the average ratio between the simulations and measurements is applied to translate the number of 478 keV gammas per source neutron into the real counting rates. Taking into account the accuracy of the experimental results, it can be seen in Figure 2 that the simulated outcome fits well. For this reason the extra (only) simulated count rates for extreme ^{10}B concentrations, namely 3500 and 5000 ppm, are taken for granted. Figure 3 shows the measurements and the extra simulated points again together with two polynomial fits, named 'low fit' and 'high fit', respectively, which are not forced to cross the origin. The first mentioned polynomial is of the second order and based on all measurements up to 210 ppm whilst the other polynomial is of the third order and based upon the results above 374 ppm ^{10}B concentrations. After recalculating all measured values using the appropriate fit function, it turns out that the agreement is within 4%. Again, this result is acceptable regarding the accuracy of the measurements. Note that the 'high fit' curve is also based on the simulated count rates of 3500 and 5000 ppm concentrations. The two fits have an overlap in the region between 200 and 650 ppm. The maximum underestimation in ^{10}B concentration when using the 'low fit' curve is 19%. This is around 2000 ppm. In this respect, all the data of the patients treated in Petten were re-examined in order to find such high concentrations. Two patients had ^{10}B concentrations in urine samples of 2773 and 2446 ppm, which now seem to be underestimated by 11% and 16%, respectively.

4. Conclusions

The relative count rates of the 478 keV gammas coming from the ^{10}B capture reaction and measured in the PGRA facility in Petten, can be well simulated by MCNP. With the resulting verified data we could show that the second order polynomial fit, based on samples < 210 ppm ^{10}B, cannot be applied for concentrations above 300 ppm. Above this value, a third order polynomial is needed to prevent underestimations up to 19%. Unfortunately, the authors could not accomplish a single curve fit valid for the whole range of presented boron concentrations. However, by using the two curve fits, the PGRA facility can precisely measure average ^{10}B concentrations within the full range needed for BNCT nowadays. Apart from this, as the tendency in BNCT is to obtain by means of new carriers higher ^{10}B concentrations in the cancer tissue or in the by rheumatoid arthritis affected synovium, the new curve is absolutely necessary in order to prepare the facility for future trials.

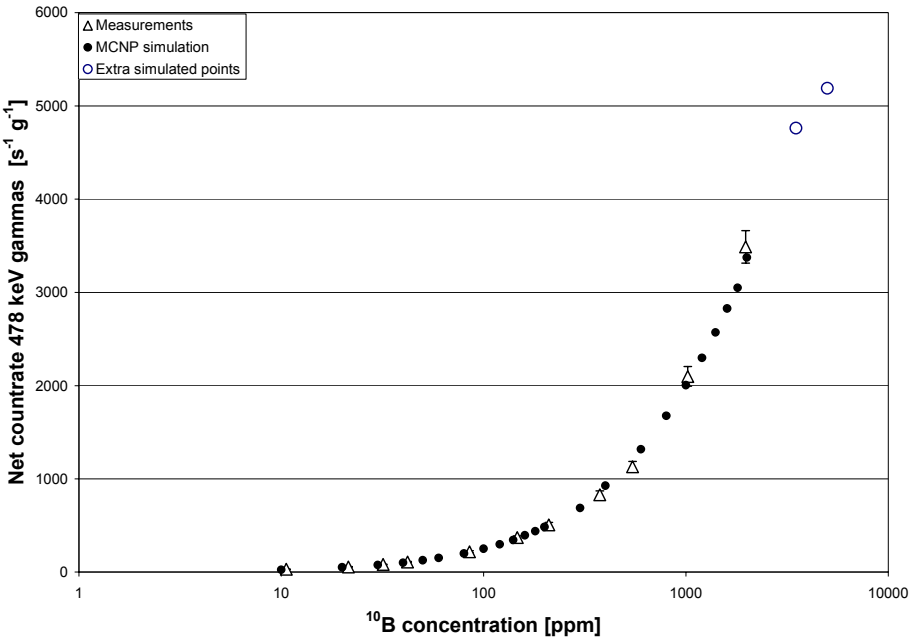

Figure 2. The measured and by MCNP simulated (up to 5000 ppm) count rates for the different ^{10}B concentrations

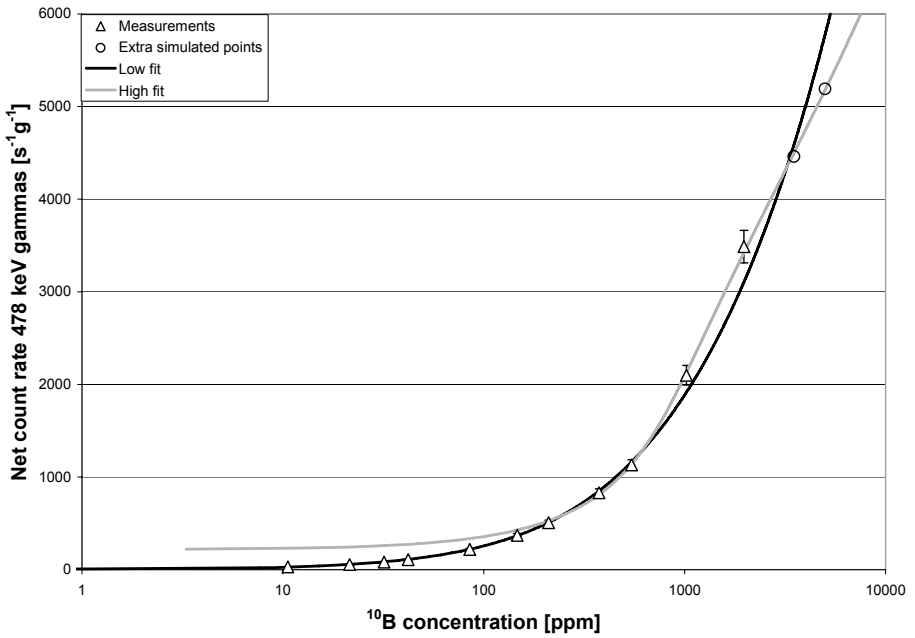

Figure 3. Measured count rates of the ^{10}B calibration solutions and two fitted polynomials. The 'low fit' curve is of the second order and based on the measurements < 210 ppm ^{10}B concentrations. The 'high fit' curve is of the third order and based on > 374 ppm measurements together with the extra simulated results for 3500 and 5000 ppm ^{10}B concentrations

References

Abrahams, K., Ratynski, W., Stecher-Rasmussen, F., Warming, E., 1966. On a System of Magnetized Cobalt Mirrors used to Produce an Intense Beam of Polarized Thermal Neutrons. Nucl. Instr. Meth., 45, 293-300.

Briesmeister, J.F., 2000. MCNP - A General Monte Carlo N-Particle Transport Code, Version 4C. LA-13709-M.

Raaijmakers, C.P.J., Konijnenberg, M.W., Dewit, L., Haritz, D., Huiskamp, R., Philipp, K., Siefert, A., Stecher-Rasmussen, F.,Mijnheer, B.J., 1995. Monitoring of blood-10B concentration for boron neutron capture therapy using prompt gamma-ray analysis. Acta.Oncol. 34, 517-523.

Stecher-Rasmussen, F., Abrahams, K., Kopecky, J., 1972. Circular Polarization of Neutron Capture Gamma-Rays from Al, Ar and Ca. Nucl.Phys., A181, 225-240.

Thellier, M., Chevallier, A., His, I., Jarvis, M.C., Lovell, M.A., Ripoll, C., Robertson, D., Sauerwein, W.,Verdus, M.C., 2001. Methodological developments for application to the study of physiological boron and to boron neutron capture therapy. J. Trace and Microprobe Techniques 19, 623-657.

Wittig, A., Michel, J., Moss, R.L., Stecher-Rasmussen, F., Arlinghaus, H.F., Bendel, P., Mauri, P.L., Altieri, S., Hilger, R., Salvadori, P.A., Menichetti, L., Zamenhof, R., 2008. Boron analysis and boron imaging in biological materials for Boron Neutron Capture Therapy (BNCT). Crit.Rev.Oncol.Hemat doi:10.101016/j. critrevonc 2008.03.004. in press.

Ye, S.J., 1999. Boron self-shielding effects on dose delivery of neutron capture therapy using epithermal beam and boronophenylalanine. Med Phys. 26(11),2488-93.

Rapid biopsy processing for secondary ion mass spectrometric (SIMS) analysis

A. Detta[1], N.P. Lockyer, M.J. Baker, J.C. Vickerman[2], G.S. Cruickshank [1]

[1] *Department of Neurosurgery, University of Birmingham, Queen Elizabeth Hospital, Birmingham, B15 2TH, UK*
[2] *Surface Analysis Research Centre, Manchester Interdisciplinary Biocentre, University of Manchester, M1 7DN, UK*

The efficacy of boron neutron capture therapy depends on the preferential accumulation of a sufficient amount of ^{10}B in the cancer cell. The determination of the presence of ^{10}B *within* the cell is thus of critical importance. One technique that shows considerable promise in this regard is secondary ion mass spectrometry (SIMS). Critical requirements of the sample preparation for high vacuum chemical imaging techniques such as SIMS are that the tissue or cell viability is preserved faithfully and chemical redistribution is minimised. For tissue samples these criteria are typically met by plunge freezing the biopsy in liquid propane, cryostating (-20 °C), thaw-mounting and freeze-drying. This process is not readily reproduced in a clinical theatre setting and is not easily applied to the tiny needle biopsies collected for routine diagnostic or other purposes. To this end, we have developed a rapid technique of tissue preservation and presentation that circumvents cryostating, and that is suitable in a clinical setting and for SIMS and complementary analysis.

Using this technique, tissue is available for SIMS analysis within 30s of removal from the patient. Importantly for sub-cellular chemical imaging, the sample temperature is maintained at -80°C or below throughout the entire processes, minimising the possibility of ionic redistribution of highly diffusible ions such as B^+. Viability was confirmed by vital dye staining and showed good preservation, especially in cell aggregates. Under H&E light microscopy, cellular morphology was excellent and architectural integrity was acceptable. Tissue integrity in SIMS is being explored by K:Na and ^{10}B uptake ratios.

The Capabilities and Limitations in the Analysis of Boron Micro-Distribution in Tumor Cells Using PIGE

K. Endo[a], Y. Shibata[a], T. Yamamoto[a]、K. Nakai[a], A. Matsumura[a], T. Sato[b], M. Oikawa[b], K. Arakawa[b], T. Kamiya[b] and K. Ishii[c]

[a]*Department of Neurosurgery, Institute of Clinical Medicine, University of Tsukuba, Ibaraki 305-8575, Japan*
[b]*Advanced Radiation Technology Center, Japan Atomic Energy Agency (JAEA), Gunma 370-1292, Japan*
[c]*School of Engineering, Tohoku University, Miyagi 980-8575, Japan*

Abstract

Micro particle-induced X-ray emission (micro-PIXE) has been applied to determine the inter- and intracellular distribution of boron (^{10}B). Because the energy of micro-PIXE from ^{10}B is too low, particle-induced gamma-ray emission (PIGE) was employed to detect gamma-rays produced by the nuclear reaction of ^{10}B (p, γ) ^{7}Be. Micro-PIGE imaging showed the distribution of boron elements in tumor tissue. Various conditions of sample preparation were compared to determine the optimal conditions to obtain clear distribution images. The result shows that the tumor BSH distribution was clearly demonstrated at a boron concentration of 250 ppm. The best measurement ranges were from 50 x 50 μm to 100 x 100μm and a measurement time from 30 to 60 minutes was required to obtain the clearest image using PIGE.

However, the intracellular micro-distribution of boron could not be clearly detected in this analysis. Improvements are therefore required in the technical methods of cell fixation and upgrading the micro-PIXE analyzing system itself.

Keywords: NCT, PIXE, PIGE, ^{10}B, micro-distribution

1. Introduction

Micro particle-induced X-ray emission (micro-PIXE) was applied to determine the inter- and intracellular distribution of boron-10 (^{10}B) in tumor cells. Because the energy of micro-PIXE from ^{10}B is too low, particle-induced gamma-ray emission (PIGE) was employed to detect the gamma-rays produced from the nuclear reaction of ^{10}B (p, γ) ^{7}Be.

Cultured 9L gliosarcoma cells grown on polycarbonate film were exposed to sodium borocaptate (BSH). To analyze the inter- and intra-cellular distribution of ^{10}B in 9L gliosarcoma cells, the cells were irradiated with a 1.7 MeV proton beam collimated to a 1 μm diameter and the emitted gamma-rays were detected. The inter- and intra-cellular distribution of ^{10}B in 9L gliosarcoma cells was directly analyzed using micro-PIGE. The results showed that the distribution of ^{10}B atoms was correctly measured. ^{10}B should have been evenly distributed in 9L gliosarcoma cells and some ^{10}B atoms showed that distribution. However, there was a significantly high background and the detection of true ^{10}B atoms was not easy. The main purpose of this study was to determine the optimal conditions to apply this technique in an *in vitro* experiment.

2. Material and Methods

Cultured 9L gliosarcoma cells were grown for 4 days on a 5 μm thick polycarbonate film. These cells were treated with 100 ppm, 250 ppm and 1000 ppm of BSH, respectively on the 3rd and 4th day. These cells were fixed on the polycarbonate film with the acute freezing on the 5th day.

The samples were analyzed to compare the distribution image of the ^{10}B atoms using the micro-PIXE analysis system with a 30 to 60 minute measuring time and a measuring range from 25 x 25 μm to 100 x 100 μm, respectively.

The peak ^{10}B atom measurement (428 Kev) was small on the measurement spectrum in comparison to the circumference background. It was possible to confirm that ^{10}B atoms were measured (**Figure 1**).

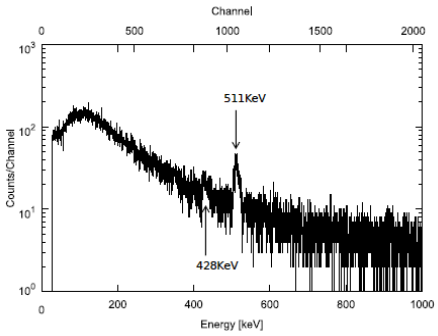

Fig.1 Energy spectrum of PIGE

The left side of **Figure 2** shows the distribution of the 9L gliosarcoma cells, made from the distribution of the sulphur (S) image as the index in measuring. The right side of **Figure 2** shows the measurement of the distribution using the ^{10}B atom channel on the spectrum.

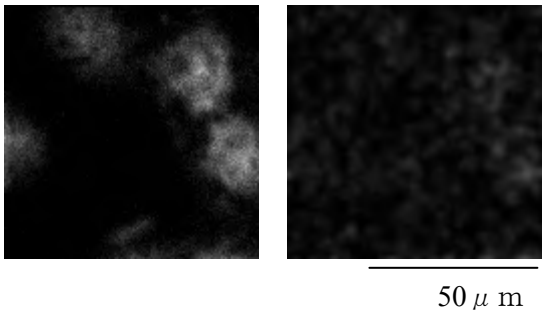

S **B**

Fig. 2 Distribution of tumor cells(S) and ^{10}B

Next, a mask was created from the distribution of sulphur and a suitable threshold value was determined. Thereafter, a PIGE spectrum was created which was specified by the masked portion and the whole spectrum was compared to the masked spectrum (**Figure 3**). It creates an energy spectrum from the data which was surrounded in the red.

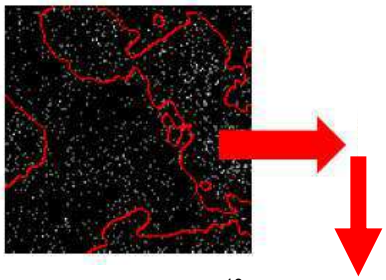

Fig.3 Distribution of ^{10}B (gray dots) and masked area (intra red line) of tumor cells (S) distribution

It was possible to confirm the presence of a correlation in the distribution of sulphur and the distribution of ^{10}B atoms because the peak (428 KeV) of ^{10}B atoms appeared more clearly in the masked spectrum (**Figure 4**).

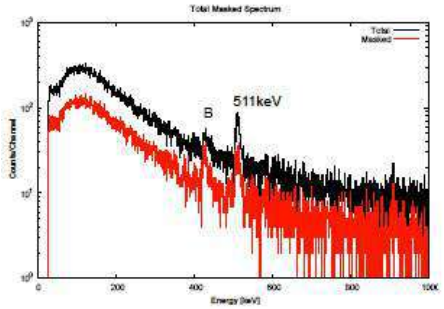

Fig.4 Total spectrum (black) and masked spectrum (red)

3. Results and Discussion

A clear correlation was observed between the distribution of tumor cells and that of ^{10}B atoms distribution when the two images in **Figure 2** were combined. This demonstrated that the ^{10}B atom was accumulating around the tumor cells.

In this *in vitro* experiment, various conditions were compared to determine the optimum conditions to yield clear distribution images. The results showed that the tumor ^{10}B distribution was clearly demonstrated at a BSH concentration of 250 ppm. The best measurement ranges were from 50 x 50 μm to 100 x 100μm and the optimal measurement time to obtain the clearest image using PIGE was from 30 to 60 minutes (**Figure 5**).

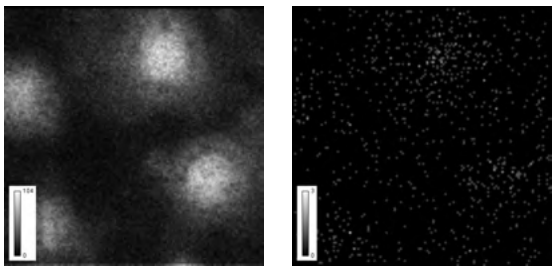

S **B**

Fig.5 Distribution of tumor cells (S) and ^{10}B

However, the intracellular micro-distribution of boron could not be clearly detected in this analysis. Improvements are necessary in the technical methods of cell fixation and upgrading the single-ended accelerator itself.

In the future, this method will be applied to analyze the intracellular micro-distribution of specific capture atoms and the development of new drugs for NCT.

4. Conclusions

It was therefore possible to measure the boron elements which were taken in by the cultured 9L gliosarcoma cells using PIGE in an *in vitro* experiment. The optimal measurement ranges were from 50 x 50 μm to 100 x 100μm, the measurement time was from 30 to 60 minutes and the optimal BSH concentration was 250 ppm to obtain the clearest image using PIGE.

Improvements are therefore necessary in the technical methods of cell fixation, while the micro-PIXE analyzing system also needs to be further upgraded.

References

Coderre J.A., Chanana A.D., Joel D.D., Elowitz E.H., Micca P.L., Nawrocky M.M., Chadha M., Gebbers J.-O., Shady M., Peress N.S., Slatkin D.N., 1998. Biodistribution of boronophenylalanine in patients with glioblastoma multiforme: Boron concentration correlates with tumor cellularity. Radiat. Res.149, 163-170.

Wegden M., Kristiansson P., Ceberg C., Munck A.F., Rosenschoeld P., Auzelyte V., Elfman M., Malmqvist K.G., Nilsson C., Pallon J., Shariff A., 2004. Nuclear microprobe analysis of the selective boron uptake obtained with BPA in brain tumour tissue. Nucl. Instr. and Meth. in Phys. Res. B 219-220, 67-71.

Endo K., Yamamoto T., Shibata Y., Tsuboi K., Matsumura A., Kumada H., Yamamoto K., Sakai T., Sato T., Oikawa M., Ohara Y., Ishii K., 2006. Demonstration of Inter- and Intracellular Distribution of Boron and Gadolinium Using Micro Particle Induced X-ray Emission (micro-PIXE). Oncol. Res. 16, 57-65.

Ceberg C.P., Brun A., Kahl S.B., Koo M.S., BRR Persson, Salford L.G.., 1995. A comparative study on the pharmacokinetics and biodistribution of boronated porphyrin (BOPP) and sulfhydryl oron hydride (BSH) in the RG2 rat glioma model. J .Neurosurgery 83, 86-92.

Chanana A.D., Capala J., Chadha M., Coderre J.A., Diaz A.Z., Elowitz E.H., Iwai J., J. Joel D.D., Jiu H.B., Ma R., Pendzick N., Peress N.S., Shady M.S., Skatkin D.N., Tyson G.W., Wielopolski L., Boron neutron capture therapy for glioblastoma multiforme: Interim results from the phase□/□ dose-escalation studies. Neurosurgery 44, 1182-1193.

Coderre J.A., Chanana A.D., Joel D.D., Elowitz E.H., Micca P.L., Nawrocky M.M., Chadha M., Gebbers J.-O., Shady M., Peress N.S., Slatkin D.N., 1998. Biodistribution of boronophenylalanine in patients with glioblastoma multiforme: Boron concentration correlates with tumor cellularity. Radiat. Res. 149, 163-170.

Coderre J.A., Elowitz E.H., Chadha M., Bergland R., Capala J., Joel D.D., Liu H.B., Slatkin D.N., Chanana A.D.,1997. Boron neutron capture therapy for glioblastoma multiforme using p-boronophenylalanine and epithermal neutrons: trial design an early clinical results. J. Neuro.-Oncol. 33, 141-152.

Accumulation of MRI Contrast Agents in Malignant Fibrous Histiocytoma for Gadolinium Neutron Capture Therapy

Takuya Fujimoto[a], Hideki Ichikawa[b], Toshihiro Akisue[c], Ikuo Fujita[a], Hitomi Hara[c], Masaya Imabori[a], Hideaki Kawamitsu[d], Masahiko Fujii[d], Masahiro Kurosaka[c] and Yoshinobu Fukumori[b]

[a]*Department of Orthopaedic Surgery, Hyogo Cancer Center, Akashi 673-0021, Japan*
[b]*Faculty of Pharmaceutical Sciences and Cooperative Research Center of Life Sciences, Kobe Gakuin University, Kobe 650-8586, Japan*
[c]*Department of Orthopaedic Surgery, Kobe University Graduate School of Medicine, Kobe 650-0017, Japan*
[d]*Department of Radiology, Kobe University Graduate School of Medicine, Kobe 650-0017, Japan*

Abstract

Neutron-capture therapy with gadolinium (Gd-NCT) has therapeutic potential, especially that gadolinium is generally used as a contrast medium in magnetic resonance imaging (MRI). The accumulation of gadolinium in a human sarcoma cell line, malignant fibrosis histiocytoma (MFH) Nara-H, was visualized by the MRI system. The commercially available MRI contrast medium (Gd-DTPA) and the biodegradable and highly gadopentetic acid (Gd-DTPA)-loaded chitosan nanoparticles (Gd-nanoCPs) were prepared as MRI contrast agents. The MFH cells were cultured and collected into three falcon tubes that were set into the 3-tesla MRI system to acquire signal intensities from each pellet by the Spin Echo method, and the longitudinal relaxation time (T1) was calculated. The amount of Gd in the sample was measured by inductively coupled plasma atomic emission spectrography (ICP-AES). The accumulation of gadolinium in cells treated with Gd-nanoCPs was larger than that in cells treated with Gd-DTPA. In contrast, and compared with the control, Gd-DTPA was more effective than Gd-nanoCPs in reducing T1, suggesting that the larger accumulation exerted the adverse effect of lowering the enhancement of MRI. Further studies are warranted to gain insight into the therapeutic potential of Gd-NCT.

Keywords: Gadolinium NCT, Chitosan, Nanoparticle, Gd-DTPA, malignant fibrosis histiocytoma (MFH), enhanced magnetic resonance imaging (MRI)

1. Introduction

Neutron-capture therapy (NCT) applied to malignant tumors utilizes the nuclear neutron capture reaction of radiation-producing agents. Coupled with several elements, it was first postulated by Locher in 1936. The most common element for NCT is boron (B-NCT), and the clinical outcome with the use of B-NCT has been good in patients with malignant melanoma (Mishima et al., 1989). Nonetheless, other more effective radiation-producing elements for NCT are still required. Gadolinium is also a radiation-producing element that provides the neutron capture reaction by thermal neutron irradiation. NCT with gadolinium (Gd-NCT) has several advantages over B-NCT, in that not only does gadolinium have a higher thermal neutron capture cross-section (66 times larger than that of boron), but it is also used as a diagnostic agent in enhanced magnetic resonance imaging (MRI) examinations and shows promise in future Gd-NCT therapy under enhanced MRI diagnosis (Fig. 1). Although the therapeutic potential of Gd-NCT has been explored in recent years, there is no study on therapy applied to musculoskeletal tumors such as sarcoma. The future success of clinical Gd-NCT trials will depend on both the visualization of tumor cells on enhanced MRI and the selectively large accumulation of gadolinium compounds in individual tumor cells. Consequently, we used a sarcoma cell line, malignant fibrosis histiocytoma (MFH) Nara-H, in this study to determine whether the accumulation of gadolinium in the cells could be detected by the MRI system. Both the commercially available MRI contrast medium (Gd-DTPA) and the biodegradable and highly gadopentetic acid (Gd-DTPA)-loaded chitosan nanoparticles (Gd-nanoCPs) prepared by a novel emulsion-droplet coalescence technique were used (Tokumitsu et al., 1999).

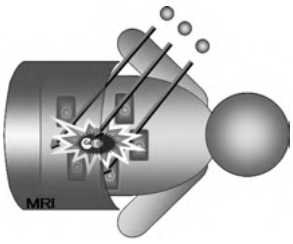

Fig. 1 Future neutron-capture therapy with gadoliniumu (Gd-NCT) under enhanced MRI diagnosis

2. Materials and Methods

The Human sarcoma cell line, malignant fibrous histiocytoma (MFH) (Nara-H), was cultured in MEM supplemented with antibiotic-antimycotic solution and FBS, and incubated in a humidified atmosphere of 5% CO_2 in air at 37 ˚C. An adequate number of cells produced in the initial culture were harvested, re-seeded in three 75 cm^2 cell-culture flasks at a density of 1000 cells/flask and cultured for 10days. When the culture reached 70% confluence, the culture medium was aspirated. The first flask was used as the control and incubated with fresh culture medium for 12 hrs. The second and third flasks were incubated for 12 hrs with Gd-DTPA and Gd-nanoCPs suspension, respectively, in fresh culture medium containing 450 μg Gd, in a humidified atmosphere of 5% CO_2 in air at 37 ˚C. The culture medium of the three flasks was then aspirated, and the cells were detached with 0.25% trypsin, washed twice with PBS to remove free Gd and Gd-nanoCPs, collected into three falcon tubes and centrifuged. The supernatant was discarded and the cells were gently washed with PBS and centrifuged again. The pellet was collected (Fig. 2) and the supernatant discarded. The three falcon tubes set in a water-filled container were, as a phantom model of tumor mass, introduced into the commercially used 3-tesla MRI system to obtain signal intensities from each pellet by the Spin Echo method (Fig. 3).

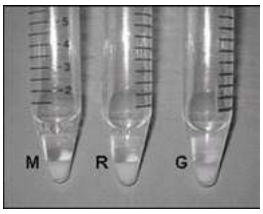

Fig. 2
The cultured cell line cells were detached and centrifuged to make the cell pellets. R, Control; G, Gd-nanoCPs; M, Gd-DTPA

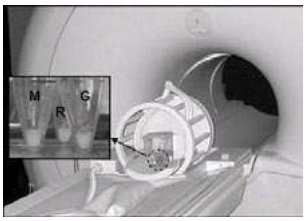

Fig. 3
Three falcon tubes were set in a water-filled container that was then, as a phantom model of tumor mass, introduced into the commercially used 3-tesla MRI system. R, Control; G, Gd-nanoCPs; M, Gd-DTPA.

The longitudinal relaxation time (T1) was calculated by changing the Repetition Time (TR) under the same Echo Time (TE). T1 was calculated from the gradient of the graph (Fig. 5). After counting the number of cells, the samples were incinerated two times in heated nitric acid. The amount of Gd in the sample was then determined by inductive coupled plasma atomic emission spectrography (ICP-AES).

3. Results and Discussion

3.1 Phantom model: Making and visualizing the cell pellets as a tumor mass under the MRI system

Although almost 5mm in diameter, the pellets responded well to the MRI examination. The phantom model was very easy to set, and the gadolinium signal intensity from the phantom tumor mass was successfully acquired under the commercially used MRI system (Figs. 3, 4). Although the pellets were very small, MR signal intensity was detected clearly and measured to the center of the pellets. No other studies have shown MR signals from malignant cell line mass. This phantom model also suggests that MR signal intensity of any other tumor cell lines can be measured through their mass. Although this phantom model showed the effect of the gadolinium on signal intensity, the MRI system could not detect the distribution of the contrast medium in the mass; in other words, whether the medium attached only to the cell membrane or accumulated inside the cell, could not be determined. The MRI contrast medium penetrates the cell membrane of glioblastoma and accumulates in the nucleus (De Stasio et al., 2001), and both Gd-DTPA and Gd-nanoCPs attach to the surface of cancer cell lines (Shikata et al., 2002). Thus, this phantom model can display the effect of gadolinium on the signal intensity in tumor cells under MRI.

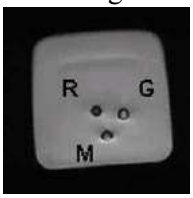

Fig. 4
The MR image from the three pellets as the phantom model. The signal intensity at the center of each pellet was measured. R, Control; G, Gd-nanoCPs; M, Gd-DTPA

3.2 Calculate the T1

The data of each specimen plotted on a graph (Fig. 5) showed a linear relation, and T1 measured from the slope of the graph was 630 (Control), 400 (Gd-nanoCPs), and 327 (Gd-DTPA) (Table 1). Although accumulation of MRI contrast medium in tumor cell lines has been described [4, 5], there is no report on whether such accumulation can enhance the signal of the cell pellet. This is the first report showing that the accumulation of the contrast medium in tumor cells was indeed visualized, and that the signal changed under the commercially used MRI system. Moreover, these data showed that the large accumulation of the contrast medium complements the enhanced effect of gadolinium.

Paradoxically, large concentrations of Gd-DTPA reduce MR signal intensity (Elaster et al., 1990), and

although our data cannot explain this phenomenon, it may not be conducive to Gd-NCT therapy, especially that both the visualization under MRI for the detection of tumors and the high accumulation are requisite for Gd-NCT therapy. In particular, the large accumulation of the MRI contrast medium in tumor lesions is a crucial factor in producing the potent energy by thermal neutrons. Further study is needed to resolve this controversy. The enhanced effect of Gd-nanoCPs has not been reported to date; however, this study showed that Gd-nanoCPs also enhanced the effect of cell mass under MRI. Even though Gd-nanoCPs include Gd-DTPA itself, their nature is different from that of the original Gd-DTPA. Further study is warranted to explain this phenomenon.

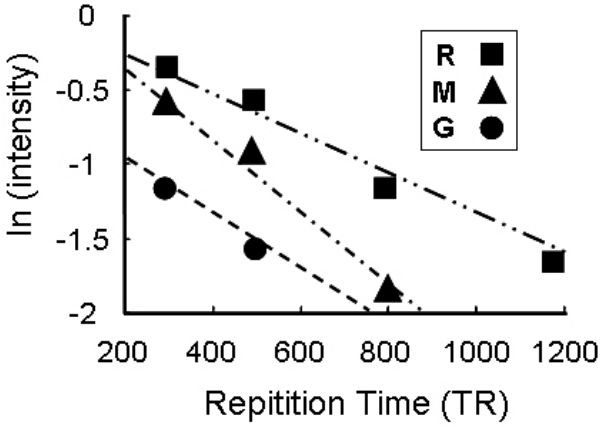

Fig. 5
The intensity data of each specimen (cell, Gd-nanoCPs, Gd-DTPA) was plotted on a graph by changing the Repitition Time (TR) under the same Echo Time (TE); each T1 was then calculated from the slope of the graph. R, Control; G, Gd-nanoCPs; M, Gd-DTPA.

	R (Control)	G (Gd-nanoCPs)	M (Gd-DTPA)
T1	630	400	327

Table 1
T1 of each specimen (R, Control; G, Gd-nanoCPs; M, Gd-DTPA) measured from the graph was 600, 400, 327, respectively.

3.3 Measurement of the Gd Concentration

The amount of gadolinium in Gd-nanoCPs and Gd-DTPA was 30.5 μg, 9.5 μg, respectively, as measured by ICP-AES (Table 2), demonstrating a larger accumulation of Gd-nanoCPs than of the commonly used Gd-DTPA in the tumor cell pellets. Gd-nanoCPs attach more easily to the surface of tumor cell lines than does GD-DTPA (Tokumitsu et al., 1999). Large accumulation of gadolinium is very conducive to Gd-NCT therapy because the neutron capture reaction by thermal neutron irradiation becomes stronger.

	R (Control)	G (Gd-nanoCPs)	M (Gd-DTPA)
Amount of Gd (micro g)	-	30.5	9.5

Table 2
The amount of gadolinium in Gd-nanoCPs and Gd-DTPA measured by ICP-AES was 30.5 μg, 9.5 μg, respectively.

3.4 Comparison between Gd-nanoCPs and Gd-DTPA

Gd-NCT has therapeutic potential, especially that gadolinium is generally used as a contrast medium in magnetic resonance imaging (MRI); thus, both diagnosis and treatment can be carried out simultaneously. Future success of clinical Gd-NCT trials will depend on both the visualization of tumor cells on enhanced MRI and selectively large accumulation of gadolinium compounds in individual tumor cells, conditions that Gd-nanoCPs satisfy. Our results showed that both Gd-DTPA and Gd-nanoCPs accumulated in sarcoma cells (Fig. 4). Furthermore, the accumulation of gadolinium in cells treated with Gd-nanoCPs was larger than that in cells treated with Gd-DTPA (Table 2). In contrast, and compared with the control, Gd-DTPA was more effective than Gd-nanoCPs in reducing T1 (Table 1). The higher numerical reduction of T1 implies that the enhancement effect on tissue was higher at enhanced MRI examination. This contrast suggested that the larger accumulation exerted the adverse effect of lowering the enhancement of MRI. Future studies are warranted to gain insight into the therapeutic potential of Gd-NCT. Finally, neither a difference in cell number nor morphological change was observed between GD-nanoCPs and the commonly used MRI contrast, Gd-DTPA. Although the Gd-nanoCPs demonstrated no toxicity to the cell, further study is warranted on this MRI agent.

4. Conclusions

The accumulation of both Gd-DTPA and Gd-nanoCPs was detected by MRI. Although Gd-nanoCPs demonstrated a smaller reduction of T1, their accumulation of gadolinium was larger than that of Gd-DTPA.

Acknowledgement

This work was supported by both Grant-in-Aid for Science Research 18659446 from Japan Society for the Promotion of Science and Grant-in-Aid from Association for Nuclear Technology in Medicine.

References

De Stasio, G., Casalbore, P., Pallini, R., Gilbert, B., Sanità, F., Ciotti, M.T., Rosi, G., Festinesi, A., Larocca, L.M., Rinelli, A., Perret, D., Mogk, D.W., Perfetti, P., Mehta, M.P., Mercanti, D., 2001. Gadolinium in human glioblastoma cells for gadolinium neutron capture therapy. Cancer. Res. 61, 4272–4277.

Elster, A.D., Sobol, W.T., Hinson, W.H., 1990. Pseudolayering of Gd-DTPA in the urinary bladder. Radiology. 174, 379–381.

Locher, G.L., 1936. Biological effects and therapeutic possibilities of neutrons. Am. J. Roentgenol. Radium Ther. 36, 1-13.

Mishima, Y., Ichihashi, M., Hatta, S., Honda, C., Yamamura, K., Nakagawa, T., 1989. New thermal neutron capture therapy for malignant melanoma: melanogenesis-seeking 10B molecule-melanoma cell interaction from in vitro to first clinical trial. Pigment Cell Res. 2, 226-234.

Shikata, F., Tokumitsu, H., Ichikawa, H., Fukumori, Y., 2002. In vitro cellular accumulation of gadolinium incorporated into chitosan nanoparticles designed for neutron-capture therapy of cancer. Eur. J. Pharm. Biopharm. 53, 57–63.

Tokumitsu, H., Ichikawa, H., Fukumori, Y., 1999. Chitosan-gadopentetic acid complex nanoparticles for gadolinium neutron-capture therapy of cancer: preparation by novel emulsion-droplet coalescence technique and characterization. Pharm. Res. 16, 1830–1835.

CR-39 neutron imaging of biological samples at clinical linac's

G. Giannini[1,2], F. Bruni[1], E. Vallazza[2], M. Bari[2], D. Iugovaz[2], G. Orzan[2], S. Reia[2], A. Beorchia[3], M. De Denaro[3], M. Severgnini[3], C. Vidali[3], R.Vidimari[3], A. Piermattei[4], A. Fidanzio[4],A. Mameli[4], L.Tommasino[5], P. Borasio[6], U. Ricardi[7], S.Anglesio[8], A. Zanini[9],P. Chiari[10], M. Prest[11]

[1] *Physics Department, University of Trieste, Italy*
[2] *INFN–Trieste, Italy*
[3] *AOU "Ospedali Riuniti", Trieste, Italy*
[4] *Istiutto di Fisica - Università Cattolica S. Cuore - Roma, Italy*
[5] *Consultant, Istituto di Fisica- UCSC - Roma, Italy*
[6] *Department of Clinical and Biological Sciences "S. Luigi Orbassano", University of Torino, Italy*
[7] *University of Torino, Italy*
[8] *ASO Molinette Torino, Italy*
[9] *INFN–Torino, Italy*
[10] *Nuclear and Theoretical Physics Department, University of Pavia, Italy*
[11] *University of Insubria, Como, Italy*

Abstract

CR-39 track-etch detectors have been used for obtaining ^{10}B thermal neutron capture induced images of biological, including human lung previously perfused with ^{10}BPA, samples.

Thermal neutrons production by means of a photo-neutron converter installed in front of the head of clinical linear accelerators is the method recently developed in Italy within the PhoNeS (Photo Neutron Source) collaboration and already tested at several hospital linac's (Trieste, Roma, Como, Torino, Rionero in Vulture, Campobasso, Salisburgo, Aviano). Such a method was applied for the present study at the Torino Molinette Elekta SLIT 25 MV e-linac with the PhoNeS converter since December 2007.

The group has used already calibrated CR39 extensively used also for dosimetric measurements. Several biological samples (thickness ~10μm, area ~ 1cm^2), prepared by the clinical and biological units, have been positioned between couples of CR39 layers (37 x 13 x 1 mm^3 in size) within the PhoNes cavity and irradiated with ~10^{11} n cm^{-2} thermal neutron fluence, operating the linac at 400 MU/min (nominal pre-conversion dose rate) and integrating a total of ~7·10^4 MU in ~3 h ~10^4 s .

After etching the CR39 layers, 2h in NaOH (6N) at 90 ^{o}C, ~10 μm diameter holes, corresponding to α and ^{7}Li products of neutron capture by ^{10}B, are clearly observed at the microscope with densities of the order of 1-2 x10^3 mm^{-2} following the features of the corresponding previously overlaying tissues. A specific sideways illumination procedure has allowed the recording of digital photographic camera high resolution images which are made available for comparison with histological ones and the determination of tissue ^{10}B concentrations.

Keywords: CR39, Boron, Imaging, BNCT, LINAC .

1. Introduction

Neutron autoradiography with track-etch detectors is an effective method for determining ^{10}B uptake in tissues. It allows to establish ^{10}B concentration ratios in tumor and healthy tissues for BNCT treatments as it has extensively been shown in recent successful applications at nuclear reactors also in Italy (see for example: Pinelli T. et al. 2002; Altieri S. et al. 2004, 2005, 2006; Bortolussi S. et al. 2006; Zonta A. et al. 2006).

In the last few years it has been demonstrated the possibility to produce sizable thermal neutron fluxes by passive photo-neutron converters mounted in front of the head of radiotherapy e-linacs in hospitals (Giannini et al. 2006; Bevilacqua et al. 2007). Measurements have been performed in various hospitals and comparisons with simulations have shown the reliability of the method. The obvious advantages of the availability of neutrons in clinical environments open the way to a wider range of medical, biological, chemical and physical

contributions to the research in BNCT in order to extend it to more oncological applications, to find new pathologies to treat, new carriers to exploit and new combined methods with other therapies to test.

In particular this paper shows how the neutron autoradiography technique by means of track-etch detectors allows imaging of ^{10}B in biological samples of oncological relevance for BNCT studies. The specific application has been carried out by a wide multidisciplinary collaboration among several Italian universities and other research institutes active in their respective fields.

2. The photo-neutron converter

The photo-neutron converter, first patented by the University of Trieste in 2004, is based on a high Z lead target, on which the gamma field is impinging, surrounded by low A neutron moderating materials: polyethylene slabs, heavy water in carbon fiber boxes and graphite blocks, plus some other shielding like B_4C, lead and plastic cover. The converter, about 300 kg in weight, is modular and thus easy to be transported, installed at and removed from clinical e-linac heads.

Two prototype devices have been built in Italy within the INFN-PhoNeS (Photo Neutron Source) collaboration and already tested at several hospital e-linac's (Trieste, Roma, Como, Torino, Rionero in Vulture, Campobasso, Salisburgo, Aviano).

For the present study one PhoNeS photo-neutron converter was installed at the Torino Molinette Elekta SLIT 25 MV e-linac since December 2007.

Fig.1: The PhoNeS photo-neutron converter.

The installed configuration is able to produce, inside an irradiation cavity, a thermal neutron flux ~ 10^7 cm^{-2} s^{-1}, with low gamma and fast neutron contamination (more details in: Zanini et al., 2008).

In the case of the installation at Aviano, CRO (Centro di Riferimento Oncologico) a Fuji-ND neutron imaging plate was used to map the thermal neutron field; in fig.2 the color coded intensity figure is superimposed on the of the device.

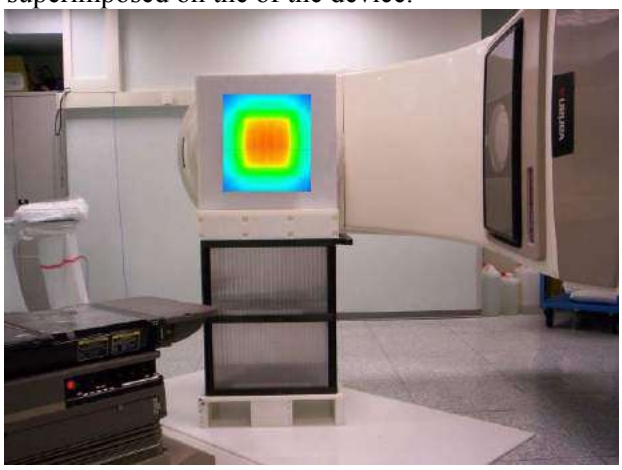

Fig.2: Thermal neutron field color coded image.

3. Material and Methods

3.1 The CR-39 track-etch detectors

The CR-39, polyallyl diglycol carbonate (PADC) Tastrak was purchased from TASL (Track Analysis Systems Ltd, Bristol, UK) with the following characteristics: rectangular shape, 37 x 13 x 1mm^3 in Size, density 1.30 g cm^{-3}. CR-39 is a clear plastic sensitive to tracks of highly ionizing particles such as alpha or ^7Li from neutron capture on ^{10}B . Following exposure, the tracks develop, after etching in solutions such as caustic alkalis, holes about ~10 μm in diameter.

3.2 CR-39 calibration

For the calibration of the CR-39 a method based on the use of a known ^{10}B content thin (25μm) commercially available organic scintillator (BC-454, 10% natural boron by Saint-Gobain) was applied. An absolute calibration was performed a few yers ago with such a method by some of the authors at the TRIGA MARK II nuclear reactor in Pavia by exposing the CR-39 based detectors to a neutron fluence of (1.70 ± 0.17) x 10^7 n/cm^2 (± 1SD) resulting in (7.8 ± 1.4) x 10^{-4} (± 1SD) tracks/neutron (Mameli et al. 2008).

Relative calibrations have been repeated now by comparing the results with the ones of BDT bubble neutron detectors (Bubble Tech. Ind., 2003) and BDS spectrometers confirming a good agreement within the declared 10-20% resolution.

3.3 *Human lung samples*

The human lung samples have been obtained from two patients by the S. Luigi Orbassano surgical team

(Borasio P. et al., 2008) after 2 h perfusion with a boronophenylalanine ^{10}BPA 300mg/kg solution.

3.4 *Preparation of the samples on the CR-39*

The biological samples (thickness ~10 μm, area ~ 1cm^2), prepared by the clinical and biological units of our team, have been positioned in direct contact between couples of CR-39 plastics layers and secured at the edges with tape.

4. Biological samples neutron irradiation

The prepared biological samples within double CR-39 plastics have been positioned inside the thermal neutron irradiation cavity.

Fig.3: The samples in the cavity.

The cavity has then been closed with the extra neutron reflecting heavy water carbon fiber boxes and a polyethylene slab.

Fig.4: The final closed cavity ready for irradiation.

A specific CR-39 calibration with the known boron content method was performed before actually installing the samples in the cavity but in the exact same configuration in order to establish the real neutron fluence delivered with only 2000 MU.

The final irradiation of the samples with a ~10^{11} n cm^{-2} thermal neutron fluence was then obtained by operating the e-linac at 400 MU/min (nominal pre-conversion dose rate) and integrating with some pauses a total of ~7 x 10^4 MU in ~3 h ~10^4 s.

After the exposure the CR39 layers were chemically etched for 2h in NaOH (6N) at 90 ^{o}C.

In this way ~10 μm diameter holes, corresponding to the α and ^{7}Li products of the neutron capture by ^{10}B, are clearly observed at the microscope with densities of the order of 1-2 x 10^3 mm^{-2} reproducing the features of the tissues deposited on the detectors themselves.

5. Results

All the 20 CR-39 detectors have been analyzed at the microscope and pictures have been taken with a camera for comparison of normal and neutron images finding also the ^{10}B concentration. For measuring the hole density and size distribution the commercial program Image-Pro-Plus © has been used, obtaining images as the following one.

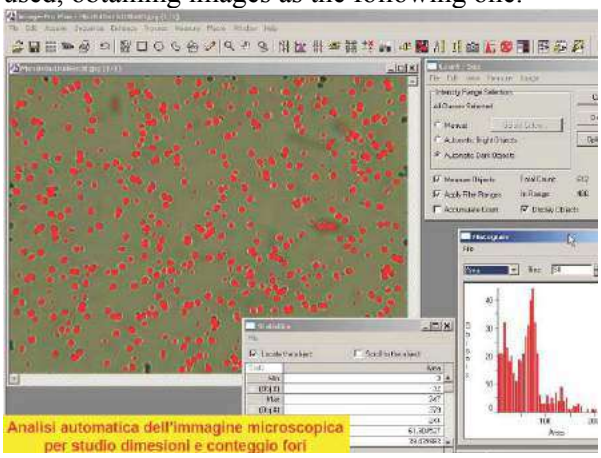

Fig.5: Automatic analysis of hole size and density.

6. Imaging results

A specific sideways illumination procedure has allowed the recording of digital photographic

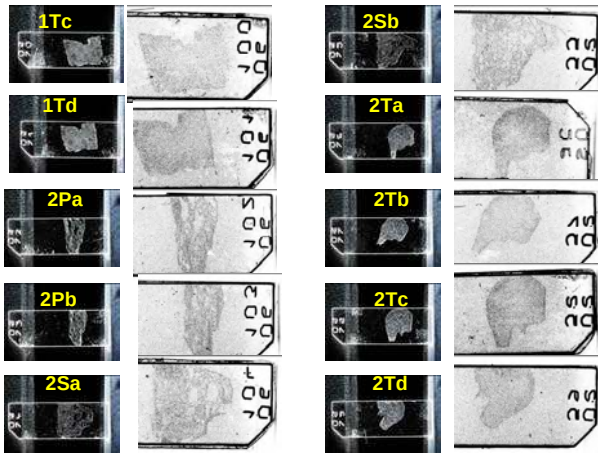

Fig.6: Sample photographic and neutron images.

camera high resolution images which can be compared with the histological ones and allow to determine the ^{10}B concentration in the tissue.

The images in fig.7-8 present the histology, the transmitted and diffused light pictures of the samples and the corresponding neutron autoradiography with CR-39 images.

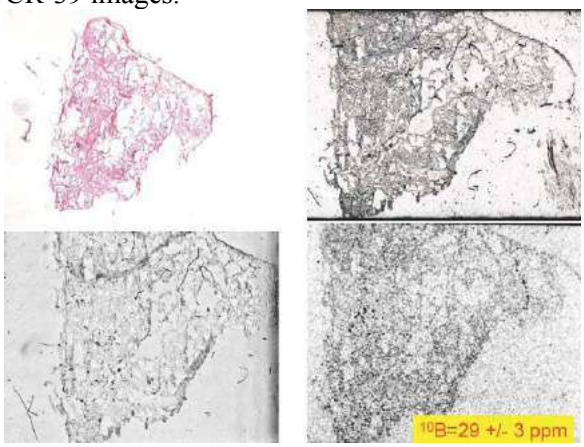

Fig.7: Healthy tissue.

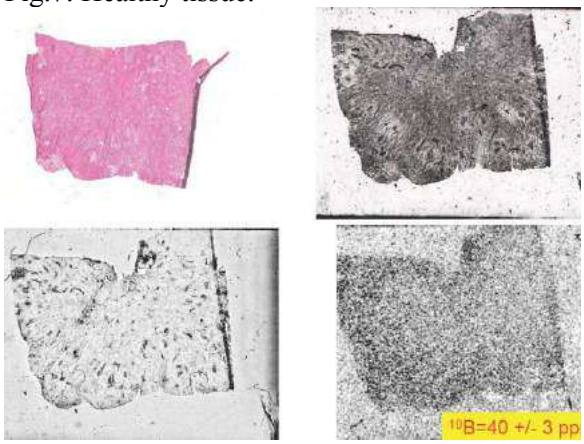

Fig.8: Tumor tissue.

For these two samples preliminary ^{10}B concentrations of 29 +/- 3 ppm and 40 +/- 3 ppm respectively have been obtained.

7. Conclusion

The method of neutron autoradiography on CR-39 track-etch detectors has been successfully applied to obtain images of human lung tumor and healthy tissue showing the capability of determining ^{10}B concentration with neutrons produced in hospital with clinical e-linac's.

References

Altieri S. et al., "Neutron radiography of human liver metastases after BPA infusion", 11th World Congress on Neutron Capture Therapy (October 2004, Boston USA)

Altieri S. et al., "Boron concentration imaging for BNCT", 5th International Conference on Isotopes. Brussels 25-29 April 2005.

Altieri S. et al., "Boron absorption imaging in rat lung colon adenocarcinoma metastases, Journal of Physics: Conference Series 41 (2006) 123-126

Bevilacqua R., et al. "PhoNeS: A novel approach to BNCT with conventional radiotherapy accelerators", Nuclear Instruments and Methods in Physics Research A 572 p. 231-232 (2007).

Borasio P. et al. "A novel approach to the study of 10B uptake in human lung by ex-vivo BPA perfusion" – 13th International Congress on Neutron Capture Therapy 2-7 November 2008 Florence, Italy.

Bortolussi S. et al., "Boron uptake measurements in metastatic tumours in rat lung", Advances in Neutron Capture Therapy, proceedings of 12th International Congress on Neutron Capture Therapy, October 9-13 2006 Takamatsu, Kagawa, Japan 91-94

Bubble Technology Industries, 2003. "Instruction Manual for the Bubble Detector Spectrometer (BDS)". Chalk River, Ontario, Canada, 2003

Giannini G., "Dispositivo convertitore da radiazioni gamma a neutroni termici e/o epitermici per uso in terapia fotoneutronica", Brevetto Universita' di Trieste MI2004A001301, 28/06/2004

Giannini G. et al. A. "Photoneutron Source for In-Hospital BNCT Treatment: feasibility study" – 12th International Congress on Neutron Capture Therapy 9-13 Ottobre 2006 Takamatsu, Kagawa, Japan.

Mameli A. et al., "CR-39 detectors based thermal-neutron flux measurements in the PHONES project" Nucl. Instr. & Meth. B, in press, accepted for publication10/6/2008.

Pinelli T. et al., "TAOrMINA: from the first idea to the application to the human liver", in W.Sauerwein, R.Moss, A.Wittig, eds Research and Development in Neutron Capture Therapy. Bologna, Monduzzi Editore, 1065-72 (2002).

Zanini A., et al. "Characterization of a Thermal Cavity in the PhoNeS photo-neutron converter for BNCT research" – 13th International Congress on Neutron Capture Therapy 2-7 November 2008 Florence, Italy.

Zonta A. et al., "Clinical lessons from the first applications of BNCT on unresectable liver metastases", Journal of Physics: Conference Series 41 (2006) 484-495.

Biological Evaluation of Boronated Unnatural Amino Acids as New Boron Carriers

G.W. Kabalka[1,*], M.-L. Yao[2], S.R. Marepally[2], S. Chandra[3]

[1,2]*Departments of Radiology and Chemistry, The University of Tennessee, Knoxville, TN, USA,*
[3]*Cornell SIMS Laboratory, Department of Earth and Atmospheric Sciences, Snee Hall, Cornell University, Ithaca, NY, USA*
**Corresponding author: Tel. +1-865-974-3260; fax: +1-865-974-2997; E-mail address: kabalka@utk.edu (G.W. Kabalka)*

Abstract

There is a pressing need for new and more efficient boron delivery agents to tumor cells for use in boron neutron capture therapy (BNCT). A class of boronated unnatural cyclic amino acids has shown a remarkable selectivity toward tumors in animal and cell culture models, far superior to currently used agents in clinical BNCT. One of these amino acids, 1-amino-3-boronocyclopentanecarboxylic acid (ABCPC), has shown a tumor to blood ratio of 8 and a tumor to normal brain ratio of nearly 21 in a melanoma bearing mouse model (1). This work represents further biological characterization of this compound for tumor targeting in an EMT6 murine mammary carcinoma mouse model and a T98G human glioblastoma cell line. Female BALB/c mice bearing EMT6 tumors were injected with the fructose complex form of racemic mixtures of *cis*- and *trans* isomers of ABCPC in identical concentrations.

Boron concentrations were measured in the tumor, blood, brain, skin, and liver tissues at 1, 3, and 5 hr post injection. These observations revealed a remarkable difference in racemic mixtures of *cis* and *trans* isomers in tumor targeting by boron. This implies that further separation of the L and D forms of this compound may enhance tumor targeting to an even higher degree than that provided by the racemic mixtures. Since the uptake measurements were made in homogenized tumor and normal tissues, little is known about the subcellular location of the boron arising from the various isomeric forms of the amino acid. To study subcellular delivery of boron from ABCPC in T98G human glioblastoma cells, we employed secondary ion mass spectrometry (SIMS) based technique of ion microscopy, which is capable of quantitatively imaging isotopic (elemental) gradients in cells and tissues at 500 nm spatial resolution. The T98G cells were exposed to the nutrient medium containing 100 ppm boron equivalent of a mixture of both L and D isomers of ABCPC in the form of a fructose complex for 1 hr.

Following this treatment, the cells were fast frozen, freeze-fractured, and freeze-dried for SIMS analysis. Within an hour of exposure, ABCPC provided partitioning of intracellular to extracellular boron of 3/1. SIMS imaging revealed that boron from ABCPC was distributed throughout the cell, including the nucleus. This level of boron delivery within an hour of exposure is superior to *p*-boronophenylalanine (BPA) and sodium borocaptate (BSH), which have been previously studied by SIMS in the same cell line (2,3). These encouraging observations provide compelling support for further isomeric separations of ABCPC into the D and L forms for enhanced tumor targeting and continued testing of these compounds as new boron carriers in BNCT.

Keywords: Amino acids; BNCT; Boron biodistribution, SIMS

1. Introduction

Boron neutron capture therapy (BNCT) of cancer depends on the selective targeting of sufficient quantities of boron-10 (approximately 30 μg/g of tumor) to the tumor cells for effective killing via the boron neutron capture fission reaction (4,5). Since the lethal reaction produced in BNCT is limited to a range of less than a single cell diameter, BNCT is potentially capable of killing individual cancer cells while sparing the neighboring normal cells. Extensive international efforts have been made by physicists, chemists, clinicians, and biologists for over 50 years focused on the development and testing of BNCT in the treatment of cancer (6-12). Clinical interest in BNCT has focused primarily on the treatment of high-grade gliomas, either cutaneous primaries or cerebral metastases of melanoma, and, most recently, head and neck and liver cancer (9, 12-16**)**.

The clinical success of BNCT depends on two factors: (i) selective targeting and delivery of sufficient quantities of ^{10}B atoms to tumor cells and (ii) a neutron flux sufficient to achieve the required nuclear reaction while minimizing damage to healthy tissue. Early BNCT clinical trials were disappointing since they failed to achieve either of these goals (5). However, significant advances in the modification of nuclear reactors and in selectively tumor-seeking boron-containing agents have been made in recent years (9,17). To minimize damage to normal tissues, the quantity of boron in tumor cells must exceed that found in surrounding normal cells by at least a factor of three (18,19). In BNCT, the cell killing efficiency is enhanced by intranuclear localization of ^{10}B, where the resulting fission products have a greater probability of damaging the DNA (20). Consequently, the development of microanalytical techniques capable of accurately analyzing subcellular concentrations at the parts-per-million (ppm) level of boron is critically needed in BNCT. Single cell and subcellular measurements are also necessary for understanding mechanistic aspects of boron delivery, as well as for identifying the partitioning of boron between the blood and the tumor cells.

Although two BNCT agents, BPA and sodium borocaptate (BSH), are being used in clinical trials in Europe and Japan focused on brain tumors, melanomas, head and neck tumors, and liver metastases, there is increasing emphasis on the need of better tumor-targeting BNCT agents (9-11). It is believed that the amino acids are preferentially taken up by growing tumor cells (21). Efforts at the University of Tennessee have focused on the synthesis of boronated unnatural amino acids as potential boron carriers to tumor cells (1,11). The logic for the synthesis of these boron carriers came from positron emission tomography (PET) studies of glioblastoma multiforme (GBM) and metastatic malignant melanoma patients using fluorine-18 labeled BPA and carbon-11 labeled 1-aminocyclobutanecarboxylic acid (22, 23). These studies revealed that cyclic amino acids localize in GBM and metastatic malignant melanoma tumors more avidly than BPA. The fact that 1-aminocycloalkanecarboxylic acids cross the blood brain barrier (24) provided further impetus to us for focusing on the synthesis of boronated unnatural cyclic amino acids as boron carriers in BNCT with potential for targeting the infiltrating glioblastoma cells in the normal brain.

In initial biodistribution studies in mice tumor models, three unnatural boronated amino acids have shown significantly improved selectivity for targeting the tumor cells when compared to BPA (**1**). The boron analogue of one of these unnatural amino acids, 1-amino-3-boronocyclopentanecarboxylic acid (ABCPC), has shown a tumor to blood ratio of 8 and a projected tumor/normal brain ratio of nearly 21 (1). The demonstrated boron delivery by this unnatural amino acid is far superior to that of BPA and BSH, the compounds currently used in clinical BNCT. The present work presents further isomeric separation and characterization of this compound for tumor targeting in an EMT-6 murine mammary carcinoma mouse model and the T98G human glioblastoma cell line.

2. Experimental section

Synthesis, separation, and biodistribution of 1-amino-3-boronocyclo-pentanecarboxylic acid (ABCPC) in EMT-6 murine mammary carcinoma mouse model

The structure of boronated amino acids under study are shown in Fig. 1. BPA is listed as Compound **1**. Several boronated amino acids, Compounds **2-7** (Figure 1), have been prepared and their *in vivo* biodistribution determined in previous studies (1, 25). The data for the cyclic five membered ring analogue, **5** (ABCPC), was striking, exhibiting a nearly 22:1 ratio of boron concentration for tumor to brain at the two hour time point, dropping to 7.3 after six hours (1). It is important to note that all of the amino acids were synthesized as racemic and diastereomeric mixtures. For compounds **3**, **4** and **5**, four isomers were present in the injectate (*cis* and *trans* isomers along with each of their enantiomers.) [Two stereoisomers (enantiomers) were present in each of the injectates of **2**, **6** and **7**.]

Thus, we reasoned that a single enantiomer of **4** and **5**, as well as a single isomer of **7** might exhibit enhanced selectivity and elevated concentrations in the tumor. To test the hypothesis, we carried out preliminary studies in which compound **5** was separated into two pairs of racemates, **8a**, **8b** and **9a**, **9b** (Figure 2).

We were able to prepare the hydantoin precursor **10** to amino acids **8a**, **8b** and **9a**, **9b** using their previously reported methodology (25). Attempts to isolate the two racemates by column chromatography on alumina were unsuccessful due to decomposition of the borate ester. Fortunately, we discovered that the racemates (**8a**, **8b** and **9a**, **9b**) could be readily separated by recrystallization using methanol as solvent. The stereochemistry of the enantiomeric pair **11a**, **11b** was confirmed by x-ray crystallography. Hydrolysis of hydantoins, **11a** and **11b**, in the presence of hydrochloric acid (12 *M*), gave amino acids **8** (**a** and **b**) and **9** (**a** and **b**), respectively [See Figure 3 for a synthesis scheme. For clarity, only one isomer of each racemic pair is shown.]

The racemic amino acids (**8** and **9**) were solubilized as the fructose complex following procedures previously described for the amino acid BPA (22). Briefly, 1 millimole of **8** or **9** was combined with 1.1 millimoles of fructose in ~1 ml of water. The pH was adjusted by addition of 10 *M* NaOH, added dropwise with stirring, until the pH reached 9.5-10.0 and all solids dissolved. The pH was then adjusted to 7.4 with aqueous HCl. The final volume was adjusted to 4 ml by addition of water and the solution was sterilized by passage through a 0.22 μm syringe filter. The boron concentration in the injection solutions was 1.87 mg B/ml for isomer **8** and 2.12 mg B/ml for isomer **9**. Both compounds contained natural abundance boron. All boron concentrations quoted below represent the total boron concentration.

The biodistribution of racemates **8** and **9** was evaluated in the EMT-6 murine mammary carcinoma in collaboration with Dr. Jeffrey Coderre, Dr. Y. Chung, and Dr. K. Riley of the Massachussetts Institute of Technology for carrying out the *in vivo* biodistribution studies on compounds **8** and **9**. Female BALB/c mice were injected subcutaneously on the flank with 1 x 10^6 EMT-6 tumor cells in a volume of 0.1 ml. After 8–10 days the tumors had reached a diameter of ~5 mm and were used for the biodistribution study. Five tumor-bearing mice were used at each of the following time points: 1, 3, and 5 hours post injection. Each mouse received an injection of 0.2 mL into the retro-orbital sinus while under brief isofluorane anesthesia. At the indicated time points, the mice were euthanized by isofluorane overdose, their blood removed directly from the heart, and tumor and normal tissues collected for boron analysis.

Subcellular SIMS studies of ABCPC in T98G human glioblastoma cells

The T98G human glioblastoma cells were exposed for 1 hr to a nutrient medium containing 100 ppm boron equivalent of compound ABCPC as a mixture of both L and D-isomers in the form of a fructose complex. Following this treatment, the cells were fast frozen, freeze-fractured using our sandwich method, and freeze-dried prior to SIMS analysis (**26-27**).

3. Results and discussion

The biodistribution data for racemate **8** show no difference between tumor and blood at any of the time points (Figure 4). The boron concentration in liver is higher than that in tumor or blood at 1 hour (tumor/liver boron concentration ratio ~0.4:1) and decreases to nearly the blood level by 5 hours post-injection.

Racemate **9**, however, shows a tumor boron concentration that is significantly greater than blood at all time points (Figure 5). At 1, 3 and 5 hours post-injection, the tumor/blood boron concentration ratios for racemate **9** are 2.8 ± 0.8, 2.4 ± 0.6 and 1.8 ± 0.5, respectively. With racemate **9**, the normal tissues, skin and brain were similar to blood at 1 hour. The boron concentration in liver was higher than that in tumor at 1 hour.

A direct comparison of the biodistribution of compound **9a** (as a racemate) with BPA and BSH in Balb/c mice bearing implanted EMT-6 mammary carcinomas (26) is shown in Fig. 6 at the time of maximum concentration in the tumor. These observations unequivocally show that the compound **9a** is at least as efficient as BPA in delivering boron to EMT-6 tumors but its time dependent uptake characteristics are quite different than BPA (Fig. 5-6). It should also be noted that compound **9a** delivered approximately the same amount of boron to the tumor at the peak tumor concentration at 1 hr from less than one-half of the dose in comparison to BPA (Fig. 6).

The compound **9a** (as a racemate) is clearly superior to BSH in delivering boron to EMT-6 tumors in mice. The observations for boronated unnatural amino acids also indicate that these compounds, like any other BNCT agents, will differ in tumor targeting depending on the type of tumor and the ways of delivery (9, 26).

Figure 7 contains examples of SIMS analyses of 1-amino-3-boronocyclopentane carboxylic acid (ABCPC), using a mixture of both the L-and D-forms, in T98G human glioblastoma cells. The high ^{39}K and low ^{23}Na signatures in individual cells indicate the absence of toxicity to the cells and reveal healthy, well-preserved cells after treatment with ABCPC. The cell nucleus is identified in one cell by a dotted black line in the ^{40}Ca and ^{11}B images. The characteristic lower concentrations of total calcium in nuclei of cells, as compared to the cytoplasm, clearly reveal the position of the nucleus in each cell in the field of view. SIMS analysis reveals that the boron-11 from ABCPC is present in all cells and is distributed with minor heterogeneity. The ^{11}B is clearly present in the nucleus of each cell. It should be noted that this distribution is distinctly different than the boron distribution observed for BPA in this cell line (3). The perinuclear, mitochondrial-rich region that distinctly shows lower boron concentrations from BPA does not show this characteristic for ABCPC. The superiority of ABCPC for boron delivery to T98G human glioblastoma cells is evident from the data in Table 1, as ABCPC delivers at least twice as much boron to cell interiors when compared to BPA, within 1 hr of treatment. A similar comparison with BSH (not shown here, see data on BSH in reference 2) also indicates ABCPC to be far superior in boron delivery to T98G cells within an hour of exposure. Further isomeric separations of ABCPC may enhance boron delivery to even higher levels than observed for the isomeric mixture.

4. Conclusion

The present study further characterizes boronated unnatural amino acids as new and more efficient boron carriers to tumor cells. This preliminary study provides compelling support for further isomeric separations and testing of subcellular level boron distributions in both *in vitro* and animal models

Acknowledgements

The authors wish to thank Drs. Jeffrey Coderre, Y. Chung, and K. Riley of the Massachussetts Institute of Technology for carrying out the *in vivo* biodistribution studies in BALB/c mice. This study was funded by the U.S. Department of Energy.

References:

1. Kabalka, G.W., Wu, Z.Z., Yao, M-L., and Natarajan, N. The synthesis and in vivo biodistribution of novel boronated unnatural amino acids. Appl. Radiat. Isotopes 61: 1111-1115, 2004.
2. Chandra, S., Lorey, D.R.,II, and Smith, D.R. Quantitative subcellular secondary ion mass spectrometry (SIMS) imaging of boron-10 and boron-11 isotopes in the same cell delivered by two combined BNCT drugs: In vitro studies on human glioblastoma T98G cells. Radiat. Res. 157: 700-710, 2002.
3. Chandra, S. and Lorey, D.R., II. SIMS ion microscopy imaging of boronophenylalanine (BPA) and $^{13}C^{15}N$-labeled phenylalanine in human glioblastoma cells: relevance of subcellular scale observations to BPA-mediated boron neutron capture therapy of cancer. Int. J. Mass Spect. 260: 90-101, 2007.
4. Godwin, J.T., Far, L.E., Sweet, W.H., and Robertson, J.S. Pathological study of eight patients with glioblastoma multiforme treated by neutron-capture therapy using boron 10. Cancer 8: 601-615, 1955.
5. Sweet, W.H. Early history of development of boron neutron capture therapy of tumors. J. Neuro-oncol. 33, 19-26, 1997.
6. Hatanaka, H. Boron neutron capture therapy for tumors. In: Glioma. A.B.M.F. Karim and E.R. Lewis (Eds.) Springer: Berlin. pp. 233-249, 1991.
7. Coderre, J.A. and Morris, G.M. The radiation biology of boron neutron capture therapy. Radiat. Res. 151: 1-18, 1999.
8. Kabalka, G.W., Nichols, T.L., Smith, G.T., Miller, L.F., Khan, M.K., and Busse, P.M. The use of positron emission tomography to develop boron neutron capture therapy treatment plans for metastatic malignant melanoma. J. Neuro-oncol. 62: 187-195, 2003.
9. Barth, R.F., Coderre, J.A., Vicente, M.G.H., and Blue, T.E. Boron neutron capture therapy of cancer: current status and future prospects. Clin. Cancer Res. 11: 3987-4002, 2005.
10. Li, T., Hamdi, J., and Hawthorne, M.F. Unilamellar liposomes with enhanced boron content. Bioconjugate Chem., 17: 15-20, 2006.
11. Kabalka, G.W. and Yao, M-L. The synthesis and use of boronated amino acids for boron neutron capture therapy. Anti-Cancer Agents in Medicinal Chemistry 6: 111-125, 2006.
12. Pellettieri, L. H-Stenstam, B., Rezaei, A., Giusti, V., and Skold, K. An investigation of boron neutron capture therapy for recurrent glioblastoma multiforme. Acta Neurol. Scand. 117: 191-197, 2008.
13. Cordoso, J.E., Trivillin, V.A., Heber, E.M., Nigg, D.W., Calzetta, O., Blaumann, H., Longhino, J., Itoiz, M.E., Bumaschny, E., Pozzi, E., and Schwint, A.E. Effect of boron neutron capture therapy (BNCT) on normal liver

regeneration: towards a novel therapy for liver metastases. Int. J. Radiat. Biol. 83: 699-706, 2007.
14. Dagrosa, M.A., Thomacz, L., Longhino, J., Perona, M., Calzetta, O., Blaumann, H., Rebagliati, R.J., Cabrini, R., Kahl, S., Juvenal, G.J., and Pisarev, M.A. Optimization of boron neutron capture therapy for the treatment of undifferentiated thyroid cancer. Int. J. Radiat. Oncol. Biol. Phy. 69: 1054-1066, 2007.
15. Kankaaranta, L., Seppala, T., Kovinoro, H., Saarilhti, K., Atula, T., Collan, J., Salli, E., Kortensniemi, M., Uusi-Simola, J., Makitie, A., Seppanen, M., Minn, K., Kotilnoto, P., Anterinen, I., Savolainen, S., Kouri, M., and Joensuu, H. Boron neutron capture therapy in the treatment of locally recurred head and neck cancer. Int. J. Radiat. Oncol. Biol. Phy. 69: 475-482, 2007.
16. Wittig, A., Malago, M., Collette, L., Huiskamp, R., Buhrmann, S., Nievaart, V., Kaiser, G.M., Jockel, K.H., Schmid, K.W., Ortmann, U., and Sauerwein, W. A. Uptake of two ^{10}B-compounds in liver metastases of colorectal adenocarcinoma for extracorporeal irradiation with boron neutron capture therapy (EORTC Trial 11001). Int. J. Cancer 122: 1164-1171, 2008.
17. Soloway, A.H., Tjarks, W., Barnum, B.A., Rong, F.-G., Barth. R.F., Codogni, I.M., and Wilson, J.G. The chemistry of neutron capture therapy. Chem. Rev. 98: 1515-1562, 1998.
18. Fairchild, R.G. and Bond, B.P. Current status of boron-10 neutron capture therapy: enhancement of tumor dose via beam filtration and dose rate, and the effects of these parameters on minimum boron content- A theoritical evaluation. Int. J. Radiat. Oncol. Biol. Phys. 11: 831-835, 1985.
19. Zamenhof, R.G., Kalend, A.M., and Bloomer, W.D. BNCT: looking for a few good molecules. J. Natl. Cancer Inst. 84: 1290-1291, 1992.
20. Gabel, D., Foster, S., and Fairchild, R.G. The Monte Carlo simulation of the biological effect of the $^{10}B(n,\alpha)^{7}Li$ reaction in cells and tissue and its implications for boron neutron capture therapy. Radiat. Res., 111: 14-25, 1987.
21. Wittig, A., Sauerwein, W.A., and Coderre, J.A. Mechanisms of transport of *p*-borono-phenylalanine through the cell membrane in vitro. Radiat. Res., 153: 173-180, 2000.
22. Hubner, K.F., Thie, J.A., Smith, G.T., Kabalka, G.W., Keller, I.B., Cliefoth, A.B., Campbell, S.K., and Buonocore, E. Positron emission tomography (PET) with 1-aminocyclobutane-1-[^{11}C]carboxylic acid (1-[^{11}C]-ACBC) for detecting recurrent brain tumors. Clin. Positron Imag. 1: 165-169, 1998.
23. Nichols, T.L., Kabalka, G.W., Miller, L.F., Khan, M.K., and Smith, G.T. Improved treatment planning for boron neutron capture therapy for glioblastoma multiforme using fluorine-18 labeled boronophenylalanine and positron emission tomography. Med. Phys. 29: 2351-2358, 2002.
24. Aoyagi, M., Agronoff, G.W., Washburn, L.C., and Smith, O.R. Blood-brain-barrier transport of 1-aminocyclohexane carboxylic acid: a nonmetabolizable amino acid for in vivo studies of brain transport. J. Neurochem. 50: 1220-1226,1988.
25. Kabalka, G. W., Das, B. C., and Das, S. Synthesis of novel boron containing unnatural cyclic amino acids as potential therapeutic agents. Tetrahedron Letters 42: 7145-7146, 2001.
26. Chandra, S., Morrison, G.H., and Wolcott, C.C. Imaging intracellular elemental distribution and ion fluxes in cultured cells using ion microscopy: A freeze-fracture methodology. J. Microsc. (Oxford), 144: 15-37, 1986.
27. Chandra, S., Smith, D.R., and Morrison, G.H. Subcellular imaging by dynamic SIMS ion microscopy. Anal. Chem., 72: 104A-114A, 2000.
28. Miura, M., Morris, G.M., Micca, P.L., Lombardo, D.T., Youngs, K.M., Kalef-Ezra, J.A., Hoch, D.A., Slatkin, D.N., Ma, R., and Coderre, J.A. Boron neutron capture therapy of a murine mammary carcinoma using a lipophilic carboranyltetraphenylporphyrin. Radiat. Res. 155: 603-610, 2001.

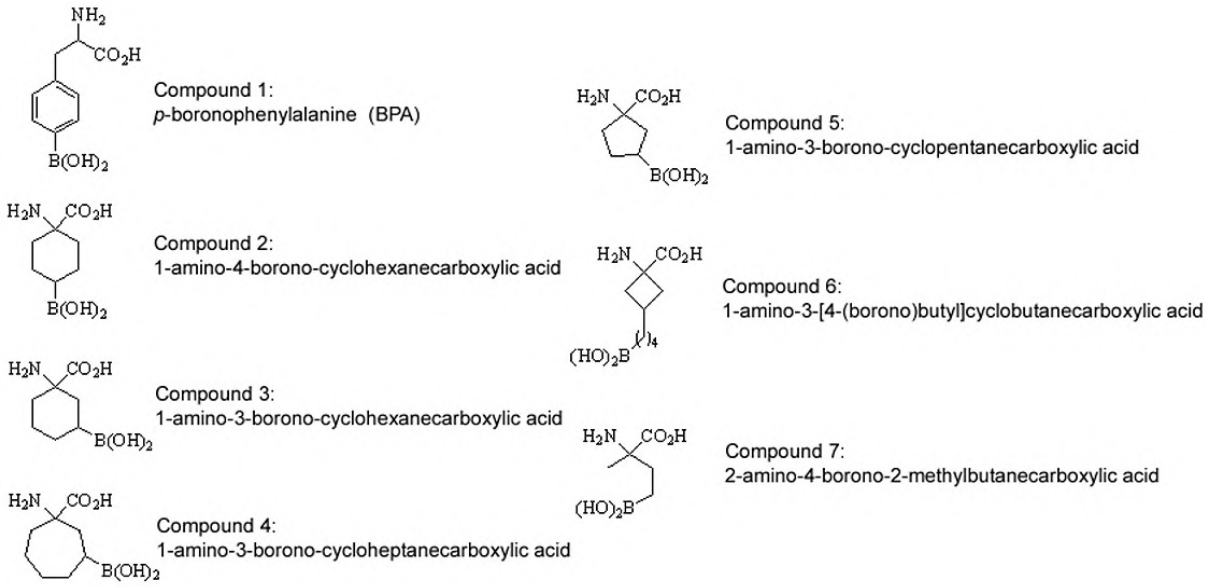

Fig. 1. Structures of BPA (**1**) and six boronated unnatural amino acids (**2-7**)

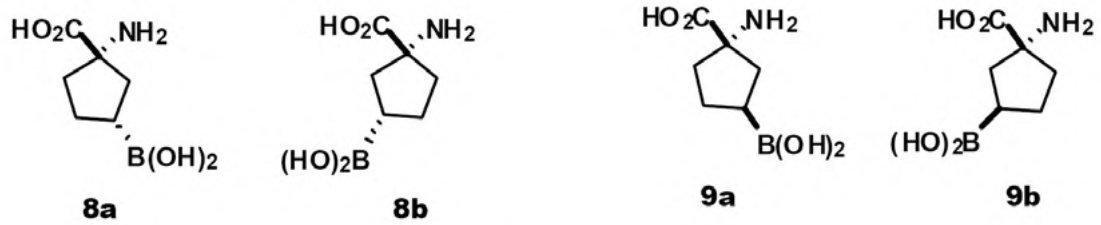

Fig. 2. Target molecules; *cis* and *trans* isomers of the cyclopentanecarboxylic acids (parent compound **5**)

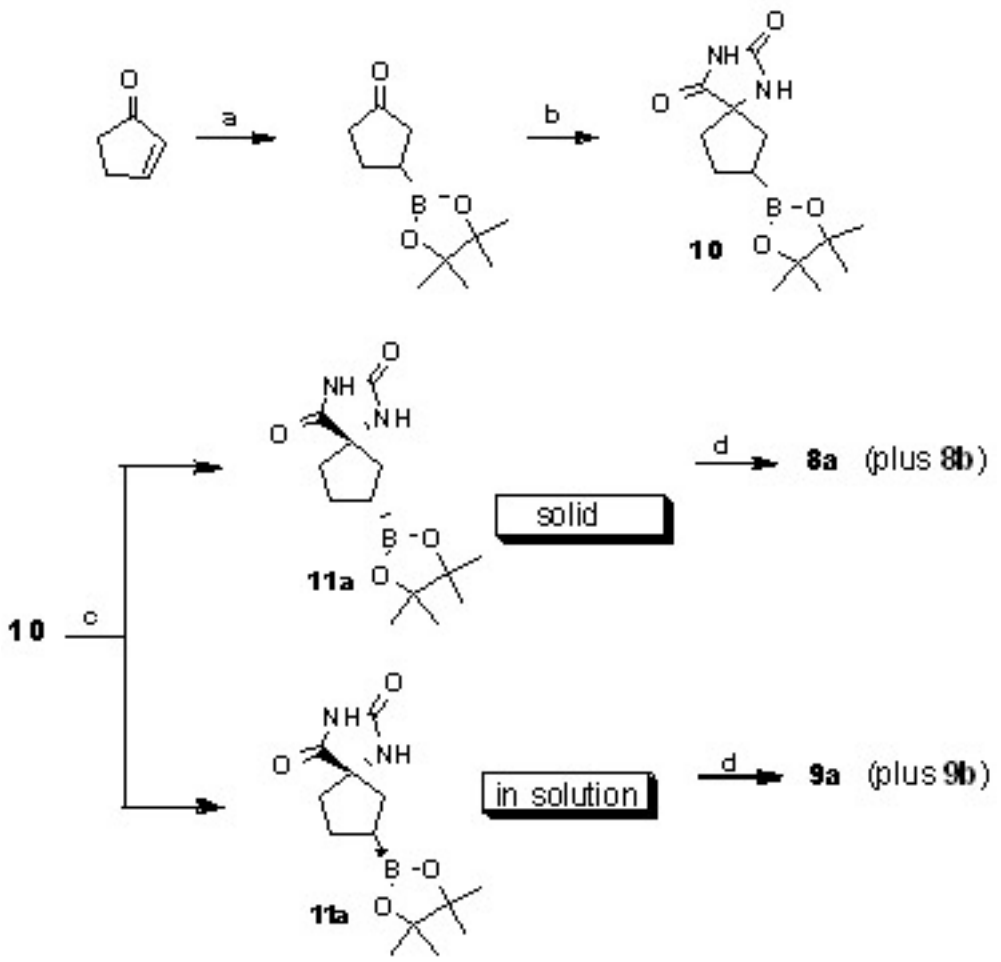

Fig. 3. Syntheses and separation of **8** and **9** (as racemates). Reagents and conditions: (a) CuCl, Bu_3P, DMF, rt; (b) $(NH_4)_2CO_3$, KCN, EtOH/H_2O (1:1), 60 °C; (c) separation of diastereoisomers **8a** and **8b** in methanol; (d) HCl (12 *M*), 150 °C

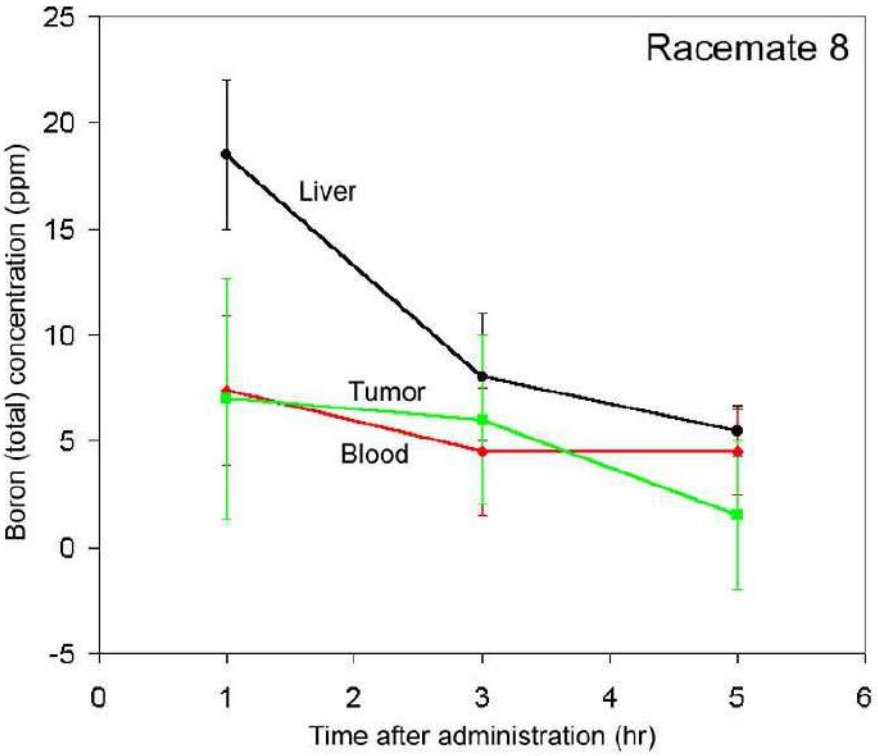

Fig. 4. Biodistribution of Compound **8a** (as a racemate)

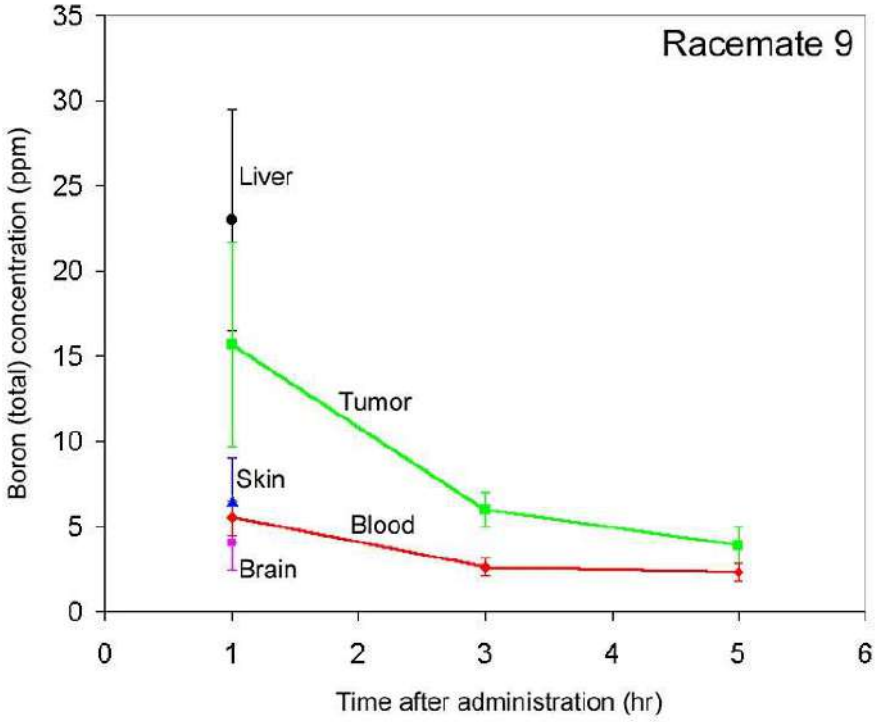

Figure 5. Biodistribution of Compound **9a** (as a racemate)

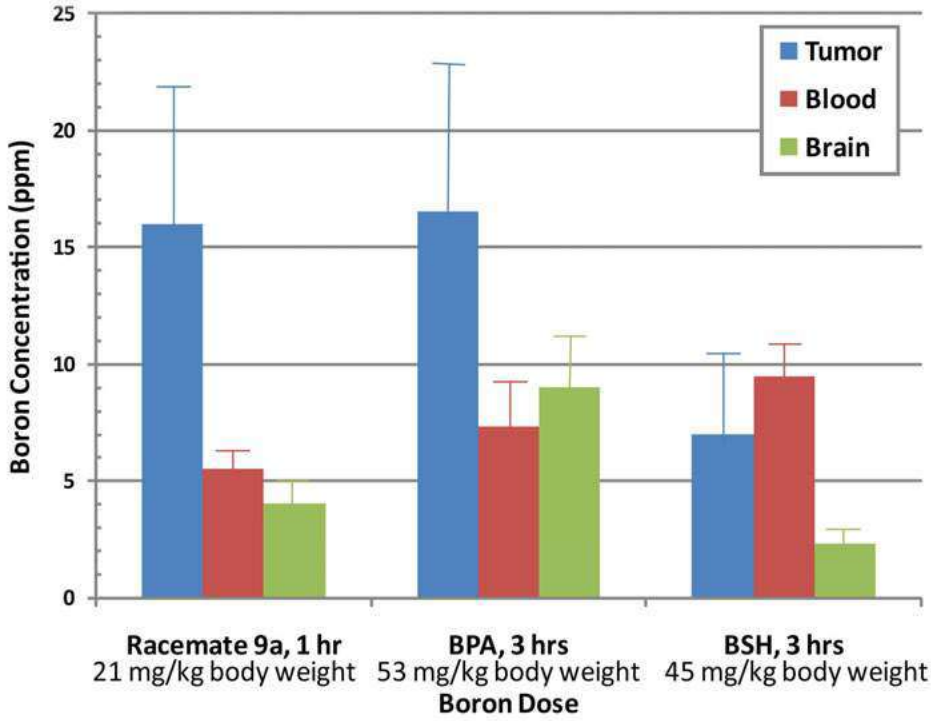

Fig. 6. A comparisons of boron concentrations in (mean ± SD) in tumor, blood, and brain from single injection of a boronated unnatural amino acid (compound 9a as a racemate), BPA, and BSH at the time of maximum concentration in the tumor. Five mice were used for observations on compound 9a

			μg/g Boron (wet weight)		
1 hr. Exposure	Cellular Potassium (mM)	Cellular Sodium (mM)	Nucleus	Mitochondria-Rich Perinuclear Cytoplasm	Remaining Cytoplasm
ABCPC (L + D)	168 ± 15	18 ± 4	303 ± 69	370 ± 77	361 ± 55
BPA	171 ± 20	14 ± 3	136 ± 55	109 ± 15	176 ± 57

Table 1. Quantitative SIMS imaging of T98G human glioblastoma cells after 1 hr treatment with 100 μg/ml boron equivalent of the fructose complex form of 1-amino-3-boronocyclopentane carboxylic acid (ABCPC in both L- and D-forms). Concentrations of potassium and sodium are expressed as mean ± SD on a cellular scale. Concentrations of boron are expressed as mean ± SD in three subcellular compartments: nucleus, mitochondria-rich cytoplasm, and the remaining cytoplasm. SIMS observations were made in more than five imaging fields containing more than 30 cells. The dry weight concentrations obtained by SIMS measurements from individual freeze-dried cells were converted into wet weight concentrations by assuming 85% cell water content. A direct comparison of compound 5 with L-*p*-BPA treatment of 110 μg/ml boron equivalent of the fructose complex for 1 hr is also shown in this table for this cell line by listing the data on BPA from reference 3.

Toward prompt gamma spectroscopy for monitoring boron distributions during extra corporal treatment of liver metastases by boron neutron capture therapy: A Monte Carlo simulation study

R. Khelifi[a], V.A. Nievaart[c], P. Bode[b], R.L. Moss[c], G.C Krijger[b]

[a] *Département de Physique, Université Saâd Dahlab, BP: 270 Route de Soumaa, Algeria*
[b] *Department of Radiation, Radionuclides and Reactors, Faculty of Applied Sciences, Delft University of Technology, Mekelweg 15, 2629 JB Delft, the Netherlands*
[c] *Institute for Energy, Joint Research Centre, European Commission, Westerduinweg 5, 1755 ZG Petten, The Netherlands*

Abstract

A Monte Carlo calculation was carried out for Boron Neutron Capture Therapy (BNCT) of extra corporal liver phantom. The present paper describes the basis for a subsequent clinical application of the prompt gamma spectroscopy set up aimed at in vivo monitoring of boron distribution. MCNP code was used first to validate the homogeneity in thermal neutron field in the liver phantom and simulate the gamma rays detection system (collimator and detector) in the treatment room. The Gamma ray of 478 keV emitted by boron in small specific region can be detected and a mathematical formalism was used for the tomography image reconstruction.

Keywords: BNCT, Prompt gamma spectroscopy, radiotherapy, MCNP

1. Introduction

Boron Neutron Capture Therapy (BNCT), a binary modality selective form of radiation therapy (Coderre et al., 1999), is based on the ^{10}B (n,α) ^{7}Li reaction: the emission of a high energetic α particle and a recoiling Li particle after thermal neutron capture in ^{10}B.

After the first successfully treatment of diffuse liver metastases at the TRIGA reactor in Pavia (2001), the Essen- Petten group investigates an extra corporal irradiation at the BNCT irradiation facility at the HFR (High Flux Reactor) Petten (The Netherlands). The technique known as prompt gamma spectroscopy (PGS) that may provide the possibility to no invasive measure boron uptake at the time of treatment. In 93.9% of the 10B(n,α)7Li reactions, the lithium nucleus is left in an excited state, which is followed by the emission of a 478 keV gamma (Figure.1) Thus a photon detector with sufficiently high spectral resolution can be used as a probe for the reaction rate of neutron capture in boron.

The principles for boron concentration determination aimed at the *in vitro* situation in a similar experimental setup were demonstrated in preceding works (Kobayashi, et al., 2000, Matsumoto, et al., 1991, Verbakel, 2002).

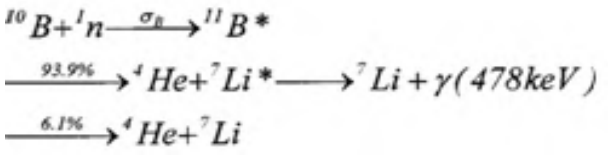

Figure 1. Simplified decay chains following neutron capture reactions in boron and hydrogen. The neutrons captured are mainly of thermal energy (0.025 eV) as the capture cross sections. An asterisk indicates that the nucleus is in an excited state. The disintegration of the excited boron-11 nucleus follows two branches

A set up constituted by a rotating PMMA (perspex) container with a liver, surrounded by PMMA and graphite for liver BNCT has already been performed in HFR, Petten, the Netherlands providing homogeneity in thermal neutron field in the liver phantom (Nievaart et al., 2006). Thus treatment of an isolated liver with thermal neutrons is promising.

It is necessary during BNCT treatment to perform spatial determinations of each dose contribution, both in tumour and in healthy tissue. In this work, the feasibility of boron distribution measurements during treatment by BNCT has been studied for the set up with a liver phantom and the gamma ray telescope of Petten (Verbakel W., 2002, Valda et al.,2005). To achieve this objective, the telescope with germanium detector was simulated using Monte Carlo code MCNPc2 to collect the prompt gamma rays (478 keV) produced during the BNCT. Within the phantom, the tumour is represented by small sphere with 65 ppm ^{10}B and it is positioned in four positions for our study. Using a GeHP detector in a telescope, gamma ray 478 keV emitted by small specific region can be detected and the reconstruction formalism can calculate absolute boron concentrations using the simulated gamma ray rates.

2. Set up for liver radiotherapy

The Set up for liver radiotherapy consist on a spherical liver irradiation holder on Perspex material (PMMA), which is confined in graphite Box of 20 cm thickness. A cylindrical hole of air is simulated in the graphite which permits the prompt gamma rays produced in the liver to reach the telescope on the top of the treatment room (Figure 2). Within the phantom, the tumour is represented by small sphere with 65 ppm ^{10}B and it is positioned hazardous for our study.

The fixed parameter are all source related: neutron energy spectrum, intensity and a maximum radius of the irradiation beam, i. e. 80mm. Note that at the edge of this disk shaped beam, the neutron intensity drops steeply. An average liver has a weight of around 1.7 kg and would fit in an imaginary cube with sides of 1200 mm. From Figure 2 it can be seen that the liver has to be irradiated from more than one side in order to get an homogeneous thermal neutron field. By extrapolating the idea of irradiating a body from more sides, the step to irradiate a rotating body which is rotational- symmetric seems straightforward (Nievaart et al., 2006).

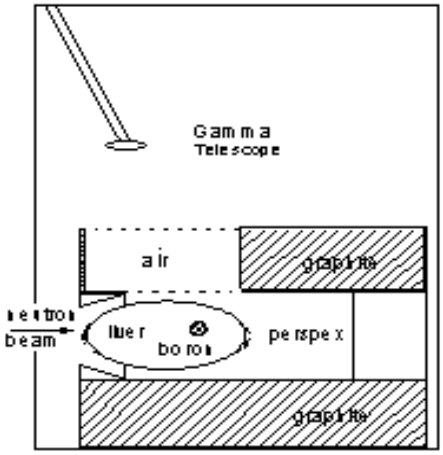

Figure 2. A part of the simulated treatment room in Petten

3. Results and discussion

3.1. Position of the liver set up

Considering the good agreement between the old version of the liver set sup and the new version (Figure 3), liver BNCT was used to studying a boron reconstitution in tumour using the simulated gamma ray telescope.

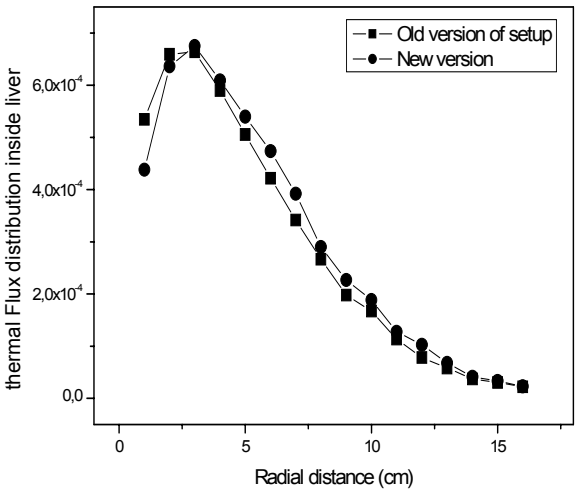

Figure 3. Thermal flux distribution along depth of the liver phantom (x,0,0)

The flux distribution was calculated using the mean density by simulated inside a liver phantom a cylinder boron with 0.7 cm of a radius containing 65 ppm of boron. The curve shows that thermal flux decrease drastically from: 7.09×10^{-4} to 4.71×10^{-7} n/cm^2 within 10 cm of distance inside the liver phantom (Figure 4).

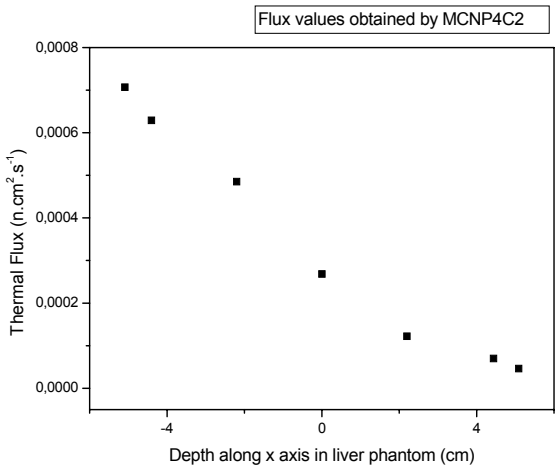

Figure 4. Thermal flux distribution along depth of the liver phantom (x,0,0)

The rotation of the system around y axis has reduced the decrease of thermal flux only to 2.69 n/cm^2.

The central axis of the gamma telescope obliges us to tacking back the liver set up of 10 cm from the neutrons source. The flux calculation by MCNP 4C2 in the liver was found comparable to the optimized values given by (Nievaart et al., 2006): 3.1 – 4.4 x 10^8 n/cm^2.s.

3.2. Study of the gamma response

Taking into account the dimensions of the telescope, the germanium detector, polyethylene and lead collimator given by constructor, the gamma rays telescope was simulated and added in the treatment room (Figure 2).

For the optimization of the graphite thickness, the gamma ray issued from the boron capture (478 KeV) reaction can reach the detector situated at 133 cm from the set up reference.

The problem with this set up was the attenuation of these gamma rays inside the 20 cm thickness of the graphite neutron reflector. To contouring this problem an air cylinder hole with a diameter of 10 cm was added to the previous set up simulation.

In this study, the densities of gamma rays (478 KeV) reached the detector and the neutron density in the liver versus the thickness of the graphite (top part of the set up) was simulated (Figure 5).

The mean thermal neutron flux was found constant during graphite thickness variation. For all simulation, The MCNP 4c2 was carried out for number of history of 10^7 and for each run, the CPU time was 52 minutes. The gamma rays densities for both 778 keV were obtained with very large errors respectively 3 %. Figure 5 shows the variations of the gamma rays. The 778 keV gamma ray start decreasing at 5 cm of graphite.

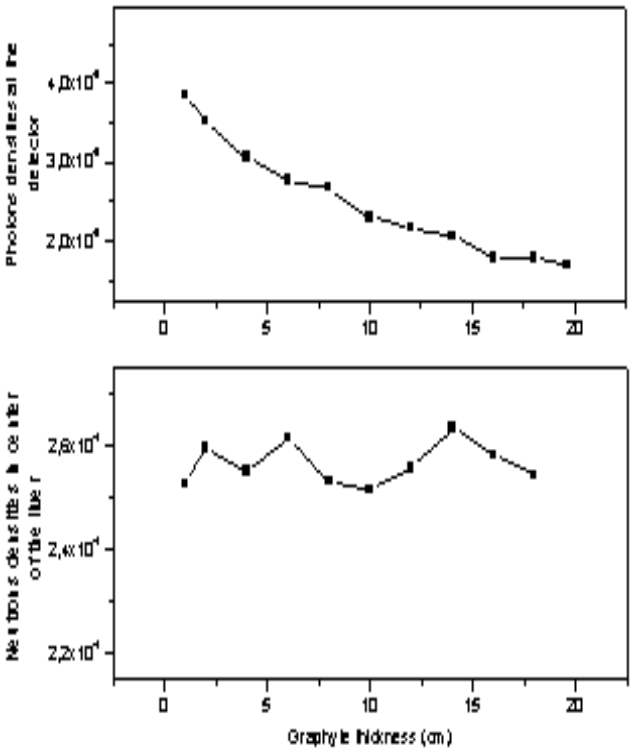

Figure 5. Photons densities of 778 keV gamma rays versus graphite thickness

3.3. Tomography

Using the optimum value of graphite thickness (0 cm: hole in graphite), the scanning process in 2 D will be studied by using a polyethylene cylinder filled with water and 65ppm of boron. Rotation around y axis of the liver holder allows us to get 24 (rotation step of 15 degrees) positions of the tumour and healthy tissue; then total gamma rays are detected.

Reconstruction consists of y_0 and z_0 coordinate, radius of the tumour and boron concentration. The model was used by Verbakel et al., 1997.

Nom linear function has been adjusted to our simulated data for 24 rotation angle. The simulated boron counts by MCNP using F4 tally and the best fitted function are represented in figure 6. The number of simulated events is such that the statistical fluctuations of the counting process can be neglected.

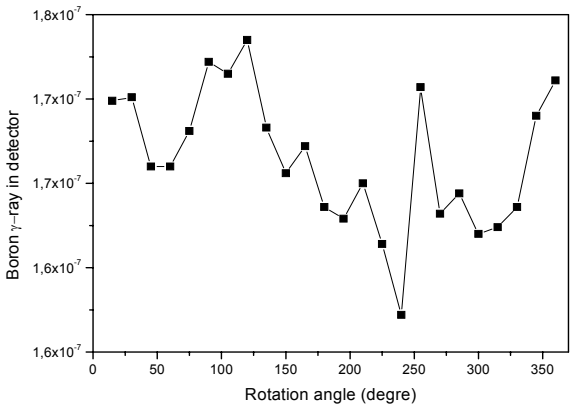

Figure 6. The 24 calculations of boron counts and the fitted function of tomography calculation

In the present work some assumptions were used (i.e. homogenous distribution of boron in tumour and healthy tissue,.. there is only one cylindrical tumour in the liver). Good agreement is found between mathematical estimation and the real parameters of position y_o and z_o radius of tumour r_o and concentration C_t used for our MCNP simulation.

Table 1 shows some high and acceptable deviation between the reconstruction and the real values. The tumour position gives 11% -13 % deviation. For tumour size 21% and 17% for tumour concentration.

	Real values	Calculated values
Y_o (cm)	1,50	1,68
Z_o (cm)	2,00	2,24
R_t (cm)	0,70	0,84
C_t (ppm)	65,0	76,0

Table1: Results of the reconstruction estimation and the real parameters

4. Conclusion

In the present work we have established by simulation with Monte Carlo MCNP code, a basis for a subsequent clinical application of the PGS setup aimed at *in vitro* monitoring of boron uptake in BNCT patients.

The next step will be the improvement of the mathematical algorithm of the reconstruction of tumour in the liver and the benchmarking with experimental measurement in High Flux Reactor (HFR), Petten, the Netherlands

References

Coderre, J. A., Morris, G. M., 1999, The radiation biology of boron neutron capture therapy Radiation Res. 151 (1-18).

Kobayashi T. , Sakurai Y., and Ishikawa M. , "A noninvasive dose estimation system for clinical BNCT based on PG-SPECT Conceptual study and fundamental experiments using HPGe and CdTe semiconductor detectors," Med. Phys. **27**, 2124–2132 (2000).

Matsumoto T., Aoki M., and Aizawa O., "Phantom experiment and calculation for in vivo 10boron analysis by prompt gamma ray spectroscopy," Phys. Med. Biol. 36, 329–338 (1991).

Nievaart VA, Moss RL, Kloosterman JL, van der Hagen T.H.J.J., van Dam H., Malago M., Sauerwein W. . 'Design of a rotating facility for extra corporal treatment of an explanted liver with disseminated metastases by boron neutron capture therapy with an epithermal neutron beam at the HFR in Petten'. Radiation Research 166, 81-88(2006).

Valda, A., Minsky D.M., Kreiner A. J.,Burlon A. A. and Somacal H. Development of tomographic system for online dose measurement in BNCT. Brazilian Journal of Physics, Vol. 35, n_o. 3B, September, 2005.

Verbakel, W. Design and validation of gamma ray telescope for in vivo dosimetry during BNCT. Ph.D Thesis, 2002.

Verbakel W. and F. Stecher-Rasmussen F., "A Gamma-ray telescope for on-line measurements of low boron concentrations in a head phantom for BNCT," Nucl. Instr.. Methods Phys. Res. A 394, 163–172 (1997).

Aromatic aminoacid analogues mimetic of BPA transport : use of *O*-(2-[^{18}F]fluoroethyl)-*L*-tyrosine in experimental animal model of F98 Glioma

Luca Menichetti[1], Lorena Gaetano[2], Giuseppe Daquino[3], Luca Cionini[4], Marino Mazzini[5], Piero A.Salvadori[1]

[1] *Department of PET and Radiopharmaceutical Chemistry, C.N.R. Institute of Clinical Physiology, Pisa, Italy*
[2]. *University School for Advanced Studies S.Anna, Pisa, Italy*
[3] *Joint Research Centre, European Commission, Petten, The Netherlands*
[4] *Unit of Radiotherapy, AOUP-University Hospital, Pisa, Italy*
[5].*Department of Mechanical, Nuclear and Production Engineering , University of Pisa, Italy*

A number of recent applications demonstrated the potential of radiolabeled aromatic aminoacids with Positron Emission Tomography (PET) for brain tumour imaging: the mechanism is similar to other metabolic substrate and it is based on their specific accumulation in neoplastic cells, probably linked to an increased expression of amino acid transporters, but not due to their incorporation in proteins.

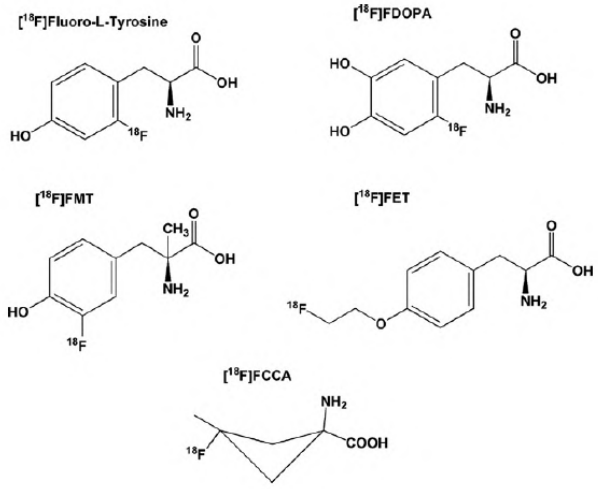

Although fluorine-18 (109.7 min half-life) is the most interesting radionuclide for the preparation of PET radiopharmaceuticals, the labeling of amino acids with fluoride-18 is often difficult, particularly in aromatic positions (the use of the molecular F_2, is on the contrary chemically unsuitable and is limited to a few PET centres provided of special equipment and cyclotron targets). An alternative way of labelling aromatic systems with fluorine-18 involves the introduction of a fluoroalkyl group to an aromatic position, rather than by direct labelling with a fluorine atom. In this class a promising molecule for its applicable in neurooncology is the *O*-(2-[^{18}F]fluoroethyl)-L-tyrosine (FET), one the first ^{18}F-labeled amino acids.

The tracer demontrated high in vivo stability, low uptake in inflammatory tissue and suitable uptake kinetics for clinical imaging.

The main objective of this work is to demonstrate the feasibility of a novel approach for experimental BNCT, with a special focus to *micro*imaging for the real assessment of the homogeneity and extent of accumulation of these class of aminoacid in tumour and surrounding healthy tissue. The goal of this study is then to use the FET to screen tumours lesions in experimental model with a small field of view PET, so called, *micro* PET. The *micro* PET-FET approach could lead to the assessment of the transport and the net influx and accumulation of FET molecule, as analogue to BPA. A correlation between BPA and FET pharmacokinetic, mainly linked to different affinities of transporters, could give numeric parameters useful for the assessment of boron loading in tumour and healthy tissues. The study present study was performed on implanted rats at the 3rd week after the tumour implantation (F98 glioma cell line).

In the frame of this project was developed a simple and convenient remote controlled, one-pot synthesis module for FET, based on an automated Gilson module (mod. *Aspec XL*) with opportune hardware and software modifications performed in our laboratories. The radiosynthesis was performed via no-carrier-added ^{18}F-fluorination of N-trityl-*O*-(2-tosyloxyethyl)-L-tyrosine-tert-butylester with subsequent deprotection under nonaqueous conditions in the presence of tetra-butyl ammonium hydrogen carbonate/carbonate. Deprotection of the intermediate FET derivative is performed in presence of trifluoroacetic acid in trichloromethane followed by solid-phase extraction. The FET containing HPLC eluent can be used for studies without purifications. The radiochemical purity is not less than 98% and the typical uncorrected radiochemical yield is higher than 40%; the total synthesis time is less than 90 min.

Determination of boron distribution in rat's brain, kidney and liver

[a,b]Ali Pazirandeh*, [c]Behnam Jameie, [b]Maysam Zargar

[a]*Nuclear Science and Technology Research Institute, AEOI*
[b]*Nuclear Engineering Department, Islamic Azad University*
[c] *Neuroscience Lab, Cellular & Molecular Research Center, Iran University of Medical Sciences,* Tehran Iran
Pzrud193@seiau.ir

Abstract

In an experiment on a rats' brain after transcardially injection of a neutral solution of boron, the animals were sacrificed and the brain were removed. The coronal sections of certain area of brain were prepared by freezing microtome. The slices were sandwiched within two pieces of CR-39. The samples bombarded in a thermal neutron field of TRR pneumatic facility. The alpha tracks registered on CR-39 after being etched in NaOH. The boron distribution was determined by counting alpha tracks found on rat's liver, kidney and brain slices showing quite different distributions.

Keywords: Boron-10, Borax, CR-39 plastic, alpha track counting

Introduction

Boron neutron capture therapy is a well known technique for destroying malignant tumor tissues as a result of a nuclear reaction of $^{10}B(n,\alpha)^{7}Li$ with Q-value of 2.31MeV (93.7% 1.47MeV alpha plus 0.478MeV gamma ray and 6.3% 1.98MeV only alpha) and the rest is carried by lithium ion. Their short range of the ions in tissue (5-9μm) restricts radiation damage to the cells in which boron absorption takes place. In BNCT, it is important that the boron compound selectively concentrate in tumor cells to destroy tumor cells without significant damage to the surrounding normal tissues. Practically the boron carrier is concentrated mainly in tumor but some remained in blood and surrounding tissues.

As a general rule, high boron concentration in tumor is advantageous because it is more effective in destruction of malignant cells. On the other hand, high boron concentration decreases thermal neutron flux in the tumor because of high absorption and consequently $^{10}B(n,\alpha)^{7}Li$ reaction decreases.

For treatment of deep seated brain tumors, epithermal neutron flux should be used to avoid thermal neutron absorption in healthy tissues before tumor, therefore epithermal neutrons beam is used. Epithermal neutrons passing through brain toward tumor slow down and become thermalized. Thermal neutrons are very easily absorbed by B-10 (3836b) as compared with epithermal neutron absorption (~10 b) see Fig. 1. Figure 1 shows simulated deposited energy in brain and tumor and beyond that as epithermal neutrons slow down in brain and induce different reactions. Therefore, the distribution of boron concentration in brain and tumor is important factor in destruction of malignant cells with least damage to healthy tissues.

* pazirand@khayam.ut.ac.ir; TelFax: +9821-44869655-6;
+9821-44817194 OR +9821-88004781
P.O.Box 1943, Tehran 19395, IRAN

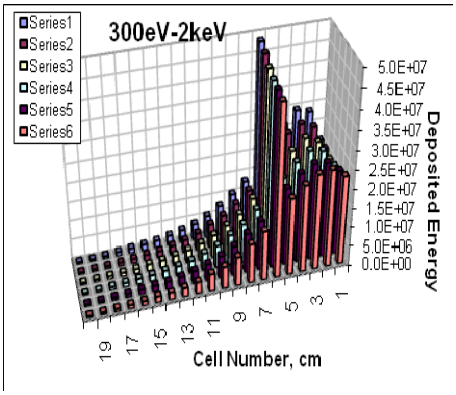

Fig. 1. Simulated deposited energy in brain and tumor

In this paper the results of an experiment to determine distribution of boron in rat's brain, kidney and liver were presented. The measurements performed on rats using a solution of a mixture of boric acid and borax with PH nearly 7. Bench *et. al.* 2004 and Gregoire *et. al*.,1993 have tried boric acid as boron carrier. The measurements showed that boron concentration was high and not uniform in liver, medium and patches of boron in kidney and low – nearly uniform in brain.

2. Experimentation

Animal models for human brain tumors have played a significant role in experimental neuro-oncology for almost four decades (Barth *et.al.* 2003, Weisacker *et.al*. 1981). Many have used rat's brain tumor model for human, have provided much information that has helped us to better understanding human brain tumors and potentially led to better clinical treatment (Nano *et.al.*2004). Normally two popular compounds sodium borocaptate or BSH ($Na_2B_{12}H_{11}SH$) and boronophenylalanine BPA are used as boron carrier but some have used boric acid. (Bennie 2004; Gregoire 1993). In this study, we have measured boron distribution in rat's brain, kidney and liver using a mixture of boric acid and borax with a proportion makes it neutral. Two solutions were prepared: (1) 1g boric acid plus 250mg borax in 70ml water (2) 2g boric acid plus 500mg borax in 50ml water. Adult male Sprague-Dawely rats were used in this study, to measure the boron distribution in brain, kidney and liver (Table 1).

Table 1. Some information about rats used in experiment

3	No. of rats
Male	sex
240, 280,300	Weight(g)
60,70,75	Age(d)

Ten minutes after induction of anesthesia by Ketamine (o.7ml/kg), 1ml of boron solution was injected transcardially via left ventricle, the animals left alive until the heart was still beating the second injection also carried out in left ventricle in the same dose. After 15 minutes, the animals were scarified. Immediately, the brain, kidneys and the liver were removed and frozen. By using freezing microtome, coronal sections of 10μm were prepared. To keep the slices intact, they were treated by H.CHO-formaldehyde. Certain sections from different parts were sandwiched with two pieces of CR-39 (allyl diglycol carbonate) plastic can record 1.48MeV α-particles and 0.83MeV ^{7}Li particles generating in $^{10}B(n, \alpha)\ ^{7}Li$ reaction, as well as 0.59MeV protons originating from $^{14}N(n,p)^{14}C$ reaction, where ^{14}N is the biological abundant nuclide(Ogura *et.al.* 2004). Some of the recoil protons are due to $^{1}H(n,n')^{1}H$ reaction in the tissue and in the plastic itself are because of epithermal neutron scattering from hydrogen nucleus, were recorded. The sandwiched brain slices were bombarded in the thermal neutron pneumatic facility of Tehran Research Reactor (TRR) in a neutron flux of $10^{6}n/cm^{2}.s$ for 15m. Thermal neutrons captured by ^{10}B may lead to production of high energy alpha particle. Some alpha particles produced in the slices may escape and travel into the plastic CR-39. After the irradiation, plastic pieces were etched in 6.25 mole NaOH at 65^{o} C for an hour. The etched CR-39 viewed on a PC based optical microscopy equipped with a digital camera revealed the ion tracks, alpha, lithium and protons. The boron distribution is assessed by scanning alpha tracks. Figure 1 shows typical ion tracks on the plastic of forebrain slice.

3. Results

As indicated above, boron density was measured in brain slices under certain conditions to be as close to *in vivo* density as possible. Figure 2 shows the photo of the removed rat's brain. Figs. 3-5 are ion tracks registered on plastic CR-39 of rat's liver, kidney and brain respectively.

The larger tracks are due lithium, medium size are alpha and small ones are identified as recoiled protons. Figs 6-9 are relative distributions of combined alpha and lithium tracks registered on CR-39 are obtained from brain slices irradiated in flux at pneumatic facility. The result of experiment revealed that due to brain structure the relative boron concentration varies as shown in Figs. (6-9).

4. Conclusions

We find from data the pattern of distribution of ^{10}B could be very important from the therapeutic point of view. The accurate measurement of ^{10}B distribution in biological models with sensitivity in the ppm range is essential for evaluating the potential usefulness of various ^{10}B-delivery compounds. For this purpose, we can easily recognize ^{10}B-rich regions in the sample by a cursory glance at the digital camera photo.

Acknowledgment

The authors would like to thank Tehran Research Reactor Operating Staff for irradiating samples and Cellular and Molecular Research Center of Iran University of Medical Sciences for technical support.

References

Awad Diaa Iene, Lutz Tabod, Silke Lutz, Wessolowski Holger, Gabel Detlef, 2005, Interaction of $Na_2B_{12}H_{11}SH$ with liposomes: Influence on zeta potential and particle size, Journal of Organomettalic Chemistry 690, 2732-2735.

Barth Rolf F., Yang Weilian, Coderre Jeffrey A.2003, Rat brain tumor models to assess the efficacy of boron neutron capture therapy: a critical evaluation, Journal of Neuro-Oncology 62, 61-74

Bench Bennie J.,Johnson Rebecca, Hamilton Craig, Gooch Joey, Wright John R., Advin self-associates with boric acid gel suspensions: an affinity boron carrier that might be developed for boron neutron capture therapy; J. Colloid and Interface Science, 270, 2, 315-320.

Gregoire V., Begg A.C., Huiskamp R., Verrijk R., Bartelink H. 1993; Selectivity of boron carriers for BNCT: pharmacological studies with borocaptate sodium, -borono phenylalanine and boric acid in murine tumors; Radiotherapy and Oncology, 27,1,46-54.

Ogura K., Yanagie H., Eriguchi M., Lehmann E.H., Kuelne G., Bayon G., Kobayashi H. 2004, Neutron capture auto radiographic study of the biodistribution of ^{10}B in tumor-bearing mice. Applied Radiation and Isotopes 61, 585-590

Rosanna Nano, Sergio Barni, Patrizia Chiari, Tazio Oinelli, Francesca Fossati, Saverio Altieri, Cecielia Zonta, Ubaldo Prati, Laura Roveda, and Aris Zonta,2004, Efficiency of boron neutron capture therapy on liver metastases of colon adenocarcinoma: Optical and ultra structural study in the rat; Oncology Reports 11,149-153

Suzuki Minoru, Nagata Kenji, Masunaga Shinichiro, Kinashi Yuko, Sakurai Yoshinori, Maruhashi Akira, Ono Koji, 2004, Biodistribution of ^{10}B in a rat liver tumor model following intrarterial administration of BSH/ degradable starch microspheres (DSM) emulsion, Applied Radiation and Isotopes 61, 933-937.

Weisacker M., Deen DF, Rosenblum, Hoshino T., Gutin PH, Barker M: 1981;The 9L rat brain tumor: description and application of an animal model. J. Neurol. 224, 183-192

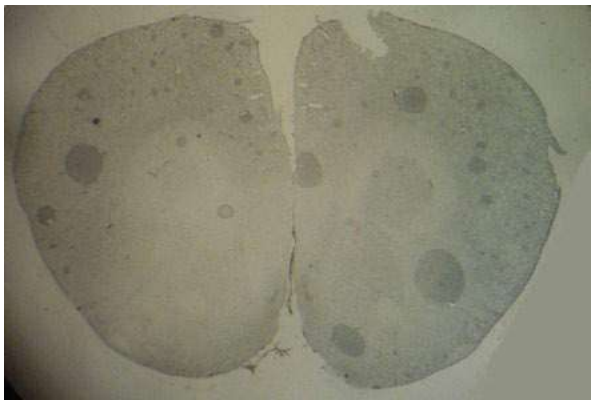

Fig. 2. Rat forebrain cut

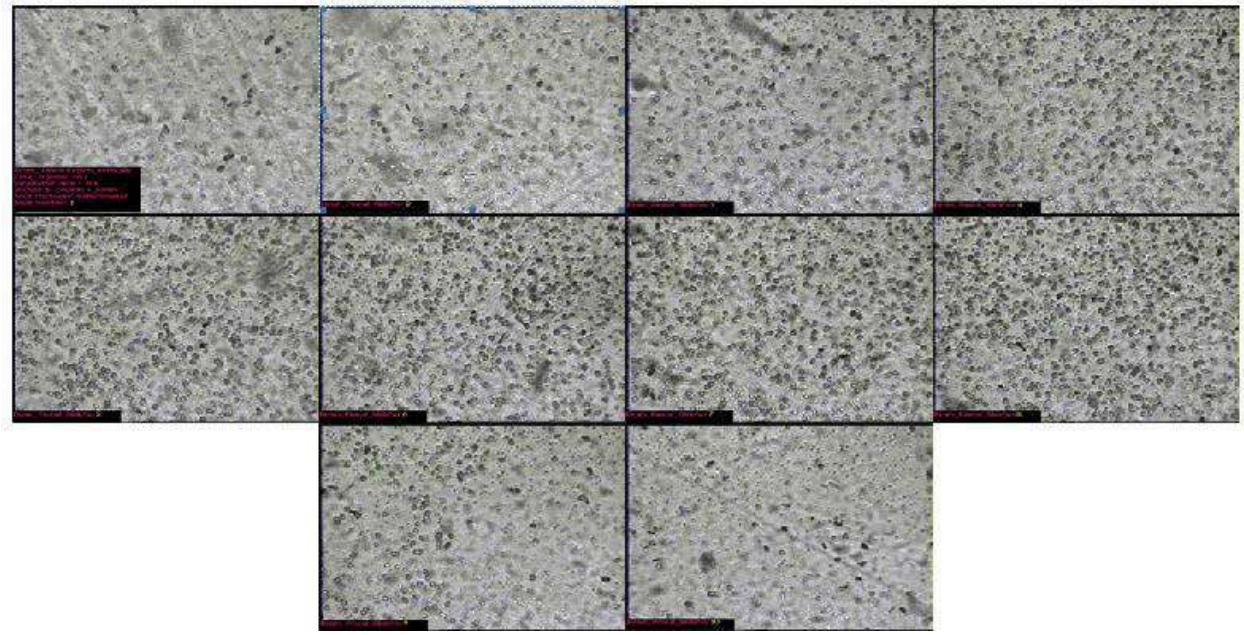

Fig. 3. Rat's brain slice ion tracks on plastic CR-39 using solution No. 2

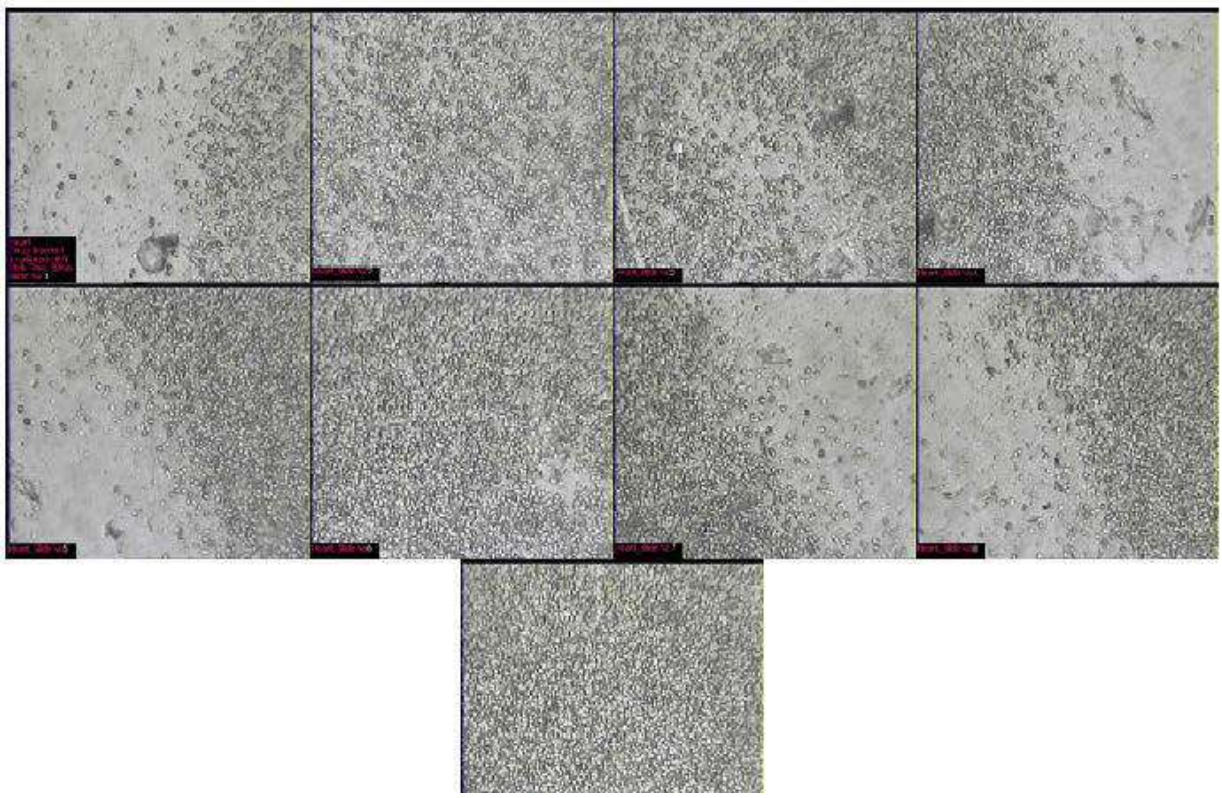

Fig. 4. Rat's liver slice ion tracks on plastic CR-39 using solution No. 2

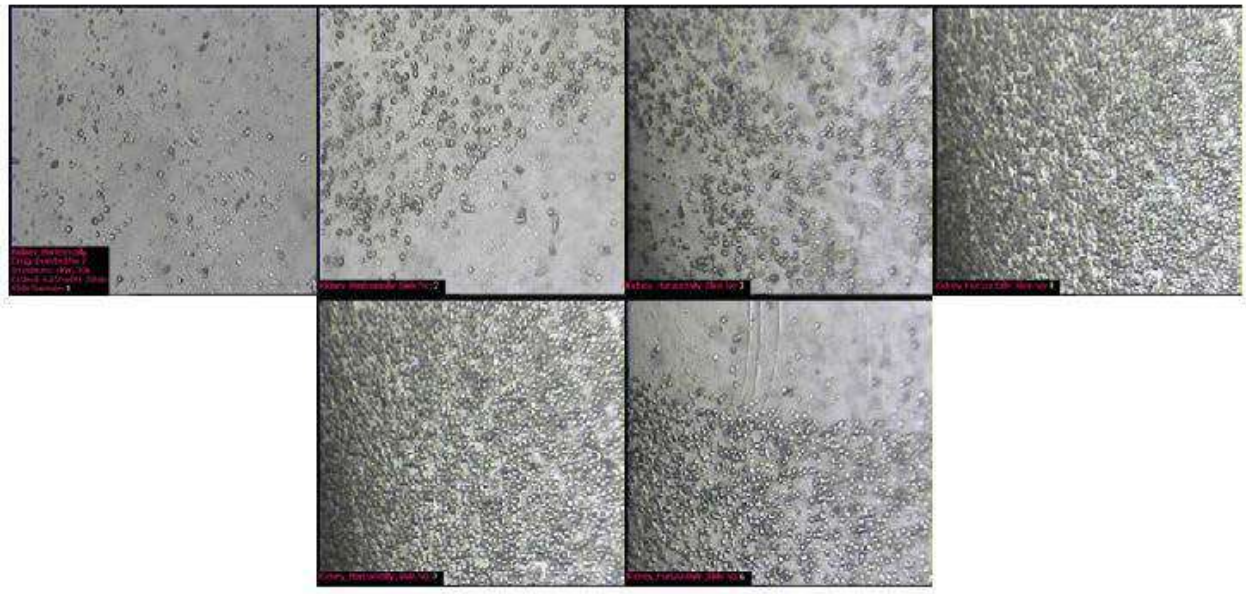

Fig. 5. Rat's kidney slice ion tracks on plastic CR-39 using solution No. 2

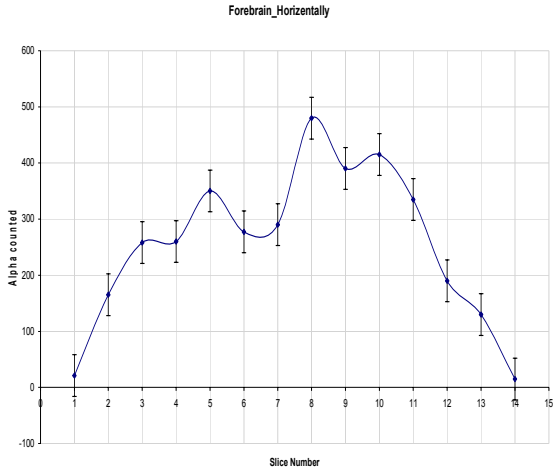

Fig. 6. Forebrain-horizontal brain slice Compound No.2

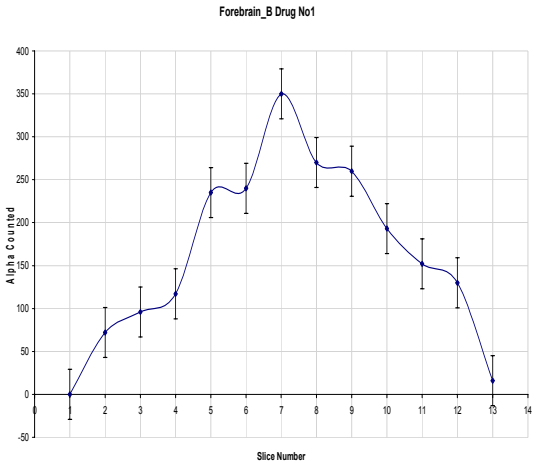

Fig. 7. Forebrain-horizontal brain slice Compound No.1

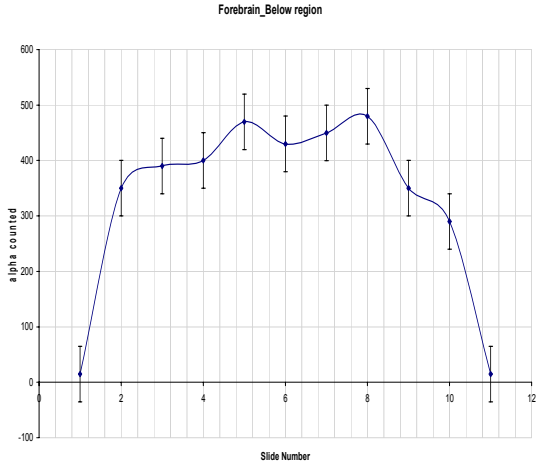

Fig. 8. Forebrain-horizontal lower brain slice Compound No.2

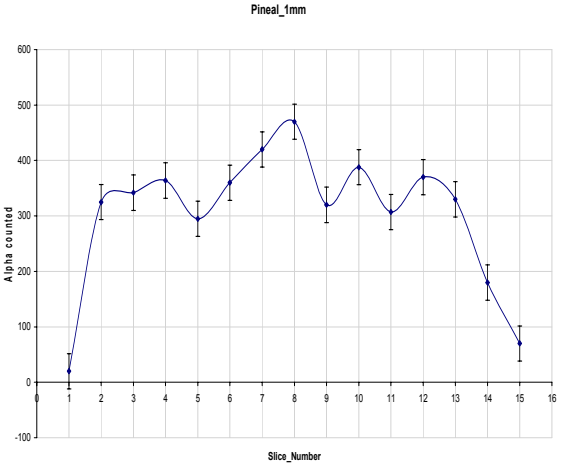

Fig. 9. Bineal-horizontal brain slice Compound No.2

Study of a Monolithic Silicon Telescope for BNCT Applications

Pola A.[1,2], Agosteo S.[1,2], Fazzi A.[1,2], D'Angelo G.[1,2], Introini M.V.[1,2], Pirovano C.[1], Varoli V.[1,2]
Altieri S.[3,4], Stella S.[3,4], Bortolussi S.[3,4], Bruschi P.[3,4]

[1]Dipartimento di Ingegneria Nucleare, Politecnico di Milano, via Ponzio 34/3, 20133 Milano,Italy.
[2]Istituto Nazionale di Fisica Nucleare, Sezione di Milano, via Celoria 16, 20133 Milano, Italy.
[3] Dipartimento di Fisica Nucleare e Teorica, Università di Pavia , via Bassi 6, 27100 Pavia, Italy.
[4] INFN, Sezione Pavia, via Bassi 6, 27100 Pavia, Italy.

The aim of this work is to study the feasibility of employing a monolithic silicon telescope for measuring the boron concentration in histological samples for BNCT (boron neutron capture therapy) applications. At the LENA reactor (Pavia, Italy) this information is derived by irradiating with thermal neutrons an histological sample (doped with boron) placed on a surface barrier silicon diode. This device measures the distribution of the energy deposited by alphas and ^{7}Li ions generated by neutron absorption on boron. The lower energy part of the spectrum is distorted by secondary electrons (produced by photon background) and by protons generated via the ^{14}N(n,p) reaction in tissue.

The monolithic telescope consists of a ΔE and an E stage built on the same chip, about 2 μm and 500 μm thick, respectively. The ΔE – E structure permits to discriminate between different types of particles. This feature can be exploited to improve the accuracy of the boron concentration estimate.

A detector with a sensitive area of 1 mm^2 was irradiated (in vacuum) bare, faced with a boron implanted silicon chip (standard by NIST) and coupled to a thin sample of rat lung charged with boron. The contribution of protons generated via direct interaction of neutrons with the detector (nitrogen in the dead layer) was estimate. Alphas and lithium ions produced by neutron capture on boron resulted to be well-separated. Moreover, events due to protons generated in tissue by neutron capture on nitrogen were identified and discriminated. The minimum detectable energy was reduced to about 40 keV.

A direct comparison of the estimate of boron concentration in an histological sample obtained with the monolithic silicon telescope and with the silicon diode (present technique) will be presented and discussed.

Neutron autoradiography with a silicon detector in a hospital environment

S. Scazzi[a], F. Basilico[b], D. Bolognini[a], P. Borasio[c], P. Cappelletti[d], P. Chiari[e], V. Conti[f], M. Frigerio[d], G. Giannini[g], S. Gelosa[d], V. Mascagna[a], A. Mattera[a], P. Mauri[b], A. Monti[d], A. Mozzanica[h], A. Ostinelli[c], M. Prest[a,] W. Sauerwein[i], E. Vallazza[g], A.Zanini[l]

[a]*Universitas Studiorum Insubriae, Como, and INFN, Milano Bicocca, Italy*
[b]*Institute of Biomedical Technologies,CNR Milano, Italy*
[c]*Department of Clinical and Biological Sciences "S. Luigi Orbassano", University of Torino, Italy*
[d]*S. Anna Hospital, Como, Italy*
[e]*Department of Nuclear and Theoretical Physics, University of Pavia, Italy*
[f]*Università degli Studi di Milano and INFN, Milano, Italy*
[g]*University of Trieste, Physics Department and INFN, Trieste, Italy*
[h]*Paul Scherrer Institute, Villigen, Switzerland*
[i] *Strahlenklinik,University of Essen, Essen, Germany*
[l]*INFN, Torino, Italy*

Abstract

In the framework of the INFN PhoNeS project a system to perform neutron imaging has been developed and tested at the radiotherapy unit of the S. Anna hospital in Como with a Varian Clinac 2100C/D. Imaging is performed by neutron autoradiography with a non depleted self-triggering microstrip silicon detector, exploiting neutrons photo-produced by the Linac. Some boron doped samples were put on the surface of the detector and irradiated: the alpha particles produced in the reaction $^{10}B(n,\alpha)^{7}Li$ are detected and the result is a 1D scan of boron concentration. Dedicated readout electronics allows to acquire the data in the inter-bunch period in order not to blind the detector with the primary gamma beam. This real-time system is independent from the specific molecule containing the boron and it allows studying its concentration in cells using different carriers. The imaging detector has been tested with different samples: solutions of boric acid with different concentrations, boron resin, biological samples of urine containing BPA and BSH and finally with ^{10}BPA-Fructose complex perfused human lung samples. The paper will present the results in terms of minimum detectable concentrations and kinetic curves. The measurements uncertainty is <10% and can be improved using better techniques to deposit the samples on the support. The minimum detected concentration of ^{10}B was 5 ppm/cm^2 and the spatial resolution can be easily improved to 50 μm even if this is not a constraint.

Keywords: Silicon, imaging, boron, Linac

1. Introduction

The two main limits of BNCT are the need of a thermal neutron flux and the lack of a carrier having all the desired features. The PhoNeS (Bevilacqua et al., 2007) project (INFN-PRIN05) has faced the first problem trying to find an alternative way to produce neutrons. At the moment such a beam is available only at nuclear reactors which are not the ideal structure to perform a radiation therapy both from the medical and safety point of view. The possibility to have a thermal neutron source in a hospital environment would be a great opportunity for the development of BNCT. The main goal of this project has been to build a converter+moderator system to photoproduce neutrons via giant dipole resonance. The flux obtained has been characterized in terms of intensity and energy spectrum (Conti et al., 2007): the intensity is a factor 10 lower than the needed value but can be increased modifying the configuration of the prototype and exploiting the Linac at its maximum power (for example, eliminating the flattening filter which degrades the intensity of the beam). The energy spectrum is the optimal thermal spectrum for BNCT (Conti et al., 2007). On the wave of these good results it has been decided to face also the second problem of BNCT: the study of boron carriers. An imaging system has been developed to measure the boron concentration in samples in real time and in a hospital environment

exploiting the neutron flux photoproduced by the linear accelerator. This set-up will allow a systematic characterization of boron carriers. In section 2, the imaging system is described while section 3 is dedicated to the analysis of the systematic study on the sample preparation and to the results of the absolute calibration and of the first tests with biological samples.

2. The measurement set-up

The imaging detector is a Hamamatsu 9.5×9.5 cm^2 microstrip silicon detector (Prest et al., 2003) consisting of 768 strips with a physical pitch of 121 μm (a one floating strip readout scheme has been adopted). The sample is positioned on the surface of the detector and irradiated with the thermal neutron beam. The detector is contained in an iron box on the treatment couch (figure 1).

The irradiation is performed without the PhoNeS prototype but with a layer of 6 cm of PMMA (PolyMethylMethAcrylate, a tissue equivalent material) and 0.5 cm of cerrobend (a combination of bismuth 50%, lead 26.7% tin 13.3% and cadmium 10%) on the iron box: this is due to the fact that the PhoNeS prototype does not allow to position the detector horizontally; a MCNP4B-GN simulation has demonstrated that the neutron flux in these conditions is enough for these tests.

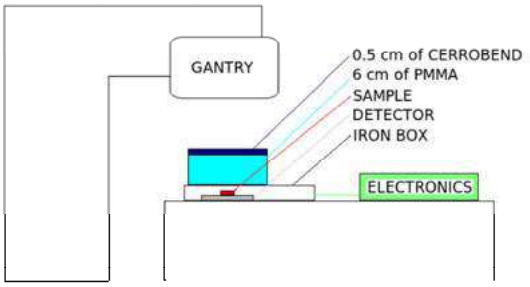

Figure 1. Scheme of the measurement set-up

The α particles emitted in the boron neutron capture reaction are detected by the system producing a 1D scan of the boron concentration contained in the sample. The detector is used unbiased in order to reduce the gamma background; this has been demonstrated with a GEANT3 simulation which also gave information on the maximum "useful" layer of the samples: the sample has to be thinner than 5 μm, otherwise the self- absorption of the αs takes place.

The data acquisition is performed exploiting the pulsed nature of the beam produced by the linac: particles are emitted in bunches with a rate of 100-300 Hz and during the inter bunch period only thermal neutrons (which are slow) survive while the photons of the primary beam are not present. A dedicated readout electronics system is used to perform this acquisition in anti-coincidence with the primary photon beam. The silicon detector is readout by three self triggering TAA1 ASICs (produced by Gamma-Medica-IDEAS) that are controlled with a dedicated repeater board.

3. Measurements and results

Two sets of measurements have been performed: in the first phase qualitative tests have been made to verify the capability of the system to detect the boron contained in the samples. A boron resin sample (with a high concentration) has been used for the very preliminary measurements (figure 2) and is still used to check the detector performance before each data taking session. Then measurements with solutions of boric acid have been performed and the first problem has been met: the sample preparation process is very important to obtain successful results.

The present choice is to make drops of the boron solution evaporate on a support; the first supports were made of paper but in this case the solution is absorbed by the paper itself and the α particles cannot go out from the sample and release energy in the detector; plastic supports have been identified as the best ones because the boron dust remains on the surface. Also the accuracy of the volume of the spots has to be good to know the deposited concentration: a micropipette is used which can deposit volumes in the range of 0.5-10 μl (figure 2).

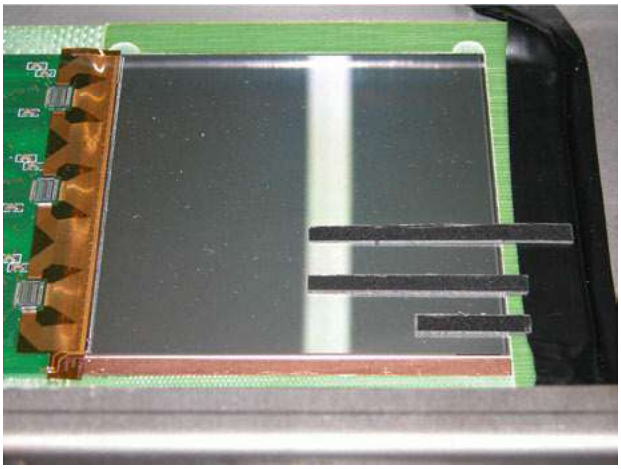

Figure 2. Photo of the silicon detector with resin samples positioned on its surface

Figure 3. Photo of the micropipette and of a typical sample with columns with a different number of spots

Another critical aspect is the homogeneity of the boron solution: in the first attempts when the water was evaporated a crystallization effect took place and the boron dust deposit resulted non homogeneous causing the self absorption of the αs. Thus it has been decided to irradiate the boron solution with ultrasounds that break the bonds of the molecules making the solution very homogeneous (see spots shown in figure 4).

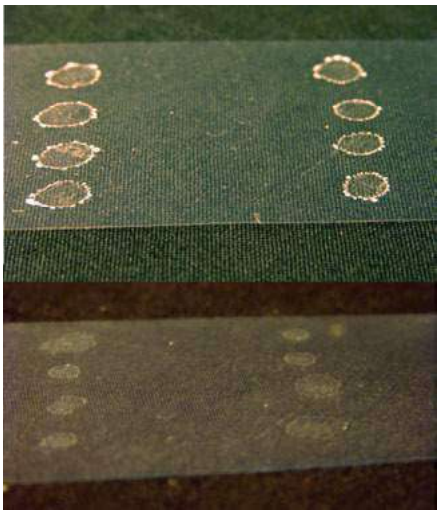

Figure 4. Photo of the evaporated spots with the crystallization effect and with the homogeneous solution

Once identified the sample preparation procedure, quantitative measurements have been performed: an absolute calibration has been made with a solution of 100 ppm of ^{10}B (columns with a different number of spots have been prepared to obtain equivalent total concentrations of 200, 400 and 600 ppm). Figure 5 shows the plot obtained for the 600 ppm sample: six identical columns have been positioned on six different parts of the detector.

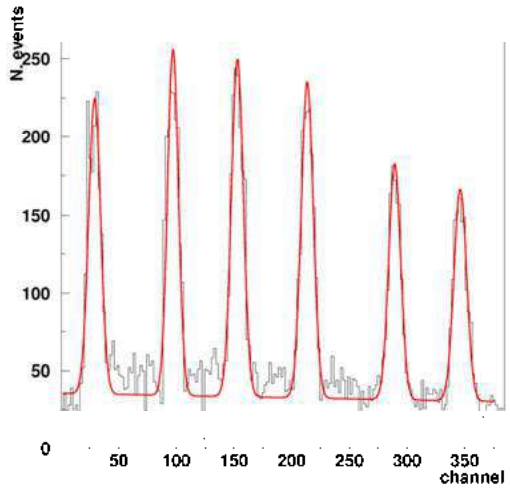

Figure 5. Plot obtained for the 600 ppm sample with the fit of the six columns

The activity of the columns is computed fitting the plot with six Gaussians and a linear function for the background.

To check the independence of the system from the solution, other measurements have been performed with a solution of 50 ppm (in columns of 100, 200 and 300 ppm) and the points are positioned on the calibration curves obtaining a measurement uncertainty lower than 10% as shown in figure 6. The minimum detected concentration of ^{10}B with the solution of boric acid is 5 ppm/cm^2.

Finally, measurements on biological samples have been performed: patients have been administered BPA and BSH and their urine has been taken at different times from the uptake. The samples have been irradiated and the neutron autoradiography has been obtained allowing to reconstruct the kinetic curve. The results have been compared with measurements of the same samples performed with a mass spectrometry system by the CNR of Milano. They are in good agreement (figures 7 and 8) and the feasibility of kinetic studies with this imaging system has been demonstrated.

Other biological samples (thanks to a collaboration with the S. Luigi hospital, Orbassano) have been used: a lung has been explanted, perfused with a solution of BPA and then frozen and cut in thin layers. The results from this set of measurements are not conclusive because of the low concentration of boron contained in the sample.

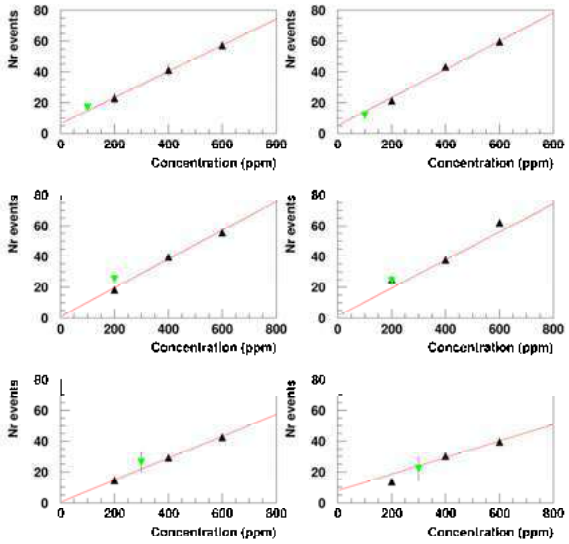

Figure 6. Comparison of the spots prepared with a 50 ppm solution with the calibration curves obtained with the 100 ppm solution; the six plots correspond to six different regions of the detector

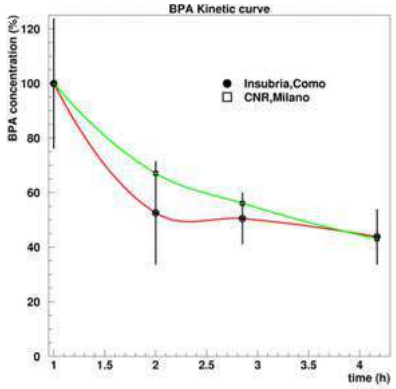

Figura 7. Comparison of the kinetic curve of BPA obtained with the silicon detector and with a mass spectrometry system

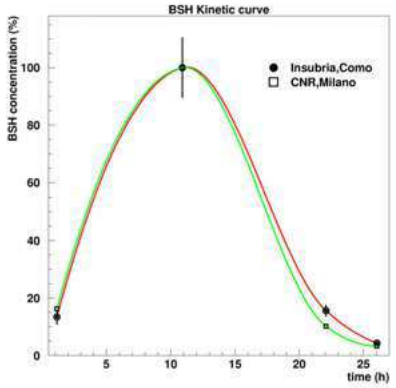

Figura 8. Comparison of the kinetic curve of BSH obtained with the silicon detector and with a mass spectrometry system

4. Conclusions

A real time boron imaging system has been characterized both in qualitative and quantitative terms. The system allows to obtain the measurement of the boron present in different types of samples in a few minutes using a hospital neutron source. The results are good: the system is able to detect the boron with a measurement uncertainty < 10% and a spatial resolution of 120 μm that can be increased to 50 μm using a silicon detector with strips having this width. The minimum detected amount of boron is 25 ng. Several improvements are foreseen: a vacuum system will allow not to position the sample on the detector (making the sample re-usable); a smaller version of the PhoNeS converter+moderator prototype is being designed to increase the neutron flux positioning the detector in the cavity; several other methods of sample preparation are being tested.

References

Bevilacqua, R., et al., 2007. PhoNeS: a novel approach to BNCT with conventional radiotherapy accelerators. Nucl. Instr. and Meth. in Phys. Res. A 572, 231-232.

Conti, V., et al., 2007. A time of flight detector for thermal neutrons from radiotherapy Linacs. Nucl. Instr. and Meth. in Phys. Res. A 581, 88-90, doi: 10.016/j.nima.2007.07.145.

Prest, M., et al., 2003. The AGILE silicon tracker: an innovative γ-ray instrument for space. Nucl. Instr. and Meth. in Phys. Res. A 501, 280-287.

Determination of boron in tissue using neutron-autoradiography and ICP-MS

Christian Schütz[1], Saverio Altieri[2], Silva Bortolussi[2], Vicent Carsí Caballer[1], Frieder Enzmann[3], Gabriele Hampel[1C], Shahin Minoushehr[4], Sven Nagels[5], Gerd Otto[4], Sabrina Stella[3]

[1]*Institut für Kernchemie, Johannes Gutenberg-Universität Mainz, Fritz-Strassmann-Weg 2, D-55128 Mainz, Germany*
[2]*Dipartimento di Fisica Nucleare e Teorica, Università degli Studi di Pavia, Via Bassi 6, 27100 Pavia (PV), Italy*
[3]*Institut für Geowissenschaften, Johannes Gutenberg-Universität Mainz, Becherweg 14, D-55128 Mainz, Germany*
[4]*Klinikum der Johannes Gutenberg-Universität Mainz, Abteilung für hepatobiliäre, pankreatische und Transplantationschirurgie, Langenbeckstr. 1, D- 55131 Mainz, Germany*
[5]*Forschungszentrum Karlsruhe GmbH, Hauptabteilung Sicherheit, Postfach 3640, D-76021, Karlsruhe, Germany*

Due to the encouraging results of the BNCT research on non-resectable liver metastases in Pavia, Italy, within the recent years, a close cooperation was formed between the University of Mainz, Germany, the Research Center Karlsruhe, Germany, and the University of Pavia. Expecting a clinical study of samples provided by 15 patients that suffer from liver-metastases of colorectal carcinoma, two methods for tissue analysis have been prepared. The boron concentration in the tissue is evaluated in Mainz by two different analytical methods: Neutron-autoradiography using CR-39 films and ICP-MS. CR-39 films overlaid with tissue slices which contain ^{10}B are irradiated at the TRIGA Mainz and the TRIGA Pavia and then analyzed.
The University of Mainz is equipped with a TRIGA Mark II reactor and a university hospital, which is an ideal situation for BNCT treatment in the way it was performed in Pavia, Italy, in 2001 and 2003.
In cooperation with the BNCT group in Pavia, a method for autoradiographical analysis of tissue samples was developed. Until now, neutron-autoradiography was mostly used for qualitative analysis. We will present a method for both qualitative and quantitative analysis that is based on graphical data only. This method consists of several algorithms designed especially for this purpose.
The samples are provided by the university hospital of the University of Mainz. After a BPA infusion, liver samples are taken from different positions and depths of the organ, then frozen in liquid nitrogen and cut to thin slices (10 – 40 µm).
The CR-39 films are irradiated in the thermal column of the reactor with a fluence of $\Phi = 3.15 \cdot 10^{11}$ n/cm² at a thermal reactor power of 1 kW. The films are then developed by placing them in NaOH (3 M) for different times between 60 and 120 minutes at 70 °C. Before doing so, they are cleaned in an ultra-sound bath for 10 minutes. Images of the films are taken with a light-microscope and then examined by means of several algorithms.
The algorithms were created using MATLAB as the program code and work fully automatically for quantitative analysis. The algorithms correct attributes like contrasts, exposure to light, particle borders etc. and then via segmentation render the tracks caused by the ionized radiation. Thus, the picture is converted into a matrix that is fit for further analysis.
Using the features of the program it is possible to determine the nature of the different tracks, the etching speed of the different tracks, their size, number and the area they cover. Hence it is possible to determine also the concentration the concentration.
The determination of the boron concentration is assisted by measurements with an ICP-MS (Agilent 7500). The tissue samples are digested and liquefied in a microwave oven and then prepared for the measurement by the ICP-MS.
We will present the neutron-autoradiography including the mathematical algorithms, the comparison measurements with ICP-MS and first results of the study.

T2 Corrected Quantification of L-*p*-Boronophenylalanine-Fructose Complex Using Proton MR Spectroscopy

Yamamoto Y[1], Isobe T[2], Shibata Y[1], Yamamoto T[1], Anno I[3]
Nakai K[1], Shirakawa M[1], Matsumura A[1]

[1] *Department of Neurosurgery, Institute of Clinical Medicine, Graduated School of Comprehensive Human Sciences, University of Tsukuba, 1-1-1 Tennodai, Tsukuba, 305-8575 Ibaraki, Japan*
[2] *Comprehensive Cancer Center, Institute of Clinical Medicine, Graduated School of Comprehensive Human Sciences, University of Tsukuba, 305-8575 Japan*
[3] *Department of Radiological Sciences, Ibaraki Prefectural University of Health Sciences, 4669-2 Ami, Ami-Machi, Inashiki-Gun, 300-0394 Japan*

Abstract

In this study, we aimed to establish T2 corrected quantification method of L-*p*-boronophenylalanine-fructose complex (BPA-F) concentration using proton magnetic resonance spectroscopy (MRS). The cylindrical water phantoms containing BPA-F, Choline (Cho), Creatine (Cr), N-acetyl-aspartic acid (NAA) were used for the experiments. We prepared BPA-F at the concentrations of 1.5, 3.0, 5.0, 7.5 and 10 mmol/kg. Also we made Cho, Cr and NAA at the concentration of 3.0, 5.0 and 3.0 mmol/kg respectively. The signal intensities of BPA-F and internal water were corrected by T2 relaxation time. The absolute concentrations of BPA-F were calculated by proton MRS using an internal water signal as a standard. The major BPA-F peaks were detected between 7.1 and 7.6 ppm. Mean T2 relaxation time was 314.3 ± 10.8 ms in BPA-F, 885.1 ± 39.7 ms in internal water. The calculated BPA-F concentrations were almost same as the actual concentration of BPA-F and the correlation coefficient was 0.99. Our BPA-F quantification method was very simple and non-invasive, also it had high accuracy. Therefore, our results indicate that proton MRS can be potentially useful technique for in vivo BPA-F quantification in boron neutron capture therapy (BNCT).

Keywords: L-p-Boronophenylalanine-Fructose Complex (BPA-F), Magnetic Resonance Spectroscopy (MRS), Quantification, T2 relaxation time

1. Introduction

Boron neutron capture therapy (BNCT) is a radiation therapy using α-ray and Li particles. The charged particles attack only tumor cells containing boron-10. Therefore, BNCT is a tumor-selective radiation therapy at the cellular level (Yamamoto et al., 2008). Quantitative information regarding local boron-10 concentrations is crucial to determining the optimal timing of the neutron irradiation and to calculating the radiation dose for the treatment planning. As a boron-10 carrier, L-*p*-boronophenylalanine-fructose complex (BPA-F) is widely used in clinical BNCT for malignant brain tumor and skin melanoma, as well as head and neck cancer. In the clinical case, BPA-F tumor uptake and systemic distribution were determined by the pharmacokinetic analysis of discontinuous venous blood samples. The concentrations of boron-10 in tumor-cells were estimated using empirical data models. Empirical data models depend on brain-to-blood, tumor-to-brain, and tumor-to-blood boron-10 concentration ratios. One of the problems is that the uptake and distribution of boron-10 varies among patients and that large uncertainties exist regarding the tumor-to-blood boron-10 concentration ratio. Recently, positron emission tomography (PET) has been used for determining boron-10 uptake and distribution in pretreatment rehearsal studies (Nicholas et al., 2002). In addition, PET examination with ^{18}F-labeled BPA-F can demonstrate boron-10 mapping in the brain. However, this rehearsal infusion is different from the BPA-F administration during actual treatment because PET examination requires only a low dose of ^{18}F-labeled BPA-F.

In addition, the synthesis of ^{18}F-labeled BPA-F is very complicated and limited. We have only two institutions that can synthesize ^{18}F-labeled BPA-F in Japan. Therefore, a new method enabling us to directly determine BPA-F concentration in vivo will improve the accuracy of BNCT. Proton magnetic resonance spectroscopy (MRS) is a noninvasive and

in vivo biochemical assay allowing us to determine and quantify brain metabolites (Isobe et al., 2002). According to previous studies (Zuo et al., 1999), the resonance signals of BPA-F can be detected by using proton MRS. In addition, it is possible to quantify BPA-F concentrations in a phantom. However, in these studies, the correction of relaxation time was insufficient. In the present study, we aimed to establish a T2 corrected quantification method for BPA-F concentrations using proton MRS.

2. Materials and Methods

2.1 Phantoms

We used five phantoms containing BPA-F, Choline (Cho), Creatine (Cr), and N-acetyl-aspartic acid (NAA). We prepared five phantoms containing BPA-F at five different concentrations (1.5, 3.0, 5.0, 7.5 and 10 mmol/kg), and Cho, Cr, and NAA at the same concentrations of 3.0, 5.0 and 3.0 mmol/kg, respectively. The inside of the phantom was filled with saline. Figure 1 shows the BPA-F phantoms that we made. The phantom consisted of a cylindrical acryl tray and a glass chamber.

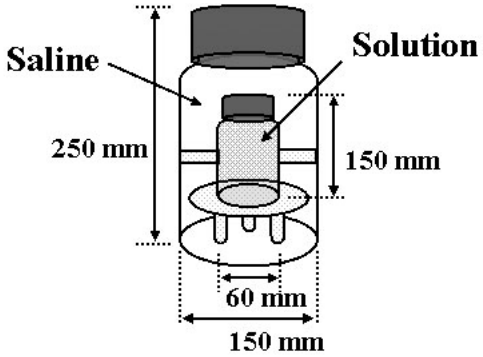

Fig. 1. The phantoms containing BPA-F

2.2 Proton MRS

Proton MRS was performed using a clinical 1.5-T superconducting magnetic resonance (MR) whole-body system (Gyroscan ACS-NT Intera; Philips Medical Systems, Amsterdam, Netherlands) equipped with a circularly polarized head coil.

Data were acquired by using a point-resolved spectroscopy (PRESS) sequence. The PRESS sequence used an asymmetrical timing scheme, as shown in Fig. 2. TE was calculated using the following equations, and the value for τ_1 was fixed at 6.89 ms:

$$TE = 2\tau_2 \qquad (1)$$

$$\tau_2 = \tau_1+\tau_3 \qquad (2)$$

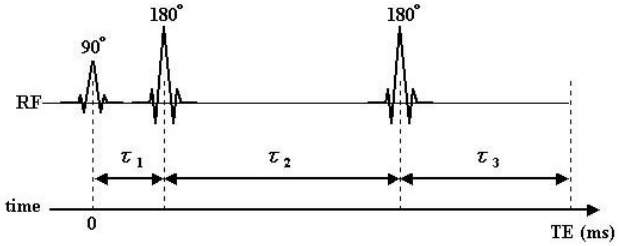

Fig. 2. The timing scheme of the PRESS sequence

The spectral width was 1000 Hz. The number of data points was 512. The number of signals averaged (NSA) 128 in BPA-F and 16 in internal water. Water suppression was performed using chemical-shift-selective (CHESS) pulses with a bandwidth of 60 Hz when measuring the BPA-F. When measuring the internal water, water suppression was not performed. The field homogeneity was optimized over the selected volume of interest (VOI) by observing the proton MR signal of the internal water with a spatially selective PRESS sequence and automatic shimming. The typical full width achieved at half maximum was 3 Hz for all measurements.

For locating the VOI, we carried out T2-weighted MR imaging in three orthogonal planes. The VOI of 20 x 20 x 20 mm^3 (8 ml) was placed in the center of the phantom in all measurements.

Spectral data processing included zero-filling (1024 data points), apodization (Gaussian filtering: 3 Hz, Exponential filtering: -1 Hz), Fourier transformation, and zero- and first-order phase corrections by means of standard Philips software (Philips Medical Systems, Amsterdam, Netherlands).

2.3 Measurements of T1 relaxation time

T1 relaxation times of BPA-F and internal water were determined with TR 900, 1000, 1200, 1500, 2000, 2500, 3000, 4000, 5000, 6000, 8000, and 10000 ms, TE 30 ms.

The corrections for the T1 relaxation were calculated using the following equation.

$$M_{S\_T1} = M_{\infty} \times \left\{1+\exp\left(\frac{-TR}{T1}\right)-2\times\exp\left[\frac{-(TR-\tau)}{T1}\right]\right\} \qquad (3)$$

M_{S_T1} is the signal intensity to a given TR, M_∞ is the signal intensity at TR = ∞, and τ is TE / 2.

2.4 Measurements of T2 relaxation time

The T2 relaxation times of BPA-F and internal water were determined with TR 2000 ms, TE 30, 230, and 490 ms.

The signal intensities of BPA-F and internal water were corrected by the T2 relaxation time using the following equation.

$$M_{S\_T2} = M_0 \times \exp\left(\frac{-2\tau}{T2}\right) \qquad (4)$$

M_{S_T2} is the signal intensity to a given TE, M_0 is the signal intensity at TR = 0, and τ is TE / 2.

2.5 Determination of BPA-F Concentration

The absolute concentrations of BPA-F were calculated by proton MRS using an internal water concentration of 100 % (55.56 mol/kg wet weight) as a standard.

The concentrations of BPA-F were calculated using the following equation.

$$C_{BPA-F} = C_{water} \times F_{cor} \times \left(\frac{S_{BPA-F}}{S_{water}}\right) \qquad (5)$$

$C_{BPA\text{-}F}$ is the concentration of BPA-F, C_{water} is the concentration of internal water, $S_{BPA\text{-}F}$ is the signal intensity of the BPA-F, and S_{water} is the signal intensity of internal water. $S_{BPA\text{-}F}$ and S_{water} were corrected for both T1 and T2 relaxation times. F_{cor} is the calculated correction factor

3. Result and Discussion

We have identified several characteristic resonances. The chemical shift of BPA-F in the phantom was corrected using the chemical shift of the Cho peak (3.22 ppm) as a standard. The major BPA-F peaks were detected between 7.1 and 7.6 ppm.

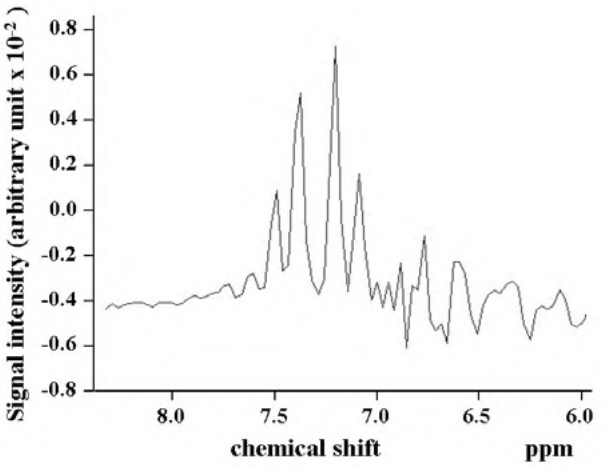

Fig. 3. The spectrum of BPA-F (10 mmol/kg) with TR 2000 ms, TE 30 ms. Several BPA-F peaks were observed. For quantification of BPA-F, we used the peaks of BPA-F between 7.1 and 7.6 ppm

Figure 3 shows the spectrum of BPA-F between 6 and 8 ppm. We considered that some big BPA-F peaks were well-suited to quantification of BPA-F, while others were essentially obscured by resonance signals from brain metabolites.

We measured the T1 and T2 relaxation times of BPA-F and internal water for corrections of signal intensity. The T1 relaxation time was 751 ms in BPA-F and 2855 ms in internal water. The T2 relaxation time was 314.3 ± 10.8 ms (mean ± standard deviation (SD)) in BPA-F and 885.1 ± 39.7 ms in internal water.

When the PRESS sequence was used, we experienced an inversion of the BPA-F peak at different TE as a result of J-coupling. We have previously discussed in detail the methods for calculating BPA-F concentrations and T2 relaxation times (Matsumura et al., 2005). We therefore calculated the T2 relaxation time using three different TEs, which were determined according to our previous examinations. As a result, the T2 relaxation time that we calculated was similar to the values obtained in previous studies (Heikkinen et al., 2003).

Figure 4 shows the relationship between calculated and actual concentrations of BPA-F in the phantom. The calculated BPA-F concentrations were almost the same as actual concentration, and the correlation coefficient was 0.99.

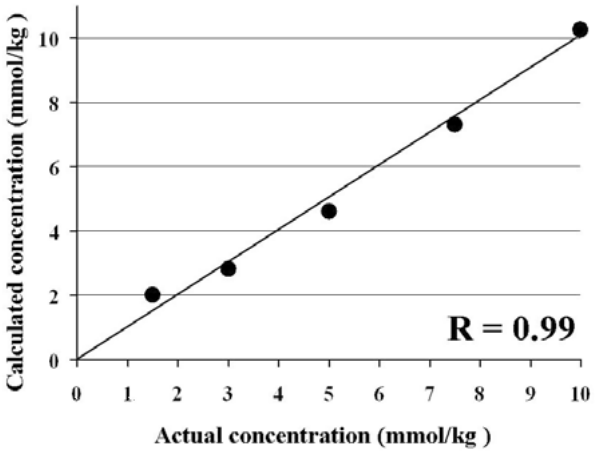

Fig. 4. The relationship between calculated and actual concentrations of BPA-F in the phantom

In our study, BPA-F concentrations were underestimated at 1 / 0.5114 times lower than actual concentrations. In other words, a signal loss occurred for BPA-F due to J-coupling and the PRESS sequence. When the PRESS sequence used an asymmetrical timing scheme, the resonance signals of metabolites with j-coupling were changed (Schick et al., 1995). Therefore, for proper quantification, we determined the correction factor (F_{cor}) in equation 5 considering these effects and the number of protons in BPA-F.

Our BPA-F quantification method is very simple and noninvasive, and its accuracy is very high. We therefore believe that this method may be applied to clinical cases utilizing BNCT.

In recent years, the analysis of proton MRS has been performed automatically using the LC Model (Provencher, 2001). The LC Model will clarify any arbitrariness in the analysis as well as shortening the analysis time. In addition, high magnetic field MR systems have a high signal-to-noise ratio. In the future, the quantification of BPA-F using proton MRS will be more accurate and useful with the utilization of high magnetic field MR systems and automatic analysis using the LC Model.

4. Conclusions

We were able to quantify the concentrations of BPA-F in a phantom using a 1.5-T clinical MR machine. Our results indicate that proton MRS is a potentially useful technique for in vivo BPA quantification in BNCT.

Acknowledgements

This study was supported in part by a Grant-in-Aid from the Ministry of Education, Science and Culture, Japan (20390379)

References

Yamamoto, T., Nakai, K., Matsumura, A., 2008. Boron neutron capture therapy for glioblastoma. Cancer Lett. 262 (2), 143-152.

Nichols, T, L., Kabalka, G, W., Miller, L, F., Khan, M, K., Smith, G, T., 2002. Improved treatment planning for boron neutron capture therapy for glioblastome multiforme using fluoline-18 labeled boronophenylalanine and positron emission tomography. Med. Phys. 29, 2351-2358.

Isobe, T., Matsumura, A., Anno, I., Yoshizawa, T., Nagatomo, Y., Itai, Y., Nose, T., 2002. Quantification of cerebral metabolites in glioma patients with proton MR spectroscopy using T2 relaxation time correction. Magn. Reson. Imaging. 20, 343-349.

Zuo, C, S., Prasad, P, V., Busse, P., Tang, L., Zamenhof, R, G., 1999. Proton nuclear magnetic resonance measurement of p-boronophenylalanine (BPA): a therapeutic agent for boron neutron capture therapy. Med. Phys. 26 (7), 1230-6.

Matsumura, A., Isobe, T., Takano, S., Kawamura, H., Anno, I., 2005. Non-invasive quantification of lactate by proton MR spectroscopy and its clinical applications. Clin. Neurol. Neurosurg. 107 (5), 379-84.

Heikkinen, S., Kangasmäki, A., Timonen, M., Kankaanranta, L., Häkkinen, A, M., Lundbom, N., Vähätalo, J., Savolainen, S., 2003. 1H MRS of a boron neutron capture therapy 10B-carrier, L-p-boronophenylalanine-fructose complex, BPA-F: phantom studies at 1.5 and 3.0 T. Phys. Med. Biol. 48, 1027-1039.

Schick, F., Nägela, T., Klose, U., Lutz, O., 1995. Lactate quantification by means of press spectroscopy-influence of refocusing pulses and timing scheme. Magn. Reson. Imaging. 13, 309-19.

Provencher, S, W., 2001. Automatic quantitation of localized in vivo 1H spectra with LCModel. NMR. Biomed. 14(4), 260-264.

Boron concentration measurement in lung tissue by charged particles spectrometry

S. Altieri[1,2], S. Bortolussi[1,2], S. Stella[1,2], M. Gadan[1], N. Protti[1] , A. De Bari[1,2] and P. Bruschi[1]

[1]*Department of Nuclear and Theoretical Physics, Pavia University, Italy*
[2]*National Institute for Nuclear Physics, INFN, Section of Pavia, Italy*

The measurement of the boron concentration in tissues is one of the fundamental aspects of Boron Neutron Capture Therapy. This work describes a method based on the spectroscopy of the charged particles emitted in the reaction $^{10}B(n,\alpha)^{7}Li$ induced by thermal neutrons. Thin slices of tissue containing ^{10}B are cut at low temperatures, deposited on mylar supports and irradiated under vacuum in a thermal neutron field. The charged particles emitted by the sample are collected by a silicon detector and their spectrum is analyzed. The mass stopping power of the irradiated tissue is used to calculate the mass of the sample from which the charged particles originated. In this way the boron concentration can be determined by relatively easy calculations. In this paper the potentiality and the limits of this technique are described and an example of an application to the measurement of the boron concentration in rat lung tissues is presented.

BIOLOGY

Biodistribution and Imaging studies on F98 rat glioma by convection enhanced delivery of transferrin targeting PEG liposomes encapsulating both BSH and iodine contrast agent

Shiro Miyata[a], Shinji Kawabata[a], Naosuke Nonoguchi[a], Kunio Yokoyama[a], Atsushi Doi[a], Yuzo Kuroda[a], Naokado Ikeda[a], Taro Yamashita[a], Kyoko Iida[a], Toshihiko Kuroiwa[a], Satoshi Kasaoka[b], Hiroyuki Yoshikawa[b], Shin-Ichi Miyatake[a]

[a]*Department of Neurosurgery, Osaka Medical College, 2-7 Daigaku-machi, Takatsuki City, Osaka, 569-8686, Japan*
[b]*Faculty of Pharmaceutical Sciences, Hiroshima International University, 5-1-1, Hirokoshingai, Kure City, Hiroshima, 737-0112, Japan*

Abstract

Introduction: In the last ICNCT we reported the effectiveness of transferrin (TF) targeting PEG liposome encapsulates BSH [TF-PEG liposome {BSH}], with regard to its ability to target tumor cells and to accumulate more boron atoms in tumor tissue. However, systemic administration of these compounds has some problems, including unexpected boron distribution to other organs, limited accumulation by blood brain barrier, infiltrative nature of gliomas, and so on. To solve these problems, in the present study we adopted convection enhanced delivery (CED) as the way of drug administration. Furthermore we developed a novel liposomal boron delivery drug which encapsulates not only BSH but also iodine contrast agent (Iomeprol), so that it has become possible to trace the distribution of these drugs by clinical imaging. We evaluated two boron carieers, PEG liposome encapsulates both BSH and Iomeprol [PEG liposome {Iomeprol, BSH}] and TF-PEG liposome {Iomeprol, BSH} administered by CED as a boron delivery system into the rat brain tumor model. **Methods**: We prepared F98 brain tumor bearing rats and administered each boron carieer, PEG liposome {Iomeprol, BSH} and TF-PEG liposome {Iomeprol, BSH} by CED over 30 min at a rate of 0.33 μl/min. In the definite time after CED, we performed computed tomography (CT) scan to evaluate the distribution of these drugs and euthanized them. And then we evaluated the boron concentration of tumor, normal brain and blood by inductively coupled plasma-atomic emission spectrometry (ICP-AES). **Results**: The difference of tumor boron concentration between PEG liposome {Iomeprol, BSH} and TF-PEG liposome {Iomeprol, BSH} showed the largest at 24 h after CED, and the values at that time were 22.5 $\mu g^{10}B/g$ in PEG liposome {Iomeprol, BSH} and 82.2 $\mu g^{10}B/g$ in TF-PEG liposome {Iomeprol, BSH}. **Conclusions**: We showed the effectiveness of TF-PEG liposome {Iomeprol, BSH}. Especially the combination of CED and TF-PEG liposome {Iomeprol, BSH} enables a precise targeting on the tumor tissue and following the trace of the drugs by clinical CT imaging.

Keywords: transferrin, convection enhanced delivery (CED), liposome, iodine contrast agent, F98 glioma

1. Introduction

Nowadays, some therapeutic modalities such as stereotactic radiosurgery, Intensity Modulated Radiation Therapy (IMRT) and heavy particle therapy have been developed, so that today even malignant brain tumors have become curable for some patients. However, for a few decades, there has been little improvement in the prognosis for patients with malignant gliomas because of their nature of intensive invasion toward the surrounding normal tissue. Surgical resection and following fractionated external beam radiation therapy are now selected as the standard therapy against these tumors.

To overcome this infiltrative nature, in just the infiltrative region, it is necessary to accumulate high concentration of mediators such as anticancer drugs or dose enhancement drugs into tumor tissue, keeping high contrast against the surrounding normal tissue.

We have so far focused on, studied and developed BNCT which can achieve 'tumor selectivity'.

In the last meeting of the ICNCT we reported the effectiveness of transferrin (TF) targeting PEG liposome encapsulates BSH [TF-PEG liposome {BSH}], with regard to its ability to target tumor cells and to accumulate more boron atoms in tumor tissue (Doi et al., 2008). However, systemic administration of these compounds has some problems, including unexpected boron distribution to other organs, limited accumulation due to blood brain barrier (Vogelbaum, 2005), infiltrative nature of gliomas, and so on. To solve these problems, in the present study we adopted convection enhanced delivery (CED) as the way of drug administration (Bobo et al., 1994).

Furthermore we developed a novel liposomal boron carieer which encapsulates not only BSH but also iodine contrast agent (Iomeprol; Iomeron, Eizai, Japan), so that it has become possible to trace the distribution of drugs by clinical imaging (Rousseau et al., 2007). We evaluated two boron carieers, PEG liposome encapsulates both BSH and Iomeprol [PEG liposome {Iomeprol, BSH}] and TF-PEG liposome {Iomeprol, BSH} administered by CED into rat brain tumor model.

2. Materials and Methods

2-1. Boron compounds

BSH was purchased from Katchem, Ltd. (Czecho). Iomeprol (Iomeron, Eizai, Japan) was used as iodine contrast agent. PEG-liposome {Iomeprol, BSH} and TF-PEG liposome {Iomeprol, BSH} were provided by one of us. (Maruyama et al., 2004).

2-2. Cell line and brain tumor models

F98 rat glioma cell line, provided by Rolf F. Barth M.D. (Ohio State Univ., Colombus, OH, USA), was maintained in Dulbecco's Modified Eagle Medium (DMEM) with 10 % fetal bovine serum (FBS) with penicillin and streptomycin at 37 ^{o}C in an atmosphere of 5 % CO_2. All materials for culture medium were purchased from Invitrogen Corporation (Carlsbad, CA, USA).

Male Fischer 344 rats (200-230 g) were anesthetized with intraperitoneal injection of pentobarbital sodium (50 mg/kg) and placed in a stereotactic frame. A midline incision was made in the scalp, and the skull target (3.5 mm right to bregma) was identified. A hand-held drill was used to create a small burr hole at this location.

The Hamilton infusion syringe (model 1700 RN) was secured in the clamping device of the stereotactic frame. The associated needle was first inserted to a depth of 6.0 mm from the skull and then withdrawn to its target depth in the brain (5.5 mm from the skull surface). Ten thousand F98 cells diluted in 10 µl of DMEM were then injected over approximately 10 min. The needle was maintained in place for 1 min after infusion and withdrawn slowly. The skull hole was sealed with bone wax, and the scalp was sutured. Under these conditions, the procedure results in 100 % tumor uptake and a median survival time of 23 days.

2-3. Boron concentration study

In vitro assay

For in vitro boron uptake studies, F98 glioma cells were used. One million F98 glioma cells were seeded onto the 100 mm culture dish with culture medium (see above). After incubation for 24 h at 37 ^{o}C, the medium was replaced with DMEM containing 10 µg^{10}B/ml PEG liposome {Iomeprol, BSH} or TF-PEG liposome {Iomeprol, BSH}, and the cells were incubated for an additional 6 h at 37 ^{o}C. Following this, the medium was removed, the cells were washed twice with phosphate buffered saline (PBS), and digested with trypsin. After digestion, medium was added, the cells were counted and sedimented. Cells were overnight dissolved with nitric acid at room temperature and boron uptake was determined by inductively coupled plasma-atomic emission spectrometry (ICP-AES).

In vivo assay

Ten days after tumor implantation, F98 brain tumor bearing rats were generally anesthetized and placed in a stereotactic frame as previously described. They were administered each boron carieer, PEG liposome {Iomeprol, BSH} and TF-PEG liposome {Iomeprol, BSH} by CED over 30 min at a rate of 0.33 µl/min. Total amount of boron administered to each rat was 20 µg^{10}B. In the selected time (0 h, 24 h, 48 h and 72 h) after CED, rats were performed computed tomography (CT) scan to evaluate the distribution of these drugs and euthanized. And then we evaluated the boron concentration of tumor, normal brain and blood by ICP-AES.

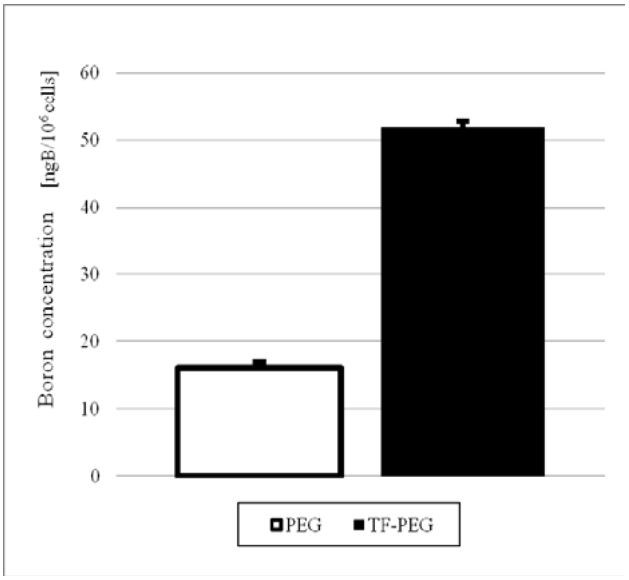

Fig. 1. Boron concentration of F98 glioma cells, 6 hours after incubation under media including 10 μg^{10}B/ml of each boron carieer

3. Results and Discussions

3-1. *in vitro* assay

The boron concentration of F98 glioma cells 6 h after exposure to each boron carieer, PEG liposome {Iomeprol, BSH} and TF-PEG liposome {Iomeprol, BSH} was 16.1 and 51.9 ng^{10}B/10^6 cells, respectively. (Fig. 1) In our laboratory there are data about in vitro boron uptake studies on C6 rat glioma cells and U87Δ human glioma cells. PEG liposome {BSH} and TF-PEG liposome {BSH} were used as boron carieers in both studies. The results showed that in both cells, boron concentration of the cells was significantly higher in TF-PEG liposome {BSH} group than in PEG liposome {BSH} group. Moreover, in boron retention studies, boron concentration of the cells kept higher in TF-PEG liposome {BSH} group until at least 12 h after removal of boron carieer and changing medium.

3-2. *in vivo* assay

Biodistribution data for PEG liposome {Iomeprol, BSH} and TF-PEG liposome {Iomeprol, BSH} after CED administration to F98 brain tumor bearing rats are summarized in Table I. The boron concentration of tumor was higher in TF-PEG liposome {Iomeprol, BSH} group than in PEG liposome {Iomeprol, BSH} group at every time point. (Fig. 2) Especially at 24 h after CED, in TF-PEG liposome {Iomeprol, BSH} group, both the mean tumor boron concentration (82.2 μg^{10}B/g) and tumor to normal brain ratio (274) were the largest of all the time points.

On the other hand, the boron concentrations of blood and contralateral normal brain were less than 1.0 μg^{10}B/g. Wu et al. reported that the amount of boron retained by F98$_{EGFR}$ gliomas 24 h after CED administration of boronated cetuximab (BD-C225) was 77.2 μg^{10}B/g, with normal brain and blood boron values < 0.5 μg^{10}B/g.

Table I. Biodistribution data for PEG liposome {BSH, Iomeprol} and TF-PEG liposome {BSH, Iomeprol} after CED administration to F98 brain tumor bearing rats

Boron carieer	Time (hours)[a]	Boron concentration (μg^{10}B/g)				Tumor to Brain ratios	
		Tumor	Brain (ipsi.)[b]	Brain (contra.)[c]	Blood	Ipsi.	Contra.
PEG liposome {Iomeprol, BSH}	0[d]	28.5±13.2	0.6±0.6	0.3±0.1	0.4±0.2	47.5	95
	24	22.5±6.1	1.7±1.5	1.0±0.6	0.4±0.1	13.2	22.5
	48	8.5±7.9	1.5±0.7	0.4±0.3	0.4±0.1	5.7	21.3
	72	4.9±4.6	0.2±0.1	0.2±0.1	0.5±0.2	24.5	24.5
TF-PEG liposome {Iomeprol, BSH}	0[d]	64.1±28.1	2.1±2.5	0.4±0.2	0.6±0.3	30.5	160
	24	82.2±18.6	0.7±0.4	0.3±0.2	0.6±0.1	117	274
	48	41.2±14.4	1.2±1.0	0.9±0.6	0.9±0.1	34.3	45.8
	72	25.8±13.5	0.4±0.2	0.4±0.2	0.6±0.2	64.5	64.5

[a] hours after CED administration of each boron carieer
[b] ipsilateral normal brain
[c] contralateral normal brain
[d]The time point of 0 means the point just after sacrifice.
Each point represents the mean±SD

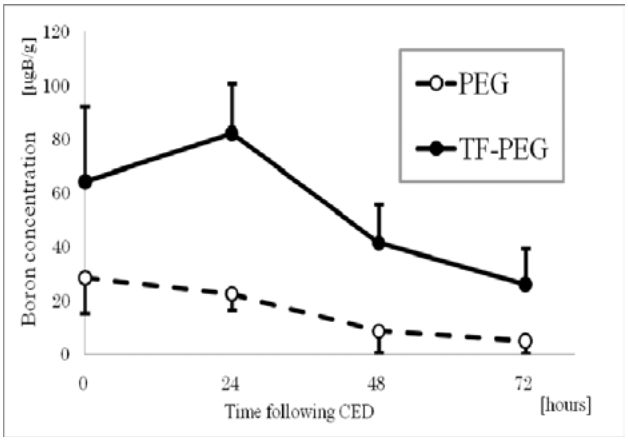

Fig. 2. Boron concentration of the tumor in the selected time after CED administration of each boron carieer, PEG liposome {BSH, Iomeprol} and TF-PEG liposome {BSH, Iomeprol}

They also showed that the mean absorbed dose delivered to $F98_{EGFR}$ tumors and contralateral normal brain was 27.5 Gy and < 1.9 Gy after CED of BD-C225 (Wu at al., 2007), respectively. In the present study, neutron irradiation was not carried out, but on the basis of their data, it is estimated that the absorbed dose might be achieved as the same level as theirs.

3-3. Imaging assay

Boron distribution can be estimated by CT scan because of synchronizing with Iomeprol. The usefulness of imaging by CT scan has been confirmed. We now attempt to obtain the excellent image of contrast enhanced brain tumor. It is theoretically possible to estimate the boron concentration in any tissue on CT image by using Hounsfield Unit.

4. Conclusions

We showed the effectiveness of TF-PEG liposome {Iomeprol, BSH} as a liposomal boron carieer for BNCT. Especially the combination of CED and TF-PEG liposome {Iomeprol, BSH} enables a precise targeting on the tumor tissue and following the trace of the drugs in clinical CT imaging.

Acknowledgements

This work was supported by Grants-in-Aid for Scientific Research for young researchers (B) (18791030 to S.K. and 20791022 to N.I.), by Grants-in-Aid for Scientific Research (C) (20591728 to S.K.), and by Grants-in-Aid for Scientific Research (B) (19390385 to S-I.M.) from the Japanese Ministry of Education, Science and Culture and by the Eisai Science Foundation to S.K.. We thank Kaori Kuroda for technical assistance.

References

Bobo, R.H., Laske, D.W., Akbasak, A., Morrison, P.F., Dedrick, R.L., Oldfield, E.H., 1994. Convection-enhanced delivery of macromolecules in the brain. Proc. Natl. Acad. Sci. USA. 91, 2076-2080.

Doi, A., Kawabata, S., Iida, K., Yokoyama, K., Kajimoto, Y., Kuroiwa, T., Shirakawa, T., Kirihata, M., Kasaoka, S., Maruyama, K., Kumada, H., Sakurai, Y., Masunaga, S., Ono, K., Miyatake, S., 2008. Tumor-specific targeting of sodium borocaptate (BSH) to malignant glioma by transferrin-PEG liposomes: a modality for boron neutron capture therapy. J. Neurooncol. 87(3), 287-94.

Maruyama, K., Ishida, O., Kasaoka, S., Takizawa, T., Utoguchi, N., Shinohara, A., Chiba, M., Kobayashi, H., Eriguchi, M., Yanagie, H., 2004. Intracellular targeting of sodium mercapto-undecahydrododecaborate (BSH) to solid tumors by transferrin-PEG liposomes, for boron neutron-capture therapy (BNCT). J. Control Release. 98, 195-207.

Rousseau, J., Boudou, C., Esteve, F., Elleaume, H., 2007. Convection-enhanced delivery of an iodine tracer into rat brain for synchrotron stereotactic radiotherapy. Int. J. Radiation Oncology Biol. Phys. 68, 943-951.

Vogelbaum, M., 2005. Convection enhanced delivery for the treatment of malignant gliomas: symposium review. Journal of Neuro-Oncology. 73, 57-69.

Wu, G., Yang, W., Barth, R.F., Kawabata, S., Swindall, M., Bandyopadhyaya, A.K., Tjarks, W., Khorsandi, B., Blue, T.E., Ferketich, A.K., Yang, M., Christoforidis, G.A., Sferra, T.J., Binns, P.J., Riley, K.J., Ciesielski, M.J., Fenstermaker, R.A., 2007. Molecular targeting and treatment of an epidermal growth factor receptor-positive glioma using boronated cetuximab. Clin. Cancer. Res. 13(4), 1260-1268.

Do the Various Radiations Present in BNCT Act Synergistically? Cell Survival Experiments in Mixed Alpha-Particle and Gamma-Ray Fields

Ben Phoenix[1], Andrew J. Mill[1], David L. Stevens[2], Mark A.Hill[2,] Bleddyn Jones[3], Stuart Green[3]

[1] *Department of Physics and Astronomy, University of Birmingham, UK*; [2]*Radiation Oncology and Biology, University of Oxford, UK*; [3] *University Hospital Birmingham, UK*.

Abstract

A novel irradiation setup has been created at the Medical Research Council in Harwell which allows simultaneous irradiation of cells by cobalt-60 gamma-rays and plutonium-238 alpha-particles. The setup allows for variation of dose and dose rates for both sources along with variation of the alpha-particle energy. Cell survival measurements have been carried out for mixed alpha-particle and gamma-ray fields using V79-4 cells and compared with the results from exposures to the individual components under identical conditions. Doses for the two components were chosen to be approximately equally effective, *i.e.* 0.5, 1.0, 1.5 and 2.0 Gy of alpha-particles and 3.5, 5.4, 7.1 and 8.6 Gy of gamma rays, producing respectively surviving fractions of 0.4, 0.15, 0.08 and 0.03. Following irradiation cells were left for 2 hours at 37°C to allow for cellular repair before processing.

The survival curve obtained for the mixed field exposures was found to be only slightly different from that obtained by addition of the individual surviving fractions; the survival curve parameters fitted to the linear-quadratic model being $\alpha = (0.423 \pm 0.038)$ Gy^{-1}, $\beta = (0.0242 \pm 0.0047)$ Gy^{-2} for the mixed fields and $\alpha = (0.407 \pm 0.078)$ Gy^{-1}, $\beta = (0.0224 \pm 0.0095)$ Gy^{-2} for the addition of the individual components.

Thus it appears that there are no significant synergistic effects of combined alpha-particles and gamma-rays under the conditions of these experiments.

1. Introduction

BNCT involves a whole range of radiation qualities from high-LET (α-particles and ^{7}Li recoil nuclei) to low-LET γ-rays. RBE or compound, cRBE factors have been determined, albeit with large uncertainties, for the individual components (Coderre and Morris 1999). However, these take no account of any possible synergy between the different components which could result in a greater biological effect than would be the case for independent action of the different radiation types present. The possibility of such synergistic interactions has important implications for treatment planning in BNCT and in other mixed field therapies. It would also complicate the interpretation of clinical results particularly when comparing data from different BNCT facilities having different mixes of high and low-LET components.

There have been a number of publications reporting the effects of mixed radiation fields. Unfortunately, the evidence is not clear, with many authors reporting synergism and others no effect. In some cases experimenters have used sequential irradiations, e.g. neutrons followed by X-rays, while in just a few cases have experimenters used truly simultaneous irradiations as would be the case in BNCT. There appears to be significant evidence that the effects of combined neutrons and X- or γ-rays are synergistic (McNally *et al*. 1984, 1985; Higgins *et al*. 1983, 1984; Ngo *et al*. 1977; Railton *et al*. 1975) for cell killing *in vitro* and for effects *in vivo* (Joiner *et al*. 1984) whether given simultaneously or sequentially. However the evidence for mixed fields involving α-particles is equivocal with only a few reports in the literature (Barendsen *et al*. 1960; Bird *et al*. 1983; McNally *et al*. 1988) and for experimental conditions which are not directly comparable with each other.

The experiments described here have been carried

out in order to clarify the question of synergism between α-particles and low-LET radiation. A novel irradiation setup has been used to simultaneously irradiate V79-4 Chinese hamster cells *in vitro* with ^{60}Co γ-rays and ^{238}Pu α-particles. The setup allows for variation of dose and dose rates for both sources as well as variation of the α-particle energy. The endpoint measured in these investigations was loss of reproductive integrity (cell survival).

2. Materials and methods

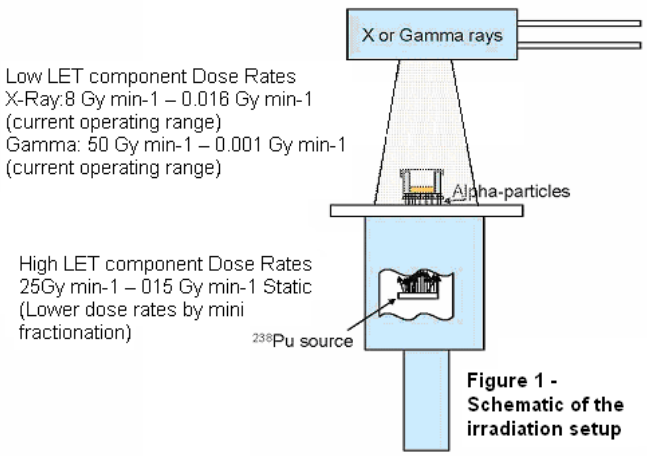

Figure 1 - Schematic of the irradiation setup

The ^{238}Pu α-particle source has been previously described (Goodhead *et al*. 1991). The setup used allowed irradiation from below with 3.2 MeV (LET: ~120 keV μm^{-1}) α-particles and from above with ^{60}Co γ-rays (see Figure 1). The dose-rates were adjusted so that the irradiation times for both sources were identical, the longest exposure (the highest dose) lasting about 10 minutes. The irradiations were carried out at a temperature of 10°C. The dose rate of the γ-ray source was measured prior to each set of irradiations. The required build-up depth for the ^{60}Co γ-rays was ensured by adding additional medium (to a total of 4 cm^3) to the Hostaphan dishes onto which cells were plated giving a total depth of medium above the cells of 5 mm.

In order to allow penetration of the α-particles from below, cells were plated onto thin-based (2.5 μm thick polyethylene terephthalate) Hostaphan dishes two days prior to irradiation with two dishes used per dose point. Cells were in log-phase growth at the time of exposure. All dose points were handled in triplets; γ-ray only, corresponding α-particle only and mixed γ-ray and α-particle. The corresponding doses were chosen to give as near as possible identical surviving fractions when processed immediately. These were 3.4, 5.4 7.1 and 8.6 Gy for ^{60}Co γ-rays and 0.5, 1.0, 1.5 and 2.0 Gy for ^{238}Pu α-particles. The experiments were carried out over a five-week period involving several repeat measurements; between 3 and 5 determinations per dose-point. The order in which the irradiations were carried out during the day was varied between weeks as was the order within 'triplets'. The plating efficiencies of the controls were >97% throughout the experiments.

Post irradiation, cells were maintained at 37 °C in an atmosphere of 5% CO_2 in air for two hours to allow for cellular repair before processing. Plating densities were estimated to give 150 colonies per Petri dish with five dishes per dose point. Post plating, the dishes were incubated at 37 °C in an atmosphere of 5 % CO_2 with each 'triplet' under identical conditions. After seven days dishes were fixed with methanol and stained with methylene blue. Colonies, containing more than 50 non-giant cells, were counted by eye and surviving fractions calculated.

3. Results

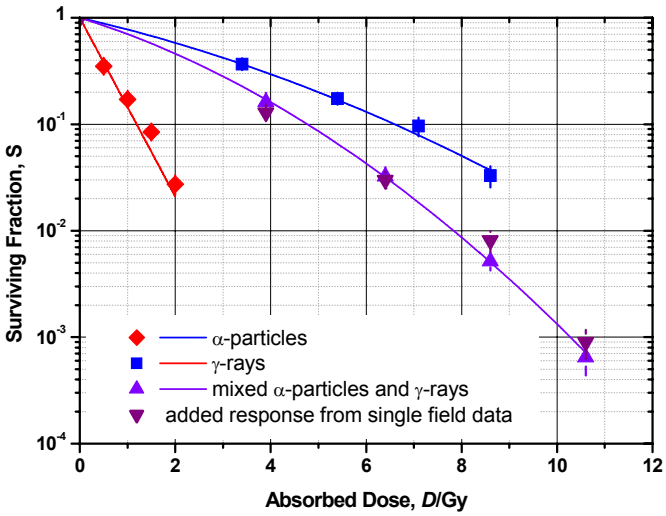

Figure 2. V79 survival curves for irradiation with ^{60}Co γ-rays, ^{238}Pu α-particles and mixed irradiations

Survival curves for single and mixed field irradiations are shown in Figure 2. Surviving fractions have been fitted to the linear-quadratic model:

$$S = \exp(-\alpha D - \beta D^2)$$

where S is surviving fraction and D is the absorbed dose. The solid lines in Figure 2 are the fitted curves.

Values obtained for the survival curve parameters, α and β are given in Table I. A comparison of measured and calculated surviving fractions for mixed field irradiations are shown in Table II.

Table I - Calculated survival curve parameters for the relationship, $S = \exp(-\alpha D - \beta D^2)$ for the survival curves given in Figure 1.

Radiation Regime	α /Gy^{-1}	β / Gy^{-2}
^{60}Co γ-rays	0.237 ± 0.017	0.0170 ± 0.0040
^{238}Pu α-particles	1.933 ± 0.039	-
Mixed γ-rays and α-particles	0.319 ± 0.043	0.0344 ± 0.0055)*

*Fit may not be meaningful since the ratio of α-particle to γ-ray dose changes slightly through the dose range

Table II - Comparison of mixed ^{60}Co γ-rays and ^{238}Pu α-particles surviving fractions.

Dose, *D* /Gy	Measured	Calculated from Single Field Data	Calculated from Survival Curve Parameters
3.9	0.161 ± 0.024	0.129 ± 004	0.140
6.4	0.0324± 0.0029	0.0300± 0.050	0.0245
8.6	(5.16± 0.65) x 10^{-3}	(8.11± 1.76)) x 10^{-3}	4.33 x 10^{-3}
10.6	(6.49± 2.12) x 10^{-4}	(8.99± 2.74) x 10^{-4}	7.74 x 10^{-4}

4. Discussion and Conclusions

Under the experimental conditions described above no significant synergy between the two radiation qualities is observed. This is at variance with previously reported mixed field data involving neutrons and suggests that the interaction which leads to a synergistic, dose enhancement, effect in a combined neutron and low-LET field is not present or possible in a mixed field where the high-LET component is due to α-particles. One possible explanation is that while neutrons do induce sub-lethal damage this is not necessarily the case for α-particles. Thus, for mixed neutron and X- or γ-ray fields the synergism that is involved may be due to the interaction of sub-lethal damage, while such an interaction may not be possible with mixed fields involving α-particles. To some extent this hypothesis is supported by data from Furusawa *et al*. (2002) who find no synergism between irradiation with heavy ions (LET range 86 keV μm^{-1} to 442 keV μm^{-1}) and X-rays.

BNCT as a synergistic interaction between the low-LET field and the boron capture products (α-particles and ^{7}Li recoil nuclei) would lead to complications in treatment planning.

It is important to expand on these data using different mixes of the high- and low-LET components to determine how general these findings are. For example, the data of McNally *et al*. (1988) suggest that synergy may be more prominent for higher α-particle doses in conjunction with large X-ray to α-particle dose ratios. In the experiments described here the doses of α-particles and γ-rays were chosen on the basis of having an approximate equivalent effect on cell survival. MCNP calculations for treatment depths of several centimetres suggest that at a concentration of 15 ppm of ^{10}B (the typical level for healthy tissue in BNCT), the absorbed dose contribution by the low-LET component is approximately equal to the absorbed dose from α-particles. While at a typical tumour concentration of 52.5 ppm of ^{10}B, α-particles are responsible for approximately 75% of the absorbed dose. Currently, further experiments are being developed using doses of α-particles and X-rays which closely match these proportions. Results from this work will also be presented.

References

Barendsen, G. W., Beusker, T. L. J., Vergroesen, A. J. and Budke, L. (1960) Effects of Different Ionizing Radiations on Human Cells in Tissue Culture, *Radiation Research*, **13**, 841-849.

Bird, R. P., Zaider, M., Rossi, H. H., Hall, E. J., Marino, S. A., and Rohrig, N. (1983) The Sequential Irradiation of Mammalian Cells with X Rays and Charged Particles of High LET. *Radiation Research*, **93**, 444-452.

Coderre, J. A. and Morris, G. M. (1999) The radiation biology of boron neutron capture therapy, *Radiation Research*, **151**, 1 - 18.

Furusawa l, Y. Aoki M. and Durante, M. (2002) Simultaneous Exposure of Mammalian Cells To Heavy Ions and X-rays, *Advanced Space Research*, **30**, 877-884.

Goodhead, D. T., Bance, D. A., Stretch A. and Wilkinson, R. E. (1991) A Versatile Plutonium-238 Irradiator for Radiobiological Studies with α-particles, *International Journal of Radiation Biology*, **59**, 195 – 210.

Higgins, P. D., Deluca, P. M., JR., Pearson, D. W. and Gould, M. N. (1983) V79 Survival following Simultaneous or Sequential Irradiation by 15-MeV Neutrons and ^{60}Co Photons, *Radiation Research* **95**, 45-56.

Higgins, P. D., Deluca, P. M., JR. and Gould, M. N. (1984) Effect of Pulsed Dose in Simultaneous and Sequential Irradiation of V-79 Cells by 14.8-MeV Neutrons and ^{60}Co Photons, *Radiation Research* **99**, 591-595.

Joiner, M. C., Bremner, J. C., Denekamp, J. and Maughan, R.L. (1984) The Interaction between X-rays and 3 MeV Neutrons in the Skin of the Mouse Foot, *International Journal of Radiation Biology*, **46**, 625 – 638.

McNally, N. J., de Ronde, J. and Folkard, M. (1988) Interaction between X-ray and α-particle Damage in V79 Cells, *International Journal of Radiation Biology*, **53**, 917 – 920.

McNally, N. J., de Ronde, J. and Hinchliffe, M. (1984) The Effect of Sequential Irradiation with X-ray s and Fast Neutrons on the Survival of V79 Chinese Hamster Cells, *International Journal of Radiation Biology*, **45**, 301 – 310.

McNally, N. J., De Ronde, J. and Hinchliffe, M. (1985) Survival of V79 Cells Following Simultaneous Irradiation with X-rays and Neutrons in Air or Hypoxia, *International Journal of Radiation Biology*, **48**, 847 -855.

Ngo, F. Q. H., Han, A. and Elkind, M. M. (1977) On the Repair of Sub-lethal Damage in V79 Chinese Hamster Cells Resulting from Irradiation with Fast Neutrons or Fast Neutrons Combined with X-rays, *International Journal of Radiation Biology*, **32**, 507 – 511.

Railton, R., Lawson, R. C. and Porter, D. (1975) Interaction of γ-ray and Neutron Effects on the Proliferative Capacity of Chinese Hamster Cells, *International Journal of Radiation Biology*, **27**, 75 – 82.

Molecular targeting of the epidermal growth factor receptor for boron neutron capture therapy of EGFR positive gliomas

W. Yang[1], R.F. Barth[1], G. Wu[1], W. Tjarks[2], P. Binns[3] and K. Riley[3]

[1]*Departments of Pathology and*
[2]*College of Pharmacy, The Ohio State University, Columbus, Ohio 43210*
[3]*Nuclear Reactor Laboratory and Department of Nuclear Engineering, Massachusetts Institute of Technology, Cambridge, Massachusetts 02215, USA*

Abstract

In the present report we have summarized studies carried out over the past 5 years on molecular targeting of the epidermal growth factor receptor (EGFR) and its mutant isoform, EFGRvIII, for BNCT of the F98 rat glioma. EGF or the monoclonal antibodies (mAbs), cetuximab (IMC-C225) and L8A4, which recognize wild-type EGFR and EGFRvIII, respectively, were heavily boronated using PAMAM dendrimers (BD) linked to the targeting vehicles by means of heterobifunctional reagents. Boronated EGF or mAbs were administered intracerebrally (i.c.) by either intratumoral (i.t.) injection or convection enhanced delivery (CED), either alone or in combination with i.v. BPA, following which BNCT was initiated. The best survival data were obtained in rats bearing $F98_{EGFRvIII}$ gliomas that had received CED of BD-L8A4 either alone or in combination with i.v. BPA. Studies carried out in rats bearing composite tumors demonstrated that it was essential to target both receptors in order to obtain an optimal therapeutic effect. Based on these observations, we have concluded that EGFR targeting vehicles are useful, but not stand-alone boron delivery agents due to the heterogeneity of EGFR expression in brain tumors. However, they could be quite useful in combination with BPA and BSH.

Keywords: Molecular targeting, epidermal growth factor receptor, monoclonal antibodies, IMC-C225 and L8A4

1. Introduction

The gene encoding the epidermal growth factor receptor (EGFR) and its mutant isoform, EGFRvIII, frequently are overexpressed in malignant gliomas, and both are low or undetectable in normal brain (Mendelesohn et al., 2006). We have been interested in using either boronated EGF (Barth et al., 2002) or anti-EGFR mAbs (Yang, et al., 2006; Wu, et al., 2007) as delivery agents for BNCT. Initially, we developed a method for the site-specific linkage of a heavily boronated PAMAM or "starburst" dendrimers (BD) to either EGF or mAbs (Wu, et al., 2004). Following i.t. injection, the bioconjugate delivered greater than 15 μg B/g of tumor to rats bearing EGFR-expressing F98 gliomas (Barth et al., 2002; Yang et al., 2006). In order to improve i.c. administration, we employed CED. This is an innovative technique for local delivery of therapeutic agents to brain tumors by applying a pressure gradient (bulk flow) to drive an infusate through the extracellular fluid compartment. This results in delivery to larger areas of brain and tumor at higher concentrations than otherwise would be attainable by i.t. injection (Yang et al., 2002). In the present report, we will summarize our studies on molecular targeting of EGFR using BD-EGF and BD-mAbs, administered by CED, for BNCT of the $F98_{EGFR}$ and $F98_{EGFRvIII}$ gliomas.

2. Materials and Methods

2.1. Preparation of boronated conjugates

EGF or the mAbs, cetuximab (C225) and L8A4, which recognize wildtype EGFR and EGFRvIII, respectively, were boronated with a methylisocyanato polyhedral borane anion ($Na(CH_3)_3NB_{10}H_8NCO$), using a procedure described in detail by us (Wu et al., 2004).

2.2 F98 Glioma model and biodistribution studies

The $F98_{EGFR}$ and $F98_{EGFRvIII}$ glioma models were produced by transfecting the parental F98 glioma with the human genes encoding either wildtype EGFR or EGFRvIII (Yang, et al. 2002 and 2006). One hundred thousand $F98_{EGFRvIII}$ or $F98_{EGFR}$ glioma cells were implanted stereotactically into the caudate nucleus of CD-Fischer rats, as described in

detail elsewhere (Barth et al., 2002). Twelve to 14 d later, biodistribution studies were carried out in rats bearing either $F98_{EGFRvIII}$ or $F98_{EGFR}$ gliomas. Animals received ^{125}I-labeled BD-EGF, BD-L8A4 or BD-C225 either by i.t. injection or CED and were euthanized at 6 and 24 hours following administration. Biodistribution of the bioconjugates was determined by means of γ-scintillation counting (Yang et al., 2002) and boron concentrations were determined by means of direct current plasma-atomic emission spectroscopy (DCP-AES).

2.3. Therapy experiments and dosimetry

Fourteen days following stereotactic implantation of 10^3 F98 glioma cells, BNCT was performed at the Nuclear Reactor Laboratory, Massachusetts Institute of Technology (MIT), Cambridge, MA. Rats were randomized on the basis of weight into experimental groups of 8-11 animals each as shown in Table 2. BNCT was initiated 24 h after i.c. CED of 10 μL of the bioconjugate (40 μg of ^{10}B per animal) and 2.5 h after i.v. administration of BPA (500 mg/kg b.w.).

Dosimetric measurements and BNCT were carried out at the MITR-II reactor in the M011 irradiation facility, as previously described in detail (Barth et al., 2002, Yang, et al., 2006). For dosimetric calculations, boron concentrations were determined in a separate group of animals by DCP-AES in tumor, normal brain and blood 24 h after CED of BD-L8A4 or BD-C225 and 2.5 h after i.v. injection of BPA. Animal irradiations were performed with the reactor operating at a power between 4.0 and 4.8 MW. These took between 6.9 and 8.6 min to deliver a thermal neutron fluence of 2.64 x 10^{12} n.cm^{-2} to complement previous dose prescriptions. After completion of BNCT, the animals were returned to The Ohio State University in Columbus, OH for clinical monitoring.

3. Results

3.1 Tissue boron concentrations and dosimetry

Boron concentrations in tumor, brain and blood following CED of the bioconjugates, are summarized in Table 1. Tumor boron values ranged from 22.3-77.2 μg/g following CED of the bioconjugates alone and 32.7-87.9 μg/g in combination with i.v. BPA. The highest value was obtained with BD-C225. Normal brain values ranged from 2.4 to 5.1 g/g and the corresponding blood values were undetectable (<0.5 μg/g).

Table 1. Boron concentrations and physical radiation doses delivered to tumor, brain and blood

		Boron Concentrations (μg/g)[a]			Absorbed dose (Gy)[b]		
Delivery Agent	Tumor Type	Tumor	Brain	Blood	Tumor	Brain	Blood
CED BD-EGF	$F98_{EGFR}$	22.3±4.3	3.1±1.5	<0.5	6.6	2.6	1.9
i.t. BD-EGF	$F98_{EGFR}$	11.7±1.6	2.9±1.0	<0.5	4.4	2.6	1.9
CED BD-EGF + i.v. BPA	$F98_{EGFR}$	36.2±6.9	5.1±1.5	5.5±3.2	10.0	3.1	1.9
CED BD-C225	$F98_{EGFR}$	77.2±14.8	<0.5	<0.5	19.5	1.9	1.9
i.t. BD-C225	$F98_{EGFR}$	50.8±5.7	<0.5	<0.5	13.4	1.9	1.9
CED BD-C225 + i.v. BPA	$F98_{EGFR}$	87.9±16.5	4.3±1.5	5.7±1.3	21.9	2.7	3.1
CED BD-L8A4	$F98_{EGFRvIII}$	32.7±3.6	<0.5	<0.5	9.2	1.9	1.9
CED BD-L8A4 + i.v. BPA	$F98_{EGFRvIII}$	44.5±11.1	4.2±0.5	5.2±1.3	12.0	2.7	2.7
CED BD-C225 +BD-L8A4	$F98_{EGFR}$ +$F98_{EGFRvIII}$	24.4±3.6	2.4±1.7	<0.5	7.3	2.5	1.9
i.v. BPA	F98	10.7±1.7	3.8±1.1	5.2±1.3	4.2	2.6	2.9
Irradiation controls [c]	F98	None	None	None	1.9	1.9	1.9
Untreated controls [d]	F98	9.2±1.3	<0.5	<0.5	0	0	0

[a] Boron concentrations in the tumor bearing cerebral hemisphere.

[b] Physical dose estimates include contributions from γ photons, ^{14}N (n, p)^{14}C and ^{10}B (n,α) ^{7}Li reactions.

[c] These animals were given the vehicle alone, followed by neutron irradiation.

[d] These animals only received the bioconjugate without neutron irradiation.

Based on these total boron concentrations, the calculated mean absorbed physical doses delivered to the tumors ranged from 6.6 to 19.5 Gy following CED of the bioconjugate alone, and 10.0 to 21.9 Gy in combination with i.v. BPA, compared to 4.2 Gy following i.v. BPA alone (Table 1).

3.2 Therapeutic response of glioma bearing rats following BNCT

The survival data following BNCT are summarized in Table 2. The MSTs of rats bearing $F98_{EGFR}$ gliomas that had received BD-EGF or BD-C225 by i.t injection were equivalent (43±3 d), compared to 54±15 d following CED without i.v. BPA and 71±11 d with it ($p<0.005$).Untreated or irradiated control animals had MSTs of 25±3 d and 31±4 d, respectively, compared to 40±5 d for rats that had received i.v. BPA. The best survival data were obtained in rats bearing $F98_{EGFRvIII}$ gliomas that had received CED of BD-L8A4 either alone or in combination with i.v. BPA (70±11 d and 86±16 d, respectively). Rats bearing composite tumors consisting of a 1:1 mixture of $F98_{EGFR}$ and $F98_{EGFRvIII}$ glioma cells, and which received both mAbs, had a MST of 55±5 d compared with 36±1 d for BD-L8A4 and 38±2 d for BD-C225 alone ($p<0.0001$). The latter were not significantly different from irradiated controls (34±1 d).

These results indicated that it was essential to target *both* receptors in order to obtain an optimal therapeutic effect (Yang et al., 2008).

4. Discussion and Conclusions

In the present study, we have shown that CED of the boronated bioconjugates, BD-EGF, BD-C225 and BD-L8A4 in combination with i.v. administration of BPA, produced a doubling in MST compared to that of irradiated control animals and a ~1.5X increase in MST compared to that of rats that received either i.v. BPA or the boronated bioconjugates alone. The increased MSTs of animals that received the boronated bioconjugates by CED, either alone or in combination with i.v. BPA, were associated with a widening of the range (40-180 d) in contrast to the narrow range in survival times that was seen in all other groups. This broadening of the range probably was the result of non-homogenous distribution of ^{10}B within the tumor. Improving the delivery of BPA and sodium borocaptate (BSH), by means of intracarotid injection and blood-brain barrier disruption, had a significant impact on enhancing survival (Barth et al., 1997). Intracarotid administration of BPA and BSH could have a similar effect on enhancing the efficacy of these bioconjugates.

Table 2. Survival times following BNCT and CED of bioconjugate with or without BPA

Delivery Agent	N[a]	Tumor Type	Survival Times (days)			% Increased Life Span[b]	
			Range	Mean±SE	Median	Mean	Median
CED BD-EGF	11	$F98_{EGFR}$	40-92	54±15	50	116	100
i.t. BD-EGF	11	$F98_{EGFR}$	34-64	43±9	42	72	68
CED BD-EGF + i.v. BPA	10	$F98_{EGFR}$	44-180(1)[c]	69±38	55	176	120
CED BD-C225	11	$F98_{EGFR}$	39-88	55±4	50	107	92
i.t. BD-C225	9	$F98_{EGFR}$	33-58	43±3	41	62	58
CED BD-C225 + i.v. BPA	11	$F98_{EGFR}$	42-180 (1)	71±11	58	170	123
CED BD-L8A4	11	$F98_{EGFRvIII}$	41-180(1)	70±11	58	168	123
CED BD-L8A4 + i.v. BPA	10	$F98_{EGFRvIII}$	42-180 (2)	86±16	65.5	225	152
CED BD-C225 +BD-L8A4	10	$F98_{EGFR}$ +$F98_{EGFRvIII}$	37-87	55±5	51	97	89
i.v. BPA	10	F98	33-48	40±5	40	60	60
Irradiation controls	10	F98	24-37	31±4	32	24	28
Untreated controls [d]	8	F98	20-29	25±3	25	-	-

[a] N designates the number of animals per group.
[b] Percentage of increased lifespan was defined relative to mean and median survival times of untreated controls.
[c] The numbers in parentheses were the number of rats surviving 180 days.
[d] Although there were small differences in the MSTs of $F98_{WT}$, $F98_{EGFR}$ and $F98_{npEGFRvIII}$, these were not statistically significant.

One of the most important challenges facing both basic and clinical researchers is how to achieve a more uniform microdistribution of ^{10}B within the tumor and how to reduce both subject-to-subject variations in boron uptake. BD-EGF has a molecular weight of ~35 kD compared to ~205 kD for the bioconjugates. Although its lower molecular weight would improve its diffusion within the tumor following CED, BD-EGF only would target those tumor cells that express wildtype EGFR and not EGFRvIII. On the other hand, most EGFR positive gliomas variably express these receptors and there are significant numbers of receptor negative cells. Our studies have shown that in order to effectively treat composite tumors, it is necessary to target both EGFR and EGFRvIII expressing cells. Since human GBMs also have substantial numbers of EGFR(-) cells, it also would be necessary to use either BPA alone or in combination with BSH to target receptor (-) cells.

How then might boronated mAbs be used for molecular targeting of EGFR for BNCT of brain tumors? One very important advantage of BNCT is its ability to selectively deliver high linear energy transfer radiation to the level of individual cancer cells in the same radiation field. In contrast, photon irradiation is a physically, rather than biologically, targeted therapeutic modality, and tumor and normal cells in the field of radiation would receive an equal dose. Therefore, one could envision using BNCT in combination with photon irradiation to deliver an added radiation dose to the tumor with little additional dose delivered to the normal brain.

Acknowledgments

The studies described in this report were funded in part by grants from the U.S. Department of Energy and the National Institutes of Health. We would like to thank all of our other collaborators, who have been involved in these studies. Special thanks are due to Laura Martz for expert secretarial assistance in the preparation of this manuscript.

References

Barth, R.F., Yang, W., Rotaru, J.H.,Moeschberger, M.L., Joel, D.D., Nawrocky, M.M., Goodman, J.H., Soloway, A.H., 1997. Boron neutron capture therapy of brain tumors: enhanced survival following intracarotid injection of either sodium borocaptate or boronophenylalanine with or without with or without blood-brain barrier disruption. Cancer Res. 57, 1129-1136.

Barth, R.F., Yang, W., Adams, D.M., Rotaru, J.H., Shukla, S., Sekdio, M., Tjarks, W., Fenstermaker, R.A., Ciesielski, M., Naworcky, M.M., Coderre, J.A., 2002. Molecular targeting of the epidermal growth factor receptor for neutron capture therapy of gliomas. Cancer Res. 62, 3159-3166.

Mendelesohn J., Baselga J., 2006. Epidermal growth factor receptor targeting in cancer. Semin. Oncol. 33, 369-385.

Wu, G., Barth, R.F., Yang, W., Ciesielski, M.J., Fenstermaker, R.A., 2004. Site-specific conjugation of boron-containing dendrimers to anti-EGF receptor monoclonal antibody cetuximab (IMC-C225) and its evaluation as a potential delivery agent for neutron capture therapy. Bioconjug. Chem. 15, 185-194.

Wu, G., Yang, W., Barth, R.F., Kawabata, S., Swindall, M., Bandyopadhyaya, A.K., Tjarks, W., Khorsandi, B., Blue, T.E., Ferketich, A.K., Yang, M., Christoforidis, G.A., Sferra, T.J., Binns, P.J., Riley, K.J., Ciesielski, M.J., Fenstermaker, R.A., 2007. Molecular targeting and treatment of an epidermal growth factor receptor-positive glioma using boronated cetuximab. Clin. Cancer Res. 13, 1260-1268.

Yang, W., Barth, R.F., Adams, D.M., Ciesielski, M.J., Fenstermaker, R.A., Shukla, S., Tjarks, W., Caligirui, M.A., 2002. Convection enhanced delivery of boronated epidermal growth factor for molecular targeting of EGF receptor-positive gliomas. Cancer Res. 62, 6552-6558.

Yang, W., Barth, R.F., Wu, G., *et al.*, 2006. Molecular targeting and treatment of EGFRvIII-positive gliomas using boronated monoclonal antibody L8A4. Clin. Cancer Res. 12, 3792-3802.

Yang, W., Gong, W., Barth, R.F., *et al.*, 2008. Molecular targeting and treatment of composite EGFR and EGFRvIII-positive gliomas using boronated monoclonal antibodies. Clin. Cancer Res. 14, 883-891.

Boron Neutron Capture Therapy (BNCT) Inhibits Tumor Development from Field-Cancerized Tissue: An Experimental Study that Supports a New Application of BNCT

Andrea Monti Hughes[a], Verónica A. Trivillin[a], Elisa M. Heber[a], Emiliano Pozzi[b], David W. Nigg[c], Osvaldo Calzetta[d], Herman Blaumann[d], Juan Longhino[d], Susana I. Nievas[e], Romina F. Aromando[f], Maria E. Itoiz[a,f], Amanda E. Schwint[a]

[a] *Department of Radiobiology, National Atomic Energy Commission (CNEA), Buenos Aires, Argentina*
[b] *Department of Research and Production Reactors, Ezeiza Atomic Center, CNEA, Buenos Aires, Argentina*
[c] *Idaho National Laboratory, Idaho Falls, Idaho, USA*
[d] *Department of Nuclear Engineering, Bariloche Atomic Center, CNEA, Rio Negro, Argentina*
[e] *Department of Chemistry, CNEA, Buenos Aires, Argentina*
[f] *Department of Oral Pathology, Faculty of Dentistry, University of Buenos Aires, Buenos Aires, Argentina*

Abstract

We previously demonstrated the efficacy of BNCT mediated by boronophenlyalanine (BPA), GB-10 ($Na_2{}^{10}B_{10}H_{10}$) and (GB-10 + BPA) to control tumors, with no normal tissue radiotoxicity, in the hamster cheek pouch oral cancer model. Herein we developed a new field-cancerization model in the hamster cheek pouch to explore the long-term potential inhibitory effect of the same BNCT protocols on the development of second primary tumors from field-cancerized tissue. Clinically, second primary tumor recurrences occur in field-cancerized tissue, causing therapeutic failure.

We performed boron biodistribution studies followed by *in vivo* BNCT studies, with 8-months follow-up. All 3 BNCT protocols induced a statistically significant reduction in tumor development from field-cancerized tissue, reaching a maximum inhibition of 77-100%. The inhibitory effect of BPA-BNCT and (GB-10 + BPA)-BNCT persisted at 51% at the end of follow-up (8 months), whereas for GB-10-BNCT it faded after 2 months. Likewise, beam-only elicited a significant but transient reduction in tumor development. No normal tissue radiotoxicity was observed. At 8 months post-treatment with BPA-BNCT or (GB-10 + BPA)-BNCT, the field-cancerized pouches that did not develop tumors had regained the macroscopic and histological appearance of normal (non-cancerized) pouches.

A potential new clinical application of BNCT would lie in its capacity to inhibit local regional recurrences.

Keywords: BNCT, oral cancer, field-cancerization, hamster cheek pouch, locoregional recurrences

1. Introduction

We previously evidenced a remarkable therapeutic success of BNCT mediated by BPA, GB-10 or (GB-10 + BPA) to treat hamster cheek pouch tumors with no normal tissue radiotoxicity (1, 2, 3). Despite the success of the BNCT protocols employed in these studies to treat tumors, a still unresolved challenge lies in controlling field-cancerized tissue. Second primary tumor locoregional recurrences that arise in field-cancerized tissue are a frequent cause of therapeutic failure (4). Within this context, the hamster cheek pouch oral cancer model poses a unique advantage in that tumors are induced by periodic, topical application of the carcinogen dimethyl-1,2-benzanthracene (DMBA), a process that mimics the spontaneous process of malignant transformation. Carcinogenesis protocols lead to the development of what has been termed globally "premalignant tissue" which gives rise to the formation of tumors. Thus, this mode of tumor induction provides a tumor model surrounded by premalignant tissue, allowing for the study of the phenomenon of field-cancerization (5, 6). In the present study we developed a model of field-cancerization in the hamster cheek pouch that allows for long-term studies and mimics field-cancerization in humans. Having developed the model of field-cancerized tissue tailored for long-term follow-up, the central aim of the present study was to evaluate the

potential inhibitory effect of BNCT mediated by BPA, GB-10 or (GB-10 + BPA) on the development of second primary tumors from hamster cheek pouch field-cancerized tissue, employing the same protocols that proved highly successful in controlling hamster cheek pouch tumors with no normal tissue radiotoxicity in previous studies (1, 3). The clinical rationale of this study was to search for a BNCT protocol that is therapeutic for tumor, not radiotoxic for the normal tissue that lies in the neutron beam path, and exerts the desired therapeutic effect on field-cancerized tissue, in terms of inhibition of the development of second primary tumors, without exceeding its radiotolerance.

2. Materials and Methods

Field-cancerization model: Initial studies evaluated the adequacy of different carcinogenesis protocols in the hamster cheek pouch to yield a model of field-cancerization amenable to long-term studies and that would guarantee tumor development in ≥80% of the animals. We treated 85 animals with the selected protocol, i.e. topical application of 0.5% DMBA in mineral oil in the right cheek pouch, twice a week for 6 weeks, and then assigned them to the different groups for boron biodistribution studies and *in vivo* BNCT studies.

Boron biodistribution studies: We employed the boron compounds and the administration protocols that were proved therapeutically effective in previous tumor control studies (7, 8, 3) (6 animals/group): 1) BPA (15.5 mg B/kg) ip, sacrifice at 3 h; 2) GB-10 (50 mg B/kg) iv, sacrifice at 3 h; 3) Combined administration of BPA (31 mg B/kg) as fractionated ip injections; GB-10 (34.5 mg B/kg) iv, sacrifice 3 h post-administration of GB-10 and 1.5 h after the last ip injection of BPA. Blood and tissue (premalignant pouch tissue, normal pouch tissue, liver and kidney) samples were processed for ICP-OES boron measurements.

In vivo BNCT: The hamsters were transported by plane to Bariloche, a city 1600 km south-west of Buenos Aires, to be irradiated with the thermalized epithermal beam at the RA-6 Reactor. There were a total of 67 cancerized hamsters. Thirty-three animals were divided up into 4 experimental groups, i.e. **BPA-BNCT** (n=8), **GB-10-BNCT** (n=9), **(GB-10 + BPA)-BNCT** (n=9) and **beam-only** (n=7). The remaining 34 cancerized hamsters were sham irradiated and served as controls. An additional group of 40 normal (non-cancerized) hamsters were transported to perform BNCT studies aimed at evaluating normal pouch tissue response. Thus, groups of 10 normal hamsters were treated with each of the four experimental protocols, i.e. BPA-BNCT, GB-10-BNCT, (GB-10+BPA)-BNCT and beam-only. In all the cases, the everted pouch and, inevitably, part of the head were placed at the beam port, which is 15 cm in diameter. The rest of the body was shielded by the lead and borated polyethylene of the beam delimiter. The average flux of thermal neutrons at the position of the pouch was $3.4 \pm 0.3 \times 10^8$ neutrons / (cm^2 s). Table 1 presents the total physical absorbed doses and irradiation times for each experimental protocol.

	Beam-only	GB-10-BNCT	(GB-10+BPA)-BNCT	BPA-BNCT
Irrad. time	75 min.	75 min.	35 min.	55 min.
Premalig. tissue	4.2±0.1	7.2±1.8	4.4±1.5	4.3±1.8
Normal tissue	4.2±0.1	7.6±1.0	4.7±1.7	4.5±2.8

Table 1: Total Physical Absorbed Doses (Gy) (mean ± SD)

Follow-up: Premalignant tissue response and potential tumor development from premalignant tissue were assessed weekly by visual inspection and tumor volume assay (when pertinent) for 8 months after treatment with the 4 different experimental protocols. Likewise, normal pouch tissue response was assessed in the normal (non-cancerized) hamsters treated with each of the 4 experimental protocols. Controls (cancerized hamsters submitted to sham-irradiation) were followed in the same way. The clinical signs and body weight of the animals were monitored regularly. At different time-points, 1-2 animals per protocol that had already developed second primary tumors were killed humanely for histological analysis of tumor, premalignant pouch tissue and normal pouch tissue.

The quantitative end-points that were evaluated were the accumulated percentage of animals that developed second primary tumors from premalignant tissue, % inhibition induced by the different treatment protocols referred to tumor development from sham-irradiated field-cancerized tissue, volume of tumors that did eventually develop from field-cancerized tissue and T50 (the time to appearance of tumors in 50% of the hamsters).

When pertinent, statistical analysis of the data was performed employing the Repeated Measures ANOVA experimental design. At selected, representative time-points the different treatment groups and the control group were compared employing a Chi-square test with Yates' correction. Statistical significance was set at $p \leq 0.05$.

3. Results

Boron Biodistribution Studies: Table 2 presents the most relevant boron content absolute values and ratios for each of the boron compound administration protocols. In all the cases, absolute boron uptake in premalignant tissue fell within a therapeutically useful range. The boron content ratio premalignant tissue / normal pouch tissue revealed no preferential uptake by premalignant tissue.

	GB-10	GB-10 +BPA	BPA
Premalig. tissue	24.4 ± 9.7 (n=23)	45.1 ± 15.3 (n=24)	19.7 ± 9.4 (n=23)
Normal tissue	27.6 ± 17.8 (n=6)	49.8 ± 20.4 (n=6)	21.9 ± 10.9 (n=6)
Blood	18.1±7.3 (n=6)	24.2±11.1 (n=8)	4.8±2.4 (n=6)
Premalig.tissue / Normal tissue	0.9/1	0.9/1	0.9/1

Table 2: Boron concentration (ppm) (mean ± SD)

In vivo BNCT

Evaluation of radiotoxicity: None of the cancerized or normal (non-cancerized) animals treated with any of the experimental protocols exhibited clinical signs of radiotoxicity throughout the follow-up period. In some cases, the premalignant pouch tissue treated with the BNCT protocols exhibited early, slight and reversible mucositis that resolved by the third week post-treatment. The normal pouches treated with the experimental protocols were indistinguishable from untreated normal pouches on visual inspection and on histological analysis until the last time-point evaluated.

Tumor development from precancerous tissue: Fig. 1 shows the accumulated percentage of animals that developed second primary tumors from field-cancerized tissue at representative time-points for each of the treatment protocols and controls. The development of second primary tumors from field-cancerized tissue in controls (cancerized, sham-irradiated animals) represents the kinetics of tumor development in the model of field-cancerization developed herein. At 2 weeks post-treatment the beam-only, BPA-BNCT and (GB-10 + BPA)-BNCT protocols exerted a reduction in tumor development vs. controls. However, this difference did not reach statistical significance. At 1 month and 2 months post-treatment all 4 treatment groups exhibited significantly lower values than controls (p=0.001 and p=0.03 respectively). At 4, 6 and 8 months post-treatment, the values corresponding to BPA-BNCT and (GB-10 + BPA)-BNCT were similar in both groups and significantly lower than controls (p<0.05, p=0.015 & p=0.002 respectively).

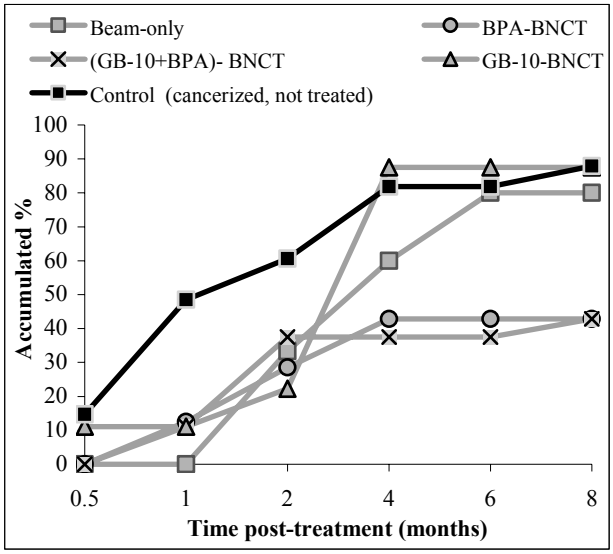

Fig. 1. Accumulated % of animals that developed second primary tumors

At these time-points, the GB-10-BNCT and beam-only groups no longer differed from controls (p>0.05). Based on these data, we calculated the percentage inhibitory effect of the different treatment protocols on the development of second primary tumors from field-cancerized tissue at representative time-points, referred to tumor development in the control group (Table 3). All 3 BNCT protocols induced an inhibitory effect on tumor development from field-cancerized tissue, reaching a maximum 77-100% inhibition. The inhibitory effect of BPA-BNCT and (GB-10 + BPA)-BNCT persisted at 51% at the last time-point evaluated (8 months). The inhibitory effect of GB-10-BNCT disappeared after 2 months. Similarly to GB-10-BNCT, beam-only exerted a transient inhibitory effect that faded after 2 months.

The values of T50 further supported the inhibitory effect observed for all 4 experimental protocols, in particular for BPA-BNCT and (GB-10 + BPA)-BNCT, i.e. Control: 4-5 weeks; GB-10-BNCT: 9-10 weeks; Beam-only: 11 weeks; BPA-BNCT: not reached within the follow-up period of 32 weeks; (GB-10 + BPA)-BNCT: not reached within the follow-up period of 32 weeks.

At 8 months post-treatment with BPA-BNCT or (GB-10+BPA)-BNCT, the field-cancerized pouches that did not develop tumors had regained the macroscopic and histological appearance of normal (non-cancerized) pouches (Fig. 2).

Time post-treatment (months)	Beam-only	GB-10-BNCT	(GB-10 + BPA) -BNCT	BPA-BNCT
0.5	100 %	26 %	100 %	100 %
1	100 %	77 %	77 %	73 %
2	46 %	64 %	38 %	52 %
4	27 %	0 %	54 %	48 %
6	2 %	0 %	54 %	48 %
8	9 %	0 %	51 %	51 %

Table 3: Percentage inhibitory effect

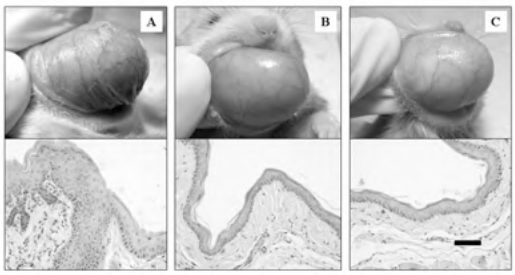

Fig. 2: (A) Control (not treated) field-cancerized pouch; (B) field-cancerized pouch 7 months post-BPA-BNCT; (C) normal pouch (non cancerized, not treated). Below, in each case, we show the corresponding characteristic light microscopy images (40X, H&E). Bar: 70μm

4. Discussion and Conclusions

All the BNCT protocols employed herein exerted a marked, statistically significant effect on the development of second primary tumors from field-cancerized tissue with no normal tissue radiotoxicity. The inhibitory effect of GB-10-BNCT lasted for approximately 2 months, whereas in the case of BPA-BNCT and (GB-10 + BPA)-BNCT a 51% inhibition persisted at the last time-point evaluated (8 months post-treatment).

The differential effect of BNCT on premalignant tissue and normal tissue cannot be attributed to preferential boron uptake by premalignant tissue and might be due to one or more of the following effects: differences in CBE values, preferential microlocalization of BPA in premalignant foci at a higher risk of malignant transformation and vascular targeting of GB-10-BNCT that would impair the process of angiogenesis associated to tumor microenvironment development. The effect of GB-10-BNCT would fade similarly to the effect of beam-only. The overall more conserved structure and function of premalignant tissue blood vessels compared to tumor blood vessels would reduce the CBE value for GB-10 in premalignant tissue, compared to its known efficacy in tumor (3).

Overall, the inhibitory effect on field-cancerized tissue could be due to the cellular and/or vascular targeting of foci of precancerous change more liable to malignant transformation (9), to the effect on the tissue microenvironment (10) or both.

The present study provides, for the first time, evidence that BNCT induces a long-term marked inhibitory effect on tumor development from field-cancerized tissue, with no normal tissue radiotoxicity and without exceeding field-cancerized tissue radiotolerance. Furthermore, we showed that BNCT is capable of reverting at least the histological hallmarks of premalignancy. Thus, the BNCT protocols that were previously proved effective to control established tumors would also inhibit locoregional recurrences caused by the development of tumors in field-cancerized tissue, suggesting a novel application of BNCT.

Acknowledgements

This work was partially supported by DOE through Idaho National Laboratory.

References

1)Kreimann E.L., Itoiz M.E., Longhino J., Blaumann H., Calzetta O., Schwint A.E., 2001b. Boron neutron capture therapy for the treatment of oral cancer in the hamster cheek pouch model. Cancer Res. (Advances in Brief) 61, 8638-8642.

2)Trivillin V.A., Heber E.M., Itoiz M.E., Nigg D., Calzetta O., Blaumann H., Longhino J., Schwint A.E., 2004. Radiobiology of BNCT mediated by GB-10 and GB-10 + BPA in experimental oral cancer. Appl. Radiat. Isot. 61, 939-945.

3)Trivillin V.A., Heber E.M., Nigg D.W., Itoiz M.E., Calzetta O., Blaumann H., Longhino J., Schwint A.E., 2006. Therapeutic success of Boron Neutron Capture Therapy (BNCT) mediated by a chemically non-selective boron agent in an experimental model of oral cancer: A new paradigm in BNCT radiobiology. Radiat. Res. 166, 387-396.

4)Smith B.D. and Haffty B.G., 1999. Molecular markers as prognostic factors for local recurrence and radioresistance in head and neck squamous cell carcinoma. Radiat. Oncol. Investig. 7(3), 125-144.

5)Schwint A.E., Savino T.M., Lanfranchi H.E., Marschoff E., Cabrini R.L., Itoiz M.E., 1994. Nucleolar organizer regions in lining epithelium adjacent to squamous cell carcinoma of human oral mucosa. Cancer 73, 2674-2679.

6)B.J.M. Braakhuis, M.P. Tabor, J.A. Kummer, C.R. Leemans, R.H. Brakenhoff, 2003. A genetic explanation of slaughter's concept of field cancerization. Cancer Res. 63, 1727-1730.

7)Kreimann E.L., Itoiz M.E., Dagrosa A., Garavaglia R., Farías S., Batistoni D., Schwint A.E., 2001a. The hamster cheek pouch as a model of oral cancer for boron neutron capture therapy studies: selective delivery of boron by boronophenylalanine. Cancer Res. 61, 8775-8781.

8)Heber E., Trivillin V., Nigg D., Kreimann E.L., Itoiz M.E., Rebagliati R.J., Batistoni D., Schwint A.E., 2004. Biodistribution of GB-10 (Na(2)(10)B10H10) in an experimental model of oral cancer in the hamster cheek pouch. Arch. Oral Biol. 49, 313-324.

9)Heber E.M., Aromando R.F., Trivillin V.A., Itoiz M.E., Nigg D.W., Kreimann E.L., Schwint A.E., 2007. Therapeutic effect of boron neutron capture therapy (BNCT) on field cancerized tissue: inhibition of DNA synthesis and lag in the development of second primary tumors in precancerous tissue around treated tumors in DMBA-induced carcinogenesis in the hamster cheek pouch oral cancer model. Arch. Oral Biol. 52, 273-279.

10)Laconi E., Doratiotto S., Vineis P.. The microenvironments of multistage carcinogenesis, Seminars in Cancer Biology (2008), doi: 10.1016/j.semcancer.2008.03.01

A novel boronated-porphyrin as a radio-sensitizing agent for boron neutron capture therapy of tumours: *in vitro* and *in vivo* studies

G.Jori[a], M.Soncin[a], E.Friso[a], M.G H.Vicente[b], E. Hao[b], G.Miotto[c], P.Colautti[d], D.Moro[d], J.Esposito[d], G. Rosi[e], E.Nava[e], C.Fabris[a]

[a]*Department of Biology, University of Padova, Via U. Bassi 58/B, 35121 Padova, Italy*
[b]*Department of Chemistry, Louisian State University, Baton Rouge, LA 70803, USA*
[c]*Department of Biochemistry, University of Padova, Viale G. Colombo 3, 35131 Padova, Italy*
[d]*INFN, Laboratori Nazionali di Legnaro, Viale dell'Università 2, 35020 Legnaro, Pd, Italy*
[e]*ENEA C.R. Casaccia, Via Anguillarese 301, 00123 S. Maria di Galeria, Roma, Italy*

Abstract

A water-soluble [meso-tetra(4-nido-carboranylphenyl)porphyrin] (H_2TCP) bearing 36 boron atoms was studied for its accumulation and its radio/photo-sensitization efficiency towards murine melanotic melanoma cells. The amount of H_2TCP in the cells increased with the porphyrin dose in the incubation medium up to 100 μM with no significant dark toxicity. Fluorescence microscopy observations showed that the porphyrin was largely localized intracellularly.

Based on these "in vitro" results our investigations were pursued using the B16F1 melanotic melanoma subcutaneously transplanted in C57BL6 mice as "in vivo" model. Phormacokinetic studies were performed by injection of H_2TCP intratumorally (1 mg/kg) and intravenously (10 mg/kg). At 0.5 h after i.t. administration or at 24 h after i.v. injection, the amountsof ^{10}B in the tumour were about 60 ppm and about 6 ppm, respectively. The distribution of H_2TCP in the tumour after intravenous or intratumoural injection was also assessed by fluorescence microscopy analyses.

Under these conditions, preliminary BNCT studies were carried out using a new thermal column called HYTOR (HYbrid Thermal spectrum sHifter TapirO Reactor) inserted in the fast nuclear reactor Tapiro at Enea Casaccia, Italy. The mice were exposed to HYTHOR radiation field for 20 min at a reactor power of 5 kW. In spite of different amounts of ^{10}B in the tumour at the irradiation time, a similar significant delay in tumour growth (5-6 days) was induced by neutron irradiation in intratoumorally and intravenously injected mice.

The response of the melanotic melanoma to H_2TCP-BNCT was compared with that obtained by irradiation after intraperitoneal injection of boron-phenylalanine.

Keywords: Photodynamic Therapy, Boron Neutron Capture Therapy, Porphyrin, Melanotic Melanoma

1. Introduction

Photodynamic therapy (PDT) and boron neutron capture therapy (BNCT) are binary therapies for cancer treatment that involve the activation of a tumour-localized sensitizer with red light, in PDT (Dougherty et al., 1998), or with low energy neutrons, in BNCT (Barth et al., 2005). The cytotoxic agents generated in PDT are reactive oxygen species (ROS), mainly $^1O_2$, whereas in BNCT short lifetime particles are formed via the ^{10}B-neutron capture nuclear reaction. The toxic effect of these species have limited ranges in tissues and, then, restricted to their site of generation. The combination of BNCT and PDT using a single drug has added advantages in that it can be easy to deliver with minimal invasiveness, while leading to increased therapeutic effect due to the targeting of different mechanisms of tumour cell destruction. This combined technique could be particularly attractive for the treatment of brain tumours and malignant melanoma. Ideal bydual sensitizers should to be amphiphilic long wavelength absorbing chromophores of high boron content, display a high affinity for tumour tissues and persist there for a considerable amount of time, have a low intrinsic toxicity, but became toxic upon activation by low energy neutrons and red light.

In this paper we describe our findings on the affinity for tumour cells in vitro and for tumour tissues in vivo of a water-soluble meso-substituted tetra(nido-carboranylphenyl) porphyrin (H_2TCP) carrying 36 boron atoms per molecule. Moreover, the efficiency of H_2TCP in photosensitising melanotic cells and its radiosensitising properties towards the subcutaneously transplanted melanoma have been investigated.

2. Materials and methods

2.1 Porphyrin

H_2TCP, (tetra(4-nido-carboranylphenyl) porphyrin was prepared by chemical synthesis at the Department of Chemistry, Louisiana State University in Baton Rouge, USA. The chemical structure and the purity of the porphyrin were characterized by standard spectroscopic and chemical analytical techniques (Vicente et al., 2002).

2.2 In vitro studies

The cell line B16F1, used in our studies, is a pigmented variant of murine melanoma B16 (Graf et al., 1984) which differs because of its highly metastatic potential. For the uptake experiments $2 \cdot 10^5$ B16F1 cells were seeded and grown for about 20 h in Dulbecco's Modified Eagle's Medium containing 10% Foetal Calf Serum. Cells were incubated with H_2TCP at the desired concentration for different periods (1-24 h).

At the end of the incubation, the cell monolayer was washed and then trypsinized. The cells were collected and resuspended in 2% sodium dodecyl sulphate. The amount of porphyrin was calculated by spectrophotofluorimetric analysis The uptake of the porphyrin by the cells was expressed as nmoles of photosensitizer per mg of cell protein.

In the phototoxicity experiments, after 24 h incubation with 1-20 μM porphyrin, the cells were irradiated for 1-15 min with 600-700 nm light (20 mW/cm^2). The cell survival was determined by means of the trypan blue exclusion test at 18-24 h after the end of irradiation.

Fluorescence microscopy observations were performed at 24 h after dark incubation of the cells with 10 μM H_2TCP.

2.3 In vivo studies

B16F1 cells were subcutaneously transplanted in C57/BL6 mice. Pharmacokinetic studies were performed by intratumoural (i.t.) and intravenous (i.v.) injection of H_2TCP and the recovery of porphyrin in the tumour and selected tissues was determined by spectrophotofluorimetric analysis.

The distribution of H_2TCP in the tumour after i.t. or i.v. injection of the porphyrin was assessed by fluorescence microscopy investigations.

Preliminary BNCT studies were carried out using HYTOR (HYbrid Thermal spectrum sHifter TapirO Reactor), a new thermal column inserted in the fast nuclear reactor Tapiro at Enea Casaccia, Italy (Esposito et al., 2008). The tumour-bearing mice were exposed to the radiation field for 20 min at a reactor power of 5 kW after i.t. and i.v. injection of H_2TCP. The effectiveness of H_2TCP-BNCT in delaying the tumour growth was compared with that obtained by irradiation of melanoma bearing mice after intraperitoneal injection of boron-phenylalanine-fructose.

3. Results

The amount of H_2TCP in the melanoma cells increased with the porphyrin dose in the incubation medium up to at least a100 μM concentration with no significant cytotoxic effect in the dark (data not shown). Moreover, as one can see in Fig. 1, the H_2TCP uptake increased with the incubation time reaching a plateau value corresponding with the recovery of 0.4 nmoles of H_2TCP per mg of cell proteins after 24 h incubation with 20 μM porphyrin.

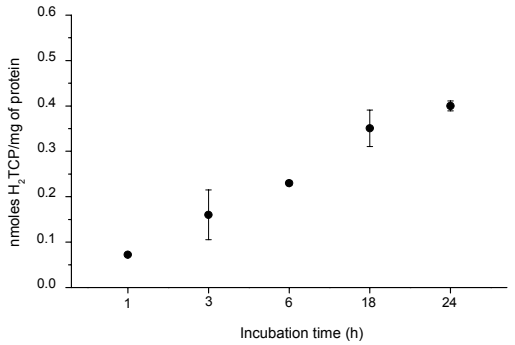

Fig. 1 Effect of the incubation time on the uptake of 20 μM H_2TCP by B16F1 melanotic melanoma cells. Average of three experiments ± standard deviation

The exposure of the H_2TCP -loaded cells to 600-700 nm light wavelengths for different times after 24 h incubation resulted in a drop of cell survival, as shown in Fig. 2.

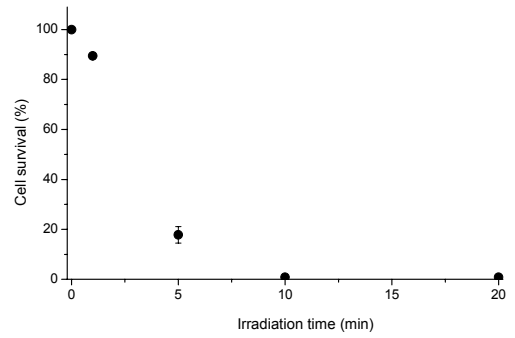

Fig. 2 Effect of the irradiation time on the survival of B16F1 cells incubated for 24 h with 20 μM H_2TCP. Irradiations were performed with 600-700 nm light (20 mW/cm^2). Values represent mean ± standard deviation of 3 experiments

In particular, the porphyrin-promoted photo-process yielded an essentially complete cell lethality after 10 min-irradiation in the presence of a 20 μM photosensitizer concentration.

Fluorescence microscopy observations showed that the porphyrin was largely localized intracellularly, exhibiting a discrete distribution in

the cytoplasm with a pattern which was closely similar to that observed for the endosomal probe Lucifer yellow (Fig. 3).

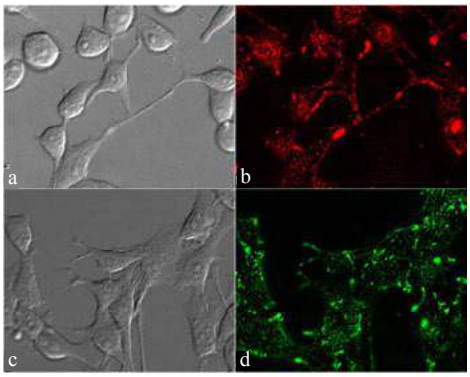

Fig. 3 Fluorescence micrographs of cells after 24 h incubation with 10 μM H_2TCP. Image **b** shows the dotted red fluorescence distributed throughout the cytoplasm (excitation at 420 nm and fluorescence detection between 650-700 nm); image **d** shows the fluorescence distribution observed after incubation with 10 mM Lucifer Yellow (excitation at 425 nm and fluorescence detection between 500-550 nm)
a and **c**: bright field images
b and **d**: fluorescence images

The biodistribution in selected tissues of melanotic melanoma-bearing mice were comparatively studied for H_2TCP injected by two different modalities. The recovery was determined in: the melanotic lesion, the skin (peritumoural tissue), lung, kidney and liver (to identify the main pathway of porphyrin elimination from the body), and spleen (since hydrophobic drugs are known to be efficiently taken up by the components of the reticuloendothelial system) (Jori, 1989). The boron concentrations in the tumour after i.v. injection of 10 mg H_2TCP/kg of body weight (2.6 mg ^{10}B/kg), was found to be about 6 ppm. As expected, liver and spleen represent the main sites of porphyrin accumulation, in agreement with what observed for a variety of porphyrin derivatives (Fig 4A).

In order to reduce the risk of non-selective damage following exposure to the thermal neutron beam a group of animals was intratumourally injected with 1 mg/kg of H_2TCP (0.26 mg ^{10}B/kg). As one can see in Fig.4B, at 30 min after administration, the recovery of ^{10}B in the tumour was about 60 ppm; under these conditions only traces of porphyrin were detected in serum, liver and spleen, indicating that only minor amounts of the radiosensitizing agent leaked into the general blood circulation.

The experiments of thermal neutron irradiation on melanotic melanoma in C57BL/6 mice were performed at 0.5 h after intratumoural administration of 1 mg/kg H_2TCP or at 24 h after intravenous injection of 10 mg/kg H_2TCP.

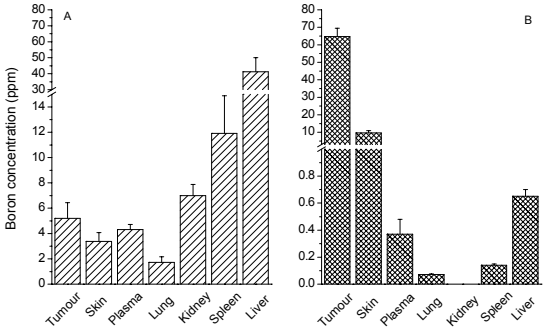

Fig. 4 Recovery of boron from tumour and selected normal tissues of mice bearing B16F1 melanotic melanoma. The mice were i.v.-injected with 10 mg/kg H_2TCP (A) or i.t.-injected with 1 mg/kg H_2TCP (B).

As shown in Fig. 5, no significant difference in the rate of tumour growth was observed between control untreated mice and mice that had been exposed to the thermal neutron flux for 20 min. without prior injection of H_2TCP. On the other hand, a limited delay in tumour growth (5-6 days) was induced by thermal neutron irradiation in the two groups of porphyrin-injected mice. The delay was practically identical for the intratumourally and intravenously injected mice in spite of different amounts of ^{10}B in the tumour at the irradiation time. Instead, a significantly delay was observed in the tumour growth of mice irradiated 1 h after intraperitoneal injection of 200 mg/kg boron-phenylalanine

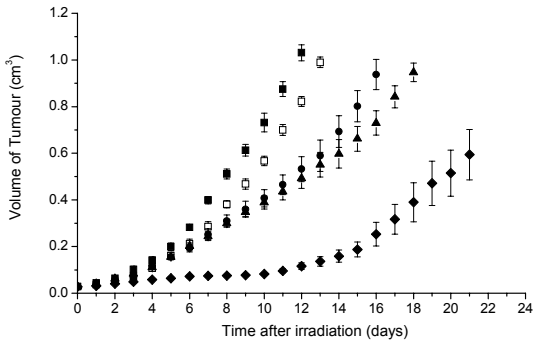

Fig. 5 Rate of tumour growth for C57BL/6 mice bearing a subcutaneously transplanted B16F1 melanotic melanoma exposed to thermal neutrons (5 kW) for 20 min.
■ uninjected and unirradiated control mice
□ only irradiated mice
● irradiated 0.5 h after i.t-injection of 1 mg/kg H_2TCP
▲ irradiated 24 h after i.v-injection of 10 mg/kg H_2TCP
◆ irradiated 1 h after i.p-injection of 200 mg/kg BPA-F
Each point represents the average of 12 mice ± standard error

4. Conclusions

Several carboranyl–porphyrin derivatives are being considered as sensitisers for a dual, possibly combined, application in BNCT and PDT of specific tumours (Renner et al., 2006). The tumour-localized tetrapyrrole compound can be sequentially activated by low energy neutrons to generate mainly α and Li particles and by red light wavelengths to produce singlet oxygen and other reactive oxygen species. Such hyper-reactive intermediates are characterized by a short travel path in a tissue, hence the overall process is often characterized by a high degree of selectivity as regards tumour damage. The tetra-(carboranylphenyl)porphyrin studied in the present investigation appears to be particularly promising. In actual fact, the presence of four carborane moieties does not appreciably affect the photosensitising efficiency of the porphyrin, at least on the basis of the extensive photoinactivation of melanotic melanoma cells after exposure to relatively low red light doses (6 J/cm^2). The high efficiency of the photoprocess can be ascribed at least in part to the partitioning of the photosensitising agent in several subcellular membranes, as suggested by the distribution pattern observed at the fluorescence microscope (Fig. 3).

The pharmacokinetic results presented in this paper fully confirm the findings obtained in our (Friso et al., 2006) and other (Miura et al., 2001) laboratories showing that porphyrin derivatives bearing up to four carborane cages can be systemically injected *in vivo* with no detectable toxic effects, while their overall biodistribution is closely similar with that typical of non-boronated porphyrins. In particular, the amount of ^{10}B-loaded porphyrin which is accumulated in the melanotic melanoma is sufficient to induce an appreciable tumour response after thermal neutron irradiation. In spite of an about ten-fold difference in the endotumoral boron concentration., there is no detectable difference in the tumor response after intratumoral or intravenous administration of the H2TCP. It appears reasonable to hypothesize an inhomogeneous ditribution of the porphyrin among the various compartments of the melanoma, especially in the case of the intratumorally delivered radiosensitizer.

The overall radiosensitizing efficiency of H2TCP is still appreciably lower than that observed for BPA (Fig.5). On the other hand, it is possible to enhance the anti-melanoma activity by combining the BNCT treatment with the photodynamic therapeutic activity which typical of porphyrins. Studies aimed at explaining this development are in progress in our laboratory.

References

Barth, R.F., Coderre, J.A., Vicente, M.G.H., Blue, T.E., 2005. Boron neutron capture therapy of cancer: current status and future prospects. Clin. Cancer Res. 11, 3987-4002.

Dougherty, T.J., Gomer, C.J., Henderson, B.W., Jori ,G., Kessel, D., Korbelik, M., Moan, J., Peng, Q., 1998. Photodynamic therapy. J Natl Cancer Inst. Jun 17;90(12):889-905.

Esposito, J., Ceballos, C., Soncin, M., Fabris, C., Friso, E., Moro, D., Colautti, P., Jori, G., Rosi, G. Nava, E., 2008. Feasibility of BNCT radiobiological experiments at the HYTHOR facility. Nucl. Inst. and Meth. in Phys. Res. B. 266, 2587-2593.

Friso, E., Roncucci, G., Dei, D., Soncin, M., Fabris, C., Collutti, P., Esposito, J., Rossi, C.R., Nitti, D., Borsetto, L, Jori, G., 2006. A novel ^{10}B-enriched carboranyl-containing phthalocyanine as a radio- and photo-sensitising agent for boron neutron capture therapy and photodynamic therapy of tumours: *in vitro* and *in vivo* studies. Photochem. Photobiol. Sci. 25, 39-50.

Graf, L.H., Kaplan, P., Silagi, S. 1984. Efficient DNA-mediated transfer of selectable genes and unselected sequences into differentiated and undifferentiated mouse melanoma clones. Somat. Cell. Mol. Genet. 10, 139-151.

Jori G., 1989. *In vivo* transport and pharmacokinetic behaviour of tumour photosensitisers In *Photosensitising Compounds: their Chemistry, Biology and Clinical Use*, Bock,G., Harnett, S., (eds) Ciba Foundation Symposium 146, London. 173-186.

Miura, M., Morris, G.M., Micca, P.L., Lombardo, D.T., Youngs, K.M., Kalef-Ezra, J.A., Hoch, D.A., Slatkin, D.N., Ma, R., Coderre, J.A., 2001. Boron neutron capture therapy of a murine mammary carcinoma using a lipophilic carboranyltetraphenylporphyrin. Radiat. Res., 155, 603-610.

Renner, M.W., Miura, M., Easson, M.W., Vicente, M.G., 2006. Recent Progress in the Syntheses and Biological Evaluation of Boronated Porphyrins for BNCT. Anti-Cancer Agents Med. Chem. 6(2), 145-158.

Vicente, M.G.H., Nurco, D.J., Shetty, S.J., Osterloh, J., Ventre, E., Hegde, V., Deutsch. W.A., 2002. Synthesis, dark toxicity and induction of in vitro DNA photodamage by a tetra(4-nido-carboranylphenyl)porphyrin. J. Photochem. Photobiol. B: Biol. 68, 123-132.

High-LET Dose and Microscopic Uncertainties in an Irradiated Cell Population

Gustavo A. Santa Cruz

Comisión Nacional de Energía Atómica
Av. del Libertador 8250 (1429), Buenos Aires, Argentina

Abstract

The probability distribution of specific energy deposited by radiation in a microscopic site is described by the microdosimetric multi-event density function and thus applies only to an infinite population of sites. The mean of this density function is the dose *D*. However, when a cell irradiation is performed, a finite sample of such volumes is implicated. The (unknown) average dose actually deposited in them will be different from *D*, and some measure of how close the point estimate is likely to be to the true value is necessary.

In this work, we show that a (1-α)% confidence interval for the sample average dose can be calculated knowing the population mean dose *D* and the microdosimetric quantity z_D, the dose-mean specific energy.

As an example, a hypothetical survival experiment where ^{10}B thermal neutron capture reactions are produced is analyzed. For a spherical cell nucleus 10 microns in diameter and a uniform distribution of boron reactions, the z_D value is 0.41 Gy. In order to get a 95% confidence interval for the sample average ^{10}B dose of length no more than 2%, the number of cells to be seeded for a given survival point is $N=1.57\text{x}10^4/[DS(D)]$, where *D* is the dose in Gy for that point and *S*(*D*) the survival due only to the boron component. Compared to photons, the number of cells needed to achieve an uncertainty of 2% at 1 Gy of ^{10}B dose is two orders of magnitude larger. Likewise, if a survival point is measured by considering for example a hundred surviving cells, the total uncertainty is 25% for a mean ^{10}B dose of 1 Gy. If the microdistribution of reactions is not uniform, both z_D and *D* must be calculated on a microdosimetric basis. This shows the importance of taking into account the stochastic aspects for specifying dose uncertainties associated to survival points, especially when high-LET radiation and low doses are involved.

Keywords: Microdosimetry, Cell survival, BNCT

1. Introduction

Since reporting only the point estimate of a population parameter obtained from a sample is usually unsatisfactory, some measure of how close the point estimate is likely to be to the true value is required. One possibility is to report both the estimate and its standard deviation (STD). If the estimator has (at least approximately) a normal distribution, it is possible to be quite confident that the true value lies within 2 or 3 STD around the estimated value.

Let $x_1 \ldots x_n$ be the values of a series of random samples, taken from a normal distribution $N(\mu,\sigma)$. The point estimate of the mean

$$\bar{x} = \frac{1}{n}\sum_{i=1}^{n} x_i \qquad (1.1)$$

is also a random variable and it has normal distribution:

$$\bar{x} \sim N\left(\mu, \sigma/\sqrt{n}\right) \qquad (1.2)$$

Therefore

$$Z = \frac{\bar{x}-\mu}{\sigma/\sqrt{n}} \qquad (1.3)$$

has a standard normal distribution, $N(0,1)$. The probability that *z* lies within $-z_{\alpha/2}$ and $z_{\alpha/2}$ is:

$$P\left(-z_{\alpha/2} \le z \le z_{\alpha/2}\right) = 1-\alpha \qquad (1.4)$$

The interval

$$\left(\bar{x} - z_{\alpha/2}\frac{\sigma}{\sqrt{n}}, \bar{x} + z_{\alpha/2}\frac{\sigma}{\sqrt{n}}\right) \qquad (1.5)$$

is a $100(1-\alpha)\%$ confidence interval for the mean μ of a normal population when σ is known. It indicates that if repeated samples are taken from the population, $100(1-\alpha)\%$ of the time these random intervals will cover the true mean.

The fixed (not random) interval

$$\left(\mu - z_{\alpha/2}\frac{\sigma}{\sqrt{n}}, \mu + z_{\alpha/2}\frac{\sigma}{\sqrt{n}}\right) \qquad (1.6)$$

will contain, $100(1-\alpha)\%$ of the time, the sample average, $\bar{x}$.

Let $x_1, ...x_n$ be a random sample from a population having mean μ and STD σ. If n is large (n > 30), $\bar{x}$ has approximately a normal distribution, by virtue of the central limit theorem (CLT) (A. Papoulis, 1991).

2. Materials and Methods

2.1 Microdosimetry

If we irradiate a large sample of identical sites (e.g., cells, nuclei, etc), and we calculate the first two moments of the single-event density function of the specific energy, we can associate the following values for the mean and STD σ (ICRU Report 36, 1983):

$$\mu = D;\ \sigma = \sqrt{z_D D} \qquad (2.1)$$

where z_D is the single-event dose-mean specific energy. In this case, the average dose imparted to the sample, $\bar{D}_n$, (i.e., the average dose among the elements that constitute the sample, as if each site were conceived as a "detector"), will lie in the interval

$$\left(D - z_{\alpha/2}\sqrt{\frac{z_D D}{n}}, D + z_{\alpha/2}\sqrt{\frac{z_D D}{n}}\right) \qquad (2.2)$$

$100(1-\alpha)\%$ of the time (see Eq. (1.6)). Let L be the "length" of the interval (2.2). Then

$$L/D = 2z_{\alpha/2}\sqrt{\frac{z_D}{nD}} \qquad (2.3)$$

Assume we want to associate to the mean dose D an interval such that it represents a fraction 2δ of D. The number n of sites to be considered in the sample in order to have the sample average $\bar{D}_n$, lying within an interval $\pm\delta D$ around D, $100(1-\alpha)\%$ of the time is:

$$n = \left(\frac{z_{\alpha/2}}{\delta}\right)^2 \frac{z_D}{D} \qquad (2.4)$$

The interval given by (2.2) represents only the uncertainty associated to the random fluctuations in the specific energy imparted to a *finite* sample of cells, even in the ideal case where the population dose D is known with infinite precision.

2.2 Survival experiments

Despite the initial number of cells irradiated in a survival experiment, the relevant information is obtained only from the cells with clonogenic capacity (i.e., a subset of the total cells seeded in the dish). This final number of surviving cells can be, in general, relatively small. Indeed, this subset of cells constitutes the sample of the infinite population, and if the population mean dose D is assigned to the survival point, an interval should be included in order to report the range within which the sample average dose $\bar{D}_n$ can reasonably be expected to lie.

In order to simplify this analysis we assume that the surviving cells represent an unbiased sample of the population, i.e., that the cells surviving were exposed to the same specific energy distribution that the inactivated cells, which is of course a debatable assumption. In other words, every cell in the irradiated population is supposed to have an equal chance of being "selected" for surviving.

2.3 "A priori" calculations

Before the experiment, let us assume that we want to keep the length of the interval equal to $2\delta D$ around D. Let n_S be the number of cells that we "expect" will survive after a dose D. Then, from Eq. (2.4), the number N of irradiated cells to seed should be at least

$$N = \frac{n_S}{S(D)} = \left(\frac{z_{\alpha/2}}{\delta}\right)^2 \frac{z_D}{DS(D)} \qquad (2.5)$$

or in terms of δ

$$\delta = z_{\alpha/2}\sqrt{\frac{z_D}{NDS(D)}} \qquad (2.6)$$

On the other hand, the number of inactivated cells, $n_I = n_S\left[(1-S(D))/S(D)\right]$, will have associated a

confidence interval of length

$$L_I = 2z_{\alpha/2}\sqrt{\frac{z_D D}{n_I}} = L_S\sqrt{\frac{S(D)}{1-S(D)}} \qquad (2.7)$$

where $L_S = 2\delta D$.

2.4 "A posteriori" calculations

Conversely, if subsequent to the experiment, we find that n_S cells survived after irradiation with a dose D, the relative length of the confidence interval will be given by Eq. (2.3), with $n = n_S$.

3. Results

3.1 ^{10}B reactions

Let us consider microdosimetric spherical volumes of 10 microns in diameter, representing for instance the cell nuclei. For such volumes and a uniform boron microdistribution, the dose-mean specific energy is $z_D = 0.41$ Gy. For a 95% confidence interval, $z_{\alpha/2} = 1.96$. If we consider for example 100 cells surviving, the relative length of the 95% confidence interval, L_S/D, is given by:

$$L_S/D = \left[25/D(Gy)^{1/2}\right]\% \qquad (3.1)$$

This is the uncertainty in the sample average dose that should be assigned to the survival of 100 cells at dose D, strictly associated to the stochastic aspects of energy deposition.

On the other hand, let us consider a "fixed" (or desired) uncertainty δ of 1%. Then, by Eq. (2.4):

$$n_S = \left(\frac{1.96}{0.01}\right)^2 \frac{0.41\ \text{Gy}}{D(\text{Gy})} = \frac{1.57\ 10^4}{D(\text{Gy})} \qquad (3.2)$$

and in consequence, the number N of cells to seed should be at least equal to:

$$N = \frac{1.57\ 10^4}{D(\text{Gy})S(D)} \qquad (3.3)$$

Figure 1 shows the dependence of N with dose, for a simple exponential survival curve with slope α of 1.2 Gy^{-1}. The percentages represent the δ values and the curves are calculated in order to obtain 95% confidence intervals.

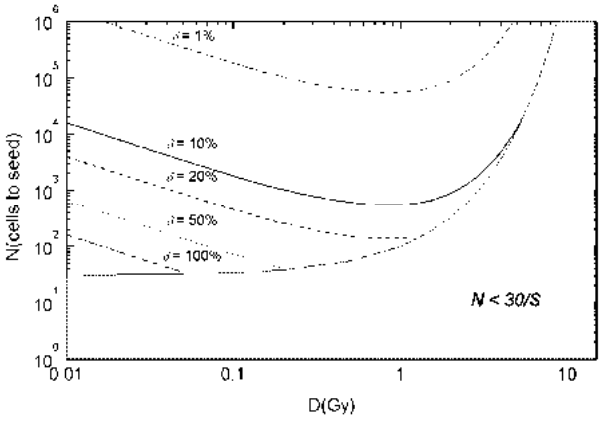

Figure 1. Minimum number of cells to be considered as a function of dose and for different levels of uncertainty. The gray area represents the region where the conditions imposed by the CLT are not satisfied

The gray area is the region where the CLT cannot guarantee the approximate normal distribution for the point estimate of the mean (less than 30 cells surviving, or N<30/S). The different curves are lower limits for N.

For instance, if we want to have a sample of surviving cells whose dose average value lies (95% of the time) within 20% (δ = 10%) around 4 Gy, the minimum number of cells to seed is approximately 4800, with an expected number of surviving cells of about 40 (just above the limit imposed by the CLT).

It can be shown that the minimum value for N occurs when $D = \alpha^{-1}$.

A probably more convenient representation is illustrated in Figure 2. We plot the number N of cells to seed as a function of the surviving fraction S, for different δ values. For comparison, a photon curve with δ = 1% is included.

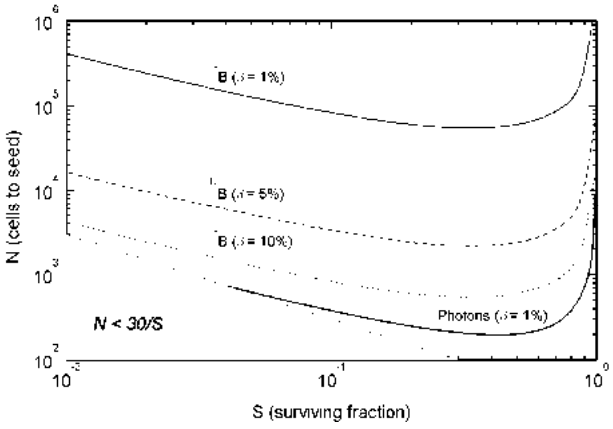

Figure 2. Idem as in figure 1, but as a function of the surviving fraction, for ^{10}B reactions and for photons

The above calculations are also valid for the case of a boron compound that distributes non-uniformly at cellular scale. However, the dose D can no longer be associated with kerma, since the conditions for Charged Particle Equilibrium (CPE) are not satisfied. Considering a bi-valued boron microdistribution model, where two different boron reaction rates are supposed to occur inside and outside the microscopic volume, the non-equilibrium dose and STD are functions of the accumulation ratio $a = c_I / c_O$, the ratio of boron concentrations inside vs. outside the site (G. A. Santa Cruz, 2004):

$$D(a) = \eta(a) K\left(\max\{c_O, c_I\}\right) \qquad (3.4)$$

$$\sigma_z(D,a) = \sqrt{z_D(a) D(a)} \qquad (3.5)$$

where $\eta(a)$ is called Microscopic Dose Correction Factor (MDCF). In Eq. (3.4) it is assumed that the kerma is calculated with the highest boron concentration, resulting in an MDCF always less than one. Figure 3 shows the minimum number of cells to seed as a function of the surviving fraction for different ^{10}B microdistributions, considering a 10 microns site and δ = 10%. For this size, extrasite distributions present the smallest z_D, and in consequence, are less affected by randomness. Conversely, intrasite distributions present the highest z_D values, and a higher number of cells to seed will be required in order to obtain the same level of uncertainty. In this calculation, S is calculated as a function of the actual dose $D(a)$, not kerma.

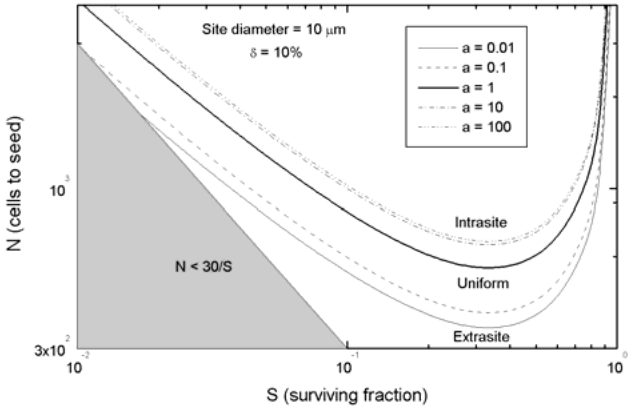

Figure 3. N vs. S for different boron microdistributions and a fixed δ = 10%. Site diameter = 10 μm

4. Conclusions

It is worthy to remark that the dose uncertainty derived from microdosimetric considerations would actually provide additional information for the analysis of a survival experiment that is not considered in general, i.e., the fundamental aspects of heavy ion energy deposition at the microscopic level.

If we consider a non-uniform boron microdistribution, the quantity z_D (which is sensitive to the accumulation ratio and to the size and shape of the site as well) will influence the dose uncertainty, even though the number of cells and dose were kept the same.

The "*a posteriori*" viewpoint is possibly a suitable approach for living tissues. If we consider for example a tumor mass with a small number of well-perfused regions, although the cells in those regions will probably get a good boron uptake and in consequence be exposed to high doses, the surviving tumor cells will have associated large dose uncertainties, since the confidence interval is inversely proportional (see Eq. (2.6)) to the initial number of clonogenic cells (small) and to the surviving fraction (low).

When a structured normal tissue is irradiated (e.g. skin), and the toxicity rests on the interdependence between different cell populations, usually the most affected one will drive the effect of the whole tissue. If the surviving fraction of this critical population is low, we will have again the same situation mentioned above. This would imply that it could not be possible to associate a specific dose value to the observed effect, but a broad range of doses instead.

Acknowledgements

The author is indebted to Sara J. Gonzalez, for her suggestions and comments.

References

ICRU Report 36, Microdosimetry. ICRU, Bethesda, MD (1983).

Papoulis A., Probability, Random Variables and Stochastic Processes, 3rd ed., McGraw-Hill, New York (1991).

Santa Cruz G. A. and Zamenhof R. G., "The Microdosimetry of the ^{10}B Reaction in Boron Neutron Capture Therapy: A New Generalized Theory." Radiat. Res., 162(6), pp.702-710 (2004).

Development and Characterization of a Small Animal Irradiation Facility for Boron Neutron Capture Therapy (BNCT) Research at the RA-3 Research Reactor: Application to BPA-BNCT for Oral Cancer

E. Pozzi[a], D.W. Nigg[b], M. Miller[c], S.I. Thorp[c], E.M. Heber[d], V.A. Trivillin[d], L. Zarza[a], G. Estryk[a], A. Monti Hughes[d], R.F. Aromando[e], M.E. Itoiz[d,e], A.E. Schwint[d]

[a] *Research and Production Reactors, National Atomic Energy Commission, Ezeiza Atomic Center, Argentina*
[b] *Idaho National Laboratory, Idaho Falls, USA*
[c] *Instrumentation and Control Department, National Atomic Energy Commission, Ezeiza Atomic Center, Argentina*
[d] *Department of Radiobiology, National Atomic Energy Commission, Constituyentes Atomic Center, Argentina*
[e] *Department of Oral Pathology, Faculty of Dentistry, University of Buenos Aires, Argentina*

Abstract

The National Atomic Energy Commission of Argentina (CNEA) has constructed a thermal neutron source for use in BNCT applications at the RA-3 research reactor facility located in Buenos Aires. The aim of the present study was to perform a dosimetric characterization of the facility and undertake radiobiological studies of BNCT in an experimental oral cancer model. The free-field neutron flux spectrum was measured at the irradiation location by nuclear activation techniques. The thermal neutron flux was also measured employing self-powered neutron detectors (SPND). The free-field thermal flux was 7.1 x 10^9 n cm^{-2} s^{-1} and the fast neutron flux was 2.5 x 10^6 n cm^{-2} s^{-1}, indicating a very well thermalized neutron field with negligible fast neutron dose. The gamma dose rate at the irradiation location was 4.8 ± 0.5 Gy/h. Having previously demonstrated the efficacy of BNCT to treat tumors in the hamster cheek pouch oral cancer model at the RA-6 Reactor hyperthermal neutron facility, we performed radiobiological studies of BNCT mediated by BPA, GB-10 or (GB-10 + BPA) in the same model at the new RA-3 facility. In order to shield the body of the animal from the neutron flux while exposing the everted cheek pouch bearing the tumors, we developed an enclosure fabricated from plates composed of a 6 mm layer of lithium carbonate enriched to 95 % in lithium-6 sealed between thin sheets of Lucite. The hamster pouch bearing tumors is everted out of the enclosure and onto a protruding shelf. A Lucite hamster phantom was constructed for measurements to determine the spatial distribution of the thermal and above-thermal flux based on activation of copper-gold flux wires and foils. The wire measurements showed that the thermal neutron flux at all locations within the shield container is at least a factor of 20 lower than the flux on the shelf. Groups of tumor-bearing hamsters were submitted to BPA-BNCT (33 tumors), GB-10-BNCT (11 tumors), (GB-10 + BPA)-BNCT (13 tumors) or beam only (15 tumors) treatments employing the shielding device. Normal (non-cancerized) hamsters were treated similarly to evaluate normal tissue radiotoxicity. The total physical dose delivered to tumor with the BNCT treatments ranged from 6 to 8.5 Gy. Tumor control ranged from 73-85%, with no normal tissue radiotoxicity and significant but reversible mucositis in precancerous tissue surrounding tumors. RA-3 is a useful, novel irradiation facility for BNCT-related small-animal studies. The therapeutic success of different BNCT protocols in treating experimental oral cancer at this facility was unequivocally demonstrated. Additionally, comparative studies with other facilities such as RA-6 and RA-1 will allow for enlightening radiobiological studies on the effect of the different dose components of BNCT since these other facilities have different neutron spectra than RA-3.

Keywords: oral cancer, BNCT, hamster cheek pouch, RA-3 Reactor, lithium-6 shielding

1. Introduction

The efficacy of BNCT mediated by BPA, GB-10 and (GB-10 + BPA) to treat tumors with no normal tissue radiotoxicity in the hamster cheek pouch oral hamster model was demonstrated in previous studies by our group (Kreimann et al., 2001b; Trivillin et al., 2004, 2006). These BNCT treatments were performed at the RA-6 reactor hyperthermal neutron facility located in the city of San Carlos de Bariloche, 1,600 km south-west of Buenos Aires, where our research labs are located. The National Atomic Energy Commission of Argentina constructed a thermal neutron source for use in BNCT biomedical applications at the RA-3 research reactor facility located in Buenos Aires (Miller et al., this meeting). The aim of the present study was to perform radiobiological BNCT studies to explore therapeutic efficacy and normal tissue radiotoxicity in the hamster cheek pouch oral cancer model in the novel facility, extending the necessary dosimetric characterization.

2. Materials and Methods

Physical dosimetry

A tunnel penetrating the graphite structure of the thermal column at the RA-3 reactor enables the insertion of samples into a near-isotropic neutron field (Fig. 1) while the reactor is in normal operation (Miller et al., this meeting). The free-field neutron flux spectrum was measured at the irradiation location by nuclear activation techniques employing a variety of foils to cover the energy range from thermal to about 1 MeV (Pozzi et al., 2007). Additionally, the thermal to fast neutron dose ratio was measured with bare and cadmium-covered gold foils. The thermal neutron flux was also measured employing calibrated self-powered neutron detectors (SPND).

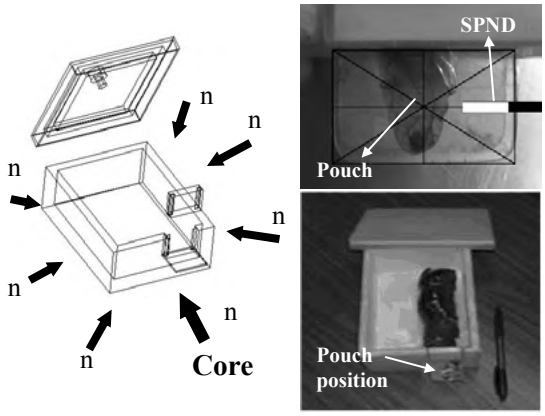

Figure 1 Thermal neutron shielding enclosure (left) with hamster phantom (lower right). Detail of a pouch positioned for irradiation, with reference of the position of SPND monitor (upper right).

Structural gamma dose rate was measured with a Far West graphite ionization chamber covered with a neutron shield of F^6Li. Physical dosimetry data (this study and Pozzi et al. 2007) and radiotolerance data extrapolated from previous studies by our lab (Kreimann et al., 2001b; Trivillin et al., 2006) suggested the convenience of constructing a shield to protect the body of the animal from the neutron flux while exposing the everted cheek pouch bearing tumors. To that end we developed an enclosure fabricated from plates composed of a 6 mm layer of lithium carbonate enriched to 95% in lithium-6 sealed between sheets of Lucite (Fig.1).

The hamster pouch is everted out of the enclosure and onto a protruding shelf. A Lucite hamster phantom was constructed for measurements to determine the spatial distribution of the thermal and above-thermal flux within the shield and at the position of the everted pouch, based on activation of copper-gold flux wires. SPND measurements showed that the influence of the shielded animal body and the very thin cheek pouch on neutron flux at the target position was negligible. Thereafter, SPNDs at the target position were employed prior to each irradiation to monitor potential local flux variations.

Radiobiological studies

Tumor induction

The right cheek pouch of young Syrian hamsters was subjected to topical application of 0.5% dimethyl-1,2-benzanthracene (DMBA) in mineral oil twice a week for approximately 12 weeks (Kreimann et al., 2001a). Once the exophytic tumors, i.e. squamous cell carcinomas, had developed, the animals were used for *in vivo* BNCT studies.

In vivo BNCT

Dosimetric calculations were based on the physical dosimetry data and previously reported boron biodistribution data (Kreimann et al., 2001a; Heber et al., 2004). Table 1 presents the boron values used for dose calculations.

Table 1

Boron concentration (mean ± SD) (ppm) for the different administration protocols			
Tissue	**BPA**[a]	**GB-10**[b]	**GB-10**[c] **+ BPA**[d]
Pouch tumor	33 ± 17	32 ± 21	63 ± 21
Precancerous tissue	20 ± 6	34 ± 17	41 ± 14
Normal pouch tissue	14 ± 5	22 ± 7	38 ± 18
Blood	12 ± 4	32 ± 6	30 ± 14

a 3 h after 15.5 mg ^{10}B /kg b.w. bolus ip; **b** 3 h after 50 mg ^{10}B /kg b.w. bolus i.v.; **c** 3 hs after 34.5 mg ^{10}B /kg b.w bolus i.v.; **d** 1.5 h after 31 mg ^{10}B /kg b.w., 3 h infusion

Groups of tumor-bearing hamsters were submitted to BNCT mediated by BPA (15.5 mg^{10}B/kg) (33 tumors); GB-10 (50 mg^{10}B/kg) (11 tumors) or the combined administration of GB-10 (34.5 mg^{10}B/kg) and BPA (31 mg^{10}B/kg) (13 tumors).

Beam only irradiations (15 tumors) were performed employing the longest exposure time. Normal (non-cancerized) pouches were irradiated similarly to evaluate potential normal tissue radiotoxicity.

Table 2 presents the estimated physical doses from the different radiation components at the target position for the different irradiation protocols. Boron dose is quoted per part per million boron by weight.
Table 3 shows the total physical absorbed doses. The combined absolute uncertainty on the total dose includes the boron concentration uncertainty.

Table 2

Physical Absorbed Doses at the Target Position (Pouch) for the Different Experimental Protocols			
	BPA- BNCT	**GB-10-BNCT**	**(GB-10 + BPA)- BNCT**
Irrad time [min]	5.0 ± 0.8	9.0 ± 0.8	3.0 ± 0.8
Gamma photons [Gy]	0.61 ± 0.07	0.95 ± 0.11	0.30 ± 0.04
Induced protons (^{14}N) [Gy]	0.35 ± 0.04	0.47 ± 0.05	0.15 ± 0.02
Boron [Gy/ppm]	0.151 ± 0.015	0.204 ± 0.021	0.066 ± 0.007

Table 3

Total Physical Absorbed Doses [Gy]			
Position	**BPA-BNCT**	**GB-10-BNCT**	**(GB-10 + BPA)-BNCT**
Pouch tumor	5.97 ± 2.67	7.94 ± 4.42	4.62 ± 1.45
Precancerous tissue	3.91 ± 0.93	8.43 ± 3.52	3.14 ± 0.97
Normal pouch tissue	3.12 ± 0.78	5.84 ± 1.50	2.95 ± 1.20
Body	0.69 ± 0.08	1.24 ± 0.13	0.40 ± 0.05

Follow-up

The tumor, precancerous and normal tissue responses were assessed by visual inspection and a tumor volume assay at 1, 7, 14, 21 and 30 days post-treatment. Body weight and clinical signs were monitored periodically. At the last experimental time-point the animals were sacrificed humanely for histological analysis of tumor, precancerous and normal tissue.

3. Results and Discussion

The foil measurements indicated that the free-field thermal flux was 7.1 x 10^9 n cm^{-2} s^{-1} and the fast neutron flux was 2.5 x 10^6 n cm^{-2} s^{-1} with estimated uncertainties of 8%, indicating a very well thermalized neutron field with negligible fast neutron dose. The measured cadmium ratio was 4100. Measured thermal neutron flux at the center of the everted pouch was 4.6 x 10^9 n cm^{-2} s^{-1}.

The gamma dose rate in air at the irradiation location was 4.8 ± 0.5 Gy/h. The copper-gold flux wire measurements corresponding to the Lucite hamster phantom showed that the thermal neutron flux at all locations within the shield container is at least a factor of 20 lower than the flux on the shelf onto which the tumor-bearing pouch is everted for irradiation.

None of the BNCT treated animals showed signs of radiotoxicity or alterations in body weight gain. No normal tissue radiotoxicity was observed. All 3 BNCT protocols exhibited marked therapeutic efficacy. Overall tumor response was expressed as partial remission plus complete remission and ranged from 73-85% (Table 4, Fig.2). Two arbitrary tumor size ranges were defined to categorize tumor size at the time of irradiation and evaluate potential size-related differential response (Table 4).

Table 4

Tumor Response for each Protocol as Indicated					
Protocol	**Tumors**	**n**	**PR**	**CR**	**OTR**
Beam Only	**Small <10mm^3**	23	23%	0%	23%
	Large ≥10mm^3	3	67%	0%	67%
	Total	**26**	**31%**	**0%**	**31%**
BPA-BNCT	**Small <10mm^3**	28	21%	50%	71%
	Large ≥10mm^3	5	60%	20%	80%
	Total	**33**	**27%**	**45%**	**73%**
GB-10-BNCT	**Small <10mm^3**	7	29%	43%	78%
	Large ≥10mm^3	4	75%	0%	75%
	Total	**11**	**45%**	**27%**	**73%**
(GB-10 + BPA)-BNCT	**Small <10mm^3**	11	36%	45%	82%
	Large ≥10mm^3	2	100%	0%	100%
	Total	**13**	**46%**	**38%**	**85%**

PR: Partial Remission, CR: Complete Remission, OTR: Overall Tumor Response (PR + CR)

Complete remission was greater in small tumors. Although overall tumor response was similar for all 3 BNCT protocols, the therapeutic efficacy of (GB-10 + BPA)-BNCT showed a trend towards improvement compared to the other two BNCT protocols (85 vs 73%), conceivably due to more homo-

geneous targeting of heterogeneous tumor cell populations (Heber et al., 2006) and the high boron content in tumor tissue (Heber et al., 2004) that allows for shorter irradiation times with the concomitant reduction in background dose and the increase in therapeutic ratio (Trivillin et al., 2006).

Beam only induced only slight partial tumor remission and no complete remission. Precancerous tissue exhibited manifest, albeit reversible, mucositis, in particular in the BPA-BNCT group. Histological analysis revealed inflammatory infiltrate and edema associated to macroscopic signs of mucositis.

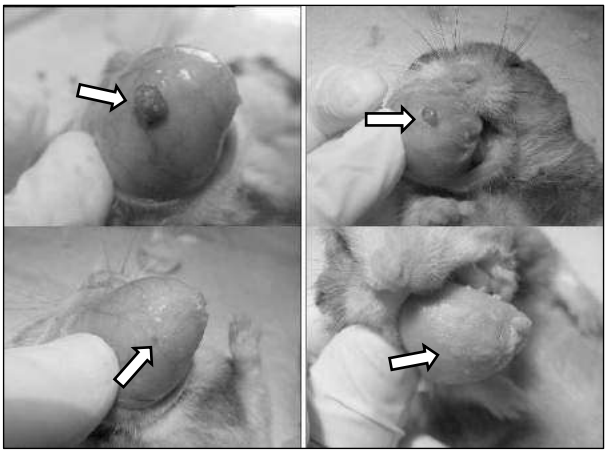

Figure 2: Representative examples of (A): partial remission (GB-10-BNCT) and (B): complete remission (BPA-BNCT). Top panel: pre-treatment; lower panel: 28 days post-treatment.

4. Conclusions

RA-3 is a useful, novel irradiation facility for BNCT-related small-animal studies. The therapeutic success of different BNCT protocols in treating experimental oral cancer at this facility was unequivocally demonstrated. Additionally, comparative studies with other facilities such as RA-6 and RA-1 will allow for enlightening radiobiological studies on the effect of the different dose components of BNCT since these other facilities have different neutron spectra than RA-3. The potential boosting therapeutic role of the non-boron dose components of BNCT suggested by previous studies by our laboratory (Trivillin et al., 2008) remains to be elucidated.

References

Miller M, Quintana J, Ojeda J, Langan S, Thorp S, Pozzi E, Sztejnberg-G.C. M, Estryk G, Nosal R, Saire E, Agrazar H, Graiño F, 2008. New irradiation facility for biomedical applications at the RA-3 reactor thermal column. (this meeting)

Heber E, Trivillin VA, Nigg D, Kreimann EL, Itoiz ME, Jiménez Rebagliati R, Batistoni D, Schwint AE, 2004. Biodistribution of GB-10 ($Na_2{}^{10}B_{10}H_{10}$) compound for boron neutron capture therapy (BNCT) in an experimental model of oral cancer in the hamster cheek pouch. *Arch Oral Biol*; 49**:** 313-324.

Trivillin VA, Nigg DW, Itoiz ME, González BN, Rebagliati RJ, Batistoni D, Kreimann EL, Schwint AE, 2006. Homogeneous boron targeting of heterogeneous tumors for Boron Neutron Capture Therapy (BNCT): chemical analyses in the hamster cheek pouch oral cancer model. EM Heber, Archives of Oral Biology 51: 922-929.

Kreimann EL, Itoiz ME, Dagrosa A, Garavaglia R, Farías S, Batistoni D, Schwint AE, 2001a. The Hamster Cheek Pouch as a Model of Oral Cancer for Boron Neutron Capture Therapy Studies: Selective Delivery of Boron by Boronophenylalanine. *Cancer Res*; 61: 8775-8781.

Kreimann EL, Itoiz ME, Longhino J, Blaumann H, Calzetta O, Schwint AE, 2001b. Boron Neutron Capture Therapy for the treatment of oral cancer in the hamster cheek pouch model. *Cancer Res (Advances in Brief)*; 61: 8638-8642.

Trivillin VA, Heber EM, Itoiz ME, Nigg D, Calzetta O, Blaumann H, Longhino J, Schwint AE, 2004. Radiobiology of BNCT mediated by GB-10 and GB-10 + BPA in experimental oral cancer. *Appl Radiat and Isotopes*; 61: 939-945.

Trivillin VA, Heber EM, Nigg D, Itoiz ME, Calzetta O, Blaumann H, Longhino J, Schwint AE, 2006. Therapeutic Success of Boron Neutron Capture Therapy (BNCT) Mediated by a Chemically Non-selective Boron Agent in an Experimental Model of Oral Cancer: A New Paradigm in BNCT Radiobiology. R*adiation Research*; 166, 387–396.

Trivillin VA, Heber EM, Rao M, Cantarelli MA, Itoiz ME, Nigg DW, Calzetta O, Blaumann H, Longhino J, Schwint AE, 2008. Boron Neutron Capture Therapy (BNCT) for the treatment of spontaneous nasal planum Squamous Cell Carcinoma in felines. Radiation and Environmental Biophysics 47 (1): 147-155.

Pozzi E, Nigg DW, Miller M, Thorp SI, Schwint AE, Heber EM, Trivillin VI, Zarza L, Estryk G, 2008. A Small-Animal Irradiation Facility for NCT Research at the RA-3 Research Reactor, Trans ANS 97**:**309-311.

Acknowledgements

This work was partially supported by the US Department of Energy, Office of Science, through Idaho National Laboratory.

The authors are indebted to the expert Radioprotection and Operation teams of RA-3.

Boron Neutron Capture Therapy of Liver and Lung Coloncarcinoma Metastases: an *in vitro* Survival Study

C. Ferrari [a], A.M. Clerici [a], C. Zonta [a], L. Cansolino [a], A. Boninella [a], S. Altieri [b,c], F. Ballarini [b,c], S. Bortolussi [b,c], P. Bruschi [b], S. Stella [b,c], J. Bakeine [b,c], P. Dionigi [a], A. Zonta [a]

[a] *Dept. of Surgery, Experimental Surgery Laboratory, University of Pavia, Pavia, Italy*
[b] *Dept. of Nuclear and Theoretical Physics, University of Pavia, Pavia, Italy*
[c] *National Iinstitute of Nuclear Physics (INFN), Section of Pavia, Pavia, Italy*

Abstract

The management of tumors disseminated in explantable organs by means of BNCT is particularly favourable. The possibility to perfuse the isolated organ, withdrawing the residual boronated compound, and to expose it entirely to the neutron flux, let BNCT to better show its peculiarity i.e. selectively kill neoplastic ^{10}B enriched cells sparing normal ^{10}B lacking tissues. Being BNCT effectiveness tightly dependent on the amount of the endocellular boron at the time of neutron irradiation, the occurrence of the discharge of a fraction during the perfusion procedure is a questionable point in terms of therapeutic efficacy. In order to investigate the incidence of the endocellular boron loss, caused by the boronated compound deprivation, the boronophenylalanine (BPA) cell uptake and its washout were checked *in vitro* on the DHDK12TRb (DHD) rat coloncarcinoma cell line and *in vivo,* on BD-IX rats, affected by liver metastases induced by DHD cells injection, following BPA removal by the organ perfusion. The dose-dependent cell survival was studied on the same cell line. Results on the DHD cells show a time and concentration dependent boron accumulation capability. Cell harvesting as like as time and temperature of permanence in boron deprived medium influence boron loss, that can reach substantial levels. Nevertheless the retained intracellular fraction results in a TD_{50} for an absorbed dose of 0,29 Gy. *In vivo* data of ongoing studies show more favourable cellular behaviour in terms of retained boronated compound suggesting that the organ perfusion cannot invalidate the BNCT therapeutic efficacy.

Keywords: Boron Neutron Capture Therapy, coloncarcinoma metastases, BPA release, cell survival

1. Introduction

The treatment of the tumours that affect whole organs, such as liver or lung, affected by diffuse metastases, is a really promising application field for Boron Neutron Capture Therapy (BNCT) (Zonta et al., 2006; Wittig et al., 2008; Suzuki et al., 2007; Altieri et al., 2006; Suzuki et al., 2006). In the special case of explantable organs, its therapeutic efficacy is maximized for two main reasons: *1)* the isolated organ can be entirely exposed to the neutron flux that can reach even non detectable micrometastases, increasing the selectivity of the therapeutic approach; *2)* the boronated compound can be removed by perfusion from the circulatory system thus sparing vessels and normal tissues from aspecific radiation damages.

Nevertheless it must be taken into account that the last advantage might turn into a problem if the perfusion procedure causes the release of the boronated compound previously uptaken by neoplastic cells.

It is well known that for successful BNCT a therapeutic radiation dose must be delivered to tumour, keeping the one absorbed by normal tissues under the tolerance levels, therefore the rate of ^{10}B concentration between neoplastic and normal cells must be kept as high as possible. Afterwards, the knowledge of all the aspects related to uptake, retention and washout of the compound delivered as boron carrier is of great interest to properly manage the therapy (Dahlström et al., 2004; Capala et al., 1996; Hsieh et al., 2006)

At the moment the boronated compounds commercially available for clinical use are the boronophenylalanine (BPA) and the sodiumborocaptate (BSH). Our *in vitro* and *in vivo* experimental experience as like as the clinical application on liver coloncarcinoma metastases are based on BPA as boron delivery agent. The evidence of the *in vitro* existence of a resistant cell fraction together with the appearance of recurrences in the clinical outcome suggest that insufficient quantities of ^{10}B were present in these cells at the moment of neutron irradiation.

This could be attributed to poor uptake or to BPA discharge caused by extracellular BPA deprivation. The aim of the present work is to quantify the supposed BPA cellular washout, subsequent to the external compound absence and to estimate the cell survival following *in vitro* irradiation in absence of external BPA.

2. Materials and methods

Boron uptake as a function of BPA concentration and time of treatment

Experiments were performed on the DHDK12TRb (DHD) rat coloncarcinoma cell line. Flasks were plated at a costant density of $3x10^6$ cells, and allowed to attach and grow for 48 h. The culture medium was removed and BPA-enriched (20, 40, 80, 160 μg ^{10}B/ml) medium was added for 4 and 18 h. At the end of the treatment time, the cells were washed three times with PBS, trypsinized and enriched by centrifugation. Samples of medium containing ^{10}B, PBS, supernatant and of the cell fraction were frozen in liquid nitrogen for subsequent boron content analyses, performed by ICP-MS and α spectrometry (Wittig et al., 2008).

Boron washout on cell suspensions as a function of temperature and time after BPA deprivation .

Cells, seeded and cultured as above described, were incubated for 4 h with 80 ppm of BPA enriched medium. At the end of the time of contact, after medium withdrawing, the cells were washed three times with PBS, harvested and resuspended for 4 h, at 4 or 37 °C, in BPA-free release medium. Cell suspensions were sampled every 30 min for the first two hours and subsequently every hour. After centrifugation the releasing medium and the cell fractions were frozen in liquid nitrogen, for ^{10}B levels measurements.

Boron washout on adherent cells as a function of temperature and time after BPA deprivation

The same treatment conditions carried out in the experiments of boron release on cell suspensions were applied to those on adherent cells. Afterwards, the cells were deprived of boron containing medium, washed three times with PBS, added of BPA-free medium and mantained at 4 or 37 °C. Replicate flasks were prepared for each of the established release observation time: 30, 60, 90, 120, 180 and 240 min. At these intervals of time, the cells were washed once in PBS, trypsinised and enriched by centrifugation. Samples of medium, PBS and cellular fractions were collected and analysed as described above.

Boron washout in rat liver as a consequence of the organ perfusion.

BD-IX rats were injected with $20x10^6$ DHD cells into the spleen to induce liver coloncarcinoma metastases which developed in about twenty days. At that time a solution of 300 mg/kg of BPA-fructose was administered by intravenous injection and two hours later the animals were anaesthetized for the liver perfusion carried out with Ringer solution at 4 °C. Samples of both neoplastic and normal tissues were taken from the perfused organ and frozen in liquid nitrogen for ^{10}B content evaluation performed on criostatic sections by means of neutron autoradiography (Altieri et al., 2008) and α spectroscopy (Wittig et al., 2008).

Cell survival related to radiation dose exposure

Exponentially growing cells were cultured for 4h in 80 ppm BPA enriched medium. At the end of the fixed time of contact the medium was replaced and cells were washed three times in PBS, harvested by trypsinization, counted and enriched by centrifugation. Cells were submitted to neutron irradiation at the concentration of $5x10^6$/ml within one hour after boron deprivation keeping cells at 4 °C. The irradiation takes place in the thermal column of the TRIGA Mark II reactor of University of Pavia, in a position where the thermal neutron flux is $1.67x10^{10}$ cm^{-2} s^{-1} at 250 kW. Immediately before irradiation, aliquots of $4x10^6$ cells are layered on a mylar disk for ^{10}B content analysis performed by α-spectrometry. Following neutron exposure cells are diluted with boron free medium for subsequent clonogenic assay. The cell survival is assessed by the rate of the plating efficiency of the irradiated cells treated with boron on that of non irradiated controls treated with boron.

The cell survival was also investigated theoretically by means of an *ab initio*, mechanistic model and a Monte Carlo code originally developed for radiation-induced chromosome aberrations. A detailed description of the model/code and its validations and applications is beyond the scope of this paper, and can be found elsewhere (see e.g. Ballarini et al. 2007 and references therein). In this context it is sufficient to mention that the current version of the model can provide simulated dose-response curves for the main aberration types (i.e., dicentrics, translocations, rings, more than 40 complex exchanges and excess acentrics) following exposure to photons, light ions and heavy ions. The model is based on the assumption that aberrations arise from clustered DNA strand

	4h			18h		
C_m ^{10}B (ppm)	C_i $^{10}B_{tot}$/ C_m ^{10}B	C_i $^{10}B_{rel}$/ C_i $^{10}B_{tot}$	C_i $^{10}B_{ret}$/ C_m ^{10}B	C_i $^{10}B_{tot}$/ C_m ^{10}B	C_i $^{10}B_{rel}$/ C_i $^{10}B_{tot}$	C_i $^{10}B_{ret}$/ C_m ^{10}B
10	2.49 ± 0.88	0.69 ± 0.09	0.79 ± 0.09	6.05 ± 0.47	0.79 ± 0.01	1.09 ± 0.34
20	1.97 ± 0.62	0.73 ± 002	0.46 ± 0.17	4.00 ± 1.26	0.80 ± 0.04	0.77 ± 0.27
40	2.14 ± 0.83	0.75 ± 0.12	0.50 ± 0.12	3.01 ± 1.43	0.82 ± 0.02	0.58 ± 0.16
80	2.25 ± 0.2	0.76 ± 0.05	0.57 ± 0.09	2.49 ± 0.29	0.77 ± 0.03	0.57 ± 0.14
160	1.81 ± 0.33	0,68 ± 0.02	0.57 ± 0.08	1.98 ± 0.13	0.70 ± 0.06	0.56 ± 0.08
Mean value	2.13 ± 0.57	0.72 ± 0.06	0.58 ± 0.11	3.50 ± 0.72	0.78 ± 0.03	0.71 ± 0.2

Tab.1 Boron concentration rates, reached by cells after 4 and 18 h of treatment, in medium enriched with icreasing boron concentrations.
C_m= boron concentration in the medium
C_i $^{10}B_{tot}$= total boron uptaken by cells
C_i $^{10}B_{rel}$= boron released by cells
C_i $^{10}B_{ret}$= boron retained by cells

breaks, and the yields of such breaks are taken from Ottolenghi et al. (1995). In the present work, the model was extended to simulate cell survival, adopting the assumption of a one-to-one correlation between the average number of "lethal" aberrations (i.e., asymmetric chromosome exchanges such as dicentrics and rings) per cell and –logS, being S the surviving fraction, as suggested by Cornforth and Bedford (1987). As a preliminary approach, the effects of cell exposure to neutrons alone were reproduced simulating cell irradiation with 35 keV/micron protons, whereas neutron exposure of cells incorporating Boron was described simulating cell irradiation with a mixed field consisting of 35 keV/micron protons and 200 keV/micron alpha particles, assuming that low-energy Litium has a biological effectiveness not significantly different from high-LET alpha particles. In the case of (simulated) mixed field irradiation, 86% of the dose was attributed to alpha particles, whereas the remaining 14% was attributed to protons, according to experimental dosimetry measurements.

3. Results

Boron uptake as a function of BPA concentration and time of treatment

Total endocellular levels of ^{10}B uptaken by DHD cells evidenced a concentration and time dependent behaviour. Total boron rate values (i.e. total boron accumulated by cells on the medium boron concentration), following 4 h treatment, showed constant levels (mean value, 2.13 ± 0,57) at any studied concentration, while 18 h contact evidenced a 3.5 mean rate value with a progressive capture rate reduction (range 6.05 ± 0,47 - 1.98 ± 0,13) that, at the highest checked concentrations overlapped the value obtained after 4 h treatment (Tab. 1).

Analyses of ^{10}B released by cells as a consequence of external boron deprivation, harvesting and cell centrifugation, showed a remarkable washout of the previously accumulated compound, which was time and concentration independent and that lead to a retained boron fraction of less than 30% (Tab.1).

The mean rate of the retained fraction on the treatment medium concentration resulted in 0.58 ± 0.11 and 0.71 ± 0.2 respectively in case of 4 h and 18 h of contact time. As evidenced by data reported in table 1 higher rate values of retained boron were reached at the lower checked concentrations and for longer incubation times while, starting from 40 ppm boron enrichment, constant concentration and time independent rates were obtained. Intracellular boron levels as a function of the medium concentration after 4 and 18 h of contact times are reported in figure 1.

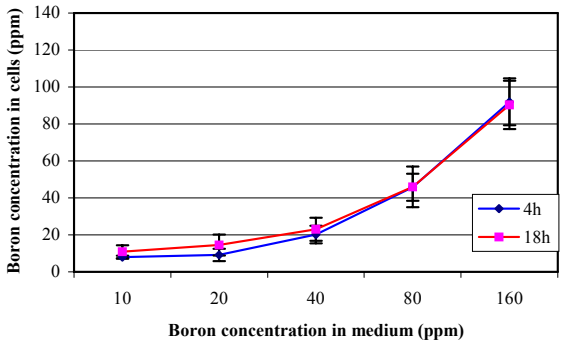

Fig.1 Intracellular boron concentration as a function of the concentration in the medium after 4 and 18 h of incubation time

Boron washout on cell suspensions as a function of temperature and time after BPA deprivation

A time and temperature dependent cellular ^{10}B efflux was evident when harvested cells suspensions are left in BPA free medium.
The constant boron elimination rate at 37 °C was 1,45 ± 0,06 h^{-1} in the first release hour and then decreased to 0,29 ± 0,15 h^{-1} in the two subsequent ones and to 1,1 ± 0,07 h^{-1} in the last observation time. Intracellular boron efflux studied at 4 °C showed, in the first 60', a constant elimination rate of 0,82 ± 0,17 h^{-1} that decreased to 0,23 ± 0,06 h^{-1} in the subsequent two hours, while no compound release was observed in the following studied intervals.

Boron washout on adherent cells as a function of temperature and time after BPA deprivation

As observed in case of cell suspensions, also adherent cells showed a time and temperature dependent ^{10}B release behaviour, as a consequence of boron enriched medium replacement with normal culture medium. The constant releasing rate in the first hour was 1,08 ± 0,5 h^{-1} and 0,67 ± 0,3 h^{-1} respectively for cells maintained at 37 °C and at 4 °C, while both rates reduced to 0,22 ± 0,08 and to 0,06 ± 0,03 in the next studied intervals. The intracellular concentration values were unmodified in the last interval time.

Boron washout in rat liver as a consequence of the organ perfusion

Data collected did not evidence a reduced intracellular boron concentration, following the organ perfusion at low temperature, neither in normal nor in neoplastic tissues.

Cell survival related to radiation dose exposure

The surviving fraction following *in vitro* thermal neutron irradiation in boron free medium plotted against the absorbed dose (Gy) is reported in figure 2.

The corresponding simulated values, obtained as described in section 2, are reported in figure 3, where the points represent simulated cell survival and the lines are fits to the experimental data, reported for comparison. For each simulation point, the statistical error is less than 5%. The agreement between simulations and data is satisfactory, especially for thermal-neutron irradiation of cells in corporating Boron.

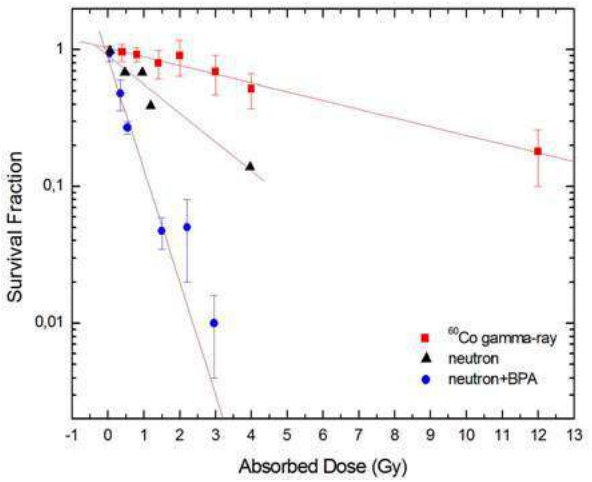

Fig. 2 Survival fraction of the DHD cells, irradiated with γ-rays from a ^{60}Co source (red squares), with thermal neutrons without boron treatment (black triangles) and with thermal neutrons after BPA treatment (blue circles)

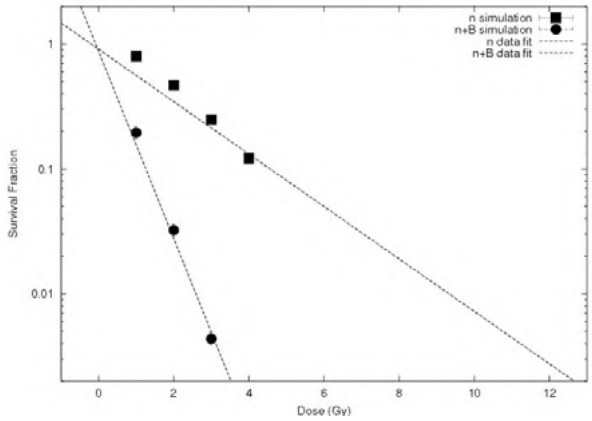

Fig. 3 Simulated cell survival following exposure to neutrons only and to neutrons plus Boron (squares and circles, respectively.
The error bars representing the simulation statistical errors are almost invisible because they are of the same size of the symbols). The corresponding experimental data fits (dashed lines) are also reported for comparison

4. Discussion and conclusions

BNCT management of diffused metastases, affecting explantable organs, can benefit, at the end of the established infusion time, of the boron carrier removal from the circulatory system, by means of the explanted organ perfusion. Experimental *in vitro* and *in vivo* studies can play an important role in assessing the extent and the kinetic of the intracellular boron release, in the absence of the external compound, thus giving important information to design the BNCT clinical applications.

Results of BPA uptake on the DHD cell line showed a remarkable accumulation rate (mean value: 2.13 ± 0,57 at 4 h; 3.5 ± 0,72 at 18 h) against gradient concentration which is function of the time of incubation. Nevertheless, the ^{10}B washout, following BPA deprivation, harvesting and centrifugation, lead to a severe, time and concentration independent, reduction of about 70% of the previously uptaken boron levels, suggesting that this is an unbound fraction exposed to diffusion processes.

Despite best accumulation rates (6,05 ± 0,47) were reached after 18 h of treatment in medium enriched with the lowest checked boron concentrations, stating the extent of the released fraction, these conditions were insufficient to cells for retaining therapeutic boron levels. Starting from 40 ppm, the endocellular ^{10}B retained was independent on the time of incubation, so having considered the lower BPA cytotoxicity with reduced times of contact (data not shown), 4 h incubation, in 80 ppm ^{10}B enriched medium, was the treatment of choice for kinetic release and survival studies.

Results of boron efflux, following BPA deprivation showed that cell suspensions, much more than adherent cells, were influenced to release the uptake boron, when kept in boron lacking medium. Moreover high temperature and time are favourable release factors. In every studied conditions, the constant of elimination rate was higher in the first hour of permanence, being the highest level (1,45 ± 0,06) the one reached by cell suspensions maintained at 37 °C.

Low temperature reduced boron loss of the first observation hour, keeping the elimination rates values constant in the subsequent studied times. Therefore, in case of neutron irradiation performed on cell suspensions, to reduce boron washout, it is highly recommendable to keep cells at 4 °C, being in this experimental conditions the constant of elimination rate reduced to 0,82 ± 0,17, thus keeping the retained boron fraction to about 25-30 ppm, which is a sufficient amount in order for BNCT to be successful and that experimentally resulted in a TD_{50} of 2,9 Gy.

The induction of clonogenic cell death was investigated also theoretically, applying a model/code of chromosome aberration induction purposely modified to reproduce the experimental irradiation conditions and to link the yield of asymmetric exchange-type aberrations to clonogenic cell death. Preliminary calculations, which need to be considered with caution due to the adopted assumptions (e.g. description of neutron plus Boron by means of alpha particles, and application of a one-to-one relationship between the yield of asymmetric exchanges and the log of the surviving fraction), are encouraging.

In vitro results show that the extracellular boron removal don't limit the therapeutic efficacy of the neutron treatment, although a relevant boronated compound loss, when adequate amounts of compound are delivered and when cells, in deprived medium, are kept at low temperature.

In vivo results don't evidence an endocellular boron decrease comparable to that obtained *in vitro*, following the organ perfusion, suggesting that the procedure can be performed without limiting the therapeutic efficacy.

References

Altieri, S., Bortolussi, S., Bruschi, P., Fossati, F., Vittor, K., Nano, R., Facoetti, A., Chiari, P., Bakeine, J., Clerici, A., Ferrari, C., Salvucci, O., 2006. Boron absorption imaging in rat lung colon adenocarcinoma metastases. J Phys: Conf Ser. 41(1), 123-126

Altieri, S., Bortolussi, S., Bruschi, P., Chiari, P., Fossati, F., Stella, S., Prati, U., Roveda, L., Zonta, A., Zonta, C., Ferrari, C., Clerici, A., Nano, R., Pinelli, T., 2008. Neutron autoradiography imaging of selective boron uptake in human metastatic tumours. Appl. Radiat. Isot. (in press)

Ballarini, F., Alloni, D., Facoetti, A., Mairani, A., Nano, R., Ottolenghi, A. 2007. Radiation risk estimation: modelling approaches for "targeted" and "non-targeted" effects. Adv. Space Res. 40, 1392-1400

Capala, J., Makar, M.S., Coderre, J.A., 1996. Accumulation of boron in malignant and normal cells incubated *in vitro* with boronophenylalanine, mercaptoborane or boric acid. Radiat. Res. 146, 554-560

Cornforth, M., Bedford, J., 1987. A quantitative comparison of potentially lethal damage repair and the rejoining of interphase chromosome breaks in low passage normal human fibroblasts. Radiat. Res. 111, 385-405

Dahlström, M., Capala, J., Lindström, P., Wasteson, A., Lindström, A., 2004. Accumulation of boron in human malignant glioma cells *in vitro* is cell type dependent. J. Neurooncol. 68, 199-205

Hsieh, C.H., Liu, H.M., Hwang, J.J., Wang, H.E., Kai, J.J., Chen, F.D., 2006. A simple model for quantification of the radiobiological effectiveness of the $^{10}B(n,\alpha)^{7}Li$ capture reaction in BNCT. Appl. Radiat. Isot. 64(3), 306-314

Ottolenghi, A., Merzagora, M., Tallone, L., Durante, M., Paretzke, H., Wilson, W., 1995. The quality of DNA double-strand breaks: a Monte Carlo simulation of the end-structure of strand breaks produced by protons and alpha particles. Radiat. Environ. Biophys. 34, 239-244

Suzuki, M., Sakurai, Y., Masunaga, S., Kinashi, Y., Nagata, K., Maruhashi, A., Ono, K., 2006. Feasibility of boron neutron capture therapy (BNCT) for malignant pleural mesothelioma from a viewpoint of dose distribution analysis. Int. J. Radiat. Oncol. Biol. Phys. 66(5), 1584-1589

Suzuki, M., Sakurai, Y., Hagiwara, S., Masunaga, S., Kinashi, Y., Nagata, K., Maruhashi, A., Kudo, M., Ono, K., 2007. First attempt of Boron Neutron Capture Therapy (BNCT) for hepatocellular carcinoma. Jpn. J. Clin. Oncol. 37(5), 376-381

Zonta, A., Prati, U., Roveda, L., Ferrari, C., Zonta, C., Zonta, S., Clerici, A.M., Pinelli, T., Fossati, F., Altieri, S., Bortolussi, S., Bruschi, P., Nano, R., Barni, S., Chiari, P., Mazzini, G., 2006. Clinical lessons from the first applications of BNCT on unresectable liver metastases. J Phys: Conf Ser. 41, 484-95

Wittig, A., Malago, M., Collette, L., Huiskamp, R., Bührmann, S., Nievaart, V., Kaiser, G.M., Jöckel, K.-H., Schmid, K.W., Ortmann, U., Sauerwein, W.A., 2008. Uptake of two ^{10}B-compounds in liver metastases of colorectal adenocarcinoma for extracorporeal irradiation with boron neutron capture therapy (EORTC trial 11001). Int. J. Cancer. 122, 1164-1171

Radiobiological Studies in a Human Cell Line of Undifferentiated Thyroid Cancer (UTC) for BNCT

MA Dagrosa[a,e], M Crivello[a], S Thorp[a], M Perona[a,e], E Pozzi[a], M Casal[b], R Cabrini[a], S Kahl[c], G Juvenal[a,e], M Pisarev[a,d,e].

[a]*Comisión Nacional de Energía Atómica, Av. del Libertador 8250, (1429) Cdad. de Buenos Aires, Argentina*
[b]*Instituto de Oncología Angel H. Roffo, Av. San Martín 5481, (1417) Cdad. de Buenos Aires, Argentina*
[c]*Dept. of Pharmaceutical Chemistry, University of California, San Francisco, USA.*
[d]*Dept. of Biochemistry, School of Medicine, University of Buenos Aires, Argentina.*
[e]*CONICET, Avda. Rivadavia 1917, (1033) Cdad. de Buenos Aires, Argentina*

Abstract

In previous studies we demonstrated the efficacy of BNCT for the treatment of UTC using ^{10}BPA (p-borophenylalanine) alone and combined with ^{10}BOPP (2,4-bis (α,β-dihydroxyethyl)-deutero-porphyrin IX). In the present work we evaluated in vitro the mechanisms of damage induced by BNCT by cytokinesis block micronuclei assay (CBMN) and by the cell fraction survival using a colorimetric assay of viability (MTT). We also calculated the relative biological effectiveness factor (RBE) of the neutron beam and the compound biological effectiveness (CBE) values for BPA and BOPP. Exponentially growing human cells of UTC (ARO) were distributed into the following groups: 1) BPA (10 ppm ^{10}B) + neutrons; 2) BOPP (10 ppm ^{10}B) + neutrons; 3) neutrons alone; 4) gamma-rays (^{60}Co). The cells were irradiated in the thermal neutron beam of the RA-3 (flux= 7.5 10^9 n/cm^2 sec). The irradiations were performed during different times in order to obtain total physical doses between 1-5 Gy (±10%). The frequency of micronucleated binucleated UTC cells and the number of MN per micronucleated binucleated cells showed a dependent dose relationship until around 2 Gy. The response to gamma rays was significantly less than the other treatments. The irradiation with neutrons alone and neutrons + BOPP showed curves that didn't differ significantly and showed less DNA damage than neutrons + BPA. A decrease in the survival fraction as a function of the physical dose was observed for all the treatments. We also observed that neutrons and neutrons + BOPP did not differ significantly and that BPA is the more effective compound. The RBE and CBE factors calculated from CBMN and MTT assays, respectively, gave the following values: beam RBE: 4.4 ± 1.1 and 2.4 ± 0.6; CBE for BOPP: 8.0 ± 2.2 and 2.0 ± 1; CBE for BPA: 19.6 ± 3.7 and 3.6 ± 1.3. These values represent the first experimental values obtained for the RA-3 in a biological model and will be useful for future dosimetric experimental studies of the application of BNCT to UTC.

Keywords: thyroid cancer, micronuclei, CBE, RBE

1. Introduction

Undifferentiated thyroid carcinoma (UTC) is a very aggressive solid tumor which represents between 5 and 10% of total thyroid cancers (Ain, 1998). BNCT has been proposed as an option for the treatment of this pathology since it lacks an effective treatment (Pisarev *et al*, 2005).

In previous studies we have shown that the cell line of human undifferentiated thyroid carcinoma (ARO) has a selective uptake of boronophenylalanine (^{10}BPA), both in vitro and after being transplanted to NIH nude mice (Dagrosa *et al*, 2002; Dagrosa *et al* 2003). Also the application of BNCT using BPA showed a complete halt of tumor growth in 100% of the animals and a complete histological cure in 50% of the mice bearing tumors smaller than 50 mm^3 (Dagrosa *et al*, 2003).

Another boron compound, the tetrakis –carborane carboxylate ester of 2,4 -bis-(α,β-dihydroxythyl)-deutero-porphyrin IX (BOPP) was studied in this animal model. The results showed that BOPP alone was not selectively accumulated by the tumor.

However, the combination of BOPP and BPA administration duplicated the amount of boron in the tumor compared to BPA alone (Dagrosa *et al*, 2005). The posterior irradiation of these animals improved significative the therapeutic response (Dagrosa *et al*, 2007).

The radiation can kill the cell by apoptosis or mitotic catastrophe. This type of death results of DNA damage non repaired o misrepaired. Little is

known about the mechanisms that play a role in the tumor damage produce by BNCT. The DNA molecule is the principal biological target that conduces to the cell death. The high LET radiation produces mostly DNA double strand break (DSBs) and is common to observe chromosomal aberrations and its citoplasmatic derivates the micronuclei (MN) (Norppa and Falck, 2003).

The dosimetric calculations in BNCT are not simple. To express the total physical absorbed dose received in the tumor in terms which permit the comparison with the conventional treatment (x-rays or gamma) the boron component has to be multiplied by compound biological effectiveness (CBE) factor. CBE is specific for different tissues and for different boron compounds and depends on a broad spectrum of variables (Coderre and Morris, 1999).

In the present work we have study the DNA lesions produce by BNCT. We also have calculated the beam RBE of RA-3 and the CBE values for BPA and BOPP in a human cell line of UTC from two different endpoints: the survival fraction and the induction of micronuclei. These factors will be used in future treatments of patients.

2. Materials and Methods

Cell line: The UTC cell line (ARO) kindly provided by Dr. G Juillard (University of California, Los Angeles) was cultured in RPMI 1640 medium supplemented with 10% bovine fetal serum (GIBCO; Invitrogen, Basel Switzerland) in a 5% CO_2-95% air atmosphere at 37º C.

Experimental design*:* The cells were seeded in an amount of 200,000-400,000 and grown in flasks with area of 25 cm^2 one day before irradiation. The exponentially growing cells were irradiated in the thermal neutron beam of RA-3 (Ezeiza Atomic Center) which has a flux of 7.5 10^9 n/cm^2 sec. Irradiations using a source of ^{60}Co with a dose rate of 1Gy/min were also performed on these cells. The irradiations in the reactor were performed during different times (at the full power of 8 MW) in order to obtain total absorbed doses between 1 and 5 Gy with an estimated uncertainty of 10%.

The cells were distributed into the following groups: 1) BPA + neutrons: the cells were incubated with BPA at a dose of 10 ppm of ^{10}B (0.925M) during 12 hr before irradiation; 2) BOPP + neutrons: the cells were incubated with BOPP at a dose of 10 ppm of ^{10}B (33μg/mL) during 16 hr before irradiation; 3) neutrons alone; 4) gamma rays. Control groups were performed by incubating the cells with boron compounds for the same periods of time but without irradiation.

Stock solutions of BOPP of 10mg/mL in 0.9% isotonic NaCl were prepared and were stored in darkness at 4ºC for no more than 24 h before administration. Boron concentration in each flask at the end of incubation was checked by inductively coupled plasma optical emission spectroscopy (ICP-OES) instrument (Perkin-Elmer, Norwalk, CT).

CBMN assay: For the CBMN assay 4 hr after treatments the cell culture medium was removed, the cells washed and placed in BPA-free culture medium. Cytochalasin B (Sigma, St Louis, MO) was added at a final concentration of 3μg/mL and the cells were grown for 48 hr for recovery of binucleated cells. The cells were then harvested by trypsinization, rinsed and submitted to mild hypotonic treatment. The centrifuged cells were placed on dry slides. After the slides were fixed with cold methanol (30 min) and one day later they were stained with Giemsa for 10 min. For each experimental point 1000 binucleated (BN) cells with well preserved cytoplasm were scored. MN were identified according to the criteria of Caria *et al* (1995) using a 500X magnification on a light microscope. Two indices were evaluated, number of micronuclei per binucleated cell (MN/BN), which represents the average number of MN per BN cell, and frequency of micronucleated binucleated cells (%MNBN) which represents the fraction of cytokinesis blocked (BN) cells with MN regardless of the number of MN per BN cell .

MTT assay: In these studies 2000 cells/well were plated in 96 well microplate with 200 μL RPMI containing 10% FBS. Following 7 days incubation at 37º C the culture medium was changed and 20μL of 3-(4,5-dimetiltiazol-2-il)-2,5-difeniltetrazolium bromuro MTT (Sigma M-2128) 0,5% P/V in PBS was added to each well. After 4 hr incubation at 37ºC the medium was removed and 200 μL of dimethylsulfoxide (DMSO) was added to solubilize the MTT- formazon product. The absorbance was reader at wavelength 540 nm.

3. Results and Discussion

The results of the induction of micronuclei in ARO cells under different treatments of irradiation are shown in Figures 1 and 2. In Figure 1 the number of MN per binucleated ARO cell (MN/BN) as a function of the physical dose is observed. The MN/BN is an important indicator of the degree of chromosomal lesions per cell. An increase in the MN/BN up 2 Gy was observed in the cells treated by neutrons and neutrons plus boron (n_{th}; n_{th} + BOPP; n_{th} + BPA). After 2 Gy approximately a kind of saturation was shown. The DNA damage produced by BNCT was significantly greater than the damage by gamma irradiation. Neutrons alone and neutrons plus BOPP did not show significative difference. On the other hand BPA was the boron compound more effective with a peak of 2 MN per cell. Figure 8 shows the frequency of micronucleated binucleated UTC cells (%MN.BN) as a function of the total physical dose. This index indicates the extension of DNA damage. The saturation in the groups irradiated with neutrons alone o neutrons plus boron was achieved before, indicating that to higher doses increase the magnitude of cellular damage but not the proportion of cells with chromosomal lesions.

The results of the surviving cell fraction as a function of the total physical dose are shown in Figure 3. The neutron irradiation of the cells showed a decrease in the cell viability. This effect was greater in the cells incubated with BPA. Neutrons alone and neutrons plus BOPP did not show significative difference.

The dose-response curves performed for the induction of micronuclei showed that both low and high LET radiation can be fitted with a sigmoidal model. One explanation for this model could be that for low doses of radiation the damage cells have only a chromosomal fragment and this has the probability of became in one MN but to high doses the cells have one o more fragment and these can be incorporated in one MN, this fact could explain the depression in the curves of micronuclei.

The beam RBE and the CBEs for BPA and BOPP were calculated from Figures 1, 2 and 3 using the following formulae (Coderre and Morris, 1999):

RBE= Dose X-rays/ Dose neutron

CBE Dose X-rays = (Dose beam) (RBE) + (Dose_^{10}B) (CBE)

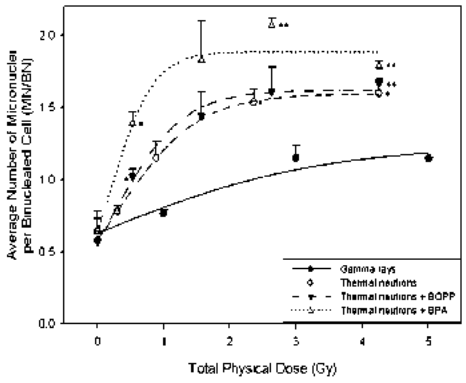

Figure 1. Average number of micronuclei per binucleated cell (MN/BN) in ARO cells under different treatments. Results are expressed as means ± SEM from two independent experiments. ** $p < 0.005$ for n_{th} + BOPP; n_{th} + BPA vs. γ. * $p < 0.05$ for n_{th}; n_{th} + BOPP; n_{th} + BPA vs γ

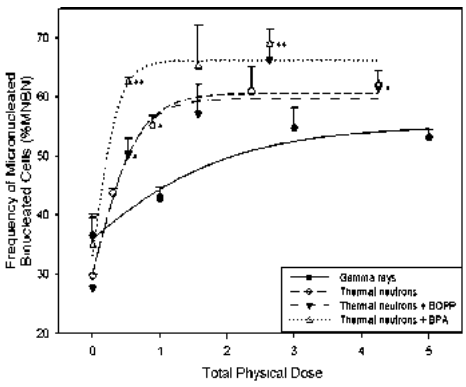

Figure 2. Frequency of micronucleated binucleated ARO cells (%MN.BN) as a function of the total physical dose. Results are expressed as means ± SEM from two independent experiments. ** $p < 0.005$ for n_{th} + BPA vs. γ. * $p < 0.05$ for n_{th}; n_{th} + BOPP; n_{th} + BPA vs. γ

The experimental values obtained are shown in Table 1. The beam RBE values were between 2.6 ± 0.7 and 4.4 ± 1.1 for CBMN assay. The survival fraction (MTT) as endpoint showed values of 2.3 and 2.4 ± 0.6. These data represent the first experimental values of relative biological effectiveness for the neutron beam of RA-3 reactor. The experimental calculated values for CBEs for BPA and BOPP were higher for the MNCB assay than the MTT assay.

The obtained values for BPA were between 12.2 ± 2.3 and 19.6 ± 3.7 for the DNA damage and approximately 3.6 ± 1.3 for surviving fraction. On the other hand the CBEs calculated for BOPP were between 2.9 ± 1.1 and 8.0 ± 2.2 when the endpoint was DNA damage and around 2.0 ± 1.0 when the endpoint was the survival fraction.

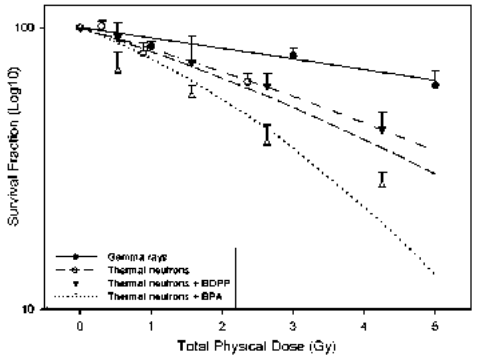

Figure 3. Survival of ARO cells under the different treatments. Data are fitted with a quadratic-linear model. Each point is the average of 6-8 wells ± SEM of two independent experiments.

Although the values obtained for RBE and CBE were higher when the endpoint studied was the DNA damage we found a good correlation between the induction of MN and the survival fraction (R=0.95; result not showed). In these studies we did not discriminate between MN originated from acentric fragment from those produce from whole chromosome. This fact could explain the different values obtained for the different endpoint. On the other hand the values obtained studying the viability from MTT assay agree with the values previously obtained in the same cell line irradiated in the neutron beam of MIT evaluating the viability whit the colony forming assay (Dagrosa *et al*, 2006).

4. Conclusions

The curves doses response performed in this work contribute to the knowledge of mechanism of cell damage/death produced by BNCT. We showed that both citotoxic and genotoxic effects produce in the cells treated by BNCT are different and higher of those produce in cell irradiated with the gamma irradiation. The results provide values of RBE for neutron beam of RA-3 and CBEs for BPA and BOPP in a human cell line of UTC that should be useful for dosimetric calculation in the application of BNCT to the treatment of this pathology.

Table 1. Experimental RBE and CBEs for UTC

Parameter	Endpoint	Beam RBE	CBE BOPP	CBE BPA
MN/BN	0.8	2.6 ± 0.7	4.6 ± 1.1	12.2 ± 2.3
	1.2	4.4 ± 1.1	8.0 ± 2.2	19.6 ± 3.7
%MN.BN	43.4	2.6 ± 0.7	2.9 ± 1.1	12.3 ± 2.3
	52.0	4.4 ± 1.1	5.1 ± 1.9	17.8 ± 3.6
Survival fraction (MTT)	65.6	2.4 ± 0.6	2.0 ± 1.0	3.5 ± 1.2
	75.8	2.3 ± 0.6	1.9 ± 1.0	3.7 ± 1.3

References

Ain KB. Anaplastic thyroid carcinoma: behavior, biology, and therapeutic approaches. Thyroid 8: 715-726, 1998.

Caria H, Chaveca T, Laires A, *et al*. Genotoxicity of quercentin in the micronucleus assay in mouse bone marrow erythrocytes, human lymphocytes, V79 cell line and identification of kinetochore-containing (CREST staining) micronuclei in human lymphocytes. Mutat Res. 343: 85-94, 1995.

Coderre JA and Morris GM. The radiation biology of boron neutron capture therapy. Radiat. Res. 151:1-18, 1999.

Dagrosa M, Chung Y, Riley K, *et al*. Compound biological effectiveness (CBE) factors in human undifferentiated thyroid cancer (UTC). In: "Advances in Neutron Capture Therapy, Proceedings of 12th International Congress on Neutron Capture Therapy". Y. Nakawaga, T. Kobayashi and H. Fukuda. Kagawa, Japan. pp 157-160, 2006.

Dagrosa MA, Thomasz L, Longhino J, *et al*. Optimization of the application of boron neutron capture therapy (BNCT) to the treatment of undifferentiated thyroid cancer (UTC). Int. J. of Radiat. Oncol. Biol. Phys 69 (4): 1059-1066, 2007.

Dagrosa MA, Viaggi ME, Jiménez Rebagliati R, *et al*. Biodistribution of boron compounds in an animal model of undifferentiated thyroid cancer for boron neutron capture therapy. Molecular Pharmaceutics 2: 152-156, 2005.

Dagrosa MA, Viaggi ME, Kreimann EL, *et al.* Selective uptake of p-borophenylalanine by undifferentiated thyroid carcinoma for boron neutron capture therapy. Thyroid 12: 7-12, 2002.

Dagrosa MA, Viaggi ME, Longhino J, *et al.* Experimental application of boron neutron capture therapy (BNCT) to undifferentiated thyroid carcinoma (UTC). Int. J. Radiat. Oncol. Biol. Phys. 57: 1084-1092, 2003.

Norppa H and Falck G.. What do human micronuclei contain?. Mutagenesis. 18(3):221-223, 2003.

Pisarev M, Dagrosa MA, Juvenal G. Application of boron neutron capture therapy too the treatment of anaplastia thyroid carcinoma: current status and future perspectives. Current Opinion Endocrinol Diabetes 12: 352-355, 2005.

Viaggi ME, Dagrosa MA, Gangitano. D, *et al*. A new animal model for human undifferentiated thyroid carcinoma in nude mice. Thyroid 13: 529-536, 2003.

Monitorisation of BNCT efficiency using biochemical oxidative stress and apoptosis parameters

Maria Iuliana Gruia, Valentina Negoita, Monica Vasilescu, Dumitru Barbos*, Rodica Anghel

Institute of Oncology Bucharest Romania
**Institue for Nuclear Research Pitesti-Romania*

Boron neutron capture therapy is based on the selective delivery of boron-10 to tumor cells. Approximately 10^9 ^{10}B atoms per tumor cell are necessary to produce four to five α particles per cell, but studies of radiation-induced apoptosis suggest that BNCT also may be cytotoxic via other mechanisms so that the required number of ^{10}B atoms actually may be less. The aim of our paper is to find new biochemical mechanisms such us the oxidative destruction involved in tumoral cell cytotoxicities mediated by oxygen reactive species.

Materials and methods RS1 hepatoma –bearing rats were given single i.p. injection of 30 mg ml^{-1} of a BPA: fructose 1.0:1.1 molar solution. Mice were anaesthesiated and irradiated 2 hours with a $1.655*10^9$ n / cm^2 epithermal fluency beam. Tumor, blood, and liver tissue sample were removed and assayed for boron biodistribution, oxidative stress and apoptosis induction.

Results Our results show preferential capture of BPA at tumoral level with a maximum value at 3 hours after the administration., the lipid peroxides level measured in blood is increasing two times at the hepatoma bearing rats than in normal control, also the caeruloplasmin Cu-oxidase activity growth from 168 I.U. to 330 I.U., the albuminic thiol-groups are decreasing from 267 μmol/l at 107 μmol/l , at at liver level of tumor bearing rats sacrificed one hour after the irradiation can be observed an increase of apoptosis rate, suggesting the implication of free radicals in the apoptotic pathway.

Conclusions The BPA administration possibly induce methabolic pathways wich involves the oxigen consumption, and after the irradiations the cytotoxicities is done by oxigen free radical production The biochemical parameters of oxidative stress can be used in monitoring the evolution of hepatoma, the modifications after BPA administration and the irradiation effects.

Bystander effect induced mutagenicity in HPRT locus of CHO cells following BNCT neutron irradiation: characteristics of Point mutations by sequence analysis

Yuko Kinashi[a], Minoru Suzuki[a], Shinichiro Masunaga[a], Koji Ono[a]

[a] *Research Reactor Institute, Kyoto University, Kumatori-cho, Sennan-gun, Osaka, Japan*

Abstract

To investigate bystander mutagenic effects induced by alpha particles during boron neutron capture therapy (BNCT), we mixed cells that were electroporated with borocaptate sodium (BSH), which led to the accumulation of ^{10}B inside the cells, and cells that did not contain the boron compound. BSH-containing cells were irradiated with alpha particles produced by the $^{10}B(n,\alpha)^{7}Li$ reaction, whereas cells without boron were only affected by the $^{1}H(n,\gamma)^{2}H$ and $^{14}N(n,\rho)^{14}C$ reactions.

The lethality and mutagenicity measured by the frequency of mutations induced in the hypoxanthine-guanine phosphoribosyltransferase (HPRT) locus were examined in Chinese hamster ovary (CHO) cells irradiated with neutrons (Kyoto University Research Reactor: 5 MW). Neutron irradiation of 1:1 mixtures of cells with and without BSH resulted in a survival fraction of 0.1, and the cells that did not contain BSH made up 99.4% of the resulting cell population. Using multiplex polymerase chain reactions (PCRs), molecular structural analysis indicated that most of the mutations induced by the bystander effect were point mutations and that the frequencies of total and partial deletions induced by the bystander effect were less than those induced by the original neutron irradiation.

The types of point mutations induced by the bystander effect of BNCT were analyzed by cloning and sequencing method. Base substitutions were 65.5%, deletions were 27.5% and insertions were 7%. Sequence analysis of base substitution shows that trasversions and transitions occurred 64.7% and 35.3%, respectively. The ratio of G:C→T:A transversion induced by 8-oxo-guanine in DNA was 2/34 of base substitution mutants. These characteristic mutations of bystander effects induced by alpha particles in BNCT were different from those typical of γ-ray radiation.

Keywords: α-particle, neutron, BSH, HPRT, point mutation

1. Introduction

We previously described the mutagenicity of thermal neutrons in CHO cells and presented evidence for the increased mutagenicity of thermal neutrons in the presence of boron (Kinashi et al., 1997 and 2000.). In BNCT experiments, boron was located both inside and outside the cells. Clinically, one problem associated with BNCT is represented by the potential mutagenic effects of the therapy on the normal cells that do not take up the boron compounds, but are located near the boron-containing tumor cells. In this study, we investigated the mutagenic effects of this therapy on cells that did not contain boron (no-boron cells), but were located near cells that contained ^{10}B following electroporation with BSH (BSH-electroporated cells). The characteristics of mutants induced by the bystander effect following BNCT neutron radiation was analyzed in c-DNA of nine exons located in HPRT locus.

2. The experiments of bystander effect in BNCT

Cell culture and electroporation

CHO K-1 (wild-type) cells were cultured at 37 °C in a humidified 5% CO_2 atmosphere in Eagle's a-minimal essential medium (MEM). CHO cells exponentially growing in MEM were trypsinized and cell suspensions containing 10 ppm BSH were

placed into the chamber (maximum effective volume of 0.8 ml) of a Gene Pulser system for electroporation (Bio-Rad Laboratories). The cells were washed twice with PBS after electroporation and the medium was replaced with MEM without the boron-containing compound. After electroporation, the viable cells were counted. The no-boron cells were also trypsinized and counted, and the BSH-electroporated cells were placed in a flask containing no-boron CHO cells at a cellular ratio of 1:1. After confirming that the cells were attached to the flask, the cells were irradiated at room temperature with neutrons from a reactor at Kyoto University. The total absorbed dose resulting from thermal or epithermal neutron irradiation was calculated by the sum of the absorbed doses. The details of the calculation method were described previously (Kobayashi et al., 1982., Kitao et al., 1975.).

HPRT mutation assays

To determine the mutant frequencies, each irradiated culture containing at least 10^6 cells was incubated in non-selective medium for 7 to 9 days to allow phenotype expression. Then, 2 x 10^5 cells were added to each of twenty 100-mm plastic dishes containing 5 mg/ml 6-thioguanine, incubated for 10 days, and the mutant colonies were counted. The mutant frequencies are expressed as the number of resistant colonies divided by the total number of viable cells, which was determined using the cloning efficiency at the time of selection.

3. Analysis of the molecular structure of the HPRT mutations and the types of point mutations using direct sequencing of PCR fragment

In the mutation analysis assay, neutron irradiation at the applied fluence resulted in a cellular survival fraction of 0.1. At this fluence, the survival fractions of the no-boron cells and the BSH-electroporated cells were 0.7 and 0.004, respectively. The cell population of the samples comprised 99.4% no-boron cells and 0.6% BSH-electroporated cells after neutron irradiation, The DNA extraction procedure has been previously described in detail (Kinashi et al., 1995).

Structural analysis of the HPRT gene was carried out using a modified multiplex PCR amplification technique. Three sets of PCRs were carried out to amplify exons 2, 3, 7/8, and 9; exons 4, 5, and 6; and exon 1. The molecular structures of the HPRT genes were divided into three categories: no change (normally sized exons 1 through 9 were present), partial deletions (the absence of between one and eight of the exons as revealed by PCR analysis), total deletion (all nine HPRT exons were missing). Fig. 1 shows the molecular structure patterns of HPRT mutations.

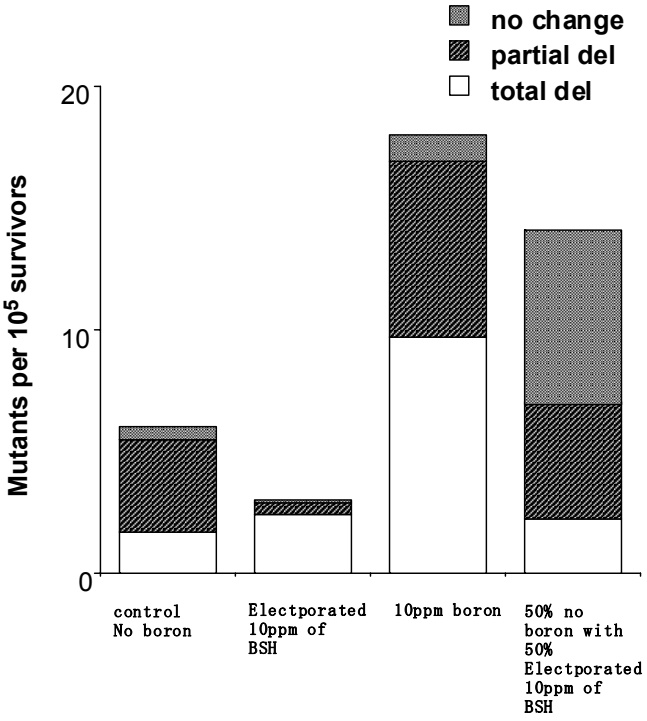

Fig.1. The molecular structure patterns of HPRT mutations. Total deletion represents all nine HPRT exons were missing. Partial deletion represent the absence of between one and eight of exons. No change means point mutation that normally sized exons one through nine were present

The molecular nature of the point mutations was analyzed by the direct sequence of PCR fragment of exon 1 and exon 9. Tables 1 and 2 represent the classes and various base substitutions induced by the bystander effect of BNCT.

Table 1. Types of point mutation induce by BNCT bystander effect

Types	BNCT Bystander	γ -ray Irradiation
Base substitution	65.5%	62%
Deletions	27.5%	30%
Insertions	7%	8%

Table 2. Patterns of base substitution

	BNCT Bystander	γ -ray Irradiation
Transition		
G:C→A:T	4	6
A:T→G:C	8	1
Total	12	7
(%)	35.3%	31.8%
Transversion		
G:C→T:A	2	10
G:C→C:G	5	4
A:T→C:G	0	1
A:T→T:A	15	0
Total	22	15
(%)	64.7%	68.2%

4. Conclusions

Due to the bystander effect, mutations were induced in the cells located near the BSH-containing cells. These mutants were not irradiated directly by α–particles. Molecular structural analysis indicated that most of the mutations induced by the bystander effect (the 4th bar in the figure) were point mutations and the frequencies of total and partial deletions induced by the bystander effect were less than those induced by the original neutron irradiation (the third bar in the figure). The cloning and sequencing analysis showed that the types of point mutations induced base substitutions were 65.5%, deletions were 27.3% and insertions were 7%.

The characteristics of mutation induced BNCT-bystander effect were similar to those typical of γ -ray-induced mutagenesis (Grosovsky et al., 1988 and Nohmi et al., 2005).

The main feature of ionizing radiation-induced base substitution pattern is a predominant of G:C→ T:A transversion. This mutation is induced by 8-oxo-guanine in DNA (Kasai et al., 1993) . It is noticed that p53 oncogene in lung cancer displays G:C → T:A transversion (Iggo et al., 1990). Our results showed that the ratio of G:C → T:A transversion induced by 8-oxo-guanine in DNA was 2/34 of base substitution mutants.

These results suggested that in BNCT the mutations caused by the bystander effect and those caused by γ -ray irradiation are induced by different mechanisms.

Acknowledgement

This study was supported by a Grant-in-Aid for Scientific Research from the Ministry of Education, Culture, Sports, Science and Technology of Japan.

References

Kinashi Y, Masunaga S, Takagaki M, Ono K. 1997. Mutagenic effect at HPRT locus induced in Chinese hamster ovary cells by thermal neutrons with or without boron compound. Mutat. Res.377, 211-215.

Kinashi Y, Sakurai Y, Masunaga S, Suzuki M, Takagaki M, Akaboshi M, Ono K. 2000. Molecular structure analysis of HPRT mutations induced by thermal and epithermal neutrons in Chinese hamster ovary cells. Radiat. Res. 154, 313-318.

Kobayashi T, Kanda K. Analytical calculation of boron-10 dosage in cell nucleus for neutron capture therapy. 1982. Radiat.Res. 91,7 7-94.

Kitao K. A method for calculating the absorbed dose near-interface from $^{10}B(n, \alpha)^{7}Li$ reaction. 1975. Radiat. Res. 61, 204-315.

Kinashi Y, Nagasawa H, Little JB. Molecular structure analysis of 417 HPRT mutations induced by restriction endonucleases in Chinese hamster ovary (CHO) cells. 1995. Mutat. Res. 326,83-92.

Grosovsky AJ, DE Boer JG, DE Jong PJ, Drobetsky EA, Glickman BW. Base substitutions, frameshifts, and small deletions constitute ionizing radiation-induced point mutations in mammalian cells. 1988. Proc.Natl.Acad.Sci.USA. 85,185-188.

Nohmi T, Masumura K. 2005.Molecular nature of intrachromosomal deletions and base substitutions by environmental mutagens. Environ.Mol.Mutagen. 45, 150-161.

Kasai H, Chung MH, Yamamoto F, Ohtsuka F, Laval J, Groolman AP, Nishimura S. 1993. Formation, inhibition of formation, and repair of oxidative 8-hydroxyguanine DNA damage. Basic.Life.Sci. 61, 257-262.

Iggo R, Gatter K, Bartek J, Lane D, Harris AL. 1990. Increased expression of mutant forms of p53 oncogene in primary lung cancer. Lancet. 335, 675-679.

Accumulation of ^{131}I-BSH in melanoma B-16 and surrounding tissues of mice following different methods of compound administration

S.N. Koryakin, V.A. Yadrovskaya, A.P. Baranov, E.V. Isaeva, S.E. Ulianenko

Medical Radiological Research Centre, Obninsk, Russia

The heightened attention is recently given to combined application of BNCT and fast neutron therapy. The local delivery of significant boron amount to tumour is a primary problem both for BNCT and for the mixed therapy. Depending on tumour localization it is reasonable to use various methods of compounds administration: intravenous, intra-arterial, intratumoral (into metastases), and pricking around the tumour zone. Not only concentration of ^{10}B in tumour tissues but also the degree of boron accumulation in tumour cells is important for the effective realization of BNCT. In this regard, the purpose of the research was to study distribution of sodium mercaptododecaborate, labeled with radioactive iodine (^{131}I-BSH), in melanoma B-16 and surrounding tissues following various methods of compound administration: intraperitoneal, single and double intratumoral and also under tumour administration. The ratio between accumulation of ^{131}I-BSH in tumour cells and intercellular space depending on method of compound administration was also studied.

The studies were carried out on male C_{57}BI/6 mice with melanoma B-16 subcutaneously implanted in hind leg. ^{131}I-BSH (0.1 ml) was administrated into tumour (single and double) and under tumour with 0.15 MBq radioactivity. Content of the labelled compound in tumour and surrounding tissues (blood, skin, muscle) was measured in 15 min, 30 min, 1 h and 3 h after the administration by the radioactivity level of decapitated under narcosis animals. The intraperitoneal (0.2 ml, 0.3 MBq) and single intratumoral (0.1 ml, 0.15 MBq) administrations of ^{131}I-BSH were performed for studies of cellular and intercellular accumulation of the compound in tumour tissue. The tumour was removed from the hind leg in 3, 6 and 12 h (after intraperitoneal administration) and in 0.5, 1 and 2 h (after intratumoral administration). Then it was comminuted and trypsinized at constant mixing (37 °C, 15 min). The cellular suspension was centrifuged for 15 min at 2000 r/min. The supernatant and the sediment were selected in tubes for radioactivity measuring.

The studies of ^{131}I-BSH distribution in melanoma B-16 and surrounding tissues by different methods of compound administration showed that the high content of ^{131}I-BSH in the tumour was reached in all cases. The most compound accumulation was observed in 1 h after administration. The percentage of administrated ^{131}I-BSH per 1 g of the tumour were 11.60±1.68 % and 11.26±0.88 % for single and double intratumoral administration, respectively, and 10.69±2.54 % for administration under tumour. In this case the ratio of radioactivity in melanoma B-16 and surrounding tissues was more than 3 for majority of mice.

The study of ^{131}I-BSH accumulation in tumour cells showed considerably larger compound accumulation in intercellular space (65.3% and 63.0%) in comparison with the cellular content (34.7% and 37.0%) in 3 and 6 h after intraperitoneal administration. The ratios became identical in 12 h. There were approximately equal compound accumulations in intercellular space and tumour cells during the study (0.5-2 h) at single intratumoral administration of ^{131}I-BSH.

The results of studies allow to consider the intratumoral administration of sodium mercaptododecaborate to be a perspective for combined application of neutron capture and fast neutron therapy.

The researches were supported by the Russian Federation President Grants Council (grant № МК-4562.2007.7) and the International Science and Technology Center (ISTC) (project № 3437).

Molecular targeting of CD44 for Mesothelioma

Chun-Man Lee[1,2], Hitoshi Fujii[2], Nagako Sougawa[1], Hiroshi Komoda[1], Akifumi Matsuyama[1], Yasufumi Kaneda[3], Yoshiki Sawa[1,2]

[1] *Medical Centre for Translational Research, Osaka University Hospital,*
[2] *Department of Surgery, and* [3]*Division of Gene Therapy Science,*
Osaka University Graduate School of Medicine, Osaka, JAPAN

Abstract

A novel BSH compound has been developed with the proteoglycan Hyaluronan (HA) for the treatment of Malignant Pleural Mesothelioma (MPM) by BNCT. On the cell surfaces, MPM cells expressed a large amount of CD44, one of major receptor of HA. The Hemagglutinating Virus of the Japan Envelope (HVJ-E) was also utilized as vehicle of ^{10}B. The new BSH compound has a high affinity and kept a high concentration of ^{10}B in MPM cells. These results suggest that the targeting of CD44 with HA represents a potentially useful strategy for BNCT of Mesothelioma.

Keywords: Mesothelima, Hyaluronan, CD44, Hemagglutinating Virus of Japan Envelope (HVJ-E)

1. Introduction

Malignant pleural mesothelioma (MPM) is an aggressive and refractory tumor caused by exposure to asbestos. The current therapy for MPM is multidisciplinary; surgery, chemotherapy, and radiotherapy. However, surgery (extrapleural pneum onectomy) is limited to locally advanced MPM. Chemotherapeutic regimens with CDDP and Pemetrexed have resulted in an improved tumor response, but the median survival is still only 12 months from the date of diagnosis. The use of radiotherapy, including intensity-modulated radio therapy (IMRT), is limited because the extent of the tumor requires large fields and it is impossible to administer tumoricidal doses without injuring the adjacent lung and mediastinal organs.[1, 2] BNCT could be a breakthrough strategy to treat MPM, because it is suitable for the treatment of diffuse and invasive tumor.[3, 4] However, the success of BNCT depends on the selective delivery of ^{10}B–atoms to tumor cells to complement the attenuation of thermal neutron.

CD44 has been used as a focus for the molecular targeting of MPM, a large amount of CD44 is expressed on MPM cells.[5, 6] HA is one of the major ligands of CD44, and possesses the various biological functions. It influences the hydration and physical properties of tissues, interacts with other extracellular matrix macromolecules, and interacts with cell surface receptors, notably CD44. So HA was utilized as carrier for tumor targeting.[7]

The Hemagglutinating Virus of Japan Envelope (HVJ-E) has also been utilized as vehicle for ^{10}B. HVJ-E possesses the high fusion ability and activates the immuno-system.[8] Thus the novel BSH compound has been evaluated for BNCT of MPM.

2. Materials and Methods

Preparation of BSH compound

HVJ-E was purified from the chorioallantoic fluid of hen's eggs by centrifugation, and the virus was inactivated by exposure to UV irradiation just before use. BSH has been used in clinical trials for treatment of malignant tumors, was obtained by Stella Chemifa Co. Ltd. (Osaka, Japan).

To incorporate BSH into HVJ-E with HA (HA-HVJ-E), 10 μl of HVJ-E suspension was added to 15 μl of 1% protamine sulfate solution, and mixed with BSH and 40 μl of 3% Tween 80 diluted with TE solution (10 mM Tris-Cl, pH 8.0, 1 mM EDTA). The mixture was centrifuged at 15,000 rpm for 15 min at 4^{o} C. Cationized HA, prepared from high molecular weight HA, and the appropriate volume of BSH encapsulated in HVJ-E was added in aqueous solution and incubated on ice for 15 min to form HA-HVJ-E. HA-HVJ-E was purified by centrifugation.

Incorporation of luciferase gene or Qdot.

The luciferase gene was incorporated into HVJ-E in the same procedure of BSH incorporation. Qdot ITK Carboxyl Quantum Dots were incorporated into HVJ-E by electroporation. The mixture was centrifuged at 15,000 rpm for 15 min at 4 °C.
After washing the pellet with 1 ml of balanced salt solution to remove the detergent and unincorporated plasmid DNA or Qdot.

Hemagglutination assay

50 μl of HVJ-E solution serially diluted with PBS(-) was added into each 0.5% suspension of chicken red blood cells in 96 well plate, respectively. The concentrated HVJ-E caused hemagglutination. The assay was read, as the reciprocal dilution of the last well showing hemagglutination, following 1 hr incubation at 4° C.

The affinity and incorporation of HA-HVJ-E to tumor cells

MPM (MSTO-H211) cells were seeded at a density of 2E+04 cells per well, in an 8-well Lab-tek chamber slide (Nalge Nunc International) on day 0. The cells were incubated with either CD44 neutralizing antibody, high molecular weight HA, or condition medium on day 1, and incubated with Qdot, Qdot incorporated into HVJ-E, or Qdot incorporated into HA-HVJ-E at a concentration of 2.5E+08 particles per well for 1 hr. The cells were then washed with PBS and fixed with 4% paraformaldehyde before incubation in 10 μM Hoechst 33342 (Molecular Probes, Inc.) to stain cell nuclei, Cells were observed by fluorescence microscopy (BX61, Olympus Co. Ltd.).

3. Results and Discussion

Hemagglutination assay.

HVJ-E possesses hemagglutination properties and so the systemic administration of HVJ-E is restricted in clinical use. Previously the gelatin conjugate of HVJ-E was developed and this alleviated hemagglutination *in vitro* [9]. These result showed that certain polymers could alleviate the side effect of HVJ-E, so the hemagglutination ability of HVJ-E with HA was evaluated.

The hemagglutination activity of HA-HVJ-E was approximately two times lower than that of HVJ-E in chicken red blood cells. This result revealed that the stability of HA-HVJ-E in the bloodstream would be increased efficiently (Figure 1). Actually, *in vivo,* toxicity test revealed that maximum dose of HA-HVJ-E tolerated was higher than that of HVJ-E in normal mice (data not shown).

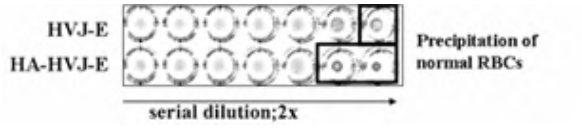

Figure 1. Hemagglutination test of chicken red blood cells.
HVJ-E and HA-HVJ-E solutions were serially diluted with PBS(-). In the far right well of HVJ-E (lowest concentration of HVJ-E), the partial precipitation of chicken red blood cells was observed, while in HA-HVJ-E wells, complete precipitation of red blood cells was observed, despite two times higher concentration of HVJ-E

The affinity and incorporation of HA-HVJ-E with luciferase expression plasmid for MPM cells

HVJ-E compounds, with luciferase expression plasmid, were co-cultured with MPM cells for only 1 hr with or without pretreatment with either CD44 neutralizing monoclonal antibody or high molecular weight HA. HA-HVJ-E, containing luciferase expression plasmid, possesses significantly higher transfection efficiency for MPM cells that express a large amount of CD44 than HVJ-E containing luciferase expression plasmid. Furthermore, the high transfection efficiency of HA-HVJ-E was significantly inhibited by pretreatment with either CD44 neutralizing monoclonal antibody or large amounts of high molecular weight HA (Figure 2).

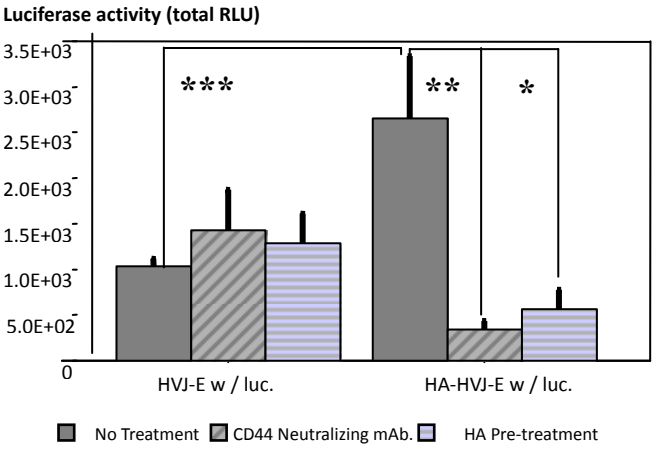

, **, ; p<0.01**

Figure 2. The affinity and incorporation of HA-HVJ-E with luciferase expression plasmid for MPM cells

HA-HVJ-E, containing luciferase expression plasmid, possesses significantly higher transfection efficiency for MPM cells that express a large amount of CD44 than HVJ-E containing luciferase expression plasmid. The high transfection efficiency of HA-HVJ-E was significantly inhibited by pretreatment with either CD44 neutralizing mAb. or large amounts of high molecular weight HA

These results show that the binding of HA-HVJ-E to MPM cells is CD44 dependent and that the affinity of HA-HVJ-E for MPM cells is significantly higher than that of HVJ-E. HVJ-E is superior vehicle for anticancer drug and gene expression plasmid, and some attempts to target tumor cells. [10,11] Therefore, BSH incorporated into HA-HVJ-E could be useful compound for BNCT of mesothelioma.

4. Conclusions

BNCT with a novel boron compound incorporated into HVJ-E with HA represents a potentially useful strategy for the treatment of mesothelioma.

References

1. D. C. Rice, W. R. Smythe, C. W. Stevens, et al, 2007. "Dose-dependent pulmonary toxicity after postoperative intensity-modulated radiotherapy for malignant pleural mesothelioma." Int J Radiat Oncol Biol Phys, 69, 350-357.

2. A. M. Allen, M. Czerminska, E. H. Baldini, et al, 2006. "Fatal pneumonitis associated with intensity-modulated radiation therapy for mesothelioma." Int J Radiat Oncol Biol Phys, 65, 640-645.

3. M. Suzuki, Y. Sakurai, K. Ono, et al, 2007. "A preliminary experimental study of boron neutron capture therapy for malignant tumors spreading in thoracic cavity." Jpn J Clin Oncol., 37, 245-249.

4. M. Suzuki, K. Endo, K. Ono, et al, in press. "A novel concept of treatment of diffuse or multiple pleural tumors by boron neutron capture therapy (BNCT)." Radioth Oncol.

5. T. Asplund and P. Heldin, 1994. "Hyaluronan receptors are expressed on human malignant mesothelioma cells but not on normal mesothelial cells." Cancer Res., 54, 4516-4523.

6. M.B. Penno, F. B. Askin, H. I. Pass, et al, 1995. "High CD44 expression on human mesotheliomas mediates association with hyaluronan." Cancer J Sci Am., 1, 196-203.

7. C. D. Meo, L. P. Donatella, V. Crescenzi, et al, 2007. "Hyaluronan as carrier of carboranes for tumor targeting in boron neutron capture therapy." Biomacromolecules, 8, 552-559.

8. M. Kurooka and Y. Kaneda, 2007. "Inactivated Sendai virus particles eradicate tumors by inducing immune responses through blocking regulatory T cells." Cancer Res. 67, 227-236.

9. H. Mima, R. Tomoshige, Y. Kaneda, et al, 2005. "Biocompatible polymer enhances the *in vitro* and *in vivo* transfection efficiency of HVJ envelope vector." J Gene Med., 7, 888-897.

10. H. Mima, S. Yamamoto, Y. Kaneda, et al, 2006. "Targeted chemotherapy against intraperitoneally disseminated colon carcinoma using a cationized gelatin-conjugated HVJ envelope vector." Mol Cancer Ther, 5, 1021-1027.

11. T. Shimbo, M. Kawachi, Y. Kaneda, et al, 2007. "Development of a transferring receptor-targeting HVJ-E vector." Biochem Biophy Commun, 364, 423-428.

In vitro neutron dosimetry of glioma and endothelial cultured cells

Luca Menichetti[1, †], Lorena Gaetano[2], Antonella Zampolli[1], Serena Del Turco[1], Cinzia Ferrari[3], Anna Maria Clerici[3] , Silva Bortolussi[4,5], Sabrina Stella[4,5], Piero Bruschi[4], Piero A.Salvadori[1], Saverio Altieri[4,5], Luca Cionini[6]

1. Department of PET and Radiopharmaceutical Chemistry, C.N.R. Institute of Clinical Physiology, Pisa, Italy
2. University School for Advanced Studies S. Anna, Pisa, Italy
3. University of Pavia, Department of Surgery, Laboratory of experimental Surgery, Pavia Italy
4. University of Pavia, Department of Nuclear Physics, Pavia, Italy
5. National Institute for Nuclear Physics (INFN), Section of Pavia, Italy
6. Unit of Radiotherapy, AOUP-University Hospital, Pisa, Italy

† Corresponding Author: luca.menichetti@ifc.cnr.it

Abstract

To fully develop its potential BNCT requires the combination of a suitable thermal/epithermal neutron flux together with a selective extraction of ^{10}B-boron nuclei in the target tissue. The latter condition is the most critical to be realized as none of the boron carriers used for experimental or clinical purposes proved at the moment an optimal selectivity for cancer cells compared to normal cells. In addition to complex physical factors the assessment of the intracellular concentration of boron represent a crucial parameter to predict the dose delivered to the cancer cells during the treatment. Nowadays the dosimetry calculation and then the prediction of the treatment effectiveness are made using Monte Carlo simulations, but some of the model assumption are still uncertain: the radiobiological dose efficacy and the probability of tumor cell survival are crucial parameters that needs a more reliable experimental approach. The aim of this work was to evaluate the differential ability of two cell lines to selectively concentrate the boron-10 administered as BPA-fructose adduct, and the effect of the differential boron intake on the damage produced by the irradiation with thermal neutrons; the two cell lines were selected to be representative one of normal tissues involved in the active/passive transport of boron carriers, and one of the tumor. Recent in vitro studies demonstrated how BPA is taken by proliferating cells, however the mechanism of BPA uptake and the parameters driving the kinetics of influx and the elimination of BPA are still not clarified. In these preliminary studies we analyzed the survival of F98 and HUVEC cells line after irradiation , using different thermal fluencies at the same level of density population and boron concentration in the growing medium prior the irradiation. This is first study performed on endothelium model obtained by a primary human cell line (HUVEC). The perspective application of this work is to develop a model able to foresee the effects produced by different combination of boron influx with a thermal neutron fluencies, applying a standardized radiobiological methodology, and in particular to continue the investigation of the radiobiological effects on the endothelium model as the main tissue involved in the transport of boronated molecules.

Keywords: BNCT, BPA, glioma, endothelium, cell dosimetry, radiobiology.

1. Introduction

Boron Neutron Capture Therapy (BNCT) is a binary treatment modality based on the use of low energy neutrons able to produce a lethal damage only to cells loaded with a sufficient number of boron-10 nuclei, while a tolerable damage occurs in cells where no boron influx occurs. The main condition required to make BNCT effective is that boron carriers are selectively targeted to tumour cells in order to have the higher effective dose able to minimize the probability of tumor cell survival. Different tumour types would potentially benefit from this kind of approach: those with high radioresistance and for which other treatment modalities are usually ineffective to control loco regional disease, such as Glioblastoma and Melanoma. The condition leading to tumor recurrences is represented by the survival of even a small amount of tumor cell after the treatment. At the present stage this represents a crucial aspect even in BNCT. At least in theory this could be overcome using novel boronated drugs or eventually

proactive molecules, yielding target to non-target ratio (*T/N*) of boron concentration higher than 5:1 that represents the best result obtainable with the di-hydroxyboryl-phenylalanine (BPA). The screening of new boron delivery agents and the comparative evaluation of their effects in vitro and in vivo require the development of reference methods to predict the ^{10}B-content in cells and the subsequent dosimetry to predict the cell survival probability. This study is focusing on the development of procedures able to assess the radiobiological damage induced in different cell phenotypes.

The present study has also been devised to compare the biological properties of different thermal /epithermal neutron beams using validated reference methods: the collaboration between Centers working on BNCT is often hindered by methodological differences that make difficult if not impossible the comparison between different experimental data sets.

In this study the production of specific dose-effect curves has been optimized in cells of Glioma (line F98) and Endothelium (Human Umbilical Vein Endothelial Cells, HUVEC) with/without the incorporation of BPA-fructose adduct (BPA-fr) used as reference compound.

We already investigated the incorporation of 10-boron in these two cell phenotype, and set up a methodology based on capillary electrophoresis-electrospray mass spectrometry (EC-ESI-MS) and HR-ICP-MS for the quantification of intracellular ^{10}B-BPA [1]. Different studies showed that BPA is taken up more actively by proliferating cells [2], probably because BPA may follow the pathway of essential (aromatic) amino acids which are extracted by cells with higher metabolic activity. Differences in the radiobiological effects of BNCT in quiescent and proliferating cells have been shown with indirect assays. This differential effect was more significant for BPA than with sulfhydrylborane (BSH), a compound extensively used in BNCT [2-3] but lacking a metabolic mechanism of uptake [4-5]. For BPA the observation of a dependence of Boron uptake from the cell cycle [2, 5], suggests a higher Boron uptake in replicating cells. However, the mechanism of BPA uptake and release is still unclear, in particular the correlation of the final intracellular Boron concentration with active and/or passive membrane transport.

The present study is then aiming to investigate the cell damage and the survival fraction with BPA-fr under controlled condition taking into account the BPA-fr intracellular concentration. On the basis of the kinetic of BPA uptake and release in the aforementioned cell lines, the *survival fraction* (*SF*) has been experimentally calculated.

The *SF* has been used to estimate the incremental value of the cytotoxic damage, linked to the effective intracellular concentration of boron-10. The study of the radiobiological damage at higher neutron doses is still ongoing.

2. Material and Methods

2.1 Cell culture

Glioma F98 Cells: Rat F98 glioma (ATCC) closely resemble human high-grade brain tumors and is widely used to model in vivo the behavior of glioblastoma F98 cells were maintained in Dulbecco´s Modified Medium (DMEM) containing HEPES (25 mmol/L) antibiotics, and 10% heat-inactivated fetal calf serum. Complete medium change was routinely performed every 3 days. Cells were used between 25th and 35th passage in log-phase. F98 glioma cells have been obtained and propagated in vitro. Doubling time of F98 cell line was very short (18.2 hours) in the exponential phase of growth.

A first experimental set up was characterized using cultured F98 cells and BPA-fr. Cells were seeded in 96 well plates containing DMEM (Dulbecco's Modified Eagle's Medium). Cell culture media were from BioWhittaker, Cambrex Europe. Cell proliferation Kit I (MTT) was from Roche Applied Science. All other reagents were purchased from Sigma.

HUVEC: Human umbilical vein endothelial cells were isolated from umbilical cords, harvested enzymatically with Type I A collagenase 1 mg/mL as described, and maintained in Medium 199 (M199), containing HEPES (25 mmol/L), heparin (100 mg/mL), epidermal growth factor (EGF) (20 ng/mL), L-glutamine (2 mmol/L), antibiotics, and 10% heat-inactivated fetal calf serum.

Once grown to confluence, cells were collected with trypsin/EDTA, subcoltivated on 1% gelatin-coated flasks and used at second passage in log phase. HUVEC or F98, plated in 96 well with 100 μL of complete culture media, were incubated with BPA-fr (0-110 μg of ^{10}B equivalent) until the neutron irradiation. Cells were then quickly washed twice in a controlled environment close to the reactor to remove boron compounds and previous medium. After the irradiation performed over a precise and fixed time length, the cells were allowed to grow for 5 days, when proliferation and viability were assessed with a colorimetric assay.

Briefly, 3-(4,5-dimethylthiazole-2-yl)-2,5-diphenyl *tetrazolium* bromide (MTT) salts were added to the culture medium. HUVEC were incubated with MTT salts for 4 hr, while F98 were incubated with MTT for 2.5 hrs. Then 100 μL of 10%SDS in 0,01M HCl were added and plates were kept in the incubator overnight to allow for complete solubilisation of *formazan* crystals. Absorbance was read with a microplate spectrophotometer.

2.2 Neutron Irradiation

The irradiation experiments were performed at the LENA laboratory, using a fully characterized thermal neutron field with low gamma background (Triga Mark II reactor, LENA, University of Pavia). The reference conditions have been considered at 250 kW in air:

$\Phi(n)$ thermal $_{(E < 0.2\ eV)} = 1.4 \cdot 10^{10}\ cm^{-2} \cdot sec^{-1}$

$\Phi(n)$ ephitermal $_{(0.2 < E < 3.5\ MeV)} = 3.3 \cdot 10^{7}\ cm^{-2} \cdot sec^{-1}$

$\Phi(n)$ fast1 $_{(3.5 < E < 8.2\ MeV)} = 2.0 \cdot 10^{6}\ cm^{-2} \cdot sec^{-1}$

$\Phi(n)$ fast2 $_{(E > 8.2\ MeV)} = 9.4 \cdot 10^{4}\ cm^{-2} \cdot sec^{-1}$

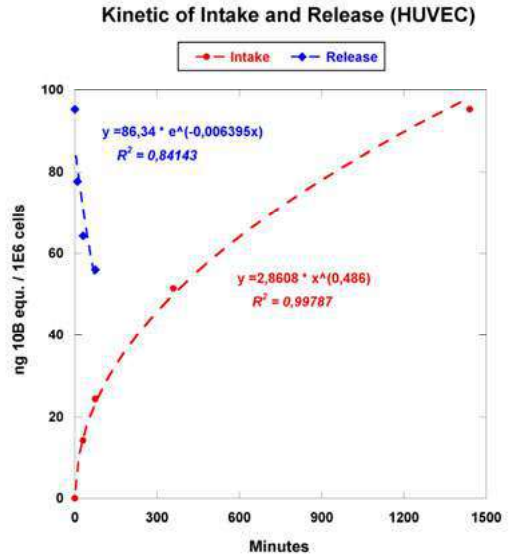

Fig.1: Kinetic curves representing the intake and release of BPA-fr at 110 µg ^{10}B equiv. in HUVEC cell cultures. Typical curves were obtained for F98 and HUVEC cells at different boron concentration in the growing medium [1]

2.3 Survival analysis

Chemosensitivity and antiproliferative effects of BPA-fr were assessed using MTT assay after neutron irradiation. SF values at different BPA-Fr concentrations were investigated: no cytotoxic effects were detected at concentration up to 110 µg·ml-1 ^{10}B-equivalent in the control samples. Uptake and efflux (*wash-out*) of BPA-fr were calculated and these data were considered as a key parameter in the design of the experimental protocol. The kinetic of incorporation of ^{10}B-BPA fructose adduct in F98 and HUVEC cell types was already evaluated in previous study by us and a methodology based on capillary electrophoresis-electrospray mass spectrometry and HR-ICP-MS for the quantification of cellular ^{10}B-borono-phenylalanine intake was already validated [1]. On the basis of this findings to maximize the intracellular boron concentration (cells in different cellular cycle phase probably exhibit different uptake of aminoacid analogues) [2, 5], the incubation time of ^{10}B-BPA was set up to 18 hours at 110 µg·ml^{-1} ^{10}B-equivalent in the growing medium.
The change in proliferative capacity induced by neutron irradiation was assessed with a viability test (MTT assay) on 96 multiwell plate. For each cell line a control set, without boron-10 added (i.e. a solution of fructose was used to compensate any effect of dilution of the medium), was compared with two different irradiated sets. In one of this two sets the incubation medium was maintained (*BPA +*); in the other the incubation medium was removed just before the irradiation (*BPA –*). In this case the medium was gently replaced with fresh normal medium without boron added: this sample was used to isolate the effect of the neutron capture of intracellular boron excluding any contribution of dose linked to boron-10 present in the growing medium. To take into account the kinetic of efflux of the intracellular BPA-fr, the medium changing, washing and operations prior to irradiation were standardized in 10±2 minutes for each sample set. The survival fraction for each set was plotted as a function of total absorbed dose. Each 96 multiwell plate contains the treated sample (BPA+ or BPA-) and a control sample (added only with a fructose solution in the same proportion of BPA-fr solution).

F98 Tests

BPA (+)	BPA (-)
BPA-fr maintained in the medium	BPA removed (medium change)
Conc.10B eq. = 89 ppm	Conc.10B eq. = 85 ppm during irradiation

HUVEC Tests

BPA (+)	BPA (-)
BPA-fr maintained in the medium	BPA removed (medium change)
Conc.10B eq. = 12 ppm	Conc.10B eq. = 10 ppm during irradiation

Table 1. Experimental sample sets of F98 and HUVEC cells. BPA-fr was maintained in the growing medium (BPA +) or removed just before the irradiation (BPA -): the two above conditions modify the intracellular boron concentration during the irradiation

3. Results

3.1 Neutron Dosimetry

The fluence measurements were performed during each experiment using two methods**:** on line with a Self Powered Neutron Detector (SPND) [9] and by means of an indirect measurements based on the activation of Cu wires placed in selected positions of

each multiwell plate [10-11]. The dose component due to ^{14}N thermal neutron capture was estimated, assuming that the nitrogen content in the different samples was 3% by weight.

F98 cultured Cell (96 multiwell plate)

Reactor power (kW)	γ dose (Gy)	p dose (Gy)	B dose[1] (Gy)	Total dose (Gy)
5	0,0082	0,0104	0,3486	0,3672
10	0,0164	0,0208	0,6972	0,7344
20	0,0328	0,0416	13,944	14,688

1(Max boron concentration in cells, 89.4 ppm)

HUVEC cultured Cell (96 multiwell plate)

Reactor power (kW)	γ dose (Gy)	p dose (Gy)	B dose[2] (Gy)	Total dose (Gy)
5	0,0082	0,0104	0,0468	0,0654
10	0,0164	0,0208	0,0936	0,1308
20	0,0328	0,0416	0,1872	0,2616

2(Max boron concentration in cells, 12.0 ppm)

Table 2. Absorbed doses (Unit, *Gy*); the assessment of the dose was performed for every positions in the 96 multiwell plate taking into account the experimental flux perturbations

3.2 Cell survival

MTT assay has been performed on irradiated sample cells with/without boron-10. The first experimental point corresponding at $1.68 \cdot 10^{11}$ cm^{-2} thermal neutron fluence showed to have no measurable effects in vitro on both F98 and HUVEC cell line (sublethal dose), while increasing the fluence from $3.36 \cdot 10^{11}$ cm^{-2} to $6.72 \cdot 10^{11}$ cm^{-2} the antiproliferative effects on both cells was detected. Therefore the optimal fluence to perform radiobiological studies was $6.72 \cdot 10^{11}$ cm^{-2}. The dose range according the different boron concentration was 0-14 Gy for the F98 line and 0-0.26 Gy for HUVEC line. The total absorbed doses are reported in Table 2.

F98 Dose-3 (BPA+)

OD (BPA+)	SE	OD(Fructose)	SE
1.3916	0.0420	1.8786	0.0343

F98 Dose-0 Control Sample (BPA +)

OD (BPA+)	SE	OD(Fructose)	SE
2.1483	0.0653	2.1024	0.0419

F98 Dose-3 (BPA-)

OD (BPA-)	SE	OD(Fructose)	SE
1.6939	0.0310	1.9343	0.0441

F98 Dose-0 Control Sample (BPA -)

OD (BPA-)	SE	OD(Fructose)	SE
2.0462	0.0370	2.0881	0.0407

HUVEC Dose-3 (BPA+)

OD (BPA+)	SE	OD(Fructose)	SE
0.3444	0.0026	0.4254	0.0040

HUVEC Dose-0 Control Sample (BPA +)

OD (BPA+)	SE	OD(Fructose)	SE
0.4520	0.0048	0.4723	0.0047

HUVEC Dose-3 (BPA-)

OD (BPA-)	SE	OD(Fructose)	SE
0.4162	0.0066	0.4739	0.0039

HUVEC Dose-0 Control Sample (BPA -)

OD (BPA-)	SE	OD(Fructose)	SE
0.4788	0.010	0.5382	0.0089

Table 3. Absorbance Values expressed as Optical Density, OD of treated and control samples (control samples were added with an equivalent fructose solution free of boron). Standard Error (SE) are reported

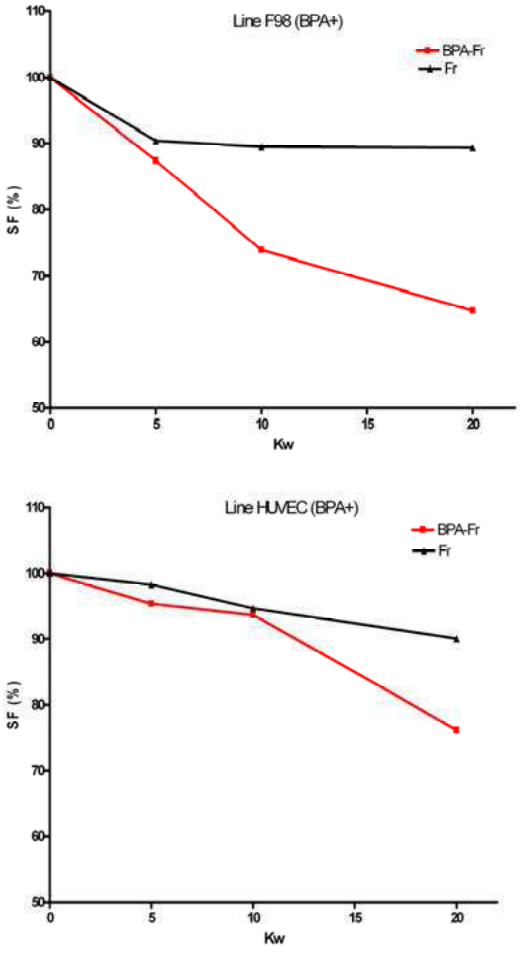

Figure 2. Viability curves reporting the survival fraction (SF%) of the cell population after irradiation at different neutron fluences, corresponding to 0, 5, 10, 20 kW of the reactor power (for the dose calculation see table 2). Typical curves of line F98 and HUVEC with BPA(+) present in the growing medium during the irradiation

F98 Cell line (dose unit, Gy)

kW[1]	Control[2]	SF	BPA(+)	SF
20	0.074	0.894	14.688	0.648
kW	Control[1]	SF	BPA(-)	SF
20	0.074	0.926	13.984	0.828

1, Dose-3, Fluence 6.72·10E+10 n·cm^{-2}; 2, Fructose solution

HUVEC Cell line (dose unit, Gy)

kW[1]	Control[2]	SF	BPA(+)	SF
20	0.074	0.762	0.262	0.901
kW	Control[1]	SF	BPA(-)	SF
20	0.074	0.893	0.233	0.948

1, Dose-3, Fluence 6.72·10E+10 n·cm^{-}; 2, Fructose solution

Table 4. Survival fractions (SF) of treated and control samples at dose-3 (corresponding at a fluence of 6.72 ·10^{11} n·cm^{-2} thermal neutron, LENA reactor)

The evaluation of the effect of neutron irradiation on the proliferative capacity with MTT assay was performed after 6 cell cycles. SF has been calculated for BPA(+), BPA (-) and fructose sample sets (see table 4) considering as reference data those of samples non irradiated samples maintained in the same conditions (dose-0). Our first data demonstrate that sole neutron irradiation of sample determined a very low variation of the survival fraction, while the irradiation after incorporation of ^{10}B-BPA at 110 μg·ml^{-1} ^{10}B-equivalent resulted in a significant increase of the lethal effect leading to a differential cell damage.

4. Discussion

In this study we considered separately the component linked to the neutron irradiation and those deriving from the neutron capture reactions in cell culture were the boron-10 was present as intracellular only *(BPA–)*, or in the growing medium *(BPA+)*. In order to establish a methodology to correlate the survival fraction with the dose and the intracellular boron concentration, it was mandatory to control every environmental and experimental condition.

In this study all the irradiation experiments were performed maintaining a constant temperature in the multiwell plates, verifying the geometry during the irradiation, and performing the experiment on the same time interval after replacing the medium (table 1).

Due to the prevalence of the high LET radiation (table 2) delivered after neutron capture, we expected that the most relevant killing effect was linked to the differential accumulation of boron and hence to the different dose released at cellular level [6-8].

For this reason, having a different intracellular boron concentration, glioma and endothelial cells in the same irradiation conditions demonstrated to have different values of cell survival. Indeed the HUVEC cells showed a significant lower damage, linked to a very lover concentration of intracellular boron-10 (10-12 ppm). In the range of neutron dose hereby studied, the survival probability of F98 cell lines decreased clearly with the intracellular boron incorporation, while the less amount of boron inside the HUVEC cell do not lead a similar effect. Nevertheless we cannot exclude at this stage that different cell morphology, cell volume and BPA trafficking for F98 and HUVEC may influence the cell survival in the same conditions of neutron fluence and boron concentration [13-14].

In spite of a lower intake of BPA-Fr (starting from the same concentration in the growing medium) and the same physical dose exposition (due to gamma and protons) HUVEC cell showed a measurable amount of lethal damage, probably linked to their relative higher radiosensitivity.

This finding represent the first study performed on endothelium model obtained by human endothelial cells in experimental BNCT. Further data will be achieved increasing the neutron dose in the same conditions of incubation and exposition to ^{10}B-BPA-fr in the growing medium. Our future research plan includes a wider characterization of the experimental models preliminary described in the present paper, with particular reference to endothelium cell cultures.

Whenever this target will be achieved it will provide the necessary reference data set for BNCT modelling developments in terms of both irradiation procedures and evaluation of new more effective boron compounds.

References

1. "Capillary electrophoresis-electrospray mass spectrometry and HR-ICP-MS for the detection and quantification of (10)B-boronophenylalanine ((10)B-BPA) used in boron neutron capture therapy." Aurélien Pitois, Laura de Las Heras, Antonella Zampolli, Luca Menichetti, Ramon Carlos, Guido Lazzerini, Luca Cionini, Pietro Salvatori, Maria Betti, Anal Bioanal Chem. Dec 22; :1-10, 2005
2. "Cell cycle dependence of boron uptake from two boron compounds used for clinical neutron capture therapy", F. Yoshida, *et al.*, Cancer Letters 187, 135–141, 2002
3. "Current Status of Neutron Capture Therapy", J. A. Coderre, *et al.*, IAEA-TECDOC-1223, , Annex 6, IAEA, 2001
4. "Impact of the p53 Status of the Tumor Cells on the Effect of Reactor Neutron Beam Irradiation, with Emphasis on the Response of Intratumor Quiescent Cells", Shin-ichiro Masunaga, Koji Ono, Akihisa Takahashi, Yoshinori Sakurai, Ken Ohnishi, Toru Kobayashi, Yuko Kinashi, Masao Takagaki and Takeo Ohnishi, Jpn. J. Cancer Res. 93, 1366–1377, 2002
5. "Biodistribution of boronophenylalanine in patients with glioblastoma multiforme: boron concentration correlates with tumor cellularity" Coderre, J.A., Chanana, A.D., Joel, D.D., Elowitz, E.H., Micca, P.L., Nawrocky, M.M., Chadha, M., Gebbers, J.O., Shady, M., Peress, N.S., Slatkin, D.N., Radiat. Res. 149 (2), 163–170, 1998
6. "A simple model for quantification of the radiobiological effectiveness of the 10B(n,a)7Li capture reaction in BNCT" C.H. Hsieh, H.M. Liu, J.J. Hwang, H.E. Wang, J.J. Kai, F.D. Chen Applied Radiation and Isotopes 64 306–314, 2006
7. "A comparative study of the radiobiology of BNCT beams", A.J. Mason, D.T. Beynon, J.W. Hopewell, J.Capala, P.M. Munck af Rosenschold, Dedalo Ed. Proceedings Int. Workshop on Neutron Capture Therapy: State of the art", 125-128, 2003
8. "Radiobiological evidence suggesting heterogeneous microdistribution of boron compounds in tumors: Its relation to quiescent cell population and tumor cure in neutron capture therapy", Koji Ono, Shin-Ichiro Masunaga Yuko Kinashi, Masao Takagaki, Mitsuhiko Akaboshi , Toru Kobayashi and Keizo Akuta, Int J.Rad. Oncol. Biol. Ph. 34, Issue 5, 1081-1086, 1996
9. "Implantable self-powered detector for on-line determination of neutron ux in patients during NCT treatment", M.E.Miller, L.E.Mariani, M.L.Sztejnberg Goncalves-Carralves, M.Skumanic, S.I.Thorp, Appl. Radiat. Isot. 61, 1033-1037, 2004
10. "Effective Cross Sections Values of Well Moderated Thermal Reactor Spectra", C.H.Wetscott, Report AECL n.1101, 1960
11. C. H. Wetscott, W. H. Walker, T. K. Alexander, "Effective Cross Section and Cadmium Ratios for the Neutron Spectra of Nuclear Reactors", in Proceedings of the International Conference on the Peaceful Uses of Atomic Energy, Geneva, 1958, P/202 70, 1959
12. "Boron analysis and boron imaging in biological materials for Boron Neutron Capture Therapy (BNCT), Andrea Wittig, Jean Michel, Raymond L. Moss, Finn Stecher-Rasmussen, Heinrich F. Arlinghaus, Peter Bendel, Pier Luigi Mauri, Saverio Altieri, Ralf Hilger, Piero A. Salvadori, Luca Menichetti, Robert Zamenhofk, Wolfgang A.G. Sauerwein, Critical Reviews in Oncology /Hematology 68 66–90, 2008
13. "Microdosimetric study for interpretation of outcomes from boron neutron capture therapy clinical trials", T. L. Nichols, L. F. Miller, G. W. Kabalka and T. M. Dudney, Radiat Prot Dosimetry.;126(1-4):645-7, 2007
14. "A simple model for quantification of the radiobiological effectiveness of the 10B(n,a)7Li capture reaction in BNCT", C.H. Hsieh, H.M. Liu, J.J. Hwang, H.E. Wang, J.J. Kai, F.D. Chen, Applied Radiation and Isotopes 64 306–314, 2006

Acknowledgments

We thank Professor Marino Mazzini (Department of Mechanic Nuclear and Production Engineering, University of Pisa) for having strongly believed in this project and supported it. We also thank the two staffs at LENA reactor and the Laboratory of experimental surgery (Department of Surgical Sciences) in Pavia for the support during the experiments. We thank finally Mr. Guido Lazzerini (CNR Institute of Clinical Physiology, Pisa) for the expertise in cell cultures.

Cell Survival Measurements, with and without Boron, in an Accelerator Produced Epithermal Neutron Beam: A Proposal for a Radiobiological Intercomparison of BNCT Facilities

Ben Phoenix[1], Zamir Ghani[1], Stuart Green[2], Richard Hugtenburg[1], Andrew Mill[1]
Cecile Wojnecki[2]

[1] *Department of Physics and Astronomy, University of Birmingham, UK*
[2] *University Hospital Birmingham, UK*

The accelerator-based BNCT facility at Birmingham has been previously used for cell survival measurements and data from these irradiations presented at earlier ICNCT conferences (Mason 2004). The purpose of the work to be presented here is to extend these data using more clinically relevant conditions of temperature, growth conditions and cell lines. A further aim is to establish a standard simple and reproducible protocol for the international comparison of the biological effectiveness of different BNCT facilities.

Three cell lines are being used for these experiments: V79 Chinese hamster cells and M095K and M095J human glioma cells. V79 cells are widely used in radiobiology research, and the use of these for international comparisons is ideal. However, M095K and M095J cells are of more relevance for BNCT purposes.

Initial results for irradiations with V79 cells in 50 ppm of boron-10 (as boric acid) indicate an approximate 8 to 10-fold increase in cell killing at all depths over non-borated cells. This is in broad agreement with previous data using a reactor-based neutron beam (Mill 1994).

A standard set-up and protocol for comparison purposes will be presented. This will be based on a large rectangular water phantom maintained at a temperature of 37°C. V79 cells will be irradiated attached to T25 flasks placed at set depths within the water phantom and containing two different concentrations (0 and 50 ppm) of boron-10 (as boric acid). It is hoped that a number of groups will participate in a biological inter-comparison of their BNCT irradiation facilities.

Study of Hela cell Damage Effect Induced by ^{7}Li Ions Irradiation

Wang Xiao, Kong Fuquan, Shi Xiaopei, Zhang Xuefeng, Xu Wenge, Sui Li, Zhao Kui

China Institute of Atomic Energy, P.O. Box 275-10, Beijing 102413,China;

NCT is an experimental form of treatment that requires the infusion of an element such as Boron or Gadolinium and exposure of the patient to a Neutron Beam from a nuclear reactor.

It is a two component or binary system, based on the nuclear reaction that occurs when the stable isotope ^{10}B is irradiated with low energy or thermal neutrons to yield highly energetic particles including 1.47MeV of helium-4 (^{4}He) nuclei (i.e., α particles) and 0.84MeV of recoiling Lithium-7 (^{7}Li) ions. The emitted α particles and ^{7}Li ions are largely high linear energy transfer (LET), producing more severe damage than low LET (such as X-rays, γ-rays and electron) radiation resulting in the increase of cell death. The short range in tissue of these two particles (<10 μm) allows localized energy release in tumor cells, saving the surrounding healthy tissue. These particles exhibit characteristics of high energy transfer (LET) radiation and have enhanced biologic effects. Therefore, It is essential to study the mechanism of tumor cell damage induced by α particles and ^{7}Li ions radiation. Here, α particles and Lithium ions were produced by ^{241}Am radiation source and HI-13 tandem accelerator at China Institute of Atomic Energy (CIAE) respectively to simulate ionizing radiation in Boron Neutron Capture Therapy (BNCT) process. The effects of heavy ion radiation on Hela cells were investigated with a 30MeV ^{7}Li irradiation.

The results showed: Under the ^{7}Li irradiation，the proliferation of cells was decreased; The G1 and G2/M of cells was inhibited; The cells had some apoptosis. After ^{7}Li ions irradiation, Survival fraction of cells was decreased with radiation dose increasing. The apoptosis of cells also ncreased. A damege effect was observed after irradiation.

Inhibition of Tumor Growth of Mouse Colon Cancer Cell Line by Boron Neutron Capture Therapy & Immunotherapy

H. Yanagie [1,2], K. Kakimi[2,3], A. Hosoi[2,3], A. Ogata[2], Y. Sakurai[2], K. Mouri[2], K. Eguchi[2], Y. Morishita[4], A. Shinohara[5], H. Sugiyama[2], S. Takamoto[2,6], M. Eriguchi[2,7], and H. Takahashi[1,2]

[1] *Department of Nuclear Engineering & Management, Graduate School of Engineering, The University of Tokyo,Tokyo, JAPAN,*
[2] *Cooperative Unit of Medicine & Engineering, The University of Tokyo Hospital, Tokyo, Japan*
[3] *Department of Immunotherapeutics (Medinet), The University of Tokyo Hospital, Tokyo, Japan*
[4] *Department of Human & Molecular Pathology, Graduate School of Medicine, The University of Tokyo, Tokyo, Japan*
[5] *Department of Hygenes, School of Medicine, Jyuntendo University, Tokyo, Japan*
[6] *Department of Cardiac Surgery, The University of Tokyo Hospital, Tokyo, Japan*
[7] *Department of Microbiology, Syowa University School of Pharmaceutical Sciences, Tokyo, Japan*

Corresponding Author: Hironobu Yanagie, MD, PhD ; TEL: +81-3-5800-9194 ; FAX: +81-3-5800-9195 ; E-mail: yanagie@n.t.u-tokyo.ac.jp

Abstract

Cytotoxic effects of locally injected ^{10}B entrapped cationic liposome (COATSOME-EL) on mouse colon cancer were evaluated with thermal neutron irradiation.

^{10}B entrapped COATSOME-EL was prepared. After thermal neutron irradiation of mice injected with ^{10}B entrapped COATSOME-EL, 2 x10^6 immature dendritic cells (DC) were injected intratumorally (IT). Colon26 tumor growth was suppressed in the groups of BNCT and BNCT with DC injections relative to controls. After one month observation of tumor growth, the splenocytes of tumor bearing mice were isolated, and were transferred to other same strain mice by intravenous injection. Then, half million of colon26 cells were challenged. The growth of colon26 tumors was highly suppressed in mice that received spleen cells from DC-treated mice, suggesting that anti-tumor immunity was induced by DC treatment.

These data show that direct DC immunotherapy can enhance the anti-cancer effect of BNCT and have promising clinical application in near future .

Keywords : Boron neutron capture therapy, Immunotherapy, Dendritic cell

1. Introduction

The cytotoxic effect of BNCT is due to a nuclear reaction between ^{10}B and thermal neutrons (^{10}B + $^{1}n \rightarrow {}^{7}Li$ + ^{4}He + 2.31 MeV (93.7%) / 2.79 MeV (6.3%)). The resultant lithium ions and α particles are high linear energy transfer (LET) particles which give important biological effect. Their short range in tissue (5 - 9 μm) restricts radiation damage to those cells in which boron atoms are located at the time of neutron irradiation.

Liposomes can contain a large amount of ^{10}B compound, which can be delivered to tumor cells. We have reported that ^{10}B atoms delivered by immunoliposomes are cytotoxic to human pancreatic carcinoma cells (AsPC-1) with thermal neutron irradiation *in vitro* (Yanagie, 1991), and intratumoural injection of boronated immunoliposomes can increase the retention of ^{10}B atoms in tumour cells, and suppress tumor growth *in vivo* under thermal neutron irradiation (Yanagie, 1997).

Dendritic Cells (DCs) are potent antigen-presenting cells that can both activate innate and acquired immune responses, so it is now being focused on the role of DCs in eliciting antitumor immunity and in potential therapeutic applications. For example, administration of DCs loaded ex vivo

with tumor-associated antigens can elicit antitumor immunity resulting in tumor regression in various murine tumor models, and DCs pulsed with tumor derived peptides, proteins, genes or tumor lysates, as well as DCs fused with tumor cells, have all been studied as therapeutic cancer vaccines (Chang, 2002). Candido et al had reported that they evaluated the effect of IT injections of bone marrow derived DCs on the subcutaneous growth of the murine MT-901 breast tumor (Candido, 2001). They demonstrate that DCs can efficiently uptake apoptotic MT-901 tumor cells and that local injections of DCs alone can result in regression of this breast tumor *in vivo*, which is dependent on host CD8 T-cell immunity.

Recently, it has been reported that combined immuno and radiation therapy results in effective tumor growth suppression. Radiation therapy is currently applied in the treatment of a wide array of human cancers. Recent evidence indicates that besides exerting direct toxic effects on tumor cells, ionizing radiation also exhibits various immunomodulatory effects. Inflammatory responses are triggered within irradiated tissues recruiting DCs to sites of inflammation. At the site, DCs acquire antigens, undergo maturation, and then migrate to the draining lymph node, where they present processed antigens to T cells. Irradiated tumor cells have been shown to serve effectively as a source of Tumor Associated Antigens (TAAs) to elicit specific T-cell responses *in vitro* when processed and presented by DCs (Strome, 2002).

In this study, we prepared the cationic liposome (COATSOME-EL) as the effective ^{10}B carrier to deliver the boron atomes into the cancer cells as the manner of gene delivery systems, and we evaluated the synergic anti-cancer effects of immune-responces with dendritic cells intratumoral injection after BNCT.

2. Materials & Methods

Chemicals

Sodium salt of undecahydro-mercaptocloso-dodecaborate ($Na_2{}^{10}B_{12}H_{11}SH$) was obtained by Wako Chemical Co. Ltd. (Tokyo, Japan).

Preparation of Liposomes containing ^{10}B-compound

A cationic empty liposome (COATSOME EL-C-01 : Nichiyu liposome Co. Ltd.) is composed with L-a-dipalmitoyl phosphatidylcholine (26 μmoles), cholesterol (20 μmoles), and stealylamine (4 μmoles). BSH (10mg/ml) solution was added to the COATSOME EL-C-01, and made the *^{10}B-liposome solution* (Yanagie, 1999). The boron concentration entrapped in COATSOME-EL vesicles was determinated by ICP-Masspectroscopy of Jyuntendo University.

Generation of Bone Marrow-Derived DCs

Bone marrow cells obtained from femurs and tibias of BALB/c mice were cultured in RPMI 1640 medium supplemented with 10% FCS, 12.5 mM HEPES, 5×10^{-5} M 2-mercaptoethanol, 1×10^{-5} M sodium pyruvate, 1% NEAA, 10 mg/ml Penicillin/Streptomycin and 20 ng/ml GM-CSF (PeproTech, Rocky Hill, NJ) for 7 days.
On day 7, DCs were harvested by gentle pippetting, washed twice with PBS and resuspended at 1×10^7 cells/0.1 ml PBS for intratumoral injection (Saji, 2006).

Splenocytes

Spleen cells, harvested from BALB/c mice, were treated with ammonium chloride-potassium lysis buffer (0.83% ammonium chloride,0.1% KHCO3, and 0.004% EDTA) for 5 min to deplete erythrocytes and washed twice with HBSS. They were then enumerated and resuspended in HBSS for injection (Saji, 2006).

BNCT procedure

The Colon26 (1×10^6) cells were injected subcutaneously into the back of the male BALB/C mice (Nihon SLC). Ten days after injection, when an average diameter of 10 mm was reached , 150 μl of ^{10}B-liposome solution were injected (IT). The mice injected with ^{10}B-liposome solutions were irradiated with thermal neutrons (2×10^{12} n/cm^2) at JRR4 reactor of Japan Atomic Energy Research Institute.

DC treatment

On day 10, when the tumors reached an average diameter of 10 mm, BNCT on mice IT injected with ^{10}B entrapped liposome was performed and, at that time, syngeneic DCs(1×10^7 cells/mouse) were injected IT with the schedule 1 (day 0, day 3 , day 6), or schedule 2 (day 0, day 3, day 6, day9, day 12, day 15, day 18). After BNCT+DCs injections, the effect of treatment was calculated on the basis of tumor volume and morphological findings of the tumors at 4-day intervals.

ELISPOT Assay.

Tumor-specific T cell responses were evaluated by ELISPOT assays. Erythrocyte-depleted splenocytes harvested from treated or control mice

40 days after tumor inoculation or from age matched naive mice (5 x 10^4 splenocytes in 100 µl of CM) were placed into each well and incubated for 24 h at 37°C, 5% CO_2 in the absence or presence of irradiated (60 Gy) Colon26 tumor cells (5 x 10^3 cells in 100 µl of CM). The assays were performed and developed using anti-mouse IFN-γmAb according to the kit manufacturer's instructions (BD Pharmingen). All experiments were performed in duplicate and the data correspond to the mean value.

Adoptive Transfer Model

Splenocytes harvested from treated mice on day 40 after tumor inoculation were transferred intraveneously to syngeneic mice. Two days after spleen cells transfer, Colon26 cells (5 x 10^5 cells) were injected subcutaneously. The effect of anti-tumor immunity was evaluated on the basis of tumor volume (Saji, 2006).

Animal Etics

The procedures for the tumor implantation and the sacrifice of the animals were in accordance with approved guidelines of the Institution's Animal Ethics Committee.

3. Results & Discussion

In order to evaluate that local BNCT followed by IT-DC can inhibit primary tumor growth, BALB/c mice were injected s.c. with Colon26 tumor cells. On day 10, the tumors reached an average diameter of 10 mm, BNCT on IT with ^{10}B entrapped liposome was done at that time and syngeneic DCs were injected intratumorally with the schedule 1 (day 0, day 3 , day 6), or schedule 2 (day 0, day 3, day 6, day9, day 12, day 15, day 18). On schedule 1, although the tumors grew rapidly following treatment with saline alone, and IT-DC, the group treated BNCT + IT-saline and the combination of BNCT + IT-DC resulted in significant suppression of tumor growth (Figure 1). Almost all animals treated with BNCT + It-saline, and BNCT + IT-DC became tumor-free. On schedule 2, 30% tumor growth suppression was achieved on IT-DC group, and also the group treated BNCT + IT-saline, and the combination of BNCT + IT-DC resulted in significant suppression of tumor growth compared to non-treated group (Figure 2).

Because both components of the combined treatment, BNCT+DC, are delivered directly to the tumor, we investigated whether this protocol could induce a systemic antitumor response. It has been reported that *in vitro* tumor-specific IFN-γ production by host-derived T cells correlated with systemic antitumor immunity *in vivo*. We evaluated whether treatment of Colon26 tumor-bearing mice with BNCT+DCs could elicit tumor-specific IFN-γ secreting T cells using ELISPOT assays. Splenocytes retrieved on day 40 after tumor inoculation from mice subjected to the BNCT+ 3 times DCs combined therapy showed slightly activated tumor-specific IFN-γ-secreting cells, while schedule 2 with BNCT+ 7 times DCs resulted in significantly more tumor-specific IFN-γ-secreting cells compared with splenocytes from control groups (data not shown).

To examine whether tumor-specific immune response was induced in BNCT-DC treated mice, splenocytes harvested from treated mice on day 40 after tumor inoculation were transferred i.v. to syngeneic mice, and, Colon26 cells (5 x 10^5 cells) were injected subcutaneously. In tumor challenged mice, that received spleen cells from DC-treated mice and BNCT-treated mice, tumor growth was suppressed by 25%. Fifty % reduction in tumor growth was observed in mice that received spleen cells from BNCT+DCs treated mice (Figure 3).

Celluzzi *et al.* had reported that it is possible that radiation augments the antitumor efficacy of DC administration by modifying tumor cells to become more immunogenic (Celluzzi, 1998). This would allow *ex vivo*-generated functional DCs to acquire TAAs from irradiated tumor cells more efficiently than they would acquire them from nonirradiated tumor cells. One of the hallmarks of inflammation is an increase in the permeability of the local vasculature that leads to recruitment of circulating leukocytes into surrounding tissues. Recently, it has been shown that necrotic tumor cells can serve as a source of multiple TAAs to pulse DCs as effectively as apoptotic tumor cells (Kotera, 2001).

In these experiments, our data indicate that DC administration combined with BNCT induces tumor antigen-specific cellular-mediated immune responses in tumor bearing mice. DCs combined with BNCT of a solitary tumor confers protection against tumor rechallenge. It is thought that tumor antigens derived from necrosis, apoptosis, and inflammation induced by BNCT had been presented to DCs in BNCT+DCs combined therapy. The growth of Colon26 tumors was highly suppressed in mice that received splenocytes from BNCT+DCs treated mice.

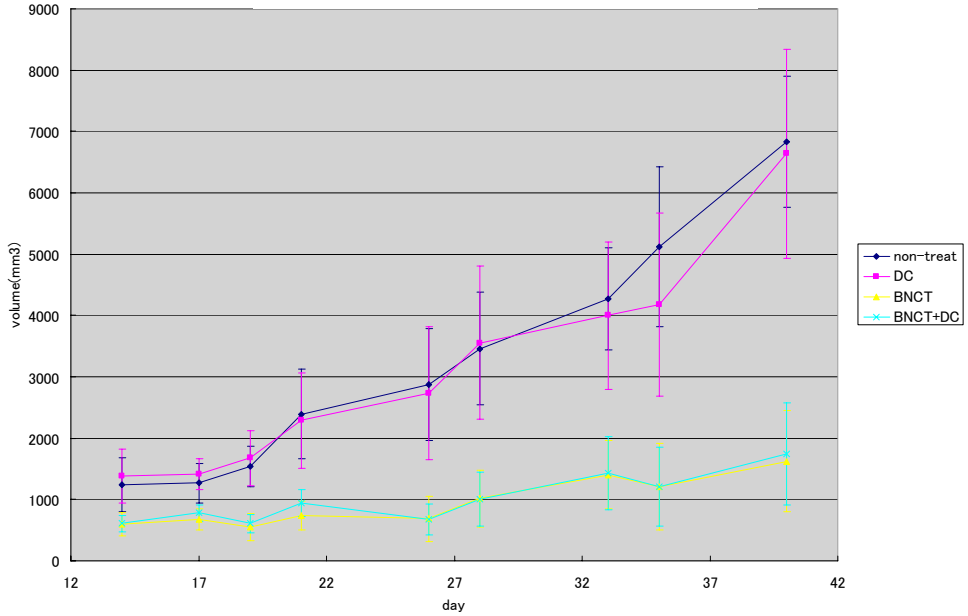

Figure 1. Effect of combination treatment with BNCT and IT-DC on Colon26 tumors

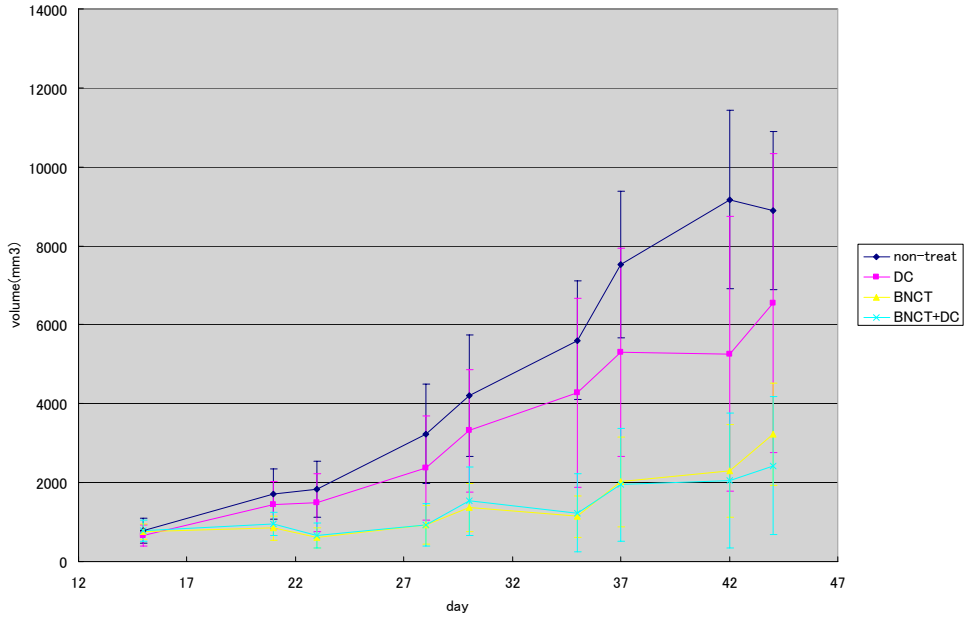

Figure 2. Enhancement of tumor growth suppression with increased intratumoral injections of DCs on BNCT and IT-DC treatments

Regulatory T cells and suppressor macrophage will be necessary to delete in the adoptive splenocytes for more stimulation the anti-tumor immunity (*not clear)*. We hope to apply this direct DC immunotherapy for enhancing the BNCT effects in clinical trials.

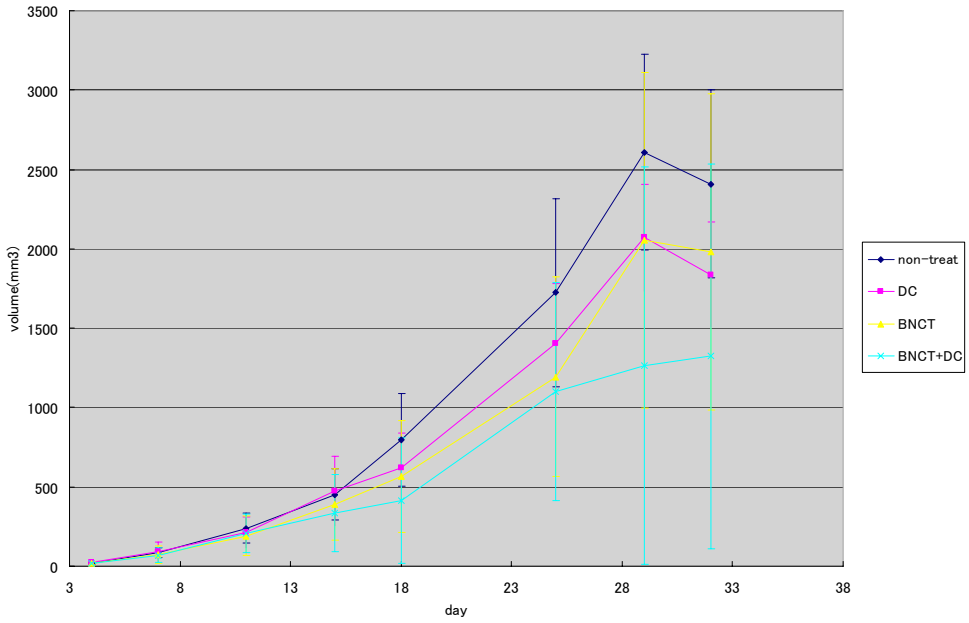

Figure 3. Tumor growth suppression with adoptive immunity by BNCT+DCs on new challenging Colon26 tumor

4. Conclusion

Colon26 tumor growth was suppressed in the groups of BNCT and BNCT with DC injections relative to controls. The growth of colon26 tumors was highly suppressed in mice that received spleen cells from DC-treated mice, suggesting that anti-tumor immunity was induced by DC treatment. Direct DC immunotherapy can enhance the anti-cancer effect of BNCT and have promising clinical application in near future.

References

Candido, K. A., et al., 2001. Local administration of dendritic cells inhibits established breast tumor growth: implications for apoptosisinducing agents, Cancer Res., 61: 228–236.

Celluzzi, C. M., and Falo, L. D., Jr., 1998. Physical interaction between dendritic cells and tumor cells results in an immunogen that induces protective and therapeutic tumor rejection, J. Immunol., 160: 3081–3085.

Chang, A. E., et al., 2002. A Phase I trial of tumor lysate-pulsed Dendritic cells in the treatment of advanced cancer, Clin. Cancer Res., 8: 1021–1032.

Friedman, E. J., 2002. Immune modulation by ionizing radiation and its implications for cancer immunotherapy, Curr. Pharm. Des., 8: 1765–1780.

Kotera, Y., Shimizu, K., and Mule, J. J., 2001. Comparative analysis of necrotic and apoptotic tumor cells as a source of antigen(s) in dendritic cell-based immunization, Cancer Res., 61: 8105–8109.

Nikitina, E. Y., and Gabrilovich, D. I., 2001. Combination of γ-irradiation and dendritic cell administration induces a potent antitumor response in tumor-bearing mice: Approach to treatment of advanced stage cancer, Int. J. Cancer, 94: 825–833.

Quarmby, S., Kumar, P., and Kumar, S., 1999. Radiation-induced normal tissue injury: Role of adhesion molecules in leukocyte-endothelial cell interactions, Int. J. Cancer, 82: 385–395.

H Saji H, et al., 2006. Systemic Antitumor Effect of Intratumoral Injection of Dendritic Cells in Combinationwith Local Photodynamic Therapy, Clin Cancer Res, 12(8), 2568-2574.

Strome, S. E., et al., 2002. Strategies for antigen loading of dendritic cells to enhance the antitumor immune response, Cancer Res., 62: 1884–1889.

Yanagie H, et al., 1991. Application of boronate anti-CEA immuno liposome to boron neutron capture therapy model, Brit. J. Cancer, 3(4): 522 - 526.

Yanagie H, et al., 1997. Inhibition of human pancreatic cancer growth in nude mice by boron neutron capture therapy, British Journal of Cancer, 75 (5) : 660 - 665.

Yanagië H, et al., 1999. Neutron capture autoradiographic determination of ^{10}B distributions and concentrations in biological samples for boron neutron capture therapy, Nucl. Instr. Meth., A 424, pp.122-128.

BNCT for oral squamous cell carcinoma with p53 gene mutation

Yusei Fujita[1], Akitoshi Kamida[1], Itsuro Kato[1], Koji Ono[2], Minoru Suzuki[2], Yoshinori Sakurai[3], Takeo Ohnishi[4], Ken Ohnishi[4], Yoshiaki Yura[1]

[1]*Department of Oral and Maxillofacial Surgery II, Osaka University Graduate School of Dentistry, Osaka 565-0871, Japan*
[2]*Radiation Oncology Research Laboratory, Research Reactor Institute, Kyoto University, Osaka 590-0494, Japan*
[3]*Radiation Life Science, Research Reactor Institute, Kyoto University, Osaka 590-0494, Japan*
[4]*Department of Biology, Nara Medical University, Nara 634-8521, Japan*

Abstract

Mutation in p53 tumor suppressor gene is a genetic alteration frequently observed in oral squamous cell carcinoma (SCC). We examined the effect of boron neutron capture therapy (BNCT) on oral SCC cells showing either wild-type P53 (SAS/neo) or mutated-type p53 (SAS/mp53). When SAS/neo and SAS/mp53 cells were subjected to BNCT using boronophenylalanine (BPA) as a boron compound, a greater suppressive effect on colony formation was observed in SAS/neo cells as compared with SAS/mp53 cells. Flow cytometric analysis revealed that there was no increase of cells at G0/G1 in SAS/mp53 cells, although the proportion of cells at G2/M was increased after an interval. Examined by immunoblot analysis, the expression of p21 was markedly increased after BNCT in SAS/neo cells, but not in SAS/mp53 cells. Wee1 and cdc-2 were elevated after BNCT in both cell lines. These results suggest that oral SCC cells with mutated p53 cells are more resistant to BNCT than those with wild-type p53. The resistance of oral SCC cells with mutated p53 is ascribed in part to the lack of apoptotic cell death subsequent to G1 arrest.

Keywords: BNCT, p53, mutation, SAS/neo, SAS/mp53

Introduction

Oral SCC patients are generally treated with surgery in combination with radiation therapy and/or chemotherapy. It has been shown that the p53 gene serves a critical role in maintaining genomic stability during the cell cycle checkpoint in G1 and G2/M transition by the suppression of gene errors. p53 also participates in apoptosis thus controlling the sensitivity of cells to ionizing radiation therapy. Loss of p53 function in certain cancer cells can lead to resistance to radiation therapy. However, whether the p53 gene can affect the sensitivity of oral SCC cells to BNCT had not been studied so far. In the present study, we examined the effects of BNCT on cell survival, apoptosis and cell cycle in oral SCC cells showing wild-type p53 or mutated type p53.

Material and methods

Cells

SAS cells derived from human SCC of the tongue were cultured in Dulbecco's modified Eagle's medium containing 10 % fetal bovine serum at 37° C. SAS cells showed the phenotype of wild-type p53. Plasmid pC53-248, which contains mutated p53 (mp53) gene (codon 248, from Arg to Trp248), was used to produce a dominant negative mp53 protein. Plasmid pCMV-Neo-Bam, which contains neo-resistance marker, was used as a control.

Boron compound and BNCT for cultured cells

^{10}B-enriched (>98%) BPA was purchased from Boron Biologicals, Inc. and converted to a fructose complex to increase its solubility. The concentration of the aqueous suspension of BPA was adjusted to 250 mg/ml (21.28 mg ^{10}B/ml).

SAS cells were incubated in the presence of 50 ppm of BPA for 2 h and then exposed to thermal neutron beam irradiation for 2 h at Kyoto University Research Reactor. The neutron fluence was measured by radioactivation of gold foils on the front and back of the dishes. The average fluence of the thermal neutrons was 2.1 x 10^{12} n/cm^2 and the average flux was 2.3 x 10^9 n/cm^2/s at 5 MW. Thermoluminescent dosimeters were used for gamma-ray dosimetry. BNCT was performed at a physical dose of 6 Gy.

Colony formation assay

Cells were plated in 6-well plates at the density of 500 cells/well. The colonies obtained 7 days after BNCT were fixed with methanol and stained with 1 % crystal violet. Colonies composed of more than 30 cells were counted. The surviving cell fraction was determined by dividing the number of colonies in the treated culture by that in the unirradiated control culture.

Flow cytometric analysis

Cells were harvested and fixed in 70 % ethanol at -20° C for 24 h. The cells were then resuspended in 1 ml of PBS solution containing 10 mg/ml propidium iodide (PI) and RNase and incubated for 20 min at room temperature. Samples were then analyzed on a Becton Dickinson FACSort flow cytometer. From an analysis of DNA histograms, the percentages of cells in the sub-G1, G0/G1, S, and G2/M phases were evaluated.

Hoechst staining

Trypsinized cells were fixed in 70 % ethanol at -20° C. After removing the ethanol and washing in PBS, the cells were stained with 1 mM DNA binding dye Hoechst 33342. Cells were visualized in a Nikon Microphot-FXA fluorescence microscope.

Immunoblot analysis

Cells were washed in PBS and lysed in a buffer containing 20 mM Tris-HCl (pH 7.4), 0.1 % sodium dodecyl sulfate, 1 % Triton X-100, 1 % sodium deoxycholate and protease inhibitor cocktail.

After sonication on ice and subsequent centrifugation at 15,000 g for 10 min at 4° C, the supernatant was collected and the protein concentration was determined using a Protein Assay Kit.

The effect of BNCT on the cell cycle

Proteins (20 μg) were electrophoresed through a polyacrylamide gel and transferred to a polyvinylidene fluoride membrane by electroblotting. The membrane was probed with antibodies and antibody-binding was detected using an enhanced chemiluminescence kit according to the manufacturer's instructions. Antibodies used were as follows: mouse monoclonal rabbit antibodies against p53, p53 phosphorylated at serine 15, p21, and β-actin and rabbit polyclonal antibodies against cdc2, and cdc2 phosphorylated at tyrosine 15. The β-actin expression was assessed to ensure equal protein loading.

Results

Effect of BNCT on the colony formation of oral SCC cells

SAS/neo and SAS/mp53 cells were treated with BNCT and the survival ratios were measured by colony formation. In both cell lines, the survival ratios were decreased in a dose-dependent manner, but the suppressive effect was more prominent in SAS/neo cells. At a dose of 6 Gy, the survival ratios in SAS/neo cells and SAS/mp53 cells were 8 % and 36 %, respectively (Fig.1).

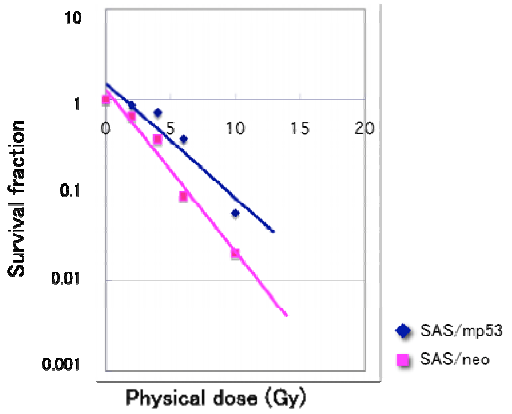

Fig.1. Effect of BNCT on cell survival

Effect of BNCT on cell cycle

SAS/neo cells were treated with BNCT and then subjected to flow cytometric analysis. The proportion of cells at G0/G1 was increased at 6 h after BNCT, but that of G2/M was increased from 12 h. In SAS/mp53 cells, there was no increase of cells at G0/G1, although cells at G2/M were increased at 12 h after BNCT. Increase of sub-G1 peak indicating apoptotic cells was observed from 6 h in SAS /neo cells, while it occurred from 48 h in SAS/mp53 cells (Fig.2).

Effect of BNCT on apoptotic cell death

To determine whether BNCT could induce apoptotic cells with DNA fragmentation, Hoechst 33342 staining was performed. In SAS/neo cells, the proportion of apoptotic cells at 6 h after BNCT was over 3.7 %. In the case of SAS/mp53, apoptotic cells were found at a control level, but the proportion was increased to 2 % from 48 h after BNCT (Fig.3).

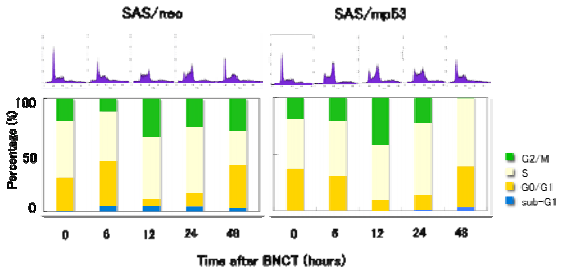

Fig. 2. Effect of BNCT on cell cycle

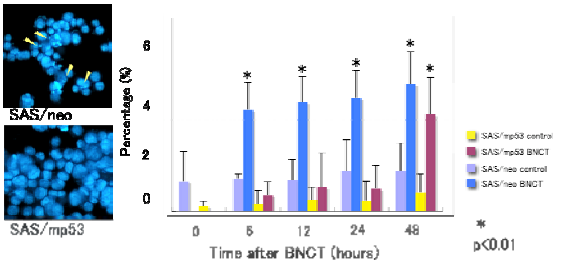

Fig. 3. Effect of BNCT on apoptotic cell death

Effect of BNCT on G1 checkpoint- and G2 checkpoint-related proteins

Proteins prepared from BNCT-treated cells were subjected to immunoblot analysis for G1 checkpoint-related proteins, p53 and p21. In SAS/neo cells, the expression and phosphorylation of p53 were increased after BNCT and a maximal phosphorylation level was achieved at 6, 24 and 48 h after BNCT (Fig.4a). The expression of p21 was markedly increased at 6 h after BNCT in SAS/neo cells, but not in SAS/mp53 cells.

Wee1 protein kinase that phosphorylates cdc-2 at its threonine-14 and tyrosine-15 residues is involved in the G2 checkpoint. The expression of Wee1 was elevated from 12 to 24 h after BNCT in both cell lines (Fig.4b). The phosphorylation level of cdc2 was markedly elevated from 12 to 24 h and returned to the initial level at 48 h in SAS/neo, and a transient increase was observed at 12 h after BNCT in SAS/mp53 cells.

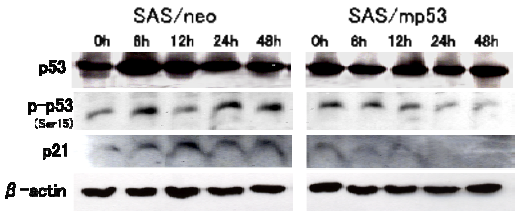

Fig.4a. Effect of BNCT on G1 checkpoint-related proteins

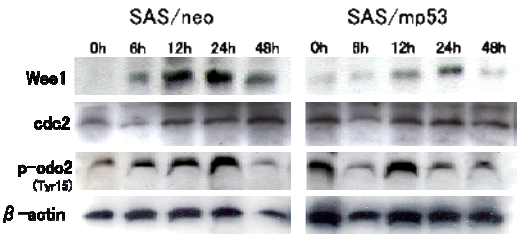

Fig.4b. Effect of BNCT on G2 checkpoint-related proteins

Discussion

It was reported that ionizing radiation efficiently induced apoptosis in SAS/neo cells, but hardly induced apoptosis in SAS/mp53 cells. Consistent with these results, we found that SAS/mp53 cells survived 6 Gy BNCT at a higher ratio than SAS/neo cells. Thus, the expression of functional p53 must be required for efficient growth suppression of oral SCC cells by BNCT.

We found that BNCT affected cells cycle and induced G1 and G2 arrests in SAS/neo cells. Apoptosis subsequent to G1 arrest was also observed. In contrast, only G2 arrest was induced in SAS/mp53 cells and apoptosis became prominent at late time after BNCT. Thus, it is considered that p53 is associated with the induction of G1 arrest and G1 arrest-related apoptosis. Hoechst 33342 staining revealed the DNA fragmentation of BNCT-treated

SAS/mp53 cells as well as SAS/neo cells. This indicates that BNCT induced apoptosis in both cell lines, although the intervals after BNCT are different.

Cell cycle of oral SCC cells is regulated by the function of checkpoint-related proteins. As expected, the G1 checkpoint-related proteins, p53 and p21, were not altered in SAS/mp53 cells. G2 checkpoint-related proteins, Wee1 and cdc-2, were elevated at 12 h after BNCT in both cell lines.

These results suggest that oral SCC cells with mutated p53 cells are more resistant to BNCT than those with wild-type p53. The resistance of oral SCC cells with mutated p53 is ascribed in part to the lack of apoptotic cell death subsequent to G1 arrest.

BNCT would inhibit oral SCC cells by p53-dependent and p53-independent mechanisms.

References

Kamida A et al., "Effects of boron neutron capture therapy on human oral squamous cell carcinoma in a nude mouse model." Int J Radiat Biol. 2006 Jan;82(1):21-9.

Obayashi S et al., "Delivery of (10)boron to oral squamous cell carcinoma using boronophenyl- alanine and borocaptate sodium for boron neutron capture therapy. Oral Oncol." 2004 May;40(5):474-82.

Kato I et al., "Effectiveness of BNCT for recurrent head and neck malignancies." Appl Radiat Isot. 2004 Nov;61(5):1069-73.

Takahashi A et al., "p53-dependent thermal enhancement of cellular sensitivity in human squamous cell carcinomas in relation to LET." Int J Radiat Biol. 2001 Oct;77(10):1043-51.

Yasumoto J et al., "Analysis of apoptosis-related gene expression after X-ray irradiation in human tongue squamous cell carcinoma cells harboring wild-type or mutated p53 gene." J Radiat Res (Tokyo). 2003 Mar;44(1):41-5.

Masunaga S et al., "Impact of the p53 status of the tumor cells on the effect of reactor neutron beam irradiation, with emphasis on the response of intratumor quiescent cells." Jpn J Cancer Res. 2002 Dec;93(12):1366-77.

Feasibility study of the utilization Boron Neutron Capture Therapy (BNCT) in diffuse rat Lung Metastases

J.G. Bakeine[a], M.Di Salvo[a], S. Bortolussi[a,b], S.Stella[a,b], P. Bruschi[a], A. Bertolotti[c], R. Nano[c], A.Clerici[d], C. Ferrari[d], C. Zonta[d], A.Zonta[d], A Marchetti[e] and S.Altieri[a,b]

[a] *Dept. of Nuclear and Theoretical Physics, University of Pavia,Pavia, Italy*
[b] *National Iinstitute of Nuclear Physics (INFN), Section of Pavia, Pavia, Italy*
[c] *Department of Animal Biology, University of Pavia, Italy*
[d] *Dept. of Surgery, Experimental Surgery Laboratory, University of Pavia, Pavia, Italy*
[e] *Scientific Research Office, Fondazione San Matteo University Policlinic, Pavia, Italy*

Abstract

In order for BNCT to be eligible for clinical application in lung tumour disease, three fundamental criteria must be fulfilled; there must be selective uptake of boron in the tumour cells in respect to surrounding healthy tissue, biological effectiveness of the radiation therapy and minimal damage or collateral effects of the irradiation on the surrounding tissues. In this ongoing study, we evaluated the biological effectiveness of BNCT by *in vitro* irradiation of rat colon-carcinoma cells previously incubated in boron-enriched medium. One part of these cells was re-cultured *in vitro* while the other was inoculation via the inferior vena cava to induce pulmonary metastases in a rat model.

We observed a post-irradiation cell viability of 0,05% after 8 days of cell culture. At four months follow-up, all animal test subjects that received irradiated cells were alive while no animal survived beyond one month in the control group that received non-treated cells. ($P<0.001$ Kaplan-Meier). These preliminary finds strongly suggest that BNCT has a significant lethal effect on tumours cells and post-irradiation surviving cells lose their malignant capabilities. This radio-therapeutic potential warrants the investigation BNCT in *in vivo* lung tumour metastases.

Keywords: Boron Neutron Capture Therapy, coloncarcinoma metastases, BPA release, cell survival

1. Introduction

Boron Neutron Capture Therapy (BNCT) and clinical rationale

An ideal therapy for metastatic lung disease would be one whereby all tumour cells are selectively destroyed without damaging normal tissue. Despite today's state-of-the-art treatment strategies -surgery, radiation therapy and chemotherapy- very little progress has been made in terms of survival, and overall prognosis for these patients remains poor. As such, metastatic lung disease remains the leading cause of tumour death in the western world. For this reason any efforts to identify and validate new effective therapeutic procedures for lug cancer is timely and essential.

BNCT is an experimental form of binary radiotherapy based on thermal neutron radiation with the potential to preferentially deliver a lethal radiation dose to tumour cells while sparing normal tissue after the infusion of a boronated drug that can selectively load the tumour cells with ^{10}B [1,2]. This selective potential of boron uptake in the tumour with respect to healthy surrounding tissues makes BNCT an extremely attractive technique in the cure of tumours that affect whole vital organs that are surgically inoperable, not responsive to current radio-chemotherapy, or micro metastases that are not visible with state-of-the-art radiological diagnostic tools.

The physical principle of BNCT is simple and elegant. The binary radiation therapy modality brings together two components that when kept separate have only minor effects on cells. The thermal neutron capture reaction where non-radioactive isotope ^{10}B atoms that have absorbed low energy neutrons (>0.5eV) disintegrate into alpha (^{4}He) particles and recoiled lithium nuclei (^{7}Li), [$^{10}B(n,\alpha)^{7}Li$]. These particles deposit large amounts of energy along their very short path (<10 μm). Given that a sufficient number of Boron atoms are loaded in a tumour cell, on thermal neutron. irradiation, the subsequent nuclear reaction triggered causes irreversible damage to the DNA, leading to cell apoptosis.

It is therefore straightforward that the limitation to the successful outcome of BNCT is that a sufficient number of ^{10}B atoms must accumulate in the tumours, and that the concentration gradient of ^{10}B atoms between the tumours and surrounding normal tissues must be large to permit irradiation of the tumour regions with an efficient neutron dose which must be tolerable to the surrounding normal tissues which are also inevitably irradiated.
In our previous work on boron pharmacokinetics using a rat model with metastatic lung disease, we observed a maximal boron concentration ratio of lung tumour to healthy lung tissue of 4.5 four hours after of intra-peritoneal BPA infusion [5,6].
Coderre et al [8] investigated post-irradiation damage in healthy lung after whole-thorax thermal neutron irradiation in a rat model previously infused with p-boronophenylalanine (BPA). They determined that at radiation dose of 7.0 ±0.5 Gy, fifty percent of the animal subjects (ED_{50}) had a positive histological response of atinic pneumonitis. (And suggested this to be dose-limiting toxicity). In view of the findings in the studies mentioned above, the objective of this study was to test if there is a rationale for BNCT in metastatic lung disease when neutron radiation doses are administered within these limits.
In this study we associate three sets of experiments. In the first set, rat colon carcinoma cells were incubation in BPA containing medium and subsequently under went *in vitro* thermal neutron irradiation followed by post irradiation cell culture to determine the biological effectiveness of BNCT.
In the second set of experiments the *in vitro* post irradiated cells were inoculated via the inferior vena cava of rat subjects in order to induce lung metastases and their survival endpoint was determined.
In the third set of experiments *in vitro* post irradiated cells were inoculated via the inferior vena cava of rat subjects which were sacrificed at a monthly interval and pulmonary histology endpoint as a function of time was determined.
We report the results of our findings and an attempt to draw working conclusions on the feasibility of BNCT in lung metastases are presented.

Methods

In vitro cell irradiation

DHD/K12/TRb colon-carcinoma cell line obtained from a 1,2 dimethyhydrazine-induced colon adenocarcionoma in syngeneic BDIX rats, selected and cloned for their capacity to induce progressive and metastatic tumours in syngeneic host [7] were cultured in medium composed of a mixture (50:50 v/v) of HAM's F10 and DMEM low glucose addition with 10% FBS and 1% Gentamycin. Cells were incubates for 4 hours in medium supplemented with BPA to a final concentration of 80μg/ml and then rapidly rinsed three times in PBS to remove any un-absorbed BPA and normal medium was replaced. Thereafter, the cells were subjected to thermal neutron radiation in the TRIGA Mark II reactor of the University of Pavia at a power of 250 KW for 10 minutes. The thermal neutron flux in the irradiation position was 1.7 x 10^{10} cm^{-2} s^{-1}. Irradiated cells without boron enrichment acted as controls.

Post-irradiation cell viability

Irradiated and non irradiated control cells with and without boron enrichment were plated in 5 replicate Petri dishes for each selected concentration which ranged from 10 x 10^5 and 50 x 10^5 case of boron enriched irradiated cells and from 50 to 250 in all the other remaining conditions under investigation. Colonies were allowed to grow in complete medium for 8 days, thereafter fixed, stained and counted. Only colonies containing more than 50 cells were regarded as having arisen from a surviving cell and so counted. The plating efficiency (PE) is calculated by dividing the number of colonies formed by the number of cells plated. The cells survival is expressed as the ratio of PE of irradiated cells to that of the controls.

In vivo studies

After *in vitro* cell irradiation in the TRIGA Mark II reactor as described above, a suspension of 1.5 x 10^6 cells were inoculated in the inferior vena cava of BDIX rats (Group A) via laparotomy. A total of 12 animals were inoculated with these treated cells.
In a second group of BDIX rats (Group B) that acted as positive controls, animals were inoculated with 1.5 x 10^6 cells of non-irradiated cells. While a third group of 5 rats inoculated with 0.9% water saline as placebo acted as negative controls. The animals were followed up to determine their survival.
All surgical procedures were carried out in general anaesthesia in aseptic conditions as outlined by the Animal Ethics and Experimental Committee of the University of Pavia.

Pulmonary histological for metastatic disease as function of time

At a one monthly interval after the day of inoculation, one animal each from the group inoculated with irradiated cells and the other with non-irradiated cells were respectively sacrificed using a lethal dose of general anaesthesia. The lungs were removed and conserved in 10% formalin. After fixation in paraffin, tissue specimen were sliced, placed on glass slides and analysed by light microscopy after standard haematoxylin-eosin staining. Animals that died before their programmed sacrifice date underwent necropsy and lung tissue was harvested for histological exam as above.

Results

***In vitro* BNCT leads to significant tumour cell failure to proliferate**

Assessing survival of cells after radiation depends on the demonstration that they retain the ability to produce a large number of progeny, i.e., to produce a colony. One of the commonest ways to assess cell survival is the in vitro plating assay. Cells cultured for 4 hours in medium enriched with 80 ppm BPA and irradiated with thermal neutrons for 10 minutes at 250 KW received a radiation dose of about 34 Gy resulting in 0,05% cell survival being 94% (PE=29%) that of boron enriched non radiated cells and 31% of the PE of control boron-lacking non irradiated cells. This positive result suggests that BNCT treated cells failure to repair radiation damage and to proliferate.

***In vitro* BNCT treated tumour cells do not induce lung metastases in an animal model**

To indirectly evaluate the efficiency of BNCT in an animal model, 5 BDIX rats each inoculated with 1.5 x 10^6 of boron-loaded irradiated cells (Group A) were followed up to determine the clinical outcome. Five rats inoculated with non-irradiated cells (Group B) and 5 rats inoculated with 0.9% water saline placebo (Group C) acted as positive and negative controls respectively. At 4 months follow-up, the time of the write-up of this report, all the animal subjects in group A and C which received treated cells and placebo respectively were alive. Animal subjects in group B that received non-irradiated died within one month of inoculation. The survival data of the three groups are summarized in Kaplan-Meier graph 1.

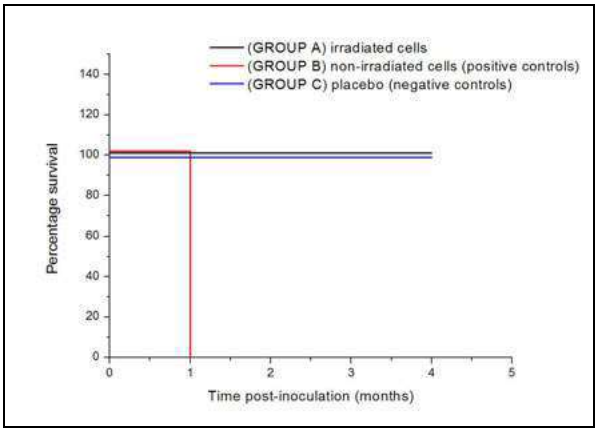

Fig.1. Kaplan-Meier graphic representation of rat subject survival in 3 groups investigated. At 4 month follow-up survival in Group A (n=5) was100% compared to Group B (n=5) which was 0% ($p < 0.001$)

Histological evaluation lung tissue of as a function of time.

In order to evaluate the presence of metastatic spread at the tissue level, lung tissue was harvested from a sacrificed animal from group A and B at a monthly interval for histological examination. Since all animals in Group B died at one month, lung tissue was harvested from one animal at day 25 and the rest at necropsy. In this ongoing study, we report on histological findings of tissue harvested at one month.

Histological specimens from group A revealed the absence of tumour however there was altered lung tissue characterised by atelectasis and emphysema (Fig. 2A).

The histology of Group B rat sacrificed at day 25 showed the presence of tumour cannon balls and emphysema (Fig. 2B) while histology from Group B rats at necropsy at 30 days depicted large tumour cannon balls that substituted almost 90% of lung tissue (Fig. 2C) hence the ensuing respiratory failure and death.

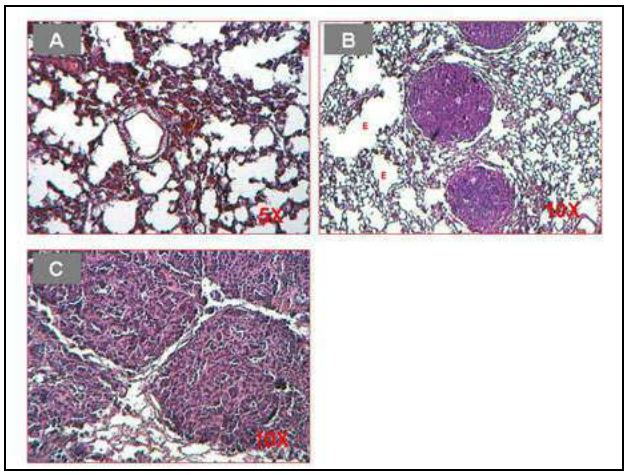

Fig. 2(A) representative histology of lung tissue from Group A at one month after inoculation with treated tumour cellls showing the absence of metastatic tumour disease but emphysema and atelectasis lung changes. **2(B)** Lung histology of rat from group B sacrificed at day 25 depicting the presence of tumour cannon balls and emphysema (E). **2(C)** histology at necropsy of rat from group B depicting the evolution of the cannon balls that substituted nearly 90% of lung tissue leading to respiratory failure and death

Discussion

In this study we evaluated the radio-biological efficiency of BNCT at the cellular level. The study design adopted assumed ideal pharmaco-dynamics so as to elucidate the maximum effect of BNCT at a predetermined thermal neutron dose. By incubating tumour cells in boron-rich medium it was assumed that maximal absorption would take place since the whole cell surface was awash with BPA. Subsequent *in vitro* irradiation also assumed maximal neutron beam exposure without beam attenuation with distance as is likely to occur solid organ irradiation.

Since the irradiation cannot be escalated beyond a given threshold due to the undesirable side effects it would cause *in vivo* to highly radio-sensitive structures like gastro-intestinal mucosa and lung, we sought to determine whether there was a rationale in investigating BNCT using the neutron dose below these threshold limits.

Although we present preliminary results, two straight forward observation can be made from this study at this point in time.

An insignificant but not negligible number of tumour cells are resistant to BNCT even under the ideal irradiation exposure at the predetermined neutron dose. However post-irradiation surviving cells lost their malignant capability and were unable to induce metastatic lung disease in the animal modal as evidenced by survival curves and histology above (Graph 1 and Fig 1). It is postulated that they were weeded out by the host immune system but caused lung structure changes.

Conclusion

Given that one rat month is equivalent to 2.5 human years, and that the inoculated rats have so far survived for 4 months, therapeutic application of BNCT *in vivo* lung tumour metastases should be investigated.

Reference

[1] J.A. Coderre, J.C. Turcotte, K.J. Riley, P.J. Binns, O.K. Harling and W.S. Kiger III. Boron Neuton Capture Therapy: cellular targeting of higher energy transfer radiation. Tech. Cance Res. Treat. 2, 355-375 (2003)

[2] R. F. Barth, J.A Coderre, M:G. Vicente and T.E. Blue. Boron neutron capture therapy of Cancer: current status and future prospects: Clin. Cancer Res. 11, 3987-4002 (2005)

[5] S. Altieri, S. Bortolussi, P.Bruschi, P. Chiari, F. Fossati, A Facoetti, R. Nano, A. Clerici, C- Ferrari, A. Zonta, C. Zonta, A. Marchetti, E. Solcia, G. J. Bakeine, O. Salvucci, in Y. Nakagawa, T.Kobyashi, H. Fukuda (Editors), Advances in Neutron Capture Therapy (Takamatsu, Japan 2006) pp 91-94.

[6] S. Bortolussi. Boron Neutron Capture Therapy of disseminated tumours. Scientifica Acta1, No. 1, 123-128 (2007)

[7] A. Cagnard, M.S. Martin, M.F. Michel and F. Michel. Interaction between two cellular subpopulations of a rat colonic carcinoma when inoculated in a sygeneic host. Int. J. Cancer. 36 273-273. 1985

[8]J.L. Kiger, W.S. Kiger, III, H. Pateal, P.J. Binns, K.J. Riley, J.W. Hopewell, O.K Harling and J.A Coderre. Effects of boron neutron capture therapy on the normal lungs of rats. J. Applies radiation and isotopes. 61: 969-973 2004

Selective Uptake of P-Boronophenylalanine by Osteosarcoma Cells for Boron Neutron Capture Therapy

C. Ferrari [a], C. Zonta [a], L. Cansolino [a], A.M. Clerici [a], A. Gaspari [a], S. Altieri [b,c], S. Bortolussi [b,c], S. Stella [b,c] , P. Bruschi [a], P. Dionigi [a], A. Zonta [a]

[a] *Dept. of Surgery, Experimental Surgery Laboratory, University of Pavia, 27100 Pavia, Italy*
[b] *Dept. of Nuclear and Theoretical Physics, University of Pavia, 27100 Pavia, Italy*
[c] *National Institute of Nuclear Physics, INFN, Section of Pavia, 27100 Pavia, Italy*

Osteosarcoma is the most common non hematologic cancer type that develops in bone. Current osteosarcoma treatment relies on surgical resection associated with adjuvant chemotherapy and frequently requires the entire limb amputation. The incidence of distal recurrences reduces the survival rate to less than 60%. These poor data request to set up a new therapeutic approach aimed to restrict the surgical removal meanwhile acting a radical treatment. Boron neutron capture therapy (BNCT) could be a valid alternative or integrative option in case of osteosarcoma management.

In this particular application field two main characteristics of BNCT could be turned in advantage: the selectivity of the therapeutic action and the possibility to deprive the circulatory system from the residual boronaded compound. Aim of the present work is to investigate the feasibility of employing BNCT to treat knee osteosarcoma. An animal tumor model was developed in Sprague-Dawley rats by means of an intrafemoral injection of UMR-106 osteosarcoma cell line at the condyle site. The tumour to normal tissue ^{10}B ratio was determined injecting boronophenylalanine (BPA) as boron carrier. The endocellular compound uptake was previously *in vitro* checked on the referred cell line and results evidence an adequate cell accumulation capability.

Despite preliminary *in vivo* data don't completely support the required prerequisite for BNCT applicability, they encourage us to express a positive judgement.

NUCLEAR ENGINEERING

Performance of a New Composite Single-Crystal Filtered Thermal Neutron Beam for Neutron Capture Therapy Research at the University of Missouri

John Brockman[a], David W. Nigg[b], M. Frederick Hawthorne[a], Charles McKibben[a]

[a] *University of Missouri, Columbia, MO USA*
[b] *Idaho National Laboratory, Idaho Falls ID USA*

Abstract

Parameter studies, design calculations and initial neutronic performance measurements have been completed for a new thermal neutron beamline to be used for neutron capture therapy cell and small-animal radiobiology studies at the University of Missouri Research Reactor. The beamline features the use of single-crystal silicon and bismuth sections for neutron filtering and for reduction of incident gamma radiation. The calculated and measured thermal neutron flux produced at the irradiation location is on the order of 9.5×10^8 neutrons/cm^2-s, with a measured cadmium ratio (Au foils) of 106, indicating a well-thermalized neutron spectrum with sufficient thermal neutron flux for a variety of small animal BNCT studies. The calculated combined epithermal and fast-neutron kerma of the beam is approximately 1.0×10^{-11} cGy-cm^2, and the calculated incident gamma kerma is approximately 4.0×10^{-11} cGy-cm^2.

Keywords: BNCT, Neutron Source, Thermal, Activation

1. Introduction

The University of Missouri (MU), the Idaho National Laboratory (INL), the National Atomic Energy Commission of Argentina (CNEA), and the University of Missouri Research Reactor (MURR) are collaborating under the leadership of the MU International Institute for Nano and Molecular Medicine in a new initiative to further the development of improved BNCT agents and treatment protocols for an array of non-traditional tumor types. A key first step of this effort has been the design and construction of a new thermal neutron beam irradiation facility for cell and small-animal radiobiological research at the MURR. Here we present the beamline design with the results of pertinent neutronic calculations as well as initial neutronic performance measurements.

2. Facility Description

The MURR reactor features a compact light-water cooled and moderated fully-enriched annular cylindrical core composed of eight plate-fuel elements. The licensed power level is 10 MW. The outer diameter of the core is approximately 30 cm (1 ft), with an active height of 60.96 cm (2 ft). The core is surrounded by a beryllium reflector, followed by a graphite reflector, all located in a deep pool of light water surrounded by a heavy concrete biological shield. Details of the new beamline design are shown in Figure 1. It is located in an existing 15.24 cm (6") diameter MURR beam tube, referred to as Beamline E, which extends from the outer surface of the beryllium reflector, through the graphite reflector, and out through the biological shield wall as shown in the figure. Key features of the new beamline include the use of a single-crystal silicon neutron filtering section followed by a single-crystal bismuth section in a manner similar to that reported by Kim et al. (2007), but without cryogenic cooling of the crystals. The irradiation location is just downstream of the bismuth filter section, at a distance of approximately 3.95 meters from the central axis of the reactor. A shielding enclosure surrounds the exit port of the beamline as shown. A hydraulic lift inside this shield enclosure enables the remote placement of samples or animals being irradiated. The single-crystal silicon section in the beamline provides the bulk of the spectral filtering, while the bismuth section provides some final neutron filtering along with its key function of reducing the incident gamma component in the beam. When the beam is not in use, the bismuth filter section rotates out of the beamline and is replaced by a Pb, steel, boral and polyethylene laminated shutter.

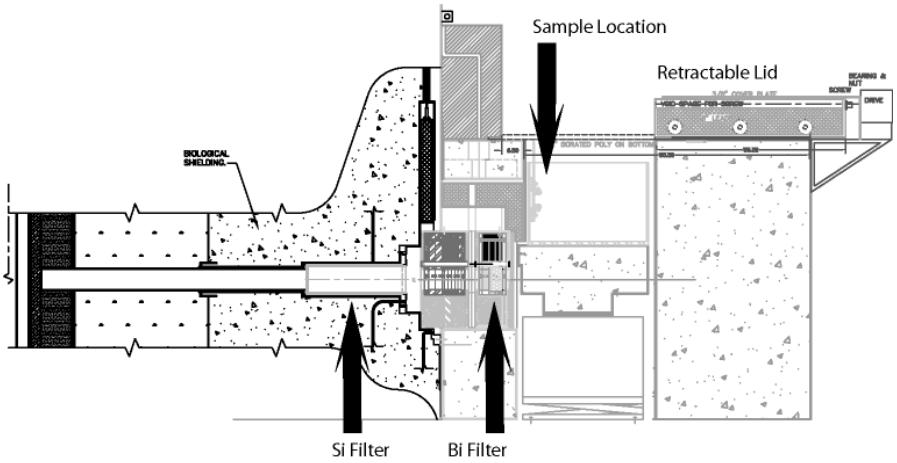

Figure 1. MURR thermal beamline design detail, shown in a closed configuration to allow access to samples.

3. Computational Methods and Models

A discrete-ordinates model of the coupled reactor core and beamline was developed using the DORT (Rhoades et al., 1993) code, using a highly forward-biased angular quadrature set consisting of 315 angular directions. The BUGLE-80 47-neutron, 20-gamma group cross section library (Roussin, 1980) was employed with the DORT computations, in keeping with previous practice at the INL for analysis of a number of other NCT neutron facilities worldwide. Modeling of the MURR with the two-dimensional cylindrical geometry option in DORT required a vertically-oriented model for the core, coupled at the outer boundary of the bismuth reflector to a separate, horizontal, model for the beamline. The thermal scattering cross sections for amorphous bismuth and silicon in the BUGLE-80 library were adjusted to account for the single-crystal form of these materials using correction factors computed using an MCNP (Briesmeister, 1999) model of the beamline. This model employed special cross section sets for the single-crystal bismuth and silicon regions that were provided to MU and INL for this study by the Korean Atomic Energy Research Institute (Lee, 2007). These modified cross sections were prepared (Kim et al., 2007) according to models described by Freund (1983).

Several parameter studies were conducted, varying the thicknesses of the silicon and bismuth filter sections to find an optimum that maximized the thermal neutron flux while maintaining the fast-neutron and gamma components of the beam within acceptable ranges. These computations led to the conclusion that the silicon filtering section should be 50-55 cm in thickness along the beamline, while the bismuth section should be 8-10 cm in thickness.

Neutron spectra at the irradiation location are shown in Figure 2 for the unfiltered beamline, for the beamline with 50 cm of silicon only, and for the fully-filtered Si(50cm)/Bi(8cm) configuration. The total calculated thermal neutron flux (0 – 0.414 eV) delivered to the irradiation location by the fully-filtered beam (Si/Bi) with the reactor at 10 MW was approximately 9.6 x 10^8 neutrons/cm^2-s with an estimated uncertainty of approximately 10%. The DORT calculations yielded a combined epithermal and fast-neutron dose rate of 0.7 cGy/min and an incident gamma dose rate of 2.3 cGy/min.

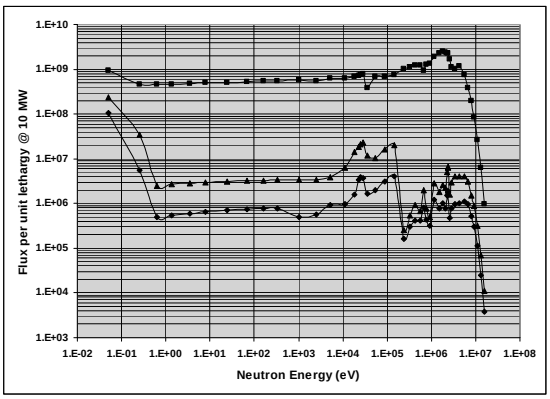

Figure 2. Computed unfiltered (■), silicon-filtered (▲), and Si+Bi filtered (♦) neutron spectra at the irradiation location for the MURR thermal beam.

Table 1. Preliminary performance results for the thermal-neutron BNCT facility at MURR

	Voided Beamline	8 cm Bi Crystal	50 cm Si Crystal	50 cm Si + 8 cm Bi
Saturation Activity, Bare Gold Foil (Bq/atom)	1.31×10^{-12} (5%)	3.82×10^{-13} (5%)	2.38×10^{-13} (5%)	8.67×10^{-14} (5%)
Saturation Activity , Cd Covered Gold Foil (Bq/atom)	4.11×10^{-13} (5%)	7.49×10^{-14} (5%)	3.64×10^{-15} (5%)	8.21×10^{-16} (5%)
Difference in Saturation Activity, Bare-Cd (Bq/atom)	8.95×10^{-13} (8%)	3.07×10^{-13} (5%)	2.34×10^{-13} (5%)	8.59×10^{-14} (5%)
Measured Thermal Flux (n/cm^2-s)	9.80×10^{9} (11%)	3.36×10^{9} (8%)	2.56×10^{9} (8%)	9.41×10^{8} (8%)
Calculated Thermal Flux from DORT (n/cm^2-s)	9.38×10^{9} (10%)	3.81×10^{9} (10%)	2.22×10^{9} (10%)	9.62×10^{8} (10%)
Cadmium Ratio (Bare/Cd)	3.19 (7%)	5.10 (7%)	65.4 (7%)	105.6 (7%)
Wire saturation activity ratio (Au/Cu)	36.4	28.4	22.4	22.4

Note: Reactor power is 10 MW. Uncertainties (1σ) are shown in parentheses.

4. Measurements and Results

Basic beam performance measurements for an initial configuration of the beamline with 50 cm of single-crystal silicon and 8 cm of single-crystal bismuth in place, but without the rotating shutter, were focused on quantifying the thermal neutron flux intensity and the approximate spectral quality. Measurements were conducted using gold foils with and without cadmium covers as well as with flux wires composed of natural copper alloyed with 1.55% gold by weight. Some scoping measurements to estimate the gamma dose rate at the irradiation location were also performed using Landauer TLD-100 dosimeters. Initial measurements were conducted for the following beamline filter arrangements: 1) the open, unfiltered, beamline, 2) the bismuth filter and no silicon filter, 3) the silicon filter and no bismuth and, 4) the silicon filter, followed by the bismuth filter. This allowed independent evaluation of the performance of each of the two filter components separately, and in combination. The activation foils and wires and the gamma dosimeters were placed in the center of the beamline at the approximate axial location of the irradiation position in the planned final configuration. After irradiation, the absolute activities of the foils and wires were measured using a high-purity germanium detector and converted to saturation activity per atom in the usual manner.

The results of the preliminary measurements are listed in Table 1. The "measured" thermal flux values given in Table 1 were obtained by dividing the difference between the bare and cadmium-covered foil activities by a computed (MCNP) effective average thermal (0-0.414 eV) cross section for the bare foils (91.3 b ± 3%). The statistical uncertainties associated with the saturation activities shown in Table 1 are approximately 2% (1σ), including both the counting statistics for the foil being measured as well as the uncertainty associated with the detector calibration. In addition, based on the observed reproducibility of the foil measurements for each beamline configuration, it is estimated that there is an additional systematic uncertainty of approximately 3% associated with the saturation activities in Table 1, largely caused by foil positioning uncertainty.

The silicon filter increased the cadmium ratio from 3.1 in the voided beamline case to 65.4 indicating that it is effectively removing epithermal and fast neutrons while transmitting thermal neutrons. The measured thermal flux with both the silicon and bismuth filters in place was 9.40 x 10^8 n/cm^2·s with a Cd ratio of 105.6, indicating a well-thermalized beam with sufficient thermal neutron flux for a variety of small animal BNCT studies. The measured cadmium ratios for the various configurations are very consistent with expectations and show the anticipated trend toward greater thermalization of the beam as filter components are added. The ratios of gold activity to copper activity induced in the flux wires for each configuration confirm the spectral trends shown by the foil data. This ratio approaches a theoretical minimum of approximately 22 (i.e. the corresponding thermal cross section ratio) as the beam is thermalized by the various filter combinations.

The preliminary gamma dose measurements using the Landauer TLD-100 dosimeters were suspect, due to potential neutron sensitivity of these particular dosimeters as well as issues related to prompt gamma emission from some of the temporary beamstop shielding materials that were, of necessity, present during the measurements.

5. Conclusions

Parameter studies, design calculations and initial performance measurements have been completed for a new thermal neutron beamline for neutron capture therapy cell and small-animal radiobiology studies at the University of Missouri Research Reactor. Results indicate that typical single-fraction irradiations to the required total accumulated dose for clinical relevance (6-10 Gy) can be conducted in an hour or less, depending on the tissue boron content, which is typically in the range of 20-100 parts per million by weight. Once the rotating beam shutter and the permanent beamstop shielding components have been installed, a much more comprehensive set of activation measurements will be conducted to characterize the neutronic performance of the final system. The incident gamma component of the MURR neutron source will also be measured using a set of FarWest^{TM} paired ion chambers, in keeping with international recommendations (Järvinen and Voorbrack, 2003).

6. References

Breismeister, J.F., 1999. "MCNP – A General Monte Carlo N-Particle Transport Code, Version 4C, LA-13709-M, Los Alamos National Laboratory, USA .

Freund, A.K., 1983. Cross Sections of Materials used as Neutron Monochromators and Filters, Nuclear Instruments and Methods, **243:**495-501.

Järvinen, H., and Voorbraak, W.P., 2003. Recommendations for the Dosimetry of Boron Neutron Capture Therapy, Report 21425/03 55339/C, NRG Petten, The Netherlands.

Kim, Myong-Seop et al., 2007. Development and characteristics of the HANARO neutron irradiation facility for applications in the boron neutron capture therapy field, Phys. Med. Biol. **52** 2553-2566

Lee, Byung-Chul, 2007. Korea Atomic Energy Research Institute, Private communication.

Rhoades, WA, et. al., 1993. TORT-DORT: Two and Three-Dimensional Discrete-Ordinates Transport, Radiation Shielding Information Center, Oak Ridge National Laboratory, CCC-543.

Roussin, R.W., 1980. BUGLE-80 Coupled 47-Neutron, 20 Gamma-Ray P3 Cross Section Library, DLC-75, Radiation Shielding Information Center, Oak Ridge National Laboratory, USA.

Acknowledgements

This work was supported by the University of Missouri Institute for Nano and Molecular Medicine. The University of Missouri Research Reactor organization provided essential logistics, engineering and machine shop support. Some in-kind material contributions were made by the US Department of Energy through the Idaho National Laboratory.

New irradiation facility for biomedical applications at the RA-3 reactor thermal column

M. Miller[a], J. Quintana[b], J. Ojeda[b], S. Langan[b], S. Thorp[a], E. Pozzi[b], M. Sztejnberg[a], G. Estryk[b], R. Nosal[b], E. Saire[b], H. Agrazar[b], F. Graiño[b]

[a] *Instrumentation and Control Department, National Atomic Energy Commission, Argentina*
[b] *RA-3 Nuclear Reactor, National Atomic Energy Commission, Argentina*

Abstract

A new irradiation facility has been developed in the RA-3 reactor in order to perform trials for the treatment of liver metastases using BNCT. RA-3 is a production research reactor that works continuously 5 days a week. It had a thermal column with a small cross section access tunnel, not accessible during operation. The objective of the work was to perform the necessary modifications to obtain a facility to irradiate a portion of the human liver left lobe. This irradiation facility had to count on a highly thermalized neutron spectrum, a thermal flux of around 10^{10} n cm^{-2} s^{-1} as isotropic and uniform as possible, the possibility of introducing on-line instrumentation, and no interference in the regular production. The main modifications consisted of obtaining an access tunnel inside the thermal column with the suitable dimensions, reducing gamma dose rate in the irradiation position, and constructing properly shielded entrance gates enabled through a logical control for the safe operation with the reactor at full power (safe introduction and withdraw of samples). Conventional activation foils techniques and a neutron shielded graphite ionization chamber were used for the preliminary characterization of the irradiation site in air. The facility was constructed and resulted very practical and easy to use. The operation was authorized by radioprotection personnel after checking that the levels of radiation had no significant changes compared to the registered before the modification. A highly thermalized and homogenous irradiation site was obtained. Measures in the empty cavity showed a thermal flux near 10^{10} n cm^{-2} s^{-1}, a Cadmium ratio of 4100 for Gold foils and a gamma dose rate of around 5 Gy h^{-1}.

Keywords: BNCT thermal irradiation facility, ex-situ treatment, biological sample irradiation

1. Introduction

A new concept of BNCT was applied in 2001 by the University of Pavia (Pinelli et al., 2002). Unlike previous treatments, where patient's tumors were irradiated in-situ with external collimated beams of thermal or epithermal neutrons, the new idea considered the resection of the zone to be treated, its irradiation with thermal neutron inside a nuclear reactor thermal column and finally its re-implantation. This condition allows the immersion of the biological sample in a near isotropic neutron radiation field providing a reasonable uniformity (especially for small samples) in all the volume.

This is an important requirement for diffused and multifocal tumors. University of Pavia applied this idea to an entire liver with multifocal unresectable metastasis. Due to flux non uniformity along the organ the treatment included its irradiation in two positions rotated 180º. Results were promising. Based on these ideas, an alternative technique was proposed by a liver surgeon of the Roffo Institute (Cardoso et al., 2007). It was based on ex-situ irradiation and partial liver autograft that has the advantage for the patient of the absence of an anhepatic phase. Besides, treating a small portion, instead of the whole organ, would provide better uniformity during neutron irradiation.

In order to carry out this treatment in the frame of the Argentine BNCT project, it was decided to construct a new irradiation facility in the thermal column of the RA-3 reactor at the Ezeiza Atomic Center which is near to the Roffo Institute (one hour's drive), where surgeries would be done. The goal was to obtain a highly thermalized neutron spectrum, with a thermal flux of around 10^{10} n cm^{-2} s^{-1} (to reach required doses in a time of the order of 10 minutes, analog to the Italian experience).

The additional requirements were a neutron flux as isotropic and uniform as possible and a gamma flux as low as possible. Such facility would also be

adequate to treat other organs ex-situ and to perform experiments with biological samples like cells or small animals' irradiations.

This work presents a description of the facility and a preliminary gamma and neutron characterization of the irradiation site in air.

2. Description of the new facility and physical characterization of the space for samples.

RA-3 is an open pool up to 10 MW power reactor whose main activity is radioisotopes production. For this reason it works continuously five days a week. At one side of the pool it has a graphite thermal column but, before modification, the access into the column during reactor operation was not possible. In order to obtain availability during regular production, it was decided to construct additional shields and shutters to allow for sample introduction with the reactor at full power. Additionally, the possibility of introducing on line instrumentation for neutron and gamma measurements was considered. Figure 1 shows a diagram of the new facility.

The thermal column is constructed with graphite as its main material. It is about 3 m long and it has a squared section that increases by steps from the nearest end to the core to the other end where the section is 2 m x 2 m (1). In the center and along 1 m inside the thermal column there is an air tunnel of squared cross section. The original dimension of this section was 10 cm x 10 cm, but as it was not big enough to introduce the liver to be irradiated; it was increased up to 15 cm x 15 cm (2). In order to reduce gamma emission from the core, a Bismuth block with a squared section of 20 cm x 20 cm and with a thickness of 10 cm (3) was set at the end of this tunnel. Additionally, a lead block was originally installed at the end of the column, near to the core (4). At the other end, an iron door closes the column and shields radiation from it. This door has a squared section of 2 m x 2 m and is 0.5 m thick (5). In the center of this door an air tunnel aligned with the air tunnel of the graphite and with the same dimensions was constructed. Between the graphite and the external door there is an air space of about 0.5 m (6).

In contact with the door, a new external shield (Fig. 2) was constructed for sample insertion (7). It is composed of a 1.1 m long central air tunnel, aligned with the door and graphite air tunnels (also with the same cross sectional dimensions) (9), surrounded with lead walls with a thickness of about 10 cm (8). Inside the air tunnel there is a movable carrier sample tray of Zircaloy-4 (Zy-4) (10). On this tray there is a Bismuth block with a cross section of 15 cm x 15 cm and 10 cm thick (11), a Bismuth base of 15 cm x 2 cm x 18cm which supports the samples (12) and graphite blocks for neutron reflection (13). The space for samples over the Bismuth base has a dimension of 15 cm x 11 cm x 18 cm (14).

By moving the tray it is possible to insert and extract samples in the column. The Bismuth block is at the end of the tray and has two functions. When it is inside, during sample irradiation, it is an additional shield for gamma emissions from the core and when it is outside it is a radioprotection shield for samples insertion and extraction in the space for samples. A door with lateral movement in the upper part of the external shield (15) was constructed to introduce samples in this space.

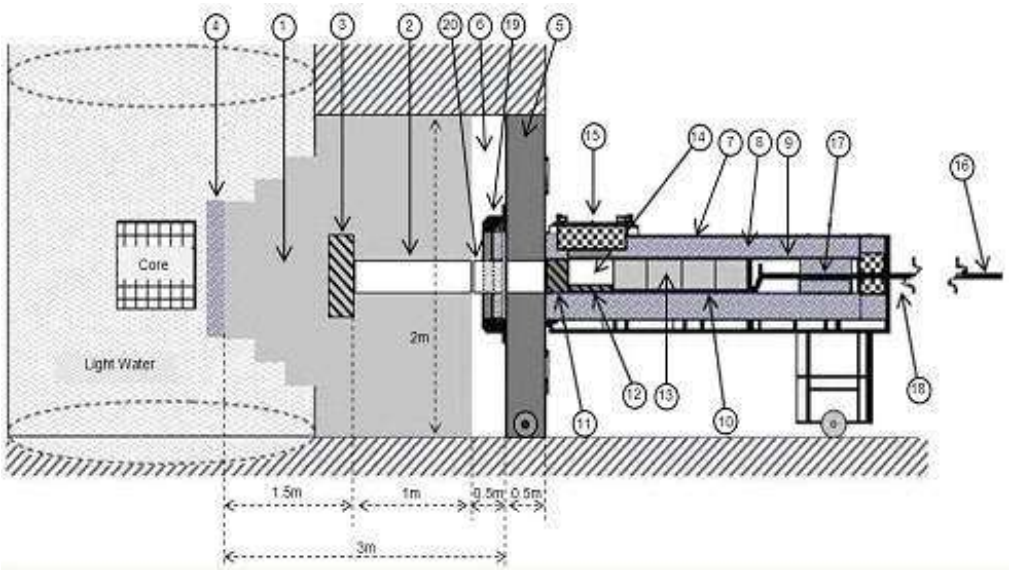

Figure 1. Schematic representation of the facility

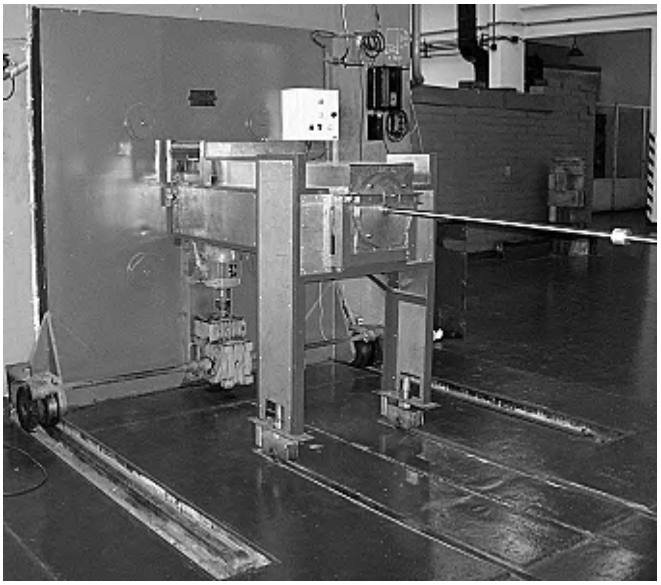

Figure 2. View of the external shield

The mentioned upper door was made of lead (10 cm thick) and covered with Stainless Steel. Figure 3a is a photograph of the door when it is closed and Fig. 3b is a photograph of the door when open and the space for samples. A long Zy-4 tube (as it can be seen in Fig. 2) was joined to the tray in order to introduce and extract it (16). Cables for on-line instrumentation of the samples can go trough this tube.

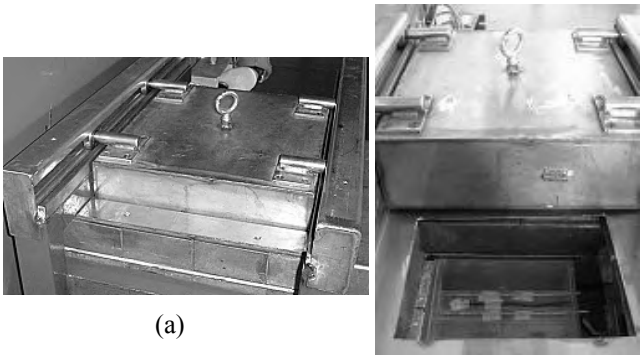

(a) (b)

Figure.3. Detail of the upper door
(a) Closed
(b) Open. View of the space for sample

An additional and independent movable shield was constructed at the end of the tray (17) of Cadmium and Lead. During irradiation it is placed inside the air tunnel of the thermal column door as radioprotection shield. A second tube of Stainless Steel was joined to this shield to allow its displacement (18). This second tube surrounds the Zy-4 tube.

On the internal side of the column door a movable gamma and neutron shield (shutter) (19) was mounted. Figure 4 shows a diagram of the shutter. It has a squared section of 20 cm x 20 cm (to cover the air tunnel of the door) and was constructed with Lead, Cadmium and paraffin wax. It has a lateral movement commanded by an external control. On one lateral side of the shutter a movable bridge (20) was mounted. This bridge accompanies the lateral movement of the shutter. In this way, when the shutter is open, the bridge is aligned with the air tunnels of the column door and the thermal column.

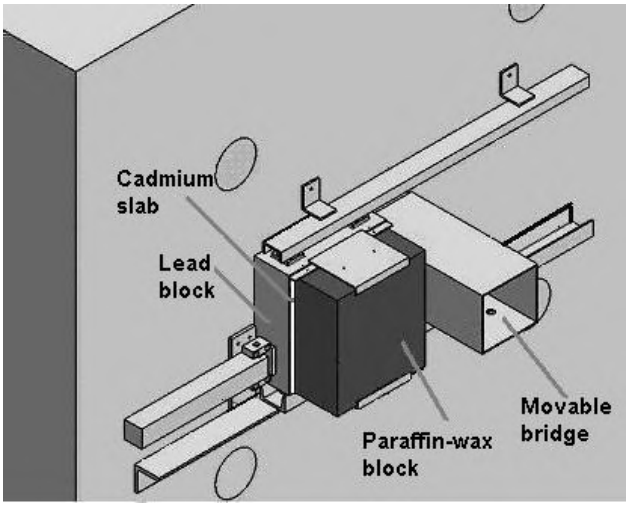

Figure 4. Movable shield (shutter)

To irradiate a sample, it must be first introduced in the space for samples (upper door open) with the shutter closed. Then, with the upper door closed, the shutter can be opened and the carrier sample tray and the movable shield can be introduced by pushing the corresponding tubes. A logical control for the safe operation was developed to enable or not the opening of the shutter according to the positions of the tray and the upper door. Associated with this logical control a panel with light indicators was mounted on the external side of the column door.

The following measurements were performed in the space for samples in air, with the tray in the nearest position to the core, and with the reactor at a power of 8 MW.

a) To measure thermal to fast neutron ratio bare and under Cadmium cover Gold foils were used.

b) To measure the thermal flux in different positions of the space for samples, bared Cobalt and Gold foils and a calibrated SPND were used.

c) To evaluate the uniformity it was measured the ratio between the neutron flux in both extremes of

the space for samples (nearest and farther from the core) with Cobalt and Gold foils and Copper with Gold wires.

d) To estimate structural gamma dose rate it was used a Far West graphite ionization chamber covered with a neutron shield of ^{6}LiF.

3. Results and discussion

The facility was constructed during 2005 and its use started in 2006 after checking that the levels of external radiation had no significant changes compared to those registered before the modification.

Concerning characterization studies, the measured cadmium ratio was 4100 and the ratio between epicadmium (epithermal + fast) to thermal neutron flux was 0.03% (Pozzi et al., 2007) which shows that a highly thermalized spectrum was obtained.

Measured thermal flux in the nearest position to the core was $(9\pm1)10^{9}$ n cm^{-2} s^{-1} which fulfills the expected value in order to deliver required doses in a few minutes.

Regarding uniformity, a ratio of 80 % along the space for samples (18 cm) for the thermal flux in air was obtained.

The free-in-air gamma-ray dose rate resulted (5.6±0.5) Gy/h. It will contribute with a dose per thermal neutron fluence unit of 1.7 10^{-13} Gy cm^{2} n^{-1}.

Due to its final characteristics and high availability, several biological experiments have been able to be performed up to now. Among these experiments one can find irradiations of small animals (hamsters and rats), different tumoral cells (thyroid and melanoma), and, in particular, a preliminary characterization of in-tissue neutron flux inside portions of cow and pig livers simulating human liver left lobe. Results of these last tests, presented in another work (Gadan et al., 2008), showed a very good uniformity of the neutron flux along the samples.

4. Conclusions

As a consequence of the very well thermalized spectrum available in the new facility the contribution from fast neutron to overall dose can be considered as negligible for typical BNCT assays.

Structural gamma dose rate also resulted low enough to assume that its importance in total dose will not be a limiting factor.

The small decrease of the neutron flux in air inside the space for samples as well as the results from preliminary tests of the neutron profile in portions of livers showed that an acceptable uniformity can be obtained, without rotating or moving the sample during its irradiation.

Acknowledgements

The authors wish to thank Dr. S. Altieri for the useful discussions related to gamma characterization.

Especial thanks go to the Radioprotection and Operation teams of the RA-3.

References

Pinelli, T., Zonta, A., Altieri, S., Barni, S., Braguieri, A., Pedroni, P., Bruschi, P., Chiari, P., Ferrari, C., Fossati, F., Nano, R., Ngnitejeu Tata, S., Prati, U., Ricevuti, G., Roveda L. and Zonta, C., 2002. "Taormina: From the First Idea to the Application to the Human Liver", Research and Development in Neutron Capture Therapy. Proceedings of the 10th International Congress on Neutron Capture Therapy: 1065-1072

Cardoso, J., Trivillin, V., Heber, E., Nigg, D., Calzetta, O., Blaumann, H., Longhino, J., Itoiz, M., Bumaschny, E., Pozzi, E., Schwint, A., 2007. "Effect of Boron Neutron Capture Therapy (BNCT) on Normal Liver Regeneration: Towards a Novel Therapy for Liver Metastases", International Journal of Radiation Biology Oct; 83(10): 699-706

Pozzi, E., Nigg, D., Miller, M., Thorp, S., Schwint, A., Heber, E., Trivillin, V., Zarza, L., Estryk, G., 2007. "A Small-Animal Irradiation Facility for Neutron Capture Therapy Research at the RA-3 Research Reactor", Proceedings of the ANS Winter Meeting. Research Reactor, Trans ANS **97:**309-311.

Gadan, M., Crawley, V., Thorp, S., Miller, M., 2008. "Preliminary liver dose estimation in the new facility for irradiation of biological samples at the RA-3 Reactor". Proceedings of the 13th ICNCT.

Reactor based BNCT facilities: current status and future prospects

Iiro Auterinen[1], Leena Kankaantanta[2]

[1] *VTT Technical Research Centre of Finland, Espoo, Finland*
[2] *Department of Oncology, Helsinki University Central Hospital, Helsinki, Finland*

Until now few nuclear research reactor-based neutron beams have been available to treat patients with neutron capture therapy (NCT), however an increasing effort exists to develop accelerator-based neutron sources for NCT essential for a wide use of NCT at specialized radiation therapy centers around the world. Today, dependent on reactor facility-based BNCT, the clinical trials studies are planned to test the efficacy and safety of NCT in a wider spectrum of malignancies. Extensive clinical trials in BNCT are currently conducted only at two facilities, the JRR-4 in Japan and the FiR 1 in Finland. For multicenter trials and in case of a rapid extension of BNCT more neutron facilities should be opened for clinical trials. In several cases nuclear reactors may also be a competitive neutron source for new BNCT facilities.

A nuclear reactor offers an intense and reliable source of neutrons for BNCT. Modernization and refurbishment of an existing reactor or construction of a new research reactor might open possibilities for a new BNCT facility. Other possible advantages are a reasonable additional cost of the reactor operation to be covered by the BNCT activity and availability of skilled personnel to develop and operate a BNCT beam facility. The major prerequisite is interaction with a research hospital with radiation therapy units.

In this work the current status and future prospects of the existing and planned reactor-based BNCT facilities are evaluated. Past, current and future activities at the existing and planned BNCT facilities are reviewed. Emphasis is put on the analysis of the research and development environment and business plans for BNCT. Location of the reactor, its availability for BNCT and appropriate treatment environment are of importance. The capabilities of the facilities, like beam properties and patient positioning, are analysed from the viewpoint of application of BNCT to various tumour sites.

This work is done in collaboration with and to support the Technical Working Group on Research Reactors (TWGRR) at the IAEA.

Preliminary Modeling of BNCT Beam Tube on IRT in Sofia

S. Belousov[a], K. Ilieva[a]

[a]*Institute for Nuclear Research and Nuclear Energy of the Bulgaria Academy of Sciences, Tsarigradsko 72, Sofia, Bulgaria*

Abstract

The technical Design of the research reactor IRT in Sofia is in progress. It includes an arrangement for BNCT facility for tumor treatment. Modeling of geometry and material composition of filter/collimator for the BNCT beam tube on IRT has been carried out following the beam tube configuration of the Massachusetts Institute of Technology Reactor (Harling, 2002) and taking into account an ability to include the tube into IRT reactor geometry. The results of neutron and gamma transport calculations performed for the model have shown that the facility will be able to supply an epithermal neutron flux of about 5.10^9 n/cm^{2}s, with quality, which is close to the best value reached in the world until now. For the BNCT beam tube collimator an analysis of its shape optimizing in accordance with the results obtained for TAPIRO research reactor in Italy (Nava, 2005) have been performed.

Keywords: BNCT, Beam tube design, Moderator/Filter, Collimator

1. Introduction

The pool type research reactor IRT in Sofia is nowadays at the stage of reconstruction from IRT-2000 – the previous reactor design operated until 1989. New technical design of the reactor includes arrangement of BNCT facility that is being in considered. We have a unique ability to use worldwide existing experience in development of our beam design. The selected reactor core configuration and beam design provide positioning of the fuel assemblies just at the entrance of the beam tube so that a fission converter is not needed.

Modeling of geometry and material composition of filter/moderator for the BNCT beam tube on IRT has been carried out following the beam tube construction of the Massachusetts Institute of Technology Reactor (MITR) (Harling, 2002) that design was very consistently substantiated in available publications. Collimator design has been analyzed taking into account an ability to include the BNCT tube into the IRT-2000 geometry and following known recommendations concerning collimator shape optimizing (Nava, 2005).

It was expected obtaining beam performance at the IRT similar to the MITR taking into account that MITR converter power is very close to the power released in the two rows of the IRT core fuel assemblies (FA) (~ 80 kW at 200 kW full IRT core power) located at the entrance of the IRT beam tube and similarity in the collimators length.

2. Geometry description

The working drawing of the horizontal cross section of the IRT reactor is presented in Figure 1. The BNCT tube adjusted to the reactor vessel is planned to be replaced with the thermal column that existed in the IRT-2000 design. The stepwise boundaries in the concrete biological shielding of the previous graphite thermal column can be seen in Figure 1. The inside dimension of the BNCT rectangular beam tube (filter/moderator region) is 52 cm horizontally, and 67 cm in the vertical direction. This area fully comprises the core area (neutron source) dimensions at the entrance of the tube. According to the fuel meat distribution in the FA the neutron source size is limited by 28.6 cm and 60 cm correspondingly.

It was allowed that the beam collimator output could be located at the surface about 60 cm inside the biological shielding outer surface. This depth coincides with the thickness of the outer graphite block of the thermal column of IRT-2000. All graphite blocks of the thermal column will be withdrawn during the IRT-2000 dismantling and the gaps between the BNCT tube and the existing biological shielding will be filled with a heavy concrete. The collimator shortening is favorable for preserving beam intensity but some structural analysis will be needed for the approval of the concrete shielding construction modification.

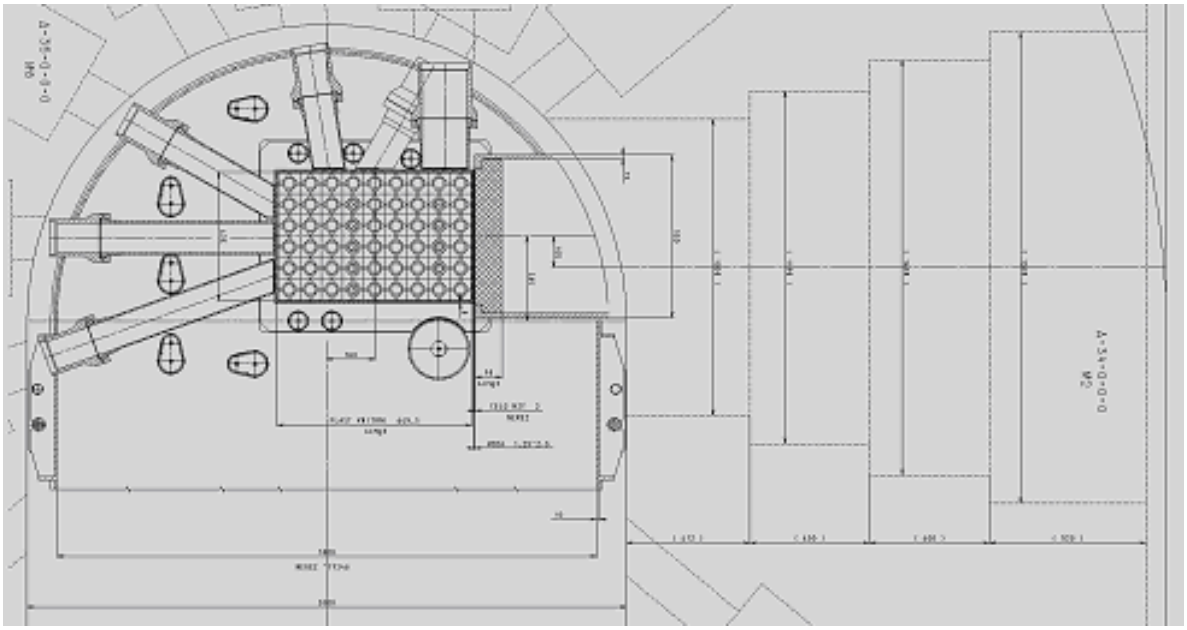

Figure 1. IR T reactor horizontal cross section

3. Modeling and calculations

The BNCT tube calculation was carried out by MCNP code (Briesmeister, 2000). The calculation was performed by two stages. At the first stage criticality calculation was used for determination of the critical positions of the control rods and definition of the neutron surface source at the entrance of the BNCT tube for the next stage calculation.

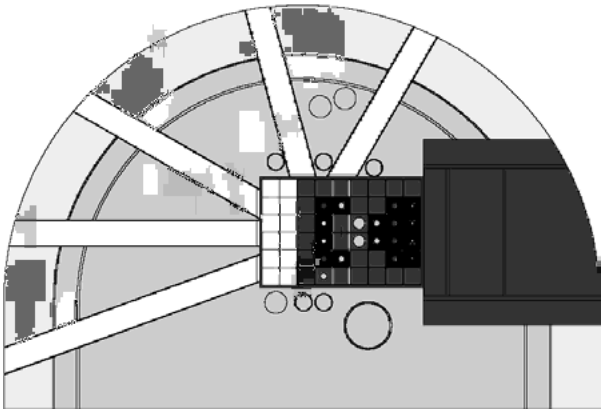

Figure 2. MCNP model for the IRT criticality and BNCT neutron source calculation

A horizontal cross section of the MCNP model horizontal used for the first stage of calculations is presented in Figure 2. The model includes reactor vessel with 54 cells filled by 16 fuel assemblies (6FA and 8FA – six and eight tubes fuel assemblies, Figure 3, IRT-4M type LEU FA (Apostolov, 2006)) adjusted to the vessel side at the BNCT tube entrance and surrounded by 26 beryllium blocks (Be). The model includes part of surrounding the reactor vessel pool and about 30 cm of biological shielding (heavy concrete). The neutron source on the surface coinciding with entrance aperture of the BNCT beam tube was stored in the external file and used at the next stage.

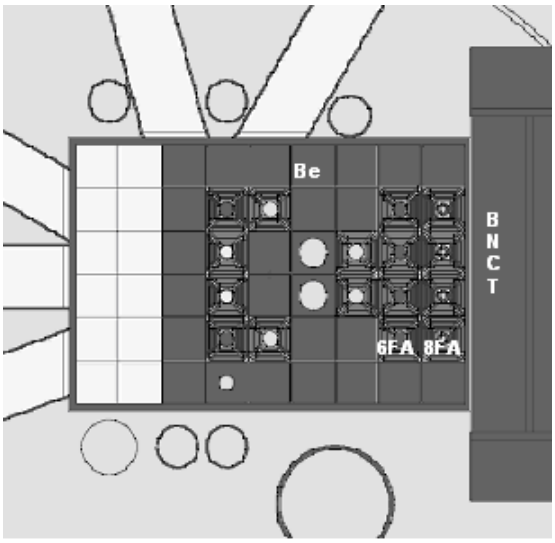

Figure 3. MCNP model (fragment) for the IRT criticality and BNCT neutron source calculation

The second stage MCNP model cross section is illustrated in the Figure 4. The model is presented against a background with the IRT working drawing to show how the model is incorporated into the existing geometry. The beam neutron flux values calculated by both models at a distance of about 40 cm from the beam entrance aperture were consistent to within 1%.

The calculation model filter/moderator design and the lead reflector thickness were chosen to be the same as those used at the MITR.

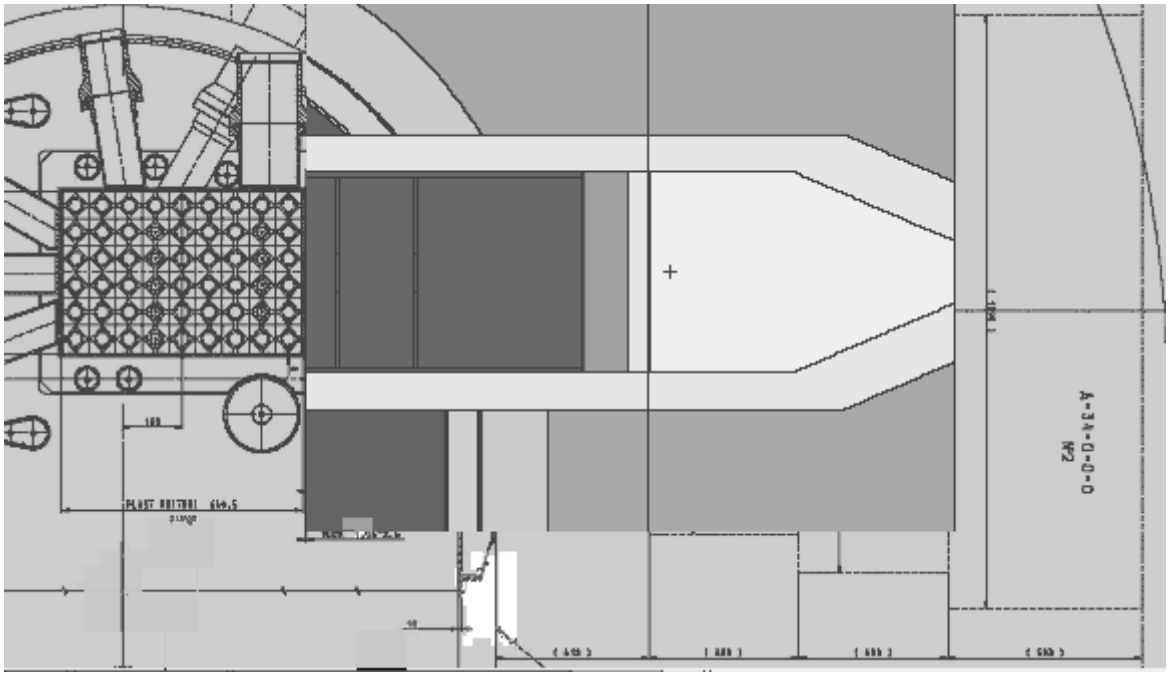

Figure 4. IRT reactor cross section and MCNP model for BNCT tube calculation

Different collimator surface shapes (pyramid, cone, and parabolic), length (L) and half angle (θ) of narrowing to the output aperture were analyzed for the purpose of the design optimization. The collimator length L = 90 cm corresponds to the basic option when collimators' output is located at the surface about 60 cm inside the biological shielding (Figure 4) outer surface.

The first stage criticality calculation was carried out without application of any variance reduction technique (VRT). The mesh based weight windows VRT was applied at the second stage. The second stage calculations were carried out in neutron, and neutron-photon mode.

4. Results and analysis

The calculation results for epithermal neutron flux - φ_{epi} (neutrons with energy between 0.5 eV and 10 keV), at the BNCT beam output (with area of 225 cm^2) are presented in Table 1.

Table 1. Calculated BNCT beam performance

Collimator design	φ_{epi}, $cm^{-2}s^{-1}$
Pyramid, L=90cm, θ = 17°	4.0E+9±4%
Cone, L=90cm, θ = 21°	5.0E+9±4%
Pyramid, L=90cm, θ = 21°	4.6E+9±4%
Cone, L=124cm, θ = 16°	2.7E+9±4%
Cone, L=72cm, θ = 27°	6.2E+9±4%

From Table 1, it is seen that the considered design produces beam with intensity similar to that of the MITR beam. Using a basic collimator with a length equal to 90 cm, a cone shape is the most appropriate although the results for the cone and pyramid shapes practically coincide for the same angle θ in the limits of statistical uncertainty. The results for the different cone collimator length provide an ability to assess the impact of collimator extension. The flux intensity decreases by more than a factor of two when increasing the collimator length from 72 to 124 cm.

To evaluate the efficiency of application of parabolic collimator shape (Nava, 2005) in the IRT beam configuration the results obtained for cone (L=90cm, θ = 21°) were compared with those for parabolic inside surface collimator (Figure 5).

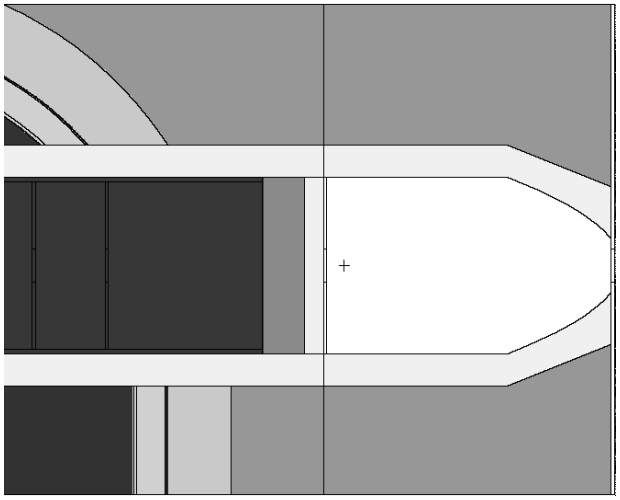

Figure 5. MCNP model for IRT BNCT tube with parabolic collimator shape

The results of comparison for beam performance including "in-air" soft tissue (ICRU 46, 1992) doses (fast neutron − D_{fn}, and photon doses − D_{γ}) and beam collimation (currant to flux ratio − J_{epi}/φ_{ep}) evaluation are illustrated in Table 2.

Table 2. Parabolic and cone collimator IRT BNCT beam performance

Collimator	Cone	Parabolic
φ_{epi}, E+9 $cm^{-2}s^{-1}$	4.63±0.3%	4.78±1.0%
D_{fn}/φ_{epi}, E−11 cGy cm^2	2.10±1.0%	2.24±1.0%
D_{γ}/φ_{epi}, E−11 cGy cm^2	0.55±1.0%	0.63±1.0%
J_{epi}/φ_{epi}	0.704±1.0%	0.665±1.0%

It is seen from Table 2 that parabolic collimator shape advantage in the IRT geometry for epithermal flux intensity is about 3% that is considerably less than the advantage obtained for TAPIRO reactor (Nava, 2005).

5. Conclusions

A preliminary modeling of the BNCT beam tube at the IRT, Sofia reactor using the MITR beam tube design is performed. The modeled beam performance at the IRT, Sofia is similar to the MITR facility and meets the existing requirements (IAEA-TECDOC-1223, 2001). The basic collimator length is selected on the basis of the IRT, Sofia construction design and worldwide existing experience. The beam intensity sensitivity to the collimator length and angle of narrowing is evaluated. It is obtained that application of parabolic collimator shape is not advantageous for the IRT, Sofia BNCT beam.

In the analyzed model of the IRT, Sofia BNCT tube the materials thickness in filter/moderator region exactly coincides with that for MITR. Further investigation has to include analysis of the beam performance sensitivity to different materials thickness aiming optimization of the beam tube performance for specific IRT, Sofia geometry conditions. Additional collimator optimizing analysis for the beam performance including extenders application will be carried out too. The BNCT beam optimizing (energy range, output aperture dimension and configuration providing required treatment flexibility) will be done and in accordance with the last achievements known from the BNCT experienced institutions (Auterinen, 1992).

Additional investigations concerning shutter design are needed. The approved nominal power of the IRT, Sofia is 200 kW but the safety analysis recently completed shows that the IRT, Sofia could be operated safely even at 1MW power level. That has to be kept in mind during shutter design development.

Summarizing the aforementioned discussion we could conclude that we have all potentials to create a facility with properties comparable or even better than existing ones at least based on research reactor operated at the same level of power.

Simultaneously we have not to forget that the beam design has to be performed in a close collaboration with the IRT construction designer and in consistency with construction limitation that could arise in the process of the design realization.

References

Apostolov, T.G., Belousov S.I., Hanan N.A., Matos J.E., 2006. Analyses of the IRT, Sofia Initial LEU Core Performance. 28th International Meeting on Reduced Enrichment for Research and Test Reactors, Cape Town, South Africa, October 29 – November 2. http://www.rertr.anl.gov/

Auterinen, I., Hiismäki, P., 1992. Epithermal BNCT neutron beam design for a Triga II reactor. Proceedings of the 5th ISNCT. Columbus, OH, USA, 14 – 17 September. Plenum Press (1993), 81 – 84.

Briesmeister, J.F., 2000. MCNP – A General Monte Carlo N-Particle Transport Code Version 4C. LA-13709-M.

Harling, O.K., Riley, K.J., Newton, T.H., Wilson, B.A., Bernard, J.A., Hu, L-W., Fonteneau, E.J., Menadier, P.T., Ali, S.J., Sutharshan, B., Kohse, G.E., Ostrovsky, Y., Stahle, P. W., Binns, P.J., Kiger III, W.S., Busse, P.M., 2002. The Fission Converter-Based Epithermal Neutron Irradiation Facility at the Massachusetts Institute of Technology Reactor. Nucl. Science and Eng., 140, 223-240.

IAEA-TECDOC-1223, 2001. Current status of neutron capture therapy. IAEA.

International Commission on Radiation Units and Measurements, 1992. Photon, Electron, Proton and Neutron Interaction data for Body Tissues. ICRU 46.

Nava E., Burn, K.W., Casalini, L., Petrovich, C., Rosi, G., Sarotto M., Tinti, R., 2005. Monte Carlo Optimization of a BNCT Facility for treating Brain Gliomas at the TAPIRO Reactor**.** Radiat. Prot. Dosim., 116 (1-4), 475-481.

Redesign of the RA-6 reactor BNCT facility

H. Blaumann[a], J. Longhino[a], O. Calzetta[b]

[a] *Unidad de Actividad de Energía Nuclear, Centro Atómico Bariloche, S. C. de Bariloche, 8400 Río Negro Argentina*
[b] *Agencia Brasileño-Argentina de Contabilidad y Control de Materiales Nucleares*

Abstract

The pool type reactor RA-6, located in Bariloche, Argentina, is undertaking a conversion to low enrichment core, with a power uprate to 2 MW. The BNCT facility has been widely used for experimental models development and human clinical trials during the last ten years. The hyperthermal BNCT beam is then under redesign, in order to make the most of the upcoming increase in reactor power. This task was performed by using the transport code MCNP5 v1.40, from the criticality calculation of the new core configuration, filtering calculation and final beam conformation at the external port. Several issues were evaluated for the performance (final filtering, shutting system, beam conformation).

Keywords: Beam Design, MCNP, Hyperthermal Beam, Calculated Fluxes and Doses.

1. Introduction

The RA-6 reactor is located at Bariloche Atomic Center. Designed and constructed fully in Argentina, since its commissioning in 1982 to 2006 it has been operated with a 90% ^{235}U enrichment core, at 500kW nominal power. It was devoted to research, development and teaching activities. In 1997, an Epithermal BNCT Beam was commissioned. Later, in order to fit the requirements for clinical trials on skin melanoma models, a partial-thermalization stage was added, becoming the *'Hyperthermal'* beam in service up to 2007 (Blaumann et al., 2004). This Beam was used for human cancer models in animals (Trivillin et al., 2006), and eight irradiations in a clinical trial on humans (Gonzalez et al., 2006).

As the low enrichment core conversion is taking place, the original core was dismantled late 2007, and a new, 20% enriched uranium core is foreseen to be commissioned mid-2008. In this new configuration, an increase in thermal power to 2MW was sought, in order to enhance prior capabilities and advance on other topics (isotope production, diffractometry, etc). As a four-fold power increase, and then flux level increase, will take place, the BNCT facility can be largely improved both in beam intensity and in quality.

2. Objectives of the redesign

From the experience gathered through the years of use of the facility, some aspects regarding usability were sought to be optimized.

Most importantly, the limitation for the positioning of patients, due to the external surface of the Initial Beam port which was flat-top and did not allow a variety of postures for the irradiation of extremities was undesirable. A protruding end of the collimator, allowing a separation from the shielding wall to the irradiation position was therefore considered a must.

For the in-phantom configurations (similar to clinical cases), the thermal flux achieved at the maximum was roughly 10^9 n cm^{-2}sec^{-1}. As this value implied patient's irradiation periods from 40 to 80 minutes, it was sought to increase this intensity by a factor of two, thus reducing irradiation times by at least this proportion.

As the initial configuration had fast neutron and gamma contamination of 1.35 and 3.0 cGy/min respectively in the free in-air beam, a reduction in these values was sought.

Finally, a beam-shutter system was considered, in order to try to of uncouple the reactor schedule from the irradiation schedule. The final criteria for the shutter system performance was to reduce the free-in-air dose rates at 2MW power to those found in the initial configuration with the reactor shut down, allowing controlled transit into the irradiation room.

The objectives of adding a collimator and beam shutters meant lengthening the beam line and these together with improved beam purity tend to in

conflict with the desired increase in intensity of the redesigned beam. This clearly implied that the final design would be a compromise between beam quality and intensity as well as irradiation room allowance.

3. Methods and models

All calculations were performed with MCNP5, v1.40, using ENDF B-V and VI point libraries. The new, 20% $^{235}U_3Si_2$ enriched fuel elements were modeled into a 20 Fuel Elements core, and a track-by-track source of neutrons and photons was recorded from a criticality calculation in the core/BNCT filter boundary. This source was then transported in a separate calculation through the unmodified internal filter, obtaining the final track source at the pool surface, in front of the irradiation room (Figure 1).

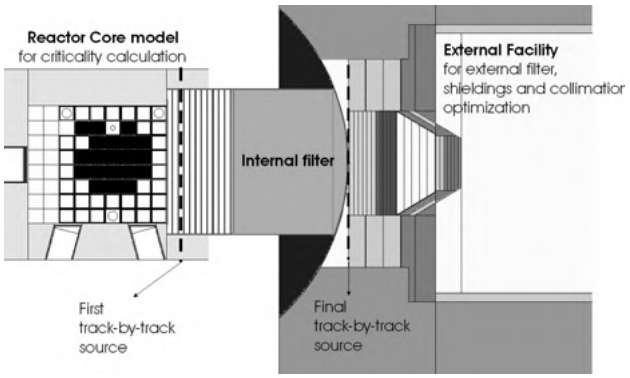

Figure 1: Schematic of the geometries used in the optimization

The external filtering and collimation of the beam, and the peripheral shieldings were optimized from an initial conceptual design. This comprised a neutron filtering stage of PTFE (Optimum Thickness –OT–: 15cm), partial neutron thermalization in Acrylic (OT: 22mm) and the final gamma shielding with Bismuth (OT: 98mm). The collimation was performed through a composite material of lead/borated polyethylene called Polyboron which formed a hollow cone, protruding 15cm from the shielding wall. This peripheral wall was in turn 20cm thicker than in the initial configuration, due to an increase in both neutron and gamma shielding. The overall design distance from the core to the new irradiation position was ~20cm longer than before.

The conceptual design of the shutter system included originally two stages; a solid block of Polyboron and a water filled conical box, inserted into the collimator. Early on in the analysis, a third stage was added: a lead replacement for the protruding part of the collimator.

Three simulations were performed for each analyzed variation; Full power with Phantom, Full Power free-in-air, and Full power with shutters closed (?)(if shutters included).

4. Shutter System model.

The cases involving independent shutter systems were analyzed first. The goal was to assure radiant fields in the 'closed' situation with about the same intensity as those present in the initial configuration during positioning of patients. The goal doses were then those measured free-in-air at the center of the beam for the initial configuration (i.e: $\dot{D}n = \sim 0.00005$cGy/min, $\dot{D}\gamma = 0.0003$cGy/min).

Although the Reactor primary shutdown system was still planned as the most secure means of ending an irradiation session, the shutter system should provide a secondary way of finishing an irradiation, forcing the evaluation of devices with actuation times lower than one minute. A Three-Staged Shutter was considered optimum for this problem. The final configuration is shown in Figure 2.

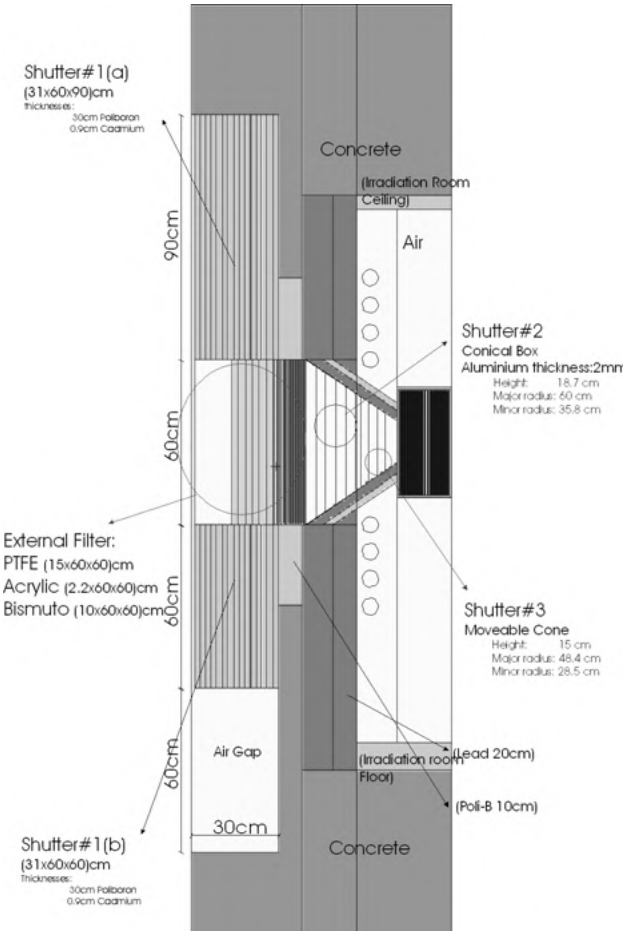

Figure 2: XZ cut of the optimal design with a three staged shutter system

Shutter #1, placed next to the pool tank, was designed as neutron moderator/neutron shielding, being of 30cm of Polyboron and 0.6mm of cadmium. As this is thicker than the PTFE+Acrylic –which, are of no use as shielding materials– this Shutter was part of fail-safe, gravity driven system, in which the therapeutic field is obtained by raising the block, and the beam is closed passively by letting the block lower. As this block is considerably larger than the materials conceptually included, large cavities in the shielding wall were needed, a follower was attached, and the overall complexity of the system increases. The alternative of placing this block separately from the PTFE+Acrylic filtering stage was discarded as the added separation of the irradiation position lowered the beam intensity too much.

Shutter#2 is a thin aluminium walled conical box, inserted into the collimator. This box is filled with distilled water when shutter is acted. The filling was thought as gravity driven, estimating the delay in the action in ~1 minute.

Shutter#3 is solid lead, truncated cone, 15 cm in height, reproducing the geometry of the hollow collimator. Its actuation should be mechanical, with a delay of seconds.

Figures of Merit (Thermal flux, Fast neutron and Gamma dose rates) were taken from a cylindrical tally placed at the beam centerline, 3cm in radius and 1cm thick (if phantom present, including 5mm of acrylic and 5mm of water) or 3cm thick (if free-in air). These results from the three simulations are presented in Table I.

Table I: Outstanding parameters at the beam aperture for the three dosimetric models. Relative statistical uncertainty (1 STD) is also reported

	ϕ_{th} [n/cm²sec]		D_n [mGy/min]		D_g [mGy/min]	
Open w/ Phantom	1.47E+09	0.7%	7.57	5.3%	72.23	0.8%
Open w/o Phantom	4.57E+08	<0.1%	7.03	0.4%	10.95	0.2%
Closed Shutters	3.07E+03	0.3%	0.007	1.0%	0.003	6.5%

As the doses in the closed situation are ten-fold the objective, and due to the huge size of the devised Shutter#1, along with the impact on the fluxes, this model is considered impractical.

5. Simpler Shutter system for non therapeutic condition

The reduction of the performance implied in the complete Shutter System was not accepted, though the widening of available irradiation schedules was still desirable. For this reason, the usual method of ending was again considered, but, in view of the effectiveness of Shutter#2 and #3, the use of these two stages, along with operative restrictions of the reactor's schedule was studied in order to reproduce equivalent allowance without complete shutdown of the reactor.

The final optimum design does not include the models of Shutter#2-#3, instead of that, a conical *Stopper* was designed, including PoliB, Cd and lead. Also, by extracting the Shutter #1 and associated gaps, the Beam flux intensity increases as well as the peripheral contaminations decreases. Optimum Configuration is shown in Figure 3.

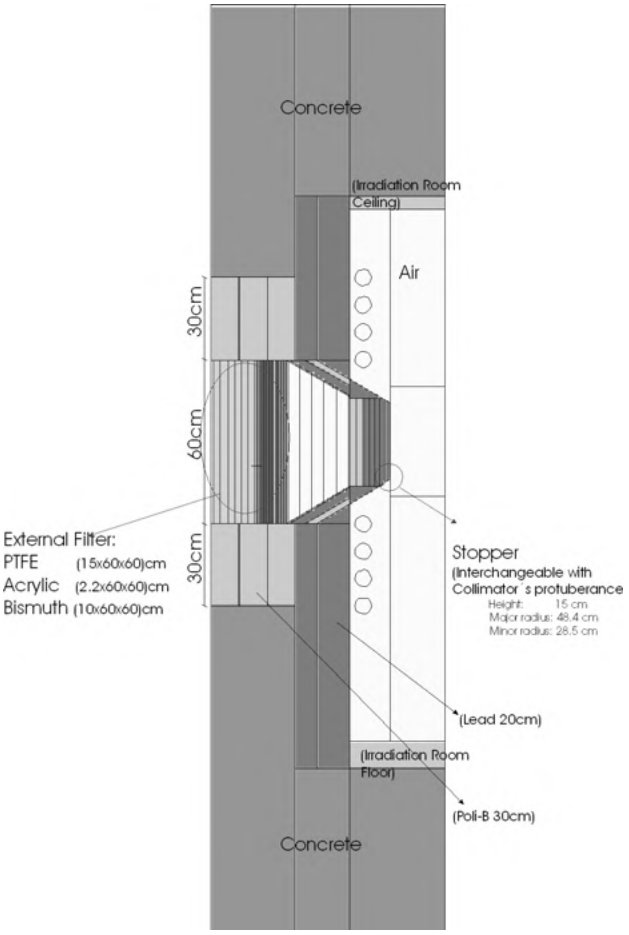

Figure 3: XZ cut of the optimal design with a stopper

The figures of merit calculated for this configuration are shown in Table II.

Table II: Outstanding parameters at the beam aperture for the three dosimetric models. Relative statistical uncertainty (1 STD) is also reported

	ϕ_{th} [n/cm²sec]		D_n [mGy/min]		D_g [mGy/min]	
Open w/ Phantom	1.81E+09	0.7%	9.00	4.6%	84.7	1.0%
Open w/o Phantom	5.62E+08	<0.1%	7.74	0.1%	10.20	0.1%
Stopper **Full power**	7.61E+05	<0.1%	0.123	0.1%	0.009	0.3%

6. Discussion and Results

As seen in the tables, the simplification of the shutting system increases the intensity of the therapeutic fluxes more than the associated contamination. Thus, the figures of merit favor the second model. It is clear that the *Stopper* cannot functionally turn off the beam at full power; but by applying a simultaneous power reduction (down to 1% of Full Power), the calculated doses could become very similar to those of the actuated Complete Shutting system. The desired doses, can be obtained by shutting the reactor down, as with the old beam. This offers a method for patient positioning not explored up to now by our group.

In the final design, maximum dose rates values in a model of the reference water-filled phantom were about 0.9 and 10 cGy/min for gamma and fast neutron respectively, while the thermal flux was 1.9×10^9 n/cm²sec. This comprises an in-phantom increase in the foreseen thermal dose rate of ~80%, whilst decreasing the fast neutron contamination 33%, and increasing the gamma dose rate in 10% compared with the current hyperthermal beam.

7. Conclusions

Based on a previous conceptual design, all enounced objectives were analyzed, and two optimal configurations were modeled and calculated. Evaluation was performed based upon the same integral merit figures for three dosimetric models: Open Beam with and without reference phantom, and Closed Beam –with the corresponding closing method– only free-in-air. In every case, radiant contamination decreases whilst flux intensity increases at irradiation position.

The configuration that included a three–staged shutter system was such that its implementation is difficult and costly in terms of flux. On the other hand, the second, simpler configuration including a radiation 'stopper' rendered higher flux intensities.

The effects of a larger, more complex three stage shutter system can be achieved by lowering the reactor power, without shutting down.

Based on the aforementioned results, the optimal design based on the stated objectives should dismiss the inclusion of shutters that lengthen the beam line too much. A less effective shutter, referred to as the stopper together with lowering the reactor power can achieve the same objective. Also, the new configuration of the external filtering, collimation and peripheral shielding results in a cleaner and more intense therapeutic BNCT beam.

References

Blaumann H., González S., Longhino J., Santa Cruz G., Calzetta O., Bonomi M., Roth B., 2004. Boron Neutron Capture Therapy Of Skin Melanomas At The RA-6 Reactor: A Procedural Approach To Beam Set Up And Performance Evaluation For Upcoming Clinical Trials. Medical Physics, 31(1). pp 70-80.

González S., Casal M., Santa Cruz G., Bonomi M., Jiménez Rebagliati R., Carando D., Blaumann H., Dagrosa M., Longhino J., Calzetta Larrieu O., Feld D., Castiglia S., Roth B., Menéndez P., Batistoni D. and Liberman S., 2006. Detailed Dosimetry and Clinical Outcome Analysis for the Argentine BNCT Trials of Cutaneous Nodular Melanomas. Kagawa, Japan. (12th ICNCT)

Trivillin, Heber, Nigg, Itoiz, Calzetta, Blaumann, Longhino, Schwint, 2006. Therapeutic success of Boron Neutron Capture (BNCT) mediated by a chemically non-selective boron agent in an experimental model of oral cancer: A new paradigm in NCT radiobiology. Radiation Research vol 166. pp 387-396.

Program for reconstruction of experimental equipment of tangential horizontal experimental channel (HEC) No7 of IR-8 reactor at RRC "Kurchatov institute" for medical, biological and physical research using capillary neutron optical systems (CNOS)

G.I. Borisov[1], R.I. Kondratenko[1]

[1]*RRC "Kurchatov Institute", Moscow, Russia*

For the tailoring of neutron and photon beam spectra a thin hydrogen-containing scatterer that we developed earlier and set of filters that slow down and absorb fast neutrons will be used. The scatterer will be situated inside the channel on the axis of reactor core. Such neutron source produces beams with the most advantageous spectrum for NCT, CNOS and medical and biological in vivo studies.
We plan the construction of medical block for NCT with thermal and epithermal in the physical hall of the reactor. The traditional collimators will be used for tailoring of broad beams and for in vasion NCT the cone-shaped focusing CNOS will be used to achieve high neutron flux density. The distance from the axis of the reactor core to the channel end is 2.5m. Thermal neutrons flux density at the end of the channel after the biological shielding will be 3·109 1/cm^{2}s, and for epithermal – 109 1/cm^{2}s given the reactor power of 8 MW. The ratio of thermal neutrons flux to the 2.2 MeV neutrons flux is equal to 80. Kerma of fast neutrons is equal to 8·10-13 Gy·cm^2.
The second end of the HEC No7 is planned to be equipped with various CNOS for tailoring of focused, qausiparallel, and extra clean thermal neutrons beam along with the set of collimators for tailoring of beams with various intensities and spectral composition. The distance from the axis of the reactor core to this end of HEC is 6.5m.
Using these neutron beams and other equipment various experiments will be conducted: a wide range of medical and biological in vivo studies including NCT, fundamental and applied studies for solid state and nuclear physics, neutron radiography. HEC No7 experimental equipment is designed for broad range of specialists in various spheres of science and technology.

Neutron Field Characterization for Accelerator Based BNCT with Low Energy Neutron Spectrometer Based on Position Sensitive ^{3}He Counter

Isao Murata[1], Hiroyuki Miyamaru[1], Itsuro Kato[2], Yoshiharu Mori[3]

[1] *Division of Electrical, Electronic and Information Engineering, Graduate School of Engineering, Osaka University, Japan*
[2] *Department of Oral and Maxillofacial Surgery II, Graduate School of Dentistry, Osaka University, Japan*
[3] *Kyoto University Research Reactor Institute, Kyoto University, Japan*

At present development of new neutron sources based on a particle accelerator is underway would wide for boron neutron capture therapy (BNCT). Though nuclear reactors were used for a long time as the neutron source, accelerator based neutron sources have recently been advantageous taking into account its easy-to-use and acceptable performance. However, when using an accelerator, various secondly particles would be emitted simultaneously and act as a troublesome background, and initially produced neutrons have a high energy and thus should be moderated largely. Moreover, in these circumstances, patients should be positioned close to the neutron source to keep a strong neutron flux intensity so that the BNCT will be completed within about 1 hour. This indicates that inside a relatively narrow space neutrons should be moderated, simultaneously shielding unnecessary secondary particles. Since this is not an easy job, it is known that it becomes quite hard to make an acceptable background-free neutron field for BNCT.

It consequently means, characterization of such neutron fields will have to be a critical issue to confirm the availability of the neutron sources for BNCT. In the present study, a low energy neutron spectrometer has been thus designed and developed to figure out the accelerator based neutron source performance.
As well known, a technique to measure neutron spectrum over 10 keV is already established, e.g., with a scintillation detector. However, below 10 keV there was no straightforward way. In the present study, an easy-to-use low energy neutron spectrometer is aimed at so as to cover quite a wide dynamic range of 6 decades from thermal to epi-thermal region. This wide dynamic range is a crucial requirement especially for BNCT.
The presently proposed spectrometer is based on a ^{3}He proportional counter, which is 50 cm long by 5 cm in diameter with a gas pressure of 0.3 MPa. It is quite unique that the spectrometer is set up in parallel with the incident neutron beam and a reaction depth distribution is measured by it as a position sensitive detector. Recently, a prototype detector has been developed and the signal test is now underway. The present paper summarizes how and why the present spectrometer would play a critical role in BNCT, together with the feasibility and design study result, and the fabrication process details.

Performance of a New Composite Single-Crystal Filtered Thermal Neutron Beam for Neutron Capture Therapy Research at the University of Missouri

John D. Brockman[1], David W. Nigg[2], M. Frederick Hawthorne[1] , Charles McKibben[1]

[1] *University of Missouri, Columbia, MO USA*
[2] *Idaho National Laboratory, Idaho Falls ID USA*

The University of Missouri (MU) Institute for Nano and Molecular Medicine, the Idaho National Laboratory (INL) and the University of Missouri Research Reactor (MURR) have undertaken a new collaborative research initiative to further the development of improved boron delivery agents for BNCT. The first step of this effort has involved the design and construction of a new thermal neutron beam irradiation facility for cell and small-animal radiobological research at the MURR. In this paper we present the beamline design with the results of pertinent neutronic design calculations. Results of neutronic performance measurements, initiated in February 2008, will also be available for inclusion in the final paper.

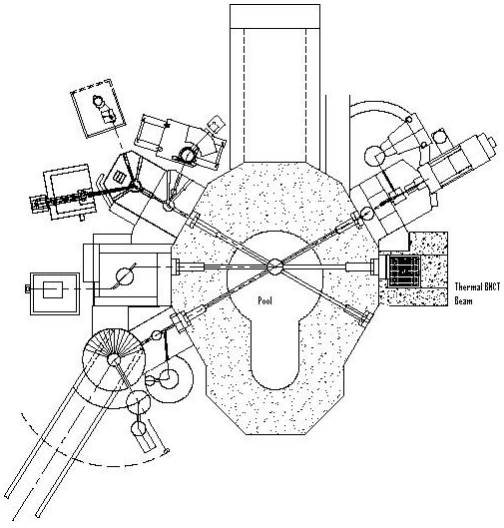

Figure 1. MURR core, shielding, and beamlines.

The new beam will be located in an existing 152.4 mm (6') diameter MURR beam tube extending from the core to the right in Figure 1. The neutron beam that emanates from the berylium reflector around the reactor is filtered with single-crystal silicon and single-crystal bismuth segments to remove high energy, fission spectrum neutrons and reactor gamma ray contamination. The irradiation chamber is downstream of the bismuth filter section, and approximately 3.95 m from the central axis of the reactor.

There is sufficient neutron flux available from the MURR at its rated power of 10 MW to avoid the need for cryogenic cooling of the crystals. The MURR operates on average 150 hours per week, 52 weeks a year. In order to take advantage of 7800 hours of operation time per year the small animal BNCT facility will incorparate a shutter constucuted of boral, lead, steel and polyethylene that will allow experimenters to access the irradiation chamber a few minutes after irradiation.
Independent deterministic and stochastic models of the coupled reactor core and beamline were developed using the DORT two-dimensional radiation transport code and the MCNP-5 Monte Carlo code, respectively. The BUGLE-80 47-neutron, 20-gamma group cross section library was employed for the DORT computations, in keeping with previous practice for analysis of a number of other NCT neutron facilities worldwide. The standard ENDF/B Version 6.8 cross section libraries were used with MCNP, except that special calculated cross section sets for the single-crystal bismuth and silicon filters in the MCNP calculations were provided to MU and INL specifically for this study by the Korean Atomic Energy Research Institute and, independently, by North Carolina State University. Cross sections for the amorphous bismuth and silicon files on the BUGLE-80 library used with DORT were modified to account for the single-crystal form of these materials using correction factors computed using MCNP.
A number of parameter studies were conducted, independently varying the thicknesses of the silicon and bismuth filter sections to find an optimum that maximizes the thermal neutron flux while maintaining the fast-neutron and gamma components of the beam within acceptable ranges. Both the DORT and MCNP beamline optimization computations led to the conclusion that the silicon filtering section should be approximately 55 cm in thickness and the bismuth section should be 8 cm in thickness. The total estimated thermal neutron flux delivered to the irradiation location by the filtered beam, integrated to 0.414 eV, is approximately 9.0×10^{8} neutrons/cm^2-s. The calculations also yielded an epithermal and fast-neutron kerma of approximately 1.0×10^{-11} cGy-cm^2.
Construction of the beamline is currently underway and initial foil activation measurements to characterize the free-field neutron flux spectrum at the irradiation location were undertaken in February 2008. Measured results obtained so far indicate that the neutronic performance of the beam is within the expected range.

Specific Features of Implementation of a Clinical Base for Neutron Capture Therapy of Cancer at the IRT MEPhI Reactor

A.A.Portnov[1], K.N.Zaitsev[1], V.A.Savkin[1], V.I.Kvasov[1], V.A.Kamnev[1], A.A.Liogenky[1], V.K.Sakharov[1], V.S.Troshin[1], O.V.Mishcherina[1], V.F.Khokhlov[2], V.N.Kulakov[2], I.N.Sheino[2], V.N.Mitin[3]

[1] *Moscow Engineering Physics Institute (State University), Moscow, RF*
[2] *State Research Center – Institute of Biophysics, Moscow, RF*
[3] *Russian Cancer Research Center of RAMS, Moscow, RF*

An irradiation base has been implemented at the IRT MEPhI Research Reactor for research in the field of neutron capture therapy (NCT) of malignancies.
An irradiation room was built at the horizontal tangential channel HEC-4 with a thermal neutron beam, for preclinical NCT studies. Currently, on this facility, preclinical NCT studies are carried out in cell cultures, small laboratory animals, and dogs with spontaneous malignancies. Over 80 dogs have undergone the NCT procedure with use of ^{10}B-containing (boronphenylalanine) and Gd-containing (Dipentast) compounds.
However, this facility is inapplicable for clinical trials, as the restricted size of the irradiation room prevents location of a human patient; also, the spectrum of the channel contains no epithermal neutrons necessary for treating deep-seated tumors, primarily brain tumors. In order to solve these problems, it was proposed to build an irradiation unit for clinical NCT studies on the HEC-1 channel that extends through the thermal column.
For this purpose, the thermal column is being redesigned, i.e. dismantling major part of graphite and replacing it with the unit of combined aluminum-based shaper of the thermal / epithermal neutron spectrum. For this, the axis of the channel is shifted for 25 cm from its initial position in order to decrease the contribution of the direct radiation of the core.

The existing shutter will be replaced with a shutter of a new rotary design; a special collimating device will be installed at the outlet of the beam. The proposed reconstruction design is based on computational studies under MCNP-4c2. The prospective beam is supposed to provide epithermal, and thermal neutrons, or their combination in required proportion with use of a ^{6}Li-containing filter. The calculations have shown feasibility of a beam of thermal and/or epithermal neutrons of more than 1.0×10^{9} n/cm^{2}s with concomitant total dose of fast neutrons and photon radiation not more than $8 \cdot 10^{13}$ Gy per unit thermal or epithermal neutron flux. Basic results of the calculations have been confirmed in experimental studies.

This neutron beam will be the base of a clinical NCT irradiation facility for the treatment of both surface and deep-seated tumors. Currently, a detail design of the reconstruction has been developed; the rotary shutter with the collimator, and blocks of the combined epithermal neutron spectrum shaper have been manufactured.

After the reconstruction of the HEC-1 channel and construction of the irradiation room at the IRT MEPhI Reactor, the first Russian base for specialized experimental and clinical studies on NCT of malignant tumors will be created. Works on implementation of the medical NCT base are supposed to be completed by 2010.

Simulations studies for the radiation shielding of a treatment room for AB-BNCT

A.A. Burlon[a,b], D.Fondevila[c], A.J. Kreiner[a,b,d]

[a]*Departamento de Física, Comisión Nacional de Energía Atómica, Av. Gral Paz 1499 (1650), San Martín, Buenos Aires, Argentina*
[b]*Escuela de Ciencia y Tecnología. Universidad Nacional de Gral. San Martín, M. De Irigoyen 3100 (1650), San Martín, Buenos Aires, Argentina*
[c]*VIDT Centro Médico, Vidt 1924 (1425), Ciudad Autónoma de Buenos Aires, Argentina*
[d]*CONICET, Avda. Rivadavia 1917(C1033AAJ), Ciudad Autónoma de Buenos Aires, Argentina*

Abstract

This work presents two independent MCNP simulation studies dealing with the radiation shielding for a treatment room of an Accelerator-Based source for Boron Neutron Capture Therapy (AB-BNCT). In the first one, the dose was calculated at various positions within the room walls using neutrons generated by the ^{7}Li(p,n)^{7}Be reaction at 2.5 MeV in order to determine the required protection for staff and personnel outside of the treatment room. The results show good agreement with data presented in the literature (Costes et al., 1996) for 1% ^{10}B loaded walls. Furthermore, we have evaluated the dose outside of the room walls for other ^{10}B concentrations and for ^{6}Li as a neutron absorber which does not produce gamma contamination. From our calculations, walls of about 1 m thickness keep the dose rates below 25 μSv/hr. In the second study, the neutron and gamma fluences around a phantom patient head were calculated with and without inner wall shielding. In this case the inner walls of the treatment room were covered with other shielding materials such as polyethylene loaded with 5% ^{6}LiF. Significant decreases in the thermal neutron and gamma doses were obtained for the shielded case which appears as a useful method to diminish the unwelcome dose on the patient.

Keywords: Treatment room, Radiation Shielding, AB-BNCT, MCNP Simulations

1. Introduction

The radiation shielding design of a treatment room has to accommodate two different concerns: radiation protection of the facility staff and personnel outside of the treatment room, and the radiation protection of the patient within, avoiding undesirable contamination in the dose delivered to the patient due to interactions in the wall such as the 2.2 MeV gamma background from neutron capture in hydrogen present in the concrete and low energy backscattered neutrons. The two independent MCNP studies presented in this work aim at optimizing a properly shielded room associated to an accelerator neutron source for BNCT which is now under development at the Comisión Nacional de Energía Atómica (CNEA) in Argentina (Kreiner et al., 2007).

2. Materials and Methods

2.1 Radiation protection of personnel outside of the treatment room

MCNP simulations were done using a neutron source model for the ^{7}Li(p,n)^{7}Be reaction at 2.5 MeV with a total yield of 8.83×10^{11} neut/mA·s. Biological equivalent doses were computed by converting the neutron and gamma fluence to equivalent dose at differents depths in a single thick wall. Although a more realistic approach is to calculate for each thickness the dose immediately outside the wall, the effect of this (as was pointed out by Costes et. al) is to increase the dose by no more than a factor of two (from contributions due to the backscatter within the wall) while the simulation time is greatly reduced. This is acceptable for radiation protection purposes implying a conservative design. So, the neutron doses were calculated at different depths within the wall in spherical cells having a radius of 0.9 cm and spaced 5 cm apart.

The room was modeled as it appears in Costes et al. (1996) (Fig. 1): with 200 cm thick concrete walls having a density of 2.35 g/cm^3 and the composition given in Table I.

H	O	Si	Ca	Na	Mg	Al	S	K	Fe
0.5	49.0	32.0	8.2	1.8	0.3	4.6	0.1	2.0	1.2

Table I. Elemental composition of the concrete in wt.% (taken from Costes et al.)

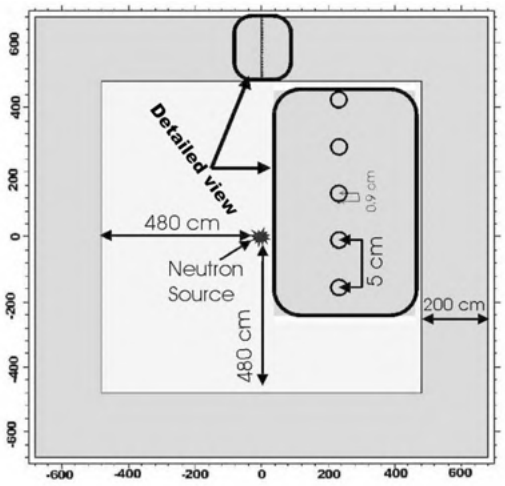

Fig 1. Geometry for MCNP simulations (as was proposed by Costes et al.) with an expanded view of the dose tally cells

.

The equivalent neutron dose was obtained from the MCNP simulated neutron fluences using the conversion fluence-to-dose factors from Belogorlov et al. (1982). These conversion factors were calculated by Belogorlov by considering the energy deposition in a semi-infinite slab of tissue from a monoenergetic neutron beam (Costes et al., 1996) (see Fig 2). While, for the gamma dose a weigthed factor of 1 was considered.

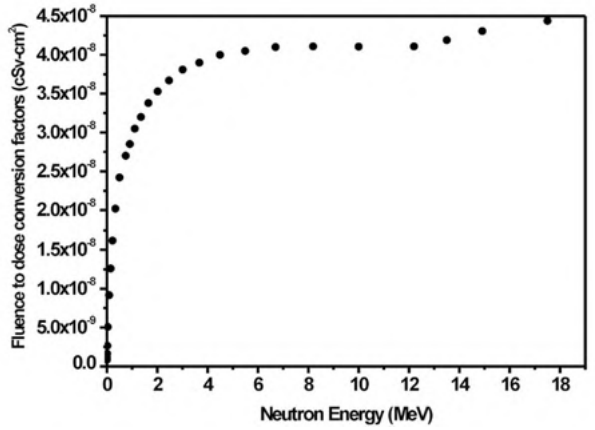

Fig 2. Belogorlov´s factors to convert the simulated neutron fluence to equivalent dose (Costes et al., 1996, Belogorlov et al., 1982)

Equivalent doses were obtained as a function of wall thickness (i.e., of the position of the cell within the wall) for 1% of ^{10}B (as is presented by Costes et al.) and for 10 % ^{10}B. As an alternative, we calculated the dose outside the room for ^{6}Li loaded walls (1, 5, and 10%) instead of boron. A maximum occupational radiation level of 5 REM (= 5 cSv) was considered as the limit for a yearly operating cycle of 2000 hours, resulting in a maximum allowable dose equivalent of 25 μSv/hr. A proton current of 100 mA was used to represent the source term (Costes et al., 1996).

2.2. Radiation protection of the patient.

The second study aims at minimizing the neutron and gamma contamination transmitted to the patient from the room walls. In order to simulate the neutron and gamma fluences, a geometry as shown in Fig. 3 was adopted. This design (with the inner side of the walls now covered with polyethylene loaded with 5% ^{6}LiF) corresponds to an optimized beam shaping assembly (BSA) taken from Burlon et al. (2005) (Fig. 4A). The fluences were simulated in an angular array of tally cells around the head phantom, in two cases: with and without ^{6}LiF shielding (Fig. 4 B).

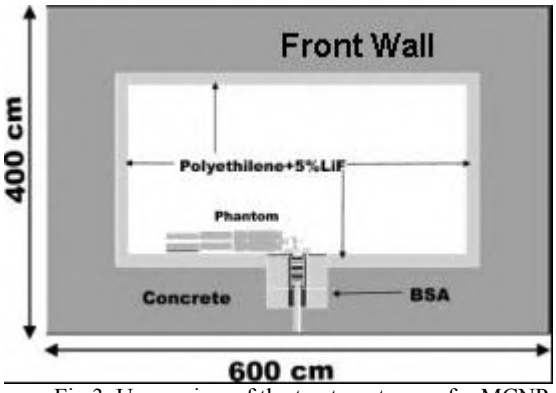

Fig 3. Upper view of the treatment room for MCNP simulations. The ceiling and the floor are also covered with slabs of polyethylene +5% ^{6}LiF

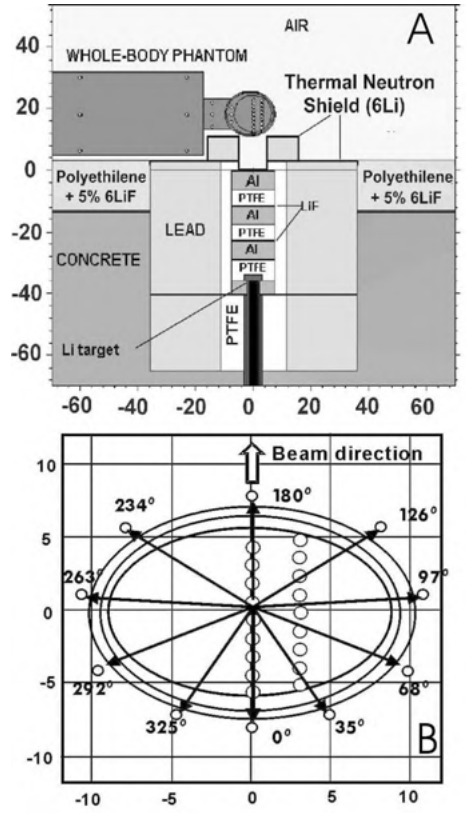

Fig 4. Geometry to simulate the wall contamination around the phantom head (detailed view at bottom)
(Dimensions are in cm)

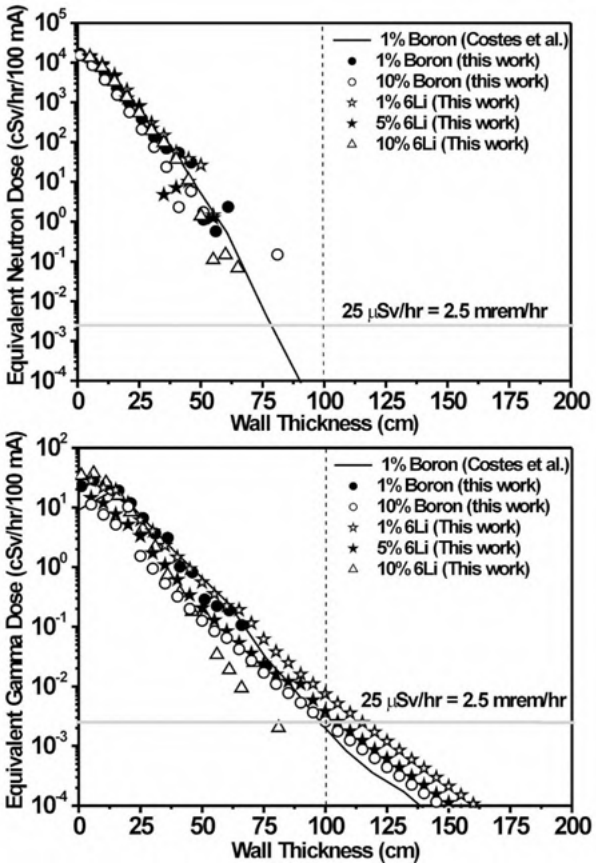

Fig 5. Equivalent Neutron and Gamma doses for different wall thicknesses.

3. Results

3.1 Radiation protection for personnel outside of the treatment room.

Figure 5 shows the equivalent doses calculated for neutrons and gammas. A good agreement can be seen with Costes et al. (in the case of 1% ^{10}B). There is no significant decrease in the neutron and gamma dose for increasing boron concentrations. The neutron dose for ^{6}Li shows a similar trend, but a significant decrease in the gamma dose is evident for 10% ^{6}Li (no gammas are emitted in the neutron capture in Li). The allowed occupational level of 25 μSv/hr (in the case of gamma dose) is reached with a wall of 100 cm thickness while the neutron dose stays below this value for such a wall.

3.2. Radiation protection of the patient.

Figure 6 shows the results from the simulations of the second study. A significant decrease in the thermal neutron and gamma doses can be seen when the inner side of the walls are shielded with LiF loaded polyethylene, in particular at positions which are facing the front wall (around the 180^{o} position-see Fig 3) where the wall contamination is dominant.

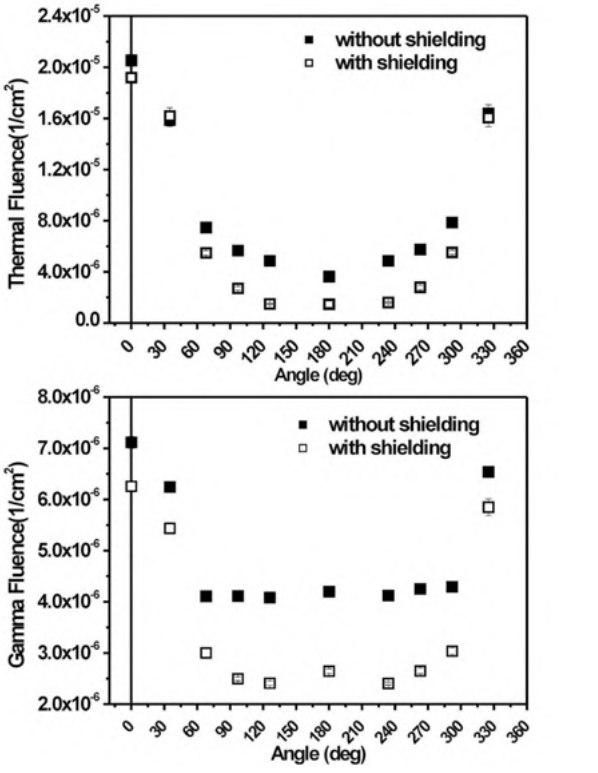

Fig 6. Thermal neutron and gamma fluence around the head phantom with and without shielded walls (No significant differences were observed for epithermal and fast neutron fluences for the shielded and unshielded cases)

4. Discussion and conclusions

4.1 Radiation protection for personnel outside of the treatment room.

A concrete wall loaded with 1% Boron of about 100 cm thickness seems to be sufficient to protect the personnel outside the treatment room from the gamma and neutron dose generated within. But the presence of ^{10}B in the treatment room walls contributes with the emission of the 478 keV neutron capture gamma ray which increases the required shielding. Moreover, this gamma ray from the walls is undesirable if a system is planned to measure the 478 keV boron capture gamma rays emitted by the patient during irradiation. Hence, ^{6}Li appears as an advantageous alternative to boron. An equivalent neutron shielding is obtained for a similar wall thickness with 5-10 % ^{6}LiF loading but the gamma dose is lower than the boron one for a thickness less than 100 cm.

Figure 7 shows the asymptotic behavior of the wall thickness (in order to reach gamma dose levels of 25 μSv/hr) and Figure 8 plots the neutron dose for different thicknesses for 1% ^{6}Li concentration and 50% ^{6}Li concentration (the last one only shown as an asymptotic value). In both cases the thickness is about 100 cm or less.

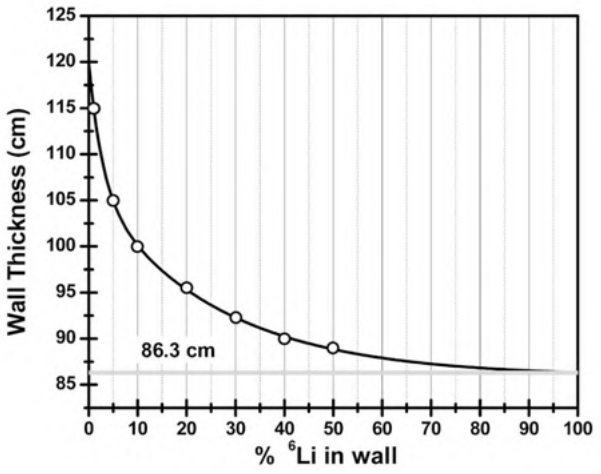

Fig 7. Wall thickness (for a gamma dose level of 25 μSv/hr) as a function of ^{6}Li concentration

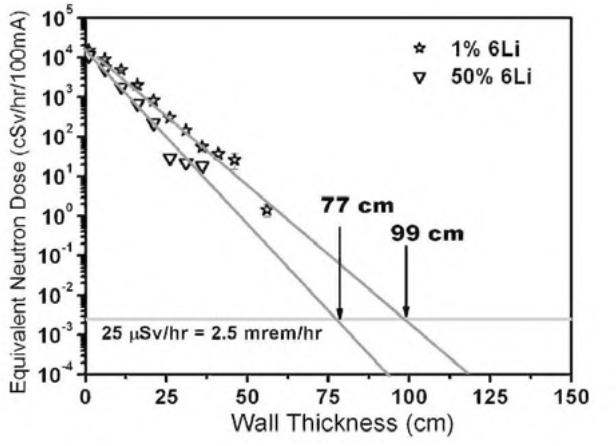

Fig 8 Equivalent Neutron dose at different depths within the front wall for two ^{6}Li concentrations

4.2. Radiation protection of the patient.

Polyethylene loaded with 5% 6LiF reduces the undesirable thermal and gamma dose on the patient, specially the contamination from the front wall. Also, this compound could be used as a shielding material to avoid the radiation emission to the outside of the room.

Our conclusion is that it is far more convenient to shield the treatment room walls with lithiated polyethylene slabs rather than mix the LiF into the concrete.

References

Belogorlov E, Golovachik,V, Lebedev, V, Potemkin, E, 1982. Depth Dose And Depth Dose Equivalent Data For Neutrons With Energy From Thermal Up To Several TeV, Nucl. Instrum. Methods 199, 563–572.

Burlon, A.A, Kreiner, A.J., Valda, A.A., Minsky, D.M., Somacal, H.R., Debray, M.E., Stoliar, P.A., 2005. Optimization of a neutron production target and a beam shaping assembly based on the 7Li(p,n)7Be reaction for BNCT. Nucl. Instrum. Methods B 229, 144–156.

Costes, S.V., Donahue, R.J., Vujic, J., 1996. Radiation shielding and patient organ dose study for an Accelerator-Based BNCT facility at LBNL. LBL Report 39450, 1–16.

Kreiner, A.J., Kwan, J.W., Burlon, A.A, Di Paolo, H., Henestroza, E., Minsky, D.M., Valda, A.A., Debray, M.E., Somacal, H.R., 2007. A Tandem-Electrostatic-Quadrupole for Accelerator-Based BNCT. Nucl. Instrum. Methods B 261, 751–754.

Design study to further optimise the Birmingham orthogonal accelerator epithermal neutron beam

Z. Ghani[1], S. Green[2], C. Wojnecki[2]

[1] *School of Physics and Astronomy, University of Birmingham, United Kingdom*
[2] *Department of Medical Physics, University Hospital Birmingham, United Kingdom*

A detailed study has been carried out on comparing various moderator and reflector materials in order to quantify any improvements that can be made to the current Birmingham facility.
The motivation for optimising and re-modelling the treatment facility was to maximize the dose to tumour tissue while keeping the weighted dose to healthy brain tissues below 12.5 Gy. Five key indices were calculated for three moderator materials (Fluental, MgF_2 and Teflon) and two reflector materials (Graphite and Lead):

1. Treatment Time
2. Therapeutic Ratio (TR) at 6.5cm into the brain
3. Max TR is the ratio of Maximum Tumour Dose to Maximum Tissue Dose
4. Advantage Depth (AD) and
5. Skin dose

Changing the graphite reflector to one made of lead (for 25 cm Fluental moderator) delivered a substantial improvement. It resulted in an increase in beam quality in terms of Therapeutic Ratio and AD. The AD increased from 9.1 to 9.8 ±0.1cm, the TR at 6.5 cm deep from 2.23 to 2.75 and the max TR from 5.34±0.05 to 5.40±0.05, with a 10 % reduction in treatment time from 198 minutes to 176 minutes.
In order to increase the dose rates obtained with the MgF_2 moderator / lead reflector, and thus reduce the treatment time, it becomes necessary to compromise beam quality. By moving to a shorter moderator depth of 18.1 cm treatment time was brought down from 258 minutes to 146 minutes. The change in other key indices being AD from 9.1±0.1 to >10cm, the TR from 2.23 to 2.76 and the max TR from 5.34 ±0.05 to 5.26 ±0.03 when compared to the current facility.
Further calculations will be presented to show that the addition of a Li-Si filter does not affect our choice of the optimum length of moderator and reflector, and to quantify the effect of an additional patient collimator on beam performance indices.

BNCT of explanted livers using a suitably shaped neutron spectrum and irradiation box.

V. Giusti[1,2], K. Skold[2]

[1] *Department of Mechanical, Nuclear and Production Engineering, University of Pisa, Pisa, Italy*
[2] *Hammercap Medical AB, Stockholm, Sweden*

A combination of a suitably shaped irradiation box and neutron energy spectrum to treat explanted livers is here presented. Thermal neutrons have a very low penetration capability inside the human tissue thus, in order to get an as much as possible uniform distribution of thermal neutron flux inside the irradiated organ, a mix thermal/epithermal neutron beam has been found more appropriate. Moreover, to flat the neutron distribution it turned out to be useful also adopting an irradiation box with concave lateral walls. Computational results obtained taking as reference the research beam that was available at the Studsvik BNCT facility (Sweden) are here reported.

The thermal neutron flux inside the irradiation box along the beam axis is distributed within -5%/+7% of its average value. The total dose to the healthy tissue is distributed within -3%/+5%. Limiting the maximum health tissue dose to 10 Gy-eq, at a reactor power of 150 kW the irradiation time is equal to 11 minutes while the total tumor dose ranges between 43.5 and 50.0 Gy-eq.

Modification of the thermal column of the TRIGA Mainz for the treatment of liver metastasis

Gabriele Hampel[1], Arturo Lizon Aguilar[2], Prof. Knorr[3], Shahin Minouchehr[5], Sven Nagels[4], Gerd Otto[5], Christian Schütz[1], Birgit Wortmann[2]

[1]*Institut für Kernchemie, Johannes Gutenberg-Universität Mainz, Fritz-Strassmann-Weg 2, D-55128 Mainz, Germany*
[2]*Evonik Energy Services GmbH Essen, Rüttenscheider Str. 1-3, D-45128 Essen, Germany*
[3]*TU Dresden, Instiut für Energietechnik, D-01062 Dresden*
[4]*Forschungszentrum Karlsruhe GmbH, Hauptabteilung Sicherheit, Postfach 3640, D-76021, Karlsruhe, Germany*
[5]*Transplantationschirurgie, Johannes Gutenberg-Universität Mainz, D-55131 Mainz, Germany*

In 2001 the BNCT method was successfully applied for the extracorporeal treatment of liver metastases at the University of Pavia. Due to this promising result the BNCT project shall be established at the University of Mainz in a close collaboration with the University of Pavia.

The requirements for the therapy in Mainz are ideal: Like the TRIGA reactors in Finland (Espoo) and Italy (Pavia), the TRIGA Mainz is well suited for BNCT. Its irradiation facility is easily accessible, there is sufficient flexibility concerning irradiation times and it is located close to Mainz Medical University Hospital.

The TRIGA Mainz can be operated in the steady state mode with a maximum power of 100 kW_{th} and in the pulse mode with a peak of 250 MW_{th} for a period of less than 100 ms. It has four beam tubes and a thermal column which shall be reconstructed for the treatment of an explanted organ. Therefore, medical and technical requirements as well as the legal regulations must be considered.

In order to determine the optimal parameter for the planned therapy and for the design of the thermal column calculations were done using the MCNP-code as well as the transport code ATTILA. On the basis of the calculations, the reconstruction of the thermal column will be carried out.

The irradiation facility must provide a homogenous thermal neutron field over the organ and a negligible gamma field at the irradiation position. To guarantee constant irradiation conditions in the thermal column during the treatment, online monitoring of the gamma and neutron component is desirable. The irradiation, handling and transport time for the explanted liver should be as short as possible. To maintain the organ in adequate extracorporeal conditions during the irradiation time, a special confinement which allows the placement of the organ in the thermal column and ensures storage of about 4 °C during the irradiation must be designed.

Two possible configurations are being discussed for the irradiation of the liver. An overview of the concept for of the reconstruction of the thermal column will be given as well as an schedule of the whole procedure.

Construction Design of a PGNAA Facility for Boron Concentration Measurement in THOR

Shiang-Huei Jiang[a], A. Y. Chen[a], C. K. Huang[a], H. M. Liu[b], K. B. Chen[b], and J. J. Peir[b]

[a]*Department of Engineering and System Science, National Tsing Hua University, Hsinchu, Taiwan*
[b]*Nuclear Science and Technology Development Center, National Tsing Hua University, Hsinchu, Taiwan*

Abstract

MCNP4C code was used to carry out a series of design calculations for a PGNAA beam in the E-2 beam tube with a length of around 4 meters and a diameter of 8 inches in the THOR. Because that a filter consisting of 30-cm graphite and 20-cm bismuth will suppress the thermal neutron fluence rate by three orders of magnitude, a simple concrete collimator plug with a length of 158.75 cm and an aperture of 2 inches was adopted to construct the PGNAA beam. The fluence rate at the beam exit was calculated to be 1.55 x 10^8 neutrons $cm^{-1}s^{-1}$ for reactor operated at around 1 MW. The counting rate of the detector system for a sample containing 1 μg of ^{10}B was estimated to be around 20 cps.

Keywords: PGNAA beam, Construction design, Monte Carlo calculation, ^{10}B concentration

1. Introduction

For Boron Neutron Capture Therapy (BNCT) animal or clinic trials the information of boron concentration in blood is a prerequisite. In order to accurately measure the boron concentration in blood as a function of time after boron compound infusion a Prompt Gamma Neutron Activation Analysis (PGNAA) facility was designed and is being under construction in the E-2 beam port nearby the BNCT epithermal neutron beam of the Tsing Hua Open-pool Reactor(THOR). ^{10}B has a huge thermal neutron absorption, namely, $^{10}B(n,\alpha)^7Li$ cross section (3840 barns). The reaction product ^7Li is left at the first excited state with a branching ratio of about 94 percent. Through the measurement of the 0.48-MeV gamma rays emitted from the de-excitation of the excited ^7Li nuclides, the concentration of ^{10}B in the sample irradiated by thermal neutrons can be determined. The design objectives of the PGNAA neutron beam, therefore, are both to pursue a thermal neutron fluence rate at the exit of the beam as high as possible with a level at least higher than 1.0 x 10^7 neutrons $cm^{-2}s^{-1}$ and to reduce the fluence rates of the contaminated fast neutrons and gamma rays to a level as low as possible. MCNP Monte Carlo code was applied in this work to conduct design calculations of the PGNAA beam line. A series of calculations have been carried out for different beam line configurations with and without filter materials. In order to ensure a maximum thermal neutron fluence rate at the beam exit higher than 1.0 x 10^7 neutrons $cm^{-2}s^{-1}$ and taking into account the fabrication practice, cylindrical concrete collimator plugs with a length of 158.75 cm and an aperture of 2 inches were adopted to construct the PGNAA beam at the E-2 beam port of the THOR.

2. Materials and Methods

2.1. Description of the E-2 beam of the THOR

THOR is a 2-MW swimming pool research reactor with TRIGA fuels. There are six horizontal neutron beam tubes extending from the core edge through the water pool and concrete shield for neutron experiments, three at east side and three at west side. The E-2 beam tube consists of two sections with a total length of about 4 meters. The front section has a diameter of 8 inches and a length of 230 cm with part passing through the water pool and part in the concrete shield. The following rear section all in the concrete shield has a diameter of 10 inches and a length of 158.75 cm. Figure 1 shows the layout of the E-2 beam tube in the THOR.

The neutron spectrum at the core edge was measured by multi-foils activation method at one of the six vertical irradiation tubes at the north side of the core edge (Niu, 1981). Figure 2 shows the measured neutron spectrum at the core edge which will be used as the neutron source spectrum for the design calculations of the PGNAA beam at the E-2 beam port. From the source neutron spectrum it was

found that the fractions of thermal (< 0.414 eV), epithermal (0.414 eV – 7.2 keV) and fast (> 7.2keV) neutrons were 70%, 9%, and 21%, respectively.

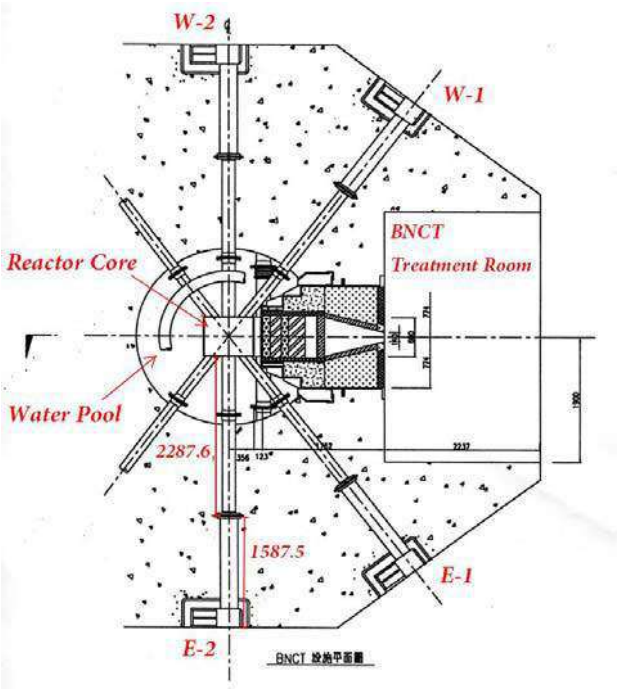

Fig. 1 Layout of the E-2 beam tube in the THOR.

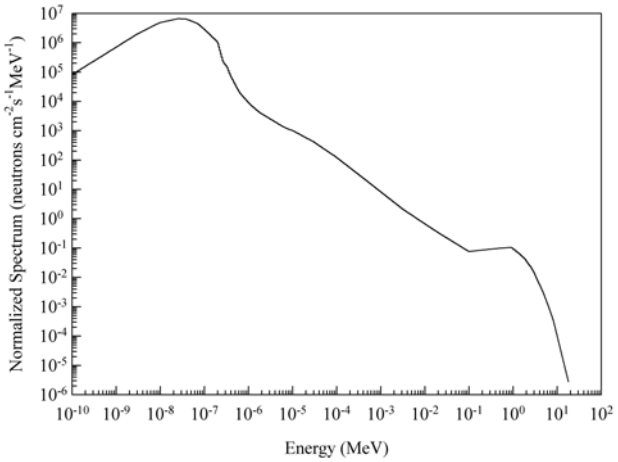

Fig. 2 Neutron spectrum at the core edge of the THOR.

2.2. MCNP Monte Carlo Calculations

MCNP4C code (Briesmeister, 2000) was used for the design calculations of the PGNAA beam. The geometry and material of the E-2 beam tube were modeled exactly in the input file of the code. The neutron source from the reactor core was treated as a disk source of 100 cm in diameter located at the front end of the beam tube. The spectrum of the neutron source was taken from Fig. 2 and the angular distribution was assumed to be a cosine distribution. In the design of PGNAA beams, filters consisting of graphite and bismuth were normally embedded in the beam (IAEA, 2007). Graphite is used to moderate the fast neutrons and to increase the fraction of thermal neutrons. Bismuth is used to attenuate gamma rays coming directly from the reactor core. The effects of these filters and their installing locations were invested. The boundary crossing estimator (the F2 tally) was used to score the neutron as well as the secondary gamma-ray fluence rates at the beam exit and the fluence rate was normalized to unit source strength.

3. Results and Discussions

PGNAA beams with the embedded filter consisting of 30-cm graphite and 20-cm bismuth at the front and middle regions and without the filter were investigated. Figure 3 shows these three geometry models in the MCNP calculations. Note that the collimator consisting of 10-cm Pb and 20-cm PE with 40%w Li_2CO_3 at the exit end of the beam tube has an aperture of 6 cm x 6 cm.

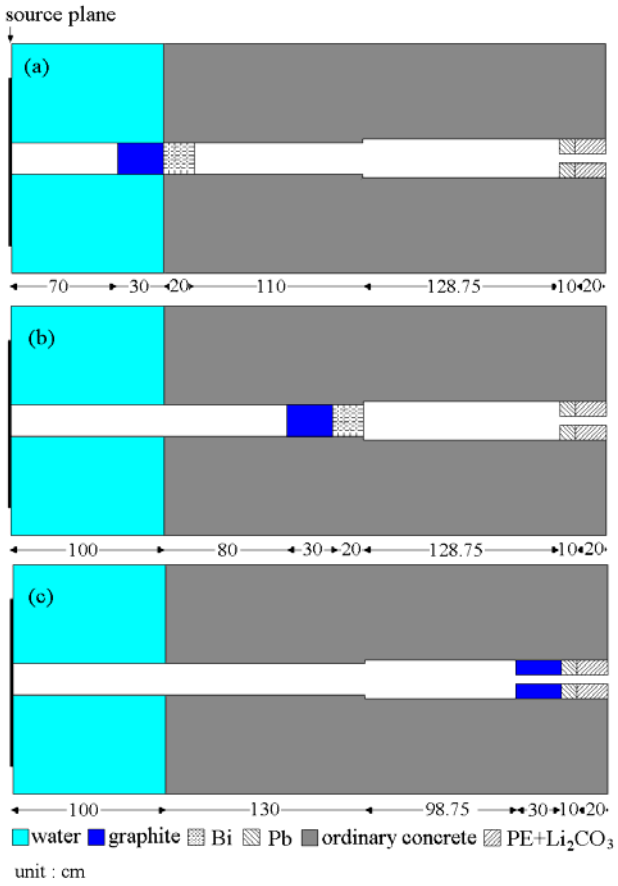

Fig. 3 Geometry models of three PGNAA beam configurations.

The calculated neutron and secondary gamma-

ray fluence rates at the beam exit for the three beam configurations are listed in Table I. The neutron fluence rate at the beam exit for the beam with no filter essentially comes directly from source neutrons without any collision, i.e., the line-of-sight component. Therefore, the thermal neutron fraction of about 70% is almost the same as that of source neutrons. It can be seen from Table I that the existence of the filter really suppresses the neutron fluence rate by about three orders of magnitude. The moderation effect of the filter is not significant as shown by the thermal neutron fraction. The other purpose of the filter, i.e., to attenuate the source gamma rays was not studied in this work. The secondary gamma-ray fluence rate equals roughly neutron fluence rate for beams with filter and is about 7% of the neutron fluence rate even for the beam without filter. For a further inspection, the neutron fluence rates along the beam length for the three beams were calculated and the thermal neutron fluence rates were plotted in Fig. 4.

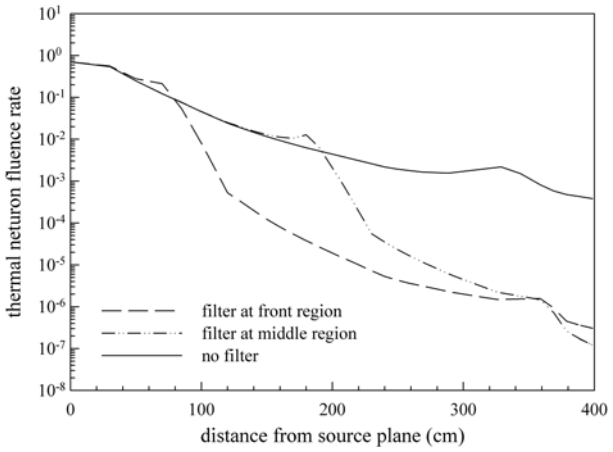

Fig. 4 Distributions of thermal neutron fluence rate along the beam length.

Before the exit collimator, the thermal neutron fluence rate for the beam with filter at the middle region is higher than that for the beam with filter at the front region, however, at the beam exit the reverse is true. Clearly, this is attributed to the divergent angular distribution of neutrons emergent from the filter.

In order to ensure a maximum thermal neutron fluence rate higher than 1.0 x 10^7 neutrons $cm^{-2}s^{-1}$ and taking into account the fabrication practice, cylindrical concrete collimator plugs of 158.75 cm in length and 25.4 cm in diameter with apertures of 1- and 2-inches diameters, respectively were adopted to construct the PGNAA beam at the E-2 beam port of the THOR. Figure 5 shows the geometry model of the PGNAA beam with concrete collimator for MCNP calculations. A shorter collimator plug with a length of 100 cm was also calculated for comparison. The thermal neutron fluence rate at the beam exit were found to be 3.82 x 10^7 and 1.55 x 10^8 neutrons $cm^{-2}s^{-1}$ for collimators with 1″- and 2″-aperture, respectively and 1.09 x 10^8 and 4.03 x 10^8 neutrons $cm^{-2}s^{-1}$ for 100-cm collimator plug for the disk source with a strength of 10^{12} neutrons $cm^{-2}s^{-1}$, which corresponds to the reactor operating at a power around 1 MW. At the distance of 10 cm away from the beam exit the thermal neutron fluence rate decreases about 10 percent. The counting rate for a sample containing 1 μg of ^{10}B irradiated at the location 25 cm away from the beam exit of the PGNAA beam constructed by a concrete collimator plug with a length of 158.75 cm and an aperture of 2 inches measured by a high purity germanium detector (HPGe) with a relative efficiency of 35% set at a distance of 25 cm from the irradiated sample is estimated to be 21.2 counts per second (cps), where the detection efficiency for the 0.48-MeV gamma rays from $^7Li^*$ is assumed to be a factor of two higher than that for 1.333-MeV gamma rays from ^{60}Co and the effect of detector collimator is not taken into account.

Table I Neutron fluence rates at the beam exit for three PGNAA beam configurations.

	Filter at front region		Filter at middle region		No filter	
	Fluence rate	RE	Fluence rate	RE	Fluence rate	RE
Thermal neutron	3.64E-07	2.97%	1.71E-07	0.62%	4.29E-04	2.07%
Epi- neutron	1.29E-08	23.17%	1.50E-08	2.72%	6.60E-05	5.36%
Fast neutron	6.07E-08	12.53%	5.35E-08	3.22%	1.22E-04	4.09%
Total neutron	4.38E-07	3.10%	2.39E-07	0.89%	6.17E-04	1.75%
Gamma-ray	3.43E-07	6.25%	2.11E-07	0.97%	4.41E-05	6.18%

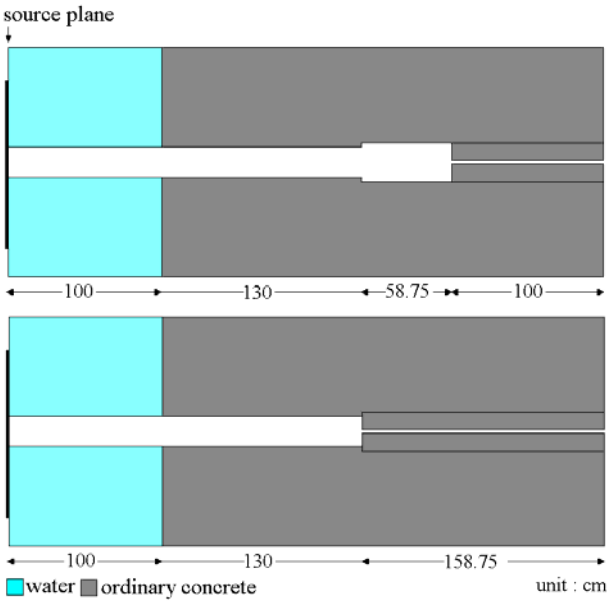

Fig. 5 Geometry models of the PGNAA beams with concrete collimators.

4. Conclusions

In order to accurately measure the boron concentration in blood a PGNAA facility was designed and is being under construction in the E-2 beam port of the THOR. MCNP4C computer code was used to perform the design calculations. It was found that a graphite-bismuth filter with a thickness of 50 cm will suppress the neutron fluence rate at the beam exit by three orders of magnitude.

In order to ensure a maximum thermal neutron fluence rate at the beam exit and taking into account the fabrication practice, a cylindrical concrete collimator plug with a length of 158.75 cm and an aperture of 2 inches was adopted. The thermal neutron fluence rate at the beam exit was calculated to be 1.55 x 10^8 neutrons $cm^{-2}s^{-1}$ for reactor operated at a power around 1 MW. The counting rate of the detector system for a sample containing 1 μg of ^{10}B was estimated to be around 20 cps.

Acknowledgements

This work was supported by the booster program of 2007-2008 of National Tsing Hua University, Hsinchu, Taiwan, R.O.C..

References

Briesmeister, J.F, (Ed.), 2000. MCNP - A General Monte Carlo N-Particle Transport Code, Version 4C. LA-13709-M. Los Alamos National Laboratory, USA.

IAEA, 2007. Database of Prompt Gamma Rays from Slow Neuton Capture for Elemental Analysis, IAEA, Vienna.

Niu, H. C., 1981. Neutron Spectrum Measurement for the Tsing Hua Open-pool Reactor, Master Thesis, Department of Nuclear Engineering, National Tsing Hua University.

Performance measurement of the SOF detector for boron neutron capture therapy

Masao Komeda[1], Hirokai Kumada[1] , Masayori Ishikawa[2], Takemi Nakamura[1],
Kazuyoshi Yamamoto[1], Akira Matsumura[3]

[1] *Department of Research Reactor and Tandem Accelerator, Japan Atomic Energy Agency, Japan*
[2]*Department of Medical Physics, Hokkaido University Hospital, Japan*
[3] *Department of Neurosurgery, University of Tsukuba, Japan*

Abstract

The thermal neutron flux can be easily measured in real time by using the SOF (Scintillator with Optical Fiber) detector. However the irradiation damage under high-intensity neutron flux causes the deterioration of the SOF detector due to the plastic scintillator in which ^{6}LiF is blended.

After irradiating the SOF detector for 4 hours (thermal neutron fluence approximately 2.0×10^{13} neutrons/cm^2), the sensitivity of the SOF detector decreased by 3.0%. After irradiating the SOF detector for 2 months (thermal neutron fluence approximately 6.4×10^{14} neutrons/cm^2), the sensitivity was reduced to 42%. Supposing that the thermal neutron fluence is 2×10^{12} (neutrons/cm^2) on the surface of a patient in a BNCT treatment, the sensitivity of the SOF detector is reduced by approximately 0.3 %. This report presents investigations on the deterioration of the SOF detector in irradiation experiments.

Keywords: SOF, irradiation damage, deterioration, plastic scintillator, BNCT

1. Introduction

The SOF detector (Ishikawa et al., 2006) (Ishikawa et al., 2005) has recently been developed as a small-sized neutron beam monitor. It is composed of a plastic scintillator in which ^{6}LiF is blended and an optical fiber. Because the SOF detector is small-size and rapid-response, it can be used to measure the thermal neutron flux in real time easily during the BNCT treatment. However the irradiation damage of the plastic scintillator by neutron and alphamay be the cause of deterioration of the SOF detector. This report indicates deterioration of the SOF detector by irradiation experiments that consist of correcting measurements and deterioration measurements. Both correcting and deterioration measurements were carried out at the JRR-4 reactor (Japan Research Reactor No.4) (Torii et al., 2000). In the correcting experiments, the method of correcting of the SOF detector is introduced and estimated. In the deterioration measurements, the SOF detector is irradiated for long time and deterioration is estimated.

2. Material & Methods

(1) Correcting measurements

The correcting measurements were performed by using a gold wire attached on the tip of the SOF located in a water phantom that was set in front of the beam collimator. Fig.1 shows a cross-section drawing of the JRR-4 reactor and the neutron irradiation facility. Fig.2 shows the water phantom. Fig.3 shows the probe of the SOF detector and the gold wire.

The SOF detector with the gold wire was installed in the water phantom through a guide tube and irradiated. After a ten-minutes irradiation, the SOF with the gold wire was pulled out and the correction factor was calculated by comparing data of the SOF detector with the activation of the gold wire. The correction measurements were carried out 4 times in a day. The correction factor (Cf) is calculated as follows: $Cf = \Phi_{gold} / N_{SOF}$ where Φ_{gold} is the fluence by the gold wire and N_{SOF} is the number of counts on the SOF detector. The measured value of the SOF detector decreases as sensitivity of SOF decreases. Therefore the value of Cf is increasing as sensitivity is decreasing. In short, the sensitivity is proportional to 1/Cf.

In this irradiation field, the thermal neutron flux is 1.6×10^{8} (neutrons/cm^{2}s) and the cadmium ratio is 15.

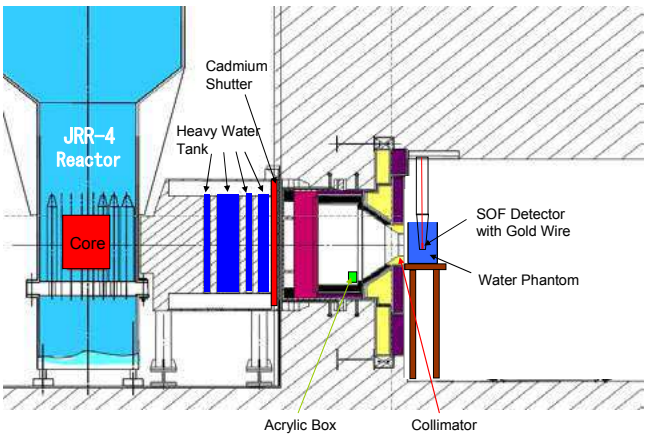

Fig.1. Cross-section drawing of the JRR-4 reactor and the neutron irradiation facility

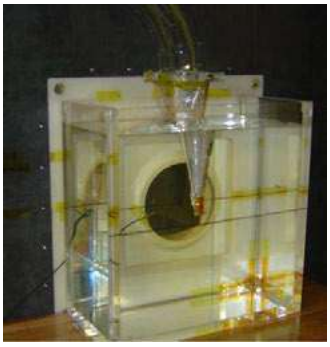

Fig. 2. Water phantom

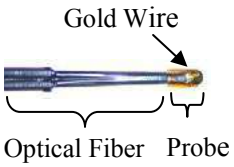

Fig. 3. Probe of the SOF detector and gold wire

(2) Deterioration measurements

The deterioration measurements were carried out at higher flux than that of the correcting measurements. An acrylic box (a 4 cm side cube) was used as a moderator in the location shown in Fig.1. The SOF detector was installed in the acrylic box (Fig.4). The thermal neutron flux was 2.3×10^{9} (neutrons/cm^{2}s) and the cadmium ratio was 4.4 in the hole of the acrylic box. The SOF detector was irradiated for about 4 hours from reactor start up to shut down. The deterioration was estimated by monitoring data of the SOF detector. Because monitoring data decreased approximately linearly, the deterioration was calculated by the inclination.

In addition, the SOF detector was used for about 2 months. The deterioration was estimated by the correction factors that were measured with a gold wire at the first day and the last day. The fluence of the SOF was calculated by using an average value of those two correction factors.

Fig. 4. Acrylic box and SOF detector

3. Results

(1) Correcting measurements

The measurements were carried out 4 times for the SOF detector. Results are shown in Fig.5. The error associated with this method of correcting measurement is approximately 4%. The declination setting of the gold wire and the SOF detector could have caused the error. In these correcting measurements, a clear deterioration could not be found. It is difficult to estimate deterioration in the case of small deterioration because correcting method with gold wire has small error.

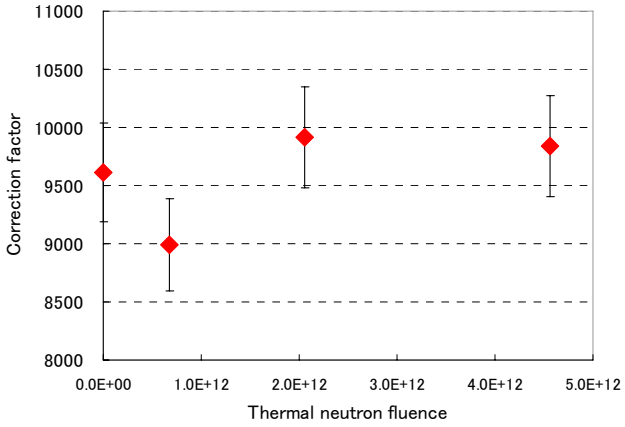

Fig .5. Results of correcting measurements

(2) Deterioration measurements

Fig.6 shows the result of a deterioration measurement. The measured values from 97 min. to 282 min. were declining though the reactor power was stable. It is considered that the reason of the declining is deterioration. The degree of deterioration was estimated by calculating the inclination between 97 min. and 282 min. in the Fig.6. Therefore it was found that sensitivity decreased by approximately 3% for thermal neutron fluence of 2×10^{13} (neutrons/cm^2).

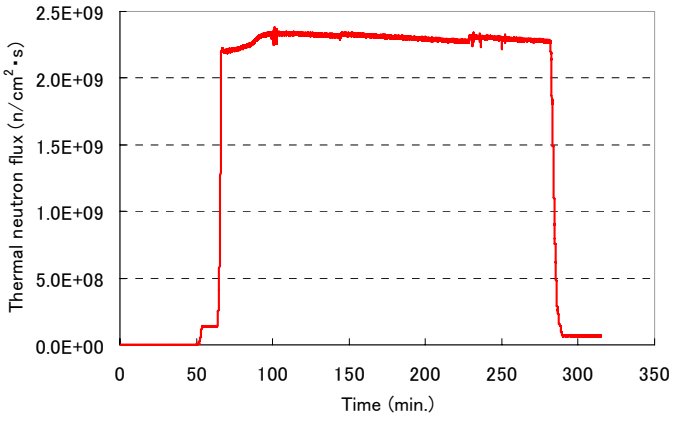

Fig. 6. Results f a deterioration measurement

In addition, the SOF detector that was used at the above deterioration measurement was used for about 2 months. Then thermal neutron fluence was approximately 6.4×10^{14} (neutrons/cm^2). Results of correcting measurements at the first measurement and the last measurement were shown on Table1, where the total fluence was estimated by monitoring data of the SOF detector. Then correction factor was applied as the average value of first and last correcting measurements.

Table 1. The result of monitoring by the SOF detector

Irradiation days	15 days
Total fluence	6.4×10^{14} n/cm^{-2}
Initial correction factor ①	4100
Final correction factor ②	10000
②／①	2.4

Table1 shows that the sensitivity of the SOF detector decreases to 42% (=1/2.4 × 100) for a thermal neutron fluence of 6.4×10^{14} neutrons/cm^2. Fig.6 shows that the sensitivity decreased to 97% for a thermal neutron fluence of 2.0×10^{13} neutrons/cm^2. Applying this result of the sensitivity to the neutron fluence of 6.4×10^{14} neutrons/cm^2, the sensitivity is 0.97^{32}=0.38=38%. The value is roughly in accordance with the value in Table1.

4. Conclusions & Discussions

The deterioration measurement indicated that the sensitivity of the SOF detector decreased by approximately 3% for a thermal neutron fluence of 2.0×10^{13} neutrons/cm^2. Though the deterioration could be mainly caused by the irradiation damage of the plastic scintillator, the irradiation damage of the optical fiber is also thought to be large. It is necessary to investigate the irradiation damage of an optical fiber in the future. It is also considered that the amount of ^{6}LiF in the SOF detector influences the irradiation damage. Now we are investigating the influence of changing the amount of ^{6}LiF.

Supposing that the thermal neutron fluence on the surface of a patient is 2×10^{12} neutrons/cm^2 in a BNCT treatment, as the result of the deterioration measurement, it is considered that the sensitivity of the SOF detector is reduced by approximately 0.3 %.

The SOF detector can measure only thermal neutron flux. It can not measure the epi-thermal neutron beam mostly used at present in JRR-4. It is necessary to investigate the method to measure epi-thermal beam by using SOF detector in the future.

The SOF detector is not suitable for monitoring absolute value of high neutron flux because of the deterioration problem. Therefore we considered a combination with a Self Powered Neutron Detector (SPND) (Hilborn, 1964), which has practical accomplishment for high flux measurements. While the SPND has the advantage of being strong against deterioration, it has the disadvantage of a very slow response. Therefore we are now considering a beam monitor that is strong against deterioration in high neutron flux field and has fast response by composing the SOF detector with the SPND.

References

Ishikawa, M., Ono, K., Matsumura, A., *et al.*, 2006. Development of a real-time thermal neutron monitor and its clinical application. Proceedings of ICNCT12.

Ishikawa, M., Kumada, H., Yamamoto, K., *et al.*, 2005. Development of a wide-range paired scintillator with optical fiber neutron monitor for BNCT irradiation field study. Nuclear Ins. Meth. Phys. Res., Vol. A-551, 448-457.

Torii, Y., Yamamoto, K., Kishi, T., 2000. The BNCT irradiation facility of JRR-4. Proceedings of ICNCT9.

Hilborn, J.W., 1964. Self-Powered Neutron Detectors for Reactor Flux Monitoring. Nucleonics, 22.

Study of irradiation port position for accelerator beam shaping assembly operated $^{7}Li(p,n)^{7}Be$ neutron producing target

Oleg E. Kononov[1], Michel V. Bokhovko[1], Victor N. Kononov[1]

[1] *Institute of nuclear and neutron phisic, State Scientific Center of Russian Federation - Institute for Physic and Power Engineering*

Two possible position of irradiation port – on beam axis and under 90 degree to proton beam axis for accelerator based beam shaping assembly is discuss. Results of calculated absorbed dose distribution from the point of view beam shaping assembly optimisation are presented. Possible optimum configuration of BSA is discuss. Results of neutron spectra measurement are presented for optimised beam shaping assembly with irradiation port located under 90 degree to proton beam axis. Discussed results of absorbed dose measurements at accelerator KG-2.5 with water phantom and beam shaping assembly with irradiation port under 90 degree to proton beam axis. Advantage of 90 degree irradiation port positioning is discussed.

Transport of high-intensity proton and deuteron beams through a TESQ accelerator

P. Levinas[a,c] , A.J. Kreiner[a,b,c] and E. Henestroza[d]

[a]*Departamento de Física, Comisión Nacional de Energía Atómica, Av. Gral Paz 1499 (1650), San Martín, Buenos Aires, Argentina.*

[b] *Escuela de Ciencia y Tecnología. Universidad Nacional de Gral. San Martín, M. De Irigoyen 3100 (1650), San Martín, Buenos Aires, Argentina.*

[c]*CONICET, Avda. Rivadavia 1917(C1033AAJ), Ciudad Autónoma de Buenos Aires, Argentina.*

[d] *Ernest Orlando Lawrence Berkeley National Laboratory, University of California, Berkeley, USA*

Abstract

Within the frame of an ongoing project to develop a Tandem-ElectroStatic-Quadrupole (TESQ) accelerator facility for Accelerator-Based (AB)-BNCT at the Atomic Energy Commission of Argentina in Buenos Aires we discuss the transport of a high-intensity proton and deuteron beam. The project goal is a machine capable of delivering 30 mA of 2.4 MeV protons to be used in conjunction with a neutron production target based on the ^{7}Li(p,n)^{7}Be reaction, slightly beyond its resonance at 2.25 MeV and to be ultimately installed at a hospital site. This important ion current is necessary given the values of the relevant neutron production nuclear cross sections. For these intense beams, composed by charged particles of equal sign, there are significant repulsive space charge effects. Hence it is convenient to resort to devices capable of providing strong and effective transverse focusing, independently of the accelerating fields. In this work we describe in some detail the transport calculations performed through the focusing and accelerating electrostatic quadrupoles and axially symmetric structures. The geometry and voltages along the column were selected using as a guide the solutions to the envelope equations and a selfconsistent calculation of the beam propagation was performed.

Keywords: Accelerator-Based BNCT (AB-BNCT), Tandem Electrostatic Quadrupole accelerator, Beam transport, acceleration and focusing.Envelope equations. Selfconsistent 3D Warp calculations.

1. Introduction

Within the frame of an ongoing project to develop a Tandem-ElectroStatic-Quadrupole (TESQ) accelerator facility for Accelerator-Based (AB)-BNCT at the Atomic Energy Commission of Argentina in Buenos Aires (Kreiner et al., 2007) we discuss the transport of high-intensity proton and deuteron beams. Neutron production is based on the ^{7}Li(p,n)^{7}Be reaction, slightly beyond its resonance, at 2.3 MeV and also on the ^{9}Be(d,n)^{10}B reaction at about 1.2 MeV (to be implemented through a single-ended machine). The machine being designed and constructed is a folded TESQ with a terminal at 1.2 MV. Hence, the project aims at developing a machine capable of delivering a proton beam of about 2.4 MeV and 30 mA. This high ion current is required given the values of the relevant neutron production nuclear cross sections. For these intense beams, constituted by charged particles of equal sign, there are significant repulsive space charge effects. Hence, it is convenient to resort to devices capable of providing strong and effective transverse focusing, independently of the accelerating fields. In this work we describe in some detail the calculations performed through the focusing and accelerating electrostatic quadrupoles and axially symmetric structures.

2. Materials and Methods

Most existing DC electrostatic accelerators can produce only a few mA of beam current, limited by the column design. For sufficiently high space-charge densities, as implied by a size limited multi-mA beam, particles carrying the same charge will repel each other, causing the ion beam to self-expand. Hence high beam current density needs strong transverse focusing. In a conventional

Pierce column, the longitudinal electric field E_z is proportional to $V^{1/4}$ (Anderson et al., 1994), V being the voltage along the machine referred to the ion source voltage, which is proportional to the kinetic energy of the particles. Thus, the threshold of electrical breakdown along the beam axis limits beam focusing.

In this regard, for a given value of peak electric field, ESQ´s have a much stronger focusing capability than the aperture lenses used in conventional Tandem accelerators (Kwan et al., 1997). This is accomplished by effectively decoupling the two functions: longitudinal acceleration in the gaps between the quadrupoles and transverse focusing within each quadrupole. The strong transverse field in an ESQ not only focuses the beam but also suppresses secondary electrons, and associated induced X-rays, preventing them from cascading downstream and minimizing the risk of electrical breakdown. The alternating compression and decompression of the beam in successive quadrupoles in both x and y-axes of the ESQ chain produces a net beam focusing effect. In fact, for a given current density and our geometry (this geometry can be seen in more detail in the contribution by Kreiner et al. in these proceedings), the peak longitudinal focusing field required in a Pierce column is about 4 times larger then the transverse pole tip field required for the ESQ (Anderson el al., 1994).

As an intermediate step of this project, we shall first produce a 1.2 MeV deuteron beam to hit a thin Be target to produce neutrons through the ^{9}Be(d,n) reaction (see Kreiner et al., these proceedings), hence the interest of also studying the transport of deuterons through the accelerator.

3. Results

In a first step, we utilize the Kapchinskii-Vladmirsky (KV) envelope equations (Lawson, 1988; Humphries, 2002) to study the force balance between focusing achieved by quadrupole doublets and defocusing caused by space charge and finite emittance. The envelope equation approach for our TESQ accelerator has already been described in previous publications (Kreiner et al., 2007 and 2007a). We propose here a modular geometry and a gradual adjustment of the focusing (quadrupole) voltages, while maintaining fairly constant the acceleration field and the beam radius -averaged over a quadrupole doublet-. Finally, we use the code WARP (Friedman et al., 1992; Grote et al., 1996) to simulate the transport of the beam with a realistic geometry and without constraining the form of the distribution function. This is performed in a self-consistent way, meaning that the beam propagation is done by taking into account both applied and self-generated fields, the latter being dependent on the evolution of the beam itself. This is accomplished by the following procedure: First the Laplace equation is solved and particles are propagated throughout the structure, without considering any space charge forces. The positions at each time step are stored and a density function is created. Then the Poisson equation is solved considering the electrodes and this density function, electrical fields are calculated and particles are propagated once again. A new density function is then created, and the process is repeated until convergence is reached.

The strategy to make a first estimate of the voltages along the column consists in balancing the main repulsive effect, due to space-charge, with the focusing action of the quadrupoles: this leads to a scaling law proportional to $E^{1/4}$ for the quadrupole voltages, for a given quadrupole length, being E the kinetic energy of the particles at a given position along the accelerator. The voltage differences between all electrodes along the accelerating tube, including the quadrupole electrodes, can only be adjusted to multiples of 10 kV, due to the design of the high voltage supplies. To preserve a modular design we have restricted ourselves to just two different quadrupole sizes. 9 quadrupoles of 20.3 cm length and the rest of 31 cm length. The shorter quadrupoles are useful to reduce the phase advance per cell at lower energies, minimizing envelope oscillations and providing a more stable transport (Lawson, 1988). In the end only two values of focusing voltages where used, one for the short quadrupoles section and one for the large quadrupoles section, due to the high voltage supplies restriction (Table 1). The pole tip (or bore hole) radius of the quadrupoles is 5 cm, roughly 5 times larger than the actual beam radius, which implies a safe operation.

In the actual simulation a 200 keV semi-gaussian beam was injected, accelerated and transported through the system. This kind of beam corresponds to a uniform distribution in position (within a given range) and gaussian in velocities. The chosen normalized emittance value (for both x and y) is 0.253 π.mm.mrad (see Kreiner et al., 2007). The extraction and pre-acceleration to 200 keV will be carried out using a cylindrical geometry, with the exception of the matching section just before the quadrupoles. The purpose of this section is shaping the beam in a way that it is

suitable for transport through the quadrupole structure.

In Fig. 1 and Fig. 3 we can see that the beam radius remains approximately constant throughout the entire structure, and in Fig. 2 and Fig. 4 that the beam propagates without essentially incrementing its normalized effective emittance. The effect of the bending magnets and the stripper in the high voltage terminal is yet to be taken into account when performing future calculations.

Nquad	DVquad [kV]	DVaccel [kV]
1	40	20
2	40	30
3	40	30
4	40	20
5	40	30
6	40	30
7	40	20
8	40	30
9	40	30
10 to 25	30	70

Table 1. Focusing (DVquad) and accelerating voltages (DVaccel) applied along the column. Nquad is the index of the quadrupoles, starting at the lowest energy

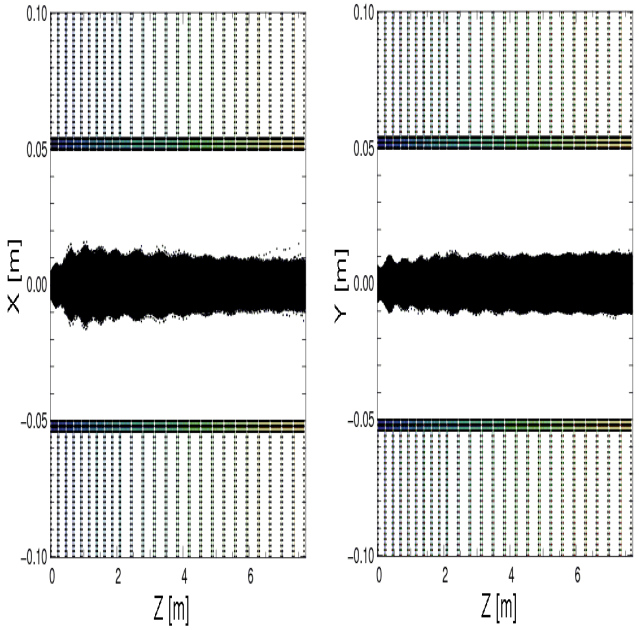

Fig. 1. XZ and YZ projections for a 30 mA proton beam (Z is the propagation axis). In the lower and upper part of the figure we see the successive quadrupoles along the machine. Their pole tip radius is 5 cm

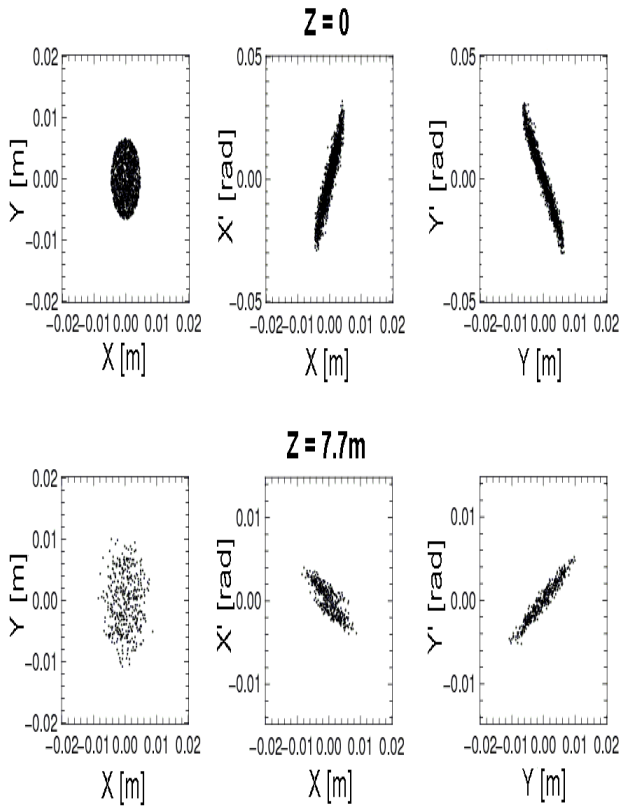

Fig. 2. Projections on different trace space planes of the proton beam at the beginning (Z=0) and ending (Z=7.7 m) of the accelerator

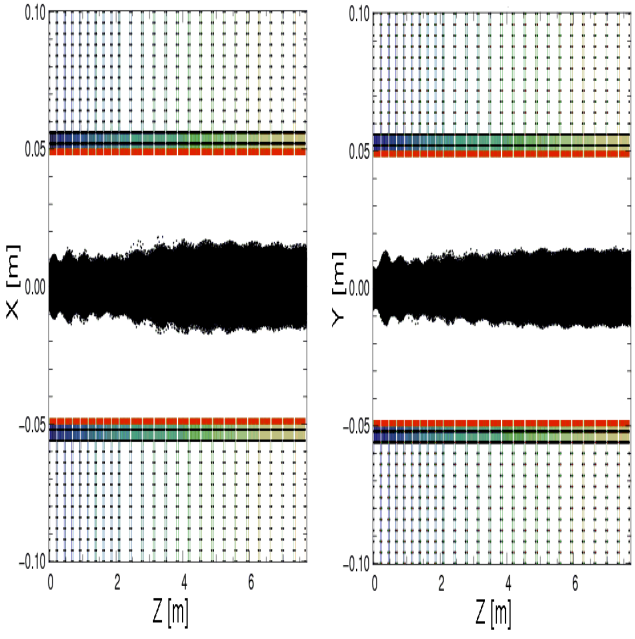

Fig. 3. Projections on the XZ e YZ planes for a deuteron beam

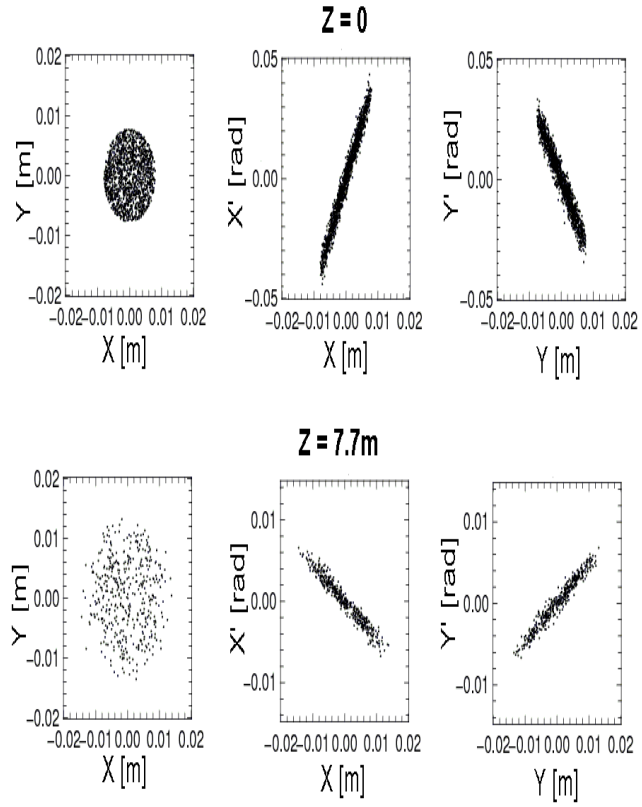

Fig. 4. Projections on different planes of the deuteron beam at the beginning (Z=0) and ending (Z=7.7 m) of the accelerator

4. Summary and conclusions

In previous publications the propagation of the beam through the TESQ accelerator was assessed using the KV envelope equations with a schematic description of the external electrostatic fields (namely the fields due to perfect quadrupoles, and the accelerating gaps, but without solving Poisson's equation with the complete geometry). In this contribution we have gone a step further and have calculated the selfconsistent propagation of proton and deuteron beams using the 3D code WARP. The results show that the chosen design for the TESQ accelerator can be used for guiding and accelerating a 30 mA beam.

References

Anderson O.A., E. L. Alpen, J. W. Kwan, R. P. Wells, G. J. Devries, A. Faltens and L. L. Reginato, 1994. ESQ-focused 2.5 MeV DC Accelerator for BNCT, in Proceedings of the Fourth European Particle Accelerator Conference, 2619-2621.

Friedman A., D. P. Grote, I. Haber, Three Dimensional Particle Simulation of Heavy Ion Fusion Beams, 1992. Phys. Fluids B. 4, 2203.

Grote D.P., A. Friedman, I. Haber, 1996. Three-Dimensional Simulations of High Current Beams in Induction Accelerators with WARP3d, Fus. Eng. & Des., 32-33, 193. 193-200.

Humphries S. Jr., 2002. Charged Particle Beams.

Kreiner, A.J., Kwan, J.W., Burlon, A.A, Di Paolo, H., Henestroza, E., Minsky, D.M., Valda, A.A., Debray, M.E., Somacal, H.R., 2007. A Tandem-Electrostatic-Quadrupole for Accelerator-Based BNCT. Nucl. Instrum. Methods B 261, 751–754 and references therein.

Kreiner, A.J., H. Di Paolo, A.A. Burlon, J.M. Kesque, A.A. Valda, M.E.Debray, Y. Giboudot, P. Levinas, M. Fraiman, V. Romeo, H. Somacal, D. Minsky, 2007a. Accelerator-Based Boron Neutron Capture Therapy and the Development of a Dedicated Tandem-Electrostatic-Quadrupole. VII Latin American Symposium on Nuclear Physics and Applications. AIP Conf. Proc. 947, 17-24.

Kwan, J.W., E. Henestroza, C. Peters, L.L. Reginato, and S.S. Yu, 1997. Designs of a DC ESQ Accelerator for BNCT Application, *Application of Accelerators in Research and Industry*, AIP Press, 1313-1315, and references therein.

Lawson, J.D., 1988. *The Physics of Charged-Particle Beams*. Clarendon Press, Oxford.

Prompt Gamma Neutron Activation Analysis of ^{10}B and Gd in Biological Samples at the MEPhI Reactor

V.F.Khokhlov[1], K.N.Zaitsev[2], V.N.Beliayev[2], V.N. Kulakov[1], V.I.Kvasov[2], A.A.Lipengolts[2], A.A.Portnov[2]

[1] *State Research Center – Institute of Biophysics, Moscow, Russia*
[2] *Moscow Engineering Physics Institute (State University), Moscow, Russia*

Abstract

The purpose of the work was to build a prompt gamma neutron activation analysis (PGNAA) facility at the MEPhI Reactor for the analysis of the content of various elements for NCT. The facility was implemented on a monochromatic neutron beam. Methods of quantitative ^{10}B and Gd measurement have been developed for pharmacokinetic studies. The facility is capable of measuring 1 μg of ^{10}B in biological samples with an error of not more than 10%. The detection limit of the facility is 0.3 μg of ^{10}B.

Keywords: BNCT, PGNAA, Research Reactor, Monochromator

1. Introduction

NCT studies on the prospective irradiation base with two neutron beams on separate channels of the MEPhI nuclear research reactor [1] will require tools and methods for the measurement of the quantitative content of the elements used in NCT, such as ^{10}B and Gd. Among all the element analysis techniques, preference was given to prompt gamma neutron activation analysis (PGNAA) as a nondestructive method with minimum sample preparation, and sufficient sensitivity and detection limit for NCT.

2. Materials and Methods

The quantitative analysis of elements by PGNAA is based on the registration of prompt gamma radiation emitted in the reaction of neutron capture by an element. The intensity of prompt gamma radiation of certain energy is proportional to the quantity of a particular element. For ^{10}B, it is 478-keV gamma-rays emitted in the $^{10}B(n,\alpha\gamma)^{7}Li$ reaction; for gadolinium, those are the 182 keV and 944 keV lines from the $^{157}Gd(n,\gamma)^{158}Gd$ reaction. The PGNAA facility at the MEPhI Research Reactor has been implemented on the radial horizontal channel HEC-9. The need for the use of the radial channel for the PGNAA facility is caused by the following fact: the experiments carried out on the single tangential channel of the MEPhI Research Reactor used for experimental NCT irradiations of dogs with spontaneous tumors have shown that the neutron beam of this channel fails to meet the PGNAA demands concerning the intensity of the background photon radiation and number of fast neutrons. In order to produce a neutron beam with characteristics necessary for PGNAA, the following plan was used to deliver the neutron beam to the irradiation position of samples to be measured. The neutron beam from the core is shaped by a lead collimator to a monocrystal of pyrolitic graphite [2]. The monochromatic neutron beam with an energy of 0.049 eV is deflected to an aluminum neutron guide with a rectangular section of 22x96 mm and 868 mm long. The neutron guide passes through the biological shielding consisting of a borated polyethylene layer of 600 mm thick and a lead layer of 200 mm thick located in a rectangular two-section steel tank. In order to decrease the interaction of neutrons with the steel walls of the shielding tank, a neutron collimator of a rectangular section of 15x44 mm and 600 mm long made of borated polyethylene is installed at a depth of 200 mm from the outlet of the neutron guide. The sample to be examined is placed in a fluoroplastic holder in the irradiation position. The irradiation position is surrounded with a lead shield of 50 mm thick lined with ^{6}Li-containing plastic inside. A semiconductor coaxial detector from hyper pure germanium manufactured by CANBERRA is used to register prompt radiation. The detector has a lead shield of 50 mm thick and is located at a distance of 70 mm from the irradiation position "looking" at the irradiation position through a collimator of 18 mm in diameter in the lead shield.

A plug from $^{6}Li_2CO_3$ is inserted into the collimator to protect the detector against scattered neutrons.

3. Results and Discussion

The plan of extraction of the neutron beam described above has allowed producing a monochromatic neutron beam with a flux of neutrons in the irradiation position of $2.7x10^6$ n/cm^{2}s at a reactor power of 2.5 MW. The cross-section of the neutron beam is a rectangle of 15x44 mm, with nonuniformity of the neutron flux not more than 10%. Standard samples representing aqueous solutions of 1.5 ml with a known content of the element to be analyzed placed in cylindrical polyethylene containers with an internal diameter of 9-mm have been prepared for an assessment of the sensitivity of ^{10}B and Gd measurements. By the slope angles of the calibration lines, the sensitivity of the element measurement was determined to be 254 cps/mg for ^{10}B, 57 cps/mg by the 182 keV line and 18 cps/mg by the 944 keV line, respectively, for Gd. The detection limit calculated by formula (1) is 0.3 μg for ^{10}B, and 2 μg for Gd in a measurement of 15 hours long.

$$DL = \frac{3 \cdot \sqrt{S_{bg}}}{T \cdot w} \quad (1),$$

where S_{bg} – background sum of counts under the peak in question (counts), T – counting time (sec.), w – sensitivity for the particular line of the element(cps/mg).

The performance of the PGNAA facility on HEC-9 of the MEPhI Research Reactor allows determining ^{10}B quantities of 1 μg, and Gd of 3 μg in a 2-hour measurement with an error of not more than 10%. The time and accuracy of measurement largely depends on the nature of the sample, its geometrical dimension, and homogeneity of distribution of the element being analyzed. The impact of the geometrical dimension of the sample and homogeneity of distribution of the element being measured on the accuracy of the analysis was assessed in a measurement of neutron flux distribution in a cylindrical polyethylene container with a 9-mm internal diameter filled with aqueous solution of boric acid with ^{10}B concentration of 100 μg/ml. For this purpose, the plate of the solid-state track detector (SSNTD) CR-39 parallel to the neutron beam axis was placed in the container in its cross-section, and then the container was irradiated with neutrons. The neutron capture by ^{10}B nuclei results in a reaction that produces two charged particles: an alpha-particle and a ^{7}Li nucleus, which hit the SSNTD leaving tracks on its surface visible with use of a light microscope after etching. The density of tracks on the SSNTD surface is obviously proportional to the neutron flux. The distribution of the track density in the diametral plane of the container parallel to the neutron beam axis is shown in Figure 1.

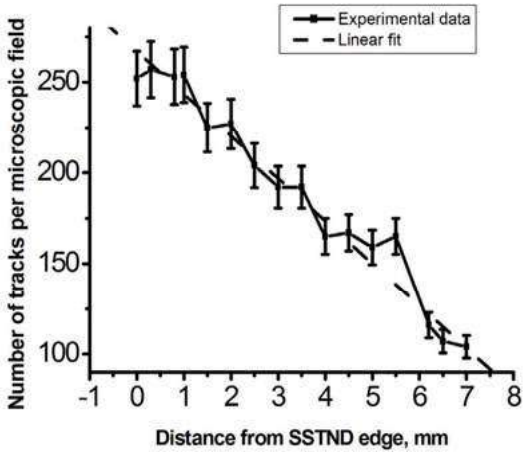

Figure 1. Distribution of tracks on the SSNTD surface along the neutron beam axis

The results of the measurement have shown that the neutron flux in the container with water can be fitted with a straight line, and the value of the flux at the front and rear walls of the container differs by a factor of 2.7. Thus, in case of nonuniform distribution of the element being determined in biological tissue samples with a geometrical dimension along the neutron beam longer than 5 mm, the difference in the intensity of the prompt radiation line of a particular element could reach 30% and more.

The linearity of the neutron flux inside the sample being measured allowed suggesting a new system of calculation of the element content based on the assumption that the entire amount of the element being analyzed is in a certain effective point, which is legitimate for a linear neutron flux. In order to determine the location of the effective centre of an element, two measurements are carried out, with the sample in the second measurement turned by 180° regarding the first measurement.

The quantity of the element measured is calculated by formula (2)

$$N = \frac{N_0 \cdot (k+1) \cdot I}{2k \cdot I_0} \quad (2),$$

where N_0 – known quantity of the element in the reference sample, I – intensity of the prompt radiation line from the sample being measured, I_0 – intensity of the prompt radiation line from the reference sample, $k = I/I_{180}$, where I_{180} – intensity of the prompt radiation line from the sample turned by 180° regarding the first measurement. Model experiments with artificial inhomogeneities and with a known content of the element being measured in a water sample have shown the applicability of the suggested technique.

On the facility, ^{10}B and Gd content was measured in samples of various tissues of mice, with intravenous administration of boronphenylalanine and intratumoral administration of the gadolinium-containing compound Dipentast. The measurements have shown the possibility to measure simultaneously the content of ^{10}B and Gd in samples of biological tissues. Also, the distribution of the Na salt of aminoacid derivative of cobalt bis(dicarbollide), Na[8-$H_2NCH(COOH)CH_2CH_2OCH_2CH_2O$-3,3′-Co(1,2-$C_2B_9H_{10}$)(1′,2′-$C_2B_9H_{11}$)] (DCC-AA) [3] positioned as a promising boron-containing BNCT compound [4,5,6] in various tissues and organs of rats has been studied [4].

4. Conclusions

The NRA facility on the horizontal channel HEC-9 of the MEPhI Research Reactor is capable of online measuring the quantitative content of such elements as ^{10}B and Gd in the range of concentrations significant for NCT. The pharmacokinetics study of BPA, DCC-AA, and gadolinium-containing compound Dipentast in small laboratory animals has shown serviceability of the PGNAA facility on the MEPhI Research Reactor for such problems.

The suggested approach of calculation of the quantitative element content by the intensity of relevant prompt gamma radiation lines will allow a more precise estimation of the neutron capture element content in tissues and organs with a nonuniform distribution of the neutron capture compound resulting either from the irregularity of its administration (e.g., at intratumoral administration), or composite heterogeneous structure of the tissue itself.

Implementation of the PGNAA facility at the MEPhI Reactor is a required and important step on the way of creation of a medical and research NCT centre at the MEPhI Research Reactor.

References

[1] Zaitsev K.N., Portnov A.A., Sakharov V.K. et al. 2007. Development of the Technology of Neutron Capture Therapy for the Treatment of Malignancies and Preclinical Studies at the IRT MEPhI Reactor. Inzhenernaya Fizika (Rus.). 2, p.122.

[2] Riley K.J., Harling O.K. 1998. An Improved Prompt Gamma Activation Analysis Facility Using A Focused Diffracted Neutron Beam. Nucl. Instr. Meth. V. **143**. pp.414-421.

[3] Sivaev I.B. et al. 2002. Synthesis of functional derivatives of the [3,3′-Co(1,2-$C_2B_9H_{11})_2]^-$ anion. J. Organomet. Chem, 649(1), pp. 1-8.

[4] Bregadze V.I. et al., 2004. Cobaltcarborane derivatives for NCT, 11-th World Congress on NCT, Boston, MA, USA, October 11-15, p. 19.

[5] Kulakov V.N., 2004 et al. Experimental pharmaokinetic studies of Gd and ^{10}B-containing ompounds at the MEPhI reactor, 11-th World Congress on NCT, Boston, MA, USA, October 11-15, p. 39.

[6] Bregadze V.I. et al. 2005. Comparative efficiency of two derivatives of anion cobalt bis(dicarbollide) in NCT of melanoma. Scientific session of MEPhI – 2005. Collected papers. M: MEPhI. V.5, pp. 27-29.

[7] Zaitsev K.N., Kvasov V.I., Lipengolts AA., Portnov A.A., Bregadze V.I., Kulakov V.N., Khokhlov V.F., Sheyno I.N., Nasonova T.A., 2008. Pharmacokinetic estimation of aminoacid derivative of cobalt bis(dicarbollide) as a prospective compound for NCT. Scientific session of MEPhI – 2008. Collected papers. M: MEPhI. V.3., pp. 34-36.

Increase the Beam Intensity for BNCT by Changing the Core Configuration at THOR

Hong-Ming Liu[a], Jinn-Jer Peir[a], Y.H. Liu[b], P.E. Tsai[b], S.H. Jiang[b]

[a] *Nuclear Science and Technology Development Center, National Tsing Hua University, Taiwan*
[b] *Engineering and System Science Dept., National Tsing Hua University, Taiwan*

Abstract

In this article, we will consider several core configurations and run the core calculation with MCNP to obtain the neutrons distribution in reactor core. Therefore, neutrons produced in core will be traced along the BNCT beam to obtain the neutron intensity at the beam exit. Comparing the neutron intensities both in core and at the BNCT beam exit for several core configurations, the preliminary results show that the BNCT beam intensity can be increased without decreasing the neutron intensity in core. Based on these simulation results, the fuel elements were rearranged during the annual repair period in 2007. The epithermal neutron flux at the center of BNCT beam exit in air was measured again, and the results showed that the beam intensity increased by 50%.

Keywords: BNCT, THOR, MCNP, core configurations

1. Introduction

Before the thermal column was remodeled as epithermal neutron beam for BNCT in 2004, the Tsing Hua Open-pool Reactor (THOR) was mainly used for radioisotopes production and neutron activation analysis. The vertical tubes (VT-A ~ VT-E) inside the reactor were used for radioisotopes production and neutron activation analysis. Figure 1 shows the core configuration in 2004. The graphite assemblies were arranged around the core boundary for reflecting the neutrons back and for saving the necessary nuclear fuels in core.

THOR was dedicated to medical purpose. Boron Neutron Capture Therapy (BNCT) was chosen as another utilization additional to the I-131 radioisotope production. The BNCT beam conceptual design and reconstruction were performed step by step to meet the criteria for BNCT clinical trial. All the tasks were completed in 2004. The epithermal neutron flux at the center of BNCT beam exit in air was measured. The experimental result was only 5.66×10^{8} n/cm^2/sec at 1MW reactor power, much lower than the simulation results based on the conceptual design (Liu et al., 2004).

In order to balance both utilizations for radioisotope production and BNCT research at fixed reactor power at THOR, the average thermal neutron flux inside the vertical tubes should be maintained while we try to increase the BNCT beam intensity. MCNP-4C was used for core calculation. Several THOR core configurations were considered and the fuel assemblies were rearranged to make sure that the beam intensity for BNCT reach the clinical criteria, and keep the radioisotopes production rate high enough at the same time.

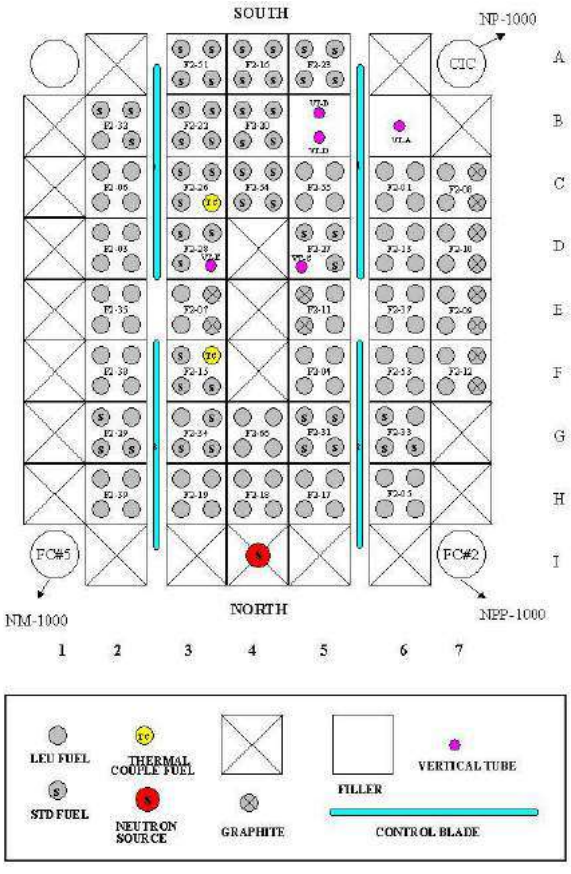

Figure 1 THOR core configuration in 2004

2. Materials and Methods

2.1 THOR and BNCT Beam

The Tsing Hua Open-pool Reactor (THOR) is TRIGA-conversion type with maximum reactor power of 2 MW. Two types of TRIGA fuels are used at THOR, the standard type (8.5 wt-% uranium and 20% enriched) and the long life type (20 wt-% uranium and 20% enriched). Each fuel assembly consists of four fuel rods. The fuel specifications are summary in Table 1.

THOR is normally operated at 1 MW ~1.5 MW depending on experimental demands. The reactor power can be controlled by four control blades composed of B_4C. Currently, the I-131 radioisotope production and the BNCT research are two major utilizations for this reactor. The radioisotopes are activated using the vertical tubes located around the south side in core while the BNCT facility is a horizontal neutron beam distant from the core center about 2 meters located at north side.

The BNCT beam at THOR was remodeled from the thermal column in 2004. This beam was composed of FLUENTAL, aluminum, cadmium, bismuth, and lead to provide high intensity of epithermal neutrons and low contaminations from the gamma rays and fast neutrons. The distance from the core center to the beam exit is about 2 meters, and the beam aperture is 14 cm in diameter.

Table 1 Specifications of TRIGA fuels

	Standard type	Long Life type
	8.5/20	20/20
Fuel composition	U-$ZrH_{1.6}$	U-$ZrH_{1.6}$-Er
Overall length	30.0 in. (76.2 cm)	30.0 in. (76.2 cm)
Outside clad diameter	1.375 in. (3.492 cm)	1.375 in. (3.492 cm)
Fuel outside diameter	1.333 in. (3.386 cm)	1.333 in. (3.386 cm)
Fuel length	20 in. (50.8 cm)	20 in. (50.8 cm)
Weigh of single rod	3.54 kg	3.85 kg
Weight of ^{235}U	45 g	120 g
^{235}U content	8.5 wt-%	20.0 wt-%
^{235}U enrichment	20.0 %	20.0 %
Er content	0.0 wt-%	0.5 wt-%
Cladding thickness	0.020 in. (0.051 cm)	0.020 in. (0.051 cm)
Lattice pitch in assembly	1.53 in. (3.887 cm)	1.53 in. (3.887 cm)
Volume fraction of Zr rod	0.021	0.021
Volume fraction of fuel	0.577	0.577
Volume fraction of clad	0.0363	0.0363
Volume fraction of Water	0.3657	0.3657

2.2 MCNP Simulation

MCNP-4C code (Briesmeister, 2000) was used for THOR core calculation. The fuel rods in reactor core were modeled in great detail but the surrounding structures were simplified as a big water ball for simulation. The attitudes of four control blades were adjusted variable to make sure the value of k_{eff} for a KCODE criticality calculation approximate to 1.

To evaluate both the radioisotope production rate and the BNCT beam intensity, the thermal neutron flux inside the vertical tubes (VT-B~VT-E) and the fast neutron flux in the first row facing to the BNCT facility (I3~I5) were tallied for indication. All the results were then normalized to the total fissions inside the fuel rods.

2.3 Neutron Flux Measurement

The neutron fluxes at the center of BNCT beam exit in air were measured by using the two foils method (Raaijmakers et al., 1995). MnNi foil (88 % Mn in Ni) of 0.1 mm thickness and AuAl foil (1% Au in Al) of 0.2 mm thickness were simultaneously irradiated. Another Cu foil of 0.1 mm in thickness was also irradiated at the same time for normalization. If a simplified two-group model of the neutron energy spectrum consisting of a Maxwell spectrum coupled with a 1/E spectrum is

used, the saturation reaction rates of the foils due to the irradiation with neutrons can be expressed as:

$$\alpha_{Mn} = \varphi \cdot \sigma_{Mn} + \theta \cdot I_{Mn}$$
$$\alpha_{Au} = \varphi \cdot \sigma_{Au} + \theta \cdot I_{Au} \quad (1)$$

where α_{Mn} and α_{Au} are the saturation reaction rates per unit mass of foil of $^{55}Mn(n,\gamma)$ and the $^{197}Au(n,\gamma)$ reactions, respectively; σ_{Mn} and σ_{Au} are the thermal neutron cross sections of the $^{55}Mn(n,\gamma)$ and the $^{197}Au(n,\gamma)$ reaction, respectively; I_{Mn} and I_{Au} are the resonance integrals of the $^{55}Mn(n,\gamma)$ and the $^{197}Au(n,\gamma)$ reaction, respectively; φ is the thermal neutron flux and θ is the intermediate neutron flux per unit lethargy.

The reaction rates were determined by using a high purity germanium detector (HPGe). The efficiency of HPGe detector was calibrated by using the Eu-152 standard source.

3. Results and Discussions

Fig. 1 was the THOR core configuration in 2004. The epithermal neutron flux at the center of the BNCT beam exit in air was measured to be 5.66×10^8 n/cm^2/sec at a reactor power of 1.0 MW. Since the epithermal neutron flux is lower than our design criteria ($\varphi_{epi.} > 1.0\times 10^9$ n/cm^2/sec), three fuel assemblies were added to replace the external source and graphite assemblies on the first row (I3~I5) facing to the BNCT facility. Figure 2 shows the THOR core configuration in 2006.

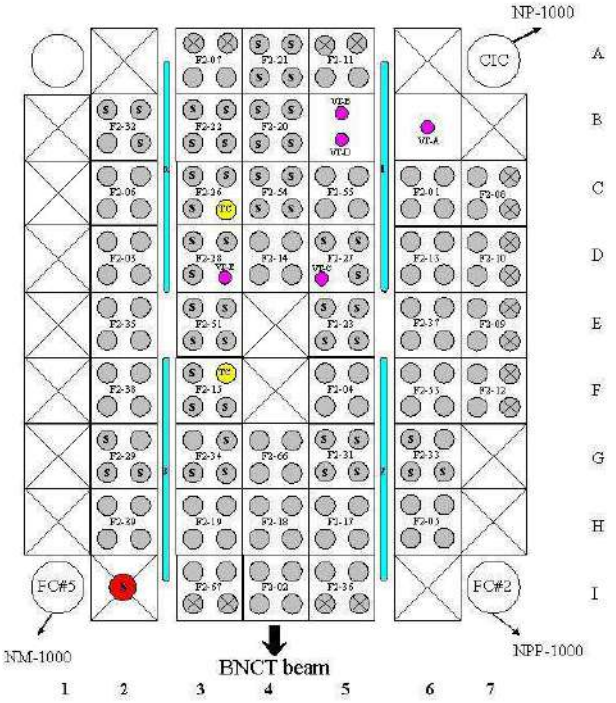

Figure 2 THOR core configuration in 2006

MCNP core calculations were performed to compare the neutrons distribution in core for core configurations in 2004 and in 2006. The simulation results were shown in Table 2.

Comparing the results for core configurations in 2004 and in 2006, the average fast neutron fluxes on the first row facing to the BNCT facility (I3~I5) increase from 1.018×10^{13} to 1.484×10^{13} n/cm^2/sec (~45% increase). That means more fission neutrons nearby the BNCT facility. On the other side, the average thermal neutron fluxes in these vertical tubes used for radioisotopes activation decrease from 1.643×10^{13} to 1.409×10^{13} n/cm^2/sec (~14% decrease).

The experimental data also shows that the epithermal neutron flux at the center of BNCT beam exit in air increase from 5.66×10^8 to 9.20×10^8 n/cm^2/sec (~62% increase). Due to the neutron spectrum for core configuration in 2006 at the first row facing to the BNCT facility is harder than the spectrum for core configuration in 2004, the increase percentage of the epithermal neutron flux for BNCT beam exit is larger than the increase percentage for the average fast neutron flux on the first row facing to the BNCT facility.

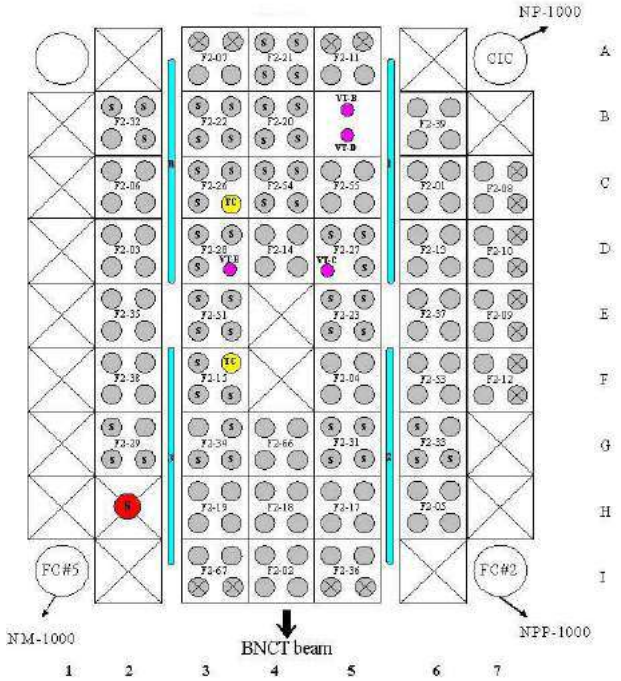

Figure 3 THOR core configuration in 2008

The neutrons distribution in core is inclined to the north side (BNCT beam) because of three fuel assemblies were added to the first row facing to the BNCT facility. This phenomenon also results in an average thermal neutron flux decrease inside the vertical tubes for fixed reactor power. Then, the radioisotopes production rate will decrease about

14% for such situation.

In order to balance two major utilizations of BNCT research and radioisotopes production at THOR, the core configuration was changes again by replacing one vertical tube (VT-A) with fuel assembly. Figure 3 shows the core configuration in 2008.

The simulation results and the experimental data were also shown in Table 2. Although the epithermal neutron flux for BNCT beam decrease slightly from 9.20×10^8 to 8.92×10^8 n/cm^2/sec (~3% decrease), the average thermal neutron flux inside the vertical tubes can increase from 1.409×10^{13} to 1.586×10^{13} n/cm^2/sec (~13% increase). If THOR is operated at 1.2 MW, the epithermal neutron flux for BNCT beam can reach 1.07×10^9 n/cm^2/sec that can meet the design criteria for BNCT clinical trials.

Table 2 MCNP simulation results in THOR core and experimental data for BNCT beam exit in air

Position	Neutron energy	Core-2004	Core-2006	Core-2008
VT-B	Thermal	1.332×10^{13}	1.308×10^{13}	1.679×10^{13}
VT-C	Thermal	1.947×10^{13}	1.506×10^{13}	1.578×10^{13}
VT-D	Thermal	1.351×10^{13}	1.348×10^{13}	1.602×10^{13}
VT-E	Thermal	1.940×10^{13}	1.472×10^{13}	1.485×10^{13}
I-3	Fast	1.084×10^{13}	1.363×10^{13}	1.128×10^{13}
I-4	Fast	9.021×10^{12}	1.675×10^{13}	1.521×10^{13}
I-5	Fast	1.067×10^{13}	1.415×10^{13}	1.332×10^{13}
BNCT beam exit in air	Thermal	4.28×10^7	7.588×10^7	1.12×10^8
	Epithermal	5.66×10^8	9.20×10^8	8.92×10^8

4. Conclusions

In order to balance both utilizations of radioisotope production and BNCT research at THOR, the average thermal neutron flux inside the vertical tubes should be maintained while we try to increase the epithermal neutron flux for BNCT beam. Take several core configurations into consideration and perform the MCNP core calculations, the results show that the epithermal neutron flux at the center on BNCT beam exit in air can be increased by 50% while the average thermal neutron flux inside the vertical tubes is only decreased by 3%.

Acknowledgement

This study was supported by the National Science Council of the Republic of China under contract number NSC96-2221-E-007-063.

References

Briesmeister, J.F., 2000. MCNP—A General Monte Carlo N-Particle Transport Code Version 4C, Los Alamos National Laboratory.

Liu, Y.-W.H., Huang, T.T., Jiang, S.H., Liu, H.M., 2004. Renovation of epithermal neutron beam for BNCT at THOR. Applied Radiation and Isotopes, 61, 1039-1043.

Liu, Y.H., Nievaart, S. Tsai, P.E., Moss, R., Liu, H.M., Jiang. S.H., 2008. Coarse-Scaling Adjustment of Fine-group Neutron Spectrum of Epithermal Neutron Beams in BNCT using Multiple Activation Detectors. To be published.

Raaijmalers, C.P.J, Konijnenberg, M.W., Verhagen, H.W., Mijnheer, B.J., 1995. Determination of dose components in phantoms irradiated with an epithermal neutron beam for boron neutron capture therapy. Med. Phys. 22 (3), 321-329.

Conceptual design of a liquid metal small fast reactor for BNCT

Tetsuo Matsumoto[1], and Yuriko Uchida[2]

[1] *Atomic Energy Research Lab., Musashi Institute of Tech., Kawasaki-shi, Japan*
[2] *Department of Nuclear Engineering System, Musashi Institute of Tech., Tokyo, Japan*

The fourth generation reactor with high economical efficiency, high safety, high amount minimization of wastes, and nuclear proliferation resistance has been studied throughout the world. Five concepts of a supercritical-pressure light water cooled reactor, a lead alloy-cooled fast reactor, a very high temperature reactor, a high temperature gas cool reactor, and a molten salt reactor are presented. These innovative atomic power systems are superior to the physical performance of the present light water reactor system. Development of these reactor system aims at attaining social targets, such as a contribution to the economic society by reservation of energy security, maintenance of the technical base by activation of the atomic power industry, and creation of new industry, and much more improvement in social receptiveness. In order to reduce the investment risk of a building program and electricity demand with uncertainty, development of a small modular type reactor has been considered from view points of technical program as well as social and institutional maintenance. A small modular type reactor is generally less 350 MWe, and is called for corresponding to multi-purpose use such as high-temperature heat supply, hydrogen manufacture and neutron use as well as the power generation.

In this paper, the conceptual design of the lead-alloy cooled fast reactor ENHS+ was studied for consideration of both a high burn-up reactor using spent fuels of PWR and medical use by BNCT in reference to the ENHS(The encapsulated Nuclear Heat Source) which is currently examined at U.S. Department of Energy. The results are as follows:

1) The optimal fuel composition (93%U(1.5%EU)+7%Pu) was determined by use of general PWR spent fuels, and the reactor core design was done with nuclear calculation code (SRAC2003 and SLAROM/CITATION-FBR), and KCODE in MCNP for an ENHS+ reactor core. An effective multiplication factor (burn-up=0) was 1.026, and the critical state could be resulted in maintaining for 30 years or more.
2) Another design study of epithermal neutron beam for BNCT installed at ENHS+ reactor was carried out using Monte Carlo transport code MCNP. An AlF3 /PbF2 was used as a neutron filter /moderator. The beam hole was surrounded by Li-poly. To absorb extra neutrons outside the reactor shield. The void layer inside the beam hole was prepared to avoid attenuation of the beam intensity as well as improvement of beam directionality. The irradiation position was at distance of 248 cm from the core. An epithermal neutron beam with an intensity of $1x10^{10}$, and fast neutron dose and gamma-ray dose per an epithermal neutron of $2x10^{-15}$ and $4x10^{-15}$ $Gycm^2n^{-1}$, respectively , could be produced at irradiation port for the power of 25MWt .

These results would suggest the conceptual design of next generation reactor with multipurpose use.

Building of Scientific Information System for Supporting BNCT Development in Bulgaria

Mladen Mitev[a], Krassimira Ilieva[a], Tihomir Apostolov[a]

[a] *Institute for Nuclear Research and Nuclear Energy of the Bulgarian Academy of Sciences, Boul. Tsarigradsko shossee 72, Sofia, Bulgaria*

Abstract

Building of Boron Neutron Capture Therapy (BNCT) facility is foreseen within the reconstruction of the Research Reactor IRT (IRT) of the Institute for Nuclear Research and Nuclear Energy of the Bulgaria Academy of Sciences (INRNE). The development of BNCT at IRT plays a very significant role in the plan for sustainable application of the reactor. A centralized scientific information system on BNCT is being built to the INRNE with purpose to collect and sort as the new information so knowledge accumulated during more then thirty years history of BNCT. This BNCT information system will help the creation and consolidation of a well informed and interconnected interdisciplinary team of physicists, chemists, biologists, and radio-oncologists for establishing BNCT cancer treatment in Bulgaria. It will strengthen more intensive developing of the national network as well as its enlargement to the Balkan region countries. Acquainting with the opportunity for BNCT cancer treatment will be addressed to the public at large. Human, social and economical results due to the BNCT for many patients from Balkan region are expected.

Keywords: BNCT, knowledge management, scientific information system, national network, young scientists

1. Introduction

The Research Reactor IRT (IRT), Sofia, of the Institute for Nuclear Research and Nuclear Energy of the Bulgarian Academy of Sciences (INRNE) is in a process of reconstruction. The design includes an arrangement of Boron Neutron Capture Therapy (BNCT) facility. The development of BNCT for head and neck cancer, and liver cancer is one of the main tasks in the Program for sustainable application of the reactor. The IRT has the support of the Bulgarian government, projects of the PHARE program, the IAEA project BUL/4/014 "Refurbishment of the Research Reactor", and the US Department of Energy in the frame of the RERTR and RRRFR programs. As a part of the BNCT policy development is a creation and maintaining of Scientific Information System supported by the National Fund "Scientific Investigations".

2. Necessity of Scientific Information System

BNCT has been carried out in the USA, Japan, Netherlands, Germany, Finland, Italy, the Czech Republic, Argentina, etc. It has more than thirty years history. A big amount of information and knowledge is collected during this period. A lot of new information on BNCT is published periodically in the scientific journals.

In Bulgaria, feasibility studies within the national network of the INRNE, the Medical University in Sofia, the National Centre of Radiobiology and Radiation Protection, the Institute of Experimental Pathology and Parasitology and Institute of Electronics of the Bulgarian Academy of Sciences, and the Faculty of Physics of Sofia University have been carried out. Contacts with institutes experienced in BNCT as the EC JRC, Petten, the Netherlands, the VTT, Finland and the NRI-Rez, the Czech Republic, have been established. Design calculations of the BNCT tube have been done. Modeling of geometry and material composition of filter/collimator for the BNCT beam tube on IRT has been carried out following the beam tube configuration of the Massachusetts Institute of Technology Reactor (Harling, 2002) and taking into account an ability to include the tube in to IRT reactor geometry. (Belousov, 2008). The calculation results have shown that the designed IRT BNCT beam tube could provide epithermal neutron flux

with intensity about 5.10^9 n/cm^{2}s (that is close to the highest levels realized up to now at the existing BNCT installations) with needed beam.

Expert visits to the INRNE and to experienced institutes have been realised. Very useful information and experience has been shared during the visits to INRNE of Dr. Raymond Moss from JRC-IE, Petten and Dr. Iiro Auterinen from VTT, Finland. During scientific visits, Bulgarian researchers have been acquainted with the BNCT facilities at High Flux Reactor at JRC-IE, Petten, the FiR-1 in Finland, the TRIGA Mark II at Pavia, the TAPIRO in Casaccia and the LVR-15 at NRI/Rez, the Czech Republic. Bulgarian researchers take also part on almost every workshop on BNCT organised from JRC-IE, Petten.

Promising young specialists are also involved in the BNCT development. Ms.Sci. and Ph.D. theses on the design and dosimetry issues of BNCT are carried out. Their works have to be made available to the public at large and to the research community from all areas of science that are connected with BNCT.

The INRNE together with the Technical University in Sofia have proposed to the Ministry of Education a new programme for education of students in nuclear technology application for obtaining Master of Science Degree of the Technical University in Sofia. The dosimetry methods and techniques needed for BNCT application are also included in the educational programme.

Necessity to collect and sort the accumulated information and exchanged experience by a centralized Scientific Information System on BNCT has been aroused. This Scientific Information System has a purpose to help the creation and consolidation of a well-informed and interconnected interdisciplinary team of physicists, chemists, biologists, and radio-oncologists for establishing BNCT cancer treatment in Bulgaria. It has to strengthen the developing of the national network as well as its enlargement to the Balkan region countries as well as to acquaint the public at large with the opportunity for BNCT cancer treatment.

The BNCT Scientific Information System is necessary for supporting the continuous access of the Bulgarian researchers jointly working in BNCT to the national requirements, norms, legislation, regulations, ethical rules and/or codes of conduct the BNCT. It has to provide access to the international journals on BNCT. The information base, together with the mobile equipment has to put into practice the necessary on-line connection between the researches in this interdisciplinary area while preserving their mobility.

3. The BNCT Scientific Information System

Scientific information base has been developed with purpose to foster the development of BNCT at the reconstructed Research Reactor IRT. It has been built as a subsystem to the INRNE Intranet. The information system is based on a server and set of notebooks and is implemented to the INRNE information network (Fig.1).

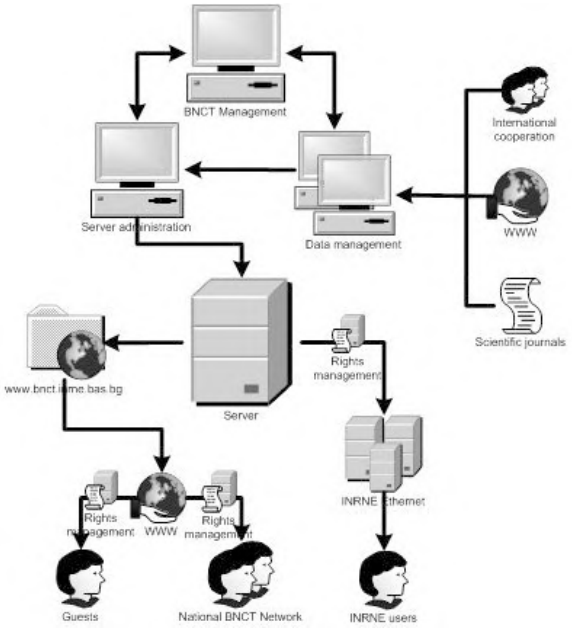

Figure 1. BNCT Scientific Information System

It provides reliable access to the specific data, periodic publications, and a possibility for continuous exchange of information relating BNCT of the researchers from the national BNCT network, jointly working on BNCT development in Bulgaria. The information system also supplies easy and fast access to the basic and current information to the young specialists just starting with BNCT.

The information can help the sustainable development and application of BNCT in Bulgaria. Huge amount of the work in collecting, reviewing and sorting of the data is done from graduated student and young scientists working at INRNE. The Information system is now part of the INRNE network. INRNE has a reliable information network, maintained by well-trained IT specialists thus provides stable Internet connection for the new information system, and this assures an access of the collaborators from the BNCT scientific network to the incoming information and the BNCT database. The INRNE handles the software and hardware maintenance of the information system through the specialists from Information Technologies Department. The BNCT team is engaged to collect and review the available data and put it on the server. A database management system and interface for web access is created.

Through the BNCT Scientific Information System, it is possible to obtain recent data from the leading periodic journals as:

- Radiation Research – RRS, USA
- Medical Physics – AAPM, USA
- Nuclear Technology – ANS, USA
- Nuclear Science and Engineering – ANS, USA
- International Journal of Radiation Oncology * Biology * Physics – ASTRO, USA and EU.

Differentiated access to the stored data has been created. The popular data is stored on a web page and is accessible to the public at large. The specific data, together with the copyrighted and patients related materials are put into scientific database that is available only to INRNE staff and the members of the national BNCT Network.

The popular titles and presentations are put on the web server to give the public at large the opportunity to become familiar with BNCT as a cancer treatment modality. The basic goal of the web page is to receive the public acceptance for the development of BNCT on the reconstructed reactor IRT. The webpage also contains the history of BNCT, and short information for the INRNE BNCT team, together with contact information. It can be found on the server references to the projects' reports, activities and events on BNCT in Bulgaria like:

- Determination of The Beam Parameters and Evaluation of Irradiation Time for Clinical Purposes (2003)
- INRNE - JRC Conference - Information Days (2003)
- Workshop on BNCT carried at INRNE, Sofia, by Dr. Raymond Moss from IE-JRC, Petten (2007)
- Workshop on BNCT carried at INRNE, Sofia, by Dr. Iiro Auterinen from VTT Finland (2007)
- Workshop on BNCT carried at Plovdiv University, Plovdiv, by Dr. Iiro Auterinen from VTT Finland, (2007)
- Scientific visits of INRNE specialists at IE-JRC, Petten and VTT, Finland (2007)
- Feasibility Study for Building BNCT Facility on IRT Research Reactor (2008),
- etc.

There are also hyperlinks to the websites of the major BNCT investigators in the European Union, like JRC-IE, Petten, the Netherlands, the BONECA Corporation, Finland, the INFN, Pavia, Italy and the NRI/Rez, the Czech Republic, where additional information on BNCT can be found. Special section contains the Bachelor and Master thesis that are done at INRNE from graduating students, giving them the possibility to publish their work and present themselves to the scientific community.

The specific scientific data, as well as the copyrighted materials are accessible only through INRNE Ethernet. More than one hundred titles, presentations and technical reports are stored in the database. The content is divided into six sections:

- Clinical Matters and Biomedical Applications
- Radiobiology
- Chemistry and Pharmacology
- Boron Imaging
- Nuclear Physics and Engineering
- Medical Physics

Search engine is also provided for fast and efficient access to the specific information necessary in the daily engagements of the scientists. Further development of web interface that will allow the authorized users to access the data from around the world is in progress.

The information system provides sustainable information basis for the researchers involved in BNCT, as well as for the young researchers interested in this vast interdisciplinary area.

4. Conclusions

BNCT Scientific Information System is being built with purpose to support the development of BNCT for medical application in Bulgaria. Data on BNCT available until now are collected and put into the information database. The system provides access to international journals where publications on BNCT and its applications for tumor and other diseases treatment could be found. The web server interface will make possible the access of the researchers jointly working on BNCT to the national requirements, norms, legislation, regulations, ethical rules and/or codes related with the BNCT. The sorted data will help the students and the young researchers, just starting in the field of BNCT to enter quickly into this interdisciplinary area. The system will help the more intensive development of the national BNCT network as well as its enhancement to the other Balkan countries. The systems' power and flexibility allows further improvement by integrating a centralized formal information system that will manage the process of establishment of the BNCT on the IRT. It will play a very important role for the development and application of BNCT in Bulgaria. Human, social and economical results due to the BNCT for many patients from Balkan region are expected.

Acknowledgements

The BNCT Scientific Information System has been built under the project NIK 2/2007 between of the National Fund "Scientific Investigations" to the Ministry of Education and Science of Republic of Bulgaria.

References

Harling, O.K., Riley, K.J., Newton, T.H., Wilson, B.A., Bernard, J.A., Hu, L-W., Fonteneau, E.J., Menadier, P.T., Ali, S.J., Sutharshan, B., Kohse, G.E., Ostrovsky, Y., Stahle, P. W., Binns, P.J., Kiger III, W.S., Busse, P.M., 2002. The Fission Converter-Based Epithermal Neutron Irradiation Facility at the Massachusetts Institute of Technology Reactor. Nucl. Science and Eng., 140, 223-240.

Belousov, S.I., Ilieva, K.D., 2008. Preliminary Modeling of BNCT Beam Tube on IRT in Sofia. Thirteenth Congress on Neutron Capture Therapy, Florence, Italy.

On accelerator Based Neutron Sources and Neutron Field Characterization with Low Energy Neutron Spectrometer Based on Position Sensitive ^{3}He Counter

Isao Murata[a], Hiroyuki Miyamaru[a], Itsuro Kato[b], Yoshiharu Mori[c]

[a]*Division of Electrical, Electronic and Information Engineering, Graduate School of Engineering, Osaka University, Japan*
[b]*Department of Oral and Maxillofacial Surgery II, Graduate School of Dentistry, Osaka University, Japan*
[c]*Kyoto University Research Reactor Institute, Kyoto University, Japan*

Abstract

At present development of new neutron sources based on particle accelerators is underway world-wide for BNCT. Though nuclear reactors were used for a long time as the neutron source, accelerator based neutron sources have recently been advantageous taking into account its easy-to-use and acceptable performance. However, when using an accelerator, various secondary particles would be emitted simultaneously and act as a troublesome background, and initially produced neutrons have a high energy and thus should be moderated largely. Moreover, in these circumstances, patients should be positioned close to the neutron source to keep enough neutron flux intensity so that the BNCT will be completed within about 1 hour. This requires that inside a relatively narrow space neutrons should be moderated, and simultaneously unnecessary secondary particles should be shielded. Since this is not an easy job, it is known that it becomes quite hard to make an acceptable background-free neutron field for BNCT. It consequently means that characterization of such neutron fields will have to be a critical issue to confirm the availability of the neutron sources for BNCT. In the present study, a low energy neutron spectrometer has been thus designed and is now being developed to measure the accelerator based neutron source performance. The presently proposed spectrometer is based on a ^{3}He proportional counter, which is 50 cm long by 5 cm in diameter with a gas pressure of 0.5 MPa. It is quite unique that the spectrometer is set up in parallel with the incident neutron beam and a reaction depth distribution is measured by it as a position sensitive detector. Recently, a prototype detector has been developed and the signal test is now underway. In this paper, the feature of the accelerator based neutron sources is outlined and importance of neutron field characterization is discussed. And the developed new low energy neutron spectrometer for the characterization is detailed.

Keywords: BNCT, accelerator based neutron source, low energy neutron spectrometer; position sensitive proportional counter, ^{3}He detector

1. Introduction

Research aiming at boron neutron capture therapy (BNCT) is underway world-wide. As is well known, the BNCT is one of the most promising therapies for cancer comparing with other therapies like gamma (cyber) knife, ion beam radiotherapy and so on. Especially in Japan, the research and development have positively been carried out for years partly because traditionally the number of cancer patients is quite large in Japan. Recently, the therapy is beginning to be conducted more regularly by using a nuclear reactor. In Japan, there are two nuclear reactors available for BNCT, in which one is JRR-4 of Japan Atomic Energy Agency in Ibaraki prefecture, and the other is KUR of Kyoto University in Osaka Prefecture. These are experimental nuclear reactors for nuclear engineering research, and thus there exist a lot of restrictions when used. For example, patients should reserve the machine time well in advance. Also, the machine time is not flexible so that an emergency treatment is normally not accepted. Moreover, because the nuclear reactors available are located only in Ibaraki and Osaka prefectures, patients and their doctors should go to one of the two facilities even if they live very far from the two facilities.

Under these circumstances, investigation of accelerator based neutron sources is in progress. It is obviously difficult to construct a nuclear reactor in a hospital because of a severe problem of public acceptance. However, accelerators are already accepted in hospitals as a radioisotope source for

positron emission tomography (PET), for example. As an available accelerator for BNCT research in Japan, a fixed field alternating gradiant (FFAG) accelerator has been constructed in Kyoto University, named FFAG-ERIT (Emittance Recovery Internal Target) (Mori et al., 2006), which has already produced neutrons even as a test operation at present. After characterizing the neutron field, irradiation tests for BNCT are planned in the next phase. By the author's group, a new low energy neutron spectrometer for the characterization of FFAG-ERIT has been designed and is now being developed. As is well known, neutron field characterization is a crucial issue even in a nuclear reactor. As described in Sec. 2, in the case of accelerators the situation will be getting worse. The characterization of the neutron field will be indispensable in advance. However, the characterization is not an easy job, because there is no direct technique to measure the neutron energy spectrum particularly in the lower energy region. The new spectrometer being developed in the present study will thus be a general-purpose neutron spectrometer, which is able to be utilized in various applications as well as in BNCT.

In the present paper, the feature of the accelerator based neutrons sources is outlined and importance of the neutron field characterization is discussed. Details of a new low energy neutron spectrometer based on a position sensitive ^{3}He proportional counter being developed for the characterization are described.

2. Nuclear reactor and accelerator as a neutron source for BNCT

The fundamental difference between nuclear reactor and accelerator is the intensity of their neutron fluxes. In the nuclear reactor, even an experimental reactor, the thermal neutron flux of more than 10^{13} $sec^{-1}cm^{-2}$ can be achieved in the core. On the other hand, in the accelerator based neutron source, even if integrated over the whole solid angle of 4π, the incident neutron intensity is more-or-less 10^{13} sec^{-1}. Moreover, in this case, the incident neutron energy is much higher than thermal neutron except for ^{7}Li(p,n) reaction with low energy incident protons. The neutrons should be moderated down to thermal energy. Hence, the thermal neutron flux intensity becomes around 10^{9} $sec^{-1}cm^{-2}$ at the highest, which is known to be the lowest level applicable for BNCT.

The above facts lead to the following discussion: (1) In the case of the nuclear reactor, the distance between the neutron source and a patient can be kept long enough to supply a large space for neutron filters and shielding material. A part of the space, being on the line between the neutron source and the patient, attenuates the direct high energy neutrons and gamma-rays from the neutron source. Also this enough space allows us to set up a sufficient amount of moderator "not" in the same place as the radiation shield, i.e., not on the line between the neutron source and the patient, so that neutrons are well moderated to supply an ideal thermal neutron irradiation field for BNCT, simultaneously shielding other background radiations. (2) In the case of the accelerator, because the intensity is not so high, the patient should be positioned close to the neutron source, typically within around 1 m. In this narrow space, a moderator system to moderate the incident neutron energy down to the thermal energy region should be set up, and at the same time a shielding system is placed "at the same place" as the moderator to attenuate high energy neutrons from the target and secondary neutrons and gamma-rays produced in the surrounding material. It is not trivial to combine moderating and shielding material in the same limited space.

The problem to be solved is how to decrease the background radiation, because the thermal neutron intensity itself could be increased if approaching the neutron source. However, in return, the background intensity is also going up absolutely and relatively against the thermal neutron intensity. This is a principal difficulty in case of applying accelerators to BNCT. The FFAG-ERIT, which has been constructed in Kyoto University, would have an ability to overcome it. The ERIT is an emittance recovery internal target. In this technique, a target is positioned inside the accelerator ring, meaning transmitted particles through the target are once again accelerated and focused by the ionization cooling technique. In other words, at the target region, there is no need to prepare a beam dump which normally produces a large amount of background radiations. In addition, using a thin target a large (cross section)/(stopping power) ratio can be achieved. This can facilitate the heat removal difficulty in the target.

In any case, the point is to prepare an appropriate technique to characterize the neutron field in order to discuss applicability of the neutron source to BNCT in various neutron source facilities.

3. Low energy neutron spectrometer

In the present study, a general-purpose low energy neutron spectrometer has been designed and is now being developed for characterization of the neutron field in accelerator based neutron sources

like FFAG-ERIT. In the following sections, the principle and brief description of the spectrometer is presented. The more details are found elsewhere (Murata and Miyamaru, 2008).

Principle of the spectrometer

It is difficult to directly obtain spectral information for low energy neutrons. In this study, we consider another physical quantity which is directly related to the neutron energy. It is obvious that the neutron-nuclear cross section can be used for this purpose, because it is a function of the neutron energy. Consequently, the position of a reaction event in a neutron detector shall depend on the neutron energy. If the reaction cross section is larger, the distance from the detector entrance to the position at which the reaction occurs becomes smaller, and vice versa. In other words, the reaction position "distribution," measured by the detector, varies with the incident neutron energy. If selecting ^{10}B or ^{3}He as the detection medium, the neutron energy and the reaction cross section share a one-to-one correspondence in the low energy region. Figure 1 shows the reaction cross section of ^{3}He, for example. Fortunately, ^{10}B and ^{3}He in gas are already available at present for a neutron detector.

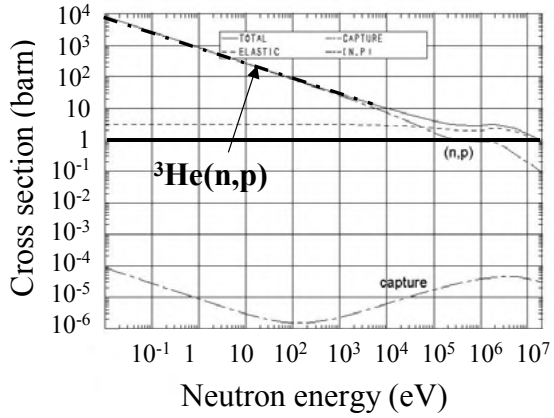

Fig. 1. Reaction cross section of ^{3}He cited from JENDL-3.3. Neutrons are detected by ^{3}He(n,p) reaction

Figure 2 shows the schematic design figure of the present neutron spectrometer. The neutron detector is a proportional counter having one wire in a cylindrical casing. Because we wish to measure the reaction position of the neutron in the detector, the detector is operated as a position sensitive counter. This kind of detector is already available (Fischer, 1977). However, such a detector provides information on the one- or two-dimensional position where an incident neutron enters. In other words, the detector is arranged in such a way that neutrons enter from a direction perpendicular to the detector axis. On the other hand, in the present spectrometer, the reaction position (depth) should be measured to finally determine the neutron energy. The detector should thus be fixed so that neutrons reach the detector, parallel to the detector axis, as shown in Fig. 2. This spectrometer is unique in this aspect.

Neutrons enter the detector parallel to the detector axis from either side of it. Charged particles will be emitted because of nuclear reactions of neutrons with ^{10}B or ^{3}He. Their charges are collected by the electric field formed by the anode wire after appropriate electron multiplication. The detector consists of two output connectors on both ends. Generally, the difference (ratio) in the amount of charges collected at both ends indicates the reaction position in the detector.

The obtained reaction position distribution can be converted into the energy spectrum by unfolding process using the detector response function. The detector response function is defined as the reaction position distribution in the detector for each neutron energy. As mentioned earlier, a one-to-one correspondence for the neutron energy and the reaction position distribution is a crucial requirement to properly unfold the distribution, because the unfolding process is equivalent to solving an inverse problem.

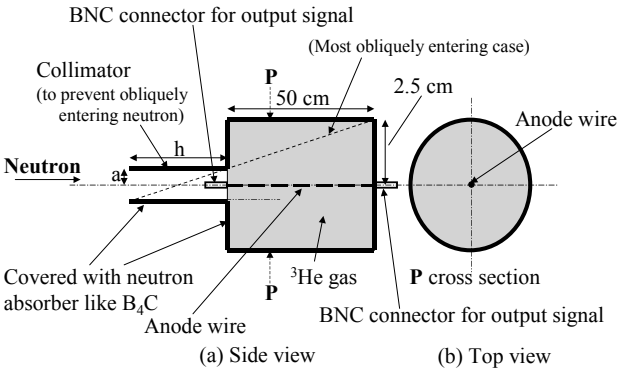

Fig. 2. Schematic design figure of the spectrometer. *a* and *h* are determined so as to prevent neutrons from entering the side wall

Spectrometer design

As the detection gas, ^{3}He and BF_3 are a candidate suitable for the present spectrometer. ^{3}He was finally employed taking into account an important requirement of BNCT that the measurable energy should be as high as possible. More practically, the n/γ discrimination problem is surely a drawback in the use of ^{3}He. However, for ^{3}He, a higher pressure is acceptable compared with ^{10}B and also the cross section is inherently larger by a factor

of 1.4. Consequently, the detection sensitivity of ^{3}He is much better than BF_3.

For the gas pressure, it is possible to utilize ^{3}He gas up to around 1 MPa. Since the present spectrometer is a prototype, 0.5 MPa was adopted. For the diameter, 5 cm was employed with the same reason, though finally over 10 cm is aimed at. For convenience of use, a 50 cm long proportional counter is employed, though a longer one is desired in order to improve the detection performance of higher energy neutrons. For BNCT, the dynamic range is set enough wide, i.e., from thermal to around 10 keV (~6 orders of magnitude). However, the realization is not so straightforward, because the efficiency becomes very small around there. Nevertheless, as a final goal, unfolding up to 10 keV is aimed at for BNCT in the present study. As shown in the next section, for this purpose, various experimental approaches are planned.

Fig. 3. Photo of the prototype low energy neutron spectrometer. A BNC connector is seen in both ends of the spectrometer.

Spectrometer fabrication

A prototype spectrometer has been developed by the author's group at Osaka University in collaboration with OHYO KOKEN KOGYO CO., LDT.(http://www.oken.co.jp/web_oken/indexen.htm). Figure 3 shows a photo of the developed spectrometer. As described earlier, the spectrometer has a BNC connector in both ends to measure the detection position distribution, and is placed so that neutrons reach the detector, parallel to the detector axis. The connector can thus hamper the neutron detection and distort the measured neutron spectrum. However, numerical correction of the distortion of the measured detection position distribution is possible. Though the present prototype spectrometer is 50 cm long, according to the manufacturer of the present spectrometer, a longer one could be produced; however, it seems to be easier to increase the gas pressure than making a longer counter.

We have started neutron measurements with the present prototype spectrometer to test the spectrometer performance and the unfolding process. For the detection position identification a simple method of estimating the position from the ratio of charges detected at both ends. We have plans of neutron measurements in order to confirm feasibility of measuring over-keV neutrons, i.e., detector response measurements with mono-energetic neutrons of 8 keV (^{45}Sc(p,n)) and 23 keV(^{9}Be(γ,n) by decay gamma-rays of ^{124}Sb). After checking the whole spectrometer system, the neutron spectrum measurement is planned at the accelerator based neutron source of FFAG-ERIT.

4. Conclusions

A low energy neutron spectrometer has been designed and is now being developed to characterize the low energy neutron field of the accelerator based neutron sources particularly for BNCT. The proposed spectrometer is based on a ^{3}He proportional counter and aims at covering the neutron energy from thermal to keV region, i.e., around 6 decades. The spectrometer is 50 cm long by 5 cm in diameter with the gas pressure of 0.5 MPa. Recently, the prototype detector has been completed and the signal test is now in progress. After checking the whole spectrometer system, the neutron spectrum measurement is planned at the accelerator based neutron source of FFAG-ERIT, Kyoto University. The present spectrometer is a general-purpose low energy neutron spectrometer, which would be utilized for various neutron measurements in nuclear reactors, accelerators and even in the environment.

Acknowledgement

This study is being conducted in part with the support of Grants-in-Aid for Scientific Research by JSPS, Scientific Research (B), [Contract No. 19360429].

References

Fischer, B. E., 1977. A Digital Processor for Position Sensitive Detectors. Nucl. Instr. and Meth. 141, 173.

Mori, Y., 2006. Development of FFAG accelerators and their applications for intense secondary particle production. Nucl. Instr. and Meth. A562, 591-595.

Murata, I., Miyamaru, H., 2008. Low Energy Neutron Spectrometer Using Position Sensitive Proportional Counter – Feasibility Study Based on Numerical Analysis. Nucl. Instr. and Meth. A589, 445-454.

Concept of a BNCT line with underwater in-pool fission converter at reactor MARIA in Świerk

K. Pytel[a], K. Andrzejewski[a], N. Golnik[a], J. Ośko[a]

[a]*Institute of Atomic Energy, 05-400 Otwock-Świerk, Poland*

Abstract

BNCT facility in the Institute of Atomic Energy in Otwock-Świerk is now under construction at the horizontal channel H2 of the research reactor Maria. Measurements of the neutron energy spectrum performed at the front of the channel H2, shown that flux of epithermal neutrons (above 10 keV) at the irradiation port was far below 10^9 n $cm^{-2}s^{-1}$ so it was too low to be directly used for the BNCT treatment. Therefore, a fission converter, will be placed between the reactor core and the treatment port. The optimum position for the converter is either close to the front of the channel (near the reactor core) or at the mouth of the channel. The concept with the converter in the reactor pool, near the front of the H2 channel was finally chosen. The uranium converter will consist of densely packed fuel elements with enrichment of 10% and will be placed in the region of the graphite reflector of the reactor. Preliminary calculations showed that the total neutron flux at the entrance to the converter will be about 10^{13}n $cm^{-2}s^{-1}$ and flux of epithermal neutrons at the entrance to the filter/moderator of the beam will be about $2 \cdot 10^9$ n $cm^{-2}s^{-1}$.

Keywords: BNCT, reactor facility, fission converter.

1. Introduction

BNCT research program started in Poland in 2001, in collaboration of the Institute of Atomic Energy in Świerk with the Institute Maria Curie Oncology Centre in Warsaw. The MARIA reactor in Świerk is to be used as the neutron source for the planned Polish BNCT facility.

The underwater neutron line for BNCT was mounted along the H2 horizontal beam tube axis of the reactor. The line consisted of two pneumatic caissons coupled with a pneumatic system for emptying/refilling. The neutron spectrum of the beam contained mostly thermal neutrons, so a fission converter was designed at the mouth of the channel, before the filter/moderator assembly.

After six years in the reactor pool, one of the caissons was broken. It was decided to remove both caissons and to replace them by one pipe coupled with the same pneumatic system as before. A new concept of an underwater, in pool fission converter has been elaborated.

2. Reactor MARIA in Świerk

The multipurpose high flux research reactor MARIA is a pool type reactor, water and beryllium moderated with graphite reflector. The reactor has pressurised channels containing concentric six-tube assemblies of fuel elements.

The fuel channels are situated in a matrix, made of beryllium blocks and enclosed by lateral reflector made of graphite blocks in aluminium cans. The nominal power of the reactor is 30 MW(th). Thermal neutron flux is $4.0 \cdot 10^{14}$ $cm^{-2}s^{-1}$ resulting in output thermal neutron flux of horizontal channels of $3\text{-}5 \cdot 10^9$ $cm^{-2}s^{-1}$.

The reactor reached its first criticality in 1974. It was in operation until 1985 when it was shut down for modernisation. In 1993 it was put into operation again.

The modernisation encompassed refurbishment and upgrading of technological systems. In particular, the efficiency of ventilation and cooling systems was improved. In February 2005, a lot of 84 MR-6 type fuel assemblies with 36% enrichment in U-235 was supplied and actually only MR-6 type fuel assemblies with 36% enrichment in U-235 are loaded in the reactor core. There are two kinds of assemblies - the old ones with 540 g contents of U-235 and the new ones with 430 g of U-235.

The reactor has been designed with a high degree of flexibility. The MARIA reactor is equipped with vertical channels for irradiation of target materials, a rabbit system and seven horizontal neutron beam channels, marked in Figure 1 as H2 to H8 (Krzysztoszek et al., 2005). Channel H1 is not used.

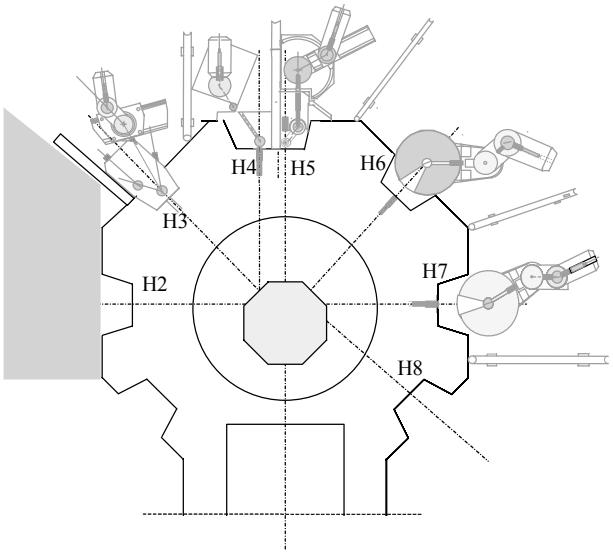

Figure 1. Experimental facilities at the horizontal channels of the reactor MARIA and the room for the BNCT facility at the H2 beam. Channels H3 to H7 are equipped with instruments for neutron physics. The H8 is for neutron radiography

3. First design of the NCT beam line at H2 channel

Flux of the epithermal neutrons from the reactor MARIA is too low to be directly used for the treatment. Therefore two pneumatic caissons were constructed, in order to form the underwater neutron line for NCT (Golnik and Pytel 2006).

Both caissons were designed as suitably shaped, welded aluminium boxes (Golnik et al., 2002), coupled with a pneumatic emptying/refilling system. For the time of irradiation, the caissons were filled with nitrogen and then refilled with water, in order to restore the biological shield of the reactor.

Measurements of the neutron energy spectrum performed at the front of the channel H2, after construction of the underwater line, confirmed that the dominating component in the spectrum was due to thermal neutrons. Therefore, a fission converter has to be used. Initially, the converter was designed as an arrangement containing ^{235}U, placed between the reactor core and the treatment port, but a serious damage in one of the caissons forced re-consideration of the design.

The most important advantages of present design were low thermal power of the fission converter and low burning of the fuel in the converter. There were however also disadvantages, observed in practice:

– The primary beam should be broad, so the caissons had to be designed as boxes of very complicated shapes. With such design, it was not possible to avoid presence of water between caissons. This resulted in considerable attenuation (scattering) of the primary beam. The beam was also attenuated by connector pipe of the horizontal channel.
– The shielding of the external fission converter had to be very heavy, even if the working load was assumed to be moderate.

Taking into account the considerations mentioned above and also the practical problems associated with the reconstruction of the damaged caisson, it was concluded that an alternative solution with underwater fission converter will be realised.

4. NCT beam line with underwater fission converter

Earlier calculations performed by K. Pytel, (Golnik et al., 2002, Golnik and Pytel, 2006) showed that the optimum position for the fission converter at the H2 channel was either close to the front of the channel (near the reactor core) or at the mouth of the channel. According to the new concept the uranium converter will be placed in the reactor pool, near the front of the H2 channel (Figure 2).

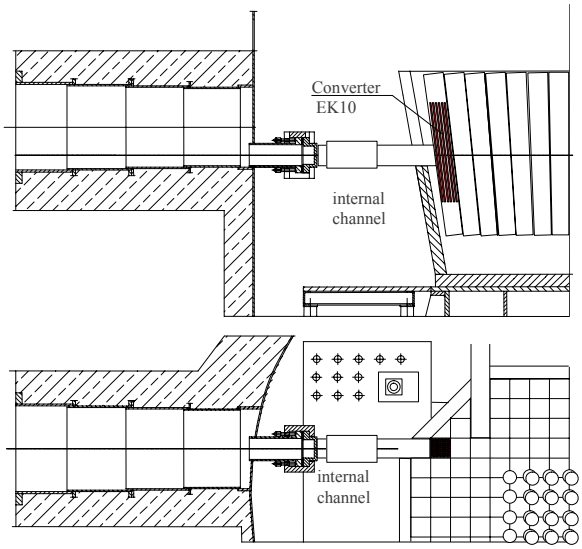

Figure 2. Schematic view of the NCT beam line proposed design o at the reactor MARIA in Poland. (upper panel – side view, lower panel – top view)

Tubular design of the internal channel makes the construction resistant to mechanical load, especially to the load associated with filling the system with nitrogen and refilling with water.

The converter will consist of densely packed fuel elements EK-10 with enrichment of 10% and will be placed in the region of the graphite reflector of the reactor. The fuel rod is shown in Figure 3 and its elemental composition is described in Table 1.

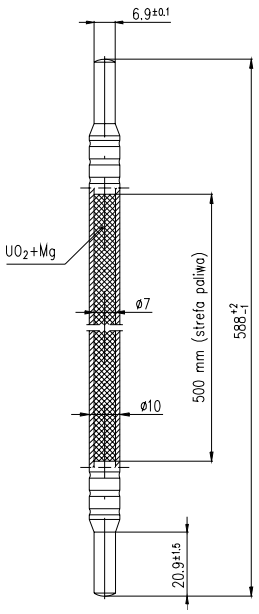

Figure 3. Schematic view of the EK-10 fuel element

Table 1. Elemental composition of the EK-10 fuel element. *For the fuel containing part (500 mm)

Material	Mass [g]
^{235}U	8.05
^{238}U	73.33
Mg	13.03
O	12.19
Al	64.4/54.1*

Before the fuel elements can be mounted in the converter, they have to be re-tested. Special attention will be paid to leak tightness.

There are several important requirements which should be taken into account at the design stage. Some of them are mutually controversial.

- Maximum efficiency of the converter can be reached at the maximum number of the installed fuel elements.
- Proper cooling conditions can be ensured by an appropriate water flow, so the resistance to flow has to be reduced and the number of the fuel elements has to be limited.
- The water flow shunt through the converter cannot exceed about 5% of the total discharge of water in cycle.
- The requirement of the minimum resistance to water flow leads to the openwork design of the fuel element separator, which, on the other hand, has to be strong enough to ensure the needed strength for mechanical load due to the fuel weight and forces associated with the water flow.

It was shown (Pytel at al., 2008) that the conditions described above can be ensured when the fuel elements are placed in the triangle lattice with the distance of 12 mm (Figure 4).

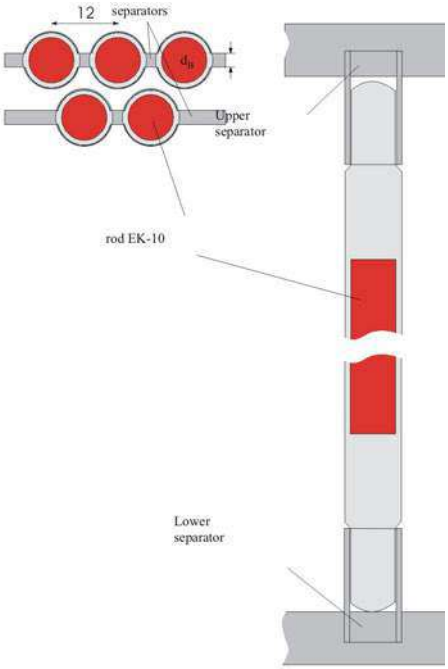

Figure 4. (Pytel et al., 2008). Triangle lattice with separators for the EK-10 fuel elements

In order to minimize the neutron activation of the fuel in the converter, there has to be a possibility to remove the converter and to replace it with an aluminium dummy, for the time when the beam at the channel H2 is not used. This means that both, the converter and the dummy have to be easy removable from the converter socket. There has to be also the place in the water pool, near the BNCT facility, where the converter can be safely stored.

Thermal and neutron load for the fuel rods in the converter are highly inhomogeneous. The maximum loads are in the rod, which is the closest to the reactor core. In order to equalize these loads, the converter will be designed in such a way that it will be possible to mount it also after turn by 180° around the vertical axis.

There will be a considerable increase in the water temperature near the elements with the highest workload. Therefore, the converter socket will be designed in such a way that it will be possible to connect also a measuring probe with two thermocouples, which will measure the temperature increase in the converter. The probe will be placed near the fuel element with the highest workload.

The flux and neutron spectra will be monitored by means of activation foils and wires, attached to the converter socket.

The most important are the positions near the fuel element with the highest workload and the surface adjacent to the internal channel.

Preliminary calculations showed that the total neutron flux at the entrance to the converter will be about 10^{13}n cm^{-2}s^{-1} and flux of epithermal neutrons at the entrance to the filter/moderator of the beam will be of about $2 \cdot 10^{9}$ n cm^{-2}s^{-1}.

5. Conclusions

A new design was proposed for the BNCT line in the reactor MARIA. It was shown that the underwater uranium converter placed in the reactor pool at the edge of the reflector may serve as an efficient source of epithermal neutrons.

The converter will be constructed with low-enrichment reactor fuel EK-10. Cooling of the converter will be ensured by cooling circuit of the reactor pool.

The beam of epithermal and fast neutrons will be extracted through the tubular internal channel filled with nitrogen. Such design is advantageous comparing with the extraction of thermal neutrons, because of lower scattering and absorption of epithermal and fast neutrons by construction materials of the channel and by possible gaps, filled with water.

References

Golnik, N., Pytel, K., Dąbkowski, L., 2002. A concept and state of the art. of irradiation facilities for NCT at research reactor MARIA in Poland. In: "Research and Development in Neu-tron Capture Therapy", Eds: W. Sauerwein, R. Moss, A. Witting, Monduzzi Editore, 191 – 195.

Golnik, N., Pytel, K., 2006. Irradiation facilities for BNCT at research reactor MARIA in Poland. Pol. J. Med. Phys. Eng. 12(3), 143-153.

Krzysztoszek, G., Gołąb, A., Jaroszewicz, J., 2005. Operation of the MARIA research reactor. Annual Report of the Institute of Atomic Energy, Świerk, Poland. 2005, 15-19.

Pytel, K., Owsianko, I, Andrzejewski, K., 2008. Reconstruction of the BNCT channel at the MARIA reactor. Report of the Institute of Atomic Energy, Świerk, Poland.

Specific Features of Implementation of a Clinical Base for Neutron Capture Therapy of Cancer at the IRT MEPhI Reactor

A.A.Portnov[a], K.N.Zaitsev[a], V.A.Savkin[a], V.I.Kvasov[a], V.A.Kamnev[a], A.A.Liogenky[a], V.K.Sakharov[a], V.S.Troshin[a], O.V.Mishcherina[a], V.F.Khokhlov[b], V.N.Kulakov[b], I.N.Sheino[b], V.N.Mitin[c]

[a] *Moscow Engineering Physics Institute (State University), Kashirskoe shosse, 31, 115409 Moscow, Russia*
[b] *State Research Center – Institute of Biophysics, Zhivopisnaya ul., 46, 123182 Moscow, Russia*
[c] *Russian Cancer Research Center of RAMS, Kashirskoe shosse, 24, 115478 Moscow, Russia*

Abstract

Based on full-scale computational studies of the IRT MEPhI Reactor model in 3D geometry using the code MCNP-4c, the optimum variant for the renovation of the reactor thermal column and creation of a medical channel for NCT has been selected. It has been shown that to reduce the dose rate from fast neutrons and photon radiation to the desired levels, the beam axis should be shifted off the centre of the core. Optimization calculations determined the geometry and composition of the neutron beam shaping area, as well as the arrangement of special filters for decreasing the flux of gamma-rays to meet the requirements for NCT.

Keywords: Nuclear reactor, thermal and epithermal neutron beam, NCT.

1. Introduction

An irradiation center is being arranged at the IRT MEPhI Research Reactor for studies in the field of neutron capture therapy (NCT) of malignancies. The center has two neutron beams on separate channels of the nuclear reactor.

On the horizontal tangential channel HEC-4, an irradiation room with a thermal neutron beam outlet has been built for preclinical NCT trials. For the time being, preclinical studies on cell cultures, small laboratory animals, and dogs with spontaneous tumors have been carried out on this beam. Over 80 dogs underwent the NCT treatment with use of compounds containing ^{10}B (boronphenylalanine) and Gd (Dipentast) (Mitin et al., 2008).

However, this facility is inapplicable for clinical trials, since the size of the irradiation room is too limited for accepting a human patient; also, the spectrum of the HEC-4 channel contains few epithermal neutrons for the treatment of deep-seated tumors. With the purpose to solve these problems, an irradiation room for clinical NCT studies has been designed on the horizontal channel HEC-1 extended through the thermal column of the reactor.

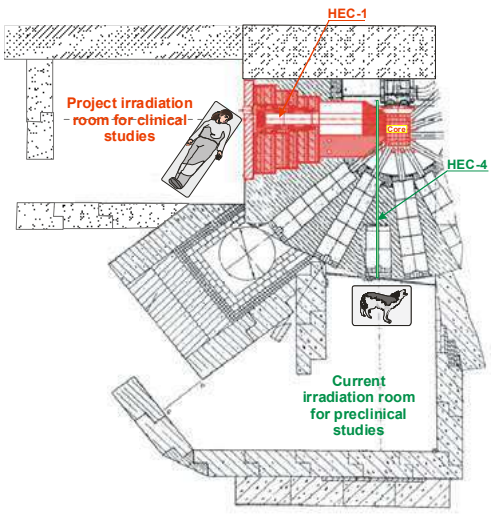

Fig. 1. Layout of the channels of the designed NCT base at the IRT MEPhI Reactor

2. Materials and methods

The medical channel has been designed on the basis of the results of full-scale computational studies using the MCNP-4b and MCNP-4c2 codes (Briesmeister et al., 1997, 2000) that are intended for solving radiation transport problems in real three-dimensional geometry.

Taking into account the complexity of the solution for this problem caused by a significant thick-

ness of the protective structures, various methods of non-analog simulation that reduce the variance of the results were used in the calculations. Those methods included splitting and Russian roulette, the use of importance functions of separate computational cells, and local estimation of the flux.

The time of calculations was selected in terms of the statistical error of the results not exceeding 5% for separate energy groups of neutrons in the region of thermal energies, and not exceeding 20% for photons and fast neutrons.

The geometrical computational model described the geometry of the channel structure and adjacent elements to the greatest extent practical.

The material composition of separate areas of the design accepted in the calculations fully complied with the actual materials of the structure. The neutron and photon interaction cross-sections in the pointwise MCNP format were taken from the libraries of neutron cross-sections ENDL-85 and ENDF/B-V, ENDF/B-VI.

In order to take into account the specific character of interactions of neutrons with energies below 4 eV, scattering functions $S(\alpha,\beta)$ for hydrogen, carbon, and beryllium at room temperature were used.

Photon interaction cross-sections for all elements were taken from the mcplib2 library based on data reported by E.Storm and H.I.Israel, 1967.

In order to assess the reliability of the results, neutron flux distributions and their functionals along the beam axis were calculated using the codes MCNP-4c and TORT (Rhoades et al., 1987) for a simplified model of the channel identical for both codes. The results of these thermal neutron flux calculations comply well with each other both in the shaping region, and along the channel length.

The experimental data from measurements of the thermal neutron flux, as well as absorbed photon dose rates in the vertical channels located in the thermal column of the reactor were compared with the results obtained by MCNP-4 calculations. The difference between the measured and calculated thermal neutron fluxes in all points of interest inside the channels does not exceed the experimental accuracy.

In view of the contribution of prompt fission photons, the maximum difference between the measured and calculated values of photon dose rates does not exceed 30%, which is also considered satisfactory.

The comparisons of the experimental and computational results have shown that the generated starting package of MCNP correctly reflects the geometry of the system, thus making it applicable for further calculations of particular structures of the channel.

3. Results and discussions

The schematic design of the channel is represented in Fig. 2. The axis of the channel is shifted to maximum possible extent in the horizontal plane off the core centre (for 220 mm) providing the effect of the tangential position. The structure of the channel consists of three basic areas: - the area of pre-shaping of beam parameters, - the area of beam extension through the protective (primary) shutter; - and the area of fine adjustment of the beam parameters formed in the additional shutter.

The main beam filter is an aluminum block adjacent to the head of the thermal column in the direction of the channel axis. The length of the block is ~ 600 mm. There is a recess formed in the graphite stack surrounding the block; the size of the recess is 400 x 400 mm^2 in cross-section and 520 mm long. Before the primary shutter, a lead block of 60 mm thick is installed. This recess and the graphite surrounding it along the perimeter are sealed with a thin (6 mm) plate of an aluminum alloy. Its primary purpose is to prevent massive losses of water from the reactor pool in case of emergency loss of containment of the thermal column casing.

The computational studies have shown that the most suitable materials for the use in the pre-shaping area are aluminum (Al) and Fluental® ($Al+AlF_3$). Fluental® is not manufactured in Russia, and also its thermal conductivity coefficient is low, which will cause a substantial increase of temperature.

Aluminum has therefore been selected as the most suitable material to form the required parameters of a medical beam. This material is available, easy to work with, has a high fusion temperature, and a low activation cross section. The area of fine adjustment of the beam is implemented as a cylindrical “socket” of ~ 150 mm in diameter in a component called the additional shutter. Into this “socket”, a fixture with collimating and filter elements can be installed. The remaining space in the TC recess is filled with elements (blocks) of biological shielding.

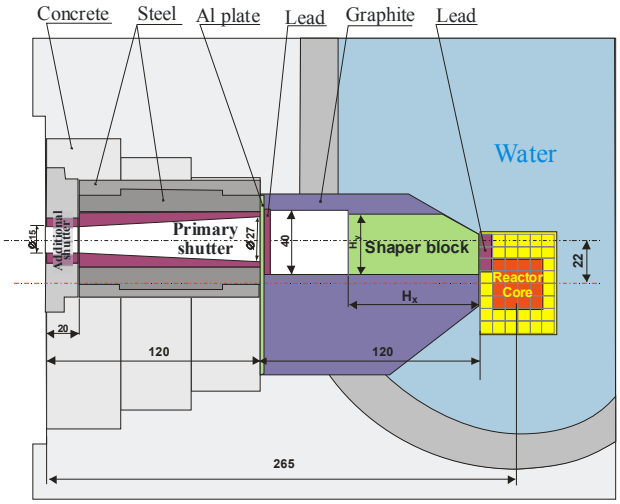

Fig. 2. Draft design layout of the HEC-1 channel

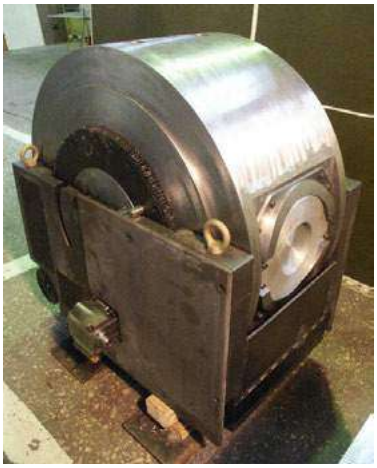

Fig. 3. Primary shutter

This additional shutter is a concrete slab lined with corrosion-resistant steel, in which a through orifice of 150 mm in diameter is made, coaxial to the beam orifice in the primary shutter in its "open" position. A bushing with collimating filters can be inserted in this orifice.

When selecting among the alternate implementations of the channel, preference has been given to engineering solutions that reduce the fraction of fast neutrons in the beam to maximum possible extent, which results in an increase in the photon dose rate at the channel outlet. The calculations, however, show that the photon dose rate can be reduced by installing filters in the channel, with an associated decrease in the thermal neutron flux. The optimum relation of beam characteristics will be chosen experimentally after installing basic elements of the structure.

Transport of the neutron beam to a patient, as well as its reliable and safe control is provided with use of a primary shutter representing a rotary disk with an orifice serving as a neutron guide. The shutter is arranged in a steel stepped casing equipped with wheels and installed on a rail way inside the stationary shielding. The type of the primary shutter and its size were chosen based on construction considerations, provision for acceptable speed of operation and ease of manufacture using the applied materials. Selecting the composition of the materials and their geometry in the shutter was based on providing maximum effective protection in the closed state. Direct paths of radiation through the gaps around the shutter and around the device that moves during repair or other operations, and the installed shielding, have been minimized. As a result, a "wheel-type" shutter was selected, which is pictured in Figure 3. The basic component materials are steel, zirconium, and heavy concrete.

Computational studies on the equivalent dose rates in different points at distances of 0, 10, and 35 cm from the outer surface of the facility with the shutter closed ranged from 0.95 μSv/h to 1.5 μSv/h, below the maximum permissible dose of 12 μSv/h for personnel. The total dose is distributed rather uniformly over the outer surface of the facility, slightly decreasing with distance from the surface. The contributions of neutron and photon components in the total dose are approximately equal, which may attest to the optimal choice of materials used as a shielding. Thus, the shutter device together with the additional lead shield at the channel outlet provides safe conditions for work on the facility, when the shutter is closed.

The results of the computational studies demonstrate that replacing part of the graphite in the reactor thermal column with the aluminum block of the thermal and epithermal neutron spectrum shaper has no effect on the distribution of neutron fields in the reactor core or the water pool. Thus, such a redesign of the thermal column (TC) causes no changes of nuclear physical characteristics of the IRT MEPhI Reactor.

The calculated results show that the generated nuclear heat is effectively removed to the reactor pool water. The temperature in the components of the beam shaping area does not exceed 300°C.

The most comprehensive description of the neutron beam in terms of its NCT application is obtained from the results of estimation of the spatial distribution of biologically weighted dose inside a tissue-equivalent phantom positioned at the beam outlet. In this case, the quality of the neutron beam for neutron capture therapy can be characterized with the therapeutic ratio (TR) estimated as the ratio of dose rate in tumor to maximum dose rate in healthy tissue.

The quality of the HEC-1 and HEC-4 beams for NCT was assessed based on calculations of the TR (Fig. 4) in a fashion similar to that reported by Liu et al. (2004).

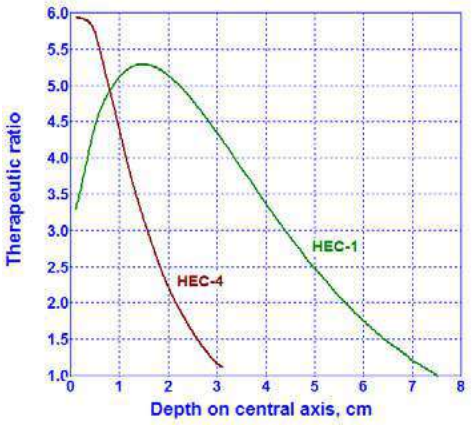

Fig. 4. Therapeutic ratio distribution along the axis of a phantom in the HEC-1 and HEC-4 beams. Boron-10 concentration in tumor to normal tissue: 65/18 ppm

The data presented show that the NCT procedure on the HEC-4 channel will be effective for tumors as deep as 3 cm. At the HEC-1 channel, it is possible to treat tumors up to a depth of 7 cm.

Table 1 shows experimental data for the existing channel HEC-4 and calculated data for the channel HAC-1 being redesigned with the geometry and composition described above.

Table 1. Characteristics of the beams of the NCT irradiation base at the IRT MEPhI Reactor

Characteristic	HEC-4*	HEC-1**
Thermal neutron flux, n/cm^2/s	6.7E+08	1.2E+09
Epithermal neutron flux, n/cm^2/s	1.4E+08	1.1E+09
Fast neutron dose rate, Gy/s	1.4E-03	5.1E-04
Fast neutron dose /Thermal flux, Gy*cm^2/neutron	2.1E-12	4.3E-13
Fast neutron dose /Epithermal flux, Gy*cm^2/neutron	1.0E-11	4.7E-13
Photon dose rate, Gy/s	1.8E-04	5.2E-04
Photon dose rate / Thermal flux, Gy*cm^2/neutron	2.6E-13	4.3E-13
Photon dose rate / Epithermal flux, Gy*cm^2/neutron	1.3E-12	4.7E-13

* Experimental data, ** Estimated data

4. Conclusions

Engineering specifications for the renovation of the channel were developed. A technology was developed for dismantling and installation of materials and structures of the medical channel in the thermal column of the IRT MEPhI reactor. The basic structures are planned to be assembled in 2008.

The engineering specifications developed allow proceeding to further stages in the implementation of the NCT irradiation base at the IRT MEPhI reactor.

References

Briesmeister, J.F., Ed., 1997. MCNP - A General Monte Carlo N-Particle Transport Code, Version 4B, Los Alamos National Laboratory Report, LA-12625

Briesmeister J. F., Ed., 2000. MCNP - A General Monte Carlo N-Particle Transport Code, Version 4C, LA-13709-M

Liu, Y.-W.H., Huang, T.T., Jiang, S.H., Liu, H.M. 2004. Renovation of epithermal neutron beam for BNCT at THOR. Appl. Radiat. Isot. 61, pp. 1039-1043.

Mitin, V.N., Kulakov, V.N., Khokhlov, et al. 2008. Comparison of BNCT and GdNCT Efficacy in Treatment of Canine Cancer. In: Proceedings of ICNCT-13, 2008.

Rhoades, W.A., Childs R.L., 1987. The TORT three-dimensional discrete ordinates transport code. ORNL-6268

Storm, E., and Israel, H.I. 1967. Photon Cross Sections from 0.001 to 100 MeV for Elements 1 through 100. Los Alamos Scientific Laboratory Report LA-3753

Characterization of a Thermal Cavity in the PhoNeS photo-neutron converter for BNCT research

A. Zanini[a], P. Borasio[b], O. Borla[a,g], E. Durisi[c,a], U. Ricardi[c], R. Ragona[c] , S. Anglesio[d] , M. Prest[e] and G. Giannini[f]

[a]*Istituto Nazionale Fisica Nucleare Sezione Torino (Italy)*
[b]*Università di Torino, Dipartimento di Scienze Cliniche e Biologiche. S. Luigi Orbassano (Italy)*
[c] *Università degli Studi di Torino (Italy)*
[d] *AOU San Giovanni Battista Torino (Italy)*
[e]*Universitas Studiorum Insubriae, Como, and INFN, Milano Bicocca, (Italy)*
[f] *University of Trieste Physics Dept. and INFN–Trieste, (Italy)*
[g]*Institute for Scientific Interchange Foundation Torino (Italy)*

Abstract

Recently, a feasibility study demonstrates that it is possible to obtain interesting thermal and/or epithermal neutron fluxes (> 1E7 cm^{-2} s^{-1}) using a dedicated photo-neutron converter applied to the high energy (> 18 MV) e-linac head. In this work, neutrons produced by Giant Dipole Resonance (GDR) reaction in high Z core (lead) are moderated to lower energies in a closed treatment cavity, suitably shaped to obtain uniform neutron field and low gamma and fast neutron contaminations. The experimental results concerning the cavity characterization, obtained at Elekta Precise 25MV accelerator, are presented. Neutron spectrometry and dosimetry is carried out by passive detectors while gamma contamination is evaluated with GAF Chromic EBT film. All the experimental results are compared with Monte Carlo (MC) simulations performed with MCNP-GN code. Moreover, accurate measurements of neutron and gamma background, inside and outside the treatment room, are performed, as well as the evaluation of the residual activation. The encouraging results show that this device could represent the first in-hospital neutron source for BNCT research and application, useful for exposure to thermal neutrons of cells and biological samples.

Keywords: BNCT, LINAC, photoneutron production, MCNP.

1. Introduction

BNCT clinical trials on brain tumours, diffused melanoma and liver metastasis gave very encouraging results, both for patient survival time and quality of life. Unfortunately the possibility to widely investigate new boron carriers as well as the different tumour sensitivity to the therapy is dramatically reduced by the limited number of available neutron sources. In fact, at present, only research nuclear reactors can provide the intense neutron field suitable for clinical application.

Some recent studies in Italy propose to use high-energy electron linear accelerators (e-LINAC), currently used in gamma radiotherapy, as photoneutron sources for in-hospital medical applications. Neutrons are produced by Giant Dipole Resonance (GDR) reactions (Followill et al., 2002) from high-energy photons on high Z targets. As already demonstrated in feasibility studies (Giannini et al., 2006), it is possible to design a photoneutron converter, constituted by high Z core surrounded by a moderator of low Z materials, easy to be installed and removed at the e-LINAC head. The moderator is shaped to produce a thermal field inside an irradiation cavity. A simple prototype, easy to be transported and installed at the head of existing accelerator, inside a radiotherapy hospital department, has been manufactured and tested in many hospitals (Bevilacqua et al., 2007). With this simplified facility, the resulting thermal neutron flux is ~1E7 $cm^{-2}s^{-1}$, depending on linac energy and structural characteristics.

In this work the characterization of a closed cavity is described: the material choice and geometry are accurately investigated to optimize the energy spectrum shape and to obtain uniform thermal neutron field inside the cavity. The specific aim is to provide a suitable facility for in-hospital research and experiment on cells and biological samples of interest in BNCT application.

By using this kind of facility it could be possible to study the distribution of boron compound in tumour cells (peripheral area or nucleus), to analyse the behaviour of different ^{10}B carriers, to investigate the effectiveness of BNCT treatment on different pathologies according to the indications of medical staff. The experimental data carried out at Radiotherapy Department in Molinette Hospital of Turin (Italy) are presented.

2. The neutron photoconverter prototype

Different types of neutron photoconverters have been studied by simulation code (MCNP-GN) during the feasibility study (Giannini et al., 2006).

A small prototype of photoconverter, easy to be installed and removed from the accelerator head and suitable to be transported to different radiotherapy departments, has been manufactured (INFN of Trieste Mechanical Laboratory).

The main characteristics of the small prototype (Fig. 1) are: graphite blocks external moderator (60x75x30 cm^3), lead target (30x30x10 cm^3), moderators in polyethylene (30x30x3 cm^3), carbon fibre box of different shape and dimension filled with heavy water (D_2O 99% purity), and irradiation cavity (20x20x10 cm^3), total weight about 300 kg, total assembly time about 2 hours. Layers of polyethylene, lead and B_4C have been placed all around the photoconverter surface to minimize the neutron and gamma undesired component outside the cavity.

Fig.1. The neutron photoconverter prototype

3. Material and methods

3.1 The MCNP-GN code

The simulation code MCNP-GN (NEA-1733), especially developed for (γ,n) photoproduction in linac accelerators (Zanini et al., 2004), has been used to treat the electromagnetic cascade and the photoneutron production and transport. The used simple photo-reaction model assumes that the dominant neutron emission mechanism is evaporation, with a Maxwellian neutron energy distribution and an isotropic angular distribution at lower energy; a small (10%) direct neutron knockout component for E_n>2 MeV is also considered. Both (γ,n) and (γ,2n) channels are treated and since photonuclear cross sections are a factor 100 lower than for atomic processes, suitable variance reduction techniques are used.

3.2 The BDS spectrometer

Experimental measurements of neutron spectra have been performed inside the irradiation cavity with BDS spectrometer, based on superheated bubble detectors manufactured by BTI, Ontario, Canada. Six thresholds are available (10, 100, 600, 1000, 2500 and 10000 keV); the upper energy limit is always 20 MeV. A suitable unfolding code, BUNTO especially developed to process the BDS responses, is used. The thermal component has been measured by BDT detector (Bubble Technology Industries, 2003) sensitive to neutrons with energy from 0.025 eV to 0.4 eV.

3.3 GAFChromic EBT film

The photon dose has been measured in the irradiation cavity by using GAFChromic EBT film useful for the assessment of the absorbed dose of high-energy photons. The film has been designed for use in the 1cGy to 800cGy dose range. The response to photons is energy-independent in the MeV range and measurements at energies down to about 30keV reveal that the sensitivity changes by less than 10%. An accurate calibration of the GAF detector against a 515 cm^3 ionization chamber has been carried out (Fig. 2) to check the behaviour of GAF in presence of an intense neutron field.

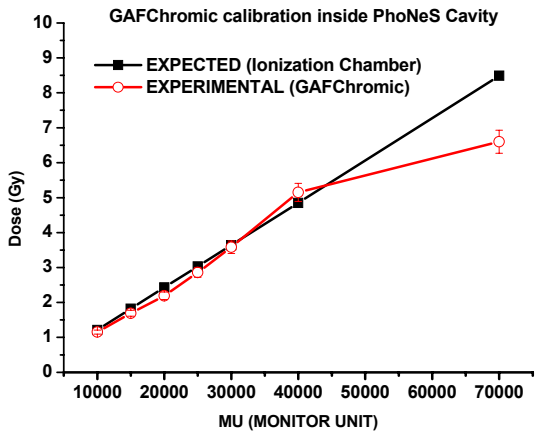

Fig. 2. GAFChromic calibration

It is evident a very good agreement with the ionization chamber data and the saturation plateau, typical for GafChromic EBT film, for absorbed dose greater than 5 Gy.

4. The thermal cavity characterization

The main goal of the characterization is to obtain inside the cavity a thermal neutron field of suitable intensity and energy spectral distribution, in view to irradiate biological samples.

In order to maximize the thermal neutron component a closed cavity solution has been chosen. Two carbon fibre boxes filled with heavy water and a polyethylene pane have been used (Fig.3a and Fig.3b). In this way it is possible to exploit the low neutron absorption cross section and the high scattering cross section on carbon.

The new Phones photoconverter has been installed at the head of the ELEKTA PRECISE 25MV accelerator in Radiotherapy Department of San Giovanni Battista Molinette Hospital (Turin).

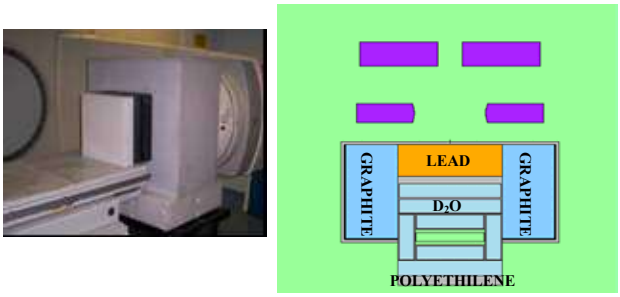

(a) (b)

Fig. 3. (a) The PhoNeS closed cavity; (b) MCNP-GN simulation of PhoNeS prototype: closed cavity

The simulation results (Fig. 4) and experimental data (Fig. 5 and Table 1) demonstrate that with respect to an open cavity it is possible to increase the thermal neutron component, and obtain an uniform neutron field and a better thermal to fast neutron ratio.

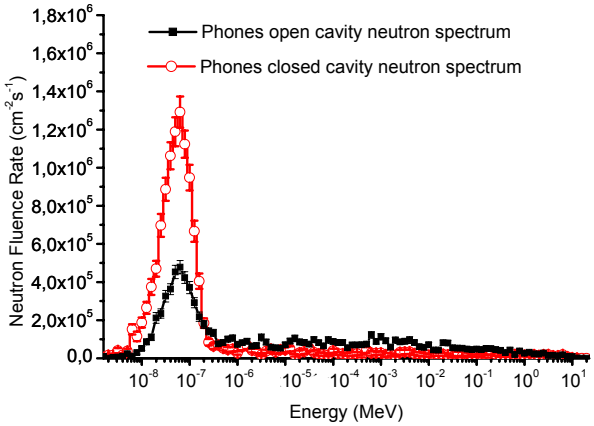

Fig. 4: Open and closed cavity neutron spectra comparison (MCNP-GN).

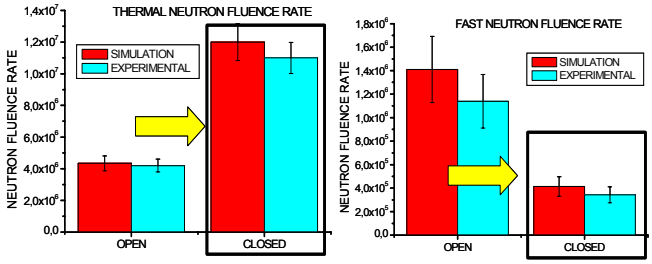

Fig. 5. Neutron fluence rate: open and closed cavity. Left: thermal neutrons. Right: fast neutrons

Table 1. Measurements of thermal and fast neutron fluence rate in open and closed cavity

	$\phi_{thermal}$ ($cm^{-2}s^{-1}$)	ϕ_{fast} ($cm^{-2}s^{-1}$)
Open cavity	(4.2±0.8)E6	(1.2±0.2)E6
Closed cavity	(1.1±0.2)E7	(4.1±0.8)E5

In MCNP-GN calculation the simulated neutron fluence rate is given per electron particle source. To obtain a fluence rate per second it is necessary to multiply by a conversion factor depending on the duty cycle of the LINAC. Typical ELEKTA LINAC working values gives a conversion factor of about 1E14 e^-/s.

From the results presented above it is evident that with the simple PhoNeS facility it is possible to obtain a significant thermal neutron fluence rate (~1.1E7 cm^{-2} s^{-1}) with a very low fast neutron contamination (4%). It is also interesting to stress that PhoNeS neutron spectrum is comparable in shape with a typical thermal neutron reactor spectrum (Fig. 6), (even if. the flux intensity is two order of magnitude lower).

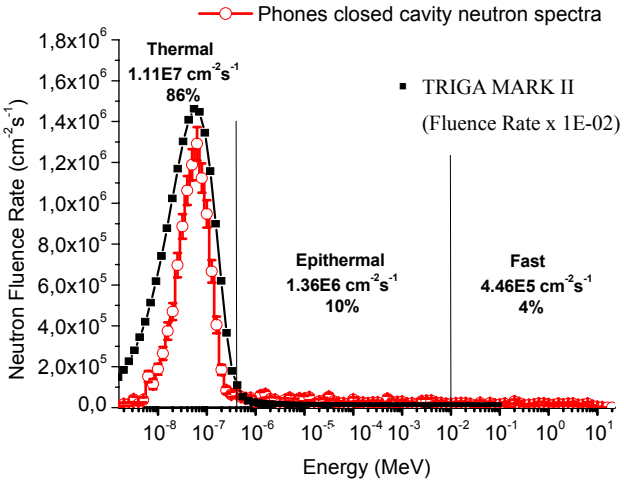

Fig. 6. Comparison of PhoNeS with Triga Mark II reactor neutron spectrum

The experimental neutron fluxes obtained by using the BDS spectrometer and BDT detectors is compared to the simulation results. Also the experimental gamma component has been evaluated with GAFChromic EBT film previously calibrated. In Table 2 the integral values of gamma and neutron components in different energy range are reported. A good agreement between the experiment and simulation is observed.

Table 2: Integral values of gamma and neutron components in different energy range.

	$\phi_{thermal}$ ($cm^{-2}s^{-1}$)	$\phi_{epithermal}$ ($cm^{-2}s^{-1}$)	ϕ_{fast} ($cm^{-2}s^{-1}$)	$D\gamma$ (Gys^{-1})
MCNP	(1.0±0.2)E7	(1.4±0.4)E6	(4.5±0.1)E5	(5.1±0.5)E-4
EXP	(1.1±0.2)E7	N.A.	(4.1±0.8)E5	(7.0±0.7)E-4

The free beam parameters D_γ/ϕ_{hyper}= 4E-11Gycm^2 and D_{fast}/ϕ_{hyper}= 4E-12Gycm^2 (D_γ = gamma dose, ϕ_{hyper} = hyperthermal (thermal + epithermal) fluence rate and D_{fast} = fast neutron dose) have been also evaluated.

5. Biological sample irradiation trials

After the assessment of the good performances of Phones closed cavity as in-hospital neutron source, a first important biological sample irradiation trial on human primary lung adenocarcinoma, previously perfused with BPA (Borasio et al., 2008), has been carried out. Three hours irradiation time allowed to reach a thermal neutron flux of ~1.0E11 cm^{-2}.

CR-39 track-etch detectors have been used for obtaining ^{10}B thermal neutron capture induced images. Fig. 7a and Fig. 7b show the histological sample on CR-39 detector and the corresponding image obtained after thermal neutron irradiation (3 hours) and etching of CR-39 layer with NaOH at 90 ^oC (2 hours). The etched track image shows a pattern that correspond to the tissue characteristics. It is possible to evaluate the ^{10}B concentration in the sample by counting the tracks (after CR-39 detector calibration) (Giannini et al., 2008).

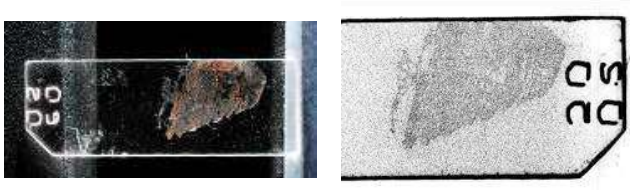

(a) (b)

Fig.7: (a) Histological sample on CR-39 detector, (b) corresponding image of sample after irradiation.

6. Conclusions

The obtained results indicate that the PhoNeS closed cavity could provide ~1.1E7 $cm^{-2}s^{-1}$ thermal neutron fluence rate with a spectrum comparable in shape to the neutrons from a nuclear reactor, an uniform distribution of thermal neutron field and a better thermal to fast neutron ratio compared to an open cavity. This device could represent the first in-hospital neutron source, suitable for irradiating, in reasonable time (about 3 hours), cells or biological samples of interest for BNCT and could be used to analyse the behaviour of different ^{10}B carriers. Moreover, as demonstrated in a previous feasibility study (Giannini et al., 2006), further improvements can be easily obtained using a high energy e-linacs, suitably modified to maximize the photoneutron production (Felici et al., 2007) and an optimized photoconverter. In this way a hyperthermal neutron flux >E9 $cm^{-2}s^{-1}$ suitable for BNCT clinical application could be obtained.

References

Bevilacqua, R., et al., 2007. PhoNeS: A novel approach to BNCT with conventional radiotherapy accelerators. Nuclear Instruments and Methods in Physics Research A 572, 231-232.

Borasio, P., et al., 2008. A novel approach to the study of ^{10}B uptake in human lung by ex-vivo BPA perfusion. 13th International Congress on Neutron Capture Therapy, Florence, Italy.

Bubble Technology Industries, 2003. Instruction Manual for the Bubble Detector Spectrometer (BDS). Chalk River, Ontario, Canada.

Followill, S., et al., 2002. Neutron source strength measurements for Varian, Simens, Elekta, and General Electric linear accelerators. American College of Medical Physics (PACS Numbers: 87.53Qc, 87.52.Ln).

Giannini, G., et al., 2008. CR-39 neutron imaging of biological samples at clinical linac's. 13th International Congress on Neutron Capture Therapy Florence, Italy.

Giannini, G., et al., 2006. A. Photoneutron Source for In-Hospital BNCT Treatment: feasibility study. 12th International Congress on Neutron Capture Therapy 9-13 Takamatsu, Kagawa, Japan.

Zanini, A., et al., 2004. Monte Carlo simulation of the photoneutron field in linac radiotherapy treatments with different collimation systems. Physics in Medicine and Biology, 49, 1-12.

Felici, G., et al., 2007. Progetto di un LINAC da con fascio da 25 MeV e 100 mA (2 KW potenza media) dedicato alla fotoproduzione di neutroni per la BNCT nell'ambito del progetto PHONES. Atti del congresso V Congresso AIFM.

NEUTRON SOURCES

The BSA modeling for the Accelerator-Based BNCT facility at INFN LNL for treating shallow skin melanoma

C. Ceballos[a,b] and J. Esposito[a]

[a] *INFN Laboratori Nazionali di Legnaro, Via dell'Università, 2, I-35020, Legnaro(PD), Italy*
[b] *Centro de Aplicaciones Tecnlógicas y Desarrollo Nuclear, 5ta y30, Miramar, Playa, Ciudad Habana, Cuba*

Abstract

The SPES-BNCT ongoing project of the *Istituto Nazionale di Fisica Nucleare* (INFN) is aimed at the construction at the *Laboratori Nazionali di Legnaro* (LNL) of an Accelerator-Based (AB), high flux thermal neutron beam facility devoted to Boron Neutron Capture Therapy (BNCT) experimental treatment of extended skin melanoma, in the framework of SPES (Selective Production of Exotic Species) project. The neutron source will be produced via the ^{9}Be(p,xn) reactions by a 5 MeV, 30 mA proton beam into a thick beryllium target. The resulting neutron spectrum is slowed down using a Beam Shaping Assembly (BSA), which modeling is in an advanced neutronic design stage. An overview on the BSA current status, based on the Be neutron converter prototype designed and already constructed, is here reported.

Keywords: AB-neutron source, ^{9}Be(p,xn) reaction, BNCT facility, BSA, MCNPX.

1. Introduction

The studies carried out in the last years for developing an Accelerator-Based BNCT (AB-BNCT) irradiation facility are mainly focused on neutron sources based either on the ^{7}Li(p,n) nuclear reaction, both at threshold energy (1.89 MeV protons with a neutron mean energy of about 35 keV) and around 2.5 MeV proton energy, with 500 keV neutron mean energy (Bleuel et al., 1998; Blue et al., 2003) or, alternatively, on the ^{9}Be(p,xn) reaction at around 4 MeV, with neutron mean energy of 1.15 MeV (Pisent et al., 2006). On the other hand different, deuteron-induced reactions, i.e. ^{9}Be(d,n) and ^{12}C(d,n) (Colonna et al., 1999) as well as ^{2}H(d,n) and ^{3}H(d,n) fusion reactions due to new sealed tube generators recently developed have also been proposed (Cerullo, et al., 2002; Martin et al., 2004, Durisi et al. 2007).

The AB-BNCT project of the Legnaro National Laboratories (LNL-INFN), named SPES-BNCT, has been developed in accordance with the Veneto regional oncology center IOV (Padua, Italy) and is mainly devoted to the experimental treatment of skin melanoma tumor with a combined BNCT plus Photodynamic (PDT) therapy. This project is part of a larger one for Selective Production of Exotic Species (SPES) for nuclear physics research on neutron-rich short-living isotopes (Prete, 2007). The neutron source will be driven by a high intensity proton beam (5 MeV, 30 mA) delivered by the RFQ accelerator developed within the TRASCO (TRAsmutazione SCOrie) nuclear waste transmutation program for ADS reactors (Pisent et al., 2004), currently under the final construction stage at LNL, on a thick Be target which was selected as proton-neutron converter material. More detailed information about the target prototype which has been developed and already constructed for the SPES-BNCT project has been reported by Esposito et al. (2008). Because of the relatively high average neutron energy (~1.5 MeV) which is expected by p+Be reactions at the nominal TRASCO RFQ output energy, the design of a Beam Shaping Assembly (BSA) capable to produce the requested thermalized, as well as high-flux collimated neutron beam, represents a real challenge. An overview on the irradiation facility neutronic design status is here reported.

2. The BSA modeling current status

As a general rule, the neutron beam shaping and filtering assembly design must take into account the real-scale geometry of the neutron converter and the supporting structure effects on the neutron and gamma transport. The experience gained in the last years at LNL labs with the 5 MeV, 1μA demonstration facility (Agosteo et al, 1997) driven by the CN Van de Graaff accelerator, revealed quite useful for the next facility neutronic design.

The treatment of shallow tumors with the SPES-BNCT facility requires an eminently thermal neutron beam, with a limited non-thermal and gamma doses contaminations. A set of *in-air Figure Of Merit (in-air FOM)* beam reference parameters, given at the irradiation port, which in our case has a fixed area of 10x10 cm^2, have at this purpose been

developed in the BNCT community as a quick and useful method to compare the calculated parameters at the neutronic design stage. The more stringent and widely accepted recommended goals here adopted, as well as the related energy group ranges, are listed in table 1 (IAEA, 2001). An extensive set of computational studies has therefore started from the original demonstration facility configuration, all accommodating the final, full-scale, Be target prototype modeling developed. The MCNPX v.2.6b code (Hendricks, 2006) was used for BSA modeling. During all simulations, the protons were not transported, being the neutrons generated directly on the target beryllium surface, following the expected RFQ beam power parabolic profile hitting the target. However, due to the lack of a full set of experimental, double-differential neutron yielding spectra at the required 5 MeV proton energy, a complete set of available experimental data set at 4 MeV (Howard et al., 2001) have been used instead. Different BSA configurations were investigated, in order to get the fulfillment of the required parameters from table 1.

The study was done taking into account the well known neutron slowing down properties, the *moderating power* ($\xi\Sigma_s$) and the *moderating ratio* ($\xi\Sigma_s/\Sigma_a$) mainly, of a set of selected materials, as well as their radiative capture cross section features. Three-most important stages are worth to be mentioned here for the neutronic design evolution. In all the three configurations reported the irradiation port has been placed 90° with respect to the proton beam incoming direction, in order to limit both the hard (E>1MeV) neutron spectrum fraction and getting a more compact-size moderation volume. After a preliminary assessment study using the Reactor Grade (RG)-graphite as unique moderator material, because of large availability, a configuration (named stage I) was produced, in order to limit the relatively high prompt gamma emission level estimated. For such a configuration the first step of the neutron slowing down takes place in a heavy water (D_2O) tank which surrounds the neutron converter. Heavy water was chosen instead of light water because of its best moderation ratio known among candidate materials and the lower gamma production from neutron radiative capture. The system is then inserted in a RG-Graphite volume, acting as both additional moderator and reflector system. Lead layers were finally used for gamma shielding. On the effort to get an improvement of the thermal beam fraction at the irradiation port, while minimizing the neutron flux on all other facility side walls, an intermediate configuration was reached (stage II). In this case Bi was used instead of Pb as gamma shielding for the patient-facing wall only. The Pb and Bi slabs play the role of shielding the gamma rays that are generated by the neutrons production-moderation-absorption process inside all the BSA volume.

BNCT beam port parameters		Required limits
Φ_{th}	$[cm^{-2}s^{-1}]$	$\geq 1 \cdot 10^{9}$
Φ_{th} / Φ_{total}		> 0.9
$\dot{K}_{n\ epi\text{-}fast} / \Phi_{th}$	$[Gycm^2]$	$\leq \sim 2 \cdot 10^{-13}$
$\dot{K}_{\gamma} / \Phi_{th}$	$[Gycm^2]$	$\leq \sim 2 \cdot 10^{-13}$
Thermal energy group	Φ_{th}	E< ~ 0.5 eV
Epithermal energy group	Φ_{epi}	0.5 eV ≤E≤10 keV
Fast energy group	Φ_{fast}	E > 10 keV

Tab.1. BNCT in-air beam port recommended goals for the BSA facility of the SPES-BNCT project

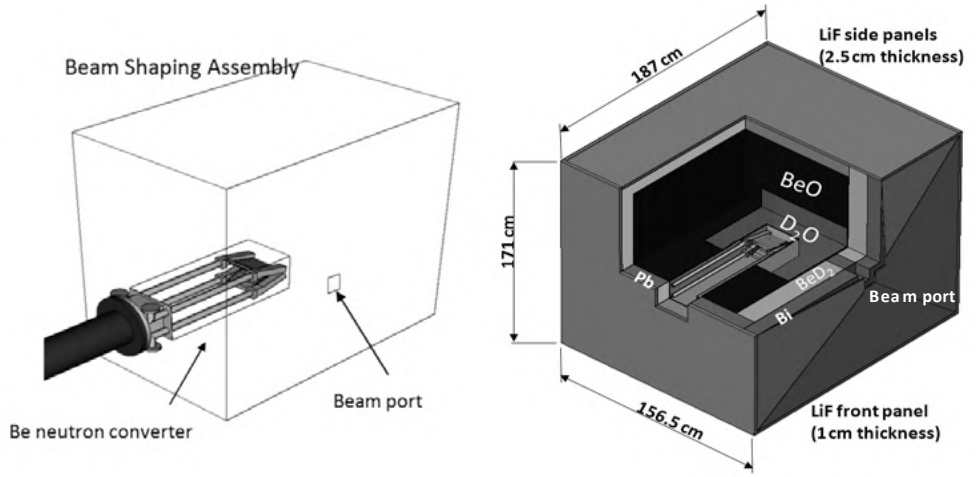

Fig.1. Real-like geometry modeling of the final Be neutron converter developed, inserted inside the BSA volume (left). The current BSA configuration proposed, housing the Be neutron converter (right): MCNPX 3D geometry model

Although both materials have similar mass attenuation coefficients, Bi thermal neutron capture cross section is nonetheless almost the half of that from Pb. Moreover the resulting radiative capture prompt gamma spectrum contribution generated is "softer" than that of lead (319.7 keV against 7367 keV for the most intense line respectively). Another improvement, in neutron slowing down, was the use of a 15 cm thick BeD_2 slab placed on the irradiation port direction only, because of its good moderation properties, while providing a low albedo for thermal neutrons. Such a solution revealed able to limit the backscattering of neutrons next to being thermalized, which would otherwise end up absorbed before reaching the irradiation port. The facility was then surrounded by 2.5cm thick Lithiated-Polyethylene (Li-nat(7.5wt%)-CH_2) panels, for increasing the capture of the thermal neutrons that escape from outside the irradiation port area. Graphite was still used as main moderator-reflector. Finally, as a further improvement step, Figure 1 shows the current BSA configuration (right), from now on called "Stage III". Figure 1 (left) shows the actual geometry of the Be neutron converter. This BSA is basically made of a (70x70x50 cm^3), Teflon (CF_2)-made, heavy water-filled tank, which volume surrounds the neutron converter, being larger towards the irradiation port. The tank itself is inside a beryllium oxide (BeO) structure instead of the former RG-Graphite. This choice revealed a good solution for increasing the thermal flux (Φ_{th}) at the beam port above the limit reported on table 1, while keeping a very high Φ_{th}/Φ_{tot} ratio. This is due to BeO remarkable albedo property for better confining and moderating the neutrons inside the BSA volume. This neutronic design fulfills the requirement to let neutrons being thermalized and directed towards the irradiation port, while keeping a low absorption rate. Another important improvement is the use of a 2.5 cm thickness of hydrogen-free lithium fluoride (LiF) flat panels around five out of six walls of the BSA. The panel covering the beam port wall side is instead of 1 cm thickness and shaped as a truncated pyramid, with a central squared hole that corresponds to the irradiation port area. Such panels efficiently absorb the thermal neutrons that escape throughout walls, based on the $^6Li(n,^4He)^3H$ reaction. In this way the reduction of gamma contamination from the irradiation beam may be achieved since the $^1H(n,\gamma)^2H$ (radiative capture) reactions are avoided. Furthermore, the truncated-pyramid shape of LiF panel allows for the thermal neutrons coming through the Bi slab surface from outside the irradiation port area, but on its direction (solid angle), to be used for the therapy, while all the others are mostly absorbed.

Beam port data	Stage I	Stage II	Stage III
Φ_{th} ($\times 10^9 \cdot cm^{-2}s^{-1}$)	1.55±0.006	0.69±0.02	1.17±0.003
Φ_{th}/Φ_{total}	0.83	0.99	0.99
$\dot{K}_{n\ epi\text{-}fast} / \Phi_{th}$ ($\times 10^{-13}$ Gy·cm^2)	1.89±0.08	0.08±0.008	0.008±0.002
$\dot{K}_{\gamma} / \Phi_{th}$ ($\times 10^{-13}$ Gy·cm^2)	1.50±0.08	1.08±0.03	1.38±0.003

Tab.2. Summary of beam port parameters calculated for the main different BSA configurations investigated (see text)

3. Results

Table 2 shows the value of the reference parameters calculated at the irradiation port for the three BSA configurations mentioned. In all simulations the dose rates were calculated using the fluence-to-kerma conversion factors from ICRU-63 data for neutrons and ICRU-46 ones for gammas. It can be seen that the current (Stage III) BSA

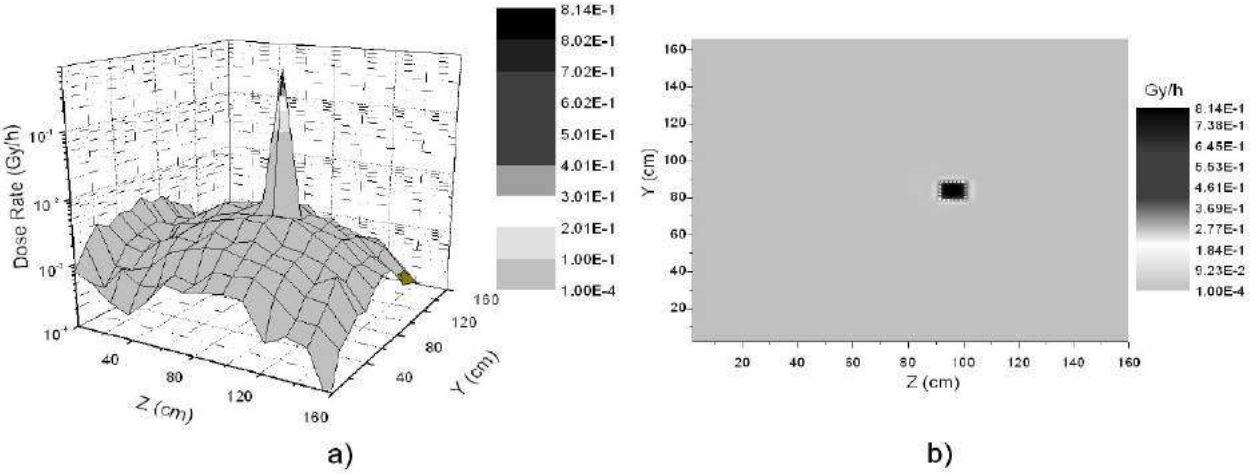

Fig. 2. (a) 3D (b) 2D plot of the thermal neutrons dose rate distribution over the beam port wall

Beam component	Beam Port (x 10^{-3} Gy/h)	Rest of Wall (x 10^{-3} Gy/h)	Beam port fraction vs. total (%)
Thermal	700 ± 1.8	1.90 ± 0.04	99.7
Epithermal	0.07 ± 0.01	0.014 ± 0.001	98
Fast	0.26 ± 0.07	0.083 ± 0.001	97
Gamma	580 ± 12.8	53 ± 0.27	92

Tab. 3. Average dose rates calculated at beam port position area and over the rest of the wall for each beam component for the current BSA proposed

configuration, fulfills all the in-air reference limits from table 1. Table 3 reports the fraction of the total dose rate at the irradiation port and the rest of the wall for each component of the beam for the last configuration. It can be seen that the beam is well collimated on the irradiation port area, while the contribution outside of it is kept quite low, as requested by the beam design specification. Figure 2 shows the plot of the thermal neutron dose rate distribution only over the patient-facing wall, which includes the irradiation port. The dashed square on the 2-D image indicates the irradiation port area. Here again, it can be seen that the neutron beam is peaked on the irradiation port, so the total body dose might be minimal.

4. Conclusions

The present computational MCNPX modeling of the proposed irradiation facility for the SPES-BNCT project, based on a 4 MeV proton-driven Be neutron source, would already be able to provide a well collimated and highly thermal neutron beam. At present stage, the design was based on in-air figures of merit specifications for a BNCT irradiation facility, fulfilling all of them. For the next stage calculations will be referred to the more correct in-phantom figure of merits, taking into account the complete structure of the irradiation room, apart from the BSA. Further improvements are also in progress for better shielding the gamma radiation level. In addition, an experimental project is planned by LNL to complete the measurements of the neutron yielding spectra from the ^{9}Be(p,xn) reaction, using a thick target and 5 MeV proton beam. When the whole data set will be available, the current model will be implemented and minor facility modifications are expected to be made.

References

Agosteo, S., Bodei, G., Colautti, P., Corrado, M.G., d'Errico, F., Monti, S., Silari, M., Tinti, R., 1997, An accelerator-based thermal neutron source for BNCT", *Advances in Neutron Capture Therapy*, Vol. 1, pp. 483-489, B. LARSSON et al., Ed., Elsevier Science, Zurich, Switzerland

Bleuel, D., Donahue, R. J., Ludewigt, B. A., Vujic, J., 1998. Designing accelerator-based epithermal neutron beams for boron neutron capture therapy. Med. Phys. 25, 1725-1734.

Blue, T., Yanch, J., 2003. Accelerator-based epithermal neutron sources for boron neutron capture therapy of brain tumor. Journal of Neuro-Oncology, 62, 19-31.

Cerullo, N., Esposito, J., Leung, K.N., Custodero, S., 2002. An Irradiation Facility for BNCT Application Based on a RF-Driven D-T Neutron Source and a New Beam Shaping Assembly, Rev. Sci. Instr., 73, (10), 3614-3618.

Colonna, N., Beaulieu, L., Phair, L., Wozniak, G. J., Moretto, L. G., Chu, W. T. , Ludewigt, B. A., 1999. Measurements of low-energy (d,n) reactions for BNCT, Med. Phys. 26, 793-798.

Durisi, E., Zanini, A., Manfredotti, C., Palamara, F., Sarotto, M., Visca, L., Nastasi, U., 2007. Design of an epithermal column for BNCT based on D–D fusion neutron facility, NIMA, 574, 2, 363-396.

Esposito, J., Colautti, P., Fabritsiev, S., Gervash, A., Giniyatulin, R., Lomasov, V.N.,, Makhankov, A. Mazul, I., Pisent, A. Rumyantsev, M., Tanchuk, V., Tecchio, L., 2008. Be target development for the accelerator-based SPES-BNCT facility at INFN Legnaro, this proceeding.

Hendricks, JS, et al., 2006. MCNPX, version 2.6b Los Alamos National Laboratory Report. LA-UR-06-3248.

Howard, W. B., Grimes, S. M., Massey, T. N., Al-Quraishi, S.I., Jacobs, D. K., Brient, C. E., Yanch, J.C., 2001. Measurement of the thick-target ^{9}Be(p,n) Neutron Energy Spectra. Nuc. Sci. Eng., 138, 145-160.

IAEA, 2001. Current Status of Neutron Capture Therapy, IAEA-TECDOC-1223, International Atomic Energy Agency, IAEA, Vienna, Austria

Martin, G., Abrahantes, A., 2004. A conceptual design of a beam-shaping assembly for boron neutron capture therapy based on deuterium-tritium neutron generators. Med. Phys. 31, 1116-1122.

Pisent, A, Colautti, P, Esposito, J., De Nardo, L., Conte, V., Agosteo, D., Jori, G.., Posocco, P.A., Tecchio, L.B., Tinti, R., Rosi, G.., 2006. Progress on the accelerator based SPES-BNCT project at INFN Legnaro. J. Phys.: Conf. Ser. 41, 391-399, doi: 10.1088/1742-6596/41/1/043

Pisent, A. Comunian, M., Palmieri, A. Fagotti, E., Lamanna, G.V., Mathot, S., 2004. The TRASCO SPES-RFQ, Proc.of the LINAC Conference, Lübeck, Germany, 69-71.

Prete, G., 2007. SPES Advanced Exotic Ion Beam facility at LNL, Technical Design Report, INFN-LNL-220 (2007).

Collaborative Characterization of the KG 2,5 Accelerator Epithermal Neutron Beam in Obninsk

Iiro Auterinen[1], Oleg Kononov[2], Tom Serén[1], Victor Kononov[2] and Michael Bokhovko[2]

[1] *VTT Technical Research Centre of Finland*
[2] *IPPE, Obninsk, Russia*

A comprehensive measurement campaign was carried out in May-June 2007 with the aim of characterizing the accelerator-based epithermal neutron beam in Obninsk, Russia.

Measurements were performed with activation detectors and ionization chambers both free-in-air and in a water phantom. VTT and IPPE used their own chambers and activation foils and all the activity measurements were performed on site. This exercise provides an opportunity to intercalibrate equipment and methods and also to compare the results with those obtained at other facilities.

The results of the measurement campaign will be presented and compared to MCNP calculations performed at IPPE. Conclusions about the clinical suitability of the beam will be drawn.

Feasibility Study for the Upgrade of a Compact Neutron Generator for NCT Application

S. Custodero [a], K. Leung, [b, c], F. Mattioda [a]

[a] *EUROSEA Committee, via Livorno 60, I-10144 Torino, Italy*
[b] *Lawrence Berkeley National Laboratory, 1 Cyclotron Road, Berkeley, CA, USA*
[c] *Department of Nuclear Engineering, University of California, Berkeley, CA, USA*

Abstract

In 2001 an agreement between the Italian non-profit association EUROSEA Committee (Turin) and the Plasma and Ion Source Technology Group at Lawrence Berkeley National Laboratory (LBNL) was signed for the development of a prototype of Compact Neutron Generators (CNG) for medical uses. At the end of 2004 this prototype called EUROSEA 001 was installed and tested at the Experimental Physics Department of Turin University. This prototype is designed to produce a D-D neutron yield of $1 \cdot 10^{11}$ n/s and its dimensions do not exceed 50 cm.

Since 2006 EUROSEA Committee and the Plasma and Ion Source Technology Group at LBNL investigated different approaches for upgrading the neutron generator Model EUROSEA 001: the most promising are presented in this paper. The goal is to increase the neutron yield from $1 \cdot 10^{11}$ n/s to more than 10^{12} n/s without changing the size of the neutron generator.

Keywords: compact neutron generator, neutron source, neutron yield upgrade

1. Introduction

The Plasma and Ion Source Technology Group at Lawrence Berkeley National Laboratory (LBNL) in the USA has been developing Compact Neutron Generators (CNG) for medical and industrial applications based on the nuclear fusion reactions for the last decade.

In 2001, an agreement between the Italian non-profit association EUROSEA Committee (Turin) and LBNL was signed for the development of a prototype of CNG for medical uses. At the end of 2004 this prototype called EUROSEA 001 was installed and tested at the Experimental Physics Department of Turin University (see fig. 1).

The CNG is basically composed of three main elements: a source of deuterium ions, a low voltage electrostatic accelerator and a titanium target. This prototype is designed to produce a D-D neutron yield of $1 \cdot 10^{11}$ n/s and its dimensions do not exceed 50 cm.

Since 2006 EUROSEA Committee and The Plasma and Ion Source Technology Group at LBNL have investigated different approaches for upgrading the present neutron generator EUROSEA 001. The goal is to increase the neutrons yield from $1 \cdot 10^{11}$ n/s to more than $1 \cdot 10^{12}$ n/s without changing the size of the neutron generator.

This can be achieved acting on the ion source chamber (namely modifying the shape and number of the windows where D+ ions are extracted) or on the target (namely changing the target material and the nuclear reactions occurring).

This is very important for a therapeutic application of the NCT because the increase of the neutron production will allow a sensible reduction of the treatment time for the patient. By this way, the upgraded CNG, together with dedicated neutron moderators, can be an interesting source for NCT application, providing both epithermal and thermal neutrons.

The modifications proposed do not affect the main characteristics of EUROSEA 001, namely:

- high compactness (dimensions do not exceed 50 cm.);
- safety (neutron production is stopped when the electrical supply is turned off);
- simplicity of assembly and operation throughout the life cycle.

Fundamental aim of this work is to preserve the main EUROSEA 001 characteristics passing to the upgrade CNG version.

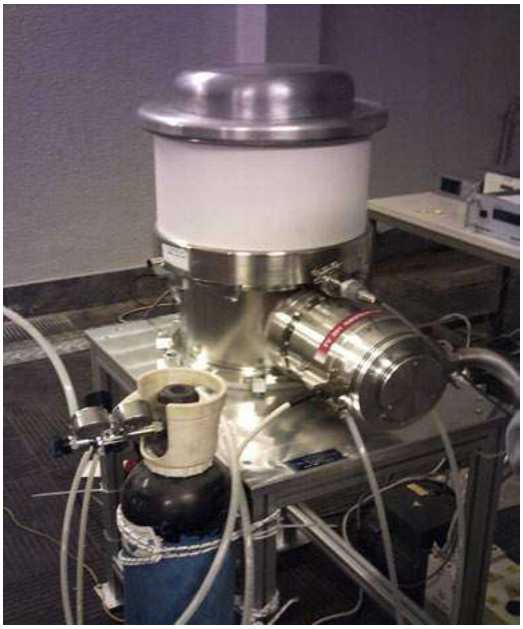

Fig. 1. CNG EUROSEA model 001

2. EUROSEA model 001

The compact neutron generator EUROSEA 001 allows to produce until $1 \cdot 10^{11}$ n/s operating with 300 mA deuterium ions current @ 120 kVolt. It is basically composed of three main elements (Fig. 2):

- a source of deuterium ions;
- a low voltage electrostatic accelerator;
- a titanium target where nuclear fusion reactions between the deuterium nuclei occur resulting in the generation of fast neutrons.

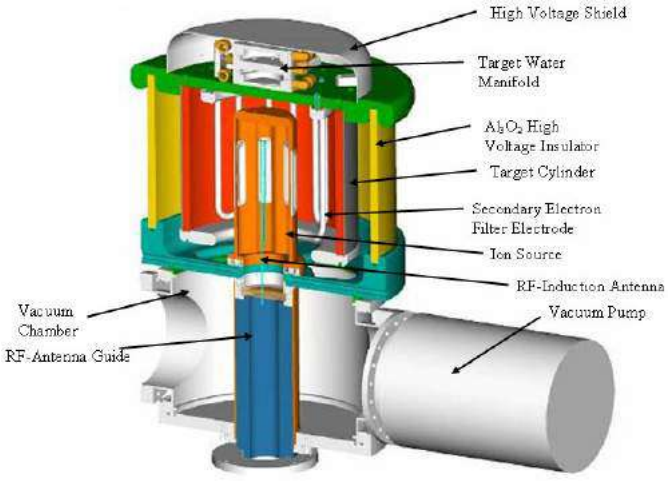

Fig. 2. CNG EUROSEA model 001 – main parts and components

The radio frequency antenna (13.5 MHz) is used to produce deuterium ions which, properly accelerated by the potential difference in vacuum chamber, hit the target (at 120 kV) generating neutrons.

The ion source chamber has a cylindrical shape and is placed in the centre of the system. The target is an aluminium cylinder, coaxial with the source and with the inner surface covered by a titanium layer. The deuterium ions are extracted from some windows on the source chamber wall and hit the titanium target, where the nuclear fusion reactions among deuterium nuclei occur with generation of fast neutrons.

The complete configuration of the Compact Neutron Generator system also includes the following auxiliary systems:

1. radio frequency (RF) and High Voltage supplies (HV);
2. cooling system to remove thermal power;
3. moderator which allows slowing down fast neutrons and addressing them toward the treatment area optimizing their energy in order to irradiate efficiently the tumour mass.

3. EUROSEA 001 upgrade by ion source chamber modification

In order to improve the neutron output to more than $1 \cdot 10^{12}$ n/s without changing the size of the neutron generator, one option is to increase the D+ ion energy and the D+ ion beam current (for example, by operating the source at a beam power of 180 kV and 1 A) that reaches the target.

This can be accomplished by drilling more apertures on the ion source chamber (see figure 3): by this way a higher D+ ion current is accelerated toward the target.

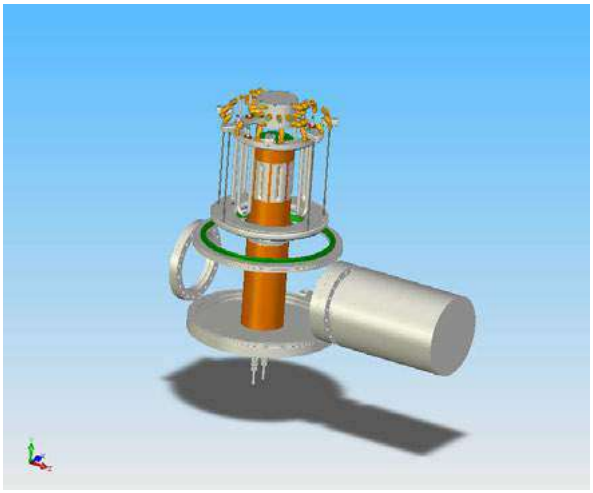

Fig. 3. Apertures on the ion source chamber

The beamlets arrive at the target surface where the D + D fusion reactions take place. In order to keep the beam power density on the target at about 600 kW/cm^2 (optimum power density for the best neutron production) there are two criteria that must be observed:

- the beamlet has to be spread out such that the beam spot size on the target is bigger than the beam size at the source exit;
- the ion source must be capable of producing enough beam current to meet the neutron source requirement.

The fulfillment of the first criterion requires a detailed design of the ion source chamber and its apertures from the optical and mechanical point of view.

Calculations show that, operating the CNG at 120 kV, in order to produce a D-D neutron source of 10^{12} n/s, the accelerated D+ ion beam current should be about 3 A.

In this upgrade approach one does not have to modify other components except the ion source chamber. This replacement can be easily done for EUROSEA model 001.

4. EUROSEA 001 upgrade by target material modification

In order to improve the neutron output of an order of magnitude ($1 \div 2 \cdot 10^{12}$ n/s) without changing the size of the neutron generator, a second option is to change the target material and to employ other reactions for neutron production instead of the D-D reaction.

An interesting material seems to be lithium and the nuclear reaction is D + Li.

In particular, two reactions are interesting from the neutron production point of view:

- $D + {}^{7}_{3}Li \rightarrow n + {}^{8}_{4}Be$;
- $D + {}^{7}_{3}Li \rightarrow n + {}^{4}_{2}He + {}^{4}_{2}He$.

Several data of cross-sections are available for D+ ion energy higher than 750 keV. Data for D+ ion energy less than 250 keV are taken from papers listed as references.

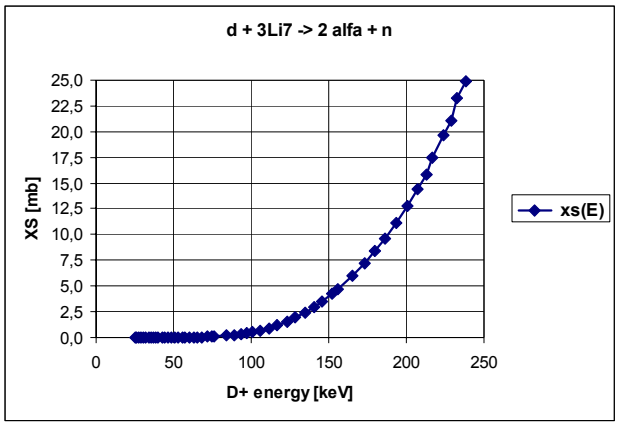

Fig. 4. Cross-section for ^{7}Li(D,2α)n reaction as function of D energy

Then it is possible to estimate the neutron production using the following formula:

$$Y = \frac{(I/e) \cdot a_r \cdot \rho \cdot (N_A / A) \cdot \sigma}{(dE/dx)}$$

where:

Y = yield in n/s;
I = deuterium current;
e = elementary charge = 1.6E-19 C;
a_r = atomic ratio;
ρ = target density in g/cm^3;
N_A = Avogadro's number;
A = atomic weight;
σ = microscopic cross section of the nuclear reaction at a given deuterium energy;
dE/dx = stopping power for deuterium in the target at a given deuterium energy.

The National Institute for Standard and Technology (NIST) reports stopping power value for several target materials and different incoming charged particles (assuming that D+ behaves as H+).

One can find the following results for Li-nat (92.5% Li-7, ρ = 0.53 g/cm^3, melting Temperature = 180 C):

- Y (0,12 MeV D+) = 1.77E+06 neutrons per μC. For 300 mA EUROSEA001 deuterium current Y (0,12 MeV D+, 300 mA D+) = 5.31E+11 neutrons/s;
- Y (0,18 MeV D+) = 5.66E+06 neutrons per μC. For 300 mA EUROSEA001 deuterium current Y (0,18 MeV D+, 300 mA D+) = 1.70E+12 neutrons/s

One can find the following results for LiF (ρ = 2.64 g/cm^3, melting Temperature = 870 C):

- Y (0,12 MeV D+) = 2.37E+06 neutrons per μC. For 300 mA EUROSEA001 deuterium current Y (0,12 MeV D+, 300 mA D+) = 7.12E+11 neutrons/s;
- Y (0,18 MeV D+) = 7.59E+06 neutrons per μC. For 300 mA EUROSEA001 deuterium current Y (0,18 MeV D+, 300 mA D+) = 2.28E+12 neutrons/s.

Better neutron output can be achieved with higher deuterium ion energy. Nevertheless, also for energy of 120 keV, it seems possible to have a neutron output increase of an order of magnitude with respect to EUROSEA 001 one.

5. Applications

Both options seem to be able to give a neutron output increase of an order of magnitude without changing the size and the cost of the compact neutron generator.

This gives the possibility to have:

- intense fast neutron beams using the CNG by itself;
- high epithermal and thermal neutron fluxes coupling the CNG with suitable moderating material assemblies devoted to slow down fast neutrons and to select the neutron energy range more effective for tumor treatment.

The achievement of suitable neutron beams and fluxes for NCT treatment and the fulfillment of all the NCT requirements needs a detailed neutronic and mechanical design of the moderating material assemblies to be coupled with the CNG.

Some examples have already been presented at:

- Protons, Ions and Neutrons in Radiations Oncology International Symposium, Munich, 6-7 July 2007;
- International Workshop on Accelerator based Neutron Sources for Medical, Industrial and Scientific Applications, Turin, 23rd May 2008.

A poster on *Thermal Neutron Flux for NCT Application by means of Compact Neutron Generators* is available in this conference.

6. Conclusions

Eurosea Committee and Lawrence Berkeley National Laboratory have investigated different approaches for upgrading the neutron generator Model EUROSEA 001.

In particular, two approaches showed to be very interesting:

- To increase the D+ ion beam current and energy by ion source chamber modification;
- To change the target material and employ other reactions for neutron production.

Both option seem to allow a neutron output increase of an order of magnitude, namely, to pass from $1 \cdot 10^{11}$ n/s (EUROSEA 001) to more than 10^{12} n/s without changing the size and the cost of the compact neutron generator.

Then, combining the two options, it seems possible to improve the CNG EUROSEA 001 till to reach a **neutron output of about 10^{13} n/s.**

References

BNL nuclear reaction database (http://www.nndc.bnl.gov/exfor/exfor00.htm).

M.A.Hofstee, A.K.Pallone, F.E.Cecil, J.A.Mcneil, C.S.Galovich, Measurement of low energy (d,n) reactions on light nuclei important to astrophysics, Nuclear Physics, Section A Vol.688, p.527 (2001).

S. Custodero, F. Mattioda, Thermal neutron flux for NCT applications using the Compact Neutron Generator EUROSEA 001, Protons, Ions and Neutrons in Radiations Oncology International Symposium, Munich, 6-7 July 2007.

S. Custodero, F. Mattioda, The Compact Neutron Generator Prototype EUROSEA 001, International Workshop on Accelerator based Neutron Sources for Medical, Industrial and Scientific Applications, Turin, 23rd May 2008.

The National Institute for Standard and Technology (NIST) database (http://physics.nist.gov/PhysRefData/Star/Text/contents.html).

Verbeke JM et al. Appl. Rad. Isot. 53 p.801-809 (2000).

Beam shaping assembly with thick liquid lithium target for neutron production in BNCT

G. Bengua[a], T. Kobayashi[b], K. Tanaka[c], M. Ishikawa[a]

[a] *Medical Physics Department, Hokkaido University Hospital, Sapporo, Japan*
[b] *Kyoto University Research Reactor Institute, Osaka, Japan*
[c] *School of Medicine, Sapporo Medical University, Sapporo, Japan*

Abstract

The feasibility of using thick flowing liquid lithium as target for neutron production in irradiation facilities for BNCT application was studied, assuming the neutron production with the $^{7}Li(p,n)^{7}Be$ reaction at 2.5 MeV incident protons. In particular, a Beam Shaping Assembly (BSA) using D_2O as moderator and Pb gamma absorber were investigated by comparing the gamma Protocol Depth (PD(γ)), the Heavy Charged Particle Protocol Depth (PD(HCP)) and the Treatable Protocol Depth (TPD) corresponding to the selected target and BSA component thicknesses. All simulations were carried out using the Monte-Carlo n-particle transport code (MCNPX), while the BNCT absorbed dose components were calculated based on a protocol for intra-operative BNCT. A TPD of as much as 3.72 cm may be achievable at the suitable combination of the moderator and gamma absorber thicknesses. The best D_2O moderator thickness for the target assembly configuration considered in this study is about 10 cm, while the Pb gamma absorber thickness is around 2 cm. The thickness of the liquid lithium target for all the calculations was assumed to be 1mm, which is thicker than the range of 2.5 MeV protons in lithium that is only about 0.25mm.

Keywords: Accelerator, $^{7}Li(p,n)^{7}Be$ reaction, Thick liquid target, Beam shaping assembly

1. Introduction

The design of target assemblies for accelerator-based neutron sources utilizing the $^{7}Li(p,n)^{7}Be$ near threshold reaction has mainly considered lithium targets which are thinner than 10 μm, in order to minimize the gamma rays produced in the target (Bengua, G. et al., 2006; Kobayashi, T. et al., 2007; Tanaka, K. et al., 2002). From these studies, we foresee a number of problems that would arise from using thin solid targets. One of them would be the need for the constant target replacement due to its fast degradation.

We have considered liquid targets to effectively remove the heat generated in the target system due to proton bombardment. For a liquid target, the practically achievable thickness of the flowing lithium layer should be larger than 1 mm. It is therefore necessary to investigate the best irradiation system that can be constructed based on these assumptions of using a relatively thick lithium target.

The proton energy for neutron production assumed in this work was 2.5 MeV in order to take advantage of the higher neutron yield at proton energy above the peak resonance of the $^{7}Li(p,n)^{7}Be$ reaction.

However, at this proton energy, the generated neutrons have energies higher than the requirements for BNCT and therefore an appropriate moderating material and thickness has to be placed between the target and the phantom.

Additionally, the thick target we assumed in our simulations is expected to generate gamma rays from (p,p'γ) and (p,γ) reactions in the target, thus an effective gamma absorber has to be included in the beam shaping assembly (BSA). For this study, we selected lead (Pb) as the gamma absorbing material.

The main objective of this research was to investigate the suitable configuration of the target-assembly and the BSA for an accelerator-based neutron source that uses a 1 mm-thick flowing liquid lithium metal target and mono-energetic 2.5 MeV incident proton energy.

We report here the results of our preliminary investigation aimed at the initial optimization focused on the assessment of the proper dimensions of the D_2O neutron moderator and of the Pb gamma absorber. Also considered here is the effect of using a fluorinated material as a target coolant.

2. Methods

A. *Target assembly design and Simulation Parameters*

The irradiation system modeled in our simulations is shown in Fig. 1. The geometry for the lithium target used here are the same as those applied in near-threshold $^{7}Li(p,n)^{7}Be$ neutron production study by Kobayashi, T., et al., (2008)

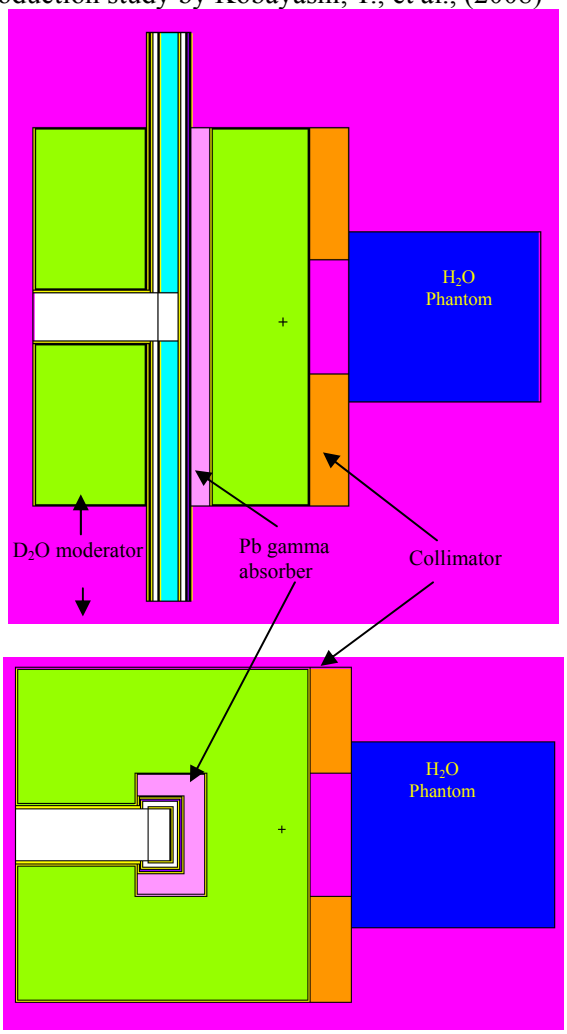

Fig. 1. The irradiation system modeled in this study which is composed of the target-assembly, the beam shaping assembly and water phantom

The target-assembly included a 1 mm thick lithium target and a layer for target cooling. On the other hand, the BSA is composed of a layer of lead, for absorbing gamma rays generated at the target, a D_2O moderator surrounding the gamma absorber, and a lithiated polyethylene collimator which is 40 mm thick. Also shown is the water phantom representing a human head phantom under neutron irradiation.

Neutron production in the lithium layer was limited to a cross-sectional area having 3 cm diameter. The neutron energy and angular distributions were calculated through the Fortran code developed by Lee and Zhou (1999) while those of the gamma rays generated in the lithium target from proton-induced reactions were obtained using equations derived from experimental data (Lee, C.L. et al., 2000). Neutron and gamma-ray transport calculations within the entire irradiation system were carried out by means of Monte Carlo n-particle transport code (MCNPX) (Waters, L.S., 2002).

The range of D_2O moderator thicknesses evaluated here was from 5 cm to 20 cm while the gamma absorber thicknesses were from 1 cm to 3 cm. We likewise checked how a layer of target cooling material (fluorinated) would affect the dose distribution in the water phantom. In the simulations, we used C_2F_4 for the layer of fluorinated material.

B. *Calculation of BNCT Absorbed Dose Components*

Absorbed doses were computed from the particle fluence at each mesh tally in the water phantom with the ^{10}B concentration in the tumor set at 30 ppm and in the normal tissue at 10 ppm. The tissue composition was assumed to be H(11.7%), C(12%), N(2%) and O(74.2%) by weight percent (Snyder, W.S. et al., 1975). Conversion of particle fluence to absorbed dose was carried out using the conversion factors for gamma rays and Heavy Charged Particle (HCP) interactions derived by Hubbell (1999) and Caswell and Coyne (1980), respectively.

The dose to normal tissue from HCP was taken as the sum of the $^{10}B(n,\alpha)^{7}Li$ reaction at 10ppm ^{10}B concentration, $^{14}N(n,p)$ and (n,n) reactions in H, C, and O. The dose to tumor from HCP was computed in the same manner, differing only in the ^{10}B concentration which was set to 30 ppm. The gamma ray dose was computed from the sum of the dose from capture gamma rays in the phantom and the dose from contaminant gamma rays in the neutron field coming from the target assembly and the BSA.

C. *Criteria for Optimization*

The dose distributions in the water phantom obtained from various BSA configurations were evaluated using the protocol based optimization criteria we introduced in a previous study, namely, the gamma Protocol Depth (PD(γ)), the HCP Protocol Depth (PD(HCP)) and the Treatable Protocol Depth (TPD) (Bengua, G. et al., 2004). These indices were defined based on the protocol by Nakagawa et al. (2003) which sets the tumor treatable dose for HCP to 15 Gy, the normal tissue tolerance dose to HCP at 15 Gy and the normal tissue tolerance dose to gamma rays at 10 Gy.

3. Results and Discussion

The results reported here are based on the assumption of a thick lithium layer in the target-assembly in order to allow the use of flowing liquid lithium as target for neutron production. The practically usable thickness for this type of target will be about 1 mm and this thickness has been applied in all the geometry for the target-assembly in our simulations. The optimization carried out in this study was limited to the moderator and the gamma absorber layer of the BSA, while the engineering aspects of implementing the flowing liquid lithium target will be discussed in a separate publication.

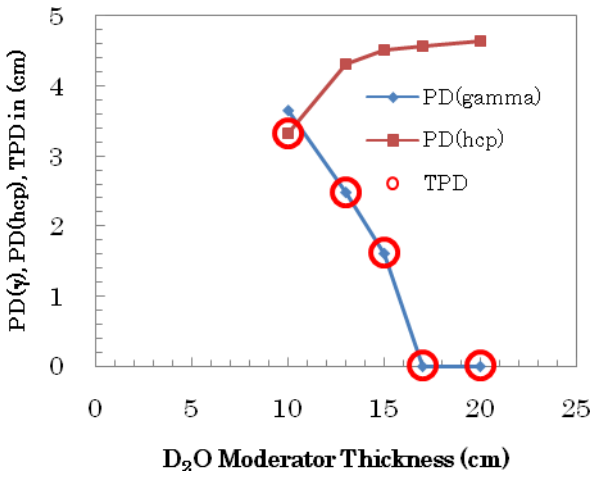

Fig. 2. The effect of moderator thickness on PD(γ), PD(HCP) and TPD for a target assembly configuration shown Fig. 1 using a gamma absorber thickness of 1cm

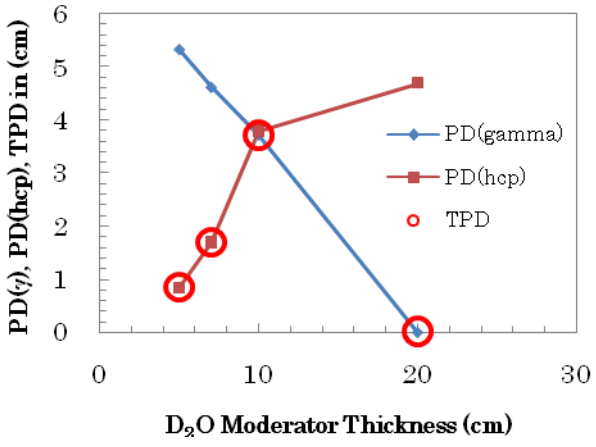

Fig. 3. The effect of moderator thickness on PD(γ), PD(HCP) and TPD for a target assembly configuration shown Fig. 1 using a gamma absorber thickness of 2 cm

Shown in Fig. 2 is the effect of the moderator thickness on PD(γ), PD(HCP) and TPD for a fixed gamma absorber thickness of 1 cm.

The monotonically decreasing PD(γ) for thicker moderators is brought about by the lower difference between the neutron dose to tumor and the gamma ray dose to healthy tissues due to loss in neutron fluence. On the other hand, the increasing PD(HCP) is a result of the relatively lower average neutron energy when thicker moderators are used.

From Fig. 2 it appears that the optimum moderator thickness for a 1 mm lithium target and a 1 cm gamma absorber is about 10 cm.

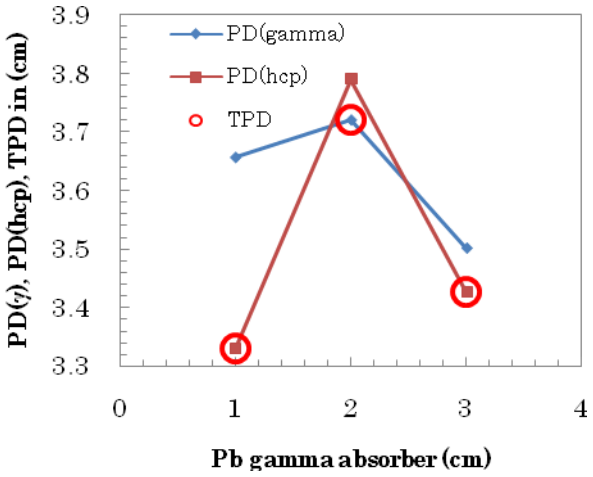

Fig. 4. The effect of the Pb gamma absorber thickness on PD(γ), PD(HCP) and TPD for a target assembly configuration shown Fig. 1 at a D_2O thickness of 10 cm

We also looked at the effect of using a thicker gamma ray absorber in the BSA, the result of which is shown in Fig. 3. Here we can see that the maximum TPD increased from 3.33 cm to 3.72 cm when the gamma absorber thickness was brought from 1 cm to 2 cm, respectively. The moderator thickness corresponding to the maximum TPD was again about 10 cm thick.

Figure 4 illustrates the effect of the thickness of the Pb gamma ray absorber on the PD(γ), PD(HCP) and TPD for three absorber thicknesses. Here we can see that the deepest TPD is achieved when the Pb layer is set to 2 cm.

Tab. 1. Effect of coolant layer on PD(γ), PD(HCP) and TPD for the target assembly configuration in Fig. 1

Coolant	PD(γ)	PD(hcp)	TPD
fluorinate	3.72	3.79	3.72
Air	3.68	3.37	3.37

Comparing the PD(γ), PD(HCP) and TPD parameters when the coolant layer of target assembly is filled with both a fluorinated material and with just air as target coolant, we get a higher TPD for the former. This may be due to the additional moderating and scattering effect on the neutron beam by the fluorinated layer.

4. Summary

Thick liquid lithium targets may be usable in target assemblies for neutron production in BNCT. This, however, will require a suitable combination of moderator material and thickness and also a dedicated gamma absorber in the BSA. Our calculations have shown that the best D_2O moderator thickness will be about 10cm while the Pb gamma absorber thickness will be around 2cm for the irradiation system considered in this study. In our future investigations, we also intend to evaluate other possible moderating materials and gamma absorbers.

References

Bengua, G., Kobayashi, T., Tanaka, K. et al., 2006. TPD-based evaluation of near threshold mono-energetic proton energies for the ^{7}Li(p,n)^{7}Be production of neutrons for BNCT, Phys. Med. Biol. **51**, 4095-4109.

Bengua G., Kobayashi T, Tanaka K and Nakagawa Y, 2004. Evaluation of the characteristics of boron-dose enhancer (BDE) materials for BNCT using near threshold ^{7}Li(p,n)^{7}Be direct neutrons. Phys. Med. Biol. **49**(5), pp. 819-831.

Caswell, R.S. and Coyne, J.J., 1980. Kerma factors for neutron energies below 30 MeV. Radiat. Res., 83, 217-254.

Hubbell, J.H., 1999. Review of photon interaction cross- data in the medical and biological context. Phys. Med. Biol., **44**, R1-R22.

Kobayashi, T., Bengua, G., Tanaka, K., et al. 2007. Variations in lithium target thickness and proton energy stability for the near-threshold ^{7}Li(p,n)^{7}Be accelerator-based BNCT, Phys. Med. Biol. **52**, 645-658.

Kobayashi, T., Bengua, G.., Tanaka, K., et al., 2008 Neutrons for BNCT from the Near Threshold 7Li(p,n)7Be on a Thick Li-target, Proc. of ICNCT-13.

Lee, C.L. and Zhou, X.L., 1999. Thick target neutron yields for the ^{7}Li(p,n)^{7}Be reaction near threshold.Nucl. Instr. Methods Phys. Res. B, **152**, . 1-11.

Lee CL, Zhou XL, Kudchadker RJ, Harmon F and Harker YD, 2000. A Monte Carlo dosimetry-based evaluation of the ^{7}Li(p,n)^{7}Be reaction near threshold for accelerator boron neutron capture therapy. Med. Phys., **27**(1), pp. 192-202.

Nakagawa Y, Pooh K, Kobayashi T, et al., 2003. Clinical review of the Japanese experience with boron neutron capture therapy and a proposed strategy using epithermal neutron beams. Journal of Neuro-Oncology, 62, pp. 87-99.

Snyder, W.S., Cook, M.J., Nasset, E.S., Kahrhausen, L.R., Howells, G.P. and Tipon, L.H., 1975. Report of the Task Group on Reference Man (Oxford:Pergamon).

Tanaka, K., Kobayashi, T., Sakurai, Y., Nakagawa, Y., Ishikawa, M. and Hoshi, M., 2002. Irradiation characteristics of BNCT using near-threshold ^{7}Li(p,n)^{7}Be direct neutrons: application to intra-operative BNCT for malignant brain tumors. Phys. Med. Biol., **47**, . 3011-3032.

Waters, L.S., ed., 2002. MCNPX User's Manual Version 2.4.0 LA-CP-02-408. Los Alamos National Laboratory, Los Alamos, New Mexico.

A comparison between a TESQ accelerator and a reactor as neutron sources for BNCT

A.A. Burlon[a,b] and A.J. Kreiner[a,b,c]

[a]*Departamento de Física, Comisión Nacional de Energía Atómica, Av. Gral Paz 1499 (1650), San Martín, Buenos Aires, Argentina.*
[b]*Escuela de Ciencia y Tecnología. Universidad Nacional de Gral. San Martín, M. De Irigoyen 3100 (1650), San Martín, Buenos Aires, Argentina.*
[c]*CONICET, Avda. Rivadavia 1917(C1033AAJ), Ciudad Autónoma de Buenos Aires, Argentina.*

Abstract

In this work, the performance of an accelerator-based neutron source design has been compared with that of a modern fluoride-filtered reactor-based epithermal beam having near-optimal quality for treatment of deep seated tumours in relation to its applicability for BNCT. The accelerator is a Tandem-ElectroStatic-Quadrupole (TESQ) accelerator which is a design under development at the Comisión Nacional de Energía Atómica (CNEA) in Buenos Aires, Argentina based on the ^{7}Li(p,n)^{7}Be reaction, relatively close to its energy threshold. The reactor is the Massachusetts Institute of Technology reactor upgraded with a Fission Converter Beam (MIT-FCB) and improved with an 8mm thick ^{6}Li Filter. The comparison has been done by means of data reported on the MIT-FCB + ^{6}Li Filter performance and MCNP simulations on our TESQ design considering the doses delivered in a human phantom by both devices. The results show a deeper advantage depth (AD) for the TESQ which turns out to be a promising alternative to a reactor-based BNCT treatment. Our calculations show that the TESQ facility may reach a 98% Tumour Control Probability at 6.4 cm inside the brain in a 27 minutes treatment keeping the maximum healthy tissue RBE dose at 11.6 RBEGy (considering 12.5 RBEGy as the maximum allowed healthy tissue dose) utilizing 34 cm of moderator and a 30 mA proton beam for an optimized patient position in front of the emerging neutron beam.

Keywords: Accelerator-Based BNCT (AB-BNCT), ^{7}Li(p,n)^{7}Be reaction, Reactor based BCNT, Tandem Electrostatic Quadrupole accelerator, MCNP simulations.

1. Introduction

Within the frame of Accelerator Based BNCT (AB-BNCT), a project to build a Tandem-ElectroStatic-Quadrupole (TESQ) accelerator is under development (Kreiner et al., 2007) in Argentina based on the ^{7}Li(p,n)^{7}Be reaction, slightly beyond its resonance, at 2.3 MeV. The project aims at developing a machine capable of delivering a proton beam of about 2.5 MeV and 40 mA to irradiate a Li metal (or a refractory Li compound) target in order to produce the therapeutic neutron beam after appropriate beam shaping. In this work, (Burlon and Kreiner, 2008) we compare the performance of such a beam with the Massachusetts Institute of Technology reactor upgraded with a Fission Converter Beam (MIT-FCB) and improved with the installation of a ^{6}Li filter, which produces a near-optimal quality beam for the treatment of deep seated tumors (Riley et al, 2003 and Binns et al., 2007). By means of MCNP simulations, dose distribution studies in a head phantom model have been made for the TESQ beam in order to compare it with the MIT-FCB.

2. Materials and Methods

To compare the performance of the TESQ beam with the MIT-FCB + ^{6}Li filter (Fig.1), the TESQ target geometry was translated into an MCNP input to be run in dedicated computers. We simulated the geometry corresponding to an optimized Beam Shaping Assembly (BSA) including the patient phantom and the treatment room. The BSA consists of a moderator composed by successive slabs of aluminum, Teflon and LiF as a thermal neutron absorber and a lead mantle as neutron reflector (Burlon et al., 2005) as is shown in Fig. 2.

Two moderator thicknesses were studied: 34 and 40 cm, and a 40 mA, 2.3 MeV uniform proton beam of 10 cm diameter on a Li metal target was

considered. For the TESQ, the doses were calculated in a longitudinal array of spherical tally cells (1 cm diameter) located within the head phantom to evaluate the delivered doses at different depths along the central axis while for the MIT-FCB + ^{6}Li filter the longitudinal axis dose measurements (corresponding to a converter power of 83 kW) reported were considered for comparison (Binns et al., 2007).

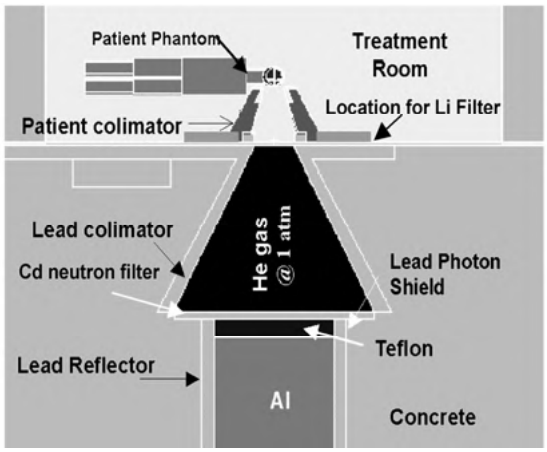

Fig. 1. Geometry of the MIT-FCB +^{6}Li Filter reactor (from Binns et al, 2007)

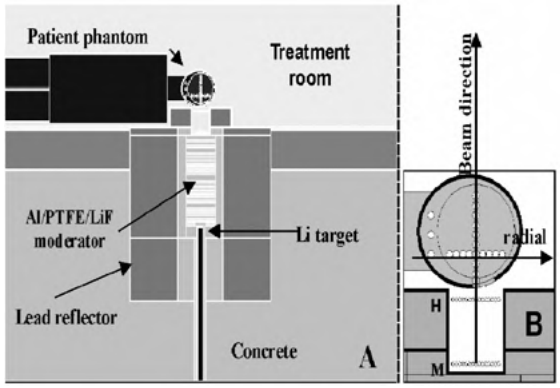

Fig. 2 Geometry of the TESQ-BSA designed to be simulated with MCNP

For the MCNP TESQ-BSA dose calculations, the following conditions were adopted: (a) RBE-doses were calculated assuming 65 ppm and 18 ppm for the ^{10}B concentration in tumor and healthy tissue respectively as adopted by Binns et al., while there is no boron concentration in the skull; (b) cRBE's of 1.3 and 3.8 were considered for the boron dose in healthy tissue (brain and scalp) and tumor respectively; (c) For the thermal energy range (En < 0.5 eV) the considered reactions were $^{10}B(n,\alpha)^{7}Li$ and $^{14}N(n,p)^{14}C$ (cRBE of 3.2) , for the epithermal range (0.5eV<E_n<10keV), $^{10}B(n,\alpha)^{7}Li$, $^{14}N(n,n')^{14}N$ (cRBE of 2), and, for the fast neutron range (E_n >10 keV), $^{1}H(n,n')^{1}H$ (cRBE of 3.2), respectively and the photon dose.

All the absorbed doses were weighted with their respective cRBE value and added to obtain the total cRBE-dose rate in both tumor and healthy tissue.

3. Results

Fig. 3 gives the respective total tumor and healthy tissue dose rates. For the MIT-FCB + ^{6}Li Filter an Advantage Depth (AD) of 9.9 cm is reported by Binns while for the TESQ arrangements the AD's are of 10.5 cm (for 34 cm BSA) and 10.7 cm (for 40 cm BSA). Moreover, it can be seen that the maximum total tumor dose rates are reached at similar depth (near 3 cm).

As another way to assess our results, Tumor Control Probability (TCP) curves have been plotted in Fig. 4 as a function of the maximum delivered healthy tissue dose for both facilities (Burlon et al., 2005 and Wheeler et al., 1999) and all the three curves stay below the maximum allowed healthy tissue dose of 12.5 RBEGy, being the MIT-FCB + ^{6}Li Filter one the best.

However, at deeper positions in the brain (that means going towards the AD) the TCP curves for TESQ stay to the left of the MIT ones. In particular, a position at 6.8 cm appears as the limit for which a 98% TCP can be reached with the TESQ delivering 12.5 RBEGy to the healthy tissue while a higher dose to the normal brain (for the same TCP) is delivered for the MIT-FCB +^{6}Li Filter reactor as shown in Fig. 5.

4. Discussion and conclusions

From Fig. 4, it can be seen that for a depth of 3 cm, a higher TCP (98%) can be obtained with the MIT reactor than for TESQ (preferably with a 40 cm BSA) while keeping all the doses in healthy tissue under their maximum allowed value of 12.5 RBEGy. But for deeper positions (near to the AD, see Fig. 5) the TESQ-BSA curves show a better behavior than the MIT ones, as a result of their larger AD.

In conclusion, TESQ with this BSA and a 40 mA proton beam could provide a properly shaped neutron beam for the treatment of a 3-4 cm deep tumor with high TCP and up to a depth of 10.7 cm and shows a relatively better behavior for positions beyond about 7 cm. The estimated treatment times at the 3 cm position for both TESQ configurations with a 40 mA proton beam and a TCP of 98% are (24±1) minutes (for a 34 cm moderator) and (41±1) minutes (for a 40 cm moderator).

In the figures of merit of Fig. 6, the maximum doses delivered to the normal tissue (associated to a 98% TCP) are plotted as a function of the treatment time at different depths in brain.

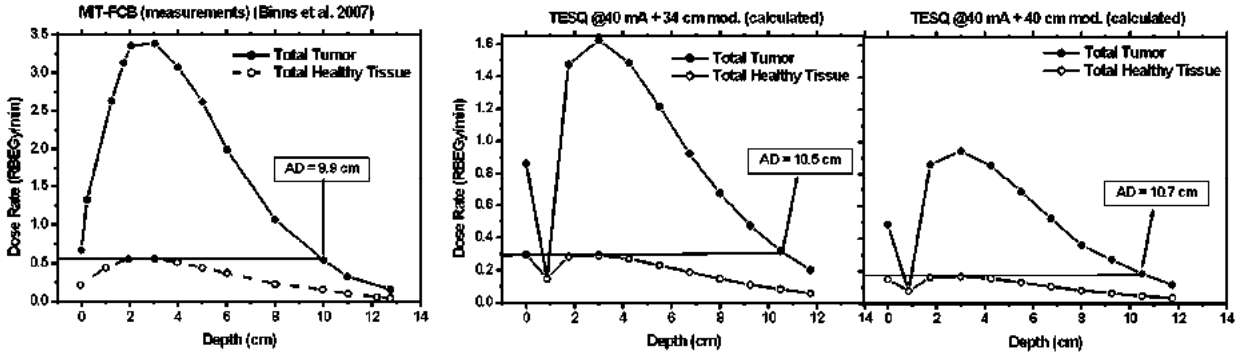

Fig. 3 Doses rates and Advantage Depths (A.D) for MIT-FCB + ^{6}Li Filter (Binns et al., 2007) and both TESQ-BSA options

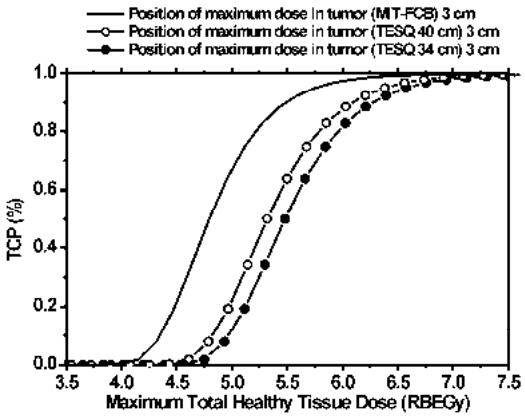

Fig. 4 Tumor Control Probability curves as functions of the maximum delivered dose in healthy tissue at 3 cm in brain for both the MIT-FCB +^{6}Li Filter and TESQ-BSA options

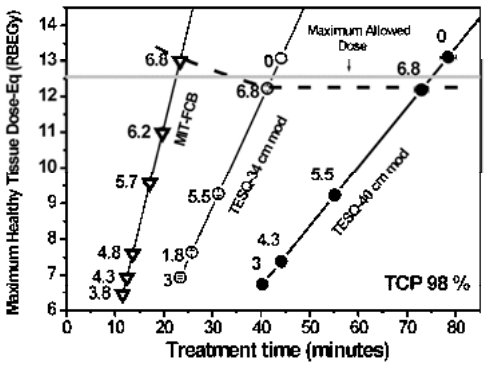

Fig. 6. Figures of merit for both TESQ-BSA options and MIT-FCB + ^{6}Li Filter for a 98% TCP. Each point is labeled with its depth in brain. The dashed line connects the 6.8 cm depth positions

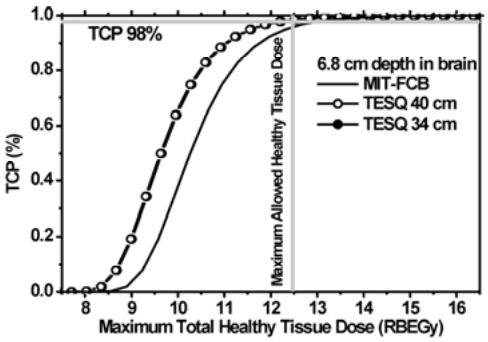

Fig. 5. TCP curves as a function of the maximum delivered dose to the healthy tissue at 6.8 cm depth in brain

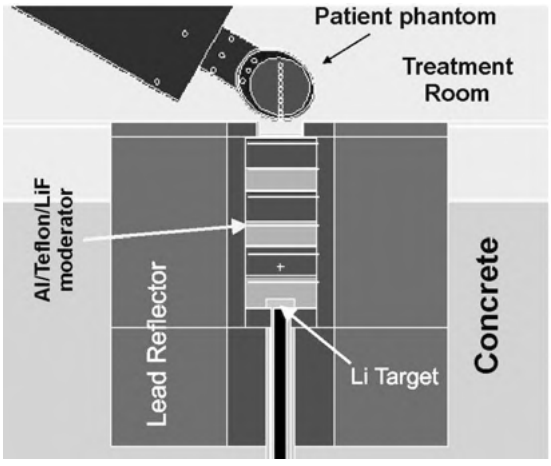

Fig. 7. Repositioning of the patient in the TESQ BSA

Although the smallest treatment times are obtained by MIT-FCB + ^{6}Li Filter, for deeper positions the TESQ provides a 98% TCP while keeping the tissue dose under 12.5 RBEGy (as is shown by the 6.8 cm connecting dashed line). As an improvement of our TESQ-BSA, the patient can be brought closer to the output port as shown in Fig 7.

The repositioning implies a rotation of the phantom to avoid that its shoulder makes contact with the output port.

At this new position, the dose profiles were recalculated for both moderator thicknesses and for 40 mA (Fig 8) and the figures of merit for both moderator thicknesses and for 40 mA and 30 mA

primary proton beams (Fig. 9). Then, our TESQ facility may reach an AD of about 11.5 cm and 98% Tumour Control Probability at 6.4 cm inside the brain in a 27 minutes treatment keeping the maximum healthy tissue RBE dose at 11.6 RBEGy (considering 12.5 RBEGy as the maximum allowed healthy tissue dose) utilizing 34 cm of moderator and a 30 mA proton beam.

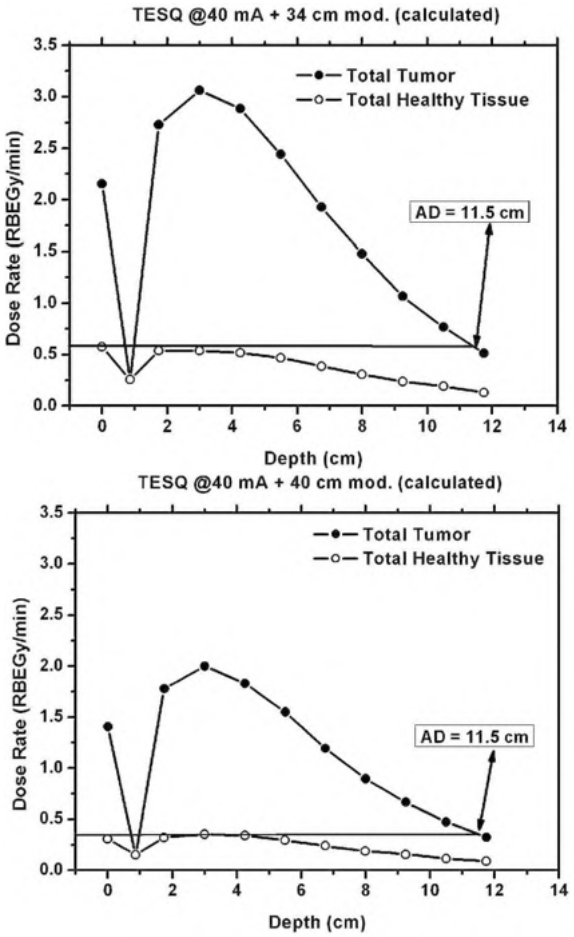

Fig. 8 Doses rates and Advantage Depths (A.D) for both TESQ-BSA options at the improved patient position

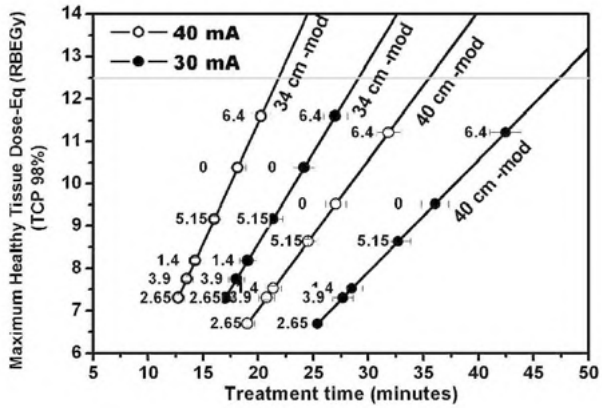

Fig. 9. Figures of merit for both TESQ-BSA options and 30 and 40 mA for a 98% TCP at the improved patient position. Each point is labeled with its depth in brain

Since an accelerator can be sited in a hospital environment, is safer as far as operating conditions are concerned, easier-to-operate and of lower cost than a reactor, our present results provide an additional justification for the ongoing efforts to develop such a machine as a means to achieve further progress in the field of BNCT.

References

Binns, P.J., Riley, K.J., Ostrovsky, Y., Gao, W., Albritton, J.R., Kiger, W. and Harling, O., 2007. Improved dose targeting for a clinical epithermal neutron capture beam using optional ^{6}Li Filtration. Int. J. Radiation Oncology Biol. Phys. 67(5), 1484-1491.

Burlon, A.A, Kreiner, A.J., 2008. A comparison between a TESQ accelerator and a reactor as a neutron sources for BNCT. Nucl. Instrum. Methods B 266/5, 763-771.

Burlon, A.A, Kreiner, A.J., Valda, A.A., Misnky, D.M., Somacal, H.R., Debray, M.E., Stoliar, P.A., 2005.Optimization of a neutron production target and a beam shaping assembly based on the 7Li(p,n)7Be reaction for BNCT. Nucl. Instrum. Methods B 229, 144–156.

Kreiner, A.J., Kwan, J.W., Burlon, A.A, Di Paolo, H., Henestroza, E., Minsky, D.M., Valda, A.A., Debray, M.E., Somacal, H.R., 2007. A Tandem-Electrostatic-Quadrupole for Accelerator-Based BNCT. Nucl. Instrum. Methods B 261, 751–754.

Riley, K.J., Binns, P.J., Harling, O.K., 2003. Performance characteristics of the MIT fission converter based epithermal neutron beam. Phys. Med. Biology. 48, 943-958.

Wheeler, F., Nigg, D., Capala, J., Watkins, P., Vroegindeweij, C., Auterinen, I., Seppala, T., Bleuel, D., 1999. BNCT: Implications of neutron beam and boron compound characteristics. Med. Phys. 26 (7) , 1237-1244.

Thermal Neutron Flux for NCT Application by means of Compact Neutron Generators

S. Custodero [a], F. Mattioda [a]

[a] *EUROSEA Committee, via Livorno 60, I-10144 Torino, Italy*

Abstract

At the end of 2004 EUROSEA 001, the first prototype of Compact Neutron Generators (CNG) developed by the Plasma and Ion Source Technology Group at Lawrence Berkeley National Laboratory (LBNL) for the Italian non-profit association Eurosea Committee of Turin, was installed and tested at the Experimental Physics Department of Turin University. This prototype is designed to produce a D-D neutron yield of $1 \cdot 10^{11}$ n/s and its dimensions do not exceed 50 cm.

EUROSEA 001 and its upgrade version can provide thermal neutrons for tissue sample irradiation tests and therapeutic applications respectively. To this end, the CNGs have to be coupled with a moderating-reflecting assembly devoted to slow down fast neutrons (2.45 MeV) and to increase thermal neutron population.

An extensive set of MCNP simulations have been performed. The results show that the CNGs, coupled with a suitable moderating-reflecting assembly, give thermal neutron fluxes matching all the spectral purity parameters for NCT application, for instance, liver cancer treatment and other medical applications.

Keywords: compact neutron generator, thermal neutron, liver cancer treatment

1. Introduction

In 2001, an agreement between the Italian non-profit association Eurosea Committee (Turin) and The Plasma and Ion Source Technology Group at Lawrence Berkeley National Laboratory (LBNL, California, USA) was signed for the development of a prototype of Compact Neutron Generators (CNG) based on fusion reactions for medical uses.

The CNG is basically composed of three main elements: a source of deuterium ions, a low voltage electrostatic accelerator and a titanium target. The radio frequency antenna (13.5 MHz) is used to produce deuterium ions which are properly accelerated by the potential difference in vacuum chamber. The deuterium ions are extracted from some circular apertures on the source chamber wall and they hit the titanium target (at ~120 keV energy), where nuclear fusion reactions between the deuterium nuclei occur resulting the generation of fast neutrons.

At the end of 2004 this prototype called EUROSEA 001 was installed and tested at the Experimental Physics Department of the Turin University. The prototype is capable of producing a D-D neutron yield of $1 \cdot 10^{11}$ n/s and its dimensions do not exceed 50 cm.

Then, Eurosea Committee and Lawrence Berkeley National Laboratory have investigated different approaches for upgrading the present neutron generator Model EUROSEA 001. The goal is to increase the neutrons yield without changing the size of the neutron generator. This is very important for a therapeutic application of the NCT because the increase of the neutron production will allow a sensible reduction of the treatment time of the patient.

EUROSEA 001 and its upgrade version can provide thermal neutrons for tissue sample irradiation tests and for therapeutic applications respectively.

In order to set up a suitable assembly for the production of thermal neutron fluxes, the CNGs have to be coupled with a moderating-reflecting assembly devoted to slow down fast neutrons (2.45 MeV) and to increase thermal neutron population.

To meet this goal the proposed assembly presents a central region containing the CNG

(*neutron source*), an inner moderating region (*moderator*) devoted to slow down fast neutrons and an outer reflecting region (*reflector*) devoted to limit thermal neutron leakage via back-scattering process.

The assembly proposed has been studied by means of MCNP code version 4C. Neutron and photon fluxes have been evaluated inside the inner moderating region in several points. Neutron and photon fluxes have been evaluated and compared with the recommended values for the application of NCT. An extensive set of simulation have been performed. The results show that the CNGs, coupled with a suitable moderating-reflecting assembly, give thermal neutron fluxes matching all the spectral purity parameters for NCT application (for instance in case of liver cancer treatment) in the dedicated irradiation region.

2. EUROSEA model 001

The compact neutron generator EUROSEA 001 allows to produce until $1 \cdot 10^{11}$ n/s operating with 300 mA deuterium ions current @ 120 kVolt. It is basically composed of three main elements (Fig. 1):

- a source of deuterium ions;
- a low voltage electrostatic accelerator;
- a titanium target where nuclear fusion reactions between the deuterium nuclei occur resulting in the generation of fast neutrons.

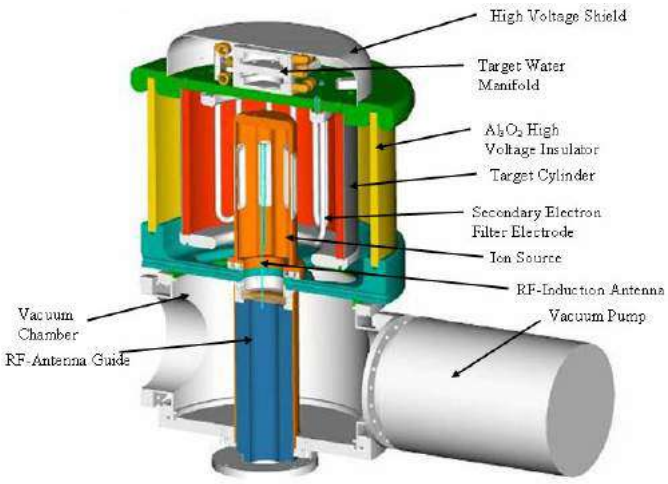

Fig. 1. CNG EUROSEA model 001 – main parts and components

The complete configuration of the Compact Neutron Generator system also includes the following auxiliary systems:

- radio frequency (RF) and High Voltage supplies (HV);
- cooling system to remove thermal power;
- moderator which allows slowing down fast neutrons and addressing them toward the treatment area optimizing their energy in order to irradiate efficiently the tumour mass.

The main characteristics of the prototype are:

- high compactness (dimensions do not exceed 50 cm.);
- safety (neutron production is stopped when the electrical supply is turned off);
- simplicity of assembly and operation throughout the life cycle.

3. EUROSEA 001 upgrade

In order to improve the neutron output without changing the size of the neutron generator, two main one options are available:

- to increase the D ion beam current and energy (for example, by operating the source at a beam power of 180 kV and 1 A);
- to change the target material and employ other reactions for neutron production instead of the D-D reaction.

Further details are available in the paper *Feasibility Study for the Upgrade of a Compact Neutron Generator for NCT Application,* presented in this Conference.

In the first upgrade approach one does not have to modify other components except the ion source chamber. This replacement can be easily done for EUROSEA model 001.

4. Production of thermal neutrons using EUROSEA 001 and its upgraded version

In order to set up a suitable assembly for the production of thermal neutron fluxes to be used for irradiation of samples of liver tissue and other medical applications, the Model EUROSEA 001 UPGRADE can be considered as a very interesting thermal neutron source provided that it is coupled with a moderating-reflecting assembly devoted to slow down fast neutrons (E_n = 2.45 MeV).

Some examples have been presented in the Protons, Ions and Neutrons in Radiations Oncology International Symposium, Munich, 6-7 July 2007 and in the International Workshop on Accelerator based Neutron Sources for Medical, Industrial and Scientific Applications, Turin, 23rd May 2008.

The assembly presented in this work presents is characterized by:

- a central region containing the Model EUROSEA 001 (*neutron source*);
- an inner moderating region (*moderator*) in heavy water (ρ=1.1 g/cm^3) devoted to slow down fast neutrons, with reduced neutron capture;
- an outer reflecting region (*reflector*) in graphite (^{12}C, ρ=1.8 g/cm^3) or Teflon (CF_2, ρ= 2.25 g/cm^3) devoted to limit thermal neutron leakage, reflecting the neutrons toward the *moderator*.

The assembly proposed has been studied by means of MCNP code version 4C.

Neutron and photon fluxes have been evaluated inside the inner moderating region in some points where small irradiation regions (an air sphere having 1 cm radius) could be placed. In the position labelled as "A", the neutron and photon fluxes have been evaluated and compared with the recommended values for the application of NCT (Tab. 1). The case with a bigger irradiation region (a 15 x 8 x 2 cm^3 air box) shielded by 1 cm of bismuth is also presented in Table 1.

Fig. 2 shows a view of EUROSEA 001 and the irradiation region. Figures 3, 4 show a planar and axial view of the proposed assembly.

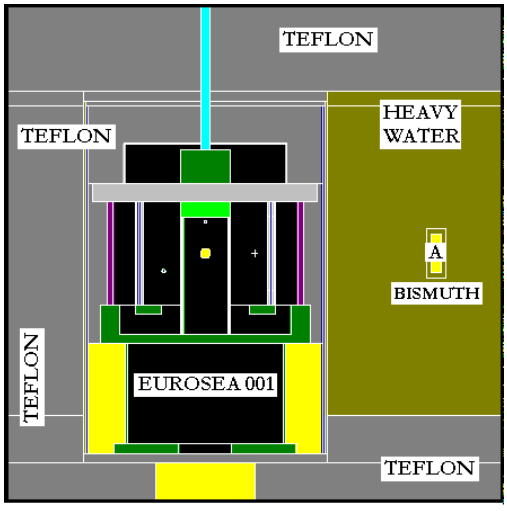

Fig. 2. EUROSEA 001 and the irradiation region

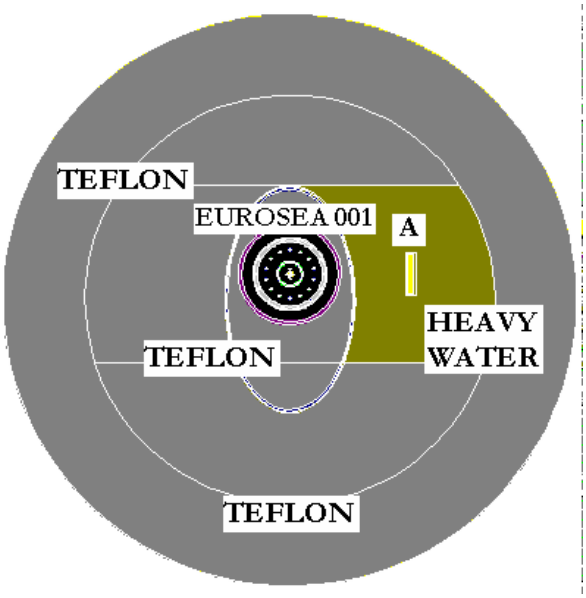

Fig. 3. Planar view of the assembly based on CNG EUROS EA 001

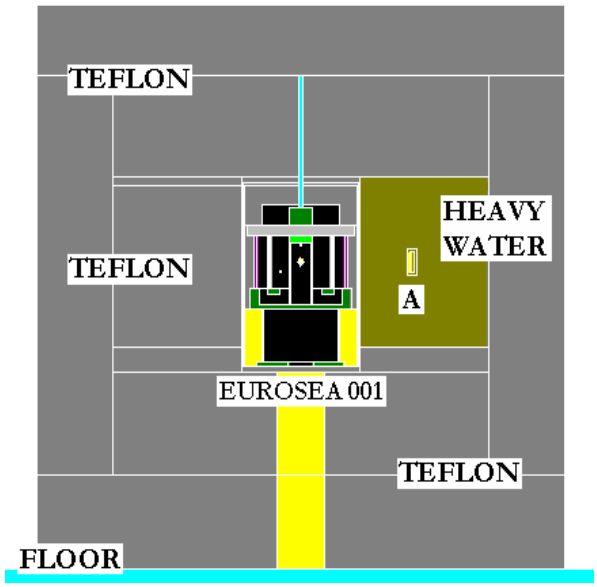

Fig. 4. Axial view of the assembly based on CNG EUROSEA 001

In order to evaluate the possibility to obtain suitable thermal neutron fluxes for diagnostics and/or therapeutic applications of NCT, an extensive set of MCNP simulations have been performed.

They have been evaluated:

- neutron fluxes as function of neutron energy;
- photon fluxes as function of photon energy;
- dose rates due to neutrons as function of neutron energy;
- dose rates due to photons as function of photon energy.

Results are reported in Table 1 for a neutron yield of $2x10^{12}$ n/s. This neutron output is available using an upgraded version of CNG EUROSEA 001.

		R = 1 cm SPHERE IRRADIATION REGION	1 cm Bi shielded 15 x 8 x 2 cm BOX IRRADIATION REGION	LIMIT FOR NCT
Φ_th [> 0,4 eV]	[n cm^{-2} s^{-1}]	**1,19 E+09**	**1,09 E+9**	> 1 E+9
Φ_epi [0,4 eV > 10 keV]	[n cm^{-2} s^{-1}]	1,16E+08	1,01E+08	-
Φ_fast [> 10 keV]	[n cm^{-2} s^{-1}]	2,24E+07	1,87E+07	-
Φ_total	[n cm^{-2} s^{-1}]	1,33E+09	1,21E+09	-
Φ_th / Φ_total	[%]	89,6	90,2	> 90%
Φ_th / Φ_fast	-	53,3	58,1	-
D_n	[mGy h^{-1}]	5,88E+02	8,34E+02	-
D_γ	[mGy h^{-1}]	1,29E+03	6,84E+02	-
D_n_fast / Φ_th	[Gy cm^2]	1,25 E-13	1,99 E-13	< 2 E-13
D_γ / Φ_th	[Gy cm^2]	3,02 E-13	1,74 E-13	< 2 E-13

Table 1. EUROSEA 001 UPGRADE based Facility: neutron and photon fluxes in position "A"

The maximum width, length and height of the proposed assembly do not exceed 250 cm. In the proposed assembly there are about:

- about 220 liters of heavy water (D_2O);
- about 8 m3 of graphite (^{12}C) or Teflon (CF_2) for a weight of 15 tonn.

The main problems connected with the location of proposed assembly based on EUROSEA 001 inside a suitable bunker, the shielding and structures activation have been already studied but not discussed in this report.

It is important to note that, using the CNG EUROSEA 001 and its upgraded versions coupled with a suitable moderating-reflecting assembly, the thermal neutron flux matches all the parameters for the application of NCT in the irradiation region.

Using EUROSEA 001 it is possible to perform the irradiation of tissue samples or in-vitro cells in hospitals.

Once the upgraded version of EUROSEA 001 will be available, it is possible to perform irradiation of tissue samples and tumour treatment in hospitals without relying on the conventional nuclear reactors.

5. Conclusions

At present CNG EUROSEA 001 is placed inside the bunker of the former accelerator of the Experimental Physics Department, University of Turin, Italy.

As shown in this work, EUROSEA 001 and its upgrade version can provide thermal neutrons for tissue sample irradiation tests and therapeutic applications respectively. To this end, the CNGs have to be coupled with a moderating-reflecting assembly devoted to slow down fast neutrons (2.45 MeV) and to increase thermal neutron population.

An extensive set of MCNP simulations have been performed. The results show that the CNGs, coupled with a suitable moderating-reflecting assembly, give thermal neutron fluxes matching all the spectral purity parameters for NCT application, for instance, liver cancer treatment.

Then, In order to set up a suitable device for the production of thermal neutron fluxes to be used for irradiation of tissue samples and tumour treatment, EUROSEA 001 can be considered as a very interesting neutron source.

Further improvements of the performance of the system seem possible using a little more complicated geometric configurations and different materials such as reactor grade graphite.

References

S. Custodero, N. Leung et al., Upgrade of a Compact D-D Neutron Generator for NCT Application, 12th ICNCT, Japan, October 8-13, 2006

S. Custodero, F. Mattioda, Thermal neutron flux for NCT applications using the Compact Neutron Generator EUROSEA 001, Protons, Ions and Neutrons in Radiations Oncology International Symposium, Munich, 6-7 July 2007.

S. Custodero, F. Mattioda, The Compact Neutron Generator Prototype EUROSEA 001, International Workshop on Accelerator based Neutron Sources for Medical, Industrial and Scientific Applications, Turin, 23rd May 2008.

Be target development for the accelerator-based SPES-BNCT facility at INFN Legnaro

J. Esposito[a], P. Colautti[a], S. Fabritsiev[b], A. Gervash[b], R. Giniyatulin[b], V.N. Lomasov[c], A. Makhankov[b], I. Mazul[b], A. Pisent[a], A. Pokrovsky[d], M. Rumyantsev[b], V. Tanchuk[b], L. Tecchio[a]

[a] *INFN Laboratori Nazionali di Legnaro, Via dell'Università 2, I-35020, Legnaro(Padova), Italy*
[b] *STC SINTEZ, D.V. Efremov Scientific Research Institute, Metallostroy, 196641, St.Petersburg, Russia*
[c] *SEI, St Petersburg State Polytechnic University, Polytechnicheskaja, 195251, St Petersburg, Russia*
[d] *SRIIAR, Scientific Research Institute of Atomic Reactors,* 433510, *Dimitrovgrad, Russia*

Abstract

An accelerator-driven thermal neutron source for BNCT application, planned to be installed at the INFN Laboratori Nazionali di Legnaro (LNL), is in progress in the framework of SPES (Selective Production of Exotic Species) research program. The most critical element of such a facility is the construction of a reliable neutron converter based on the ^{9}Be(p,xn) nuclear reaction, working at high power level (150 kW) and 5 MeV beam energy, due to the SPES driver constraints. Two original, beryllium-based, target concepts have been designed for such a purpose. The status of art about the neutron converters developed, as well as the test results performed so far on prototypes constructed is here reported.

Keywords: Accelerator-based BNCT, Neutron Source, Beryllium Target, ^{9}Be(p,xn) reaction

1. Introduction

An accelerator-driven, high flux thermal neutron beam facility, devoted to perform Boron Neutron Capture Therapy (BNCT) experimental treatments on skin melanoma tumor, is planned to be installed in the next years at the INFN Legnaro labs. The LNL BNCT project is part of a larger one, named SPES (Selective Production of Exotic Species) that will allow a research program both in nuclear and interdisciplinary physics (Prete, 2007). The neutron facility will be driven by a high intensity RFQ proton accelerator (Pisent et al., 2004), currently under the final construction stage at LNL, developed within the TRASCO (TRAsmutazione SCOrie) nuclear waste transmutation program. Moreover the proton source TRIPS (TRasco Intense Proton Source) (Ciavola et al., 2001), commissioned and built at INFN-LNS lab, was transferred to LNL in fall 2005 where it has been further improved and has begun to produce stable and high quality beams since mid 2007 (Fagotti et al., 2008). The proton source and the RFQ installed at LNL will represent a unique facility, able to deliver 30 mA, 5 MeV beam which will be used as a stand-alone system for the BNCT facility as well. The status on the Beam Shaping Assembly (BSA) modeling, currently under way at LNL, in order to slow the neutrons generated by the target down to thermal energy range (E_n<0.5 eV), is reported by Ceballos et al. (2008). In the present report the neutron converter developed for such a facility and the tests so far performed on prototypes constructed are discussed.

2. The neutron converter development

The main low energy, proton-induced nuclear reactions considered to yield a neutron source, i.e. ^{7}Li(p,n)^{7}Be, ^{9}Be(p,n)^{9}B and ^{13}C(p,n)^{13}N, have been taken into account at the target design stage for the accelerator-based SPES-BNCT facility. A summary of main nuclear, as well as physical and thermal properties of materials selected may be found elsewhere (Bair et al., 1981, Colonna et al., 1999, Taskaev et al., 2006). A R&D stage has therefore started in 2002 at LNL in order to design a neutron converter able to fulfill the TRASCO RFQ driver beam specifications. At last beryllium revealed to be the best solution, due to the neutron yielding (~10^{14} s^{-1}) and spectrum features (E_n<3.2 MeV) expected at the fixed RFQ output power, as well as the related engineering solutions available for a reliable solid target. After neutronic as well as technological feasibility studies lasted two years, the design of an original, beryllium-based target, shown in Figure 1 was therefore produced from the collaboration between LNL and the STC Sintez of Efremov Institute in S. Petersburg, (Russia) (Makhankov, et al, 2004). The first, full-scale half-target prototype, also shown in Figure 1, was finally assembled by the end of 2004. The target main structural components are based on a zirconium alloy (Zr + 2.5% Nb), while the neutron converter is basically made of beryllium tiles which are brazed on 10 mm outer diameter, 1 mm thickness, cooling pipes. These latter are produced by casting of bronze (CuCrZr) alloy

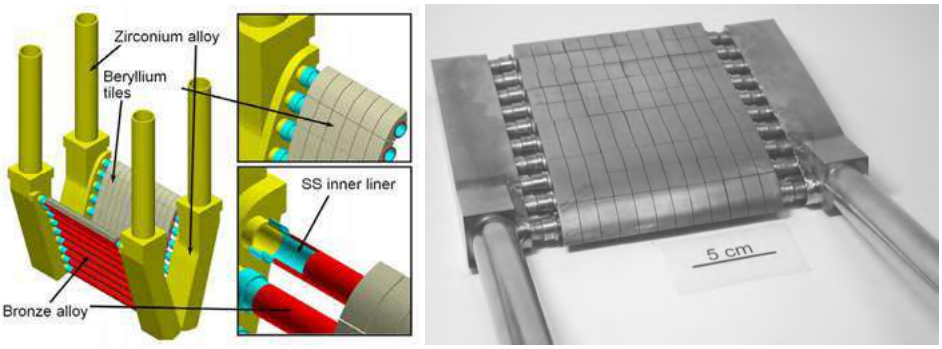

Fig. 1. The first Be-tiles based neutron converter concept developed: final target layout (left). First, full-scale, half target prototype constructed (right)

onto 0.3 mm thickness SS pipe, thus avoiding the corrosion of copper alloy by the coolant, with the following quenching and ageing manufacturing process. Such a pipe structure allows for the application of the well-developed Be-Cu joint technology. On the other hand the peculiar V-shaped like target profile has been selected to meet the design criteria to get a compact neutron yielding volume, while removing the total heat load impinging (150 kW). The spot area is limited at 130x170 mm^2 on each target half, which fulfills the main requirement of a peak-power density as low as ~0.7 $kWcm^{-2}$ (along beam axis direction), providing proper engineering safety margins. The maximum power density lies along the centerline of each target half surface, while reducing at the extremities, as shown in Figure 2, following the SPES RFQ parabolic beam power profile. Due to the geometry of the cooling system full turbulent flow conditions are achieved (Re ~$4 \cdot 10^4$) with the light water speed of 4 ms^{-1}. In such a way a heat transfer coefficient as high as $6 \cdot 10^4$ $Wm^{-2}K^{-1}$ is gained. The coolant inlet temperature is fixed at 20°C, with a mass flow rate of 10.8 m^3h^{-1}, while the working water pressure being 0.3 MPa. Notwithstanding the first prototype constructed, a new technological research program started, aiming at constructing a neutron converter made of bulk beryllium only. All the target system: manifolds, cooling pipes, and the neutron converter layer have, therefore, to be manufactured starting from a full Be block. The main advantage of such a solution is less assembling parts and considerably less brazing joints. Moreover, the same neutron yielding of Be-tile converter would be provided, with an improvement in the neutron moderating power due to beryllium target itself. In such a way a higher neutron flux per unit accelerator current may be provided at the beam port. On the contrary a significant cut in the prompt capture gamma yielding by target structural materials is gained as well. After a feasibility study by LNL and Efremov Institute, the first full-scale prototype, shown in Figure 3, was assembled on mid 2005. The new target positively passed the preliminary He leakage tests in late summer 2005, thus proving the proper manufacturing process adopted. The Be-bulk neutron converter works with a slightly larger beam spot area (120x210 mm^2) on each target half, in order to lower the peak power density down to 0.5 $kWcm^{-2}$, thus obtaining larger engineering safety margins.

3. Thermal stress analyses

A detailed coupled thermal-mechanical analysis has been performed on target models during the design study to assess the maximum working temperatures and the related mechanical stresses and

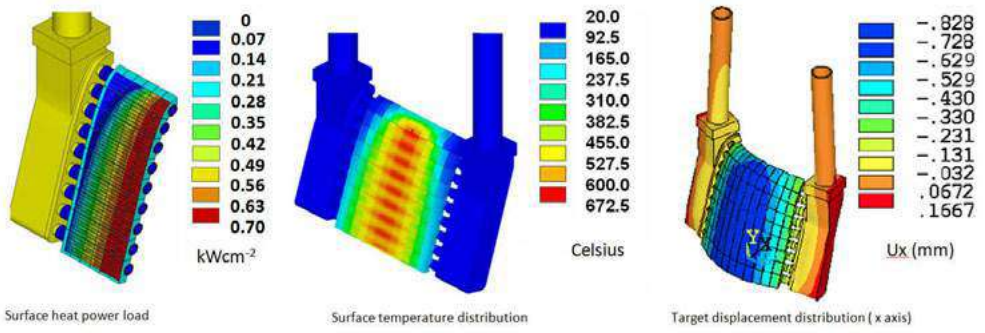

Fig. 2. Be-tiles target model for thermal stress calculation response in steady state operation: heat power distribution on surface (left). Resulting temperature distribution (center). Induced target deformations (displacements along beam normal direction) (right). ANSYS® code

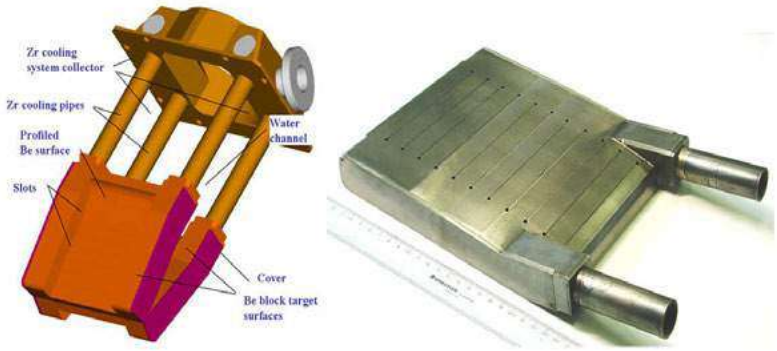

Fig. 3. The Be-bulk type neutron converter developed: final target layout (left) with beam collimator. First, real-scale, half target prototype constructed (right)

deformations induced, under both static and cycling loading operating conditions. The main results of steady state thermal analysis are reported in Figure 2 for the Be-tiles target model only. The maximum temperatures calculated in the different target components: beryllium hitting surface (673°C), Cu-alloy pipes (362°C), SS pipe liners, (344°C) and Zirconium alloy cooling feed system (21°C), are well below the corresponding melting points. The average temperature estimated in Be material is about 400°C. Moreover the stress intensities and deformations calculated at loading (beam on) and unloading (beam off) stages in all structural parts have turned out to be within the allowable design limits. The target model also fulfills the other critical design requirement to pass the limit of 2000 hrs lifetime, under 200 thermal cycles (the beam is on and off per each run).

4. The e-beam test results on target prototypes

After a preliminary series of thermal-stress tests performed on Be-tiles and Be-bulk mock-ups under different power density levels up to 1.1 $kWcm^{-2}$, both target prototypes constructed were finally tested at the High Heat Flux (HHF) Tsefey facility at the Efremov Institute, which maximum electron beam power available is 60 kW. The electron scanning beam was tuned to heat the target surface with a power deposition having a parabolic profile, quite close to the real one which will be provided by the RFQ proton accelerator. The first, full-scale, Be-tiles based half-target prototype, successfully passed the preliminary series of both operative and critical scanning e-beam tests with power densities up to 0.8 $kWcm^{-2}$ in March-July 2005. After 2000 thermal cycles (ten times higher than requested) the target inspection has shown no any visible damage or cracks on Be tiles. The second, full-scale half target prototype developed (Be-bulk) has undergone the same operative and critical power test conditions in fall 2006, with peak power densities ranging from the designed 0.5 $kWcm^{-2}$ up to 0.7 $kWcm^{-2}$ (see Fig. 4). As a result the half target positively passed the test: no visible damage (cracks) has been observed by the visual inspection on the heated surface. Therefore this second target version may be considered as a possible alternative solution for the BNCT facility.

5. Status on the radiation damage tests plan

The basic knowledge about the mechanical properties degradation the Be target undergoes during operation (i.e. hardening and embrittlement), is fundamental for the assessment of both the target reliability, and the lifetime estimation. For such a goal MCNPX calculations have been performed on

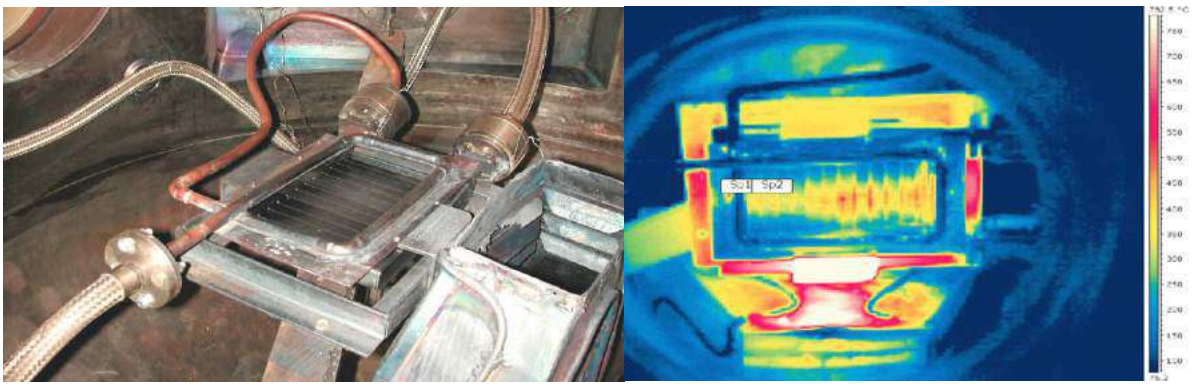

Fig. 4. Be-bulk target prototype mounted on support inside the Tsefey electron beam testing facility (left). Target surface temperature measured with IR camera during each thermal cycle (right)

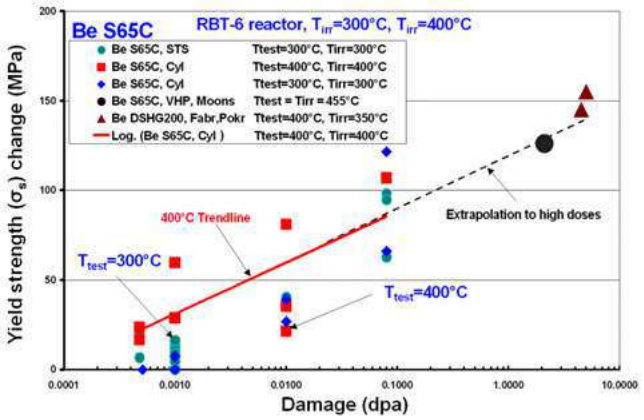

Fig. 5. Radiation hardening effect on Be-S65C alloy irradiated and tested both at 300 ºC and 400 ºC

the last version of the irradiation facility modeling, including the real-like target geometry (Ceballos et al., 2008). The results point out that the damage due to the neutron fluence level expected (10^{19} cm^{-2}), is estimated to be 0.05 dpa (displacement per atom) after the scheduled 2000 hrs of operation. On the other hand the related damage due to the high intensity RFQ proton beam inside the first layers (≤ 300μm) from the Be surface, is estimated to be within 0.1÷1 dpa. Therefore it would be reasonable to investigate the radiation resistance of the Be alloy in the dose range of 10^{-3}÷0.1 dpa, where the material bulk properties should change. Taking into account the two different processes involved, a radiation damage test has therefore been planned in two basic steps. The first one, based on the neutron irradiations at different fluence levels inside Material Testing Reactor (MTR) facilities has already been completed. A given number of two standard STS planar and cylindrical type specimens were manufactured from the same beryllium target material (Be S65C alloy). Four irradiation facilities were loaded with specimens and inserted in a proper channel inside the core of the RBT-6 MTR at Dimitrovgrad (Russia), rated 6 MW nominal power where a $\Phi_{total}=5\cdot10^{13}cm^{-2}s^{-1}$ fluence rate is available. In such a place the fraction of neutrons with energy higher than 0.1 MeV is about $N_{0.1}/N_{tot}=0.6$. Such a parameter, which gives the quality of neutron spectrum used for radiation damage testing, is in close agreement with the one expected in the target region inside the BNCT facility at the given operating condition ($N_{0.1}/N_{tot}=0.63$). The local neutron fluence has been measured for each facility using the standard foil activation technique, while the irradiation temperature has been controlled during all the experiments long to be 300°C and 400°C within ±15ºC (close to the target operative average temperature) by a system of local thermocouples. Both unirradiated and irradiated samples were then standard tensile tested in the temperature range (20-400)°C. Temperature-damage dependencies of the mechanical properties of Be alloy were obtained within the range (20-400)°C at different neutron fluence levels. The main results plotted in Figure 5 point out that, in the investigated damage interval of 0.005–0.1 dpa, the Be alloy retains its strength and ductile bulk properties within the allowable limits. Additional information may be found in (Esposito, et al, 2008). The second step of the planned radiation damage tests using proton beams are scheduled to be completed in 2008.

References

Prete, G., 2007. SPES Advanced Exotic Ion Beam facility at LNL, Technical Design Report, INFN-LNL-220 (2007).

Pisent, A. Comunian, M., Palmieri, A. Fagotti, E., Lamanna, G.V., Mathot, S., 2004. The TRASCO SPES-RFQ, Proc.of the LINAC , Lübeck, Germany, 69-71. JaCoW eds.

Ciavola, G., Celona, L., Gammino, S., 2001. First Beam from the TRASCO Intense Proton Source (TRIPS) at INFN-LNS, Proc. of the PAC, Chicago, U.S.A, P. Lucas and S. Webber eds. 2406- 2408

Fagotti, E., Palmieri, A., 2007. Results of SPES source improvements, LNL Annual Report, INFN-LNL-222(2008), ISSN 1828-8545, 171-172

Ceballos, C., Esposito, J., 2008. The BSA modeling for the Accelerator-Based BNCT facility at INFN LNL for treating shallow skin melanoma, this proceeding.

Colonna, N., Beaulieu, L., Phair, L., Wozniak, G. J., Moretto, L. G., Chu, W. T. , Ludewigt, B. A., 1999. Measurements of low-energy (d,n) reactions for BNCT, Med. Phys. 26, 793-798.

Bair, J.K., Miller, P.D., Wieland, B.W., 1981. Neutron Yields from the 4-12 MeV Proton Bombardment of ^{11}B, ^{13}C and ^{18}O as Related to the Production of ^{11}C, ^{13}N and ^{18}F, App. Rad. Isot., 32, 389-395.

Taskaev, S ., Bayanov, B., Belov, V. Zhoorov, E., 2006. Development of lithium target for accelerator based neutron capture therapy, Advances in Neutron Capture Therapy 2006. Proceedings of ICNCT-12. Nakagawa, Y.; Kobayashi, T.; Fukuda, H. (Eds). International Society for Neutron Capture Therapy, 81– 84.

Makhankov, A. et al., 2004. An accelerator based thermal neutron source for BNCT application, Proc. of EPAC 2004, Lucerne, Switzerland, July 5-9, 2004, p. 2745-2747, European Physical Society. Accelerator Group (EPS-AG) eds, ISBN 92-9083-231-2 (Web version)

Esposito, J. et al., 2008. The SPES-BNCT project: Investigation of radiation damage effects in Be neutron converter prototype" LNL Annual Report, INFN-LNL-222(2008), ISSN 1828-8545, 173-174

High Power Accelerator-Based Boron Neutron Capture with a Liquid Lithium Target and New Applications to Treatment of Infectious Diseases

S. Halfon[a,b], M. Paul[b], D. Steinberg[c], A. Nagler[a], A. Arenshtam[a], D. Kijel[a], I. Polacheck[d], A. Rubinstein[e] and M. Srebnik[f]

[a]*Soreq NRC, Yavne, Israel 81800*
[b]*Racah Institute of Physics, Hebrew University, Jerusalem, Israel 91904*
[c]*Biofilm Laboratory, Institute of Dental Sciences, Faculty of Dentistry, Hebrew University-Hadassah*
[d]*Clinical Microbiology and Infectious diseases, Hadassah-Hebrew University Medical Center*
[e]*Department of Pharmaceutics, School of Pharmacy, Hebrew University of Jerusalem, Jerusalem 91120, Israel*
[f]*Department of Medicinal Chemistry and Natural Products, School of Pharmacy, Hebrew University, Jerusalem, 91120, Israel*

Abstract

A new conceptual design for Accelerator-based Boron Neutron Capture Therapy (ABNCT) facility, based on the high-current low-energy proton beam from the linear accelerator at SARAF (Soreq Applied Research Accelerator Facility) incident on a windowless forced-flow liquid-lithium target, is described. The liquid-lithium target, currently in construction at Soreq NRC, will produce a neutron field suitable for deep-tissue BNCT, through the reaction ^{7}Li(*p,n*)^{7}Be. The liquid-lithium target is designed to overcome the major problem of solid lithium targets, namely to sustain and dissipate the power deposited by the high-intensity proton beam. Together with diseases conventionally targeted by BNCT, we propose to study the application of our setup to a novel approach in treatment of diseases associated with bacterial infections and biofilms, *e.g.* inflammations on implants and prosthetic devices, Cystic Fibrosis, infectious kidney stones. Feasibility experiments evaluating the boron neutron capture effectiveness on bacteria annihilation are taking place at the Soreq nuclear reactor.

Keywords: Accelerator-based BNCT, target, liquid lithium, infectious diseases.

1. Introduction

Suitable neutron sources for BNCT have been limited for many years to nuclear reactors (Harling et al., 2003). A reactor can produce a sufficient neutron flux for therapy, around 10^{9} cm^{-2}s^{-1} at irradiation facility beam port, for reasonable therapy duration (30-90 min) (Barth et al., 2005). However, the source energy spectrum is usually moderated to the thermal range, when superficial tumors treatments are requested. The optimization of the neutron energy spectrum for the maximum benefit to the patient in therapy of deep-seated tumors has been studied in the last fifteen years (Bisceglie et al, 2000). The epithermal neutrons, lying in the energy range 0.5 eV<E<10 keV, have been assessed as ideal for therapy of such tumors.

2. Accelerator-based BNCT

A neutron source based on a low-energy, high-current light-ion accelerator has the potential for meeting the requirements for a clinical BNCT facility (Blue et al. 2003). The flexibility to choose the target material and the ion energy and current allows the design of the most suitable neutron field (energy spectrum and flux) for therapy. Accelerators are also of small size, which can be located in hospitals with simplified licensing and regulations, reasonable cost and good public acceptability. The main efforts in the last years to design a neutron converter for an accelerator-based BNCT facility have been mainly focused on the use of lithium through the reaction ^{7}Li(*p,n*)^{7}Be (Blue et al. 2003) (Lee et al., 2000) (Kononov, et al., 2003) at proton energies of 1.9-2.5 MeV. The major advantage of this reaction consists in its low-energy neutron spectrum (mean neutron energy in the range of 34-326 keV). Neutrons lying in such an energy range require less moderation volumes in order to get to the desired BNCT neutron spectrum than those generated in other target materials suggested for this purpose, such as beryllium and carbon (Blue et al. 2003). Moreover smaller moderator volumes imply fewer neutron losses due to capture reactions, with higher neutron intensity per unit accelerator current. The lithium target neutron yield allows the use of smaller and cost-effective accelerators with a current of ~5 mA (Lee et al., 2000).

However, despite the excellent neutronic qualities of the ^{7}Li(p,n)^{7}Be reaction, a reliable a lithium target, working under beam power levels considered for such a purpose, has been considered as very difficult to build because of the mechanical, chemical and thermal properties of lithium (low melting point of 180 °C and low thermal conductivity of 85 W/m-K at 300 K), the major problem being to remove the thermal power generated by the high-intensity proton beam.

3. Liquid-Lithium Target

A Liquid-Lithium Target (LiLiT) based on a windowless forced liquid-Li flow, is designed to produce neutrons through the ^{7}Li(p,n)^{7}Be reaction and serve as power dump for a high-intensity proton beam (~2 MeV, 2- 4 mA). The proton beam will be obtained from the SARAF superconducting linear accelerator (Nagler, et al., 2006), currently in construction at Soreq NRC. The design of the target is based on a prototype liquid-lithium loop that has been developed at Argonne National Laboratory for use as a fragmentation target and a stripper in a new generation of heavy-ion accelerators. The lithium flow has been successfully tested for power dissipation, using a 1 MeV, 20 kW electron beam (Reed et al., 2004). The intensive research for IFMIF (a 250 mA, 40 MeV deuteron accelerator (Ida et al., 2002)) has been exploited as well. The liquid-lithium loop (Fig. 1) is designed to generate a stable lithium jet at a velocity higher than 20 m/s, on a concave supporting wall with free surface towards the incident proton beam. The liquid lithium flow at a temperature of 225 °C is driven by an electromagnetic induction pump. The local temperature rise due to full beam power is expected to be between 80 to 100°C, minimizing risks of evaporation, bubble formation or instabilities. The lithium flow is collected into a containment tank (Fig. 1B) in which a heat exchanger dissipates the beam power. In order to study the conditions of the jet, an experiment was conducted with water, of similar hydrodynamic properties as liquid Li. The water velocity was up to 26 m/s and the simulation results showed a stable water film with minimal waviness. ^{7}Be will be produced in the lithium target by the interaction of the proton beam with lithium, through the reaction ^{7}Li(p,n). This nuclide has half life of 53 days and emits a 478 keV gamma radiation. The ^{7}Be atoms are expected to accumulate in the colder parts of the loop (Kato et al., 1998), the cold trap and the heat exchanger; a proper shielding of these areas will reduce the ^{7}Be dose risk.

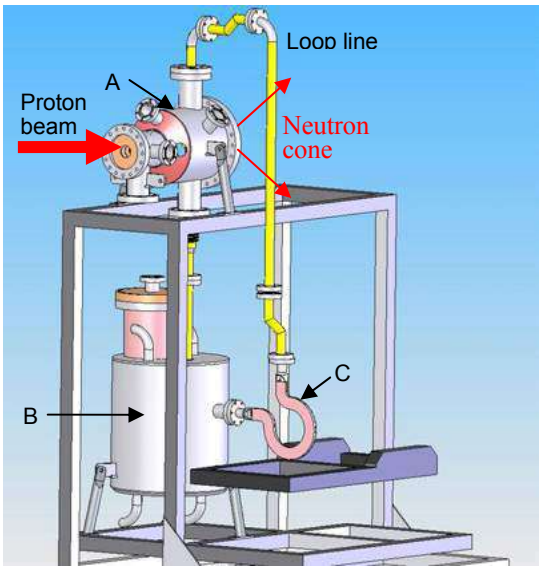

Fig. 1. Liquid lithium loop design: A- Target chamber (with lithium nozzle), B- Lithium containment tank (with heat exchanger and ^{7}Be cold trap), C- Electro magnetic pump loop (the pump is not illustrate)

4. Neutron production and tailoring

For an incident proton energy $E_p \approx 1.91$ MeV, the emitted neutrons are forward-collimated into a cone with a full-opening angle of ± 60°, average energy of 42 keV and total yield of $2.4\text{x}10^{10}$ n/mA. At higher energies ($E_p \approx 2$ MeV) neutrons are also emitted at rear angles, but most of them are still emitted at angles smaller than ± 51°, the average energy of which is 75 keV and the total yield is $1.1\text{x}10^{11}$ n/mA (Lee et al., 1999). A moderator/reflector assembly will be built to get a neutron beam having both spectrum and fluence rate requested for the treatment. Thus the assembly is designed to: (*i*) moderate the fastest neutrons to below 10 keV; (*ii*) filter out the neutrons with energy lower than 0.5 eV; (*iii*) reduce γ-ray contamination. The facility design must provide a fluence rate of usable neutrons (0.5 eV-10 keV) sufficient to provide therapeutic doses in reasonable times (30-90 min). Water as a moderator and Al_2O_3 as a reflector have been shown to be ideal for ^{7}Li(p,n) near-threshold BNCT (Kudchadker, 1996). A conceptual model of our liquid-lithium target and moderator-reflector assembly is shown on figure 2. The moderator geometry is based on Lee et al., 2000, where Monte Carlo calculations showed that near threshold, a 5-mA proton beam can produce therapeutically useful neutron beams with a water moderator. Graphite, LiF, MgF_2, CaF_2, C_6F_6 and Teflon are also considered as alternative moderators

due to the extreme reactivity of liquid lithium with water and the associated safety requirements. The photon production in the target include mostly 478-keV γ rays from inelastic proton scattering ($p,p'\gamma$). The addition of a layer of lead or bismuth between the target and the moderator is considered in order to attenuate the γ-ray intensity at the patient station. As thermal-neutron shield, a ^{6}Li thin sheet (0.01-0.03 cm) between the moderator and the patient or phantom would be most effective (Lee et al., 2000). Cadmium is not viable for this purpose, despite its high thermal neutron absorption cross section, since it produces large number of thermal-neutron capture γ- rays.

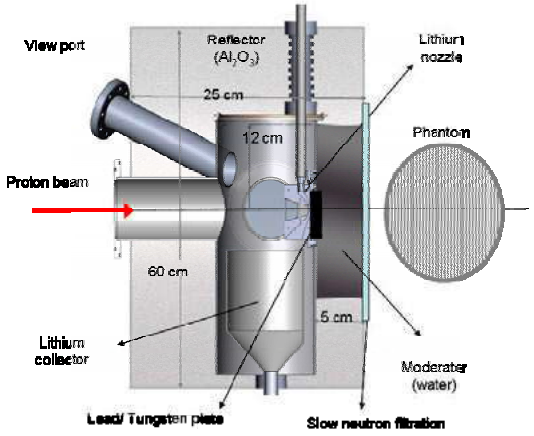

Fig. 2. Conceptual model of our liquid-lithium target (LiLiT) with moderator/ reflector assembly for BNCT

5. BNCT of infectious diseases

Accelerator-based BNCT can in principle be applied in a wide variety of clinical problems. We are presently investigating a novel approach for the treatment of infectious diseases stemming from biofilms. Biofilms are composed of microorganisms in a hydrated polymeric matrix of their own synthesis, attached to a biological or non-biological surface such as medical implants or devices.

The mode of growth of this microorganism, composed mainly of bacteria and fungi, is not completely understood. Bacteria in biofilms have however different characteristics than in their regular mode of growth. For example, they can be up to 1500 times more resistant to antibiotics and immune chemicals. Biofilms are associated with many infectious diseases and inflammatory processes such ear, nose and throat (ENT) infections, implant infections, bacterial endocarditis, bacterial kidney stones, cystic fibrosis to name a few of a growing list of maladies.

The BNCT methodology described here can be beneficial in this context. We envision that BNCT will significantly degrade biofilms on medical devices, in cavities and other organs and prosthetic implants and will provide a non-invasive procedure that is less threatening to the patient, cost effective and at the same time will help to reduce resistance to common antibiotics.

6. Preliminary experiments

In order to study the feasibility of the concept, we are conducting experiments evaluating the effectiveness of boron neutron capture for killing bacteria, using the Soreq NRC nuclear reactor. Previous studies performed pointed out that an efficient BNCT treatment requires a local fluence of 10^{12} n/cm^2 on targeted cells and a ^{10}B concentration of ~20 µg/g at target cells (or ~10^9 atoms/cell) (Barth et al., 2005). In these conditions, 2 or 3 neutron capture events are occurring in the target cell or within the range of the ionizing particles produced. Studies on the radiobiology of α-particles (Raju et al., 1993) also showed that the number of α's (with energy similar to that produced by ^{10}B neutron capture) required for one lethal lesion per cell, is in the range of 2-6 (depending on the cell type and their nucleus size).

Following these results, our experimental conditions of thermal neutron flux (applicable since no tissue penetration is required), irradiation time and boron concentration were set to ensure at least one $^{10}B(n,\alpha)^{7}Li$ reaction to occur at the bacterium periphery. The neutron flux was measured at several locations in the reactor experimental hall, using the gold activation method.

The reactor tangential tube was found to be the most suitable for the experiment, with a neutron flux >10^7 n/cm^{2}s^{-1}, a cadmium ratio of ~8 and relatively low gamma radiation (<100 R/h). Since the neutron flux is relatively low, the irradiation time was set to 6-8 hours and the ^{10}B concentration was 4.5 µg/g. We evaluated that in these conditions there would ensure around one $^{10}B(n,\alpha)^{7}Li$ reaction within a 5 µm radius of each bacterium.

Small polyethylene ampoules containing the bacteria *Streptococcus mutans* in Brain Heart Infusion (BHI) media and boron compound (FOX6) (Jabbour, et al., 2004) at different concentrations were placed in the tangential tube and exposed to the neutron flux from the Soreq reactor. Control samples (no neutron irradiation) were prepared in the same way.

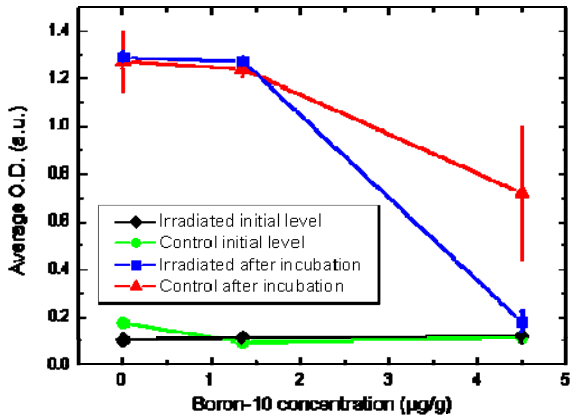

Fig. 3. Average optical density (O.D.) as a function of ^{10}B concentration for a 6.25 hr. neutron irradiation of samples (see text) and for control samples, before and after 20 hr. incubation

Preliminary results of these experiments are shown in figure 3. The optical density (O.D.) of the solution containing bacteria in aqueous phase is a measure of the amount of bacteria present, when the background sample (BHI) is set as O.D. zero. In figure 3 the average O.D. of samples that were irradiated with neutrons for 6.25 hours and then incubated at 37 °C for 20 hours is shown together with the O.D. from identical control samples, incubated for the same time. The O.D.'s were measured before and after the incubation.

A minor effect on bacteria growth in the highest ^{10}B concentration was measured in the control group (although the standard deviation is large). The irradiated group shows a significant reduction in the O.D. at ^{10}B concentration of 4.5 µg/g.

The growth of bacteria was affected by the combined irradiation and ^{10}B, but there was no total elimination of the bacteria. It is possible that the damage is not a direct killing of the bacteria, but a damage influencing bacteria growth. We are pursuing the study of the effect of BNC on bacteria killing and growth at the Soreq nuclear reactor.

7. Conclusions

The concept of a windowless liquid-lithium jet target is potentially suited to produce an epithermal neutron flux by bombardment of a high-intensity (mA range) proton beam and we are presently building a prototype target. The utilization of BNCT for the treatment of biofilm and bacterial diseases is under investigation.

References

Barth, R.F. et al., 2005. Boron neutron capture therapy of cancer: current status and future prospects. Clin. Cancer. Res., **11**, 3987-4002.

Bisceglie, E. et al., 2000. On the optimal energy of epithermal neutron beams for BNCT. Phys. Med. Biol. **45**, 49-58.

Blue, T.E. et al., 2003. Accelerator-based epithermal neutron sources for boron neutron capture therapy of brain tumors. J. Neurooncol **62**, 19-31.

Harling, O. and Riley, K., 2003. Fission reactor neutron sources for neutron capture therapy- a critical review. J. Neurooncol **2**, 7-17.

Ida, M. et al., 2002. Thermal hydraulic characteristics of IFMIF liquid lithium target. Fusion Engineering and Design **63-64**, 333-342.

Jabbour, A. et al., 2004. Synthesis and Evaluation of Oxazaborolidines for Antibacterial Activity against *Streptococcus mutans*. J. Med. Chem. **47**, 2409-2410.

Kato, Y. et. al., 1998. Impurity control in liquid lithium loop for IFMIF target facility. Journal of Nuclear Materials 258-263, 394-399

Kononov, E. et al., 2003. Neutron source for boron neutron capture therapy based on the reaction ^{7}Li(p,n)^{7}Be near threshold. Atomic Energy, **94**, 417-420.

Kudchadker, R.J., 1996. Optimized accelerator based epithermal neutron beams for boron neutron capture therapy. Ph.D. dissertation, University of Missouri- Columbia.

Lee, C.L., Zhou, X.L., 1999. Thick target neutron yields for the ^{7}Li(p,n)^{7}Be reaction near threshold. Nucl. Instr. and Meth. in Phys. Res. B **152**, 1-11.

Lee, C.L. et al., 2000. A monte carlo dosimetry-based evaluation of the ^{7}Li(p,n)^{7}Be reaction near threshold for accelerator boron neutron capture therapy. Med. Phys. **27**, 192-202.

Nagler, A., et al., 2006. Statues of the SARAF project. Proc. of Linac 2006, Knoxville, Tennessee, USA, MOP054, 168-170.

Raju, M.R. et al., 1993. Radiobiology of alpha particles IV, cell inactivation by alpha particles of energies 0.4-3.5 MeV. Radiation Research **133**, 289-296.

Reed, C.B. et al., 2004. A 20 kw beam-on-target test of a high-power liquid lithium target for RIA. Nucl. Phys. A **746,** 161c-165c.

The Study of Physics and Thermal Characteristics for In-hospital neutron irradiator (IHNI)

Ke-Guotu[1] Sun-Ziyong[1] Lv-Zheng[1] Shen-Feng[1] Liu-Tiancai[1] Zhou-Yongmao[2]

[1] *China Institute of Atomic Energy, Beijing, 102413, China*
[2] *China Zhongyuan Engineering corporation, Beijing, 10083, China*

Abstract

The IHNI is designed for Boron Neutron Capture Therapy (BNCT) based on Miniature Neutron Source Reactor(MNSR). The reactor with thermal power 30Kw is an undermoderated reactor of pool-tank type, and UO_2 as fuel, light water as coolant and moderator, and metallic beryllium as reflector. The fission heat produced by the reactor is removed by the natural convection.

The paper gives the calculating results of critical mass and the worths of central control rod, auxiliary control rod, reactivity regulator and neutron beam equipments. The parameters at thermal and small thermal ports and at epithermal port were calculated by optimizing combination of kinds of material by MCNP code. The dynamic feature research was done by RELAP5 code when the reactivities of 3 mk, 4.5mk and 6mk were inserted respectively. The results shown that the reactor power can be limited to safe level by itself owing to the Doppler effect of fuel element and moderator negative temperature effect when the 6mk reactivity was inserted to reactor.

KEYWORDS: MNSR LEU BNCT NAA

1 Introduction

The INHI[1] is composed of an innovated Miniature Neutron Source reactor (MNSR) of 30kW; two neutron beams, one of it is thermal neutron beam and the other is epithermal neutron beam; and the corresponding neutron capture treatment(NCT) medical research and treatment facility. A great number of optimizing Calculations have been done through program MCNP for the material, geometry and size of the neutron energy regulator, neutron reflector, and the gamma ray attenuator. The reactor design is gained of the maximum ratio value of irradiation flux (at port) to reactor unit power.

2 Decrease the uranium enrichment of MNSR

The fuel meat of present MNSRs adopts high enrichment uranium, which is advantageous for high neutron flux obtained. But the alteration of fuel from HEU to LEU is a worldwide tendency for ensuring the nuclear facilities are utilized as peace purpose.

When the fuels rods are replaced with low enrichment uranium, the quantity and the arrangement of rods are also changed for assurance the criticality of the reactor. At the same time, the side-shields of the core are adjusted to fit the demand of facilities.

Fig.1 shows a diagram of INHI. However, which percent of enrichment of uranium should be adopted and how many fuels rods should be install in core are optimized considering the criticality, the life-time of the reactor, the flux, etc. Many cases are calculated and the results are shown in table 1.

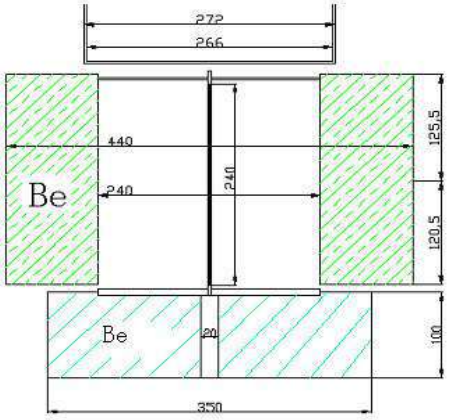

Fig. 1. The structure of INHI

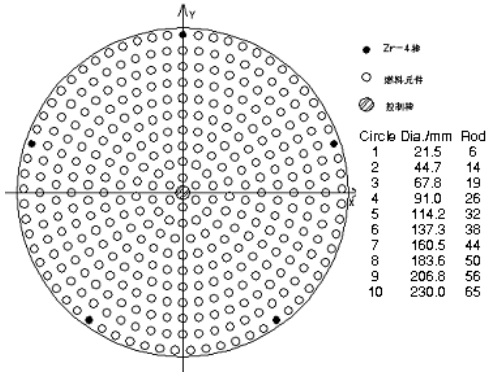

Fig. 2. The fuel arrangement

Table 1. The results of critical calculation

^{235}U Enrichment	$H/^{235}U$	Quantity of fuel	Load of ^{235}U(g)	K_{eff}		
				The thickness Beryllium up-shield 110mm		No up-shield
				Bottom Be shield 50mm	Bottom Be shield 100mm	Bottom Be shield 100mm
13 %	180	324	1308.00	1.082543	1.091542	1.071206
	190	310	1251.49	1.076762	1.085678	1.065526
	200	296	1194.97	1.070002	1.078822	1.058891
14 %	180	304	1321.65	1.085804	1.094784	1.074499
	190	291	1265.13	1.079590	1.088481	1.068399
	200	278	1208.62	1.072355	1.081148	1.061289
15 %	180	287	1336.85	1.088185	097140	1.076923
	190	274	1276.29	1.081107	1.089966	1.069968
	200	262	1220.40	1.073879	1.082643	1.062860

The natural cooling manner is adopted when the reactor is operating. For a given reactor power, when more fuels rods are loaded, the heat released from one rod is lower, as the result, the reactor would be safer if more fuels rods are loaded. Additionally, the Keff shown in table1 are too large for a MNSR, despite the accessories are not considered. Thus the final parameters of the reactor are as follow, 12.5%wt enrichment of uranium-235, 350 lattices of fuels elements are prepared.

The arrangement of fuel rods is shown in fig. 2.

3 INHI Facilities[2]

3.1 Neutron beam equipments and design target

The INHI facility contains two sets of filters—thermal neutron beam facility and epithermal neutron beam facility. For thermal neutron beam facility the moderator is adopted graphite, and aluminum and Al_2O_3 are adopted in epithermal neutron beam facility to slightly moderate the fast neutrons coming from the reactor core into epithermal neutrons (0.4eV~10keV). Another materials, FLUENT Al (30%Al, 69%AlF_3, 1%LiF), are also attempted for epithermal neutron beam, but it was not adopted finally for its high price.

The structure of INHI and its two neutron beam equipments are shown in fig. 3. The gamma shielding materials are bismuth and lead and Plumbum-Poly as well, boron-poly and lithium-poly are adopted for neutron shielding.

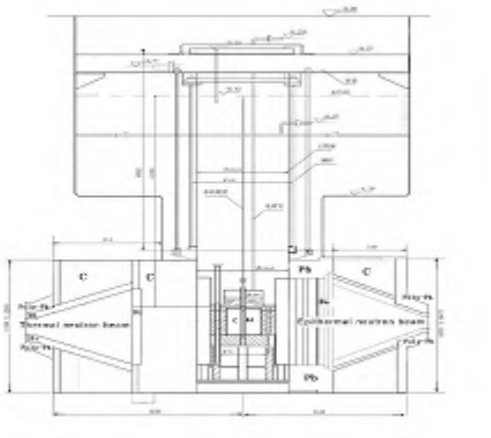

Fig. 3. The structure of INHI

The design targets of BNCT facilities are
For thermal neutron beam

- ✧ Thermal neutron flux at the beam tube exit $>1\times10^{9}$n/cm^{2}-s
- ✧ The dose due to fast neutrons and epithermal neutrons $<1\times10^{-11}$cGy/(thermal flux)
- ✧ The dose due to gammas $<2\times10^{-11}$cGy/(thermal flux)

For epithermal neutron beam

- ✧ Epithermal neutron flux at the beam tube exit $>5\times10^{8}$n/cm^{2}-s
- ✧ The dose due to fast neutrons $<2\times10^{-12}$cGy/(epithermal flux)

The dose due to gammas $<2\times10^{-12}$cGy/(epithermal flux)

3.2 Calculation results

The main results of two neutron beam equipments are listed in table 2 and 3, when the power of the reactor is 30kW.

At the exit of the radiation filters, the thermal neutron flux is calculated as 2.14×10^{9}n/cm^{2}-s in thermal neutron beam equipment, and the epithermal neutron flux is calculated as 4.0×10^{8}n/cm^{2}-s in epithermal neutron beam equipment.

Using the RELAP5 code, the dynamic feature research was performed when the reactivities of 3 mk, 4.5mk and 6mk were inserted respectively. See fig. 4.

When a certain amount of positive reactivity is inserted into the reactor suddenly, the power will be increased suddenly, however, it will turn to the normal value due to the negative temperature effect. Fig.4 shows that the maximum peak power value for 4.5mk reactivity release is 110.72kW.

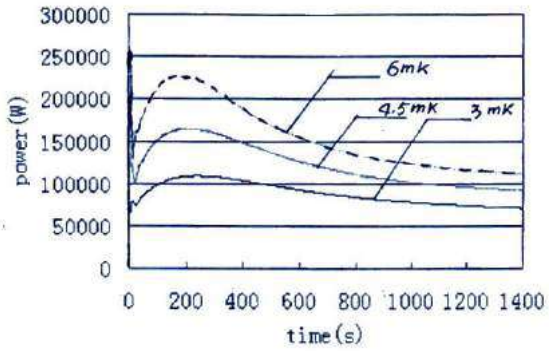

Fig. 4. Power changes with the reactivity release

Table 2. The results of the exit of thermal neutron beam

Characteristics	Unit	Results
ϕ_{th} **(<0.4eV)**	n.cm^{-2}.s^{-1}	2.14×10^{9} (±0.41%)
ϕ_{epi} **(0.4eV-10keV)**	n.cm^{-2}.s^{-1}	9.12×10^{7} (±1.39%)
ϕ_{f} **(>10keV)**	n.cm^{-2}.s^{-1}	2.56×10^{7} (±2.66%)
$\boldsymbol{\phi_n}$	n.cm^{-2}.s^{-1}	2.26×10^{9} (±0.40%)
$\boldsymbol{\phi_\gamma}$	γ.cm^{-2}.s^{-1}	2.63×10^{7} (±1.10%)
$\dot{D}_{epi}$	cGy.s^{-1}	6.72×10^{-4} (±2.95%)
$\dot{D}_{f}$	cGy.s^{-1}	3.57×10^{-2} (±3.78%)
$\dot{D}_{\gamma}$	cGy.s^{-1}	2.09×10^{-2} (±1.13%)
$(\dot{D}_f+\dot{D}_{epi})/\phi_{th}$	Gy.cm^2	1.70×10^{-13}
$\dot{D}_\gamma/\phi_{th}$	Gy.cm^2	9.73×10^{-14}
$\phi_{th}/(\phi_f+\phi_{epi})$		18.36
$\boldsymbol{J_n^+/\phi_n}$		0.798
$\boldsymbol{J_n^+}$	n.cm^{-2}.s^{-1}	1.80×10^{9}

Table 3. The results of the exit of epithermal neutron beam

Characteristics	Unit	Results
ϕ_{th} **(<0.4eV)**	n.cm^{-2}.s^{-1}	1.56×10^{7} (±2.29%)
ϕ_{epi} **(0.4eV-10keV)**	n.cm^{-2}.s^{-1}	4.00×10^{8} (±0.56%)
ϕ_{f} **(>10keV)**	n.cm^{-2}.s^{-1}	3.60×10^{7} (±1.69%)
$\boldsymbol{\phi_n}$	n.cm^{-2}.s^{-1}	4.52×10^{8} (±0.54%)
$\boldsymbol{\phi_\gamma}$	γ.cm^{-2}.s^{-1}	1.91×10^{7} (±1.35%)
$\dot{D}_f/\phi_{epi}$	Gy.cm^2	5.60×10^{-13}
$\dot{D}_\gamma/\phi_{epi}$	Gy.cm^2	1.95×10^{-13}
ϕ_{epi}/ϕ_{th}		25.59
$\boldsymbol{J_n^-/\phi_n}$		0.830
$\boldsymbol{J_n^-}$	n.cm^{-2}.s^{-1}	3.75×10^{8}

4 Conclusion

The present design of both the reactor core and two sets of neutron beam equipment achieve the requirements of the applications. The study also provides a new way to utilize MNSR which is mainly used for NAA, training and teaching, testing of nuclear instrumentation now.

When a certain amount of positive reactivity is inserted into the reactor suddenly, the power will be increased suddenly, however, it will turn to the normal value due to the negative temperature, the IHNI also has the inherent safety.

The design parameters of IHNI can satisfy the requirement of BNCT, but the final loading need to be determined by the zero power experiment.

Reference

[1] Design and construction of the In-Hospital Neutron Irradiator-I. Zhou yongmao,Gao Zhixian, Li Yiguo. Proceedings of ICNCT 2006, P557.

[2] The conceptual calculation for the Neutron Beam Device at <In-Hospital Neutron Irradiator>. Jiang Xinbiao, Zhu Yangni, Gao Jijin. Proceedings of ICNCT 2006, P576

Neutrons for BNCT from the Near Threshold ^{7}Li(p,n)^{7}Be on a Thick Li-target

Tooru Kobayashi[a], Gerard Bengua[b], Kenichi Tanaka[c]

[a] *Kyoto University Research Reactor Institute, Osaka, Japan*
[b] *Medical Physics Department, Hokkaido University Hospital, Sapporo, Japan*
[c] *School of Medicine, Sapporo Medical University, Sapporo, Japan*

Abstract

The near threshold ^{7}Li(p,n)^{7}Be reaction for 1.900 MeV incident mono-energetic protons on a thick Li-target was studied as a possible practical implementation of an accelerator-based neutron source for BNCT. Neutron fields from near threshold reactions on thick targets are usually not considered suitable for BNCT because they are highly contaminated with gamma rays. Results of our parametric survey using Monte Carlo simulation showed that one of the practical approaches to near threshold neutron production via the ^{7}Li(p,n)^{7}Be reaction would be to include an effective gamma ray shield if thick targets are to be used. A 1 mm-thick Li-target having a 50 mm width and 50 mm height could be constructed more easily than a thin Li-target of a few micrometers. Candidate gamma absorbers are Bismuth and/or Lead and the chosen BDE (boron-dose enhancer) is Polyethylene. The optimum thickness of the gamma absorber was determined by means of the Protocol Depths: PD(hcp), PD(gamma) and the Treatable Protocol Depth: TPD. For an incident mono-energetic 1.900 MeV proton beam and a polyethylene BDE thickness fixed at 1.19 cm, the deepest TPD occurs when the Pb thickness is around 5 cm, and Bi thickness is around 6 cm, respectively. From the relationship between the value of TPD and the Pb(or Bi) thickness and a realistic proton current for BNCT, a practical suitable thickness of Pb or Bi layer could be around 3 cm.

Keywords: Accelerator, Near-threshold, ^{7}Li(p,n)^{7}Be reaction, Thick target, Direct neutron usage

1. Introduction

The neutron irradiation systems (NIS) for boron neutron capture therapy (BNCT) using accelerators are now under development (Blue T. et al., 2003). The properties of neutron fields from accelerators depend on both the type of neutron production reaction, such as ^{7}Li(p,n)^{7}Be, Be(p,xn), (p,spallation) of Ta or W and the incident proton energy being considered practically which is from 1.900 MeV to 50 MeV. The NIS for BNCT can be categorized in two types i.e. one is the usage with neutrons coming from beam shaping assembly (BSA) which we call "moderated neutron usage"; the other is the usage without BSA which we call "direct neutron usage (DNU)". We have been investigating the DNU which is deemed to be advantageous for hospital-based implementation because of its simpler and compact design (Tanaka K, et al., 2002). Practically there is only one choice for DNU, that is, to use the near threshold ^{7}Li(p,n)^{7}Be neutron. In earlier studies, the lithium target (Li-target) thickness for DNU had to be chosen as thin as possible to minimize the production of gamma rays in the target assembly (Lee CL, et al., 2000). This thickness was assumed in order to satisfy the practical requirements for the duration of usage and beam intensity. However, the expected degradation of the Li-target from ion-impact, operating temperatures and other factors could lead to the loss of efficiency for BNCT and the periodical replacements of the Li-target are needed in actual operation.

In our previous study, we investigated the conditions for a practical implementation of a Li-target system using the near threshold ^{7}Li(p,n)^{7}Be reaction for BNCT (Bengua G, et al., 2006) (Kobayashi T, et al., 2007). In this work, we now consider a flowing liquid metal target with a thickness of over 1 mm as a reliable target system. For the early stage of this research, we have assumed that the incident protons in the ^{7}Li target are mono-energetic. The treatable protocol depth (TPD) combined with the boron dose enhancer (BDE) of polyethylene was the primary index of evaluation applied in this study (Tanaka K, et al., 2002) (Bengua G, et al., 2004).

2. Methods

A. Li-target and Particle Transport Geometry

The neutron-producing target assembly considered in this work consists of a thick lithium layer with stainless steel for structural support. For the feasibility study on the use of thick Li-target,

only the lithium thickness was fixed at 1 mm which is large compared with the range of 1.900 MeV mono-energetic protons which is about 0.25 mm. Both neutron production and gamma ray production occurs within the thick Li-target.

The energy and angular distributions of neutrons generated via the $^{7}Li(p,n)^{7}Be$ reaction were obtained from Lee et al.'s program (Lee CL, et al., 1999). Gamma ray yields from the Li-target were computed based on the formula derived from empirical data of Lee (Lee CL, et al., 1999) and Kiss (Kiss AZ, et al., 1985). Neutron and gamma ray transport in both the target assembly and the water phantom were handled by means of the MCNPX Version 2.40 code where mesh tallies were used to determine the flux distributions (Waters LS, ed., 2002).

Statistical errors for the tallies were kept below 5% and the S(α,β) treatment of thermal neutron scattering was used. The calculation geometry for this study is shown in Fig. 1.

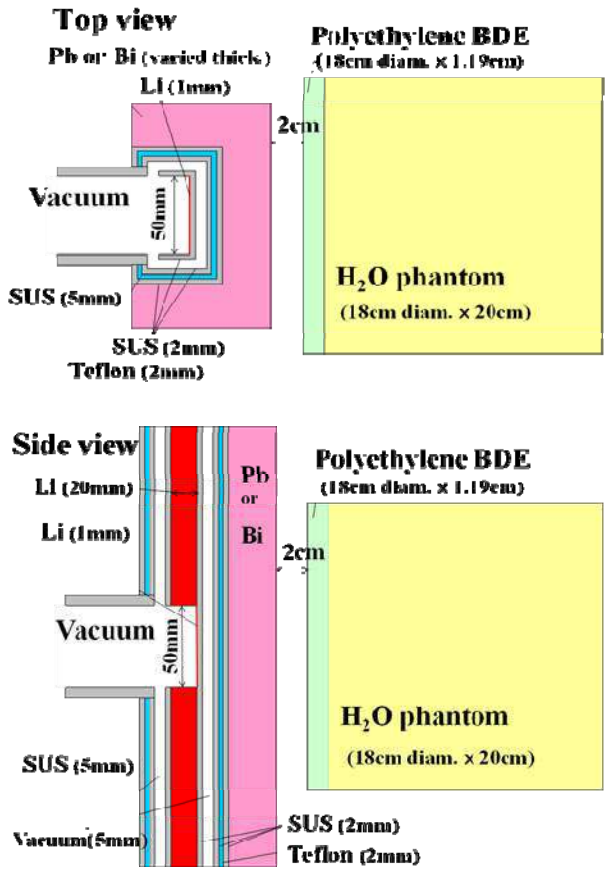

Figure 1. The irradiation set-up as represented in the MCNPX input file. Shown here are the target assembly and its structure, the BDE and phantom

The gamma ray absorber (Pb or Bi) was arranged between the housing of Li-target system and polyethylene BDE. SUS stands for stainless steel.

B. Absorbed Dose Calculation for BNCT

The absorbed dose from heavy charged particles (HCP) was computed from the neutron flux generated by MCNPX for each mesh tally in the water phantom. Conversion of particle flux to dose was carried out using the conversion factors for HCP interactions given by Caswell and Coyne (Caswell RS, et al. 1980). The total dose to normal tissue due to HCP was taken as the sum of the $^{10}B(n,\alpha)^{7}Li$ reaction at 10 ppm ^{10}B concentration, $^{14}N(n,p)^{14}C$ and elastic scattering on H,C,N and O. The total dose to tumor was computed in the same manner, differing only in the ^{10}B concentration which was set at 30 ppm. The gamma ray fluxes resulting from both the capture gamma rays of neutrons and the gamma rays from the Li-target were converted into absorbed doses using the dose conversion factors given by Hubbell (Hubbell JH, 1999). Their sum was designated as the total gamma ray dose to both tumor and healthy tissue. Here, tissue composition was assumed to be: H(11.1%), C(12.7%), N(2%) and O(74.2%) by weight percent for the absorbed dose calculation (Snyder W. S. et al., 1975).

C. Dose Evaluation Indices

From the distribution of the HCP dose to tumor, the HCP dose to healthy tissue and the Gamma ray dose to healthy tissue, the Protocol Depths PD(γ) and PD(hcp) were defined. PD(γ) is defined as the central axis depth where the dose to tumor from HCP is 15 Gy and the gamma ray dose to healthy tissue is 10 Gy. PD(hcp) is the central axis depth for which the dose to tumor and the dose to healthy tissue from HCP are both 15 Gy. TPD was defined as either PD(γ) and PD(hcp), whichever is smaller. The HCP and gamma ray dose protocols to be applied for tumor and healthy tissue were taken from the intra-operative BNCT protocol as given in Table I.

Table I. Dose protocol of the intra-operative BNCT for brain tumor (Physical doses)

	HCP	γ	HCP+γ
Treatable Dose (Gy)	15	*	*
Tolerance Dose (Gy)	15	10	*

**No particular dose is currently specified in the protocol*

In this study, the dependence of PD(γ), PD(hcp) and TPD on the Pb or Bi thickness was investigated for a polyethylene BDE thickness of 1.19 cm. The polyethylene BDE used here had the same diameter as the water phantom and was placed adjacent to the water phantom such that the BDE surface facing the neutron beam was always 20 mm away from the outside surface of the Pb or Bi layer.

3. Results and Discussion

A Li-target thicker than 0.25 mm will produce a constant yield of neutrons and gamma rays because all incident protons are stopped in it. All the dose components from the target assembly will be constant for as long as the incident proton energy remains the same. The Pb or Bi layer influences the neutron and gamma ray fields in the phantom i.e. the energy spectrum and the intensity will change according to the thickness of Pb or Bi layer.

Figures 2 and 3 show the variation of TPD for 1.19 cm polyethylene BDE according to the thickness of Pb layer and Bi layer, respectively. Tables II and III show the PD values and their respective necessary proton currents for 1 hour irradiation of BNCT. For an incident mono-energetic 1.900 MeV proton beam and a polyethylene BDE with a constant thickness of 1.19 cm, the deepest TPD was obtained when the Pb layer thickness was around 5 cm, and the Bi layer thickness was around 6 cm. From the relationship between the value of TPD and the thickness of Pb (or Bi), for a realistic proton current, a suitable thickness of the Pb or Bi layer would be around 3cm.

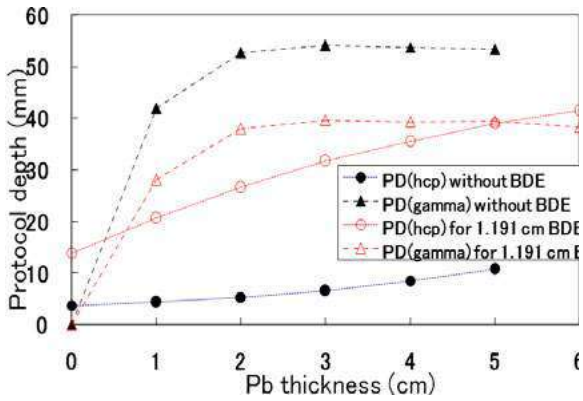

Figure 2. The PD(γ) and PD(hcp) as functions of the Pb thickness when BDE of 1.19 cm thickness is used

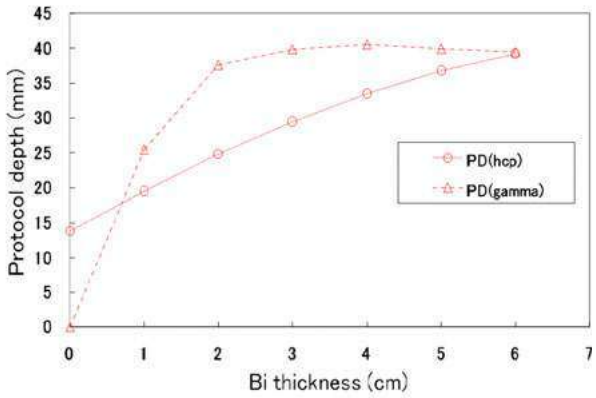

Figure 3. The PD(γ) and PD(hcp) as functions of the Bi thickness when BDE of 1.19 cm thickness is used

In our early studies, we defined TPD_{max} which is a convenient index for evaluating neutron irradiation field for BNCT (Bengua G, et al., 2006). TPD_{max} is estimated from the TPD vs BDE thickness curve for a specific BDE material, for example, TPD_{max} of polyethylene or TPD_{max} of carbon.

Therefore if we want to know the precise thickness of the Pb or Bi layer using the value of TPD_{max}, we need further simulation calculations in order to obtain the relationship between TPD and the thickness of the BDE.

However, the present results provide some suitable information to evaluate the gamma ray shielding materials for target systems of near threshold $^{7}Li(p,n)^{7}Be$ reaction using Pb or Bi.

Table II. The PD(hcp), PD(γ) and TPD as functions of the Pb thickness when BDE thickness of 1.19 cm.

BDE Thickness (cm)	Pb Thickness (cm)	PD(hcp) (mm)	PD(γ) (mm)	**TPD (mm)**	Necessary proton current *1 (mA)
0	0	3.8	**0.0**	**0.0**	1.3
0	1.0	**4.4**	41.9	**4.4**	2.7
0	2.0	**5.4**	52.6	**5.4**	4.6
0	3.0	**6.6**	54.1	**6.6**	7.2
0	4.0	**8.6**	53.7	**8.6**	10.7
0	5.0	**10.8**	53.5	**10.8**	15.1
1.19	0	13.9	**0.0**	**0.0**	1.9
1.19	1.0	**20.7**	28.1	**20.7**	6.6
1.19	2.0	**26.6**	37.9	**26.6**	10.2
1.19	3.0	**31.8**	39.6	**31.8**	14.8
1.19	4.0	**35.5**	39.4	**35.5**	20.8
1.19	5.0	**39.1**	39.5	**39.1**	28.4
1.19	6.0	41.5	**38.4**	**38.4**	34.4

*1: necessary proton current for 1 hour Irradiation for BNCT.

Table III. The PD(hcp), PD(γ) and TPD as functions of the Bi thickness when BDE thickness of 1.19 cm.

BDE Thickness (cm)	Bi Thickness (cm)	PD(hcp) (mm)	PD(γ) (mm)	**TPD (mm)**	Necessary proton current *1 (mA)
1.19	0	13.9	**0.0**	**0.0**	1.9
1.19	1.0	**19.5**	25.5	**19.5**	6.3
1.19	2.0	**24.8**	37.6	**24.8**	9.3
1.19	3.0	**29.4**	39.9	**29.4**	13.2
1.19	4.0	**33.5**	40.6	**33.5**	18.2
1.19	5.0	**36.8**	39.9	**36.8**	24.6
1.19	6.0	**39.2**	39.5	**39.2**	32.1

*1: necessary proton current for 1 hour Irradiation for BNCT.

For an actual accelerator system, the stability of the proton energy could vary slightly from the intended energy. This is critical for the near threshold ^{7}Li(p,n)^{7}Be neutron production since neutron yields and angular distributions at this proton energy range vary dramatically. We will investigate the effect of Gaussian proton beams using TPD_{max} in near future.

4. Conclusions

For an incident mono-energetic 1.900 MeV proton beam and a polyethylene BDE with fixed thickness of 1.19 cm, the deepest TPD was achieved with Pb and Bi thicknesses of around 5 cm and 6 cm respectively. From the relationship between the value of TPD and the Pb (or Bi) thickness and the necessary proton current for BNCT, a suitable thickness of the Pb or Bi layer for a practical implementation of the design considered in this study would be about 3 cm.

References

Bengua G, Kobayashi T, Tanaka K, et al., 2006. TPD-based evaluation of near threshold mono-energetic proton energies for the ^{7}Li(p,n)^{7}Be production of neutrons for BNCT, Phys. Med. Biol. 51, pp. 4095-4109.

Bengua G, Kobayashi T, Tanaka K and Nakagawa Y, 2004. Evaluation of the characteristics of boron-dose enhancer (BDE) materials for BNCT using near threshold ^{7}Li(p,n)^{7}Be direct neutrons. Phys. Med. Biol. **49**(5), pp. 819-831.

Blue T and Yanch JC, 2003. Accelerator-based epithermal neutron sources for boron neutron capture therapy of brain tumors. Journal of Neuro-Oncology, **62**, 19-31.

Caswell RS and Coyne JJ, 1980. Kerma factors for neutron energies below 30MeV. Radiat. Res., 83, pp. 217-254.

Hubbell JH, 1999. Review of photon interaction cross- data in the medical and biological context. Phys. Med. Biol., 44, R1-R22.

Kiss AZ, Koltay E, Nyako B, Somorjai E, Anttila A and Raisanen J, 1985. Measurements of relative thick target yieldsfor PIGE analysis on light elements in the proton energy interval 2.4–4.2 MeV. J. Radioanal. Nucl. Chem. **89**, pp.123–41.

Kobayashi T, Bengua G., Tanaka K, et al., 2007 Variations in lithium target thickness and proton energy stability for the near-threshold ^{7}Li(p,n)^{7}Be accelerator-based BNCT, Phys. Med. Biol. 52, pp. 645-658.

Lee CL and Zhou XL, 1999. Thick target neutron yields for the ^{7}Li(p,n)^{7}Be reaction near threshold. Nucl. Instr. Methods Phys. Res. B, **152**, pp. 1-11.

Lee CL, Zhou XL, Kudchadker RJ, Harmon F and Harker YD, 2000. A Monte Carlo dosimetry-based evaluation of the ^{7}Li(p,n)^{7}Be reaction near threshold for accelerator boron neutron capture therapy. Med. Phys., **27**(1), pp. 192-202.

Snyder WS, Cook MJ, Nasset ES, Kahrhausen LR, Howells GP and Tipon LH, 1975. Report of the Task Group on Reference Man(Oxford:Pergamon)

Tanaka K, Kobayashi T, Sakurai Y, Nakagawa Y, Ishikawa M and Hoshi M, 2002. Irradiation characteristics of BNCT using near-threshold ^{7}Li(p,n)^{7}Be direct neutrons: application to intra-operative BNCT for malignant brain tumors. Phys. Med. Biol., **47**, pp. 3011-3032.

Waters LS, ed., 2002. MCNPX User's Manual Version 2.4.0 LA-CP-02-408. Los Alamos National Laboratory, Los Alamos, New Mexico.

Development of a Tandem-ElectroStatic-Quadrupole accelerator facility for BNCT

A.J. Kreiner[a,b,c], V. Thatar Vento[a], P. Levinas[a,c] , J. Bergueiro[a], H. Di Paolo[a,b], A.A. Burlon[a, b], J.M.Kesque[a], A.A. Valda[a,b], M.E. Debray[a,b], H.R. Somacal[a,b], D.M. Minsky[a, b], L. Estrada[a], A. Hazarabedian[a], F. Johann[a], J.C. Suarez Sandin[a], W. Castell[a], J. Davidson[a,c], M. Davidson[a,c], Y. Giboudot[a], M. Repetto[a], M. Obligado[a], J.P. Nery[a], H. Huck[a,b], M. Igarzabal[a], A. Fernandez Salares[a].

[a]*Departamento de Física, Comisión Nacional de Energía Atómica, Av. Gral Paz 1499 (1650), San Martín, Buenos Aires, Argentina*
[b]*Escuela de Ciencia y Tecnología. Universidad Nacional de Gral. San Martín, M. De Irigoyen 3100 (1650), San Martín, Buenos Aires, Argentina*
[c]*CONICET, Avda. Rivadavia 1917(C1033AAJ), Ciudad Autónoma de Buenos Aires, Argentina*

Abstract

In this work we describe the present status of an ongoing project to develop a Tandem-ElectroStatic-Quadrupole (TESQ) accelerator facility for Accelerator-Based (AB)-BNCT at the Atomic Energy Commission of Argentina in Buenos Aires. The project final goal is a machine capable of delivering 30 mA of 2.4 MeV protons to be used in conjunction with a neutron production target based on the ^{7}Li(p,n)^{7}Be reaction slightly beyond its resonance at 2.25 MeV. These are the specifications needed to produce sufficiently intense and clean epithermal neutron beams, based on the ^{7}Li(p,n)^{7}Be reaction, to perform BNCT treatment for deep-seated tumors in less than an hour. An electrostatic machine is the technologically simplest and cheapest solution for optimized AB-BNCT. The machine being designed and constructed is a folded TESQ with a high-voltage terminal at 1.2 MV intended to work in air. Such a machine is conceptually shown to be capable of transporting and accelerating a 30 mA proton beam to 2.4 MeV. The general geometric layout, its associated electrostatic fields, and the acceleration tube are simulated using a 3D finite element procedure. The design and construction of the ESQ modules is discussed and their electrostatic fields are investigated. Beam transport calculations through the accelerator are briefly mentioned. Likewise, work related to neutron production targets, strippers, beam shaping assembly and patient treatment room is briefly described.

Keywords: Accelerator-Based BNCT (AB-BNCT), Tandem Electrostatic Quadrupole accelerator, Electrostatic design, Accelerator tubes.

1. Introduction

Within the frame of Accelerator-Based BNCT (AB-BNCT), a project to build a Tandem-ElectroStatic-Quadrupole (TESQ) accelerator facility is under development in Argentina (Kreiner et al., 2007) based on the ^{7}Li(*p,n*)^{7}Be reaction, slightly beyond its resonance, at 2.3 MeV. The machine being designed and constructed is a folded TESQ with a terminal at 1.2 MV intended to work in air, to avoid the need for a pressure vessel and for an insulating gas installation. The project aims at developing a machine capable of delivering a proton beam of about 2.4 MeV and 30 mA to irradiate a Li metal (or a refractory Li compound) target in order to produce the therapeutic neutron beam after appropriate beam shaping.

In this work, we report on the present status of the project.

The general geometric layout, its associated electrostatic fields, and the acceleration tube are simulated using a 3D finite element procedure. The design and construction of the ESQ modules is discussed and their electrostatic fields are calculated. Beam transport calculations through the accelerator are briefly mentioned (see Levinas et al., in these proceedings). Likewise, work related to strippers and neutron production targets is briefly described. To give a complete picture of the work being done in the frame of this project, progress on the beam shaping assembly and design of a patient treatment room is also mentioned (see Burlon et al., these proceedings).

2. Materials and Methods

The TESQ accelerator general layout has already been presented in previous publications (see Kreiner et al., 2007, fig. 1). It consists of a series of stacked cylindrical boxes which are separated by 200 kV in voltage and 40 cm air gaps (a total of 6 to reach 1.2 MV). A partial view of this structure is shown in fig. 1. These boxes house generators, driven by insulating rotating shafts, connected to electric motors (two motors of about 70 kW each) placed at ground potential, which provide the necessary power to feed the high-voltage supplies (100 kV and 60 mA units) which will energize the whole installation.

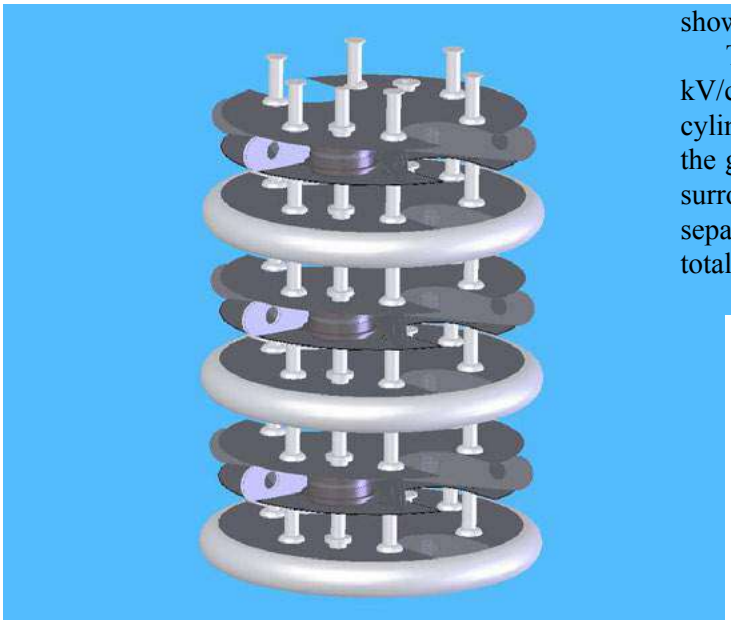

Figure 1. Partial view of high-voltage column showing 6 boxes (3 open with generators and 3 closed, surrounded by semitoroidal shields). The successive boxes are separated by 6 posts

These boxes are traversed vertically by the up and down-going acceleration tubes (only holes for them are shown in fig.1), which are made of slices of borosilicate glass and stainless steel.

The electrostatic fields have been calculated by means of 3D finite element and other numerical codes and a detailed design has been made paying special attention to the avoidance of sharp edges and points to limit the fields to safe values. The criteria have been to limit the fields on metal surfaces in air to values not exceeding 12 kV/cm, to 5 kV/cm at the interfaces between insulators and air (the room which will house the machine will have controlled temperature and humidity, about 20 ^{0}C and 35% respectively) and to 45 kV/cm on metal surfaces in vacuum. We shall address the geometric layout of the column and the accelerator tube composed of focusing quadrupoles and accelerating gaps.

The simulation of the transport and acceleration of the 30 mA proton and deuteron beams through the tube is accomplished by means of self-consistent 3D Vlasov-Poisson calculations (Humphries, 2002), which are only briefly mentioned here (see Levinas et al., these proceedings).

3. Results

Fig. 2 shows the general geometric layout of the high-voltage column. It is being built as a right cylinder of 2.5 m diameter crowned at its upper ending by a partly hemispherical (radius r is 1.85 m), cylindrical and semi-toroidal (r=0.60 m) dome at 1.2 MV (the 180^0 bending magnet within the dome is not shown).

The maximum field can be kept below 12 kV/cm. The column consists of a series of stacked cylindrical boxes (30 cm in height to accommodate the generators and the high-voltage power supplies), surrounded by semi-toroidal surfaces, which are separated by 200 kV in voltage and 40 cm air gaps (a total of 6 to reach the 1.2 MV dome).

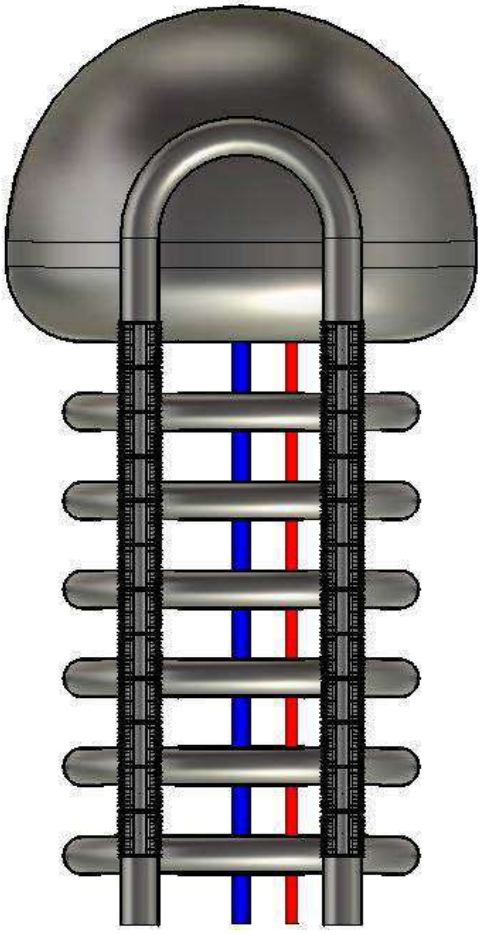

Fig. 2 Vertical cut of the column and dome through the mid-plane, showing the two tubes with connection within the dome, one post and one rotating shaft (right). The height is about 7 m

The distance to the wall (a cylindrical grounded Faraday cage, not shown) is also optimized in order to keep the electrostatic field at its minimum value. In our case the required distance from the box column is 3.5m. The height from ground to roof turns out to be about 10 m.

Figs. 3 and 4 show details of two and one focusing and accelerating tube sections respectively. Each tube section is 35 cm long and consists of slices of borosilicate glass (diameter of 30 cm and thickness along the tube axis of 3.15 cm) bonded to stainless steel electrodes and end-flanshes. The electrodes are protruding to the inside, with a curved geometry, in order to block the direct view of the beam by the insulating glass walls.

To the outside they are terminated in rings to limit the maximum field at the sharp edges. In addition, the tubes house a series of quadrupole focusing elements. These are made of semi-cylindrical rounded-edge stainless steel pieces which are held in place by both conducting and insulating supports. The total voltage across the two tube sections, located between the mid-planes of two consecutive boxes, is designed to be 200 kV. The voltage between poles for each quadrupole is typically between 20 to 40 kV, and the voltage between poles of consecutive quadrupoles (accelerating gaps) is of the order of 70 keV for most of the tube. This last voltage is responsible for acceleration along the machine.

Fig. 5 shows the equipotential lines in a transverse mid-plane cut inside a tube section, where the quadrupole character is apparent. Here the function is only to transversely focus the beam.

The simulation of the transport and acceleration of the 30 mA proton beam through the tube is done using the self-consistent 3D code WARP (Friedman et al., 1992) (this work is described in more detail in these proceedings, see Levinas et al.).

As an intermediate step we shall first produce a 1.2 MeV deuteron beam to hit a thin Be target to produce neutrons through the ^{9}Be(d,n) reaction. This reaction, in the bombarding energy range 1.2 to 1.1 MeV is a very interesting source of low-energy neutrons, due to the strong population of excited states at 5 MeV in the residual nucleus ^{10}B (Guzek et al., 1997).

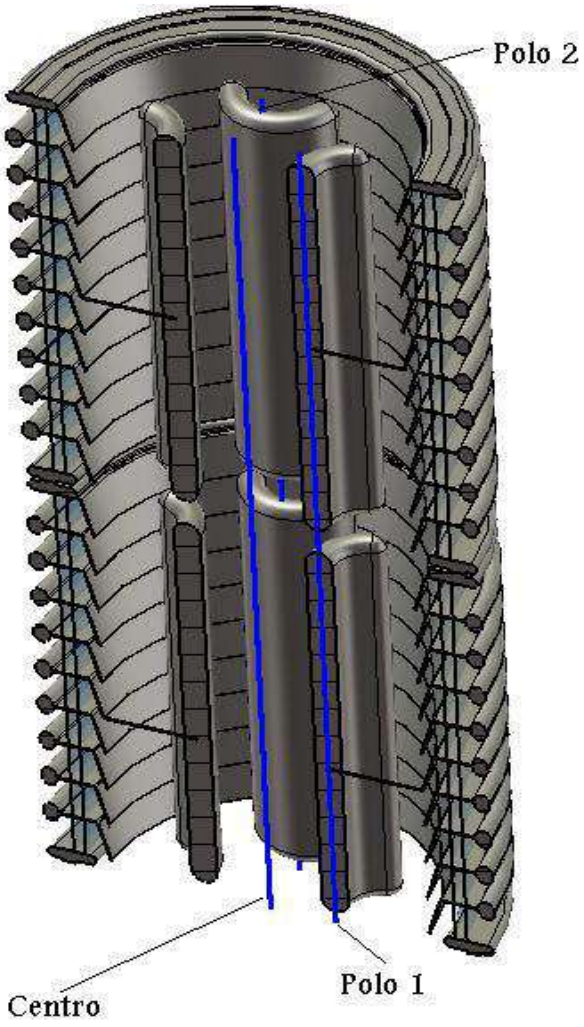

Fig. 3 Vertical cut of two consecutive tube sections through their mid-plane, showing three (partial) quadrupole electrodes, the protruding shielding electrodes, the grading rings outside and the transparent insulating glass slices

Fig. 4 View of an entire tube section showing all four quadrupole electrodes

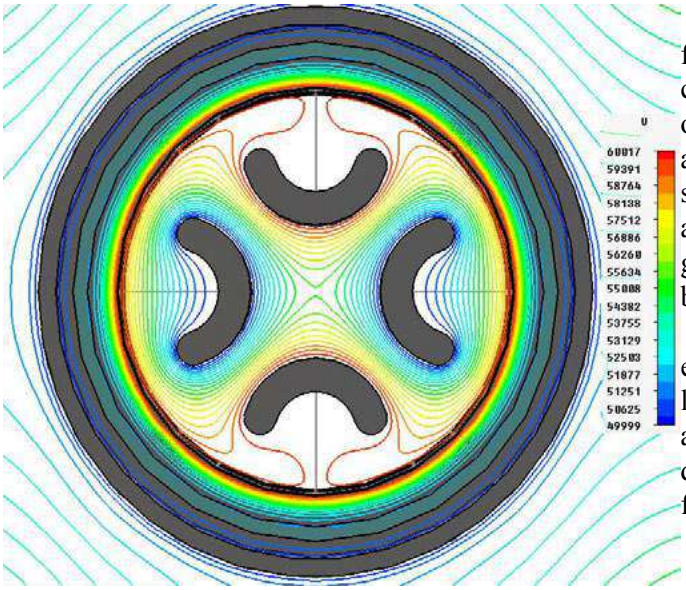

Fig. 5 Equipotential lines in the transverse mid-plane of a quadrupole

In relation to this possibility we are studying thin Be targets and likewise stripper materials (for the TESQ final design). To test their durability and study different alternatives we have used the heavy ion microbeam of our TANDAR tandem accelerator, which provides beams of comparable fluence rate to those expected for the TESQ facility (i.e., about 10 mA/cm^2). Our preliminary results indicate that Be foils about 1 μm thick would last at least for a few hours when subjected to a 30 mA, 1-2 MeV proton beam. In fact, the best present-day carbon strippers withstand about 40 mAh (Zeisler et al., 2008), a number which starts to turn a solid stripper into a realistic option for the operation of a BNCT TESQ. As far as targets are concerned we are studying different alternatives from solid Li metal, refractory compounds like Li_2O and liquid Li. The liquid Li option is very attractive provided the temperature is not higher than about 250^{0}C (in order to keep the vapor pressure sufficiently low) and a very efficient LN_2 trap is installed next to the neutron production target (Scott, 2007). Also an optimized beam shaping assembly (BSA) and a patient treatment room is being designed (see Burlon et al., these proceedings). It is shown that an optimized BSA in conjunction with a 30 mA beam from our TESQ accelerator would have a larger advantage depth that the MIT fission converter facility (11.5 vs 9.9 cm), and would allow an optimized treatment of tumors at 6.4 cm inside the brain in a 27 minutes treatment (see also Burlon et al., 2008).

4. Discussion and conclusions

A Tandem-ElectroStatic Quadrupole accelerator facility for AB-BNCT is being designed and constructed at CNEA, Argentina. The general layout of the facility, the accelerator column, the accelerating tube and several other susbsystems like strippers, neutron production targets, beam shaping assembly, treatment room, power and high voltage generation and ion sources are being defined and built.

Since an accelerator can be sited in a hospital environment, is easier and safer to operate and of lower cost than a reactor, our present results provide an additional justification for the ongoing efforts to develop such a machine as a means to achieve further progress in the field of BNCT.

References

Burlon ,A.A. and Kreiner, A.J., 2008. A comparison between a TESQ accelerator and a reactor as neutron sources for BNCT, Nucl. Instrum. and Methods B 266, 763–771.

Friedman, A., D. P. Grote, I. Haber, 1992.Three Dimensional Particle Simulation of Heavy Ion Fusion Beams, Phys. Fluids B. 4, 2203.

Guzek J., Tapper U., McMurray W., Watterson J., 1997. Characterisation of the ^{9}Be(d,n)^{10}B Reaction as a Source of Neutrons Employing Commercially Available Radio Frecuency Quadrupole (RFQ) Linacs, Proceedings-SPIE, The International Society for Optical Engineering, Vol 2867, 509-512.

Humphries S. Jr., 2002. Charged Particle Beams.

Kreiner, A.J., Kwan, J.W., Burlon, A.A, Di Paolo, H., Henestroza, E., Minsky, D.M., Valda, A.A., Debray, M.E., Somacal, H.R., 2007. A Tandem-Electrostatic-Quadrupole for Accelerator-Based BNCT. Nucl. Instrum. Methods B 261, 751–754 and references therein.

Kwan, J.W., E. Henestroza, C. Peters, L.L. Reginato, and S.S. Yu, 1997. Designs of a DC ESQ Accelerator for BNCT Application, *Application of Accelerators in Research and Industry*, AIP Press, 1313-1315, and references therein.

Zeisler, S.K. and Vinder, J., 2008. Multilayer carbon foils for cyclotron beam extraction. Nucl. Instrum. and Methods A 590, 18–21.

Scott, M.C., 2007. University of Birmingham, private communication

The Physics Experimental Study for In-hospital Neutron Irradiator

Li-Yiguo[1] Xia-Pu[1] Zou-Shuyun[1] Zhang-Yongbao[1] Lv-Zheng[1]
Zhou-Yongmao[2] Liu-Tong[3] Xu-Wenze[3] Gao Zi-xian[4]

[1] *China Institute of Atomic Energy, Beijing,102413,P.O.Box 275-75,China*
[2] *China Zhongyuan Engineering corporation, Beijing,100083,China*
[3] *Beijing Capture Tec. Co., No 8, Fuchenmenwai Street,Beijing, 100037,China*
[4] *Beijing Tiantan Hospital, No. 6, Tiantanxilu,Beijing,100050*

Abstract: $MNSR_S$(Miniature Neutron Source Reactor) are low power research reactors designed and manufactured by China Institute of Atomic Energy (CIAE). $MNSR_S$ are mainly used for NAA, training and teaching, testing of nuclear instrumentation. The first MNSR, the prototype MNSR, was put into operation in 1984, later, eight other $MNSR_S$ have been built both at home and abroad. For $MNSR_S$, highly enriched uranium(90%) is used as the fuel material.

The In-hospital neutron irradiator(IHNI) is designed for Boron Neutron Capture Therapy(BNCT) based on Miniature Neutron Source Reactor(MNSR). On the both sides of the reactor core, there are two neutron beams, one is thermal neutron beam , and the other opposite to the thermal beam, is epithermal neutron beam. A small thermal neutron beam is specially designed for the measurement of blood boron concentration by the prompt gamma neutron activation analysis(PGNAA).

In this paper, the experimental results of critical mass，worth of the top Be reflectors，worth of the control rod, neutron flux distribution and other components worth were measured, the experiment was done on the Zero Power Experiment equipment of MNSR.

KEYWORDS: MNSR LEU BNCT NAA

1 Description of equipment[1,2]

The reactor with thermal power 30kW is an undermoderated reactor of pool-tank type, and UO_2 with enrichment of 12.5% as fuel, light water as coolant and moderator, and metallic beryllium as reflector. The fission heat produced by the reactor is removed by the natural convection.

Fig. 1 shows the figure of the experimental equipment. One central control rod is in the center of reactor core, one auxiliary control rod and two reactivity regulators are in the side beryllium reflector.

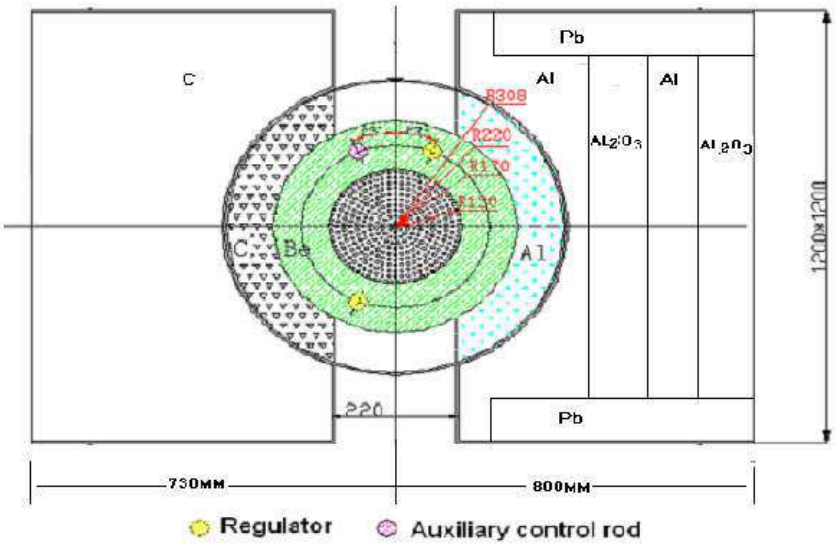

Fig. 1 The diagram of the experimental equipment

1.1 Reactor

The upper and lower grid plates are linked by five tie rods, ten rows of 351 lattices are concentrically arranged, the central lattice is reserved for central control rod. While the five tie rods are uniformly arranged at the tenth row. The rest lattices are for fuel element and dummy elements(see fig. 2).

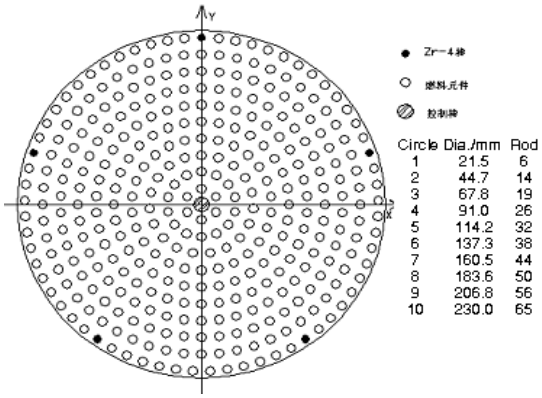

Fig. 2 The fuel arrangement

The UO_2 is used as the fuel meat with density 10.6g/cm^3, ^{235}U enrichment is 12.5%, the dimension is 4.2mm×240mm. The cladding material is Zr-4 alloy with wall thickness 0.4mm and 256mm in length(8mm end plug at up end,7mm end plug at lower end, 1mm Helium gas between the up end and fuel meat)

The central control rod :

1) Guide tube: inner dia. 9mm, outer dia. 12mm , length: 258mm

2) Meat: Cd tube outer dia. 4.0mm, inner dia. 2.0mm, length 280mm; inside Cd tube: Al rod φ2.0×280 (mm)

3) Outside Cd tube S.S tube outer dia. 5mm , wall thickness：0.5mm, total length: 450mm

The fuel Cage:

1) Dia：240mm, heiqht: 240mm; 2) Top core plate: Zr-4 alloy thickness: 2mm, lower core plate: Zr-4 alloy thickness: 4mm.

1.2 Side Be reflector

The dimension：inner dia. 240mm , outer dia. 440mm, height：246mm

1.3 Bottom Be reflector

The dimension: dia. 350mm, thickness：100mm, central hole of 20mm in diameter.

1.4 Top Be reflector

The Al alloy tray for Top Be reflector：inner dia. :266mm, outer dia. 270m , height：140mm , bottom thickness：2mm.

The dimension of top Be reflectors：dia.: 264mm, hole dia.: 20mm , total thickness：111mm.

1.5 Auxiliary control rod

The auxiliary control rod is arranged at the radius of 170mm in the side Be, it consists of three parts, the up part: Cd tube outer dia.25.0mm , inner dia.23.0mm; Inside Cd tube: Al rod φ23.0×250 (mm) ; the middle part: Al rod dia. 25mm; the lower part: Be rod dia. 25. The outside tube : Al tube outer φ28.0×534mm.

1.6 Reactivity regulator

The two reactivity regulators are arranged inside Beryllium. The dimension of regulator：Cd tube outer dia.30.0mm , inner dia.28.0mm, height 250mm; Inside Cd tube: Al rod φ28.0×250 (mm) ; Outside Cd tube: Al tubeφ33.0×260 (mm.

1.7 Neutron beam equipment

For thermal neutron beam equipment, the graphite is adopted as moderator, and aluminum, Lead and Al_2O_3 are adopted in epithermal neutron beam equipment.

2 Zero power experimental results

The experiment was done in the MNSR zero power equipment, some parameters were measured.

2.1 Critical mass

Two ways of extrapolation and insertion were used for the measurement of critical mass. The results are 296.8 fuel elements, the fuel elements in the outermost circle are not uniformly arranged.

2.2 Worth of the central control rod

The worth was measured by the period method. Insert a part of the rod in the reactor, measured the worth by the same method again. Do it Alternately, the total worth of the rod was measured finally(see Fig .3). The total worths of the central control rod of calculation and experiment are 6.0mk and 6.4mk respectively

.

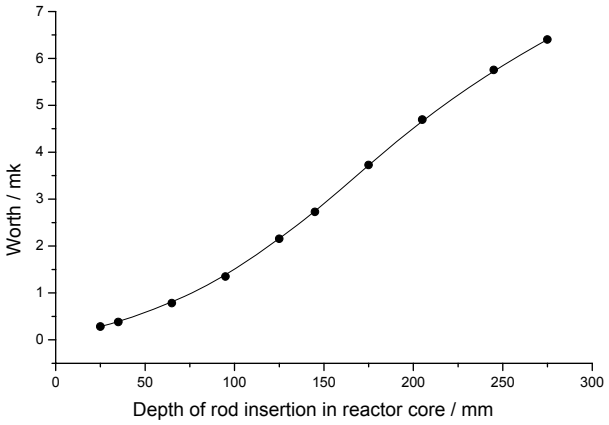

Fig. 3 Central control rod worth

2.3 Worth of the top Beryllium reflectors

By the period method, the worth was also measured. Add the piece of top Be, measured the worth; and then, take out the fuel element from the reactor core, add the top Be, measured the worth again; Do it Alternately, the total worth of the rod was measured finally(see Fig.4). The total worths of the top Be reflectors calculation and experiment are 17.6mk and 16.11mk respectively**.**

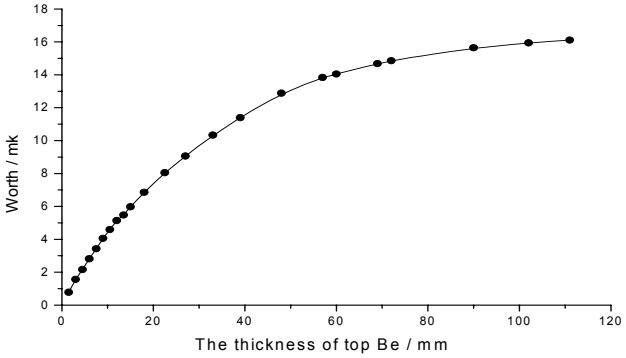

Fig. 4 Top Be worth

2.4 Relative neutron flux distribution

Using the Mn activation method, the neutron flux distribution in the reactor core was measured. The Mn foils were put in the height of 120mm from the up surface of the lower plate at the different position in the radial direction, the Mn foils were put between the 4th circle and 5th circle at different position for the measurement of axis neutron flux. the activity was measured by γ spectrum equipment. See fig.5.

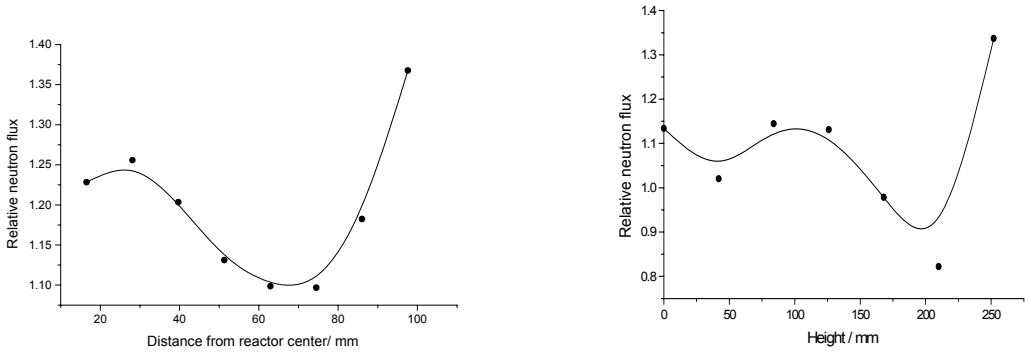

Fig. 5 Neutron flux distribution in the reactor core(Radial and axial)

2.5 Worth of auxiliary control rod(ACR), reactivity regulator(RR) and neutron beam equipment(NBE), see Table 1

Table 1 The Worths of ACR,RR and NBE

ACR/mk		RR /mk		NBE/mk	
Experiment	Calculation	Experiment	Calculation	Experiment	Calculation
-3.78	-5.8	-8.07	-6.4	-0.17(-6.7)*	-0.45(-7.8)*

*: epithermal neutron beam equipment

3 Conclusion

The design limit of the excess reactivity of the reactor is not more then 4.5mk. At the initial state of reactor, one reactivity regulator and the lower part of auxiliary control rod are in the reactor, when the loading is 299 fuel elements in the reactor core, the responding reactivity(measured) of reactor is 1.25mk. The worth of one fuel element is 1.2mk, so the excess reactivity for the loading of 302 fuel elements is 4.85mk(no consideration of the end worth of the central control rod). Consideration of the -0.5mk of end worth of central control rod, the excess reaxtivity for the loading of 302 fuel elements is 4.35mk, so the final loading at the initial state of reactor is 302 fuel elements, the rest lattices will be filled by fuel elements of ^{238}U.

Reference

[1] Design and construction of the In-Hospital Neutron Irradiator-I. Zhou yongmao,Gao Zhixian, Li Yiguo. Proceedings of ICNCT 2006, P557.

[2] The conceptual calculation for the Neutron Beam Device at <In-Hospital Neutron Irradiator>. Jiang Xinbiao, Zhu Yangni, Gao Jijin. Proceedings of ICNCT 2006, P576.

A neutron producing target for BINP accelerator-based neutron source

B. Bayanov[a], E. Kashaeva[b], A. Makarov[c], G. Malyshkin[b], S. Samarin[b], and S. Taskaev[a]

[a] *Budker Institute of Nuclear Physics, 11 Lavreniev ave., Novosibirsk, Russia*
[b] *All-Russian Research Institute of Technical Physics,13 Vasiliev str., Snezhinsk, Russia*
[c] *Novosibirsk State University, 2 Pirogov str., Russia*

Abstract

An innovative accelerator-based neutron source for BNCT has just started operation at the Budker Institute of Nuclear Physics, Novosibirsk. One of the main elements of the facility is a lithium target producing neutrons via the threshold ^{7}Li(p,n)^{7}Be reaction at 25 kW proton beam with energies of 1.915 MeV or 2.5 MeV. The design of an optimal target and results of investigation of radiation blistering of the lithium layer were presented at previous NCT Congresses. During the last two years the neutron target had been manufactured, assembled and placed in the facility. Optimization of the target is carried out with the Monte Carlo simulation code MCNP. In the report, the design of the target is discussed, results of all previous investigations are summarized, results of target testing and neutron generation are described, and results of simulation of neutron spectra are presented.

Keywords: target, lithium, neutron capture therapy, epithermal neutrons

1. Introduction

In 1998 at the Budker Institute of Nuclear Physics (BINP) an original source of epithermal neutrons has been conceived based on the tandem accelerator with vacuum insulation, suitable for widespread use of BNCT in clinical practice (Bayanov et al., 1998). It is intended to generate neutrons with the threshold reaction ^{7}Li(p,n)^{7}Be bombarding a lithium target with a 1.915 MeV 10 mA proton beam. At present moment the accelerator has been constructed (Kudryavtsev et al., 2008), and the first experiments on generating neutrons have been carried out (Bayanov et al., 2008). In this work the results of these experiments are presented.

2. Summary of previous investigations

Four neutron-producing charged particle reactions have been proposed for use in accelerator-based BNCT: ^{7}Li(p,n), ^{9}Be(p,n), ^{9}Be(d,n) and ^{13}C(d,n) (Blue and Yanch, 2003). The best reaction for epithermal neutron generation is ^{7}Li(p,n): neutron production from this reaction is high and the relatively soft spectrum requires less moderation than those generated in other reactions. This reaction is going to be used by us in spite of the poor mechanical, chemical, and thermal properties of lithium metal.

Pure lithium is more effective for neutron generation as compared with lithium hydride, oxide, nitride or fluoride (Lee and Zhou, 1999). However it requires efficient heat removal to avoid melting (lithium melting temperature is 182 °C) so as to prevent the undesirable release of ^{7}Be. A liquid metal coolant is preferable to water at a high power density. However during thermal tests with gallium as a coolant, target damage occurred due to the high chemical activity of gallium (Belov et al., 2002). Then it was found that the target size for near-threshold generating mode could be increased up to 10 cm without any negative consequence on the neutron beam characteristics (Bayanov et al., 2005). It was experimentally demonstrated in (Bayanov et al., 2004) that water cooling is the best one for a target of 10 cm diameter, and that the lithium target could run up to 10 mA proton beam before melting.

As a result of proton bombardment of lithium an undesirable flux of 478 keV γ-rays appears (Savidou et al., 1999). To decrease it appreciably, the production via evaporation of a thin lithium layer is needed – from 5 to 100 μm thickness for protons with energies from 1.915 to 2.5 MeV. This thickness of lithium layer slows down the protons to 1.882 MeV – the threshold energy for neutron generation. Then the protons can be absorbed without γ-radiation in any metal heavier than aluminum.

New techniques have been proposed and developed to evaporate thin lithium layers (Bayanov et al., 2006), to facilitate the evaporation process (Bayanov and Taskaev, 2007) and to measure the radial distribution of the evaporated lithium layer thickness (Bayanov et al., 2008). It was determined that evaporated lithium density corresponds to the metal lithium density.

A 10% decrease in the neutron yield per unit

current has been observed within 3 h after firing a proton beam on a lithium target in the experiment at the Birmingham accelerator, U.K. (Brown et al., 2002). This decrease may be caused by a change in the lithium layer composition as a result of its interaction with residual gas since the neutron yield, e.g., in lithium nitride is a factor 1.66 lower than in pure lithium. We investigated the dependence of the secondary negative ion yield on the layer depth for lithium layers exposed under different vacuum conditions using the secondary-ion mass spectrometry method (Bayanov et al., 2008). It was found that changes in the lithium layer composition as a result of its interaction with the residual gas could not be the cause for the 10% observed decrease in neutron yield. During these experiments the evaporated layer was ascertained to consist of pure lithium.

Monoenergetic proton absorption in a metal results in radiation damage. The appearance of blistering on different metals was experimentally examined. It was found that the beam with the design parameters blistered copper in less than one hour. For metals that have a good level of hydrogen solubility, this time increases by more than a factor of 100 times.

3. Simulations

During the first experiments on neutron generation, a target with good thermal removal characteristic was used. Fig. 1 illustrates the target general view.

In 2007 T. Kobayashi and G. Bengua made MCNP calculations on the acceptability of this target for neutron-capture therapy (Bengua et al., 2006). They have proved that it is useful to replace a stainless steel backing by a tungsten one, to use heavy instead of light water and to use a polyethylene boron dose enhancer.

Then the numerical simulation of protons, neutrons and γ-quanta transporting in the neutron-generating target and its environment was made. The simulation was performed with PRIZMA program (Arnautova et al., 1993). To understand better the physical nature of this process, all calculations were made for two different geometrical models: a full target geometry (Fig. 2) and a simplified one where a part of the target below the backing *1* was absent. The water phantom 20 cm in diameter and 20 cm height has been placed 2 cm below the target. All obtained results were averaged over 5 cm diameter and over a depth of 5 – 10 cm.

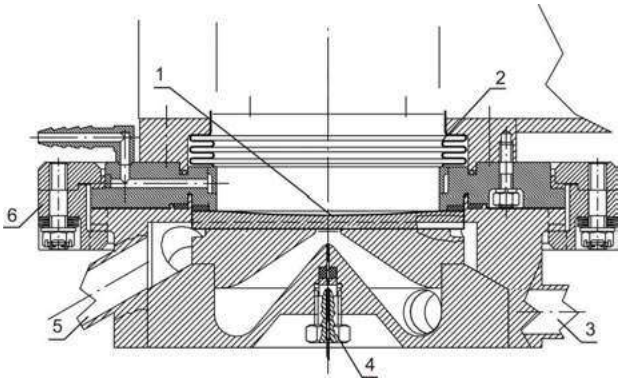

Fig. 1. Target for BINP accelerator neutron source: 1 – backing with lithium layer, 2 –bellow, 3 – water input, 4 – thermocouple, 5 – water output, 6 – bayonet.

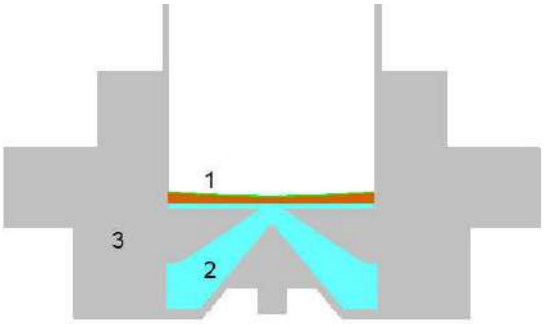

Fig. 2. Calculational model of the target: 1 – copper backing 10 cm in diameter with thin lithium layer, 2 – water, 3 – stainless steel.

Figs. 3 and 4 illustrate results of neutron flux calculations on the surface of the phantom for the simplified and full target geometries in the case of near-threshold neutron generation (proton energy: 1.915 MeV, current: 10 mA, lithium thickness: 10 μm). As a result of scattering in the constructional materials of the target and in the coolant, the neutron spectrum became softer and more appropriate for neutron-capture therapy without losses in flux density. Still a considerable flux of neutrons with energies around 60 keV is present. Obviously, the use of iron backing is inadmissible for optimal target geometry due to the presence of windows in the scattering cross-section. Using an orthogonal neutron beam is a possible way of softening the spectrum.

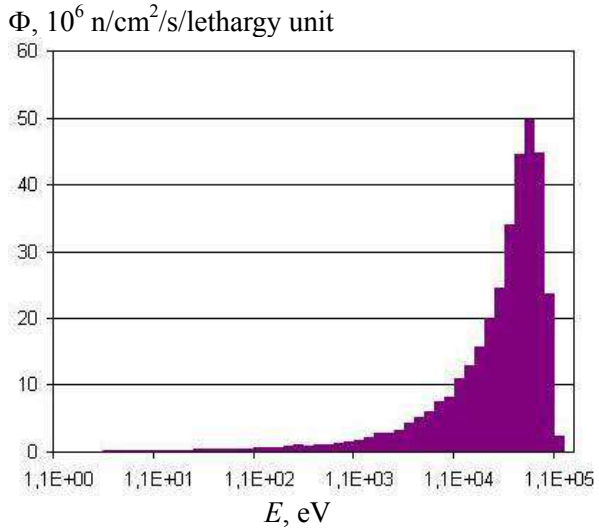

Fig. 3. Neutron energy spectrum for simplified target geometry.

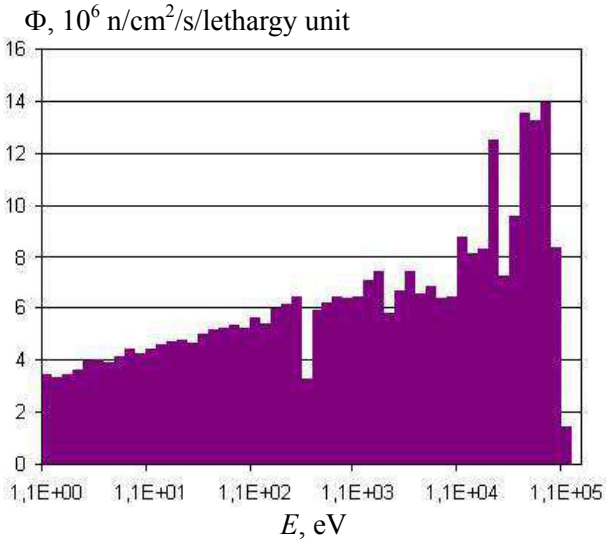

Fig. 4. Neutron energy spectrum for full target geometry.

Fig. 5. Target substrate with lithium after neutron generation. The mark left by the beam can be seen on the left.

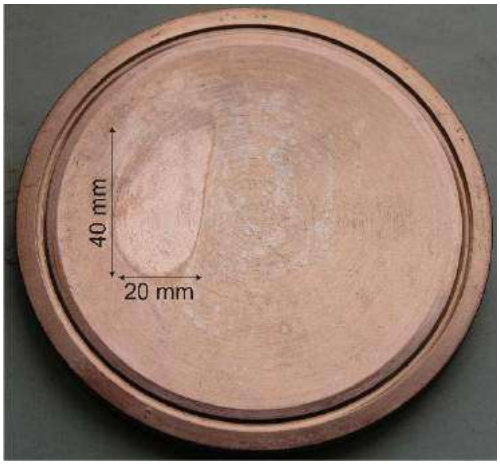

Fig. 6. Target substrate without lithium after neutron generation. The mark left by the beam can be seen on the left.

4. Neutron generation

Recently neutron generation at the facility was first achieved (Bayanov et al., 2008). The target used in the conducted experiments is shown in Fig. 1. To ensure radiation protection, the beam current was limited to 140 μA. At the same time the beam was fixed (not sweeping) and Figs. 5 and 6 show the marks left by the beam. The beam is 2 cm in diameter, in good agreement with calculations. At this beam size the power density on the target is about half the design value. The critical changes in the lithium layer were not observed thus indicating an adequate heat removal.

5. Conclusions

In this work the authors have summarized the results of all previous investigations that concern the choice of the neutron generation reaction, the design of the heat-removal system, the determination of the lithium layer thickness, the employment of new evaporation techniques to produce the lithium layer, the study of the lithium layer characteristics and the analysis of the blistering.

During first experiments on neutron generation it has been demonstrated that the target is acceptable in respect to providing the necessary level of heat removal. Calculations of the neutron flux and spectrum are in agreement with the measurements. Studies are ongoing to find possible drawbacks in the target design and to discover ways to improve it.

References

Arnautova, M., Kandiev, Ya., Lukhminsky, D., Malyshkin, G., 1993. Monte-Carlo Simulation in Nuclear Geophysics: Comparison of the PRIZMA Monte Carlo Program and Benchmark Experiments. Nuclear Geophysics, 7, 407-418.

Bayanov, B., Belov, V., Bender, E., Bokhovko, M., Dimov, G., Kononov, V., Kononov, O., Kuksanov, N., Palchikov, V., Pivovarov, V., Salimov, R., Silvestrov, G., Skrinsky, A., and Taskaev, S., 1998. Accelerator-based neutron source for the neutron-capture and fast neutron therapy at hospital. Nucl. Instr. and Meth. in Phys. Res. A413, 397-416.

Bayanov, B., Belov, V., Kindyuk, V., Oparin, E., Taskaev, S., 2004. Lithium neutron producing target for BINP accelerator-based neutron source. Applied Radiation and Isotopes 61, 817-821.

Bayanov, B., Belov, V., Taskaev, S., 2005. Neutron producing target of the accelerator based neutron source for neutron-capture therapy. Preprint BINP 2005-4, Novosibirsk, Russia.

Bayanov, B., Belov, V., Taskaev, S., 2006. Neutron producing target for accelerator based neutron capture therapy. Journal of Physics 41, 460-465.

Bayanov, B. and Taskaev, S., 2007. Lithium container. PCT/RU2007/000276.

Bayanov, B., Zhurov, E., and Taskaev, S., 2008. Measuring the Lithium Layer Thickness. Instr. and Exper. Techniques 51, 147-149.

Bayanov, B., Taskaev, S., Obodnikov, V., Tishkovskii, E., 2008. Effect of the residual gas on the lithium layer of a neutron-generating target. Instr. and Exper. Techniques 51, 438-442.

Bayanov, B., Burdakov, A., Chudaev, V., Ivanov, A., Konstantinov, S., Kuznetsov, A., Makarov, A., Malyshkin, G., Mekler, K., Sorokin, I., Sulyaev, Yu., and Taskaev, S., 2008. First neutron generation in the BINP accelerator based neutron source. Proc. of this Congress.

Belov, V., Fadeev, S., Karasyuk, V., Kononov, V., Kononov, O., Kuksanov, N., Kraynov, G., Petrov, Y., Pidyakov, V., Rachkov, V., Salimov, R., Silvestrov, G., Smirnov, G., Taskaev, S., and Villeval'd, G., 2002. Neutron producing target for accelerator based neutron source for NCT. Research and Development in Neutron Capture Therapy. Eds.: W. Sauerwein, R. Moss, and A. Wittig. Monduzzi Editore, 247-252.

Bengua, G., Kobayashi, T., Tanaka, K., Nakagawa, Y., Unesaki, H., 2006. TPD as a future of merit for the evaluation of near threshold mono-energetic proton energies for the ^{7}Li(p,n)^{7}Be production of neutrons for BNCT. Advanced in Neutron in Neutron Capture Therapy 2006, Y. Nakagawa et al., Eds., 288-291.

Blue, T. and Yanch, J., 2003. Accelerator-based epithermal neutron sources for boron neutron capture therapy of brain tumors. Journal of Neuro-oncology 62, 19-31.

Brown, A., Forsey, K., and Scott, M., 2002. The design and testing of a high power lithium target for accelerator-based boron neutron capture therapy. Research and Development in Neutron Capture Therapy, W. Sauerwein et al., Eds., Italy, Bologna: Monduzzi Editore, 277-282.

Kudryavtsev, A., Belchenko, Yu., Burdakov, A., Davydenko, V., Ivanov, A., Khilchenko, A., Konstantinov, S., Krivenko, A., Kuznetsov, A., Mekler, K., Sanin, A., Shirokov, V., Sorokin, I., Sulyaev, Yu., Tiunov, M., 2008. First experimental result from 2 MeV proton tandem accelerator for neutron production. Rev. Sci. Instr. 79, 02C709.

Lee, C., Zhou, X., 1999. Thick target neutron yields fot the ^{7}Li(p,n)^{7}Be reaction near threshold. Nucl. Instr. and Meth. in Phys. Res. B 152, 1-11

Savidou, A., Aslanoglou, X., Paradellis, T., Pilakouta, M., 1999. Proton induced thick target c-ray yields of light nuclei at the energy region E_p = 1.0 ± 4.1 MeV. Nucl. Instr. and Meth. in Phys. Res. B 152, 12-18.

Pulsed Neutron Source for Boron Neutron Capture Therapy Initial Simulation Results

M.Ramos [(a)], F. Longo [(b)], V. Gribkov [(c)], G. Giannini [(b)], M. Chernyshova [(d)], C. Tuniz [(e)]

[a] *Institute of Nuclear Science, Miramar # 502, Havana, Cuba*
[b] *University of Trieste and INFN, Trieste, Italy*
[c] *A.A. Baikov Institute of Metallurgy and Material Sciences, Russ. Ac. Sci., Russia*
[d] *Institute of Plasma Physics and Laser Microfusion, Poland*
[d] *International Center for Theoretical Physics ICTP, Trieste, Italy*

Abstract

In this work a feasibility study of the use of irradiation by neutron pulses generated by a Dense Plasma Focus device for BNCT treatment is presented. The use of short powerful neutron pulses in BNCT could in principle produce the desired effect with a considerably lower total absorbed dose. Through Monte Carlo (MC) simulations this experimental configuration could be described and each pulsed deposited dose and dose power estimated. A detailed MC simulation based on the Geant4 toolkit was implemented to evaluate the neutron pulse characteristics (pulse duration and spectrum) after its penetration through a moderator. Then, the neutron flux and dose deposition in a human phantom was studied. A second MC simulation step is performed to evaluate the dose deposition in a cluster of healthy and cancer cells.

Keywords: Neutron Pulses, Plasma Focus Device, BNCT, dose deposition, Geant4.

1. Introduction

The use of short and powerful neutron pulses for Boron Neutron Capture Therapy (BNCT) could reduce the total dose absorbed by the patient. A Dense Plasma Focus device (DPF) emits very short and intense pulses of fast neutrons (2.5- or 14-MeV energy neutrons from D-D or D-T nuclear reactions respectively). The interaction of this very powerful neutron beam with cells during a few nanoseconds can produce diverse effects on the biochemical functions of the cells (1). The inducing of synergetic effects within the cells, e.g. producing a high concentration of secondary particles (free radicals, ions, and electrons), may result in a collective action of them.

Nevertheless to the authors' knowledge, pulsed neutrons have not so far been used in BNCT, but it is known (2) that the use of nanosecond neutron pulses in radiation chemistry and biology could produce the desired effect with a considerably lower total absorbed dose. Gribkov et al (3) have studied the possibility of using pulsed radiation in biological applications.

The biological effects of radiation depend on the dose and the spatial distribution of the microscopic energy deposition. To verify the recent studies of the interactions of pulsed radiation with biological tissues (2) in the context of BNCT treatment, we introduced in our model the effects of the temporal profile of the beam (pulsed or continuous radiation).

This paper will focus on the development of a detailed simulation of interaction of pulsed radiation generated by a DPF with tissue to estimate the absorbed dose by the cells for this dynamic case. The simulation was carried out by means of the Geant4 code, a toolkit to simulate the interaction of radiation with matter, originally developed for nuclear and particle physics. The experimental

simulation was developed in two fundamental steps. The first consists in the modeling of the pulsed neutron source itself. The second is the development of a biological model to quantify the interaction of the pulsed neutron beam with a tissue.

2. Model

The simulation process includes: geometry of the system, materials involved, and physical processes governing particle interactions.

In the first stage a DPF was simulated. Using Geant4(4) for the simulation of the system geometry, DPF was implemented following the same features for the DPF construction originally developed by Gribkov et al. (Fig. 1). The neutron source was taken with neutrons produced from the D-D reaction, i.e. with energy E=2.45 MeV, and it had a flux $\Phi=10^9$ neutron/cm^2.

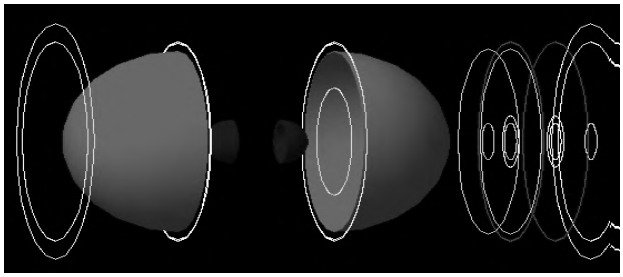

Fig.1. Plasma Focus Device geometry simulated in Geant4. The internal diameter of the spherical anode of the device's chamber is 60 mm. The external diameter of the spherical anode of the device's chamber is 120 mm

In the Geant4 model, the pulsed neutron source was generated. The specific capability of Geant4 to keep track of temporal evolution of the different processes was used to verify the temporal evolution signature of short neutron pulses at different distances from the source.

This model includes the development of a human phantom placed at 3 meters from the pulsed neutron source, and the evaluation of Dose deposition in the phantom produced by each neutron pulse. The energy deposition is found by placing a detector in the phantom to measure the energy deposited in the body.

Neutron thermalization was studied in detail. For this case, a point neutron source surrounded by a water sphere with 0.5 cm radius was considered. An energy detector was placed at the sphere surface. The resulting neutron spectrum was calculated and subsequently used in the simulation of the interaction process of them with the cell cluster at the second stage of our computing.

3. Geometry of the modeled cell cluster

A close packed structure of 14 spheres made from homogeneous material, whose composition was defined using the parameters of table 1. from ICRU (5) was used. The arrangement of the cells in the cluster was optimized to use less space (6) (see figure 2). Each cell had a diameter of 13 μm. The cell composition used in our model was that defined by ICRU (5) (table1), but we included a Boron concentration of 30 ppm of boron per gram of tissue.

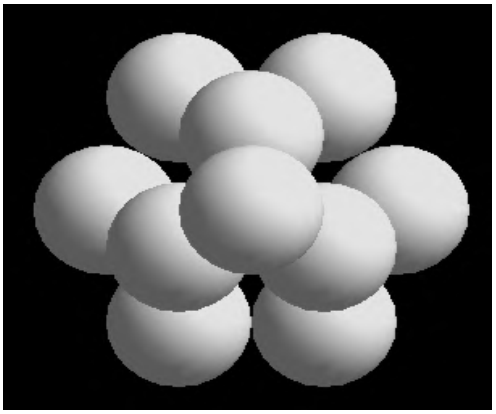

F*ig 2. Image of cell cluster as simulated by Geant4. Dimension of the cell cluster is around 26 μm diameter, arranged in order to minimize the space occupied by each cell. The cells in the cluster were surrounded by water*

Table1.

Cell Medium						
	Hydrogen	Carbon	Nitrogen	Oxygen	Phosphorus	Boron
Tissue (%by atom)	59.59	11.109	4.039	24.239	1.009	0.0029

4.Conclusions

In this section we present general results obtained with our simulation.

First, we found that the dose is distributed almost homogeneously among the cells within the cluster. The small differences in dose deposition between the cells of the cluster may arise from the differences in the small number of neutron tracks through each cell. We found that it's number of neutron tracks through the cells rather than the energy of the neutrons to determine the dose deposition. More intensive simulation are planned to understand this issue.

The result from this model suggests that one should plan the *in vitro* experiment in mammalian cells using a pulsed neutron source taking into account the dose deposition distributed around the tissue.

More specific results are presented and discussed in the conference.

References

1. V.A. Gribkov, M.A. Orlova., 2000 .Enzyme Activation and Inactivation Induced by Low Doses of Irradiation, Applied Biochemistry and Biotechnology. 88. 243-255.

2. V.A. Gribkov, A.V. Dubrovsky, M.A. Orlova, M. Scholz., 2005. Opportunities Afforded by New Generation of Pulsed Radiation Sources in Flash Radiation Physics and Chemistry. Research Journal of Chemistry and Environment. 9. 11-19.

3. V. A. Gribkov, A. V. Dubrovsky, M. Scholz, et al., 2006. PF-6 – an effective plasma focus as a source of ionizing radiation and plasma streams for application in material technology, biology and medicine. Nucleonika. 51. 55-62.

4. S. Agostinelli et al., Geant4—A simulation toolkit, Nuclear Instruments and Methods in Physics Research A 506 (2003) 250-303

5. ICRU, 1989.Tissue Substitutes in Radiation Dosimetry and Measurements. Report 44, International Commission on Radiation Units and Measurements, Bethesda, MD.

6. V.J. Petteri, L. Juha, K. Antti, I. Sami, S. Jiri, S. Sauli, 2001.Comparison of different cell-cluster models for cell-level dosimetry. Acta oncologica, 40. 92-97.

High Energy Proton Application to BNCT Neutron Source (1) - Outline of J-PARC project and Transmutation Experimental Facility -

Toshinobu Sasa[1], Yoshihisa Tahara[2], Mamoru Baba[3], Hitoshi Yokobori[4]

[1] *J-PARC Center, Japan Atomic Energy Agency*
[2] *Department of Nuclear Reactor Design, Engineering Development Co. Ltd., Japan*
[3] *Cyclotron and Radioisotope Center, Tohoku University*
[4] *Advanced Reactor Technology Co., Ltd.*

Japan Atomic Energy Agency and High Energy Proton Accelerator Research Organization (KEK) precede the Japan Proton Accelerator Research Complex (J-PARC) project. J-PARC consists of a 600 MeV proton linac, a 3 GeV synchrotron, a 50 GeV synchrotron and research facilities for basic science like particle physics and applied sciences. Within the project, Transmutation Experimental Facility (TEF) is planned to build in the second phase of the project. TEF aims at studying the physics and engineering feasibility of accelerator driven system (ADS) that is suitable for transmutation of long-lived radioactive wastes. TEF consist of two buildings; Transmutation Physics Experimental Facility (TEF-P) and ADS Target Test Facility (TEF-T). Because of the requirement of low-power operation of critical assembly in TEF-P, beam dump will be located at the end of the beam transport system for TEF-P. In the present plan, a 400MeV-30kW proton beam will be delivered to the beam dump.

It is well known that the proton-induced spallation reaction is an endoergic reaction and is convenient to obtain bright neutron source for basic science. It is also useful for Boron Neutron Capture Therapy (BNCT) which is conducted using fission reactors, and an accelerator driven BNCT neutron source will be realized because the spallation neutron has an energy spectrum similar to that of fission neutron. Hence, we are proposing a BNCT neutron source facility using the beam dump of TEF-P. The neutron spectrum provided by the spallation reaction will also be useful for various simulations such as neutron effects for soft and hard errors of micro-electronic devices.

In the presentation, outline and the current plan of J-PARC and TEF will be presented and installation plan of spallation target and beam ports specialized for BNCT will be discussed.

The INR Neutron Sources for Neutron Capture Therapy

S.V. Akulinichev, L.V. Kravchuk, V.M. Skorkin

Institute for Nuclear Research of the RAS, 60-th October Anniversary pr.7a, Moscow 117312, Russia

Abstract

Liquid-crystalline DNA-Gd nanoparticles, as a potential carrier for NCT were investigated using the spallation neutron source and the fusion neutron reaction $T(D,n)^4He$. The spallation neutron source are based on impulse beam provided by the high-current proton linac. This source produces fast neutrons with an average intensity up to 10^{15} n/s and an average neutron energy of 0.5 MeV. Secondary photons from irradiated DNA-Gd nanoparticles have been detected by Xenon gamma spectrometer. The radiobiological effectiveness of the nanoparticles have been investigated using fast neutrons of the compact D-T neutron source.

Keywords: Neutron source, spallation, NCT*, DNA-Gd, nanoparticle*

1. Introduction

Yevdokimov (2005) has proposed nanoarticles of liquid-crystalline dispersions formed by the cholesteric double-stranded DNA and Gd ions as a potential platform for Neutron Capture Therapy. Each nanoparticle contains 10^8 gadolinium atoms and the corresponding natural gadolinium concentration in the biomaterial is about 250 μg/g (^{157}Gd concentration is about 40 μg/g).

In Neutron Capture Therapy (NCT), the therapeutic effect of the gadolinium compound the main radiation effect is caused by electrons and gamma rays derived from the $^{157}Gd(n, \gamma)^{158}Gd$ reaction (Greenwood, 1978). During neutron irradiation, secondary radiation (γ- ray, electron, X-ray) are produced by nuclear reactions in the material. The secondary particles have a range in tissue above of 30 μm and can induce a tissue dose and DNA double strand breaks (DSB) in tumor cell nucleus when the DNA-Gd nanoparticles are located on the surface of tumor cells. The secondary radiation generated and crossing the cell nucleus are enough to lead to lonogenic death.

Neutron capture therapy of oncology diseases requires the use of neutron beams having a specific quality. In the treatment of deep seated tumours by NCT epithermal neutron beams, lying in the energy range (0.5 eV – 10 keV) are required. Requirements to the neutron beams are formulated by health physics and approved by the proper methods of treatment. Fast neutron beams, having energies higher than 10 keV, can be used for neutron capture therapy after being moderated.

The nuclear reactor is the most powerful stationary source of neutrons (Zaitsev, 2004). However, a powerful reactor is very complex and expensive facility whose maintenance needs strong requirements to nuclear safety. The problems of the development of a neutron source for NCT based on the compact and inexpensive accelerator are the subject of intense discussions.

2. The spallation neutron sources of the INR linac.

The neutron sources of the Institute for Nuclear Research of the Russian Academy of Sciences (INR RAS) are based on the pulsating beam provided by the high-current proton linac of the Moscow Meson Facility (MMF) of the INR RAS.

The INR linac is foreseen to accelerate protons and H^- ions up to 600 MeV with the average current up to 500 μA. Pulse current is 50 mA, beam pulse duration (0.3 – 100) μs and beam pulse repetition rate up to 100 Hz. The secondary spallation neutrons are produced when hydrogen ions interact with the target nuclei of tungsten.

The spectrum of the evaporation neutrons at angle of 90^o from tungsten target of the RADEX facility irradiated by protons with energy 300 MeV is shown in Fig.1.

The contribution of the cascade neutrons is about of 1%.

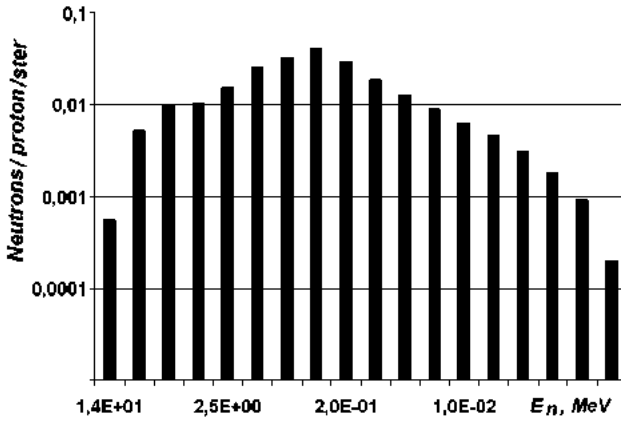

Fig. 1. The spectrum of the evaporation neutrons at angle of 90^o from W target hit by 300 MeV protons

The irradiation facility RADEX at the beam-stop is placed on the direct card track of the proton beam (Fig. 2). The RADEX irradiation facility has vacuum proton channel (Ø 20 cm), tungsten target (Ø 30 cm) and vertical neutron channel (Ø 6 cm and 4m length).

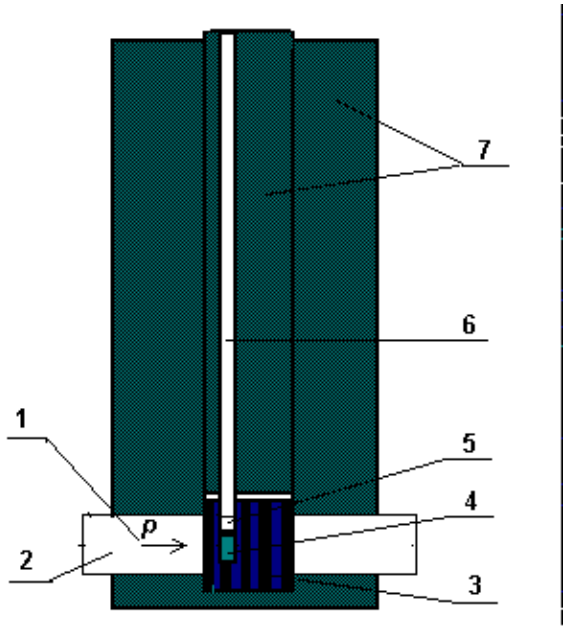

Fig.2. The RADEX Beam Stopper: 1- proton beam; 2 - vacuum channel; 3- tungsten target; 4 - moderator 5 - irradiated channel; 6 - vertical channel; 7 - iron shield

The tungsten target is placed 4 m beneath the surface of the beam-stopper. The vertical channel is placed between the tungsten target and surface of the beam-stopper. The spallation reactions result in the yielding of 10^{15} n/s fast neutrons from the target. The irradiated channel is placed into the tungsten target. The neutron flux level available in the irradiated channel is up to ~10^{13} n·cm^{-2}s^{-1}.

The neutron beams of the RADEX facility can be used for neutron capture therapy after being moderated. The moderator materials are placed into the irradiated channel of the RADEX facility. A Monte-Carlo transport program, MCNP-4B, was used to calculate the fluxes of the thermal, epithermal, fast neutrons and gamma beam components out the vertical channel for H_2O, D_2O and C moderator materials.

The neutron spectrum calculated out from the vertical channel is shown in Fig. 3.

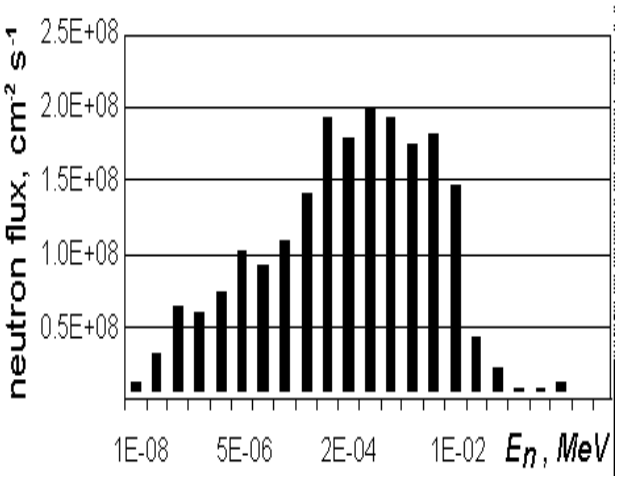

Fig.3. Spectrum of the neutrons out vertical channel of the facility RADEX

The RADEX irradiation facility has been used for registration of the secondary photons from neutron radiative capture by DNA-Gd nanoparticles. Biology samples containing 1 mg DNA-Gd nanoparticles were placed over the vertical channel and irradiated by thermal neutrons of the neutron of the RADEX facility. The average current onto W target was 10 μA. The characteristic gamma peaks at the energy above 1 MeV have been registed by Xenon gamma spectrometer (Dmitrenko, 1999).

3. The compact D-T neutron source.

The other compact D-T neutron source available produces up to $5\cdot10^{12}$ s^{-1} fast neutrons (about 15 MeV) using the fusion neutron reaction T(D,n)^{4}He threshold reaction. Current of deuteron beam (400 keV) used onto tritium target is 20 mA.

The D-T neutron source could be employed for neutron capture therapy experimental investigations by using an irradiation facility consisted of the tungsten neutron converter, a bismuth reflector, a graphite and polyethylene moderator. The thickness of W converter and Bi reflector is about 10 cm. Thickness of graphite moderator is about 20 cm.

A Monte-Carlo transport program, NCNP4B, was used to calculate the fluxes of the thermal, epithermal, fast neutrons from such a system shown in Fig.4.

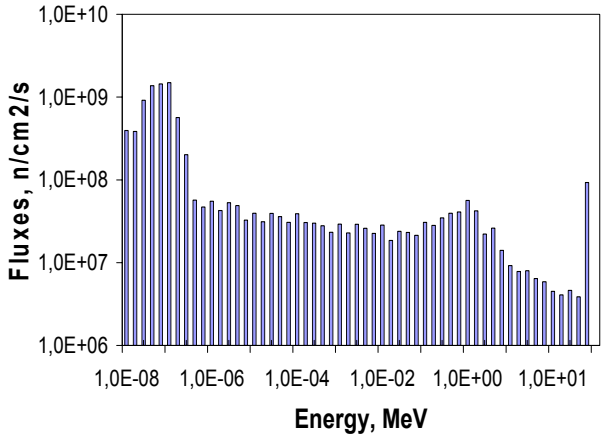

Fig.4. Spectrum of the neutrons from moderator system of the neutron generation

We have investigated the radiobiological effectiveness (RBE) of the secondary photon and electron radiation, generated after the thermal neutron capture by the DNA-Gd nanoparticles.

The amount of 0.1 ml of a cell suspension, containing about 10^7 cells, has been piled up on the inner surface of biological samples. The amount of (DNA-Gd) particles, containing about 0.5 mg of the natural gadolinium, was injected into the biomaterial of a given sample. The resulting nanoparticle density was of the order of 10^3 particles per cell (Gd concentration is about 5 mg/g). In such a case we may expect the DNA DSB and the killing of all cells provided the thermal neutron fluence is about 10^{11} n·см$^{-2}$. This result agrees with the estimations of Goorley (2004).

The biological samples containing cell suspension and DNA-Gd nanoparticles have been irradiated into the polyethylene phantom by neutrons from the D-T neutron source (Andreev, 1999). In this source primary neutrons with the energy about 15 MeV and the total intensity of ~ $2\cdot10^{11}$ n/s are generated in the tritium target, irradiated by the initial deuteron beam with the current of ~ 2 mA.

The biological samples were fixed at the depth of 5 cm in the polyethylene phantom of the size 20 ×20×20 cm^3. The polyethylene phantom was placed in moderator system consisted of the tungsten converter, bismuth reflector and polyethylene.

Monte-Carlo calculations were performed for evaluating the neutron spectrum the fluxes of the thermal, epithermal, fast neutrons and gamma rays in the biological samples. The estimated integral thermal, epithermal, fast neutron and gamma ray fluxes in the biological samples are of $1.4\cdot10^8$ n·см$^{-2}$·s^{-1}, $2.9\cdot10^7$ n·см$^{-2}$·s^{-1}, $3.5\cdot10^7$ n·см$^{-2}$·s^{-1}, $5.9\cdot10^7$ n·см$^{-2}$·s^{-1} correspondingly.

We might expect that the killing of a major part of tumor cells in biological samples with nanoparticles should be due to secondary electrons and photons. However, a certain amount of fast neutrons was still reaching the biological samples.

In order to extract the net biological effect of the thermal neutron capture in the nanoparticles, we have identically irradiated two sets of biological samples: one with the nanoparticles containing gadolinium and a another one without it.

The thermal and fast neutron fluxes for each biological sample were measured by means of the neutron activation analysis. For these purposes standard calibrated samples of pure niobium, indium, manganese, lanthanum have been used. In all experiments these standard samples were placed between the biological samples. In the experiment under consideration the fast neutron flux for the neutron energy above 0.3 MeV was estimated as $(1\text{-}3)\cdot10^7$ n·см$^{-2}$·s^{-1}. The experiment thermal neutron flux in the same experiment was about $1.5\cdot10^8$ n·см$^{-2}$·s^{-1}. This result agrees with the our estimated neutron fluxes.

Irradiation time of the biological samples was (15-60) minutes. The thermal neutron fluence was of the order of $(0.5\text{-}5)\cdot10^{11}$ n·см$^{-2}$.

The resulting absorbed dose delivered by the secondary electrons and photons, emitted after the thermal neutron capture by (DNA-Gd) nanoparticles, was (10-20) Gy. This dose of the secondary photons and electrons results in an average 1 DSB/cell. The fast neutron fluence on biological samples did not exceed of $5\cdot10^{10}$ n·см$^{-2}$. The gamma radiation dose from thermal neutron capture by the polyethylene phantom did not exceed of 0.1 Gy.

When gadolinium atoms were present into biological samples, was the killing of all cells when exposed to about $1\cdot10^{11}$ n·см$^{-2}$ of thermal neutrons. The kill-effect was no observed in the biological samples without gadolinium.

5. Conclusions

Further studies are needed to determine optimal Gd-157 concentrations as a function of neutron fluence and irradiation time.

We want to acknowledge the special effort of A.V. Andreev who provided important support for the measurements.

References

Yu. M. Yevdokimov et al., 2005, Particles of liquid-crystalline dispersions formed by (nucleic acid-rare earth element) complexes as a potential platform for neutron capture therapy. Int. J. Biol. Macromol.370, 165-173.

R.C. Greenwood, C.W. Reich, H.A.Baader et al., 1978., Collective and two-quasiparticle states in ^{158}Gd observed though study of radiative neutron capture in ^{157}Gd. Nucl. Phys. A 304, 327-428.

K.N. Zaitsev, A.A. Portnov, O.V. Mishcherina et al., 2004. Neutron capture therapy at t he MEPhI reactor**,** International Journal of Nuclear Science and Technology. 83-101.

V.V. Dmitrenko, A.G. Dvornyak V.M. Gratchev et al, 1999 Nucl. Instr. and Meihod. A 442.326-330-326.

T. Goorley, R. Zamenhof, H. Nikjoo, 2004, Calculated DNA Damage from Gadolinium Auger Eletrons and Relation to Dose Distributions in a Head Phantom. Int. J. Radiat. Biol., v.80, p. 933-940**.**

A.V. Andreev, S.A. Makarov, 1999. Analysis of multicomponent systems by fast neutron activation, Chechoslovak Journal of Physics. 49, part 1, 377-379

Perspectives for the Application of Plasma Focus Technology to Neutron Capture Therapy

G. Grasso[a], F. Rocchi[a], M. Sumini[a], A. Tartari[b]

[a] *Nuclear Engineering Laboratory of Montecuccolino, University of Bologna, via dei Colli 16, 40136 Bologna (BO), Italy*
[b] *Physics Department, University of Ferrara, and INFN Ferrara, via Saragat 1, 44100 Ferrara (FE), Italy*

Abstract

One of the major problems in the widespread diffusion of neutron capture therapy installations, both for research and treatment purposes, is the lack of safe neutron sources. By safe it is meant a source that satisfies at least three requirements: 1) doesn't rely upon even small quantities of fertile/fissile materials; 2) doesn't rely upon the strong emissions of radioisotopes; 3) can be switched off and turned on at will. In 2002 we presented a preliminary design for a thermal neutron source based on the Plasma Focus (PF) technology for TAORMINA-like treatment protocols. The PF technology in fact satisfies all the three requirements mentioned above. PF machines can produce fast neutrons by triggering D-D or D-T nuclear fusion reactions in a repetitively generated pulsed plasma discharge. Deuterium and Tritium are used at fairly low values of pressure (a few hundred Pa), so that only small amounts of these gases are required. The typical neutron yield per discharge is proportional to the square of the input energy E which is stored in a high voltage capacitor bank. For D-D reactions and for E = 50 kJ, the neutron yield results to be about $2.5 \cdot 10^{10}$ n/discharge, while for D-T reactions at the same input energy the yield is about $2.5 \cdot 10^{12}$ n/discharge. For these values of E it is possible to build PF machines capable of 1 Hz discharge repetition rates with a continuous workload up to total neutron yields for a D-T plasma of about $3 \cdot 10^{14}$ n in 2 minutes. In the present paper we present a different PF design which can accommodate two special types of irradiators, one that can be used to provide thermal neutrons for TAORMINA-like treatments, and another that can provide epithermal neutrons for standard protocols. The PF end-user can shift between these two at will depending on the day-by-day needs. Evaluations of the performances of the two irradiators will be presented by Montecarlo (MCNP code) simulation of the neutron transport processes.

Keywords: Plasma Focus, MCNP, thermal spectrum, epithermal spectrum

1. Introduction

One of the major problems in the widespread diffusion of neutron capture therapy (NCT) installations, both for research and treatment purposes, is the lack of safe neutron sources. By safe it is meant a source that satisfies at least three requirements: 1) doesn't rely upon even small quantities of fertile/fissile materials; 2) doesn't rely upon the strong emissions of radioisotopes; 3) can be switched off and turned on at will. The first requirement stems out from the great procedural simplification in the licensing, commissioning and management of a neutron source that doesn't involve the use of fertile/fissile materials in comparison with one that on the contrary uses them. Not all the medical research centres interested in NCT can afford the burden of dealing with either a critical or slightly subcritical nuclear reactor as a neutron source. The second requirement is directly connected to the risks associated with personnel exposure to ionizing radiations or with environment contamination which a sealed neutron source brings with itself. Among the desiderata of a good neutron source for NCT applications is for sure a high emission intensity; however the higher is the intensity, the higher are the associated risks. The third requirement is related to the ease of use of the source itself. While there exist many neutron sources that satisfy only one of these requirements (a subcritical reactor can be switched off by turning off the primary source of neutrons consisting f.i. in a proton accelerator), very few exist that satisfy all of them (the aforementioned subcritical reactor must contain large amounts of highly enriched uranium which might pose severe problems related to the proliferation issue). In 2002 (Benzi et al., 2004) we presented a preliminary design for a thermal neutron source based on the Plasma Focus (PF) technology for TAORMINA-like treatment protocols. The PF technology satisfies all the three requirements mentioned above. PF machines can produce fast

neutrons by triggering D-D or D-T nuclear fusion reactions in a repetitively generated pulsed plasma discharge. Deuterium and Tritium are used at fairly low values of pressure (a few hundred Pa), so that only small amounts of these gases are required. Typically a single PF impulse consists in the preliminary and relatively slow (a few seconds) storaging of energy in a high voltage capacitor bank (15-30 kV) and in the subsequent extremely rapid (a few ms) discharge of this energy onto a gas load. The initial power delivered to the capacitor bank is therefore compressed in space and time, this being the main reason to include the PF in the class of the so called pulsed power devices. The high voltages used in the process are able to generate a plasma from the initially neutral gas; this plasma is then arranged in a thin sheath that is forced by the self-induced electromagnetic forces to implode onto itself. During this implosion PF devices are able to generate the necessary plasma conditions to trigger nuclear reactions between the ion species of the plasma. In case of a PF which uses deuterium, D-D fusion reactions are used as sources of 2.45 MeV neutrons; if a mixture of deuterium and tritium is used then fusion reactions produce 14 MeV neutrons. The neutron emission source can practically be considered point-like, isotropic and monochromatic. At the end of the rapid energy discharge the plasma species recombine and the gas is taken to its initial state, ready for another pulse. These pulses can be repeated for some time at a given repetition frequency f which varies according to the technological characteristic of the PF considered. In all PF devices however the average number of neutrons produced per shot depends only on the square of the input energy E according to a well-known scale law. For D-D reactions and for E = 50 kJ, the neutron yield results to be about $2.5 \cdot 10^{10}$ n/discharge, while for D-T reactions at the same input energy the yield is about $2.5 \cdot 10^{12}$ n/discharge. For these values of E it is possible to build PF machines capable of 1 Hz discharge repetition frequencies with a continuous workload up to total neutron yields for a D-T plasma of about $3 \cdot 10^{14}$ n in 2 minutes. Considering that to turn off a PF it is enough to avoid to store further energy in the capacitor bank, and that the amounts of tritium are very small (a few hundreds Pa in volumes of some tens of litres), it can safely be concluded that PFs satisfy the three conditions mentioned above concerning safe neutron sources for NCT applications. In the present paper we present a PF design which can accommodate two special types of irradiators, one that provides thermal neutrons for TAORMINA-like treatments, and another that can provide epithermal neutrons for standard protocols. The PF user can shift between these two at will depending on the day-by-day needs.

2. PF geometry and irradiators

The design here presented comprises a core unit, the PF itself, surrounded by a neutron reflector, and an upper part, the so called irradiator, which can be changed according to the neutron spectral needs. The whole system is cylindrical, with a diameter of 100 cm. Figure 1 shows a scheme of the core with the thermal neutron irradiator; the PF itself is made by the volumes labelled with numbers 1 to 9; volumes 4, 5 and 6 are occupied by the PF work gases; the other volumes are occupied by structural materials (T91 stainless steel). All the PF ancillary devices (capacitor bank, power supply etc.) are not shown. Volume 21 is occupied by the explanted organ to be irradiated (filled with water in the calculations reported below); all the remaining volumes are filled with BeO.

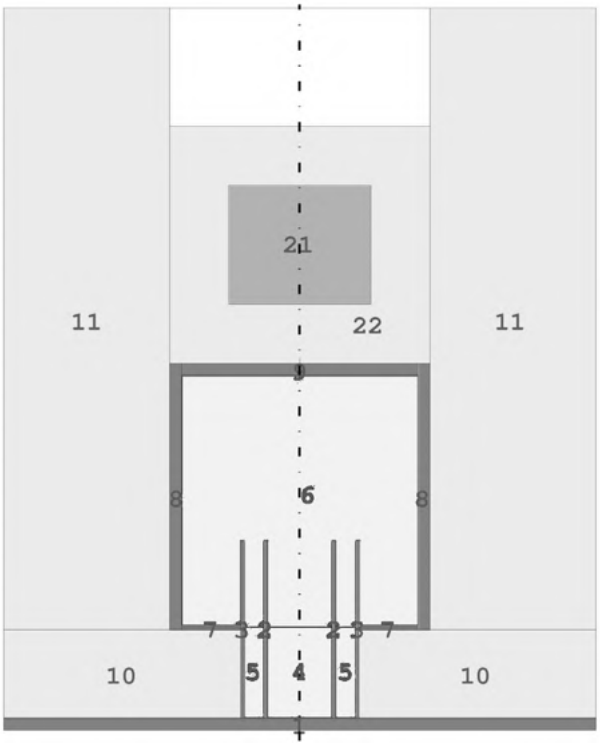

Figure 1. Schematic drawing of PF geometry with thermal neutron irradiator

The height of the system up to the upper level of volume 22 is 1 m. Volume 11 has been kept 20 cm taller to improve the neutron reflection towards volume 21. BeO was used instead of polyethilene as neutron reflector because the second would have acted in the sense of lowering the energy of the reflected neutrons more strongly than the first, and this isn't an optimized design for a core unit which

has to supply also epithermal neutrons. Figure 2 shows a schematic drawing of the PF geometry with the epithermal neutron irradiator. It can be seen that the core unit (below volume number 31) is exactly the same as that in Figure 1.

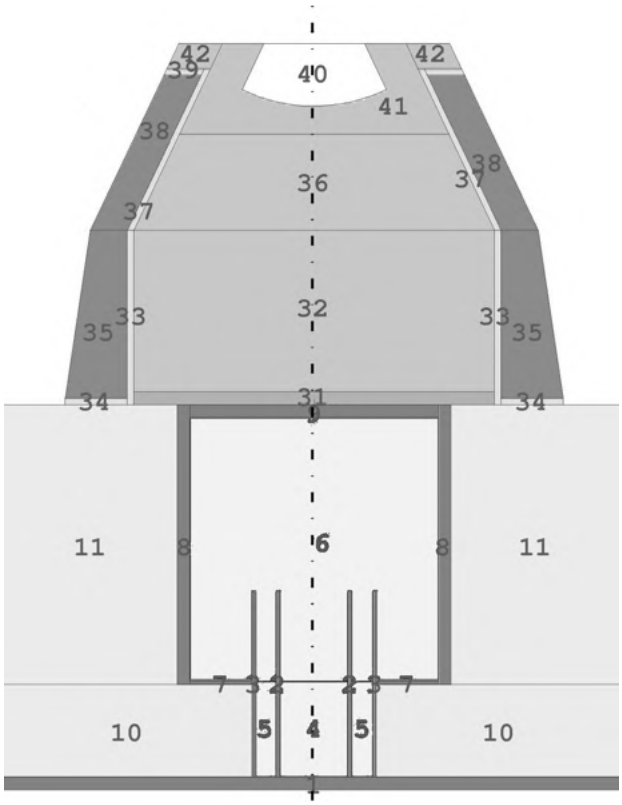

Figure 2. Schematic drawing of PF geometry with epithermal neutron irradiator

The neutron irradiator (volumes with label numbers higher than 31) for epithermal applications is taken from the optimal design configuration validated by Montagnini et al. (2002). Volume 40 is the irradiation cavity, shaped to accommodate the head of a patient or the body of a guinea pig. Volume 31 is filled with AlF_3 and volumes 32 and 36 are filled with a mixture of AlF_3 and LiF. These materials exhibit the highest spectrum shifting properties: the ratios between the fast-to-epithermal energy groups transfer cross section and the removal cross section from the epithermal group are about 2.3 and 2 for AlF_3 and LiF respectively. LiF has also a (n,t) cross section which is rather high for thermal neutrons, so that it can also act as a high-pass neutron filter with energy cut-off at the thermal/epithermal threshold. Volumes 31, 32 and 36, which act as an epithermal column, are surrounded by a Ni reflector (volumes 35 and 38); between the epithermal column and its reflector a thin layer of LiF (volumes 33 and 37) is also placed, to minimize the gamma ray emission from the thermal neutron captures of Ni. Volumes 41 and 42 are filled with Bi which acts as a shield to protect volume 40 against any other gamma rays which could be generated parasitically in the system.

3. Evaluation of the neutronic properties

The evaluation of the neutronic properties of the system has been carried out with four MCNP 5 simulations, two for each PF neutron source energies. For the sake of convenience three neutron energy groups have been defined: 1, up to 0.4 eV (thermal); 2, between 0.4 eV and 0.1 MeV (epithermal); 3, higher than 0.1 MeV (fast). Figure 3 shows the evaluated neutron energy distributions for 2.45 MeV and 14 MeV source particles (A curves), averaged over the volume 21 of Figure 1, and their respective energy integrals (B curves), for the thermal neutron irradiator.

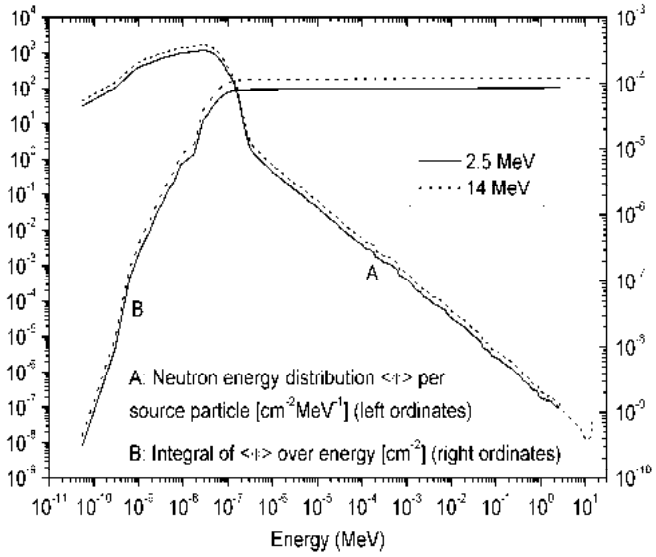

Figure 3. A: neutron energy distribution per source particle, averaged over volume 21 (see Fig. 1). B: integral of A over energy

It can be seen that the 14 MeV distribution presents the same features of the 2.45 MeV one; this is due to the fact that the moderation properties of the system are exactly the same for the two monochromatic source energies; however the 14 MeV distribution is always slightly higher than that at 2.45 MeV; this is due to the fact that the 14 MeV neutrons have a higher probability than the 2.45 MeV ones of inducing (n,2n) reactions in T91 and in ^{9}Be. The (n,2n) threshold for ^{16}O is too high, being at about 16.7 MeV; that for ^{56}Fe (main isotope in T91) is at about 11.4 MeV, so that only neutrons from the 14 MeV source are capable of triggering (n,2n) reactions. The threshold for ^{9}Be is at about 1.9 MeV, so that both sources are able in principle to generate extra neutrons, however the ratio $\sigma_{n,2n}$(14 MeV)/$\sigma_{n,2n}$(2.45 MeV) is about 20, so that more

extra neutrons are produced by ^{9}Be from 14 MeV neutrons than from 2.45 MeV ones. Since all these extra neutrons are produced only by energetic primary neutrons, they are produced very near the PF source so that they are all subject to the same slowing down kernel of the primary neutrons and therefore don't induce differences in the final energy distributions. The overall result of the simulations is that the neutrons available for thermal BNCT applications are roughly 10^{-4} those provided by the source. Figure 4 shows a map of the thermal fluence per 2.45 MeV source neutron in the midplane of volume 21 (see Fig. 1). It can be seen that the spatial distribution is not uniform, with a gradient along the axial direction expressed by a variation of about a factor 9. It can also be seen the beneficial effect of the lateral reflectors which increase the fluence profiles near the edges of the volume.

Table 1. Performance of PF & epithermal irradiator

Source Energy (MeV)	Energy Groups	J^+ @ PF exit [#]	J^+ @ irradiator exit [#]	$\langle\Phi\rangle$ in volume 40 [cm^{-2}]
2.45	1	2.10e-2	2.46e-5	1.14e-7
	2	2.64e-1	2.86e-3	1.34e-5
	3	2.20e-1	2.92e-5	1.71e-7
14	1	2.42e-2	2.42e-5	1.00e-7
	2	2.63e-1	2.96e-3	1.39e-5
	3	2.15e-1	3.19e-4	1.34e-6

Table 1 summarizes some results pertaining to the epithermal irradiator system. The first column shows the source energy while the second presents the three energy groups. The third and fourth columns give the integral J^+ of the partial neutron current in the upward direction over the surfaces of volumes 31 and 40 (see Fig. 2) respectively. The last column shows the average fluence per source particle in volume 40. Roughly 10^{-5} neutrons per source neutron are available for epithermal NCT; the epithermal component of the spectrum is particularly pure, being about two order of magnitudes higher than the undesired thermal and fast ones. No strong differences are present between the results pertaining to the 2.45 MeV and the 14 MeV sources. It is evident, by analyzing the J^+ that the epithermal irradiator acts as a spectrum shifter; in fact while it reduces the thermal and fast components of the spectrum by 3 to 4 orders of magnitude, it lowers the epithermal contribution by only 2 orders of magnitude. In this way it can be considered a good epithermal column for the system.

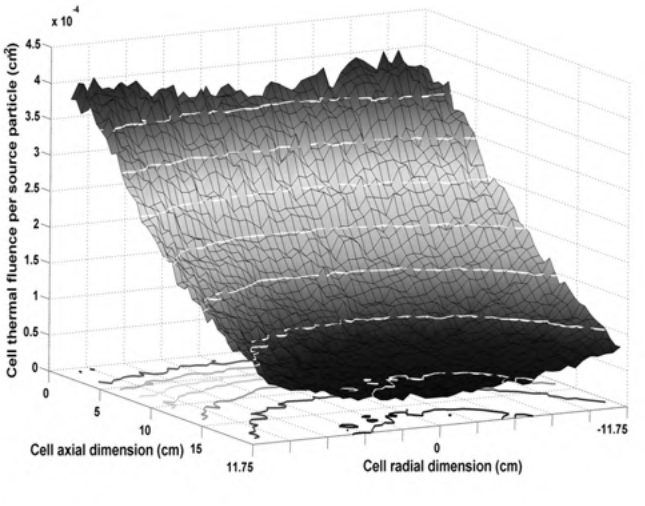

Figure 4. Map of the thermal fluence per 2.45 MeV source neutron in the midplane of vol. 21 of Fig. 1

4. Conclusions

Using the results of the previous section it is possible to estimate the fluences attainable with a PF. Assuming a realistic machine, working at f = 1 Hz and having a bank energy of 50 kJ, source fluences of about $3\cdot10^{14}$ neutrons in 2 minutes of continuous workload are possible with a D-T gas mixture. In these 2 minutes then it is possible to deliver thermal fluences of about $3\cdot10^{10}$ n/cm^2 with the thermal irradiator and epithermal fluences of about $3\cdot10^{9}$ n/cm^2 with the epithermal irradiator. While these values are not yet enough for a TAORMINA-like protocol and for a standard epithermal treatment, they are more than enough to carry out experiments on guinea pigs. It would be possible to increase the fluences of about a factor 10 if the capacitor bank energy were increased up to 150 kJ. A PF, however not dedicated to the production of neutrons, with 150 kJ bank energy and f = 1 Hz is presently under construction as a joint effort of the universities of Bologna and Ferrara (PFMA-1).

References

Benzi, V., Mezzetti, F., Rocchi, F., Sumini, M., 2004. Feasibility analysis of a Plasma Focus neutron source for BNCT treatment of transplanted human liver. Nucl. Inst. Meth. B 213, 611-615.

Montagnini, B., Cerullo, N., Esposito, J., Giusti, V., Mattioda, F., Varone, R., 2002. Spectrum shaping of accelerator-based neutron beams for BNCT. Nucl. Inst. Meth. A 476, 90-98.

Epithermal Neutron Generator Using J-PARC 400 MeV Protons

Yoshihisa Tahara[a], Toshinobu Sasa[b], Mamoru Baba[c], Hitoshi Yokobori[d], Shinji Abe[a]

[a]*Engineering Development Co., Ltd., 1-1-1, Wadasaki-cho, Hyogo-ku, Kobe, 652-8585, Japan*
[b]*J-PARC Center, Japan Atomic Energy Agency, 2-4, Shirane, Shirakata, Tokaimura, Naka-gun, 319-1196, Japan*
[c]*Cyclotron and Radioisotope Center, Tohoku University, 6-3 Aoba, Aramaki, Aoba-ku, Sendai 980-8578, Japan*
[d]*Advanced Reactor Technology Co., Ltd., 16-5, Konan 2-chome, Minato-ku, Tokyo, 108-0075, Japan*

Abstract

An epithermal neutron generator for BNCT has been studied, which utilizes the spallation reaction induced by 400 MeV protons in J-PARC. Moderators and a collimator were optimized by neutronics calculations with the MCNPX code and a high epithermal neutron flux was obtained at the exit of the collimator.

Keywords: BNCT, J-PARC, Accelerator, proton, tantalum, spallation

1. Introduction

A proton linear accelerator is being constructed in J-PARC (Japan Proton Accelerator Research Complex), which is a joint project of JAEA (Japan Atomic Energy Agency) and KEK (High Energy Accelerator Research Organization). A Transmutation Experimental Facility (TEF) and a beam dump for the high energy beam is also planned to be constructed in the second stage of construction.

In the near future, high energy protons become available for physics experiments and Boron Neutron Capture Therapy (BNCT) in J-PARC.

So, a feasibility study on BNCT using such high energy protons has been done.

We have already shown that neutrons produced from high energy (p, n) reactions of tantalum can be used for BNCT, which are moderated into epithermal neutrons by iron and Fluental (Yonai et al., 2003 & 2004, Tahara et al., 2006). In the studies, a proton beam of 300μA at 50MeV was assumed because such a high current is planned at the Cyclotron and Radioisotope Center (CYRIC) of Tohoku University.

Based on the above studies, we have designed a neutron generator using a cyclotron available in the accelerator market which can produce a 30 MeV/ 700 μA proton beam (Tahara et al., 2006, Unno et al., 2006, ICNCT-12).

The present study aims to establish the concept of a neutron source for BNCT to make efficient use of a 400 MeV proton beam drawn into the beam dump. The beam current available is 75 μA, i.e., total power of 30 kW.

This paper describes brief overview of J-PARC and a conceptual design of neutron generator using 400 MeV protons.

2. J-PARC

JAEA has been conducting a design study of the accelerator-driven system (ADS) to transmute minor actinides and long-lived fission products to reduce the radiological burden and disposal amount of high-level radioactive wastes (Sasa, 2004). To solve technical issues of ADS, the construction of TEF is planned under the framework of J-PARC project

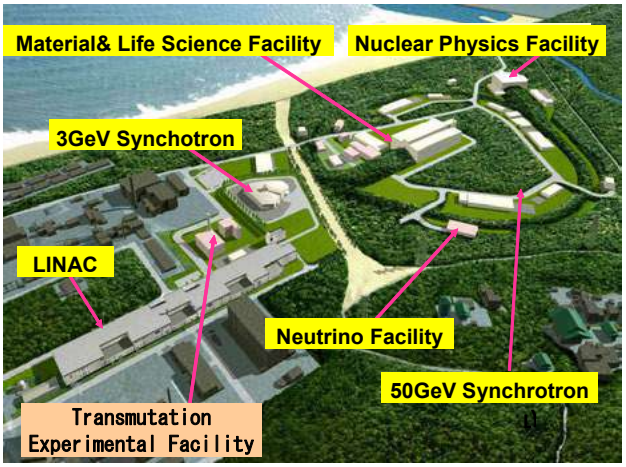

Fig. 1 Site plan of J-PARC Project

* Corresponding author's e-mail address is tahara@lax.kuramae.ne.jp.

(JAERI, 2000). J-PARC consists of a 600 MeV proton linac, a 3 GeV synchrotron, a 50 GeV synchrotron and research facilities for basic science, hadron physics, material science, and life science as shown in **Fig.1**. TEF is illustrated in **Fig.2**, which consists of two buildings: Transmutation Physics Experimental Facility (TEF-P) (Oigawa, 2001) and ADS Target Test Facility (TEF-T) (Sasa, 2005) .

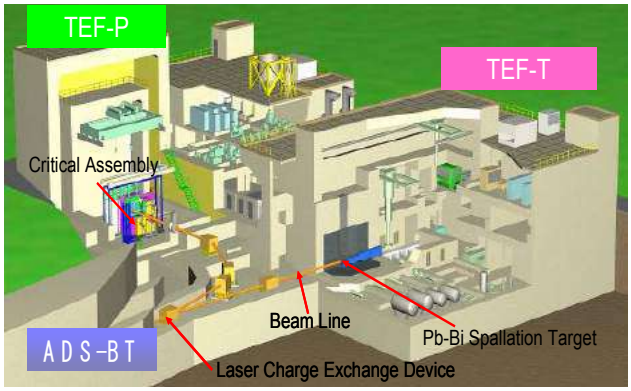

Fig. 2 Transmutation Experimental Facility

TEF-P is a critical/subcritcal assembly which can accept up to the beam power of 600 MeV-10 W at subcritical state. The purposes of TEF-P are the experimental validation of the data and method to predict neutronics of the ADS with spallation neutron source, the demonstration of the controllability of the system driven by a high-power proton accelerator, and the basic research of reactor physics for transmutation of long-lived radioactive nuclides. Another building called TEF-T is a facility to take data for engineering design of ADS using a 600 MeV-200 kW proton beam, which employs the Pb-Bi spallation target. The purposes of TEF-T are R&D for the irradiation damage of the beam window, the compatibility of the structural material with flowing liquid Pb-Bi and to accumulate experiences in operation of the high power spallation target.

Because of the requirement of low-power operation in TEF-P, the beam dump has to be installed at the end of the beam line for TEF-P as shown in **Fig. 3**. In the first stage of construction, a 400MeV-30kW proton beam is planned to be delivered to the beam dump. The delivered beam is planned to use in various research fields not only for the reactor engineering but also physics and medical applications. The multipurpose experimental area is beside the shield of the beam dump and its spallation neutrons can be supplied for engineering or scientific experiments. Additional removable spallation neutron source for BNCT is also planned in front of the beam dump. The horizontal and vertical beam ports are planned to easily irradiate any tumor location. Neutron spectrum can be changed by adjusting moderator thicknesses.

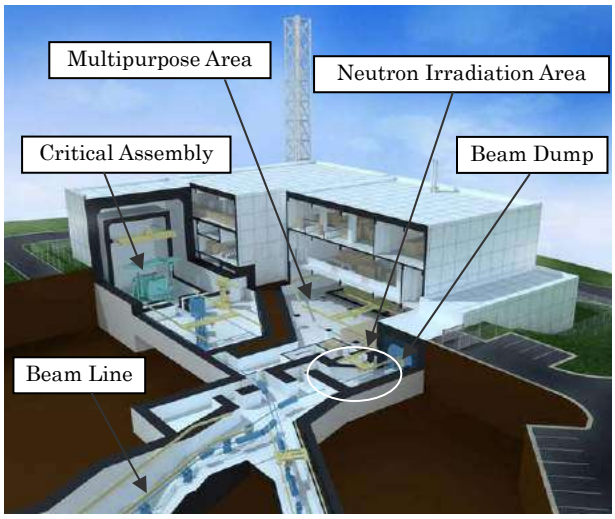

Fig. 3 Latest plan of TEF-P with beam dump

3. Epithermal Neutron Generator

The feature of this neutron source is to use spallation reaction of tantalum induced by high energy protons, while a Li or Be target uses low energy protons.

The population of backward neutrons produced by spallation reactions is less than that of forward ones in the high energy region. Thus, the use of backward neutrons, in our case 90 degrees against the proton beam axis, reduces patient damage due to high energy neutrons.

A newly proposed neutron generator is illustrated in **Fig.4**. It consists of a tantalum target with a cooling system, iron and Fluental moderators, a lead neutron reflector, and a collimator.

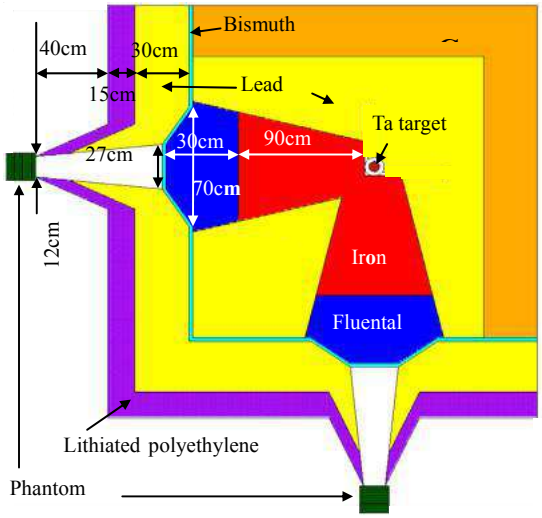

Fig. 4 Epithermal Neutron generator for BNCT

Protons flow along the z axis in Fig.4 from the back of the plane of the figure. The neutron source is assumed to be placed just before the beam dump.

The shape and size of the collimator and moderators were optimized to obtain high RBE dose and a deep dose distribution in the phantom. The moderator assembly is a column which consists of iron and Fluental. The collimator is made up from lithiated polyethylene (LiF dispersed polyethylene) and thick lead because the collimator has functions of neutron shielding as well as collimating a neutron beam. It also has a shape of a frustum of a cone from the easiness of setting a patient. In the dose evaluation, the Monte Carlo code MCNPX (LA-CP-02-408, 2002) was used with nuclear data libraries ENDF/B-VI ($E \leq 20$MeV) and LA150 ($20\text{MeV} \leq E$) (Chadwick et al., 1999). The resultant thicknesses of iron and Fluental moderator are 90 cm and 30 cm, respectively. The obtained neutron spectrum is shown in **Fig.5**.

The free beam characteristics are represented by three factors: for the 100% ^{6}Li collimator case, the integral value of epithermal flux Φ_{epi} is 1.07×10^{9} ($cm^{-2}s^{-1}$) and very close to the IAEA criteria of 1.0×10^{9} ($cm^{-2}s^{-1}$); the ratio of fast neutron flux Φ_{th} to epithermal neutron flux Φ_{epi} is 0.07 and almost same as the IAEA criteria value of 0.05; the ratio of gamma dose D_{γ} to epithermal neutron flux is 1.4×10^{-13} (Gy•cm^{2}) and less than the IAEA criteria value of 2×10^{-13} (Gy•cm^{2}).

These show that the quality of the epithermal neutron beam almost meets the requirements for BNCT (IAEA- TECDOC-1223, 2001).

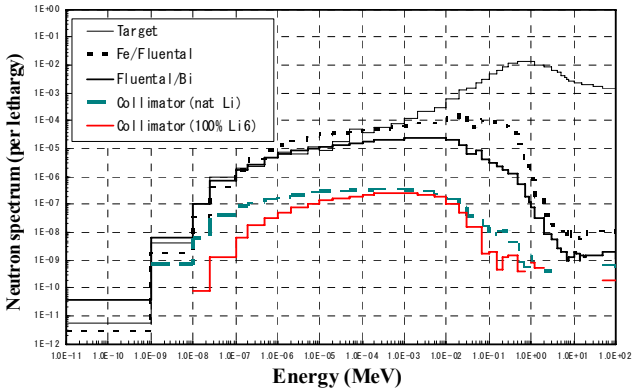

Fig. 5 Neutron spectrum at the exit of collimator

Equivalent doses of tumor and normal tissues in the phantom were calculated using MCNPX results and a kerma factor according to the procedure described by Yonai (2003). The phantom has the form of a column 16 cm in diameter and 16 cm long and is placed immediately close to the aperture of the collimator. In this calculation, values of 13 ppm and 45.5 ppm were assumed for the ^{10}B concentrations in normal tissue and in tumor tissue, respectively. Soft average tissue of an adult male is assumed as the phantom material (ICRU Report, 1989).

The RBE weighted dose distributions were calculated for normal and tumor tissues along with the center axis of the phantom, where a therapeutic time of one hour was assumed according to the IAEA TECDOC 1223 recommendation. The result is shown in **Fig.6** for ^{natural}Li collimator case.

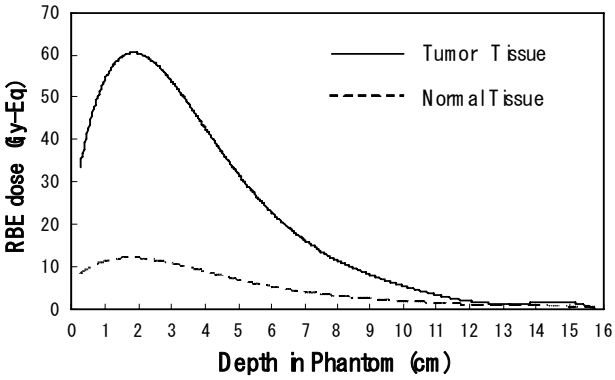

Fig. 6 Dose distributions in the phantom for tumor and normal tissues.

The maximum dose of 60 Gy-eq is achieved for tumor tissue and a RBE dose greater than 30 Gy-eq can be delivered to tumor tissue within a depth of 5.3 cm in the phantom. A sufficient dose for killing tumor tissue necessitates at least 22 to 30 Gy-eq in the case of partition irradiation (Feinendegen, 1997).

The maximum permissible irradiation time, which is usually called therapeutic time, can be calculated by equating weighted dose to the maximum tolerance value for normal tissue. The beam current required for one hour treatment can then be calculated to be 45μA. It is roughly a half of the total beam current. Therefore, the proton beam current is so strong that more sophisticated idea, e.g. neutron and gamma shielding, neutron shutter, can be incorporated into the design. The remaining beam current of 30μA or less may be disposed into the beam dump through the target. The heat load on the target will be mitigated in this way. The target structure will be also studied to maintain the integrity of the target.

Layout plans of the neutron generator were also considered for one floor type and two floors type (Tahara et. al., ICNCT-12, 2006).

This neutron source can be also designed as a multipurpose one by extracting neutrons directly or through moderators depending on the purpose of its use: BNCT, soft error evaluation, nuclear data measurements and shielding experiments etc.

6. Conclusions

This study shows that high intensity epithermal neutrons suitable for BNCT can be obtained by moderating high energy neutrons produced by spallation reactions using 400 MeV protons in J-PARC.

The construction of the two facilities TEF-P and the beam dump are planned in the second phase of construction of J-PARC. Discussions on necessity of such facilities and what kinds of equipments are useful to the facilities have been just started. Hence, this is the good time to discuss the application of 400-MeV protons to the neutron source for BNCT as an effective use of high energy protons to the beam dump.

Acknowledgements

The authors gratefully acknowledge the contributions of N. Akana and C. Hondo of Shibata Kako Sekkei Co., Ltd. for their support of calculations.

References

Chadwick, M. B., Young, P. G., Chiba, S., *et al.*, 1999. Cross-section evaluation to 150 MeV for accelerator-driven systems and implementation in MNCPX, Nucl. Sci. Eng., 131, p.293.

Feinendegen, L. E., 1997. Report on the Workshop: The Clinical State of Boron Neutron Capture Therapy 1997, United States Department of Energy, Office of Science of Biological and Environmental Research Medical Science Division.

IAEA-TECDOC-1223, 2001. Current status of neutron capture therapy. International Atomic Energy Agency.

ICRU Report 44, 1989. International Commission on Radiation Units and Measurements; Tissue Substitutes in Radiation Dosimetry and Measurement.

JAERI-Tech 2000-003, 2000. The Joint Project for High-Intensity Proton Accelerators (in Japanese). The Joint Project Team of JAERI and KEK.

LA-CP-02-408, 2002. MCNPX User's Manual Version 2.4.0, Los Alamos National Laboratory.

OIGAWA, H., et al., 2001. Conceptual Design of Transmutation Experimental Facility. Proc. of Global2001, Paris, France.

SASA, T., et al., 2004. Research and development on accelerator-driven transmutation system at JAERI. Nuclear Engineering and Design 230, 209-222.

SASA, T., et al., 2005. Conceptual Study of Transmutation Experimental Facility (2) Study on ADS Target Test Facility (in Japanese). JAERI-Tech 2005-021.

Tahara, Y., Oda, Y., Shiraki, T., Tsutsui, T., Yokobori, H., Yonai, S., Baba, M., Nakamura, T., 2006. Engineering Design of a Spallation Reaction-Based Neutron Generator for Boron Neutron Capture Therapy. J. Nucl. Sci. and Technol., Vol.43, No.1 p.9.

Tahara, Y., Abe, S., Akiyama, Y., Kamei, Y., Tsutsui, T., Yokobori, H., Unno, Y., Baba, M., 2006. A BNCT Neutron Generator using a 30MeV Proton Beam. Proc. of 12th Int. Cong. on Neutron Capture Therapy, ICNCT-12, pp.327-330, October 9-13, 2006 in Takamatsu, Kagawa, Japan.

Unno, Y., Yonai, S., Baba, M., Itoga, T., Kamada, S., Tahara, Y., Yokobori, H., 2006. Benchmark Experiments on Neutron Moderator Assembly for Cyclotoron-Based Boron Neutron Capture Therapy. ibid., pp.331-334.

Yonai, S., Aoki, T., Nakamura, T., Yashima, H., Baba, M., Yokobori, H., Tahara, Y., 2003. Feasibility study on epithermal neutron field for cyclotron-based boron neutron capture therapy. Med. Phys. 30 [8], p.2021.

Yonai, S., Itoga, T., Baba, M., Nakamura, T., Yokobori, H., Tahara Y., 2004. Benchmark experiments for cyclotron-based neutron source for BNCT," Proc. of 11th Int. Cong. on Neutron Capture Therapy, Boston, MA, U.S.A., p.997.

An epithermal neutron generator based on the Be(p,n) reaction using a 30 MeV proton cyclotron accelerator at KURRI

H. Tanaka[a], Y. Sakurai[a], M. Suzuki[a], T. Takata[a], S. Masunaga[a], Y. Kinashi[a], G. Kashino[a], Y. Liu[a], T. Mitsumoto[b], S. Yajima[b], H. Tsutsui[b], A. Maruhashi[a], and K. Ono[a]

[a]*Research Reactor Institute, Kyoto University, Asashiro-nishi 2-1010, Kumatori-cho, Osaka 590-0494, Japan*
[b]*Sumitomo Heavy Industries, Osaki 2-1-1, Shinagawa, Tokyo, 141-6025, Japan*

Abstract

In order to generate epithermal neutrons for Boron Neutron Capture Therapy (BNCT), we proposed the method of filtering and moderating fast neutrons, which are emitted from the reaction between a beryllium target and 30 MeV protons accelerated by a cyclotron accelerator, using an optimum moderator system composed of iron, lead, aluminum, and calcium fluoride. At present, the epithermal- neutron source is under construction since June 2008 at Kyoto University Research Institute. This system consists of a cyclotron accelerator to supply a proton beam of about 1 mA at 30 MeV, a beam transport system, a beam scanner system for heat reduction on the beryllium target, a target cooling system, a beam shaping assembly and an irradiation bed for patients.

In this article, an overview of the Cyclotron-Based Neutron Source (CBNS) and the properties of the treatment neutron beam optimized by using the MCNPX Monte Carlo code are presented. The distribution of the RBE (Relative Biological Effectiveness) dose in a phantom shows that, assuming a ^{10}B concentration of 13 ppm for normal tissue, this beam could be employed to treat a patient with an irradiation time less than 30 minutes and a dose less than 12.5 Gy-eq to normal tissue. The CBNS might be an alternative to the reactor-based neutron sources for BNCT treatments.

Keywords: cyclotron-based neutron source, proton cyclotron, Be(p,n) reaction

1. Introduction

At first, the BNCT treatments using KUR (Kyoto University Research Reactor) were adapted for malignant melanoma and brain tumors. The widespread application to the treatment of other diseases such as recurrent head and neck tumors, liver tumors (Suzuki et al., 2007) and mesothelioma (Suzuki et al., 2006) using epithermal neutrons has resulted in an increased number of clinical trials. In order to obtain good results for deep tumors, a higher dose is required. Moreover, a sufficient neutron yield obtained by using an accelerator-based neutron source that can be located near a hospital would be useful for further developments of BNCT.

Yonai et al. (2003) and Tahara et al. (2006) are already investigating a neutron source using spallation reactions that occur for 30-50 MeV protons incident on a tantalum target. The possibility of exploiting the reaction of several tens of MeV protons incident on a beryllium target, was excluded because of the fast neutrons contamination of the treatment beam. However, a sufficient epithermal neutron yield based on the Be(p,n) reaction could be obtained with an optimum beam-shaping assembly. Our system has the advantage of a larger neutron yield and a lower activation of the target material in comparison with the spallation reactions involving heavy materials.

The neutron transport for optimum treatment beams was simulated by using the Monte Carlo calculation code MCNPX (Pelowitz, 2005). This article reports an overview of the epithermal neutron generator and calculated parameters in phantom.

2. Cyclotron-Based Neutron Source (CBNS)

2.1. Cyclotron accelerator and Beryllium target

The cyclotron accelerator (HM-30) manufactured by Sumitomo Heavy Industries is employed to provide a ~1 mA, 30 MeV proton beam. In the HM-30 hydrogen negative ions are accelerated and protons up to 30 MeV are derived by the charge conversion in a carbon foil stripper. The proton beam derived from HM-30 is led to a beryllium target via a beam transport system. A uniform 120 mm × 120 mm proton beam at the beryllium target is shaped by a controlling magnetic field of two scanning magnets.

Table I shows the characteristics of Be, W, and Ta target materials when irradiated by a 1mA, 30MeV proton beam.

Target	Melting point (°C)	Boiling point (°C)	Thermal conductivity (W/m/K)	Neutron yield (/s/cm²/mA)	Gamma ray yield per one neutron
Be	1278	2970	201	1.90E+14	0.02
Ta	3017	5458	57.5	1.27E+14	0.93
W	3422	5555	174	9.65E+13	1.40

The neutron and gamma ray yields were estimated by using the MCNPX code and the cross-section data of ENDF/B-VII, physical model, and la150 for Be, Ta, and W, respectively. In comparison with the other materials listed in Table I, Be shows the highest neutron yield, the smallest gamma-ray yield per neutron, the highest thermal conductivity and a high melting point. A 1 mA, 30 MeV proton beam has a 30 kW power. Such a large heat input needs a target-cooling system. In our system, a Be target is directly cooled by pure compressed water. The compressed water flows through a spiral graphite water channel. 30 MeV protons with a range of 5.8 mm in Be penetrate a 5.5 mm-thick Be target and inject in the compressed cooling water in order to prevent blistering of the target.

With regard to the experimental results for the thermal resistance of a Be target, Tadokoro et al. (2006) indicated that a heat input of 500 W/cm^2 leads to a temperature less than 500 ^{o}C. The irradiation area should be expanded to 60 cm^2 for a heat input of 500 W/cm^2 under 30 kW operation. The area of 144 cm^2 scanned by two scanning magnets is sufficient for heat reduction on the target.

In order to evaluate the target activation resulting from one year of operation a 2-h irradiation per day with a 1 mA proton current was assumed. The neutron- and proton-induced activation of the three above materials was calculated by using the IRACM code (Tanaka et al., 1997). The nuclei produced in a W target have higher activity and longer half lives than Be and Ta targets. Immediately after the daily operation, the activation rate of a Ta target is four order of magnitude higher than that of a Be target. The period required for the Ta target until the ambient dose rate becomes 1 mSv/h is twice of that required for the Be target. Considering the above-mentioned results in terms of neutron yield, thermal properties, and activation level, the Be target was chosen.

2.2. Beam-shaping Assembly (BSA)

Yanch et al. (1991) found out that for BNCT treatments at a 10 cm depth in the head, the most effective neutron energy is 10 keV and the most effective neutron energy range is between 4 eV and 40 keV.

In the reaction between 30MeV protons and a Be target, the neutrons that are emitted in the forward direction have an energy of up to 28 MeV. In order to reduce the neutron energy to the epithermal energy range, a BSA composed of a moderator and a shaper has been employed. The moderator is used to reduce the energy from the maximum value of 28 MeV with low capture cross section. The shaper is used to obtain the 10 keV optimum energy mentioned above.

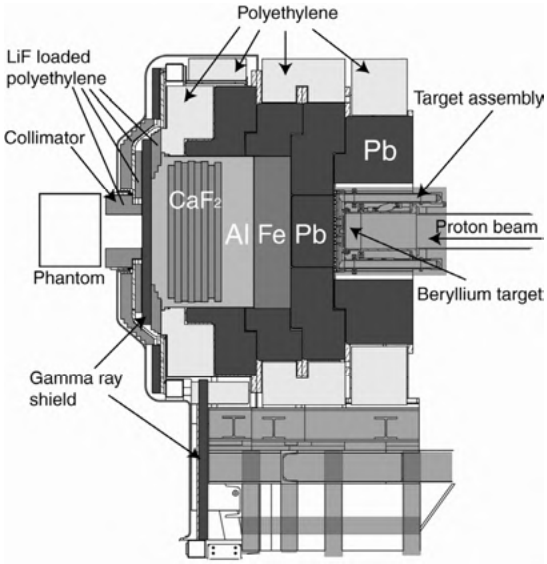

Fig. 1 Schematic layout of the BSA to obtain an epithermal neutron beam using a 30-MeV proton beam incident on a beryllium target

Fig.1 shows the schematic layout of the BSA. The moderator materials are Pb and Fe. The Pb component, used as a breeder and a reflector for high energy neutrons, was installed near the target. The Fe component, mainly used as a moderator, was installed after the Pb component. With regard to the shaper, AlF_3 is often used in the design of an epithermal neutron generator (Liu et al., 2004) and the material density should be high in order to form a compact BSA. It is difficult to increase the AlF_3 density because it sublimes at a temperature of 1040 ^{o}C under atmospheric pressure. Therefore, we focused on Al and CaF_2 instead of AlF_3.

The optimum thickness of each component was determined through the calculation of the dose distribution in the phantom composed of soft average tissue of adult male (ICRU-44) by using the MCNPX code.

In order to prevent the exposure of the patient to the fast-neutron radiation, the moderator, the shaper and the front surface of the collimator are surrounded by polyethylene blocks.

Furthermore, in order to accurately set the patient in the position determined by the treatment planning system, an X-ray tube and an imaging plate are installed. The pair of X-ray tube and imaging plate can be moved to the neutron beam side and an image of the "beam's eye view" can be obtained. Laser markers are also installed; the irradiation position is set by a marking on the skin.

3. Results and Discussion

All the following results are related to a 1 mA, 30 MeV proton beam.

3.1. Free beam properties

Fig. 2 shows the CBNS neutron flux spectrum under the free-air condition evaluated at the surface of the gamma-ray shield in comparison with the KUR one, which is most-often used in the BNCT treatments (Sakurai and Kobayashi, 2000). The CBNS neutron spectrum has a peak in the 10-20 keV energy range. In this article, the definition of the epithermal energy range is from 0.5 eV to 40 keV. The energy region below 0.5 eV is defined as the thermal region; that above 40 keV, as the fast-neutron region.

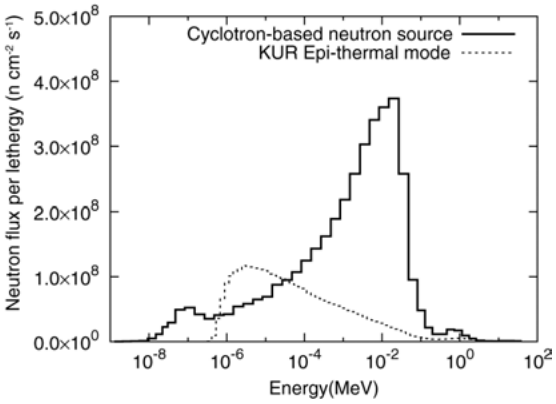

Fig. 2 Comparison between the CBNS neutron spectrum and the KUR one

The fast-neutron and gamma-ray dose contaminations per epithermal neutron for CBNS under the free-air condition are 5.84×10^{-13} and 7.75×10^{-14} Gy·cm^2, respectively. Each absorbed dose value was obtained by using the neutron flux at the gamma-ray shield and the flux-to-dose conversion factors published in ICRP-74. The human tissue components were assumed to be H: 11.1, C: 12.6, N: 2.0, and O: 74.3 (wt %). The fast-neutron and gamma-ray dose contaminations per epithermal neutron for KUR under the free-air condition are 9.10×10^{-13} and 2.40×10^{-13} Gy·cm^2, respectively (Sakurai and Kobayashi, 2000). With regard to the fast neutrons and gamma rays contaminations the CBNS facility is superior to KUR one.

3.2 Beam characteristics in phantom

Fig. 3shows the evaluation of the CBNS neutron flux components in a phantom located in front of the collimator.

The diameter of the collimator aperture and phantom are 16 cm and 26 cm, respectively. The maximum value of thermal neutron flux is 2.3×10^9 cm^{-2}·s^{-1} at a depth of 2.3 cm in phantom.

The prescribed dose is determined by the differential boron accumulation in tumor and normal cells (T/N ratio) and the boron concentration in the blood of the patient.

The RBEs assumed for nitrogen, hydrogen and gamma rays are 3.0, 3.0, and 1.0, respectively.

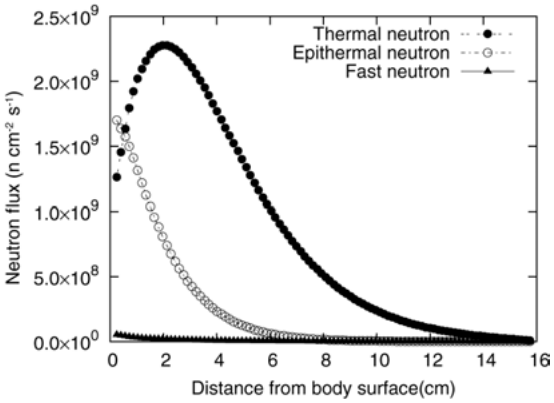

Fig. 3 Neutron flux components (thermal, epithermal and fast) in phantom

The compound biological effectiveness (CBE) factors for tumor and normal brain are 3.8 and 1.35, respectively. The T/N ratio of 3.5 is employed. The boron concentration is assumed to be 13 ppm. The therapeutic time is determined by the dose limit for the normal brain of 12.5 Gy-eq. Fig. 4 shows the distribution of the RBE dose components in the phantom. Under the above hypotheses, the RBE dose in tumor reaches a maximum value of 57 Gy-eq at a depth of about 2.3 cm in phantom and the irradiation time is less than 30 minutes. The sufficient dose for killing the tumor is at least 30 Gy-eq. The CBNS facility can treat a tumor located within a depth of 5.5 cm, with the RBE dose of 30 Gy-eq by single irradiation. With regard to the irradiation of deeper tumors, the bilateral irradiation can be adopted to raise the prescribed dose. At a depth of 8 cm, the RBE dose is about 15 Gy-eq. Therefore CBNS can treat tumors situated at almost all the positions in the brain by using the bilateral irradiation.

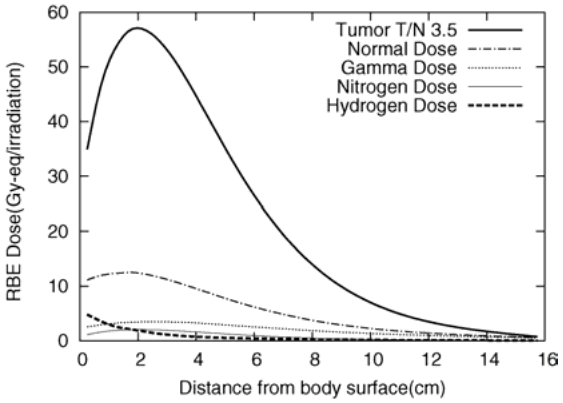

Fig. 4 RBE dose components in phantom

4. Conclusions

By means of Monte Carlo simulations a moderator and a shaper have been optimized for the high energy neutrons emitted from the Be(p,n) reaction with a 1 mA, 30 MeV proton beam. With regard to the fast neutrons and gamma rays dose contamination, CBNS is superior to the current KUR facility. From the evaluation of the dose distribution in a phantom the irradiation time using CBNS turns out to be about 30 minutes. CBNS becomes a powerful tool for treating deep tumors by using the bilateral irradiation. The CBNS facility is now under construction and the aim is to establish it at KURRI by 2009. KUR also will restart in the middle of 2009. Thus KURRI will have both the reactor- and the accelerator- based neutron sources for BNCT. The treatment using CBNS will be performed on the basis of the optimization presented in this article. The accelerator-based neutron source can be located near the hospital; this work could lead to future developments of BNCT.

References

Liu, Y.W.H., Huang, T.T., Jiang, S.H., Liu, H.M., 2004 Renovation of epithermal neutron beam for BNCT at THOR, App. Rad. Isotope, 61, 1039-1043

Pelowitz, D.B., 2005. MCNPX user's manual - Version 2.5.0, Los Alamos National Laboratory Report LA-CP-05-0369

Sakurai, Y. and Kobayashi, T., 2000, Characteristics of the KUR Heavy Water Neutron Irradiation Facility as a neutron irradiation field with variable energy spectra, Nucl. Instrum. Methods A453 569-596

Sakurai, Y. and Ono K., 2007. Improvement of dose distribution by central beam shielding in boron neutron capture therapy, Phys. Med. Biol. 52 7409-7422

Suzuki, M., Sakurai, Y., Hagiwara, S., Masunaga, S., Kinashi, Y., Nagata, K., Maruhashi, A., and Ono, K., 2007, First attempt of boron neutron capture therapy(BNCT) for hepatocellular carcinoma, Jpn J Clin Oncol,37(5) 376-381

Suzuki, M., Sakurai, Y S., Masunaga, S., Kinashi, Y., Nagata, K., Maruhashi, A., and Ono, K., 2006. Feasibility of boron neutron capture therapy (BNCT) for malignant pleural mesothelioma from a viewpoint of dose distribution analysis, Int. J. Radiation Oncology Biol. Phys., Vol. 66, No. 5, pp. 1584-1589

Tadokoro, T., Kawakubo, Y., Seki, H., Tayama, R., Umegaki, K., Baba, M., Kobayashi, T., 2006. Feasibility Study on a Common Use Accelerator System of Neutron Production for BNCT and Radionuclide Production for PET, Advances in Neutron Capture Therapy 2006 (Proceedings of ICNCT-12)304-307

Tahara, Y., Oda, Y., Shiraki, T., Tsutsui, T., Yokobori, H., Yonai, S., Baba, M., Nakamura, T., 2006. Engineering Design of a Spallation Reaction-Based Neutron Generator for Boron Neutron Capture Therapy, J. nucl. Sci. and Tech., Vol.43, No.1, 9-19

Tanaka, S., Fukuda,M., Nishimura, K., et. al, 1997. A Code System to Calculate induced Radioactivity Produced by Ions and Neutrons, JAERI-Data/Code 97-019

Yanch, J.C., Zhou, X.L., Brownell, G.L., 1991, A Monte Carlo Investigation of the Dosimetric Properties of Monoenergetic neutron Beams for neutron Capture Therapy, Radiation Research 126,1-20

Yonai, S., Aoki, T., Nakamura, T., Yashima, H., Baba, M., Yokobori, H., Tahara,Y., 2003. Feasibility study on epithermal neutron field for cyclotron-based boron neutron capture therapy, Med. Phys. 30(8), 2021-2030

First neutron generation in the BINP accelerator based neutron source

B. Bayanov[a], A. Burdakov[a], V. Chudaev[a], A. Ivanov[a], S. Konstantinov[a], A. Kuznetsov[a], A. Makarov[b], G. Malyshkin[c], K. Mekler[a], I. Sorokin[a], Yu. Sulyaev[a], and S. Taskaev[a]

[a] *Budker Institute of Nuclear Physics, 11 Lavreniev ave., Novosibirsk, Russia*
[b] *Novosibirsk State University, 2 Pirogov str., Russia*
[c] *All-Russian Research Institute of Technical Physics,13 Vasiliev str., Snezhinsk, Russia*

Abstract

Pilot innovative facility for neutron capture therapy was built at Budker Institute of Nuclear Physics, Novosibirsk. This facility is based on a compact vacuum insulation tandem accelerator designed to produce proton current up to 10 mA. Epithermal neutrons are proposed to be generated by 1,915 MeV protons bombarding a lithium target using ^{7}Li(*p*,*n*)^{7}Be threshold reaction. The results of the first experiments on neutron generation are reported and discussed.

Keywords: epithermal neutrons, lithium target, neutron capture therapy, tandem accelerator

1. Introduction

In 1998 at Budker Institute of Nuclear Physics an original source of epithermal neutrons had been offered on a base of the tandem accelerator with vacuum insulation VITA, suitable for wide use of BNCT in clinical practice (Bayanov et al., 1998). It is offered to carry out generation of neutrons as a result of threshold reaction ^{7}Li(*p*,*n*)^{7}Be while dumping the 1.915 MeV 10 mA proton beam on lithium target. At present moment the accelerator is constructed (Kudryavtsev et al., 2008). In this work the results of the first experiments on generating neutrons are presented.

2. Gamma-registration system

A γ-detector based on NaI Ø6×6 cm and Photonis XP3312B photomultiplier with the power supply optimized for spectrometer problems were used to register γ-radiation from lithium target. All elements of the detector are covered by metal shells and reliably protected from magnetic fields and electromagnetic noises. Stability of the power supply voltage is about 0.1%. This detector was placed inside a lead shield with wall thickness ~10 cm at 222 cm distance under the lithium target and covered with borated polyethylene when necessary. The collimator port size was 10×15 mm. The spectral analysis of scintillation impulses from γ-detector is carried out with the help of a high-speed spectrometer ADC, installed in the computer. The resolution of the ADC is 4096 channels at the amplitude of input impulses from -50 mV to -4 mV and speed of signal analysis is up to $4 \cdot 10^{5}$ imp/s. The software allows us to observe a spectrum accumulation in real time, to save and to display saved spectrums as well as to set the exposition time. Preliminary calibration of γ-spectrometer was carried out with the help of the ^{40}K spectral line registered in the gamma background and using a calibrated radioactive source ^{60}Co with activity $5.66 \cdot 10^{7}$ Bq and energy of γ-quanta 1173 and 1332 keV, and ^{137}Cs with activity $2.15 \cdot 10^{8}$ Bq and energy 662 keV. The calibration confirmed the spectrometer system linearity and showed that NaI crystal has 9.5% energy resolution and provides full absorption of energy for ~37% of 662 keV gammas, that is close to the 447 keV spectral line.

3. Experimental results

For radiation safety the proton beam current on the target has been limited by size using a collimator to an order of ~100 μA. The proton current on the target was measured indirectly by the coolant heating.

In Fig. 1 the spectrum registered at energy of protons lower than neutron generation threshold is shown. At energy of the proton beam 1.7 MeV the bright spectral line with energy 477 keV related to excitation of lithium nuclei by protons is visible. The γ-quanta with lower energy are also visible. These quanta are related to the work of the accelerator and-or hitting the proton beam on constructional materials. Turning off the magnet directing the protons to the lithium target results in the situation that only a background radiation from working accelerator remains in a spectrum.

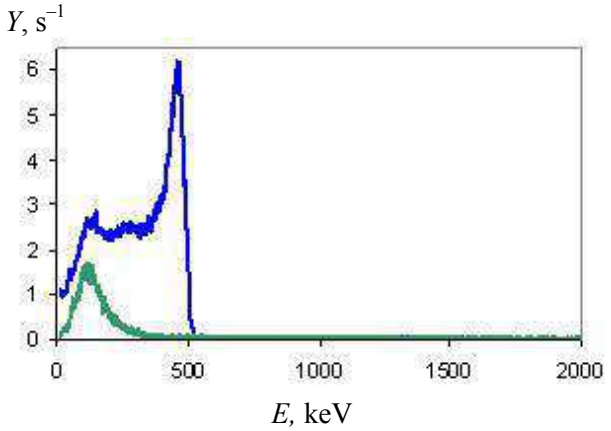

Fig. 1. Gamma spectra at the proton beam energy of 1.7 MeV (top curve); the spectrum at beam dumping on a wall of the vacuum chamber (bottom curve)

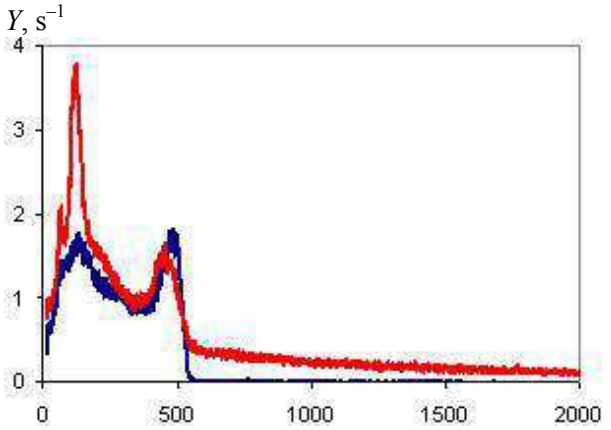

Fig. 2. Gamma spectra in case of the detector covered with borated polyethylene at dumping 1.92 MeV (top curve) and 1.7 MeV (bottom curve) proton beam on the lithium

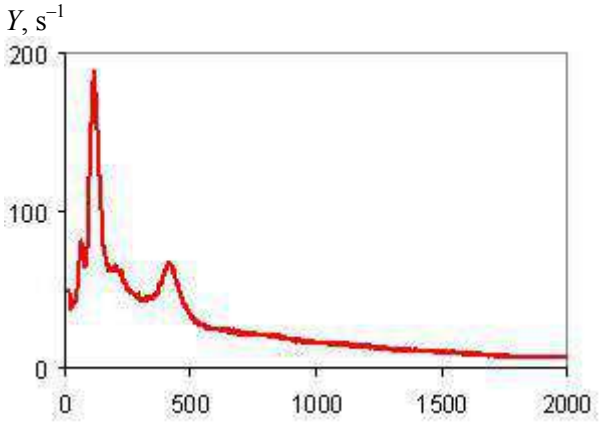

Fig. 3. Gamma spectrum in case of the detector without borated polyethylene protection at dumping 1.92 MeV proton beam on the lithium

At proton energy increased up to 1.92 MeV, neutrons start to be generated and γ-quanta from activated elements of the accelerator construction appear in a spectrum (Fig. 2). We should notice that the detector has been covered with borated polyethylene to attenuate the neutron flux. The total count speed has increased ~2 times in comparison with the subthreshold mode. When the borated polyethylene is removed from the detector, the signal increases considerably (Fig. 3) that is associated with capture of neutrons by iodine. This sort of sensitivity of NaI detector to neutrons allows us to use it as activation detector as well.

4. Usage of NaI as activation detector

^{127}I natural isotope has some resonances of neutron capture with energies from 20 eV to 1 keV with cross-sections about tens of barn. Resonant integral of capture $\int \sigma \frac{dE}{E} = 140$ barn. As the epithermal neutrons are of interest for neutron capture therapy the use of NaI as activation detector seems to be the ideal case.

Process of neutron capture by iodine-127 is accompanied by instant emission of 1.6 γ-quanta of which 0.3 have energy lower than 430 keV, and the others – from 4 to 6.7 MeV. It is proved in the measurements that spectral peaks are obviously visible at energies 63, 115, 202 and 416 keV which are in good agreement with transition energies between excitation levels in ^{128}I.

The ^{128}I isotope appeared as a result of neutron capture which decays with a half-life time of 25 min. In 6.4% of cases decay takes place by electron capture without any radiation, in 93.6% through a β^- decay with emission of electron having energy up to 2.12 MeV. Apart from the radioisotope ^{128}I there is another radioisotope, ^{24}Na which appears in the scintillator with a speed level estimated to be of the order of 2% with respect to iodine. Fig. 4 shows the spectrum registered by the activated detector. Such spectrum is specific for β^- decay.

The measurement started 13 minutes after the termination of neutron generation and stopped at the 106-th minute, with an average count speed registered of 2000 s^{-1}. When estimating the neutron yield it is necessary to consider that the part of the activated nuclei decay during the time interval of measurement for the reason that time of neutron generation and time of spectral measurements are comparable to iodine half-decay period. About $2 \cdot 10^7$ nuclei of ^{128}I were estimated to be inside the scintillator by the measured activity. As generation of neutrons was carried out within 420 seconds,

the speed of activation turns out to be equal to $5.4 \cdot 10^4$ s^{-1}. It was calculated by MCNP code that at the proton current of 100 μA the neutron capture reaction rate for iodine should be $3.77 \cdot 10^4$ s^{-1}, while for sodium $0.058 \cdot 10^4$ s^{-1}. Hence it turns out that the proton beam current was equal to 140 μA in the experiment, that is in good agreement with current measurements.

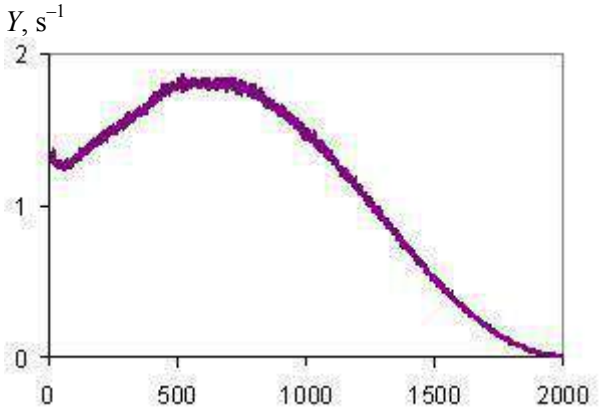

Fig. 4. Gamma spectrum of the activated detector (the measurement started 13 minutes after the termination of neutron generation and lasted 93 minutes)

5. The lithium target activation

As each neutron yielded in reaction $^7Li(p,n)^7Be$ is accompanied by the occurrence of ^7Be radioactive nuclei, the total yield of neutrons can be determined by measuring the remaining activity of lithium target. After the termination of neutron generation the target with lithium layer has been taken out and placed 21 cm over NaI detector. In Fig. 5, the measured γ-spectrum of the activated target is presented on which the 477 keV peak of γ-quanta from beryllium decay is obviously visible. The measured count speed for this peak was 4.1 events in a second. Given that only 37% of γ-quanta were found in the peak of full absorption, the target radiates $2.6 \cdot 10^4$ s^{-1} γ-quanta, and activity of beryllium turns out to be $2.6 \cdot 10^5$ Bq. In the given experiment the irradiation of the target with current 140 μA within 7 minutes was preceded by irradiation with approximately 2 times lower current within 6 minutes. Calculations show that the target activation reached 2.9 10^5 Bq, in good agreement with previous estimation. As the rate of decay of ^7Be radioactive nuclei is $1.51 \cdot 10^{-7}$ s^{-1} the quantity of generated neutrons is $2 \cdot 10^{12}$, and the average neutron yield makes $2.9 \cdot 10^9$ s^{-1}.

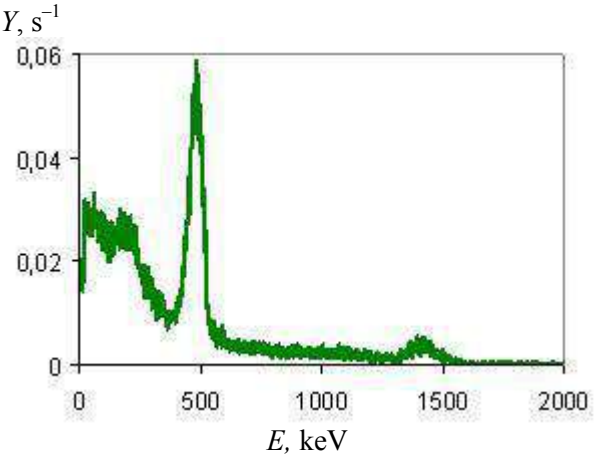

Fig. 5. Gamma spectrum of the activated target

6. Primary analysis of the generated neutron spectrum

For the primary analysis of the generated neutrons spectrum we used bubble detectors BDT and BD100R (Bubble Technology Industries, Canada). Detector BDT is a flask 19 mm in diameter 145 mm length and 58 g weight filled with polymer containing droplets of superheated liquid which structure is matched so that the detector has the maximum sensitivity at the thermal energies of neutrons $\sim 10^{-3}$ bubble/neutron·cm^2. BD100R detector, on the contrary, is sensitive to neutrons with energy more than 100 keV. In Fig. 6 two BDT detectors after neutron generation are shown. In the experiments performed the number of bubbles scored in BDT detector was 20 times greater than in BD100R one. Such a ratio corresponds to the expected spectrum with average energy 40 keV, realized in near-threshold mode.

Fig. 6. The BDT detectors after neutron generation

7. Conclusion

At Budker Institute of Nuclear Physics the first experiments on generation of neutrons for BNCT are carried out by means of tandem-accelerator VITA. The neutron yield is defined by means of a γ-detector using a NaI scintillator through the measurent of the remaining activity of the target and as activation detector itself. The average neutron yield determined in the experiments is $2.6 \cdot 10^9$ s^{-1} at the proton beam current ~140 μA that is in good agreement with theoretical value. Preliminary conclusions about the spectrum of neutrons are made using bubble detectors and correspond quite well to theoretical predictions. A more detailed investigation of the neutron spectrum is planned in the future using time-of-flight technique.

References

Bayanov, B., Belov, V., Bender, E., et al., 1998. Accelerator-based neutron source for the neutron-capture and fast neutron therapy at hospital. Nucl. Instr. and Meth. in Phys. Res. A413, 397–416.

Kudryavtsev, A., Belchenko, Yu., Burdakov, A., et al., 2008. First experimental result from 2 MeV proton tandem accelerator for neutron production. Rev. Sci. Instr. 79, 02C709.

Design of an Accelerator-Based Neutron Source for Neutron Capture Therapy

R. Terlizzi[1,2], N. Colonna[1], P. Colangelo[1], A. Maiorana[2], S. Marrone[1], A. Rainò[1], G. Tagliente[1], V. Variale[1]

[1] *Istituto Nazionale Fisica Nucleare and Dipartimento Interateneo di Fisica, Università di Bari, 70126 Bari, Italy*
[2] *IRCSS "Casa Sollievo della Sofferenza", U.O. di Fisica Sanitaria, 71013 San Giovanni Rotondo, Italy*

Abstract

The Boron Neutron Capture Therapy is particularly indicated in the treatment of the deep-seated tumours. In order to use this therapy in the hospitals, neutron beams of suitable energy, current and compactness are needed. In this contribution the advantages and disadvantages of several neutron beam choices are illustrated in terms of therapeutic gains. In detail the GEANT-3/MICAP simulations show that high tumour control probability, with sub-lethal dose at healthy tissues, can be achieved by using neutron beams of few keV energy having a flux of about 10^9 neutrons/(cm^{2}s). To produce such neutron beam, the feasibility of a proton accelerator is investigated. In particular an appropriate choice of the radiofrequency parameters (modulation, efficiency of acceleration, phase shift, etc.) allows the development of relatively compact accelerators, having a proton beam current of 30 mA and an energy of 2 MeV, which could eventually lead to setup hospital-based neutron facilities.

Keywords: BNCT; Neutron Source; RFQ accelerator.

1. Introduction

One of the most promising treatment using hadron particles for the care of the deep-seated tumors is the Boron Neutron Capture Therapy (BNCT). In fact thanks to the high depth of penetration of the neutrons in the tissues and in the bones, BNCT could be useful in the treatment of high-grade gliomas and specifically Glioblastoma Multiforme (GBM), extremely resistant to all current forms of therapy including surgery, chemotherapy, radiotherapy, immunotherapy and gene therapy after decades of intensive research (Barth et al, 2005).

This hadron-therapy is a two-component modality mainly based on the radiation damage produced by the high Linear Energy Transfer (LET) particles emitted in the capture reaction: $^{10}B(n,\alpha)^7Li$ (Barth et al, 2005). To obtain a high tumor control probability with minimal collateral effects on healthy tissues, an adequate concentration of ^{10}B has to be selectively accumulated in tumor cells by means of specific borated compounds. Then the patient is irradiated with neutron beams of energy and intensity suitably chosen so that the maximum density of thermal neutrons is reached in the proximity of the tumor area.

Clinical BNCT trials are currently undergoing at nuclear reactors (Harling and Riley, 2003); however, the development of high intensity accelerators could lead to high quality, safe and cost effective epithermal neutron sources for this therapy. In fact, compared to nuclear reactors, accelerator-based sources allow the production of epithermal neutron beams with higher spectral purity. In addition the compactness and the small size of low-energy accelerators may enable the operation of BNCT facilities in metropolitan areas and in the hospitals.

In this context, our study reports the characteristics and the feasibility of a low energy and high-current proton accelerator. Making appropriate choices in terms of reaction, energy and beam shaping, this machine can be used to produce the epithermal neutron beams useful for BNCT treatments. In the next section the optimal parameters for the neutron beams are indicated while section 3 illustrates the accelerator design.

2. Optimal energy of therapeutic neutrons

The optimal energy of a neutron beam for the treatment of deep-seated tumors can be investigated by means of simulations of the dose distribution in tissues. To this end, we have used the GEANT/MICAP package (Bisceglie et al, 2000).

Then the quality of the neutron beam is assessed by analyzing several figures of merit (e.g. the therapeutic gain) of the dose distribution, as a function of the neutron energy.

A realistic description of the geometry and composition of the head model is used. In fact the head is represented as a 7.6 cm radius sphere. The skull (calcium) is 0.54 cm thick while the remaining part of the sphere contains the brain. The tumour size is a 1 cm thick section of the brain and is located at 3, 5 and 7 cm depth inside the head. The brain tissue is composed in weight by: water (83.25%), carbon (14.90%) and nitrogen (1.84%) plus other minor elements. The thumoral tissue has the same composition of the brain but a larger contribution of B which replaces the oxygen atoms. In detail ^{10}B is included in concentrations of 10 (normal tissue) and 43 (tumour tissue) parts-per-million. These loading are typical of boronophenylalanine (BPA), a ^{10}B-carrier that together with sodium borocaptate (BSH) are the only boron delivery agents used in the clinical trials. Although, at this time no single ^{10}B-carrier fulfills all the criteria for a successful boron delivery agent (low systemic toxicity, tumor concentration, rapid clearance from blood and normal tissue, etc.), the BPA and BSH safety administration has been established (Hawthorne and Lee, 2003). At the same time the relative biological effectiveness (RBE) values of 1.6 and 2.3 are chosen for protons and α-particles, respectively. The dependence of the biological effect on the microdistribution of ^{10}B should require the use of compound biological effectiveness (CBE) factors that are drug dependent (Coderre and Morris,1999). Because it is very difficult to simulate the true bio-distribution of each drug, we have calculated only the RBE equivalent dose.

Fig. 1(a) shows the therapeutic gain (TG) as a function of the neutron energy in all three tumor depths considered. TG is defined as the ratio between the dose released to the tumor and the maximum dose to the normal tissues. The analysis of the TG allows the estimation of the optimal neutron energy range for different tumor locations, see Fig.1(b). The maximum therapeutic effect is always achieved by using neutrons of energy between 1 and 3 keV. Neutrons of lower energy thermalize at depths smaller than the tumor location, while for higher energies, recoiling protons lead to a sharp increase of the dose released to normal tissues, in particular to the brain surface.

3. Accelerator-based BNCT

The production and the collimation of monoenergetic neutron beams with energies of a few keV and suitable flux is not an easy task. In the case of reactor-based sources, the energy distribution of the neutron beam can be optimized by an appropriate choice of the material and geometry of the beam shaping assembly (BSA) made of filters, moderators and collimators. It is possible to improve the quality of the epithermal neutron beam by using an accelerator and a suitable proton or other induced reaction for neutron production. The choice of the beam energy and of the target is mainly dictated by the need of high yield of low energy neutrons (E_n < 1 MeV), and small contamination of the neutron beam (mainly, protons, electrons and γ-rays).

Furthermore, to minimize the size and the cost of the accelerator, a low energy injector of the primary beam has to be chosen, while the target should present good mechanical and thermal properties.

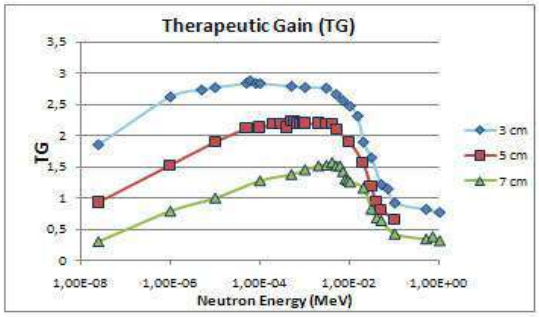

(a)

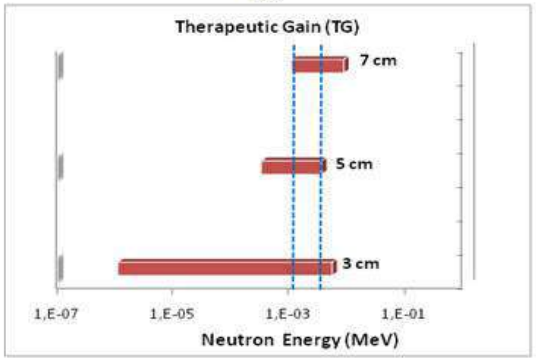

(b)

Fig. 1. (a) TG is shown as a function of neutron energy for tumour depths of 3, 5 and 7 cm. TG is defined as the ratio between the dose released to tumour and the maximum dose irradiated to normal tissues. (b) The maximum therapeutic effect is obtained with neutrons of energy between 1 and 3 keV

Finally, a stable residual isotope should be produced in the reaction, to reduce safety problems associated with storage and disposal of the targets.

Several approaches can be used in the choice of the proton beam energy and conversion target. A class of suitable neutron sources is represented by the near-threshold reactions. In this case, the low yield of neutrons is compensated by their low energy, permitting moderation for clinical application. The maximum achievable epithermal neutron flux for the $^{7}Li(p,n)^{7}Be$ near-threshold reaction (proton energy in the range between 1.89 and 1.95 MeV) is about 8×10^{7} neutrons/(cm^2 s mA). Since to complete a treatment in one hour 10^{9} neutrons/(cm^2 s) must be delivered (Zimin and Allen, 2000), the proton beam current, required in conjunction with that reaction, is in the range of 10-30 mA.

Accelerator neutron sources based on the near threshold $^{7}Li(p,n)^{7}Be$ reaction require a small size moderator because neutrons emitted from the lithium target have neutron energies peaked between 100 and 800 keV. This energy range is definitively low, compared to other nuclear reaction producing neutrons, but it is still too much for BNCT (Liskien and Paulsen, 1975). The optimal configuration of a BSA has been estimated by means of simulations in a 3D geometry. Neutron transport through different moderator/reflector systems has been performed with the GEANT 3.21 code. The overall therapeutic gain and the number of neutrons moderated in suitable energy (efficiency in percentage) are shown in Fig. 2 as a function of moderator thickness for different materials. These results suggest that a close to optimal TG, together with an efficiency greater than 15%, could be obtained by using a moderator/reflector assembly of BeO/Al_2O_3, 10 cm thick.

The production of epithermal neutron beams for BNCT requires a proton accelerator of high current (10 mA) and low energy (2–2.5 MeV). A radio frequency quadrupole (RFQ) accelerator would be well suited for this purpose, since it can be assembled in a very efficient and compact way. An RFQ uses electrical radio-frequency focusing and is able to capture, bunch and transmit high current ion beams with a reduced space-charge effects. In fact, for a low-energy beam, the space-charge forces increase causing the blow-up of beam emittance. RFQ can be used to bunch the beam adiabatically (Schempp, 1995). Several parameters (synchronous phase, acceleration efficiency etc…) can be chosen so that as the velocity increases, the geometrical length of the bunch remains nearly constant while the bunch spacing increases. This keeps the bunch from being spatially compressed, resulting in a reduction of the space-charge effects. Finally, if the parameters of the accelerator are chosen properly, RFQ bunching nearly eliminates the focusing difficulties. In order to sustain acceleration of high intensity ion beam by adiabatic bunching, it is necessary to design a structure of RFQ cells with four sections. Bunching is started in the shaper section, while adiabatic bunching is realized in the gentle buncher section. The designed final energy is achieved in the acceleration section.

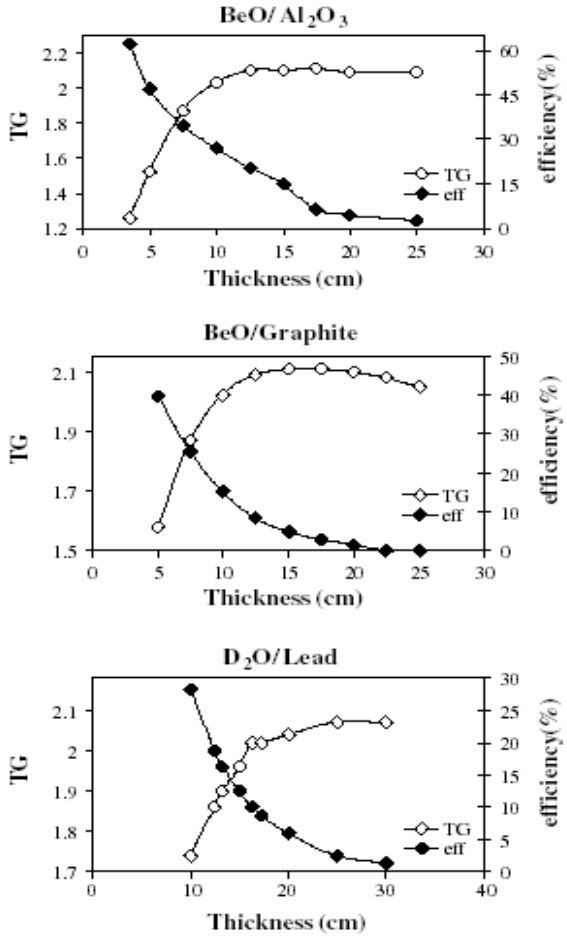

Fig. 2. The overall therapeutic gain (TG) and the efficiency are shown as a function of the moderator/reflector thickness. A therapeutic gain close to 1.9 with an efficiency greater than 15%, can be obtained by a moderator/reflector assembly of BeO/Al_2O_3, 10 cm thick

The feasibility of an RFQ-based neutron source for BNCT has been estimated using Trace 3-D code (Crandall, 1987), an interactive beam-dynamics software that calculates the envelope of bunched beams, including linear space-charge forces, through a user defined transport system.

The following parameters have been assumed: an initial proton energy of 80 keV, a current of 30 mA, a voltage range of 68 kV, a radius for the RFQ cell of 3 mm and a radio-frequency of 352 MHz. The beam envelope for the whole RFQ system provided by Trace 3-D code is shown in Fig. 3. A total of 135 cells are necessary to produce a final proton energy of 2.0 MeV for an estimated length of 2.47 m.

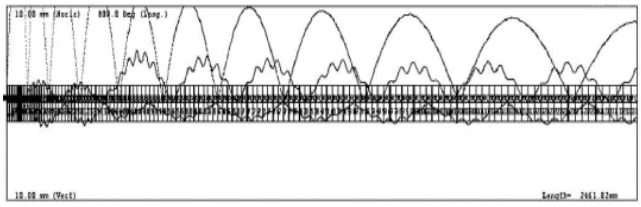

Fig. 3. Beam envelope calculated by Trace 3-D for an RFQ system of 135 cells, designed for accelerating a proton beam of 30 mA current at the final energy of 2 MeV. The three curves represent the envelopes in the phase-space planes. The total length of the accelerator results 2.47 m

4. Conclusions

The feasibility of an accelerator-based neutron source (ABNS) for producing therapeutic beams for BNCT have been investigated. A possible solution could be based on the use of ^{7}Li(p,n) near threshold reaction, or other low-energy (p,n) or (d,n) reactions (Colonna et al, 1999). The use of a compact RFQ linac would allow the production of the high current proton beam needed for BNCT, leading to hospital-based BNCT facilities. Some progresses have been made in the last few years, and accelerator-based facilities are now becoming a reality (Culbertson et al, 2004). Nevertheless, continuing efforts have to be devoted on target manifacture and cooling, in order to improve the neutron beam quality to the level required for BNCT. It is foreseable that, thanks to the ongoing research on ABNS in many countries, high quality therapeutic beams will become increasingly available in the near future.

References

Barth, R.F., Coderre, J.A., Vincente, M.G.H., and Blue, T.E., 2005.Boron Neutron Capture Therapy of Cancer: Current Status and future prospects. Clin Cancer Res 11(11) June 1.

Beynon, T., Forcey, K.S., Green, S., Cruickshank, G., and James N., 2002**.** Status of the Birmingham accelerator based BNCT facility. In: M.W. Sauerwein et al. Research and Development in Neutron Capture Therapy, Bologna: Monduzzi Editore, International Proceeding Division;. P. 225-8.

Bisceglie, E., Colangelo, P., Colonna, N., Santorelli, P., Variale, V., 2000. On the optimal energy of epithermal neutron beams for BNCT, Phys. Med. Biol. 45 p.49.

Coderre, JA., Morris, GM., 1999. The radiation biology of boron neutron capture therapy. Radiat. Res; 151: 1-18.

Colonna, N., Beaulieu, L., Phair, L., Wozniak, G.J., Moretto, L.G., Chu, W.T., Ludewigt, B.A., 1999. Measurements of low-energy (d,n) reactions for BNCT. Boron Neutron Capture Therapy, Med. Phys. 26, 793.

Crandall, K.R., 1987. Trace 3-D documentation, Los Alamos National laboratory,.

Culbertson, C.N., Green, S., Mason, A.J., Picton, D., Baugh, G., Hugtenburg, R.P., Yin,Z., Scott, M.C., Nelson, J. M., 2004. In-phantom characterization studies at the Birmingham Accelerator-Generated epithermal Neutron Source (BAGINS) BNCT facility, Applied Radiation and Isotopes 61, 733.

Harling, O., Riley, K., 2003. Fission reactor neutron sources for neutron capture therapy-a critical review. J Neurooncol;7-17.

Hawthorne, MF., Lee, MW., 2003. A critical assessment of boron target compounds for boron neutron capture therapy. J of Neuroncol; 62:33-45.

Liskien, H., Paulsen, A., 1975. Atom Data Nucl. Data Tables 15 p. 57.

Schempp, A. , 1995. Research application of RFQ linacs, Nucl. Instr. and Meth. B 99 p. 688.

Starling, WJ., RFI Linac for accelerator-based neutrons. Abstracts of the 11th World Congress on Neutron Capture Therapy; 2004 Oct 11-5; Boston, MA. p.45.

Zimin, S., Allen, B.J., 2000. Study of moderator thickness for an accelerator based neutron irradiation facilities for boron neutron capture therapy using ^{7}Li(p,n) reaction near threashold. Phys. Med. Biol. 45, 59-67.

Opportunity of using neutron pulsed sources with combined boost neutron capture therapy

Stepan Ulyanenko

Medical Radiological Research Center, Koroleva, 4, Obninsk, Russia, 249036

Abstract

For prognosis further development of neutron and neutron capture therapy is necessary to continue study of construction of biological response to pulsed radiation. Radiobiological and biophysical experiments at BARS-6 (pulsed reactor, dose rate up to 10^7 Gy/s), pulsed neutron generators (duration of an impulse from 1 nanosecond to μs), and also linear accelerator KG-2,5 and reactor BR-10, conduct to the conclusion, that influence of a dose rate (in the given range of absorbed doses) neutron radiation on formation of radiobiological effects allows us to consider sources of pulsed neutron radiation as promising installations for neutron therapy.

Introduction

The problem of powerful pulsed action of neutron radiations upon biological tissue is one with both fundamental and practical aspects. In the fundamental one it is connected with an investigation of short transient processes taking place inside the objects at different stages of their evolution after an irradiation by powerful short flashes of ionizing radiation – at the physical stage (characteristic lead time of the processes ~10^{-15}-10^{-9} s), at the chemical one (~10^{-11}-10^{-6} s), during the biological and radiobiological processes. Here we have to define also the parameter "relative biological efficiency" (RBE) of pulsed radiation action in radiation biology and nuclear medicine. In practice it provides new opportunities in diagnostics and therapy ensured by different nature of action of powerful short-pulse irradiation on objects by penetrating radiation. All these phenomena are related to the sphere of natural sciences that is devoted to investigation of effects on matter of the action of different forms of radiation of very high power.

At present time the use of pulsed sources of ionizing radiation in biological and medical physics is increasing. Pulsed transfer of energy is characterized firstly by the high flux and secondly by the interference of secondary and primary processes taking place in the case when the irradiating pulse duration and the time elapse of the corresponding secondary processes inside the irradiated objects (including dosimetric systems) are comparable. These features cause also additional difficulties in dosimetry and planning of therapeutic procedures. It requires rechecking the methods widely used in dosimetry, radiobiology and radiotherapy by continuous irradiation before assimilating pulsed irradiation.

Neutron capture therapy (NCT) utilizes thermal (epithermal) neutron interactions with a substance of high specific capture cross-section resulting in secondary local irradiation of a target (tumor cells). NCT neutron accelerators, generators and nuclear reactors serve as sources of neutron fields. An absorbed dose in a target with neutron capture therapy is formed by radiation of quite broad energy spectrum including densely and sparsely ionizing radiations (both as primary, and as secondary). Interaction of radiations of different energies can produce synergetic effect.

Choice of optimal source of neutrons for NCT is based not only on physico-dosimetric parameters (the flux, a power spectrum, contribution of accompanying photon radiation), but on parameters of stable formation of therapeutic beams, type of radiation and availability of neutron sources.

The important feature of significant number of physical research installations generating neutron beams is the pulsed character of radiation in a wide frequency range, various forms of the pulse.

Role of a dose rate in formation of therapeutic effect is still a key problem in teletherapy as a whole and neutron capture therapy in particular.

Radiotherapy

According to the state-of-the-art data ~70 % of oncological patients need radiation therapy (together with surgery and chemical-therapeutic methods). Gamma-rays and neutron radiation fluxes here have their own special niches in cancer treatment (together with ionizing particle beams of other nature – protons, muons, etc.). These fluxes of different quasi-particles are used for irradiation of different types of tumors positioned at various

depths. In particular, neutron therapy is prescribed to about 30% of oncological patients. This type of therapy is applied in more than 20 countries over the world. With a correct choice of patient for the therapy it produces at least 20% enhancement of immediate and long-term positive treatment results. Recently the development of new methods of neutron therapy is underway – neutron capture therapy combined thermal neutron therapy plus fast neutron therapy, and a complex gamma-ray/neutron therapy. Some problems in this field are poorly studied. These issues relate to dosage for the intermediate layers of organism while deeply located tumor is under irradiation, to neutron scattering and penetration within organism, combined irradiation modes, etc. Therapeutic efficiency of neutron radiation versus dose rate (or dose power in particular for short irradiations) and pulse frequency is virtually not studied. In accordance with some theoretical concepts namely pulsed radiation influence upon tumor may be especially effective because within the short pulse duration repair and recovery processes have not enough time to take place, and various effects of cumulative influence and synergism are possible.

Side by side with oncology a series of very new applications of neutrons in various fields of clinical practice is developed. From 1985 up to 2002 about 500 patients with different malignancies have been treated in Medical Radiological Research Center (MRRC) with fast reactor neutrons (Gulidov I., Mardynsky Y., Tsyb A. et al., 2001).

The further increase of neutron cancer therapy efficiency is based on accumulation of new radiobiological data, improvements in clinical methods, development of physical and dosimetry support of the studies, creation of new neutron sources for therapy as well as the equipment for formation of radiation fields with optimal space and temporal parameters for neutron and combined neutron capture therapy (Britten R.A., Peters L.J., Murray D., 2001).

Equipment, techniques and dosimetry

Isotopes, nuclear fission reactors, cyclotrons, linear and other-type accelerators are currently used as neutron and gamma-ray sources for therapeutic purposes. Although they find an important success, a number of specific parameters of the irradiation used should be improved (neutron biological efficiency, dose depth distribution, lower overall dose, stability, availability, cost, dimensions and ecological compatibility of the sources, possibility of multi-field, multi-beam and rotational irradiation, etc.).

Apparatus and medical lines for developing neutron radiotherapy include the following tasks:

- size of sources and cost reduction;
- source ecological compatibility, in particular, safe location of source at clinic;
- study of mechanism of neutron action and effects upon human body with respect to individual organs and organism as a whole;
- study of combined neutron and gamma-ray effects upon tissues including the effects while simultaneously employing chemical therapy;
- study of the dependency of these effects on source parameters (particle energy spectrum, dose rate, power and value, pulse duration and frequency, etc.).

Pulsed neutron generator ING-031 (All-Russian Research Institute of Automatics, Moscow) and nuclear reactor BARS-6 (IPPE, Obninsk) were used to obtain original experimental data used in the report. Technical characteristics of pulsed neutron generator ING-031: Neutron (D-T) fluence $5 \cdot 10^{10}$ - n/s, Accelerating voltage - 150 kV, Ion current - 5 mA, Variable pulse frequencies- 1-100Hz, Pulse duration - 1.0 μs, Target – grounded, Power input - 0.6 kW.

Pulsed nuclear reactor BARS-6 has two active zones, control, protection and radiation monitoring systems, as well as support equipment. Reactor may operate in continuous and pulse regimes. Mean energy of neutrons generated by the reactor – 1.44 MeV, pulse duration is equal to 65 μs, dose power up to 10^8 Gy/s.

Nickel detectors (NP-2M) in the form of disks of 10 and 50 mm diameter and 1.0 mm thickness were used for measurement of the fast neutron fluence during the pulse. This method allows to determine fast neutron fluence with the statistical accuracy equal to ± 16% (confidence probability $\alpha = 0.95$). Fluence of thermal and epithermal neutrons were measured by a conventional method with the help of gold foils. Neutron flux was determined by the activation detector method as well as by track detectors using a fission set (^{235}U, ^{238}U, ^{237}Np) of DKN-2 (VNIIFTRI, Mendeleyevo), the latter have been wrapped either by a ^{10}B-sphere (1g/cm^2) and/or by a ^{112}Cd shell (thickness 0,7 mm). For activation detectors the ^{27}Al and ^{58}Co elements were adopted. Additionally the 27012, DKS-101, TLD dosimeters and proportional counters were used for measurements of gamma component of the radiation field. Also chemical dosimeters Fricke and FBX were used.

Doses of gamma radiation were estimated using thermoluminescent dosimeters (IKS-A). Mean measurement error was 30% at $\alpha = 0.95$. Additionally ferrous sulphate dosimeters, which determine the total effect of neutron and gamma radiation, were used for these dose measurements. In this case the gamma radiation effect was excluded from the total effect due to measurements made by IKS-A gamma dosimeters. Because of small gamma contribution to the total dose the error of the neutron dose determination was less than 15%.

Chemical dosimeters were generally used for measurement of radiation fields at the reactor BARS-6. Use of these methods on neutron generator ING-031 is limited by their insufficient sensitivity and rather large sample volumes of the chemical solution used. Thus, new methods directed both to increase sensitivity and reduce volume of chemical dosimeters are now under development. One of clear advantages of chemical dosimetry is that the chemical solution is a good enough model of a biological object. For the dosimetric support two different chemical systems differing in their sensitivity by a factor of 25 were used: namely standard Fricke dosimeter and its modified variant – dosimeter FBX – because there is no single chemical dosimeter with a wide working range from 0.7 Gy up to 1500 Gy, required for carrying out experiments with biological objects. Both these solutions are considered to be tissue-equivalent dosimetric systems.

As a result of the original researches provided by us on the reactor BARS-6 a difference in the effects of pulsed and stationary modes (for the same integral neutron yields) at a physical-chemical level (products of radiolysis of water) is shown. An increase in sensitivity of the chemical dosimeters to neutrons is possible by introducing into them isotopes having large neutron capture cross-section, for example, ^{10}B. To reveal the effect of introducing the boron we used the standard chemical solution FBX. The irradiation of samples was made both in pulsed and continuous modes. At each exposure the qualitative and quantitative structure of ionizing radiation in a pulsed operational mode of a reactor was identical to the structure in a continuous mode. The difference irradiated samples with and without boron solutions allows to estimate the contribution of the neutron capture events to the final effect. This data provide a natural opportunity to interpret as a positive influence on the magnitude of the final effect, the neutron-capture events from ^{10}B. It gave an opportunity to make a comparison of the influence of pulsed and stationary modes on the tissue-equivalent test-structure with greater accuracy. Change of a mode of an irradiation leads to a change both of amplitudes of each curve and of the order of an arrangement of curves. It is shown that the neutron-capture effect depends not only on the character of an irradiation (pulsed/continuous), but also on the structure of the mixed gamma-neutron field. It is necessary to emphasize in particular that the specificity of pulsed irradiation affects already the chemical stage of the effect. It appears that in spite of the fact that the value of the dose power changes equally in different points of the irradiated volume, changes not only disproportionately, but even in different directions.

Some radiobiological aspects of pulsed radiation effect

At present the advantage of neutron radiation application in therapy of different histological forms and locations of malignant tumors is already an incontestable fact not only for oncologists and radiobiologists but also for specialists of other fields related to medicine - physicists, mathematicians, etc. Owing to this cooperation, new neutron sources are being designed; methods and criteria for estimation of irradiation effectiveness are being developed; the schemes of their use in oncotherapy are being validated (Musabaeva L.I., 1985).

The increase efficiency of neutron use for beam therapy is based on accumulation of new radiobiological data, perfection of clinical methods, development of physico-dosimetric support of researches, production of new neutron therapeutic sources and facilities for shaping the radiation field to achieve optimal spatio-temporal conditions of neutron therapy.

In spite of a considerable number of studies, the question of the role of neutron radiation in beam therapy of tumors at various locations is still open. The discrepancy of the received data is possible to explain by the differences in neutron beam characteristics and energy, the insufficient adaptability of some neutron sources for medical purposes, the absence of the common concept of dose fractionation, the small number of individual groups of patients, the inclusion in one group of patients with various locations of the tumor, the insufficient analysis of the criteria of patient selection for neutron therapy (Tsyb A.F., Mardynsky Yu.S., Ulyanenko S.E. et al. 2003).

Results of studies on comparison of efficiency of pulsed and continuous radiation are scarce and contradictory. This concerns in particular pulsed neutron radiation for average interval doses (therapeutic) rather than destructive doses.

Increasing interest in the problem of pulsed neutron effect is due to both fundamental aspects and a number of actual practical problems. Fundamental aspects are the study of fast biological and radiobiological processes, the RBE definition of radiations with high and ultrahigh rate dose (Obaturov G.M., Sokolov V.A., Ulyanenko S.E. et al., 1997). The applied problems are rather diverse. So, in some of the studies, the advantage of application of high-LET radiations with high rate dose including pulsed radiations was proved on the basis of theoretical preconditions with the purpose of increasing the efficiency of the beam therapy (Zhestyanikov V.D., 1979, Hall E.J., Brenner D.J., 1991). Personnel at the cyclotrons and the pulsed nuclear reactors are subject to a higher background radiation (pulse character) while standards of radiation safety and estimations of radiation risk of pulsed effects are practically absent (Edwards A.A., 1999).

Influence of the time irradiation on radiobiological effects connects both with first formations of radiation damage and at their realizations in observable radiobiological effects (Sevan'kaev A.V., Zherbin A.V., Obaturov G.M. et al., 1979). So, the change in the radiobiological effect (cell survival, chromosomes aberrations formation, etc.) at dose rates of gamma radiation 5-200 mGy/min was caused repair of radiation damage during irradiation. At higher DR ($0.3\text{-}10^5$ Gy/min) the absence of DR effect was explained from the fact that the damage repair time is greater than the formation time. At very high dose rates ($> 10^9$ Gy/min) effects connected with the kinetics of processes related to the physical and chemical stages of radiation effects are observed.

In the current research for investigation of biophysical and radiobiological aspects of effect of pulsed neutron and x-ray radiation the studies on various biological objects: sub-cellular structures, microorganisms cells with various repair genotype, mammals and human cells, small laboratory animals with tumor are carried out.

Conclusion

Thus general methodological approaches to complex studies of biophysical phenomena of the action of pulsed neutron and gamma-ray radiations are stated.

Performed experimental investigations concerning the influence of dose rate on biological efficiency of ionizing radiations have demonstrated different responses of biological systems to pulsed and continuous exposure at equal absorbed doses. Thus quantitative and directional difference of the effect depending on the kind of biological object was observed. Existing material on the damage induced by pulsed and continuous radiations do not allow to give a definite answer as to what stage a qualitative difference between the effects produced by those different types of radiations begins to exist. Further experimental and theoretical studies are needed to understand the problem.

Now the studies at the reactor BARS-6 on accumulation of statistical data for each of the biotest-systems are being carried out. A following stage of researches will be studying the biological efficiency of the pulsed neutron generator ING-031 at various irradiation regimes, also pulsed x-ray and neutron radiation with pulse length of some nanoseconds. The obtained data will allow to define and compare the biological efficiency of various pulsed sources for determination of biophysical and radiobiological aspects of pulsed radiation effects in comparison with the effects of continuous radiation.

References

1. Britten R.A., Peters L.J., Murray D., 2001. Biological factors influencing the RBE of neutrons: implications for their past, present and future use in radiotherapy. Radiation Research, 156, 125-135.
2. Edwards A.A., 1999. Neutron RBE values and their relationship to judgment in radiological protection. J. Radiol. Prot., 19 (2), 193-195.
3. Gulidov I., Mardynsky Y., Tsyb A. et al., 2001. Neutrons of nuclear reactors in treatment of tumors. MRRC RAMS, Obninsk, 132 p.
4. Hall E.J., Brenner D.J., 1991. The dose-rate effect revisited: radiobiological considerations of importance in radiotherapy. Int. J. Radiation Oncology.Biol.Phys, 21, 1403-1414.
5. Musabaeva L.I., 1985. Neutron therapy in oncology. Med. Radiol. (Moscow), 30 (9), 57-63.
6. Obaturov G.M., Sokolov V.A., Ulyanenko S.E. et al., 1997. The topical problems radiobiology of neutron. Radiation biology Radioecology, 37 (4), 475-481.
7. Sevan'kaev A.V., Zherbin A.V., Obaturov G.M. et al., 1979. Cytogenetic effects induced by neutrons in lymphocyte of peripheral blood in vitro. Genetics, 15 (6), 1046-1060.
8. Tsyb A.F., Mardynsky Yu.S., Ulyanenko S.E., et al. 2003. Neutrons in treatment of malignant tumours.Obninsk, BIST, 112 p.
9. Zhestyanikov V.D., 1979. DNA repair and its biological importance. Leningrad, Nauka, 285p.

Accelerator-Driven Sub-Critical Multiplier for BNCT

Francesco Ganda[a], Jasmina Vujic[a], Ehud Greenspan[a] and Ka-Ngo Leung[b]

[a]*Department of Nuclear Engineering, University of California at Berkeley, CA, USA*
[b]*Lawrence Livermore National Laboratory, Berkeley, CA, USA*

Abstract

The primary objective of this work is to assess the feasibility of using a small, safe and inexpensive $k_{eff} \leq 0.98$ subcritical fission assembly (SCM) to multiply the treatment neutron beam intensity attainable from a compact D-D fusion neutron source delivering ~10^{12} n/s. The goal is to reduce the treatment time for deep-seated brain tumors to about one hour, if a compact BNCT facility is to be used. The paper describes the optimal SCM, as well as two optimized beam shaping assemblies (BSA), one for maximizing the dose rate to a deep seated tumor and the other for maximizing the total dose that can be delivered to a deep seated tumor.

Keywords: BNCT, Compact Neutron Source, Sub-critical Multiplier, Beam Shaping Assembly, MCNP

1. Introduction

A novel, highly compact, fusion neutron source (CNS) based on a coaxial electrostatic accelerator is under development at the Lawrence Berkeley National Laboratory [1, 2]. This source is designed to generate ~10^{12} D-D n/s. This source intensity is an order of magnitude too small for Boron Neutron Capture Therapy (BNCT) applications. The primary objective of this project is to assess the feasibility of using a small, safe and inexpensive subcritical fission assembly to multiply the fusion neutrons by an order of magnitude, thus developing a highly compact neutron source for BNCT (and potentially also for other medical and industrial applications) that could treat deep-seated brain tumors in approximately one hour.

Possible advantages of using a Sub-Critical Neutron Multiplier (SCM) include the following: (a) Earlier commercialization of the CNS for BNCT. (b) Making it possible to attain the needed neutron source intensity using a D-D CNS; (c) Reducing the total power needed for operating a CNS.

The SCM considered is small and has low power – approximately 0.5 kW relative to 200 kW that will be deposited by the ion beam on the target of the ~10^{12} n/s D-D CNS. At that low power level it is possible to design the SCM to be passively super-safe. It can be designed in such a way that will not enable it to become critical under any circumstances. Passive cooling will ensure that the fuel will maintain its integrity and fission products will not be released. It will use a relatively small amount of low enriched uranium (i.e. ≤20%) so it will not be of proliferation concern.

The optimization effort focuses on, primarily, two components of the BNCT facility – the SCM and the Beam Shaping Assembly (BSA). Reflector/shield optimization was undertaken as well.

2. Compact Neutron Source (CNS)

The CNS under development at the Lawrence Berkeley National Laboratory by H. Koivunoro [2] is designed to generate up to ~10^{14} D-T n/s or up to ~10^{12} D-D n/s. It is based on a newly developed radio frequency (RF) driven multicusp ion source that is simple to operate and has long lifetime. The cylindrical source consists of a RF-driven D-D or D-T plasma. A 2 MHz or a 13.56 MHz RF-discharge produces the deuterium and/or tritium ions at the center of the cylindrical device. The RF-discharge yields a high-density plasma with a high fraction of mono-atomic ion species (D^+ for D-D and 50% D^+ + 50% T^+ for D-T). It enables attaining high neutron yield with low gas pressures (few mTorr). A vacuum contained within a quartz vacuum chamber is used for high voltage insulation around the target cylinder. The vacuum line, RF power, cooling water, and pulsed high voltage are brought in through a vacuum feed-through at one end of the cylindrical assembly. The ions are accelerated through the extraction grid to an energy of 100 keV or higher. The cylindrical geometry of the source is advantageous for holding high voltage due to the uniform distribution of the electric field equi-potential lines between the electrode and target cylinders. Because this target is wrapped around the source of deuterium ions, there is a large target area in a small space compared to an accelerator with flat plate target. This geometry also leads to a very high current limit as a result of the large beam extraction area. The ion beam impinges on a titanium coated copper or aluminum target

where either the 2.45 MeV D-D or 14 MeV D-T neutrons are generated. Having in mind known difficulties in working with tritium (it is expensive and presents a health hazard), we decided to focus on a D-D neutron source. With a 200 kV extraction voltage and a 1 A beam current, this source produces an isotropic source of 2.45 MeV neutrons at about 1.1×10^{12} n/s. Though the maximum extracted beam current from the deuterium source is approximately 27 A, the size and cost of the power supply as well as the cost of electricity becomes excessive beyond 400 kW, which corresponds to a 2A current at 200 keV. This will provide a neutron source intensity of 2.3×10^{12} n/s and will require an effective target length of 40 cm. Based on our previous studies [1], this neutron source intensity is an order of magnitude short of the intensity needed for BNCT of deep brain tumors. Thus, without a SCM it is not likely that a D-D CNS could be developed to generate up to $\sim 10^{14}$ n/s.

3. Study plan

Three optimization studies were performed: optimization of the sub-critical neutron multiplier (SCM), optimization of the beam-shaping assembly (BSA) and optimization of the reflector. The SCM optimization objective is to maximize the current of neutrons that leak out from the SCM in the direction of the patient, without exceeding a maximum permissible k_{eff} of 0.98. Minimizing the required uranium inventory is another objective of this study. The SCM design variables used include the SCM shape and dimensions, fuel thickness and moderator thickness.

The objective of the BSA optimization is to maximize the tumor dose rate using the optimal SCM while maintaining a tumor-to-normal tissue dose ratio of at least 20 to 12.5 (corresponding to the tumor control dose and to the healthy tissue dose limit). The BSA design variables include its shape, dimensions and composition.

The reflector optimization is, in fact, an integral part of the SCM optimization and of the BSA optimization. The reflector design variables are composition and thickness. The overall design objective is to get a treatment time that does not significantly increase beyond one hour when the effective multiplication factor of the SCM is $k_{eff} = 0.98$.

4. Optimization of the SCM and of the reflector

By definition, $k_{eff} = k_\infty * P_{NL}$, where P_{NL} is the non-leakage-probability. To maximize the effectiveness of the SCM, it is desirable to maximize the leakage probability, P_L, in the direction of the patient. To accomplish this it is first needed to find the highest possible k_∞ subjected to the $k_{eff} \leq 0.98$ constraint.

The optimal SCM configuration was found with the help of SWAN [4] and MCNP [3]. The SCM was made of 0.05 cm thick aluminum clad slabs of metallic uranium with water in between the fuel slabs. The fuel and the water were assumed at room temperature. The optimal fuel and water gap thicknesses were found to be, respectively, 0.06 cm and 0.84 cm. The corresponding maximum k_∞ is 1.7267[a].

To minimize the neutron radial leakage probability from the SCM and thereby to maximize the axial leakage probability, a good reflector is needed. BeO was selected as the preferred choice based on a companion study that compared the reflection properties of many materials that surround a small spherical thermal critical assembly[b]. The results are summarized in Figure 1.

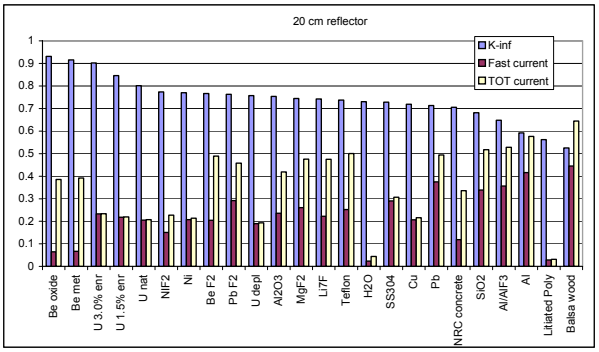

Figure 1. Comparison of the effectiveness of various materials as reflectors 20 cm thick

The use of a BeO reflector minimizes the amount and cost of the required uranium and contributes to the safety of the facility: the replacement of BeO or part thereof with any other material, possibly as a result of an accident, will result in a negative reactivity effect. The BeO reflector thickness chosen was 62 cm; it offers close to an infinite reflector characteristics.

In order to improve the "source utilization factor" or source effectiveness, defined as the fraction of neutrons emitted by the CNS that reach the sub-critical multiplier, the SCM geometry was

[a] The k_∞ calculated by studying a representative unit cell, as we did here, does not account for the spectrum alteration induced by the reflector, CNS and BSA. The effect of these components is expected to be pronounced because of the small dimentions of the SCM and its high surface to volume ratio. In principle the k_∞ optimization study should have been re-done each time a change was made to any of these components. For practrical reasons no such re-optimization was done; the optimal unit cell geometry was kept throughout the study.

[b] The critical assembly examined is a minimum mass spherical core made of a mixture of $UZrH_{1.6}$ with 20% enriched U.

designed so as to increase the solid angle by which the SCM "views" the CNS (in Figure 2): it was arranged as a "cup" shape that surrounds the CNS on three sides. The CNS, orientated axially, is surrounded by two 20.995 cm long[c] cylinders of aluminum-clad 20% enriched U fuel having the optimal water-to-fuel volume ratio. There are 6 vertical cylindrical plates, 16.75 cm in radius: k_{eff} is 0.98. The required uranium amount is 8.5 kg and its cost is about \$57,400[d].

The required SCM power level is estimated at 400 W when driven by a 10^{12} D-D n/s neutron source. This translates into consumption of only about 0.5% of the initially loaded ^{235}U atoms during 50 years of continuous operation. It thus appears that the SCM could operate continuously for the entire lifetime of the machine without refueling. Also as desired, cooling the SCM does not pose a challenge; it may be accomplished passively; i.e., without resorting to forced circulation.

4. Optimization of the BSA

The BSA was optimized based on the results of previous studies [1], which established that neutrons with energy below 1 keV and above 20 keV are not desirable as their tumor dose to normal tissue dose ratio is too low. Additionally, the gamma-rays are undesirable as they deliver the same dose to the healthy tissue as to the tumor. The most important parameter is the dose rate (Gy/hour); the higher it is the better. At the same time it is desirable to have large maximum dose, large H/L dose ratio and large lethality range.

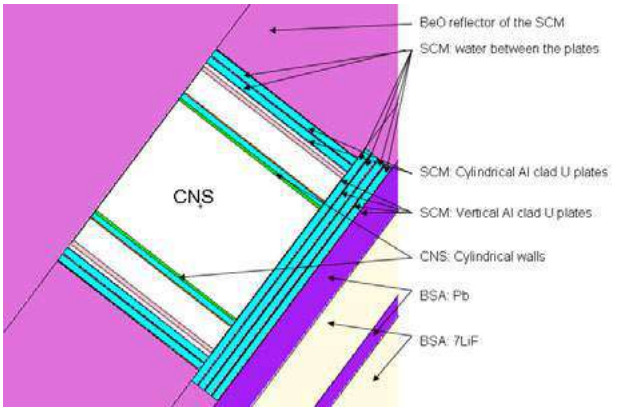

Figure 2. Cross sectional view of the "cup shape" SCM that surrounds the CNS

Two optimal BSA designs were identified; one for maximizing the dose rate and the other for maximizing the total dose that can be delivered to a deep seated tumor. The former offers the minimum treatment time whereas the latter offers the largest lethality. The former features a harder neutron spectrum and relatively high neutron dose component to the skin while in the latter the neutron, gamma-ray and boron dose components in the skin are comparable. The corresponding maximum dose rates that can be delivered to the tumor are 10.1 Gy/hour and 51.8 Gy.

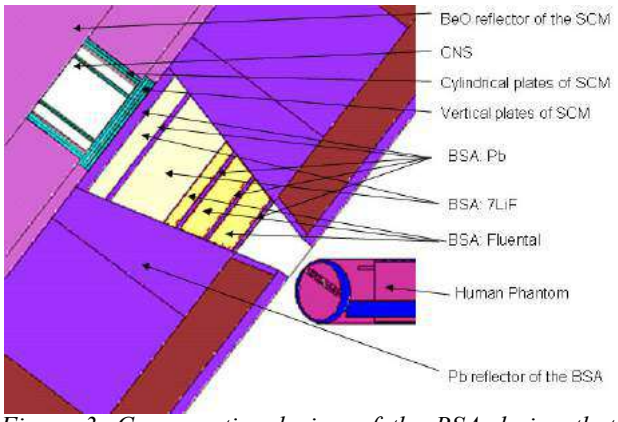

Figure 3. Cross sectional view of the BSA design that maximizes the dose rate

The BSA design that maximizes the dose rate, illustrated in Figure 3, is 51.1 cm long. It has a truncated conical shape with the large base, 23.3cm in radius, interfacing the SCM and the small base 9.74cm in radius, near the patient. The cone angle is 14.9 degrees. The BSA is made of the following segments, starting from the SCM: 3.5 cm lead, 6 cm ^{7}LiF, 1.5 cm lead, 17 cm ^{7}LiF, 4 cm fluental[e], 1 cm lead, 8 cm fluental, 1 cm lead, 8 cm fluental, 0.9 cm lead and 0.1 cm ^{6}LiF. The last 19 cm of the cone towards the patient are surrounded by a 1 mm thick ^{6}LiF. The reflector is made of lead, and fills the space between the BSA cone and a coaxial cylinder that is 77 cm in radius.

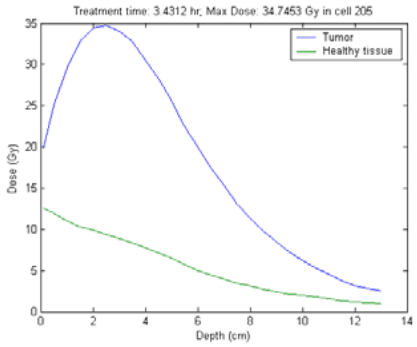

Figure 4. Total dose to the healthy tissue (L) and to the tumor (H) as a function of depth for the BSA design that maximizes the dose rate

[c] As long as the CNS they surround

[d] The costs of the uranium parts of the SCM mentioned throughout this work are based on the assumptions of availability of uranium at 50 \$/kg and of SWU (Separating Working Units) at 110 \$ each; the enrichment of the tails is assumed at 0.25 %.

[e] Fluental is Al/AlF_3 (40%/60%). Fluental is chosen over ^{7}LiF to cut down the undesirable fast neutron component: the aluminum contained in this material features relatively high scattering cross section above ~30 KeV; it is higher than that of ^{7}Li and higher than the cross section below ~30 keV.

The sides of the collimator are lined with a 2.1 cm thick lead collar, continuing the conical shape of the BSA.

This BSA offers the highest tumor dose rate (H) of 10.1 Gy/hour/1E+12n/s; it can deliver a lethal dose of 20 Gy or higher to the tumor in the first 6 cm of the brain (Figure 4) in 3.4 hours if the CNS intensity is $1x10^{12}$ n/s or in 1.5 hours if the CNS intensity is $2.3x10^{12}$ n/s. The neutron dose component to the healthy tissue is significantly larger than the gamma dose component (Figure 5).

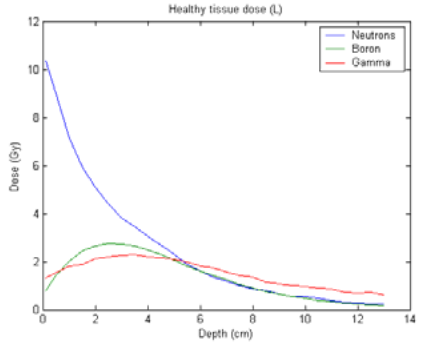

Figure 5. Components of the healthy tissue dose (L) for the BSA design that maximizes the dose rate

The BSA design that maximizes the total dose is 53.1 cm long of truncated conical shape with the same conical angle and same base dimensions as of the previously described BSA. The BSA is made of the following segments, starting from the SCM: 3.5 cm lead, 27.4 cm ^{7}LiF, 20 cm fluental, 0.1 cm ^{6}LiF and 2.1 cm lead. The cone is surrounded on the side by a 1 mm thick ^{6}LiF in the last 21 cm towards the patient. The reflector is made of Al_2O_3, filling the space between the side of the BSA cone and a coaxial cylinder 35 cm in radius; lead surrounds the alumina reflector with a coaxial cylinder 77 cm in external radius. The sides of the collimator are shielded by a 2.1 cm thick lead collar, continuing the conical shape of the BSA.

The maximum tumor dose of about 51.8 Gy is reached at 2.5 cm depth in about 10 hours with the CNS intensity of $1x10^{12}$ n/s. The different relative contributions to the healthy tissue dose, shown in Figure 6, are balanced.

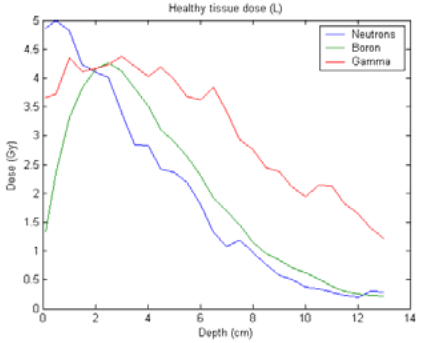

Figure 6. Components of the healthy tissue dose (L) for the BSA design that maximizes the total dose

A separate calculation was performed with the SCM substituted by vacuum, using the BSA that offers the highest dose rate. The resulting dose rate is only 0.56 Gy/hr, requiring a treatment time of 60 hours with the CNS intensity of $1x10^{12}$ n/s. This implies that the SCM increases the treatment dose rate by a factor of about 18.

4. Conclusions

The study identified the optimal design of a passively cooled SCM made of 20%-enriched, aluminum clad metallic uranium fuel.

Two optimal BSA designs were identified; one for maximizing the dose rate and the other for maximizing the total dose that can be delivered to a deep seated tumor. The maximum dose rate that can be delivered by the former is 10.1 Gy/hour and the maximum dose that can be delivered by the latter is 51.8 Gy.

The study concludes that the addition of a SCM makes it possible to increase the treatment beam intensity by a factor of 18 – from 0.56 Gy/hour to 10.1 Gy/hours, with the CNS intensity of $1x10^{12}$ n/s., Therefore, a practical BNCT facility based on the optimal system identified in this study could deliver the desired tumor dose in less than an hour, if either one of the following approaches is adopted: (1) Irradiating the patient in 3 to 4 one-hour sessions; (2) Irradiating the patient using 3 or 4 beams simultaneously; or (3) Increasing the permissible SCM maximum k_{eff} to 0.995. However, if the CNS intensity of $2.3x10^{12}$ n/s could be achieved, above mentioned remedies would not be needed.

References

1. J. M. Verbeke, J. Vujic, and K. N. Leung, "Neutron Beam Optimization for Boron Neutron Capture Therapy Using the D-D and D-T High-Energy Neutron Sources," Nuclear Technology, 129, 257 (2000).
2. H. Koivunoro, T-P Lou, J. Reijonen and K-N Leung, "A Compact Neutron Generator Based on D-D or D-T Fusion Reaction for BNCT," Proceedings of the10th International Congress on Neutron Capture Therapy for Cancer, Essen, Germany, 8 - 13 September 2002.
3. Oak Ridge National Laboratory "RSICC Computer Code Collection MCNP4C: Monte Carlo N-Particle Transport Code System", Radiation Safety Information Computational Center, 3-150 p.p., Jul 2000.
5. Y. Karni, D. Regev, E. Greenspan, S. Goluoglu, L.M. Petrie and C.M. Hopper, "The SMORES Capability for Minimum Critical Mass Determination," ICNC2003, Tokai-Mura, Japan, Oct. 20-24, 2003.

Overview of the IBA Accelerator-Based BNCT System

E. Forton, F. Stichelbaut, A. Cambriani, W. Kleeven, J. Ahlback, Y. Jongen

Ion Beam Applications s.a., Chemin du Cyclotron 3, Louvain-la-Neuve, Belgium

Abstract

During the last few years, IBA started the development of an accelerator-based BNCT system. The accelerator is a Dynamitron built by RDI in the USA and will produce a proton beam of 20 mA at 2.8 MeV. Neutrons will be produced by the $^{7}Li(p,n)^{7}Be$ nuclear reaction by directing the proton beam on a thin lithium target. The neutron energy spectrum will be tailored using a dedicated beam shaping assembly (BSA) surrounding the target.

This presentation makes a summary of the present status of the development. After a description of each subsystem, some design issues, solutions and experimental tests will be discussed.

For instance, the high proton current on target induces blistering problems and cooling issues. Both of these can be tackled by a careful choice of the materials and a good target design. Other tests include activation measurements with a low current neutron beam shaped with a close-to-final but versatile BSA design.

According to all tests performed so far, the future BNCT system should fulfill the design specifications.

Keywords: accelerator-based BNCT, dynamitron, target, BSA.

1. Introduction

The IBA Company has started the development of a complete system for BNCT based on a low-energy high-current proton accelerator.

The accelerator is a Dynamitron developed to produce a 3 MeV, 20 mA proton beam. Two types of treatment rooms are possible; one boasts a fixed beam line, the other one has an isocentric gantry. Neutrons are produced by the $^{7}Li(p,n)^{7}Be$ reaction and the resulting neutron flux will be tailored using an optimized beam shaping assembly (BSA).

The resulting neutron intensity will correspond to a thermal neutron flux above 2.10^{9} n/cm^{2}.s at a depth of 2.5 cm in tissue along the neutron beam axis. Figure 1 shows a schematic drawing of the IBA BNCT facility.

2. Accelerator and beam lines

Dynamitrons (refer to e.g. [1] for the operating principle) are linear accelerators initially designed for the acceleration of high intensity electron beams. The source can be changed to accelerate other types of particles. In the case of the BNCT Dynamitron (Figure 2), an ECR source is used. Currents above 35 mA of 30 keV protons and molecular hydrogen have been measured at source exit. A permanent magnet will filter out molecular hydrogen to select protons and inject them in the accelerator.

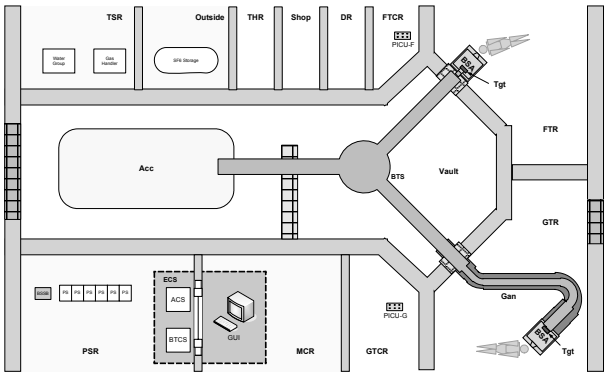

Figure 1. Symbolic layout of the BNCT facility. Another design proposes to vertically mount the accelerator in order to minimize the facility footprint

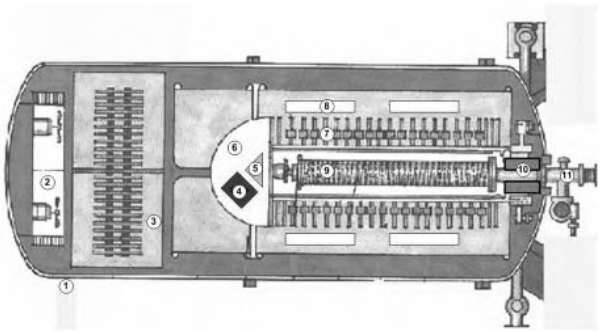

Figure 2. Layout of the dynamitron. The ECR source and selection magnet are pictured as a dark square and grey triangle, respectively

Acceleration voltage will range from 1.9 to 2.8 MV. Beam lines have been designed using Transport[2], magnets have been modelled using the Vector Fields TOSCA/OPERA package[3]. Both the beam line layout and magnet design are influenced by the high intensity of the beam. As an example, beam stops placed around the switching magnet require a large beam spot at that place (about 8 cm diameter) in order to lower the dumped power density. This, in turn, implies that the switching magnet has a large gap (12 cm) and a broad pole.

3. Target

There are two critical issues on the target design, namely the heat load and hydrogen-implantation issues. Both are due to the high proton current.

At 2.8 MeV, a 20 mA proton beam induces a 56 kW heat load on target. The beam spot will be enlarged using scanning magnets, and the target surface will be increased by means of tilted panels. The power density on target will hence not exceed 450 W/cm². The lithium layer will be 55 µm thick, such that protons will leave it as their energy become lower than the Li(p,n) threshold. This way, protons will loose the remaining energy in the target substrate, which has a higher melting point. The target panels will be water-cooled using an array of microchannels. Total water flow will be about 20 l/min for an average water velocity of 10 m/s in the channels. Numerical computations predict that the lithium temperature will remain around 120-130 °C, well below the melting point (180.54 °C). Heat load tests on a prototype microchannel cooling plate proved that these values are reasonable.

At 20 mA, Hydrogen ion implantation leads to the so-called “blistering” phenomenon.

After some time, hydrogen concentration within the target material becomes so high that bubbles create cracks and damage the target surface (Figure 4). This phenomenon appears at fluences in the 10^{18} 1/cm² range for most materials. Collaborations with the University of Namur (Facultés Universitaires Notre Dame de la Paix, Namur, Belgium) and the Budker Institute for Nuclear Physics (Novosibirsk, Russia) have proven that some materials are more suitable regarding this aspect. Iron and Tantalum are among them and Iron has been chosen for machining and welding properties, as well as availability and price. Despite a careful choice of the target material, blistering cannot be avoided.

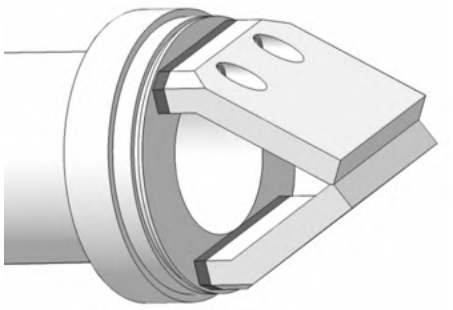

Figure 3. Drawing of the end of a beam line, with the water-cooled target panels on which a 55 µm Lithium layer has been evaporated (side panels not pictured)

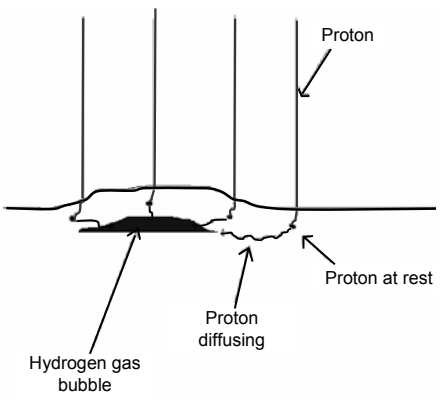

Figure 4. Principle of blistering. Heavy hydrogen implantation in the target creates bubbles and cracks

Hence, it has been decided that the targets should be changed on a regular basis, about every month. Dedicated target handling system and target cooling vault are required as the Beryllium activity will rise up to about 30 Ci, and Beryllium lifetime is 53.3 days.

4. Beam shaping assembly

The design of the BSA [4] is based on the original work of D. Bleuel from LBNL [5] and has been pursued using the Monte Carlo simulation code MCNPX [6]. Design goals were the following:

- A maximal dose of 12 Gy-eq anywhere in healthy tissues;
- A maximal dose in healthy tissues of 8 Gy-eq at skin level;
- An advantage depth in tumor tissues of at least 8 cm;
- A maximal thermal neutron flux of 2.10^9 n/cm^2.s, at a depth of 3 cm inside the brain.

Several materials and dimensions have been considered for the moderator and the reflector. Based on the simulations, ideal BSA characteristics are:

- The moderator will be made of MgF_2 with a density of at least 2.54 g/cm^3;
- The moderator radius will be 20 cm;
- The moderator length will be adjusted based upon the MgF_2 density to reach a maximal dose value of 8 Gy-eq at skin level in healthy tissues;
- The reflector will be made of Lead with a radial thickness of 30 cm;
- The delimiter will consist of Polyethylene with 7.5% Lithium;
- The beam energy will be set to 2.8 MeV.

The neutron beam should then have the following main characteristics:

- The dose in tumour reaches a maximal value of 50 Gy-eq at a depth of about 3 cm inside the brain.
- The corresponding thermal neutron flux is $2\ 10^9$ n/cm².s for a 20 mA incident proton beam (cf. Figure 5).
- The advantage depth is equal to 8.5 cm.

An experimental benchmarking of the BSA performance has been carried out with the Van De Graaff generator at the Catholic University of Louvain (UCL, Louvain-la-Neuve, Belgium). Neutrons are produced by a 5 µA, 2.8 MeV proton beam impinging a simple target made of a 250 µm Lithium foil glued on a water-cooled flange.

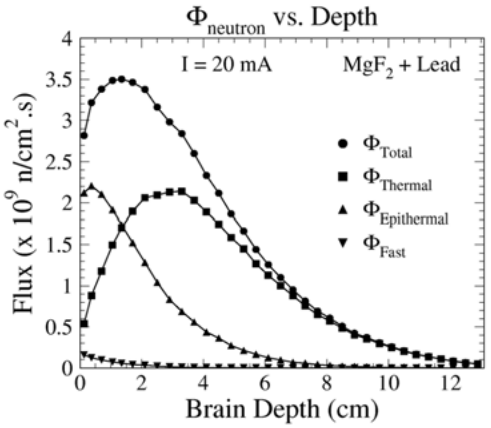

Figure 5. Depth Evolution of the total neutron flux and its thermal (E_n<0.5 eV), epithermal (0.5 eV < E_n < 10 keV) and fast (E_n>10 keV) components

For these tests, a BSA prototype has been build. The prototype dimensions are close-to-final, with a 40 cm diameter, 30 to 40 cm thick neutron moderator.

The neutron field has been characterized by means of activation measurements on thin gold foils. Gold presents the advantage of high neutron capture cross section, suitable half life (2.7 days), simple analysis of the decay gamma spectrum (a single 411 keV photon emitted in 95 % of the decays), limited neutron or gamma self-shielding. ASTM recommendations[7] have been followed. During irradiation, these foils are placed in a tissue-equivalent plastic phantom. Due to the low intensity of the beam, relatively long (~24h) irradiations have been carried out. Relatively long measurement times are also required for the subsequent counting with a calibrated HPGE detector.

First activation measurements were performed with a Teflon moderator. Teflon has been chosen for its well known characteristics, uniformity and because its chemical composition is as close as possible to MgF_2. Figure 6 and 7 show typical results of an activation measurement: both the activation-depth and cross profile measurements agree with Monte Carlo predictions. Experimental error bars are of the order of 8-10 %, dominated by stochastic errors.

The moderator has been subsequently replaced with isostatically pressed MgF_2 discs (40 cm diameter, 10 cm thick each). Despite a good overall density and purity of the material, first measurements where surprising as the depth activation profile did not match Monte Carlo predictions, indicating the beam was more intense and more energetic than foreseen.

Xray pictures and CT scans of the discs put forward severe non-uniformities.

Many centimeter-sized cavities were observed in every MgF_2 discs, mostly located in the middle region of them. We are convinced these cavities are responsible of the bad experimental results, as a rough modelling of the cavities in MCNPX leads to a much better agreement between predictions and experiments (Figure 8).

In addition to proton beam current monitoring, final BSA design will include fission chambers for neutron measurement. Those will allow detecting problems in the neutron yield. The performance of the chosen chamber in the moderated neutron beam has been verified and matches MCNPX estimations.

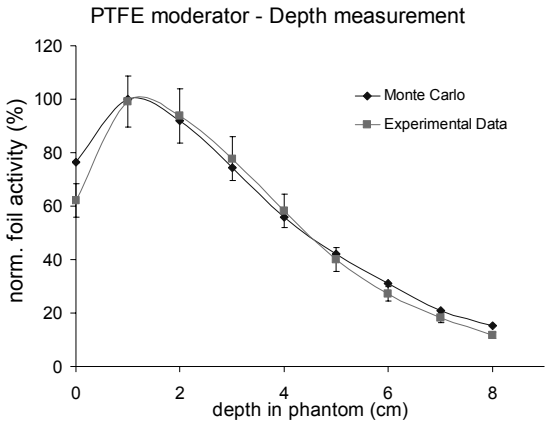

Figure 6. Comparison of predicted and measured activation profiles as a function of depth in a TEP phantom (bare foils, Teflon moderator)

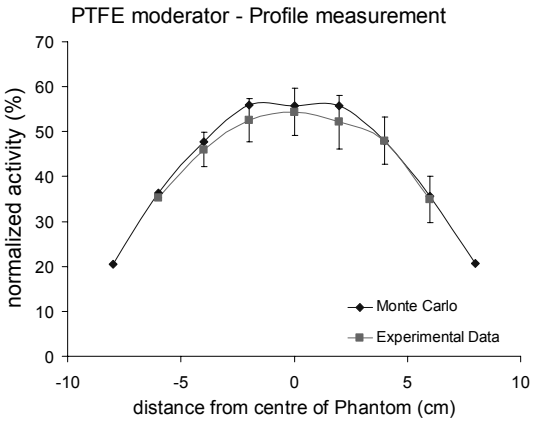

Figure 7. Comparison of predicted and measured activation profiles as a function of radial distance, at 3cm depth in a TEP phantom (bare foils, Teflon moderator)

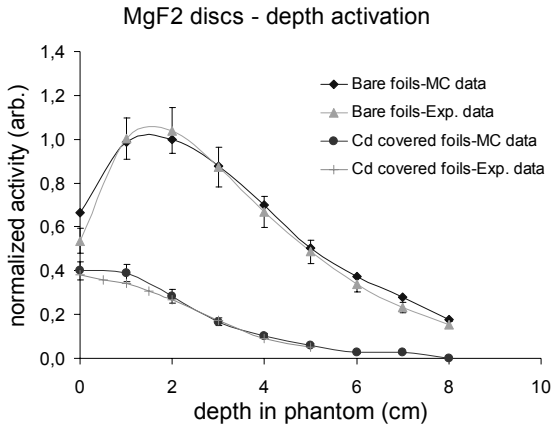

Figure 8. Comparison of predicted and measured activation profiles as a function of depth in a TEP phantom (MgF_2 moderator). Upper curves correspond to bare gold foils; lower curves correspond to Cd-covered foils

6. Conclusions

IBA proposes a Dynamitron-based system whose characteristics (neutron intensity and energy spectrum) are well suited for efficient BNCT.

The design of the whole system is deeply influenced by the high power proton beam. Beam lines are designed in order to cope with specific issues regarding beam power. Even more stringent constraints are put on the target, and despite extensive studies on blistering, it has been decided that targets should be changed about every month.

The BSA will be a crucial element for the quality of the radiation field. The emphasis put on the treatment quality together with the highest possible epithermal neutron flux lead IBA to an innovative design in terms of the choice of material for the moderator (MgF_2) and the reflector (Lead). A prototype facility has been build. Further improvements on the MgF_2 quality are required, but experimental measurements on the neutron beam agree with the Monte Carlo predictions, indicating that the MCNPX model of the neutron beam behaves in a realistic way.

References

[1] M. R. Cleland, "Industrial applications of electron accelerators", CAS proc. CERN yellow report 2006-012 (2006).

[2] K.L. Brown et Al. "Transport, a Computer Program for Designing Charged Particle Beam Transport Systems". CERN yellow report 73-16 (1973).

[3] Vector Fields Limited, Oxford, UK.

[4] F. Stichelbaut, "Design of a Beam Shaping Assembly for an Accelerator-Based BNCT System", ICNCT12 proceedings, Kagawa (2006).

[5] D. L. Bleuel, "Determination and Production of an Optimal Neutron Energy Spectrum for Boron Neutron Capture Therapy", Ph.D. thesis, University of California at Berkeley (2003).

[6] "MCNPX User's Manual version 2.5.0", LA-CP-05-0369, April 2005.

[7] ASTM international, "Annual book of ASTM standards, vol 12.02" (revised annually).

BEAM DOSIMETRY

Preliminary characterization of the epithermal beam at the TAPIRO reactor

Elisabetta Nava[a], Stefano Agosteo[b,c], Maurizio Angelone[d], Roberto Bedogni[e], Kenneth W. Burn[a], Marco Caresana[b,c], Lodovico Casalini[a], Giorgio Curzio[f], Francesco d'Errico[f], Adolfo Esposito[e], Paolo Ferrari[g], Orlando Fiorani[h], Armando Foglio Para[b,c], Grazia Gambarini[c,i], Gianfranco Gualdrini[g], Andrea Pola[b,c], Giancarlo Rosi[h], Alfonso Santagata[h], Alba Zanini[j]

[a]*ENEA, Bologna Research Centre, Via Martiri di Monte Sole 4, 40129 Bologna, Italy*
[b]*Politecnico di Milano, Department of Energy, Piazza Leonardo da Vinci 32, 20133 Milan*
[c]*INFN Sezione di Milano,Via Celoria 16, 20133 Milan, Italy*
[d]*ENEA, Frascati Research Centre, Via Enrico Fermi 45, 00044 Frascati (Roma), Italy*
[e]*INFN LNF, Via E. Fermi40, 00044 Frascati (Rome), Italy*
[f]*University of Pisa, DMNP, Via Diotisalvi 2, 56126 Pisa, Italy*
[g]*ENEA, Radiation Protection Institute, Via dei Colli, 16, 40136 Bologna, Italy*
[h]*ENEA, Casaccia Research Centre, Via Anguillarese 301, 00123 S. Maria di Galeria (Rome), Italy*
[i] *University of Milan, Department of Physics, Via Celoria 16, 20133 Milan, Italy*
[j]*INFN Sezione di Torino, Via Pietro Giuria 1, 10125 Turin, Italy*

Abstract

The characterisation of the epithermal neutron beam at the 5 kW fast reactor TAPIRO (ENEA, Italy) began in 2007. The status of the beam-characterization activities is presented in this paper. The neutron fluence rate and the gamma dose were measured free in-air to verify the design parameters. The thermal and epithermal neutron fluence rates were measured with activation techniques by using bare and cadmium-covered gold foils. The spatial homogeneity of the neutron beam over the beam aperture was verified using TLDs and two sets of gold foils. The spectral fluence of fast neutrons was assessed at the beam port with a Bonner sphere spectrometer and a set of bubble detectors. Also, some preliminary measurements of the gamma dose component were carried out with ionization chambers. Monte Carlo calculations were performed and the results were compared with the experimental data. Further work is required to complete the experimental program.

Keywords: epithermal column, activation technique, neutron spectrometry, MCNP

1. Introduction

An epithermal BNCT facility was installed at the TAPIRO 5 kW fast reactor (ENEA, Italy) in 2006. A detailed description of the configuration of the epithermal column can be found elsewhere (Burn et al., 2006).

In order to perform the characterization of the epithermal neutron beam, an irradiation area has been set up in the reactor hall. The irradiation area is shielded to allow safe operation up to 500 W in reactor nominal power (i.e. 10% of its maximum nominal power). This paper discusses the preliminary characterization of the radiation field which was performed from October 2007 up to February 2008.

2. Materials and methods

The neutron fluence rate and gamma dose were measured free in-air to verify the design parameters (Burn et al., 2006). These measurements were performed across the standard 12×12 cm^2 beam aperture.

The thermal and epithermal neutron fluence rates were measured with activation techniques at nine positions across the beam aperture. Two irradiations were performed in air, by exposing separately bare and cadmium-covered gold foils in the different positions. An aluminium holder was used for the gold foils in order to minimize the positioning uncertainty.

The activity of the gold foils was measured with

a 2"×2" NaI(Tl) scintillator. The epithermal (0.5 eV – 20 keV) fluence rate was assessed through the resonance integral (i.e. by assuming a 1/E spectral distribution for the slowing-down neutrons). The efficiency of the NaI(Tl) detector was calculated with the MCNP code (Briesmeister, 1997). The following sources of non-statistical uncertainty were accounted for: scintillator efficiency, thermal and resonance fluence depression factors, cadmium factor, target weight, reactor power. These measurements provided also some information about the spatial homogeneity of the thermal (labelled "1st set" in section 3) and epithermal neutron components over the aperture.

The uniformity of the thermal neutron component was verified also by means of a further independent measurement using another set of nine gold foils (measuring the relative activities) located along the horizontal and vertical axes of the beam aperture. This measurement (labelled "2nd set" in section 3) was performed using an HPGe (high-purity germanium) detector calibrated by means of a standard set of gamma-ray calibration sources absolutely calibrated at ±1.5%.

The spectral fluence of fast neutrons was measured with a Bonner sphere spectrometer (BSS). The BSS consists of five polyethylene spheres (47, 97, 147, 201, 253 mm in diameter), housing a gold foil at their centre. The 47, 97 and 147 mm spheres are covered with a cadmium layer 0.5 mm in thickness. The response of the BSS (Figure 1) was calculated with the MCNP code and was verified for two spheres at the INFN-Legnaro National Laboratories through irradiation with quasi-monoenergetic neutron fields. The experimental data unfolding was assessed with a code based on the formalism described in (Matzke, 1994) for the GRAVEL code.

The consistency of the reconstructed spectrum with the experimental data (i.e. the saturation activity of the gold foils irradiated inside the polyethylene sphere) was checked by folding the BSS response with the unfolded spectral fluence. Each sphere was irradiated at a certain position so that the distance between the gold foil inside the sphere and the centre of the beam aperture was 90 cm (Figure 2).

The activity of the gold foils contained in each sphere was measured with a 2"×2" NaI(Tl) scintillator. It should be underlined that the BSS responses were calculated against an expanded and aligned beam of neutrons and therefore they cannot be applied for reconstructing a different situation.

In the present case, only the three smaller spheres gave consistent results because the neutron field from the aperture (120×120 mm^2) irradiates partially the two larger spheres (201 and 253 mm in diameter).

A set of bubble detectors was also employed for measuring the fast neutron spectrum. The measurements were performed at the beam aperture and at 10 cm from the beam port (Figure 3), by using the passive bubble detector spectrometer (BDS) (Bubble Technology Industries, 2003). The data were analysed by means of the BUNTO unfolding code (Zanini et al. 2004).

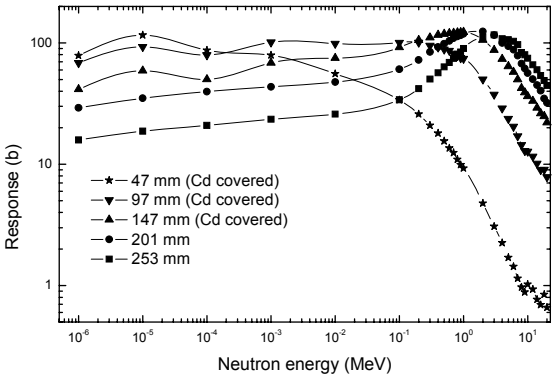

Figure 1. The response of the BSS, consisting of five polyethylene spheres housing a gold target at their centre. The values are in barn (10^{-24} cm^2)

Figure 2. One of the Bonner spheres located in front of the beam aperture

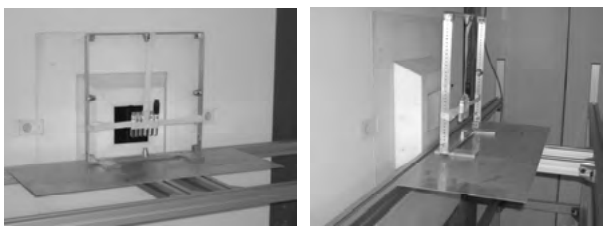

Figure 3. Bubble detectors located in front of the beam aperture (left) and 10 cm far from the aperture (right)

Further measurements of the thermal neutron fluence rate and of the gamma dose were performed using TLD-600 (^{6}LiF:Mg,Ti) and TLD-700 (^{7}LiF:Mg,Ti) detectors that have similar sensitivity to photons but very different sensitivity to thermal neutrons. Both detectors have a negligible sensitivity to epithermal and fast neutrons. When exposed in the epithermal neutron beam, both photons and thermal neutrons give a contribution to the TLD-600 and TLD-700 response with different relative percentages. The shape of the experimental glow curves is exploited for separating the gamma dose and the thermal neutron fluence. The irradiations were performed by positioning the dosemeters at the centre of the beam aperture and at 3 cm from the centre along the horizontal and vertical axes. These measurements allowed to further verify the spatial distribution of the thermal neutron fluence rate.

Finally, a measurement of the gamma dose component at the beam aperture was carried out by means of an ionization chamber calibrated at the Secondary Standard Centre of the Polytechnic of Milan.

The reactor power was monitored during the irradiations by using a reference ionization chamber inserted inside the TAPIRO reactor (close to the core). The current of the ionization chamber, which is linearly correlated with the reactor power, was measured with a Keithley 614 electrometer interfaced with a personal computer.

Most measurements have been compared with the calculated values obtained with the Monte Carlo code MCNP5 (X5 Monte Carlo Team - LANL, 2003). Data libraries based on ENDF/B-VI.8 and ENDF/B-VI.6 were employed.

3. Results

As already mentioned, the spatial uniformity of the thermal neutron component over the beam aperture (12×12 cm^2) was verified using two sets of gold foils (two independent measurements) and a number of TLDs at some selected points along the horizontal and vertical axes of the beam port. The uniformity of the epithermal neutron component was verified by exposing separately bare and cadmium-covered gold foils in the different positions.

The thermal and epithermal measured values are compared with the calculated ones in Figure 4 and Figure 5, respectively. All the data are normalized to the value at the centre of the beam aperture.

The neutron fluence rate resulted to be fairly uniform over the whole beam aperture except for two positions along the vertical axis and one position along the horizontal one that show a thermal component about 15-25% lower than that measured in the central position.

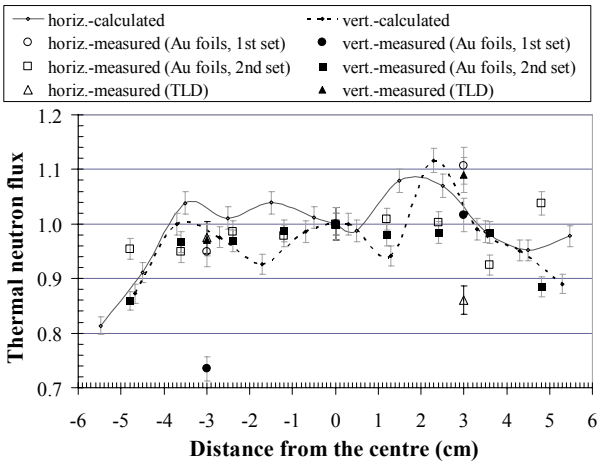

Figure 4. The thermal neutron component distribution compared with the calculated values. The data are normalized to the value at the centre of the beam aperture. (Note that the two sets of gold measurements are totally independent)

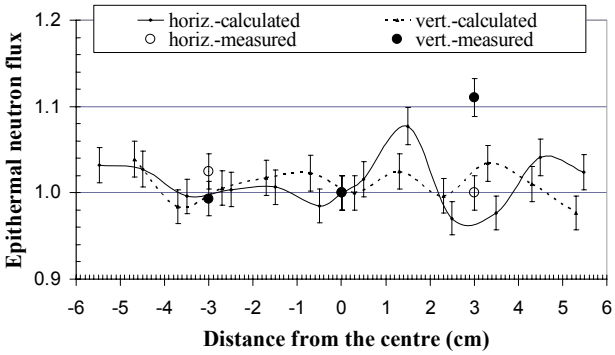

Figure 5. The epithermal neutron component distribution compared with the calculated values. The data are normalized to the value at the centre of the beam aperture.

Table I shows the comparison between the calculation (statistical uncertainties below 5%) and the measurement of the following free beam parameters: the thermal fluence rate (below 0.5 eV), the epithermal fluence rate (0.5 eV - 20 keV) and the fast (above 20 keV) neutron fluence rate. All the parameters were evaluated as average values at the beam aperture per unit reactor power. The uncertainties (1σ) of the measurements account for both statistical and systematic contributions. The measured thermal (1st set of gold foils) and epithermal components resulted to be about 50% lower than the calculated values. The fast neutron fluence rate measurement turned out to be 20% higher than the calculated one.

The spectral fluence measured with the BSS at 90 cm from the beam aperture and reconstructed from the three smaller spheres is shown in Figure 6 together with the calculated one at the beam aperture. (In the near future the comparison will be made at the same position.) At 90 cm from the beam port the total fluence rate per unit power of the reactor resulted to be 4.6×10^{6} cm^{-2} s^{-1} kW^{-1}, while that integrated from 10 keV up to 7 MeV is 8.8×10^{5} cm^{-2} s^{-1} kW^{-1}.

Table I – Comparison between calculated and measured free beam parameters averaged over the beam aperture per unit reactor power (cm^{-2} s^{-1} kW^{-1})

	Calculation	Measurement
Thermal neutron fluence rate	1.6×10^{7}	$(9.0 \pm 0.27)\times10^{6}$
Epithermal neutron fluence rate	1.6×10^{8}	$(8.2 \pm 0.27)\times10^{7}$
Fast neutron fluence rate	5.2×10^{6}	$(6.4 \pm 0.6)\times10^{6}$

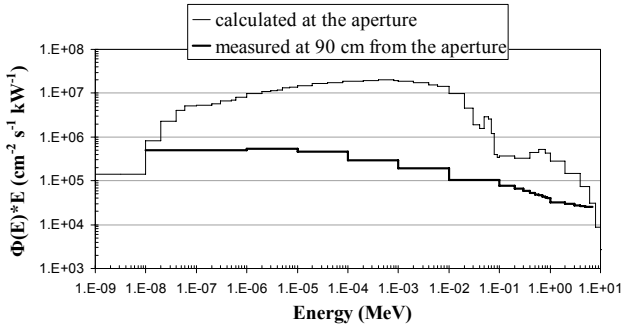

Figure 6. Calculated neutron spectral fluence rate at the beam aperture and the measured one with the BSS at 90 cm from the beam aperture

In Figure 7 the fast component (above 20 keV) of the neutron spectra shown in Figure 6 is compared with the neutron spectra measured with the BDS at the beam aperture and at a distance of 10 cm. The agreement of the spectra at the beam aperture is fairly satisfactory in the energy range between 20 keV and 1 MeV, while at higher energies the spectra show an increasing discrepancy. The shape of the spectra measured at the beam aperture is very similar to that measured at 10 cm.

The gamma air-kerma rate measured with the ionization chamber resulted to be about 0.9 Gy h^{-1} kW^{-1}.

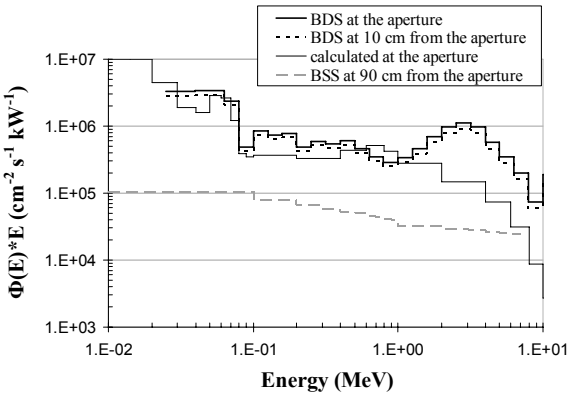

Figure 7. Comparison between the calculated and measured fast neutron spectra

4. Conclusions

The preliminary results of the characterization of the epithermal BNCT column at the TAPIRO reactor have been presented. Activation techniques, TLDs, Bonner spheres, bubble detectors and an ionization chamber were used for this purpose. The experimental data were compared with Monte Carlo calculations.

The measurements have not been completed yet because the reactor was shut down in March 2008 for maintenance. Further measurements and simulations will be performed to complete the scheduled activities and to investigate the discrepancies observed in this preliminary work.

References

Briesmeister, J.F., Editor, 1997. MCNP - A General Monte Carlo N-Particle Transport Code, Version 4B. LA-12625-M.

Bubble Technology Industries, 2003. Instruction manual for the bubble detector spectrometer (BDS). Chalk River, Ontario Canada.

Burn, K.W., Casalini, L., Martini, S., Mondini, D., Nava, E., Rosi, G., Tinti, R., 2006. Final design and construction issues of the TAPIRO epithermal column. Advances in Neutron Capture Therapy 2006 (Proceedings of ICNCT-12), 564–567.

Matzke, M., 1994. Unfolding of Pulse Height Spectra: the HEPRO Program System. Braunschweig, Germany, PTB Bericht, vol. 19.

X5 Monte Carlo Team - LANL, 2003. MCNP - A General Monte Carlo N-Particle Transport Code, Version 5, LA-UR-03-1987 (Revised 10/3/05).

Zanini, A., E. Durisi, F. Fasolo C. Ongaro, U. Nastasi, K.W. Burn, J.R.M. Annand, 2004. Neutron spectra in a tissue equivalent phantom during photon radiotherapy treatment by linacs. Rad. Prot. Dosim. 110 1-4, 157-160.

Progress in the use of gadolinium for NCT

N. Cerullo[a,b], D. Bufalino[a,c], G. Daquino[d]

[a] *Department of Mechanics, Nuclear and Production Engineering (DIMNP), University of Pisa, via Diotisalvi 2, 56126, Pisa, Italy*

[b] *Department of Production Engineering, Thermoenergetics, and Mathematical Models (DIPTEM), University of Genova, via all'Opera Pia 15/a, I-16145, Genova, Italy*

[c] *SORIT s.r.l. (Research Company for Techn. Development), via Montegrappa 15, 57100, Livorno, Italy*

[d] *JRC (European Commission), P.O. Box 2, Westerduinweg 3, 1755 ZG Petten, The Netherlands*

Abstract

The evaluation of possible improvement in the use of Gd in cancer therapy, particularly in the assessment of TPS, in reference to GdNCT, has been analyzed. At first the problem of the gadolinium compounds toxicity was reviewed identifying the Motexafin Gadolinium as the best. Afterwards, the spectrum of IC and Auger electrons was calculated using a special method. Afterwards, this electron source has been used as input of the PENELOPE code and the energy deposit in DNA was well defined. Taking into account that the electron yield and energy distribution are related to the neutron beam spectrum and intensity, the shaping assembly architecture was optimized through computational investigations. Finally the study of GdNCT was performed from two different points of view: macrodosimetry using MCNPX, with calculation of absorbed doses both in tumour and healthy tissues, and microdosimetry using PENELOPE, with the determination of electron RBE through the energy deposit. The equivalent doses were determined combining these two kinds of data, introducing specific figures of merit to be used in TPS. According to these results, the GdNCT appears to be a fairly possible tumour therapy.

Keywords: GdNCT, Gadolinium, Nanodosimetry, Auger electron, treatment planning system

1. Introduction

The GdNCT is a recently reproposed therapy, mainly based on the action of Auger and IC electrons, generated by ^{157}Gd after neutron capture.

The reference to the use of gadolinium is derived mainly from the consideration of its quite higher neutron capture cross sections (254000 barns for ^{157}Gd) vs. boron (3835 barns for B-10) that implies a huge dose delivery in proximity of the tumour region.

The research on the use of gadolinium as neutron absorber in NCT, even if appears quite complex, presents some promising future applications. The evaluation of improvements in the use of gadolinium in cancer therapy (GdNCT), through the treatment planning system (TPS) assessment, is one of the topics currently analyzed by our group. In fact the first issue is to save the patient's health ("primum non nocere"). This item suggests to deeply analyze the toxicity of gadolinium compounds and the effect on healthy tissues of parasitic reactions.

Gadolinium neutron capture reactions release a wide range of particles: prompt gamma rays, internal conversion electrons, X-rays and Auger electrons. The spectrum of the secondary particles emitted by gadolinium (mainly electrons) is complex and, among others, the presence of strong gammas spreads out the dose delivery to a broad region, thus limiting the selectivity of the therapy. The photons emitted in the (n,γ) reactions interact with the tissues but deposit energy over a longer path length than the boron reaction products. This is the main drawback of GdNCT.

However, if ^{157}Gd uptake is strictly limited to tumour bulk, having a size of the order of some cm^3 by volume, then an additional effect, in the increasing of tumour dose and in the attenuation of the capture photons yield, will be added.

Conversion and Auger electrons are also emitted after the Gd neutron capture, at hundreds of discrete energies. These electrons have energy-dependent ranges in water as short as 0.8 μm at 5 keV. However the range due to the most commonly yielded electron energies exceeds the size of a single cell. Electrons with very low energies (few tens of eV) are also emitted; having a desired short range and bringing a very high contribute to the local dose delivery in

GdNCT.

Even if the energy carried out by these electrons is limited to about 1% of total energy released by the $^{157}Gd(n,\gamma)^{158}Gd$ reaction only, their contributions is nevertheless very effective due to the high electron LET, if the emitter is bound to DNA. Therefore the DNA double-strand break occurs with consequent cell killing. Furthermore Auger cascade electrons display a very complex energy spectrum, dominated by a large number of very low-energy electrons (down to few eV) with ranges of macromolecular dimensions in biological matter.

2. Gadolinium compounds toxicity and localization in tissues

Although Gd^{3+} ions are toxic, there are some gadolinium compounds (e.g. Gd-DTPA and other chelate compounds) that show a very low toxicity. These substances are given intravenously to the patient. They are already used in MRI and considered even more safe than iodized contrast agents as far as kidney damage is concerned.

Recently a new compound, Motexafin Gadolinium (MGd) has been developed by pharmaceutical industry (Evens, 2004). MGd have been studied because it may make tumour cells more sensitive to radiation therapy, improves tumour image quality using magnetic resonance imaging and kills cancer cells. It is a type of metalloporphyrin complex, also called gadolinium texaphyrin (Gd-Tex). A number of toxicological studies have been conducted on this substance leading to the statement that its intravenous delivery is well tolerated. Furthermore in this case plasmatic concentration is maintained at high levels for longer periods in comparison to current paramagnetic contrast agents.

The dose to a biological target depends in part on the cumulated quantity of gadolinium in the target and its surroundings. The extreme short range of Auger electrons may require accurate data acquisition on the spatial localization of the emitters relative to the targets with nano-scale resolution. Unfortunately such information cannot readily be obtained even from patient, animal or cell culture studies.

De Stasio et al. (2006) made use of X-ray photo-emission electron microscopy (X-PEEM) analysis on some gadolinium coumponds (e.g. Motexafin Gadolinium) using the Spectromicroscope for Photoelectron Imaging of Nanostructures with X-rays (SPHINX) instrument but this technique was used for *in vitro* samples. Some similar analysis has been done in Japan using a single ended accelerator (Endo et al., 2004). This information plays a critical role in the evaluation of DNA damage due to gadolinium in GdNCT, and therefore is mandatory for predicting the tumour biological effects. De Stasio et al. (2006) found that in all types of samples exposed to 100 µmol/L of MGd more than 90% of cellular nuclei contain Gd. Therefore it is demonstrated that molecules like MGd are able to carry Gd atoms especially inside the tumour DNA. This result is very encouraging with regard to the possibility of using MGd, also well tolerated, in GdNCT. Furthermore it is highly probable that pharmaceutical research can drive to new and more specific compounds. In other words the therapy efficacy is highly dependent on the chemical / pharmaceutical progress.

3. Electron spectrum determination

The Auger electron spectra are discrete, reflecting the energies of orbital transitions within the atom. The analysis of this spectrum is fundamental to study the local electron transport in order to evaluate the DNA damage.

Starting from gadolinium reaction data, the IAEA BRICC code (Kibédi et al., 2005) which provides, for allowed transitions, the internal conversion coefficients for the atomic levels, has been used. The IC electron energies were determined by difference between the transition energy and atomic orbital bound energy. The Auger and Coster-Kronig emission energies have been calculated with the EADL (Evaluated Atomic Data Library) of LLNL (Perkins et al., 1994) and the associated RELAX program (Cullen, 1992). In Fig. 1 the calculated spectrum is shown. It appears that there are too many points in this figure so it is not very clear from the graphical point of view. However, all the values are available in tabular form. So this work could be used as a basis for Monte Carlo (MC) calculations in further GdNCT studies.

4. Nanodosimetry and macrodosimetry

Only 1% of neutron capture reaction energy is transported by Auger and IC electrons, but if the Gd atom is bounded to the DNA their effectiveness in killing tumour cell is very high. Molecules like MGd are able to carry Gd atoms specially inside the tumour DNA. Supposing to have an approximated knowledge of the gadolinium positioning inside the cell, the estimation of the energy fraction released by the electrons at nano-scale level, is the main issue to be sorted out. The first idea, due mainly to complex cell geometry and to the stochastic nature of the phenomena, is to use the Monte Carlo technique. The RBE of Auger electrons depends dramatically on the location of Gd inside the cells. With Monte Carlo codes it is possible to determine

microdosimetric quantities such as energy deposit and lineal energy. In fact IC and Auger electrons from Gd atoms bounded to DNA can still be tracked with the same techniques used in microdosimetry (ICRU, 1983) in spite of nanodosimetric dimensions of the target,. Calculated lineal energy spectra can be used to predict the RBE of electrons.

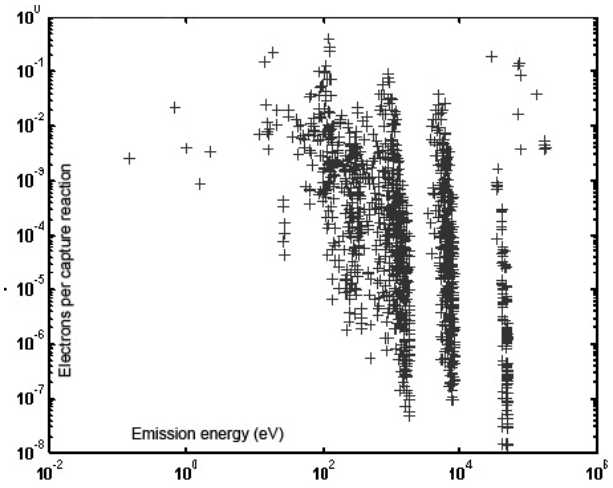

Fig.1 Number of electrons (Auger and IC) for $^{157}Gd(n,\gamma)^{158}Gd$ capture reaction

PENELOPE (Salvat et al., 2006) has been chosen for the calculations. This code performs Monte Carlo simulation of coupled electron-photon transport in arbitrary materials and complex quadric geometries. Electron kinetic energies must be in the range from 100 eV to 1 GeV. The mixed simulation algorithm for electrons implemented in PENELOPE reproduces the actual transport process to a high degree of accuracy and is very stable even at low energies. This is partly due to the use of a sophisticated transport mechanics model based on the so-called "random hinge method", with energy-loss corrections for soft events. The code is in continuous progress and our group is part of the PENELOPE users team.

The source spectrum plotted in Fig. 1 has been used in input for PENELOPE calculations simulating a fragment of DNA, approximated by a 3 nm radius cylinder, positioning the source (Gd atoms subject to neutron reaction) in various localisations (inside the DNA, on the DNA surface, near the surface etc.). The target of this analysis is to evaluate the energy deposit and the lineal energy for the electrons in each configuration. Starting from the lineal energy RBE value has been associated to electrons according to the ICRU 40 (1986) methodology.

Table 1 shows the results of the analysis in three cases.

Tab. 1 – RBE values assigned to electrons according to Gd position

Gd Position	**Mean energy released in DNA for source electron (eV)**	**Mean energy released in DNA for single neutron capture (eV)**	**Mean lineal energy (*y*) (keV/µm)**	**Associated RBE according ICRU 40 (Q)**
At the centre of cylinder	75,192	380,6	32.55	12,563
On the surface of cylinder	40.560	205,3	17,56	5,97
On the proximity of the surface but outside the cylinder	11,493	58,17	4,97	1,46

RBE value results to be higher than 1 if Gd atom is bounded to the DNA. Of course the specific RBE value to attribute to electrons depends on the Gd compound and the tissue characteristics.

The results of the nanodosimetric analysis have been used in the macrodosimetric analysis. In this case the MCNPX code (Pelowitz, 2005) simulating a Snyder phantom containing a turmour zone (Fig. 2), has been used. The calculation coupled the neutron and gamma transport, determining physical doses from neutrons (both proton recoil and $^{14}N(n,p)^{14}C$ contribution) and from gammas. Physical dose from electrons was calculated multiplying ^{157}Gd neutron capture reaction rate to the mean electron energy for capture, assuming that electrons deposit locally their energy. Weighted doses was obtained making the summation over various particle contributions, multiplying separately the values of physical doses by RBE associated to single contributions. It has been assumed RBE equal to 3.2 for proton recoil and protons coming from $^{14}N(n,p)^{14}C$ reaction. RBE for photons is equal to 1. The RBE value for Auger and IC electron contribution is a function of Gd localisation. Concentrations of 700 ppm of ^{157}Gd in tumour tissue and 10 ppm of ^{157}Gd in healthy tissues have been assumed. Adopting the hypothesis that Gd is localised almost only in the tumour DNA RBE values of 9.42 in tumour (an intermediate value between that corresponding to the centre of tumour and that corresponding to the surface) and 1 in healthy tissues have been chosen for electrons. It is worth to point out that Gd is commercially available in 86-97% ^{157}Gd enrichment. Exposing the phantom to a neutron flux of 10^9 $n \cdot cm^{-2} \cdot s^{-1}$ from a D-T based accelerator (Cerullo et al., 2005) the dose profile has been calculated and shown in Fig. 2. The treatment was bilateral (30 minutes each side).

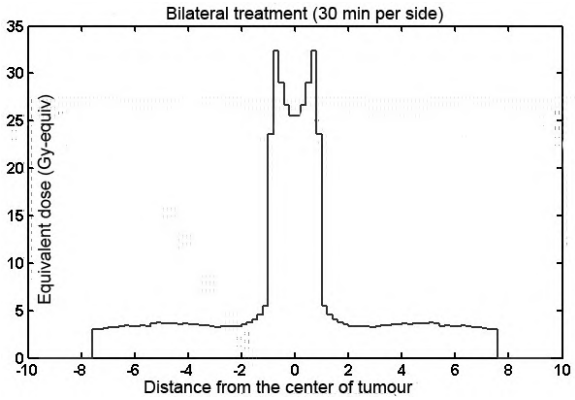

Fig. 2 – Equivalent dose in the case of bilateral treatment of a 2 cm diameter tumour positioned at the centre of the skull.

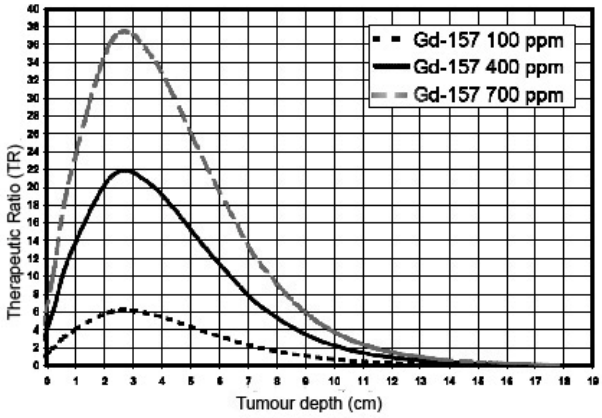

Fig. 3 – Therapeutic ratio in function of tumour depth (monolateral treatment) for various ^{157}Gd concentrations in tumour

Figure 3 shows the trend of the Therapeutic Ratio (TR). TR was calculated dividing the tumour equivalent dose (assuming tumour dimension as negligible) by the maximum value of equivalent dose in the healthy tissue.

5. Conclusions

GdNCT, maintaining its promises, appears to be a fairly possible tumour therapy. Its drawbacks, namely the toxicity of Gd compounds and the damage to healthy tissues due to the parasitic gamma radiation, have been analyzed. They can be sorted out taking into account the efforts performed in the research so far. The results of macrodosimetric calculations using Motexafin Gadolinium-like compounds incorporated in tumour cells DNA show a satisfactory increase in therapeutic ratio.

References

Cerullo N, Esposito J, Bufalino D, Mastrullo A, Muzi L, Palmerini S, 2005. Preliminary design of a Gd-NCT neutron beam based on compact D-T neutron source. Rad. Prot. Dosim., 116(1-4 Pt 2),605-8.

Cullen D.E., 1992. Program RELAX, A Code Designed to Calculate Atomic Relaxation Spectra of X-Rays and Electrons. LLNL, Livermore, California, UCRL-ID-110438

De Stasio G., Rajesh D., Ford J.M., Daniels M.J., Erhardt R.J., Frazer B.H., Tyliszczak T., Gilles M.K., Conhaim R.L., Howard S.P., Fowler J.F., Estève F., Mehta M.P., 2006. Motexafin-Gadolinium Taken Up In vitro by at least 90% of Glioblastoma Cell Nuclei, Clin Cancer Res., 12(1), pp 206-213

Endo K., Shibata,, Yoshida H., Nakai K., Yamamoto T., Matsumura A., Ishii K., Sakai T., Sato T., Oikawa M., Arakawa K., Kumada H., Yamamoto K, 2004, Analysis of Intracellular Distribution of Boron and Gadolinium in 9L Sarcoma Cells Using a Single-Ended Accelerator (Micro PIXE), Nippon Genshiryoku Kenkyujo JAERI, Review, pp. 274-275 (2004)

Evens.AM., 2004. Motexafin gadolinium: a redox-active tumor selective agent for the treatment of cancer. Curr Opin Oncol;16(6),576-80.

International Commission for Radiation Units and Measurements, 1983. Microdosimetry. ICRU Report 36.

International Commission for Radiation Units and Measurements, 1986. The Quality Factor in Radiation Protection. ICRU Report 40.

Kibédi T., Burrows T.W., Trzaskovskaya M.B., Nestor C.W. Jr., 2005. BrICC Program Package v. 2.0. Department of Nuclear Physics, Australian National University, ANU-P/1684

Pelowitz D.B., 2005. MCNPX User's Manual, version 2.5.0., LANL, LA-CP-05-0369

Perkins S.T., Cullen D.E., 1994. ENDL Type Formats for the LLNL Evaluated Atomic Data Library, EADL, for the Evaluated Electron Data Library, EEDL, and for the Evaluated Photon Data Library, EPDL. LLNL, California, UCRL-ID-117796

Salvat F., Fernández-Varea J.M., Sempau J., 2006. PENELOPE-2006: "A Code System for Monte Carlo Simulation of Electron and Photon Transport". NEA Workshop Proceedings, Barcelona, Spain, Edited by OECD, ISBN 92-64-02301-1

A detailed Monte Carlo accounting of radiation transport in the brain during BNCT

M. P. W. Chin, N. M. Spyrou

Department of Physics, University of Surrey, Guildford GU2 7XH, England

Abstract

The collision type central to BNCT is $^{10}B(n, \alpha)^{7}Li$, however, other types of nuclear reactions also take place in the patient. In addition to the major elements (H, C, N, O), minor elements such as Na, Mg, P, S, Cl, K, Ca and Fe present in body tissues also interact in neutron collisions. Detailed accounting of the above not only provides a better understanding of radiation transport in the human body during BNCT, but such knowledge affects the design of the facility, as well as treatment planning, imaging and verification for a given BNCT agent. Of the methods of investigation currently available, only Monte Carlo simulation could provide the detailed accounting and breakdown of the quantities required. We report Monte Carlo simulation of an anthropomorphic voxel phantom, the VIP-Man, and show how these quantities change with different ^{10}B concentrations in the tumour, the blood and the remaining tissues. We have chosen the ^{10}B biodistribution to be the variable of interest, since it is not accurately known, is frequently approximated and is a crucial quantity on which dose calculations are based.

Keywords: Monte Carlo, MCNPX, anthropomorphic phantom, VIP-Man, minor elements

1. Introduction

We have previously compared two Monte Carlo codes, FLUKA (Ferrari et al., 2005) and MCNPX (MCNPX User's Manual, 2005), on the simulation of the $^{10}B(n, \alpha)^{7}Li$ collision -- the underlying principle of boron neutron capture therapy (BNCT). Our study demonstrated how MCNPX produced the unexpected phenomenon of a single neutron releasing multiple 0.478 MeV photons. Despite such anomalies, the net effect after averaging over multiple histories did converge with the accepted expectation of 94% $^{10}B(n, \alpha)^{7}Li$ collisions producing a 0.478 MeV photon (Chin and Spyrou, 2007). Based on the convergence established, we now proceed with a detailed Monte Carlo accounting of different collision types with a variety of nuclei present in the heterogeneous anatomical structures during a delivery of BNCT to the brain.

While it is customary to estimate BNCT dose in terms of four contributing components from thermal neutron, fast neutron, photon and boron (Goorley et al., 2002) via calculations and simulations, the full potential of Monte Carlo has yet to be tapped. While $^{14}N(n, p)^{14}C$, $^{1}H(n, n')^{1}H$, $^{1}H(n, \gamma)^{2}H$ and $^{10}B(n, \alpha)^{7}Li$ are generally taken as the origin of the above four components respectively, many other reaction types take place with both major and minor elements in the head. Monte Carlo simulation allows the above components to be separated into further components, which could provide invaluable insights for optimising BNCT. Moreover, Monte Carlo makes it possible to extract radiation quantities at the point of collision, before further scattering takes place. Examining the particles' attributes first-hand at the time of collision is an essential preliminary to the investigation of derived secondary quantities such as dose equivalent and biological effectiveness.

2. Materials & Methods

MCNPX version 2.5.0 was used for the simulations described in this work. The heterogeneous body of a patient was represented by the VIP-Man anthropomorphic phantom comprising over 1.3×10^{6} voxels of 4 mm × 4 mm × 4 mm (Xu et al., 2000). Based on the geometry input cards downloaded from the American Nuclear Society Computational Medical Physics Working Group online database, we made modifications as described in the following paragraphs.

A voxel of tumour was introduced by adding ^{10}B into the material composition which was originally 'normal' gray matter (Fig. 1). The location was selected based on the 3D probabilistic glioblastoma multiforme location atlas (Frew et al.). As BNCT cases involve varying stages of resection with a possible combination of radiotherapy and chemotherapy, a full tumour of the order of centimetres was not modelled here.

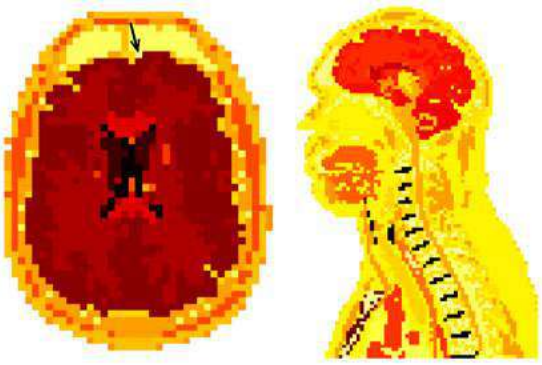

Fig. 1. A tomographic cut and a sagittal cut (not on the same scale) from the VIP-Man anthropomorphic phantom used in this work. The location of the tumour is indicated by a black arrow on the tomographic image

A lateral neutron beam simulated as a thin cross-section of radius 2.0 cm was made incident at source-to-surface distance 5 cm with its central axis intercepting the tumour. The spectrum was similar to an ideal BNCT spectrum proposed by the Berkeley group (Bleuel et al., 1998) which forms a symmetrical bell-shape curve when the energy is plotted on a log scale, ranging from 1 to 100 keV, with its peak at 10 keV.

The most recent evaluation of cross-sections for temperature 293.6 K were chosen (alternatives include 300.0 and 77.0 K) (MCNPX User's Manual, 2005). To obtain more accurate thermal neutron scattering, thermal treatment for hydrogen in light water was used for all tissues except the adipose tissue where the thermal treatment in polyethylene was used instead (Evans et al., 2001; Yonai et al., 2007). Implicit (as opposed to analog) capture was applied to achieve higher simulation efficiency. This modified sampling method, also known as implicit absorption and survival biasing, operates by reducing the weight of the particle instead of killing it in the event of an absorption. No additional variance reduction techniques were used; particle importances were uniformly unity throughout the anthropomorphic phantom.

No MCNPX *tallies* were used. All results presented here were extracted via *PTRAC* (event-by-event output) and from *Table 140* (nuclide activity for neutrons) of the standard output.

The quantities extracted were the number of neutron collisions per history and the capture ratio. Both were divided into contributing components according to the tissue type (e.g. gray matter, blood etc.) In MCNPX nomenclature, *capture* includes radiative and non-radiative captures. ^{10}B was explicitly specfied in the material composition, as opposed to the use of kerma factors (Zamenhof et al., 1996; Chadwick et al., 1999; Goorley et al., 2002; Casal et al., 2004). The simulation was repeated with different combinations of ^{10}B concentration in blood (B_B), tumour (B_T) and remaining tissues (B_R) as tabulated in Table 1, chosen according to reported values (IAEA, 2001) and also to make the following comparisons. Simulations S_{II} and S_{III} are for comparing the effects of B_R while keeping B_B and B_T constant. Similarly, the S_{IV}-S_{III} and S_V-S_{III} pairs are for comparing the effects of B_B and B_T respectively while keeping the remaining two variables constant. Each simulation comprised 120 million independent histories.

Table 1. Combinations of ^{10}B mass concentration specified in five independent simulations

Simulation	^{10}B concentration (ppm)		
	B_B	B_T	B_R
S_I	0	0	0
S_{II}	15	30	0
S_{III}	15	30	10
S_{IV}	15	50	10
S_V	10	30	10

3. Results

The weighted number of collisions per history is shown in Fig. 2. The colourscale of each pixel indicates $\log_{10} \overline{N}_{\zeta,\tau}$, where $\overline{N}_{\zeta,\tau}$ denotes the weighted number of collisions per history, ζ the element and τ the tissue type respectively. The weighted number of collisions but not the number of collisions is plotted because for some collisions the particle weighs less than unity due to the biasing caused by implicit captures. Whereas $\overline{N}_{\zeta,\tau}$ includes all collisions types, whether elastic, inelastic or capture, Fig. 3 shows the capture fraction (out of the total collisions) $\overline{C}_{\zeta,\tau}$ for the respective ζ and τ; the colourscale of each pixel indicates $\log_{10} \overline{C}_{\zeta,\tau}$.

As expected, while hydrogen recorded the highest $\overline{N}_{\zeta,\tau}$ (Fig. 2), boron recorded the highest $\overline{C}_{\zeta,\tau}$ (Fig. 3), generally, across different anatomical structures. Whereas $\overline{N}_{\zeta,\tau}$ depends on the amount of the nuclide available for collision in a given anatomical structure as well as the competing collisions posed by the remaining nuclei, $\overline{C}_{\zeta,\tau}$ is not.

On the other hand, both $\overline{N}_{\zeta,\tau}$ and $\overline{C}_{\zeta,\tau}$ are dependent on the neutron energy at the time of collision, which would have been reduced with respect to the incident energy and which varies according to the age of the neutron, as well as the nuclei it previously traversed upstream of the radiation history. For the same nuclide, carbon, for example, $\overline{C}_{\zeta,\tau}$ varied from 5.87×10^{-4} in the cerebellum to 1.50×10^{-4} in the tumour respectively.

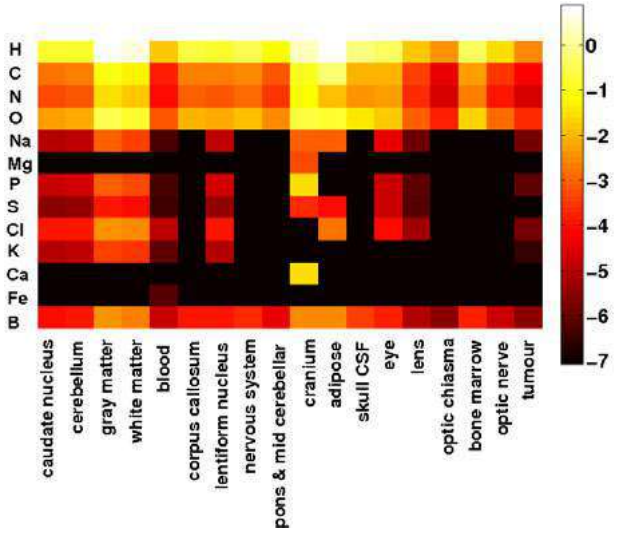

Fig. 2. Results from simulation III: the number of collisions (weighted due to implicit capture) per history for different elements in different anatomical structures in the brain

From the simulations, capture gamma rays as high as 6.49, 9.28, 7.93, 8.64, 8.58, 7.77 MeV were emitted from Na, Mg, P, S, Cl, K respectively. ^{10}B itself produced capture gamma rays as high as 11.5 MeV.

Comparing S_I with S_{III} (Fig. 4) the presence of ^{10}B in the body was found to cause increased collisions most notably in blood, followed by the remaining tissues and the tumour. In blood, the increase was due to both the major (11.85%±0.07%) and the minor (9%±2%) elements.

Effects of the addition of B_R by 10 ppm could be seen by comparing S_{II} with S_{III} (Fig. 5) where the number of collisions with the major and minor elements and ^{10}B in the blood decreased by (11.43±0.07)%, (15±2)% and (10±2)% respectively. A point to note is the larger effect from the minor elements. In the remaining tissues, collisions with the major and minor elements decreased by (6.262±0.002)% and (4.82±0.04)% respectively. Increasing B_T from 30 ppm to 50 ppm (simulations S_{III} and S_{IV}) resulted in negligible changes (<0.001% reduction) in the number of collisions in the remaining tissues.

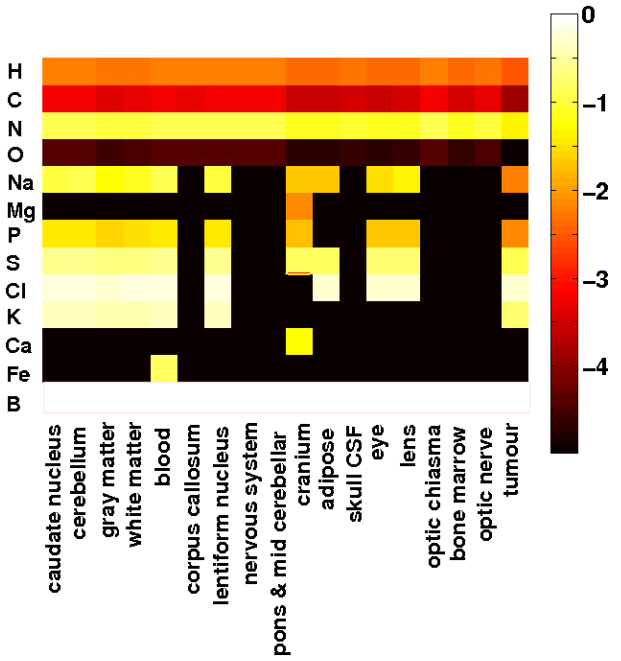

Fig. 3. Results from simulation III: the capture fraction for different elements in different anatomical structures in the brain. Boron scored the highest capture fraction (all white) across all anatomical structures

Self absorption and screening effects were found to be negligible. Assuming equal B_R and B_B (S_V) led to no significant changes in the number collisions in both the remaining tissues and the tumour.

4. Conclusions

The interplay of multiple factors as the neutron progresses through the random walk as demonstrated above complicates the 'back-of-the-envelop' calculation of $\overline{N}_{\zeta,\sigma}$ and $\overline{C}_{\zeta,\sigma}$. The presence of minor elements (besides H, C, N, O) in body tissues was found to affect radiation transport dynamics. The minor elements produced capture gamma rays more energetic than the typical 6 MV or even 18 MV radiotherapy photon beam at the depth of maximum dose (known as d_{max}).

No significant difference in the number of collisions in the remaining tissues could be observed when the ^{10}B concentration in the tumour was increased from 30 to 50 ppm, or when ^{10}B concentration in blood was increased from 10 to 15 ppm. It should be stressed that this is a study on radiation transport, not on the biology of ^{10}B uptake; each combination of ^{10}B concentration in the blood, tumour and remaining tissues was fixed as input to the Monte Carlo simulations performed here.

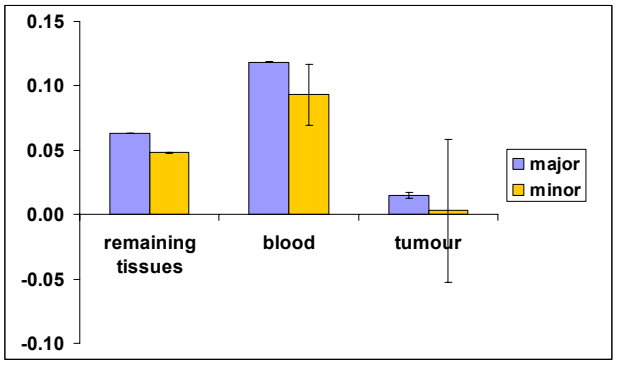

Fig. 4. Fractional change in the number of neutron collisions (with the major and minor elements) in simulation S_I with respect to S_{III}

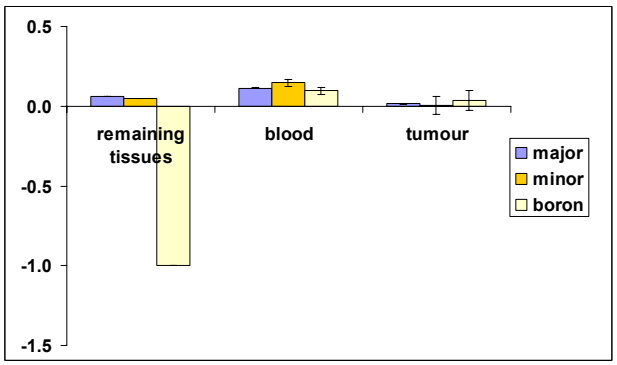

Fig. 5. Fractional change in the number of neutron collisions (with the major and minor elements as well as boron) in simulation S_{II} with respect to S_{III}

References

Bleuel, D.L., Donahue, R.J., Ludewigt, B.A., Vujic, J. 1998. Development of a neutron energy-biased in-air figure-of-merit of predicting in-phantom BNCT neutron beam characteristics. Berkeley: Lawrence Berkeley National Laboratory.

Casal, M.R., Gonsalez, S.J., Blaumann, H.R., Longhino, J., Calzetta Larrieu, O.A., Wemple, C.A., 2004. Comparison of the performance of two NCT treatment planning systems using the therapeutic beam of the RA-6 reactor. Applied Radiation and Isotopes 61, 805-810.

Chadwick, M.B., Barschall, H.H., Caswell, R.S., DeLuca, P.M., Hale, G.M., Jones, D.T.L., MacFarlane, R.E., Meulders, J.P., Schuhmacher, H., Schrewe, U.J., Wambersie, A., Young, P.G., 1999. A consistent set of neutron kerma coefficients from thermal to 150 MeV for biologically important materials. Medical Physics 26 (6), 974-991.

Chin, M.P.W., Spyrou, N.M., 2007. Event-by-event Monte Carlo tracking of neutron-nucleus collisions in neutron detectors. Trans. Am. Nucl. Soc., 288-289.

Evans, J.F., Blue, T.E., Gupta, N., 2001. Absorbed dose estimates to structures of the brain and head using a high-resolution voxel-based head phantom. Medical Physics 28 (5), 780-786.

Ferrari, A., Sala, P.R., Fasso, A., Ranft, J. 2005. FLUKA: a multi-particle transport code: CERN.

Frew, A.J., Thompson, P.M., Cloughesy, T.F., Tseng, P.B., Toga, A.W., Alger, J.R. 2008. *A 3D probabilistic glioblastoma multiforme location atlas* [cited June 2008]. Available from www.loni.ucla.edu/~thompson/HBM2004/AF_HBM2004_Atlas.pdf.

Goorley, J.T., Kiger, W.S., Zamenhof, R.G., 2002. Reference dosimetry calculations for neutron capture therapy with comparison of analytical and voxel models. Medical Physics 29 (2), 145-156.

IAEA. 2001. Current status of neutron capture therapy. Vienna: International Atomic Agency.

MCNPX User's Manual. 2005. edited by Pelowitz, D.B. Los Alamos: Los Alamos National Laboratory.

Xu, X.G., Chao, T.C., Bozkurt, A., 2000. VIP-man: An image-based whole-body adult male model constructed from color photographs of the visible human project for multi-particle Monte Carlo calculations. Health Physics 78 (5), 476-486.

Yonai, S., Baba, M., Itoga, T., Nakamura, T., Yokobori, H., Tahara, Y., 2007. Influences of neutron source spectrum and thermal neutron scattering law data on the MCNPX simulation of a cyclotron-based neutron field for boron neutron capture therapy. Journal of Nuclear Science and Technology 44 (11), 1361-1367.

Zamenhof, R.G., Redmond, E., Solares, G., Katz, D., Riley, K., Kiger, S., Harling, O., 1996. Monte Carlo-based treatment planning for boron neutron capture therapy using custom designed models automatically generated from CT data. Int. J. Radiation Oncology Biol. Phys. 35 (2), 383-397.

Angle- and energy-differential neutron spectrometry for the SPES BNCT facility

F. d'Errico[a], R. Ciolini[a], A. Di Fulvio[a], M. Reginatto[b], J. Esposito[c], C. Ceballos Sànchez[c], P. Colautti[c]

[a]*Dipartimento di Ingegneria Meccanica, Nucleare e della Produzione, Università degli Studi di Pisa, Italy*
[b]*Physikalisch-Technische Bundesanstalt, Braunschweig, Germany*
[c]*Istituto Nazionale di Fisica Nucleare - Laboratori Nazionali di Legnaro, Legnaro, Italy*

Abstract

An accelerator-driven thermal neutron facility for boron neutron capture therapy of skin melanoma is currently under construction at the Laboratori Nazionali di Legnaro. The installation relies on the production of neutrons from a thick beryllium target bombarded with 5 MeV protons. A complete set of double differential data, i.e. angle- and energy-differential neutron spectra produced by the beryllium target, is necessary for the Monte Carlo based design of the installation. For this purpose, double differential fluence measurements are currently performed with the "BINS" neutron spectrometer using 5 MeV protons at the "CN" Van de Graaf accelerator. This spectrometer uses a superheated emulsion of dichlorotetrafluoroethane which is sequentially operated at 25, 30, 35, 40, 45, 50 and 55 °C and thus provides a series of seven sharp thresholds covering the 0.1-10 MeV neutron energy interval. Deconvolution of the data is performed with the code "MAXED", which is based on the maximum entropy principle. The analysis of our first neutron spectrometry measurements at angles of 0, 40, 80 and 120 degrees supports the viability of the BINS spectrometry method for the generation of the required double differential data.

Keywords: Accelerator-based BNCT, thermal neutron beam, neutron spectrometry, superheated emulsions.

1. Introduction

In the framework of the SPES (Study and Production of Exotic Species) project of the Istituto Nazionale di Fisica Nucleare (INFN), an accelerator-driven thermal neutron facility for BNCT (Boron Neutron Capture Therapy) is currently under construction at the Laboratori Nazionali di Legnaro (LNL). The SPES- BNCT facility is designed for the treatment of skin melanoma and, at a later stage, of hepatic metastases in the explanted liver. An intense proton beam of 30 mA and 5 MeV will be used as driver source. The beam will be provided by the SPES Radio Frequency Quadrupole, which is the first accelerating stage of the planned 20 MeV superconducting linac. The proton beam will impinge on a 1 mm beryllium converter target. The target is thick enough to stop the protons completely and it generates neutrons *via* the ^{9}Be(*p,n*) reaction. The fast energy neutron spectrum resulting from the Be(*p,n*) reaction presents an average energy of 1.5 MeV and is not suitable for BNCT. Therefore, a moderating assembly ("spectrum shifter") will be necessary to slow down the emitted fast neutrons and generate a collimated thermal neutron beam. Monte Carlo simulations are used for the evaluation of the optimal selection of geometry and materials for the moderating assembly. A complete set of double differential data produced by the beryllium target, i.e. angle- and energy-differential neutron spectra, is necessary to perform these simulations. While double differential data are available in the literature for 4 MeV protons on beryllium, fluence measurements for 5 MeV protons are only available for 0° proton incidence (Howard *et al*., 2001). For this reason, extensive investigations are currently in progress at the INFN-LNL CN Van de Graaf accelerator utilizing two independent spectrometers: a monolithic silicon telescope (Agosteo *et al*., 2007) and the BINS device based on superheated emulsions (d'Errico *et al.*, 1995; d'Errico *et al*., 2008).

2. Materials and methods

The neutron spectrometry approach BINS was introduced several years ago (d'Errico *et al*., 1995) and has been tested extensively in a variety of neutron fields, including the BNCT installations at Studsvik-Nyköping (Sweden) and at Rome-Casaccia (Italy) (d'Errico *et al*., 2002). The spectrometer has

evolved significantly over the years; the current version uses superheated emulsions of dichloro-tetrafluoroethane which are sequentially operated at 25, 30, 35, 40, 45, 50 and 55 °C, and thus provide a series of seven sharp thresholds covering the 0.1-10 MeV neutron energy interval (Fig. 1).

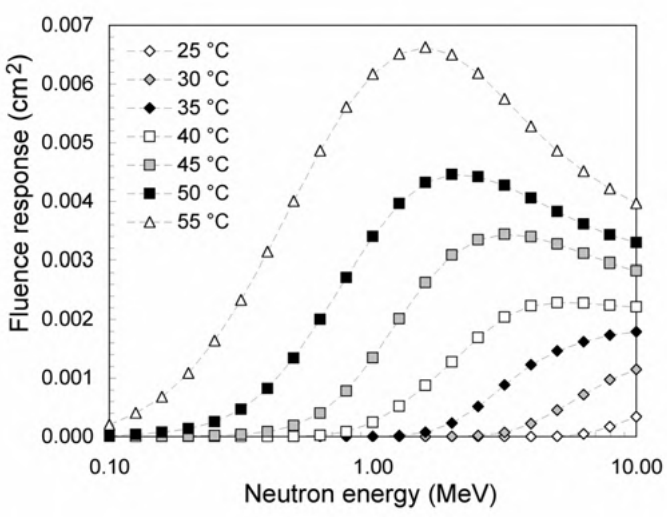

Figure 1. Response matrix of the BINS spectrometer used in the SPES-BNCT measurements

The BINS response matrix is virtually orthogonal, with threshold responses nested and spaced in quasi-isolethargic bins. This makes BINS ideally suited for spectrum unfolding using "few-channel" techniques, where the number of detectors, i.e. thresholds, is much smaller than the number of energy bins used for the unfolding.

The count rate in superheated emulsions is monitored in real time by detecting the acoustic pulses associated with bubbles vaporizations. With the current choice of piezoelectric transducers, these pulses have a relatively long duration (~10 ms) which limits the maximum practical counts rate to less than 10 s^{-1}. As a consequence, the maximum fluence rate of fast neutrons that the spectrometer can sustain is less than 10^5 cm^{-2} s^{-1}.

In order to achieve an acceptable count rate, we carried out our experiments at a constant proton beam current of about 100 nA, and we adjusted the source to detector distance between 10 and 250 cm. The measured BINS count rates were normalized to the count rate from a recoil-proton fast neutron monitor (Dennis and Loosemore, 1960) kept in a reference position.

The source to detector distance and all other functions of the spectrometer were remotely controlled using an apparatus specifically designed and built for these experiments (Ciolini et al., 2008). This system allows a complete control and monitoring of the angular spectrometer operation, i.e., setting the angular position of the detector in the (0 - 135)° range with respect to the proton beam axis, setting the distance between the SDD vial and the beryllium target in the (10 – 250) cm interval, setting the detector temperature in the (0 – 55) °C interval, and counting the number of nucleated bubbles. The above mentioned functions can all be performed without interrupting the proton beam, i.e. without varying the operational conditions of the accelerator.

The system consists of a 3 m long aluminium rail (Fig. 2) rotating around a bearing support, which is fixed to the accelerator room floor and vertically aligned with the beryllium target. The angular movement of the rail is achieved by means of a stepper motor equipped with a dedicated driver and mechanically coupled to a 40 mm diameter rubber wheel by a gear reduction system. The wheel moves along an aluminium circular rail fixed on the floor and coated with a suitable high-friction material. The detector vial is vertically held on a trolley whose motion along the rail is driven by a second stepper motor and gear belt transmission system.

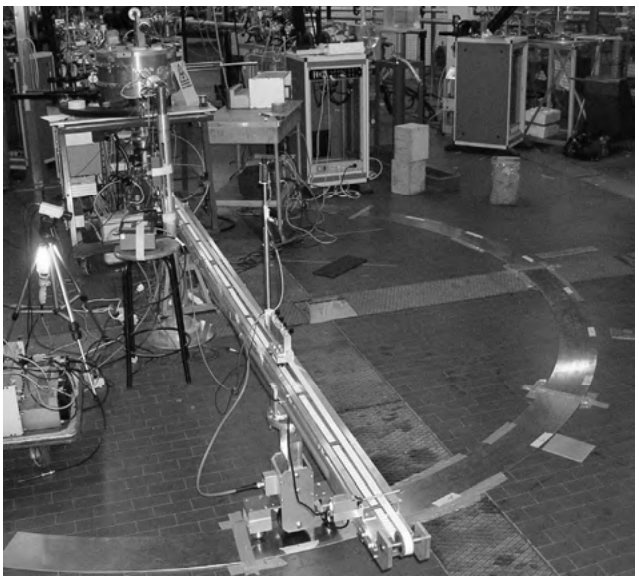

Figure 2. Overview of the SDD remote control system

The two stepper motors are controlled by dedicated software, which determines the number of steps required to achieve a desired angular and longitudinal detector position. The centre of the vial is aligned with the axis of the proton beam.

In order to perform measurements at different angles, a special holder was used keeping the beryllium target at an angle of 60 degrees with respect to the proton beam axis (Fig. 3). With this holder, source neutrons emitted in the (0 - 135)° range do not cross the edge of the holder.

The motion control system also permits the positioning of a shadow cone on the rail, aligned between the centre of the detector and the accelerator target (Fig. 4).

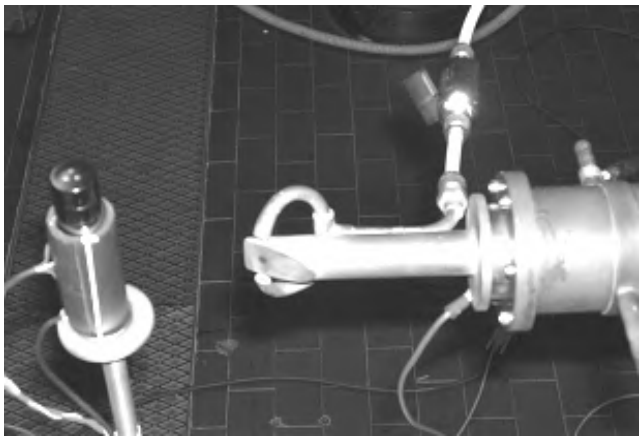

Figure 3. Detail of detector vial and beryllium target

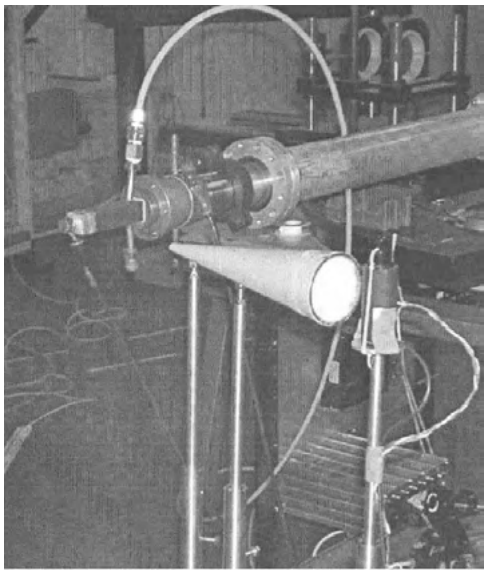

Figure 4. Measurements at 80 degrees with shadow cone in place

The shadow cone comprises an iron section followed by a high-density polyethylene section. This device virtually eliminates the exposure of the detector to primary neutrons, while allowing measurements of the neutron background due to scattering with accelerator hall walls, which is particularly pronounced at high angles. The scattered neutron contribution is then subtracted from the measurements in order to obtain the net neutron spectrum at different angles.

The unfolding code MAXED (Reginatto and Goldhagen, 1999) was used in the analysis of the measurements. MAXED is a computer program developed to apply the maximum entropy principle to the problem of unfolding neutron spectrometric measurements. The approach used in MAXED is based on information theory, and allows for the inclusion of a priori information in a well-defined and mathematically consistent way. Correct use of *a priori* information is of crucial importance for few-channel spectrometry, such as the unfolding of BINS data. In addition, the algorithm leads to a solution spectrum that can be written in closed form. This last feature permits the use of standard methods for the sensitivity analysis and the propagation of the uncertainties in the solution spectra.

3. Results and discussion

The first and preliminary results of our neutron spectrometry studies are reported in Fig. 5, showing the differential fluence distributions measured at angles of 0, 40, 80 and 120 degrees with respect to the primary proton beam axis.

Deconvolution with MAXED was performed using a flat initial spectrum and a soft upper energy cut-off of 3.2 MeV, based on the Q value of the Be(*p,n*) reaction. The response matrix used for the unfolding is based on measurements with reference monoenergetic neutron beams in the (0.144 - 19) MeV range and temperatures in the (25 - 54) °C range. Data were interpolated and extrapolated to cover the temperature range (25 - 60) °C and are therefore less accurate at 55 °C and above. However, a recalibration of the temperature controller used in our experiments at LNL revealed that the nominal temperature of 55 °C was actually closer to 56 °C. A sensitivity analysis was performed to assess the impact of perturbations in the highest operating temperatures and in the respective responses. The effect on the unfolded spectra is mainly observed in the energy region below 1.5 MeV of the results for 0 and 40 degrees. The 80 degree result is also affected to some extent, while the result for 120 degrees is virtually insensitive to the perturbations. These findings prompted a more accurate determination of the spectrometer response at higher temperatures.

While the resolution of the unfolded spectra is limited due to the few thresholds of the current spectrometer, the overall structure of the fluence distributions is well in line with the expectations.

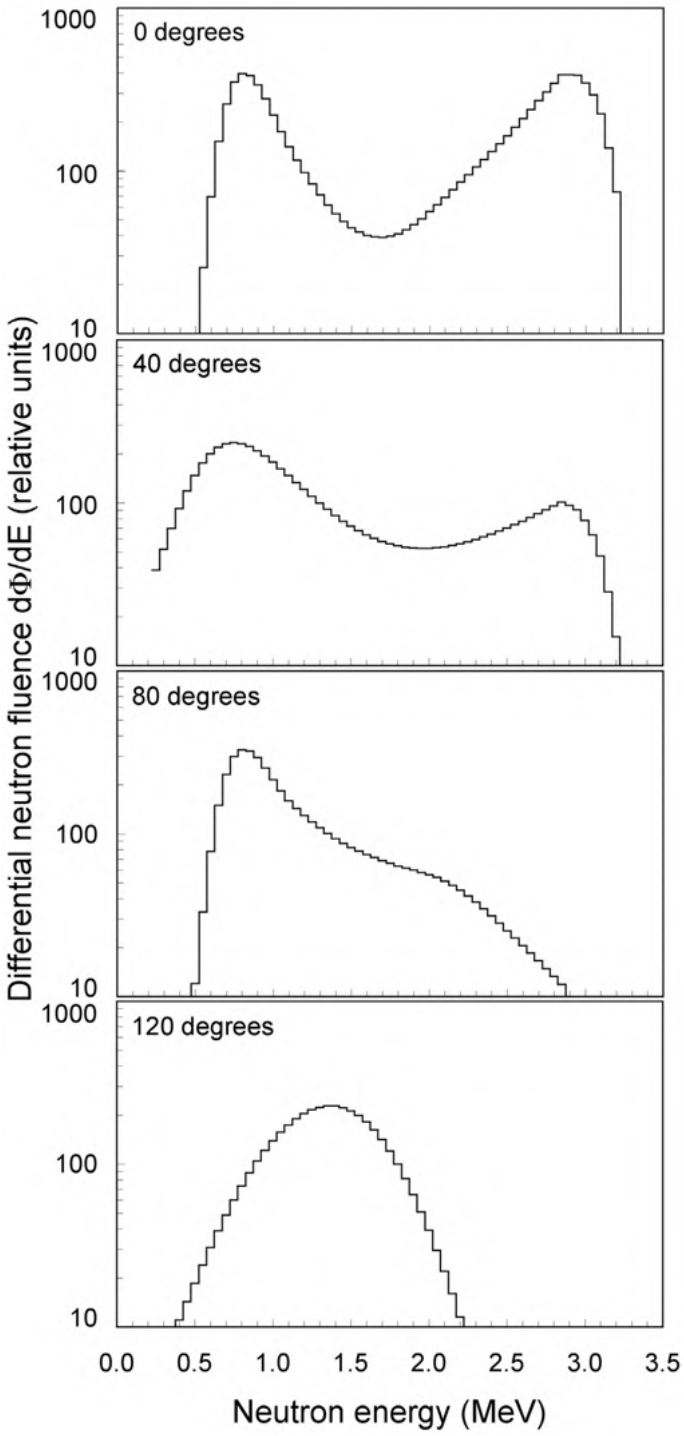

Figure 5. Double-differential spectra measured at 0-120 degrees

These first trials achieved their main objective of demonstrating the viability of the neutron spectrometer BINS, including its ancillary apparatus for the remote operation of the system, for angle- and energy-differential fluence measurements.

The tests also indicated some limitations of the current system. Primarily, the temperature control system is being enhanced for better performance at high temperatures, which will improve the overall reliability in the detection of low-energy neutrons. The spectrometer is also being augmented by including more operating temperatures between 25 °C and 40 °C, which will increase the number of thresholds and the resolution in the high energy region of the spectrum. Finally, piezoelectric sensors detecting the high-frequency harmonics emitted by the expanding bubbles are being investigated in order to increase the maximum sustainable count rate.

References

Agosteo, S., D'Angelo, G., Fazzi, A., Foglio Para, A., Pola, A., Zotto, P., 2007. Neutron spectrometry with a monolithic silicon telescope. LNL Annual Report 2006, 267-268.

Ciolini, R., d'Errico, F., Di Fulvio, A., Mazed, D., Del Gratta, A., Pazzagli, F., Esposito, J., 2008. A remote control positioning system for Be(*p,n*) angular neutron spectrum measurements with superheated drop detectors. LNL Annual Report 2007, 220-221.

d'Errico, F., Alberts, W.G., Curzio, G., Guldbakke, S., Kluge, H., Matzke, M., 1995. Active neutron spectrometry with superheated drop detectors. Rad. Prot. Dosim. 61(1-3), 159-162.

d'Errico, F., Giusti, V., Nava, E., Reginatto, M., Curzio, G., Capala, J., 2002. Fast neutron spectrometry of BNCT beams. Proc. 10th Int. Congr. Neutron Capture Therapy for Cancer, 1139-1144.

d'Errico, F., Ciolini, R., Di Fulvio, A., Reginatto, M., Esposito, J., Colautti, P., 2008. Double differential neutron spectra from 5 MeV protons on beryllium. LNL Annual Report 2007, 218-219.

Dennis, J.A., Loosemore, W.R., 1960. A fast neutron counter for dosimetry. A.E.R.E. Report R3302.

Howard, W.B., Grimes, S.M., Massey, T.N., Al-Quraishi, S.I., Jacobs, D.K., Brient, C.E., Yanch, J.C., 2001. Measurement of the thick-target ^{9}Be(*p,n*) neutron energy spectra. Nucl. Sci. Eng. 138(2), 145-160.

Reginatto, M., Goldhagen, P., 1999. MAXED, a computer code for maximum entropy deconvolution of multisphere neutron spectrometer data. Health Phys. 77, 579-583.

Radiation field characterization of the NCT research facility at IEA-R1

P.R.P. Coelho, R.O.R. Muniz*, J.F. Nascimento*, G.S.A. Silva,
P.T.D. Siqueira, H. Yoriyaz and V.J. Carneiro

Reactor Physics Area of Nuclear Engineering Center, Energy and Nuclear Research Institute, IPEN/CNEN-SP, Av. Professor Lineu Prestes, 2242, Cidade Universitária, São Paulo, Brasil

Abstract

An NCT (Neutron Capture Therapy) research facility was constructed at IEA-R1 reactor. The facility installed at beam-hole (BH) number 3 can be described to be consisted of 2 modules: - an inner BH module: with the filter, sample support and shielding arrangement sets and - an out of wall module: with biological shielding room surrounding the sample positioning/removing table. Neutron/gamma spectra can be modulated by a set of filters interposed between the reactor core and the sample position. The biological shielding at the end of the BH was designed and constructed to allow the extraction of the sample (and the inner shielding with it) even with the reactor on. This feature, together with a remote controlling sample positioning/removing system, enables controlling the sample exposure time (dose). Experiments with activation foils and thermo-luminescent dosimeters have been performed to characterize the field. Actual thermal neutron radiation conditions are 32.2 ± 0.1 Gy/h of dose rate with 25 % of gamma contamination for a 3.5 MW reactor operation power. As the sample irradiation region is inside BH, sample size is limited to a cylindrical enclosure of 30.0 cm height by 12.8 cm in diameter and therefore due to its size limit, the facility is not suited to carry any human treatment. Field modulation and time exposure control possibilities of this facility provide adequate radiation conditions to perform NCT research experiments.

Keywords: NCT, experimental facility, field modulation, TLD, activation foils

1. Introduction

IEA-R1 is a pool type multi-purpose nuclear research reactor. Its first criticality occurred in 1957 and set the origin of Energy and Nuclear Research Institute (IPEN). Since then it has been submitted to many improvements as did IPEN, which has also increased its activities, infrastructures and working power. Although IEA-R1 has not stood as the solely facility at IPEN, as many other facilities have been built, it still interprets a prominent role in the institution. The upgrade from 2 MW to 5 MW it was submitted in late nineties and the amount of work developed by many different researcher groups which use some of its beam-holes to perform their experiments can be set as examples of its importance to IPEN.

The NCT research group of IPEN starts its first feasibility studies in early nineties (Gaspar, 1994) but no experiments were carried out before the beginning of this decade. Since then the NCT group has been working in neutron beam modulation and characterization aiming to tailor it to the best conditions attainable to perform NCT experiments.

This work presents the results from simulations and experimental work done so far to fulfill this goal.

2. NCT Facility

The NCT research facility was constructed at IEA-R1 reactor and it is installed at beam-hole (BH) number 3. BH-3 is a 2.6 m long and 20.32 cm (8 inches) diameter tube which extends from one of the faces of the reactor core to the outside of the reactor pool wall.

The facility (Figure 1) can be described to be consisted of 2 modules:

- an inner BH module with the filters, sample and shielding arrangement sets. As these sets have eventually to be changed, they are settled into two movable structures. Sample irradiation cavity and shielding set lie on the most external structure

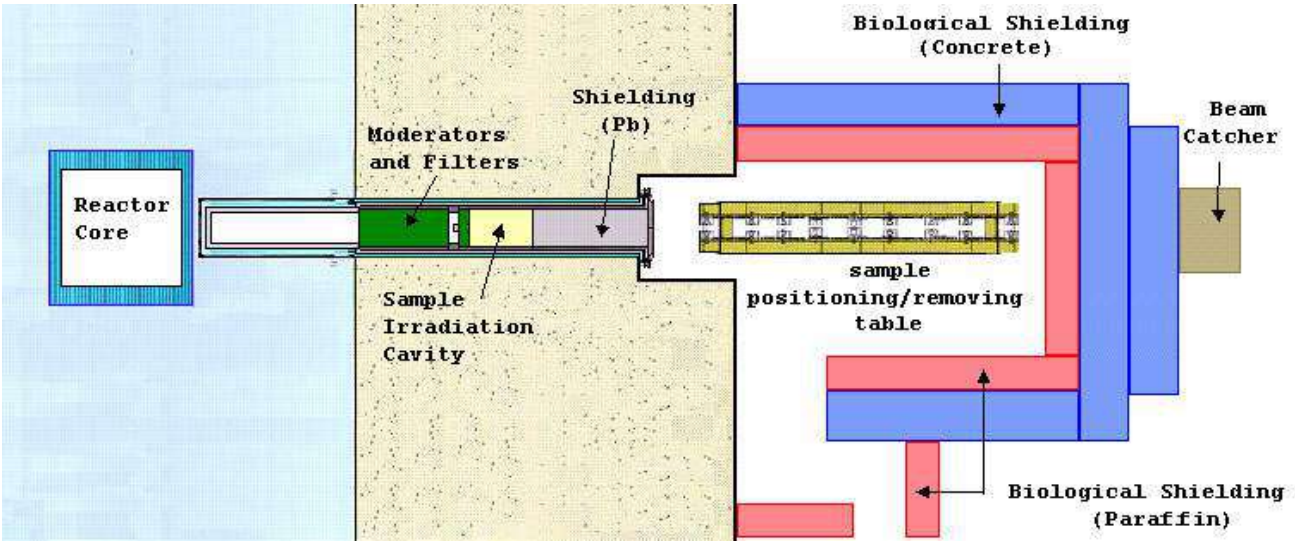

Fig. 1 – Schematic view of the NCT facility

inserted and withdrawn from the BH by a remote operating system. Although filter disks can also be placed in the mentioned structure, most part of the filters set lies on the most internal structure. It is removed from BH by manipulating a retrieving tool and is inserted back in the tube by pushing it through the forementioned remote operating system. Due to radiation safety procedures, this structure is rarely removed from its place. In order to withdraw this most internal structure, reactor core must be shutdown and moved to a different place in the pool so to attain proper radiation safety conditions.

- an out of wall module: with biological shielding room surrounding the sample positioning/removing table. Sample positioning/removing table is placed close to BH-3 exit so to stand as a support to the movable parts whenever they are outside the tube. It also performs the insertion and withdrawal of the inner BH module. The biological shielding is composed by paraffin/concrete walls and ceiling. It has been projected to attain adequate radiation conditions to allow the presence of individuals around its external vicinities even with the reactor on and with no shielding in the tube. This characteristic together with the sample changing device allows controlling sample exposure time. Sample changing device is a remote operating carriage system which grabs/carries/looses samples. Its only purpose is to place and retrieve samples from the high dose environment found in the biological shielding room.

The facility, so designed, allows the interposition of materials between the reactor and the sample irradiation cavity, providing the possibility to interfere with the radiation field the sample is subjected to. Exposure time can also be controlled by remote controlling sample positioning/removing system. Irradiation position has been projected to be inside the BH so as to get higher neutron flux. Sample irradiation cavity is a 12.8 cm diameter and 30 cm wide cylinder shaped region and therefore the NCT facility is not suited to perform any human treatment.

3. Simulations

Many sets of simulations have been carried out in order to select the best set of modulators and filters to achieve an adequate radiation field (high thermal neutron flux and low gamma contamination) to perform the NCT experiments. These simulations were the focus of previous works (Coelho, 2002; Gual, 2005).

MCNP (Brown, 1987) has been used to perform such simulations.

4. Experiments

Neutron flux has been determined through activation foils experiments.

Dose rates have been determined by thermo-luminescent dosimeters (TLD). In order to discriminate gamma and neutron contribution 3 different kinds of TLDs were used: TLD-400 (CaF_2:Mn), TLD-700 (^{7}LiF:Mg,Ti) for gamma dose measurements and TLD-600 (^{6}LiF:Mg,Ti) for neutron dose measurements. Selection of a group of TLDs with similar response functions was done for each kind before dose experiments were performed. Calibration curves were obtained up to 1,000 Gy (TLD-400 and TLD-700).

Actual thermal neutron radiation conditions are 32.2 ± 0.1 Gy/h of dose rate with 25 % of gamma contamination for a 3.5 MW reactor operation power and a set of filters constituted by approximately 22 cm of lead.

Thermal neutron flux has been quantified as $1.39 \pm 0.12 \times 10^8$ n/cm^2. Epithermal neutron flux is 2 orders of magnitude lower but fast neutron flux is as high as thermal neutron flux. Neutron flux profile along sample irradiation cavity shows higher values closer to the BH external end. These unexpected responses - odd neutron profile and high fast neutron flux - have been regarded to neutron leakage between the tubes. Figure 2 shows a schematic perpendicular view at the filter disposition quota, which as the sample positioning quota, has a wider air gap in its upper part.

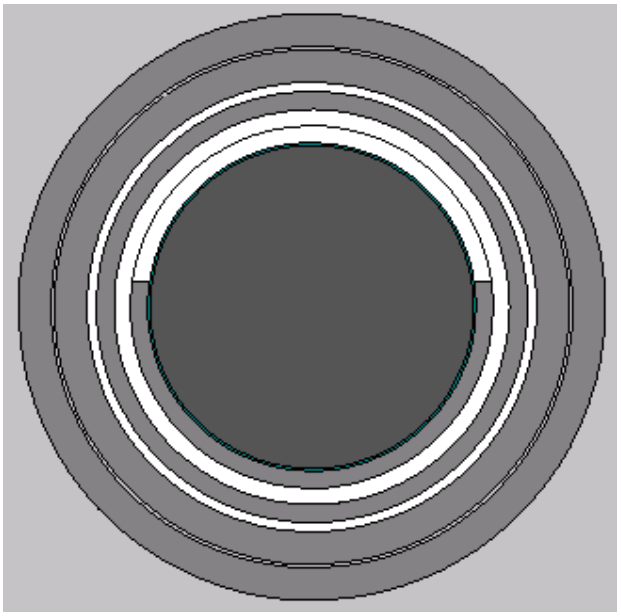

Fig. 2 – Schematic perpendicular view of the NCT facility. White: air gaps; light grey: reactor pool wall; grey: tubes (BH, Liners and moveable structure); dark grey: filters (represented by the centered disk)

5.Conclusions

IEA-R1 is an old pool type multi-purpose research reactor whose utilization has changed along the years. Although it has not been projected to perform NCT, research in this area is under progress.

Simulations have been conducted as supporting tools to better select the set of filter to be used in order to improve radiation field.

Neutron flux and doses due to neutrons and gammas have been determined in the sample irradiation position of the NCT facility.

Thermal neutron flux has been quantified as $1.39 \pm 0.12 \times 10^8$ n/cm^2.s and dose due to gamma has been determined to correspond to 1/4 of that due to neutrons (32.2 ± 0.1 Gy/h). These values reveal the feasibility to perform research experiments on NCT in this facility. The observed high fast neutron flux have shown however the necessity to improve the facility.

Acknowledgments

The authors would like to acknowledge CNPq/Brasil for supporting some of the authors*.

References

Coelho, P.R.P., et al. 2002. Neutron Flux Calculation in a BNCT Research Facility Implemented in IEA-R1 Reactor. In: Wolfgang S., Raymond M., Andrea W. (Eds.) Research and Development in Neutron Capture Therapy. Monduzzi, Bologna, pp.197 - 201.

Gaspar, P.F., 1994. *Considerações Sobre o Estudo da BNCT. Dissertação de mestrado* (Considerations in BNCT study, Master degree dissertation), IPEN.

Gual, M.R. et al. 2004, Study for neutron-DNA interaction at IPEN BNCT research facility, Braz. J. Phys., 34 (3A), 901-903.

Brown, F.B., 1987. MCNP – A general Monte Carlo N particle transport code, Report LA-UR-03-1987, Los Alamos, NM, Los Alamos National Laboratory.

The basic theory for 10B NCT with thermal neutrons

G.I. Borisov[1], R.I. Kondratenko[1], R.S. Sharikov[1]

[1]*RRC "Kurchatov Institute", Moscow, Russia*

The basis of the theory is the value of effective mass of substance irradiated by thermal neutrons as we introduce it. The values of the effective mass corresponding to the various irradiation conditions can be measured in model experiments or in certain cases theoretically calculated. The theory we introduce ties the physical conditions of irradiation, neutron, nuclear and atomic data, 10B concentration in the irradiated area to the maximum absorbed dose rate in the irradiated object by simple algebraic expressions.
The results of calculations of the following values are presented in table 1:

- The effective mass of biological tissue – Meff for the narrow neutron beam;
- Effective thickness of biological tissue – meff for the broad neutron beam (the broadness of the neutron beam is related to the diffusion length of neutron in biological tissue);
- Values of thremal neutron flux density - φth corresponding to the maximum dose rate of 30 Gy/hr given 10B concentration is 30ppm;
- Kerma of fast neutrons Kfast corresponding to 3 Gy/hr given the fraction of fast neutrons in the beam is 0.25.

Table 1.

Beam	Meff, g	meff, g/cm^2	φth, 1/cm^{2}s	Kfast, Gy·cm^2
Narrow	2,0	–	2,6·109	9,5·10-13
Broad	–	3,2	1,3·109	20·10-13

Importance functions approach to neutron beam optimization for tumor therapy

Viktor Kononov, Valeriy Korobeynikov, Oleg Kononov, Artem Korobeynikov, Nikolai Soloviev

Institute of Physics and Power Engineering
249020 Obninsk, Kaluga region, Bondarenko Sq.1
Russian Federation
korob@ippe.ru

Abstract

Calculation study has been carried out to analyze the optimal structure of neutron source for cancer tumor treating. The special approach based on so called importance functions was developed. The numbers of these important functions are made for all energy groups. Two tasks can be solved with importance function using. First is to calculate the dose distribution in tumor and healthy tissue for the source with arbitrary energy structure. The second task is to construct such a source which allows treating tumor with highest efficiency.

Keywords: Neutron beams, importance functions, malignant *tumor, Monte Carlo method, therapeutic ratio.*

1. Introduction

A wide variety of different neutron spectra can be produced by various neutron sources (reactors, accelerator tuned to different proton energies or utilizing different target materials) and various moderator assemblies. The clinical efficacy of each spectrum must be evaluated by extensive Monte Carlo modeling with program such as MCNP [5]. Generally this is done in two-step process. The first step involves modeling the "pure" beam to determine the spectrum that will be applied to the patient. The next step consists of determining the filter which will form the best neutron specter for tumor treating.

Optimizing neutron beams for treatment is primarily a matter of designing moderators and filters to produce a spectrum which limits the unwanted "background" doses while maximizing the penetration of the beam and maintaining a high enough dose rate to treat in a reasonable amount of time. Optimization studies usually have involved hundreds of Monte Carlo simulations to compare properties of different neutron beams and filter constructions.

Small changes in tumor parameters or RBE values can produce drastic changes in the performance of different neutron beams.

Usually, the only way to determine the effect of changing involved in BNCT [1-3] treatment is to return many Monte Carlo processes, each of which can take hours or days.

To accelerate the process of performing a great number of Monte Carlo simulations with different sources the importance functions approach was developed. The idea of this approach is based on the dose distributions from number of the delta neutron sources having the definite energy (energy group). The developed method of applying importance functions to reduce a Monte Carlo simulation for different variable sources is quite powerful. Using the number of such importance functions it can be defined what energy for neutron source more preferable, not only for tumor but for healthy tissue too.

2. Methodology

To treat a malignant tumor BNCT utilizes a binary method. The first step involves administering a cancer-seeking pharmaceutical that has been loaded with ^{10}B. An ideal drug is harmless to the patient and is absorbed in cancerous cells far more selectively than in normal tissue cells. The second step is irradiation of the patient by soft neutron beam. ^{10}B has a very high thermal neutron capture cross section of 4000 barns and decays immediately into high LET particles via $^{10}B(n,\alpha)^{7}Li$ reaction, as well as 480 keV γ ray in 93% of the reactions. The energy of combined high LET particles is largely confined within the diameter of a single cell, thus targeting a large radiation dose preferentially to malignant cells

without significantly irradiating dose healthy tissue. Because BNCT is a binary therapy, advances in both boron delivery and in neutron beam shaping are important to improving the quality of treatment

The total effective dose to either tumor or healthy tissue is calculated by adding different dose components, multiplied by appropriate weighting factors to obtain the total photon equivalent dose. Doses, which vary with depth in the patient body, are multiplied by relative biological effectiveness (RBE) factors, or in case of the boron dose, a compound factor (CF). These doses are calculated in small volume cells

The special approach for the calculation of so called importance functions was used. The idea of this approach is to calculate the dose distributions for number of the delta neutron sources having the definite energy (energy group). If the number of these important functions were provided for all energy groups we can solve two tasks. First is to calculate the dose distribution for the source with arbitrary energy structure. Everybody can sum these importance functions with sources weights for each energy groups:

$$D_x(\mathbf{r}) = \sum_g S_g D_x^g(\mathbf{r}), \qquad (1)$$

$$\sum_g S_g = 1, \qquad (2)$$

Where $D_x^g(\mathbf{r})$ - important function, dose distribution of x – type of irradiation (neutron, gamma, etc.) from source, concentrated in the energy group g.

S_g - Source specter.

More important (but more complicate) the second task is to create such a source which allows treating with highest efficiency. Three quantities, initially defined by Zamenhof [6] are used to provide quantitative descriptions of neutron beams for BNCT:

(1) Advantage depth (AD), which indicates the penetrability of the neutron beam;
(2) Therapeutic ratio (TR), which gives the tumor dose to maximum dose in healthy tissue;
(3) Advantage depth dose rate (ADDR), an indicator of treatment time.

The beam optimization is very complicate task which have not yet final approach and methodology. The approach, based on importance function methodology is a way to improve situation.

The calculations of importance functions were carried out by Monte Carlo code MCNP [5]. The calculations were made for all energy groups. The tumor dose and its components were calculated. The healthy tissue doses distributions were made for comparison with tumor doses too.

3. Calculation models and codes

The calculation scheme of the tissue-equivalent phantom with dimension 20x20x20 cm. Calculation study was executed with normal neutron beam. The beam has cylindrical form and neutrons spatial distribution is uniform. The diameter of beam is equal 10cm. It was supposed that ^{10}B concentration was equal 65 ppm per 1 gram tumor tissue and for healthy tissue ^{10}B concentration was equal 18 ppm per 1 gram of tissue. CBE of $^{10}B(n,\alpha)^7Li$ reaction products are 1,3 for healthy tissue and 3,8 for tumor one. In order to calculate phantom doses distribution, the Monte Carlo code MCNP was used [5]. The calculations were made in consecutive order for every energy group. Total doses were calculated in tumor and its components:

- from secondary gamma irradiation;
- from interaction with main tissue components (hydrogen, oxygen and nitrogen);
- Boron dose.

Total dose in healthy tissue for comparison with tumor one was made too.

4. Results and analysis

Doses distributions (importance functions) versus phantom depth near by central axis for some energy intervals (groups) are given on Figures 1-2. Figures 1-2 are shown that dose in tumor tissue significant greater than in healthy one. It is very important for medical application fact. Actually, radiation treatment must produce minimal harm for healthy tissue and maximal for tumor. It should be underline that such result can get for neutron sources distributed from 1eV to 60 keV only. For higher energy (greater than 60kev) situation becomes worse. For its improvement it is necessary to reduce the share of high energy neutron in initial spectra of nuclear reactors or accelerators. It can be made by special filters use.

The values of the therapeutic ratio as a function of beam energy and depth in phantom are given on Figure 3. The most preferable energy interval for treating with high efficiency is from 1keV to 10keV for wide number of tumor locations. Therapeutic ratios for optimized accelerator beam based on $^7Li(p,n)^7Be$ reaction [4] are given on Figure 3 for comparison.

The beam formed in [4] has good parameters for tumor treating. It is necessary to mark that theoretical results for ideal spectrum are extreme and "practical" beam can be only worse. AD distribution as a function of energy is given on Figure 4. The dependence AD from energy is very smooth from 1eV to 70 keV. AD for optimized beam from [4] is high enough.

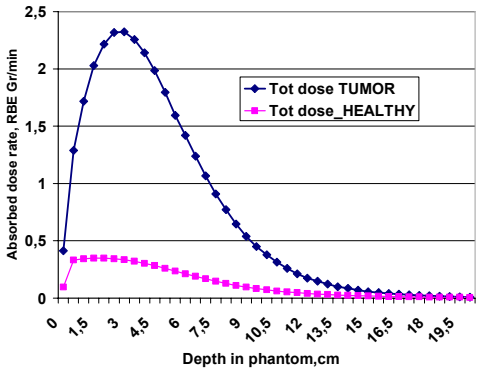

Fig. 1. Importance functions for energy interval 10-20keV

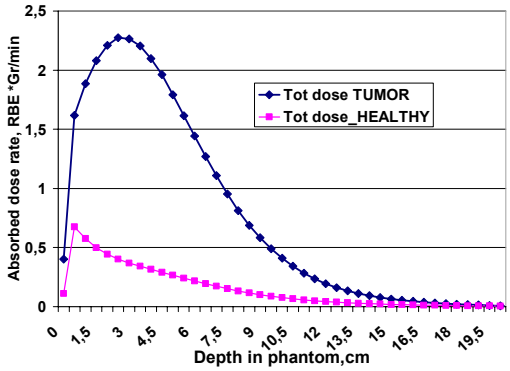

Fig. 2 . Importance functions for energy interval 30-40keV

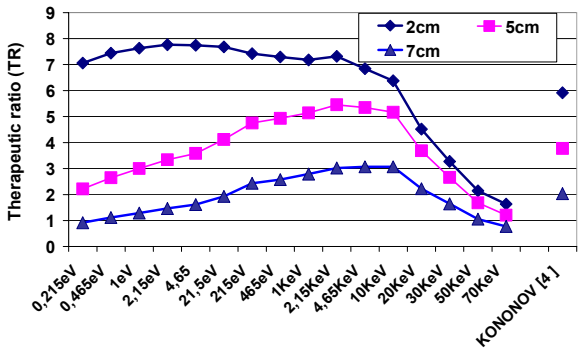

Fig. 3. Therapeutic ratio as the function of beam energy and depths in phantom

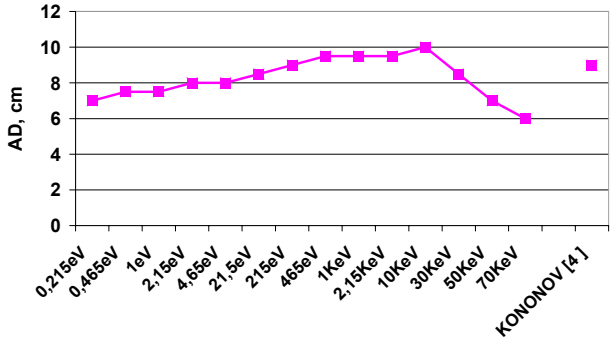

Fig. 4. Advantage depth (AD) as the function of beam energy

5. Conclusion

The developed method based on importance functions is quite powerful.

It is necessary to mark that theoretical results for ideal spectrum are extreme and "practical" beam quality can be only worse. The importance functions can be used for beam optimization.

.

References

1. IAEA, VIENNA, 2001, IAEA – TECDOK – 1223, ISS N 1011_4289, Current status of neutron capture therapy, May 2001.
2. Tsyb A.F. et al. Development of Neutron Therapy Treatment. The 5th Japan_Russian Symposium on Radiation Safety. Tokyo, 26_27 August, 1997.
3. B.F. Bayanov, M.V. Bokhovko, V.N. Kononov et al. "Accelerator-based neutron source for the neutron capture and fast neutron therapy at hospital. Nucl. Inst. and Meth. in Phys. Res. A413, 397-426, 1998.
4. O. Kononov, V. Kononov, V. Korobeynikov, N. Soloviev, M. Bokhovko, D. Sanin, W. Chu, A. Zhitnik, S. Ognev. EPITHERMAL NEUTRON SOURCE BASED ON ^{7}Li(p,n)^{7}Be REACTION OPTIMIZATION FOR NEUTRON CAPTURE THERAPY. Preprint IPPE-2984, Obninsk, 2003.
5. J. Briesmeister "MCNP – A general Monte Carlo n-particle transportation code". LA-1625-M, version 4B, LANL, 1997.
6. R. Zamenhof, B.W. Murray, G.L. Brownell. " Boron neutron capture therapy for the treatment of cerebral gliomas. I: Theoretical evaluation of the efficacy of various neutron beams". Med Phys.2, 47-60 (1975).

Neutron irradiation techniques to reduce skin dose and to improve therapeutic dose distribution using a thermal neutron filter

Hiroaki Kumada[a], Takemi Nakamura[a], Akira Maruhashi[b],Koji Ono[b], Akira Matsumura[c]

[a] *Department of Research Reactor and Tandem Accelerator, Japan Atomic Energy Agency, Tokai, Ibaraki, 319-1195, Japan*

[b] *Radiation Oncology Research Laboratory, Research Reactor Institute, Kyoto University, Osaka, 590-0494, Japan*

[c] *Department of Neurosurgery, Institute of Clinical Medicine, University of Tsukuba, Tukuba, Ibraki, 305-8575, Japan*

Abstract

In most of clinical studies of boron neutron capture therapy (BNCT) for a malignant brain tumor and for a head-&-neck cancer performed at JRR-4, dose given to a patient has been controlled according to limitation of not tolerance dose of brain but skin dose. This is attributed to the fact that component of thermal neutron included in epithermal neutron beam of JRR-4. The aim of this study is to enhance the therapeutic dose around tumor region by decreasing the thermal neutron component in the beam. To reduce the thermal neutrons, a filter which can cut the thermal neutron at just before patient was designed. Several estimations were carried out using MCNP-5 to determine optimum content and geometry of the filter. The results demonstrated that a filter consisting of 50% enriched Li-6 fluoride: 50%wt and Teflon: 50%wt (the thickness was 5mm) can reduce the thermal neutron flux at surface of a phantom approximately 30% against the conventional filter-less beam. In case of estimations applying clinical condition, application of the filter enhanced the maximum therapeutic dose about 10%, the dose at 5cm in depth about 20% than the values of the filter-less beam. However the application of the filter causes increase of irradiation time due to reduction of the neutron intensity. To make up for the shortcomings of the filter application, enhancement of the beam intensity by reducing heavy water thickness in heavy water tank was investigated. By changing the heavy water thickness from 8cm to 5cm, thermal neutron flux in the phantom increased approximately 1.4 times with the conventional beam. The results demonstrated that the combination with the filter and reduction of heavy water thickness can enhance the therapeutic dose for tumor practically. Based on the estimation results, a prototype of the thermal neutron filter was made and has been installed to JRR-4.

Keywords: BNCT, thermal neutron, JRR-4, MCNP, skin dose

1. Introduction

Clinical studies of BNCT for a malignant brain tumor (Yamamoto *et al.*, 2004) and for a head-&-neck cancer (Kato *et al.*, 2004) are being performed using JRR-4 in Japan Atomic Energy Agency (JAEA). In most of the clinical trials at JRR-4, dose given to a patient has been controlled according to limitation of not tolerance dose of brain but skin dose. This is attributed to the fact that proportion of thermal neutron component (<0.5eV) included in epithermal neutron beam of JRR-4 is higher than other reactors' one such as KURR and FiR 1. In the medical irradiation facility of JRR-4, a cadmium shutter which can cut out the thermal neutron in the beam is installed at intermediate position on beam transport line (Torii *et al.*, 2000).

Figure 1 shows a schema of cross section view of medical irradiation facility of JRR-4. A bismuth block is installed on the beam line after the Cd shutter to reduce gamma-ray from the core, and to lead neutrons to beam aperture, graphite blocks and several materials have been installed in the collimator. These materials generate thermal neutrons again, and then the proportion of the thermal neutron in the epithermal neutron beam at the beam aperture increase. We expected that reduction of the proportion of the thermal neutrons in the epithermal neutron beam contributes to decrease the skin dose and to raise the therapeutic dose around the target region consequently. The aim of this study is to investigate how to reduce the thermal neutron component in the neutron beam and how to enhance the therapeutic dose at tumor region.

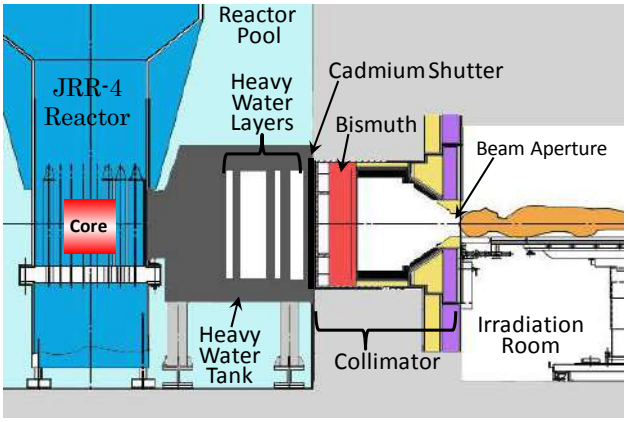

Fig. 1 Cross section view of JRR-4

2. Materials and methods

(1) Thermal neutron filter

To reduce the thermal neutron component in the beam, we approached to install a thermal neutron filter locating on beam path near beam aperture. In the investigation, enriched ^{6}Li fluoride (LiF) and Teflon compound was employed as the filter's material in consideration of technological property. The ^{6}Li has large capture cross section for thermal neutron, and doesn't generate secondary gamma-ray. And an advantage of combination with the Teflon is that the compound doesn't moderate high energy neutrons due to hydrogen free. The filter was set on the beam line just before beam aperture. Similar filtering techniques were reported and have been already applied to clinical trials in some facilities (Capala *et al.*, 2003) (Auterinen *et al.*, 2000). Figure 2 shows a schematic layout.

(2) Suitable neutron beam mode

JRR-4 can generate 32 patterns of neutron beam spectra by changing heavy water thickness in heavy-water-tank and by moving the Cadmium shutter (Cd Shutter). However at present, we have applied only three modes to clinical trials. For the epithermal neutron beam, the thickness of the heavy water is 8cm, and the Cd shutter is set in the beam line. We call the mode as ENB-8 mode.

The three modes were determined according to some protocols for brain tumor BNCT of the time. However in current BNCT, dose estimation way and contribution rate for each dose component in total dose have been also changed, because protocols applying to the epithermal neutron beam BNCT have changed with the decade-old protocols of intra-operative BNCT. Therefore, it may be possible to pick out suitable beam mode from the unvalued modes.

(3) Optimum design of the filter using MCNP

To determine optimum design of the thermal neutron filter, several estimations were carried out using MCNP-5 (Briesmeister, 2000).

In the estimation conditions, the beam aperture shape was fixed a circular shape in 10cm diameter, and the beam spectrum was applied the ENB-8 mode as the conventional irradiation condition with the epithermal neutron beam BNCT in JRR-4. And the filter was located at 10cm reactor core side from the beam aperture. The composition of the filter was set as the enriched lithium fluoride (LiF): 50%wt and Teflon: 50%wt, and the enrichment of ^{6}Li and the thickness of the filter was changed as following; the enrichment of the ^{6}Li in the LiF was changed to 7% (Natural Li), 20%, 50% and 95%, and the thickness of the filter was changed to 3, 5, 10, and 15mm.

The neutron spectra and neutron fluxes for free in air condition were calculated, and dose distributions in a cylindrical water phantom were also determined respectively, and then these results were compared with results of the conventional epithermal neutron beam (filter-less). Figure 2 shows the schematic of the irradiation condition with cylindrical phantom.

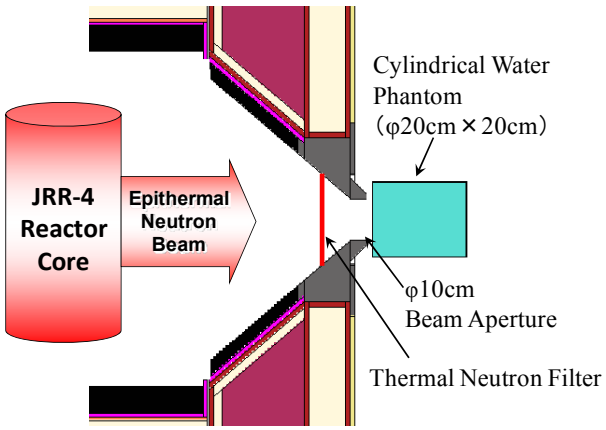

Fig. 2 Layout of the thermal neutron filter

(4) Estimation of optimum mode for the filter

To determine suitable beam mode when we apply the thermal neutron filter, some estimations for change of the beam mode were carried out using the MCNP-5. In the estimations involving the filter, the specification of the filter was fixed based on the preliminary estimations as above, and then the filter was applied. In the estimations of the optimum neutron beam mode, heavy water thickness in the heavy-water-tank was changed from 8cm (ENB-8 mode) to 5cm (ENB-5 mode). The neutron spectra for free in air condition and dose distributions in a cylindrical water phantom were calculated respectively, and then the results were compared with the results of the ENB-8 mode with the filter.

3. Results and discussions

(1) Results for the estimations of the filter

Figure 3-(a) shows the results of each neutron spectrum with several thermal neutron filters at centre of the beam aperture for the free in air condition. The results proved that application of the filter was effective to reduce rate of thermal neutron component in the beam against the conventional filter-less beam. Figure 3-(b) shows thermal neutron flux profiles on central axis in the phantom for each filter condition. The profiles were normalized with each maximum value of the thermal neutron fluxes. By using the filter consisting of the 50% enriched ^{6}Li (thickness: 5mm) or the 95% enriched ^{6}Li (thickness: 3mm), the thermal neutron flux at phantom's surface reduced approximately 37% compared with the filter-less beam. And each depth of the flux's peak with the filters shifted to deeper than the peak point of the filter-less condition, and the fluxes at deeper region were higher than the flux of the filter-less condition. The results indicated that application of the thermal neutron filter enable to reduce the surface's flux effectively and to enhance the fluxes at deeper regions. However, the intensity of the beam were reduced approximately 60% compared with the intensity of the filter-less beam.

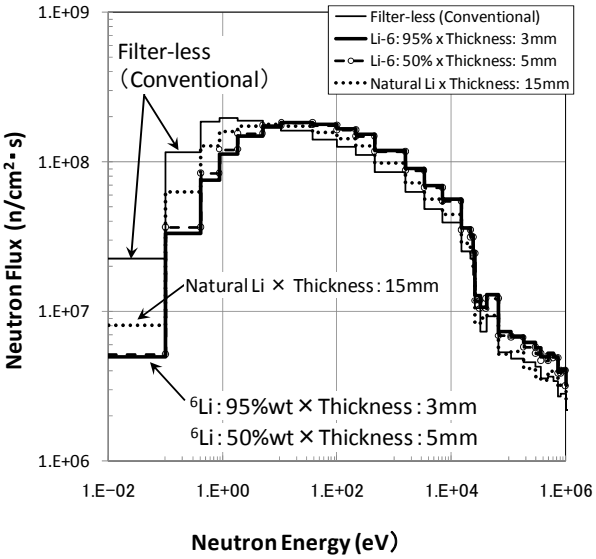

Fig. 3-(a) Neutron spectra for each condition

Based on the calculation values for the phantom irradiation, we evaluated dose distributions applying a typical clinical condition at JRR-4. In the estimation, boron concentration in blood was assumed to 24ppm, and ratios of ^{10}B concentration for tumor, normal tissue and skin with blood were set to 3.5, 1.0 and 1.2 respectively. RBE for tumor, normal tissue and skin were set to 3.8, 1.35 and 2.5 according to a head-&-neck cancer protocol using BPA. And also the RBE for fast neutron and thermal neutron were set to 2.5. Total dose (= boron dose + thermal neutron dose + fast neutron dose+ gamma-ray dose) for each organs and tumor region were determined respectively. The doses were normalized by maximum skin dose as 10Gy-Eq. Figure 3-(c) shows dose distributions on the beam's axis in the phantom for each condition. The results indicated that maximum tumor doses for each filter application increase approximately 10% than the maximum dose of the filter-less irradiation, and the peak points shifted to deeper region. The tumor doses at 5cm in deep of each condition were enhanced approximately 20% than the conventional one. The results demonstrate that the application of the filter enable to deliver higher therapeutic dose to deeper region. Irradiation time for the filter-less condition was about 19 minutes, on the other hand, the time for both of the 95%wt enriched ^{6}Li filter and 50%wt enriched ^{6}Li filter were increased to 36 minutes due to the reduction of the neutron intensity.

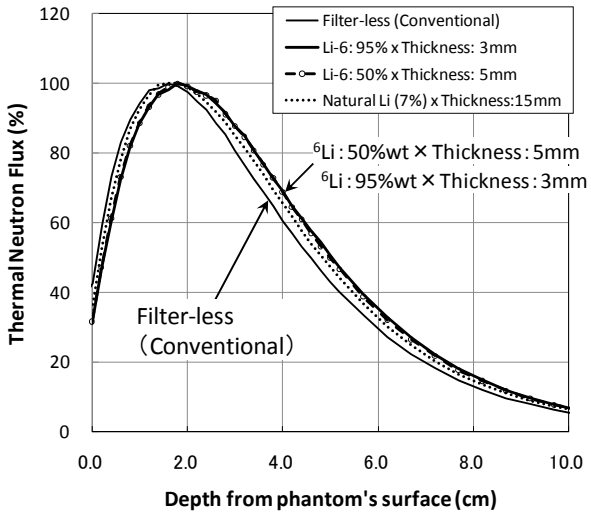

Fig. 3-(b) Thermal neutron flux profiles on beam's central axis in the phantom

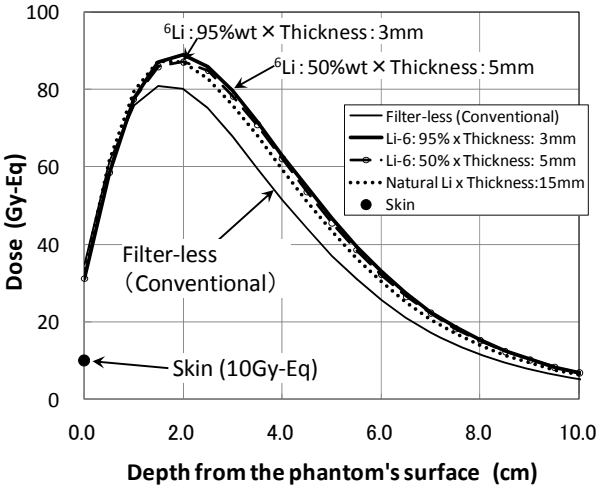

Fig. 3-(c) Tumor dose profiles on beam's central axis in the phantom

(2) Results of Optimization of neutron beam mode with the thermal neutron filter

Based on the above estimations and production cost and so on, we had chosen the 50%wt enriched ^{6}Li filter (thickness: 5mm) as a practical thermal neutron filter. And in the estimation for optimization of neutron beam mode with the thermal neutron filter, the specification of the filter had been applied.

The results for the irradiation with the ENB-5 mode demonstrated that the maximum thermal neutron flux in the phantom increased about 1.4 times compared with the flux of the ENB-8 mode. Figure 4 shows the results of dose distributions on the central axis in the phantom for several conditions. In the filter-less condition in the figure, tumor dose distributions of the ENB-5 mode were similar to the distribution of the ENB-8 mode. However, irradiation time with the ENB-5 mode shortened to 12 minutes against the time of ENB-8 mode (19min.) due to higher neutron intensity of the mode. By applying combination method between the filtering and the ENB-5 mode, eventually the maximum dose in the phantom rose approximately 12 % than the filter-less irradiation with ENB-8 mode. The irradiation time of the combination way became to be slight long as about 26 minutes compared with the conventional filter-less irradiation with the ENB-8 mode. The results proved that the combination of the ENB-5 mode could make up for the reduction of the beam's intensity from the application of the filter. In the application of the ENB-5 mode, we should pay attention increasing of high energy neutron component in the beam due to reduction of the heavy water in the tank.

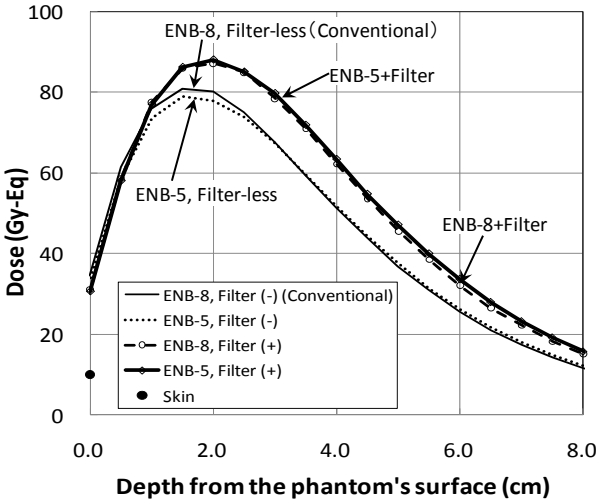

Fig. 4 Tumor dose profiles on beam's central axis in the phantom for ENB-8 and ENB-5

4. Conclusions

To reduce the thermal neutron component in the epithermal neutron beam, a thermal neutron filter consisting of enriched ^{6}Li fluoride and Teflon compound was designed. The results proved that the filter enabled to reduce the skin dose and to enhance the dose at deeper region in a body. On the other hand, the application of the filter brings on an increase of the irradiation time. To make up for the shortcomings of the filter application, changing the neutron spectrum of the epithermal neutron beam of JRR-4 was investigated. The investigation results demonstrated that the ENB-5 mode could deliver higher thermal neutron flux into the tumor region.

In accordance with the results, the specification of the thermal neutron filter for JRR-4 was fixed as following; the filter consisted of LiF: 50%wt and Teflon: 50%wt, the enrichment of the ^{6}Li in Lithium was 50%, and the thickness was set to 5mm. Then we developed a prototype of a detachable thermal neutron filter, and then the filter has been installed to the predefined position in the beam collimator of JRR-4. We will perform several characteristic measurements for the filter in order to apply the filter to the clinical trials in practical use as soon as possible. And for the application of the ENB-5 mode, the several measurements using a phantom and cell experiments are also carried out concurrently.

References

Auterinen I., seppala T., Salmenhaara S., et al., 2000, Improving the performance of the FiR 1 BNCT facility, *Abstracts of ninth international symposium on neutron capture therapy for cancer,* 43-44

Briesmeister, J. F.(Ed.), 2000 MCNP-A General Monte Carlo Code N-Particle Transport Code Version 4C, *LA-13709-M*

Capala J., Stenstam B. H., Skold K., et al., 2003, Boron neutron capture therapy for glioblastoma multiforme: clinical studies in Sweden, *J Neuro-Oncol*, 62, 135-144

Kato I., Ono K., Sakurai Y., Ohmae M.,Matsumura A., et al., 2004, Effectiveness of BNCT for recurrent head and neck malignancies, *Applied Radiation and Isotopes*, 61, 1069-1073

Torii Y., Yamamoto K., Kishi T., Hori N., Kumada H., Horiguchi Y., 2000, The BNCT irradiation facility of JRR-4, *Abstracts of ninth international symposium on neutron capture therapy for cancer*, 242-242

Yamamoto T., Matsumura A., Nakai K., et al., 2004, Current clinical results of the Tsukuba BNCT tria, *Applied Rad. Iso.* **61** 1089-93

Neutron Flux Mapping inside a PMMA and a RANDO Phantom using Indirect Neutron Radiography

P.E. Tsai[a], C.K. Huang[a], Y.H. Liu[a], H.M. Liu[b], Shiang-Huei Jiang[a]

[a]*Engineering and System Science Dept., National Tsing Hua University, Taiwan*
[b]*Nuclear Science and Technology Development Center, National Tsing Hua University, Taiwan*

Abstract

This study aims to measure the two-dimensional neutron spatial distribution inside a PMMA and a RANDO phantom for the purpose of further comparison with the treatment planning. The measurements were made by using the indirect neutron radiography, which utilized a thin copper foil and the imaging plate. The developed image provides satisfactory spatial resolution and very low statistical error (< 1%). As to the time cost, the whole procedure normally takes less than three hours. The result shows that the indirect neutron radiography can be a quick and reliable method to provide a 2D neutron spatial distribution inside a phantom.

Keywords: BNCT, indirect neutron radiography, imaging plate, neutron flux mapping

1. Introduction

The thermal neutron flux distribution inside a tumor is proportional to the boron reaction rate distribution concerned in the boron neutron capture therapy (BNCT). The boron dose delivered to a tumour, which is an important indication of the effectiveness of BNCT, is an integrated value of the boron spatial distribution multiplied by the neutron spatial distribution over the tumour volume. The more precise the neutron flux and the boron compound distribution, the more precise the boron dose. This paper will focus on the measurement of neutron flux distribution.

Generally, the flux mapping is performed by only limited number of activation detectors due to the time cost and the counting ability. Hence, the quality of the flux mapping is not satisfactory. Recently, it is demonstrated that the indirect neutron radiography (INR) can quickly and precisely picture the two-dimensional (2D) neutron spatial distribution of an epithermal neutron beam with a very high resolution (Liu et al., 2008[a]). In this study, the INR is applied to obtain the 2D neutron spatial distribution inside a PMMA and a RANDO phantom for the purpose of further comparison with the treatment planning.

2. Materials and Methods

2.1 THOR BNCT Beam

The BNCT beam of the THOR is an epithermal neutron beam with an aperture of 14 cm in diameter. The neutron fluxes at the center of the beam exit were measured to be 1.34 x 10^8 and 1.07 x 10^9 neutron-cm^{-2}-sec^{-1} (Liu et al., 2008[b]) for thermal (< 0.5 eV) and epithermal neutrons (0.5 eV < E_{epi} < 10 keV), respectively at a reactor power of 1.2 MW.

2.2 Indirect Neutron Radiography

The INR utilizes the idea of neutron activation and later development. In this study it is applied to measure the 2D neutron spatial distribution inside a phantom. The activity of the irradiated target is proportional to the product of the target cross-section and the cross neutron flux. For an epithermal neutron beam incident into a PMMA phantom, it is quickly moderated into thermal neutrons. Hence, the activity distribution over the target is the relative distribution of the concerned thermal neutron flux. As a result, the developed image can be processed into the neutron flux map after proper translation as expressed in the following equation:

$$I \propto \alpha_0 \propto \phi_n \qquad (1)$$

where I is the number of signal collected by the image reader; α_0 is the activity of the activated target at the end of irradiation; ϕ_n is the thermal neutron flux cross the target.

2.3 Experiment Setup

Concerning the availability, cost, neutron capture cross section, and the activated radionuclide properties, a 15 × 20 × 0.0125 cm^3 copper foil with purity 99.9% is chosen to be an activation converter for the neutron flux mapping. The dominant

radionuclide in the copper foil is ^{64}Cu formed from the ^{63}Cu(n,γ)^{64}Cu reaction, which is sensitive to thermal neutrons.

Measurements were performed inside a solid PMMA phantom and a RANDO phantom. The PMMA phantom is composed of PMMA slices with an area 20 × 20 cm^2 and with different thicknesses from 1 mm to 5 cm such that the copper can be put at the position of interest, and the outer dimensions are 21 × 21 × 21 cm^3. The RANDO phantom is composed of 12 slices of thickness 2.54 cm, from the shoulder to the top of head.

There are four cross-hair lasers installed in the BNCT irradiation room; all the lasers crosses through a reference point. The front laser pointing to the beam center emits a cross passing through the horizontal and vertical planes normal to the beam exit surface. The PMMA phantom with a copper foil inside is positioned against the beam exit surface and aligned according to the front laser to ensure that the beam direction is vertical to the PMMA surface. This position method is similar to the RANDO phantom.

For the BNCT beam, the intensity distribution of epithermal neutrons at the beam exit is also quite important. Therefore, a 0.5-mm thick cadmium plate was put in front of the copper foil to filter the thermal neutrons whose energies are below the cadmium cut-off energy (0.55eV).

2.4 Image Development

The radiation area detector applied in INR is an image plate (IP) which was first introduced by Fuji Film Co. in 1983 (Sonoda et al., 1983). It is comprised of phosphors whose material is BaFBr:Eu^{2+} that can trap and store the radiation energy. The IP applied in this work is type BAS-IIIs or the so-called white IP manufactured by Fuji, and the IP reader is Fuji FLA-3000 with the reading density selected to be 20 pixels per mm. The dimensions of BAS-IIIs IP are 20-cm wide and 40-cm long.

As a 2D integral-type detector, IP was chosen in this work due to its superior linearity range exceeding 5 orders and its high sensitivity which is several ten times higher than the traditional X-ray film (Thoms, 1997). Moreover, it is reusable. Such advantages make the arrangement of INR much flexible.

After the irradiation and cooling, the activated foil was placed into the IP cassette where the copper foil is attached to the surface of IP for exposure. Hence the response of IP to the radioactivity is contributed dominantly from the beta-plus and beta-minus particles accompanying the ^{64}Cu beta decay than the decay gamma rays. Such an arrangement improves the quality of image.

For minimizing the influence caused by fading phenomenon and non-uniform exposure, all the exposure are performed in a well temperature-controlled dark room (20 ± 1 °C). After the exposure, the IP was moved into the IP reader for development. All the following image process is done by Fujifilm Image Gauge software.

2.5 Linearity Calibration

When incident radiations deposit energy to IP's phosphor layer, the excited electrons are then trapped to form Fluoride-centers. The trapped electrons are stimulated using 633-nm HeNe laser and released as ~415-nm blue lights called photostimulated luminescence (PSL). Theoretically, the PSL value is directly proportional to the deposited energy caused by radiation. In order to ensure that the response of IP is directly proportional to the activity of radiation source, the linearity between the PSL value and the number of incident radiation was checked by a ^{64}Cu source which is a 2.5 by 2.5 cm^2 square, 0.1-mm thick, pure copper foil.

3. Results and Discussions

3.1 Linearity of IP

Fig. 1 shows the result of linearity calibration. The copper foil described in Section 2.3 was first irradiated and activated in the epithermal neutron beam for two hours to accumulate sufficient activity. Its activity was then determined by a well-calibrated high purity germanium detector. The exposure time was controlled to be 30 min; the time period after exposure, prior to the readout process was 10 min. From Fig 1, it is clear that the activity of ^{64}Cu is directly proportional to the PSL value.

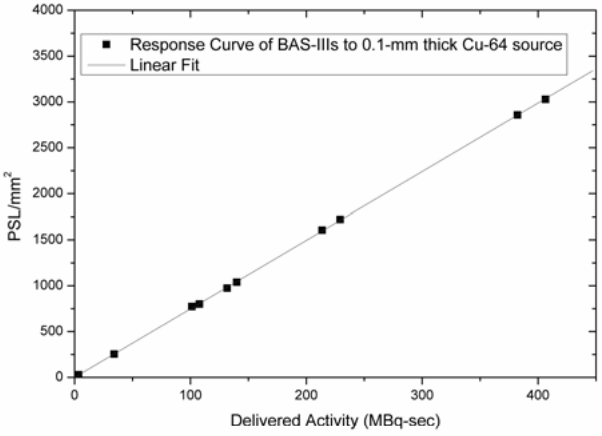

Figure 1 The linear response curve of BAS-IIIs to a 0.1-mm thick ^{64}Cu source

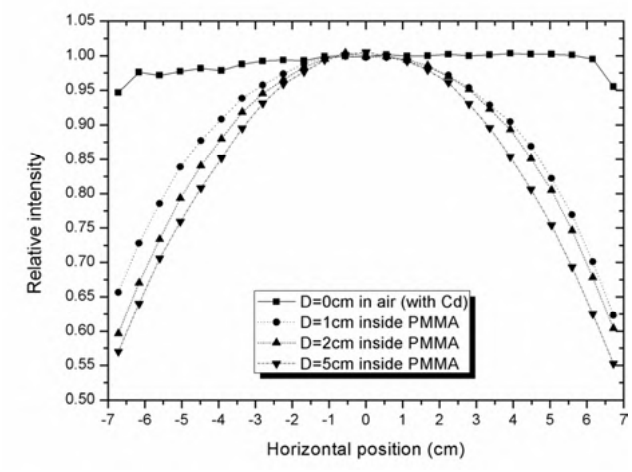

Figure 2 The comparison between the ^{64}Cu activity profiles along the horizontal axis at different depth in the PMMA phantom, and free-in-air at beam exit surface

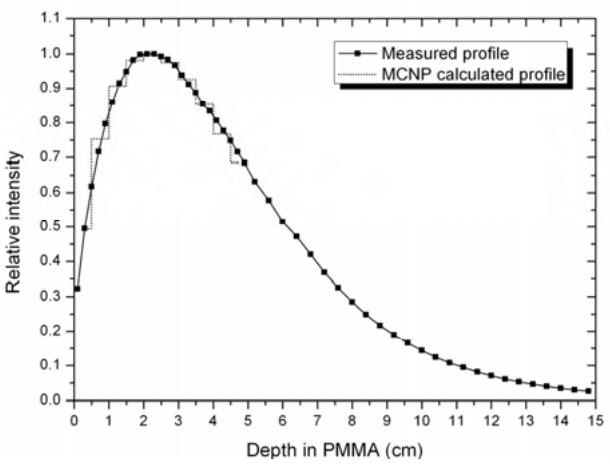

Figure 3 Measured and calculated depth profiles of the ^{64}Cu activity along the central axis of the beam

3.2 Neutron Flux Mapping in a PMMA Phantom

The copper foils were irradiated for 15 to 30 minutes, depending on the irradiation position, with a reactor power of 1.2 MW to perform the INR in a PMMA and a RANDO phantom. After one-hour cooling, the activated copper foil was exposed to the IP for 30 to 60 minutes according to the degree of activity. All the interesting measured data are with a standard deviation below 1%.

The measurements performed inside the PMMA phantom are at the depth of 1, 2 and 5 cm. The ^{64}Cu activity profiles, which are proportional to the thermal neutron distributions, along the horizontal axis of the beam aperture are shown in Fig. 2. The measured free-in-air profile (with cadmium cover) at the beam exit surface is also given in the figure.

It can be seen from the free-in-air measurement that the epithermal neutron distribution are quite uniform within a 12-cm diameter at the beam center.

When the epithermal neutron beam is incident into the PMMA phantom, owing to the scattering effect and its angular distribution, the relative intensity sharply decreases on the edge. The deeper the depth goes, the more divergent the beam is. Hence, the 90% relative intensity of the profiles is located at 4, 3.75, and 3.25 cm away from the beam center for the depths of 1, 2, and 5 cm, respectively. The measured profiles in the PMMA phantom are quite symmetric, which is consistent with the free-in-air measurement.

Due to the build-up effect of the epithermal neutrons in the hydrogen-rich phantom, the peak of the thermal neutron flux along the central axis will be a small distance away from the phantom surface. The measured profile along the center line is plotted in Fig. 3. The peak of the measured result is at 2.3 cm.

The profile calculated by MCNP (Briesmeister, 2000) is also given in the figure. All the calculated values have a statistical uncertainty below 1% within 95% confidence interval. Apparently, the calculated curve is slightly different from the measured one. This is because of the imperfect energy spectrum and angular distribution of the neutron source description applied in the calculation.

The measured 2D profile of the horizontal plane cross the central axis is shown in Fig. 4. The depths before 5 cm are much more concerned in the treatment, and therefore the resolution is higher than the rest of depths. The element size of the image before 5 cm is 0.2 (depth) x 0.6 (wide) cm^2; for the depths after 5 cm, it is 0.4 (depth) x 0.6 (wide) cm^2 per element. The hot spot emerges at the depth of 2.3 cm and the center of vertical axis. The upper 50% intensity along the center line locates between 0.4 and 6.2 cm. Please note that all the concerned elements have a statistical error less than 1%.

3.3 Neutron Flux Mapping in a RANDO Phantom

The INR can also be performed in a human-like, sophisticated phantom like RANDO phantom. To simulate the clinical treatment of brain tumor, the copper foil was positioned at the vertical plane cross the beam central axis and implanted between layer 4 and 5 (about the height of eyes) as The RANDO phantom was lying with its face side up as shown in Fig. 5(a). Fig. 5(b) shows the measured neutron spatial distribution. This result is quite delicate and can be used for the comparison with the treatment planning.

4. Conclusions

This study successfully measured the 2D thermal neutron flux distribution in the PMMA and RANDO phantom using indirect neutron radiography.

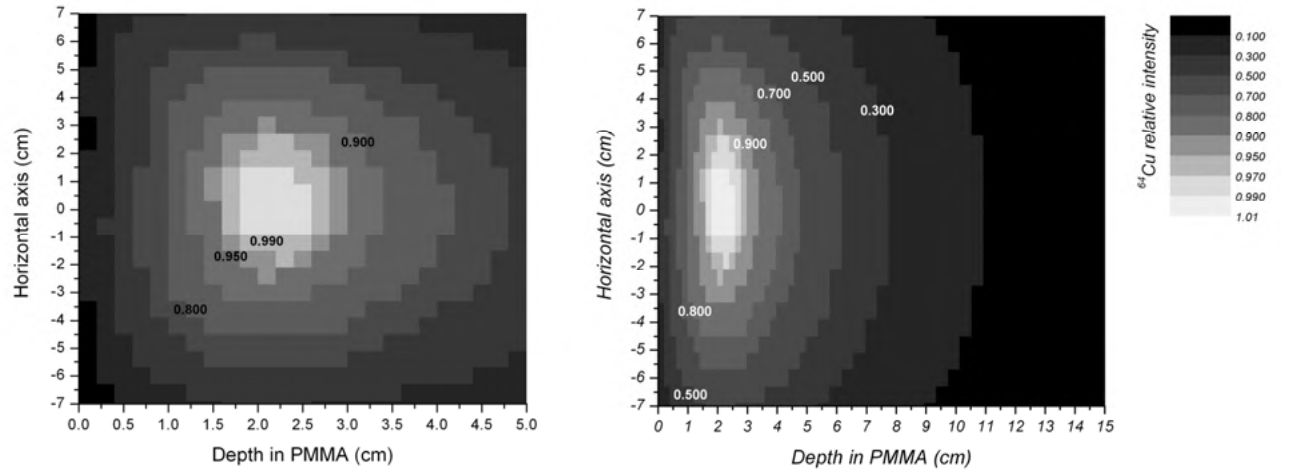

(a) (b)

Figure 4 (a) and (b): The horizontal depth profile of the ^{64}Cu relative distribution inside a PMMA phantom with different range of depths. The depth in (a) is from 0 to 5 cm; the depth in (b) is from 0 to 15 cm

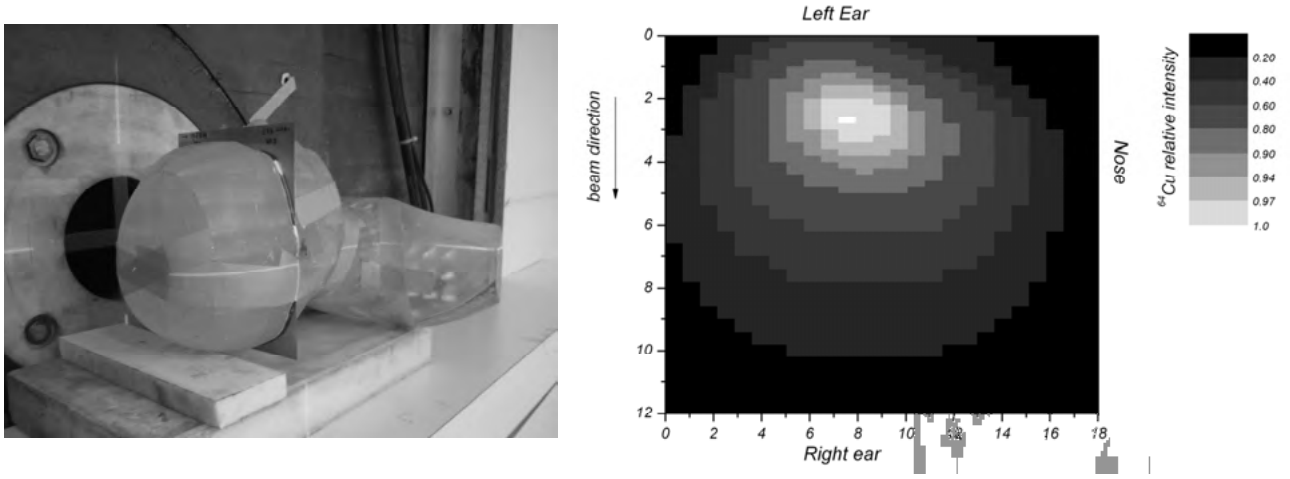

(a) (b)

Figure 5 The indirect neutron radiography was utilized in a RANDO phantom. (a) is the experimental setup, and (b) is the processed image representing the ^{64}Cu 2D relative distribution in the phantom

The procedure only takes less than 3 hours. The developed image has satisfactory resolution and very low statistical error. The hot spot emerges at the depth of 2.3 cm in the PMMA phantom. The image of the RANDO phantom is ready to be used for the comparison with the treatment planning and neutron source adjustment.

Acknowledgement

This study was supported by the National Science Council of the Republic of China under contract number NSC95-2221-E-007-135 and -136. We will like to show our sincere appreciation to Mr. Chen, Ang-Yu for his assistance in the MCNP calculations.

References

Briesmeister, J.F., 2000. MCNP—A General Monte Carlo N-Particle Transport Code Version 4C, Los Alamos National Laboratory.

Liu, Y.H., Huang, C.K., Tsai, P.E., Chen, A.Y., Liu H.M., Lee, S.C., Jiang, S.H., 2008[a]. BNCT Epithermal Neutron Beam Mapping by using Indirect Neutron Radiography. The 11th International Conference on Radiation Shielding (ICRS-11)

Liu, Y.H., Nievaart, S., Tsai, P.E., Moss, R., Liu, H.M., Jiang, S.H., 2008[b]. Coarse-Scaling Adjustment of Fine-group Neutron Spectrum of Epithermal Neutron Beams in BNCT using Multiple Activation Detectors. To be published.

Sonoda, M., Takano M., Miyahara J., Kato, H., 1983. Computed radiography utilizing scanning laser stimulated luminescence Radiology. Radiology 148, 833-838.

Thoms, M., 1997. The dynamic range of X-ray imaging with image plates. Nucl. Instrum. Methods A 264, 437-440.

Determination of the irradiation field at the research reactor TRIGA Mainz for BNCT

Sven Nagels[1], Frank Becker[1], Gabriele Hampel[2], Christian Schütz[2], Norbert Wiehl[2], Birgit Wortmann[3], Arturo Lizon Aguilar[3], Gerd Otto[4] and Shahin Minouchehr[4]

[1]Forschungszentrum Karlsruhe GmbH, Hauptabteilung Sicherheit, Postfach 3640, D-76021, Karlsruhe, Germany
[2]Institut für Kernchemie, Johannes Gutenberg-Universität Mainz, Fritz-Strassmann-Weg 2, D- 55128 Mainz, Germany
[3]Evonik Energy Services GmbH Essen, Rüttenscheider Str. 1-3, D-45128 Essen, Germany
[4]Klinikum der Johannes Gutenberg-Universität Mainz, Transplantationschirurgie, Langenbeckstr. 1, D- 55131 Mainz, Germany

The TRIGA Mainz (TRIGA = Training Research Isotope production General Atomic) is one of two research reactors operated at German universities. The TRIGA Mainz can be operated in the steady state mode with a maximum power of 100 kW_{th} and in the pulse mode with a peak power of 250 MW_{th}. With respect to a future application of the boron neutron capture therapy (BNCT) at the research reactor TRIGA Mainz the basic characteristics of the radiation field in the thermal column must be determined. So far neutron and gamma fluxes in the thermal column were determined using thermoluminescence detectors (TLD)with a new developed energy-compensation filter system as well as thin gold foils, and a semiconductor detector.

The TRIGA Mainz with a graphite thermal column provides a source of well-thermalized neutrons suitable for physical research or biological and medical irradiations. This thermal column shall be used for the irradiation of an explanted liver with thermal neutrons for a liver metastases therapy. BNCT was first realized at the TRIGA Pavia, Italy as follows: after a patient accumulates pharmaceutical ^{10}B mainly in the tumour tissue, the liver is explanted, irradiated with thermal neutrons and reimplanted (auto-transplantation).

Concerning the proximity between the transplantation centre and the treatment reactor, the TRIGA Mainz has a unique advantage in Europe.

The basic characteristics of the radiation field in the thermal column as beam geometry, neutron and gamma-ray energies, angular distributions, neutron flux as well as absorbed gamma and neutron doses must be determined in a reproducible way.

Measurements of the photon dose and the neutron flux in this mixed neutron-gamma radiation field have been performed using different TLDs, gold foils and a semiconductor detector.

The employed TLD materials were CaF_2:Tm (TLD-300) and LiF:Mg,Ti with different ^6Li concentrations and thicknesses. They have been used to determine the photon dose contributions in a plexiglass phantom and free in air over the whole length of the central radiation channel of the thermal column for reactor powers between 10 W and 100 kW.

The TLDs were analysed at the “Forschungszentrum Karlsruhe” and calibrated at the thermal neutron beam of the GKSS research reactor (GeNF) in cooperation with the PTB. This beam at GeNF provides a negligible photon dose.

The thermal column of the TRIGA Mainz shall be reconstructed to allow the irradiation of an organ with thermal and epithermal neutrons and to establish an irradiation facility for medical purposes at the reactor facility. A further aim is to measure photon and neutron dose with small and thin TLDs inside the liver during the treatment.

TREATMENT PLANNING

Neutron Beam Source Definition Techniques for NCT Treatment Planning

J.R. Albritton[a,b] and W.S. Kiger, III[b]

[a]*Nuclear Science and Engineering Department, Massachusetts Institute of Technology, 77 Massachusetts Avenue, Cambridge, MA 02139, USA*
[b]*Department of Radiation Oncology, Beth Israel Deaconess Medical Center, Harvard Medical School, 330 Brookline Avenue, Boston, MA 02215, USA*

Abstract

Constructing an accurate description of a neutron beam is critical to achieving accurate calculations of dose in NCT treatment planning. This paper compares two different methods of neutron beam source definition. The first method involves performing a detailed simulation of the neutron beam line and recording the characteristics of all particle histories to a phase space file referred to as a "surface source" for subsequent transport through the patient model. The second method involves representing the beam characteristics as a set of probability distributions using the MCNP general source definition card (SDef). Simulations in this study were performed using the MCNP Monte Carlo radiation transport code with the MIT Fission Converter beam (FCB), which has a well-validated Monte Carlo model, serving as the test neutron beam. Each source type (surface source file and SDef) was used to simulate transport of the beam through a voxel model of an ellipsoidal head phantom where doses were calculated as in a treatment planning simulation. The initial calculations with the SDef produced significant, ~12% errors in dose relative to calculations with the surface source file. Using a patched version of MCNP that could model the observed radial dependence of the relative azimuthal angle, errors in all dose components at D_{max} were reduced to levels that were not statistically significant ($P \geq 0.18$) and errors in all components except the fast neutrons were reduced to $\leq 0.8\%$.

Keywords: boron neutron capture therapy (BNCT), radiotherapy treatment planning, Monte Carlo simulation, radiation source definition

1. Introduction

Definition of the radiation source for computations is perhaps the most difficult aspect of treatment planning because it requires producing an adequately accurate representation of the 5-dimensional probability distribution describing the spatial, energy, and angular characteristics of a neutron beam. Two methods of defining a neutron beam source for NCT treatment planning involve using either binary phase space files (surface sources) or a set of probability distributions to define the radiation source characteristics at the neutron beam aperture. When using surface sources, the particle tracks stored in a phase space file from a previous simulation of the beamline are sampled in subsequent simulations of particle transport through the patient geometry. In the second method, probability distributions for the source particle variables are usually constructed from prior Monte Carlo or discrete ordinates transport calculations of the neutron beam. In the patient calculations, the probability distributions are sampled to determine starting characteristics for each source particle. In the MCNP5 code (X-5 Monte Carlo Team, 2005) used in this study, these source probability distributions are specified in the general source definition card (SDef).

Each of these methods has significant benefits and drawbacks. The primary benefit of using a surface source file is that it introduces no significant approximations into the source description, which should lead to improved dose accuracy. Disadvantages of this method include the extremely large (GB) size of the unportable binary files, lower computational efficiency, increased start-up times for parallel computations, and limitations on the number of particles that can be run which thus limits dose precision. However, an SDef does not suffer from any of these shortcomings, but may involve significant approximations and loss of information that reduce the accuracy of computed doses. The fact that the probability distributions for the source variables (energy spectrum, spatial distribution, angular distribution) may be inseparable is also problematic to constructing SDefs. Nevertheless, if the approximations inherent in constructing an SDef

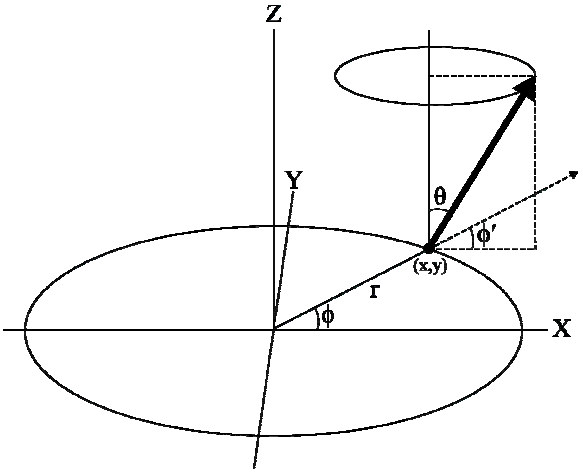

Fig. 1. Illustration of parameters used to define the particle position and direction (indicated by the bold arrow) in the SDef source representations. r and ϕ are sampled to define position (x,y). The polar angle θ and the relative azimuthal angle ϕ′, defined relative to the track's radial vector, determine particle direction

could be limited to the extent that they produce no significant differences in dose when compared to calculations with surface sources, then the use of SDefs in NCT treatment planning calculations would indeed be advantageous.

2. Materials and Methods

The neutron beam used as a test case in this study is the MIT fission converter beam (FCB) (Harling *et al.*, 2002), which has a well-validated MCNP model. A detailed simulation of the FCB beamline was conducted to produce a surface source file at the beam aperture, where the beam exits the collimator. The surface source file modeling the MIT FCB was converted into an SDef using a suite of Matlab (The Mathworks, Natick, MA) functions to read and score the track information into a 4D array of radial (r), energy (E), polar angle (θ), and relative azimuthal angle (ϕ') bins. As shown in Fig. 1, the relative azimuthal angle ϕ' is defined as the angle between the particle's radial position vector and the projection of the particle's direction onto the source plane. The circular symmetry of the FCB collimator and the emerging neutron beam permits this convenient representation of the source geometry using polar coordinates.

In the standard version of MCNP, ϕ' is sampled uniformly from $-\pi$ to $+\pi$. However, for the MIT FCB, ϕ' is not uniformly distributed. Instead, values of $|\phi'| < \pi/2$ are preferred (i.e., particles directed radially outward, away from the beam center), and this preference has a radial dependence that increases with distance from the beam center. Therefore, MCNP5 was modified to allow the radial dependence of ϕ' to be accurately modeled using a radially dependent offset cosine function and other distributions. Fig. 2 compares the radial dependence of ϕ' observed in the surface source with the fitted model.

To construct the probability distributions for the SDef, the r-E-θ phase space was broken into several rectangular regions. In each region, marginal probability distributions for each source variable (r, E, θ, ϕ') were computed from the binned track data. These marginal distributions are sampled in the SDef model and actually define the source. By graphically comparing the joint probability distributions for source variable pairs with the product of their marginal distributions, the coarse region boundaries were selected to minimize the differences and produce an accurate model of the source. Relatively few course regions for each source variable were used to reduce the complexity of the SDef. However, it should be noted that the complexity of the SDef has no significant effect on the total simulation time since most computational effort is spent tracking the particles and not in sampling the SDef.

Using the MiMMC (Multi-Modal Monte Carlo) treatment planning system (Kiger *et al.*, 2004), 4 and 10 mm voxel models of the modified Snyder head phantom were constructed. Transport

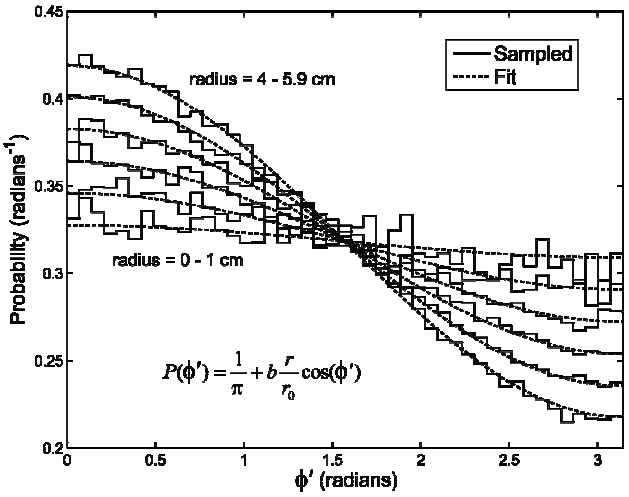

Fig. 2. Actual sampled and fitted probability distributions of ϕ' (the relative azimuthal angle) inside the beam aperture of the MIT FCB. The nonuniform distribution shows a preference for outward angles ($|\phi'| < \pi/2$). r_0 is the radius of the beam aperture, 5.9 cm, and b is a fitted constant. Radial bins range from 0 to 5.9 cm in ~1 cm steps. P(ϕ') is shown averaged over the radial bins for this comparison

simulations were performed in this phantom using MCNP5 with the 3 different source models for the MIT FCB: a surface source representation and SDef models with and without ϕ' dependence. Doses calculated in the phantom were compared by plotting isodose contours and depth vs. dose along the central beam axis. In the SDef source models, source biasing of the fast neutrons was used to improved statistics at depth in the phantom. For the comparison, dose rates calculated in the 4 mm voxel model were used for all the dose components except the incident photons, where data from the 10 mm voxel model were used to improve poor statistics resulting from the combination of limited photon track information in the surface source file and smaller voxels.

3. Results

Fig. 3 compares isodose contours and depth vs. dose plots for the 2 SDef source models to reference data computed with the surface source. Table 1 summarizes these results, reporting the error in maximum dose for the two SDef source models. Significantly elevated dose rates as much as 12.6% higher than the reference surface source results were computed with the SDef model using the standard version of MCNP, which uses a uniform ϕ' distribution. Shifts in the isodose contours to deeper depths (and higher dose rates) for all dose components are clearly evident with this model.

When the nonuniform ϕ' distribution was modeled accurately using the patched version of MCNP, the agreement between the SDef and the surface source improved dramatically, resulting in no statistically significant differences between the calculated dose rates and in good agreement in the isodose contours.

Table 1. Percent error in maximum dose rate for SDef source models compared to the surface source reference values. Uncertainties are 1 σ

	Error	
Dose Component	ϕ' Uniform	ϕ' Nonuniform
Boron	12.6 ± 0.2%	-0.1 ± 0.2%
Thermal neutron	12.5 ± 0.2%	-0.1 ± 0.2%
Induced photon	11.4 ± 0.2%	0.0 ± 0.2%
Fast neutron	5.6 ± 3.8%	-5.0 ± 3.8%
Incident photon	12.2 ± 3.0%	-0.8 ± 2.9%
Total weighted brain dose	12.4 ± 0.3%	-0.2 ± 0.3%

4. Discussion

The preference for outwardly directed particle tracks in the actual source distribution produces lower dose rates relative to an SDef with a uniform distribution of ϕ' because outwardly directed particles have a greater tendency to miss the phantom and not deposit any energy. Modeling the radial dependence of the relative azimuthal angle in MCNP produced significantly better agreement between in-phantom dose rates calculated using the surface source and SDef. Using this modification and the sophisticated Matlab tool to analyze the surface source file and construct the SDef, the approximations in source modeling were minimized to result in excellent agreement with the dose rates calculated using the surface source.

Using versions of MCNP not modified with the patch described here, the SDef source model (uniform ϕ') and surface source models have both been used at Harvard-MIT and elsewhere in clinical treatment planning. To some extent, the dose error resulting from using a uniform ϕ' distribution with the standard SDef model can be accounted for in planning system calibration by dose rate scaling. However, dose rate scaling corrects this problem only approximately since the effect of this error is not spatially uniform; i.e., with the planning system tuned to give good agreement on the central axis, agreement will be poorer laterally. This adjustment is also phantom-dependent. Within this framework, the correct solution is to properly model the nonuniform ϕ' distribution using a patched version of MCNP or a surface source file.

Acknowledgements

This research was supported by the Harvard Joint Center for Radiation Therapy Foundation.

References

Harling, O.K., *et al.* 2002. The Fission Converter Based Epithermal Neutron Irradiation Facility at the MIT Reactor. Nucl. Sci. Eng. 140, 223-40.

Kiger, III, W.S., Hochberg A.G., Albritton J.R., Lu X.-Q., 2004, Development of a Multimodal Monte Carlo Radiotherapy Planning System. Eleventh World Congress on Neutron Capture Therapy. Waltham, MA, 50.

X-5 Monte Carlo Team, 2005, MCNP - A General Monte Carlo N-Particle Transport Code, Version 5, LA-UR-03-1987, Los Alamos National Laboratory.

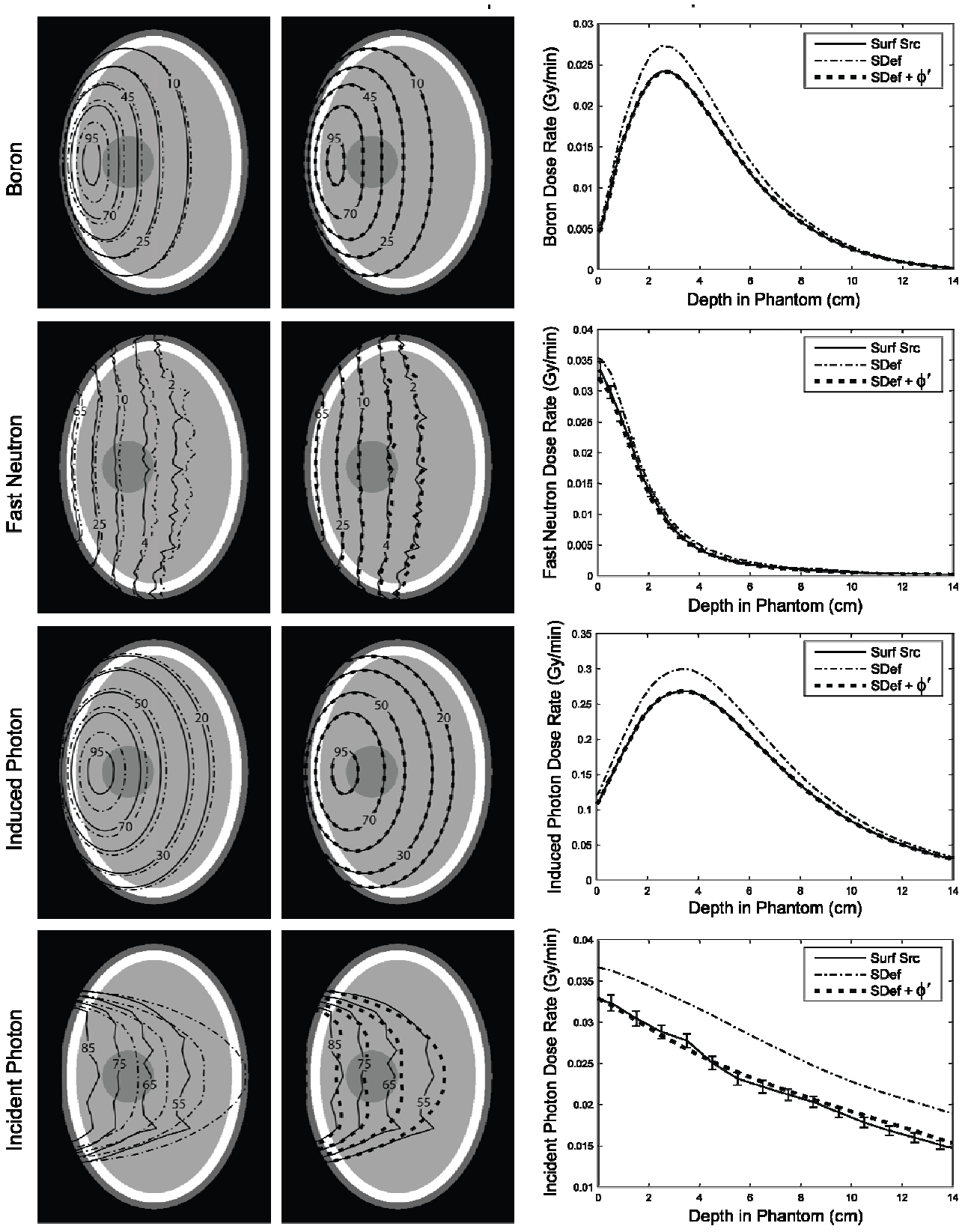

Fig. 3. Comparison of dose rates calculated in the modified Snyder head phantom using different beam source models for the MIT FCB. Solid lines represent the reference doses calculated with the surface source while dashed and dash-dot lines represent data for the SDef models with and without ϕ' dependence, respectively. Isodose labels represent a percentage of the maximum dose rate in the phantom computed with the surface source for each dose component. Error bars (1 σ) in the depth-dose plots are omitted for clarity in cases where they are negligibly small

Acceleration of Monte Carlo based treatment planning: criteria when adjoint calculations are faster

S. Nievaart[a], R. Moss[a]

[a] *Institute for Energy, Joint Research Centre of the European Commission, Petten, the Netherlands*

Abstract

Up until now, treatment planning in Boron Neutron Capture Therapy is only performed using Monte Carlo-based techniques. The conventional radiotherapy community has become more interested in such techniques, as they are impressed by the accuracy that can be achieved with Monte Carlo calculations. However, a disadvantage of the method is still the long times needed to obtain results with reliable statistics. Although computer power has become faster and cheaper over the years, it is still impossible to calculate a hundred or more different beam positions within a few days, which is the time a treatment planner in BNCT normally needs to produce an acceptable plan. With more calculated beam positions, a better treatment plan can be composed which can maximise the dose in the tumours whilst sparing the organs at risk. In normal (forward) Monte Carlo calculations, the particles start at the beam opening and travel into the tissue where they may or may not hit a target, e.g. tumour, organ at risk. In adjoint Monte Carlo calculations, the particles start at the target and travel out of the tissue to where the information is recorded. This information can be translated as if the particle started at the place of recording. With this method, the same information is gathered as with forward Monte Carlo but instantly all around the irradiated tissue. In a realistic head phantom with 10 organs at risk and 10 tumours, the adjoint techniques are 1.8 to 3.3 times faster than the forward MC calculations when 1020 different orientations of a gamma beam with a diameter larger than 5 cm are simulated. In the case of a neutron beam, the adjoint technique is faster by 6.6 to 20 times, than the forward MC. In general, in the case of small diameter beams, adjoint MC calculations are only preferable for a large number of beams and a small number of regions of interest. For larger beam sizes, the adjoint method is more favourable than the forward calculations when there are fewer beams and/or many regions of interest.

Keywords: Treatment planning, Monte Carlo, Adjoint

1. Introduction

Currently, most investigations in treatment planning focus on decreasing the computational time to obtain the doses without making concessions on the accuracy (Siebers et al. and Ulmer et al.). When less time is needed for the dose calculations, more time is available for optimization of a treatment plan. Beside BNCT, also in conventional treatment planning, Monte Carlo (MC) provides more accurately calculated dose rates in the heterogeneous human tissues (Ma et al. and Demarco et al.) than with other methods. However, currently, long calculation times prevent that the MC methods can be applied for every single beam configuration for every patient. A promising technique to reduce the variance of the MC result is applying adjoint MC. In reactor physics, an equation can be defined that is mathematically adjoint to the neutron transport equation. The solutions of this adjoint equation can be physically defined as a measure of the "importance" of a neutron in contributing to the response of the detector (Bell and Glasstone). In normal, actually called 'forward' Monte Carlo calculations, the particles start at the beam opening which is the real source, and travel into the tissue where they may or may not hit a detector. In adjoint Monte Carlo calculations, the particles start at the detector and travel out of the tissue to where the information is recorded. This information can be translated as if the particle started at the place of recording which can be a possible beam exit location. In fact, the adjoint particles can be seen as traveling backwards. In the field of irradiating materials, e.g. phantoms and patients, the adjoint method can simply provide at defined locations (points, areas, volumes) the expected detector contribution of source particles, as a function of

energy, position and starting angle. These 'detectors' can be tumours or organs at risk (OAR), which together, are mentioned as regions of interest (ROI). Since BNCT worldwide is still in a clinical trial phase, relatively not many patients are treated. As a consequence, little experience exists in positioning neutron beams and making optimal treatment plans for various locations and positions of the cancer. Especially, whenever a homogeneous thermal neutron field in a larger volume of the patient, by means of more beams, is requested. This paper will show that the adjoint MC technique can be an improvement for BNCT and can help the treatment planner in selecting optimum beam settings. However, up until recently, a major drawback of the adjoint MC approach was the inapplicability when performing BNCT with a mono- or nearly mono-directional neutron beam (meaning parallel travelling of the particles within the beam). To overcome this, two techniques are developed for the Monte Carlo code MCNP (Briesmeister), which have been discussed and published previously (Nievaart et al.). These techniques are called the 'Adjoint Point Detector Technique' and 'Legendre EXpansion Technique' and are discussed under the headings of APDT and LEXT, respectively, in Section 2. In the above mentioned paper it was concluded that application of the adjoint MC for mono-directional neutron beams enables to obtain more quickly the optimum irradiation directions and positions for a BNCT treatment plan. In case of a head phantom, for example, the smallest beams (5 cm) are calculated most quickly with forward MC for both neutrons and gammas. In the case of neutrons, the calculations for the 10 cm and 15 cm beams are respectively 6.6 and 20 times faster with the adjoint MC. For gammas, the calculation times for the 10 cm and 15 cm beam exits decrease with a factor of 1.8 and 3.3, respectively. An overview of when adjoint MC calculations are faster than the forward MC techniques, as a function of the number of ROI against the number of beams was not given in the mentioned paper, but is discussed here.

2. Set-up

The calculation times needed to obtain certain results with equal (acceptable) statistical uncertainties, using the forward and adjoint MC techniques are obtained in a patient suffering from multiple tumours in the brain, describing a real BNCT case. The total detector responses of the fluxes due to thermal neutrons and gammas in 10 randomly distributed tumours and 10 OAR are calculated. The MCNP geometry of the patient's head, with material compositions taken from ICRU46, is shown in Figure 1, as created by the program Sabrina and Scan2MCNP (West and Van Riper). The OAR are defined as described in the protocol in Petten used to treat metastatic malignant melanoma in the brain (Wittig et al.). The head phantom is surrounded by 60, evenly distributed, centre points where all adjoint detector discs are positioned. An adjoint detector disc is equivalent to the shaped surface of the beam exit disc in the forward MC calculation.

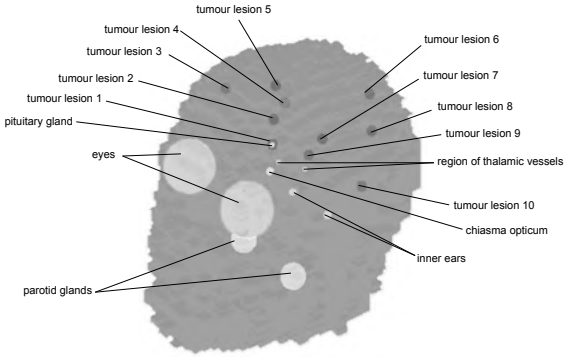

Figure 1. Phantom head with 10 OAR and 10 tumours, as is used in the calculations

At each of the 60 positions, 17 discs with different, systematically chosen orientations of their outer normals (pointing away from the phantom) are positioned. This implies that in total (60 times 17) 1020 beams are modelled around the head. All calculations, for all 1020 beams, are performed for beam diameters of 5 cm, 10 cm and 15 cm. The source energy spectrum is taken from the BNCT treatment beam, called HB11, as available in Petten (Moss). It consists of mainly 10 keV source neutrons and has a 2 degree divergence which can be regarded as mono-directional. The gamma source spectrum is arbitrary and taken uniform between 0.01 MeV and 20.0 MeV. Below follows a brief description of the techniques developed in MCNP as stated in Section 1:

APDT: Since the probability that MC particles will traverse a plane detector perpendicularly within a narrow solid angle is very small, one has to 'force' them. In MCNP this 'forcing' technique is called DXTRAN; at every event the contribution a particle will have to a certain specified region is calculated deterministically. DXTRAN can be used in forward and adjoint mode. This specified region can be defined as a point and by positioning this point far away from an opening (shaped like the adjoint detector disc = beam exit), the particle tracks will be 'stretched' whilst attracted to this point. The further away the adjoint point detector is positioned, the more perpendicular the contributions traverse the adjoint detector disc (=beam exit) shaped entrance.

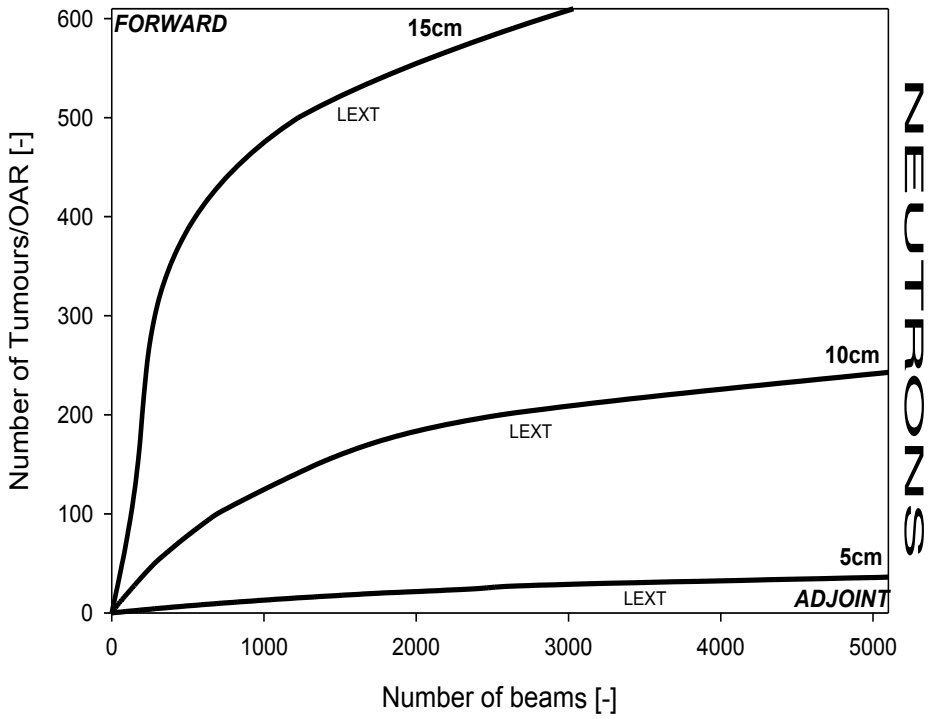

Figure 2. Number of neutron beams with different diameters vs. number of tumours/OAR for which adjoint or forward MC is preferable. For a given beam diameter, the region below the line is the area where adjoint MC is preferable

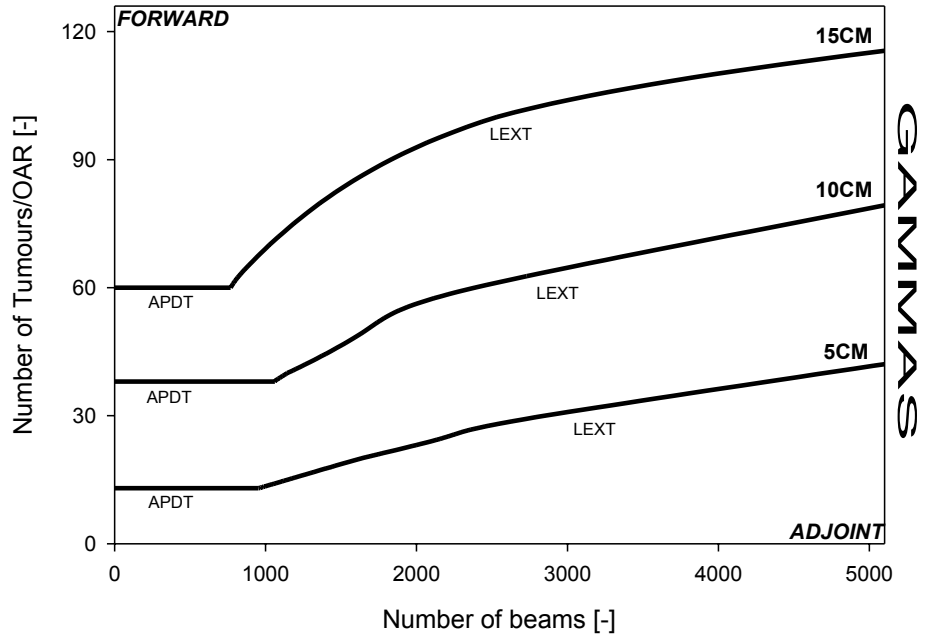

LEXT: The second technique to determine the adjoint function for the direction perpendicular to the adjoint detector disc is determined by use of the Functional Expansion Technique (Beers and Pine).

This means that adjoint particles that traverse an adjoint shaped detector plane are used to estimate the Legendre coefficients for expansion of the angular adjoint function. This provides an estimate of the adjoint function for the direction normal to the detector plane.

3. Results

An overview of when forward MC calculations are faster than adjoint MC techniques, as a function of the number of ROI against the number of beams, is given in Figures 2 and 3, for neutrons and gammas respectively. Every figure contains 3 lines belonging to each beam exit diameter. Above the line of a certain beam diameter, the calculations are faster using forward MC and faster below the line when using the adjoint MC. Figures 2 and 3 are based on scaling the calculation times of the forward MC and adjoint MC head phantom results according to:

$$\textit{Forward MC} \propto \textit{number of beams}$$
$$\textit{APDT} \propto \textit{number of beams and number of ROI}$$
$$\textit{LEXT MCNP} \propto \textit{number of ROI}$$
$$\textit{LEXT Post Proc.} \propto \textit{number of beams and number of ROI}$$

The increase of MCNP calculation time due to the increasing complexity of the geometry when more ROI are involved is not taken into account. Due to this, in reality, the LEXT adjoint results will be even better than presented because of the post processing that is performed outside MCNP. As a consequence, the post processing time does not depend on the complexity of the geometry. The exercise presented here can also be performed for a fixed beam diameter but as a function of ROI size/volume. The same kind of curves, as presented in Figures 2 and 3, can be realized although the largest beam diameters will represent the smallest ROI and vice versa.

4. Conclusions

Two adjoint MC techniques are available, which enable the simulation of mono-directional gamma, as well as neutron, beams. In this paper, the adjoint and forward MC techniques are demonstrated in a patient suffering from 10 tumours in the brain. Of course, the presented techniques could be demonstrated in other organs (e.g. liver) as well. Overall, for small diameter neutron and gamma beams (around 5cm), the adjoint MC techniques are preferred when thousands of different locations and orientations of a mono-directional BNCT beam need to be calculated and when there are no more than ten ROI. For larger beam diameters, the adjoint MC is preferable up to hundreds of ROI whenever even a 'few' hundred of beams are investigated. Of course, in general, in order to take advantage of the adjoint technique, the user has to be interested in beam positions at many locations around the irradiated patient. Further analysis in the field of treatment planning optimisation is obviously the next step.

References

Bell, G.I., Glasstone, S., 1970. Nuclear Reactor Theory, Van Nostrand Reinhold Company, New York, NY.

Beers, B.L., Pine, V.W., 1976. Functional Expansion Technique for Monte Carlo Electron Transport Calculations. IEEE Trans. Nucl. Sci. 23, No. 6.

Briesmeister, J.F., 2000. MCNP - A General Monte Carlo N-Particle Transport Code, Version 4C. LA-13709-M.

Demarco, J.J., Chetty, I.J., Solberg, T.D., 2002. A Monte Carlo tutorial and the application for radiotherapy treatment planning. Med.Dosim. 27(1), 43-50.

ICRU 46. 1992. Photon, electron, proton and neutron interaction data for body tissues. International Commission on Radiation Units and Measurements. Bethesda. MD.

Ma, C.M., Mok, E., Kapur, A., Pawlicki, T., Findley, D., Brain, S., Forster, K., Boyer, A.L., 1999. Clinical implementation of a Monte Carlo treatment planning system. Med.Phys. 26(10), 2133-2143.

Moss, R.L., 1990. Progress towards boron neutron capture therapy at the High Flux Reactor Petten. Basic Life Sci. 54, 169-83.

Nievaart, V.A., Légràdy, D., Moss, R.L., Kloosterman, J.L., Van der Hagen, T.H.J.J., Van Dam, H., 2007. Application of adjoint Monte Carlo to accelerate simulations of mono-directional beams in treatment planning for Boron Neutron Capture Therapy. Med.Phys. 34 (4), 1321-1335.

Siebers, J.V., Lauterbach, M., Tong, S., Wu, Q., Mohan, R., 2002. Reducing dose calculation time for accurate iterative IMRT planning. Med.Phys. 29(2), 231-237.

Ulmer, W., Pyyry, J., Kaissl, W., 2005. A 3D photon superposition/convolution algorithm and its foundation on results of Monte Carlo calculations. Phys.Med.Biol. 50, 1767-1790.

Van Riper, K.A., 2005. A CT and MRI scan to MCNP input conversion program. Rad.Prot.Dos. 115 No. 1–4, 513–516.

West III, J.T., 1986. SABRINA, an Interactive Three-Dimensional Geometry-Modeling Program for MCNP. Los Alamos National Laboratory Report LA10688M.

Wittig, A., et al., 2003. Early phase II study on BNCT in metastatic malignant melanoma using the boron carrier BPA, EORTC protocol 11011.

Development of a multi-modal Monte-Carlo radiotherapy planning system

Hiroaki KUMADA[a], Takemi NAKAMURA[a], Masao KOMEDA[a], Akira MARUHASHI[b]

[a] *Department of Research Reactor and Tandem Accelerator, Japan Atomic Energy Agency, Tokai, Ibaraki, 319-1195, Japan*

[b] *Department of Neurosurgery, Institute of Clinical Medicine, University of Tsukuba, Tukuba, Ibraki, 305-8575, Japan*

Abstract

A new multi-modal Monte-Carlo radiotherapy planning system (developing code: JCDS-FX) is under development at Japan Atomic Energy Agency. This system builds on fundamental technologies of JCDS applied to actual BNCT trials in JRR-4. One of features of the JCDS-FX is that PHITS has been applied to particle transport calculation. PHITS is a multi-purpose particle Monte-Carlo transport code. Hence application of PHITS enables us to evaluate doses not only for neutrons and photons but also for protons and heavy ions. Therefore, the JCDS-FX with PHITS can evaluate total doses given to a patient by a combined modality therapy. Moreover, it can be used for the study of accelerator based BNCT. To verify calculation accuracy of the JCDS-FX with PHITS, dose evaluations for neutron irradiation of a cylindrical water phantom and for an actual clinical trial performed at JRR-4 were performed, then the results were compared with calculations obtained from JCDS with MCNP. Calculations of neutron and photon fluxes and of several doses were in good agreement with JCDS calculations, these results demonstrated that JCDS-FX is applicable to BNCT treatment planning in practical use. To apply the new treatment planning system to clinical trials in practical use as soon as possible, further verifications are being performed. We will release the system to the public in the fairly near future.

Keywords: BNCT, treatment planning, Monte-Carlo, PHITS, dosimetry, JRR-4

1. Introduction

Clinical studies of boron neutron capture therapy (BNCT) are being performed at JRR-4 in Japan Atomic Energy Agency (JAEA) (Yamamoto *et al.*, 2004). At JRR-4, first, clinical trial for malignant brain tumor was begun using mixed thermal-epithermal neutron beam in 1999, then BNCT using epithermal neutron beam has been performed since 2003(Matsumura *et al.*, 2004) . Moreover clinical trials for head-&-neck cancer and for pulmonary tumor were also begun in 2004 (Kato *et al.*, 2004).

In the BNCT with mixed thermal-epithermal neutron beam, dose given to a patient was evaluated by measuring the radioactivity of Gold wires located on brain. However, the dosimetry method could not be applied to the epithermal neutron beam BNCT. Therefore, we developed JCDS (JAEA Computation Dosimetry System) as a treatment planning system for BNCT (Kumada *et al.*, 2007). Applying JCDS to treatment planning, we became to obtain detailed information for several doses and an optimum irradiation condition for the patient could be determined in advance. Practical application of JCDS enabled to perform the BNCT with the epithermal neutron beam in JRR-4.

In current BNCT studies in Japan, several trials such as combined modality therapy (BNCT and X-ray therapy), expansion of application for trunk tumor and accelerator based BNCT are being performed. By means of these innovative modalities, BNCT studies will make further progress. However, to deal with these trials, we have to carry further developments for irradiation techniques and dosimetry method. In this framework, a new multi-modal radiotherapy planning system is under development at JAEA. This system (developing code: *JCDS-FX*) builds on fundamental technologies of JCDS. JCDS-FX has several advantages for computational dosimetry work in BNCT as well as several radiotherapy treatments. This system will be released for public use in the fairly near future. Several features and performances of the new multi-modal Monte-Carlo radiotherapy planning system are presented.

2. Material and methods

2.1 JCDS fundamental system of JCDS-FX

JCDS, as fundamental software of the new treatment planning system has been developed by JAEA to perform the treatment planning.

To simulate a neutron irradiation in BNCT, first, JCDS creates a detailed three-dimensional model of a patient using both of CT and MRI image data. Then, to investigate the behavior of neutrons and photons in the model effectively, the detailed model is converted into a voxel one, and several dose components are determined using the voxel model with MCNP (Briesmeister, 2000).

JCDS in the initial version employed a voxel calculation method dividing the space into 10x10x10 mm^3 voxel cells. The current version of JCDS uses as calculation method the "Mesh Tally" function already installed in MCNP-5. The speedup by the application of the Mesh Tally calculation enabled to further downsize the voxel cell size of the calculation model. At present, JCDS can evaluate doses precisely by calculation with 2x2x2mm^3 voxel.

2.2 JCDS-FX

JCDS-FX has several features and advantages compared to JCDS. One of the features in the JCDS-FX development is that PHITS has been applied to particle transport calculation in addition to MCNP (Iwase *et al.*, 2002). Some features of PHITS are described in next section. The application of PHITS to treatment planning enables us to evaluate doses and the distributions for several radiotherapies including BNCT. Moreover a total dose given to a patient by a combined modality therapy as a combination of BNCT and proton therapy can be also evaluated. Furthermore, to study accelerator based BNCT, we are able to perform not only the design of the facility, involving proton accelerator geometry including proton-neutron target source but also a detailed dosimetry including.

Construction process for a patient model and for a voxel model has been improved through the basic technologies of JCDS and was installed to JCDS-FX. For construction process of a patient's model, JCDS-FX can load PET images in addition to CT and MRI images. By using PET data, tumor regions which may be invisible by CT or MRI are picked out properly, and then boron dose distribution can be determined according to the PET value of the region. For the process of creating a voxel model, JCDS-FX makes minute voxel model consisting of pixel based voxel cell or 1x1x1mm^3 voxel cell in addition to the conventional 2mm^3 voxel.

2.3 Feature of PHITS

PHITS, a multi-purpose particle Monte-Carlo transport code is under development by JAEA and other group researchers. The Monte-Carlo code can compute particle behavior not only for neutrons and photons but also protons and heavy ions. For neutron transport, PHITS can calculate high-energy as well as low-energy fields. For transport of the low-energy neutrons and the photons, MCNP technologies have been installed, thus, descriptions in MCNP's input such as "Cell", "Surface" and "Material" are available in PHITS input directly. In case of calculations with same nuclear data of MCNP libraries as ENDF/B, PHITS determines identical values with MCNP calculations. Hence, we can use PHITS for doses calculations in BNCT.

PHITS can generate multiple particles in source definition concurrently, though MCNP generates only one particle. Thus we can make a proper beam source including both neutrons and photons at the patient position, then doses involving primary core gamma-ray dose are able to be evaluated effectively.

2.4 Verification of dose evaluation with PHITS

In this section, verification of performance of JCDS-FX with PHITS is described. In the verification, several calculations using both JCDS with MCNP and JCDS-FX with PHITS were carried out, and each calculation result was compared.

First, to verify the characteristics of dose calculation for PHITS, irradiation condition with a cylindrical water phantom located at irradiation position in JRR-4 was set. In the calculation, neutron beam was selected Epithermal Neutron Beam mode (ENB mode) which is applied to actual BNCT at JRR-4. For definition of neuron beam in MCNP calculation, we applied phase space files (surface source files). Surface source files for each beam mode had been made in previous simulation with "SSW/SSR" function of MCNP. Particle tracks of neutrons and photons are stored in the source files. Location of the surface is shown in Figure 1. Validity of the source of ENB mode has been verified (kumada *et al.*, 2004).

By using the surface source file, calculations of neutron fluxes and several dose components in the phantom were performed accurately. On the other hand, in PHITS calculation, we have newly created a beam source data for the ENB mode in PHITS format. The surface location of the source was matched to the surface of the SSR of MCNP, and the PHITS source can generate neutrons and photons concurrently as described above. In both Monte-Carlo transport calculations, ENDF/B- VI nuclear library data was employed. Neutron and photon distributions and several dose components as Boron dose, Nitrogen dose, Hydrogen dose and gamma-ray dose were determined in the phantom by using MCNP and PHITS respectively.

Figure 1 shows the layout of the irradiation condition with cylindrical phantom.

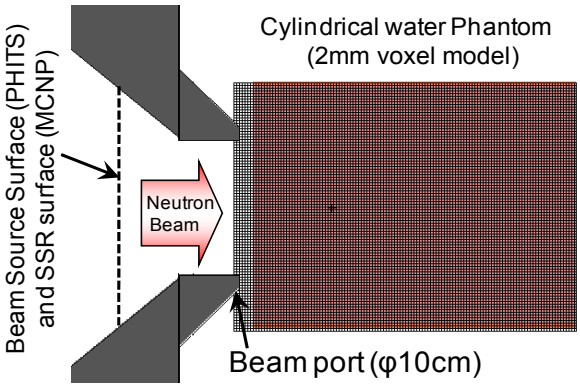

Figure 1 Calculation condition with cylindrical water phantom

Next, to confirm practical utility of JCDS-FX with PHITS for BNCT clinical trial, treatment planning for a real BNCT condition was performed. In the verification, a 3D model of a patient was created using patient's CT and MRI data, then irradiation condition of the actual previous BNCT was reconstructed properly. For PHITS calculation, the voxel model of the patient was constructed by $2mm^3$ voxel cell to match the condition of the treatment planning with JCDS. Figure 2 shows the $2mm^3$ voxel model of PHITS calculation. Several dose components and their distributions in the patient were calculated by PHITS, then total doses for tumor region and for normal tissue region were evaluated by JCDS-FX. The dosimetry results were compared with the dose evaluation results which had been determined by JCDS with MCNP.

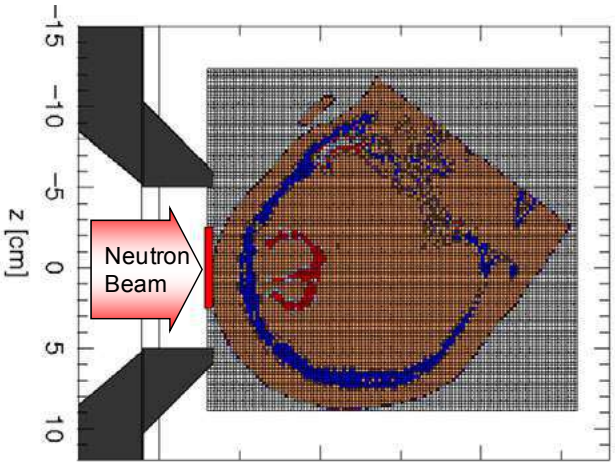

Figure 2 Patient's model created by PHITS

3. Results and discussions

3.1 Comparison results for the dose evaluation for the cylindrical water phantom irradiation

Thermal neutron flux profiles on beam central axis in the phantom are shown in Figure 3-(a) for both MCNP and PHITS calculations. Figure 3-(b) shows the photon flux profiles for each calculation. The profiles of PHITS were comparable to MCNP profiles within statistical errors. The results demonstrated that PHITS can evaluate the fluxes for both neutrons and photons properly. Figure 4-(a) shows boron dose profiles in the phantom for both calculations. For the calculations of the doses generated by neutron reactions such as boron dose and nitrogen dose, MCNP and PHITS use heating number of the ENDF/B-VI. Therefore, the dose profiles for PHITS were in good agreement with the MCNP profiles due to application of same heating number. On the other hand, gamma-ray dose profiles determined by PHITS were approximately 5% lower than MCNP profiles as shown in Figure 4-(b). The gamma-ray dose was determined by respective gamma-ray dose conversion factor installed in each code. Thus the gamma-ray dose depended on conversion factors, even if the photon fluxes were comparable. In fact, the discrepancy of gamma-ray dose is due to the difference of conversion factor. We will arrange the factor in PHITS to a suitable factor for BNCT dosimetry so the conversion factor in PHITS can be changed. At present, intercomparison between JRR-4 and KUR is being performed by collaboration with Kyoto University and JAEA. In the collaborative research, several dose evaluations in same conditions are carried out using both JCDS-FX and SERA, then, dose characteristics for both systems are analyzed. First, common conversion factor in Japan will be determined in the near future.

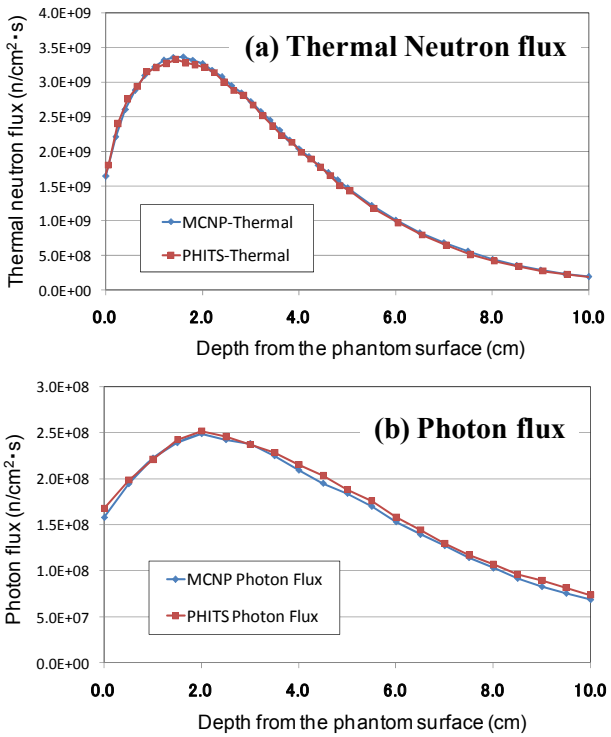

Figure 3 Profiles of thermal neutron flux and photon flux

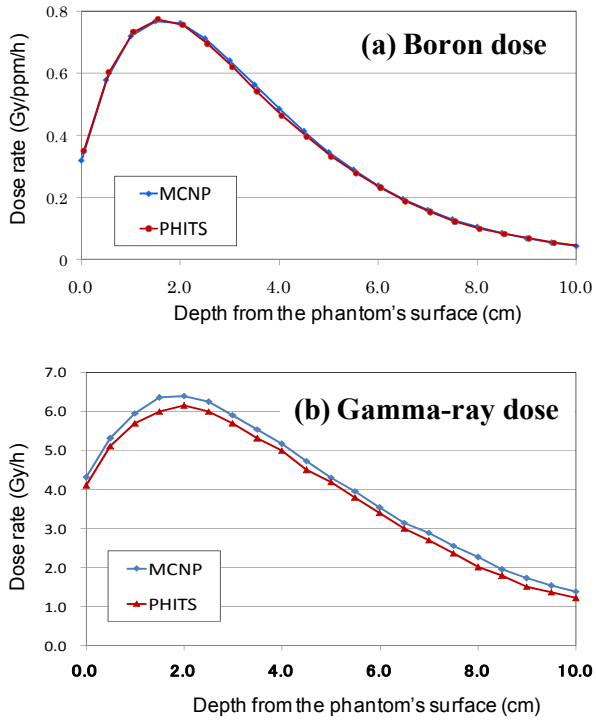

Figure 4 Profiles of dose rate for boron and gamma-ray

3.2 Results of actual BNCT dosimetry using JCDS-FX & PHITS

Figure 5 shows tumor dose distributions on patient MRI images obtained with JCDS-FX and JCDS respectively. Dose distributions around tumor region determined by JCDS-FX & PHITS were in good agreement with the distributions by JCDS & MCNP. For Dose Volume Histogram (DVH) in each treatment plan, the JCDS-FX histograms for several organs as GTV, CTV and brain were comparable to the histograms of the conventional system within each statistical error.

The calculation time of PHITS was with the same as MCNP calculation. By using a parallel computing environment, the time of the PHITS calculation becomes shorter in proportion to the CPU of the system. These results proved that JCDS-FX with PHITS can be applied to treatment planning in actual BNCT trials.

4. Conclusions

A new multi-modal Monte-Carlo radiotherapy planning system is being developed on the basis of fundamental technologies of JCDS. The system has applied PHITS. For calculations for neutron, photon and several doses, PHITS can obtain equivalent values with the MCNP calculations. However for gamma-ray dose calculation, PHITS evaluates lower values approximately 5% than JCDS-MCNP values due to difference of the gamma-ray conversion factor.

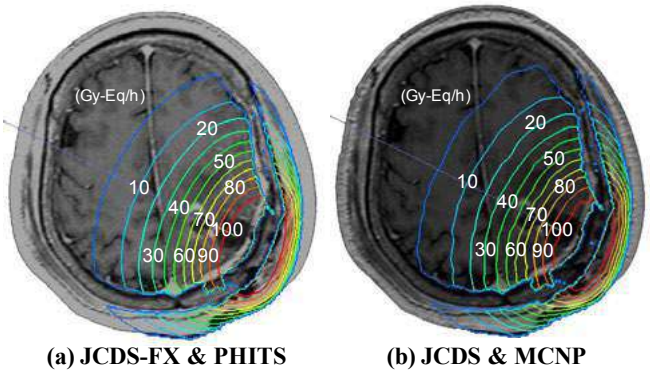

(a) JCDS-FX & PHITS (b) JCDS & MCNP

Figure 5 Comparison of tumor dose distributions

We should standardize the conversion factor, and then common CF data will be employed to all of the treatment planning for BNCT in order to allow inter-comparison of clinical data in the near future.

The comparison results for the treatment planning for the actual BNCT demonstrated that JCDS-FX is applicable to BNCT treatment planning in practical use. To apply the new treatment planning system to the clinical trials in practical use as soon as possible, we are performing further verifications of the system; procedure and structure for distribution of the system for researchers is being prepared.

References

Briesmeister, J. F.(Ed.), 2000, MCNP-A General Monte Carlo Code N-Particle Transport Code Version 4C, *LA-13709-M*

Iwase H., Niita K., Nakamura T., 2002, Development of General-Purpose Particle and Heavy Ion Transport Monte Carlo, *J. Nucl. Sci. Technol.*, 39, 1142-1151

Kato I., Ono K., Sakurai Y., Ohmae M., Matsumura A., et al., 2004, Effectiveness of BNCT for recurrent head and neck malignancies, *Applied Radiation and Isotopes*, 61, 1069-1073

Kumada H., Yamamoto K., Matsumura A., at el., 2007, Development of JCDS, a computational dosimetry system at JAEA for boron neutron capture therapy, *J. Physics: Conf. Series*, 74

Kumada H., Yamamoto K., et al., 2004, Verification of the computational dosimetry system in JAERI (JCDS) for boron neutron capture therapy, *Phys. Med. Biol.*, 49, 3353-3365

Matsumura A., Yamamoto T., Nakai K., Kumada H., Mizutani T., et. al., 2004, The new treatment protocol using epithermal neutron for intraoperative boron neutron capture therapy at JRR-4, *Abstracts of ISNCT-11*, 61

Yamamoto T., Matsumura A., Nakai K., et al., 2004, Current clinical results of the Tsukuba BNCT tria, *Applied Rad. Iso.* **61** 1089-93

Dose calculations with SERA and JCDS treatment planning systems

H. Koivunoro[a,b], H. Kumada[c], T. Seppälä[a], P. Kotiluoto[d], I. Auterinen[d], L. Kankaanranta[b], S. Savolainen[e]

[a]*Department of Physics, POB 64, FI-00014 University of Helsinki, Finland*
[b]*Department of Oncology, Helsinki University Central Hospital, Helsinki, Finland*
[c]*Dept of Research Reactor and Tandem Accelerator, Japan Atomic Energy Agency, Ibaraki 319-1195, Japan*
[d]*VTT Technical Research Centre of Finland, Espoo, POB 1000, FI-02044 VTT Finland*
[e]*HUS Helsinki Medical Imaging Center, University of Helsinki, POB 340, FI-00029 HUS, Finland*

Abstract

Three treatment planning systems developed for clinical BNCT use are SERA developed by INL/Montana State University, NCTPlan developed by the Harvard-MIT and the CNEA group and JCDS developed by JAEA in Japan. Previously, performance of the SERA and NCTPlan has been compared in various studies. In this preliminary study, the dose calculations performed with SERA and JCDS systems were compared in single brain cancer patient case with the FiR 1 epithermal neutron beam. A two-field brain cancer treatment plan was performed with the both codes. The dose components to normal brain, tumor and planning target volume (PTV) were calculated and compared in case of one radiation field and combined two fields. The depth dose distributions and the maximum doses in regions of interest were compared. Calculations with the treatment planning systems for the thermal neutron induced (^{10}B and nitrogen) dose components and photon dose were in good agreement. Higher discrepancy in the fast neutron dose calculations was found. In case of combined two-field treatment plan, overall discrepancy of the total maximum weighted dose was ~3% for normal brain and PTV and ~4% for tumor dose.

Keywords: Treatment planning, dose calculation, MCNP, SERA, JCDS

1. Introduction

The performance of MacNCTPlan (Zamenhof et al. 1996) and bnct-rtpe treatment planning systems (Nigg et al. 1997) have been compared in a phantom study by Goorley et al (2002). Wojnecki and Green (2002) performed a comparison between MacNCTPlan and SERA systems (Nigg et al. 1999, Nigg 2003) (recent version of the BNCT_rtpe) in the phantom geometries. Most recently, Casal *et al.* (2004) compared the calculations performed with the updated version of MacNCTPlan, NCTPlan (González *et al.* 2002), and SERA to the measurements in a phantom at the RA-6 reactor facility. BNCT treatment planning system JAEA Computational Dosimetry System (JCDS) is developed and have been in clinical use at Japan Atomic Energy Agency (JAEA) (Kumada et al. 2004). The calculations with JCDS have been compared to measurements and to the calculations with a general Monte Carlo n-particle code MCNP (Briesmeister 2000). To date JCDS has not been compared to other BCNT treatment planning systems.

JCDS and NCTPlan systems use MCNP code as a computational tool. MCNP uses pointwise continuous-energy cross-section libraries, whereas SERA system uses multigroup neutron and photon cross-sections. Another notable difference between the codes is that SERA produces a patient model using pixel-by-pixel uniform volume element ('univel') reconstruction method, while JCDS and NCTplan use the voxel reconstruction method for patient modelling. In the latest version of JCDS, MCNP5 is used with the mesh tally option, which has enabled more accurate calculations, since the voxel size in a patient model can be scaled down without increasing the simulation time dramatically (Kumada et al. 2007). In this study, the treatment planning calculations with SERA and JCDS programs are compared in a clinical BCNT case using the FiR 1 epithermal beam.

2. Material and methods

The dose calculations with JCDS and SERA treatment planning systems were performed for one brain cancer patient using FiR 1 epithermal neutron beam following the Finnish treatment planning protocol of BPA mediated BNCT for the recurrent brain tumors (Protocol FIN-BNCT-03, www.clinicaltrials.gov) (Joensuu et al. 2003).

The 3D patient model in SERA was created using 48 T1 weighted MR image slices of the patient imaged from the top of the head to the neck, with pixel size of 1 mm and slice thickness of 5 mm. The skin, brain, cranium, sinuses, tumor, edema and planning target volume ('PTV', including tumor, edema and marginal of about 2 cm) were segmented in the patient model and the tissue material compositions were defined according to ICRU Report 46 (ICRU 1992). The 'univel' patient model created by SERA was converted into grayscale images in order to reconstruct the same model with JCDS. In SERA calculations, the default size (1 cm^3) voxel was used in the simulation edit mesh. The JCDS patient model was created with the 2×2×2 voxels (mm) and the element size of 5×5×5 mm was applied in the edit mesh.

Two circular (ø 14 cm) (anterior and posterior to the patient) neutron fields were used in the treatment planning (Fig. 1). In the dose calculations, the weighting factors were obtained from the Brookhaven clinical trials (Chanana et al. 1999): 3.2 for hydrogen and nitrogen dose of Brook's brain material composition (corresponding to 3.16 for hydrogen and 2.68 for nitrogen in the ICRU brain material), 1.3 for ^{10}B in brain and 3.8 for ^{10}B in tumor. The ^{10}B concentration of 19 ppm in brain and 66.5 ppm in tumor was used. Exactly same FiR 1 neutron beam model (Serén *et al.* 1999, Seppälä 2002) created with the DORT code (Rhoades and Childs 1988) was used in both SERA and JCDS calculations. Only proton recoil reaction induced 'hydrogen dose' was included in the fast neutron dose calculations with the both codes. In SERA calculations, a neutron calculation of 50 million simulation particles was performed following by a biased fast neutron calculation and gamma calculation (including beam photons and neutron induced gammas). About 100 million simulation particles were used in the JCDS calculations. All the results are normalized by the Au reaction rate measurement at the thermal neutron flux maximum (2 cm) depth in PMMA phantom. Slightly different normalization factors were obtained for SERA and JCDS (0.94 and 0.956 respectively). The calculation results were compared in case of one single radiation field (the anterior field, 'field 1') and combined fields. For optimal treatment plan of the combined fields, irradiation time of the anterior and the posterior field was weighted 65:35 respectively.

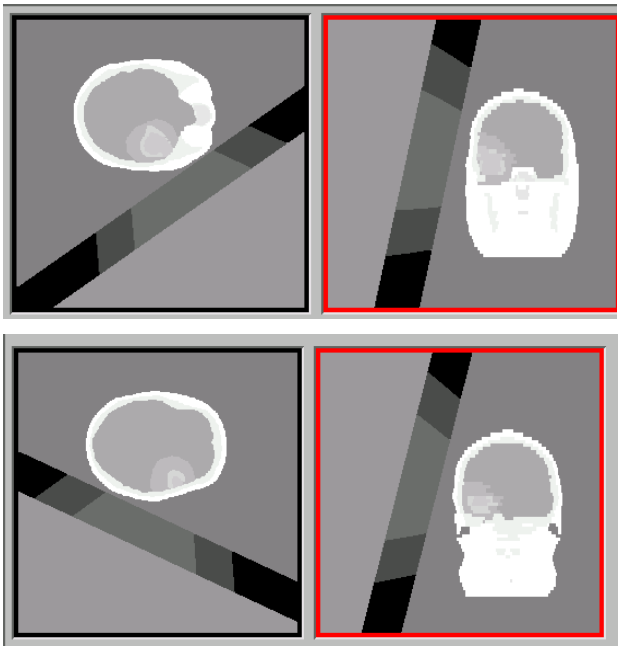

Fig. 1. The beam orientations used in the treatment planning calculations: for field 1 upper and for field 2 lower two images

3. Results and Discussion

The depth profile along the beam centerline in the patient calculated with the both codes for the anterior field 1 are shown in figure 2 for nitrogen dose, figure 3 for fast neutron dose, figure 4 for photon dose and figure 5 for thermal neutron fluence. The 'peak' showing in the depth dose curve at depths of about 1.1-1.9 cm in figures 2 and 3 is due to fact that the dose is calculated for ICRU skeleton cranium (5.0 weight-% hydrogen and 4 weight-% of nitrogen) at the location of skull in the patient model. Elsewhere the dose is calculated for ICRU brain (10.7 weight-% of hydrogen and 2.2 weight-% of nitrogen) at every point regardless of the real material in the patient model.

Difference between the JCDS and SERA calculation results for two combined neutron fields in regions of interest (brain, PTV and tumor) for photon, fast neutron (proton recoil), ^{10}B, nitrogen and total maximum doses are shown in table 1.

Overall discrepancy of the total maximum weighted dose was ~3% for the normal brain and PTV and ~4% for the tumor dose. The large (up to 22%) discrepancy in fast neutron dose have only a small effect on the total weighted dose since the fast neutron dose covers only about 1% of the total maximum tumor and PTV doses and 6% of the total maximum brain dose in FiR 1 beam. Over 90% of the total tumor and PTV doses and 94% of the total brain dose is produced by the thermal neutron induced dose components (^{10}B, nitrogen and induced photon dose) and thus accurate calculation of the thermal neutron component can be considered the most important.

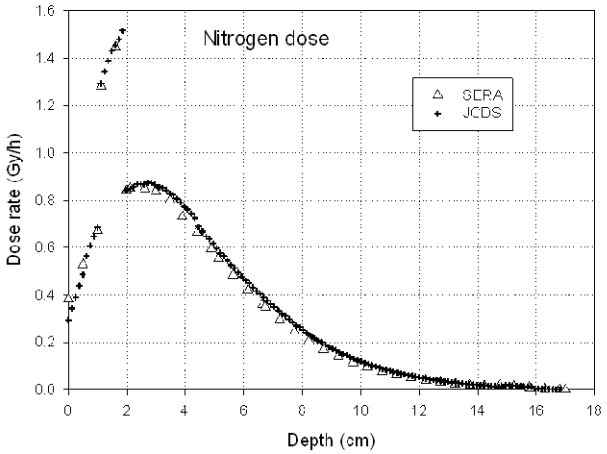

Fig. 2. *Weighted nitrogen dose for anterior field 1 in the patient along the neutron beam (ø 14 cm) axis calculated with SERA and JCDS*

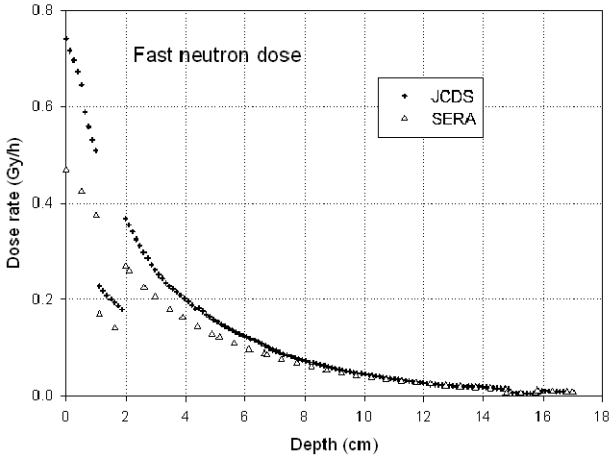

Fig. 3. Weighted fast neutron (proton recoil) dose for anterior field 1 in the patient along the neutron beam (ø 14 cm) axis calculated with SERA and JCDS

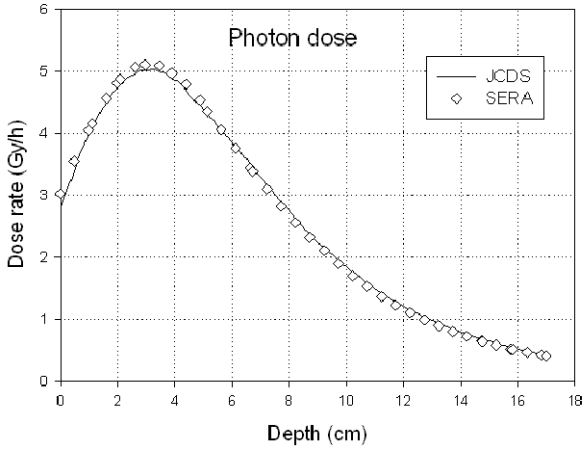

Fig. 4. Total photon dose for anterior field 1 in the patient along the neutron beam (ø 14 cm) axis calculated with SERA and JCDS

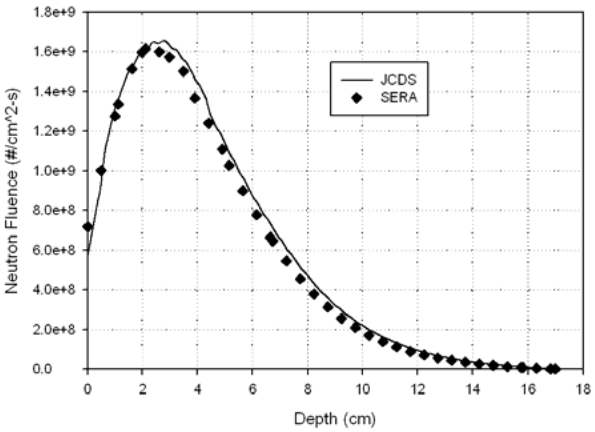

Fig. 5. Thermal neutron fluence (E < 0.53 eV) for anterior field 1 in the patient along the neutron beam (ø 14 cm) axis calculated with SERA and JCDS

Table 1. The percentage differences in dose rates between JCDS and SERA results in case of two-field treatment plan for maximum photon (D_γ), fast neutron (D_{fast}), ^{10}B (D_B), nitrogen (D_N) and total (D_{total}) dose in brain, PTV and tumor volumes. D_B is calculated for 19 ppm of ^{10}B in brain and 66.5 ppm of ^{10}B in tumor and PTV

	D_γ	D_{fast}	D_B	D_N	D_{total}
Brain	90%	78%	99%	97%	97%
PTV	95%	82%	104%	101%	103%
Tumor	95%	83%	104%	102%	104%

Since the fast neutron (E > keV) flux of the FiR 1 beam, is very low (2.9% of total with the 14 cm beam (Serén et al. 1999)), long simulation time is required to obtain low statistical error in the Monte Carlo calculations.

The statistical error of the fast neutron dose calculations with JCDS was <5%. The statistical error is not provided by SERA system, but 50 million particle histories have been found sufficient number to obtain stable dose calculation results for all the BNCT dose components at the 2 cm depth in a phantom (Seppälä 2002). Our result for fast neutron dose difference between the codes is in agreement with the previous studies considering SERA and MCNP or NCTPlan calculations (Casal et al. 2004, Goorley et al. 2002, Albritton 2001).

The underestimation of SERA fast neutron dose has been suggested to be due to different cross-section libraries used in SERA (ENDF/B-IV) and MCNP (ENDF/B-VI or VII), different forms of

cross-sections used (multigroup energy in SERA and continuous energy in MCNP) and due to fact that also other fast neutron dose components than proton recoil dose has been included in the fast neutron dose in NCTPlan calculations (unlike in this study).

4. Conclusions

In this study, the dose calculations performed with SERA and JCDS treatment planning systems were compared in a brain cancer patient case using FiR 1 epithermal neutron beam. We compared the dose components in case of two-field brain cancer treatment plan and one individual neutron field. The calculated thermal neutron flux and the thermal neutron induced dose components (^{10}B and nitrogen dose) agreed well (within 4%) with each other. The difference with the photon dose was larger (5-10%). The largest (17-22%) difference between the JCDS and SERA results was found with the fast neutron (proton recoil) dose.

References

Albritton, J.R., 2001. Analysis of the SERA treatment planning system and its use in boron neutron capture synovectomy. M.S. Thesis, Massachusetts Institute of Technology.

Briesmeister, J.F., editor 2000. MCNP - A general Monte Carlo Code N-particle transport code, Version 4C, Report LA-13709 (Los Alamos National Laboratory).

Casal, M. R., González, S. J., Blaumann, H. R., et al., 2004. Comparison of the performance of two NCT treatment planning systems using the therapeutic beam of the RA-6 reactor. Appl. Radiat. Isot. 61: 805-10.

Chanana, A. D. *et al.,* 1999. Boron Neutron Capture Therapy for Glioblastoma Multiforme: Interim Results from the Phase I/II Dose-Escalation Studies, Neurosurgery 44 (6): 1182-1192.

González, S. J., Carando, D. G., Santa Cruz, G.A., et al., 2005. Voxel model in BNCT treatment planning: performance analysis and improvements. Phys. Med. Biol. 50: 441-58.

Goorley, J. T., Kiger, W.S. 3rd and Zamenhof, R. G., 2002. Reference dosimetry calculations for neutron capture therapy with comparison of analytical and voxel models. Med. Phys. 29: 145-56.

ICRU, 1992. Radiation Dosimetry: Electron Photon, Electron, Proton and Neutron Interaction Data for Body Tissues, Report 46. Bethesda, MD. (ICRU).

Joensuu, H., Kankaanranta, L., Seppälä, T., et al., 2003. Boron neutron capture therapy of brain tumors: clinical trials at the finnish facility using boronophenylalanine. J. Neurooncol. 62: 123-34.

Kumada, H., Yamamoto, K., Matsumura, A., et al. 2004. Verification of the computational dosimetry system in JAERI (JCDS) for boron neutron capture therapy. Phys. Med. Biol. 49: 3353-65.

Kumada, H., Yamamoto, K., Matsumura, A., et al., 2006. Improvement of JCDS, a computational dosimetry system in JAEA for neutron capture therapy. In: Nakagawa Y, Kobayashi T and Fukuda H, Ed. Advances in Neutron Capture Therapy 2006, Proceedings of ICNCT-12, Takamatsu Japan October 9-13: 474-477.

Nigg, D. W., Wheeler, F. J., Wessol D. E., et al., 1997. Computational dosimetry and treatment planning for boron neutron capture therapy. J. Neurooncol. 33: 93-104.

Nigg, D. W., Wemple, C. A., Wessol D. E., *et al.,* 1999. SERA - an advanced treatment planning system for neutron therapy and BNCT. Trans. Am. Nucl. Soc. 80: 66-8.

Seppälä, T., 2002. FiR 1 Epithermal Neutron Beam Model and Dose Calculation for Treatment Planning in Neutron Capture Therapy, Ph.D. thesis. Report Series in Physics, HU-P-D103. Helsinki, Finland: University of Helsinki.

Serén, T., Auterinen, I., Seppälä, T., Kotiluoto, P., 1999 Spectrum measurements and calculations in the epithermal neutron beam at the FiR 1 BNCT facility. In: 15th European Triga Conference, VTT Symposium 1997. Salmenhaara, S. (Ed). Espoo Libella: 167-79.

Rhoades, W. A. and Childs, R. L., 1988. The DORT Two-Dimensional Discrete Ordinates Transport Code Nucl. Sci. Eng. 99: 88-89.

Wojnecki, C., and Green, S., 2002. A preliminary comparative study of two treatment planning systems developed for boron neutron capture therapy: MacNCTPlan and SERA. Med. Phys. 29: 1710-5.

Zamenhof, R., Redmond, E. 2nd, Solares, G., et al., 1996. Monte Carlo-based treatment planning for boron neutron capture therapy using custom designed models automatically generated from CT data. Int. J. Radiat. Oncol. Biol. Phys. 35: 383-97.

Comparison of different MC techniques to evaluate BNCT dose profiles in phantom exposed to various neutron fields

E. Durisi[a,b], H. Koivunoro[c,d], O. Borla[e], E. Gallio[a,b], U. Nastasi[f] and A. Zanini[b]

[a] *Experimental Physics Department, University of Torino, Via P. Giuria 1, 10125 Torino (Italy)*
[b] *INFN Torino, Via P. Giuria 1, 10125 Torino (Italy)*
[c] *Boneca Corporation, FIN-00029 HUS, Helsinki (Finalnd)*
[d] *Department of Physical Sciences, University of Helsinki, P.O .Box 64, FI-00014 Helsinki University, (Finland)*
[e] *Institute for scientific interchange foundation Torino (Italy)*
[f] *AOU San Giovanni Battista Hospital Torino, Via Cavour 31, 10123 Torino (Italy)*

Abstract

The absorbed dose in BNCT (Boron Neutron Capture Therapy) consists of several separate radiation components (gamma dose, neutron dose, proton dose and boron dose), with different physical properties and biological effectiveness. In order to assess the clinical efficacy of the beams used for the therapy, determining the dose profiles in tissue, Monte Carlo (MC) techniques are used. This paper presents a comparison between dose profiles calculated along the beam axis inside different phantoms with two techniques: Monte Carlo radiation transport code MCNP-4C2 and BNCT treatment planning program SERA (Simulation Environment for Radiotherapy Application). In this study MCNP is used as a reference tool. A preliminary test of SERA is performed using six mono-directional and mono-energetic beams (size 10x10cm^2) directed onto a simple water phantom. Then, in order to deeply investigate the effect of the different cross section libraries and of the dose calculation methodology, mono-energetic and mono-directional beams directed toward a standard Snyder phantom are simulated. Neutron attenuation curves and dose profiles are calculated with both MC codes and the results are compared. The neutron attenuation results show an agreement within 18% for energies between 1keV-100keV while greater differences are observed at 25meV and 1MeV.

Keywords: Boron Neutron Capture Therapy, dose calculation, MCNP, SERA

1. Introduction

Beams commonly used in BNCT (IAEA, 2001) include contributions by fast, epithermal and thermal neutrons, as well as gamma rays from the neutron source and from capture and inelastic scattering of neutrons in the moderator structure. In addition to this incident radiation further high and low LET radiation components are produced within the patient body such as boron (^{10}B) disintegration products (α, ^{7}Li), recoil protons from the interaction of fast and epithermal neutron with hydrogen, protons from nitrogen capture reaction and gamma rays from hydrogen capture reaction. Therefore, at every tissue location, the total physical dose consists of several separate radiation components (gamma dose D_γ, neutron dose D_n, proton dose D_p and boron dose D_B), with different physical properties and biological effectiveness. To predict the biological effect every dose contribution needs to be multiplied by its corresponding weighting factor (Coderre et al., 1999).

Monte Carlo techniques based, for example, on MCNP code are widely used to design and optimize neutron beams for BNCT. This requires the calculation of free beam parameters, dose profiles and in-phantom figures of merit. In order to get a neutron beam suitable for the treatment these values must be comparable with the recommended standards (IAEA, 2001). Moreover, in view of clinical treatments it could be useful to investigate the dose distributions inside a patient by means of specific Treatment Planning System especially developed for BNCT.

This work proposes to compare the basic features of MCNP-4C2 (Briesmeister, 2000), chosen as reference tool, and SERA (Wessol et al., 2002), developed by the INEEL/Montana State University group, in order to investigate the effects of the different cross section libraries and of the dose

calculation methodology (Albritton et al., 2006). Six mono-directional neutron beams with energies of 0.025eV, 1keV, 5keV, 10keV, 100keV and 1MeV are simulated and depth dose profiles are calculated inside a Snyder head phantom filled with water and inside a standard Snyder head already implemented in SERA.

2. Materials and Methods

A neutron source of 10x10 cm^2, with an intensity of 10^9 cm^{-2} s^{-1}, is implemented in both MC codes. A 5cm thick lithiated polyethylene delimiter is placed in front of the neutron source, and the neutrons are directed through a 10x10cm^2 beam aperture to the head phantom placed at the 5 cm distance from the beam aperture plane (Fig. 1).

Fig. 1 Cross section of the beam collimator and Snyder phantom from the top view

In the first set of simulations the phantom is filled with water, while in the second one skin, skull and brain compositions are defined as ICRU report 46 (International Commission on Radiation Units and Measurements, 1992) values for adult patient. The depth neutron attenuation curves and the depth dose profiles are calculated with both MC codes along the beam axis.

MCNP-4c2 uses pointwise continuous-energy neutron and photon cross sections based on the ENDF/B-VI data library. The S(α,β) treatment is included in all simulations to treat the chemical binding effects of hydrogen in biological materials. On the contrary, the electron transport is not taken into account in a first instance. Neutron fluence rates (tally F4) are calculated averaging over small tally volume cells (4x4x0.2cm^3) and the dose components are assessed using MCNP tally multiplier facility. The gamma dose is assessed by means of tally F6: energy deposition averaged over a cell. In the second set of simulations the ^{10}B concentration for boronphenylalanine (Coderre et al., 1999) is assumed to be 15ppm in the skin, 0 in the skull and 10ppm in brain. These concentrations are included in MC transport simulations although such levels of ^{10}B do not perturb the neutron fluence. A mean (high LET) energy release of 2.34 MeV is assumed for $^{10}B(n,\alpha)^7Li$ reaction. In order to evaluate the biological dose, weighting factors 1 for D_γ and 3.2, (w_γ and w_n) for both D_n and D_p are used. To calculate the biological boron dose, a weighting factor (w_B) of 1.3 is used in the brain, while 2.5 is employed in the skin.

SERA code uses a reconstruction technique based on a pixel by pixel uniform volume element (univel). However in this case the phantom geometry is simply defined in terms of intersections and/or unions of solid geometric shapes and included in Combinatorial Geometry (CG) file. The radiation transport calculation is based on a tailored Monte Carlo code (seraMC) specifically designed for BNCT, based on multigroup neutron and photon cross sections. The neutron and photon cross section data are taken from ENDF/B-V libraries and are pre-processed into 94 neutron energy group: 22 thermal neutron group, 40 epithermal neutron group and 32 fast neutron group. The source file requires, as input, the spectral and angular distributions of the incident neutron current from a planar square source. Therefore, the monoenergetic beam is obtained using narrow energy bins, while the monodirectionality is obtained with a narrow cosine bin spanning from 0.999990 to 1.0 as demanded by the code (Wojnecki, 2002). Neutron fluence is tallied along the beam axis in 1cm^3 voxels. The absorbed doses are calculated from the kerma factors for each radiation component. Finally in order to get the biological dose the above mentioned weighting factors are used.

3. Results and discussion

The results reported in this section are obtained processing 10^7 particles in both codes. In the first set of simulations a simple water phantom, shaped as Snyder head, is used. Fig. 2 shows the total neutron fluence rate and the thermal component in the

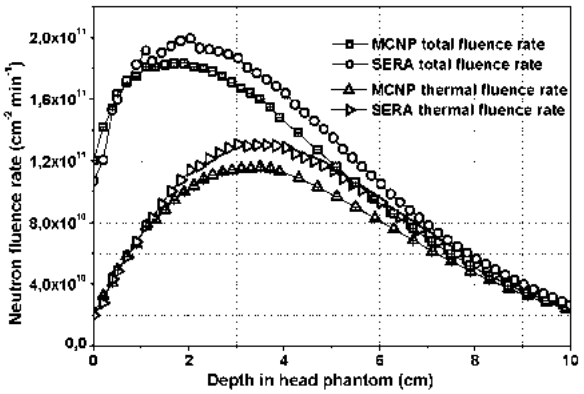

Fig. 2. Monoenergetic and monodirectional neutron beam of 5 keV. Neutron fluence rate components are calculated in water phantom along the beam axis

phantom along the beam axis obtained with MCNP and SERA using a neutron beam of 5 keV. The uncertainties, reported only in MCNP results, are stochastic and represent one standard deviation. The maximum difference is 14% for the total neutron fluence rate at 5.1 cm and 16% for the thermal neutron component at 4.7 cm. The discrepancies are due not only to the different cross section libraries but also to the tally volume size (MCNP: 3.2cm^3 vs SERA: 1cm^3). The reduction of MCNP tally cells size could improve the agreement but it would increase the computing time.

Tab. 1 summarizes the results obtained with the other monoenergetic and monodirectional beams. A general good agreement between MCNP and SERA is evident for neutron beams of 1keV-100keV. Elsewhere the greater discrepancy is due to the differences in the total cross sections used by the two codes for water (as reported by Wojnecki, 2002).

Tab. 1. Maximum % difference between neutron fluence calculated along the beam axis in the water phantom with MCNP and SERA

E_n (keV)	Max diff. Φ_{total}	Depth (cm)	Max diff $\Phi_{thermal}$	Depth (cm)
25E-6	40%	1.1	40%	1.1
1	15%	5.9	16%	5.9
5	**14%**	**5.1**	**16%**	**4.7**
10	15%	8.3	16%	4.7
100	12%	5.9	14%	4.7
1E3	33%	9.9	34%	9.9

Since different methods are used to assess the dose components (tally multiplier in MCNP, kerma factors in SERA) it is interesting to compare their profiles. A maximum difference of 11% is obtained in the gamma dose profile at 4.7 cm (Fig. 3), this is in agreement with the discrepancy in the thermal neutron fluence rate.

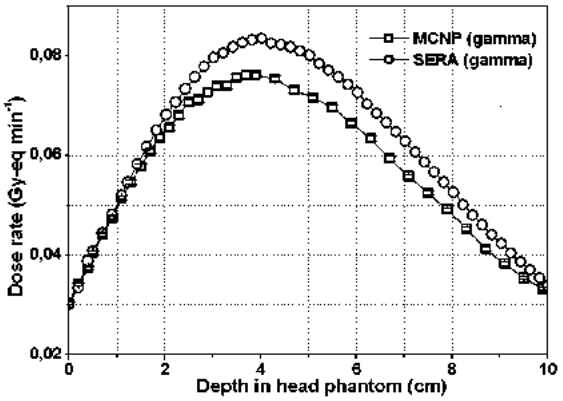

Fig. 3. Monoenergetic and monodirectional neutron beam of 5 keV. Gamma dose rate calculated in water phantom along the beam axis

Concerning the other dose components (Fig. 4), a maximum difference of -97% due to the different dose calculation method is obtained at 9.5 cm. At this depth these components are negligible in comparison to the gamma contribution, in fact the total doses are in agreement within 9%.

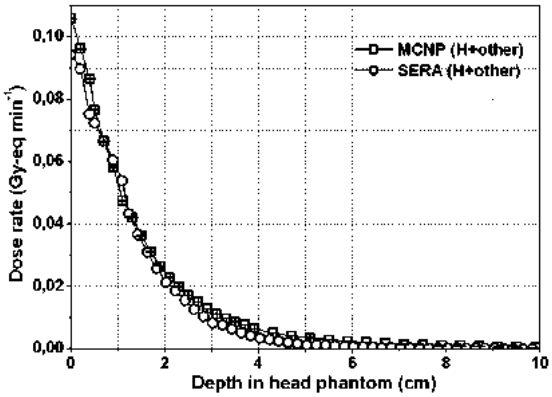

Fig. 4. Monoenergetic and monodirectional neutron beam of 5 keV. Hydrogen and Oxygen dose rate calculated in water phantom along the beam axis

Tab. 2 shows the results carried out with the other monoenergetic and monodirectional beams. The differences in the gamma doses are most likely due to the discrepancy in the thermal neutron fluence as explained above. At 25meV SERA does not provide any H and O dose because kerma factors are zero. Limitations are also encountered up to 100keV, however the differences due to H and O dose calculation methodologies does not affect significantly the total dose rate. At 1MeV the differences increase due to the different cross sections.

Tab. 2. Maximum % difference between the dose components calculated along the beam axis in the water phantom with MCNP and SERA

E_n (keV)	Max diff. Dγ	Depth (cm)	Max diff D_{H+O}	Depth (cm)	Max diff. D_{total}	Depth (cm)
25E-6	25%	6.6	-100%	-	24%	6.3
1	13%	5.1	-99%	8.3	11%	5.1
5	**11%**	**4.7**	**-97%**	**9.5**	**9%**	**4.7**
10	14%	5.9	-93%	9.9	11%	5.9
100	10%	6.7	-39%	9.9	-9%	0
1E3	27%	7.9	24%	8.7	-25%	9.5

In order to deeply investigate these tasks the same calculations are performed with a standard Snyder phantom. The neutron fluence rates results are summarized in Tab. 3. The obtained data are comparable with the ones presented above, showing significant differences only at lowest and highest energies due to the different cross section libraries.

Tab. 3. Maximum % difference between the neutron fluence calculated along the beam axis in the standard Snyder phantom with MCNP and SERA

E_n (keV)	Max diff. Φ_{total}	Depth (cm)	Max diff $\Phi_{thermal}$	Depth (cm)
25E-6	43%	9.5	43%	1.1
1	18%	5.9	21%	3.1
5	**18%**	**5.9**	**20%**	**3.9**
10	18%	5.9	18%	4.7
100	14%	5.9	19%	5.1
1E3	41%	9.9	42%	6.3

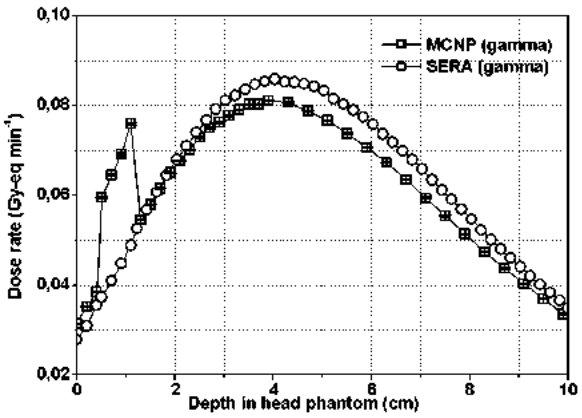

Fig. 5. Monoenergetic and monodirectional neutron beam of 5keV. Gamma dose rate calculated in Snyder phantom along the beam axis

Elsewhere the agreement could be improved reducing the MCNP tally volume sizes. As far as the dose profiles are concerned, the differences increase showing a strong influence of the cross sections and of the dose calculation method. Fig. 5 shows the comparison between gamma dose profiles calculated in Snyder head using 5 keV neutron beam. The agreement is satisfactory (9% at 5.9 cm) except in the skull where the different cross sections contribute to increase the gamma dose in MCNP. Similar behavior is noticed for the other neutron beam energies.

On the contrary, SERA overestimates (around 25% at 4.7 cm) the nitrogen dose everywhere and the differences increase in the skull as it is shown in Fig. 6. Concerning the boron dose, as expected the maximum dose corresponds to the position of the thermal neutron peak. Differences within 23% are obtained and are mainly due to the differences in the thermal neutron fluence.

4. Conclusions

In both sets of simulations SERA overestimates the neutron fluence rate and the thermal neutron component along the beam axis inside the phantom: 16% for neutron beams 1keV-100keV, greater differences at 25meV and 1MeV. This could be explained by the different cross section library used in the codes and by the difference tally volume sizes. In particular MCNP provides an average dose value on the volume cell and its reduction would increase the dose, improving the agreement between the codes. The differences in the thermal neutron components affect the gamma dose results as well as the boron dose ones (in the second set of simulations). Concerning the other components, the different methods to assess the dose do not affect in a significant way the results presented inside the water phantom while they become important when biological tissue is simulated.

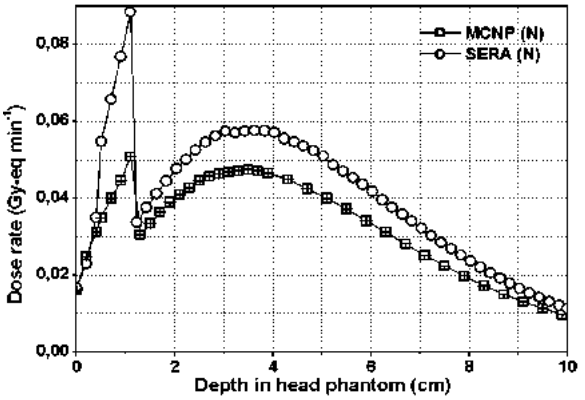

Fig. 6. Monoenergetic and monodirectional neutron beam of 5keV. Nitrogen dose rate calculated in Snyder phantom along the beam axis

References

Albritton, J.R., et al., 2006. Development of reference problems for neutron capture therapy treatment planning systems. Proceeding of ICNCT-12, 496-499.

Briesmeister, J.F., editor 2000, MCNP-A General Monte Carlo N-Particle Transport Code Version 4C, LA-13709.

Coderre, J.A., et al. 1999. REVIEW The Radiation Biology of Boron Neutron Capture Therapy. J. Rad. Res. 151**,** 1-18.

IAEA (International Atomic Energy Agency) 2001. Current status of neutron capture therapy, TECDOC-1223 Vienna.

International Commission on Radiation Units and Measurements, Photon, electron, proton and neutron interaction data for body tissues, Report 46, Bethesda, MD 1992.

Wessol, D.E., et al., 2002. SERA: Simulation Environment for Radiotherapy Applications User's Manual version 1C0. INEEL/EXT-02-00698.

Wojnecki, C. and Green, S., 2002. A preliminary comparative study of two treatment planning systems developed for boron neutron capture therapy. Med Phys 29 (8), 1710-1715.

Assessment of dose rate scaling factors used in NCTPlan treatment planning code for the BNCT beam of THOR

F.Y. Hsu[a], M.T. Liu[b], C.J. Tung[c], Y.W. Hsueh Liu[d], C.C. Chang[c], H.M. Liu[a] and F.I. Chou[a]

[a]*Nuclear Science Technology and Development Center, National Tsing Hua University, Taiwan*
[b]*Department of Radiation Oncology, Changhua Christian Hospital, Taiwan*
[c]*Department of Biomedical Engineering and Environmental Sciences, National Tsing Hua University, Taiwan*
[d]*Department of Engineering and System Science, National Tsing Hua University, Taiwan*

Abstract

Tsing Hua Open-pool Reactor (THOR) at Tsing Hua University in Taiwan has been used to investigate the feasibility and to enhance the technology of boron neutron capture therapy (BNCT) for years. A rebuilt epithermal beam port for BNCT at THOR was finished in the summer of 2004, then researches and experiments were performed to hasten the first clinical treatment case of BNCT in Taiwan in the near future. NCTPlan, a Monte Carlo-based clinical treatment planning code, was used to calculate the dose rate distributions of BNCT in this work. A self-made Snyder head phantom with a servo-motor control system was irradiated in front of the THOR BNCT beam exit. The phantom was made from a 3 mm shell of quartz wool impregnated with acrylic casting resin mounted on an acrylic base, and was filled with water. Gold foils (bare and cadmium-covered) and paired ion chambers (one with graphite wall and filled with CO_2 gas, another with A-150 plastic tissue equivalent wall and filled with tissue equivalent gas) were placed inside the Snyder phantom to measure and estimate the depth dose distributions in the central axis of the beam. Dose components include the contribution of thermal neutrons, fast neutrons, photons and emitted α particles from $^{10}B(n,\alpha)^{7}Li$ reaction. Comparison and analysis between computed and measured results of depth dose distributions were made in this work. Dose rate scaling factors (DRSFs) were defined as normalization factors derived individually for each dose component in the BNCT in-phantom radiation field that provide the best agreement between measured and computed data. This paper reports the in-phantom calculated and experimental dosimetry and the determined DRSFs used in NCTPlan code for the BNCT beam of THOR.

Keywords: BNCT, THOR, NCTPlan, Scaling factor, treatment planning

1. Introduction

An epithermal neutron test beam of Tsing Hua Open-Pool Reactor (THOR) was constructed in 1998 to investigate the feasibility of boron neutron capture therapy (BNCT). A rebuilt epithermal beam port for BNCT at THOR was finished in the summer of 2004, then researches and experiments were performed to hasten the first clinical treatment case of BNCT in Taiwan in the near future.

Dosimetry in BNCT is a complex task because it involves a mixed field of photons, thermal neutrons, fast neutrons, and neutron-induced alpha particles from boron-10 (Rogus et al., 1994). A self-made ellipsoidal head (Snyder) phantom (Harling et al., 1995) and a servo motor system were manufactured to assess the depth-doses. Depth-dose distributions for the BNCT beam for all the above dose components were measured in the phantom system using foil activation and dual ion chamber techniques.

A Monte Carlo-based clinical treatment planning code, NCTPlan (González et al., 2002, and Hsu et al., 2002), was used to compute dose-rate distributions for the THOR BNCT beam within the self-made physical Snyder phantom. Dose-rate scaling factor (DRSF) is defined here as normalization factor derived individually for each dose component in a BNCT in-phantom radiation field that provides the best agreement between measured and computed data. If measured and computed dose-rates completely agree, the corresponding DRSF would be 1. Once the DRSF for each dose component was estimated and applied in the NCTPlan treatment planning code, the computed dose-rate is brought

into optimal agreement with the measured dose-rate. DRSF values for the THOR BNCT test beam had been estimated and published in 2004 (Hsu et al., 2004). In the present work, the comparison between the in-phantom calculated and experimental dosimetry and the derived DRSFs obtained with the newest THOR BNCT beam were reported.

2. Materials and Methods

Dose components of BNCT include thermal neutrons (thermal), fast neutron (fast), photons (photon), and neutron-induced alpha particles from boron-10 (B-10). The depth-dose-rate distributions in central-axis, for each dose component, within physical and calculated versions of the ellipsoidal head phantom irradiated by the newest THOR beam were assessed by measurement and by computation using the NCTPlan code. A photograph of the physical self-made Snyder phantom used for the measurements is shown in figure 1 (left). The phantom was made of a 3 mm shell of quartz wool impregnated with acrylic casting resin mounted on a acrylic base, and was filled with water. A servo motor system was manufactured to assist the depth-dose measurements and to save the gathering time efficiently. A set-up of the servo motor system with the Snyder phantom is shown in figure 1 (right).

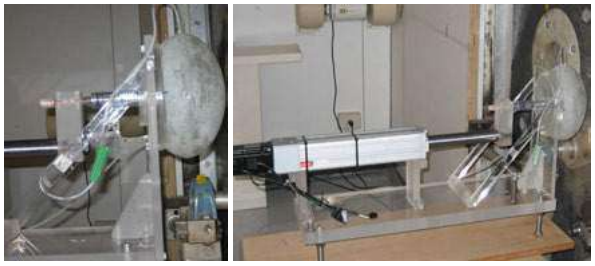

Figure 1. The self-made ellipsoidal head (Snyder) phantom (left), and the servo motor system (right)

Thermal neutron fluxes were measured using the saturated activity of bare and cadmium-covered gold foils (American Society for Testing and Materials, 1998). Thermal neutron fluxes were then converted to tissue (ICRU brain) or boron-10 dose-rates using appropriate kerma factors (ICRU, 1992 and 2000). Fast neutron and photon dose-rates were measured using paired ion chambers (IC-18WP and IC-18GWP, Far West Technology), one with graphite wall and CO_2 gas, the other with A-150 plastic tissue-equivalent (TE) wall and TE gas filling, and both with active volumes of 0.1 ml. Measurements were performed at 1 MW reactor power, with the Snyder phantom located at 10 cm apart from the physical exit plane of the beam.

For computing the doses in NCTPlan, a 14 cm diameter source model of the newest THOR BNCT beam was prepared from THOR Monte Carlo simulations using MCNP code. Corresponding dose-rates were computed using the NCTPlan code, assuming the same elemental material compositions as for the measurements. The experimental and computational irradiation conditions were made as similar as possible in order to permit a valid set of DRSF values to be derived. CT scans of the physical ellipsoidal head phantom were used as the anatomical input to NCTPlan. DRSF values were then calculated for each dose components. Figure 2 presents the beam direction assignment as shown in NCTPlan. The vertical central lines (red and blue) indicate the central axis of the beam. The dashed (red) line in the right image indicates the central line of CT image.

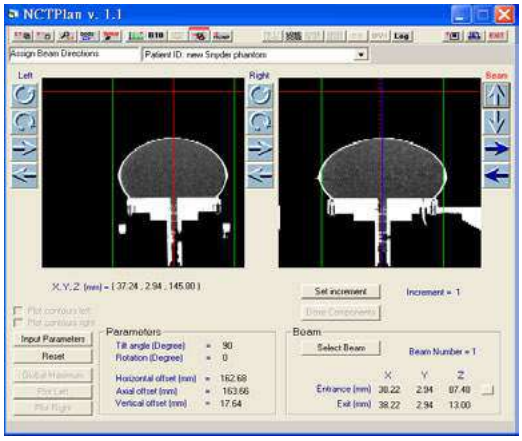

Figure 2. NCTPlan beam direction assignment function applied to the CT images of the ellipsoidal head phantom

The adjusted computed dose, D_{adj} (dose component), at any position within the ellipsoidal head phantom was then given by equation 1 to 4. For boron-10 dose-rates, boron-10 concentrations of 7.5μg/g (ppm) and 30μg/g, were assumed for normal brain and tumor tissue respectively. To compute the total biologically weighted dose (RBE dose), RBE values of 3.2 for fast neutron and thermal neutron, 0.5 for photon, 1.35 for boron-10 in normal tissue and 3.8 for boron-10 in tumor were used (Coderre, J., et al., 1993). RBE dose was determined by equation 5.

D_{adj}(thermal) = DRSF(thermal)×D(thermal) (Eq. 1)

D_{adj}(fast) = DRSF(fast) × D(fast) (Eq. 2)

D_{adj}(photon) = DRSF(photon) × D(photon) (Eq. 3)

D_{adj}(B-10) = DRSF(B-10) × D(B-10) (Eq. 4)

RBE dose = RBE(thermal) × D_{adj} (thermal)
+ RBE(fast) × D_{adj} (fast)
+ RBE(photon) × D_{adj} (photon)
+ RBE(B-10) × D_{adj} (B-10) (Eq. 5)

3. Results and Discussion

Measured biologically weighted depth-dose-rate (in the unit of RBE cGy/min) distributions for thermal neutron, fast neutron, photon, boron-10 in tumor and normal tissue, and total dose-rate in normal tissue and tumor are depicted in figure 3. The peak of total tumor or normal brain tissue dose-rates occurs at approximately 2 to 2.5 cm depth.

Depth-dose-rate distributions of all dose components determined by measurement and by NCTPlan computation, corrected with the individually derived DRSF values, are shown in figure 4. The DRSF values derived from the measured and computed depth-dose-rate distributions by least-squares criteria are as follows: 0.64 (thermal), 1.39 (fast), 0.96 (photon), 0.65 (B-10).

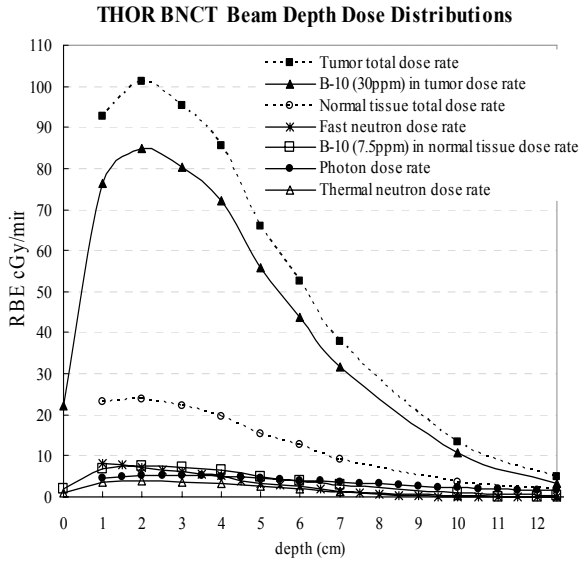

Figure 3. Experimental measured depth-dose-rate distributions of THOR epithermal test beam

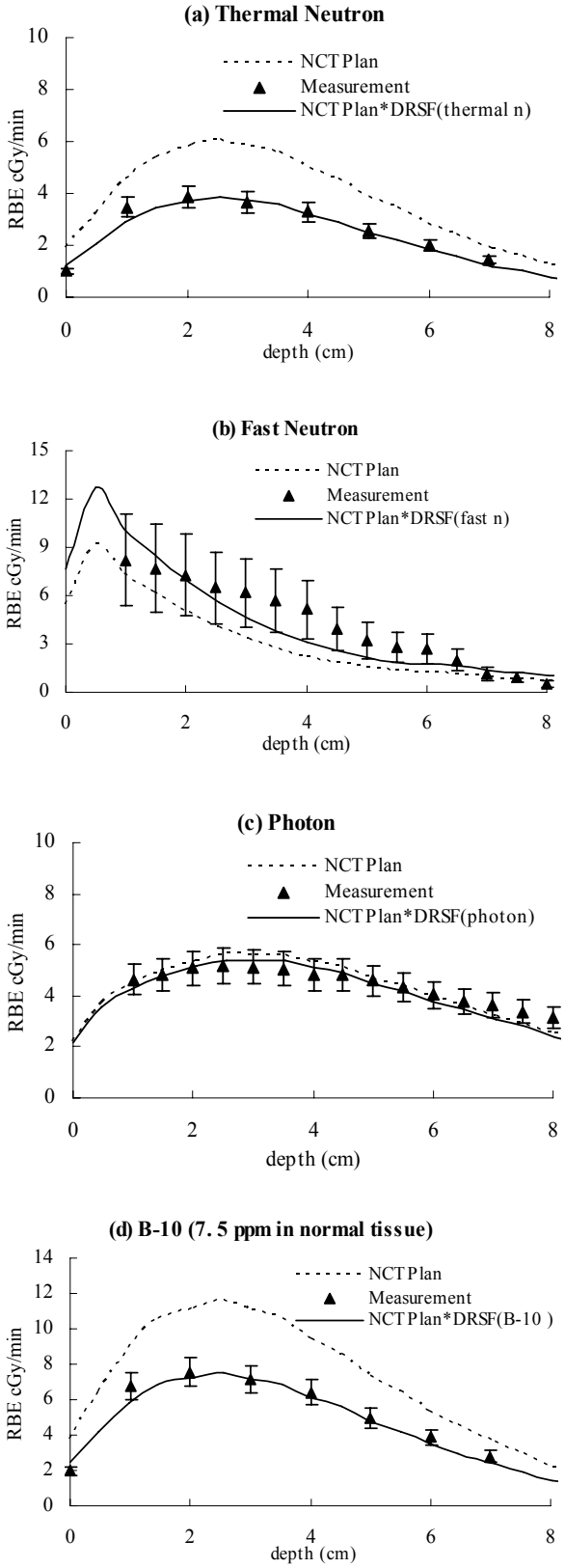

Figure 4. Depth-dose-rate distributions for all dose components acquired by measurement, unadjusted NCTPlan dose-rates, and adjusted (NCTPlan × DRSF) dose-rates: (a)thermal neutron, (b)fast neutron, (c)photon, and (d) 7.5 μg/g (ppm) ^{10}B in normal tissue

DRSF-adjusted NCTPlan computed dose-rates agree well with measured results. Average differences of each dose component are: 2.78% for thermal neutron, 5.67% for fast neutron, 4.11% for photon, and 3.21% for boron-10.

Observed differences between measured and NCTPlan computed dose-rates were found in figure 4. The main reason for the differences is that the source file configuration in NCTPlan may not properly scaled due to the physical source characteristics, such as the actual number and position of fuel elements used, degree of fuel burn-up, etc., may influence the correctness of source file used in NCTPlan. Besides, it may be due to errors in the spatial, angular, or spectral distributions of the neutron and photon sources and also potential scaling errors in the analysis of measured data having limited accuracy. In addition, inherent to the method of mixed-field dosimetry is the inevitably large systematic error uncertainty associated with the derivation of the fast neutron dose-rates. An inherent systematic uncertainty of approximately 35% in the determination of fast neutron dose-rates was estimated in this study.

In comparison, the DRSF values used for the THOR BNCT test beam were: 0.55 (thermal), 2.88 (fast), 0.53 (photon), and 0.56 (B-10). The DRSF values used for the newest THOR BNCT beam are closer to 1. This is due to the source normalization between calculated and actual sources.

4. Conclusions

Comparison and analysis between computed and measured results of depth dose distributions were made in this work. Monte Carlo-based BNCT treatment planning has been shown to be an essential computational tool for BNCT clinical trials. The determination of DRSF adjustment factors is a necessary and important aspect of these requirements. DRSF values used in NCTPlan code for the newest THOR BNCT beam were estimated. The source normalization between calculated and actual sources is strongly suggested to be performed as the beam is operational for every period of six months to eliminate or decrease the observed differences in this research. For this purpose, the experimental and computational techniques used in the current studies will be continually improved.

References

ASTM (American Society for Testing and Materials), 1998. Standard test method for determining thermal neutron reactions and fluence rates by radioactivation techniques. ASTM Protocol E262-97.

Coderre, J., Makar, M., et al., 1993. Derivations of Relative Biological Effectiveness for the High-let Radiations Produced during Boron Neutron Capture Irradiations of the 9L Rat Gliosarcoma in vitro and in vivo. Int. J. Radiat. Oncol. Biol. Phys. Vol.27, 1121-9.

González, S., Santa, Cruz, G., et al., 2002. NCTPlan, the New PC version of MacNCTPlan: improvements and verification of a BNCT treatment planning system, 10th International Symposium on Neutron Capture Therapy for Cancer, Essen, Germany.

Harling, O., Roberts, K., et al., 1995. Head phantom for neutron capture therapy, Med. Phys., 22(5), 579-583.

Hsu, F.Y., Tung, C.J., et al., 2004. Dose rate scaling factor estimation of THOR BNCT test beam, Appl. Radiat. Isotopes, 61, 881-885.

Hsu, F-Y., Palmer, M., et al., 2002. Comparison of NCTPlan and MacNCTPlan treatment planning for BNCT, 10th International Symposium on Neutron Capture Therapy for Cancer, Essen, Germany.

ICRU, 1992. Photon, electron, proton, and neutron interaction data for body tissue. ICRU Report No. 46.

ICRU, 2000. Nuclear data for neutron and proton radiotherapy and for radiation protection. ICRU Report No. 63.

Rogus, R., Harling, O., Yanch, J., 1994. Mixed field dosimetry of an epithermal neutron beams for boron neutron capture therapy at the MITR-II research reactor, Med. Phys., 21(5), 1611-1625.

MCDB Monte Carlo Dosimetry Code System and Its Applications

Deng Li[a] , Li Gang[a], Chen Chaobin[a], Zhang Liangui[b]

[a] *Lab. Com. Phys., Institute of Applied Physics and Computational Mathematics, Beijing 100088, China*
[b]*Capture Technology Ltd., Beijing 100037, China*

Abstract

MCDB (Monte Carlo Dosimetry Code for Brain) is developed for boron neutron capture therapy (BNCT). This system consists of a medical pre-processor, a dose computation and a post-processor. MCDB automatically produces the input file from CT and MRI image data. In Monte Carlo dose calculation, a several accelerated measures, such as the fast track technique, mesh tally matrix and material matrix, are increased. In this paper, we proposed a real model and are simulated by MCNP and MCDB, respectively. The almost same results as MCNP are achieved. MCDB is faster by factor of 3 in computational speed with respect to MCNP.

Keywords: MCDB, combined multi-voxel, fast tracking technique, mesh tally matrix, material matrix

1. Introduction

BNCT technique is used in treating brain tumors by artificially loading the tumor tissue with isotope Boron enriched compound and subsequently irradiation of brain by low energy neutrons. Dozens of countries in the world, such as USA, Japan and Finland etc., have begun the research. Comparisons of BNCT treatment planning software have been limited in scope and five codes are used clinically: NCTPlan, MacNCTPlan, BNCT–rtpe, SERA and JCDS.

The dose calculation is an important part of BNCT. High precision (error<5%) and rapid simulation time (<2 CPU hours) are basic requirements for clinical trials. In Frandsen et al.'s paper (2001), a rapid geometry interrogation for single uniform voxel model in computer graphics is introduced, where the fast track introduces how to find the meshes crossed by a ray. We refer their some ideas and further develop the technique to calculate the track length in each voxel quickly and easily. This technique has been extended to the multi-voxel model. In addition, Kiger et al.(2004) showed the computational time for variable size voxel, where the transport time increases in linear with decreasing of the voxel size. However, the tally and initialization times increase in exponent with deceasing of the voxel size. The new measures of reducing the initialization and tally times, such as mesh tally matrix and material matrix, are studied.

MCDB has been developed in the following aspects: (1) the modified Snyder voxel models are constructed; (2) the combined multi-voxel models are designed according to the depth-dose-rate distribution; (3) the fast track technique of suiting the single and the combined multi-voxel models is developed; (4) the mesh tally matrix and material matrix are designed; (5) parallel computation. The detail algorithm has been introduced in author's another paper (Li Deng et al., 2007). In this paper, we give a patient's example and compare the dose results and computational times between MCNP and MCDB. The test shows that the MCDB confirms the suitability of BNCT clinical trials.

2. Algorithms

In most of TPSs, Monte Carlo method and code are used for the dose calculation, such as MCNP code (Briesmeister, 1997). The flux and its response are obtained by an estimation of the track length. For obtaining the track length, the intersection of a particle ray with the surface being traversed must be found. The collision point is sampled in each cell. The statistical data shows that the time percentage is over 60~70% in all of the transport time. In addition, the initialization and tally times increase with decreasing of the voxel size. The time consume is so large that it

is difficult to satisfy the clinical requirement. Since the geometry of voxel model is very simple and mainly involves the plane. It exists some rules among the voxels, such as arithmetical relation. The neighbor relation is very clear. So it easily develops the fast track technique.

2.1 determination of the density in boundary voxel

For voxel model, two basic materials are contained on the boundary. They are usually mixed by 10% increments and produce another several hundred kinds of the new materials. This is a complex processing. It involves calculating the volume percentages, which is very difficult to be determined accurately. So we take the material of the voxel center as the material of this voxel. According to this processing, it does not increase the new material. We call this treatment as the center point method. Its validity has been proved for the models which the voxel size is less than 5 mm. The maximal mass error is less than 1%. The memories are greatly decreased.

2.2 The combined multi-voxel model design

For BNCT benchmark models (Goorley et al., 2002), the dose-rate of thermal neutron shows that dose-rate firstly rises from 0 to 2.5cm depth and the peak value appears in near of 2.5cm. Then dose-rate is rapidly down and accesses the level of enter skin at 6cm depth. For a generic epithermal beam, BNCT effect is good before 6cm depth, and is down after 6cm and very limit after 12cm depth. So the dose-rate is divided into three parts according to the depth. The Fig.1 shows the three combined models by center point method (Gang Li et al., 2006).

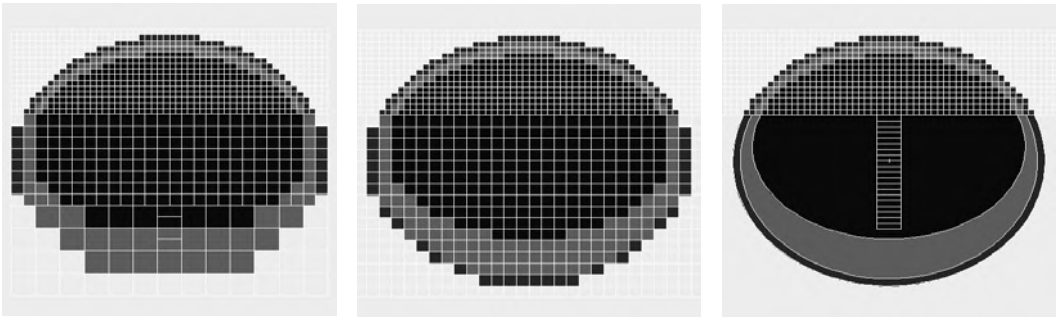

(a) (b) (c)

Fig.1 Cross sections view of the combined multi-voxel models, which are produced by MCDB

2.3 Fast track length algorithm

Firstly, each voxel mesh is mapped into a unit cube; in this case, the grid number of each mesh is expressed as (i, j, k) in integer. The mesh region is expressed as $[i-1,i)\times[j-1,j)\times[k-1,k)$. Total six neighbors mesh numbers are (i±1, j, k), (i, j±1, k), (i, j, k±1). Then, a 3-d material matrix in corresponding to the mesh number is established. The tally matrix is established in similar treatment. The tally is done for all meshes. Since the each surface of the neighbor meshes only belongs to one mesh, the case of lost particle will not happen. The new algorithm is validity for the combined multi-voxel model.

3. Test

This example is from a patient, which consists of 43 CT pictures (Fig.2 (a)). Firstly the 3-D reconstruction is done (Fig.2 (b)), then the two voxel models are designed, where one of model is CT8 which is consisted by 8×8 pixels (the total cubes = 64×64×43=176128, the size = 0.3703mm× 0.3703mm×0.3mm) and another model is CT4 which is consisted by 4×4 pixels (the total cubes=128×128×43=704512, the size=0.1852mm× 0.1852mm×0.3mm, Fig.2(c)). The neutron beam is same as benchmark models. 10 million histories are simulated and all meshes are tallied. The Fig.3 gives the comparison of the dose between MCDB and MCNP, where Fig.3 (a) gives the dose distributions of the thermal neutron, fast neutron and secondary photon of each voxel. The almost same results of MCDB and MCNP are obtained. The Fig.3 (b) gives the detail comparison of MCDB and MCNP results, where x_i is MCNP result and y_i is MCDB result. The statistical error of the photon is bigger because the voxel is too small, the secondary photons from the neutron collisions

are less than the number of the neutrons and the sample numbers do not increase (same as the benchmark 4mm voxel model). Table 1 shows the comparison of MCDB and MCNP in computing time.

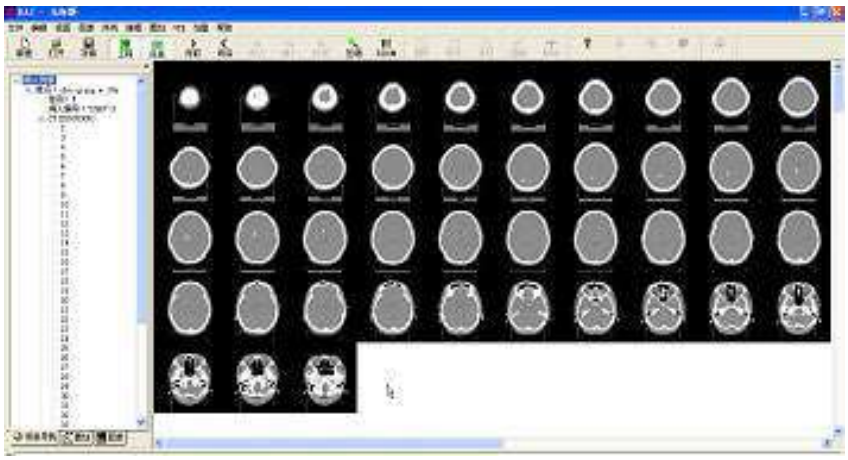

(a)

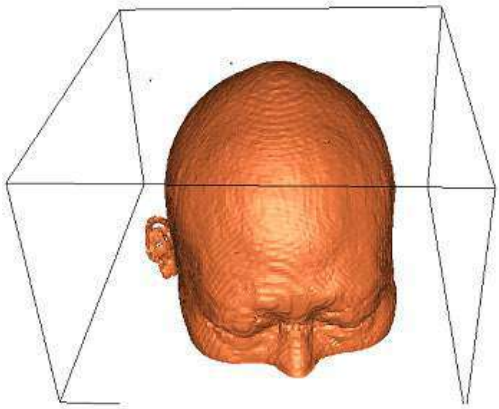

(c)

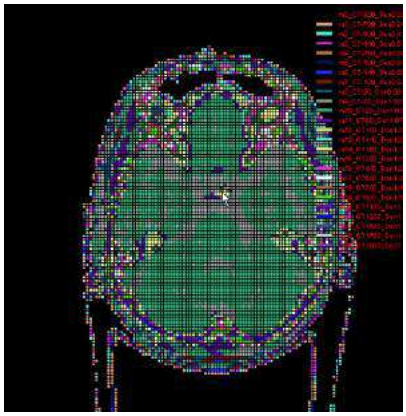

(c)

Fig.2 Cross section view of CT image and CT4 voxel model

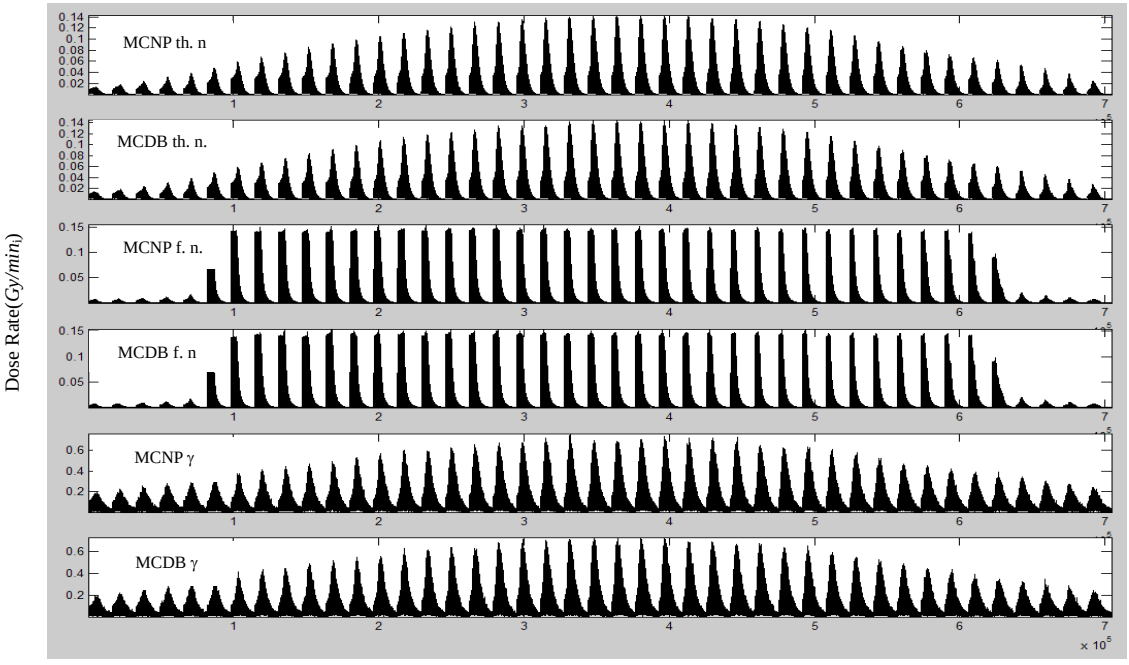

(a) The dose distributions of MCDB and MCNP about neutron and photon

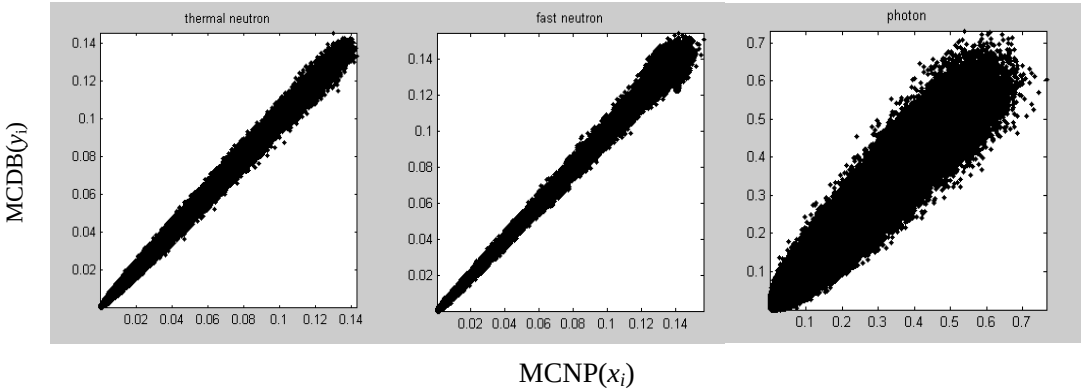

(b) The differences of MCDB and MCNP

Fig.3 Comparison of results and errors between MCDB and MCNP

Table 1 Comparison of computing times based on the CT image model

model	voxel number	geometry	tally	code	time(m)	speedup
CT8	176,128	Lattice	mesh tally	MCNP	185.26	
		Material Matrix	mesh tally matrix	MCDB	60.34	3.07
CT4	704,512	Lattice	mesh tally	MCNP	276.34	
		Material Matrix	mesh tally matrix	MCDB	81.26	3.40

Computer: Pentium IV 3.0 GHz PC machine.

4. Conclusions

MCDB TPS has shown the essential computational ability. The basic data, which is from CT and MRI images, is converted into the input file of voxel model. The material of boundary mesh is produced by center point method. The results show that it not only keeps good precision, but also saves a large amount of computational time. The combined voxels are designed and are simulated. The computation efficiency is remarkable enhanced by means of the fast track technique. The new algorithm is special valid for the mean free path over five meshes and has been expended to the multi-voxel models. MCDB is 3 times of MCNP in speed. The clinical requirement is basically satisfied. Also MCDB can do parallel computation if it is necessary.

A 30 kW BNCT reactor has been built in Beijing, China. MCDB is planning to be used in the programs**.**

Acknowledgment

This research is supported by Capture Technology Ltd.. The authors also wish to thank Prof. Y. M. Zhou.

This project is also supported by Funds of ACEP (2008B0202018, 2008B0103005) and Chinese NSAF (10576006).

References

Frandsen, M.W., 2001. Rapid Geometry Interrogation for Uniform Volume Element-Based BNCT Monte Carlo Particle Transport Simulation, Proceedings of the Eighth International Symposium on Neutron Capture Therapy, Plenum Press, New York.

Kiger III, W.S., Albritton, J.R., Hochberg A.G., et al., 2004. Performance Enhancements of MCNP4B, MCNP5, and MCNPX for Monte Carlo Radiotherapy Planning Calculations in Lattice Geometries, LA-UR-04-6972.

Li Deng, Gang Li, Tao Ye, et al., 2007. MCDB Monte Carlo Code with Fast Track Technique and Mesh Tally Matrix for BNCT. J Nucl. Sci. Tech. 44, 1518–1525.

Briesmeister, J.F. (Ed.), 1997. MCNP-a general Monte Carlo code for n-particle transport code. LA-12625-M.

Gang Li, Li Deng, 2006. Optimized Voxel Model Construction and Simulation Research in BNCT, HEP&NP, 30, 171–177.

Goorley, J.T., Kiger III, W.S., Zamenhof, R.G., 2002. Reference dosimetry calculations for neutron capture therapy with comparison of analytical and voxel models, Medical Physics, 29, 145–156.

BNCT Treatment Planning using THORplan

Hsien-Sheng Li[a], Yen-Wan Hsueh Liu[a,b], Tzung-Yi Lin[c]
S. C. Chung[a], Chin-Hui Wu[b], Hui-Ting Yu[b]

[a]*Department of Engineering and System Science, National Tsing Hua University, Hsinchu, Taiwan*
[b]*Institute of Nuclear Engineering and Science, National Tsing Hua University, Hsinchu, Taiwan*
[c]*Institute of Nuclear Energy Research, Longtan, Taiwan*

Abstract

The BNCT research group at Tsing Hua University, with the newly organized clinical team of Taipei Veterans General Hospital (TVGH), is aiming at clinical trials of GBM and head and neck cancer in two years. Improvements and verifications of the treatment planning system THORplan developed at Tsing Hua University is one of the important tasks at present. In this article THORplan is used for the treatment planning of a GBM patient assuming to be irradiated by the THOR epithermal neutron beam. The results of flux distributions, depth-dose distributions, isodose contours and DVHs for each tissue from the treatment planning system are shown with details of the features of THORplan introduced.

Keywords:BNCT, Treatment planning, CT image, THORplan

1. Introduction

THORplan is a treatment planning system developed for boron neutron capture therapy (BNCT) at Tsing Hua University, Taiwan (Liu and Lin, 2004; Chung *et al*., 2006). It reads in patient CT images and prepares input file of MCNP (Briesmeister, 2000) for the flux/dose calculation. It processes the output files of MCNP calculation for displaying dose contours, dose profiles and dose volume histograms (DVHs) for treatment planning evaluation. THORplan is recently developed with user-friendly interface by using Interactive Data Language (IDL, 2003). It consists of three modules, THORimage, THORinput, and THORdose (Lin and Liu, 2006).

2. Functions of THORplan

THORimage reads in a set of patient's DICOM format CT images. There are two ways to define tissue and organ types, using threshold CT values or through function ROI (region of interest). B-10 concentrations of each tissue can be defined in this module. THORimage module offers the function of cutting out the peripheral air region and combining the slices in order to reduce the number of cells.

CT images in DICOM format are normally 512x512 pixels. THORimage constructs a model which homogenizes each 8x8 array of pixels to be one cell. Cells of similar compositions are grouped to be assigned as one material with the average composition. The cell card, material card, and part of surface and data card of MCNP are generated in this module. THORimage can also produce a detailed voxel model (Lin, et al. 2002) by using repeated structure feature of MCNP for the purpose of benchmarking the homogeneous voxel model.

THORinput reads in neutron/photon source files, KERMA factors, cell and material cards generated by THORimage, and calculates the normal vector of source plane to generate a complete input file for MCNP. THORinput provides two options for dose calculation, the energy deposition method (F6 tally of MCNP) and the KERMA factor method (DE/DF card of MCNP).

After MCNP calculations, outputs are processed by THORdose for dose displays. User can input RBE values for neutron and photon, and CBEs for boron in normal tissues and tumor in THORdose module. THORdose can integrate two or more MCNP outputs with different irradiation time, source beam condition or boron concentrations to

become one result of treatment. Through interpolation, dose results can be available in 512x512xN, where N is the number of slices of the CT images.

The final dose distributions can be displayed in the form of 2D contour diagrams and dose-volume histograms. Dose distributions along each coordinate can be displayed by user's choice.

3. Results and Discussions

A tumor of 3 cm diameter was drawn manually by the user in the test problem as it would be done by the medical doctor in the real situation. The tumor is centered at 3.3 cm depth. The boron concentration in normal tissue, tumor and bone are set to be 10, 30 and 0 ppm, respectively. The CBE values for the tumor and normal tissue are assigned to be 3.8 and 1.3, respectively.

The neutron source for THORplan is the epithermal neutron beam from Tsing Hua Open-Pool Reactor (THOR) calibrated by measurements (Chang *et al*., 2006). The beam direction is normal to the skull and centered on the tumor. The irradiation time is set to be 1 minute. Fig. 1 is the fluence distribution along the beam direction. The maximum thermal fluence is 5.52 x 10^{10} cm^{-2}, occurs at the depth of 2.25 cm.

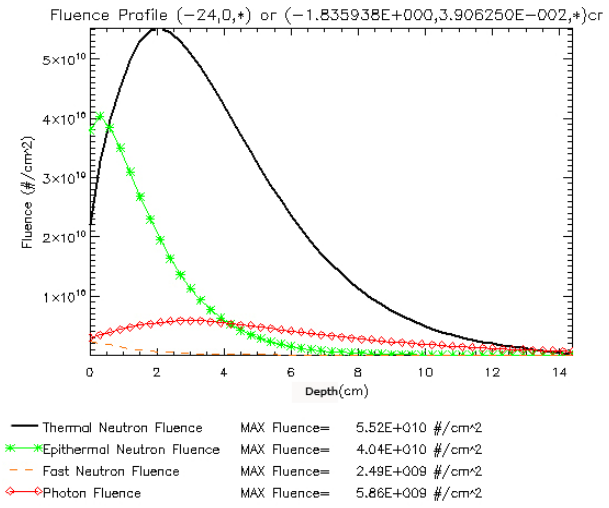

Fig. 1. Fluence distribution along the beam direction passing through the tumor region under 1 minute irradiation

Fig. 2 shows the depth-dose distribution along beam direction just outside of the tumor region (-0.2 cm away from the center of the CT image.) under 1 minute irradiation.

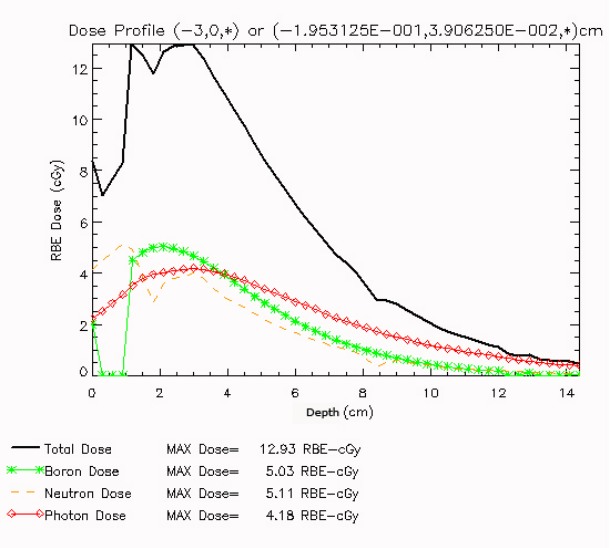

Fig. 2. Depth-dose distribution along the beam direction just outside of the tumor region under 1 minute irradiation

The RBE for neutron is 3.2, for photon is 1. The maximum dose is ~13 RBE cGy, which occurs at a depth of 1.35 cm.

The dose contribution of neutron, gamma ray and boron in normal tissue are approximately equal. The dip appear at 2 cm is due to the mix of water contain with brain in that region, which lowers the nitrogen concentration and thus the neutron dose.

Fig. 3 shows the depth-dose distribution along a line through the tumor region. The biologically weighted boron dose increases by a factor of 9 to ~ 45.3 RBE-cGy when entering into the tumor region.

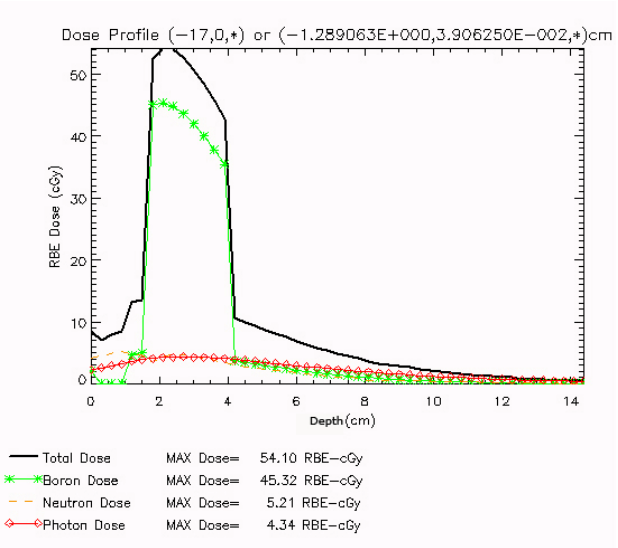

Fig. 3. Depth-dose distribution along a line through the tumor region under 1 minute irradiation

Fig. 4 is the isodose contour for CT slice at depth 2.85 cm under 1 minute irradiation. The color-filled regions represent different materials, corresponding to the anatomic structures of the dose-volume histograms (DVHs). The tumor dose in this slice ranges from 43.7 to 54.6 RBE- cGy.

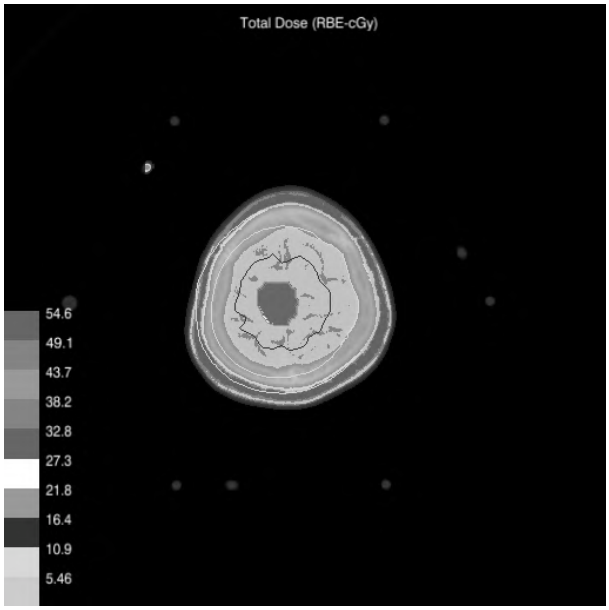

Fig. 4. Isodose contour at depth 2.85cm under 1 minute irradiation

Fig. 5 shows the dose-volume histograms (DVHs) for the tumor and the normal tissues under 1 minute irradiation. The maximum tumor dose is 54.6 RBE cGy. It shows that 100% of the tumor volume is covered by the dose rate of 68% of the maximum value. This dose is called the minimum tumor dose. It is ~37 RBE cGy in this case. The THOR beam can deliver 46.4 RBE cGy, 85% of the maximum dose, to 80% of the tumor volume in 1 minute. The maximum normal tissue dose is 13 RBE cGy. The therapeutic ratio is close to 4.

4. Future Work

Aiming at BNCT clinical trial using THOR in 2 years, THORplan will continue to be improved through discussions with the medical doctors and medical physicists in Taipei Veterans General Hospital (TVGH). The modifications of THORplan for the treatment of head and neck tumor, such as to accommodate more critical organ assignments, are already underway.

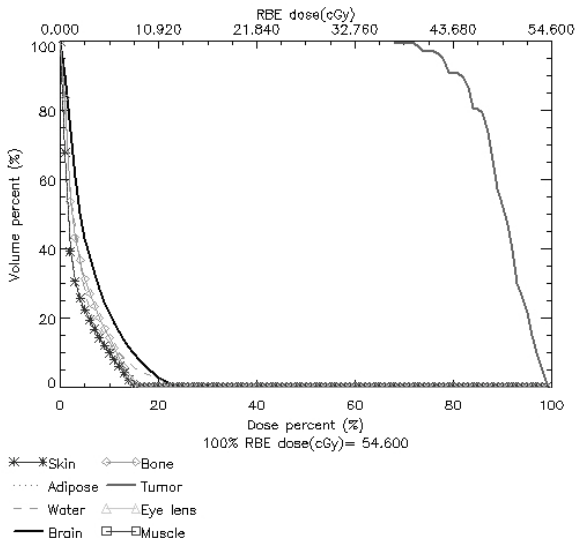

Fig.5. DVHs for tumor and normal tissues under 1 minute irradiation

References

Briesmeister, J.F., 2000. MCNP – A General Monte Carlo N-Particle Transport Code, Version 4C. LA-13709-M.

Chang, C.H., Liu,Y.H., Chen, A.Y., Jiang, S.H., Liu, Y-W. H., Liu, H. M., 2006. A study of neutron fluence rates of the BNCT beam at THOR using foil activation, Advances in Neutron Capture Therapy 2006, Proceedings of ICNCT-12, 453-456.

Chung, S.C., Liu, Y-W H., Lee, C.Y., Lin, T.Y. and Tao, Yinghua, 2006. Study of material grouping in setting Up the head model for treatment planning system for BNCT, Advances in Neutron Capture Therapy 2006, Proceedings of ICNCT-12, 527-530.

IDL, Interactive Data Language, Version 6.0, 2003. Research System, Inc..

Lin, T.Y., Liu, Y-W H., 2006. Recent development of THORplan, Advances in Neutron Capture Therapy 2006, Proceedings of ICNCT-12, 587-590.

Lin, C.Y., Teng, Y.H. and Liu, Y-W H., 2002. Comparison of homogeneous voxel model with detailed voxel model in the treatment planning dose calculations for BNCT, Research and Development in Neutron Capture Therapy, Proceeding of ICNCT-10, 579-582.

Liu, Y-W H. and Lin, T.Y., 2004. A benchmark of treatment planning System THORplan with SERA, ISNCT-11-- Eleventh World Congress on Neutron Capture Therapy, Oct. 11-15, Boston, USA.

Verification of the Accuracy of BNCT Treatment Planning System THORplan

Hsien-Sheng Li[a], Yen-Wan Hsueh Liu[a,b], Chen-Yen Lee[a], Tzung-Yi Lin[c], Fang-Yuh Hsu[d], Chung-Ching Chang[e]

[a] *Department of Engineering and System Science, National Tsing Hua University, Hsinchu, Taiwan*
[b] *Institute of Nuclear Engineering and Science, National Tsing Hua University, Hsinchu, Taiwan*
[c] *Institute of Nuclear Energy Research, Longtan, Taiwan*
[d] *Nuclear Science and Technology Development Center, National Tsing Hua University, Hsinchu, Taiwan*
[e] *Department of Biomedical Engineering and Environmental Sciences, National Tsing Hua University, Hsinchu, Taiwan*

Abstract

THORplan is a treatment planning system developed at Tsing Hua University, Taiwan for boron neutron capture therapy (BNCT) purpose. It is recently developed with user-friendly interface using Interactive Data Language. In this article the accuracy of THORplan is verified by comparing results of Snyder phantom calculation with the analytical model results of MCNP. Neutron source from THOR epithermal neutron beam is used as the source for the calculation. The thermal neutron flux calculated by THORplan is very close to the reference results. SERA overestimates thermal neutron flux by 2~5%. NCTPlan underestimates thermal neutron flux by 4 ~ 9% in most locations. The total weighted dose calculated by THORplan is accurate to within 3% except at the tissue interface. SERA overestimates the total weighted dose at depth > 1.5 cm by 2-5%. As a result of cancellation of errors, NCTPlan overestimates the total weighted dose by 2-10% at depth < 2.5 cm and underestimates it by 3% at depth > 3 cm.

Keywords: BNCT, Treatment planning, Snyder phantom, THORplan

1. Introduction

THORplan is a treatment planning system developed at Tsing Hua University, Taiwan for BNCT purpose. It reads in CT images, prepares input file of MCNP for the flux/dose calculation, and processes the output files for dose contour and dose profile displays. It is recently developed with user-friendly interface using Interactive Data Language (Lin and Liu, 2006; Chung *et al*., 2006). In this article the accuracy of the THORplan is verified by comparing results of modified Snyder phantom calculation with the analytical model results of MCNP4C (Briesmeister, 2000). Neutron source from THOR epithermal neutron beam is used as the source for the calculation. Accuracies of other treatment planning systems, SERA (Wessol, *et al.*, 2001) and NCTPlan (Gonzalez *et al.* ,2002), are also assessed. Similar work was reported earlier by Albritton (Albritton and Kiger, 2006).

2. Material & Methods

The mathematical model of modified Snyder phantom (Goorley, *et al*., 2002) is given below:

$$\left(\frac{x}{6}\right)^2+\left(\frac{y}{9}\right)^2+\left(\frac{z-1}{6.5}\right)^2=1 \quad \text{brain/skull,}$$

$$\left(\frac{x}{6.8}\right)^2+\left(\frac{y}{9.8}\right)^2+\left(\frac{z}{8.3}\right)=1 \quad \text{skull/skin,}$$

$$\left(\frac{x}{7.3}\right)^2+\left(\frac{y}{10.3}\right)^2+\left(\frac{z}{8.8}\right)^2=1 \quad \text{skin/air.}$$

Units are in cm. It can be described by continuous smooth surfaces in the MCNP code.

Based on the mathematical model an image model with 512x512 pixels per slice with total 88 slices (0.041cm pixel spacing, 0.2cm thickness) is set up for the use of treatment planning system THORplan (and SERA). For NCTPlan, the number of pixels per slice is limited to 256 x 256.

The neutron beam is directed along the z-direction. The phantom is located at 10 cm from the beam exit. Material composition of each tissue is based on ICRU Report 46 (ICRU46, 1992). Boron concentration in each material is set to 0 μg/g in this study. The comparison of thermal neutron flux will reflect the potential difference of boron dose in tumor and normal tissues. The total weighted dose calculated in this study contains neutron dose and photon dose. The RBE for neutron is 3.2, for photon is 1.

In THORplan the tally size is 0.328 x 0.328 x 0.2 cm^3, which is the same as the voxel size. In SERA, the total number of tally is limited to 30 x 30 x 30. Therefore, tally size 0.6 x 0.6 x 0.6 cm^3 is used. In NCTPlan , the tally size is 1 x 1 x 1 cm^3, the same as the voxel size. The tally size of the reference analytical model MCNP calculation is 0.656 x 0.656 x 0.2 cm^3. Tallies are done along 3 directions. The z-direction tally is along the centerline. X- and Y- direction tallies are at the depth of 2.5 cm where the maximum thermal flux occurs.

3. Results and Discussion

Fig. 1 shows the comparison of thermal neutron flux of THORplan along the centerline in the Z-direction with the reference result (i.e., the analytical model result). The 1σ statistical uncertainties of the reference results are < 1%. The result of THORplan is quite accurate, with difference ~ 1% to 2% except in the skin region where 3% difference is noted.

The same figure also shows the results of SERA and NCTPlan. At depth < 5 cm, SERA overestimates thermal neutron flux by 2~5%. NCTplan underestimates thermal neutron flux by 4 ~ 9% in most locations, and difference as large as -11.5% is observed at depth 0.9 cm.

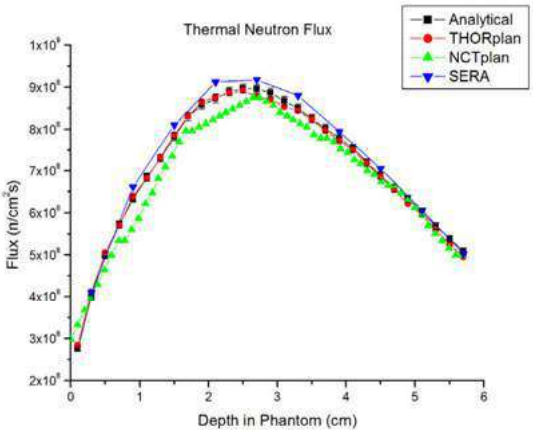

Fig. 1. Comparison of thermal neutron fluxes along the centerline in Z direction

The difference of thermal neutron flux reflects the same degree of difference in boron dose in tumor and normal tissues.

Fig. 2 to 4 show the comparisons of total weighted dose rate, neutron dose rate and gamma ray dose rate. Fig. 2 shows that total weighted dose rate of THORplan is very closed to the reference result (within 2%) except at depth corresponding to the interface of skin and bone, where difference of ~14% are observed. SERA underestimates the total weighted dose rate by 13% at depth 0.3 cm and overestimates it by 2-5% at depth > 1.5 cm. NCTPlan overestimates the total weighted dose rate by 2-10% at depth < 2.5cm and underestimates it by ~3% at depth > 3 cm.

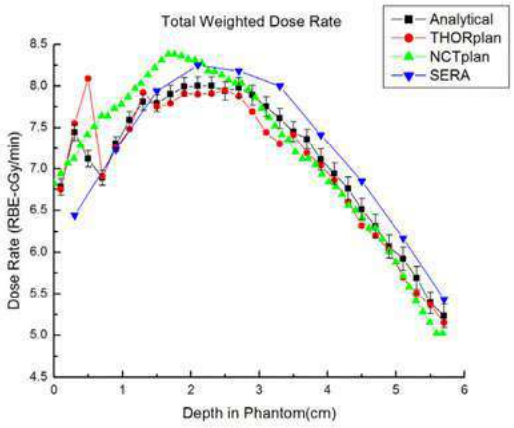

Fig. 2. Total weighted dose rate along the centerline in the Z-direction

Fig. 3 shows that neutron dose rate calculated by THORplan agrees very well with the reference results (~1%) except at the skin/bone, and bone/brain interface where 19% and 5% difference are noted. The bumps in the dose profiles of the reference result and THORplan result are due to the difference of nitrogen and hydrogen concentration between skin, bone and brain. The nitrogen atom density per unit mass of skin is slightly higher than that of bone; the hydrogen atom density per unit mass of skin is twice that of bone. The resulting effect is the total neutron dose in skin is higher than that in bone region. The bumps are more pronounced in THORplan result due to the limitation that pixels in each slice can only be assigned as one tissue, while actually it is a mixture of two tissues. No bumps is observed in dose profiles calculated by NCTPlan and SERA since brain KERMA is used through out the entire phantom. In general, SERA overestimates the neutron dose rate and NCTPlan underestimates the neutron dose rate. At depths > 1 cm neutron dose rate calculated by SERA is 3~9% higher than the reference result. The underestimation of neutron dose by NCTPlan is as large as 7~17% at depth <0.5 cm and >3 cm.

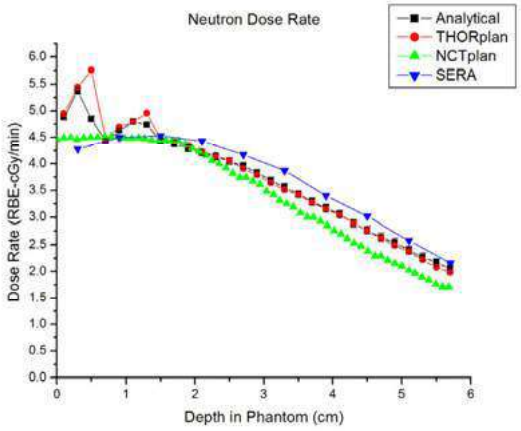

Fig. 3. Total neutron dose rate along the centerline in the Z-direction

Fig. 4 shows that gamma ray dose rate calculated by THORplan agrees with the reference result to within 3% mostly, mainly due to the statistical uncertainty ($1\sigma = 1.5\%$).

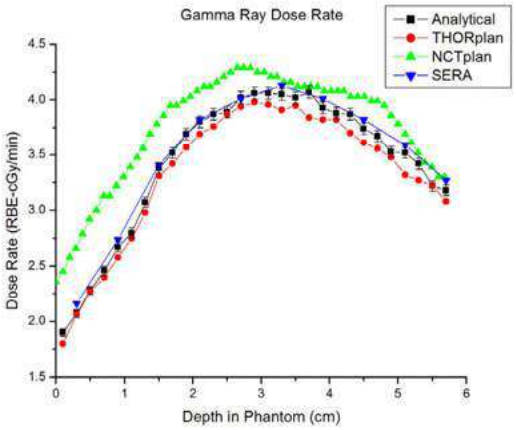

Fig. 4. Gamma ray dose rate along the centerline in the Z-direction

Overestimation of the gamma ray dose rate by SERA is <5%. NCTPlan also overestimates the gamma ray dose rate in the phantom. At depth < 3 cm, up to 29% difference is observed, which is the primary cause of overestimation of total weighted dose there.

Fig. 5 and 6 show the flux profile comparisons of THORplan with the reference results along the X–, and Y-direction at depth of 2.5 cm. The thermal neutron flux of THORplan is accurate to within 2% except at the material interface. The epithermal neutron flux is very accurate, within 1%. Similar results are found in the neutron dose comparison as shown in Fig. 7 and 8

.

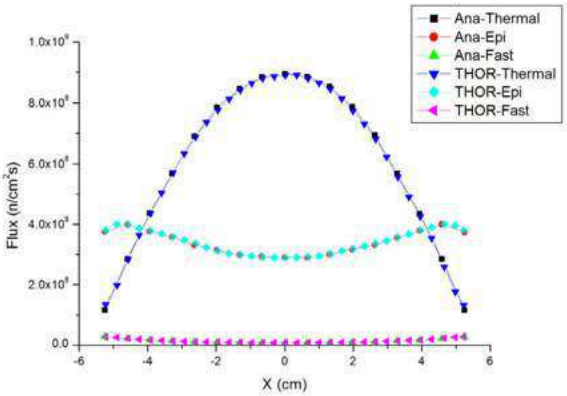

Fig. 5. Neutron flux profiles in the X-direction at depth 2.5 cm

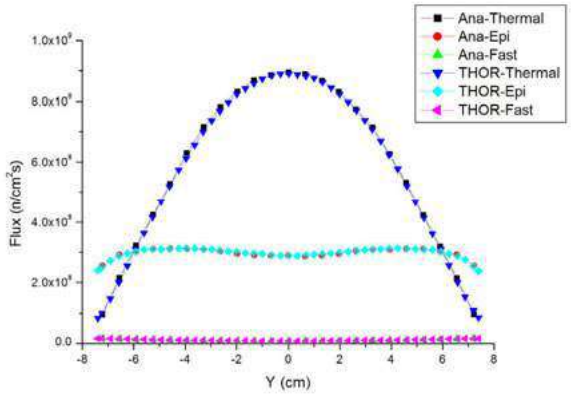

Fig. 6. Neutron flux profiles in the Y-direction at depth 2.5 cm

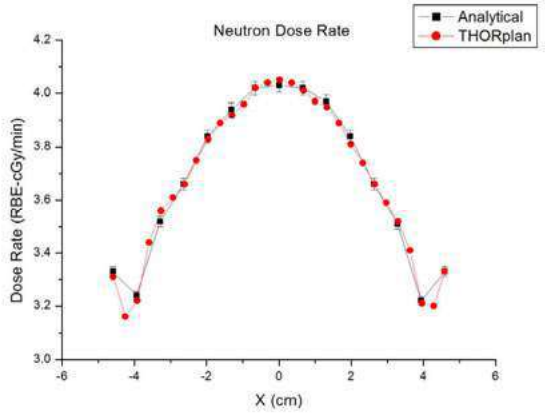

Fig. 7. Neutron dose rate profiles in the X-direction at depth 2.5 cm

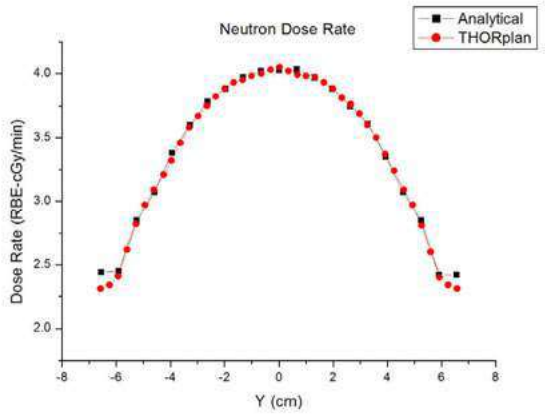

Fig. 8. Neutron dose rate profiles in the Y-direction at depth 2.5cm

4. Conclusions

The thermal neutron flux and the total weighted dose calculated by THORplan are very close to the reference results in this benchmark problem, more accurate than the existing BNCT treatment planning codes SERA and NCTPlan.

Due to the limitation of single tissue assignment for each pixel in each image slice, apparent differences of neutron dose are observed at the tissue interfaces. Although the boron concentration in each material is set to 0 μg/g in this study, the comparison of thermal neutron flux reflects the degree of difference of boron dose in tumor and normal tissues.

References

Albritton, J.R. and Kiger, W.S., 2006. Development of Reference Problems for Neutron Capture Therapy Treatment Planning Systems, Advances in Neutron Capture Therapy 2006, Proceedings of ICNCT-12, 496-499.

Briesmeister, J.F., 2000. MCNP – A General Monte Carlo N-Particle Transport Code, Version 4C. LA-13709-M.

Chung, S.C., Liu, Y-W H., Lee, C.Y., Lin, T.Y. and Tao, Yinghua, 2006. Study of material grouping in setting Up the head model for treatment planning system for BNCT, Advances in Neutron Capture Therapy 2006, Proceedings of ICNCT-12, 527-530.

Gonzalez, S.J., Santa Cruz, G.A., Kiger III, W.S. Palmer, M.R., Busse, P.M., Zamenhof, R.G., 2002, NCTPlan, the new PC version of MacNCTPlan: improvements and verification of a BNCT treatment planning system. In: Sauerwein, W., Moss, R.L., Wittig, A. (Eds.), Research and Developement in Neutron Capture Therapy, Monduzzi Editore, Bologna, Italy, pp. 557-561.

Goorley, J.T. Kiger W.S. III, Zamenhof, R.G., 2002. Reference dosimetry calculations for neutron capture therapy with comparison of analytical and voxel models, *J. Med. Phys. 29(2), 145-156.*

ICRU Report 46, 1992. Photon, electron, proton and neutron interaction data for body tissues, International Commission on Radiation Units and Measurement.

Lin, T.Y., Liu, Y-W H., 2006. Recent development of THORplan, Advances in Neutron Capture Therapy 2006, Proceedings of ICNCT-12, 587-590.

Wessol, D.E., Wemple, C.A., Wheeler, F. J., Cohen, M.T., Rossmeier, M.B., Cogliati, J., 2001. SERA: Simulation Environment for Radiotherapy Applications, User's Manual Version 1C0, INEEL/EXT-02-00698.

BNCT treatment plans and neutron dose evaluation using a Monte Carlo code

Fabiana Rossi[a], Koji Ono[b], Minoru Suzuki[b], Hiroki Tanaka[c], Maria Pia Morigi[a]

[a]*Department of Physics, University of Bologna, Italy*
[b]*Department of Radiation Oncology, Kyoto University Research Reactor Institute, Osaka, Japan*
[c]*Division of Medical Physics, Kyoto University Research Reactor Institute, Osaka, Japan*

Abstract

The aim of this study is to analyze and to optimize the dose delivered to the patient during a BNCT treatment. To do that, treatment plans for brain, lung, liver and head-neck tumors have been developed with different beam geometries using SERA (Simulation Environment for Radiotherapy Applications). For each kind of tumor, a dose analysis has been executed and a comparison among the different geometries has been done. It has been found that for brain tumors the best treatment plan is composed of three beams with a good homogeneity of dose distribution in tumoral tissue. However the absorbed doses to normal tissues are quite inhomogeneous with a mean value of about 2 Gy-Eq and variable ratios between the maximum and the minimum dose absorbed by each tissue. For liver tumors, we have noticed that three beams (anterior A, posterior P and right side R), compared with two opposite beams (AP) and two orthogonal beams (AR), provide the greatest therapeutic gain factors for tumors in the right lobe and quite similar therapeutic gain factors for tumors in the left lobe. For lung tumors, a treatment plan with six beams (compared with one using two or four beams), is the best compromise between good coverage of tumor tissue and a protection of normal tissues, with a mean of 35 Gy-Eq delivered to tumors and a mean of 5.5 Gy-Eq to the lung in which the tumor is located, which is the healthy tissue that receives the biggest dose.

Keywords: boron neutron capture therapy; brain tumors; liver tumors; lung tumors

1. Introduction

Boron Neutron Capture Therapy (BNCT) is a radiotherapy technique based on a nuclear reaction. Non-radioactive isotope ^{10}B atoms that absorb low-energy (<0.5 eV) neutrons (thermal neutrons) disintegrate into an α (^{4}He) particle and a recoiled lithium nucleus (^{7}Li). These particles deposit high energy along their very short path (<10 μm) (Coderre and Morris, 1999). If a sufficient number of ^{10}B atoms is selectively concentrated in the tumor cells and the gradient of the amount of ^{10}B atoms between the tumor and the surrounding normal tissues is large, then only malignant cells with ^{10}B will be destroyed after thermal neutron irradiation. In Japan the first clinical trials of BNCT regarded patients affected by glioblastoma multiforme, a very aggressive brain tumor. Nowadays BNCT is used in Japan not only to treat glioblastoma, but also cutaneous melanoma, tumors of the head and neck, liver cancer and, more recently, lung tumors. However, one of the obstacles to applying BNCT to many sites of malignancies is the poor penetration of thermal neutrons into the body that results in the delivery of insufficient doses to deep-seated tumors (Barth et al., 2005).

At most radiotherapy institutions, commercial-based radiation treatment planning systems are used. At the Kyoto University Research Reactor Institute in Japan, where this work was performed, the Simulation Environment for Radiotherapy Applications (SERA), a treatment planning system specialized for BNCT, has been used in clinical trials (Sakurai et al., 2002; Nigg et al., 1999).

The aim of the present study is to optimize the beam geometry conditions from the point of view of dose-distribution analysis.

2. BNCT treatment planning using the Simulation Environment for Radiotherapy Applications (SERA) system

In the present study, we have considered several patients with liver, lung and head tumors and we have designed some different plans for each one, using SERA. The SERA system requires the entry of several user-defined parameters. These parameters include the ^{10}B concentrations in the tumor and in the normal tissue, the nuclear composition of the tissues, the relative biological effectiveness (RBE) of each component of the beam, and the compound biological effectiveness (CBE) factors of the boron compound. The CBE factors were used as an alternative to RBE in evaluating the biologically absorbed dose by BNCT because different boron compounds yield variable effects on different tissues as a result of variations in the micro-distribution of the boron compounds and the morphologic character

of the target cells (Coderre and Morris, 1999).
As clearly stated in Suzuki et al. (2006), "BNCT consists of mixed radiation fields, with three types of different radiations as follows: (a) low linear energy transfer (LET) γ rays, resulting primarily from the capture of thermal neutrons by normal tissue hydrogen atoms [$^{1}H(n,\gamma)^{2}H$] and contaminating γ rays from the neutron beam port (bismuth-surface), the collimator and the irradiation room wall; (b) high LET protons, produced by the scattering of fast neutrons [$^{1}H(n,n)^{1}H$] and from the capture of thermal neutrons by nitrogen atoms [$^{14}N(n,p)^{14}C$]; and (c) high LET, heavier-charged particles, i.e. ^{4}He nuclei and ^{7}Li ions, released as products of boron neutron capture reactions (BNCR) with ^{10}B [$^{10}B(n,\alpha)^{7}Li$]".
For the dose evaluation we have used the following formula:

$$D_{tumor(normal)} = CF_{tumor(normal)} \times D_{B,tumor(normal)} + \\ + RBE_n \times D_n + RBE_\gamma \times D_\gamma$$

where D_B is the absorbed dose due to the $^{10}B(n;\alpha)^{7}Li$ reaction, D_n and D_γ are those for neutrons and gamma rays. CF stands for compound factor, while RBE_n and RBE_γ are the values of the relative biological effectiveness for neutrons and γ-rays respectively.

In order to calculate the ^{10}B concentrations in the healthy tissue and tumor, we have considered a ^{10}B concentration of 24 ppm in the blood, for patients with lung and brain tumors, and a ^{10}B concentration of 15.3 ppm for patients with liver tumors. The value of ^{10}B concentration in the tumor was then assumed to be 84 ppm for brain and lung tumors and 197 ppm for liver tumors (this value was obtained from experimental studies in animal). These values for ^{10}B concentrations were used in dose calculation by the SERA system. Table 1 summarizes the RBE and CBE factors used in the present study.

Table 1. RBE and CBE factors used for conversion of physical dose (Gy) to photon-equivalent dose (Gy-Eq)

BNCT dose component	Tumor	Brain	Lung	Liver
$^{10}B(n,\alpha)^{7}Li$	3.8	1.3	2.3	0.94
γ-ray	1	1	1	1
$^{14}N(n,p)^{14}C$	3.2	3.2	3.2	3.2
H RBE	3.2	3.2	3.2	3.2
Tissue to blood	3.5	1	1	1

The treatment planning included the following steps: first, computed tomography (CT) images of each patient were put into the SERA system. On each CT scan slice, the gross tumor volume and the volume of adjacent normal tissues, such as heart for lung tumor or eyes for brain tumor, were delineated. By this process, a 3-D geometric description of the patient was constructed. The incident neutron beam direction and the collimator size were then defined and oriented relative to the anatomy. After the ^{10}B concentrations in the tumor, or normal tissue, and the values for the RBE or CBE were entered, the SERA system was run for the dose calculation. The treatment planning code was run on Sun Blade 1000, Model 2750 (Sun Microsystems, Santa Clara, CA). The SERA system simulates about 4000000 source neutrons and 4000000 source photons and requires a processing time of 15-30 minutes for each field.

3. Multiple beam treatment planning: brain tumors

A patient with a tumor in the left side of the brain was taken into account. After putting the MR (Magnetic Resonance) images of the patient inside the SERA system, the volumes for the tumor, target (the 2 cm extension of tumor) and edema, as tumoral tissue, and brain, sinus, ventricles, eyes, skull and scalp, as normal tissue, were delineated. After the contouring, all the data for the RBE parameters and material were set. Next, the beam geometry was defined. Some different geometries were tried: three beams (i.e. a left lateral beam, a posterior beam and a superior vertex beam), two beams (i.e. a left lateral beam and a superior vertex beam), only one left lateral beam. We have used a ^{10}B concentrations of 24 ppm for lung and 84 ppm for tumor.

4. Multiple beam treatment planning: liver tumors

A patient with multiple liver tumors was examined. The first plan was made using two opposite anterior-posterior beams: the first one had a collimator size 2 cm larger than the whole liver; the second one had a collimator size 2 cm larger than the liver right lobe and not included the spinal cord. The second plan was made using two orthogonal anterior-right beams: both of them had a collimator size 2 cm larger than the whole liver. The third plan was made using anterior-posterior-right beams: the first and the third beams had a collimator size 2 cm larger than the whole liver, while the second one had a collimator size 2 cm larger than the liver right lobe and not included the spinal cord. For each plan, beams were equally weighted and plans were normalized to deliver a mean dose of 5 Gy-Eq to the whole liver.

5. Multiple beam treatment planning: lung tumors

A patient with four tumors all along the left lung was taken into consideration. The first tratment plan was composed of one single beam for the two upper tumors and of another beam for the two lower tumors. The second plan was two incident beams for the upper and lower tumors. The third one was three incident beams for the upper and lower tumors. We have used a ^{10}B concentrations of 24 ppm for lung and 84 ppm for tumor.

6. Comparison of the treatment plans and dose-volume histogram (DVH) analysis

The SERA system can provide DVH data for the volume of each tumor or for the other organs. For comparison, all treatment plans were normalized; the maximum, mean and minimum doses to the tumors and to the healthy organs were assessed for each plan. In particular, the doses delivered to 5% and 95% of the volume (D_{05} and D_{95}) were adopted as the representative doses for the maximum and minimum dose, respectively. Also the mean value and the ratio D_{05}/D_{95} were calculated in order to estimate the homogeneity of the dose distribution.

7. DVH analysis for brain tumors

In table 2, the DVH analysis for all the tissues is summarized (only the case of three beams was considered because other geometries were not enough satisfactory).

Table 2. Summary of DVH data for each tissue

Tissue	D_{95} [Gy-Eq]	Mean dose [Gy-Eq]	D_{05} [Gy-Eq]	D_{05}/D_{95}
Tumor	28.1	34.7	41.4	1.5
Target	17.1	27.2	37.2	2.2
Edema	25.4	33.6	41.9	1.7
Brain	1.1	2.9	4.7	4.1
Right eye	0.7	1.3	1.8	2.5
Left eye	2.8	3.4	3.9	1.4
Ventricles	1.4	2.1	2.8	2.0
Sinus	0.5	0.9	1.4	2.7
Scalp	0.8	2.5	4.2	5.6
Skull	0.5	1.3	2.1	4.7

It can be noticed that tumoral tissues receive a bigger dose than normal tissues; in fact, when we deliver a mean dose of 2.1 Gy-Eq to the normal tissues, the mean dose received by the tumoral tissues is 31.8 Gy-Eq. We can also notice that the dose distribution is quite homogeneous in the tumor and edema volume, but it is strongly inhomogeneous for other organs such as brain and right eye.

The indication of homogeneity is given by the ratio between the minimum and maximum dose values (if it is near 1, it means that the dose distribution is quite homogeneous), but it must be noticed that for small organs even a low value of this parameter indicates a big gradient in dose distribution. It must be noticed that neutrons can't pass a big thickness of material, so volumes near the surface are better reached by neutrons. This is one of the reasons of the better homogeneity for the tumor. For brain, instead, the value of homogeneity isn't representative because we must consider that not all the volume ($1.4x10^3$ cm^3) is tumoral tissue. The total volume of organs must be considered also in the clinical aspects to try to estimate the possibility of damage caused by the irradiation.

8. DVH analysis for liver tumors

As the position in which tumors are located is expected to affect the dose distribution in the tumors, the DVH analysis was made differently for the right and the left lobes.

We noticed that, for right tumors, the use of ARP-beams delivers the biggest mean dose (65.1 Gy-Eq) to the tumors with a significant difference compared with the AP (45.6 Gy-Eq) condition and also the gain factor is the biggest one (6.1) with a significantly difference compared with the AP (3.8) and AR (4.5) conditions. For the left lobe, instead, the biggest dose (65.1 Gy-Eq) is delivered from the AP conditions, but there is not a significant difference in the gain factor (ratio between the minimum dose to the tumor and the maximum dose to the healthy tissue) among the three conditions. As far as the whole liver is concerned, the most important condition is the homogeneity of thermal neutron fluence. We have found that the use of ARP-beams gives the highest inhomogeneity.

9. DVH analysis for lung tumors

In Figure 1 an example of DVH for tumor and lung is shown.

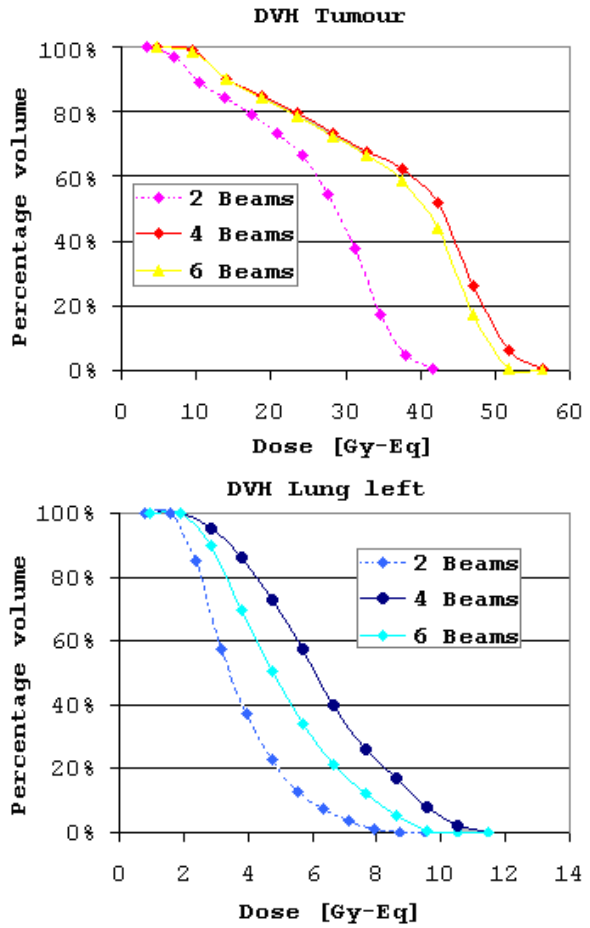

Figure 1. dose-volume histograms for tumor and normal lung

We have noticed that using 2 beams, the tumoral tissues are worse covered by radiation; instead, the use of 4 or 6 beams is quite similar, even if when using 4 beams the maximum dose is the biggest one. As far as the normal tissue is concerned, it can be noticed that for the right organs, such us liver, right lung and right kidney, the number of beams is indifferent for the dose distribution. Similarly, when we consider the homogeneity in each volume, we notice that the three plans are quite similar: each one, in fact, is highly inhomogeneous. The three plans, instead, are different if we consider the left organs such us left lung, heart and left kidney. For the left organs, in fact, the plan with 4 beams delivers the biggest dose to these tissues. With regard to the other two plans, the use of 6 beams delivers a bigger dose than the plan with only 2 beams, but if we consider the average dose in healthy tissues, we notice that the difference is not so big to compromise the organs. Therefore, we can say that the plan with 6 beams is the better compromise between good coverage of tumor tissue and a protection of normal tissues.

10. Conclusions

For brain tumours in the left hemisphere, the use of three beams delivers a mean dose less than 3 Gy-Eq to normal tissues (except for the left eye) and a dose bigger than 30 Gy-Eq to tumour, but there is a great inhomogeneity in the dose distribution inside the organs at risk.

For liver tumours, we have noticed that three beams (APR), compared with two opposite beams (AP) and two orthogonal beams (AR), provide the greatest therapeutic gain factors for tumours in the right lobe and quite similar therapeutic gain factors for tumours in the left lobe.

For tumours in the left lung, a treatment plan with six beams, compared with two and four beams, is the best compromise between good coverage of tumor tissue and a protection of normal tissues, with a mean of 35 Gy-Eq delivered to tumours and a mean of 5.5 Gy-Eq to the left lung, that is the healthy tissue that receives the biggest dose.

References

Barth, R.F., Coderre, J.A., Vicente, M.G.H., Blue T.E., 2005. Boron Neutron Capture Therapy of Cancer: Current Status and Future Prospects. Clinical Cancer Research 11, 3987-4002.

Coderre, J.A., Morris G.M., 1999. The radiation biology of boron neutron capture therapy. Radiat. Res. 151, 1-18.

Nigg, D.W., Wemple, C.A., Wessol, D.E., Wheeler, F.J., 1999. SERA, an advanced treatment planning system for neutron therapy and BNCT. Trans. Am. Nucl. Soc. 80, 66-68.

Sakurai, Y., Kobayashi, T., 2002. Controllability of depth dose distribution for neutron capture therapy at the Heavy Water Neutron Irradiation Facility of Kyoto University research Reactor. Med. Phys. 29, 2338-2350.

Suzuki, M., Sakurai, Y., Masunaga, S., Kinashi, Y., Nagata, K., Maruhashi, A., Ono, K., 2006. Feasibility of Boron Neutron Capture Therapy (BNCT) for malignant pleural mesothelioma from a viewpoint of dose distribution analysis. Int. J. Radiation Oncology Biol. Phys. 66, 1584-1589.

Suzuki, M., Sakurai, Y., Masunaga, S., Kinashi, Y., Nagata, K., Ono, K., 2004. Dosimetric study of boron neutron capture therapy with borocaptate sodium (BSH)/Lipiodol emulsion (BSH/Lipiodol-BNCT) for treatment of multiple liver tumors. Int. J. Radiation Oncology Biol. Phys. 66, 1584-1589

MEDICAL PHYSICS/DOSIMETRY

A preliminary inter-centre comparison study for photon, thermal neutron and epithermal neutron responses of two pairs of ionisation chambers used for BNCT

Antoaneta Roca[a], Yuan-Hao Liu[b], Cecile Wojnecki[c,d], Stuart Green[c,d]
Sander Nievaart[a], Zamir Ghani[d], Ray Moss[a]

[a] *Institute for Energy, Joint Research Centre: P.O. Box 2, Petten, 1755 ZG, The Netherlands*
[b] *ESS Dept., National Tsing Hua University: Hsinchu 30013, Taiwan*
[c] *Department of Medical Physics, University Hospital Birmingham, United Kingdom*
[d] *School of Physics and Astronomy, University of Birmingham, United Kingdom*

Abstract

The dual ionisation chamber technique is the recommended method for mixed field dosimetry of epithermal neutron beams. Its importance has been long recognised and it has featured highly in the dosimetry exchange programme of the MIT BNCT group.

This paper presents initial data from an ongoing inter-comparison study involving two identical pairs of ionisation chambers used at the BNCT facilities of Petten, NL and of the University of Birmingham, UK. The goal of this study is to evaluate the photon, thermal neutron and epithermal neutron responses of both pairs of TE(TE) (Exradin T2 type) and Mg(Ar) (Exradin M2 type) ionisation chambers in similar experimental conditions. At this stage, the work has been completed for the M2 type chambers and is intended to be completed for the T2 type chambers in the near future.

Photon calibration: The photon responses of the ionisation chambers were obtained in 6 and 10 MV clinical photon beams at the University Hospital Birmingham. Photon calibration factor ratios, in terms of dose to water (Petten/Birmingham) of 1.077 ± 0.006 and 1.029 ± 0.005 were found for the M2 and T2 type chambers, respectively.

Thermal neutron response: The thermal neutron sensitivities of the M2 type ionisation chambers were determined using the thermal neutron beam available at the Low Flux Reactor, Petten. Ratios of the integrated charge measured for each chamber indicate a ratio (Petten/Birmingham) of 0.980 ± 0.007 for the M2 chambers.

BNCT epithermal neutron beam: Measurements in a reference PMMA cubic phantom were performed using the M2 type ionisation chambers in the epithermal neutron beam of the High Flux Reactor, Petten. At a depth of 2.5 cm, a ratio of the integrated charge for the chambers yields a sensitivity ratio (Petten/Birmingham) of 0.985 ± 0.008.

Keywords: BNCT dosimetry, ionisation chamber, inter-comparison

1. Introduction

Boron Neutron Capture Therapy (BNCT) is a two-step technique: accumulation of a boron compound in the tumour and irradiation with a tailored thermal or epithermal neutron beam directed at the boron-containing tumour. The potential efficacy of BNCT is a significant function of the neutron beam characteristics.

In this sense, accurate, consistent and reliable dosimetric procedures are of great importance. Due to the complexity of the mixed neutron-gamma ray beam, the accuracy of the dose delivered to a patient required in conventional radiotherapy is difficult to achieve in BNCT applications. Up to now different kinds of detectors are employed: ionisation

chambers, TLDs, gel dosimeters, semiconductor detectors and activation foils. Because of the different radiation components present in such mixed fields, dosimetric procedures include use of three or more of these detectors, in order to evaluate separately each dose component produced by the beam in the tissue.

In all the mentioned techniques, translation of the measured quantity to the dose absorbed in the tissue is not straightforward. The complexity of the problem is well known and as a consequence standard dosimetric procedures are needed to provide better precision and hopefully accuracy in BNCT.

In 2003, following the work of different partners from the major BNCT groups in Europe, a report on recommendations and guidance for BNCT dosimetry has been produced (Voorbraak). This report indicates the paired-ionisation chamber technique (PICT) as the recommended method for measurement of in-phantom distributions of gamma-ray and neutron doses. It is perhaps the best of the few possible techniques for BNCT beam dosimetry. Its importance has long been recognised and featured highly in the dosimetry exchange programme of the MIT BNCT group (Riley, 2002). Within the PICT technique one of the chambers is neutron sensitive and the other one is relatively neutron insensitive, so the neutron and gamma absorbed dose are determined separately.

It seems a simple approach, but it is not straightforward, and sometimes statistical fluctuations can produce physically unrealistic solutions. A major difficulty is that both chambers respond more or less to both photons and neutrons of all energies in the beam, while one of the chambers should be sensitive only to photons and the other one to photons and fast neutrons. In order to have still the 'pure' response of these detectors to the designated radiation components in the beam, the recommendation suggests that epithermal and thermal neutron response components of the detector signal should be treated separately. This requires calibration of the detectors in a high intensity thermal neutron field, but of which only a few are available in Europe. The methodology for the thermal calibration has been studied (Raaijmakers et al, 1996, Baugh, 2003) but not clearly established, and the methods for calibration of the thermal neutron facilities themselves also need uniformity.

Despite all these efforts for a standardization of the paired-ionisation chamber method for the dosimetry of BNCT, the technique suffers from some disadvantages which can be overcome by very careful inter-comparison measurement campaigns.

In this sense, to improve the pair ionisation chamber methodology, this paper presents an inter-comparison study involving two identical pairs of ionisation chambers used in the epithermal and thermal neutron facilities: Petten, NL. The goal of this study is to evaluate the photon, thermal neutron and epithermal neutron responses of both pairs of TE(TE) and Mg(Ar) ionisation chambers in similar experimental conditions.

2. Materials and methods

Two nominally identical pairs of ionisation chambers from Exradin have been used: magnesium ionisation chambers flushed with argon gas of purity 99.999% (Mg(Ar), M2 type) and tissue-equivalent chambers flushed with tissue-equivalent gas, consisting of 3.2% nitrogen, 32.4% carbon dioxide and 64.4% methane by partial pressure (TE(TE), T2 type). All chambers have a sensitive volume of 0.53 cm^3 and a wall thickness of 1 mm. The gas flow through the chambers was controlled by a flow meter and a flow rate of 10 ml/min was used. The chambers were flushed for at least one hour before the measurements started. The accumulated charge over a 60s period was measured using two Farmer electrometers of type 2670A. The ICs were operated at a voltage of -250 V (Petten chambers) or a voltage of +300 V (Birmingham chambers). Corrections for temperature, pressure and leakage current have been performed.

2.1. Photon calibration

The measurements were performed in 6 and 10 MV clinical photon beams, using an Elekta Precise linac, at the Queen Elizabeth University Hospital of Birmingham. Ionisation chambers were placed in a polymethylmethacrylate PMMA framed water phantom of dimensions 40cm x 40 cm x 20 cm (W x H x L), with a PMMA wall thickness of 1.2 cm at 2.5 cm and 5 cm depth and a 24 cm diameter entrance window of 0.5cm thick. A check source was employed before and after every set of measurements to detect possible changes in the performance of the chambers.

The photon calibration factors were calculated in terms of dose to water using the average response of each chamber at 2.5 and 5 cm depth in the phantom, and the corresponding dose delivered.

2.2. Thermal neutron sensitivity

The measurements were performed in the 'pure' thermal neutron field available at the Low Flux Reactor (LFR) in Petten, The Netherlands. This field has a large thermal neutron fluence and a low gamma-dose rate contamination, less than 1 Gy/h (Vroegindeweij, 1997) The thermal neutron flux was determined by foil measurements to be 7.162×10^8 cm^{-2} s^{-1} free-in-air at the position of the chamber irradiation, for a reactor power of 30 kW. The detectors have been positioned free-in-air, in the centre of the field, with the beam axis perpendicular to the chamber axis. Each chamber was irradiated bare and with a 6 mm ^{6}Li cap (see Figure 1). The thermal neutron flux is assumed to be reduced to zero by the lithium cap and any gamma ray production is neglected.

The thermal neutron response of each ionisation chamber was determined from the difference between the reading of the chamber obtained without a build-up cap and the reading obtained when using the ^{6}Li cap. Both chambers were used with a voltage of -250 V. Nevertheless, the Birmingham chambers were tested for + 300 V and less than 1% difference in the average readings was found.

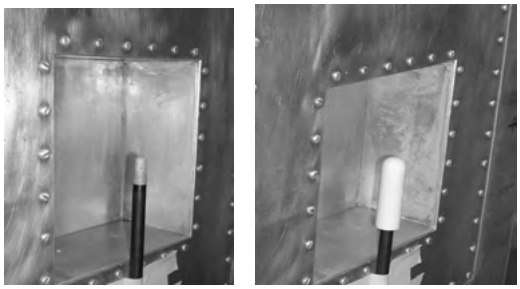

Figure 1. *Bare ionisation chamber (left) and ionisation chamber with Li-6 cap (right) in the centre of the thermal neutron beam at the LFR Petten*

During the irradiation of the TE(TE) from Birmingham, the detector exhibited a strange behaviour. The measurements were unstable and the recordings were of the same order of magnitude as the noise.

2.3. BNCT epithermal neutron beam

The measurements were performed using the clinical epithermal neutron beam at the High Flux Reactor (HFR) in Petten, The Netherlands. The ionisation chambers were irradiated at 2.5 cm depth along the central beam axis in a 15 x 15 x 15 cm^3 PMMA phantom. The phantom to beam-exit distance was 30 cm. As in the LFR measurements, all chambers were used with a voltage of -250 V. The Birmingham ones were checked for the possible polarity effect when used with +300 V.

As in the case of the LFR measurements, the TE(TE) chamber from Birmingham could not be used properly due to the stated reasons.

3. Results

The results from the photon calibration measurements are listed in table 1. Photon calibration factors are presented as ratio between each type of ionisation chamber from Petten and the corresponding chamber from Birmingham (Petten/Birmingham).

Table 1. *Photon calibration factor ratios (Petten/Birmingham) for the M2 and T2 type chambers*

Detector	Ratio of the photon calibration factors Petten/Birmingham
M2 type	1.077 ± 0.006
T2 type	1.029 ± 0.005

The photon calibration factor ratios show slightly higher photon sensitivity for both the M2 and T2 chambers from Petten compared to the Birmingham ones. Nevertheless, each chamber shows a very good stability in time regarding their photon sensitivities. The photon sensitivities for the ionisation chambers from Birmingham agreed within 1.1% with previous results obtained in the same clinical photon beam. The photon sensitivities of the ionisation chambers from Petten agreed within 3% with the previous results obtained in a ^{60}Co gamma-ray field.

Ratios of the raw data measured for the Mg(Ar) chamber in the thermal neutron beam facility (LFR) and in the BNCT epithermal neutron facility (HFR) are presented in table 2.

Table 2. *Ratios of the response of the M2 type chambers (Petten/Birmingham) in the LFR and in the HFR*

M2 type	LFR	HFR
Ratio Petten/Bham	0.980 ± 0.007	0.985 ± 0.008

The response of the M2 chambers in the LFR is presented as thermal neutron sensitivities (calculated as shown above), while in the HFR is presented as the response of the chambers to the mixed neutron-gamma beam.

The two Mg(Ar) ionisation chambers have the same sensitivity to thermal neutrons and react identically when exposed to epithermal neutrons. The ratio of the raw data shows less than 2% variability between the two M2 type chambers.

4. Conclusions

This study intends to confirm the reproducibility and uniformity of the behaviour of two identical pairs of ionisation chambers in routine use for dosimetric measurements at two different BNCT facilities. At this stage of the study, the work has been completed for the M2 type chambers only and is intended to be completed for the T2 type chambers in the near future. At present, the reproducibility and the agreement of the response of Mg(Ar) ionisation chambers when exposed to photon, thermal neutron and epithermal neutron field, and of the TE(TE) chambers when exposed to photon field, has been confirmed. Due to some technical problems of the Birmingham TE(TE) chamber appeared during the measurement campaign, it was not possible to complete the comparison for the TE(TE) chambers, as done for the Mg(Ar) ones. But it is intended to be completed in the near future. It is also intended to fully understand and clarify the methodology for the thermal calibration procedure, to work further with the raw data included in this study.

There remains a need for further work to allow these chambers to be used in the optimum way as standard methodology in BNCT epithermal neutron beams. In this direction, further work is planned in the near future, to use the two pairs of chambers in the thermal and epithermal neutron beams in the Birmingham accelerator-based BNCT facility. A more comprehensive comparison can be done after that, with the aim to have a complete understanding, then to implement and use of the technique.

References

Baugh, G., 2003. Reference Dosimetry for BNCT, Report MSc, Medical and Radiation Physics, University of Birmingham School of Physics and Astronomy.

Raaijmakers, C.P.J., Watkins, P.R.D., Nottelman, E.L., Verhagen, H.W., Jansen, J.T.M., Zoetelief, J. and Mindheer, B.J., 1996. The neutron sensitivity of dosimeters applied to boron neutron capture therapy. Med. Phys. 23**,** 1581-1589.

Riley K.J., Binns P.J., Greenberg D.D. and Harling O.K., May 2002. A Physical Dosimetry Intercomparison for BNCT," Med. Phys. 29 (5), 898-904.

Voorbraak W.P. and Järvinen H., 2003. Recommendations for the Dosimetry of Boron Neutron Capture Therapy (BNCT), Report 21425/03.55339/C, NRG, Petten.

Vroegindeweij C., 1997. Micro- and macroscopic modelling of Boron Neutron Capture Therapy, PhD Thesis, Delft University of Technology.

Evaluation of all dose components in the LVR-15 reactor epithermal neutron beam using Fricke gel dosimeter layers

G. Bartesaghi[a], J. Burian[b], G. Gambarini[a], M. Marek[b], A. Negri[a] and L. Viererbl[b]

[a]*Department of Physics - University of Milan, and INFN, via Celoria 16, 20133 Milan, Italy*
[b]*Department of Reactor Physics, Nuclear Research Institute Řež, plc, Czech Republic*

Abstract

Dosimetric evaluation in BNCT neutron beams are very challenging because of the presence of distinct radiation components having different biological effectiveness. Fricke gel dosimeters in the form of layers are chemical dosimeters based on Fricke solution that are suitable to reconstruct bidimensional distributions of the absorbed dose; in accordance with their chemical composition and applying suitably developed algorithms, they can provide dose images of the different radiation components. These dosimeters, based on tissue equivalent porcine skin gelatine, are shaped in the form of layers (3 mm thick) and inserted in water equivalent phantoms.
After the description of the applied method, this work presents the results obtained at the epithermal column of the BNCT facility at the Nuclear Research Institute of Řež (Czech Republic). The measured dose distributions are shown in comparison with data taken by means of other dosimeters (TLDs) and with calculations carried out with the Monte Carlo code MCNP5. Despite the not negligible uncertainties in parameters utilised for the analysis of the acquired images, the agreement with the results obtained by means of different techniques is satisfying.

Keywords: gel dosimetry, dose components separation

1. Introduction

For a given neutron source for BNCT treatments, it is fundamental to characterize the radiation field determining the dose distribution in a water equivalent phantom. Unlike the conventional radiotherapy case, carried out with photon or electron beams, the radiation field produced by a BNCT beam in a water equivalent material is composed of four distinct components, each one having a different radiobiological effectiveness. In order to foresee the therapeutic effects of a BNCT treatment and to evaluate the complication probability in the healthy tissues, it is necessary to evaluate separately the absorbed dose due to each radiation component.

The therapeutic dose distribution, that is the absorbed dose due to boron capture, is mainly determined by means of in-phantom thermal fluence measurements carried out with activation foils (Rogus et al., 1994). As far as the separation between photon and fast neutron dose is concerned, the most popular dosimeters are dual ionization chambers (Munck af Rosenschöld et al., 2002) and thermoluminescence dosimeters (TLDs) (Kessler et al., 2001); the achievable accuracy is not completely satisfactory, and therefore the use of more than one independent method for gamma and fast neutron dose evaluation is recommended (Voorbraak et al., 2003).

An experimental method based on radiochromic laboratory-made gel dosimeters in the form of layers, allowing to achieve valuable planar images of the different dose components, has been proposed (Gambarini et al., 2000) and is continuously improved. With these dosimeters, based on Fricke solution, images of boron, photon and fast neutron dose with areas up to 13x15cm^2 can be obtained.

Fricke gel dosimeters have been employed for in-phantom dose measurements performed at the epithermal column of the LVR-15 experimental reactor of the Nuclear Research Institute of Řež (CZ).

This paper shows the results obtained, in comparison with data taken by means of TLDs and with Monte Carlo (MC) calculations performed using the MNCP5 code (LANL, 2003).

2. Fricke gel layer dosimeters

The dosimeters, based on Fricke solution in tissue equivalent porcine skin gelatine, are shaped in form of layers (3 mm thick) and are produced with different areas, until 13x15cm^2. The gel dosimeter standard composition is: ferrous sulphate [1mM $Fe(NH_4)_2(SO_4)_2 \cdot 6H_2O$)]; sulphuric acid [25mM H_2SO_4]; porcine skin [3% of the final weight] as gelling agent and Xylenol Orange [0.165mM $C_{31}H_{27}N2Na_5O_{13}S$] as metal ion indicator.

A CCD camera system is used to measure the gel optical density, before and after irradiation; the difference of visible light optical absorbance around 585nm is proportional to the absorbed dose. Therefore, by pixel-to-pixel elaboration of the acquired grey level images, it is possible to obtain dose images. A dedicated software in the programming environment MATLAB® (The MathWorks Inc, Natick MA, USA) has been developed to amend artifacts due to small defects in the gel structures, inhomogeneous illumination of the sample (Carrara, 2007) and, recently, also non uniform thickness of layers.

The measurements have been performed by irradiating the dosimeters in a cylindrical (h: 14 cm, d: 16 cm) water-equivalent phantom or in a standard (50x50x25 cm^3) water phantom; the phantoms were put close to the beam collimator aperture (d: 12 cm), with the gel layers positioned along the beam axis (see figs. 1 and 2).

Fig. 1. The cylindrical water-equivalent phantom put closed to the beam mouth. Two 16x14 cm^2 dosimeters are inserted vertically on the cylinder axis

Fig. 2. A couple of 16x14cm^2 positioned in the 50x50x25cm^3 water phantom. The beam aperture (d: 12cm) is visible

The chemical composition of the dosimeters can be varied with respect to the standard one; a couple of standard and boron added (usually with 40 ppm of ^{10}B) dosimeters, irradiated in the same position inside the phantom, is used to determine the boron dose distribution, taking into account the different sensitivity of Fricke gel to photons and to heavy charged particles. The method for gamma and fast neutron dose separation is based on a couple of standard and heavy-water-made dosimeters (Gambarini et al., 2001), exploiting the different recoil energy of protons and deuterons.

3. Experimental results

The boron dose distribution in the water phantom has been measured with a 15x13cm^2 couple of dosimeters. The obtained dose distribution is shown in fig. 3; in this plot, the origin of the "depth" axis corresponds to the collimator-border plane, and the beam central axis intersects the "width" axis at 7.5cm.

The on-axis profile is compared in fig. 4 with calculations performed with MCNP5. The experimental geometric set up was simulated, taking into account the spectral and spatial characteristics of the neutron source (Burian et al., 2006); the number of boron captures along the central axis was calculated.

The boron dose reaches a maximum value at around 2cm of depth, corresponding to the maximum of thermal neutron fluence.

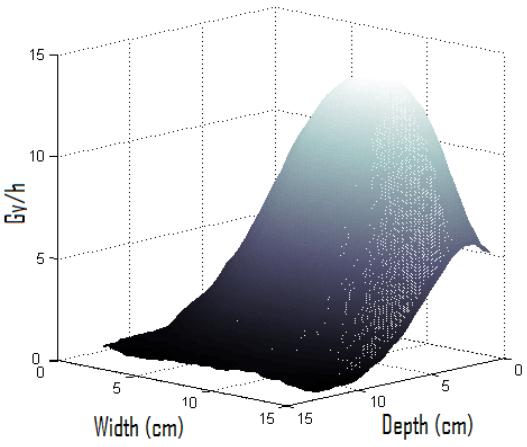

Fig. 3. Boron dose distribution in the water phantom, in a 15x13cm^2 surface along a central plane containing the beam axis

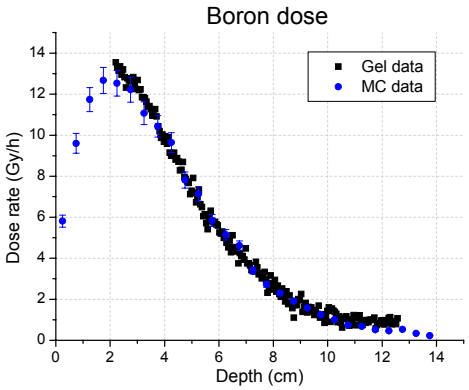

Fig. 4. On-axis boron dose distribution measured in the water phantom. The number of ^{10}B captures were computed by means of MC simulations; MC data are shown normalized at 3.75 cm depth. The first 2 cm of the boron dose are not measured, corresponding to the plastic wall of the water phantom

The gamma and the fast neutron dose components were measured with a couple of 12x6cm^2 dosimeters inserted in the cylindrical phantom; the results are shown in figs. 5 and 6.

For intercomparison of results, in the figure showing the photon dose measured with gel dosimeters the dose values obtained with TLDs are reported too, while the fast dose is shown together with MC calculations of the relative dose, normalized at 1.25 cm of depth; in both case the agreement is very satisfying.

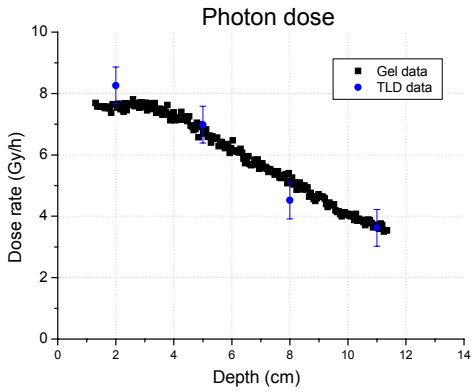

Fig. 5. On-axis photon dose distribution taken in the cylindrical phantom. Gel dosimeters measurement is compared with TLD data

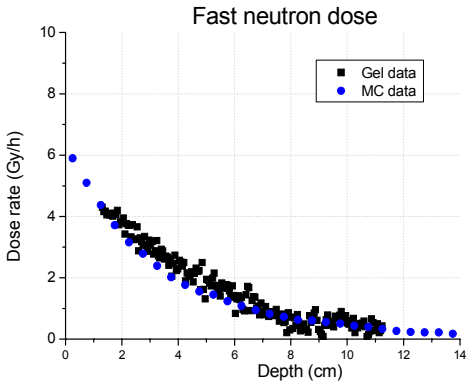

Fig. 6. On-axis fast neutron distribution taken in the cylindrical phantom. The relative fast neutron dose was calculated by means of Monte Carlo simulations; results are shown normalized at 1.25cm of depth

4. Conclusions

A campaign of measurements has been carried out in the BNCT facility of the LVR-15 reactor using Fricke gel dosimeters in form of layers; with these dosimeters, inserted in water equivalent phantoms, dose images of the different radiation components (boron, photon and fast neutrons) have been achieved.

The obtained results show a good agreement with TLD measurements and MC calculations, giving a confirmation of the reliability of the developed method based on gel dosimeters in form of layers for in-phantom dose measurements in BNCT neutron beams, achieving quantitative images of each component of the absorbed dose.

Acknowledgments

This work was supported by the National Institute of Nuclear Physics (INFN), Italy.

References

Burian, J., Flibor, S., Marek, M., Rejchrt, J., Viererbl, L., Tomandl, I., 2006. Physics for BNCT. J. of Phys: Conf. Ser. 41, 174-186.

Carrara, M., Gambarini, G., Tomatis, S., Valente, M., 2007. Dose distribution measurements by means of gel-layer dosimeters. Evaluation of algorithms for artifacts amendment. Nucl. Instr. Meth. A 579, 334-338.

Gambarini, G., Agosteo, S., Danesi, U., Garbellini, F., Lietti, B., Mauri, M., Rosi, G., 2001. Imaging and profiling of absorbed dose in neutron capture therapy, IEEE Trans.s Nucl. Sc., 48, 780-784.

Gambarini, G., Agosteo, S., Marchesi, P., Nava, E., Palazzi, P., Pecci, A., Rosi G., Tinti, R., 2000. Discrimination of various contributions to the absorbed dose in BNCT: Fricke-gel imaging and intercomparison with other experimental results. App. Rad. Isot. 53, 765-772.

Kessler, C., Stecher-Rasmussen, F., Rassow, J., Garbe, S., Sauerwein, W., 2001. Application of thermoluminescent dosimeters to mixed neutron-gamma dosimetry for BNCT. In: Hawthorne et al.: Frontiers in Neutron Capture Therapy, Kluwer Academic/Plenum Publishers, New York, Vol.2, 1165-1173.

MCNP – A General Monte Carlo N-Particle Code, Version 5, X5 Monte Carlo Team, Los Alamos National Laboratory, 2003

Munck af Rosenschöld**,** P.M., Ceberg, C.P., Giusti, V., Andreo, P., 2002. Photon quality correction factors for ionisation chambers in an epithermal neutron beam. Phys. Med. Biol. 21, 2397- 2409.

Rogus, R. D., Harling, O.K., Yanch, J.C., 1994. Mixed field dosimetry of epithermal neutron beams for boron neutron capture therapy at the MIT-II research reactor, Med. Phys. 21, 1611-1625.

Voorbraak, W.P., Stecher Rasmussen, F., Huiskamp, R., 2003. Recommendations for the Dosimetery of Boton Neutron Capture Therapy (BNCT), edited by NRG, Petten (NL).

LVR-15 Reactor Epithermal Neutron Beam parameters – results of measurements

J. Burian[a], V.Klupak[a], M.Marek[a], J.Rejchrt[a], L. Viererbl[a], G. Gambarini[b], G. Bartesaghi[b],

[a]*Department of Reactor Physics, Nuclear Research Institute Rez, plc, Czech Republic*
[b]*Department of Physics, University of Milan, Italy*

Abstract

The epithermal neutron beam of the LVR-15 reactor provides the appropriate conditions for varied BNCT activity. The principal parameters have been frequently determined. The following detectors has been used for the measurement: Set of activation monitors of different nuclides irradiated in free beam and in the water phantom, Si semiconductor detector with ^{6}LiF converter, twin ionization chambers, thermoluminescence dosimeters, gel dosimeters used for imaging of separate part of dose, neutron spectrometer of Bonner type. Obtained results of measured parameters are presented in the paper.

Keywords: BNCT, epithermal neutron beam, reactor beam dosimetry

1. Introduction

The construction of the epithermal neutron beam at a horizontal channel of LVR-15 reactor, see Fig.1, was completed in year 2000 (Burian, 2001). A group of patient was treated in the project "Pre-clinical trials of brain tumors"(Burian, 2002). In the long term the facility at the reactor is utilized for the study of physical and biological aspects of BNCT. In the part of physics the periodic verification of parameters (as international comparison, too) and the development of appropriate dosimetry methods are performed. In the part of biology the biological effectiveness of the beam has been evaluated on different biological models (cell cultures, immature rat brain, mouse intestine crypt regeneration) (Mares, 2002).

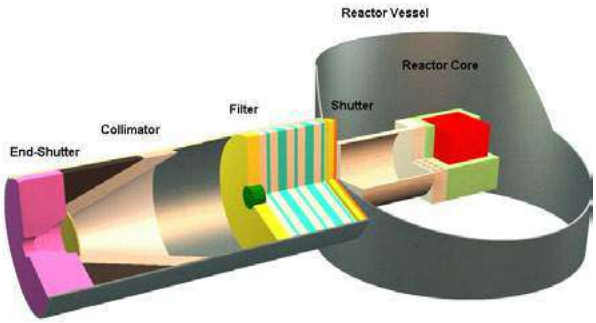

Fig. 1. The LVR-15 epithermal beam facility

2. Material and Methods

The beam properties were monitored by measurements of the neutron spectrum, neutron profile, fast neutron kerma rate in tissue, and photon absorbed dose.

Activation foils – activation of foil detectors is the basic method used for neutron spectrum determination. During the time standard set of detectors was selected, see Table 1.

Table 1 Set of activation detectors

Elem.	Mass [mg]	Conc. [%]	Measured reaction	Reaction rate [s-1]
Au	39.14	1	197Au(n,g)198Au	8.89E-14
Au	42.59	1	197Au(n,g)198Au	8.26E-14
Cu	292.71	100	63Cu(n,a)60Co 63Cu(n,g)64Cu	-- 2.92E-16
In	46.55	1	115In(n,g)116mIn 115In(n,'n)115mIn	8.72E-14 --
La	45.85	0.5	139La(n,g)140La	8.18E-16
Mn	37.31	4	55Mn(n,g)56Mn	1.11E-15
Sc	46.39	1	45Sc(n,g)46Sc	5.21E-16
Ww	43.71	0.1	186W(n,g)187W	2.91E-14
In	562.53	100	115In(n,g)116mIn 115In(n,'n)115mIn	6.52E-15 2.7E-18
Ni	1106.83	100	58Ni(n,p)58Co	9.52E-19

Neutron spectrum is evaluated using an adjustment procedure (SAND, STAYSWL, BASACF) which provides a means for combination of reaction rates with a calculated neutron spectrum resulting in determining an optimal estimation of the thermal, epithermal and fast neutron fluence rates and their uncertainties.

Semiconductor Si detector with Li converter – detectors consisted of Si diodes and neutron converters with ^{6}Li are frequently used for measurement of slow neutron fluence. After reaction of thermal neutron with ^{6}Li, triton and alpha particle are produced with total energy of 4.78 MeV (2.73 MeV for triton and 2.05 MeV for alpha particle). The Si diode works as detector of heavy charged particles. When triton or alpha particle hits the PN junction of the Si diode a signal pulse is produced on the output of the detector. From the count rate of the pulses the slow neutron fluence rate is determined. This type of detector can be used for neutron fluence rates roughly from 10^{2} cm^{-2}.s^{-1} to 10^{10} cm^{-2}.s^{-1}.

Twin ionization chambers – the neutron kerma rate in tissue and photon kerma rate in tissue both in the beam and in phantom can be determined with twin ionization chambers. They are used either as air-filled or flushed with a TE-equivalent CH_4-based gas mixture (TE chamber) or with argon (Al chamber). The chambers are calibrated in the absolute ^{137}Cs radiation beam in the units of the exposure. Responses of the chambers to the neutrons and gamma rays, respectively, are determined from measurements using different neutron and gamma sources as follows: ^{252}Cf, ^{9}Be(d,n) ,T(d,n).

Al-P glass TLD – the standard types of TLD are used to get absolute information about the gamma absorbed dose rate in the BNCT beam and in phantom measurement. The response of the detector lies in the energy range 25 keV - 7.5 MeV and the detector can measure the gamma absorbed dose up to 10 Gy. The thermal neutron correction factor derived from the measurement in a thermal neutron field has to be used.

Gel dosimeters - the Fricke gel dosimeters that are at the basis of the method are laboratory-made radiochromic gels (Gambarini, 2004); the composition of such gel dosimeters is: porcine skin in the amount of 3% of the final weight, ferrous sulphate solution [1mM $Fe(NH_4)_2(SO_4)_2$•$6H_2O$)]; sulphuric acid [25mM H_2SO_4] and xylenol-orange [0.165mM $C_{31}H_{27}N_2Na_5O_{13}S$]. These dosimeters are produced in form of layers, typically 3mm thick; they are imaged with a CCD camera system before and after irradiation, and the measured difference of optical density at 585 nm is proportional to the absorbed dose.

In order to obtain the separate evaluation of the photon (D_γ) and recoil proton (D_p) doses, gel dosimeters were prepared in pairs having different isotopic content, that is one using light water (standard dosimeter) and the other heavy water (99.9% pure); in each measurement, two such dosimeters were inserted close each to other in the phantom. This method for separation fast neutron dose by means of gel dosimeters has been now more exhaustively studied and improved.

Bonner type spectrometer – method based on a positioning thermal neutron detector behind the different thickness of polyethylene. New construction with 7 detectors in one block was tested, principal configuration see in Fig. 2.

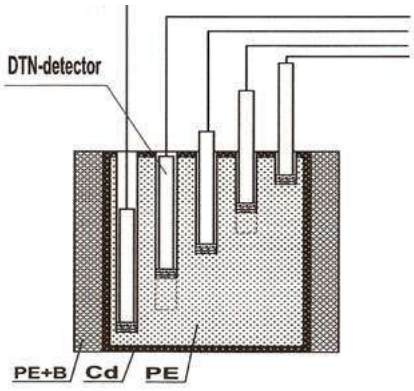

Fig. 2 Principal configuration of Bonner spectrometer in one block

The advantage of the spectrometer is that the 90% response intervals of the spheres continuously cover the epithermal part of the neutron energy range. Disadvantage of the spectrometer is its high thermal neutron efficiency resulting in the necessity to apply them at low reactor power. The spectrum adjustment procedure is analogical to the case of the activation foils.

3. Results and Discussions

The current free beam integral characteristics are as follows:

Epithermal neutron flux 6.5×10^8 /cm^{2}s

Fast neutron flux 5.5×10^7 /cm^{2}s

Thermal neutron flux 3.8×10^7/cm^{2}s

Photon absorbed dose measured in the beam axis by ionization chamber was 1.98 Gy/h, fast neutron kerma in tissue was 3.5 Gy/h. Results were received for reactor power 9 MW approximately. Neutron spectrum calculated by MCNP code adjusted with activation foil measurement see in Fig.3.

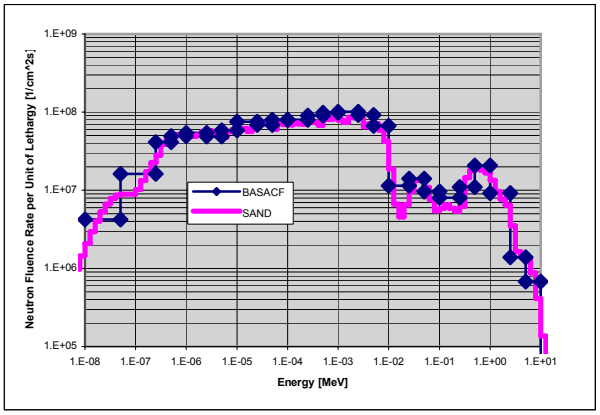

Fig. 3. Neutron spectrum, the result received with codes SAND and BASACF

Standard water phantom (400 mm width, 400 mm height, 300 mm depth) was used for measurement of neutron depth profiles. The result of calculation is demonstrated in Fig. 4.

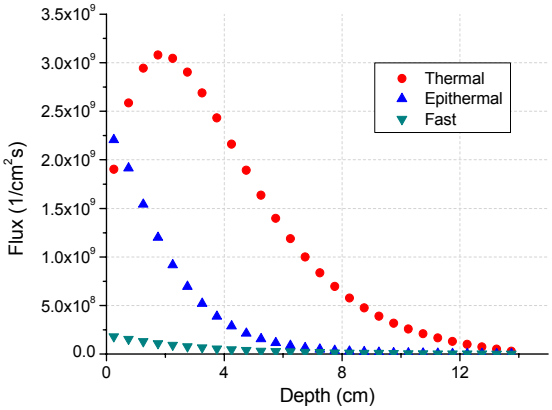

Fig. 4. Neutron fluxes at the water phantom central axis, calculated with MCNP

The thermal neutron depth profile measured with activation method, Si-Li detector and gel is shown in Fig. 5.

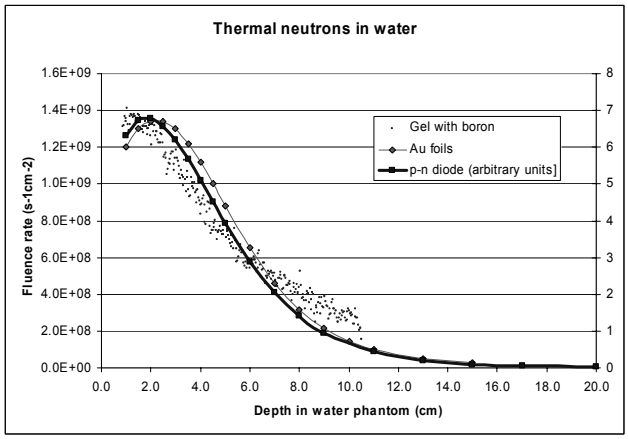

Fig. 5. Thermal neutron distribution in water

Gel dosimetry. Rectangular Fricke-gel dosimeters (13×15 cm^2) were placed in the water phantom perpendicularly to the beam mouth, in order to attain depth dose images. In Fig 6, a dosimeter ready for the irradiation is shown and in Fig. 7, a dosimeters after irradiation is visible, settled on the light source for transmittance imaging detection. In Fig. 8, the total doses measured with a gel-dosimeter made with heavy water is reported in a 2D representation.

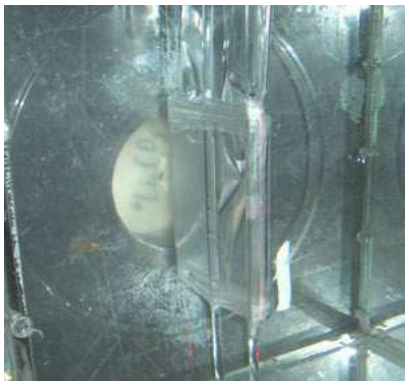

Fig. 6. Gel dosimeters in the water phantom

Fig. 7. Gel dosimeters after irradiation, placed on the light source for transmittance image detection

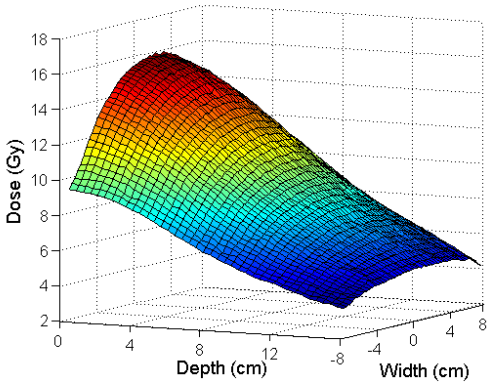

Fig. 8. 2-D representation of the total dose vs depth, obtained from the image of a gel dosimeter made with heavy water

Monoblock neutron spectrometer (MNS) of Bonner type. Response functions have been calculated with MCNP for MNS and verified by measurement with monoenergetic neutrons (Van de Graaf), isotopic sources (PuBe, Cf). The rough form of neutron spectrum was reconstructed from measurement for reactor epithermal beam, see Fig. 9.

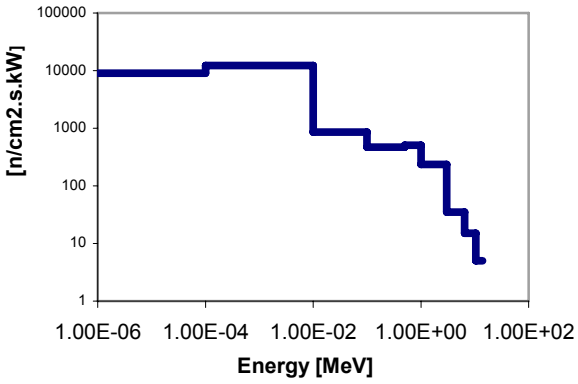

Fig. 9. Neutron spectrum - MNS of Bonner type

4. Conclusions

The epithermal neutron beam of the LVR-15 reactor provides the conditions for varied BNCT activity. The knowledge of the source parameters (energy spectrum and space distribution especially) is necessary requirement for this actions.

Acknowledgement

The work was supported by Research Project MSM 267 224 4501 of Research Centrum of NRI Rez Ltd. and Contract MPO 1H-PK2/05 of program IMPULS.

References

J.Burian, M.Marek, J.Rataj, S.Flibor, 2001. The experience from the construction of BNCT facility at the LVR-15 reactor, IAEA, Vienna, Austria, June 1999, *Current Status of Neutron Capture Therapy,* IAEA Tec-Doc 1223, p.126–131.

J.Burian, M.Marek, J.Rataj, et al., 2002. Report on the First Patient Group of the Phase I BNCT Trial at the LVR-15 Reactor. *Proceedings of 10th Int. Congress on NCT for Cancer,* Sauerwein, Moss, Wittig, Editors, Germany, pp.1107 – 1113.

G.Gambarini, V.Colli, S.Gay, C.Petrovich, L.Pirola, G.Rosi, 2004. In-phantom imaging of all dose components in boron neutron capture therapy by means of gel dosimeters, *Applied Radiation and Isotopes 61,* pp. 759-763.

V.Mareš, J.Burian, M.Marek, K.Prokeš, 2002. Assesment of the Relative Biological Effectiveness of LVR-15 Nuclear Reactor Neutron Beam by a Simple Animal Model", Acta Universitatis Purkyniana,2002, Ústi n.L.,Stud. Biol. 6, pp.5-10.

The investigation of neutron capture therapy with nanodosimetric methods

E. Gargioni, G. Hilgers, and B. Grosswendt

Physikalisch-Technische Bundesanstalt,
Bundesallee 100, 38116 Braunschweig, Germany

Abstract

The need for new quantities in dosimetry for BNCT and, in general, for hadron therapy arises from the crucial role played by the particle-track structure in causing damage to sub-cellular targets. The development of nanodosimetry is based on the assumption that initial damage to cells is related to the number of ionizations (the ionization cluster size) directly produced by single particles within short segments of DNA or in the near neighbourhood. In this work, we investigate the frequency distributions of ionization cluster sizes produced by the fissions fragments created in BNCT and present a simple procedure for connecting ionization cluster sizes directly measured in a low-pressure gas with those that are expected to be produced in short segments of DNA. We present ionization cluster-size distributions for α-particles in the energy range from 0.1 MeV to 2 MeV, measured in a nanometric volume using an ion-counting nanodosimeter and calculated with the Monte Carlo method, both using the nanodosimeter geometry and in a nanometric volume of liquid water. The good agreement between experimental data and Monte Carlo simulations confirms that nanodosimetry is a powerful tool for defining radiation quality in terms of particle-track structure.

Keywords: biological effectiveness, particle track, Monte Carlo, nanodosimetry

1. Introduction

Conventional radiation treatment planning is based on the measurement of absorbed dose to water. This macroscopic quantity is defined as an average value in regions of space which are very large with respect to the mean distance between two subsequent interactions along the track of an ionizing particle. However, radiation-induced damage to cells is strongly influenced by the pattern of inelastic interactions in sub-cellular targets, whose structure is not taken into consideration in the definition of absorbed dose. Therefore the relative biological effectiveness of ionizing radiation, which plays a crucial role in BNCT, should be defined in terms of quantities directly related to the particle track structure, thus replacing or at least supplementing absorbed dose to water.

Here we present a new dosimetric concept, which is based on the assumption that the initial radiation damage to cells is related to the number of ionizations (the ionization cluster size) directly produced by single ionizing particles within short segments of the DNA or in the near neighbourhood (Grosswendt, 2007). In particular, we define some nanodosimetric quantities, such as the frequency distribution of ionization cluster size and its moments, which can be directly measured and have shown to be directly correlated with radiation quality (Grosswendt, 2008). We investigate these nanodosimetric quantities for the fissions fragments created in BNCT by means of Monte Carlo simulations in water and present preliminary experimental results for α-particles in the energy range from 0.1 MeV to 2 MeV, measured by means of an ion-counting nanodosimeter.

2. Definition of nanodosimetric quantities

Brenner and Ward (1992) found that the yields of clusters of multiple ionization in biological sites, with a size of 2 to 3 nm, correlate well with observed yields of double-strand breaks in the DNA. As a consequence, quantities which are based on the probability for an ionizing particle to form clusters of multiple ionization in nanometric volumes can be used for tackling the metrological challenge of replacing, or at least supplementing, absorbed dose to water as a reference quantity in dosimetry. We shall refer to these quantities as nanodosimetric quantities.

The ionization cluster size v is defined as the number of ionizations that are produced in a specified cylindrical target volume of diameter D and height h by a single primary particle. The primary particle, of radiation quality Q, can either penetrate through or pass the target volume at a distance d with respect to the cylinder's main axis (see Figure 1).

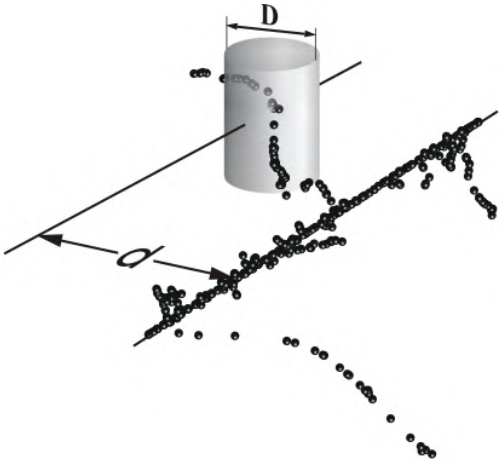

Figure 1. Ionization cluster-size formation by a primary particle passing a specified cylindrical target volume of diameter D at a distance d from the cylinder's main axis. The shown segment of the particle track represents its ionization component

The ionization cluster size can be interpreted as the result of a superposition of the ionization component of the particle track structure and of the geometric characteristics of the target volume. We can define the cluster-size distribution $P_v(Q;d)$ as the probability that exactly ν ionization are formed in the volume and the irradiation geometry defined above. Here, $P_v(Q;d)$ is normalized to unity according to Equation (1). The moments of the $P_v(Q;d)$ distribution and its sum distribution function are given by Equations (2) and (3).

$$\sum_{v=0}^{\infty} P_v(Q;d) = 1 \qquad (1)$$

$$M_{\xi}(Q;d) = \sum_{v=0}^{\infty} v^{\xi} P_v(Q;d) \qquad (2)$$

$$F_k(Q;d) = \sum_{v=k}^{\infty} P_v(Q;d) \qquad (3)$$

Nanodosimetric quantities, as defined above, cannot be directly measured in a biological target. A common practice to overcome this problem is to measure cluster-size distributions using a nanodosimeter, which consists basically of a gas-filled counter operating at low pressure.

The simplest way of relating P_v to radiobiological data is to assume that (1) water is the reference medium for approximating a biological target, (2) the probability $P_1(Q;d)$ of forming a cluster size $v = 1$ is related to the yields of single-strand breaks (SSB) in a DNA segment, and (3) the sum distribution function $F_2(Q;d)$, which corresponds to the probability of forming a cluster size $v \geq 2$, is related to the yields of double-strand breaks (DSB) in the DNA (Grosswendt *et al*, 2007).

Recently, Grosswendt (2008) calculated the ionization cluster-size formation due to electrons and light ions in nanometric target volumes of liquid water (comparable in size to a segment of the DNA) with Monte Carlo simulations (for an example, see Figure 2).

These calculations show that the probability of forming a cluster size $v = 1$, and the sum distribution function of forming an ionization cluster size $v \geq 2$ show a similar dependence on radiation quality as the radio-biological cross sections of SSB- or DSB-formation of SV40 viral DNA.

This motivates the further development of experimental techniques to directly measure ionization cluster-size distributions, in order to (1) benchmark the Monte Carlo simulations and (2) provide a new concept for characterizing radiation quality on the basis of simple, and directly measurable, nanodosimetric quantities.

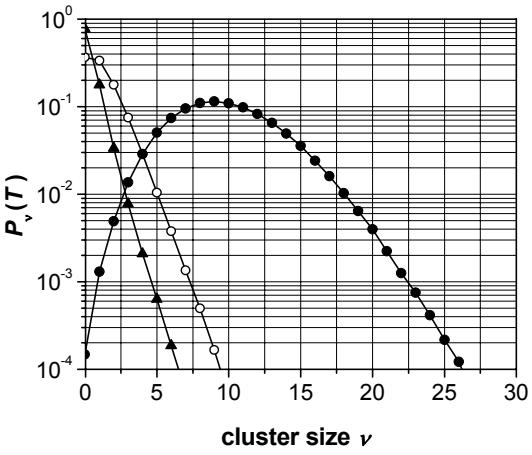

Figure 2. Ionization cluster-size distributions in water for different primary particles with the same reduced velocity: 5 MeV protons (filled triangles), 20 MeV α-particles (open circles), and 60 MeV carbon ions (filled circles). The distributions were calculated in a water cylinder, 2 nm in diameter and 2 nm in height

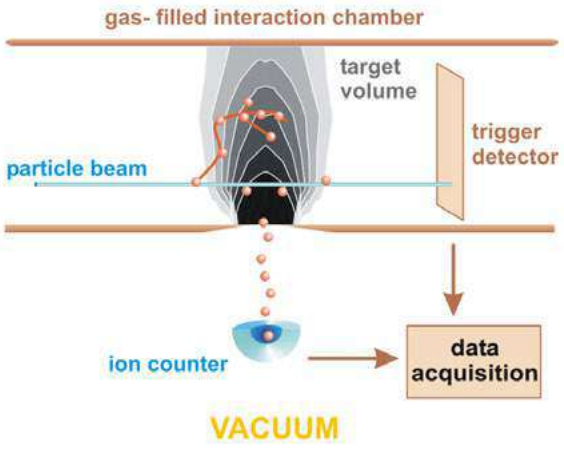

Figure 3. Schematic view of a typical ion-counting measuring device which can be applied for measuring ionization cluster-size distributions in nanometric target volumes

3. Principles of experimental nanodosimetry

A typical nanodosimeter, as developed in several institutions in the past few years (DeNardo *et al.*, 2002; Garty *et al.*, 2002a-b; Bantsar *et al.*, 2004-2006; Bashkirov *et al.*, 2006; DeNardo *et al.*, 2006), consists of a low-pressure interaction chamber, an electrode system to extract ions or low-energy electrons from the interaction chamber, an evacuated drift column which includes at its end a single-particle counter, and a primary-particle detector. When charged particles enter the interaction chamber, they penetrate through or pass aside a wall-less target volume of definite shape and size, and finally reach a trigger detector at the opposite end of the chamber. Ions or low energy electrons induced by each primary particle (and by its secondaries) within the target volume are extracted from the interaction chamber and guided into an evacuated drift chamber where they are detected by a single-particle counter. If such measurements are performed for a large number of single primary particles of radiation quality Q, the final result is the probability distribution $P_\nu(Q)$ of ionization cluster size ν.

The ion-counting nanodosimeter (ND) designed at the Weizmann Institute of Science (Garty *et al.*, 2002) is currently under further development at PTB (Hilgers *et al.*, 2007).

The actual prototype allows to measure nanodosimetric quantities for light ions as primary particles when the beam goes through the sensitive volume ($d = 0$ in Figure 1). The operating conditions allow to measure cluster-size distributions in gas volumes which simulate biological targets with diameters varying between approximately 1 nm and 4 nm (see Section 5).

We present in this work some experimental results for irradiation with monoenergetic α-particle beams in the energy range from 0.1 MeV to 2.0 MeV, which are relevant in BNCT. These measurements were carried out in a mono-energetic α–particle beam at the Van de Graaf accelerator facility of PTB.

In order to meet the needs of the measuring apparatus, the intensity of the α–particle beam is reduced to less than 100 /s by Rutherford scattering of the primary beam at an angle of 45° in a 0.1 μm gold foil.

The scattered beam is monitored by a spectrometer mounted in the symmetric scattering position at –45°. The Rutherford scattered α–particles are used for the experiment in a narrow-beam geometry and are therefore referred to as primary particles in the following.

The scattering chamber is separated from the ionization chamber of the nanodosimeter by means of a 1.2 μm mylar foil mounted on a 3 mm aperture. The diameter of the primary beam is furthermore reduced to 1 mm at the entrance of the ionization volume of the nanodosimeter, which is filled with propane at a pressure of 1.2 mbar.

The measurements of the ionization cluster size distributions are carried out with the ND operating in its pulsed mode. The DAQ-system described by Garty et al. (2002) was recently replaced by a digital storage oscilloscope (DSO).

The pulse train of the collected ions is recorded with one channel and the charge pulse of the primary particle with another channel of the DSO. Both waveforms are written to a hard disk memory and are evaluated offline after the measurements. The height of the charge pulse of the primary particle is determined numerically according to the algorithm described by Valentin et al. (1994). This allows to store the cluster size distributions as well as the energy spectra of the primary particles, which are recorded using the trigger detector of the nanodosimeter as a spectrometer. The energy calibration of the spectrometer is done using the pulse height spectra of the α-particles after their passage through the 0.1 μm gold foil and the 1.2 μm mylar foil without filling the nanodosimeter with the target gas. The energy of the α-particles leaving the mylar foil is calculated with SRIM (Ziegler, 2006). In order to obtain a good statistic in the ionization cluster size distributions, also at larger cluster sizes, up to $3x10^5$ primary events are recorded for every primary energy.

4. Monte Carlo calculation of nanodosimetric quantities

The successful use of nanodosimetric quantities to connect radiation quality and initial radiation damage to DNA is based on the assumption that the reference material for defining these quantities is liquid water. However, also for this medium, the experimental determination of cluster-size distributions is not feasible. This problem was approached in the past by Grosswendt (2004), who proposed a simple procedure to scale nanodosimetric quantities measured in a gas with those calculated in water with Monte Carlo simulations.

With this procedure, the gas pressure in the nanodosimeter is chosen in such a way that

$$(D\rho)^{(gas)} = (D\rho)^{(water)} \frac{(\lambda\rho)_{ion}^{(gas)}(Q)}{(\lambda\rho)_{ion}^{(water)}(Q)} \qquad (4)$$

In Equation (4), $D\rho$ represents the mass per area in μg/cm^2, λ_{ion} is the ionization mean free path (in cm) of radiation with quality Q, and ρ the material density in g/cm^3. Equation (4) should be independent from radiation quality and selected materials, in order to have uniquely defined dosimetric quantities.

The steps to directly measure cluster-size distributions as expected in a DNA segment are therefore (1) the experimental verification of the scaling procedure defined by Equation (4) with at least two different filling gases; (2) the determination of the appropriate nanodosimeter operating conditions for reproducing cluster-size distribution in water cylinders of different sizes; (3) the assumption, common in radiation biology, that a water cylinder, 2.3 nm in diameter and 3.4 nm in length, is equivalent to a DNA segment of approximately 10 base pairs.

Several *ad-hoc* Monte Carlo (MC) codes were developed at PTB for characterizing and further developing the ion-counting nanodosimeter [see, for example, Grosswendt and Pszona (2002), Grosswendt (2008), and references therein]. With their help, it is possible to simulate (1) the gas-filled counter, taking into account both irradiation geometry and detection efficiency, and (2) ionization cluster-size formation due to the interactions of electrons and light ions in nanometric volumes of liquid water.

These codes can simulate the transport of primary electrons at energies between about 10 eV and a few MeV, and of primary protons, α-particles or other light ions at reduced energies between about 0.15 MeV/u and 500 MeV/u. The history of each primary or secondary electron is followed, if necessary, down to the ionization threshold energy of the material, taking into account elastic electron scattering, impact ionization, as well as the most relevant excitation processes affecting electron degradation.

5. Results

The first step to verify the appropriateness of nanodosimetric quantities that are measured with a gas-filled ND is to test the validity of Equation (4) for at least two different gases. Figure 4 shows that the ionization cluster-size distribution of 1.0 MeV α-particles measured when the ND operates with nitrogen at a pressure of 1.2 mbar is equivalent to that obtained with propane at a pressure of 0.46 mbar.

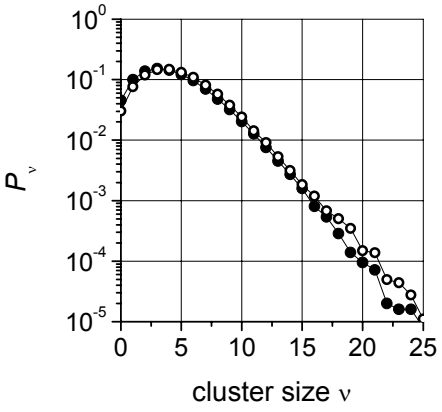

Figure 4. Ionization cluster-size distributions for α-particles at energies of 1 MeV measured with the ND for two different filling gases: nitrogen (filled circles) at a pressure of 1.2 mbar, and propane (open circles) at a pressure of 0.46 mbar. See text for more details

In Figure 5, we show an example of measured cluster-size distribution for 1.3 MeV and 0.53 MeV α-particles, together with the results of the corresponding MC-simulations. The differences in shape are due to some uncertainty in the calculation of the position-dependent detection efficiency, which is used in the MC simulation. This efficiency is determined theoretically by means of ion transport in the collecting electric field [for more details see, for example, Garty *et al.* (2002a-b)]. The agreement between experiment and simulation at 0.53 MeV is less satisfying than at 1.3 MeV, since the MC code does not accurately take into account charge-exchange processes for light ions (Toburen, 1999). As a first approximation, in fact, we assume in our model that α-particles (He^{2+}) are in equilibrium with other charge states (He^{+} and He^{0}). Therefore we calculate an average effective charge Z_{equil} for the primary beam and obtain ionization cross-section data by scaling proton cross sections with Z^2_{equil} according to the Thomas-Fermi approximation of the atom (ICRU, 1996; ICRU, 2005),

$$Z_{equil} = Z\left[1 - \exp\left(-\frac{v}{v_0 Z^{2/3}}\right)\right].$$

Here, Z and v are the atomic charge number and the velocity of the projectiles, and v_0 the Bohr velocity, $v_0 = v/\alpha$ (being α the fine structure constant).
The first moments M_1 of the experimental and simulated distributions are shown in Figure 6 in the energy range between approximately 400 keV and 2 MeV.

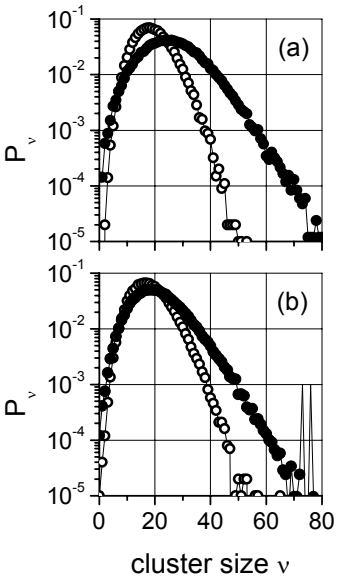

Figure 5. Ionization cluster-size distributions for α-particles at energies of (a) 0.53 MeV and (b) 1.3 MeV. Filled circles: distributions measured at the Van de Graaf accelerator facility of PTB. Open circles: results of the corresponding MC simulations. See text for more details

The agreement with the MC simulation is within 15 % for energies above 900 keV, which is compatible with the overall uncertainty in measurements and simulations.
The discrepancy, however, increases to up to 40% below 500 keV, where charge-exchange effects occur with higher probability.

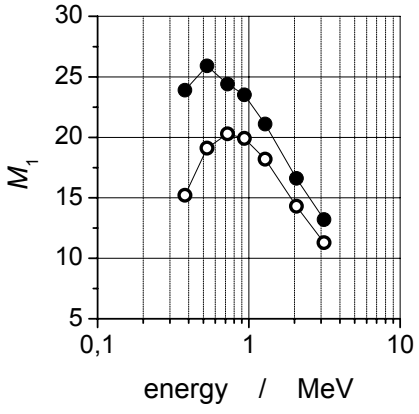

Figure 6. First moments of the ionization cluster-size distributions for α-particles as a function of the primary energy. M_1 was calculated using Equation (2) with $\xi = 1$. Symbols as in Figure 5

The second step to be achieved for connecting measurements of cluster-size distributions in gases to MC calculations in water is to determine the ND operating conditions which well reproduce MC simulations for a given water cylinder. We show in Figure 7 that for the ND working with propane at 1.2 mbar it is possible to directly measure nanodosimetric quantities which are equivalent to those in water cylinders with a diameter of approximately 3.5 nm. The difference in the first moments of the distributions are, in fact, within the overall uncertainty. Therefore, a suitable pressure adjustment can allow a direct measurement of ionization clusters that might be also found in a DNA segment, under the assumption that the latter can be simulated by means of a water cylinder. Further investigations with other filling gases and other radiation qualities will be carried out in the future.

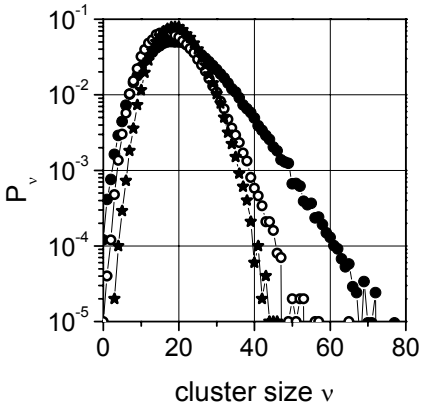

Figure 7. Ionization cluster-size distributions for 1.3 MeV α-particles. Filled circles, measured with the ND operated with propane at 1.2 mbar ($M_1 = 21.1$). Open circles, calculated with the ND geometry and working conditions as described in Section 2 ($M_1 = 18.1$). Filled stars, calculated in a water cylinder, 3.5 nm in diameter and 3.5 nm in height ($M_1 = 19.5$)

4. Conclusions

The need for new quantities in dosimetry for BNCT and, in general, for hadron therapy is a consequence of the crucial role played by the particle-track structure in causing damage to sub-cellular targets. We developed a nanodosimetric method for characterizing the BNCT radiation fields which is based on three steps: (1) the experimental verification of a simple scaling procedure for comparing cluster-size distributions measured in a low-pressure gas with an ion-counting nanodosimeter with those calculated in an equivalent water cylinder; (2) the determination of the nanodosimeter operating conditions which allow to reproduce cluster-size distribution in water cylinders of different sizes; (3) the assumption, commonly accepted in radiation biology, that a water cylinder, 2.3 nm in diameter and 3.4 nm in length, is equivalent to a DNA segment of approximately 10 base pairs.

Future investigations should aim at improving the physics of the MC codes in order to appropriately account for charge-exchange processes during the transport of light ions. This will allow an accurate investigation of α-particles with energies below 900 keV and of low-energy ^{7}Li ions. Systematic analyses of the validity of the scaling formula [Equation (4)] for any radiation quality and any low-pressure gas used in the ND will ensure that nanodosimetric quantities are related to initial damage to segments of DNA in a unique way.

References

Bantsar A., Grosswendt B., Kula J., and Pszona S., 2004. Clusters of ionization in nanometre targets for propane-experiments with a jet counter. Radiat. Prot. Dosim. 110, 845-850.

Bantsar A., Grosswendt B., and Pszona S., 2006. Formation of ion clusters by low-energy electrons in nanometric targets: experiment and Monte Carlo simulation. Radiat. Prot. Dosim. 122, 82-85.

Bashkirov V., Schulte R., Breskin A., Chechik R., Schemelinin S., Garty G., Wroe A., Sadrozinski H., and Grosswendt B., 2006. Ion-counting nanodosimeter with particle tracking capabilities. Radiat. Prot. Dosim. 122, 415-419.

Brenner D. J. and Ward J. F., 1992. Constraints on energy deposition and target size of multiply damaged sites associated with DNA double-strand breaks. Int. J. Radiat. Biol. 61, 737-748.

De Nardo L., Alkaa A., Khamphan C., Conte V., Colautti P., Ségur P., and Tornielli G., 2002. A detector for track-nanodosimetry. Nucl. Instrum. Meth. Phys. Res. A 484, 312-326.

De Nardo L., Colautti P., and Grosswendt B., 2006. Simulation of the measured ionization-cluster distributions of alpha-particles in nanometric volumes of propane. Radiat. Prot. Dosim. **122**, 427-431 (2006).

Garty G., Shchemelinin S., Breskin A., Chechik R., Assaf G., Orion I., Bashkirov V., Schulte R., and Grosswendt B., 2002a. The performance of a novel ion-counting nanodosimeter. Nucl. Instr. Meth. Phys. Res. A 492, 212 – 235.

Garty G., Shchemelinin S., Breskin A., Chechik R., Orion I., Guedes G. P., Schulte R., Bashkirov V., and Grosswendt B., 2002b. Wall-less ion-counting nanodosimetry applied to protons. Radiat. Prot. Dosim. 99, 325-330.

Grosswendt, B., 2004. Recent advances of nanodosimetry. Radiat. Prot. Dosim. 110, 789-799.

Grosswendt B., 2008. From macro to nanodosimetry: limits of the absorbed-dose concept and definition of new quantities. Proc. Workshop on Uncertainty Assessment in Computational Dosimetry, Bologna. IN PRESS.

Grosswendt B. and Pszona S., 2002. The track structure of α-particles from the point of view of ionization-cluster formation in `nanometric' volumes of nitrogen. Radiat. Environ. Biophys. 41, 91-102.

Grosswendt B., Pszona S., and Bantsar A., 2007. New descriptors of radiation qualities based on nanodosimetry, a first approach. Radiat. Prot. Dosim. 126, 432-444.

Hilgers G., Gargioni E., Grosswendt B.; Shchemelinin S., 2007. Proton induced frequency distributions of ionization cluster size in propane. Radiat. Prot. Dosim. 126, 467-470.

International Commission on Radiation Units, 1996. Secondary electron spectra from charged particle interactions. ICRU Report No. 55.

International Commission on Radiation Units, 2005. Stopping of ions heavier than helium. ICRU Report No. 73.

Toburen L., 1998. Ionization and charge transfer: basic data for track structure calculations. Radiat. Environ. Biophys 37, 221-233.

Valentin T. Jordanv, Glenn F. Knoll, Alan C. Huber, John A. Pantazis, 1994. Digital techniques for real time pulse shaping in radiation measurements. Nucl. Inst. Meth. Phys. Res. A353, 261-264.

Ziegler J.F., Ziegler M.D., Biersack J.P., SRIM – The Stopping and Range of Ions in Matter Version 2006.02, http://www.srim.org

Preliminary liver dose estimation in the new facility for biomedical applications at the RA-3 Reactor

M. Gadan[a,b], V. Crawley[a], S. Thorp[b], M. Miller[b]

[a] *Favaloro University, Argentina*
[b] *Instrumentation and Control Department, National Atomic Energy Commission, Argentina*

Abstract

As a part of the project concerning the irradiation of a section of the human liver left lobe, a preliminary estimation of the expected dose was performed. To obtain proper input values for the calculation, neutron flux and gamma dose rate characterization were carried out using adequate portions of cow or pig liver covered with demineralized water simulating the preservation solution. Irradiations were done inside a container specially designed to fulfill temperature preservation of the organ and a reproducible irradiation position (which will be of importance for future planification purposes).

Implantable rhodium based self-powered neutron detectors were developed to obtain neutron flux profiles both external and internal. Implantation of SPND was done along the central longitudinal axis of the samples, where lowest flux is expected.

Gamma dose rate was obtained using a neutron shielded graphite ionization chamber moved along external surfaces of the samples.

The internal neutron profile resulted uniform enough to allow for a single and static irradiation of the liver.

For dose estimation, irradiation condition was set in order to obtain a maximum of 15 Gy-eq in healthy tissue. Additionally, literature reported boron concentrations of 47 ppm in tumor and 8 ppm in healthy tissue and a more conservative relationship (30 ppm / 10 ppm) were used.

To make a conservative estimation of the dose the following considerations were done:

i. Minimum measured neutron flux inside the sample (~5 10^9 n cm^{-2} s^{-1}) was considered to calculate dose in tumor.
ii. Maximum measured neutron flux (considering both internal as external profiles) was used to calculate dose in healthy tissue (~8.7 10^9 n cm^{-2} s^{-1}).
iii. Maximum measured gamma dose rate (~13.5 Gy h^{-1}) was considered for both tumor and healthy tissue.

Tumor tissue dose was ~69 Gy-eq for 47 ppm of ^{10}B and ~42 Gy-eq for 30 ppm, for a maximum dose of 15 Gy-eq in healthy tissue. As can be seen from these results, even for the most conservative case, minimum tumor dose will be acceptable from the treatment point of view, which shows that the irradiation conditions at this facility have quite good characteristics for the proposed irradiation.

Keywords: BNCT, liver dose estimation, ex-situ irradiation.

1. Introduction

Taormina project (Pinelli et al, 2002) introduced a new BNCT concept to treat unresectable multifocal liver metastasis by the ex-situ irradiation of the organ and its ulterior re-implantation. Based on this protocol, a novel treatment that combines the autograft technique with the irradiation of the segments II-III of the human liver left lobe was proposed in the frame of the Argentine BNCT Project (Cardoso et al, 2007).

To estimate the expected dose for the BNCT liver treatment, it was decided to experimentally determine neutron flux and gamma dose rate profiles in samples equivalent to the segments to be treated. Irradiations were performed at the thermal column of the RA-3 reactor, where future treatments would be done (Miller et al. 2008).

In this work, results from the characterization and some calculated dose values, derived from them under conservative conditions, are shown.

2. Material and Methods

I. Neutron flux profile determination

To obtain neutron profiles, a pig liver right lobe was used as equivalent sample. This portion had similar weight, shape and dimensions to the maximum values expected in the human liver left lobe, i.e.: ~300 g, ~16 cm length, ~12 cm width and ~4,5 cm maximum height. The irradiation was performed in order to take into account all the considerations to simulate a real-case irradiation (Crawley et al., 2007). For this purpose the sample was introduced inside two polythene bags and covered with 100 cm^3 of demineralized water simulating the neutron flux attenuation by the presence of the preservation solution. The bags were closed and the ensemble was positioned into an acrylic container especially designed to maintain sample positioning and keep temperature low. The thickest part of the sample was leaning in the front surface of the container which is the nearest surface to the core, as can be seen in figure 1.

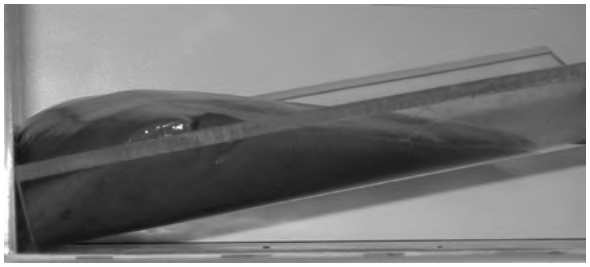

Figure 1. Detail of the position of the pig liver portion inside the container

To determine neutron flux profiles inside and outside the sample, two implantable rhodium based self-powered neutron detectors (SPND) were especially developed. Detectors had 0.2 cm of diameter and 20 cm length which allowed insertion in the sample and the possibility of covering its full extension. On the other hand, sensitive zone was 1 cm which provided the tool for a local determination. As main characteristics, detectors were watertight and had a sharp ended for easy insertion reducing tissue damage. Figure 2 shows the developed detectors.

One SPND was implanted along the central longitudinal axis of the sample, where lowest flux is expected, while the other was positioned along the longitudinal axis of the container, between the polythene bags and the container, to obtain respectively the internal and external neutron flux profiles, as can be seen in Figure 3.

Figure 2. Implantable self-powered neutron detectors

Figure 3. Sample positioned inside the acrylic container with detectors

A third not implantable SPND was positioned on the front surface of the sample, outside the bags because this point was expected to be the highest flux point.

For the determination of the flux profiles, both implantable SPNDs were positioned with their sensitive zones as close as possible to the front of the container, at around 1 cm from the surface of the sample. Then this assembly was introduced inside the thermal column to be irradiated as long as necessary to reach the saturation zone of the signal. After that, the system was withdrawn from the column, both detectors were positioned at the next point of interest and a new irradiation was carried out. This process was repeated up to complete both neutron flux profiles.

The first three points measured with the implantable SPNDs were performed every 1 cm while the last six points every 2 cm. To monitor always maximum flux, the third detector was not moved during irradiation. Currents were measured with a Keithley Electrometer Mod. 6514. Power operation of the reactor was ~8 MW.

II. Gamma dose rate profile determination

Gamma dose rate profiles were obtained using a 0.1 cc graphite ionization chamber neutron shielded with a ^{6}LiF cap. A portion of cow liver with similar shape, weight and dimensions to segments II-III of human liver, was used as equivalent sample. Same experimental setup than the used for neutron flux determination was adopted.

To evaluate the relative weight of different contributions to gamma dose rate three profiles along the longitudinal axe of the place for the sample were obtained. First profile was measured in air (structural gamma), a second profile was taken in the empty container (acrylic contribution) and the last profile included the equivalent sample (sample contribution). Each profile shows data taken in the position nearest to the core, in the center and backwards. For sample profile, measurements were done in external positions, because of detector characteristics. Currents were measured with a Keithley Electrometer Mod. 6517A. Power operation of the reactor was ~8 MW.

III. Dose estimation

Dose estimation was performed using the results of the neutron flux and gamma dose rate profiles. Irradiation time was set in order to obtain a maximum of 15 Gy-eq in healthy tissue (Pinelli et al, 2002). To make a conservative estimation, minimum measured neutron flux inside the sample was considered to calculate dose in tumor, and maximum measured neutron flux (considering both internal as external profiles) was used to calculate dose in healthy tissue. To be conservative, maximum measured gamma dose rate was used to perform gamma dose estimation for both tumor and healthy tissue. Using profiles obtained in samples of maximum expected sizes, is also a conservative condition.

Dose coming from fast neutron was neglected based on spectral characteristics of the facility (Miller et al., 2008)

Concerning boron concentration, two sets of values were used. A first calculation was performed using literature reported values of 47 ppm in tumor and 8 ppm in healthy tissue (Koivunoro et al., 2004). A second calculation was done using a more conservative relationship (30 ppm / 10 ppm). Adopted constants for calculation were: neutron (thermal) kerma factor for liver, 2.41 10^{-17} Gy m^2 (ICRU 46, 1992), RBE for N, 3.2; CBE (BPA) for tumor, 3.8 and CBE for healthy tissue 1.3 (Koivunoro et al., 2004).

3. Results and discussion

I. Neutron flux profile determination

Both internal and external neutron flux profiles are shown in figure 4. While external flux profile monotonically decreases with distance, it can be appreciated that internal flux profile presents a considerably uniformity.

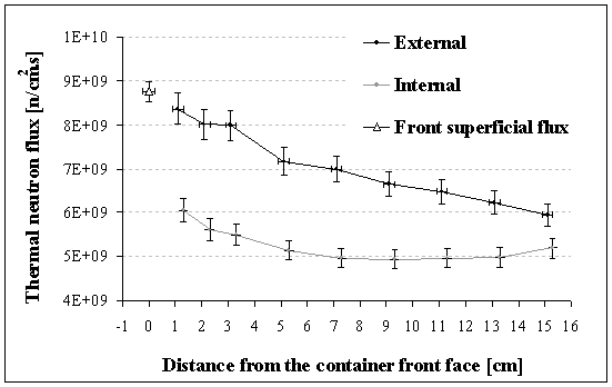

Figure 4. External and internal neutron flux profiles

This effect was related with the compensation between the narrowing of the liver lobe and the falling of the external neutron flux. The neutron flux value measured on the front surface of the sample (marked as Front superficial flux in figure 4) was $(8.7\pm0.9).10^9$ n cm^{-2} s^{-1}, and, as it was expected, it was the highest neutron flux value measured. The lowest neutron flux value measured inside the sample resulted equal to $(5.0\pm0.6).10^9$ n cm^{-2} s^{-1}. These two neutron flux values were used for dose estimation.Comparing flux measured on the frontal surface with the first value measured inside the sample (at ~1 cm), it can be seen a very important flux drop in this zone. To minimize this change and improve neutron flux and, consequently, dose uniformity in the entrance, future configurations will consider the use of a bolus of tissue equivalent material of around 1 cm width.

II. Gamma dose rate profile determination

Obtained gamma dose rate profiles are shown in figure 5. From these values, it can be said that average dose rate in air (in the space for samples) is of about 5.6 Gy h^{-1} while average increases coming from the container and sample are 3.1 and 3.8 Gy h^{-1} respectively. Relative weights of these averages in the mean total gamma dose rate (12.5 Gy h^{-1}) are ~45% (structural gamma), ~25% (container) and ~30% (sample).

The maximum measured value, obtained in the central position and equal to (13.5±1.5) Gy h^{-1}, was adopted for gamma dose rate estimation. As this is an external value, future internal gamma characterization using different techniques, should be done to improve results.

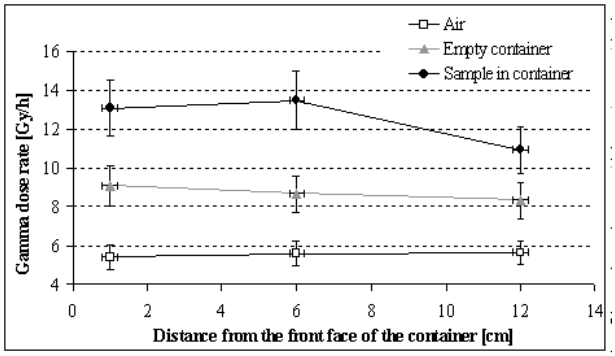

Figure 5. Gamma dose rate profiles

III. Dose estimation

Table 1 summarizes preliminary dose calculations performed by choosing irradiation time in order to have 15 Gy-eq in healthy tissue. Uncertainties are approximately ±10%.

Table 1. Estimated dose values

Tissue	^{10}B [ppm]	Irrad. Time [s]	Doses [Gy-eq]			
			γ	N	B	Tot.
Tumor	47	815	3.1	3.1	62.3	68.5
Healthy	8	815	3.1	5.5	6.4	15.0
Tumor	30	735	2.8	2.8	36.1	41.7
Healthy	10	735	2.8	5.0	7.2	15.0

These results show that, considering literature boron concentration values, tumors would receive a dose greater or equal to 68.5 Gy-eq while dose in healthy tissue would be less or equal to 15 Gy-eq. Additionally, even for the most conservative case, minimum tumor dose would be 41.7 Gy-eq, which is an acceptable value from the treatment point of view. In both considered cases, boron dose in tumor was of around the 90% of the total dose and near the 50% in healthy tissue. It is important to note that these dose results correspond to a single and static irradiation of the sample of maximum expected dimensions.

Maximum weight of gamma dose in total dose, in healthy tissue, was around 20%. A more confident estimation of gamma dose could be performed when internal dose rate values were available.

From results it can also be inferred that the maximum relative weight of the acrylic container contribution to total dose in healthy tissue is of around 5%. This contribution could be significantly reduced if Teflon were used instead but, as this maximum 5% is relatively low; it was so far preferred to keep acrylic as material due to its workability characteristics and transparency.

4. Conclusions

Neutron flux distribution obtained in samples equivalent to segments II-III of human liver irradiated in the thermal column of the RA-3 reactor, resulted uniform enough to allow the treatment of metastasis in a single and static irradiation.

Even for the most conservative conditions considered (boron concentration and sample size), treatment required doses in tumor (no matter where it were located) could be obtained without exceeding tolerance dose in healthy tissue.

References

Pinelli, T., Zonta, A., Altieri, S., Barni, S., Braghieri, A., Pedroni, P., Bruschi, P., Chiari, P., Ferrari, C., Fossati, F., Nano, R., Ngnitejeu Tata, S., Prati, U., Ricevuti, G., Roveda, L., Zonta, C., 2002. "Taormina: from the first idea to the application to the human liver", Monduzzi Editore, Research and development in Neutron Capture Therapy. Proceedings of the 10th ICNC T: 1065-1072.

Cardoso, J., Trivillin, V., Heber, E., Nigg, D., Calzetta, O., Blaumann, H., Longhino, J., Itoiz, M., Bumaschny, E., Pozzi, E., Schwint, A., 2007. "Effect of Boron Neutron Capture Therapy (BNCT) on Normal Liver Regeneration: Towards a Novel Therapy for Liver Metastases", International Journal of Radiation Biology Oct; 83(10): 699-706

Miller, M., Quintana, J., Ojeda, J., Langan, S. Thorp, S. Pozzi, E. Sztejnberg, M., Estryk, G.., Nosal, R., Saire, E., Agrazar, H., Graiño, F., 2008. "New irradiation facility for biomedical applications at the RA-3 reactor thermal column". Proceedings of the 13th ICNCT.

Crawley, V., Gadan, M., 2007. "Caracterización preliminar de la facilidad de irradiación de muestras biológicas del reactor RA-3 para la implementación del tratamiento de metástasis en hígado con BNCT", Facultad de Ingeniería y Ciencias Exactas y Naturales, Universidad Favaloro.

Koivunoro, H., Bleuel, D., Nastasi, U., Lou, T., Reijonen, J., Leung, K., 2004. "BNCT dose distribution in liver with epithermal D-D and D-T fusion-based neutron beams". Applied Radiation and Isotopes, vol. 61, 5: 853-859.

ICRU Report 46, 1992.

Dose imaging in a thorax phantom with lung-equivalent volume at the epithermal neutron beam of LVR-15 reactor

G. Gambarini[a,b], E. Vanossi[c,b], G. Bartesaghi[a,b], M. Carrara[d], M. Mariani[c], A. Negri[a,b], J. Burian[e], L. Viererbl[e], V. Klupak[e], J. Rejchrt[e]

[a] *Department of Physics, University of Milan, Italy*
[b] *INFN – National Institute of Nuclear Physics, Division of Milan, Italy*
[c] *Department of Energy, Polytechnic of Milan, Italy*
[d] *Fondazione IRCCS "Istituto Nazionale Tumori", Milan, Italy*
[e] *Department of Reactor Physics, NRI Rez, plc, Czech Republic*

Abstract

A thorax phantom has been designed, consisting of PMMA and PE layers, containing a cavity filled with a lung-substitute that is a material having good tissue-equivalence with lung. Fricke gel dosimeters have been placed in the lung-substitute volume, and the phantom has been irradiated at the epithermal column of the LVR-15 reactor of Rez. Images of the absorbed doses have been obtained for both gamma radiation and charged particles emitted in the ^{10}B reactions with thermal neutrons. Some measurements with TLDs have been performed too, in order to attain inter-comparison of results.

Keywords: Phantom, Lung, Dose imaging, Gel dosimetry, epithermal neutrons

1. Introduction

In the last years, noticeable interest has grown regarding lung cancer treatment. Nowadays, lung has been considered a candidate for boron neutron capture therapy (BNCT) application.

In order to perform reliable dosimetry aimed at validating treatment planning calculations, it is necessary to design suitable phantoms having good tissue-equivalence for neutrons and for every secondary radiation. Considering that lung density is largely lower than that of the other tissues, a preliminary study has been carried out to develop a material having proper characteristics to simulate lung tissue.

According to ICRU-44, the reference man lung density varies between 0.2 $g \cdot cm^{-3}$ and 0.5 $g \cdot cm^{-3}$ and a mean value 0.34 or 0.35 $g \cdot cm^{-3}$ is usually utilised. In this work, a gel matrix having the proper density of lung (0.34 $g \cdot cm^{-3}$) has been prepared and the tissue equivalence for both photons and thermal and epithermal neutrons has been investigated. This tissue-equivalent matrix has been obtained from a gel in which a surfactant was properly incorporated, which has the role of increasing the gel surface tension. The proper procedure has been set up, in order to attain the density of 0.34 $g \cdot cm^{-3}$. The preparation protocol has been then optimized.

The produced material has been studied in order to investigate the correctness of its properties. The mass density of the obtained material has been controlled by means of a precision balance. Both uniformity and electron density have been inspected by measurements with Computed Tomography (CT). Monte Carlo simulations have been performed in order to evaluate photon and neutron transport properties. The stability in time of the gel foam at room temperature and up to 40°C has been studied too.

Lung-equivalent phantoms of suitable design were prepared with this gel foam. A section of thorax phantom was also prepared, containing a cavity for inserting the lung substitute in which proper dosimeters can be positioned for dose imaging or mapping.

Dose distributions have been measured at epithermal neutron of the BNCT facility at the Nuclear Research Institute of Řež (Czech Republic).

2. Materials and methods

The laboratory-made lung-equivalent material is properly prepared with water, a gelling agent (gelatine) and a surfactant (sodium-dodecyl-sulfate) to increase the surface tension, as suggested by De Deene (2006). The chemical composition is the following:

Gelling agent: Porcin skin: 6% w/w
Sodium-dodecyl-sulphate: 0.15% w/w
De-ionized water : 93.85% w/w.

By means of appropriate whipping, some air is incorporated in the gel matrix and a gel foam is finally obtained, with a mass density of 0.33 $g \cdot cm^{-3}$ in agreement with ICRU 44. Mass homogeneity and electron density have been controlled by means of a computed tomography (CT) Picker PQ2000 scanner. A dedicated subroutine (written with MatLab® support) has been developed to perform 3D image reconstruction by means of the CT slices. The value of the mean relative (to water) electron density is 0.27.

Neutron transport has been controlled by means of Monte Carlo simulations, using the code MCNP-X. Examples of the obtained results are shown in Figs. 1 and 2 where the percentage depth dose (PDD) are reported, obtained for mono-energetic photon or neutron beams on a material having the composition of the gel foam and on ICRU lung respectively. The results have confirmed the satisfactory lung-equivalence for neutrons of the proposed material.

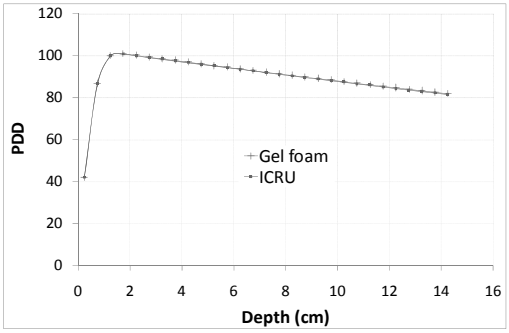

Fig. 1 – PDD for a 2.2 MeV photon beam

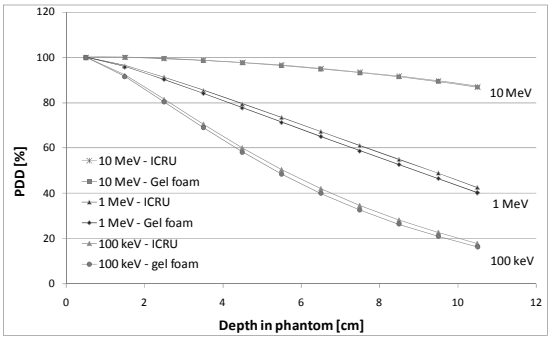

Fig. 2 – PDD for neutron beams of various energies

A phantom (named Ely) has been prepared for dose imaging in BNCT lung treatment. The phantom, shown in Fig. 3b, is made with layers of polyethylene and PMMA having thickness of 10 mm and 20 mm, suitably cut and settled to simulate part of a thorax trunk. The total thickness is of 20 cm, both height and width are 30 cm.

In this phantom, a volume having the shape of a truncated cone is filled with the lung-substitute, as shown in Fig. 3a.

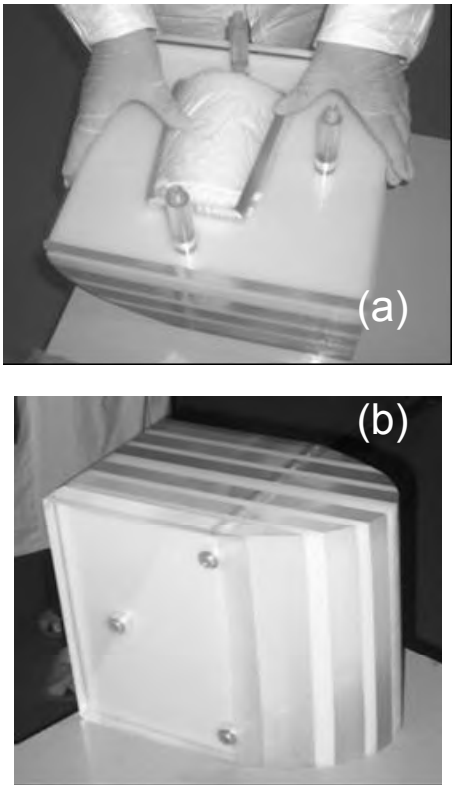

Fig. 3 - Ely phantom containing lung substitute, (a) during set up and (b) ready for exposure

For performing dosimetry measurements, the lung substitute has been cut in horizontal or vertical planes, in order to insert the suitable dosimeters. Two phantoms in the phase of set up are shown in Fig. 4.

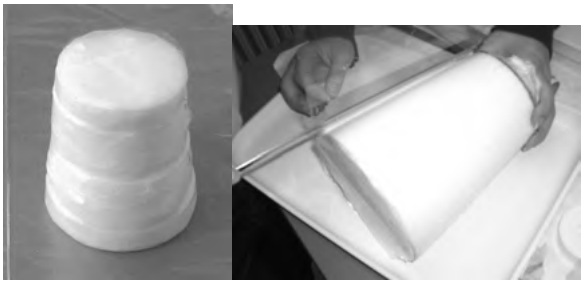

Fig. 4 – Lung phantoms, cut along (a) three horizontal planes and (b) one vertical plane, in order to place dosimeters.

Dose measurements were carried out by means of gel dosimeter layers, in order to obtain dose images. For inter-comparison of results, dose mapping with thermoluminescence dosimeters (TLD) were performed too. To this purpose, LiF:Mg,Ti (TLD-700 and TLD-600) and CaF2:Tm (TLD-300) chips were utilised. Gel dosimeters were laboratory-made Fricke gel layers having thickness of 3 mm. The absorbed dose is deduced by pixel-to-pixel manipulations of the light transmittance images detected by means of a CCD camera. By placing, in the Ely phantom's lung, couples of dosimeters having different isotopic content (Gambarini et al., 2000) and applying suitable algorithms, the images of the therapeutic dose from ^{10}B reactions and the photon dose were achieved.

In the vertical plane of the lung phantom, rectangular dosimeters were positioned, 8 cm wide and 10 cm high, as shown in Fig. 5. In the horizontal planes, circular dosimeters were placed of different diameter, near to the diameters of each sections.

Fig. 5 – Lung phantom cut in the vertical plane, in which gel dosimeters were placed

The phantom has been exposed against the collimator exit of the BNCT epithermal column of LVR-15 reactor, as shown in Fig. 6.

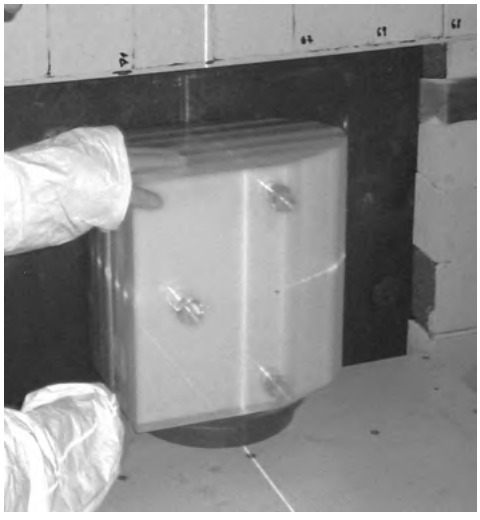

Fig. 6 – Phantom placed against the collimator exit of the LVR-15 BNCT epithermal column

3. Results

In Fig. 7, photon and ^{10}B dose images are shown in a 3D representation.

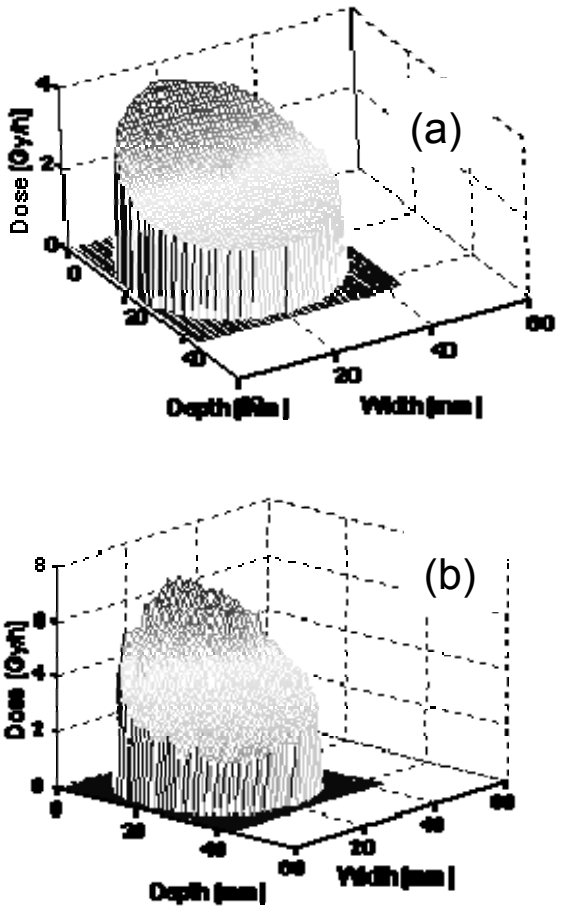

Fig. 7 – 3-D representation of (a) photon dose (b) ^{10}B dose in the central plane of the lung phantom

From the images, dose profiles have been extracted. The profiles have been compared with the results obtained with TLD chips, when available. In Fig. 8, the photon dose profile extracted from the image of Fig. 7 is reported with the results of TLD 300 measurements.

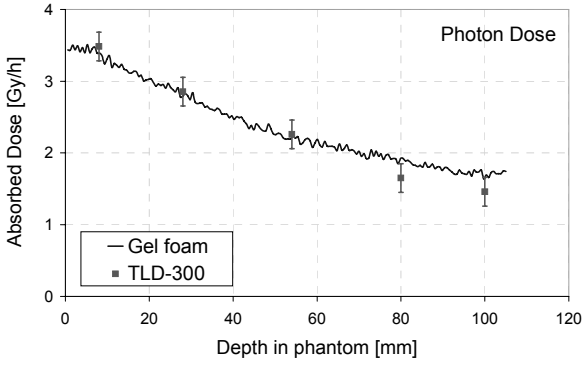

Fig. 8 – Photon dose central profile along beam axis, extracted from the image of Fig. 7

Photon and ^{10}B profiles along the beam axis, extracted from images obtained by means of vertical rectangular dosimeters inserted in the lung-substitute volume, are reported in Fig. 9.

In order to attain information that could be useful support in considering the advantages of performing the patient treatment by irradiating AP and PA, the profiles have been added to the same that were reversed. Regarding the profiles along the beam axis, this should give the same result as that obtained if the phantom at half time is rotated of 180°. The so obtained dose profiles, both for photon and ^{10}B doses, are noticeably flat. These results are reported in Fig. 9.

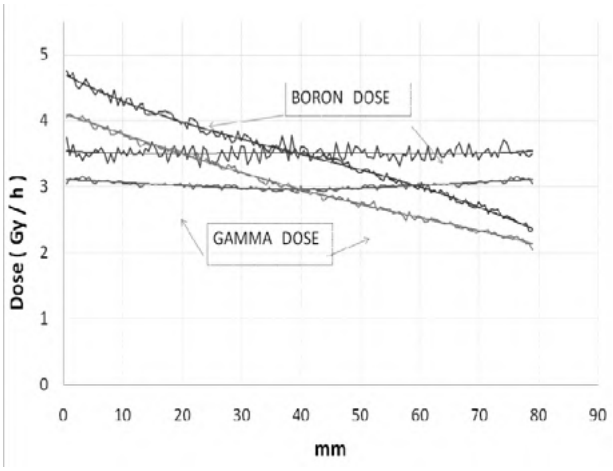

Fig. 9 – Photon and ^{10}B dose profiles along the beam axis, with the phantom irradiated from the front and with the phantom rotated 180° for the second exposure

4. Conclusions

In conclusion, the described method for lung-equivalent gel foam preparation can be useful for BNCT research in order to compose suitably shaped phantoms and carry out dosimetric measurements for lung treatments. The studied gel foam successfully simulates lung tissue properties and represents a promising material for performing reliable dosimetry in thermal or epithermal neutron fields. The obtained results can be useful for verifying the suitability of BNCT lung treatment, showing also the convenience of irradiating the patient half time from the front and half time from the back.

Further analyses of the acquired images and further measurements with the same method will give wider useful information.

Acknowledgments

This work was supported by the National Institute of Nuclear Physics (INFN), Italy.

References

De Deene Y., 2006. Three dimensional radiation dosimetry in lung-equivalent regions by use of a radiation sensitive gel foam: Proof of principle. Med.Phys. 33, 2586-2597

Gambarini, G., Agosteo, S., Marchesi, P., Nava, E., Palazzi, P., Pecci, A., Rosi G., Tinti, R., 2000. Discrimination of various contributions to the absorbed dose in BNCT: Fricke-gel imaging and intercomparison with other experimental results. App. Rad. Isot. 53, 765-772.

TLD-700 glow curve shape for determining thermal neutron fluence and gamma dose in BNCT beams

G. Gambarini[a,b] S. Agosteo[c,b], M. Carrara[d], F. Lobefalo[a], G. Rosi[e]

[a]*Department of Physics, University of Milan, Italy*
[b]*INFN Milan, Italy*
[c]*Department of Energy, Polytechnic of Milan, Italy*
[d]*Fondazione IRCCS "Istituto Nazionale Tumori", Milan, Italy*
[e]*FIS-NUC, ENEA, Casaccia, Rome, Italy*

Abstract

A simple and fast method for measuring gamma dose and thermal neutron fluence in a BNCT gamma-neutron mixed-field by means of a single thermoluminescence dosimeter (TLD-700) is proposed and tested. The method is based on the GC of the TLD-700 exposed in the mixed field, whose shape is referred to that of the gamma-calibration GC of the same TLD, and that of a TLD-600 exposed in a BNCT field, uncalibrated. Some results are reported, showing the consistency of the method.

Keywords: BNCT, neutron dosimetry, TLD-700, gamma dose, neutron fluence

1. Introduction

The measurement of the photon dose in radiation fields having suitable characteristics for boron neutron capture therapy (BNCT) requires the development of appropriate methods. In reactor thermal columns and in phantoms exposed in thermal or epithermal columns, the thermal neutron flux is very high and produces a significant contribution to the response of most dosimeters.

Thermoluminescence dosimeters (TLDs) are widely used in BNCT experiments, both for in-free-beam and in-phantom measurements. Coupled ^{7}LiF and ^{6}LiF variously doped phosphors are widely exploited. In fact, owing to the high cross section for thermal neutrons of the isotope ^{6}Li, the photon and thermal neutron sensitivity of dosimeters containing different percentages of such an isotope are different. Moreover, the relative heights of the two peaks in the dosimeter glow curve (GC), that is the thermoluminescence (TL) emission detected during dosimeter heating, are different after thermal neutron or photon irradiations. In Fig.1, the GCs of a ^{6}LiF TLD after (a) gamma and (b) thermal neutron irradiations are shown.

For gamma dose measurements, ^{6}Li depleted ^{7}LiF chips are the most commonly used TL dosimeters. In environmental or personal dosimetry, these TLDs give good results for gamma dose measures because in such radiation fields the neutron contribution is negligible. The situation is different when the same dosimeters are exposed to BNCT fields, where thermal neutron flux is high and gamma dose rate is low, because a small amount of ^{6}LiF is always present. In fact, complete removal of ^{6}LiF is not possible and pure ^{7}LiF cannot be produced. In this study, the following TLDs (by Harshaw) are considered:

TLD-600 (^{6}LiF:Mg,Ti 95.6% ^{6}LiF),
TLD-700 (^{7}LiF:Mg,Ti 99.9% ^{7}LiF).

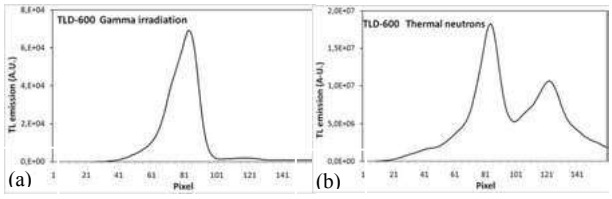

Fig. 1. GCs of a TLD-600 after (a) gamma and (b) thermal neutron irradiations

Owing to the low presence of ^{6}Li in TLD-700, both gamma rays and neutrons contribute to the TLD-700 luminescence when the neutron fluence to gamma dose ratio is that typical of BNCT neutron fields. Suitable subtraction of the neutron contribution is therefore necessary in order to obtain reliable values for the photon dose, and this problem was extensively studied by BNCT researchers (Aschan et al., 1999).

In a recent work (Gambarini et al., 2008) a

method has been proposed for achieving the evaluation of the photon dose from the GC of a TLD-700 without measurements or calculations of the thermal neutron fluence in the positions of dosimeters, but with the unique knowledge of the shape of the GC of a TLD-600 exposed in the mixed neutron-photon field.

The method has then been extended to achieve both photon dose and thermal neutron fluence from the GC of a single TLD, with the unique condition of knowing the dosimeter calibration for each radiation. The procedure is very simple and fast. The precision of the results depends on the specific mixed photon-neutron field: the contributions of photons and thermal neutrons to the TL emission must be not much different, that is none has to be largely predominant. This condition is often met in BNCT neutron fields. On the other hand, a general method for measuring both components of a mixed neutron-gamma radiation field from a single TLD, effective in whichever n-γ field, is not possible, as already revealed in 1994 by Herminghuysen et al.

2. Method

The idea of developing the method below described has originated from some peculiarities that were noticed during previous studies regarding the utilization of TLDs for BNCT dosimetry. TLDs are particularly convenient for dose or thermal neutron mapping in neutron fields, because, due to their small volume, they do not sensibly perturb the radiation field. CaF_2:Tm (TLD-300) phosphors are very convenient for measurements in large phantoms, where the gamma dose is mainly due to the 2.2 MeV photons generated by the neutron reactions with H. However, when the reactor background constitutes large part of the gamma field, their utilizations is very problematic because of the noticeable dependence of the response on photon energy, principally for energies below 100 KeV (Gambarini et al., 2004a). Moreover, they are presently not on sale. During the mentioned extensive study on LiF dosimeters, the GC of TLD-700 after in-phantom irradiation in a thermal or epithermal column designed for BNCT has been widely studied. Among other things, the contribution of photons to the TL emission of a TLD-700 has been determined by measuring the gamma dose, in the same position inside the phantom, with a TLD-300 and then multiplying by this dose value the content of all the pixels of the gamma-calibration GC (per dose unit) of the TLD-700. It was observed that, if the so obtained curve is subtracted, pixel-by-pixel, from the GC of the TLD-700, then the resulting curve, representing the contribution of thermal neutrons to the TL emission, has a shape very similar to that of a TLD-600 after exposure in a thermal neutron field, obviously with a different scale. An algorithm has therefore been formulated to obtain both thermal neutron fluence and gamma dose from the GC of a single TLD-700. The algorithm requires the calibration of the dosimeter to photons and to thermal neutrons, and the ratios between the two main peaks of the GCs of a TLD-600 irradiated with thermal neutrons and of a TLD-700 irradiated with photons. If only the TLD-700 gamma calibration is available, only the photon dose is obtained, but in a simple way, without the necessity of subtracting the thermal neutron contribution determined with another detector or by calculations.

The algorithms for obtaining gamma dose and thermal neutron fluence with a single TLD-700 were formulated by considering that, after having subtracted the instrumental background, the heights H_1 and H_2 of the two dosimetric peaks in the GC of a TLD-700 exposed to a BNCT field can be related to the gamma dose D and thermal neutron fluence Φ by the relations:

$$(1) \qquad \begin{aligned} H_1 &= D\,H_1^{\gamma} + \Phi\,H_1^{n} \\ H_2 &= D\,H_2^{\gamma} + \Phi\,H_2^{n} \end{aligned}$$

where H_1^{γ}, H_1^{n}, H_2^{γ} and H_2^{n} are the heights of the first and second peaks respectively of the gamma and thermal neutron contributions in the GC, normalised to dose and fluence units. This assertion is to some extent approximated, because thermal neutrons produce a small shift in the peak positions. However, this shift is generally smaller than the peak-position uncertainty due to common instrumental imprecision, mainly coming from small differences in the heating rate of the chips. Often a preliminary GC shift has to be performed for carrying out the following procedure.

Knowing the calibrations of the TLD-700 chips both to gamma and thermal neutrons, it is possible to obtain both gamma dose and thermal neutron fluence. By the equations (1), we arrive to two simple equations for gamma dose and thermal neutron fluence:

$$(2) \qquad D = \frac{H_2 \cdot R_n - H_1}{H_2^{\gamma} \cdot R_n - H_1^{\gamma}}$$

$$(3) \qquad \Phi = \frac{H_2 \cdot R_{\gamma} - H_1}{H_2^{n} \cdot R_{\gamma} - H_1^{n}}$$

where $R_n = H_1^{n} / H_2^{n}$

and $R_{\gamma} = H_1^{\gamma} / H_2^{\gamma}$.

The ratio R_{γ} is evaluated from a gamma calibration GC of the TLD-700. Owing to the

similarity of the shapes of the thermal-neutron-GCs of TLD-600 and TLD-700, the ratio R_n is evaluated using the heights of the first and second peaks in the GC of an uncalibrated TLD-600 exposed to a thermal neutron field. In practice, the TLD-600 can be irradiated or in-free-beam in a BNCT thermal column or in a phantom exposed to a BNCT epithermal beam. In both cases the gamma contribution, in the TLD-600 GC, is usually negligible. However, this particular must be verified, simply by checking if the R_n value is the same, within the experimental error, for TLDs-600 placed in different positions of the field. If not, a position with lower gamma-dose to thermal-neutron ratio has to be exploited. The determination of R_n is generally simple, and it can be performed only once and then utilised for whichever subsequent campaign of measurements. The only condition is, obviously, to utilise always the same parameters for the GC analysis instruments, because the GC shape depends on reading conditions, particularly on the dosimeter heating rate, as said before.

The values of H_1^{γ} and H_2^{γ} necessary for evaluating the gamma dose are taken from the gamma calibration GC of the TLD-700, normalised to dose unit.

The values of H_1^{n} and H_2^{n} necessary for evaluating the thermal neutron fluence are taken from the thermal neutron calibration GC of the TLD-700, normalised to fluence unit. If it is not possible to perform a direct thermal neutron calibration of TLDs-700 for achieving the corresponding GCs, an alternative method is possible based on the results themselves obtained with the procedures here described. This suggestion will be given in the following Section.

3. Results

In-phantom measurements have been carried out to test the method. The results have been compared with those obtained with gel dosimeters.

The phantom was made with tissue equivalent gel hold in a cylindrical polyethylene container (11 cm of height and 11 cm of external diameter) with thin walls (0.2 cm thick). The phantom was exposed in the new thermal column (Esposito et al, 2007) of the TAPIRO fast reactor of ENEA (Casaccia, Rome, Italy). The phantom is composed of two parts, suitably prepared in order to set the dosimeters in the central plane. In Fig. 2, a view of the phantom placed in the column is shown.

In the phantom, TLDs were placed in a polyethylene holder having properly shaped cavities of the dimensions of the dosimeters ($3\times3\times0.9$ mm^3) in order to avoid empty volumes inside the phantom.

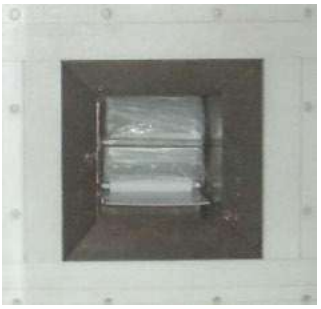

Fig. 2. View of the phantom in the thermal column

Some measurements with gel dosimeters were also carried out, for intercomparing the results. To this aim, couples of Fricke gel dosimeters in form of layers were prepared, one containing ^{10}B and one without. By means of a properly developed method (Gambarini et al., 2007), the images of gamma and boron dose were determined. From such images, the dose profiles were extracted. In Fig. 3, two examples of gamma dose profiles along the beam axis are reported, together with the gamma dose values obtained with TLDs-700 by means of the equation (2). In (a) the phantom was placed as seen in Fig. 2. In (b) the phantom was rotated, with the cylinder axis fitting the beam axis. For the ratio R_n an average value was utilised, obtained by the GCs of a few TLDs-600 previously irradiated in the thermal column, uncalibrated.

Some controls were performed on the TLD-700 GCs, to verify if the shapes of the curves resulting after subtraction of gamma contribution, evaluated by means of equation (2), truly correspond to the 'thermal-neutron-shape'.

An example of such a shape control is shown in Fig. 4, where the curves obtained during the analysis of a TLD-700 utilised for Fig. 3 (b) are reported. In Fig. 4, the higher curve is the original GC of the TLD-700 irradiated in the phantom. The dashed curve is the gamma-contribution to the GC obtained by multiplying the gamma-calibration GC (for dose unit) of the same TLD-700 by the gamma dose value obtained with the described algorithms. Of the other two curves, one is the result of the pixel-by-pixel subtraction of the two previous curves that is the original GC minus the evaluated gamma contribution; the so obtained curve is the thermal neutron contribution in the TLD response. The last curve, not very distinguishable from the previous one, is the GC of a TLD-600 of the group utilised for determining R_n.

If the result of a similar control is good as that of Fig. 4, the obtained curve for the thermal neutron contribution to the TLD-700 response can be used for calibrating the same TLD-700 to thermal neutrons, if the thermal fluence in the position of the

TLD irradiation is known, for example measured with activation foils in another experiment adopting the same geometry. This calibration can then be utilised, when a direct TLD-700 calibration to thermal neutrons is not feasible, for determining by means of equation (3) the thermal neutron fluence, besides the gamma dose, in subsequent experiments.

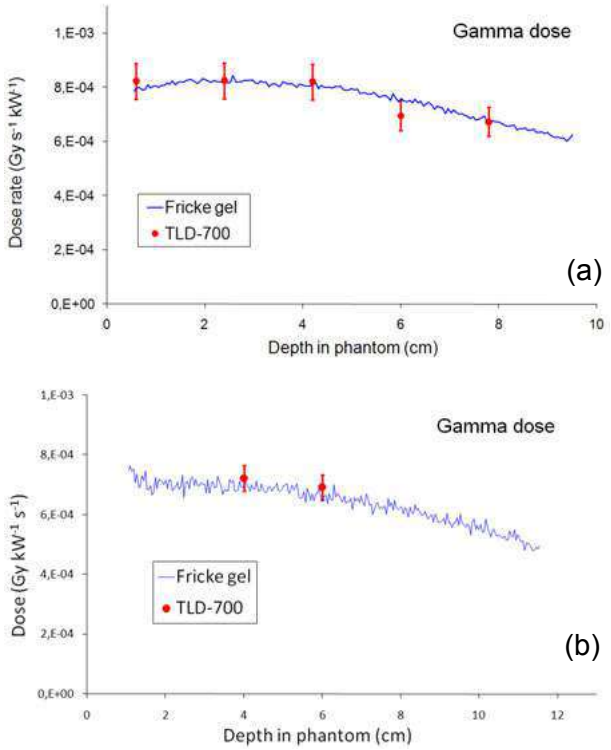

Fig. 3. Gamma dose rate profiles along the beam axis, obtained by TLDs-700 with the proposed method and measured with a Fricke gel dosimeter layer. In (a) and (b) the phantom was settled in different orientations inside the thermal column

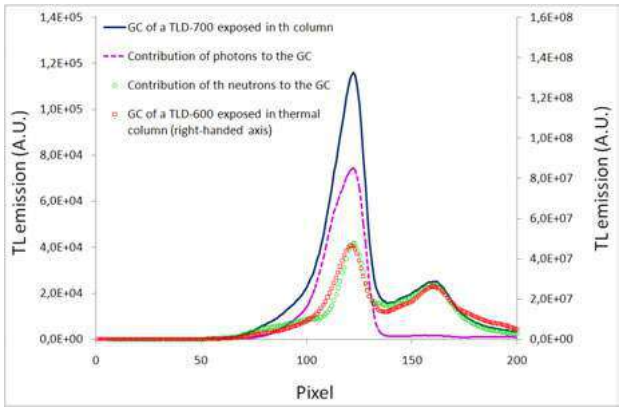

Fig. 4. GC of a TLD-700 irradiated in the cylindrical phantom exposed in the thermal column. The dashed curve is the gamma-contribution to the GC. The two short curves are the thermal neutron contribution to the TLD-700 GC and the GC of a TLD-600

4. Conclusions

The above described method for measuring both gamma dose and thermal neutron fluence utilising a single TLD-700 has shown good potentiality. The method is very simple and not much time consuming.

A noticeable peculiarity of the method is that it gives the capability of evaluating the gamma dose with a TLD-700 dosimeter in situations in which the thermal neutron contribution in the dosimeter response is not negligible, without the necessity of thermal fluence determination for performing the due correction to the dosimeter response.

The reported results show the reliability of the proposed method.

Acknowledgments

The work was supported by INFN (Italy) and by MURST (Prot. 2006029344_002).

References

Aschan, C., Toivonen, M., Savolainen, S., Stecher-Rasmussen, F., 1999. Experimental correction for thermal neutron sensitivity of gamma ray TL dosemeters irradiated at BNCT beams. Radiat. Prot. Dosim. 82, 65–69.

Esposito, J., Rosi, G., Agosteo, S., 2007. The new hybrid thermal neutron facility at TAPIRO reactor for BNCT radiobiological experiments. Radiat Prot. Dosim. 126, 69-73

Gambarini, G., Klamert, V., Agosteo, S., Birattari, C., Fiocca, M., Gay, S., Rosi, G., Scolari, L., 2004a. Study of a method based on TLD detectors for in-phantom dosimetry in BNCT. Radiat. Prot. Dosim. 110, 631–636.

Gambarini, G., Colli, V., Gay, S., Petrovich, C., Pirola, L., Rosi, G., 2004b. In-phantom imaging of all dose components in boron neutron capture therapy by means of gel dosimeters. Appl. Radiat. Isot. 61, 759-763.

Gambarini, G., Gallivanone, F., Carrara, M., Nagels, S., Vogtlander, L., Hampel,G., Pirola, L., 2008. Study of reliability of TLDs for the photon dose mapping in reactor neutron fields for BNCT. Radiat. Meas., 43, 1118-1122.

Herminghuysen, H. R., Blue, T. E., 1994. Development and evaluation of a neutron-gamma mixed-field dosimetry system based on a single thermoluminescence dosimeter. Nucl. Instrum. Meth. A 353, 420-424.

Neutron self-shielding effects and correction factors for foil activation measurements used in BNCT dosimetry

Z. Ghani[a], S. Green[a,b], C. Wojnecki[a,b]

[a] *School of Physics and Astronomy, University of Birmingham, United Kingdom*
[b] *Department of Medical Physics, University Hospital Birmingham, United Kingdom*

Abstract

Self-shielding correction factors for metal foils used to determine B and N kerma by activation analysis have been evaluated by simulation in MCNPX. Correction factors were calculated for two types of foil, one set being non-dilute (solid/metallic) foils of Au and Mn/Ni, the other being dilute foils of 1 % Mn or Au in Al. The non-dilute gold foils exhibit the largest flux depression, perturbing the flux by as much as 80 % at shallow depths and 30 % at depths approaching 10 cm. The non-dilute Mn/Ni foils cause a 5-10 % perturbation at various depths along the central axis of the phantom. Experimental data is presented to validate these simulation results. Further simulations show that the dilute foils, both MnAl and AuAl, perturb the field by less than 1 %.

Keywords: dosimetry, foil activation, self shielding, neutron flux depression

1. Introduction

It is common practice in BNCT to activate Manganese and Gold foils via the (n,γ) capture reaction to determine the thermal neutron flux. The experimentally determined reaction rates can be used, following Freudenreich's theoretical approach [Freudenreich et al. 2005], to derive the Nitrogen (N) and Boron (B) reaction rates, from which the N and B kerma can be deduced. Two types of foil are commonly used in BNCT dosimetry: non-dilute foils and dilute foils. For non-dilute metal foils, the experimentally determined reaction rates require correction for flux depression caused by self-shielding. This paper presents MCNP simulations of the flux depression caused by the non-dilute and dilute foils in a large water tank (LWT) (40 x 40 x 20 cm). An experimental comparison with dilute foils is also provided.

2. MCNP simulations

Monte Carlo simulations were carried out using MCNPX to quantify the degree of self shielding caused by non-dilute foils. Simulations directly compare self shielding effects in dilute and non-dilute foils. The simulations tallied the track length estimate of flux in both dilute and non-dilute foils at various depths in the LWT. These tallies were multiplied by the (n,γ) capture cross-sections of the Mn and Au foils respectively.

The ratio of the dilute to non-dilute saturation activities is the derived correction factor to be applied to non-dilute foils. Separate calculations were performed to determine the correction factors from dilute foils to water.

Saturation activity in the foils change rapidly with depth (as shown in figures 1 and 2). It was therefore deemed necessary to put an upper and lower bound on the simulated results caused by the ±1 mm positional uncertainty on the non-dilute foils. A cubic spline was fitted to the MCNP simulated data for the dilute foil saturation activities vs depth (not shown). Activities 1 mm either side of the assumed measured foil position were then determined.

3. Experimental validation

Experimental work has been carried out to assess the validity of these calculated correction factors in the standard LWT. Non-dilute foils were used as follows:

(a) Mn/Ni (88 % Mn by wt.) of approx 7 mm diameter and 35 mg mass.
(b) Au of approx 5 mm diameter and 50 mg mass.

Dilute foils were approximately 12 mm in diameter and 60 mg in mass [MnAl (1 % Mn by wt.), AuAl (1 % Au by wt.)].

Two rods were inserted 7 cm apart into the phantom, parallel to the neutron beam central axis. Each rod was loaded with either five dilute or non-dilute foils. With this experimental setup dilute and non-dilute foils were irradiated simultaneously overcoming any problems with irradiation reproducibility.

Each activation run was set such that the induced activity in the dilute foils was sufficient to arrive at good counting statistics (<1 %) on a HpGe detector in a reasonable time. The measured counts were converted to saturation activities per gram and the ratio of the saturation activities for dilute to non-dilute foils is the experimental correction factor.

In carrying out the experimental work it was noted that the depth at which the dilute foils were positioned had an uncertainty of ±1 mm, whereas the non-dilute foils were positioned in a far more precise manner with a positional uncertainty of < ±0.5 mm. This mandated the additional calculations described in section 2 to address the positional uncertainty of the dilute foils.

4. Results

All results are presented for the neutron field generated by the action of a 1mA proton current in the Birmingham facility described by Culbertson et al 2003. Figures 1 and 2 show the measured saturation activity per gram of activation material in the foil, for Manganese and Gold foils respectively.

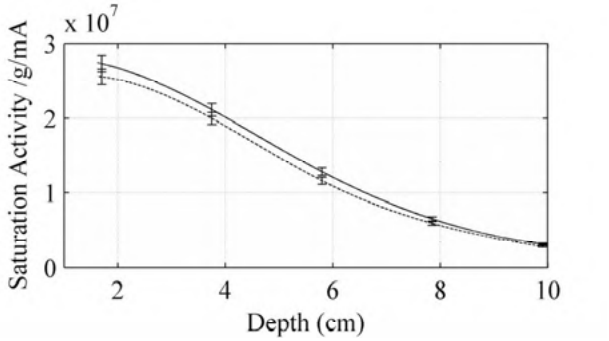

Figure 1 - Experimental saturation activity per gram/mA in non-dilute (dashed line) and dilute Mn foils (solid line) as a function of depth

These figures show that flux depression / self-shielding is a factor in both sets of foils, with the dilute foils reaching higher levels of saturation activity per gram when irradiated with an identical neutron fluence to the non-dilute foils.

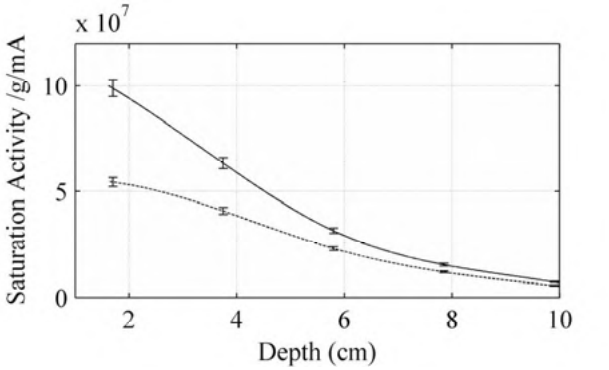

Figure 2 - Experimental saturation activity per gram/mA in non-dilute (dashed line) and dilute Au foils (solid line) as a function of depth

Figures 3 and 4 show the experimental and simulated correction factors for Mn (Figure 3) and Au (Figure 4) foils. The experimental uncertainties shown are to 2σ (i.e. a 95% confidence level).

The bounds (dashed lines) shown plotted in Figures 3 and 4 result from the simulations to assess the impact of the ±1 mm positional uncertainty on the dilute foil. Within this uncertainty bound the experimental and simulations show matching trends with depth for each foil material and similar overall values.

Further simulations for which detailed data is not presented here, show that the perturbation by the neutron flux for dilute foils is negligible and hence these foils are water equivalent.

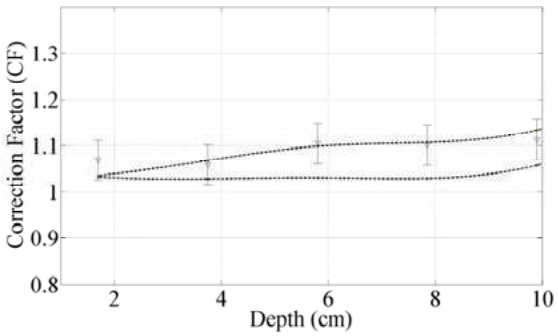

Figure 3 - Manganese foil experimental and simulated self shielding correction factors as a function of depth in LWT [triangular points represent experimental data, dashed lines represent upper and lower bounds of the MCNP simulation]

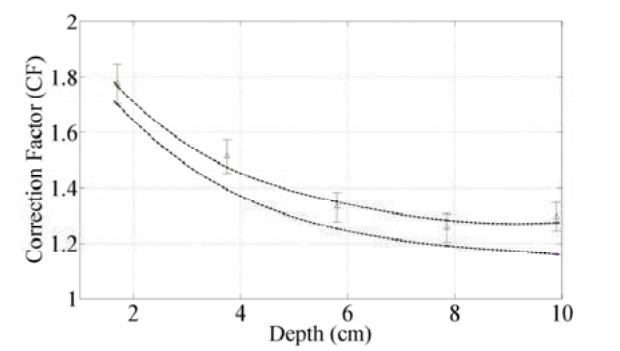

Figure 4 - Gold foil experimental and simulated self shielding correction factors as a function of depth in LWT [triangular points represent experimental data, dashed lines represent upper and lower bounds of MCNP simulation]

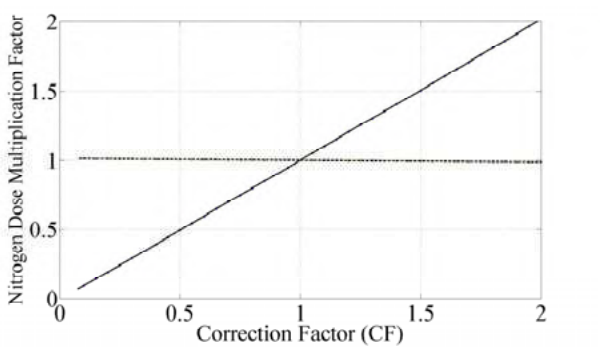

Figure 5 - Effect of Au (dashed line) and Mn (solid line) foil correction factors on the derived Nitrogen dose. [NB. No covariance is plotted here]

5. Discussion

Previous work [Culbertson et al. 2004] had reported correction factors of 5.5 % for non-dilute Mn foils and 17.5 % for non-dilute Au foils. This work also suggested that correction factors do not change significantly with depth. These results are now superceded by the current work, where for Mn the correction factor is approximately 6.5 % near the beam entrance (up to 4 cm deep) rising to 10 % at the brain midline (7 cm). For Au the correction factors are up to 80 % at 2 cm deep falling to 30 % at the brain midline.

The primary goal of Mn and Au foil activations is the derivation of the Boron and Nitrogen dose components. Further work is necessary to examine the impact of our findings on the Au/Cd difference method, but analysis has been performed for the method reported by Freudenreich [2005].

Figure 5 shows the relationship between the perturbation correction factor and kerma for the $^{14}N(n,p)$ reaction determined by the Freudenreich method. For the non dilute Mn foils used in this work, correction factors range from 6 % to 10 % with depth and require the Nitrogen dose multiplication factor ranging from 1.06 to 1.10 (i.e. the relationship between correction factor and kerma is linear for Mn foils). For the Au foils it was found that even the large correction factors that have been determined at shallow depths have relatively small (approx. 2 %) effect on the derived B and N kerma when evaluated with the Freudenreich method.

It should be noted that while this work has brought much greater understanding of the neutron flux perturbation issue, previous publications on the dosimetry results for B and N kerma [Culbertson et al. 2004] are not significantly changed, as uncertainties of ±10 % were reported.

6. Conclusions

Experimentally determined correction factors for non-dilute foils show extremely good agreement with those simulated. When using such non dilute-paired foils for dosimetry these correction factors cause a small but important correction to the derived Nitrogen and Boron dose components.

Further work would be required to generalize these results to activation wires and to dose determination using the Au / Cd difference method.

References

Culbertson, C. N., Green, S., Mason, A. J., Picton, D., Baugh, G., Hugtenburg, R. P., Yin, Z., Scott, M. C., and Nelson, J. M., In-phantom characterisation studies at the Birmingham Accelerator-Generated epithermal Neutron Source (BAGINS) BNCT facility, Applied radiation and isotopes, 2004, 61, p.733-738.

Freudenreich, W. E., Reaction rate relations of thermal / epithermal neutron activation reactions, Report 911234/05.65054/I, NRG, Petten (2005).

BNCT beam monitoring, characterisation and dosimetry

Z. Ghani[a], S. Green[a,b], C. Wojnecki[a,b], R. P. Hugtenburg[c]

[a] *School of Physics and Astronomy, University of Birmingham, United Kingdom*
[b] *Department of Medical Physics, University Hospital Birmingham, United Kingdom*
[c] *School of Medicine, University of Swansea, United Kingdom*

Abstract

Work has been recently carried out at the University of Birmingham Neutron Capture Therapy facility to relocate two neutron monitor chambers (^{235}U fission chambers - Centronic Ltd.). IEC requirements for monitoring radiotherapy beams require the chamber to be in the 'treatment' beam. The problem then arises of neutrons backscattering from patient or phantom affecting the counts at these detectors which are to be located within a 25 mm layer of Lithium polyethylene shielding surrounding the exit port of the treatment facility. The revised monitor position was chosen after detailed consideration of sensitivity to backscattered radiation and detector count-rate. Detailed design calculations with MCNPX are reported and experimental validation of final detector count rates and neutronic coupling presented.

Keywords: beam monitors, monitor chambers, neutronic coupling

1. Introduction

The University of Birmingham's experimental NCT facility is based around a 3MV Dynamitron accelerator, which is used to bombard protons onto a thick natural Lithium target to generate neutrons [Culbertson et al 2004]. Various beam monitors are used to monitor and quantify the patient dose; a Keithley electrometer is used to measure the integrated proton current onto the target, a Geiger counter to monitor the gamma ray field, and two fission chambers, a primary and a secondary, to monitor the thermal neutron flux near the beam exit port.

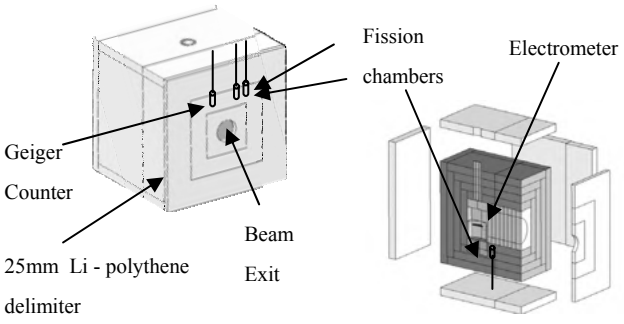

Figure 1 - showing the location of beam monitors relative to the Facilities Beam Shaping Assembly

The fission chambers were originally positioned such that they were separated from the patient / phantom by 20 mm of Li-polythene, the chambers being located in the back of the 25 mm Li-polythene beam delimiter, adjacent to the graphite neutron reflector.

It was found that the original chamber positions were susceptible to movement. Even though this movement might only be slight, the chambers were located close enough to a boundary between two surfaces (the graphite reflector and the Li-polythene delimiter) that they could easily move into high flux regions (out of the shielding). It was decided to relocate the chambers away from the boundary into a more reliable position, this being the 1st goal of the study presented in this paper.

Future plans for the NCT facility include the upgrade of the ion source to yield higher proton currents in order to produce a higher neutron flux at the beam exit port. This could cause unacceptable dead time losses in the fission chambers. Thus the 2nd goal of the relocation of the fission chambers is to reduce the count rate seen by the chambers by a factor greater than 2.

The 3rd goal is to maintain the neutronic coupling levels to less than or equal to 5 %. The coupling being the effect of 'multiple' back-scattered neutrons from patient / phantom positioned at the beam exit port, which cause the chambers to record higher count rates than those recorded for a free beam.

Thus the goals are to locate the chambers such that:

- the chamber positions are stable
- the count rate is reduced to less than half its current rate (i.e to ~approx 4000 cps at 1 mA proton current)
- the neutronic Coupling Ratios are maintained below 5 %

2. Modeling / Simulation

To investigate these requirements and to be able to quantify the neutronic coupling, MCNPX mesh tallies were used over the entirety of the shielding / delimiter surrounding the beam exit port. The simulation consisted of the entire beam shaping assembly, heavy water cooling system and outer shielding.

The Centronic pulse fission chambers used in the facility (FC05A/500/U235) are coated with 500 μgcm^{-2} of UO_2, have an active length of 0.2″ (5.1 mm) and an outside diameter 0.25″ (6.4 mm). The incoming neutrons cause the UO_2 to fission yielding high energy ionising products and generating output pulses from the chamber. The rate of pulse output is proportional to the rate of fission reactions and consequently to the neutron flux.

The neutron spectrum at the beam exit port is strongly epithermal and thus there is a need to allow for the chamber sensitivity to a spectrum of neutron energies when simulating any possible response to the movement and repositioning of these chambers. This was factored into the MCNP model by use of the tally multiplier card to multiply track length estimates of neutron flux by the ^{235}U total fission cross-section (i.e. the active detector material). The mesh tally in MCNPX was used to divide the 25 mm Lithium Polythene layer into small voxels of 1 cm x 1 cm x 0.5 cm. Transport calculations were optimised by using weight windows and tallies were resolved to less than 1 % uncertainty.

3. Neutronic Coupling Ratio

The neutronic Coupling Ratio (CR) was used as a measure of increase in neutron flux due to the presence of phantom / patient at beam exit and can be defined as:

$$CR = \frac{\text{Counts in chamber with phantom}}{\text{Counts in chamber without phantom}}$$

Simulations were carried out with and without the presence of a standard Large Water Tank (LWT) phantom (40 x 40 x 20 cm), each voxel thus recording a measure of the count rate as seen by a typical fission chamber.

4. Results

Results are presented of variations along a vertical line through the centre of the beam exit port. Separate data sets refer to the position within the 25 mm of Li-polythene where the upper-most dotted line represents the inner layer and the lower solid line the outer layer. Figure 2 shows count rate without the phantom and Figure 3 shows the count rate with the LWT. In Figure 2 the greatest detector count rates are seen at positions closer to the neutron source, while in Figure 3 the count rates are greatly increased in the open beam port due to backscatter from the phantom.

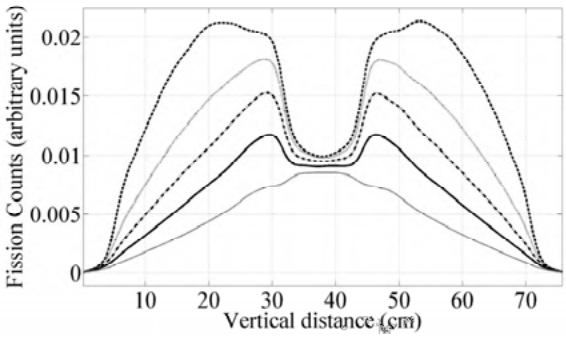

Figure 2 - Fission counts as a function of vertical position (from top of BSA) in each of the five (simulated) layers of delimiter, in the absence of any phantom

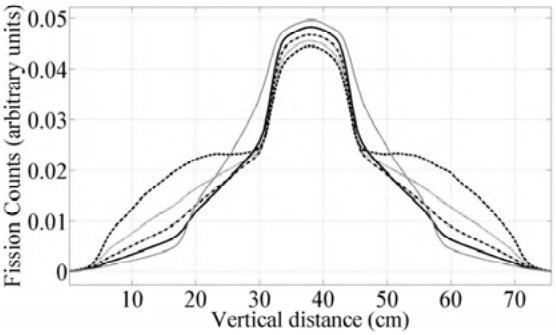

Figure 3 - Fission counts as a function of vertical position (from top of BSA) in each of the five (simulated) layers of delimeter, with large water phantom at the beam exit port

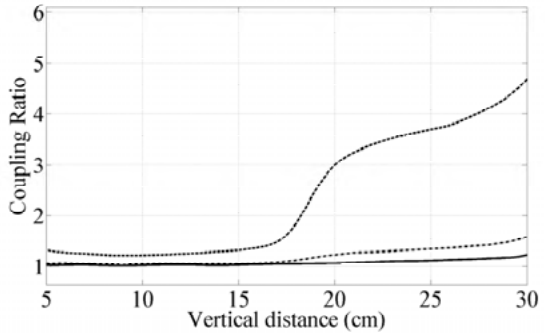

Figure 4 - Coupling Ratio (CR) as function of Depth (from top of BSA) in three layers of delimiter (middle and two extremes)

The requirement to reduce count rate in the monitor chambers suggests that the middle position in the Li-polythene delimiter would be suitable.

Figure 4 shows the coupling ratios for a restricted set of position where monitor chambers could feasibly be located. Three data sets are shown corresponding to the inner, middle and outer layers of the Li-polythene delimiter.

The requirement for CR of less than 5 % (1.05 on Figure 4) suggest that the chamber be located no closer to the phantom than the centre of the delimiter and no further from the top of the BSA than 15cm.

4. Discussion and Conclusions

The original monitor chamber position was separated from the patient / phantom by 20 mm of Li-polythene, as chambers were located in the back of the 25 mm Li-polythene beam delimiter, adjacent to the graphite neutron reflector. Experimental coupling with the chambers in this position was measured to be 2.3 ± 0.2 % with the LWT, and the corresponding MCNP simulated prediction being 2.6 ± 1 %.

Changing the monitor position to be centered within the Li-polythene delimiter, separated from the patient / phantom by 12 mm Li-polythene (instead of 20 mm) was predicted by MCNP to reduce the count-rate by a factor of 2.5 ± 0.1.

This was verified experimentally to be a factor of 2.4 ± 0.1, producing typical detector count-rates at 1 mA proton current of approximately 4000 cps. This change of position was predicted to increase the phantom coupling to no more than 3.9 %, which has been verified experimentally to be 2.3% ± 0.2.

Note that coupling is anticipated to be negligible (<1 %) for other smaller phantoms and for actual patients, but experimental validation was sought with the largest phantom which provides the greatest degree of coupling.

References

Culbertson, C. N., Green, S., Mason, A. J., Picton, D., Baugh, G., Hugtenburg, R. P., Yin, Z., Scott, M. C., and Nelson, J. M., In-phantom characterisation studies at the Birmingham Accelerator-Generated epithermal Neutron Source (BAGINS) BNCT facility, Applied radiation and isotopes, 2004, 61, p.733-738.

Tumor Control and Normal Tissue Complication in BNCT Treatments of Nodular Melanoma: A Search for Predictive Quantities

S.J. González[a, e], M. Casal[b], M.D. Pereira[b], G.A. Santa Cruz[a], D.G. Carando[c,e], H. Blaumann[a], M. Bonomi[b], O. Calzetta Larrieu[a], D. Feld[a], C. Fernández[a], S. Gossio[e], R. Jiménez Rebagliatti[a], J. Kessler[a], J. Longhino[a], P. Menéndez[b], S. Nievas[a], B.M.C Roth[b], S.J. Liberman[a]

[a]*Comisión Nacional de Energía Atómica, Av. del Libertador 8250, (1429) Cdad. de Buenos Aires, Argentina*
[b]*Instituto de Oncología Angel H. Roffo, Av. San Martín 5481, (1417) Cdad. de Buenos Aires, Argentina*
[c]*Dpto. de Matemática, Pab. I Ciudad Universitaria, UBA, (1428) Cdad. de Buenos Aires, Argentina*
[d]*Dpto. de Física, Pab. I Ciudad Universitaria, UBA, (1428) Cdad. de Buenos Aires, Argentina*
[e]*CONICET, Avda. Rivadavia 1917, (1033) Cdad. de Buenos Aires, Argentina*

Abstract

A previous work concerning tumor control and skin damage in cutaneous melanoma treatments with BNCT was extended including doses, volumes and responses of 104 subcutaneous lesions from all patients treated in Argentina. Acute skin reactions were also scored for these patients, and cumulative dose-area histograms and dose-based figures of merit for skin were calculated.

Broadening the tumor response analysis with the latest data showed that the (minimum or mean) tumor dose is not a good predictor of the observed clinical outcome by itself. However, when the tumor volume was included in the model as second explicative variable, the dose increases its significance and becomes a critical variable jointly with the volume (p-values < 0.05). A preliminary analysis to estimate control doses for two groups of tumor sizes revealed that for small tumor volumes (< 0.1 cm^3) doses greater than 20 Gy-Eq produce a high tumor control (> 80%). However, when tumor volumes are larger than 0.1 cm^3, control is very low (< 30%) even for mean doses between 20 and 40 Gy-Eq.

Some quantities based on skin doses, areas and complication probabilities were proposed as candidates for predicting the severity of the early skin reactions. With the current data, all the evaluated figures of merit derived similar results: ulceration is present among the cases for which these quantities take the highest values.

Keywords: Melanoma, Skin reaction, PEUD

1. Introduction

Dose data for tumor control of cutaneous melanomas and toxicity in normal skin are barely documented in BNCT. In conventional radiotherapy where a great amount of such data is available, dose distribution in tumors is highly homogeneous and tolerance doses (homogeneously distributed in the organ at risk) consider fractionation schemes. This is not the general situation in BNCT and particularly, is far from the CNEA clinical procedure with single-fraction neutron irradiation and dose prescriptions considering "the maximum point dose received in a 5-mm thick layer of skin".

The optimization of melanoma treatments demands prescriptions of necessarily non uniform doses that preserve normal skin while imparting therapeutic doses to tumors. In this context, we have extended a previous analysis that investigated the possible influence of tumor size and total equivalent dose on the observed local tumor response (González *et al.*, 2006). Based on all the available data for patients treated as part of the CNEA-Roffo Phase I/II clinical trial of cutaneous melanoma and the tumor analysis results, we present a preliminary estimation of control doses for two groups of tumor sizes. Regarding normal skin, we studied different factors that may be related with observed early toxicity based on an analysis of several figures of merit (FOM) derived from the skin dose distributions. The early changes in the skin occur prior to 70-120 days post-irradiation and are consequence of the depletion of the epidermal and subpapillary microvascular cell populations (Archambeau, 1987). Since the epidermis and the subpapillary dermis vary between 50 and 300 microns, we considered superficial doses instead of distributions in a layer of skin for the FOM-based

analysis. Based on each evaluated FOM, we compared the resulting patient ordering with the acute skin toxicity graded as erythema and ulceration. Finally, we discuss the consistency of our results with available reported single-fraction photon tolerance doses.

2. Materials and Methods

2.1 General considerations

Since 2003, 7 patients with subcutaneous nodular melanoma of the limbs were treated using the hyperthermal neutron beam of the RA-6 reactor at the Centro Atómico Bariloche, Argentina. The irradiations were performed in 10 anatomical areas comprising the thigh, calf, heel and foot sole. Since one patient was treated at two adjacent areas, namely the heel and foot sole, these areas were considered as only one for skin toxicity. The prescription dose in the skin was scaled from 16.5 Gy-Eq to 24 Gy-Eq. Treatment planning was carried out with NCTPlan (González *et al.,* 2002a; González *et al.,* 2005), and tumor volumes and doses were calculated using DVHTool System (González *et al.,* 2002b). To study the superficial dose distribution in the skin and compute dose-area histograms (DAH), a new Matlab-based program developed by our group was employed (Gossio *et al.*, 2008).

2.2 Tumor response analysis

Responses of 104 subcutaneous nodular lesions were analyzed with regard to different quantities such as minimum or mean photon-equivalent doses, and tumor volume. The objective response (OR) of the tumors was assessed computing tumor volumes on post treatment CT scans when possible, or by clinical inspection, external marking and photographic documentation. Local responses were graded according to WHO criteria, and complete and partial responses were considered as positive responses for the statistical analysis. A minimal follow-up of 3 months was considered for assessing responses.

A logistic regression analysis based on a generalized linear model was performed, and minimum or mean doses, either by themselves or jointly with tumor volumes, were alternatively assessed as possible predictors for the tumor response.

To preliminary estimate therapeutic doses for nodular melanomas, tumors were split into two groups according to the volume of the lesions. The division was established at 0.1 cm^3, which corresponds to a spherical tumor of about 5 mm diameter.

2.3 Normal tissue analysis

As mentioned before, early skin responses are expected to be associated with superficial doses in the epidermis and subpapillary dermis rather than the dose distribution in a layer of skin. Since we were interested in these early effects, cumulative Dose-Area Histograms (DAH) and related figures of merit (FOM) were computed to investigate their possible influence on the acute skin toxicities observed in our patients (in this work, scored as erythema or ulceration).

Eight figures of merit derived from DAHs were analyzed. These are: maximum dose to the skin, skin area that received at least some reference dose (namely, 15, 18, and 20 Gy-Eq), mean dose in the 100 and 200 cm^2 of skin that received the highest doses, the normal tissue complication probability for inhomogeneous dose distributions (NTCP), and the related probability-equivalent uniform dose (PEUD) to the skin (González et al., 2008).

Note that although all FOMs are derived from doses, and thus are correlated, they are of different nature (i.e., doses, areas and probabilities).

Reference doses used to compute skin areas were chosen based on a number of observations suggesting that doses around 18 Gy (delivered as a single fraction in fields of about 100 cm^2 in size) can be considered as a threshold for developing skin moist desquamation (ICRP Publication 85, 2001; Archambeau, 1984; Ellis, 1968 and Douglas, 1982).

The normal tissue complication probability for inhomogeneous dose distributions was computed applying the formalism of the equivalent sub-volume model presented in González & Carando (2008), using a modified version of the NTCP model for uniform doses described by the three-parameter empirical formula (see, for example, Zaider *et al.*, 1999):

$$P(D,v) = e^{-\frac{N_0}{v^k}\exp(-\alpha D)}. \qquad (2.1)$$

Here, N_0, k and α are non-negative adjustable coefficients that were determined based on Ellis (1968) and Hopewell (1990) single-fraction photon tolerance data, and v is the tissue area fraction irradiated at dose D.

The probability-equivalent uniform dose was also computed for all cases. Briefly, for a given dose distribution, the PEUD is the uniform dose throughout a given area (in this work, 100 cm^2) that gives the same complication probability as the actual dose distribution.

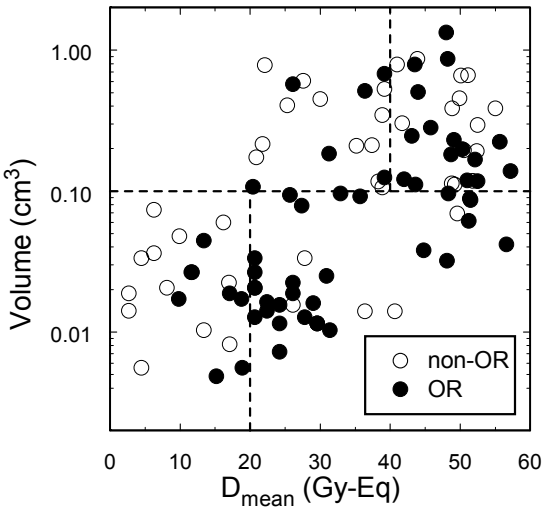

Figure 1. Tumor size vs. mean tumor dose on a semilogarithmic scale. Empty and solid symbols indicate non-objective (non-OR) and objective response (OR), respectively

3. Results and Discussions

3.1 Tumors

Neither minimum nor mean equivalent doses were found to be, by themselves, good predictors of tumor response. However, when the tumor volume was incorporated as a second explicative variable in the generalized linear model, doses (minimum or mean dose) substantially increased their significance and become critical variables together with tumor volumes (p-values < 0.05).

Figure 1 shows the distribution of volumes and mean doses of the treated lesions together with their response. A simple analysis reveals that for small volumes (< 0.1 cm^3) mean doses greater than 20 Gy-Eq produce a high tumor control (> 80%). However, when tumor volumes are larger than 0.1 cm^3, tumor control is very low (< 30%) even for mean doses between 20 and 40 Gy-Eq. The present results do not substantially differ if the minimum instead of the mean dose is considered for the analysis. For tumor volumes considered "small" in this work, minimum and mean doses are almost the same. Note that if these tumors (< 0.1 cm^3) were represented as spheres, their diameter would be about 6 mm or less. For larger volumes, minimum doses may substantially differ from mean doses. However, the tumor control rate for minimum doses ranging from 20 to 40 Gy-Eq is also low: about 40%.

3.2 Acute skin reaction

Acute skin damage developed by our patients was classified as erythema and ulceration. While erythema was an acceptable mild toxicity, skin ulceration was considered to exceed the tolerance limit even though damage was controlled with medication. Among the skin assessed areas, 6 out of 9 developed erythema. The three patients that showed ulceration were cured within one year after BNCT. Eight FOM comprising doses, skin areas, and NTCP were computed and used to sort patients by ascending order. Results of this procedure showed that all FOMs produced almost the same patient ordering, ulceration being the toxicity present among the cases for which FOMs take the highest values.

As mentioned above, figures of merit are highly correlated variables. In order to condense the information in a single parameter for each patient, a "score" was assigned averaging the 8 FOM outcomes. Figure 2 shows the patients' ordering obtained by this procedure. It can be observed that patients that developed ulceration received, on average, a higher score than patients that exhibited erythema.

Figure 3 compares three different FOM based on doses: the maximum (point) dose to the skin (D_{max}), the mean dose in the 100 cm^2 of skin that received the highest doses (D^{100}_{mean}), and the probability-equivalent uniform dose in a skin area of 100 cm^2 ($PEUD_{100}$). Furthermore, for D^{100}_{mean} and $PEUD_{100}$, dose values that show the transition between the early effects appear to be consistent with the observed range of single-fraction doses for moist desquamation (i.e., between 15 and 20 Gy for 100 cm^2 of skin), (ICRP Publication 85, 2001; Archambeau, & Ines 1984; Ellis, 1968; and Douglas, 1982). It is worthwhile mentioning that Fukuda *et al.* (1994) have reported skin reactions after BNCT treatments which are also consistent with our findings.

4. Conclusions

In a previous work, minimum and mean doses to tumors were found to be, by themselves, good

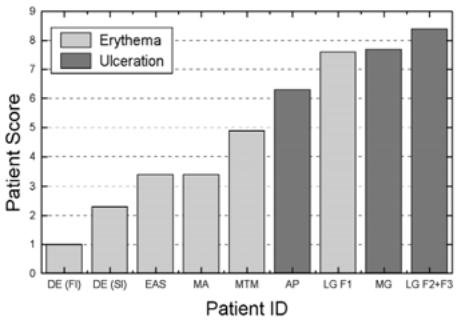

F*igure 2. Patients ordered according to the computed patient score*

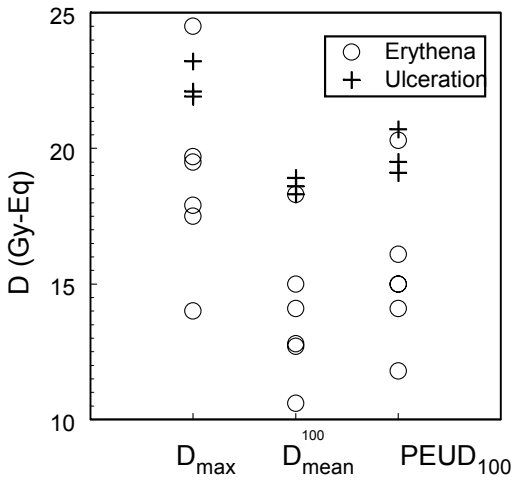

Figure 3. Evaluated figures of merit based on doses. Circles and crosses indicate patients that developed erythema and ulceration, respectively

predictors of the observed local response. The addition of new data in the present analysis made necessary to introduce the volume as a second explicative variable for responses. It is worthwhile noting that in the first analysis, 39 out of 63 nodules had very small and similar volumes. With the addition of more data comprising bigger volumes, the present analysis involved a wider range of this variable.

It was stated above that tumor size affects the chances of control for a given dose. As a part of the dose prescription, tumor volume jointly with the dose will be considered for the optimization of future treatment plans.

The different figures of merit calculated to explain skin toxicities provided very similar results, $\left(D_{mean}^{100}\right)$ and $PEUD_{100}$ being those that showed transition doses between early effects consistent with the reported tolerance data for single-fraction photon irradiations. For all FOMs, patients can be roughly divided into two distinctive groups, one with mild toxicities and the other including patients with more severe reactions. The fact that ulceration only developed in cases involving a heel or a foot sole is worthy of note. With the number of analyzed cases it is not possible to discard a particular radiosensitivity of these areas or mechanical stress as a cause.

Adding new data of normal tissue reactions to the present analysis might help to find a good predictor for the normal tissue toxicity and thus to determine a safe therapeutic dose. Since the dose distribution in the normal skin is highly inhomogeneous, an alternative quantity with more information rather than the maximum point dose to the skin will probably be considered for the new upcoming clinical trials of cutaneous melanoma. Among the candidates analyzed in this work, the mean dose in 100 cm^2 of skin and the probability-equivalent uniform dose were consist with reported conventional radiotherapy tolerance data.

Acknowledgements

M.D. Pereira is a fellow of the National Agency for Scientific and Technological Promotion of Argentina.

References

Archambeau, J.O., "Relative Radiation Sensitivity of the Integumentary System: Dose Response of the Epidermal, Microvascular, and Dermal Populations," Adv. Rad. Biol. 12, Elsevier, 1987.

Archambeau, J.O. and Ines A., "Response of Swine Skin Microvasculautre to Acute Single Exposures of X Rays: Quantification of Endothelial Changes," Rad. Res. 98, 37-51 1984.

Douglas, B.G., Implication of the quadratic cell survival curve and human skin radiation "tolerance dose" on fractionation and superfractionation dose selection. Int. J. Radiat. Oncol. Biol. Phys. 8, 1135-1142, 1982.

Ellis, F., Curr. Top. Rad. Res, Q. 4, pp. 357-397, 1968.

Fukuda, H., Hiratsuka J., Honda, C. *et al.*, "Boron Neutron Capture Therapy of Malignant Melanoma Using B-10-paraboronophenyl-alanine with Special Reference to Evaluation of Radiation Dose and Damage to the Normal Skin," Rad. Res. 138, *3*, 435-442, 1994.

González, S.J., Santa Cruz, G.A., Kiger III, W.S. *et al.*, "NCTPlan, the New PC Version of MacNCTPlan: Improvements and Verification of a BNCT TPS," *Proc. 10th ICNCT*, 557-561, Monduzzi (Ed.), Bologna, 2002a.

González, S.J., Santa Cruz, G.A., Kiger III, W.S. *et al.*, "A New Computational Tool for Constructing Dose-Volume Histograms Using Combinatorial Techniques," *Proc. 10th ICNCT*, 629-633, Monduzzi (Ed.), Bologna, 2002b.

González, S.J., Carando, D.G., Santa Cruz, G.A. *et al.*, Voxel model in BNCT treatment planning: performance analysis and improvements. *Phys. Med. Biol.* 50, 441-458, 2005.

González, S.J., Casal, M.R., Santa Cruz, G.A. *et al.*, Detailed Dosimetry and Clinical Outcome Analysis for the Argentine BNCT Trials of Cutaneous Nodular Melanomas. *Proc. 12th ICNCT,* 485-488, 2006.

González, S.J. and Carando, D.G., A general tumor control probability model for non-uniform dose distributions. *Math. Med. Biol.* 2, 171-184 2008.

Gossio, S., Carando, D.G., González S.J., A Computational Dosimetry Tool for the study of tumor doses and skin toxicities in BNCT. *Proc. 13th ICNCT,* 2008.

Hopewell, J.W., "The skin: its structure and response to ionizing radiation. Int. J. Radiat. Oncol. Biol. Phys. 57, 751-773, 1990.

ICRP Publication 85, Ch. 3 p. 26, Elsevier, 2001.

Zaider, M. and Amols, H.I., "Practical considerations in using calculated healthy-tissue complication probabilities for treatment-plan optimization," Int. J. Radiat. Oncol. Biol. Phys. 44, 439-447, 1999.

A Computational Dosimetry Tool for the Study of Tumor Doses and Skin Toxicities in BNCT

Sebastián Gossio[a], Daniel G. Carando[b,c], Sara .J. González[c,d]

[a]*Dpto. de Física, Pab. I Ciudad Universitaria, UBA, (1428) Cdad. de Buenos Aires, Argentina*
[b]*Dpto. de Matemática, Pab. I Ciudad Universitaria, UBA, (1428) Cdad. de Buenos Aires, Argentina*
[c]*CONICET, Avda. Rivadavia 1917, (1033) Cdad. de Buenos Aires, Argentina*
[d]*Comisión Nacional de Energía Atómica, Av. del Libertador 8250, (1429) Cdad. de Buenos Aires, Argentina*

Abstract

A Matlab-based computational tool was developed that helps determining tumor and skin doses in BNCT treatments. It was especially designed for cutaneous melanoma treatments and, among its features, it provides a guide for the location and delineation of tumors, a visual representation of superficial dose distributions (for both tumor and normal tissues), generates cumulative dose-volume histograms for different volumes of interest and dose-area histograms for skin. A description of the tool is presented, as well as examples of its application.

Keywords: Melanoma, treatment planning system, computational dosimetry

1. Introduction

The Comisión Nacional de Energía Atómica of Argentina (CNEA) and the oncology center Instituto Ángel H. Roffo initiated the phase I/II clinical trial of peripheral melanomas in 2003 (González *et al.*, 2004). Since then, a total of 7 patients with 88 nodular lesions in 10 anatomical areas were treated using the hyperthermal neutron beam of the RA-6 reactor at the Centro Atómico Bariloche (Menéndez *et al.*, 2008). During all these years, natural difficulties and questions regarding tumors and normal tissues were raised.

One of these questions was how to determine doses in small tumors that could not be delineated in medical images. About half of all lesions treated in Argentine clinical trials had a superficial diameter lower than 5 mm. Additionally, tumor and normal tissue mass densities are very similar, so that their gray intensity levels in CT images are not very different. Thus, the contrast between tissues is very poor and this makes it very difficult, if not impossible, to locate those nodules with small size in CT images.

Another question, of a more general nature, was how to prescribe the dose in normal skin to deliver a safe treatment while imparting doses sufficient to control tumors when dose distributions are very inhomogeneous (inhomogeneities up to 50% in 100 cm^2 of skin can be found in CNEA treatments).

These concerns motivated the development of a computational tool that helps guide physicians through location and delineation of tumors in medical images and, when this is not possible, provides an estimation of the dose delivered to the nodule. Moreover, it allows the study of normal skin dosimetry by computing cumulative dose-area histograms and specific figures of merit that cannot be obtained with the routinely used treatment planning system. In this work, we present the main features of the developed computational system and show some examples of its use. The applicability and usefulness of the present tool to other treatments are also discussed.

2. Materials and Methods

The system was programmed in Matlab (The MathWorks Inc.), using the graphical user interface capability. It is built on multiple windows devoted to different purposes. Although at present it runs under Matlab, a stand alone version of the program is planned.

As a first step, the user loads the input data involving medical images, parameters relevant to the treatment plan evaluation, and calculated physical doses (such as those generated by MCNP with NCTPlan model) (González *et al.*, 2002a; González *et al.*, 2002b).

For tumor location, only the medical images are needed. Based on these medical images, a 3D reconstruction of the patient anatomy is built (see Figure 1).

In order to facilitate location and delineation of tumors, a registration of the 3D reconstruction and a picture of the anatomy can be performed by means

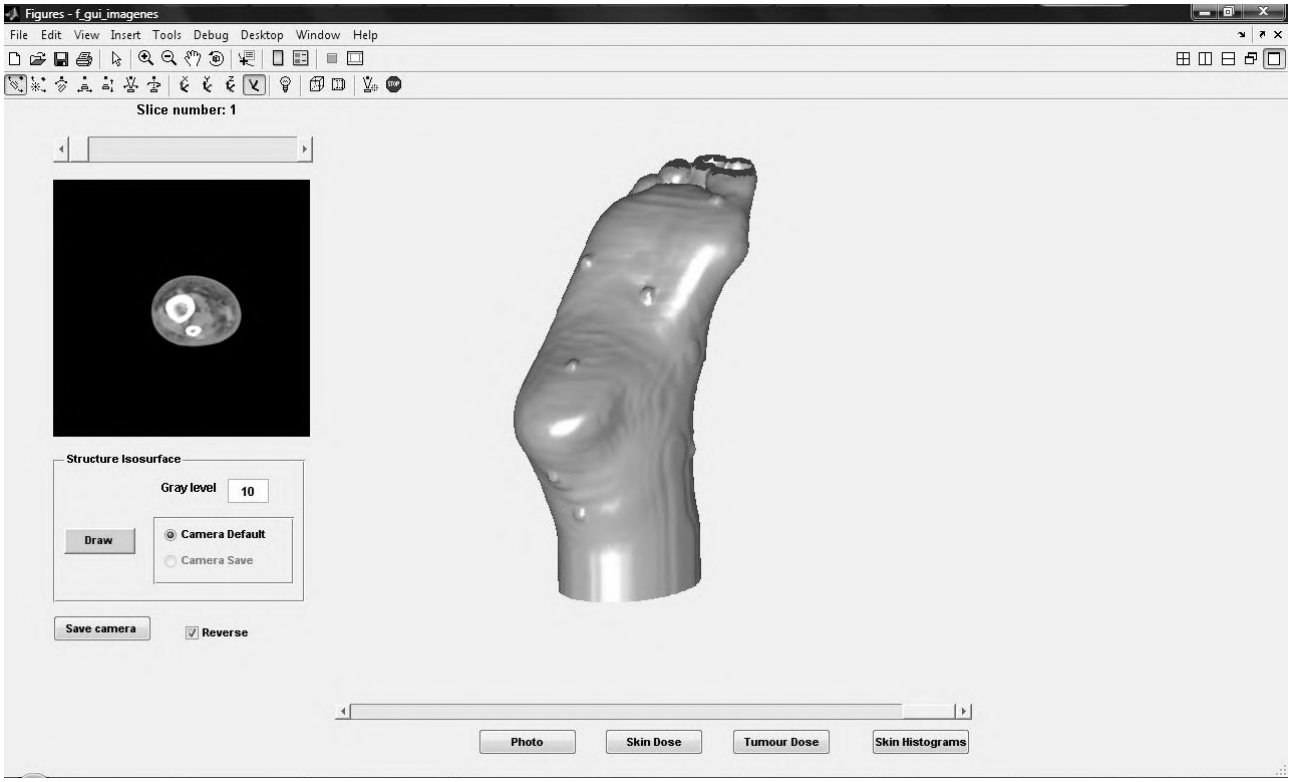

Figure 1. Reconstruction of the patient's anatomy based on the TAC images

of the fiducial markers used for treatment planning purposes. Reference marks appear both in the TAC images and in the photograph of the anatomy. Since transparency of the 3D reconstruction is controlled by the user, they can be used as registration points to achieve a good superposition. After the registration, the transparency of the 3D reconstruction can be increased to start delineation. The physician points the cursor directly on nodules in the picture. Since the 3D reconstruction is superimposed onto the picture (although not necessarily visible), the physician is actually establishing the coordinates of some points of the nodules. Then, the program identifies the TAC slices corresponding to the selected tumors and shows on each slice the physician selected points. In the following step, the physician gets the marked slices as a starting point to delineate the tumors, and can go up and down the image stack to complete the delineation of each nodule. Different filters and contrast controls are available that facilitate the identification of different tissues.

Regarding dosimetry analysis, the tool allows to compute and visualize the 3D superficial dose distribution in the reconstructed anatomy, both for tumors and skin (Figure 2). When the 3D reconstruction and a picture of the anatomy are registered, this gives a comprehensive overview of a treatment, since it allows visualizing dose distributions on skin and doses delivered to tumors. It is also possible to obtain the numerical dose value at any particular point of the anatomy surface. This has an important application: if a nodule is too small to appear in CT scans, the physician can obtain, with the help of the anatomy picture, the point tumor dose. For tumors large enough for delineation, a more accurate and complete information is obtained by the generation of cumulative dose-volume histograms. Moreover, isodose curves can be superimposed to any TAC slice.

The tool also helps study skin dosimetry. Visual information is provided by the already mentioned 3D superficial dose distribution on the reconstructed anatomy. A more quantitative analysis can be performed by means of cumulative dose-area histograms. In order to generate these histograms, areas on the anatomy surface must be computed. This is done making use of the MATLAB internal structures for surface generation.

The clinical case in Figure 3 presents several lesions of different sizes. For example, nodule 1 is large enough to appear in TAC images. However, nodules 5 and 6 are of small size, and could not be delineated. The figure shows how the doses delivered to those nodules are computed and reported by the program.

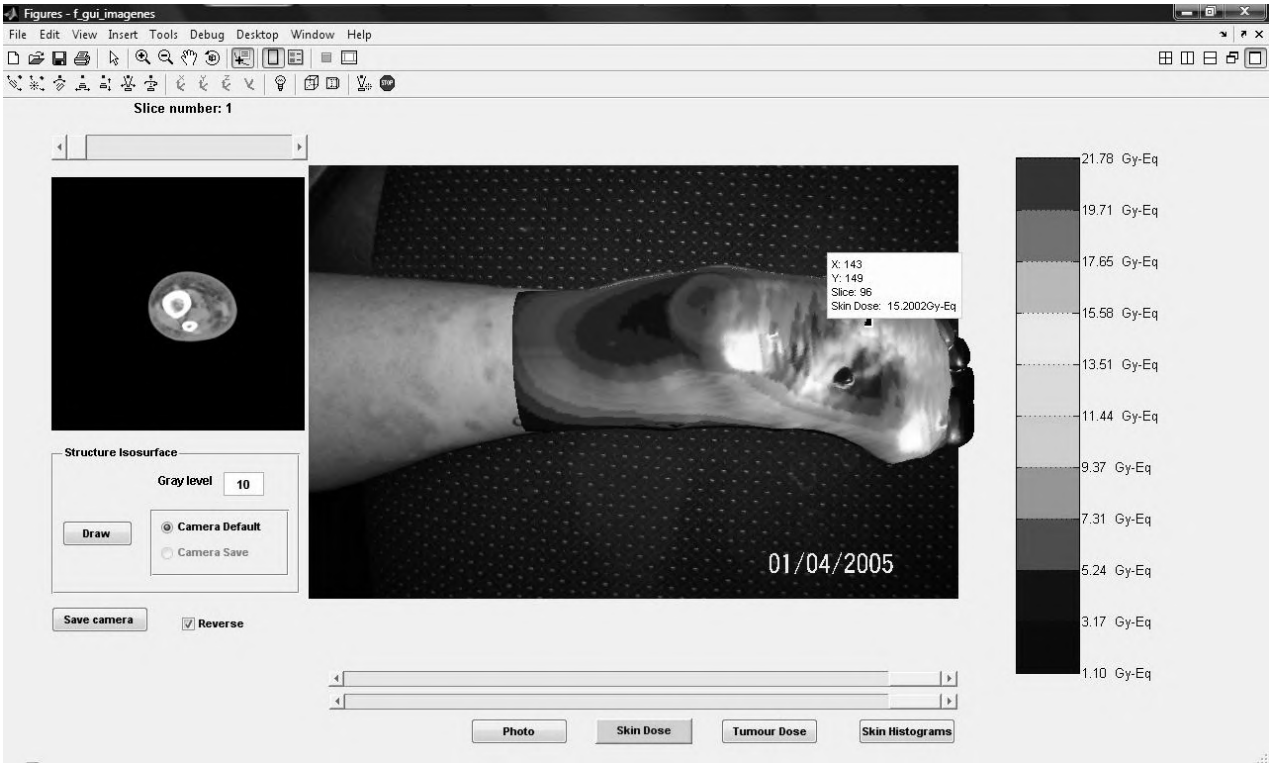

Figure 2. Registration of the superficial dose distribution for normal skin and a picture of the patient anatomy

3. Results and Discussions

The new computational tool made it possible to complete the tumor dosimetry of the Argentine treatments of cutaneous nodular melanoma, since it allowed to deal with lesions that were difficult or impossible to identify in medical images with the previous available capabilities.

It also helped performing the tumor delineation of the last clinical trials carried out in Argentina. The completion of the tumor dosimetry allowed to extend an investigation of the possible influence of tumor size and total dose on the local tumor response and to establish preliminary values of control doses for tumors in some volume range (González *et al.*, 2008).

It is worthy noticing that the visualization of the 3D dosimetry can be helpful in the treatment planning process. It provides a simple way to asses a treatment and compare different candidate plans. Skin areas with doses around tolerable limits or tumors with low doses become apparent in the visual dosimetry distribution.

A thorough description of skin dose distributions of all melanoma treatments was obtained. Cumulative dose-area histograms were generated and a set of dose-based figures of merit for skin were calculated. These figures of merit were contrasted to observed skin toxicities, in order to initiate an analysis of their possible correlation (González *et al.*, 2008).

The long term objective is to find a good predictor of skin toxicity based on dose distributions to optimize the prescription process. An accurate representation of the dose distribution in the skin is also of central importance in Dynamic Infrared Imaging (DIRI) research applied to BNCT of melanoma (Santa Cruz *et al.*, 2008).

A preliminary study based on a patient treated with BNCT and studied by means of DIRI showed consistency between the acute skin reaction, the temperature distribution and the superficial skin dose distribution.

4. Conclusions

The present work was carried out in the context of the Argentine project of BNCT treatments for cutaneous melanomas. Thus, the quantification and analysis of the dosimetry in the normal skin has been one of the main concerns.

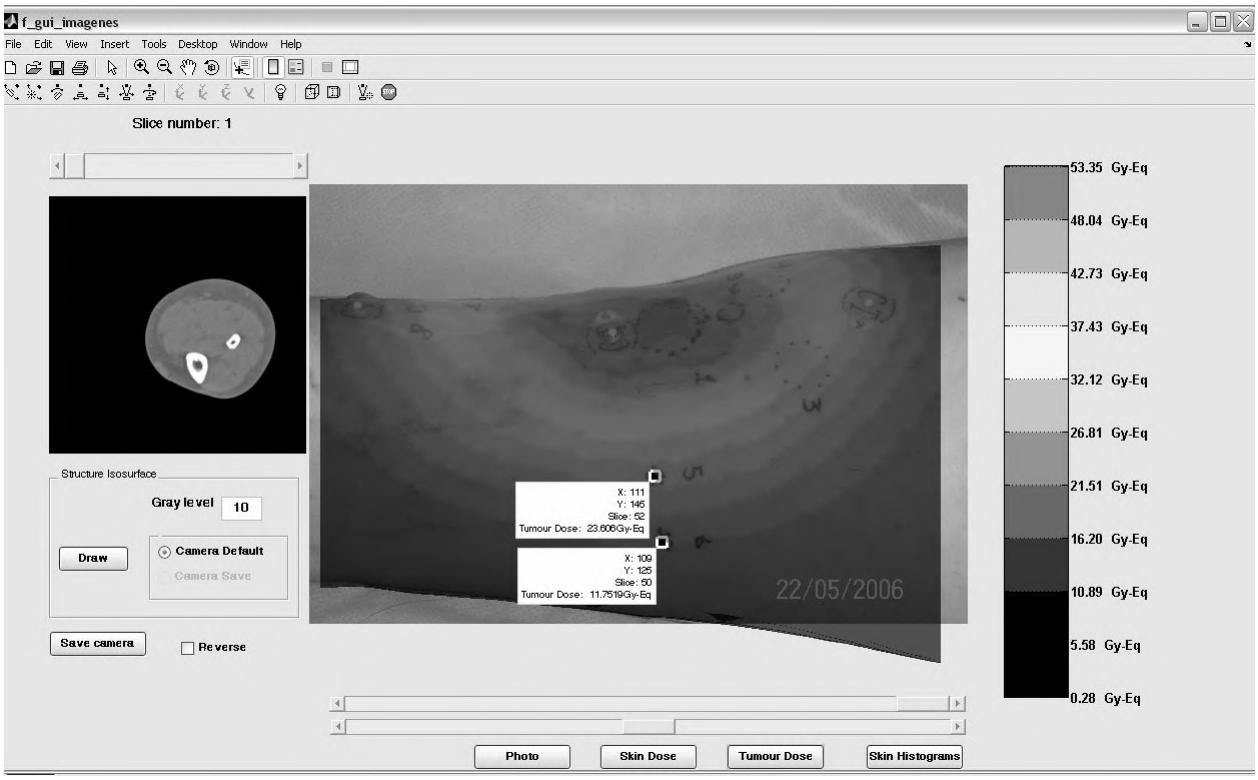

Figure 3. Nodules 5 and 6 were too small to appear in TAC images. Dose values are obtained from the superposition

The capabilities developed to this end could be useful to other BNCT applications for which skin is considered an organ at risk. All the features of the developed tool proved useful for retrospective dosimetry analysis and have potential use at the treatment planning stage.

References

González, S.J., Bonomi, M.R., Santa Cruz, G.A., *et al.*, "First BNCT treatment of a skin melanoma in Argentina: Dosimetric Analysis and clinical outcome." *Appl. Radiat. Isotopes* 61**,** 1101-1105, 2004.

González, S.J., Santa Cruz, G.A., Kiger III, W.S. *et al.*, "NCTPlan, the New PC Version of MacNCTPlan: Improvements and Verification of a BNCT TPS," *Proc. 10th ICNCT*, 557-561, Monduzzi (Ed.), Bologna, 2002a.

González, S.J., Santa Cruz, G.A., Kiger III, W.S. *et al.*, "A New Computational Tool for Constructing Dose-Volume Histograms Using Combinatorial Techniques," *Proc. 10th ICNCT*, 629-633, Monduzzi (Ed.), Bologna, 2002b.

González, S.J., Carando, D.G., Santa Cruz, G.A. *et al.*, Voxel model in BNCT treatment planning: performance analysis and improvements. *Phys. Med. Biol.* 50, 441-458, 2005.

González, S.J., Casal, M.R., Pereira, M.D. *et al.*, Tumor Control and Normal Tissue Complication in BNCT Treatments of Nodular Melanoma: A Search for Predictive Quantities. *Proc. 13th ICNCT,* 2008.

Menéndez, P.R., Roth, B.M.C., Pereira, M.D. *et al.*, BNCT for skin melanoma in extremities: updated Argentine clinical results.

Santa Cruz, G.A., Bertotti, J., Marín, J., Dynamic Infrared Imaging of Melanoma and Normal Skin in Patients Treated by BNCT. *Proc. 13th ICNCT,* 2008.

Monte Carlo modelling of the influence of boron microdistribution on BNCT microdosimetry

Richard P. Hugtenburg[1], Adam E. R. Baker[2], Stuart Green[3]

[1] *School of Medicine, Swansea University*
[2] *School of Physics, University of Birmingham*
[3] *Queen Elizabeth Medical Centre, University Hospital Birmingham NHS Trust*

Abstract

The ion transport Monte Carlo code SRIM has been used to calculate single event lineal energy spectra for the products of the boron-neutron capture reaction in a water-based medium. The event spectra have been benchmarked against spectra measured with a boron-loaded tissue-equivalent proportional counter (TEPC). Agreement is excellent and supports the use of Monte Carlo methods in understanding the influence of boron delivery on the effectiveness of boron neutron capture therapy (BNCT).

Introduction

Fundamental studies of the efficacy of boron neutron capture therapy (BNCT) including dosimetric and radiobiology studies are currently being undertaken following the commissioning of an accelerator based neutron source (Wojnecki and Green, 2002, Culbertson *et al.*, 2004). An improved understanding of the relationship between the boron microdistribution and treatment efficacy is sought, which includes the modelling of the relative biological effect (RBE) of the various components of the beam including the boron induced high-LET Li and He ions.

In this work track structure information, generated by the SRIM (Zeigler, 2004) Monte Carlo code, has been used to predict single event spectra for boron-bearing cells exposed to neutrons. These quantities are dependent on the precise microdistribution of the boron in cells. This information is compared to spectra measured using boron loaded tissue equivalent proportional counter (TEPC) microdosimeters.

Methods

Particle tracks of 1470 keV He ions and 840 keV Li ions are generated with TRIM in a liquid water medium. Figure 1 shows the dose versus depth given by the SRIM code in terms of the mean ionisation (LET). This is essentially the depth-dose distribution for a broad beam. The dose distribution computed for a 1470 keV alpha particle using the MCNPX code (Pelowitz, 2005) is shown for comparison. SRIM demonstrates much better handing of straggling and has better agreement with the range given in ICRU-37.

An additional aspect that has been examined in this work is the effect on dose-equilibrium that the use of boronated medium for in vitro experiments where the mounting material will not typically contain boron. It can be seen that uncertainties of 10-20% are anticipated in determining the dose to the nucleosome if cells are only of the order of a few micron thick with respect to the mounting plate.

Tracks generated by the SRIM code in a liquid water medium are post-processed to generate single (lineal energy) event spectra, as has been shown to improve the efficiency of simulations in general purpose codes for the examination of photon based binary-therapies (Hugtenburg, Chaoui, Pattison, 2007). Strategies to determine unbiased event spectra include the tallying of energy deposition on a regular grid in the form of a list that is further processed to determine the energy deposited within the micron dimension volume of interest.

Two models are considered for the calculation of the lineal energy spectra generated by the boron decay events in real cells; firstly the situation where boron is distributed uniformly through the cell structure, secondly where the boron only occurs outside a 2 micron diameter volume, representative of the volume of the cell nucleus. The proportion of ions entering the volume is implicitly modelled and dictated by the range of the He and Li ions, which is 0.62 to 0.32, respectively.

Only the 94% branch (Q=2.31 MeV) of the boron capture reaction has been considered in these calculations but, in principle, the 6% branch could be added. The Q value of 2.78 MeV leads to an approximately 10% decrease in LET for both ions; therefore this contribution will not be seen as a feature in the lineal energy spectra.

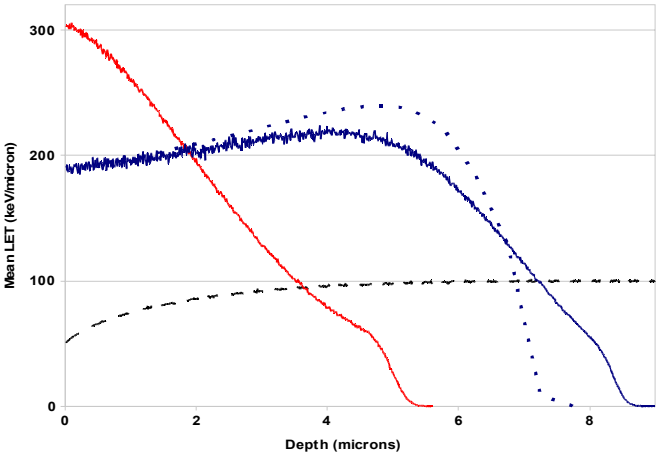

Figure 1. Dose from the boron-neutron capture reaction close to a surface where the Boron concentration falls to zero. The Monte Carlo code TRIM is used to generate track histories for 1470 keV He ions and 840 keV Li ions. Dose distributions for broad beams of Li (light solid line) and He (dark solid line) ions and compared to calculations of alpha particles with MCNPX (dotted line). Isotropically distributed sources of both ions in combination are sampled emerging from a semi-infinite boron containing medium facing a non-boron containing material (dashed line)

Quantities of boron oxide powder at typical concentrations used in BNCT (50 ppm by mass) have been introduced into the A150 wall material of one of the TEPC (Far West Technology, California). The microdosimeters are filled with a propane based tissue equivalent gas to a pressure of 89 mBar. At this pressure the effective diameter of gas volume of the proportional counter is 2 micron. It is likely that the transport of the ions through the walls is influenced by the boron nitride powder particles. This will have a small effect on the mix of He and Li particles entering the volume of interest and could also be modelled in principle with the approaches used here. It has been shown that the boron-nitride particles are approximately 15 micron diameter (Gainey, 2002).

Results

The event (lineal energy) spectra measured with the TEPC microdosimeters offer a benchmark of the Monte Carlo calculation (fig. 2). The calculated spectra are compared to the measurements made in the TEPC, where the difference between the boronated and standard TEPC represent the contributions to the spectra brought about by the He and Li products. Excellent agreement with the first model, i.e., that of the boron distributed uniformly through the medium, is demonstrated except at the high lineal energy threshold, which is in better agreement with the second model in which boron is excluded from the 2 micron diameter sensitive volume. It is understandable that the TEPC behaves in this fashion as tracks from both ions can enter the sensitive gas volume after travelling many microns but it is impossible for the tracks to originate in the gas lowering the limit on the maximum amount of energy deposited in the gas. Thus the calculated values of the threshold, according to the first inflection point below the maximum value of lineal energy, are 380 keV/micron for the first model versus 320 keV/micron for the second model; the latter being in better accord with the measured distribution.

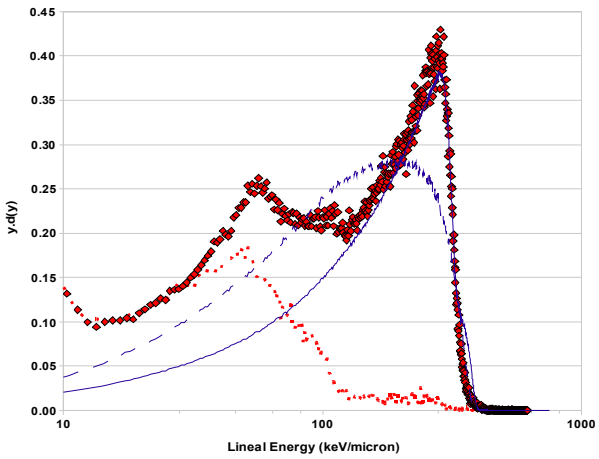

Figure 2. Measured and calculated single event (lineal energy) spectra. Boron loaded (diamonds) versus a standard, tissue-equivalent, proportional counter (dots) demonstrate contributions from the He and Li ion products of the boron-neutron capture reaction. The contributions are modelled using Monte Carlo where the boron is assumed to be uniformly distributed through the medium (solid line) and where the boron is excluded from a 2 micron diameter nucleosomal volume (dashed line). The calculated spectra are normalised such that the integral of $d(y)$ over y is 1

It is interesting to consider the effect that the large distortion in the spectra brought about by excluding the boron from the 2 micron volume, i.e. comparable to that of the cell nucleus, has on the relative biological effectiveness (RBE). A model suggested by Zamenhof (1997) proposes that a threshold value of lineal energy is needed to trigger a biological endpoint such as cell inactivation. The differences in spectra shown here suggest that large differences in RBE may occur for BNCT therapies depending on whether the targetting agent enables boron to enter the cell nucleus.

The influence of the transport of the ionised electrons on the spectra has been considered and SRIM is able to report on the spectra of ionisation events occurring within the medium. These spectra can be used with an electron transport code to determine their influence on the lineal energy spectra. As energy of electrons generated from the ionisation of the He and Li ions is less than 1000 eV and therefore a range of less than 100 nm, their effect on the spectra in a 2 micron cavity is minimal.

Conclusion

This work shows that meaningful single event spectra can be calculated with an ion transport code such as SRIM. Spectra have been used to examine differences in the radiation quality of boron neutron products as a function of microdistribution.

As well as liquid water, the code can be used to calculate tracks in a variety of media including general materials where the atomic composition is specified; therefore a more accurate model of the TEPC could be examined.

Methods are being developed to convert single event spectra into specific energy spectra in order to describe the effect of multiple events at dose levels used for in vitro experiments. The intercomparison of modelling with measured spectra and RBE from in vitro experiments will assist in devising optimized treatments. The work also supports an emerging understanding of the complex interactions between high and low-LET components of the radiation field.

References

Culbertson, C.N., Green, S., Mason, Mason, A.J., Picton, D., Baugh, G., Hugtenburg, R.P., Yin, Z. Scott, M.C., Nelson, J.M., 2004, In-phantom characterisation studies at the Birmingham Accelerator-Generated epIthermal Neutron Source (BAGINS) BNCT facility. Appl. Radiat. Isotop. 61, 733-738

Gainey, M.B., 2002. Dosimetry and Microdosimetry of the Birmingham BNCT program. Ph.D. Thesis, University of Birmingham

Hugtenburg, R.P., Chaoui, Z., Pattison, J.E., 2007. Microdosimetric event distributions in sub-cellular volumes with a general purpose Monte Carlo code, Nucl. Instrum. Meth. B 580, 157-160

Pelowitz, D. B. (Ed.) 2005, MCNPX user's manual version 2.5.0, Rep. LA-CP-05-0369, Los Alamos Natl. Lab.

Wojnecki, C., Green, S., 2002, Medical Physics 29, 1710-1715
Zeigler, J.F., 2004. SRIM-2003.Nucl. Instrum. Meth. B 219-220 1027-1036

Zamenhof, R.G., 1997. Microdosimetry for boron neutron capture therapy: A review. J. Neuro-Oncology 33**,** 81-92

Neutron Spectra Measurement and Comparison of the HFR and THOR BNCT Beams

Y.H. Liu[a], S. Nievaart[b], P.E. Tsai[a], H.M. Liu[c], R. Moss[b], S.H. Jiang[a]

[a]*Engineering and System Science Dept., National Tsing Hua University, Taiwan*
[b]*HFR Unit, Institute for Energy, Joint Research Centre, The Netherlands*
[c]*Nuclear Science and Technology Development Center, National Tsing Hua University, Taiwan*

Abstract

This paper aims to measure the spectra of HB11 (HFR) and the THOR BNCT beams by multiple activation foils. The self-shielding corrections were made with the aid of MCNP calculations. The initial spectra were adjusted by a sophisticated process named coarse-scaling adjustment using SAND-EX, which can adjust a given coarse-group spectrum into a fine-group structure, i.e. 640 groups, with excellent continuity. The epithermal neutron flux of the THOR beam is about three times of HB11. The thermal neutron flux, boron and gold reaction rates along the central axis of a PMMA phantom are calculated for both adjusted spectra for comparison.

Keywords: BNCT, spectrum adjustment, coarse-scaling, SAND-II

1. Introduction

Among the dosimetry works in the boron neutron capture therapy (BNCT), the neutron energy spectrum is one of the most important beam characteristics, which is required for the calculations of detector responses, neutron induced doses, boron dose, etc. For the purpose of beam comparison and dose information exchange, the dosimetry works have to be performed basing on the same methodology and quality. Hence, the neutron spectra of the High Flux Reactor (HFR) and the Tsing Hua Open-pool Reactor (THOR) BNCT beams were both measured using the activation technique and unfolded by the same spectrum adjustment procedure before the further dose comparison.

Multiple activation foils are applied in this study. The measured reaction rates of the foils provide an instant look at the beam intensity and reveal valuable information on the incident neutron spectrum. By a proper initial spectrum and a robust adjustment algorithm, these measured reaction rates can be used to reconstruct the neutron spectrum. Both spectra of the HFR and THOR beams were adjusted following a sophisticated process named coarse-scaling adjustment (Liu et al., 2008), which can adjust a given coarse-group spectrum into a fine-group structure, i.e. 640 groups.

Some beam characteristics were compared after the spectrum adjustment.

2. Materials and Methods

2.1 The HFR and THOR BNCT Beams

The HFR is a 45-MW, multipurpose, materials testing reactor which produces mainly radioisotopes for medical use in Europe. A specially designed filter was installed at HB11 in 1990 for BNCT purposes. The beam aperture is 12 cm in diameter. Recently its fuel was changed from the high-enriched uranium (89~93%) to the low-enriched uranium (< 20%), and therefore the spectrum of HB11 was re-measured again by this study.

The THOR belongs to the National Tsing Hua University in Taiwan. It is a 2-MW swimming-pool type reactor with TRIGA fuels built in 1959. In 2004, its thermal column was removed and reconstructed to provide epithermal neutrons. The beam aperture is 14 cm in diameter.

2.2 Activation Foils and Setup

In order to cover different energy ranges of the spectrum, multiple foils have been used in this study. In the HFR facility, a cadmium wrapped 12-foil package was irradiated. The package contains one gold foil (1 wt% Au) in front of the whole Cd capsule. In the Cd capsule, it contains InAl (0.2 wt% In), pure Sc, AuAl (1 wt% Au), WAl (1 wt% W), UAl (22.8 wt% ^{238}U), LaAl (5 wt% La), MnAl (1 wt% Mn), and CuAl (10 wt% Cu) foils in sequence. Behind the capsule are pure In, Ni and Al foils, which are used as threshold detectors.

In the THOR beam, 11 bare foils were irradiated

separately. These foils are InAl (0.2 wt% In), pure Sc, AuAl (1 wt% Au), WAl (1 wt% W), LaAl (5 wt% La), pure Co, MnAl (1 wt% Mn), CuAl (10 wt% Cu), pure In, pure Ni, and pure Al.

All the irradiations were performed at the center of the beam opening surface and were normalized by respective on-line real-time neutron monitoring system in both facilities.

2.3 Determination of RR_{mea}

The reaction rate per atom of the activation foil is proportional to the beam intensity over certain energies and is used as an indication for the spectrum adjustment. Due to that the radioactivity caused by the neutron activation is related to the degree of the resulting reaction rate, the true reaction rate per atom is thus determined experimentally from the activity of the produced radioisotope in the foil. The reaction rate per atom of the relevant reaction is then determined by a well-calibrated High Purity Germanium (HPGe) detector.

2.4 Self-Shielding Correction

The measured reaction rate per atom is not yet adequate to be used for the spectrum adjustment. Due to the unavoidable positioning of the activation detectors in the beam, the beam energy dependent spectrum is disturbed and deviates from its original condition. Most often, such a phenomenon is called the self-shielding effect (Beckurts and Wirtz, 1964). Generally, the self-shielding correction factor G is defined as:

$$G = \frac{\int_E \varphi(E)\sigma(E)dE}{\int_E \varphi_0(E)\sigma(E)dE} \quad (1)$$

In the above equation, $\varphi(E)$ is the perturbed, average neutron flux per unit energy in the foil (neutron-sec^{-1}-cm^{-2}-MeV^{-1}); $\varphi_0(E)$ is the non-perturbed neutron flux per unit energy of the incident beam; $\sigma(E)$ refers to the energy dependent microscopic cross-section of the relevant nuclear reaction (cm^2). The measured reaction rate per atom is modified to the ideal case RR_{ideal} as:

$$RR_{ideal} = \frac{RR_{mea}}{G} \quad (2)$$

where RR_{mea} is the measured reaction rate per atom determined by HPGe. The self-shielding correction factors can be calculated using the general purpose neutron transport code, MCNP (Briesmeister, 2000) as proposed by I.F. Gonçalves et al (2001). Regarding the foil package irradiated in HB11, however, the self-shielding effect will be mighty enhanced and become much more complicated. Elaborate corrections are required. For this purpose, the self-shielded groupwise cross-sections generated by MCNP are applied instead of the original cross-section library (Liu et al., 2008). The integrated self-shielding correction factor of the activation package can easily be larger than one as a result of scattering in the thick package.

2.5 Coarse-Scaling Spectrum Adjustment

The applied coarse-scaling spectrum adjustment utilizes the same unfolding algorithm as the well-known SAND-II (Berg and McElroy, 1967), but with a much more sophisticated process. Basically, it has a similar idea as the two-foil method (Beckurts and Wirtz, 1964) which adjusts the beam intensity by only two groups. For example, the 47-group, initial spectrum of the THOR beam is compressed into 11 groups according to the applied 11 activation foils. Then the 11-group spectrum is adjusted with corresponding 11-group cross-sections. The adjusted 11-group spectrum is then decompressed back to 47 groups.

However, the coarse-group spectrum is not adequate for the requirement of precise MCNP calculations of the detector responses applied in the dosimetry work, free-in-air. The deviation of the calculated results between fine-group and coarse-group can be larger than 30% (Liu et al., 2008). Hence the aforesaid adjusted 47-group spectrum is further expanded into 640 groups. The coarse-scaling adjustment is then performed again to make the SAND-II calculated reaction rates and the measured results consistent. The illustration of the whole spectrum adjustment process is plotted as a flow chart in Fig. 1. The 9-step spectrum adjustment ensures the continuity of the adjusted 640-group spectrum, which is generally a difficulty in fine-group spectrum adjustment.

To perform the coarse-scaling spectrum adjustment, a user-friendly custom-made computer program named SAND-EX has been developed for the spectrum adjustment work and analysis. SAND-EX is an extended version of SAND-II which uses the same algorithm but has extra useful accessories, such as group expansion, splitting, and compression. Another feature of this program is the easy maintainability in the cross-section library.

2.6 Beam Comparison

The adjusted spectra are compared and divided into thermal neutrons (E_{th} < 0.5 eV), epithermal neutrons (0.5 eV < E_{epi} < 10 keV), and fast neutrons (E_f > 10 keV). The fast neutron contamination is one of the concerned beam characteristics, and it is

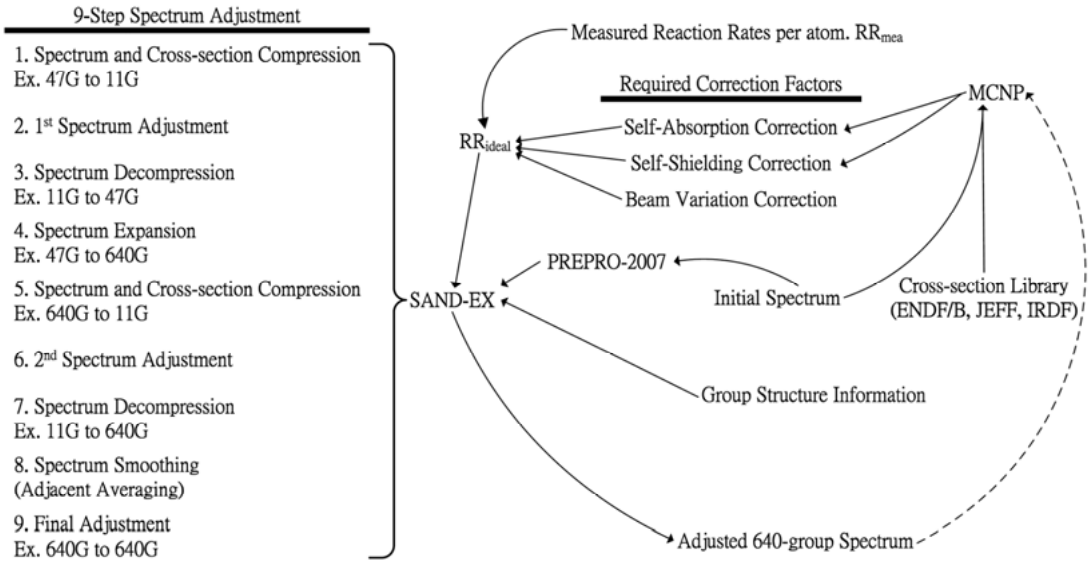

Figure 1 The flow chart of the spectrum adjustment

Table 1 Beam comparison between HB11 and the THOR

	φ_{th}	φ_{epi}	φ_{fast}	Fast Neutron Contamination
	(neutron-cm^{-2}-sec^{-1})			(Gy-cm^2-neutron^{-1})
IAEA	NA	1×10^9	NA	2×10^{-13}
HB11	1.09×10^7	3.41×10^8	2.61×10^7	3.6×10^{-13}
THOR (1.2 MW)	1.34×10^8	1.07×10^9	7.66×10^7	3.4×10^{-13}

determined using neutron kerma coefficients of adult brain.

Concerning the comparison of the adjusted spectra in a phantom, the thermal neutron flux, the boron reaction rate, and the $^{197}Au(n,\gamma)^{198}Au$ reaction rate along the central axis of a 15 x 15 x 15 cm^3 PMMA phantom are calculated by MCNP for both spectra with the same beam configuration.

3. Results and Discussions

The irradiated activation foils were measured by the local teams. The statistical error of the counting is kept below 1% for capture reactions, and smaller than 2% for threshold reactions. The necessary self-absorption and self-shielding corrections were made with the aid of MCNP calculations.

After corrections, the obtained RR_{ideal} is applied into the spectrum adjustment as illustrated in Fig. 1. The final adjusted spectra are plotted in Fig. 2 with their initial spectra for comparison. The adjusted thermal, epithermal, and fast neutron flux are listed in Table 1. The fast neutron contaminations are also given in the table. The first row contains the values suggested in IAEA TEDOC-1223 (2001). The measured ideal reaction rates and the calculated values derived by MCNP and SAND-EX are matched excellently within a maximum difference of 4%; most of them are within a difference of 2%.

The adjusted spectra are both in fine-group structure, but still show great continuity through the whole energy range. It is clear that the THOR BNCT beam is stronger than HB11. The adjusted spectra indicate that the THOR beam has a larger portion (11%) of thermal neutron than the HFR beam (2.9%); the fast neutron part, it is 6.9% in HB11 and 6.0% in the THOR. The fast neutron fluxes of the initial spectra are both underestimated. The fast neutron contaminations are higher than the IAEA suggested value, but are still acceptable.

All the calculated values in the PMMA phantom are plotted in Fig. 3; all the values have a statistical uncertainty ranging from 0.5% up to 4% (at 14 cm) in 95% confidence interval. For the purpose of comparison, all the values are normalized to their highest values. The peak of the thermal neutron curve of HB11 is deeper than the THOR. Similar result is observed in the curves of boron reaction rate. This is because the spectrum of HB11 is harder than the THOR. Besides, the curve of gold reaction rate of THOR is slightly lower than the one of HB11. It is consistent with the lower epithermal to thermal ratio of the THOR beam.

It is clear that the curve of gold reaction rate and the curve of boron reaction rate are quite different. Although the gold wire is usually applied to monitor the thermal neutron flux, it is not suitable for the

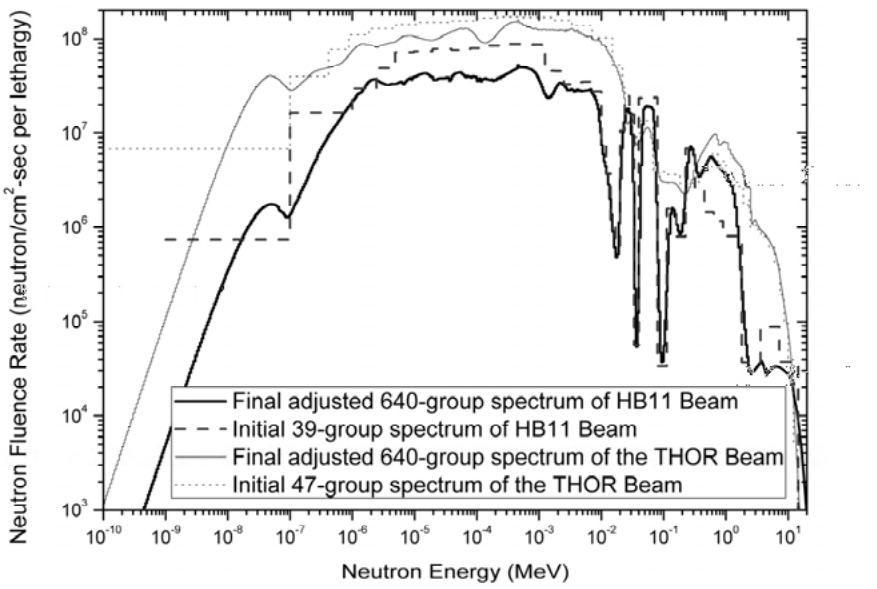

Figure 2 The adjusted spectra and the initial spectra of HB11 and the THOR BNCT beams

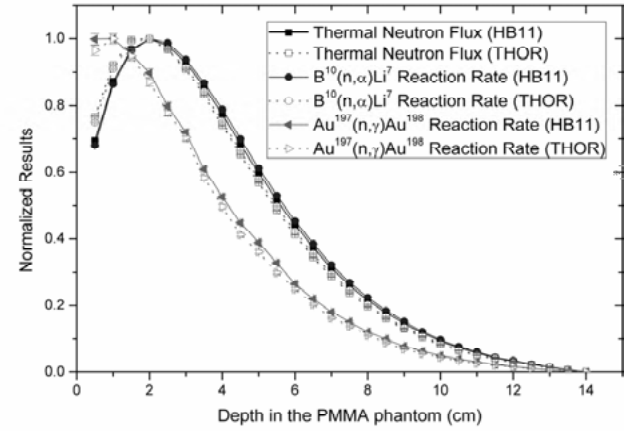

Figure 3 The calculated thermal neutron flux, boron and gold reaction rate along the central axis of the PMMA phantom

BNCT epithermal neutron beam due to its high sensitivity to the epithermal neutrons (~4.906 eV).

4. Conclusions

This paper successfully measured and adjusted the spectra of HB11 (HFR) and the THOR BNCT beams for the further dose comparison. The applied coarse-scaling spectrum adjustment ensures the continuity of the fine-group spectra adjusted from the coarse-group initial spectra.

The HB11 spectrum is harder than the THOR spectrum, which has the advantage of deeper penetration. The epithermal neutron flux of the THOR beam at 1.2 MW is about 3 times of HB11 and meets the criterion suggested by IAEA. Both beams have higher fast neutron component than their original design.

Acknowledgement

This study was supported by the National Science Council of the Republic of China under contract number NSC95-2221-E-007-135 and -136.

References

Beckurts, K.H., Wirtz, K., 1964. Neutron Physics, Springer-Verlag, New York.

Berg, S., McElroy, W.N., 1967. A Computer-Automated Iterative Method for Neutron Flux Spectra Determination by Foil Activation. SAND II (Spectrum Analysis by Neutron Detectors II) and Associated Codes. Air Force Weapons Laboratory.

Briesmeister, J.F., 2000. MCNP—A General Monte Carlo N-Particle Transport Code Version 4C, Los Alamos National Laboratory.

IAEA, 2001. Current status of neutron capture therapy. IAEA TECDOC-1223. International Atomic Energy Agency, Vienna.

Goncalves, I.F., Martinho, E., Salgado, J., 2001. Monte Carlo calculation of epithermal neutron resonance self-shielding factors in wires of different materials. Applied Radiation and Isotopes 55, 447-451.

Liu, Y.H., Nievaart, S. Tsai, P.E., Moss, R., Liu, H.M., Jiang. S.H., 2008. Coarse-Scaling Adjustment of Fine-group Neutron Spectrum of Epithermal Neutron Beams in BNCT using Multiple Activation Detectors. To be published.

Liu, Y.H., Nievaart, S., Moss, R., Liu, H.M., Jiang. S.H., 2008. Monte-Carlo Determined Self-Shielded Groupwise Cross-Sections Applied in the Epithermal Neutron Spectrum Adjustment. To be published.

Thermal neutron dosimeter by synthetic single crystal diamond devices

S. Almaviva[a], Marco Marinelli[a], E. Milani[a], G. Prestopino[a], A. Tucciarone[a], C. Verona[a],

G. Verona-Rinati[a], M. Angelone[b] and M. Pillon[b]

[a]*Dipartimento di Ingegneria Meccanica, Università di Roma "Tor Vergata", Via del Politecnico 1, I-00133 Roma, Italy*
[b]*Associazione EURATOM – ENEA sulla fusione, Via E. Fermi 45, I-00144 Frascati (Roma), Italy*

Abstract

We report on a new solid state dosimeter based on Chemical Vapor Deposition (CVD) single crystal diamond fabricated at Roma "Tor Vergata" University laboratories. The dosimeter can be used for direct neutron dose measurements in medical physics and in Boron Neutron Capture Therapy (BNCT). Two single crystal diamond detectors are fabricated in a p-type/intrinsic/metal configuration and are sandwiched together with a Boron containing layer in between the metallic contacts (see Fig. 1). Such a boron layer is used as a converting material for thermal neutrons through the $^{10}B(n,\alpha)Li$ nuclear reaction. In this way, the reaction products are simultaneously detected. Neutron irradiations were performed at the Frascati Neutron Generator (FNG) using the 2.5 MeV neutrons produced through the D(d, n)^{3}He fusion reaction. Thermal neutrons were then produced by slowing down the 2.5 MeV neutrons using a cylindrical polymethylmethacrylate (PMMA) moderator. The diamond dosimeter was placed in the center of the moderator. The products of $^{10}B(n,\alpha)Li$ nuclear reaction were collected simultaneously giving rise to a single peak. Stable performance, high reproducibility, high efficiency and resolution and good linearity were observed.

Keywords: CVD single-crystal diamond, neutron detector, solid state microdosimetry.

1. Introduction

Semiconductor detectors that incorporate neutron reactive material within the same detector offer a promising approach to neutron dosimetry. In nuclear medicine, there is a number of therapies that use the nuclear properties of matter. Among them, Boron Neutron Capture Therapy (BNCT) seems to be a promising treatment for different types of malignant tumors, based on the possibility of selective accumulation of the stable isotope ^{10}B in tumor tissue and on the high cross section of such an isotope for thermal neutrons (Barth et al, 1990). When a thermal neutron is captured by a ^{10}B atom, alpha and lithium particles are produced and release their energy within a range comparable to the size of a typical tumor cell (10-20 μm), thus the emitted radiation is limited to a single cell. In the BNCT, however, it is difficult to evaluate the delivered dose. Traditional dosimetry is based upon the use of gas proportional counters, which are quite large in size but, by variation of the gas pressure inside the detector, can simulate energy deposition by particles in sites with diameters of 2 to 100 μm (Wuu et al., 1992).

In BNCT also gel dosimeters and TLD are used for dose measurement.

An ideal dosimeter for direct neutron dose measurements in medical physics, is supposed to have particular physical and technical features such as human tissue equivalence, small size enough not to perturb the radiation field and be able to measure the macro and micro dose simultaneously at the same point in the phantom, high sensitivity in order to allow a precise real time measurement of delivered dose.

In addition, device stability, radiation hardness and linearity with dose are also required. Due to its physical properties, the use of diamond, allows to easily meet some of the above requirements.

In the last years, the fabrication and test of several types of CVD single crystal diamond neutron detectors with highly reproducible characteristics has been reported (Marinelli et al., 2005) (Marinelli et Al., 2007). In addition, the sensitivity to thermal neutron is given by depositing a boron containing layer on top of the metallic electrode of the devices.

2. Diamond dosimeter construction and experimental set up

The single detector consists of a multilayered structure obtained by a two step deposition process. A conductive boron-doped diamond homoepitaxial layer with approximately 5 Ωcm resistivity, used as a backing contact, is deposited, at first, by Microwave Plasma Enhanced CVD (MWPECVD) on a commercial low-cost synthetic HPHT type Ib single crystal diamond substrate, $4 \times 4 \times 0.5$ mm^3 in size. After that an intrinsic diamond layer is homoepitaxially grown on the doped one, which operates as detecting region. Its thickness can vary from a few microns up to more than 200 microns, depending upon the use of the detector; in our case, since the penetration depth in diamond of 1.47 MeV α-particles and 840 keV ^{7}Li ions is about few microns, a thickness of 20 - 25 μm was chosen. Each diamond layer have been oxidized, after the growth, by isothermal annealing, at 500 °C, for 1h in air, in order to remove the H_2 surface conductive layer. Finally, a circular aluminum electrode, about 3 mm diameter and 100 nm thick is deposited on the diamond surface by thermal evaporation, while annealed silver paint was utilized in order to provide an ohmic contact with the B–doped layer. A boron oxide layer, 330 nm thick, is finally deposited by vacuum thermal evaporation process on the top of the Al contact. Because of the possibility of escape of one of the reaction products from a single detector, two detectors in a sandwich configuration (Glenn F. Knoll, 1979) are commonly uses, as shown in Fig.1.

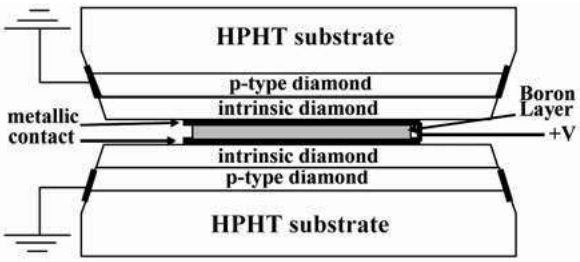

Fig. 1 - Structure of diamond dosimeter

The thin conversion layer is sandwiched between two detectors, electrically connected in parallel. If the outputs are connected together, the devices operate as a single one (diamond dosimeter).

It ought to be stressed that before to realize the evaporate boron oxide layer and thus the sandwich detector, each diamond detector is tested to check its quality.

The test is performed in vacuum for each single detector using ^{241}Am source emitting 5.5 MeV α-particles. The single detector efficiency, its resolution and long lasting stability are measured. In order to found the voltage work of the detector, a systematic investigation of both the energy resolution and the charge collection efficiency as a function of the applied voltage is performed under positive polarity.

Usually each single detector shows 100% charged collection efficiency and approximately 1% energy resolution. Charged particles entering the diamond lose their energy through Coulombic scattering, thereby creating a high-density plasma cloud of columnar ionization in the form of electron-hole pairs (Gerhard, 1999). The diamond dosimeter is biased by a positive voltage +4 V/μm on the metal contact while the boron doped diamond contact is grounded to separate the electron-hole pairs and drift the charges to their respective contacts.

The mobile charges each induce an image charge on the contacts as they move through the device, and the induced charge is integrated and measured by an external preamplifier and accompanying electronics. The charge collection efficiency and energy resolution of the diamond dosimeter was characterized using an electronic chain, consisting of an ORTEC 142A charge preamplifier, followed by ORTEC 672 spectroscopy amplifier and a multichannel analyser.

The diamond dosimeter was exposed to neutron irradiation at the Frascati Neutron Generator (FNG) using the 2.5 MeV neutrons produced by the D(d, n)^{3}He fusion reaction. These neutrons are slowed down in a cylindrical polymethylmethacrylate (PMMA) moderator with a radius of 10 cm, at the centre of which is placed the diamond dosimeter. Due to the relatively small thickness of the moderator, only a fraction of the incident neutrons are thermalized in the moderator.

Activation foils were placed inside the cylindrical moderator during the detector testing in order to determine the absolute neutron flux and spectrum at the detector position using the well established neutron spectrum unfolding technique (Pillon et al. 2004).

3. Results and discussions

The $^{10}B(n,\alpha)^{7}Li$ reaction leads to the following reaction products and branching ratio (Glenn F. Knoll, 1979):

$$^{10}B + n \rightarrow \begin{cases} 6\%: & ^{7}Li(1.015MeV) + \alpha(1.777MeV) \\ & Q = 2.792MeV\,(ground \cdot state) \\ 94\% & ^{7}Li(0.84MeV) + \alpha(1.47MeV) \\ & Q = 2.31MeV\,(excited \cdot state) \end{cases}$$

After absorption of the thermal neutron by ^{10}B, about 94% of all reaction lead to the excited state and only 6% directly to the ground state. In either case, the Q-value of the reaction is very large compared with the incoming energy of the slow neutron, so that the energy imparted to the reaction products is essentially just the Q-value itself.

As mentioned below, the primary reaction $^{10}B(n,\alpha)^{7}Li$ results in the emission of a 1.47 MeV alpha particle and 840 keV ^{7}Li ion in its first excited state. The average range for 840 keV ^{7}Li ion in boron oxide layer is 2.33 microns and the average range for a 1.47 MeV alpha particles is 4.2 microns. The energy absorbed in the single detector is simply the original particles energy minus the combined energy lost in the boron oxide film and in the metal contact of the detector during the transit. The dosimeter sensitivity increases for larger thicknesses of the converting layer. However, it is at expense of energy resolution, because the reaction products lose a not negligible and undetermined fraction of their energy in the boron oxide layer. Natural boron is used in the present experiment, containing thus 20% of the neutron interacting ^{10}B isotope.

The pulse height analysis (PHA) spectrum measured by diamond dosimeter under neutron irradiation is reported in Fig.2. It can be noticed that the approximately 2.3 MeV and 2.79 MeV peaks are well separated and correctly placed in the PHA spectrum measured; besides, their relative intensities are in good agreement with their expected reaction probabilities. The other two peaks, located at lower energies, are due to the detection of a single reaction product escaped. However, in this low energy region of the spectrum, a significant background (recoiling protons, γ ray, fast neutrons etc.) is present, so nothing can be argued from the relative intensities of the peaks.

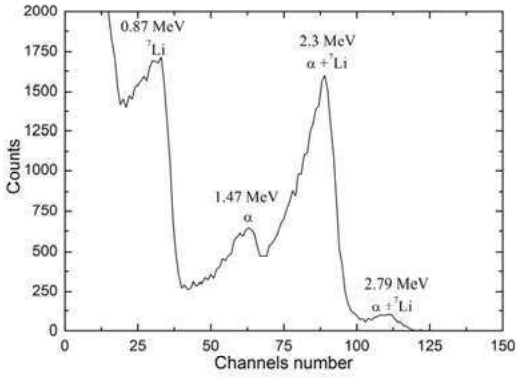

Fig. 2 - Typical PHS spectrum for a diamond dosimeter

The time irradiation profiles recorded with the CVD diamond dosimeter were compared with those recorded by the standard monitors available at FNG (NE-213 scintillator). The dosimeter count rate compared to the reference monitor is evidenced in Fig.3, where the diamond dosimeter and NE-213 normalized count rates are reported as a function of time, varying the neutron flux.

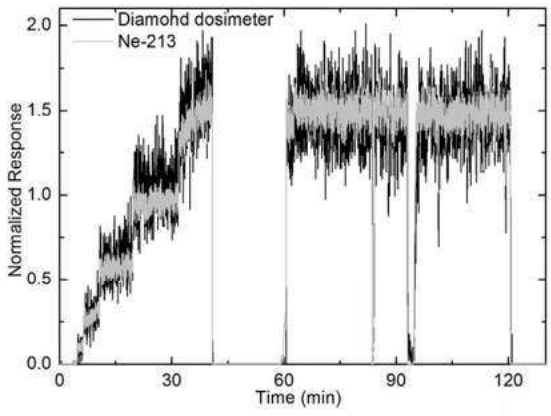

Fig. 3 – C mparison between the normalized time traces of the diamond dosimeter (black line) and the fission chamber monitor Ne-213 (gray line)

A very good correlation among the two behaviours is observed as well as a good agreement between the temporal trace of both devices. The linearity as a function of the incident thermal neutron flux was also tested by varying the neutron emission of FNG. The count rate of the diamond dosimeter was compared with the count rate of a scintillator NE-213 which is routinely used as neutron monitor at FNG.

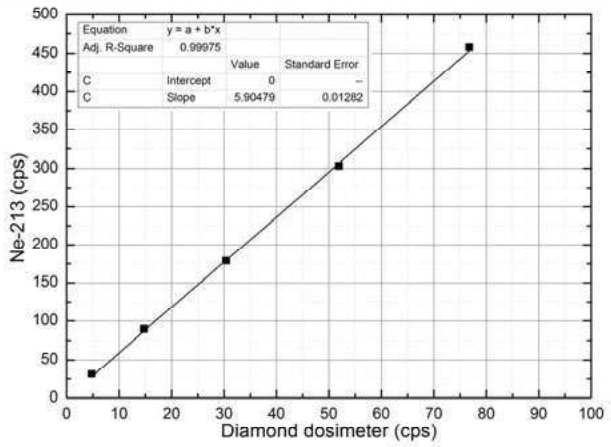

Fig. 4 - Linearity of the diamond dosimeter tested vs. NE-213

The results are reported in Fig.4. A good linear behavior is observed, with a correlation index 0.99975.

If the detector is calibrated in a reference thermal flux, by measuring the total $^{10}B(n,\alpha)^{7}Li$ counts (area under the peaks of Fig. 2) it is possible to determine the energy released in carbon (tissue) in the neutron spectrum used. The expected neutron capture probability for a given thickness of boron layer is given by $P = n\sigma L$, where n is the density of the boron atoms per cm^3, σ is the thermal neutron capture cross section of boron and L is the thickness of the boron layer. When an area A of boron layer is exposed to a neutron flux density of Φ for a time t, we expect to detect $N = P\Phi At\eta$ neutrons, where η is a parameter that corresponds to the intrinsic efficiency of the diamond dosimeter. For now, we set $\eta = 1$. In our case, the microscopic flux averaged neutron absorption cross section σ is $1162*10^{-24}$ cm^2, the atomic density of ^{10}B content in boron oxide is $n = 8.4*10^{21}$ atoms/cm^3, the thickness of boron oxide layer $L = 3.3*10^{-5}$ cm, A=0.0314 cm^2 and a neutron flux density of Φ=$1.5*10^{6}$ neutrons/cm^2s. The expected neutron capture events for diamond dosimeter is $N(Theory) = 4.8*10^{4}$. Computing the area under the peaks of experimental spectrum measured by diamond dosimeter, subtracting the background, gives us an observed $N(Experiment) = 4.2*10^{4}$.

4. Conclusions

A solid state dosimeter, based on CVD single crystal diamond in a p-type/intrinsic/metal configuration sandwiched together with a boron oxide layer in between the metallic contacts was presented and studied. Thermal neutrons are detected through the $^{10}B(n,\alpha)Li$ nuclear reaction taking place in the thin boron oxide film deposited on top of metal electrode of the single devices. The products of $^{10}B(n,\alpha)Li$ nuclear reaction were observed together as single peaks. The preliminary experimental test have shown a high thermal neutron detection efficiency, stable performance, high reproducibility and good linear behavior of the count rate versus the incident neutron photon flux. The above results strongly indicate that diamond dosimeters can be effectively used for thermal neutron monitoring in medical physics and in BNCT. Future diamond dosimeters will use enriched boron-^{10}B oxide to increase five-fold the count rate. Work is in progress to calibrate the diamond dosimeters with thermal neutrons in reference thermal fluxes as well as to test them in the BNCT beam available at TAPIRO reactor of ENEA Casaccia (E. Nava et. Al. this symposium).

References

R.F. Barth, A.H. Soloway, R.G. Fairchild, Cancer Res. 50 , 1061, 1990

C.S. Wuu, HI. Amols, P. Kliauga, L.E. Reinstein, S. Saraf, “Microdosimetry for Boron Neutron

Capture Therapy”, Radiation Research 130, 355-359, 1992.

Marco Marinelli, E. Milani, G. Prestopino, M. Scoccia, A. Tucciarone, G. Verona-Rinati, M. Angelone, M. Pillon, Appl. Phys. Lett, 86, 143509, 2005

Marco Marinelli, E. Milani, G. Prestopino, A. Tucciarone, C. Verona, G. Verona-Rinati, M. Angelone, D. Lattanzi, M. Pillon, Appl. Phys Lett 90, 183509, 2007.

Radiation Detection and Measurement, Glenn F. Knoll, 1979

Semiconductor Radiation Detectors, Lutz Gerhard, 1999

M. Pillon, M. Angelone and R. A. Forrest Radiation Physics and Chemistry, Volume 71, Issues 3-4, October-November 2004, 895-896

Gadolinium as a powerful additive for enhancing the neutron sensitivity of ESR dosimeters

M. Marrale[a,c], M. Brai[a,c] , S. Basile[a,c], G. Gennaro[a], A. Longo[a], A. Bartolotta[b,c]

[a]*Dipartimento di Fisica e Tecnologie Relative, Università degli Studi di Palermo, Viale delle Scienze, Edificio 18, 90128 Palermo, Italy*
[b]*Dipartimento Farmacochimico, Tossicologico e Biologico, Università degli Studi di Palermo, Via Archirafi 32, 90123Palermo, Italy*
[c]*Unità CNISM Palermo, Italy*

Abstract

We have studied the effect of the gadolinium addition on the neutron sensitivity of alanine and ammonium tartrate ESR dosimeters exposed to a mixed (n, γ) field mainly composed by thermal neutrons. Gadolinium has been chosen because of its very high capture cross section to thermal neutrons. The gadolinium presence hugely (up to a factor 30) enhances the sensitivity to thermal neutrons of dosimeters with gadolinium with respect to those without gadolinium for both organic molecules used. We have analysed the ESR response of these dosimeters as a function of the gadolinium concentration inside the dosimeter in order to find the optimum compromise between the increase of sensitivity to thermal neutrons and the reduction of tissue equivalence (due to high gadolinium atomic number). Our results show that a low concentration of gadolinium oxide (of the order of 5% of the total mass of the dosimeter) can significantly improve the thermal neutron sensitivity without heavily reducing the tissue equivalence. We completed our study through a Monte Carlo simulation aimed at obtaining information about the reliability of this powerful tool in predicting the response enhancement achievable with the addition of gadolinium in alanine and ammonium tartrate dosimeters. The computational values obtained through simulation have been compared with the experimental results and a good agreement has been found. These results can provide useful information for applications in Neutron Capture Therapy dosimetry.

Keywords: ESR Dosimetry, NCT, alanine, ammonium tartrate, gadolinium, Monte Carlo

1. Introduction

Along with the Neutron Capture Therapy (NCT) development and with the use of thermal neutrons for radiotherapeutic purposes, many efforts have been devoted to the beam characterization in order to optimize the therapy procedures.

Reliable dosimetric measurements should be able to determine the various components (neutronic and photonic) of the mixed beam usually employed for therapy.

Nuclei with high cross sections for thermal neutrons are needed for effective radiotherapic treatments. ^{10}B has been widely used, through its $^{10}B(n,\alpha)^{7}Li$ reaction, producing secondary particles with high LET.

More recently, ^{155}Gd and ^{157}Gd have been taken into consideration, due to their very high thermal neutron capture cross section. Nevertheless, the reaction leads to a complex pattern of secondary products. As an example, for ^{157}Gd we have:

$^{157}Gd + n_{th} \rightarrow {}^{158}Gd^{*} + \gamma$ photons + electrons

with electrons arising from both internal conversion and Auger processes, leading to energy release in the neighbourhood of the reaction site.

Both the concentration of nuclei with high cross section and the thermal neutron fluence need to be controlled in NCT.

Electron spin resonance (ESR), which detects the effects of ionizing radiations by measuring the concentrations of paramagnetic centers (free radicals) produced after exposure to radiation, has become an international standard for dose measurements using alanine dosimeters (Mehta and Girzikowsky, 1999). However, more recently new materials have been taken into consideration in order to improve the sensitivity of the ESR technique. Among these, ammonium tartrate (AT) has received particular attention due to its higher S/N ratio with respect to alanine, linear relation between radiation dose and ESR signal, and tissue equivalence (Olsson et al, 1999).

In this paper, we describe experimental results and Monte Carlo simulations concerning the addition of gadolinium to alanine and ammonium tartate pellets as a valuable tool to enhance the ESR

sensitivity of organic compounds to thermal neutrons in a mixed field of photons and neutrons.

2. Materials and methods

A blend of 94% of the active material (alanine or ammonium tartrate added or not with gadolinium in the form of its Gd_2O_3 compound), 5% of polyethylene as binder and 1% of magnesium stearate as lubricant was prepared according to the already reported procedure (Brai et al, 2007c). Various concentrations of Gd_2O_3 (up to 47%) were used. Thickness of the pellets was dependent on the gadolinium concentration, since the gadolinium oxide content modifies the density of the dosimeters which we decided to keep at constant mass.

Dosimeters were irradiated with 1.25 MeV ^{60}Co photons (using the facility at the Radiotherapy Department of the "M. Ascoli" hospital in Palermo) and with thermal neutrons (using the TAPIRO reactor at ENEA in Rome). More details can be found elsewhere (Brai et al, 2007c; Marrale et al, 2008a).

ESR measurements were performed in a TE_{102} rectangular cavity operating at approximately 9.8 GHz, and at room temperature. The peak-to-peak height h_{pp} was used as dosimetric parameter (see Fig. 1).

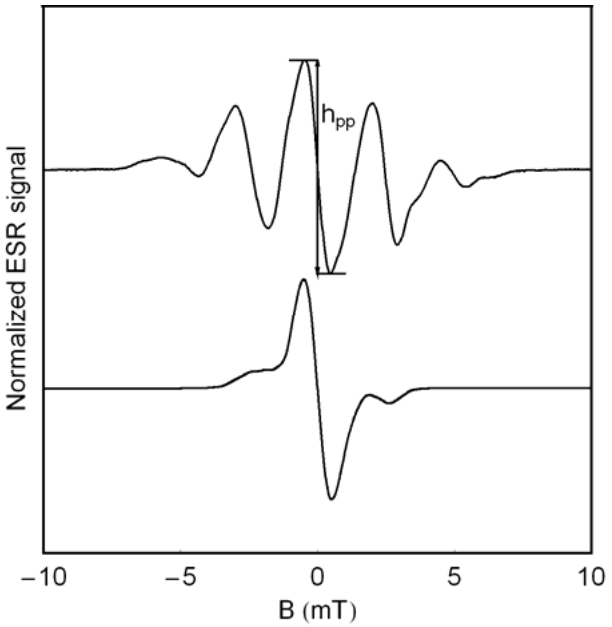

Figure 1. Pure alanine (top) and ammonium tartrate (bottom) ESR spectra

Experimental data (ESR signal) have been compared with the energy deposition inside the volume of these ESR detectors obtained by Monte Carlo simulations. The MCNP5 (Briesmeister, 2000) radiation transport code was used to perform the calculations. Neutron flux was modeled as a plane source impinging on cylindrical dosimeter along its axis. In order to better describe the features of the TAPIRO beam, the energy spectrum of the neutron source was taken into account. Target dosimeter was schematized as alternate parallel layers of gadolinium oxide and alanine or AT (Marrale et al, 2008b).

3. Results

In Figure 1 we show the ESR spectra of pure alanine (top) and pure AT (bottom). Both spectra are centered at $g \sim 2$, g being the splitting factor. It can be seen that the alanine spectrum has a wider and more complex structure than AT.

In the same magnetic field range shown in Fig. 1 the dosimeters with gadolinium oxide show a broader peak centered at $g \sim 2$, giving rise to a linear baseline. The peak-to-peak amplitude was estimated after this baseline subtraction (Brai et al, 2007a; 2007b).

Table 1 shows the photon (S_p) and neutron sensitivity (S_n) for pure and gadolinium added (47% of total mass) dosimeters. The best fit slope of the ESR signal vs gamma dose (neutron fluence) has been used as sensitivity parameter for photons (neutrons) (Brai et al, 2007c).

Table 1. Sensitivity to photons (S_p) and to neutrons (S_n) of alanine (A) and ammonium tartrate (AT) pure and gadolinium added (47% of total mass) dosimeters

Blend	S_p	S_n
A	0.362 ± 0.004	$(3.88 \pm 0.04)\times10^{-13}$
AT	0.403 ± 0.005	$(6.75 \pm 0.17)\times10^{-13}$
Gd_2O_3-A	0.670 ± 0.009	$(148.0 \pm 0.6)\times10^{-13}$
Gd_2O_3-AT	0.724 ± 0.009	$(178.0 \pm 1.5)\times10^{-13}$

These data make evident the increase of photon sensitivity (of about a factor 2 for 47% addition shown here) after the gadolinium addition.This is probably due to the increased effective atomic number.

A more dramatic role is played by gadolinium in the case of sensitivity to thermal neutrons. Its effectiveness in neutron capture processes and the large amount of free radicals produced by secondary charged particles lead to a sensitivity tens of times larger than in the pure alanine or ammonium tartrate cases.

Gadolinium addition also plays a role in decreasing the lowest measurable neutron fluence (LMF), evaluated as the fluence value which produces an ESR signal in the irradiated pellets equal to the mean value of the background in unirradiated pellets plus ten standard deviations (Currie, 1968).

In particular, the LMF values for gadolinium added alanine and ammonium tartrate are of the order of 10^{10} n_{th} cm^{-2}, i.e. two orders of magnitude smaller than in the pure cases.

As an independent check of the reliability of ESR dosimetry as a tool for discriminating gamma and neutron components of the mixed radiation field, pairs (with and without gadolinium) of dosimeters have been used to carry out a blind test. Neutron fluence has been best determined by using the dosimeter pairs of alanine and Gd_2O_3–alanine. The resulting 3% uncertainty lies well within the limiting value (5%) for application in the radiotherapeutic field.

On the other hand, the gadolinium high atomic number (Z = 64), makes its response to photons quite different from the response of soft tissue. Therefore, the gadolinium content has to be optimized in order to achieve a significant increase in sensitivity to thermal neutrons, without a significant decrease in tissue equivalence.

The tissue equivalence of gadolinium added dosimeters has been assessed through the analysis of the effective mass energy absorption coefficient $(\mu_{en}/\rho)_{eff}$, as shown in Figure 2.

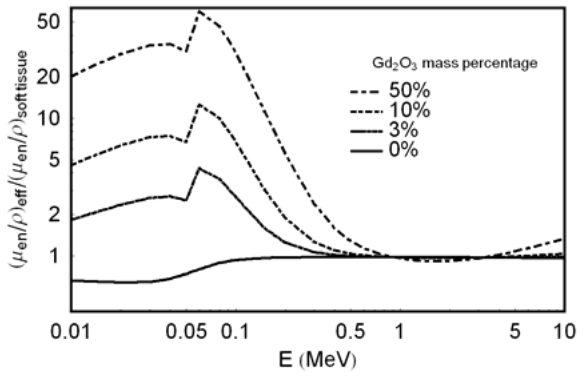

Figure 2. Effective mass energy absorption coefficient of alanine pellets for various Gd_2O_3 concentrations normalized to its tissue equivalent values

For instance, 5% gadolinium content does not significantly alter the tissue equivalence, while increasing the neutron sensitivity more than ten times. This can be seen in Figure 3, where the ESR peak-to-peak amplitude per unit mass is shown as a function of Gd_2O_3 content, both for alanine (up) and AT (bottom). Experimental data were normalized to their maximum. The signal increases with gadolinium concentration, then saturates and decreases because the high gadolinium content obviously reduces the amount of sensitive material, since the dosimeter mass is kept constant.

Figure 3 also shows the results of Monte Carlo simulations. They give information on the energy per unit mass released by neutrons inside the dosimeter. In order to compare the common trends of experimental and computational results, the Monte Carlo data have been rescaled by a factor determined minimizing the average quadratic difference of the two data series in the left region of the plot.

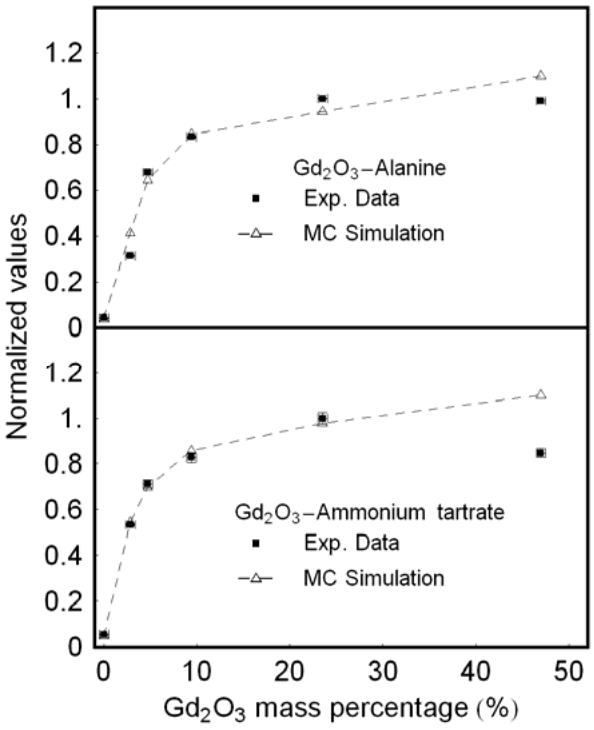

Figure 3. ESR signals per unit mass and energy released per unit mass obtained by Monte Carlo simulation

Since experimental data provide information on the number of free radicals produced by neutron interactions, the good agreement shown in Figure 3 for low Gd_2O_3 concentrations implies a proportionality of this quantity to the amount of energy released inside the dosimeters.

At high gadolinium concentrations the computed values differs from the experimental values. This effect is very evident for the highest Gd_2O_3 concentration studied (47%). A possible explanation of this difference is a saturation effect in free radicals of the sensitive materials.

The energy released inside alanine or AT is very high but not enough molecules, from which free radicals can be produced, are present. Furthermore, high spatial concentrations of free radicals could take place and this situation could lead to recombination phenomena.

Therefore, the ESR signal per unit mass decreases with increasing gadolinium content inside the pellet. However, this saturation effect is not taken into account in the Monte Carlo simulation and the computed released energy keeps increasing with gadolinium concentration.

4. Conclusions

The ESR response of alanine and ammonium tartrate dosimeters added with gadolinium oxide and exposed to mixed fields of thermal neutrons and gamma photons has been investigated.

Calibration curves to ^{60}Co gamma photons and to thermal neutrons have been obtained and the role of the gadolinium addition has been focused. In particular, because of high gadolinium cross section for neutron capture and of the secondary particles (mainly Auger and internal conversion electrons), we observed that the introduction of Gd in these organic compounds significantly increases (about a factor of 30) the sensitivity of dosimeters to neutron radiation. Since gadolinium has a high atomic number, the addition of gadolinium causes the reduction of or even the loss of tissue equivalence. Consequently, in order to provide a tissue-equivalent ESR dosimeter with improved sensitivity to thermal neutrons, a low concentration of gadolinium oxide (of the order of 5% of the total mass of the dosimeter) must be chosen.

Monte Carlo simulations have been carried out to check the reliability of this computational tool in predicting the response enhancement achievable with use of suitable additive. We found that the Monte Carlo computed values well follow the experimental data for low gadolinium level inside the dosimeter; whereas at high gadolinium concentration the difference between simulated and experimental data is larger because of the saturation effect in free radicals of sensitive materials.

These results can provide useful insight into thermal neutron dosimetry techniques and its application to NCT.

In the future we plan to make experiments with epithermal neutron beams (such as those used in NCT) and to improve the physical and geometrical modeling used in Monte Carlo calculations in order to obtain a more realistic description of the experimental set-ups.

References

Brai, M., Gennaro, G., Marrale, M., Bartolotta, A., D'Oca, M.C., 2007a. ESR response to γ-rays of alanine pellets using $B(OH)_3$ or Gd_2O_3. Appl. Radiat. Isot. 65 435–9.

Brai, M., Gennaro, G., Marrale, M., Tranchina, L., Bartolotta, A., D'Oca, M.C. 2007b. ESR response to ^{60}Co-rays of ammonium tartrate pellets using Gd_2O_3 as additive. Radiat. Meas. 42 225–31.

Brai, M., Marrale, M., Gennaro, G., Bartolotta, A., D'Oca, M.C., Rosi, G., 2007c. Improvement of ESR dosimetry for thermal neutron beams through the addition of gadolinium. Phys. Med. Biol. 52, 5219–5230.

Briesmeister, J.F., (Ed.), 2000. Los Alamos National Laboratory report LA-13709-M.

Currie, L. Limits for quantitative detection and quantitative determination. Anal. Chem. 40(3), 586–593 (1968).

Marrale, M., Brai, M., Gennaro, G., Triolo, A., Bartolotta, A., D'Oca, M.C., Rosi, G. 2007. Alanine blends for ESR measurements of thermal neutron fluence in a mixed radiation field. Radiat. Prot. Dosim. 126, 631–635.

Marrale, M., Brai, M., Gennaro, G., Bartolotta, A., D'Oca, M.C., 2008a. The effect of gadolinium on the ESR response of alanine and ammonium tartrate exposed to thermal neutrons. Radiat. Res. 169, 232–239.

Marrale, M., Gennaro, G., Brai, M., Basile, S., Bartolotta, A., D'Oca, M.C., 2008b. Exposure of Gd_2O_3-alanine and Gd_2O_3-ammonium tartrate ESR dosimeters to thermal neutrons: Experiments and Monte Carlo simulations. Radiat. Meas. 43, 471–475.

Mehta K., Girzikowsky R., IAEA reference dosimeter: alanine- ESR. In Techniques for High Dose Dosimetry in Industry, Agriculture and Medicine—Proceedings of the Symposium, pp. 299–304. IAEA-TECDOC-1070, IAEA, Vienna, 1999.

Olsson, S., Bagherian, S., Lund, E., Carlsson G. A., Lund, A., Ammonium tartrate as an ESR dosimeter material. Appl. Radiat. Isot. 50, 955–965 (1999).

Experimental feasibility studies on a SPECT tomograph for BNCT dosimetry

D.M. Minsky[a,b], A.A.Valda[a,b], A.J. Kreiner[a,b,c], S. Green[d,e], C. Wojnecki[d,e], Z. Ghani[d]

[a]*Dpto de Física, CNEA, Av. Gral Paz 1499 (B1650KNA), San Martín, Buenos Aires, Argentina*
[b]*ECyT, UNSAM, , M. de Irigoyen 3100 (1650), San Martín, Argentina*
[c]*CONICET, Av. Rivadavia 1917 (C1033AAJ), Buenos Aires, Argentina*
[d]*School of Physics and Astronomy, University of Birmingham, B15 2TT, United Kingdom*
[e]*Department of Medical Physics, University Hospital Birmingham, Birmingham, B15 2TH, United Kingdom*

Abstract

This article reports on the development of a prototype of a SPECT tomograph system for online dosimetry in BNCT based on $LaBr_3$(Ce) scintillation detectors. The setup shielding was optimized to be used in the accelerator based BNCT facility of the University of Birmingham. The system was designed and built. An image of a ^{241}Am point source was reconstructed. A projection of a phantom with two tumors with 400ppm of ^{10}B was measured at the BNCT facility.

Keywords: online BNCT dosimetry, tomography, SPECT, $LaBr_3$(Ce) scintillator

1. Introduction

In 94% of neutron captures in ^{10}B, the resulting ^{7}Li ion is emitted in an excited state and decays immediately through a characteristic 478 keV prompt gamma ray. The attenuation coefficient for this photon in tissue is about 0.1 cm^{-1}, hence this γ ray escapes from the body to a large extent. Its detection thus offers the possibility of an external measurement of the boron dose. Several approaches have been adopted for BNCT online dosimetry based on this principle. Verbakel and Stecher-Rasmussen (1997) have proposed and constructed a device named Gamma Ray Telescope that was used during BNCT clinical trials (Verbakel et al., 2003). Kobayashi et al. (2000) studied a Single Photon Emission Tomography (SPECT) device and Rosenschöld et al. (2006) reported a feasibility study for prompt gamma tomography.

In our previous work (Valda et al., 2005, Minsky et al., 2006), we designed a prototype of a SPECT system for online dose measurements in BNCT. After taking 20 projections of 41 bins the system can reconstruct boron dose maps of 21x21 voxels of 1 cm^3 size each. This dosimetry image would give spatial information not available with the current dosimetry methods and will not be hampered by the great present uncertainties in the boron concentration determination. The fluctuations in the acquisition process have been analyzed (Minsky et al., 2006) and they show that such a system is possible.

This article shows experimental work done with a prototype based on four $LaBr_3$(Ce) scintillation detectors at the BNCT facility of the University of Birmingham.

2. Prototype design

The collimator length and diameter were designed in order to maximize the detection efficiency and to obtain a resolution of 1 cm, the same size as the image pixel. The geometric detection efficiency ε and spatial resolution R of a round hole collimator are:

$$\varepsilon = \frac{\phi/2}{4(l+z)^2} \quad ; \quad R \approx \frac{\phi(l+z)}{l} \qquad (1)$$

where $\varnothing$ is the hole diameter, l the distance from collimator to object and z the collimator length. The detector-object distance (l+z) was chosen to be 60 cm, obtaining a diameter $\varnothing$=*0.5cm*, a collimator length *l=30cm*, and an efficiency ε=*4.34 10*$^{-6}$.

The detectors must be shielded in order to avoid contamination in the signal. The shielding must block not only gammas but also neutrons, since they can generate gamma contamination inside the crystals. The proposed shielding consists of several layers (fig. 1): an external layer of a material with high concentration of hydrogen (initially water) to thermalize neutrons, a second layer of lead to shield from gammas, and a layer of 95% ^{6}Li enriched lithium carbonate to capture thermal neutrons before reaching the detector.

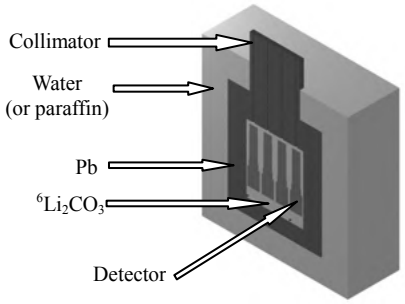

Figure 1 – Detector shielding. A material with high hydrogen content thermalizes the neutrons, a lead layer blocks gammas and a ^{6}Li layer captures thermal neutrons before reaching the detector crystal

The proposed shielding has been simulated with MCNP 5.140 (Brown et al. 2002) for different water and lead thicknesses in order to estimate the expected background under the 478 keV peak. Two different contributions to the background have been taken into account: the gamma background coming from outside the detectors and the gamma background generated inside them by neutron captures in the crystal. Since MCNP libraries do not have gamma ray production data for Br and La, the background generated inside the crystal has been estimated by generating a source distributed in the crystal with the spectra obtained per capture and the intensity calculated from the neutron flux. The expected background is shown in figure 2.

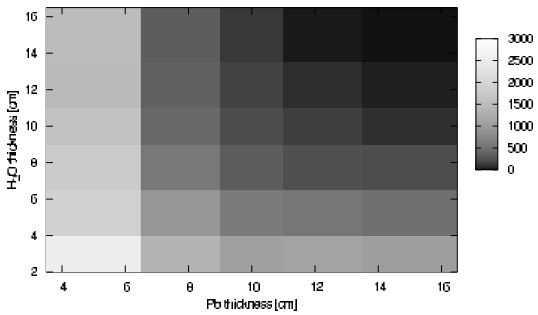

Figure 2 – Expected background under the 478keV peak vs. the water and lead thicknesses

The background decreases with the lead thickness due to attenuation of the external gamma rays, and it also reduces with the water thickness since it prevents captures in the crystal and the subsequent gamma production. Due to weight and space limitations, the shielding lead and water layers have been chosen to be 10 cm thick each. As this shielding is insufficient, lithium was added to the external layer: ^{6}Li will capture neutrons preventing them from producing gammas by reacting with hydrogen, lead and the detector crystal. For practical purposes the external layer has been replaced by paraffin since it can be loaded with significant amounts of natural Li_2CO_3.

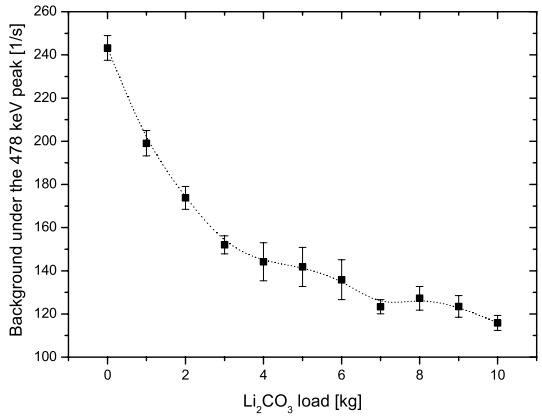

Figure 3 – Background as a function of Li_2CO_3 mass content in the 70 kg paraffin layer

Figure 3 shows how the background is reduced with the increase of Li_2CO_3 content.

In the present BNCT facility, as the setup shielding increases in size, the collimator axis (i.e., the tomographic image plane) moves away from the neutron beam port. The expected boron capture rate per unit volume was simulated for different phantom-port distances and as a function of the depth inside the phantom for a concentration of 100ppm (fig. 4)

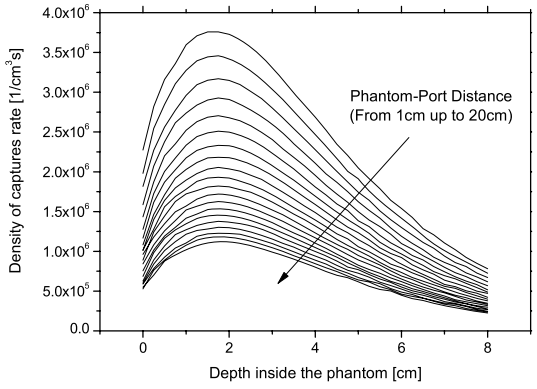

Figure 4 – Neutron captures in boron for different phantom-port distances and vs depth inside the phantom

In the present system we worked with a paraffin layer of 70 kg loaded with 10 kg of Li_2CO_3. Under this condition the expected background count rate is 120 cps. Considering the detector intrinsic efficiency, the global detection efficiency is about 10^{-6}, so for the proposed system, a signal of 3 cps for a 1 cm^3 tumor with 100 ppm of ^{10}B is expected.

3. Experimental Results

The built prototype is shown in fig. 5. The collimator resolution has been tested with a system adapted to CdZnTe detectors; figure 6 shows the measured and simulated responses.

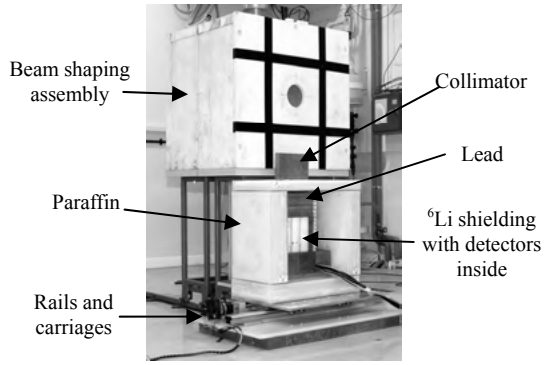

Figure 5 – Experimental setup with the shielding partially removed

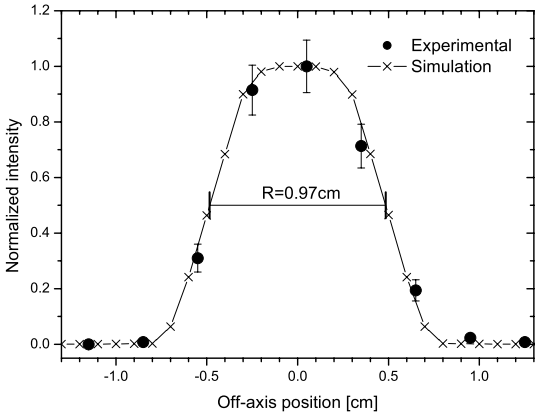

Figure 6 – Comparison of experimental spatial resolution of the collimators with simulations

A simple phantom containing a ^{241}Am point source has been used to test the reconstruction algorithm. The source was placed in a 9.22 cm radius cylindrical phantom at 4 cm from its axis.
The acquisition and reconstruction scheme was as in the designed final setup: 20 projections of 41 bins each reconstructed on a 21×21 image matrix using the expectation-maximization maximum-likelihood algorithm. The reconstructed image is shown in figure 7.

The γ background was measured with the system mounted at the BNCT accelerator facility of the Birmingham University and a spurious 478 keV peak was found. Those photons came from captures in the photomultiplier tube which is made of borosilicate. A 2mm Cd layer between the paraffin and the lead reduced this unwanted peak and also the background (fig. 8).

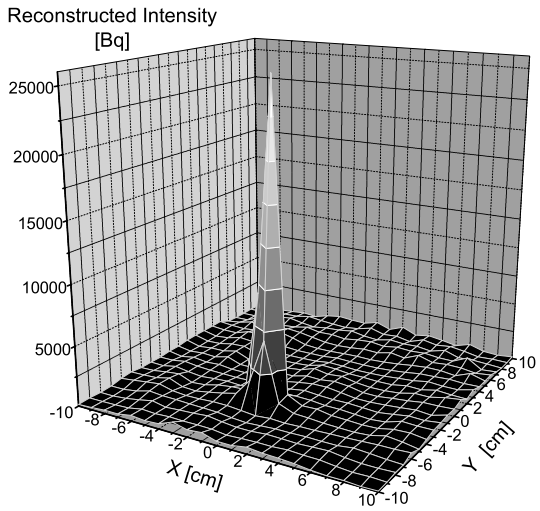

Figure 7 – Reconstructed image of a phantom with a point ^{241}Am source

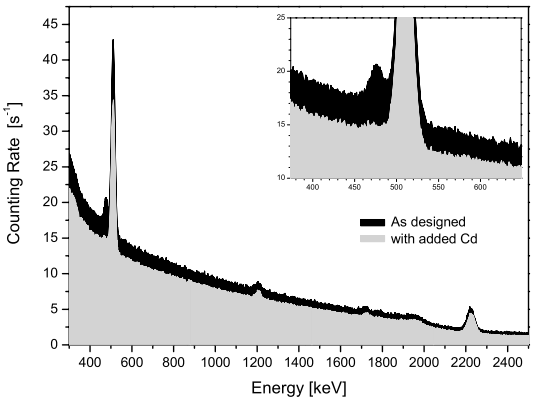

Figure 8 – A Cd layer between paraffin and lead reduced the spurious signal coming from neutron captures in the photomultiplier tube

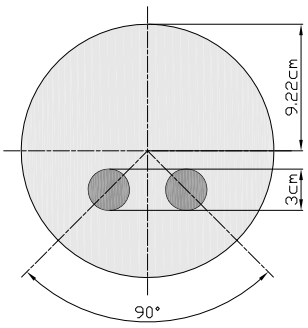

Figure 9 – Cross section of the water-filled cylindrical phantom with 2 tumors with 400ppm of ^{10}B used in the experiments

A projection of the water filled phantom containing two cylindrical tumor models (400ppm ^{10}B and 3cm in diameter each) has been measured (fig. 9).

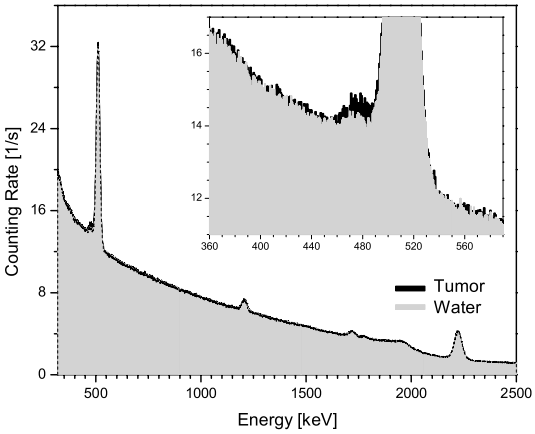

Figure 10 – Spectra measured at Birmingham's BNCT facility from a tumor and at a water region

Fig. 10 shows the difference between the tumor and a pure water region. The small 478 keV peak in the water measurement is thought to be due to the remaining captures in the photomultiplier tubes.

The projection spectra have been adjusted with a simple model: an exponential background, a Gaussian 478 keV peak and a Gaussian 511 keV annihilation peak. The measured profile across the phantom and the tumor models is shown in fig. 11.

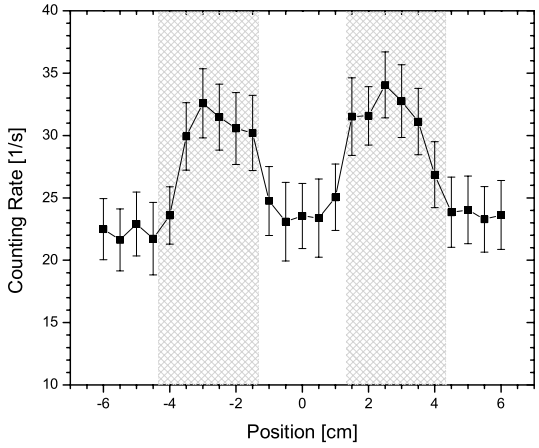

Figure 11 – Measured profile of a phantom with two tumors. The shaded areas indicate tumor positions

The resulting profile shows a baseline caused by the neutron captures in the photomultiplier. After subtracting this baseline the comparison with MCNP simulations shows a very good agreement (fig. 12).

4. Conclusions

A prototype of a SPECT system for online dose measurements in BNCT has been designed by numerical simulations. The system has been built and tested at the Birmingham University BNCT facility and a profile of a phantom has been measured. This measurement shows very good agreement with the simulations. Although the background must be further reduced, this work shows the feasibility of such a system.

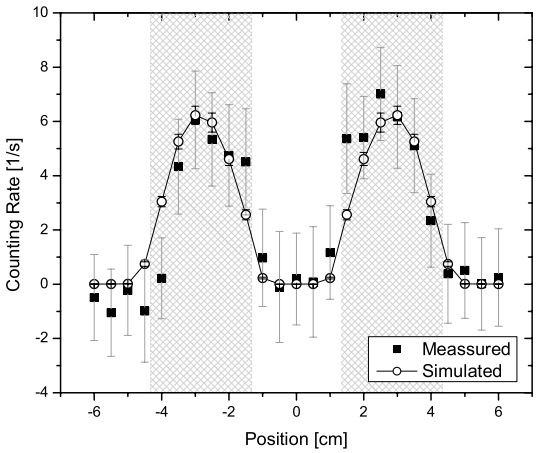

Figure 12 – After subtracting the baseline the measured projection and the MCNP simulations show good agreement. The shaded areas indicate tumor positions

References

Brown, F.B., et al., 2002. MCNP VERSION 5. Los Alamos Tech. Report LA-UR-02-3935.

Kobayashi, T., Sakurai, Y., Ishikawa, M. 2000. A noninvasive dose estimation system for clinical BNCT based on PG-SPECT - Conceptual study and fundamental experiments using HPGe and CdTe semiconductor detectors. Med Phys. 27(9), 2124–2132.

Minsky et al., 2006. Design of a SPECT tomographic image system for online dosimetry in BNCT. Advances in Neutron Capture Therapy 2006- Proceedings of the ICNCT-12, 405-408.

Munck af Rosenschöld P., et al., 2006. Prompt gamma tomography during BNCT - A feasibility study. Journal of Instrumentation 1, 1-10.

Valda, A. et al., 2005. Development of a Tomographic System for Online Dose Measurements in BNCT (Boron Neutron Capture Therapy). Br. Jour. Phys. 35(3B), 785-789.

Verbakel, W. F. A. R., Stecher-Rasmussen, F., 1997. gamma-ray telescope for on-line measurements of low boron concentrations in a head phantom for BNCT. Nucl. Instrum. Methods A 394(1-2), 163–172.

Verbakel, W. F. A. R., et al., 2003. Boron concentrations in brain during boron neutron capture therapy: in vivo measurements from the phase I trial EORTC 11961 using a gamma-ray telescope. Int. J. Radiation Oncology Biol. Phys., 55(3), 743-756.

Construction of an analytic dosimetry tool for BNCT

Josselin Morand[1,2,3], Raymond Moss[1], Wolfgang Sauerwein[2], Sabet Hachem[3]

1: European Commission Joint Research Centre PO Box 2 1755 ZG Petten, The Netherlands
2: Universitätsklinikum Essen, Hufelandstrasse 55 45122 Essen, Germany
3: Université de Nice-Sophia Antipolis 28 Avenue Valrose 06108 Nice Cedex 2, France

Abstract

The intention of this work is to provide the basis of a methodology to build a deterministic model of the $^{10}B(n,\alpha)^{7}Li$ reaction rate distribution in Boron Neutron Capture Therapy (BNCT), as a function of space variables, boron concentration and other variables, such as incidence angle. The model has to be valid in homogeneous isotropic environments and also in different kinds of heterogeneous environments, to be extended eventually to the human body, so that for a given variable set, the reaction rate is known.
The main part of the work is based on precise calculations with the MCNPX code. Calculations are made in different possible cases in order to determine how the different variables interact with each other. The first step is to build the analytic function in a simple homogeneous environment. This construction is done with statistical estimation and numerical methods such as least squares estimation. These methods are combined with the analytic solution of the radiation transport equation. The calculations are then extended in more complex heterogeneous environments in order to construct the dependence of the variables with each other.
The second point is to determine analytically the dependence of the reaction rate with the different variables and know which characteristics of the reaction rate function vary or not with the environment. The dependence is also determined using numerical methods, first in simple environments, then in more complex environments. The study of interaction and dependence leads to the construction of a valid model, as an explicit function of all the chosen variables. This model is an "eigenfunction" of the environment, gives for a given boron concentration the reaction rate that determines the dose. This model is implemented in a code written in C, named ALDEDO.

1 Introduction

The $^{10}B(n,\alpha)^{7}Li$ reaction rate is very important in BNCT. Knowing precisely the alpha reaction rate distribution leads to a better cartography and helps to improve the treatment planning. Using an analytic formula for the reactions rate can reduce the treatment planning time when compared to using Monte-Carlo methods alone. Moreover, recent work [1] can be elegantly completed with such an approach.

2 Materials and methods

As the measurements and experiments are long to be proceeded, only simulations will be used. The model of the BNCT facility described [2] is used with MCNP [3]. A voxel grid is built in the phantom. For each voxel, the position and the boron concentration is known. The objective of this study is to construct an approximate analytic function of the space variables and the concentration. Different configurations are to be used, in order to know precisely the influence of every significant variable. Figure 1 shows the phantom and the voxels.

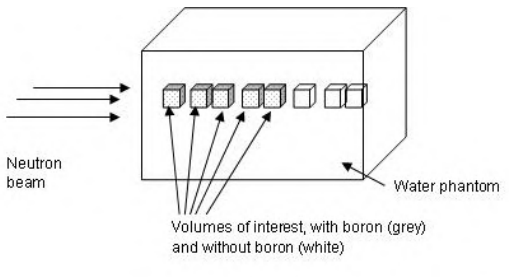

Figure 1. Presentation of the installation

3 Results in the homogeneous case

3.1 Influence of voxels shape and size

Different shapes and size for voxels are tested, in order to check if there is dependence between the reactions rate and the shape of the voxels. No significant dependence was found. In order to create a standard framework, the volumes of interest are built as spheres, with 1 cubic centimetre volume. These shapes are chosen because they are easy to handle with MCNPX. The volume is chosen because it improves the readability of the results.

3.2 Influence of boron concentration and depth

Different concentrations of boron, quoted as [B] are tested. As expected in [1], the reaction rate is a linear function of boron. Figure 2 shows the reaction rate as a function of [B]:

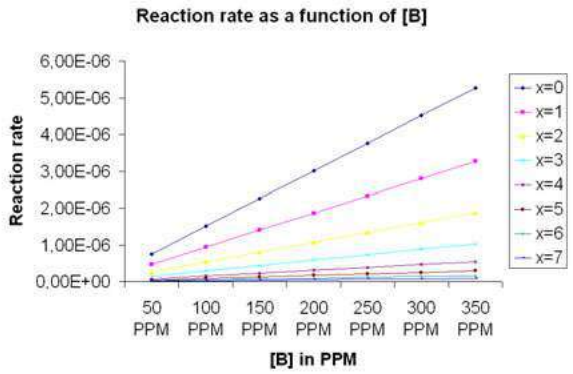

Figure 2. Reaction rate as a function of [B] for different positions

It is reasonable to write *R([B])=a*[B]*. The slope *a* can be determined with statistical methods.
The slopes of the lines change with depth. Figure 3 shows the slopes as a function of depth, for different concentrations

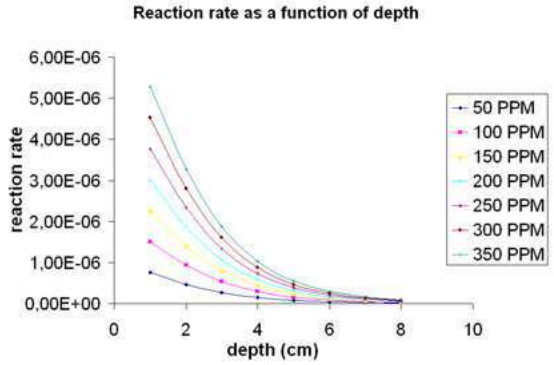

Figure 3. Reactions rate as a function of depth for different concentrations

The reaction rate is considered as a decreasing exponential function of the depth. It is reasonable to consider then $R(x)=c*e^{-b*x}$. The coefficients *b* and *c* can be determined with statistical methods, such as exponential regression.
For each depth, the slope is calculated, in order to construct the relationship between the depth and the reaction rate. Results are shown on figure 4.

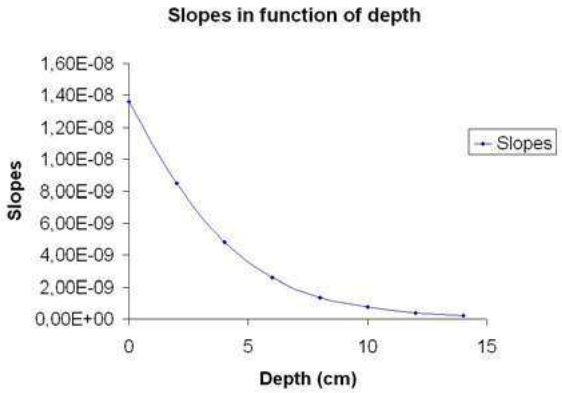

Figure 4. Slopes as a function of depth

Exponential regression indicates that the slope as a function of depth is clearly a decreasing exponential function of the depth. This statement leads to the analytical formula: $R(x,[B]) = a'*[B]*e^{-bx}$, where a' and b can be determined with statistical methods. This formula is relevant with the general radiation transport equation presented in [4].

3.3 Influence of other space variables

The same study is processed for a multidimensional case, in order to determine if the variables influence each other, and then to construct the analytic function. Figure 5 shows the voxel grid, figure 6 shows the reaction rate as a function of depth for different transversal values in the source plane.

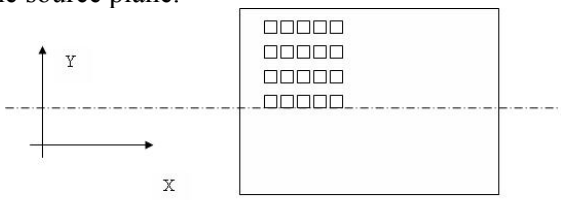

Figure 5. The grid in the source plane

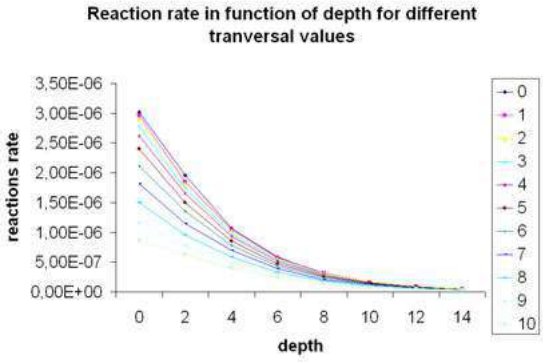

Figure 6. Reaction rate as a function of depth for different y values, at a fixed [B]=200 PPM

The shape of reaction rate does not change with the different y-values. This implies that there exist 2 functions *f* and *g*, as *R(x,y,[B])=[B]*f(x)*g(y)*. Thus, the reaction rate is a separate variable function. This structure of the reaction rate function is very important for the construction of the analytical function.
The main problem is the correct identification of the different functions. This can be done using numerical methods, such as least squares methods. It is meanwhile necessary to know the reaction rate at different positions in order to construct a precise function.
The same study has been further processed to 3 dimensions, leading to the same conclusion and the following formula:
*R(x,y,[B])=[B]*f(x)*g(y)*h(z)*.

3.4 Influence of material

Changing the material changes the order of magnitude of the reaction rate, but not the mathematical formulation. This means that using other material changes the initial conditions of the system.

3.5 Influence of geometry

The same study is processed with the axis of the phantom making an angle with the axis of the beam. The results given by the data generation are compared to the reference case and lead to the following formulation of the reaction rate function:
$R(x,y,[B])=\cos(\alpha)*[B]*f(x-x_0)*g(y-y_0)*h(z-z_0)$,
where (x_0, y_0, z_0) are the coordinates of the rotation centre.

3.6 Validity zone and the influence of collimation

The analytical function developed above is valid only over a limited zone in the phantom. It is necessary to know the dimensions of that validity zone.
Experimental values are compared to the analytical function with the following error calculation: $\varepsilon = \frac{R_{\exp} - R_{analyic}}{R_{\exp}}$. The validity threshold is fixed at 10%.
Studies show that there exists one limit zone beyond which the relative numerical error becomes a linear dimension of the space variables x, y and z. Then, the relative numerical error becomes too large for the model to be trusted.
The study is processed with three circular collimators whose diameters are 8 cm, 12 cm and 15 cm.
Results lead to the following formulation of the validity domain: a cube of dimension $a\frac{\sqrt{2}}{4}$, where *a* is the diameter of the collimator.
Inside this zone, the numerical error is considered as a random variable, following a normal law, consistent with the Kolmogorov-Smirnov goodness-of-fit test.

3.7 Example of construction: the analytic model at the HFR BNCT facility

In the Petten case, the formulation of the reaction rate is

$$R(\alpha,[B],x,y,z) = \cos(\alpha) * a_0[B]e^{-bx} * (a_1 y^2 + a_2 y + a_3) * (a_4 z^2 + a_5 z + a_6)$$

where a_i are the coefficients determined by numerical method, from the values given by the simulations and experiments.

4 Results in heterogeneous cases

The heterogeneous case is more complex, due to the changes of material. These changes induce modifications in the reaction rate. It is necessary to study those modifications.
The first step is a study of the reaction rate in a heterogeneous phantom made of water and Teflon, with the configuration shown in figure 7.

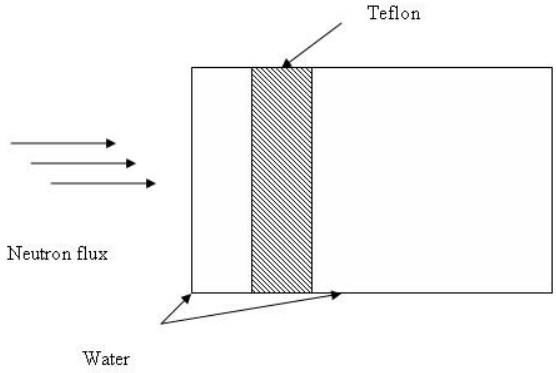

Figure 7. Sketch of the heterogeneous phantom

Heterogeneous phantoms are nominated X_Y, where X is the thickness of the first water layer and Y is the thickness of the Teflon layer.
Introducing a discontinuity in the phantom creates a discontinuity in the reaction rate function.

4.1 Comparison

The comparison between the reference phantom and the heterogeneous phantom shows that it is not possible to use the superposition principle in a heterogeneous environment. The reaction rate function at depth in the heterogeneous case **is not** the superposition of the reaction rate of the reference case. This statement is due to the neutron fluence, which behaves exactly the same.
Some elements do not vary. The shape of the reaction rate as a function of depth follows an exponential function. The exponential attenuation is calculated in the reference phantom and the heterogeneous phantom, and the results are identical in both cases.

4.2 Invariance of integration

The reaction rate is integrated in the validity zone as a function of space variables. The integrate leads to the table in figure 8:

X_Y	Integrate
3_1	3,54E-04
3_2	3,58E-04
3_3	3,59E-04
3_4	3,61E-04
3_5	3,62E-04
5_1	3,49E-04
5_2	3,53E-04
5_3	3,55E-04
5_4	3,58E-04

Figure 8. Integration of the reaction rate for different phantom size

The results are oscillating, due to the uncertainty in the results (8%), but can be considered as **constant**. This statement means that whatever the configuration of the heterogeneous multilayer phantom, the integration of the reaction rate function is constant. This statement has to be considered as a strong condition for the setting up of a robust mathematical problem.

4.3 Conception of the reactions rate in the heterogeneous case

The first step is to identify the homogeneous zones. For each zone, the reaction rate analytical function is constructed, using the least square method or more modern methods, such as genetic algorithm, in each of those zones with respect to the limit condition: the reaction rate at the border have to be the same.

5 The code ALDEDO

The method developed here is implemented in a code written in C, for UNIX and Windows systems, named ALDEDO, for **AL**pha **DE**terministic **DO**simetry. ALDEDO is designed for calculations of reaction rates in a voxels grid, using a spatial boron concentration. ALDEDO returns a voxel grid with the spatial reaction rate, in the MIRD format, presented in [5]. Further versions of ALDEDO will include more mathematical function to identify the reaction rate function, such as least squares function and genetic algorithms to construct a more precise analytical description of the reaction rate.

6 Conclusions

Elements of a new dosimetry approach are presented. This approach is based either on measurements or simulations and allows construction of an analytical reaction rate function in a delimited confidence zone. The major issues are now the mathematical construction of the function, which can be solved with very recent progress in applied mathematics, and the construction of such a function in the very complex environment of biological tissues.

7 References

- [1] A. Wittig, et al., Boron analysis and boron imaging in biological materials for Boron Neutron Capture Therapy (BNCT), Crit. Rev. Oncol./Hematol. (2008), doi:10.1016/j.critrevonc.2008.03.004
- [2] R.L. Moss , O. Aizawa, D. Beynon, R. Brugger, G. Constantine, O. Harling, H.B. Liu and P. Watkins, "The Requirements and Development of Neutron Beams for Neutron Capture Therapy of Brain Cancer", J.Neuro-Oncology, March, 1997
- [3] MCNPX user's manual, version 2.3.0, april 2002
- [4] B. Dörschel, V. Schuricht, J. Steuer, The physics of radiation protection, Nuclear Technology Publishing, England, 1996
- [5] Wesley E. Bolch et al., in collaboration with the MIRD Committee, Society of Nuclear Medicine: E.E. Watson (Chair), J.S. Robertson, MIRD Pamphlet No. 17: The Dosimetry of Nonuniform Activity Distributions — Radionuclide S Values at the Voxel Level

BNCT dosimetry performed with a mini twin TEPC

D. Moro[a,b], P. Colautti[a], J. Esposito[a], V. Conte[a], L. De Nardo[b], A. Ferretti[a], C. Ceballos[a]

[a] *LNL-INFN viale dell'Università 2, I-35020 Legnaro, Padova, Italy*
[b] *Physics Department of Padova University, via Marzolo 8, I-35131 Padova, Italy*

Abstract

The BNCT radiation field is complex because different beam components are mixed, each one having different relative biological effectiveness (RBE). Microdosimetry with tissue-equivalent proportional counters (TEPC) has proven to be an ideal dosimetric technique for mixed radiation fields, because it is able both to measure the absorbed dose and to assess the radiation field relative biological effectiveness with good accuracy. An ideal detector for BNCT should contain two TEPCs, one detector loaded with, while the other one without ^{10}B in order to record all beam components with a unique measurement. Moreover, such a detector should be of tiny size in order to be able to measure in the intense BNCT radiation fields without significant pile-up effects. TEPCs have been shown to be pretty good dosimeters for mixed radiation fields. In this paper the first mini twin-TEPC counter for BNCT is presented, as well as first measurement at the new HYTHOR thermal irradiation facility at TAPIRO nuclear reactor and comparison with related Monte Carlo calculations.

Keywords: BNCT, Microdosimetry, TEPC, HYTHOR.

1. Introduction

It is well known that BNCT dosimetry is complex because different radiation components are present, both directly and indirectly ionizing, the biological effectiveness of which is different. The actual BNCT dosimetric protocol (Binns et al., 2005) suggests the use of the well known standard t*win chamber* method (ICRU, 1977) for measuring the D_n/D_γ ratio, coupled with neutron fluence spectral measurements performed with the activation method. However, other recent radiobiological measurements performed in 7 NCT centres (Gueulette, 2006) point out that the D_n/D_γ ratio is poorly correlated with the radiation field biological effectiveness. The possibility to use tissue-equivalent gas proportional counters (TEPC) has been investigated since 1992 (Wuu, 1992). TEPCs have in fact optimal dosimetric performances in mixed radiation fields. They can be calibrated by using an internal alpha source or the so-called proton edge (Pihet, 1992). Moreover, the D_n/D_γ ratio can be measured with good accuracy without the need to know the neutron field kerma factors (Waker, 1985). Commercial TEPCs have centimetric size: too large to be used in the intense BNCT radiation fields. The counting rate a TEPC can stand without experiencing spectral distortions is of about $10^4 s^{-1}$, while in BNCT the charged-particle fluence rate in 1 cm^3 sensitive volume can easily exceed $10^6 s^{-1}$. The smallest counters successfully used in BNCT centres have sensitive volume size of 2.5 mm (Burmeister , 2003).

In this paper a novel counter made of two mini TEPCs is reported, the features of which had been successfully tested with proton beams (De Nardo, 2004, De Nardo 2004).

2. The mini twin-TEPC

In figure 1 the layout of the mini twin-TEPC constructed at the Legnaro Laboratories is shown. The sensitive volumes are the 2 cylinders of 0.9 mm of diameter and height, surrounded by the A-150 plastic cathodes (in black in the figure). One of the two cathodes is loaded with 50 ppm of ^{10}B. To get such a doping level the A-150 plastic was converted to a fine dust and 271.3 μg of natural metallic boron were added for 1 g of plastic. Everything was then mixed for 20 hours before moulding. The tissue-equivalent propane gas enters into counters following the dark grey- light grey pipe line. The anode wires are gold plated tungsten 10 μm thick. The entire insulator components are made of Rexolite® plastic. The external cup is a 0.2 mm thick titanium sleeve. The total external diameter is 2.7 mm. More details about the twin TEPC are published elsewhere (Moro, 2007). In figure 2 the twin TEPC has been inserted in a transparent plastic sleeve.

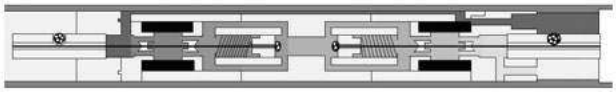

Fig. 1. Layout of the mini twin-TEPC, see text

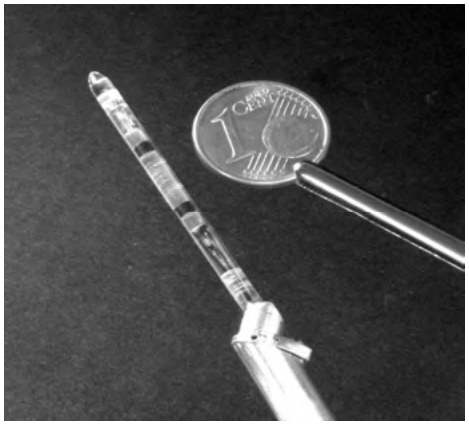

Fig. 2. Mock-up of the twin-TEPC inserted inside a transparent plastic sleeve. The two mini TEPCs are the black cylinders

3. Twin TEPC lineal energy calibration

TEPC are usually calibrated in *y* (lineal energy): the ratio of the energy imparted by an ionising event and the sensitive volume mean chord (ICRU, 1983). In figure 3 a microdosimetric spectrum collected with and without-^{10}B TEPC of the counter of figure 1 is shown. The spectrum was collected at the TAPIRO reactor in the HYTHOR irradiation cavity, which is used for BNCT radiobiology (Esposito, 2008). The spectrum shows two sharp slopes at about 12 and 150 kev/µm; they are called "electron edge" (e-edge) and the "proton edge" (p-edge). The p-edge is caused by the stopping power maximum at low proton energy. In propane TE, 100 keV protons have the maximum stopping power value that is 100 keV/µm, which means 150 keV/µm of lineal energy. For simulated site less than 1 µm the sensitive volume diameter becomes smaller than the 100 keV proton range. Therefore, the p-edge becomes constant. Differently from protons, the electron maximum stopping power is of electrons with energy close to the ionisation threshold and range of few nanometres. Therefore, the e-edge is caused by the so-called exact stoppers. They are electrons, the range of which is exactly the sensitive volume maximum chord. The e-edge value increases with the simulate site decrease. In figure 3, the dashed line shows two peaks of the second derivative. The *y*-values of the second derivative maxima correspond to the p-edge value (De Nardo, 2004) and to the e-edge value (Moro, 2003) respectively. While the p-edge values at different simulated site can be easily calculated, the e-edge values are poorly known. We have used a TEPC equipped with an internal alpha source, to determine the e-edge at different simulated site sizes. The TEPC gamma spectrum was first calibrated with alpha source, the energy spectrum of which had been previously measured, and then multiplied by the mean-energy per ion pair ratio W_e / W_α. The second derivative maximum in the 10-20 keV/µm region was then determined. Similar procedure was applied also by using the p-edge maximum for calibrating the TEPC. In this case, neutron beams of the p(4.4 MeV) +Li and p(5 MeV)+Be reactions were used. These low-energy neutron beams give rise in fact to a very sharp p-edge, because of the small yield of heavier ion events. The figure 4 shows the e-edge values measured with the two different techniques. For simulated site size bigger than 1 µm, the e-edge values measured with the two different calibration techniques do not show significant differences. At lower simulated site sizes, e-edge values after p-edge calibration are slightly smaller than e-edge values after alpha calibration. This difference is possibly due to some alpha δ-ray escape when smaller site is simulated. The thick line in figure 4 is a best fit of all the experimental data, the equation of which is:

$$e-edge = 12.18\,y^{-0.391}$$

where both the e-edge and *y* are in keV/µm.

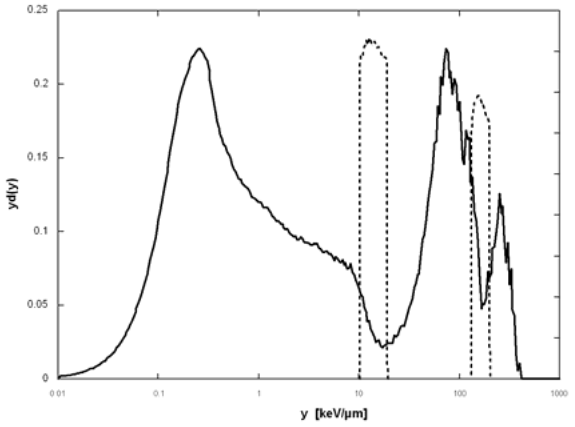

Fig.3. Thick line: 1 µm microdosimetric spectrum of the HYTHOR BNCT radiation field. Dashed line: second derivative of the spectrum. See text

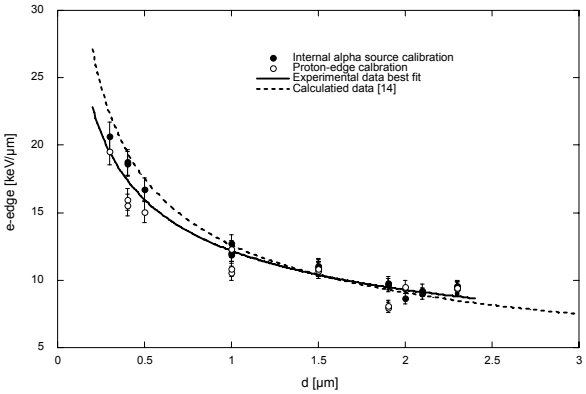

Fig. 4. Electron edge values at different simulated site sizes. See text

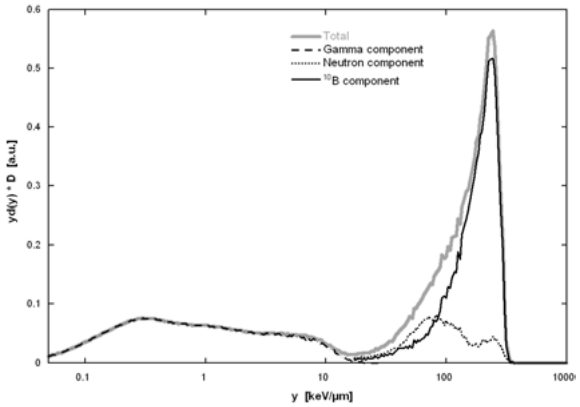

Fig. 5. HYTHOR dose-weighted microdosimetric spectrum and its components at 1µm site size

The dashed line is the best fit of e-edge calculated values based on electron extrapolated ranges (Crossman, 1994). The agreement with experimental data is pretty good.

3. Microdosimetric spectra of HYTHOR

In figure 5 first measurements taken with the twin TEPC in HYTHOR are shown. HYTHOR is a thermal column designed for small animal BNCT radiobiology (Esposito, 2008). It is inserted in the TAPIRO nuclear reactor of ENEA Casaccia research centre. The two microdosimetric spectra of twin TEPC can be processed to give the spectral components due to gamma rays, neutrons and the ^{10}B fragment. The areas under the curves of figure 5 are proportional to the main three dose components.

4. Twin TEPC Monte Carlo model

An extensive set of computational studies has been performed on the twin TEPC detector in order to calculate the absorbed dose components in HYTHOR. Starting from the former HYTHOR Monte Carlo model used for the neutronic design study (Esposito, 2007) of the irradiation facility a model of twin-TEPC detector (fig.6) has been included in the full 3D geometry. The detector position with respect to the irradiation box, the geometrical as well as material configuration, have been reproduced as closely as needed to the real one. Particle transport within the whole irradiation system was performed with the MCNPX 2.6b code (Hendricks JS, 2006). Mesh tallies were used to determine both the neutron and gamma fluxes distribution inside the irradiation cavity. A proper number of particle histories was set in order to let the relative errors for the flux and dose tallies below 0.05.

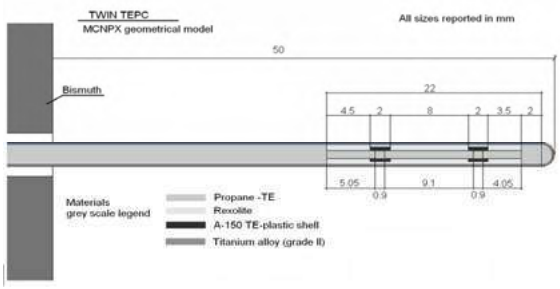

Fig. 6. Cutaway view of twin-TEPC Ti-probe part entering inside the Bi-irradiation cavity and housing the two detectors. The two mini TEPCs are the black dots. MCNPX geometry model

Moreover to get a proper transport at thermal energy ranges the S(α,β) model was used in addition to the standard free gas treatment to account for thermal neutron scattering in the TE detector materials. The twin TEPC gas ports and the front-end electronic box is located outer of irradiation chamber. Only the twin TEPC titanium sleeve enters inside the irradiation cavity.

5. Data comparison and discussion

The spectra of figure 5 have been used to calculate the gamma, D_g, the neutron, D_n, and the ^{10}B fragments, D_{bnc}, dose rates in A-150 plastic (the TEPC cathode material). D_{bnc} is calculated by subtracting the neutron component of the without-boron spectrum from the neutron component of the with-boron spectrum and multiplying the difference by the factor 2. The factor 2 takes into account that the helium and lithium ions are always emitted at 180°. Therefore, only one of them enters into the TEPC sensitive volume at any nuclear reaction. In table 1 experimental and calculated dose rate data are shown. The experimental error in table 1 is the overall uncertainty calculated by propagating all the uncertainties (the statistical ones and the systematic ones) (Moro, 2003). The calculated errors are only the statistical uncertainties. Calculated and measured neutron doses are pretty the same.

Tab. 1. Experimental and calculated absorbed dose rate components in A-150 plastic

	twin-TEPC Dose rate measurement [Gy/hr]	MCNPX Dose rate calculation [Gy/hr]
D_g	5.0 ± 0.5	3.94 ± 0.10
D_n	1.72 ±0.1	1.75 ± 0.03
D_{bnc}	20.5 ± 1	30.73 ± 0.2

The experimental gamma dose is significantly higher than the calculated one. That is possibly due to the fact that not all the counter components have been modelled. For instance, the counter gold electrical contact is a gamma source, which has not been taken into account in MC model. The experimental D_{bnc} is definitely smaller than the calculated one. This could have two reasons. Part of the ions could not be able to cross the 1 µm sensitive volume. Their *y*-values would be therefore underestimated, consequently the absorbed dose. On the other hand, helium and lithium ions could lose part of their energy inside the metallic boron grains. In such a case, the slowing-down spectrum would be shifted to lower energies and the dose delivered in the gas sensitive volume would be lower. To check the plausibility of this last hypothesis, we have used the scanning electron microscopy (SEM) to measure the grain size of the boron used to dope the A-150 plastic. After having analysed different pictures (see figure 7), the powder elementary grain size was measured to be quite small, 0.17 ±0.02 µm. However, the powder was observed to be rather sticky. It aggregated easily in blobs the size of which was of few micrometers.

6. Conclusions

A mini twin TEPC has been constructed. It has been able to measure microdosimetric spectra and all the dose components in a neutron field with thermal neutron fluence rate of 3.5 10^9 $cm^{-2}s^{-1}$. Comparison with calculated data suggests that measurements at 1 µm underestimate the D_{bnc}. If further measurements at smaller simulated sites confirmed this result, it ought to be concluded that part of the ion energy is stopped in the metallic boron powder. In such a case, the effective ^{10}B content in the cathode wall would be measured in a known thermal neutron field.

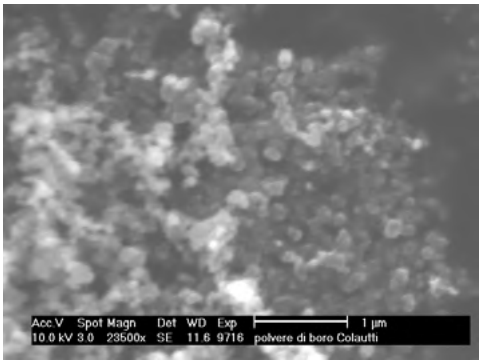

Fig. 7. SEM image of the boron powder distribution in A-150 plastic

Acknowledgements

The mini twin TEPC has been manufactured by Mr. Maurizio Geronazzo. We are in debt with Gary Johnson of the college physician and surgeons of the Columbia University of N.Y. for all the suggestions and the assistance during the counter construction.

References

Binns, P.J. et. al., 2005. An international dosimetry exchange for boron neutron capture therapy, part I: absorbed dose measurements, Med. Phys. 32, 3729-3736.

ICRU, 1977. Neutron Dosimetry for Biology and Medicine, Report 26, ICRU Publications, PO Box 30165, Washington, DC 20014, USA,

Gueulette, J. et al., 2006. Quality assurance (QA) program in BNCT: RBE of 7 NCT beams for intestinal crypt regeneration in mice. Advances in Neutron Capture Therapy 2006. Proceedings of ICNCT-12. Nakagawa, Y.; Kobayashi, T.; Fukuda, H. (Eds). International Society for Neutron Capture Therapy, 81– 84.

Wuu, C.S. et al., 1992. Microdosimetry for boron neutron capture therapy,. Rad.Res. 139, 355-359.

Pihet, P. et al, 1992. Critical assessment of calibration techniques for low pressure proportional counters used in radiation dosimetry. Rad.Prot.Dosim. 44, 115-120.

Waker, A.J. et al., 1985. Experimental uncertainties in microdosimetric measurements and an examination of the performances of three commercially produced proportional counters. NIMA, 234, 354-360.

Burmeister, J. et al.. 2003. Microdosimetric intercomparison of BNCT beams at BNL and MIT Med.Phys. 30, 1231-2139

De Nardo, L. et al., 2004. Mini-TEPCs for Radiation Therapy. Rad. Prot. Dos. 108, 345-352.

De Nardo, L. et al., 2004. Microdosimetric Assessment of Nice Therapeutic Proton Beam Biological Quality. Physica Medica XX, 71-77.

Moro, D. et al.,2007. Two miniaturized TEPCs in a single detector for BNCT microdosimetry. Rad.Prot.Dosim. 122, 396-400.

ICRU, 1983 report 36. *Microdosimetry*.

Esposito, J., et al., 2008. Feasibility of BNCT radiobiological experiments at the HYTHOR facility. NIMB 266, 2587-2593

De Nardo L et al. *BNCT Microdosimetry at the Tapiro Reactor Thermal Column*. Radiation Protection Dosimetry 110, 579-586, 2004.

Crossman, J.S.P., et al., 1994. Inherent calibration of microdosimeters for dose distributions in lineal energy. Rad.Prot.Dosim. 55, 295-298

Esposito, J. et al., 2007. The new hybrid thermal neutron facility at TAPIRO Reactor for BNCT Radiobiological Experiments. Rad. Prot. Dos., 126, 69-73.

Hendricks, J.S, et al.,2006. MCNPX, version 2.6b Los Alamos National Laboratory Report. LA-UR-06-3248.

Moro, D. et al., 2003. Statistical and overall uncertainties in BNCT microdosimetric measurements. Legnaro report. LNL-INFN (REP) 199/2003.

Implications for Clinical Treatment from the Microdosimetry of Boron Neutron Capture Therapy

T. L. Nichols[a], G. W. Kabalka[b], L. F. Miller[c], and A. Johnson[d]

[a]*Department of Physics and Astronomy, The University of Tennessee, Knoxville, Tennessee, 37901*
[b]*Department of Chemistry, The University of Tennessee, Knoxville, Tennessee, 37901*
[c]*Department of Nuclear and Radiological Engineering, The University of Tennessee, Knoxville, Tennessee, 37901*
[d]*Rush University Medical Center, Chicago, Illinois 60612*

Abstract

Boron neutron capture therapy has now been used for several malignancies. Most clinical trials have involved glioblastoma multiforme. There have been a few studies on malignant melanoma that has metastasized to the brain. The glioblastoma results have been encouraging but have not achieved the success that many expected.

The results for malignant melanoma have been very promising but with too few patients for conclusions to be drawn. Since these early trials, there have been treatments on undifferentiated thyroid carcinoma, hepatic metastases from adenocarcinoma of the colon, and head and neck malignancies.

These tumors also responded well to boron neutron capture therapy. Glioblastoma is an infiltrative tumor with distant individual tumor cells, which would imply that the therapy fails due to those distant individual cells but the recurrence is on the edges of the main tumor body.

The microdosimetry of boron neutron capture therapy can provide an explanation for this observation. Codes written to examine the microdosimetry of boron neutron capture therapy have been used to explore the effects of near neighbor cells.

The near neighbor cells can contribute a significant additional dose depending on the geometry. Different geometries have been explored and demonstrate that tumors that grow by direct extension have a greater near neighbor effect. Whereas, infiltrative tumors lose this near neighbor dose which can be a significant decrease in dose for cells that do not have optimal boron loading.

These results help to understand prior results and imply that tumors with small closely packed cells that grow by direct extension will be the most amenable to boron neutron capture therapy.

Keywords: microdosimetry, boron neutron capture

1. Introduction

Boron neutron capture therapy (BNCT) is now being applied to a number of different tumors. It was originally used to treat glioblastoma multiforme and later was used to treat malignant melanoma(Barth et al 2005). The results for glioblastomae has been mixed with most showing modest improvement. The results for malignant melanoma have showed clear benefits from BNCT. Early results from other tumors show promise as well(Kankaanranta et al 2007, Kennedy et al 2004, Kinashi et al 2007). Most clinical studies have used borono-phenylalanine (BPA) as the delivery molecule for boron-10. Glioblastoma is an aggressive tumor with modest clinical efficacy but other aggressive malignancies treated with BNCT are demonstrating better efficacy.

The macroscopic explanation for the differences in efficacy has been elucidated by using ^{18}fluoro-borono-phenylalanine (FBPA) positron emission tomography (PET) scans to construct BNCT treatment plans(Kabalka et al 2003, Nichols et al 2002, Takahashi et al 2003). The treatment plans generated with from the FBPA PET scans differ significantly from those generated by conventional treatment plans. The isodose curves generated with FBPA PET scans are more compact around the glioblastoma than are the isodose curves for conventional treatment plans. The dose delivered to the region around the tumor periphery is substantially less than conventional treatment planning would predict. The glioblastomae recur in the tumor periphery where the dose is lower. This is because glioblastoma is an infiltrative tumor so that the periphery will have a substantial load of widely separated tumor cells. The isolated tumor cells may not accumulate BPA at the same rate as the main tumor and cells in all areas could be in a G_0 phase accumulating poorly.

The same effect is seen with FBPA PET scans based treatment plans for melanoma. Melanoma grows locally by direct extension so that tumor cells tend to be close together and not as separated. The cells on the periphery are next to the tumor body and receive a higher radiation dose. FBPA PET scan generated treatment plans provide a macroscopic explanation. The presence of tumor cells in the G_0 phase within a tumor or tumor cells far from the tumor and so widely separated must receive a lethal dose. Microdosimetry is required to understand these situations.

2. Methods

Programs were written in FORTRAN to place spheriodal cells in a body centered cubic geometry and to calculate the dose for the boron (n,α) and nitrogen (n,p) reactions in three regions that have independent user determined boron concentrations. The regions are the cell nucleus, the cell cytoplasm, and the interstitium. This interstitial region models the true interstitium between cells as well as normal cells and tumor cells with boron concentrations the same as normal cells and the actual interstitium. Thus, in this model, the interstitial dose would correspond to the dose to tumor cells that accumulates BPA as normal cells. The cells can be spheres to eccentric prolate ellipsoids. The nuclei can reflect the geometry of the cell or can have an independent shape. The nuclei can be concentric or eccentric from the cell center. The nuclear center can be randomly offset from the cell center or the offset can be user defined. Cells are separated by a user defined or loop variable distance (cell edge to cell edge). The nitrogen (n,p) dose, which is homogeneous, can be turned off to better examine the effects of the boron (n,α) reaction.

The dose to the individual cell nuclei and cytoplasm are calculated and output individually. The dose for the entire microdosimetric region is calculated and can be plotted to understand the data. Stopping powers, calculated with SRIM2008 available from www.srim.org, are integrated along the ion paths to determine the energy deposition.

3. Results

Figure 1 shows a typical set of dose curves for spherical cells of radius 5 μm and spherical nuclei of radius 4 μm with concentric nuclei. The cells are arranged as a body centered cubic and increasingly separated edge to edge. The graph demonstrates a higher dose when the cells are just touching compared with an approximately 15% reduction in the nuclear dose at large separations. The change in the interstitial dose shows a similar effect of ~50% decrease in dose from the no separation to widely separated.

The effects of boron loading and separation are shown in Figure 2. The cells are once again spherical cells of radius 5 μm and nuclei of radius 4 μm. The boron concentration is 10 ppm in both cases for the interstitial region and either 100 ppm or 200 ppm for the cytoplasm and nuclei. The nuclear is high in both cases whether closely packed or widely separate. The interstitial dose demonstrates more variation with doses of ~5 Gy when cells are widely separated.

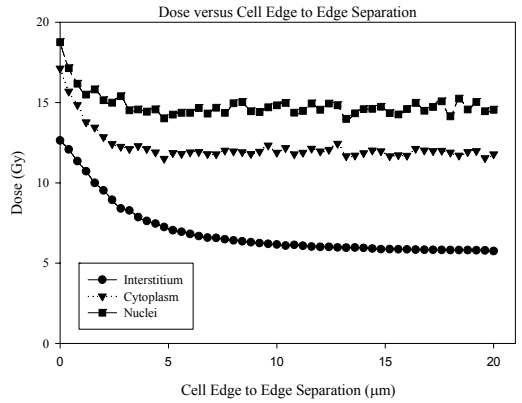

Figure 1. Dose versus cell edge to edge separation for spherical cells of radius 5 μm and nuclei of radius 4 μm for boron concentrations of 10 ppm in the interstitium, 50 ppm in the cytoplasm, and 50 ppm in the nuclei. The dose includes contributions from the boron (n,α) and nitrogen (n,p) reactions

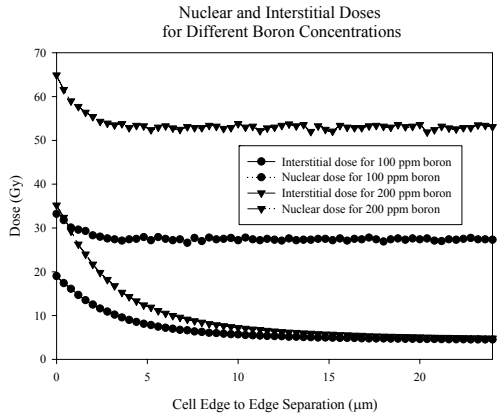

Figure 2. The dose for the three regions of interest for typical cell sizes of radius r_c = 5.0 μm with spherical concentric nuclei of radius r_n = 4.0 μm and boron concentrations that are potentially achievable with new boron carrier molecules of 200 ppm in the cells and 100 ppm in the cells with 10 ppm in both cases

4. Discussion

Figure 1 demonstrates that when cells are closely packed that the nuclei receive an additional dose from the neighboring cells resulting in an approximately 15% increase from the situation where cells are widely separated. The implication is that closely packed cells add to the damage of their neighbors. More importantly, the dose to the interstitium that models tumor cells not accumulating BPA has twice the dose when the cells are closely packed. Thus, tumors can have cells within the tumor in a resting G_0 phase and not accumulate boron but still be destroyed. Non-BPA laden tumor cells in the periphery of the tumor and widely separated will likely receive a non-lethal dose. The tumor cells on the edge of a glioblastoma will not receive a lethal radiation dose unless the boron loading of the cell is higher than possible with current boron carriers as demonstrated in Figure 2.

The clinical implications from this data are important. First, densely packed tumors that spread by direct extension are more likely to be killed by BNCT than infiltrative tumors. Infiltrative tumors will require better boron carriers (Kabalka et al 2004) that concentrate in all tumor cells in high concentrations. Clinically, tumors that tend to metastasize late, spread by direct extension, and concentrate boron as demonstrated in a pretreatment boron carrier labeled PET scan.

References

Barth RF, Coderre JA, Vicente MG, Blue TE. 2005. Boron neutron capture therapy of cancer: current status and future prospects. *Clin Cancer Res* 11: 3987-4002

Kabalka GW, Nichols TL, Smith GT, Miller LF, Khan MK, Busse PM. 2003. The use of positron emission tomography to develop boron neutron capture therapy treatment plans for metastatic malignant melanoma. *J Neurooncol* 62: 187-95

Kabalka GW, Wu ZZ, Yao ML, Natarajan N. 2004. The syntheses and in vivo biodistribution of novel boronated unnatural amino acids. *Appl Radiat Isot* 61: 1111-5

Kankaanranta L, Seppala T, Koivunoro H, Saarilahti K, Atula T, et al. 2007. Boron neutron capture therapy in the treatment of locally recurred head and neck cancer. *Int J Radiat Oncol Biol Phys* 69: 475-82

Kennedy AS, Nutting C, Coldwell D, Gaiser J, Drachenberg C. 2004. Pathologic response and microdosimetry of (90)Y microspheres in man: review of four explanted whole livers. *Int J Radiat Oncol Biol Phys* 60: 1552-63

Kinashi Y, Sakurai Y, Masunaga S, Suzuki M, Nagata K, Ono K. 2007. Evaluation of micronucleus induction in lymphocytes of patients following boron-neutron-capture-therapy: a comparison with thyroid cancer patients treated with radioiodine. *J Radiat Res (Tokyo)* 48: 197-204

Nichols TL, Kabalka GW, Miller LF, Khan MK, Smith GT. 2002. Improved treatment planning for boron neutron capture therapy for glioblastoma multiforme using fluorine-18 labeled boronophenylalanine and positron emission tomography. *Med Phys* 29: 2351-8

Takahashi Y, Imahori Y, Mineura K. 2003. Prognostic and therapeutic indicator of fluoroboronophenylalanine positron emission tomography in patients with gliomas. *Clin Cancer Res* 9: 5888-95

Monte Carlo simulations of the current obtained with ionisation chamber detectors in mixed fields of neutrons and gammas

Antoaneta Roca[a,b], Yuan-Hao Liu[c], Ray Moss[a] and Sander Nievaart[a]

[a] *Institute for Energy, Joint Research Centre; P.O. Box 2, Petten, 1755 ZG, The Netherlands*
[b] *Faculty of Physics, University of Bucharest, P.O. Box MG-1, 76900, Romania*
[c] *ESS Dept., National Tsing Hua University; Hsinchu 30013, Taiwan, R.O.C.*

Abstract

It needs no introduction that good measurements regarding BNCT dosimetry are of vital interest. Above all, calculations for patient treatment planning are initially based on these measurements. Closely related, well understood dosimetry of mixed neutron and gamma fields is necessary to explain the outcomes of the many experiments performed. It is believed that the sometimes confusing and incomprehensible outcomes in BNCT research are due to incorrect dosimetry, i.e. misleading measurements. A popular detector used to describe the absorbed neutron and gamma doses is the ionisation chamber. To understand better the behaviour and intricacies of this detector, the collected and measured current is directly simulated with MCNPX. This Monte Carlo code is able to track neutrons, gammas and electrons all around and in the ionisation chamber. The calculated dose deposited by the electrons in the gas is proportional to the current measured. Protons and alphas emanating from the wall and/or gas materials due to nuclear reactions can also cause ionisations and thus add to the current. A custom-made program has been written to simulate this contribution. The issue in this study is that a disagreement between simulated and measured current can be caused by the computer code and/or measurement set-up and/or unknown influences of source and/or materials. Therefore, the model of the ionisation chamber as well as the neutron and gamma source descriptions are validated step-by-step. After having obtained enough confidence in the model it can be concluded that ionisation chamber measurements can be significantly affected by neutron interactions (this is energy dependent). Neutrons can increase the measured current due to unknown and unconsidered beta-, proton- and/or alpha-producers in the wall material and gas; this dose component does not exist without the presence of the ionisation chamber.

Keywords: dosimetry, BNCT, ionisation chamber, Monte Carlo

1. Introduction

The efficacy of BNCT treatment depends strongly on the accuracy of characterizing the applied irradiation beam. BNCT beams contain mostly epithermal neutrons, but there are also some gammas and fast neutrons present. Within the patient/phantom, the neutron spectrum changes rapidly as the incident epithermal neutrons scatter and thermalize, and a gamma field is generated from neutron capture in hydrogen. In consequence, the resulting radiation field is complex - a mixed neutron-gamma field. Dosimetry of these types of beams is often performed with two ionisation chambers, i.e. the so-called Paired Ionisation Chamber Technique (PICT). Within this technique the neutron and gamma absorbed dose are determined separately because one of the chambers is neutron sensitive and the other one is relatively neutron insensitive. It seems a simple approach, but using PICT for the dosimetry of the mixed neutron-gamma beam is not straightforward. Despite previous investigations (Raaijmakers, 1996) on how thermal and fast neutrons influence the chambers, it is still not clear why sometimes small negative doses are observed after subtraction from the PICT results. Computer simulations might help to understand the behaviour of the ionisation chambers in radiation fields, whether or not mixed, for a correct interpretation of the dosimeter response and for the clarification of the mentioned problems.

The authors propose to investigate the PICT with the Monte Carlo code MCNPX (Pelowitz, 2005) by simulating the current obtained with ionisation chambers.

This code is chosen because it is capable of simulating neutrons, gammas and charged particle types such as protons and alphas. Additionally, MCNPX includes the energy deposition tally (F6) for electrons which is specifically used in all calculations presented in this paper. The ionisation chambers studied here and applied in Petten are the magnesium chamber flushed with argon gas (Mg-Ar), aluminum chamber flushed with argon gas (Al-Ar) and the tissue-equivalent plastic chamber flushed with tissue-equivalent gas (TE-TE).

As a preliminary but necessary investigation of the present work, the models of the Mg-Ar and TE-TE chambers were verified in a well characterized field of gamma rays coming from a cobalt-60 source (Roca, 2007). After that, the current obtained in the chambers in the mixed Petten BNCT field could be studied.

The results of the measured and simulated current are obtained with three types of ionisation chambers in a polymethylmethacrylate (PMMA) phantom.

2. Materials and methods

The TE-TE, Mg-Ar and Al-Ar ionisation chambers were irradiated in the BNCT beam having a diameter of 12 cm. The neutron spectrum can be characterized as consisting mainly of 10 keV neutrons with a 13 times less fast neutron (up to 20 MeV) and a 31 times less thermal neutron component. The primary gammas in the beam travel parallel and the spectrum can be characterized as uniform between 1 and 9 MeV. The mixed neutron and gamma source is verified regularly using multiple foils, thermoluminescent (TLDs) and Fricke gel dosimeters (Gambarini, 2007). The TE-TE and Mg-Ar chambers (manufactured by Exradin) have a sensitive volume of 0.53 cm^3, a wall thickness of 1 mm and the measurements were carried out with a Farmer Dosemeter 2670 of which the potential is set at -250 V. The Al-Ar chamber (manufactured by PTW) has a sensitive volume of 1 cm^3, a wall thickness of 0.5 mm and the measurements were carried out using a Standard Imaging electrometer MAX4000 with the potential set at +300 V. The ionisation chambers were positioned at the beam centre-line, at 2.5 cm depth in a 15 x 15 x 15 cm^3 PMMA phantom. The phantom to beam-exit distance was 30 cm (see Figure 1). Due to the presence of hydrogen in PMMA, the neutrons will moderate and thermalize. In fact, in this set-up, the chambers are irradiated in a thermal and epithermal neutron field.

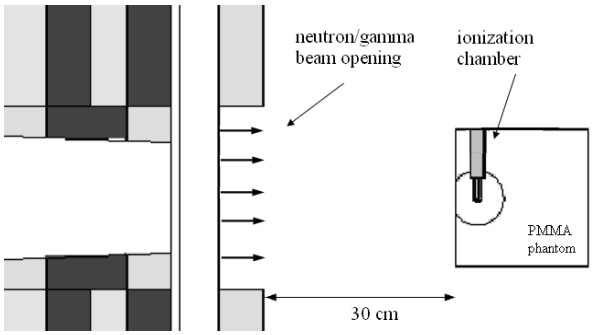

Figure 1. *MCNPX model of the experimental set-up: the ionisation chamber in the PMMA phantom in front of the beam*

The ionisation chambers were modeled according to technical drawings with designs provided by the manufacturers.

All possible neutron/gamma reactions with the ionisation chambers were individually evaluated. Each type of chamber (TE-TE, Mg-Ar and Al-Ar) had to be studied separately and all individual components contributing to the signal of each detector identified and calculated.

For all the chambers there is a common process of producing electrons by primary and neutron induced gammas, which is handled in the same manner in MCNPX: the average energy deposited by the electrons in the gas is calculated with a tally called F6:E in MCNP mnemonics. The electron tracks are only simulated in a spherical volume (diameter of 3 cm), set around the sensitive part of the ion chamber. The Integrated Tiger Series (ITS) energy indexing algorithm was used for the simulations as recommended by Schaart et al. (2002).

The result of the tally is in MeV/g which can be translated into the number of electron-ion pairs via the mass of the gas and its W value for electrons needed to create such a pair.

Finally with the beam intensity and the elementary charge the current obtained due to electrons is known. Since MCNPX cannot simulate electric fields, it is assumed that all ionisations in the sensitive gas volume are collected at the anode.

This assumption holds already for the experience with the cobalt-60 source as mentioned above. Apart from this electron component in the current, there are other charged particles that produce current in the gas, due to different interactions specific for each chamber. They are treated accordingly and added to the previous result, as described below.

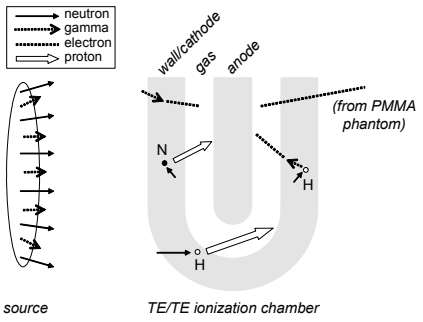

Figure 2. *Schematic overview of the set-up with origin of electron and proton contributions*

For the TE-TE chamber, irradiated with the Petten beam, the additional current is produced by the protons from $^{1}H(n,n)^{1}H$ and $^{14}N(n,p)^{14}C$ reactions (see Figure 2).

The protons released from thermal neutron reactions with nitrogen together with recoiling protons from hydrogen, induced by fast and epithermal neutrons, are a problem for MCNPX as protons cannot be tracked below 1 MeV. A custom written program called PPICC (Proton Produced Ionisation Chamber Charge) is developed that calculates, separately from MCNPX, the deposited energy and thus the current produced by the protons in the TE gas. For this it uses the stopping powers for protons in TE plastic and gas. The proton from the nitrogen reaction is released isotropically with an energy of 585 keV. In case of recoiling protons, more information is needed about the energy and direction of the incoming elastically scattering neutron. Finally the current produced by the protons in the chamber is derived. The appropriate W value related to protons is taken from Waibel and Willems.

For the Mg-Ar and Al-Ar chambers, apart from the electrons originating from primary and neutron induced gammas, there is a supplementary current due to the charge produced by the neutrons that activate the material of the chamber itself (prompt gammas from neutron capture and gammas from the decay of unstable isotopes from neutron capture) (see Figure 3).

The prompt and delayed gamma components were calculated separately. MCNPX can calculate directly the prompt gammas but not the delayed gammas. This second contribution was calculated from MCNPX-derived reaction rates of ^{27}Mg, ^{56}Mn and ^{28}Al.

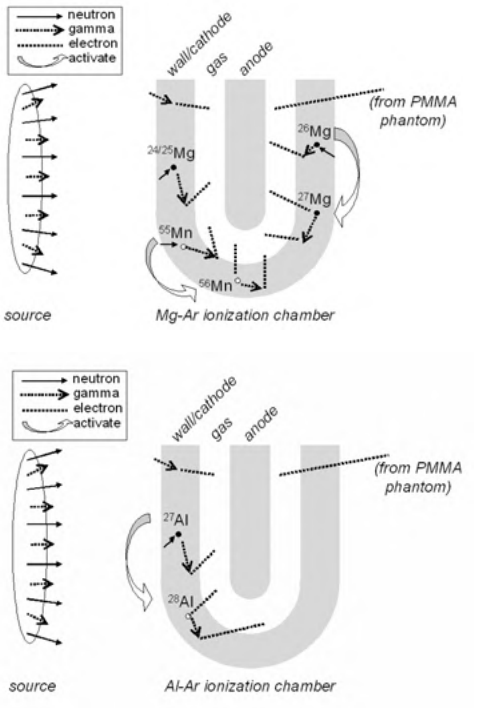

Figure 3. *Schematic overview of the Al-Ar and Mg-Ar ionisation chambers set-up with all chamber interactions*

With the corresponding beta and (delayed) gamma spectra (ICRU, 1989) the energy deposited in the gas, and then the current produced in the chamber, can be calculated.

3. Results

The simulated current produced by the electrons originating from primary gammas ($I_{primary\_gamma}$) and induced gammas ($I_{n\_induced\_gamma}$) for all three chambers are presented in the first two rows of Table 1. The total simulated current produced in the TE-TE chamber by protons from the $^{14}N(n,p)^{14}C$ reaction and from the $^{1}H(n,n)^{1}H$ reaction is presented in the Table 1 as $I_{nitrogen\_proton}$ and I_{recoil_proton} respectively. The simulated current produced in the Mg-Ar and Al-Ar chambers by the neutrons causing activation of the chamber material itself (I_{n_decay}) is also listed. Finally, the experimental results at 2.5 cm depth in the PMMA cubic phantom are presented in the same table.

Table 1. *Experimental and simulated current components obtained in TE-TE, Mg-AR and Al-Ar ionisation chambers*

PMMA phantom 2.5 cm depth	Current (pC/s)		
	TE-TE	**Mg-Ar**	**Al-Ar**
Sim. $I_{primary\_gamma}$	4.58	6.23	12.13
Sim. $I_{n\_induced\_gamma}$	10.55	13.67	25.49
Sim. $I_{nitrogen\_proton}$	5.03		
Sim. I_{recoil_proton}	2.60		
Sim. $I_{n\_induced\_gamma*}$		0.01	0.40
Sim. I_{n_decay}		0.17	15.40
Sim. I_{total}	22.76	20.08	53.42
Experiment I_{total}	22.03	25.10	65.80

***** only from the ionisation chamber

The presented results of the MCNPX calculations have a statistical uncertainty less than 2% in the 95% confidence interval. As all experiments are only repeated five times per experiment, the measure for the uncertainty is chosen to be provided by the ratio of the maximum value to the minimum value, which is a maximum of 1.004 for all the three chambers. Following further the recommendations from the ICRU Report 45 (ICRU, 1989) the statistical uncertainty in the experiments can be regarded to be less than 1%.

4. Conclusions

The good agreement between the simulated and experimental current obtained with the TE-TE ionisation chamber in thermal/epithermal neutron fields mixed with gammas, proves that the MCNPX model supplemented with PPICC is correct. This has been proved also by free-in-air results, which are not presented in this paper. The detailed simulation of Mg-Ar and Al-Ar chambers in the mixed field provides every component of the total measured current. The difference between the total measured current and the total calculated current for the Mg-Ar is 5.02 pC/s and for the Al-Ar chambers is 12.38 pC/s. Unfortunately, at the moment we are unable to explain these discrepancies, although we have investigated many possible reasons which might be the cause: the simulation code, the measurement set-up or unknown 'impurities' in the materials producing additional current.

The authors concluded that most probably there is an unknown element in both metals which is contributing significantly to the current and therefore needs further study.

In the near term, we plan to simulate the PICT and investigate in detail all aspects related to the neutron and gamma dose components. Finally, the overall outcome can be used to improve BNCT beam dosimetry.

References

Gambarini, G., Daquino, G.G., Moss, R.L., Carrara, M., Nievaart, V.A. and Vanossi, E., 2007. Gel dosimetry in the BNCT facility for extra-corporeal treatment of liver cancer at the HFR Petten. Rad. Prot. Dosimetry 126, 1-4.

International Commission on Radiation Units and Measurements, 1989. Clinical Neutron Dosimetry Part I. Report 45. Bethesda. MD.

Pelowitz, D.B., ed. 2005. MCNPX User's Manual. Version 2.5.0. LA-CP-05-0369.

Raaijmakers, C.P.J., Watkins, P.R.D., Nottelman, E.L., Verhagen, H.W., Jansen, J.T.M., Zoetelief, J. and Mijnheer, B.J., 1996. The neutron sensitivity of dosimeters applied to boron neutron capture therapy. Med. Phys. 23**,** 1581-1589.

Roca, A., Nievaart, V.A., Moss, R.L., Stecher-Rasmussen, F. and Zamfir, N.V., 2007. Validating a MCNPX model of MG(AR) and TE(TE) ionisation chambers exposed to ^{60}Co gamma rays. Rad. Prot. Dosimetry, Published online on Dec 16.

Schaart, D.R., Jansen, J.M., Zoetelief, J. and De Leege, P.F.A., 2002. A comparison of MCNP4C electron transport with ITS 3.0 and experiment at incident energies between 100 keV and 20 MeV. Phys. Med. Biol. 47, 1459–1484.

Waibel, E., Willems, G., 1992. W values for low-energy protons in methane-based tissue-equivalent gas and its constituents. Phys. Med. Biol. 37, 249–259.

Testing of a gel equivalent to liver to perform neutron characterizations

E. Pozzi[a], M. Gadan[b], S. Thorp[b], S. Bortolussi[c], M. Miller[b]

[a] *RA-3 Nuclear Reactor, National Atomic Energy Commission, Argentina*
[b] *Instrumentation and Control Department, National Atomic Energy Commission, Argentina*
[c] *Department of Nuclear and Theoretical Physics, University of Pavia, Italy*

Abstract

Several characterizations are needed in the frame of the project of irradiation of sections II-III of the human liver left lobe. For trials including neutron irradiation, samples remain with a certain level of activity that avoids their promptly disposal. To not use biological materials, that degrades and add the requirement of proper conservation up to their safe disposal, gel phantoms with non-residual activation were developed and their behavior under neutron irradiation was studied and compared to the one already obtained in previous studies using a pig liver.

Considering that response to neutrons depends mainly on the hydrogen content of the human tissue, materials chosen to construct phantoms equivalent to sections II-III of the liver left lobe were demineralized water and 2% agarose ($C_{12}H_{14}O_2(OH)_4$). The solution, still in its liquid phase, was poured into specially designed polyethylene bags in order to reproduce the portion of liver to be treated. To cover the variability range of sizes and weights in humans, three phantoms were prepared: 180, 240 and 300 g.

Implantable rhodium based self-powered detectors were used to obtain neutron flux profiles in the developed phantoms, both external and internal. Implantation of SPND was done along the central longitudinal axis of the samples, where lowest flux is expected. Irradiations were carried out under the same conditions that are previewed for the liver, i.e. inside the same acrylic container and covered with demineralized water to simulate preservation solution.

Phantoms construction was quite simple and its durability very good. Handling in order to insert instrumentation was easy.

Obtained internal neutron profile resulted very similar to the obtained for the pig liver, which showed that it is possible to use the phantoms to perform neutron characterizations.

Keywords: tissue equivalent phantom, BNCT, ex-situ treatment

1. Introduction

The Argentine BNCT project is developing the tools to treat liver metastasis with ex-situ irradiation. Unlike the treatments performed in Italy, where the whole liver was irradiated (Pinelli et al., 2002), the local idea considers just the irradiation of the segments II-III of the liver left lobe (Cardoso, et al., 2007). In order to characterize neutron flux distribution in samples equivalent to these segments, neutron flux measurements were done using the right lobe of a pig liver in the irradiation facility that will be used for the future treatments. The selected pig lobe is very similar in shape, weight, density and elemental composition to the human liver portion to be treated (Crawley et al, 2007). But, this kind of biological tissues degrades very fast, with the impossibility of reproducing measurements, and additionally, remains with a certain level of activity after irradiation that adds the requirement of proper conservation up to its safe disposal. Based on the use of tissue equivalent gels to perform dosimetry in BNCT treatments, (Gambarini et al., 1997, 2006), it was considered very convenient to develop and construct gel phantoms to evaluate neutron flux distribution solving the problems derived from working with biological tissues. The main hypothesis considered to develop these phantoms was that the thermal neutron transport is mainly dominated by the interactions between neutrons and the hydrogen contained in the biological tissues. As water content in tissue is about 80%, a gel phantom constructed just with water and agarose (C, O, H) could be enough to evaluate neutron flux distribution.

With these elemental materials, phantoms would be free of activity after irradiation.

This work describes the constructive method of this kind of phantoms, presents the comparison that shows that these phantoms have a similar neutron behavior than the obtained using a pig liver lobe and finally, shows thermal neutron profiles obtained in phantoms with different weights and dimensions in order to cover the range of variability of the segments II-III of the human liver left lobe.

2. Materials and methods

Material chosen for phantom construction was a solution of demineralized water and 2% in weight of agarose ($C_{12}H_{14}O_2(OH)_4$). This solution, still in its liquid phase, was poured inside polyethylene bags, previously partially thermo-sealed trying to reproduce the shape of the portion of liver that is expected to be treated. Three different phantoms of 180g, 240g and 300g were prepared, in order to cover variation of weight and dimensions of the segments II-III of the human liver left lobe. As the weight of the previously irradiated pig liver lobe was 310g (Crawley et al, 2007), the 300g phantom was used to compare neutron profiles and determine their equivalence.

To obtain neutron profile in phantoms, each one was introduced inside two polyethylene bags, where 100 cm^3 of demineralized water was added. In this way the effect of both autograft bags and preservation solution on neutron transport was simulated. The complete array was then placed inside an acrylic container, especially designed to avoid undesired displacement of the sample and to keep temperature during irradiation between the limits established by hypothermal preservation (Crawley et al., 2007). As the procedure followed with the pig liver, the widest part of the phantom was put forward in the box (nearest to the reactor core), as can be seen in Figure 1.

Implantable calibrated SPND were used to obtain internal and external neutron flux profiles (Crawley et al, 2007). Both detectors were aligned with the longitudinal axis of the sample one inside the gel and the other between the external bag and the container, as can be seen in *Figure 2*. This array was introduced in the irradiation facility of the RA-3 reactor (Miller et al., 2008). Electrometers Keithley models 6514 and 6517A were used to measure currents delivered by the detectors. Measuring sequence started with sensitive zone of both detectors as close as possible to the front of the container, at around 1 cm from the surface of the sample.

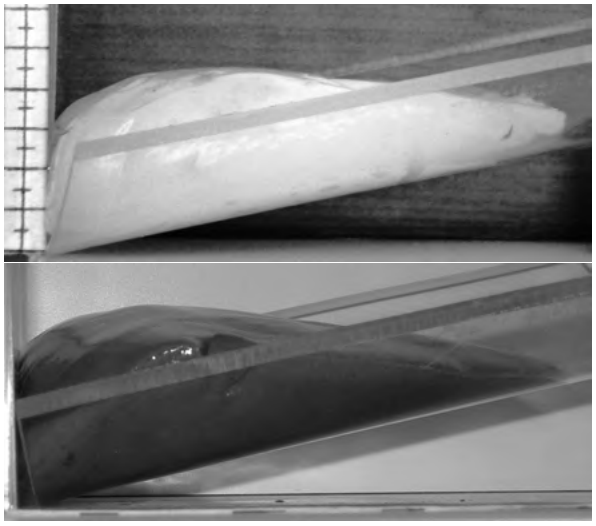

Figure 1. *Gel phantom (300g) and liver (310g) positioned as to be irradiated*

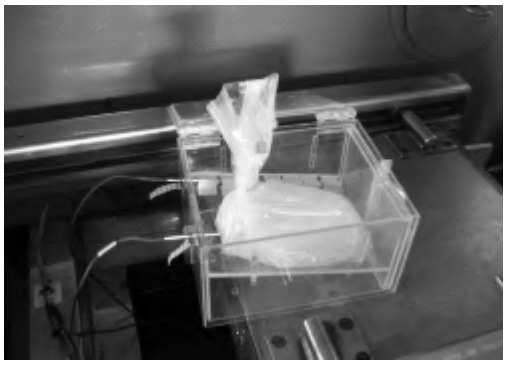

Figure 2. *Sample with detectors before irradiation*

All the system was introduced in the thermal column and irradiated as long as necessary to reach the saturation zone of the signal. After that, the system was withdrawn from the column, detectors repositioned in the next location of interest, and new irradiation was carried out. The process was repeated up to complete the full length of the samples.

Profiles obtained using the three phantoms were compared to evaluate the influence of size in neutron distribution.

3. Results and discussion

I- Phantom construction and performance

The developed phantoms resulted of easy construction. Once poured into the mould, the solution remains in its liquid phase for approximately one hour which represents time enough to give extra adjustments to the final shape.

The 2% agarose solution resulted adequate to

obtain solid phantoms that were able to keep their shape for a considerable time without loosing significant water content, problems that presented phantoms constructed previously with lower agarose content (0.5 and 1%).

Concerning neutron characterization, it was very simple to insert instrumentation in the phantoms and their use as replacement of liver resulted convenient, especially for long term experiments, mainly because of the lack of decomposition.

II-Comparison liver-gel

Figure 3 shows internal neutron profiles obtained for the 300g gel and for the 310g pig liver lobe previously irradiated (Crawley et al, 2007). Flux values were normalized to compensate for the difference of thermal flux in air (external profiles) registered during characterizations. *Figure 4* presents for comparison, values relative to maximum measured flux for both phantom and pig liver.

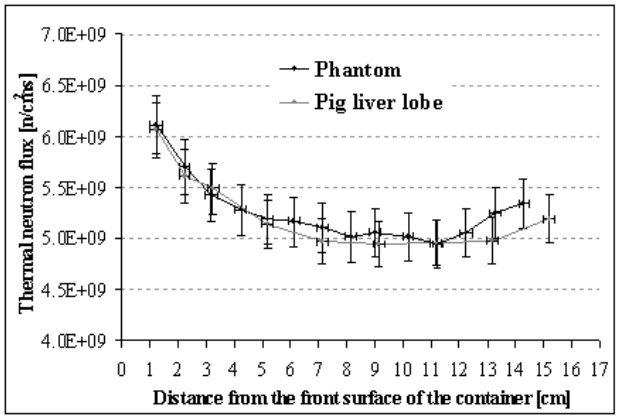

Figure 3. *Internal neutron flux profile obtained for the 300g phantom and the pig liver lobe*

Minimum flux value in the two cases, was $(5.0\pm0.2).10^9$ n/cm^2.s registered at a distance of approximately 11 cm from the front face of the container.

Comparing curves point by point, it can be seen that a very good agreement between profiles was obtained, with differences not greater than 5% between flux in gel and flux in pig liver, for the same distance to the front face of the container, what was the goal of the present work. It is also possible to see that for both samples, maximum variation for flux inside the sample, defined as [(1-minimum flux/maximum flux)x100], was approximately 20%.

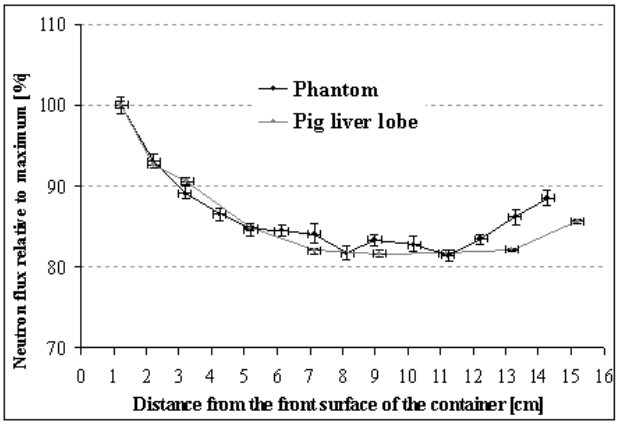

Figure 4. *Neutron profiles normalized to the maximum measured value for the 300g phantom and the pig liver lobe*

III-Neutron profiles in phantoms

Figure 5 to Figure 7 present neutron flux profiles obtained for each phantom, following the same procedure based on implantable SPND. For all the weights tested, internal and external fluxes as a function of position are shown.

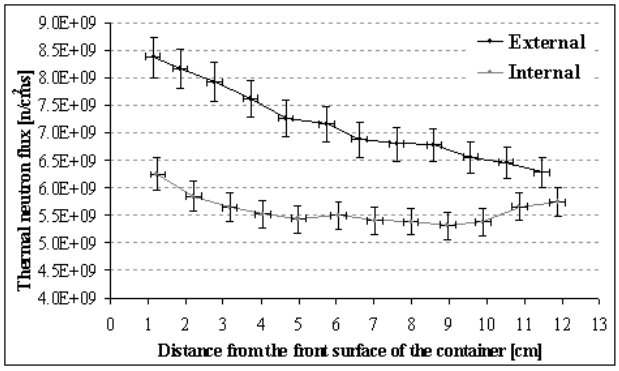

Figure 5. *Neutron flux profile inside and outside the 180g gel phantom*

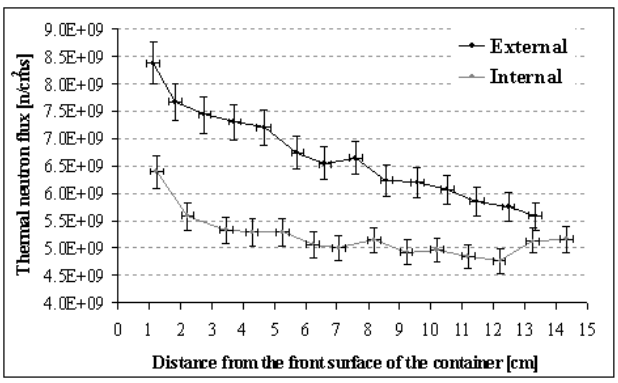

Figure 6. *Neutron flux profile inside and outside the 240g gel phantom*

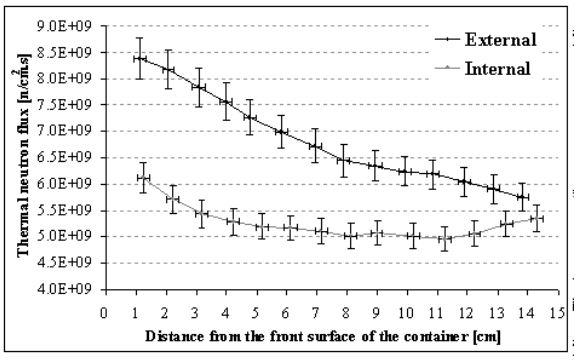

Figure 7. *Neutron flux profile inside and outside the 300g gel phantom*

It is possible to see that, for the three phantoms, external neutron flux decreases monotonically as long as the distance from the front face of the container (side nearest to the core) increases. On the other hand, the relative internal profile resulted quite uniform. This can be explained considering that there is a kind of compensation effect between the flux gradient in the container (as the external profile shows) and the narrowing of the sample.

In order to compare results in the phantoms, the following parameters were considered and summarized in *Table 1*:

i- maximum flux measured in the sample (Φ_{max})
ii- minimum flux measured in the sample (Φ_{min})
iii- distance where Φ_{max} was obtained (d_{max})
iv- distance where Φ_{min} was obtained (d_{min})
v- % flux ratio between extremes (FR_{ex})
vi- % maximum flux variation = $1-\Phi_{min}/\Phi_{max}$ (MFV)

Table 1. *Comparative values*

	180g	**240g**	**300g**
Φ_{max} [nv]	$(6.3\pm0.3).10^9$	$(6.4\pm0.3).10^9$	$(6.1\pm0.3).10^9$
Φ_{min} [nv]	$(5.3\pm0.2).10^9$	$(4.8\pm0.2).10^9$	$(5.0\pm0.2).10^9$
d_{max}	~1 cm	~1 cm	~1 cm
d_{min}	~9 cm	~12 cm	~11 cm
FR_{ex}	8%	20%	20%
MFV	15%	25%	19%

For the three phantoms, data also show very similar values for the internal fluxes in the first position, with a maximum difference of 5% while maximum difference for minimum fluxes resulted near 10%.

4. Conclusions

The very good agreement between the 300g phantom and pig liver neutron profiles, the very low level of activity post irradiation and the property to keep their shapes for long time let us affirm that the constructed gel phantoms can be adopted as very convenient replacements of biological samples in this kind of neutronic studies.

Additionally, it could be seen a high neutron flux uniformity inside the simulated organs and not significant differences for the range of variability in dimensions expected.

Acknowledgements

The authors wish to thank the invaluable help of the RA-3 Operation and Radioprotection staff.

References

Pinelli, T., Zonta, A., Altieri, S., Barni, S., Braguieri, A., Pedroni, P., Bruschi, P., Chiari, P., Ferrari, C., Fossati, F., Nano, R., Ngnitejeu Tata, S., Prati, U., Ricevuti, G., Roveda L. and Zonta, C., 2002. "Taormina: From the First Idea to the Application to the Human Liver", Research and Development in Neutron Capture Therapy. Proceedings of the 10th ICNCT. 1065-1072

Cardoso, J., Trivillin, V., Heber, E., Nigg, D., Calzetta, O., Blaumann, H., Longhino, J., Itoiz, M., Bumaschny, E., Pozzi, E., Schwint, A., 2007. "Effect of Boron Neutron Capture Therapy (BNCT) on Normal Liver Regeneration: Towards a Novel Therapy for Liver Metastases", Intern. Journal of Radiation Biology Oct; 83(10): 699-706

Crawley, V., Gadan, M. A., 2007. "Caracterización preliminar de la facilidad de irradiación de muestras biológicas del reactor RA-3 para la implementación del tratamiento de metástasis en hígado con BNCT", Facultad de Ingeniería y Ciencias Exactas y Naturales, Universidad Favaloro.

Gambarini G, Monti D., Fumagalli L., Birattari C. and Salvatori, 1997. "Phantom Dosimeters Examined by NMR Analysis: a Promising Technique for 3-D Determination of Absorbed Dose". Appl Radiat and Isotopes 48, 1477-1484.

Gambarini, G., Agosteo S., Altieri S., Bortolussi S., Carrara M., Gay S., Mariani M., Petrovich C., Rosi G and Vanossi E., 2006. "Dose Imaging with Gel Dosimeters in Phantoms Exposed in Reactor Thermal Columns Designed for BNCT". Proceedings of the 12th ICNCT, 417-420.

Miller, M., Quintana, J., Ojeda, J., Langan, S. Thorp, S. Pozzi, E. Sztejnberg, M., Estryk, G., Nosal, R., Saire, E., Agrazar, H., Graiño, F., 2008. "New irradiation facility for biomedical applications at the RA-3 reactor thermal column". Proceedings of the 13th ICNCT.

An Estimation of Activation for Target Volume due to BNCT at Kyoto University Reactor

Y. Sakurai, H. Tanaka, M. Suzuki, Y. Kinashi, S. Masunaga, A. Maruhashi and K. Ono

Kyoto University Research Reactor Institute, 2-1010, Asashironishi, Kumatori-cho, Sennan-gun, Osaka 590-0494, Japan

Abstract

Quantitative simulations were performed for the activation near the target volume in boron neutron capture therapy. The epi-thermal neutron irradiation at the Heavy Water Neutron Irradiation Facility of Kyoto University Reactor was assumed. The radioactivity distribution for each nucleus in the various human tissues was calculated from the neutron flux distribution with the reaction cross-section and the decay constant. For brain tumor, the radioactivities for soft tissues such as brain, etc. just after the irradiation, arranged in descending order were Cl-38, Na-24, K-42 and P-32. For bone, the radioactivities arranged in descending order were Cl-49, Na-24, Cl-38 and K-42. The total radioactivity due to this irradiation was estimated to approximately 1.2 MBq. It was found that the dose due to these nuclei is sufficiently smaller than the limitations of the discharge criteria for nuclear medicine diagnosis and brachytherapy in Japan.

Keywords: Activation near target volume, radioactivity distribution, external exposure to public, discharge criteria in Japan, quantitative simulation

1. Introduction

Not only the (n,α) reaction of B-10, but also various activation reactions occur in boron neutron capture therapy (BNCT). The dose due to the activation near the target volume is of negligible level compared with the dose received during a BNCT clinical irradiation. But, the estimation of the dose due to the activation is important from the viewpoints of the exposures for the patient and public. Quantitative simulations were performed for the activation near the target volume in BNCT.

2. Methods

The epi-thermal neutron irradiation at the Heavy Water Neutron Irradiation Facility (HWNIF) of Kyoto University Reactor (KUR) was assumed (Sakurai and Kobayashi, 2002). The neutron flux distribution near a target volume was obtained using a dose estimation code system "SERA" (Wessol et al., 1999). The radioactivity distribution for each nucleus in the various human tissues (Synder et al., 1975) was calculated from the neutron flux distribution with the reaction cross-section in the JENDL-3.3 nuclear data library (Shibata et al., 2002) and the decay constant.

The elements important for the activation are sodium (Na), chlorine (Cl), phosphorus (P), etc., as described below. These are included in the various human tissues at the mass ratio of zero point a few percent. The activation of blood is not considered in this estimation, because the simulation of the blood circulation is complicated and difficult. The mass ratios of Na and Cl in blood are almost two times larger than those in soft tissues, and almost the same as those in brain tissue. Assuming that blood is distributed uniformly in the whole body, the mass ratio of blood is a little less than ten percent in each part.

3. Results

The result for brain tumor irradiated in the parietal lobe for one hour is described as an example. The irradiation field size is 12 cm in diameter. Figure 1 shows the contour map for Cl-38 activity density on the axial slice at the 3-cm depth just after the irradiation. The unit for each contour is Bq/cm^3. The Cl-38 distribution is relatively similar to the thermal neutron distribution.

Figure 2 shows the contour map for Na-24 activity density. In contrast with Cl-38, the value becomes larger in bone. This is caused by the following facts: The density of Cl-37, which is the origin of Cl-38, is almost the same level in bone and brain.

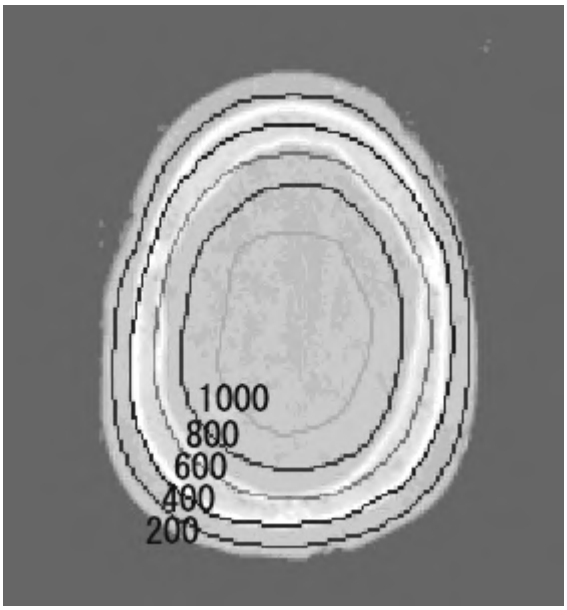

Figure 1 *Contour map for Cl-38 activity density (Bq/cm^3) just after a one-hour irradiation to brain tumor*

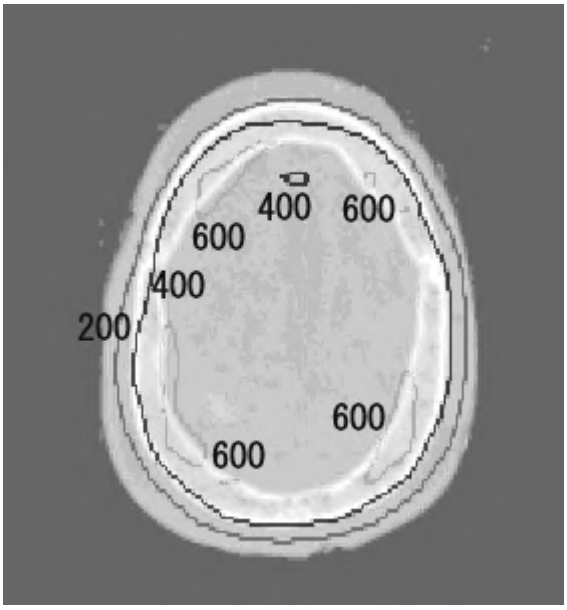

Figure 2 *Contour map for Na-24 activity density (Bq/cm^3) just after a one-hour irradiation to brain tumor*

However, the density of Na-23, which is the origin of Na-24, is 2.7 times larger in bone than in brain.

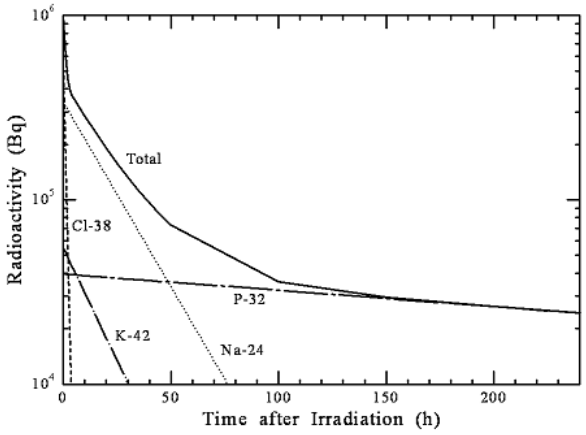

Figure 3 *Time dependence for radioactivities after a one-hour irradiation to brain tumor*

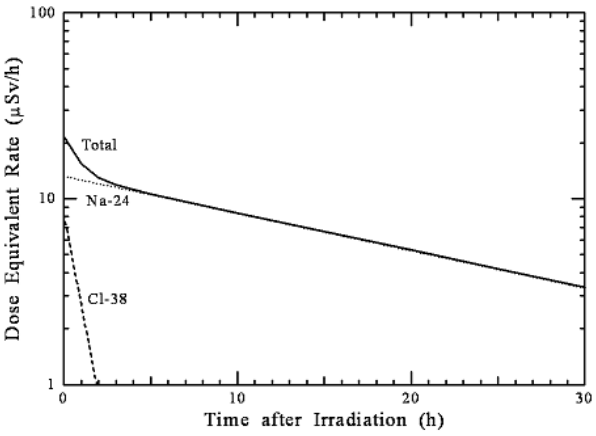

Figure 4 *Time dependence for the dose equivalent rates after a one-hour irradiation to brain tumor*

The radioactivities for soft tissues such as brain, etc. just after the irradiation, arranged in descending order were Cl-38, Na-24, K-42 and P-32. For bone, the radioactivities arranged in descending order were Cl-49, Na-24, Cl-38 and K-42. The total radioactivity due to this irradiation was estimated to approximately 1.2 MBq.

Figure 3 shows the time dependence for the generated radioactivity just after the irradiation. Here, not the biological decrease but only the physical decrease is taken into account.

The Cl-38 activity rapidly decreases just after the irradiation and the Na-24 activity is the main component within a few days. As more time elapses, P-32 activity becomes dominant.

The dose equivalent rate at 10-cm-distant from the head-top was estimated to be almost 20 μSv/h just after the irradiation. Figure 4 shows the time dependence for the dose equivalent rates. Incidentally, the contributions of beta-ray emitting nuclei such as P-32, etc. are not considered. The external exposure to the public other than the patient is mainly due to Cl-38 and Na-24.

4. Discussion

The limitations of the discharge criteria for nuclear medicine diagnosis and brachytherapy in Japan are based on the following factors. The dose exposure for the persons other than the patient is limited to 1 mSv for public, 5 mSv for comforter and carer, and 1mSv for child, per one year. For the case when the patient receives more than one diagnosis or therapy in one year, the overall exposure to the public should be estimated.

From the data in Fig. 4, the total dose exposure for an infinite time after the irradiation is estimated to approximately 0.3 mSv, even at 10-cm-distant from the head-top. It can be concluded that the effective dose exposure for persons other than the patient is sufficiently lower than the limitations described above for the discharge criteria, because the comforter or carer actually remains at a position distant from the target volume.

5. Conclusion

Gamma-ray emitting nuclei such as Cl-38 and Na-24 are important from the viewpoint of the external exposure to the public. The dose due to these nuclei is sufficiently smaller than the limitations of the discharge criteria for nuclear medicine diagnosis and brachytherapy in Japan. However, it is thought that the residual radioactivities should be recognized for a few hours for Cl-38 and for a few days for Na-24.

P-32 is particularly important from the viewpoint of the patient internal-exposure. It may remain in the patient body for a few months. The internal-dose estimation is being studied considering the biological and physiological behaviors. In addition, it is planned to insert blood circulation and metabolism of the radioactive materials into the activation and dose estimations.

References

Sakurai, Y., Kobayashi, T., 2002. The medical-irradiation characteristics for neutron capture therapy at the Heavy Water Neutron Irradiation Facility of Kyoto University Research Reactor. Med. Phys. 29, 2328–2337.

Shibata, K., Kawano, T., Nakagawa, T., Iwamoto, O., Katakura, J., Fukahori, T., Chiba, S., Hasegawa, A., Murata, T., Matsunobu, H., Ohsawa, T., Nakajima, Y., Yoshida, T., Zukeran, A., Kawai, M., Baba, M., Ishikawa, M., Asami, T., Watanabe, T., Watanabe, Y., Igashira, M., Yamamuro, N., Kitazawa, H., Yamano, N., Takano, H., 2002. Japanese evaluated nuclear data library version 3 revision-3: JENDL-3.3. J. Nucl. Sci. Technol. 39, 1125-1136.

Synder, W.S., Cook, M.J., Nasset, E.S., Kahrhausen, L.R., Howells, G.P., Tipon, L.H., 1975. Report of the task group on reference man. Pergamon Press , Oxford.

Wessol, D., Cohen, M., Harkin, G., Rossmeier, M., Wemple, C., Wheeler, F., 1999. SERA workshop lab manual. INEEL/EXT-99-00766.

A Feasibility Study of Dose Estimation with SPECT Technique after BNCT Irradiation

Y. Sakurai, H. Tanaka, M. Suzuki, Y. Kinashi, S. Masunaga, A. Maruhashi and K. Ono

Kyoto University Research Reactor Institute, 2-1010, Asashironishi, Kumatori-cho, Sennan-gun, Osaka 590-0494, Japan

Abstract

Various radioactive nuclei are generated in and around the target volume after the irradiation for boron neutron capture therapy. By measuring and estimating the distributions of these nuclei with the technique of single photon emission computed tomography (SPECT), more accurate post-irradiation dose-estimation can be expected. The feasibility study was performed mainly by simulation. The radioactivity densities for Cl-38, Ca-49 and Na-24 just after the irradiation were calculated to be 100 to 1000 Bq/cm^3 in and around the target volume. It was confirmed that these nuclei could be detected by SPECT under some conditions. Using the density differences for these generated nuclei, discrimination between soft-tissue area and bone area can be achieved. In focusing on the shallower 1-cm^3 voxel, the necessary counting-time for Na-24 was estimated to be a few tens minutes when the distance between the SPECT detector and the voxel was shortened to 6 cm.

Keywords: Post-irradiation dose-estimation, activation in human body, radioactivity distribution, imaging technique, SPECT

1. Introduction

Since December 2001, at the Heavy Water Neutron Irradiation Facility (HWNIF) of Kyoto University Reactor (KUR) (Sakurai and Kobayashi, 2002), boron neutron capture therapy (BNCT) has been expanded to the tumors of various body parts, such as neck, liver, lung, etc..

The motion ranges and shape changes of these parts are large, unlike those of head. Then, the accuracy is limited in the pre- and post-irradiation dose-estimations by the simulation based on the diagnostic imaging under a motionless and changeless condition.

In BNCT irradiations, various radioactive nuclei are generated in and around the target volume. By measuring and estimating the distributions of these nuclei with the technique of single photon emission computed tomography (SPECT), more accurate post-irradiation dose-estimation can be expected. The feasibility study by simulation calculation is reported.

2. Methods

A dose-estimation code system "SERA" (Wessol et al., 1999) was used in the simulation of the distributions of the radioactive nuclei generated near the target volume. The distributions of the respective radioactive nuclei were calculated using the neutron flux distribution obtained by SERA, with the reaction crosssections in the JENDL-3.3 nuclear data library (Shibata et al., 2002) and decay constants. Here, the physical decrease is taken into account but the biological decrease is not.

The elemental content for some human-tissues important in this study are listed in Table 1 (Synder et al., 1975).

Table 1 *Elemental content (mass percent) and density (g/cm^3) for human tissues*

	Bone	Brain	Soft tissue
H	7.19	11.1	10.5
C	25.0	12.5	23.2
N	3.00	1.33	2.49
O	46.9	73.8	63.0
Na	0.32	0.18	0.11
S	0.17	0.18	0.20
P	6.99	0.35	0.13
Cl	0.14	0.24	0.13
K	0.15	0.31	0.20
Ca	9.99	-----	-----
Density	1.5	1	1

The radioactivity distributions were simulated for bone, brain and the other soft-tissues. The estimation for blood was not performed, because it was difficult to simulate the circulation and metabolism of blood.

The simulations were performed for the typical BNCT irradiations to brain tumor and head and neck tumor. For the former irradiation, it was assumed that the neutron beam was incident to the parietal lobe and the irradiation time was one hour. For the latter irradiation, it was assumed that the neutron beam was incident to the right cheek and the irradiation time was one point five hour. The irradiation field size was 12 cm in diameter for both irradiations.

3. Results

Just after the irradiation, the total radioactivities of the gamma-ray emitting nuclei arranged in order of decreasing activity were Cl-38, Na-24 and K-42 in brain and soft tissue both for brain tumor, and head and neck tumor. In bone, the total radioactivities of Ca-49, Na-24, Cl-38 and K-42 were arranged in decreasing order.

Figures 1, 2 and 3 are the contour maps for the radioactivity densities on the axial slice at the 3-cm depth just after the irradiation for brain tumor, respectively for Cl-38, Ca-49 and Na-24. Figures 4, 5 and 6 are the contour maps for the radioactivity densities on the beam-line slice just after the irradiation for head and neck tumor. The unit for each contour is Bq/cm^3.

In Figs. 1 and 4, the Cl-38 activity density is gently distributed along the beam line. The Cl-38 activity density distributions are relatively similar to the thermal neutron flux distributions. For brain tumor, this is because the density of Cl-37, which is the origin of Cl-38, is almost the same both for bone and brain. For head and neck tumor, this is because the bone area is smaller than the soft-tissue area.

It is found that the Ca-49 activity densities are larger especially in bone, as shown in Figs. 2 and 5. This is because the Ca-48, which is the origin of Ca-49, is distributed mainly in bone.

The Na-24 activity densities are also distributed gently along the beam lines, but the values become larger in bone, as shown in Figs. 3 and 6. This is caused by that the density of Na-23, which is the origin of Na-24, is 2.7 times larger in bone than in brain and soft tissues.

4. Discussion

The radioactivity densities for Cl-38, Ca-49 and Na-24 just after the irradiation were calculated to be in the range from 100 to 1000 Bq/cm^3 in and around the target volume. Cl-38 and Ca-49 decay rapidly after the irradiation, because those half-lives are short, 37 minutes and 8.7 minutes, respectively. Meanwhile, the half-life of Na-24 is relatively larger at 15 hours, so Na-24 can be detected for a few days.

Here, the feasibility of imaging for Na-24 is discussed. For a detector of the SPECT system, it was assumed that the distance to the deepest voxel of 1 cm^3 was 20 cm, and that the effective detection-field size was 1 cm^2. The count rate for the gamma rays from the deepest voxel was estimated to be from 2×10^{-3} to 2×10^{-2} s^{-1}.

To achieve a statistical error of 10 percent, 1 to 14 hours are necessary. In focusing on the shallower voxel, the necessary counting time was estimated to be a few tens minutes when the distance between the detector and the voxel was shortened to 6 cm.

At present, the post-irradiation dose-estimation system is considered as follows. From the radioactivity distributions for Ca-49 and Cl-38, the flux distributions of neutrons, mainly thermal neutrons, are obtained, respectively for the bone and soft-tissue areas. These flux distributions are compared with the flux distribution obtained from the radioactivity distribution for Na-24. From the discrepancy between these flux distributions, the effective flux distribution, in which the motion and shape-change near the target volume during the irradiation, is estimated.

5. Conclusion

It was confirmed that imaging for the Na-24 generated under BNCT could be performed using the SPECT technique. There is a possibility that Ca-49 and Cl-38 could also be utilized for imaging, though those half-lives are short and therefore contain information only for the middle to latter phase of the irradiation. Using the density differences for these generated nuclei, discrimination between the soft-tissue area and bone area can be expected.

We are planning to quantitatively confirm the generation of these radioactive nuclei using a HPGe semiconductor detector, etc., in BNCT clinical irradiations and animal experiments, when the KUR operation is restarted in 2009. We are expecting to try the imaging using a SPECT machine if possible. In addition, we are researching the possibility to model the biological and physiological behaviors of these nuclei near the target volume.

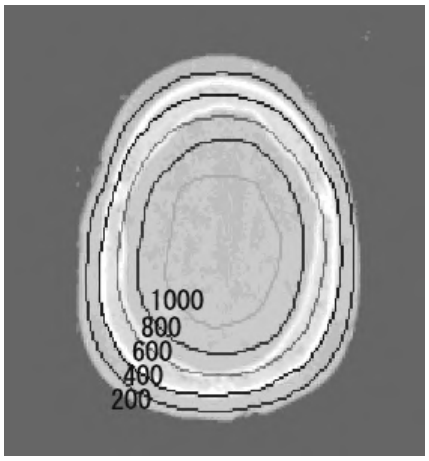

Figure 1 *Contour map for Cl-38 activity density (Bq/cm^3) just after the irradiation to brain tumor*

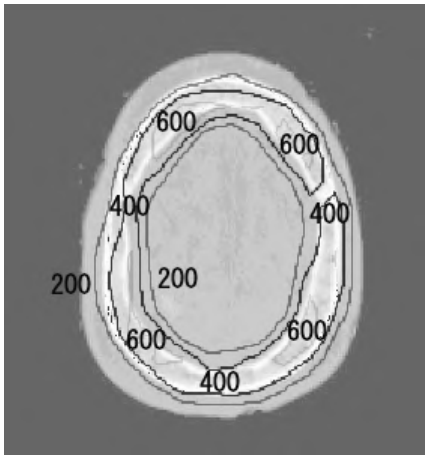

Figure 2 *Contour map for Ca-49 activity density (Bq/cm^3) just after the irradiation to brain tumor*

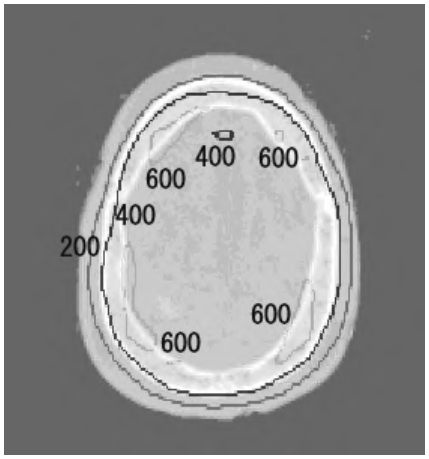

Figure 3 *Contour map for Na-24 activity density (Bq/cm^3) just after the irradiation to brain tumor*

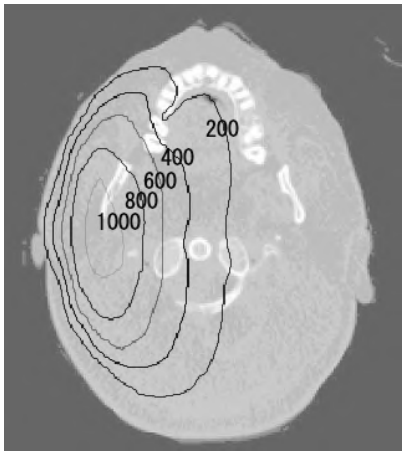

Figure 4 *Contour map for Cl-38 activity density (Bq/cm^3) just after the irradiation to head and neck tumor*

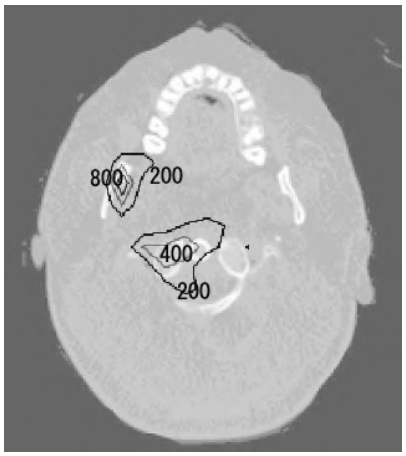

Figure 5 *Contour map for Ca-49 activity density (Bq/cm^3) just after the irradiation to head and neck tumor*

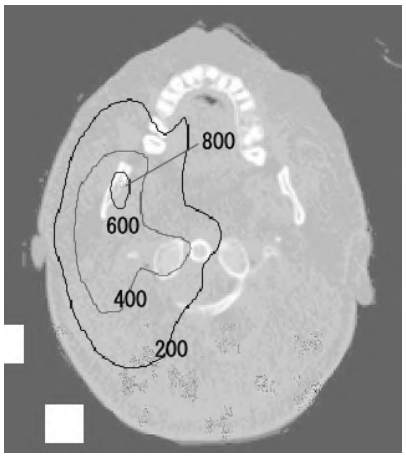

Figure 6 *Contour map for Na-24 activity density (Bq/cm^3) just after the irradiation to head and neck tumor*

References

Sakurai, Y., Kobayashi, T., 2002. The medical-irradiation characteristics for neutron capture therapy at the Heavy Water Neutron Irradiation Facility of Kyoto University Research Reactor. Med. Phys. 29, 2328–2337.

Shibata, K., Kawano, T., Nakagawa, T., Iwamoto, O., Katakura, J., Fukahori, T., Chiba, S., Hasegawa, A., Murata, T., Matsunobu, H., Ohsawa, T., Nakajima, Y., Yoshida, T., Zukeran, A., Kawai, M., Baba, M., Ishikawa, M., Asami, T., Watanabe, T., Watanabe, Y., Igashira, M., Yamamuro, N., Kitazawa, H., Yamano, N., Takano, H., 2002. Japanese evaluated nuclear data library version 3 revision-3: JENDL-3.3. J. Nucl. Sci. Technol. 39, 1125-1136.

Synder, W.S., Cook, M.J., Nasset, E.S., Kahrhausen, L.R., Howells, G.P., Tipon, L.H., 1975. Report of the task group on reference man. Pergamon Press , Oxford.

Wessol, D., Cohen, M., Harkin, G., Rossmeier, M., Wemple, C., Wheeler, F., 1999. SERA workshop lab manual. INEEL/EXT-99-00766.

BNCT beam monitoring with recombination chamber

Piotr Tulik[1,2], Natalia Golnik[2,1], Mieczysław Zielczyński[1]

[1] *Institute of Atomic Energy, Świerk, Poland*
[2] *Institute of Precision and Biomedical Engineering, Warsaw University of Technology, Warsaw, Poland*

The paper presents the new measuring method for quality assurance or *on-line* monitoring of the BNCT beam intensity and composition, using a specially designed recombination chamber.

Recombination chambers are high-pressure, ionisation chambers which operate in unsaturated mode, under conditions of initial recombination of ions. Parallel plate recombination chambers are known as the detectors which can be used in order to determine the dose rate and several parameters associated with radiation quality of mixed radiation fields. Specially designed chambers can operate correctly also at high dose rates of therapeutic beams. The system presented in the paper uses a special, double recombination chamber which contains two sets of electrode pairs. Details of the chamber design will be discussed in the paper.

The measuring method is based on continuous determination of a quantity denoted as recombination index of beam quality RIBQ. During the measurements, one of the electrode sets is polarized with the high voltage, which ensures the conditions close to saturation (few hundreds volts), while the second one with lower voltage (between 20 and 50 volts). Ionization current measured by the second set of electrodes depends on initial recombination of ions, hence on LET spectrum at the depth of the gas cavity. RIBQ is determined from the difference between ionization currents measured by the first and second sets of electrode pairs. The minimum time needed for reading and display of the data is about 1 s for the dose rate and 10 s for RIBQ. It was shown experimentally that the system can detect the change of the gamma and neutron contributions to the absorbed dose at the level of about 0.5% of the total dose.

Microdosimetry Study of THOR BNCT Beam Using Tissue Equivalent Proportional Counter

Fang-Yuh Hsu[a], Hsiu-Wen Hsiao[b], Chuan-Jong Tung[b,c], Hong-Ming Liu[a] and Fong-In Chou[a]

[a]*Nuclear Science Technology and Development Center, National Tsing Hua University, Taiwan*
[b]*Department of Biomedical Engineering and Environmental Sciences, National Tsing Hua University, Taiwan*
[c]*Department of Medical Imaging and Radiological Science, Chang Gung University, Taiwan*

Abstract

Boron neutron capture therapy (BNCT) is a cancer treatment modality using a nuclear reactor and a boron compound drug. In Taiwan, Tsing Hua Open-pool Reactor (THOR) has been modulated for the basic research of BNCT for years. A new BNCT beam port was built in 2004 and used to prepare the first clinical trial in the near future. This work reports the microdosimetry study of the THOR BNCT beam by means of the tissue equivalent proportional counter (TEPC). Two self-fabricated TEPCs (the boron-doped versus the boron-free counter wall) were introduced. This dual TEPC system was applied to measure the lineal energy distributions in air and water phantom irradiated by the THOR BNCT mixed radiation field. Dose contributions from component radiations of different linear energy transfers (LETs) were analyzed. Applying a lineal energy dependent biological weighting function, r(y), to the total and individual lineal energy distributions, the effective relative biological effectiveness (RBE), neutron RBE, photon RBE, and boron capture RBE (BNC RBE) were all estimated at various depths of the water phantom. Minimum and maximum values of the effective RBE were 1.68 and 2.93, respectively. The maximum effective RBE occurred at 2 cm depth in the phantom. The averaged neutron RBE, photon RBE, and BNC RBE values were 3.160±0.020, 1.018±0.001, and 1.570±0.270, respectively, for the THOR BNCT beam.

Keywords: microdosimetry, RBE, TEPC, BNCT, THOR

1. Introduction

Tsing Hua open-pool reactor (THOR), a 2 MW research reactor at the National Tsing Hua University in Taiwan, has been used in a feasibility study for boron neutron capture therapy (BNCT) for years. A new BNCT beam port was built in 2004 and used to prepare the first clinical trial in the near future. BNCT is a binary therapy involving two components: a boron-labeled compound that is administered to the patient and that accumulates in tumor cells; and irradiation by an epithermal neutron beam.

The neutron beam induces the ^{10}B (n,α) ^{7}Li capture reaction that emits very short-range and high linear energy transfer (LET) particles. These particles have a high probability of selectively killing the boron-loaded tumor cells.

Relative biological effectiveness (RBE) and the consequent therapeutic efficacy of BNCT are due to the energy-range properties of the secondary particles, the boron micro-distribution and the morphological properties of cells.

Because of the scale of events, microdosimetric analysis is the method of choice in modeling radiation effects. The spectrum of lineal energy, a microdosimetric parameter defined as the deposited energy per event divided by mean chord length, is an important factor in determining RBE. This work reports the microdosimetry study of the THOR BNCT beam by means of the tissue equivalent proportional counter (TEPC). The spectra of lineal energy were obtained using such paired TEPCs in free air and at various depths in a PMMA phantom. These spectra were obtained for various concentrations of boron and different site diameters. The measured lineal energy spectra revealed peaks associated with alpha particles and lithium ions from boron captures, protons from ^{14}N captures and elastic interactions, and contaminating gamma rays. The RBE values were estimated using these measured

spectra and a biological weighting function that depended on the lineal energy.

2. Materials and methods

Two 2.5 cm diameter TEPCs (the boron-doped versus the boron-free counter wall) were self-fabricated. This dual TEPC system was applied to measure the lineal energy distributions in air and water phantom irradiated by the THOR BNCT mixed radiation field. The counter walls were made of A-150 tissue-equivalent (TE) conducting plastic of 2.5 mm thickness. The filled gas was a standard TE mixture containing 55.4% propane, 39.9% carbon dioxide, and 4.7% nitrogen by molar weight. When taking the measurements, the chambers of TEPCs were filled with TE gas at the pressures of 17 Torr, corresponding to simulated cell nuclei with diameters of 1 μm.

Measurements were made using standard microdosimetry equipment, including a low-pressure gas flow system, low noise sensitive preamplifier, linear amplifier, oscilloscope, multi-channel analyzer, and multichannel analyzer (MCA). Figure 1 presents the schematic diagram of the experimental set-up for making microdosimetric measurements. Due to the wide range of lineal energy distributions for the THOR BNCT mixed radiation field, an americium-241 alpha source and a cesium-137 gamma source were chosen to calibrate the TEPCs for the radiations with different (high and low) lineal energy.

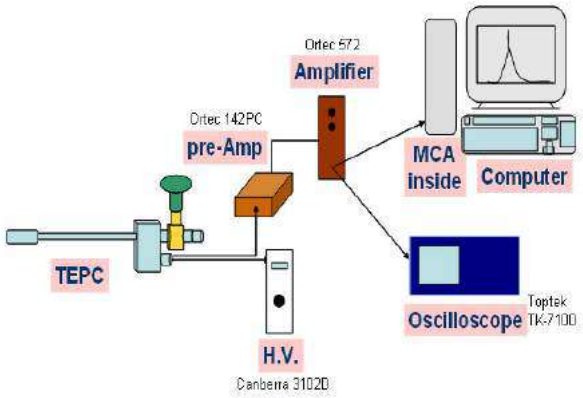

Figure 1. The schematic diagram of the experimental set-up for making microdosimetric measurements

Boron-doped (50 ppm) and boron-free counter walls for each TEPC were used to make comparative measurements. The lineal energy spectrum of the clinical BNCT beam can then be measured using such paired TEPCs in free air and at various depths in a PMMA phantom. Counters were positioned at multiple locations in a 16cm diameter by 22 cm height cylindrical acrylic head phantom to simulate the various depths of tumors in a human head. Figure 2 shows the photos of lineal energy measurements in free air and (left) and in a PMMA phantom (right). The phantom was positioned at the location of 6 cm in front of the exit of the THOR BNCT beam. Microdosimetric data at different depths (0, 2, 4, 6 , 8, and 12 cm) were measured.

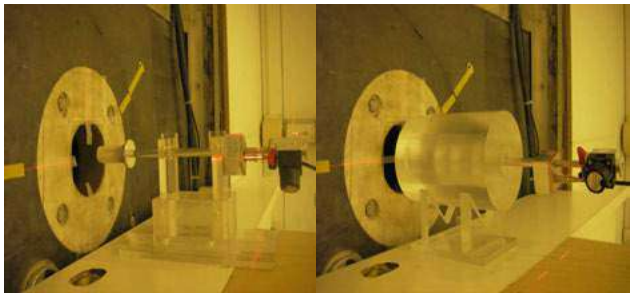

Figure 2. Photos of lineal energy measurements in free air and (left) and in a PMMA phantom (right)

To clarify the relationship between lineal energy and RBE, in 1990, Pihet et al. presented the bological weighting function, *r(y)*, by means of the observations of early radiation damage (such as regenerations of crypt cells) in rats irradiated with neutrons. *r(y)* is approximatly equal to 1 for low lineal energy, and has fluctuation for higher lineal energy. Accroding to the measured spectra of lineal energy, by means of the *r(y)* function, effective RBE could be estimated. Effective RBE is defined as equation 1.

$$\text{Effective RBE} = \frac{\int r(y)\cdot d(y)dy}{\int d(y)dy} = \frac{\int yd(y)r(y)\mathrm{d}\left[\log(y)\right]}{\int yd(y)\mathrm{d}\left[\log(y)\right]} \qquad \text{(eq. 1)}$$

If the spectrum area normalized to unit dose (eq.2), then eq.1 can be transformed to eq.3.

$$\int yd(y)\mathrm{d}\left[\log(y)\right] = 1, \qquad \text{(eq. 2)}$$

$$\text{Effective RBE} = \int yd(y)\mathrm{r}(y)\mathrm{d}\left[\log(y)\right] \qquad \text{(eq. 3)}$$

Effective RBE can be estimate by means of integration of the product of the measured (low and high) lineal energy spectrum ($yd(y)$ vs. $\log(y)$) from the boron-free TEPC and *r(y)*. The effective RBE is one of the indexes of THOR beam quality.

BNCT Dose contributions from component radiations of different linear energy transfers (LETs) were analyzed. Applying a lineal energy dependent biological weighting function, r(y), to the total and individual lineal energy distributions, the effective relative biological effectiveness (RBE), neutron RBE, photon RBE, and boron capture RBE (BNC RBE) estimated. The dosimetry of BNCT is complicated because of contribution from multiple dose components. RBE dose for each beam field could be calculated as equation 4, where RBE(BNC), RBE(neutron) and RBE(photon) are the RBE values of boron capture, neutron and photon, respectively, and D(BNC), D(neutron) and D(photon) represent physical dose of boron capture, neutron and photon, respectively. Once the effective RBE was estimate, RBE dose can be determined by equation 5.

RBE dose = RBE(BNC)×D(BNC)
+RBE(neutron)×D(neutron)
+RBE(photon)×D(photon) (eq. 4)

RBE dose = effective RBE × Σ(Physical Dose)
=effective RBE×[D(BNC)+ D(neutron)+D(photon)]
(eq. 5)

3. Results and discussion

Figure 3 depicts the lineal energy spectra of the dual TEPC (0 and 50 ppm boron-doped) system simulated 1 μm cell nuclei at 6 cm apart from THOR BNCT beam exit, measured in air. The dash line indicates the dose contribution of boron capture, which was obtained from the difference of 50 ppm Boron-doped and boron-free (0 ppm, dot line) TEPC results. Lineal energy spectrum measured by the boron-free TEPC in 2 cm depth of the PMMA phantom and *r(y)* were shown in figure 4.

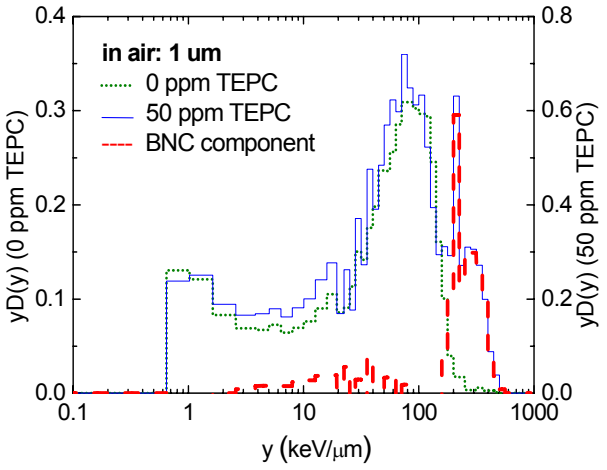

Figure 3. The lineal energy spectra of the dual TEPC (0 and 50 ppm boron-doped) system

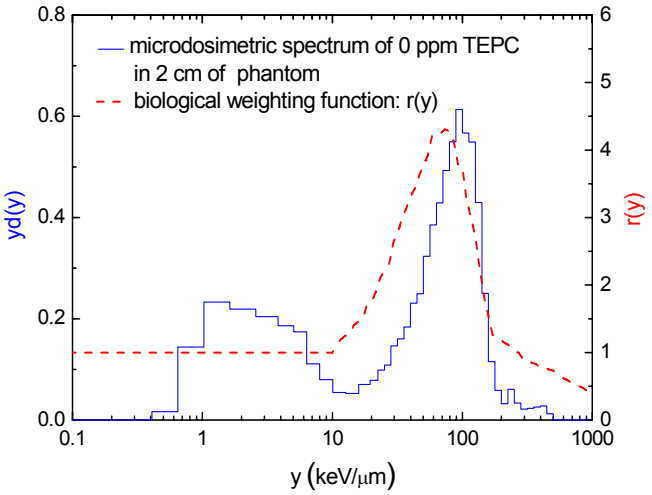

Figure 4. Lineal energy spectrum measured by the boron-free TEPC in 2 cm depth of the PMMA phantom and the bological weighting function, *r(y)*

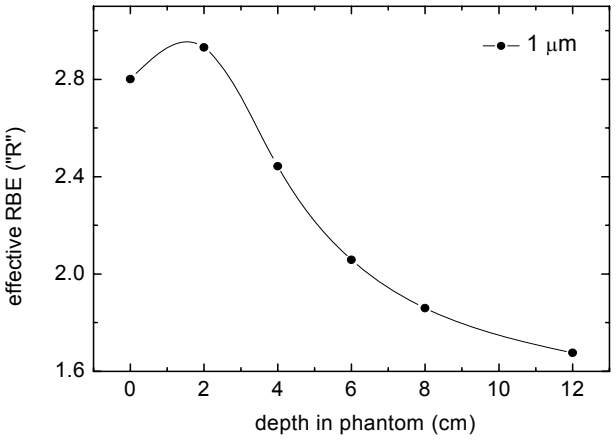

Figure 5. The effective RBE in various depths of the PMMA phantom

Effective RBE contributed from high y radiations (neutron and BNC) is more important than low y radiations (photon and electron).

Effective RBE in various depths of the PMMA phantom were estimated (represented in figure 5) by means of the measured lineal energy spectra using the boron-free TEPC and the lineal energy dependent biological weighting function, *r(y)*.

The depth is defined here as the distance from the surface of the phantom to the surface of the TEPC. The effective RBE increases from the surface of the phantom and has a maximum value at about 2 cm depth, than decrease with depth increased. The effective RBE increased due to the rich neutron fluence in shallow depth and decreased due to the poor fluence in deeper depth comparing with steady fluence for photon.

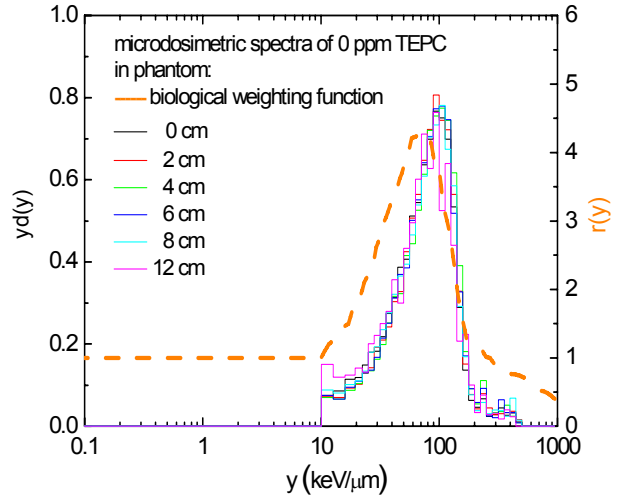

Figure 6. The lineal spectrum (y>10 keV/μm) measured from the boron-free TEPC positioned in various depths

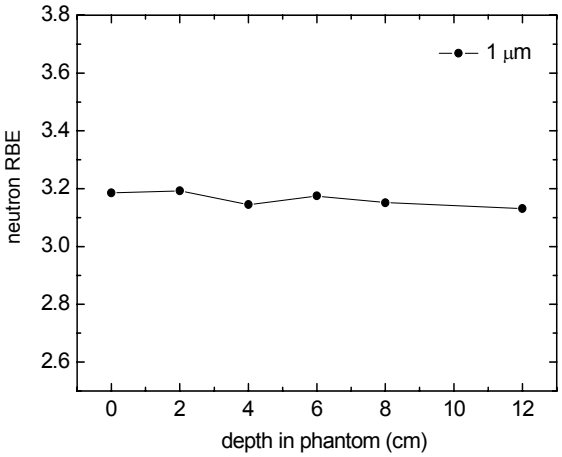

Figure 7. Neutron RBE estimated in various depths

Minimum and maximum values of the effective RBE were 1.68 and 2.93, respectively.

The RBE values for individual BNCT dose components were obtained by using the portion of lineal energy distribution for individual radiation and *r(y)*. For example, the lineal spectrum (y>10 keV/μm) depicted in figure 6, measured from the boron-free TEPC positioned in various depth, were selected to determine the neutron RBE. Estimated neutron RBE in various depths for the THOR BNCT beam is shown in figure 7. The averaged neutron RBE were 3.16±0.02. Green et al. madethe measurements in Birmingham, estimated neutron RBE was 3.40 $\pm$ 0.10. The higher the neutron RBE is, the more killing capability for the facility beam possesses.

The neutron RBE is for comparing the beam characteristics between different BNCT facilities. The boron concentration may vary in different sites, therefore, boron-free lineal spectra were chosen for the purpose of RBE estimations. It should be noted the uncertainty of applying the r(y) function derived from microdosimetric measurements made for 2 μm site (Loncol et al) to the measured results of 1 μm site in this paper.

4. Conclusions

This work reports the microdosimetry study of the THOR BNCT beam by means of the dual TEPC system. Applying the lineal energy dependent biological weighting function to the total and individual lineal energy distributions, the effective RBE, neutron RBE, photon RBE, and boron capture RBE were all estimated at various depths of the water phantom. Minimum and maximum values of the effective RBE were 1.68 and 2.93, respectively. The maximum effective RBE occurred at 2 cm depth in the phantom. The averaged neutron RBE, photon RBE, and BNC RBE values were 3.160±0.020, 1.018±0.001, and 1.570±0.270, respectively, for the THOR BNCT beam.

References

Coutrakon, G., Cortese J., et al., 1997. Micordosimety spectrum of the Loma Linda proton beam and relative biological effectiveness comparisons. Med. Phys. 24, 1499-1506.

Green, S., Gainey, M., and Wojnecki, C., 1998. Determination of an RBE for an Epithermal Neutron Beam for BNCT from Microdosimetric Measurements. ISNCT8, LaJolla, California.

Hsu, F. Y., Tung, C. J. and Watt, D. E., 2003. Microdosimetric spectra of the THOR epithermal neutron beam for boron neutron capture therapy, Radiat. Prot. Dosim., 104, No. 2, pp.121-126.

Loncol, T., Cosgrove, V., et al., 1994. Radiobiological effectiveness of radiation beams with broad spectra: microdosimetric analysis using biological weighting functions. Radiat. Prot. Dosim. 52, 347-352.

Pihet, P., Menzel, H. G., et al., 1990. Biological weighting function for RBE specification of neutron therapy beams. Radiat. Prot. Dosim. 31, 431-442.

In-phantom dose imaging with polymer gel layer dosimeters

E.Vanossi[a,b], M.Carrara[c], G.Gambarini[d,b], A. Negri[d], M.Mariani[a]

[a] *Department of Energy, Nuclear Engineering Division, Polytechnic of Milan, Via Ponzio 34/3, 20133 Milano, Italy*

[b] *INFN Milan, Via Celoria 16, 20133 Milano, Italy*

[c] *Fondazione IRCCS "Istituto Nazionale Tumori", Via Venezian 1, 20133 Milano, Italy*

[d] *Department of Physics, University of Milan, Via Celoria 16, 20133 Milano, Italy*

Abstract

Gel dosimeters in form of layers have shown noticeable potentiality for in-phantom dose and thermal flux profiling and imaging in the high fluxes of thermal or epithermal neutrons utilised for boron neutron capture therapy (BNCT). Such dosimeters give the possibility not only of obtaining spatial dose distributions but also of achieving measurements of each dose contribution in neutron fields. The various dose components are separated by means of pixel-to-pixel manipulations of pairs of images obtained with gel-dosimeters having different isotopic composition. The reliability of Polymer-gel-layer dosimeters for BNCT dosimetry has been studied. Some results obtained after the last improvements of the method are reported.

Keywords: BNCT dosimetry, Gel dosimetry, Polymer gel, Dose imaging

1. Introduction

The method for spatial determination of absorbed doses in thermal or epithermal neutron fields, based on gel dosimeters in form of layers, has revealed to be very convenient. In fact, using gel layer dosimeters it is possible, by means of a properly studied procedure, to obtain the spatial dose distribution of each dose contribution in thermal or epithermal neutron fields.

BNCT dosimetry using Fricke-xylenol-orange-infused gel dosimeters has been widely studied and experimented, giving reliable results. Polymer-gel-layer dosimeters (PGLD), in which a polymerisation process appears as a consequence of absorbed dose, have been recently tested, because of their characteristic absence of diffusion. In fact, due to the diffusion of ferric ions, Fricke-gel dosimeters require prompt analysis after exposure to avoid loss of spatial information. In this work the recent results of a study about the reliability of polymer gel in BNCT dosimetry are discussed.

In tissue exposed in the thermal column of a nuclear reactor, after injection of the boron carrier, the absorbed dose results from three main contributions: the therapeutic dose due to alpha and lithium particles released in the reaction of thermal neutrons with ^{10}B (^{10}B (n,α) ^{7}Li), the dose from protons due to the reaction of thermal neutrons with nitrogen (^{14}N (n,p) ^{14}C) and the gamma dose from the reaction of thermal neutrons with hydrogen (^{1}H (n,γ) ^{2}H and background, if not negligible). The fast neutron dose mainly due to recoil protons from elastic scattering of fast neutrons with hydrogen nuclei, is negligible in reactor thermal columns.

The experiments were carried out by exposing a phantom containing the dosimeters in the thermal column of the TRIGA MARK II reactor of the University of Pavia, where BNCT has been successfully applied to treat multiple and diffused liver metastases by means of extracorporeal exposure (Pinelli et al., 2002). Being the aim of this work the study of the feasibility of utilising gel dosimeters, a simple shape (cylindrical) was chosen for the phantom. It was however tissue equivalent (TE) and with a total mass not much far from that of a liver.

2. Materials and Methods

Polymer gel dosimeters in form of layers were used to measure the spatial distribution of the absorbed dose in a phantom exposed to a thermal neutron beam.

The dosimeters had a thickness of 3 mm and rectangular shape (12x6 cm^2). The layer holders were composed of a rectangular frame between two transparent sheets in order to allow the optical analysis of light transmittance.

In Fig. 1. some polymer gel layers after irradiation are shown.

Fig. 1. Layers of polymer gel after irradiation

The polymer gel dosimeter PAG (Polymer Acrylamide Gelatine), suitably synthesized in the laboratory, was used for the here shown measurements. The samples were always irradiated the day after the preparation. The gel composition is the same utilized by others (Baldock, 1998) with a variation in the amount of the gelling agent that was lowered to maintain the compound enough fluid to be introduced by means of a siring through the apposite holes in the holders. The gel dosimeters are prepared with the following chemical reagents: gelatine powder as gelling agent, acrylamide and N,N' methylene-bisacrylamide as monomers, tetrakis (hydroxymethyl) phosphonium chloride (THP) as antioxidant and highly purified and deionised water. The amount of each compound was the same reported in previous papers (Mariani et al., 2007; Vanossi et al., 2008) reporting the results of the first studies about the feasibility of performing BNCT dosimetry with PGLD. The method had been improved for both the dosimeter preparation protocols and the image elaboration software.

Couples of gel dosimeters were put in a cylindrical phantom and exposed in the thermal column of the nuclear reactor TRIGA MARK II of Pavia. The phantom, shown in Fig. 2., was composed of two polyethylene shells (1 mm thick) having the shape of about half-cylinder, filled with a tissue-equivalent gel obtained by dissolving in purified and deionised water the gelling agent agar in the amount of 4 % of the final weight. The two parts were assembled around the dosimeters in order to finally obtain a TE cylindrical phantom with the dosimeters in the central plane. The so obtained phantom had a height of 11 cm and a diameter of 12 cm.

In order to determine the gamma dose and the dose due to the charged particles emitted during the reactions of neutrons with ^{10}B, couples of gel dosimeters were prepared, one having the standard chemical composition and the other containing also a 40 ppm of ^{10}B. The neutron transport is determined by the whole phantom and it is not sensibly changed by the isotopic content of the dosimeters that are layers having a thickness of only 3 mm.

Fig. 2. Phantom utilised for the irradiation of gel dosimeters layers

The method for separating the various dose contributions developed using Fricke gel dosimeters (Gambarini et al., 2004) was applied to determine the different contributions of the absorbed dose. The polymer gel dosimeters were optically analysed by imaging, by means of a CCD camera, the samples placed on a plane light source. The difference Δ(OD) of optical density detected before and after irradiation, is proportional to the absorbed dose that was therefore evaluated by means of dosimeter calibrations.

The algorithms for the separation of the dose contributions take into account that the sensitivity of the dosimeters changes with LET of the radiation. For the sensitivity to the products of the reactions with ^{10}B the value 0.41 was assumed (Gambarini et al., 2002).

Gel dosimeter calibration was performed for each gel preparation. To this aim some dosimeters of each group were irradiated at different doses with a calibrated ^{137}Cs source.

3. Results

An example of gel calibration is shown in Fig. 3. where the calibration curves for a standard polymer gel and a gel added with ^{10}B are reported.

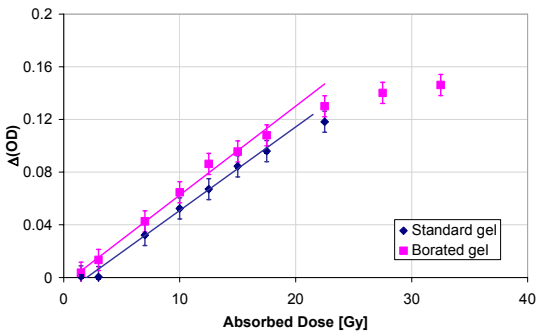

Fig. 3. Calibration curves of standard (♦) and ^{10}B-added (■) polymer gel dosimeters

Some exposures of the cylindrical phantom containing couples of polymer gel dosimeters (standard and ^{10}B-added) in the thermal column of TRIGA MARK II reactor were carried out. The phantom was placed with the cylinder axis normal to the beam axis. From the light-transmittance images of the two dosimeters by means of pixel-to-pixel elaborations using the proper algorithm, both boron and gamma dose images were obtained. An example of such results is shown in Figs. 4. and 5.

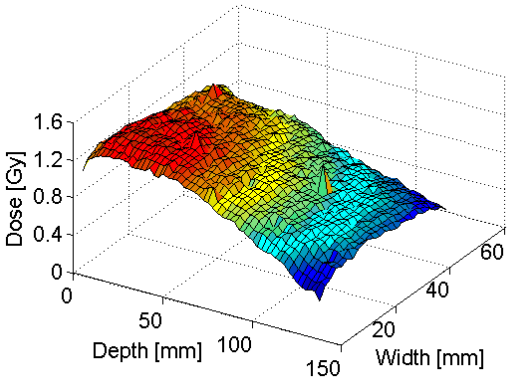

Fig. 4. Image of the gamma dose measured by means of a PGLD

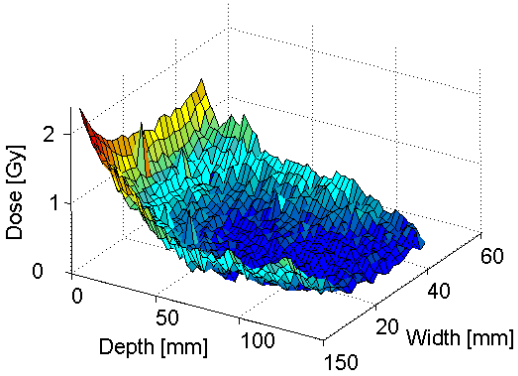

Fig. 5. Boron dose image measured by means of a PGLD

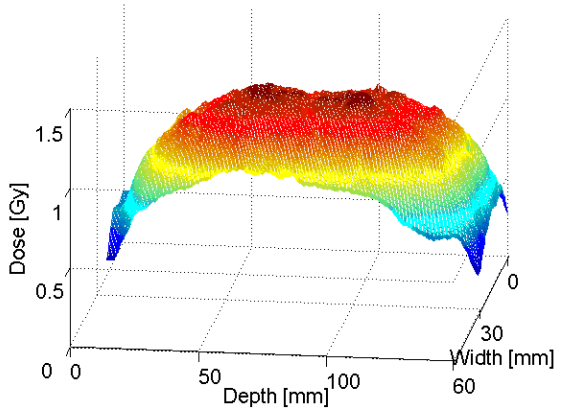

Fig. 6. Image of the gamma dose measured by means of a PGLD placed in the phantom that was rotated during the irradiation

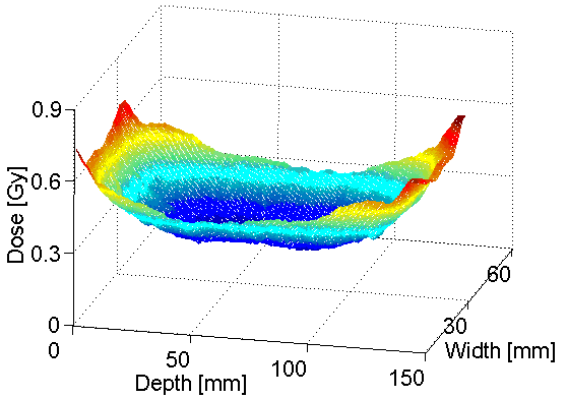

Fig. 7. Boron dose image measured by means of a PGLD placed in the phantom that was rotated during the irradiation

In one case, the phantom was rotated of 180° for similarity with the modality of liver treatment. The obtained dose images are reported in Figs. 6 and 7.

From these last dose images the profiles along the beam axis were extracted. In order to check the reliability of the here studied polymer dosimeter such profiles were compared with the corresponding profiles extracted from the images obtained by means of Fricke gel dosimeters exposed in the same phantom and in the same reactor configuration. In fact, Fricke gel dosimeters had shown to give good results both for the shapes of dose spatial distributions and their quantitative values. All profiles are reported in Fig. 8. The agreement obtained for the boron dose is noticeable. Concerning the gamma dose, the good agreement is visible for the shape of the profiles and some discordance in the absolute values. More precise results could be obtained performing more than one measurements and working with averaged images.

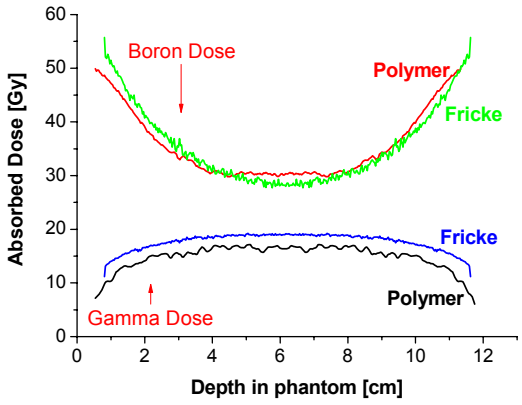

Fig. 8. Boron dose and gamma dose profiles in the central axis extracted from a polymer gel and a Fricke gel

4. Conclusions

The above reported results show that the studied PGLD can be satisfactorily utilised for imaging both gamma and boron doses in TE phantoms exposed in a reactor thermal column designed for BNCT treatments. In particular such dosimeters can be fruitfully used instead of Fricke gel dosimeters when it is not practical to get gel imaging instrumentation near to the irradiation facility as it is mandatory for Fricke gel.

Acknowledgements

The work was partially supported by the National Institute of Nuclear Physics (INFN), Italy.

References

Baldock, C., Burford, R.P., Billingham, N., Wagner, G.S., Patval, S., Badawi, R.D., Keevil, S.F., 1998. Experimental procedure for the manufacture and calibration of polyacrylamide gel (PAG) for magnetic resonance imaging (MRI) radiation dosimetry. Phys. Med. Biol. 43, 695–702.

Gambarini, G., Birattari, C., Colombi, C., Pirola, L., Rosi, G., 2002. Fricke-Gel Dosimetry in Boron Neutron Capture Therapy. Radiat. Prot. Dosim. 101, 419-422.

Gambarini, G., Colli, V., Gay, S., Petrovich, C., Pirola, L., Rosi, G., 2004. In-phantom imaging of all dose components in boron neutron capture therapy by means of gel dosimeters. Appl. Rad. Isot. 61, 759-763.

Mariani, M., Vanossi, E., Gambarini, G., Carrara, M., Valente, M., 2007. Preliminary results from a polymer gel dosimeter for absorbed dose imaging in radiotherapy. Radiat. Phys. Chem. 76, 1507–1510.

Pinelli, T., Zonta, A., Altieri, S., Barni, S., Brughieri, A., Pedroni, P., Bruschi, P., Chiari, P., Ferrari, C., Fossati, F., Nano, R., Ngnitejeu Tata, S., Prati, U., Ricevuti, G., Riveda, L., Zonta, C., 2002. TAOrMINA: From the first idea to the application to the human liver. In: Sauerwein, W., Moss, R., Wittig, A. (Eds.), Research and Development in Neutron Capture Therapy. Monduzzi, Bologna, Italy, pp. 1065–1072.

Vanossi, E., Carrara, M., Gambarini, G., Mariani, M., Valente, M., 2008. Study of polymer gel for dose imaging in radiotherapy. Radiat. Meas. 43, 442–445.

Measurement of Boron in Tumours by Neutron Capture Autoradiography following intra-arterial Administration of Boron Entrapped Water-in-Oil-in-Water Emulsion

Yanagie Hironobu[1,2], Mikado Shoji[3], Yasuda Nakahiro[4], Higashi Syushi[5], Ikushima Ichiro[5], Mizumachi Ryuji[6], Murata Yuji[6], Morishita Yasuyuki[7], Shinohara Atsuko[8], Ogura Koichi[3], Sugiyama Hirotaka[2], Ryohei Nishimura[9],Takamoto Sinichi[2,10], Eriguchi Masazumi[2,11], and Takahashi Hiroyuki[1,2]

[1]Department of Nuclear Engineering & Management, Graduate School of Engineering, The University of Tokyo,Tokyo, JAPAN, [2]Cooperative Unit of Medicine & Engineering, The University of Tokyo Hospital, Tokyo, JAPAN, [3]Department of Physics, College of Industrial Technology, Nihon University, Chiba, JAPAN, [4]Department of Physics, National Institute of Radiological Sciences, Chiba, JAPAN, [5]Miyakonojyo Metropolitan Hospital, Miyazaki, JAPAN, [6]Department of Pharmacology, Kumamoto Institute Branch, Mitsubishi Chemical Safety Institute Ltd, Kumamoto, JAPAN, [7]Department of Human & Molecular Pathology, Graduate School of Medicine, The University of Tokyo, Tokyo, JAPAN, [8]Department of Humanities, The Graduate School of Seisen University, Tokyo, JAPAN, [9]Department of Veternary Surgery, The University of Tokyo Veternary Hospital, Tokyo, JAPAN, [10]Department of Cardiac Surgery, The University of Tokyo Hospital, Tokyo, JAPAN, [11]Department of Microbiology, Syowa University School of Pharmaceutical Sciences, Tokyo, JAPAN

Corresponding Author: Hironobu Yanagie, MD, PhD ; TEL: +81-3-5800-9194 ; FAX: +81-3-5800-9195 ; E-mail: yanagie@n.t.u-tokyo.ac.jp

Abstract

The cytotoxic effect of boron neutron capture therapy (BNCT) is due to a nuclear reaction between ^{10}B and thermal neutrons. It is necessary to accumulate the ^{10}B atoms to the tumor cells selectively for effective BNCT. In order to achieve an accurate measurement of ^{10}B concentrations in the biological samples, we employed a technique of neutron capture autoradiography (NCAR) of sliced samples of tumor and normal tissues using CR-39 plastic track detectors. The CR-39 detectors attached with samples were exposed to thermal neutrons in the thermal column of the JRR3 reactor of Japan Atomic Neuclear Institute. We obtained NCAR images for VX-2 tumor in rabbit liver after injected BSH entrapped water-in-oil-in-water (WOW) emulsion by intra-arterial injection via the hepatic artery propria. The ^{10}B concentrations in the VX-2 tumor and normal liver of rabbit were estimated by means of alpha-track density measurements. In this study, we can increase the selective accumulation of ^{10}B atoms in the VX-2 tumor by intra-arterial injection of boron entrapped WOW emulsion until 7 days after injection. Therefore, we will be able to apply boron entrapped WOW emulsion to BNCT for hepatocellular carcinoma, and NCAR technique for detection of effective ^{10}B carrier in BNCT for cancer.

Keywords : Boron neutron capture therapy, Neutron capture autoradiography, WOW emulsion, Hepatocellular carcinoma, Intra-arterial administration

1. Introduction

The cytotoxic effect of BNCT is due to a nuclear reaction between ^{10}B and thermal neutrons ($^{10}B + {}^{1}n \rightarrow {}^{7}Li + {}^{4}He + 2.31$ MeV (93.7 %) / 2.79 MeV (6.3 %)). The resultant lithium ions and α particles on neutron capture reaction are high LET(linear energy transfer) particles with relatively high biological efficiency. These particles (α and ^{7}Li) destroy cells within about 10μm path length from the site of the capture reaction. It is theoretically possible to kill tumour cells without affecting adjacent healthy

cells, if the former can selectively accumulate ^{10}B atoms. So It is very important to develop selective boron delivery systems for effective BNCT therapy (Yanagie, 1991, 1997, 2004, 2006a). BNCT has been used clinically in patients with malignant brain tumours and melanoma.

Liposomes have been investigated extensively as carriers for anticancer drugs in attempts to direct active agents to tumours or to protect sensitive tissues from toxicity. We have reported that ^{10}B atoms delivered by immunoliposomes are cytotoxic to human pancreatic carcinoma cells (AsPC-1) after thermal neutron irradiation *in vitro* (Yanagie, 1991). The intra-tumoural injection of boronated immunoliposomes can increase the retention of ^{10}B atoms in tumour cells, causing suppression of tumour growth *in vivo* following thermal neutron irradiation (Yanagie, 1997). We prepared polyethylene-glycol binding liposomes (PEG-liposomes) as an effective ^{10}B carrier to obviate phagocytosis by RES.

Hepatocellular carcinoma (HCC) is difficult to cure with operation, chemotherapy, or radiation therapy. Iodized poppy-seed oil (IPSO) has a property of depositing itself selectively in the cells of HCC, and the usefulness of iodized poppy-seed oil (IPSO) for detecting or treating liver cancer was first reported. The oil has the property of depositing itself selectively in the cells of HCC. Kanematsu et al. reported a method that mixed a water-soluble antitumour agent with IPSO. In their reports, an aqueous solution of an anticancer drug, doxorubicin, was mixed with 60% urografin, a water-soluble contrast medium, before the solution was mixed with the oil (IPSO) (Kanematsu, 1989).

Higashi et al prepared a long term inseparable, water-in-oil-in-water emulsion (WOW) containing 8-60 mg of epirubicin for use in arterial injection therapy for patients with HCC (Figure 1) (Higashi, 1993, 1995). Higashi et al had reported that tumour size of HCC was reduced in six of seven patients, and a 50% or greater decrease of initial alpha-fetoprotein (AFP) levels within 14 days was observed in all four patients who showed abnomal levels of serum AFP before treatment (Higashi, 1995).

According to the Higashi's clinical results, we would like to apply BNCT to treatment of Hepatocellular Carcinoma (HCC) for increasing the selection of therapies of HCC's patients (Yanagie, 2006b). In this study, we develop BSH entrapped WOW emulsion and evaluate the emulsion as selective boron delivery carrier to cancer tissues.

The accurate measurement of ^{10}B distributions in biological samples with a sensitivity in the ppm range is essential for evaluating the potential usefulness of various boron-containing compounds for BNCT.

We applied CR-39 (polyallyldiglycol carbonate) plastic track detectors to alpha-autoradiographic measurements of the ^{10}B biodistribution in sliced whole body hepatic samples of VX-2 tumour bearing rabbit. The subsequent use of an alpha-track radiographic image analysis system enabled a discrimination between alpha-tracks and recoiled proton tracks was made by track size selection method. This enabled to estimate quantitatively the distributions of ^{10}B concentrations within the tissue sections comparing using suitable standards (Yanagie, 1999).

In this study, we performed the neutron capture autoradiography (NCAR) using CR-39 track etch detectors to qualitatively and quantitatively determine the ^{10}B biodistribution in hepatic samples of VX-2 tumours after intra-arterial injection of ^{10}B entrapped WOW emulsion.

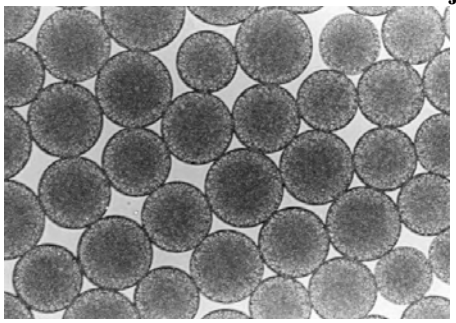

Figure 1. Microphotograph of WOW emulsion

2. Materials & Methods

Chemicals

Sodium salt of undecahydro-mercaptocloso-dodecaborate ($Na_2{}^{10}B_{12}$ H_{11} SH) was obtained by Wako Chemical Co. Ltd. (Tokyo, Japan). Iodized poppy-seed oil (IPSO, Lipiodol Ultrafluid, Kodama, Co., Ltd., Tokyo, Japan) is composed of iodized ethyl esters of the fatty acids obtained from poppy-seed oil and contains 37% iodine.

Preparation of Boron entrapped WOW emulsion

Three hundred milligrams of BSH was dissolved in 5 ml of a 5% glucose solution and filtrated of controlled pore glass membrane emulsifying into 5 ml of IPSO containing surfactant, to form the water-in-oil emulsion (WO). The WO emulsion was then emulsifyied again with aqueous phase containing 5 ml of saline and surfactant. With this double emulsifying technique, the BSH entrapped WOW emulsion was prepared (Higashi, 1995, Yanagie, 2006b).

The particle size distributions of the vesicles of WOW and IPSO microdroplets were determined with a laser-diffraction particle-size analyzer SALD-2000 (Shimadzu Corp., Kyoto, Japan). The boron concentration entrapped in WOW vesicles was determinated by ICP- Mass Spectroscopy at Jyuntendo University.

In vivo Experiments

VX-2 rabbit squamous cell carcinoma cell line was cultured in vitro supplemented with of 10% fetal bovine serum and 500mg streptomycin/penicillin in 5% CO2 condition. The VX-2 cells were inocculated onto the foot pad of the rabbits, and then, the tumours of VX-2 were formed after one week feeding. The nodules of VX-2 tumour were inocculated to left hepatic lobe of liver, then, the hepatic tumour models were constructed after two weeks feedings. After 2 weeks tumour inocculation, BSH entrapped WOW emulsions were administered with intra-arterial injections via the hepatic artery propria compared with ^{10}BSH-Lipiodol mixed conventional emulsion (^{10}BSH : 75 mg/kg rabbit) on VX-2 rabbit hepatic tumour models. One and three days after arterial injections, the boron concentrations of the tumour nodules and normal liver tissues were determinated by ICP-Mass Spectroscopy at Jyuntendo University. (Yanagie, 1999).

Preparation of standard samples and sliced mice samples

In order to examine the biodistribution of the ^{10}B entrapped WOW emulsion after intra-arterial injections to the hepatic artery propria, we carried out Neutron-Capture Auto Radiography(NCAR).

Rabbits were sacrificed 1 and 3 days after the injection of ^{10}B-WOW emulsion, and the hepatic samples were frozen at -60℃. Subsequently, the frozen samples were cut sagittally into 40 μm thick sections mounted on a thin 3M Scotch tape, freeze-dried at -20℃ for two weeks and air-dried for one more week. Thus, the dried samples were prepared Boron-containing standard samples were also prepared using drying filter paper sheets wetted by BSH solutions of four different ^{10}B concentrations(10, 50, 100, 500 ppm of ^{10}BSH), respectively. The ^{10}B concentrations of ^{10}BSH solutions were determined by ICP-Mass Spectroscopy at Jyuntendo University.

Neutron irradiation

The sliced sections were put in close contact with the CR-39 plates (HARZLAS TD-1; Fukuvi Chemical Industry, Japan) using thin adhesive tape. The set of hepatic samples of VX-2 tumour bearing rabbit were simultaneously exposed in the JRR3 reactor of Japan Atomic Energy Research Institute. The thermal neutron fluence irradiation was varied according to the experimental objectives.

For alpha track counting (i.e. ^{10}B distribution measurements) : 2.0×10^{10} n/cm^2 .
For the visible observation of NCAR image: 2.0×10^{12} n/cm^2 .

Etching procedure

For NCAR imaging utilizedα- and Li tracks as well as protons of recoiled and/or produced by ^{14}N (n, p) reaction, where ^{14}N is the biogenically abundant nuclide, the CR-39 detector plates were etched in a 7 N NaOH solution at 70 ℃ for 2 hours to reveal tracks.

3. Results & Discussion

We prepared BSH entrapped WOW emulsion. The mean ^{10}B concentration was 13000 ppm by ICP-MAS. The size of WOW was controlled to 50μm.

The ^{10}B concentration in VX-2 tumour was 141 ppm, 61 ppm by WOW emulsion after 1 day, or 3 day intra-arterial injection, respectively. The ^{10}B concentration of tumour was 58, 24ppm by Lipiodol mix emulsion after 1 day, or 3 day same injection, respectively (Table 1).

The histological staining showed the superior accumulation of the fat droplets of WOW emulsion in tumour site compared with Lipiodol mix emulsion. Electromicroscopic figure of hepatocellular carcinoma after arterial- injection chemotherapy using WOW emulsion : The microdroplets of Iodized poppy-seed oil was retained in the cytoplasm of the cancer cell in the same conformation as preparation time, but there was no accumulation of fat droplets in Lipiodol emulsion. The ^{10}B concentrations of samples were determined by ICP-Mass Spectroscopy at Juntendo University

Table 1. ^{10}B concentration of VX-2 hepatic tumour bearing rabbit model after intra-arterial injection of ^{10}B-WOW emulsion or ^{10}B-Lipiodol mix

WOW	Tumour	Normal Liver	Blood
Day-1	141.8	6.1	1.2
Day-3	61.7	4.3	0.1

Lipiodol	Tumour	Normal Liver	Blood
Day-1	58.0	14.6	0.4
Day-3	24.5	3.9	0.2

From NCAR image of sliced samples, we can estimate the ^{10}B accumulations in the organs. ^{10}B accumulations were estimated for the strongly concentrated part of the tumour at day 3 after injection by WOW emulsion. In order to show the imaging of ^{10}B accumulation in tumour, we obtained NCAR image of sliced samples of VX-2 hepatic tissues using CR-39 track etch detector. NCAR image consists of a large number of etch pits, such as proton, α- and Li tracks. The track area of the opening mouth of each etch pit as well as its position was analyzed by the automated digital imaging optical microscope (HSP-1000), whose image acquisition speed is 50-100 times faster than conventional microscope system[15]. NCAR images of tumour in hepatic tissues are shown in Fig. 2. These images were reconstructed by means of scatter plots for the *x-y* coordinate of the observed whole tracks. Each dot appearing in Fig. 2 corresponds to tracks one by one. Figure 2 shows NCAR of tumour or normal liver site of VX-2 hepatic tissues from a set of VX-2 hepatic cancer bearing rabbit that have received intra-arterial injections of 150 mg of ^{10}B by WOW emulsion or Lipiodol mix solution. The slices of sacrificed and frozen sections were prepared 3 days after injection.

It is difficalt to assess ^{10}B accumulation and distribution in the sample, because the images of Fig. 2 were contaminated by proton tracks. In order to know the efficiency of intra-arterial boron delivery carrier for BNCT, it is necessary to discriminateα- tracks from proton tracks. Generally, etch pit size of the track in the plastic track detector depends on the LET value of the incident particle. In this case, LET values for protons are less than 100 keV/ μ m. The tracks with LET greater than 100keV/ μ m are actually due to α- and Li particles from the $^{10}B(n, \alpha)^{7}Li$ reaction and the maximum values are 2.4×10^2 keV/ μ m and 3.9×10^2 keV/ μ m, respectively[16]. Therefore, two peaks of track size appear in the track area distribution, the lower peak corresponds to proton tracks, and the higher one is due to α- and Li tracks. It is considered that the contribution of Li tracks is not so large because of the short range of Li particles. The track size discrimination betweenα- and proton tracks has been done using observed track area distribution and subtracted proton tracks from Fig. 2. The results are shown in Fig. 3. The distribution of α-tracks was obtained, then we are able to recognize accurate ^{10}B accumulation and distribution in the VX-2 tumours. It is readily apparent that theα-etch pit reveals the existence of ^{10}B atoms delivered by WOW emulsion into the VX-2 tumour. Accurate ^{10}B accumulation in the VX-2

tumours was achieved by WOW emulsion. When the ^{10}B Lipiodol mix solution was injected to the tumour bearing rabbit, the accumulation of ^{10}B atoms in the tumour was small. Theα-track densities of normal liver is not detected at 3 days after intra-aterial injection, so the clearance of WOW emulsion and Lipiodol mix solution in the healthy tissue is very rapid.

The measurement of ^{10}B distributions in biological samples with a sensitivity in the ppm range is essential for evaluating the potential usefulness of various boron-containing compounds for BNCT. ^{10}B accumulations in the tumour varies by boron delivery systems, so we find the strong and weak, concentrated parts of the tumour after injection (Yanagie, 1999. It is necessary to supply the boron atoms homogeneously in the tumours for effective BNCT. The study of the microdosimetry of ^{10}B atoms is ongoing, and CR-39 radiography using track counting will be possible to determine the micro- or fine structure, i.e. *micro-autoradiography*, of ^{10}B distribution in the tumour (Ogura, 2001).

Clinically, administration of WOW emulsion drug encapsulated anti-cancer reagent in inner droplets, is surprisingly effective for both terminal and multi-originated in HCC when the drug is injected to suffered liver through a catheter inserted in liver artery. ^{10}B entrapped WOW emulsion is possible to deliver and transport the boron atoms to the cancer cell in tumour tissues. These results have shown that ^{10}B entrapped WOW emulsion is most useful for intra-arterial boron delivery carrier on BNCT to cancer. We now plan in vivo evaluation of ^{10}B entrapped WOW emulsion, and the clinical trial of BNCT for HCC patients, and hope to perform first BNCT trial with WOW emulsion in near future.

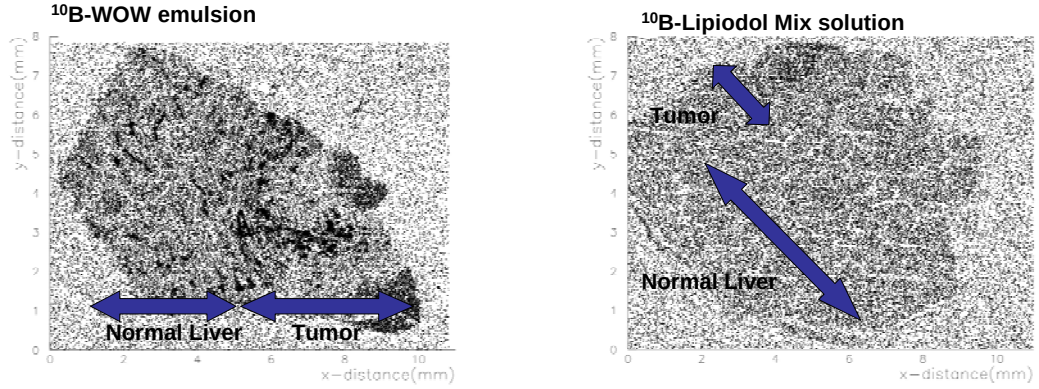

Figure 2 . Alpha and proton track etch pits distributions of the tumour after 3 days injection of ^{10}B entrapped WOW emulsion (Left) / 10B Lipiodol mix solution (Right) on VX-2 hepatic tumour bearing rabbit. This image shows tumour or normal liver site of a neutron-capture radiograph from a set of VX-2 hepatic cancers bearing rabbit that have received intra-arterial injection of 150 mg of ^{10}B. The slices of sacrificed and frozen tissues were prepared 3 days after injection.

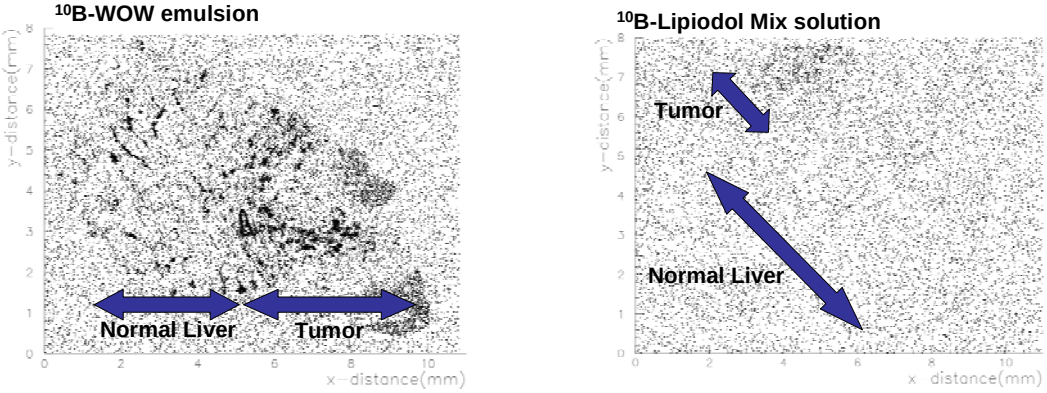

Figure 3. ^{10}B distributions of the tumour after 3 days injection of ^{10}B entrapped WOW emulsion (Left) / 10B Lipiodol mix solution (Right) on VX-2 hepatic tumour bearing rabbit. Images were obtained by the subtraction of proton track data from Fig. 2.

4. Conclusion

We will be able to apply boron entrapped WOW emulsion to BNCT for hepatocellular carcinoma, and NCAR technique for detection of effective ^{10}B carrier in BNCT for cancer.

Acknowledgements

This work was supported in part by a Grant-in-Aid from the Ministry of Education, Science and Culture, Japan (No. 11691202 and No. 11557092 to Hironobu Yanagie).

References

Higashi S, Shimizu M, Setoguchi T, 1993. Preparation of new lipiodol-emulsion containing water soluble anticancer agent by membrane emulsification technique (In Japanese with English abstract). Drug Delivery System, 8, 59-61.

Higashi S, et al, 1995. Arterial-Injection Chemo- therapy for Hepatocellular Carcinoma Using Monodispersed Poppy-Seed Oil Microdoloplets Containing Fine Aqueous Vesicles of Epirubicin. Cancer, 75, 1245-1254.

Kanematsu T, et al, 1989. A 5-year experience of lipiolization : Selective regional chemotherapy for 200 patients with hepatocellular carcinoma. Heoatology, 10: 98-102.

Ogura K, et al., 2001. Neutron capture autoradiography for a study on boron neutron capture therapy. Radiat. Meas., 34, pp.555-558.

Yanagie H, et al., 1991. Application of boronate anti-CEA immuno liposome to boron neutron capture therapy model. British J. Cancer, 3(4), 522 - 526.

Yanagie H, et al., 1997. Inhibition of human pancreatic cancer growth in nude mice by boron neutron capture therapy," British J. Cancer, 75 (5) : 660 - 665.

Yanagië H, et al., 1999. Neutron capture autoradiographic determination of ^{10}B distributions and concentrations in biological samples for boron neutron capture therapy. Nucl. Instr. Meth., A 424, pp.122-128.

Yanagie H, et al., 2004. Accumulation of boron compound of tumor with polyethylene- glycol binding liposome by using neutron capture autoradiography. Applied Radiation and Isotopes, 61:639-646.

Yanagie H, et al., 2006a. Application of boron-entrapped stealth lipsomes to inhibition of growth of Tumour cells in the in vivo boron neutron-capture therapy model. Biomed & Pharmacother, 60 : 43-50.

Yanagie H, et al., 2006b. Selective Enhancement of Boron Accumulation with Boron-Entrapped Water-in-oil-water Emulsion in VX-2 Rabbit Hepatic Cancer Model for BNCT, Proceedings of ICNCT12 (Nakagawa Y, Kobayashi T, eds), pp211-214.

Exploring a Boron-Sulphur Neutron Capture Therapy

I. Porras

Departamento de Física Atómica, Molecular y Nuclear, Facultad de Ciencias, Universidad de Granada, E-18071 Granada, Spain

Abstract

In the most commonly used version of neutron capture therapy, ^{10}B is being used to induce reactions (n,α) (Barth et al. 2005). We study the possibility of inducing a similar reaction using the nucleus of ^{33}S, for which the reaction cross section presents resonances for keV-neutrons, the highest peak occurring for 13.5 keV. By means of Monte Carlo simulation of point-like sources of neutrons of this energy, we show an enhancement effect on the equivalent dose in a four component standard tissue by the addition of both type of atoms, at the places where they are delivered. This motivates further research in a combined technique because both additions complement each other.

Keywords: neutron capture therapy, Monte Carlo simulation

1. Introduction

In a paper recently published (Porras 2008), an enhancement effect in the equivalent dose produced by a beam of 13.5 keV neutrons in water is shown when a high concentration of ^{33}S is found in the medium. As in boron neutron capture, this enhancement occurs very closely to the sulphur atom sites and is due to heavy nuclei (alpha particle and recoiling nucleus). An effect shown in this work is that the presence of sulphur-33, although producing a noticeable effect on the dose because of the (n,α) reactions induced by a small fraction of neutrons, do not reduce noticeably the neutron flux in any point of the medium. In addition to this, the low-energy neutron energies required for this effect are also in the range of the initial energies suitable for BNCT. This suggests the study of a combined technique of addition to the medium of both nuclei.

2. Material and methods

For testing the effect in human tissue of the addition of both ^{33}S and ^{10}B we have performed a simple Monte Carlo simulation of a point-like source of low energy neutron embedded in a four component standard ICRU tissue. The composition of this tissue (in mass) is the following: H: 10.1174%, O: 76.1826%, C: 11.1000% and N: 2.60%.

We have performed simulations when ^{10}B is present in the medium in an uniform concentration of 50 μg/cm^3 as a test case, and a much higher ^{33}S concentration (10 mg/cm^3**).**

As we are interested only in observing the relative effect of the sulphur addition compared with the effect of boron, the radiative capture of neutrons by either H or C has not been considered.

The cross section data for the reactions of neutrons with boron have been taken from the ENDF/B-VII (ENDF 2008) nuclear database and fitted to analytical forms. Only elastic and (n,α) processes have been considered, and described, respectively by:

$$\sigma_{tot}(B) = \left(\frac{0.611298}{E(MeV)^{0.50004}} + 1.86603 \right) \; b$$

$$\sigma_{\alpha}(B) = \frac{0.609698}{E(MeV)^{0.50014}} \; b$$

For reactions on S, and the scattering with H and O, the functions described by Porras (2008) have been employed. Finally, the cross sections for elastic scattering with C and N have been taken, for this energy range, as constants (4.75 and 9 barns, respectively).

3. Results and perspectives

As we have simulated a point-like source of neutrons, we remove the geometric factor in the equivalent dose $H(r)$ by defining the function $h(r) = 4\pi \; r^2 H(r)$. The results for this function are displayed in Figure 1.

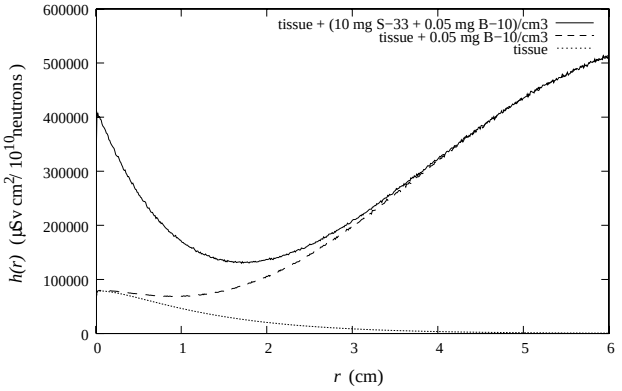

Figure 1. *Comparison of the equivalent dose produced by a point-like source of 13.5 keV neutrons in a four component tissue (dots) to the case when B-10 is added (dashes) and when both B-10 and S-33 are added to the medium (solid line)*

In this figure a comparison among (i) dose in tissue with no additions of either sulphur or boron (dots), (ii) addition of ^{10}B (dashes) and (iii) addition of both ^{10}B and ^{33}S (solid line) is illustrated. The quality factor relating the absorbed to the equivalent dose are calculated as a function of the linear energy transfer according to the ICRP recommendations in each energy deposition, as it was done in a previous paper (Porras 2008).

From the observation the figure, it can be noticed how the sulphur enhancement effect occurs in the small depth region, where the build-up of the neutron dose due to reactions in boron, which take place normally after thermalization, has not reached its maximum. This can be expected because (i) the sulphur effect is predominant the for neutrons which have not made any previous collision, and (ii) the optimum energies for boron capture are the lowest (thermal), which requires a number of previous collisions for the neutrons.

Although only qualitative, these simulations support the hypothesis of a cooperative effect between the sulphur and boron additions for neutron capture therapy. Nevertheless, they correspond to a theoretical situation that cannot be possible with the present technology. It is very difficult to deal with monoenergetic neutron sources of such a low energy (13.5 keV). No appropriate filters for using a reactor source are known, to the best of author's knowledge, for energies near this value, but there has not being a reason for investigating them in the past. Another possibility is the use of proton accelerators (Allen and Beynon 1995) on targets of materials such as Li or Sc, with a proton energy adjusted as to produce 13.5 keV neutrons in a particular direction. With respect to the sulphur carriers, our hope relies on the wide presence of sulphur in non-toxic organic compounds. The need of very high concentrations for this combined therapy suggests us the possibility of carrying nanostructures of a large number of sulphur atoms (e.g. $S_{1140}Mo_{576}$) (Tenne 2006) to the tumour cells with monoclonal antibodies.

4. Conclusions

In this work it has been shown a cooperative effect between the insertion of both ^{33}S and ^{10}B atoms in a medium, because (i) the former contributes to the absorbed dose before thermalization, (ii) the neutron flux is not noticeably reduced by sulphur, therefore almost all the neutrons are available for the capture by boron, and (iii) the regions of enhancement are different (sulphur enhances the absorbed dose before the build-up of the boron capture absorbed dose).

These facts open a new line of research in which many problems have to be solved: from designing an appropriate neutron source to finding a carrier for delivering a high concentration of ^{33}S. Some possibilities have been here discussed.

Acknowledgements

The author acknowledges financial support from the Spanish Ministerio de Educación y Ciencia under contract FIS2005-03577 and from the Junta de Andalucía (group FQM-220).

References

Allen D.A. and Beynon T.D., 1995. A design study for an accelerator-based epithermal neutron beam for BNCT. Phys. Med. Biol. 40, 807-822.

Barth R.F., Coderre J.A., Vicente M.G.H. and Blue T.E., 2005. Boron Neutron Capture Therapy of Cancer: Current Status and Future Prospects. Clin. Cancer Res. 11, 3987-4002.

ENDF 2008: Evaluated Nuclear Data File. URL: http://www.iaea.org/

Porras I., 2008. Enhancement of neutron radiation dose by the addition of sulphur-33 atoms, Phys. Med. Biol. 53, L1-L9.

Tenne R., 2006. Inorganic Nanotubes and Fullerene-Like Materials. Nature Nanotechnology 1, 103-111.

Calculations of the Dose Distribution in the Lungs of a Rat Model Irradiated in the Thermal Column of the TRIGA Reactor

N. Protti[1,2], S. Bortolussi[1,2], S. Stella[1,2], M.A. Gadan[1], A. De Bari[1,2], P. Bruschi[1], C. Ferrari [3], A.M. Clerici [3], C. Zonta [3], J. Bakeine [1], P. Dionigi [3], A. Zonta[3] and S. Altieri[1,2]

[1]*Department of Nuclear and Theoretical Physics, Pavia University, Italy*
[2]*National Institute for Nuclear Physics, INFN, Section of Pavia, Italy*
[3] *Dept. of Surgery, Experimental Surgery Laboratory, University of Pavia, Pavia, Italy*

To test the possibility to apply Boron Neutron Capture Therapy to the lung tumors, some rats are planned to be irradiated in the thermal column of the TRIGA reactor of the University of Pavia. Before the irradiation, lung metastases will be induced in BDIX rats, which will be subsequently infused with BPA. During the irradiation, the rats will be positioned in a box containing designed to shield the whole animal body except the thorax area. In order to optimize the irradiation set-up and to design a suitable holder, some MCNP calculations were performed.

A rat model was constructed using the MCNP geometry capabilities and was positioned in the box. The Teflon walls of the holder were filled with lithium carbonate and a window was opened in correspondence of the lungs zone. Different shapes of the holder and of the window were tested and analyzed in terms of the dose distribution obtained in the lungs and of the dose absorbed by the other radiosensitive structures in the rat. The results of the calculations and the best configuration of the holder will be presented and discussed.

Published by ENEA
Communication Unit
Lungotevere Thaon di Revel, 76 – 00196 Rome
www.enea.it

Editing: Giuliano Ghisu
Book cover: Cristina Lanari
Printed in October 2008 at ENEA Frascati Research Centre